Jatinder Kumar Ratan
Deepak Sahu
Nitin Naresh Pandhare
Anjireddy Bhavanam *Editors*

Advances in Chemical, Bio and Environmental Engineering

Springer

Environmental Science and Engineering

The ultimate goal of this series is to contribute to the protection of our environment, which calls for both profound research and the ongoing development of solutions and measurements by experts in the field. Accordingly, the series promotes not only a deeper understanding of environmental processes and the evaluation of management strategies, but also design and technology aimed at improving environmental quality. Books focusing on the former are published in the subseries Environmental Science, those focusing on the latter in the subseries Environmental Engineering.

More information about this series at https://link.springer.com/bookseries/7487

Jatinder Kumar Ratan · Deepak Sahu ·
Nitin Naresh Pandhare · Anjireddy Bhavanam
Editors

Advances in Chemical, Bio and Environmental Engineering

Editors
Jatinder Kumar Ratan
Department of Chemical Engineering
Dr. B. R. Ambedkar National Institute
of Technology Jalandhar
Jalandhar, Punjab, India

Nitin Naresh Pandhare
Department of Chemical Engineering
Dr. B. R. Ambedkar National Institute
of Technology Jalandhar
Jalandhar, Punjab, India

Deepak Sahu
Department of Chemical Engineering
Dr. B. R. Ambedkar National Institute
of Technology Jalandhar
Jalandhar, Punjab, India

Anjireddy Bhavanam
Department of Chemical Engineering
Dr. B. R. Ambedkar National Institute
of Technology Jalandhar
Jalandhar, Punjab, India

Preface

It is our immense pleasure to publish this book *Advances in Chemical, Bio and Environmental Engineering* in the esteemed book series "Environmental Science and Engineering". This book contains the high-quality research articles submitted in **International Conference on Chemical, Bio and Environmental Engineering (CHEMBIOEN-2021)**, organized at Dr. B. R. Ambedkar National Institute of Technology, Jalandhar (India), in August 2021. The eminent researchers have submitted their high-quality research and review articles to be published in this book, and we were delighted to handle those high-quality manuscripts. Our publication team worked days and nights and have followed a double-blind peer-review process to evaluate the potential of submitted manuscripts. The assessment of the manuscripts would not have been possible without the help and support of our esteemed peer reviewers and editors. Editors and reviewers had rejection rate of 40% to maintain the quality of this book.

This book is based on the research/review articles presented at International Conference CHEMBIOEN-2021, which was aimed to bring together leading academic scientists, researchers and research scholars to exchange and publish their experiences and research results about all aspects of Chemical, Bio and Environmental Engineering.

It also provided the premier interdisciplinary platform for researchers, practitioners and educators to present and discuss the most recent innovations, trends, concerns, practical challenges encountered and the solutions adopted in the field of Chemical, Bio and Environmental Engineering. This book focuses mainly on process design, remediation, risk assessment, nanotechnology, chemical reaction engineering, biochemical engineering, computational fluid dynamics and food and pharmaceutical engineering. This book's chapters focus on the state-of-the-art research, development and commercial prospective of recent advances in chemical sciences, innovative work in the field of Environmental Engineering, Biochemical Engineering, Chemical Engineering, Nanotechnology, Environment Impact Assessment and Green Technologies. The contents in this book cover various design concepts and control and optimization for applications in Chemical, Bio and Environmental Engineering. This book will be a useful resource for researchers, academicians

as well as professionals interested in the highly interdisciplinary field of Chemical, Bio and Environmental Engineering.

We would like to thank all the authors, reviewers, editors, publication team, organizing team, conference management team, advisory board members and patrons who supported this book to happen in the scheduled time frame. We also appreciate the continuous support and encouragement from the editors and supporting staff of the book series "Environment Science and Engineering". We are also thankful to the publisher Springer Nature for providing us an opportunity to work together. We wish to have long-term collaboration between CHEMBIOEN and Springer Nature. Finally, we would like to acknowledge Dr. B. R. Ambedkar National Institute of Technology, Jalandhar (India).

Jalandhar, India   Dr. Jatinder Kumar Ratan
                                                                                    Dr. Deepak Sahu
                                                                         Dr. Nitin Naresh Pandhare
                                                                          Dr. Anjireddy Bhavanam

Contents

Review on Synthesis of Iron Doped TiO$_2$ Nanoparticles

Rakhi Khandelwal and Shailja Tiwari

Abstract Titanium dioxide (TiO$_2$) is recognized as metal oxide semiconductor which could be extensively applied to diverse applications due to its exceptional and appropriate properties including nontoxic, excellent chemical stability, strong ultraviolet (UV) absorption, and wide band gap energy. Owing to its wide application range mass production of TiO$_2$ began in the early twentieth century by chemical methods like flame spray pyrolysis, sol gel method etc. Use of chemical method involves release of harmful chemicals in the environment so this pushed the researchers to think some alternative method for its synthesis. In last few years many researches focus on the green method (by using plant extract) for the synthesis of Titanium dioxide nanoparticles. The phytochemicals present in these natural extracts participate as capping agents or templates for the stabilization of crystalline phases and size control of the nanoparticles produced. Due to high recombination of activated electron_hole pair of TiO$_2$, it can only be excited by ultraviolet light hence to improve its light response in the visible light region metal doping has been done with Fe, Co, Ni and La. This paper is focused on the review of Fe-doped TiO$_2$ NPs. *Cymbopogon citratus* leaves extract is reported as an effective precursor for synthesis of Fe-doped TiO$_2$ NPs. This was found suitable to synthesis Fe-doped TiO$_2$ NPs with the size less than 12 $_{nm}$. It was confirmed that doping of Fe (III) ions into TiO$_2$ matrix leads to the inhibition of recombination of charge carriers, thereby enhancing photochemical quantum efficiency.

Keywords Fe-doped TiO$_2$ NPs · Green synthesis · Plant extract

1 Introduction

Titania is a commercially important inorganic material with several uses including dielectrics, paint pigments, and enhanced performance in photo catalytic applications for the removal of different organic pollutants from air and water (Vaidyanathan et al.

R. Khandelwal (✉) · S. Tiwari
Government Mahila Engineering College, Ajmer, Rajasthan, India
e-mail: rakhikhandelwal@gweca.ac.in

1

2001; Kumar and Bansal 2015, 2010a, 2010b; Li et al. 2003, 2004; Ratan and Saini 2019; Verma and Kumar 2014; Saini et al. 2020). TiO_2 has been widely employed as a promising semiconductor photocatalyst due to its large band gap, excellent chemical stability, and benign nature (Liu et al. 2014). The anatase and rutile phases of TiO_2 nanoparticles (NPs) are the two most prevalent crystal shapes. The anatase phase of TiO_2 has been discovered to have greater photocatalytic activity than the rutile phase (Liu et al. 2012). However, TiO_2's high band gap limits its practical uses under visible light, which covers a large section of the solar spectrum. Several attempts have been made to dope a transition metal ion into an anatase TiO_2 lattice in order to resolve this problem (Khairy and Zakaria 2014; Jingsheng et al. 2013; Binas et al. 2012; Cao et al. 2012). Due to its half-filled d-electronic configuration and similar ionic radius to Ti^{4+}, the Fe^{3+} ion has received a lot of interest among the numerous transition metal ions, suggesting that the Fe^{3+} ion may assimilate into the TiO_2 lattice structure (Khan and SwatiI 2016). Its usefulness is greatly enhanced as its size is reduced to nano range. Hence its wide range of applications attract researchers for the synthesis of Fe doped TiO_2 nanoparticles. Various chemical methods like chemical vapor deposition (Jian and Xudong 2011), the micro emulsion method (Shen et al. 2011), microwave assisted hydrothermal synthesis (Melis et al. 2012) and sol–gel (Valencia et al. 2013; Julkapli et al. 2014) etc. have been employed for its synthesis but chemical methods require specific conditions, hazardous chemicals and are highly expensive and also releases toxic chemicals to environment which creates a serios ecotoxicological concern. Therefore, it is the need of hour to search for some ecofriendly method for the synthesis of Fe doped TiO_2 nanoparticles. There are various green methods for the synthesis of nanoparticles which includes use of microorganisms, plant extracts etc. But unfortunately, till now research on the green methods for the synthesis of Fe doped TiO_2 nanoparticles is substantially less. In this paper we present a comparative study of chemical vs green methods used for the synthesis of Fe doped TiO_2 nanoparticles. Figure 1 shows the various methods used for the synthesis of Fe doped TiO_2 nanoparticles.

2 Chemical Methods

For the synthesis of Fe doped TiO_2 nanoparticles, researchers have used a variety of methods. In this section, we'll go through some of the chemical methods for preparing Fe doped TiO_2 nanoparticles.

2.1 Sol–gel Method

In this approach, a network is formed in the continuous liquid phase utilizing colloidal suspension (sol) and gelatin (gel). Metal alkoxides and aloxysilanes ions are utilized as a precursor for colloidal synthesis. The most commonly used compounds for silica

Fig. 1 Various method used
for the synthesis of Fe doped
TiO₂ nanoparticles
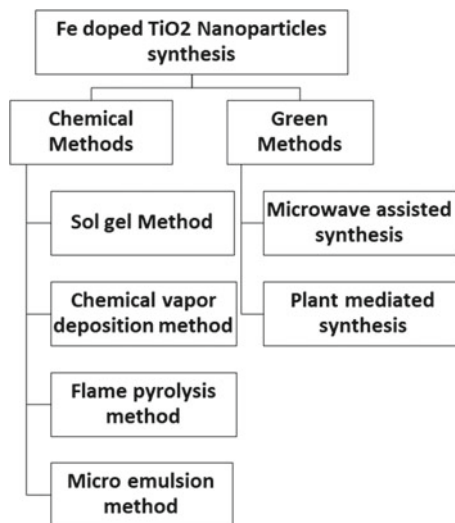
gel formation are tetramethoxysilane (TMS) and tetraethoxysilane. This process begins with the preparation of a homogenous solution of one or more suitable metal alkoxides, followed by the addition of a catalyst to start a reaction at a specified pH. As a solvent, alcohol is used. Hydrolysis, condensation, particle growth, and particle agglomeration are the four key stages of sol–gel method (Rajput 2015). So, in this method a polymeric network is formed in which metallic NPs can be retained (Pena-Pereira et al. 2012). To prepare the Fe doped TiO₂ nanoparticles by sol gel method various researchers used different precursors such as—Iron (III) Chloride 6-Hydrate, Tetra-isopropylorthotitanate, ethanol, citric acid and Acetyl acetone (Nasralla et al. 2013), Titanium tetra-isopropoxide (TTIP), Fe(NO₃)₃·9H₂O and nitric acid (Reginaldo et al. 2012), Tetra-isopropyl Orthotitanate, Ethanol, Anhydrous Ferric Chloride (FeCl₃) and Hydrochloric acid (Barkhade and Banerjee 2019). Figure 2 shows various steps of the synthesis of nanoparticles by sol gel method. Although the sol gel technique is an excellent way to make Fe doped TiO₂ nanoparticles with good purity, controlled porosity, and varying composition of Fe and Ti but still it has two major drawbacks—first, it requires an organic solvent which is hazardous to the environment and second it is a time-consuming process.

2.2 Chemical Vapor Deposition Method

In the chemical vapor deposition (CVD) method thin film of target material is deposited on a surface through the chemical reaction of gaseous molecule containing atoms useful for film formation (Pedersen and Elliott 2014). In past few decades lot of research done on the synthesis of TiO₂ and Fe doped TiO₂ nanoparticles using

Fig. 2 Preparation of Fe
doped nanoparticles by
sol–gel method
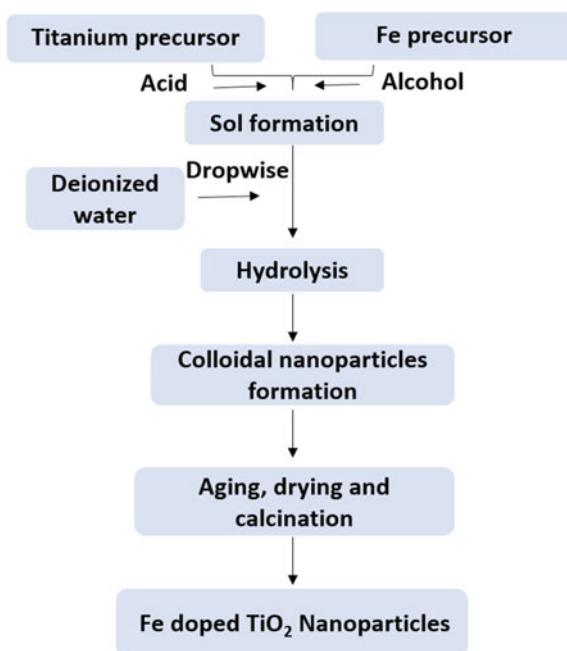
this method with the use of titanium (IV) but oxide (TBOT) as titanium precursor
and different amounts of Fe (III) salts as Fe precursor in Nitrogen gas atmosphere
(Othman et al. 2010). The surface morphology and crystal structure of nanostruc-
tures can be regulated using this approach; however, one noteworthy observation was
that the photocatalytic activity of Fe doped TiO_2 nanoparticles produced using this
method was reduced. Because of their lower photocatalytic activity, Fe^{3+} ions are
thought to have served as recombination centers for electron and hole pairs rather
as trap sites for eventual charge transfer at the interface (Othman and Abdul Rashid
2011). Figure 3 shows the preparation of Fe doped TiO_2 nanoparticles by chemical
vapor deposition method.

2.3 Flame Pyrolysis Method

The operating concept of the flame pyrolysis technique is the formation of nanos-
tructures by spraying liquid precursor directly into flame. In flame spray pyrolysis an
solution of Ti salt and Fe salt is sprayed as a fine mist, through a capillary and into a
flame. Then, small droplets are formed while the solvent burns inside the flame. The
pyrolysis step converts the salt to metal oxide, and the metal oxide atoms aggregate

Fig. 3 Preparation of Fe
doped nanoparticles by
chemical vapor deposition
method
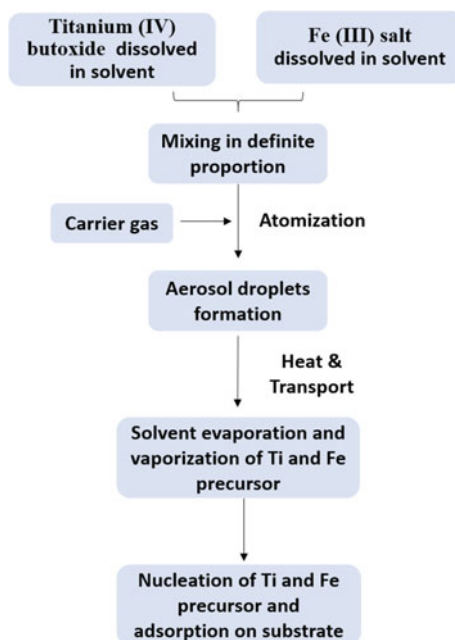
into nanoparticles, which are subsequently gathered on a substrate (Tricoli et al. 2016; Eslamian and Heine 2008). In this method titanium tetra-isopropoxide is used as the titanium precursor and iron naphthenate is used as the iron precursor (Teoh et al. 2007) and in some cases ferrocene is used as an iron precursor and (TTIP) is used as a titanium precursor (Ismail et al. 2021). Schematic representation of synthesis of Fe doped TiO$_2$ nanoparticles is shown in Fig. 4. This is a promising method for the synthesis of Fe doped TiO$_2$ nanoparticles but the process is expensive hence can not be scaled up at large level.

2.4 Micro Emulsion Method

In the microemulsion method, two microemulsions carrying the necessary reactants are mixed together to generate two microemulsions: one is a precursor emulsion and the other is a reducing agent emulsion. Reactant exchange occurs during the collision of water droplets in the microemulsion. Since this reactant exchange is too rapid, a precipitation reaction occurs in the nanodroplets, followed by nucleation growth and coagulation of primary particles, resulting in final nanoparticles that are surrounded by water and/or stabilized by surfactants (Bhagyaraj et al. 2018). For the synthesis of iron-doped TiO$_2$ nanoparticles Ti tetraisopropoxide was added to an inverse emulsion containing an aqueous solution of iron (III) nitrate nonahydrate dispersed in n-heptane, using Triton X-100 (Aldrich)

Fig. 4 Preparation of Fe
doped nanoparticles by flame
pyrolysis method
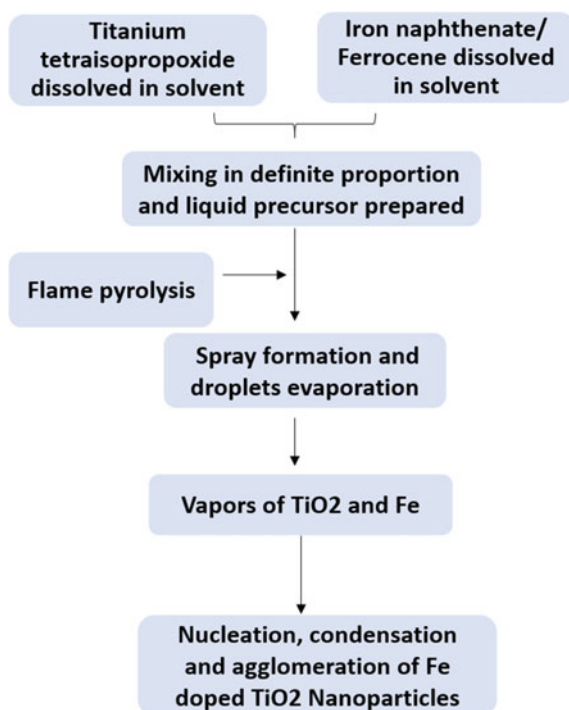
as surfactant and hexanol ascosurfactant (Fuerte et al. 2001). The microemulsion method isa simple synthetic approach it provides good control on particle size and morphology of nanoparticles, thermodynamic stability, monodispersity, homogeneity. However, there are certain issues while using the microemulsion technique such as surfactant toxicity and its need in large amount and microemulsion stability is highly sensitive that may vary with temperature and pH change. Figure 5 represents the formation of Fe dopes TiO_2 nanoparticles by microemulsion method.

Comparative analysis of all the above four chemical methods used for the synthesis of Fe doped TiO_2 nanoparticles is given in Table 1.

3 Green Methods for the Synthesis of Fe Doped TiO_2 Nanoparticles

Chemical methods employed for Fe doped TiO_2 nanoparticles need high temperature, extremely toxic reductants, and stabilising agents, all of which can be harmful to humans and when these wastes are released in water bodies, they are equally harmful for aquatic life. Green synthesis of metallic nanoparticles, on the other hand, is an environmentally benign approach that uses relatively little energy and is also cost
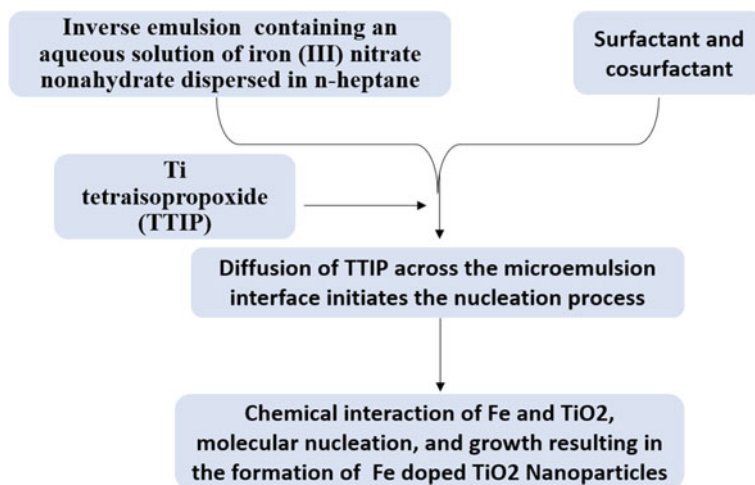
Fig. 5 Preparation of Fe doped nanoparticles by micro emulsion method

effective. Therefore, it is indeed the need of the hour to focus on the use of some eco-friendly methods for the synthesis of nanoparticles. Lot of research work has been done on the use of green methods for synthesis of nanoparticles. Various green method employed for the synthesis of Fe doped TiO$_2$ nanoparticles which mainly includes microwave assisted synthesis and synthesis by using plant extracts (Andjelkovic et al. 2014; Jahdi et al. 2020; Ricardo et al. 2019).

3.1 Microwave Assisted Synthesis

The capacity of a specific substance (i.e., solvent and/or reagents) to absorb microwave radiation and transform it into heat is the basis for this method of synthesis (Rajiv et al. 2018). A wide range of binary and ternary oxides have been prepared using this method. In the last several years, a lot of research has gone into using this method to synthesize Fe doped TiO$_2$ nanoparticles. Microwave-assisted synthesis is a more cost-effective, faster, and environmentally friendly way to make nanomaterials with excellent accuracy and performance. Controlling nucleation and growth kinetics allows for the production of nanomaterials with precise particle sizes. A microwave assisted hydrothermal synthesis approach was used to effectively synthesize Fe-doped TiO$_2$ nanocomposites. Doping TiO$_2$ with Fe resulted in a substantial increase in the visible area of TiO$_2$ photocatalytic absorption (Galema 1997; Boonyod et al. 2011). But studies also showed that for the synthesis of Fe doped TiO$_2$ nanoparticles as photocatalysts, microwave irradiation does not appear to be effective as it could not substantially increases the absorption in visible region (Esquivel et al. 2013;

Table 1 Comparative analysis of the chemical methods

Name of method	Precursor required	Operating conditions	Disadvantages	References
Sol–gel method	Tetra-isopropylorthotitanate, iron (III) chloride 6-hydrate, ethanol, citrate acid/HCl/nitric acid and acetyl acetone	High temperature	Expensive, more time consuming process, use of organic solutions that can be toxic	Nasralla et al. (2013), Reginaldo et al. (2012), Barkhade and Banerjee (2019)
Chemical vapor deposition method	Titanium (IV) butoxide (TBOT), Fe III salt	High temperature, nitrogen atmosphere	Expensive, time consuming process	Othman et al. (2010), Othman and Abdul Rashid (2011)
Flame pyrolysis method	Titanium tetraisopropoxide and iron naphthenate/Ferrocene	High temperature and Methane and oxygen supply for piolet flame	Expensive, time consuming process, safety issue during the process	Teoh et al. (2007), Ismail et al. (2021)
Micro emulsion method	Ti tetraisopropoxide and solution of Fe III nitrate, Triton X-100 as surfactant and hexanol as cosurfactant	Room temperature	Large amount of surfactant requires, expensive, wastage of chemicals which may lead harmful impact on environment	Fuerte et al. (2001)

Paola et al. 2002). Schematic preparation of Fe dopes TiO_2 nanoparticles is shown in Fig. 6.

3.2   Green Synthesis by Using Plant Extract

The use of plant extracts have become popular in recent years for nanoparticle syntheses because they are nontoxic, inexpensive, and widely available. Synthesis by using plant extracts have gained popularity as a simple, efficient, cost-effective and practical method for producing nanoparticles, as well as an ideal alternative to traditional preparation methods. In this "one-pot" synthesis process, different plants can be used to reduce and stabilize metallic nanoparticles. Many researchers have used this green synthesis method to prepare metal/metal oxide nanoparticles from plant extracts in order to further investigate their uses (Aslam et al. 2021; Khandelwal

Fig. 6 Microwave assisted synthesis of Fe doped nanoparticles
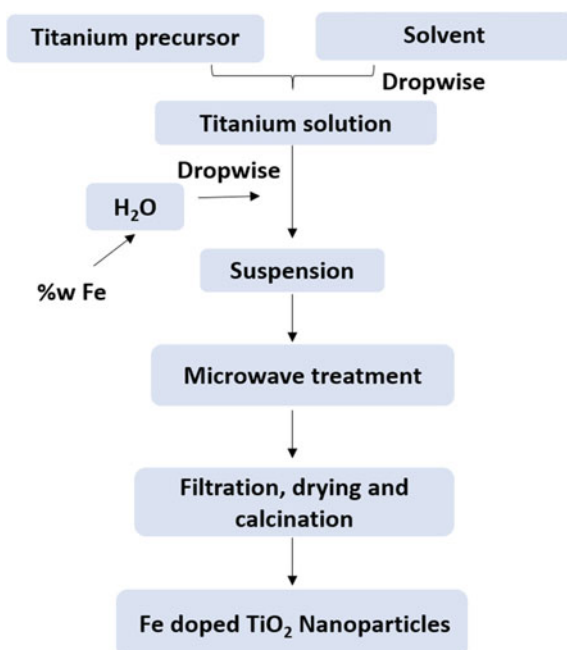
et al. 2020, 2220; Singh et al. 2018; Akintelu and Folorunso 2020). Plants have biomolecules like carbohydrates, proteins, and coenzyme with exemplary potential to reduce metal salt into nanoparticles and the proteins present in the plant extract act as a capping agent to stabilize the synthesized nanoparticles, therefore no extra stabilizing agent is required in this method. Using the plants extracts has the several advantages which can be summarized in the Fig. 7.

In past few years plant extracts using different plant parts (leaves, roots, fruits etc.) have been extensively used for the synthesis of Fe doped TiO$_2$ nanoparticles. In this method firstly the plant part is dried in the shade and then its fine powder is then subjected to a solvent extraction process using a soxhlet extractor for 6 h in approximately 500 mL of distilled water (Balakrishnan et al. 2014; Geetha and Geetha 2014). Further, this extract is used as a bio reductant and mixed with the titanium isopropoxide in a specific ratio to form the TiO$_2$ nanoparticles. Figure 8 shows the green synthesis of Fe doped TiO2 nanoparticles by plant extract.

Different plant extracts such as *Cymbopogon citratus* leave extract, *Jatropha curcas* L. (Goutam, et al. 2018), *Aloe vera* extract (Rao et al. 2015), *Ocimum tenuiflorum* Plant and *Calotropis gigantea* (Reddy et al. 2019), orange peel extract (Amanulla and Sundaram 2019) etc. Table 2 shows Comparative analysis of the synthesis of TiO$_2$ nanoparticles by using plant extracts.

Till now very few literatures is available on synthesis of Fe doped TiO$_2$ nanoparticles. As per best of our knowledge Ricardo A. Solano et al. reported their studies on *Cymbopogon citratus* leave extract for synthesis of Fe doped TiO$_2$ nanoparticles.

ADVANTAGES of GREEN SYNTHESIS by using PLANT EXTRACTS

1 Eco friendly method as no toxic chemical is used

2 Energy saving process as external experimental conditions like high temperature, pressure are not required

3 One pot synthesis, low cost process

4 Can be used for large scale production of nanoparticles
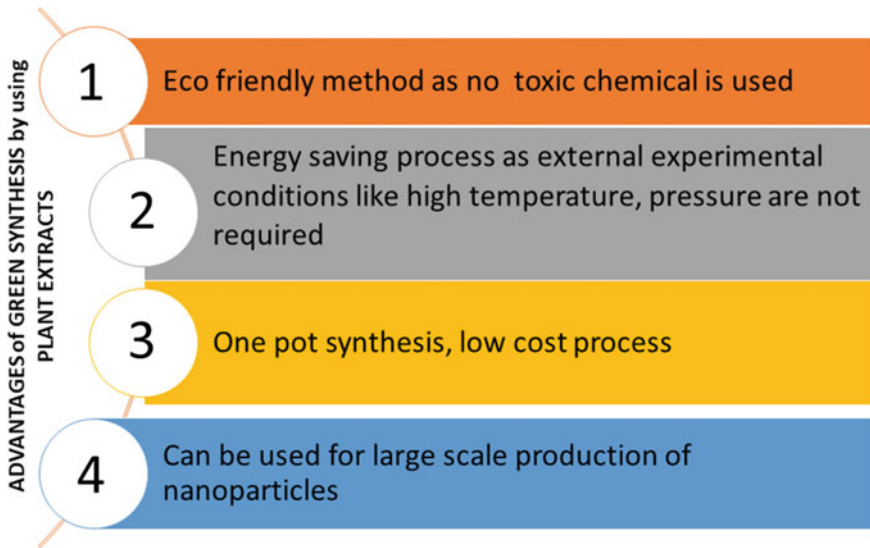
Fig. 7 Advantages of green synthesis by plant extracts

Titanium tetraisopropoxide and Fe (III) salt solutions

Plant extract

Mixing in definite proportion

Constant agitation for 30 minutes

Fe doped TiO2 Nanoparticles formed in solution

Phytochemicals present in the plant extract act as a reducing agent as well as the stabilizing agent

Filtration, Centrifugation, drying and calcination

Dry powder of Fe doped TiO2 Nanoparticles is prepared

Fig. 8 Preparation of Fe doped nanoparticles by using plant extract

Table 2 Synthesis of TiO$_2$ NPs using different plant extracts

S. No.	Plant extract used for the synthesis	Size (nm)	Morphology	References
1	*Cymbopogon citratus*	9.37–10.33	quasi-nanospheres	Ricardo et al. (2019)
2	*Jatropha curcas* L	13	Not reported	Goutam, et al. (2018)
3	*Aloe vera*	20	Irregular	Rao et al. (2015)
4	*Ocimum tenuiflorum*	19.8	Flower like structure	Reddy et al. (2019)
5	*Calotropis gigantea*	9.4	Flower like structure	Reddy et al. (2019)
6	Orange peel	21.6 and 17.3	angular nanostructure	Amanulla and Sundaram (2019)

They have successfully synthesised TiO$_2$ (anatase phase only) doped with a different molar ratio Fe^{3+}: Ti with the crystalline size between 9.37 nm and 10.33 nm. Although this method successfully synthesized the size controlled Fe doped TiO$_2$ nanoparticles but still the detailed study of the properties of nanoparticles synthesized by this method in view of their applicability is needed.

4 Summary and Future Prospective

TiO$_2$ NPs are a good semiconductor with outstanding thermal stability, optical and dielectric characteristics, biocompatibility, and non-toxicity. TiO$_2$ NPs are utilised in a variety of applications, including photocatalysis, DSSC, lithium-ion batteries, optoelectronic devices, H$_2$O$_2$ reduction, solar cells, and more. But two main problems are associated with the production and applications of these NPs are—(a) Larger energy gap (b) Harmful and expensive synthesis methods. To overcome the first problem doping of TiO$_2$ NPs may be done with some transition metals such as Co, Fe, Zn, Ni etc. Since radius of iron is similar to that of Ti^{4+} therefore it is suitable for doping in TiO$_2$. Extent of decrease in the band gap may differ with the method used for the synthesis of Fe doped TiO$_2$ nanoparticles. Second problem is with the synthesis method and that has been successfully overcame by using green methods for the synthesis. Green nanoparticle synthesis is a long-term, environmentally acceptable, low-cost method that is typically devoid of chemical pollutants and can be scaled up at large level and are very cost effective. Although various methods for nanoparticle synthesis have been successfully developed, more precise approaches are needed to overcome the limits of existing methods so that appropriate commercial application can be ensured.

Conflicts of Interest/Competing Interests The authors declare that they have no known competing financial interests.

References

Akintelu SA, Folorunso AS (2020) A review on green synthesis of zinc oxide nanoparticles using plant extracts and its biomedical applications. BioNanoScience 10:848–863

Amanulla AM, Sundaram R (2019) Green synthesis of TiO_2 nanoparticles using orange peel extract for antibacterial, cytotoxicity and humidity sensor applications. Mater Today Proc 8(1):323–331

Andjelkovic I et al (2014) Fe-doped TiO_2 prepared by microwave-assisted hydrothermal process for removal of As (III) and As (V) from water. Ind Eng Chem Res 53(27):10841–10848

Aslam M, Abdullah AZ, Rafatullah M (2021) Recent development in the green synthesis of titanium dioxide nanoparticles using plant-based biomolecules for environmental and antimicrobial applications. J Ind Eng 98:1–16

Balakrishnan B, Paramasivam S, Arulkumar A (2014) Evaluation of the lemongrass plant (*Cymbopogon citratus*) extracted in different solvents for antioxidant and antibacterial activity against human pathogens. Asia Pac J Trop Dis 4:S134–S139

Barkhade T, Banerjee I (2019) Optical properties of Fe doped TiO_2 nanocomposites synthesized by Sol-Gel technique. Mater Today Proc 18:1204–1209

Bhagyaraj SM, Oluwafemi OS, Kalarikkal N, Thomas S (2018) Synthesis of inorganic nanomaterials: advances and key technologies, 1st edn. Woodhead Publishingis, United kingdom

Binas VD, Sambani K, Maggos T, Katsanaki A, Kiriakidis G (2012) Synthesis and photocatalytic activity of Mn-doped TiO_2 nanostructured powders under UV and visible light. Appl Catal B 113–114:79–86

Boonyod S, Sutthisripok W, Sikong L (2011) Antibacterial activity of TiO_2 and Fe^{3+} doped TiO_2 nanoparticles synthesized at low temperature. Adv Mater Res 214:197–220

Cao Y, He T, Zhao L, Enjun W, Wensheng Y, Yaan C (2012) Structure and phase transition behavior of Sn^{4+}—doped TiO_2 nanoparticles. J Phys Chem C 113(42):18121–18124

Di Paola A, Marcì G, Palmisano L, Schiavello M, Uosaki K, Ikeda S, Ohtani B (2002) Preparation of polycrystalline TiO_2 photocatalysts impregnated with various transition metal ions: characterization and photocatalytic activity for the degradation of 4-nitrophenol. J Phys Chem B 106(3):637–645

Eslamian M, Heine MC (2008) Characteristics of spray flames and the effect of group combustion on the morphology of flame-made nanoparticles. Nanotechnology 19:45712

Esquivel K, Nava R, Zamudio-Méndez A, Vega González M, Jaime-Acuña OE, Escobar-Alarcón L, Peralta-Hernández JM, Pawelec B, Fierro JLG (2013) Microwave-assisted synthesis of (S) Fe/TiO_2 systems: effects of synthesis conditions and dopant concentration on photoactivity. Appl Catal B Environ 140–141:213–224

Fuerte A, Hernández-Alonso MD, Maira AJ, Martínez-Arias A, Fernández-García M, Conesa JC, Soria J (2001) Visible light-activated nanosized doped-TiO_2 photocatalysts. Chem Commun 24:2718–2719

Galema S (1997) Microwave chemistry. Chem Soc Rev 26:233

Geetha TS, Geetha N (2014) Phytochemical screening, quantitative analysis of primary and secondary metabolites of *cymbopogan citratus* (DC) stapf. leaves from Kodaikanal hills, Tamilnadu. Int J PharmTech Res 6(2):521–529

Goutam SP et al (2018) Green synthesis of TiO_2 nanoparticles using leaf extract of *Jatropha curcas* L. for photocatalytic degradation of tannery wastewater. Chem Eng J 336:386–396

Ismail MA, Hedhili MN, Anjum DH, Singaravelu V, Chung SH (2021) Synthesis and characterization of iron-doped TiO_2 nanoparticles using ferrocene from flame spray pyrolysis. Catalysts 11:438

Jahdi M, Mishra SB, Nxumalo EN, Mhlanga SD, Mishra AK (2020) Synergistic effects of sodium fluoride (NaF) on the crystallinity and band gap of Fe-doped TiO_2 developed via microwave—assisted hydrothermal treatment. Opt Mater 104:109844

Jian S, Xudong W (2011) Growth of rutile titanium dioxide nanowires by pulsed chemical vapor deposition. Cryst Growth Des 11:949–954

Jingsheng W, Yanlong Yu, Li S, Guo L, Wang E, Cao Y (2013) Doping behavior of Zr^{4+} ions in Zr^{4+}—doped TiO$_2$ nanoparticles. J Phys Chem C 117(51):27120–27126

Julkapli NM, Bagheri S, Abd Hamid SB (2014) Titanium dioxide as a catalyst support in heterogeneous catalysis. Sci World J 2014:1–25

Khairy M, Zakaria W (2014) Effect of metal-doping of TiO$_2$ nanoparticles on their photocatalytic activities toward removal of organic dyes. Egypt J Pet 23(4):419–426

Khan H, SwatiI K (2016) Fe^{3+}—doped anatase TiO$_2$ with d–d transition, oxygen vacancies and Ti^{3+} centers: synthesis, characterization, UV–vis photocatalytic and mechanistic studies. Ind Eng Chem Res 55:6619–6633

Khandelwal R, Arora SK, Phase DM, Pareek A, Kant R (2020) Study of antimicrobial activities of green synthesized silver nanoparticles. J Indian Chem Soc 97:455–459

Khandelwal R et al (2020) Anti cancer potential of green synthesized silver nano particles. In: AIP conference proceedings of 3rd international conference on condensed matter and applied physics 2220, American Institute of Physics United States

Kumar J, Bansal A (2010) Photocatlytic degradation of amaranth dye in aqueous solution using sol-gel coated cotton fabric. In: Proceedings of the world congress on engineering and computer science, vol 2, pp 20–22

Kumar J, Bansal A (2010) Photocatalytic degradation of amaranth dye over immobilized nano-crystals of TiO$_2$. In: International conference on energy and environment, pp 129–133

Kumar J, Bansal A (2015) CFD simulations of immobilized-titanium dioxidebased annular photocatalytic reactor: model development and experimental validation. India J Chem Technol 22:95–104

Li Y, White T, Lim SH (2003) Structural control and its influence on photoactivity and phase transformation of TiO$_2$ nanoparticles. Rev Adv Mater Sci 5:211–215

Li Y, White T, Lim H (2004) Low-temperature synthesis and microstructural control of titania nano-particles. J Solid State Chem 177:1372–1381

Liu L, Zhao H, Andino JM, Li Y (2012) Photocatalytic CO$_2$ reduction with H$_2$O on TiO$_2$ nanocrystals: comparison of anatase, rutile, and brookite polymorphs and exploration of surface chemistry. ACS Catal 2:1817–1828

Liu G, Yang HG, Pan J, Yang YQ, Lu GQ, Cheng H-M (2014) Titanium dioxide crystals with tailored facets. Chem Rev 114:9559–9612

Melis A, Petra L, Hopkins SC, Glenn P, Johan vander E, Susugna R, Xavier G, Glowacki BA, Isabel VD (2012) Deposition of photocatalytically active TiO$_2$ films by inkjet printing of TiO$_2$ nanoparticle suspensions obtained from microwave—assisted hydrothermal synthesis. Nanotechnology 23:165603

Nasralla N et al (2013) Structural and spectroscopic study of Fe-doped TiO$_2$ nanoparticles prepared by sol–gel method. Scientia Iranica 20(3):1018–1022

Othman SH, Abdul Rashid S (2011) Fe-doped TiO$_2$ nanoparticles produced via MOCVD: synthesis, characterization, and photocatalytic activity. J Nanomater 2011:1–8

Othman SH, Abdul Rashid S, Mohd Ghazi TI, Abdullah N (2010) Effect of Fe doping on phase transition of TiO$_2$ nanoparticles synthesized by MOCVD. J Appl Sci 10(12):1044–1051

Pedersen H, Elliott SD (2014) Studying chemical vapor deposition processes with theoretical chemistry. Theoret Chem Acc 133(5):1476

Pena-Pereira F, Duarte RMBO, Duarte AC (2012) Immobilization strategies and analytical applications for metallic and metal-oxide nano materials on surfaces. Trends Anal Chem 40:90–105

Rajiv P, Jayaseelan C, Kamaraj C, Rajasree SRR, Regina R (2018) In vitro antimalarial activity of synthesized TiO2 nanoparticles using Momordica charantia leaf extract against plasmodium falciparum. J Appl Biomed 16(4):378–386

Rajput N (2015) Methods of preparation of nanoparticles—a review. Int J Adv Eng Technol 7(6):1806

Rao KG, Ashok CH, Rao VK, CH. Chakra S, Tambur P (2015) Green synthesis of TiO$_2$ nanoparticles using Aloe Vera extract. Int J Adv Res Phys Sci 2(1A):28–34

Ratan JK, Saini A (2019) Enhancement of photocatalytic activity of self-cleaning cement. Mater Lett 244:178–181

Reddy PNK et al (2019) Structural, optical and electrochemical properties of TiO_2 nanoparticles synthesized using medicinal plant leaf extract. Ceram Int 45(13):16251–16260

Ricardo AS, Adriana PH, Maestre D, Cremades A (2019) Fe-TiO2 nanoparticles synthesized by green chemistry for potential application in waste water photocatalytic treatment. J Nanotechnol 2019:11

Santos RS et al (2012) Iron insertion and hematite segregation on Fe-doped TiO2 nanoparticles obtained from sol–gel and hydrothermal methods. ACS Appl Mater Interfaces 4:5555−5561

Saini A, Arora I, Ratan JK (2020) Photo-induced hydrophilicity of microsized—TiO_2 based self-cleaning cement. Mater Lett 260:126888

Shen X, Zhang J, Tian B (2011) Microemulsion—mediated solvothermal synthesis and photocatalytic properties of crystalline titania with controllable phases of anatase and rutile. J Hazards Mater 192:651–657

Singh J, Dutta T, Kim KH et al (2018) Green synthesis of metals and their oxide nanoparticles: applications for environmental remediation. J Nanobiotechnol 16:84

Teoh WY, Amal R, Mädler L, Pratsinis SE (2007) Flame sprayed visible light-active Fe-TiO_2 for photomineralisation of oxalic acid. Catal Today 120:203–213

Tricoli A, Nasiri N, Chen H, Wallerand AS, Righettoni M (2016) Ultra-rapid synthesis of highly porous and robust hierarchical ZnO films for dye sensitized solar cells. Sol Energy 136:553559

Vaidyanathan S, Eduardo W, Kamat PV (2001) Semiconductor—metal composite nanostructures. To what extent do metal nanoparticles improve the photocatalytic activity of TiO_2 films? J Phys Chem B 105(46):11439–11446

Valencia S, Vargas X, Rios L, Restrepo G, Marín JM (2013) Sol–gel and low-temperature solvothermal synthesis of photoactive nano-titanium dioxide. J Photochem Photobiol A 251:175–181

Verma P, Kumar J (2014) Degradation and microbiological validation of Meropenem antibiotic in aqueous solution using UV, UV/H_2O_2, UV/TiO_2 and $UV/TiO_2/H_2O_2$ processes. Int J Eng Res Appl 4(7):58–65

Microbial Degradation of Conventional Polyethylene Waste: Current Status and Future Prospective

Shilpa, Nitai Basak, and Sumer Singh Meena

Abstract Polyethylene is a polymeric substance with a wide range of applications. It is a saturated polymer expressed as C_nH_{2n}, which is an extensively used hydrocarbon polymer. The ambidexterity of these polymers arises from the fact that they are made up of cheap petrochemical feedstock, with potent catalytic-polymerization processes and generally used in food packaging, textiles, automotive components, lab equipment, etc. Urbanization and industrialization have led to the massive accumulation of synthetic plastic waste in the environment. This waste problem has been recognized as the most critical environmental challenge which is affecting the natural ecosystem. There is a steady increase in the usage of polyethylene, and this is becoming a major threat to our planet. The marine ecosystem is badly affected by polyethylene debris as different sea species suffered from an obstruction in their oesophagus which frequently resulted in death. Hence, finding a more economical and eco-friendlier solution is of utmost importance instead of traditional methods of waste management. Traditional plastic waste management methods such as chemical and physical methods are very expensive and result in the release of toxic pollutants such as furans and dioxins in the environment. Biodegradation of polyethylene waste using microbial methods is a more promising and eco-friendly solution. Several microorganisms have been reported in the past few years with the ability to degrade polyethylene, efficiently. Further, the biotic methods in combination with abiotic processes can enhance the degradation of polyethylene by manifolds. Microbial agents have been shown to ingest polyethylene by converting its complex structure into simpler carbon monomers and utilizing them as a sole carbon source. This chapter provides an overview about the plastic waste problem and discuss the role of biotechnological-based approaches and their importance in enhancing the biodegradation of polyethylene.

Keywords Synthetic plastics · Biodegradation · Microorganisms · Microbial degradation · Polyethylene

Shilpa · N. Basak · S. S. Meena (✉)
Department of Biotechnology, Dr. B. R. Ambedkar National Institute of Technology, Jalandhar, Punjab, India
e-mail: meenass@nitj.ac.in

1   Introduction

The first synthetic polymer came into existence in the year 1869 in replacement of ivory. These polymeric materials were derived from petroleum-based sources and hydrocarbons. These materials are made up of long chains of small molecules bonded together and arranged in repeated units. By the year 1950, these materials entered the commercial market globally. Polymers are categorized into different classes based on their nature and complex structure and properties (Evans and Schmalensee 2005). Based on chemical composition, polymers are sub-classified as polystyrene (PS) and polyethylene (PE). Polyethylene or commonly called polythene is a highly used plastic material in today's world. This polymeric material is primarily used in the packaging industry for different applications (such as plastic bags, containers, or geo-membranes). Reported data suggests that more than 100 million tonnes of polyethylene resins were produced annually, which accounts for approximately 34% of the total plastic market. Globally countries like China, India, Vietnam, the Philippines, and Sri Lanka annually produce around 1–1.5 million tonnes of plastics, and approximately 56% of this contributes the plastic waste. A survey on the Great Pacific Garbage Patch estimated around 80,000 tons of plastic waste in the Pacific latitudes (Lebreton et al. 2018).

Polyethylene (PE) is generally a chain of ethylene monomers. It comes under the category of thermoplastics (material that can be melted and re-casted again and again) and is low in strength. These are remarkably resistant to degradation, because of their chemical and biological inertness. With the growth and urbanization in the technological sector, the plastic industry has flourished many folds, which has led to the accumulation of plastic debris in the environment. Low-density polyethylene (LDPE) and high-density polyethylene (HDPE) are the most prominent used polyethylene types (Dey et al. 2012). LDPE is prepared using high-pressure polymerization of ethylene monomers. It is a highly durable and chemically complex material. LDPE has applicability in agricultural mulching in fields, is also used in the formation of poly-houses, and is used for the coating of paper, plastics, and in the textile sector. HDPE on the other hand is produced by the catalytic process and consists of lesser branch chains. It is usually hard, durable which makes it applicable in the sector of industries for the formation of garbage containers, jugs, carry bags, tubs, and detergent bottles (Barnes et al. 2009).

Polyethylene or plastic pollution is mainly rising due to the mismanagement of the waste material and has become a worldwide concern since 1970. Polyethylene debris has led to terrestrial as well as marine pollution, causing damage to humans, animals, and birds. Plastic bags of less than 50 microns thickness and ultra-thin bags of 15 microns have very low recovery rates. Hence, these polyethylene bags are prominent waste found in solid garbage (Danso et al. 2019). Conventional solid waste management techniques are lacking behind and are causing more damage to the ecosystem instead of resolving this problem. Physical and chemical degradation of the polyethylene involves the process such as heating, incineration, dumping, grinding, breaking, etc. But, all these processes are leading to the release of more

toxic by-products such as dioxins, furans, and persistent organic pollutants in the environment and are very expensive.

Hence, there is a need to establish a low-cost, effective and eco-friendly solution to overcome this problem. Researchers around the globe are working and emphasizing microbial biodegradation as the effective approach for the degradation of polyethylene materials. Some of the studies reported in the past few years have given enough evidence to prove the assured fragmentation of polymeric surfaces. Microbial biodegradation of polymeric structures is considered as the superior approach to degrade polymeric materials. Biodegradation is generally referred to as the process of decomposition of substance through microbial activity. This is a complicated process that involves several steps: bio-deterioration (involves the combination of biotic and abiotic factors for fragmentation of polymer structure into small fractions), depolymerization (enzymatic degradation of polymer into oligomer, monomers, and dimers). In this book chapter, we will be describing the hazardous impact of polyethylene waste on our ecosystem. This chapter mainly summarizes the important studies on PE biodegradation by microbial treatment.

2   Health Hazards of Polyethylene Waste

Polyethylene waste is one of the most prominent types of plastic waste found in solid waste and it adversely affects the ecosystem due to its hazardous health impacts on living organisms. Polyethylene waste is adversely affecting the life on land due to its excessive accumulation the landfill sites and sewage. It results in the release of toxic pollutants into the soil which affects the soil micro-biota and affecting the invertebrates in the soil along with the growth of soil microorganisms (Amobonye et al. 2021). Marine life is also affected badly by the accumulation of PE debris in oceans and water bodies (Taylor et al. 2016). The water bodies and oceans are highly contaminated with PE waste. Marine animals are widely disturbed due to the presence of toxic PE debris in marine life (Danso et al. 2019). The intestinal blockage and endocrine disruption have been observed in some of the sea animals because of the ingestion of polybags, PE bottles, and other types of PE-based polymer waste in the sea debris. It has been reported that the percentage of PE debris is more in the depths as compared to the surface of the sea.

Furthermore, PE waste has been found to interfere in the chemical communications between aquatic lives. In recent years, microplastic, which is less than 5 mm in size have attained more attention, as they are found to cause irreparable damage to the aquatic flora (Lwanga et al. 2017). These microplastic particles have the ability to agglomerate with the toxic heavy metals in the seawater. Hence, it increases the probability of the micro-sized PE materials entering the food web due to their easy ingestion by fish and sea animals because huge pollution of the world depends on seafood (Miloloža et al. 2021). This will further be problematic to humans and animals and can cause hazardous health impacts.

3 Abiotic Factor and Pre-Treatments for Enhanced Polyethylene Degradation

Several factors are responsible for the degradation of polyethylene which involves biotic, abiotic, and structural properties as listed in Fig. 1. Abiotic degradation of polyethylene material can occur because of different environmental factors such as humidity, pH, temperature, salinity, etc. Other factors such as the presence and absence of oxygen, sunlight exposure, water, environmental stress influence the degradation of polyethylene material and it can also affect the activity of microbes on its surface (Montazer et al. 2018). Weathering plays a major role in the degradation of polyethylene, as it results in the intrusion on the polymer surface which makes it easier for the microbes to intrude in the tough structure of plastics because of the functionality of the biodegradation is mainly dependent on the surface area of the polymer. The UV component of the solar spectrum initiates the ionizing radiation which has significant role in the weathering of polymeric material. Other factors which affects the weathering and degradation of PE include the quantity and quality of the solar radiation varies with geographical location, climatic changes, and time of the year (Kyrikou and Briassoulis 2007).

Temperature also plays significant role in the PE degradation and its rate of degradation, as PE waste in landfill sites and industrial composites are readily exposed to high temperatures which results in the thermal oxidation of PE and its hydrolysis (Kyrikou and Briassoulis 2007). It has been observed that the combination
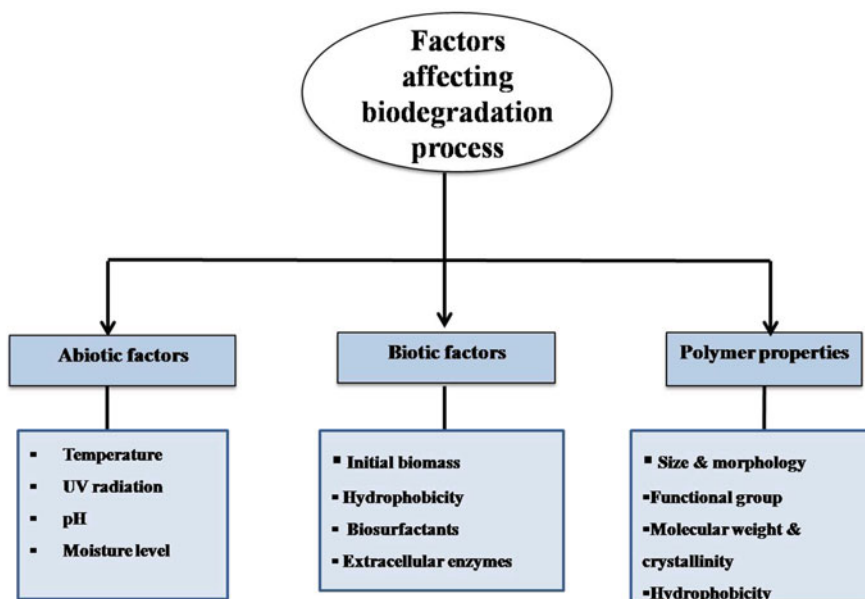
Fig.1 Different factors affecting the degradation of the process of polyethylene

of moisture and temperature effects the microbial colonization on the PE surface. Hydrophilic surfaces are more efficient in microbe colonization as compared to others (Khorasanizadeh 2013).

Photo-degradation is most commonly known abiotic factor of PE degradation. It consists of usage of light source for exposure on PE surface, it results in the photo-ionization and chain scission (Chamas et al. 2020).

Thermal UV treatment of PE films can enhance the degradation of PE by inducing the partial photolysis of PE films and causing the stimulation of weathering.

Pre-treatment of PE with pro-oxidants supports the biodegradation of PE films. Pro-oxidants results in the enhanced photo and thermal oxidation of PE which leads to the radical reaction and results in the cleavage of polymer chain (Koutny et al. 2006). Pro-oxidants such as iron, manganese, cobalt, and titanium catalyses the initiate the initial oxidation of PE materials and enhances the degradation of PE. Biodegradation study of LDPE by *Aspergillus* sp. showed that treatment with manganese stearate pre-oxidant and UV irradiation resulted in the 62% reduction in the elongation of PE films (Konduri et al. 2011). While, the Fourier transform infrared (FTIR) analysis confirmed the formation of carbonyl after biological treatment and pro-oxidant treatment on PE films (Konduri et al. 2011).

Enhanced photo-catalysis by titanium oxide (TiO_2) incorporation in the PE material has been found effective method for enhanced degradation of PE (Zan et al. 2006). This process involves the photon absorption of suitable energy causing electron generation and holes which further promotes the free radical formation and hence its oxidation followed by it biodegradation. Researchers reported the photo-catalytic degradation of LDPE by incorporation of titania nano-particles, which caused significant weight loss in PE films after 400 h of incubation (Zhao et al. 2008).

Chemical degradation by solvents or acids causes the cleavage of bond and free radical formation, for example branched chained PE materials are greatly influenced by the chemical degradation (Khorasanizadeh 2013). The mechanical factors such as shear stress, compression, and tension increase the rate of PE degradation at molecular level.

However, other factors such as crystallinity of PE plays strong role in its degradation. It has been observed the microbes attaches to the amorphous section of the PE. While, factors like size, shape, molecular weight, hydrophobicity/hydrophilicity, surface topography and types of additives utilised in manufacturing also contributes towards the degradation of PE (Wilkes and Aristilde 2017).

4   Polyethylene Biodegradation Mechanism

Biodegradation is defined as the alternation and deterioration of microbial structure through biological or microbial methods. Deterioration and degradation of polymeric structure can be defined by the measurement of its weight loss, loss in mechanical

strength, and its surface properties (Amobonye et al. 2021). Microbial deterioration of polyethylene can be one of the tangible and eco-friendly alternatives to the physio-chemical methods of degradation. The process of biological degradation of this material can be accomplished by the combination of various enzymatic and non-enzymatic methods of degradation (Ghatge et al. 2020). The efficiency of microbial degradation is directly related to the chemical, physical, and, mechanical properties of the polymer.

Biodegradation is a multistep process; (i) the microorganisms secrete the exo-enzymes or endo-enzymes which have hydrolytic and oxidative properties and functions in the initial fragmentation of the polymer into small monomers. (ii) Polymer degradation proceeds towards the assimilation which gives the end products such as CO_2, CH_4, or H_2O and cell biomass formation (iii) Mineralization occurs when the end products of the degradation are completely utilized by the microbes in the process (Bahl et al. 2020) as shown in Fig. 2.

Oxygen plays a vital role in the degradation of the polymer, as it is the terminal electron acceptor for the aerobic degradation process. Aerobic biodegradation leads to the formation of CO_2 and H_2O along with microbial biomass. In sulfidogenic conditions CO_2, CH_4, or H_2O formation occurs as a result of biodegradation (Tokiwa et al. 2009). In anaerobic conditions, H_2O, organic acids, CH_4, CO_2 are the end products of degradation. The aerobic biodegradation process is more efficient in terms of
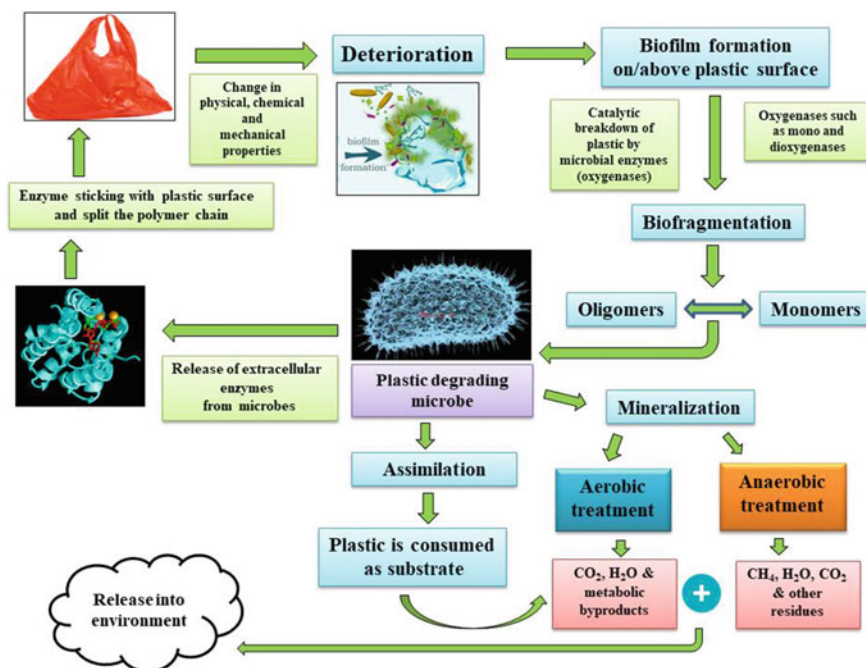
Fig.2 Schematic representation of mechanism of plastic biodegradation

energy production in comparison to the anaerobic biodegradation process. Microbes break the complex chemical structure of polyethylene through the biochemical transformation process. Aerobic degradation of the polymer can be formulation as the following reaction:

(1) $C_{Polyethylene} + O_2 + Biomass \rightarrow CO_2 + H_2O + C_{biomass}$
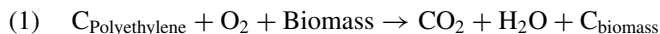
The complex mineralization of the polyethylene $C_{biomass}$ gets converted into CO_2 and H_2O by the microbial community (Gautam et al. 2007).

5 Microbes Associated with Polyethylene Degradation

The microorganisms are known for their diversified nature and wide environmental adaptability, as they consist of distinct features. A considerable number of reports have been published in the literature on the ability of microbial groups for the degradation of polyethylene as shown in Table 1. *Ideonella sakaiensis* sp., *Streptomyces* sp., *Pseudomonas* sp., *Commonas* sp, *Staphylococcus* sp., and *Bacillus* sp. are some of the majorly reported microbes, isolated from plastic dumping sites for the degradation of plastic (Ghatge et al. 2020; Kumari et al. 2009).

A recent study investigated the potential of marine bacterial strains (identified as *Bacillus* sp.) in the degradation of LDPE, and HDPE, and PVC (polyvinylchloride) (Kumari and Chaudhary 2019). Similarly, *Paenibacillus* sp. and Bacillus sp. isolated from municipal landfill soil showed the potential for the degradation of micro-sized polyethylene particles (Park and Kim 2019).

Cow dung samples have been reported in various studies for the isolation of polyethylene degradation microbes, as cow dung consists of a wide variety of microflora. Approximately 60 bacterial strains have been identified in past for the degradation of polyethylene. Likewise, some of the thermophilic and mesophilic species have also been found effective in the degradation of hydrocarbon chains of polymeric materials (Skariyachan et al. 2021).

Recently reported novel bacterial species of *Enterobacter cloacae* and *Pseudomonas* sp. which works best in consortia for the degradation of LDPE and polypropylene (PP) was isolated from cow dung samples. the formulated consortium showed the 64% and 63% weight reduction of LDPE and PP respectively in 160 days incubation. Excretion of exo-polysaccharides by the bacterial action was observed on the polyethylene structure (Skariyachan et al. 2021).

Furthermore, the *Lysinibacillus* sp. identified and isolated from soil grove sample was investigated to biodegrade the PP and PE material. The bacterial strain is capable of degrading PE and PP without any chemical and physical pre-treatment. It showed 4% and 9% weight reduction of PP and PE respectively in 26 days only. Scanning electron microscopy (SEM) showed the roughness in the surface of microbial treated material by *Pseudomonas* sp. (Jeon et al. 2021).

In addition, *klebsiella pneumoniae* was reported for the degradation of HDPE after the thermal treatment. This bacterial strain was found capable of adhering to HDPE

Table 1 Microbial communities involved in the degradation of polyethylene

Microorganism	Type of PE targeted	Source of microbe	References
Bacillus sp. and *Pseudomonas* sp.	PE carry bags	Plastic dump sites	Sangale (2012)
Aspergillus sp.	Powered LDPE	Sea water	Pramila (2012)
Pseudomonas, Bacillus sp., *Staphylococcus, Proteus, Sterptococcus, Micrococcus,* and *Aspergillus* sp.	PE bags	Sewage water soil, sludge area soil, medicinal garden soil, agriculture soil, and energy park soil	Priyanka and Archana (2011)
Aspergillus niger, Chaetomium globosum, Pullularia pullulans, and *Penicillium funiculosum*	LDPE blended with starch	Known cultures were used	Orr et al. (2004)
Pseudomonas Stutzeri	LDPE	Soil sample from plastic dumpsite	Sharma and Sharma (2004)
Aspergillus oryzae	LDPE	Known culture used	Konduri et al. (2011)
Rhodococcus ruber	LDPE	Not mentioned	Orr et al. (2004)
Rhodococcus rhodochrous	LDPE, HDPE, and linear low density polyethylene (LLDPE)	American type culture	Fontanella et al. (2010)
Serratia marscence	Polyethylene bags	Plastic waste dumpsite	Aswale and Ade (2009)
Bacillus, Listeria, Vibrio, and *Micrococcus*	LDPE and HDPE	Mangrove soil sample	Kumar et al. (2007)
Brevibacillus sp. and *Bacillus* sp.	LLDPE and LDPE	Vegetable and agricultural fields	Abrusci et al. (2011)
Staphylococcus epidermis	LDPE	Not given	Chatterjee et al. (2010)
Pseudomonas spp., *Bacillus subtilis,* and *Aspergillus niger*	Polyethylene bags waste	Soil sample from the dumping site	Nwachukwu et al. (2010)
Rhodococcus rhodochrous ATCC 29,627, *Nocardia steroids* GK 911, and *Cladosporium cladosporides* ATCC 20,251	Environmentally degradable polyethylene sample	Known cultures and their isolates	Bonhomme et al. (2003)

(continued)

Table 1 (continued)

Microorganism	Type of PE targeted	Source of microbe	References
Bacillus sp., *Streptococcus* sp., *micrococcus* sp., *Diplococcus* sp., *Pseudomonas* sp., *Staphylococcus* sp., and *Aspergillus* spp.	Polyethylene carry bags	Solid waste from municipal corporation, naturally buried polybags, and polyethylene strips buried in composite soil	Reddy (2008)
Bacillus mycoides and *Penicillium frequentans*	Biodegradable polyethylene	Different types of polyethylene dumped in soil	Seneviratne et al. (2006)
Streptococcus sp., *Micrococcus, Moraxella,* and *Aspergillus* spp.	Plastics cups and polybags	Mangrove rhizosphere soil	Kathiresan (2003)
Pseudomonas spp. (P1, P2, P3)	Polyethylene blended with vegetable starch	(i) Domestic waste disposal site (ii) Soil from textile effluent (iii) Sewage dumped soil	Nanda et al. (2010)
Streptomyces sp.	Polyethylene terephthalate powder and films	Agriculture soil	Farzi et al. (2019)
Bacillus sp. and *Paenibacillus* sp.	PE microplastic (100 mg)	Landfill site soil	Park and Kim (2019)
Bacillus amyloliquefaciens	LLDPE	Composting plant-soil sample	Novotný et al. (2018)
Pseudomonas, Bacillus, Brevibacillus, Cellulosimicrobium, Lysinibacillus, and *Aspergillus*	LDPE and PE Films	Dumpsite soil	Muhonja et al. (2018a)
Aneurinibacillus aneurinilyticus, Brevibacillus agri, Brevibacillus sp., and *Brevibacillus brevis*	Fine powders of HDPE, LDPE, and PP plastic strips and pellets	Soil samples from waste management landfills and sewage treatment plants	Skariyachan et al. (2018)

Table 1 (continued)

Microorganism	Type of PE targeted	Source of microbe	References
Enterobacter and *Pseudomonas*	LDPE	Plastic dumping landfill, Karnataka, India	Skariyachan et al. (2021)
Stenotrophomonas sp.	Poly (butylene adipate-co-terephthalate) (PBAT)	Soil sample from agriculture farms	Dey et al. (2020)
Stenotrophomonas sp.	LDPE beads	Plastic waste dumpsite near and drilling fluid site	Jia et al. (2021)
Arthrobacter sp. and *Streptomyces* sp.	PE mulch film	Soil sample from plastic dumpsite	Han et al. (2020)
Pseudomonas, Bacillus, Brevibacillus, Cellulosimicrobium, Lysinibacillus and fungi *Aspergillus*	LDPE	Dumpsite soil sample	Muhonja et al. (2018b)
Bacillus, Clostridium, Micrococcus Aspergillus, Penicillium and *Mucor*	LDPE blended with corn starch	Soil burial	Pinchuk et al. (2004)
Streptomyces sp.	PE	Soil	Abraham et al. (2017)
Acinetobacter baumanii	PE	Marine water	Pramila and Ramesh (2017)
Aspergillus sydowii	PE	Mangrove soil	Sangale et al. (2019)

surface, which causes biofilm thickness, and a decrease in the weight and tensile strength of HDPE by 18% and 60% respectively in 60 days. Surface roughness, cracks, and grooves were observed on the surface of HDPE film after the treatment by bacterial strain (Awasthi et al. 2017).

*Pseudomona*s species have also been studied identified as the potential PE degrader. *Pseudomonas fluorescens* has been reported for PE degradation in the presence of certain bio-surfactants which enhanced its polymerization and biodegradation process (Arkatkar et al. 2010).

Likewise, thermophilic bacterial strain, *Brevibacillus* sp. isolated from the dumpsite soil sample was identified as the LDPE degrader. This microbe utilizes LDPE as the sole carbon source in the medium and resulted in the 30% reduction in molecular weight after 30 days of incubation time (Hadad et al. 2005). Other bacterial strains like *Acinetobacter baumanii, Arthrobacter viscous*, *Bacillus cereus*, *Bacillus mycoides*, *Bacillus amyloliquefaciens*, *Staphylococcus xylosus*, *Nocardia asteroids*, *Microbacterium paraoxydans*, *and Staphylococcus cohnii* have also been reported as effective PE bio-degraders (Ghatge et al. 2020).

Fungal strains from genera *Fusarium, Aspergillus*, *Phanerochaete*, and *Cladosporium* have been reported as potential PE degraders (Spina et al. 2021). Generally, fungal strains are thought to be more efficient in the degradation of PE as compared to other microbial communities. Fungal strains *Aspergillus* have been reported to possess the degradation capability of LDPE sheets. In this study, the LDPE sheets were pre-treated before the degradation (El-Sayed et al. 2021). Similarly, *Aspergillu*s sp. and *Fusarium* sp. were found efficient in the degradation of LDPE. These strains showed 8–9% of weight reduction in LDPE by *Aspergillus* sp. While 5% weight reduction by *Fusarium* sp. after 60 days of incubation period (Das et al. 2014).

In recent years gut microbiome larvae have also been reported for the degradation of LDPE material without the need for any pre-treatment. The wax-worms *Galleria mellonella* and *Plodia interpunctell*a can utilize and metabolize the PE because of its structural similarity to bee-wax. But, there is a lack of information in this regard. Researchers recently reported the PE biodegradation by *Enterobacter* sp. which was isolated from the gut of wax moth *Galleria mellonella* (Weber et al. 2017). In this study, SEM and atomic force microscopy (AFM) were performed to prove the formation of microbial films around the PE surface after the treatment of 14 days by microbial strain.

Moreover, strains (*Bacillus* sp. and *Enterobacter* sp.) isolated from the gut of *Plodia interpunctell*a larvae were reported for the PE degradation. These strains caused surface disruption and reduced the hydrophobicity of PE films after 28 days. In another study, the PE biodegradation was explored by larvae of *Tenebrio molitor* (Yellow worm) (Yang et al. 2018).

The gut microbiome study conducted investigated the attachment of *Kosakonia* sp., and *Citrobacter* sp. on the PE which was ingested by the mealworms. More studies are required in this area to explore the enzymatic degradation mechanism behind the degradation of PE by gut microbes (Yang et al. 2014).

6 Microbial Enzymes for Polyethylene Degradation

Enzymatic degradation of polyethylene material occurs with the secretion of extra-cellular and intracellular enzymes on the microbial surface. The enzymes adhere to the PE surface and hydrolyze the complex structure into monomers. Some of the lignin-degrading enzymes are reported for the breakdown of PE material. Extra-cellular enzymes are the most studied enzymes till date for the degradation of PE. These types of enzymes are generally involved in depolymerisation of the oligomeric structure of PE into dimers and monomers. These enzymes work on the solid/ liquid interface of the hydrophobic surface of PE (Pathak 2017).

Manganese peroxidase (MnP), laccases, and lignin peroxidase (LiP) are some of the lignin-degrading enzymes involved in PE degradation (Wei and Zimmermann 2020). The laccases enzyme produced by the *Rhodococcus ruber* has been reported to degrade the UV pre-treated PE films(Rocha-Santos and Duarte 2015). MnP produced by *Penicillium* sp. has been found as the efficient enzyme in the degradation of PE. Furthermore, membrane weight loss has been observed in the structure of PE after treatment with laccases enzyme produced by *Trametes versicolor*. Whereas, enhanced secretion of MnP and Laccases was observed after incubation with UV treated PE films (Nishida et al. 2008). The activity of LiP by *Streptomyces* species and showed promising results in the degradation of heat-treated PE. Another enzyme, alkane hydroxylase was identified as an effective enzyme in the degradation of PE plastic isolated from *Pseudomonas* sp. (Gyung Yoon et al. 2012).

However, transcriptome analysis of the *Galleria mellonella* found the up-regulation of genes coding for lipase, carboxyl-esterase, and some of the fatty acid metabolism enzymes. The actual pathway and genes encoding for the biodegradation of PE are still unknown. But a hypothetical pathway can give a vague idea about the microbial enzymatic action on PE surface as described in Fig. 3. Microbial enzymes involved in degradation of lignin polymer have been found involved in PE degrada-tion such as manganese peroxidases and laccases. Theoretcially, as shown in Fig. 3, PE can be used as carbon source by microbes. Microbes first leads to the reduction in the molecular weight of PE. Secondly, the enzymatic action leads to the oxida-tion of terminal hydrocarbon molecules,that further get metabolized by the means of tricarboxylic acid cycle (TCA).

7 Assessment of Polyethylene Biodegradation

Analytical techniques are widely used to study biodegradation include percentage weight reduction, changes in the mechanical properties (tensile strength, stiffness, and elongation), and surface changes of polymers like PE. The visible surface changes occurring after the biodegradation of plastics evaluated using different analytical techniques. The surface changes such as roughness, pits and holes formation, and biofilm formation occur due to the microbial attack on the surface of PE that can be
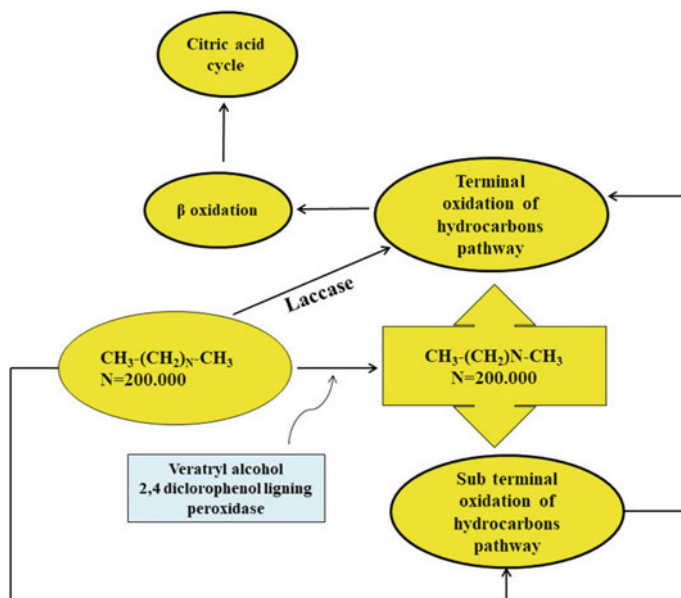
Fig.3 A schematic representation of the superficial pathway involved in the degradation of PE

assessed using high-resolution microscopic techniques i.e. SEM, AFM etc. Physical and mechanical changes in the properties of PE such as contact angle, glass transition temperature (Tg), melting temperature (Tm) can be evaluated by differential scanning calorimetry and thermogravimetric analysis (Sowmya and Thippeswamy 2014).

The biodegradation associated processes such as O_2 consumption, CO_2 formation, and substrate loss could be evaluated through infrared (IR) spectroscopy, gas chromatography (GC), total organic carbon (TOC), dissolved organic carbon (DOC), and chemical oxygen demand (COD). Various sophisticated instruments i.e. FTIR-ATR (quantifications), FT-NMR (structure determination), gel permeation chromatography (molecular estimation), vapor pressure osmometry (molecular weight estimation), chemical impendence analyzer (electrical property evaluation), atomic force microscope (surface characteristics) etc. used for characterizing different polymers.

Fourier transform infrared coupled attenuated total reflectance (FTIR-ATR) spectroscopy is one of the most rapid and sensitive techniques to quantify PE biodegradation. This technique get through thin layer of the polymer to measure carbonyl group (C=O) formed on the surfaces of the materials.

8   Conclusion and Future Prospective

The applicability and utilization of PE-based material in our day-to-day lives is massive. It is being utilized in various fields i.e. wrapping, medicine, scientific instruments, and food materials and accumulation of these hazardous materials is a great concern. Various physiochemical methods have been applied to degrade polyethylene but biodegradation serves as the best-suited approach for the degradation of PE materials. The microorganisms involved in the LDPE, HDPE biodegradation have been isolated from different sites such as agricultural, dumpsite, and mangrove soil samples. The degradation assessments are significantly important to understand the microbe influences on the degrading polymers. This chapter emphasized the use of pretreatment methods for the enhanced degradation of PE materials.

The above-mentioned studies are restricted to laboratory-scale and the large-scale production of microbes and their secreted enzymes for PE degradation is still missing. The postulated mechanism, pathways, and genes involved in the biodegradation of HDPE and LDPE involve a series of enzymatic actions but the actual mechanism is still not well understood. The reported studies gives us primary information that needs to be explored further to understand the large-scale degradation of PE. From an industrial point of view, the microbial consortia's are found to be more efficient in plastic degradation and could be beneficial candidates for large-scale degradation of polymers including polyethylene. The microbial members of consortia cultures grows symbiotically and work synergistically to follow combination of pathways to utilize the polymers i.e. PE, effectively. Further, the production of robust and efficient enzymes involved in PE degradation could be helpful for industrial-scale degradation. Further, the potential of individual or microbial consortia's need to be explored in order to degrade hazardous polymers contaminants from the environment.

Conflict of Interest   The authors of this manuscript declare that they have no conflict of interest.

References

Abraham J, Ghosh E, Mukherjee P, Gajendiran A (2017) Microbial degradation of low density polyethylene. Environ Prog Sustain Energy 36. https://doi.org/10.1002/ep.12467

Abrusci C, Pablos JL, Corrales T, López-Marín J, Marín I, Catalina F (2011) Biodegradation of photo-degraded mulching films based on polyethylenes and stearates of calcium and iron as pro-oxidant additives. Int Biodeterior Biodegradation 65:451–459

Amobonye A, Bhagwat P, Singh S, Pillai S (2021) Plastic biodegradation: frontline microbes and their enzymes. Sci Total Environ 759:143536. https://doi.org/10.1016/j.scitotenv.2020.143536

Arkatkar A, Juwarkar AA, Bhaduri S, Uppara PV, Doble M (2010) Growth of pseudomonas and bacillus biofilms on pretreated polypropylene surface. Int Biodeterior Biodegradation 64:530–536

Aswale PN, Ade AB (2009) Effect of pH on biodegradation of polythene by serretia marscence. Ecotech 1:152–153

Awasthi S, Srivastava P, Singh P, Tiwary D, Mishra PK (2017) Biodegradation of thermally treated high-density polyethylene (HDPE) by Klebsiella pneumoniae CH001. 3 Biotech 7:1–10

Bahl S, Dolma J, Jyot Singh J, Sehgal S (2020) Biodegradation of plastics: a state of the art review. Mater Today Proc 4–7. https://doi.org/10.1016/j.matpr.2020.06.096

Barnes DKA, Galgani F, Thompson RC, Barlaz M (2009) Accumulation and fragmentation of plastic debris in global environments. Philos Trans R Soc B Biol Sci 364:1985–1998

Bonhomme S, Cuer A, Delort AM, Lemaire J, Sancelme M, Scott G (2003) Environmental biodegradation of polyethylene. Polym Degrad Stab 81:441–452

Chamas A, Moon H, Zheng J, Qiu Y, Tabassum T, Jang JH, Abu-Omar M, Scott SL, Suh S (2020) Degradation rates of plastics in the environment. ACS Sustain Chem Eng 8:3494–3511. https://doi.org/10.1021/acssuschemeng.9b06635

Chatterjee S, Roy B, Roy D, Banerjee R (2010) Enzyme-mediated biodegradation of heat treated commercial polyethylene by staphylococcal species. Polym Degrad Stab 95:195–200

Danso D, Chow J, Streita WR (2019) Plastics: environmental and biotechnological perspectives on microbial degradation. Appl Environ Microbiol 85. https://doi.org/10.1128/AEM.01095-19

Das P, Solanki R, Khanna M (2014) Isolation and screening of cellulolytic actinomycetes from diverse habitats. Int J Adv Biotechnol Res 5:438–451

Dey U, Mondal NK, Das K, Dutta S (2012) An approach to polymer degradation through microbes 2:385–388

Dey AS, Bose H, Mohapatra B, Sar P (2020) Biodegradation of unpretreated low-density polyethylene (LDPE) by *Stenotrophomonas* sp. and *Achromobacter* sp., isolated from waste dumpsite and drilling fluid. Front Microbiol 11:1–15. https://doi.org/10.3389/fmicb.2020.603210

El-Sayed MT, Rabie GH, Hamed EA (2021) Biodegradation of low-density polyethylene (LDPE) using the mixed culture of aspergillus carbonarius and A. fumigates. Environ Dev Sustain. https://doi.org/10.1007/s10668-021-01258-7

Evans DS, Schmalensee R (2005) Paying with plastic: the digital revolution in buying and borrowing. Mit Press

Farzi A, Dehnad A, Fotouhi AF (2019) Biocatalysis and agricultural biotechnology biodegradation of polyethylene terephthalate waste using streptomyces species and kinetic modeling of the process. Biocatal Agric Biotechnol 17:25–31. https://doi.org/10.1016/j.bcab.2018.11.002

Fontanella S, Bonhomme S, Koutny M, Husarova L, Brusson J-M, Courdavault J-P, Pitteri S, Samuel G, Pichon G, Lemaire J (2010) Comparison of the biodegradability of various polyethylene films containing pro-oxidant additives. Polym Degrad Stab 95:1011–1021

Gautam R, Bassi AS, Yanful EK (2007) A review of biodegradation of synthetic plastic and foams. Appl Biochem Biotechnol 141:85–108

Ghatge S, Yang Y, Ahn JH, Hur HG (2020) Biodegradation of polyethylene: a brief review. Appl Biol Chem 63. https://doi.org/10.1186/s13765-020-00511-3

Gyung Yoon M, Jeong Jeon H, Nam Kim M (2012) Biodegradation of polyethylene by a soil bacterium and AlkB cloned recombinant cell. J Bioremediation Biodegradation 03. https://doi.org/10.4172/2155-6199.1000145

Hadad D, Geresh S, Sivan A (2005) Biodegradation of polyethylene by the thermophilic bacterium brevibacillus borstelensis. J Appl Microbiol 98:1093–1100

Han YN, Wei M, Han F, Fang C, Wang D, Zhong YJ, Guo CL, Shi XY, Xie ZK, Li FM (2020) Greater biofilm formation and increased biodegradation of polyethylene film by a microbial consortium of arthrobacter sp and streptomyces sp. Microorganisms 8:1–15. https://doi.org/10.3390/microorganisms8121979

Jeon J, Park S, Choi T, Park J, Yang Y, Yoon J (2021) Biodegradation of polyethylene and polypropylene by lysinibacillus species JJY0216 isolated from soil grove. Polym Degrad Stab 191:109662. https://doi.org/10.1016/j.polymdegradstab.2021.109662

Jia H, Zhang M, Weng Y, Li C (2021) Degradation of polylactic acid/polybutylene adipate-co-terephthalate by coculture of pseudomonas mendocina and actinomucor elegans. J Hazard Mater 403:123679

Kathiresan K (2003) Polythene and plastics-degrading microbes from the mangrove soil. Rev Biol Trop 51:629–633

Khorasanizadeh Z (2013) The effect of biotic and abiotic factors on degradation of polycyclic aromatic hydrocarbons (PAHs) by Bacteria in Soil. Thesis

Konduri MKR, Koteswarareddy G, Rohini Kumar DB, Venkata Reddy B, Lakshmi Narasu M (2011) Effect of pro-oxidants on biodegradation of polyethylene (LDPE) by indigenous fungal isolate, Aspergillus oryzae. J Appl Polym Sci 120:3536–3545

Koutny M, Sancelme M, Dabin C, Pichon N, Delort AM, Lemaire J (2006) Acquired biodegradability of polyethylenes containing pro-oxidant additives. Polym Degrad Stab 91:1495–1503. https://doi.org/10.1016/j.polymdegradstab.2005.10.007

Kumar S, Hatha AAM, Christi KS (2007) Diversity and effectiveness of tropical mangrove soil microflora on the degradation of polythene carry bags. Rev Biol Trop 55:777–786

Kumari A, Chaudhary DR (2019) Destabilization of polyethylene and polyvinylchloride structure by marine bacterial strain. Environ Sci Pollut Res 1507–1516

Kumari K, Aanad RC, Narula N (2009) Microbial degradation of polyethylene (PE) 66–70

Kyrikou I, Briassoulis D (2007) Biodegradation of agricultural plastic films: a critical review. J Polym Environ 15:125–150. https://doi.org/10.1007/s10924-007-0053-8

Lebreton L, Slat B, Ferrari F, Sainte-Rose B, Aitken J, Marthouse R, Hajbane S, Cunsolo S, Schwarz A, Levivier A (2018) Evidence that the great pacific garbage patch is rapidly accumulating plastic. Sci Rep 8:1–15

Lwanga E, Mendoza Vega J, Ku Quej V, de los Angeles Chi J, Sanchez del Cid L, Chi C, Escalona Segura G, Gertsen H, Salánki T, van der Ploeg M, Koelmans AA, Geissen V (2017) Field evidence for transfer of plastic debris along a terrestrial food chain. Sci Rep 7:1–7. https://doi.org/10.1038/s41598-017-14588-2

Miložoa M, Kučić Grgić D, Bolanča T, Ukić Š, Cvetnić M, Ocelić Bulatović V, Dionysiou DD, Kušić H (2021) Ecotoxicological assessment of microplastics in freshwater sources—a review. Water 13:56

Montazer Z, Habibi-Najafi MB, Mohebbi M, Oromiehei A (2018) Microbial degradation of UV-pretreated low-density polyethylene films by novel polyethylene-degrading bacteria isolated from plastic-dump soil. J Polym Environ 26:3613–3625. https://doi.org/10.1007/s10924-018-1245-0

Muhonja CN, Makonde H, Magoma G, Imbuga M (2018a) Biodegradability of polyethylene by bacteria and fungi from Dandora dumpsite Nairobi-Kenya. PLoS ONE 13:1–17. https://doi.org/10.1371/journal.pone.0198446

Muhonja CN, Magoma G, Imbuga M, Makonde HM (2018) Molecular characterization of low-density polyethene (LDPE) degrading bacteria and fungi from dandora dumpsite, Nairobi, Kenya 2018

Nanda S, Sahu S, Abraham J (2010) Studies on the biodegradation of natural and synthetic polyethylene by *Pseudomonas* spp. J Appl Sci Environ Manage 14

Nishida T, Fujisawa M, Hirai H (2008) Degradation of polyethylene and Nylon-66 by the laccase. J Polym Environ 9:103–108

Novotný Č, Malachová K, Adamus G, Kwiecień M, Lotti N, Soccio M, Verney V, Fava F (2018) Deterioration of irradiation/high-temperature pretreated, linear low-density polyethylene (LLDPE) by bacillus amyloliquefaciens. Int Biodeterior Biodegradation 132:259–267

Nwachukwu S, Obidi O, Odocha C (2010) Occurrence and recalcitrance of polyethylene bag waste in Nigerian soils. Afr J Biotechnol 9:6096–6104

Orr IG, Hadar Y, Sivan A (2004) Colonization, biofilm formation and biodegradation of polyethylene by a strain of Rhodococcus ruber. Appl Microbiol Biotechnol 65:97–104. https://doi.org/10.1007/s00253-004-1584-8

Park SY, Kim CG (2019) Biodegradation of micro-polyethylene particles by bacterial colonization of a mixed microbial consortium isolated from a landfill site. Chemosphere 222:527–533. https://doi.org/10.1016/j.chemosphere.2019.01.159

Pathak VM, Navneet (2017) Review on the current status of polymer degradation: a microbial approach. Bioresour Bioprocess 4. https://doi.org/10.1186/s40643-017-0145-9

Pinchuk LS, Makarevich AV, Vlasova GM, Kravtsov AG, Shapovalov VA (2004) Electret-thermal analysis to assess biodegradation of polymer composites. Int Biodeterior Biodegradation 54:13–18. https://doi.org/10.1016/j.ibiod.2003.11.005

Pramila R (2012) Brevibacillus parabrevis, acinetobacter baumannii and pseudomonas citronellolis—potential candidates for biodegradation of low density polyethylene (LDPE). J Bacteriol Res 4:9–14. https://doi.org/10.5897/jbr12.003

Pramila R, Ramesh KV (2017) Biodegradation of low density polyethylene (LDPE) by fungi isolated from marine water—a SEM analysis. https://doi.org/10.5897/AJMR11.670

Priyanka N, Archana T (2011) Biodegradability of polythene and plastic by the help of microorganism: a way for brighter future. J Env Anal Toxicol 1:1000111

Reddy RM (2008) Impact of soil composting using municipal solid waste on biodegradation of plastics

Rocha-Santos T, Duarte AC (2015) A critical overview of the analytical approaches to the occurrence, the fate and the behavior of microplastics in the environment. TrAC Trends Anal Chem 65:47–53

Sangale MK (2012) A review on biodegradation of polythene: the microbial approach. J Bioremediat Biodegradation 03. https://doi.org/10.4172/2155-6199.1000164

Sangale MK, Shahnawaz M, Ade AB (2019) Potential of fungi isolated from the dumping sites mangrove rhizosphere soil to degrade polythene. Sci Rep 9:1–11

Seneviratne G, Tennakoon NS, Nandasena KA, Weerasekara M (2006) Polyethylene biodegradation by a developed Penicillium-Bacillus biofilm

Sharma A, Sharma A (2004) Degradation assessment of low density polythene (LDP) and polythene (PP) by an indigenous isolate of Pseudomonas stutzeri

Skariyachan S, Taskeen N, Kishore AP, Krishna BV, Naidu G (2021) Novel consortia of enterobacter and pseudomonas formulated from cow dung exhibited enhanced biodegradation of polyethylene and polypropylene. J Environ Manage 284:112030. https://doi.org/10.1016/j.jenvman.2021.112030

Skariyachan S, Patil AA, Shankar A, Manjunath M, Bachappanavar N, Kiran S (2018) Enhanced polymer degradation of polyethylene and polypropylene by novel thermophilic consortia of *Brevibacillus* sps. and *Aneurinibacillus* sp. screened from waste management landfills and sewage treatment plants. Polym Degradation Stab 149:52–68. https://doi.org/10.1016/j.polymdegradstab.2018.01.018

Sowmya HV, Thippeswamy B (2014) Biodegradation of polyethylene by bacillus cereus. An Int J 4:28–32

Spina F, Tummino ML, Poli A, Prigione V, Ilieva V, Cocconcelli P, Puglisi E, Bracco P, Zanetti M, Varese GC (2021) Low density polyethylene degradation by filamentous fungi. Environ Pollut 274:116548

Taylor ML, Gwinnett C, Robinson LF, Woodall LC (2016) Plastic microfibre ingestion by deep-sea organisms. Sci Rep 6:1–9

Tokiwa Y, Calabia BP, Ugwu CU, Aiba S (2009) Biodegradability of plastics. Int J Mol Sci 10:3722–3742. https://doi.org/10.3390/ijms10093722

Weber C, Pusch S, Opatz T (2017) Polyethylene bio-degradation by caterpillars? Curr Biol 27:R744–R745

Wei R, Zimmermann W (2020) Minireview microbial enzymes for the recycling of recalcitrant petroleum-based plastics : how far are we ? 2020. https://doi.org/10.1111/1751-7915.12710

Wilkes RA, Aristilde L (2017) Degradation and metabolism of synthetic plastics and associated products by *Pseudomonas* sp.: capabilities and challenges. J Appl Microbiol 123:582–593. https://doi.org/10.1111/jam.13472

Yang J, Yang Y, Wu W-M, Zhao J, Jiang L (2014) Evidence of polyethylene biodegradation by bacterial strains from the guts of plastic-eating waxworms. Environ Sci Technol 48:13776–13784

Yang S-S, Brandon AM, Flanagan JCA, Yang J, Ning D, Cai S-Y, Fan H-Q, Wang Z-Y, Ren J, Benbow E (2018) Biodegradation of polystyrene wastes in yellow mealworms (larvae of tenebrio molitor linnaeus): factors affecting biodegradation rates and the ability of polystyrene-fed larvae to complete their life cycle. Chemosphere 191:979–989

Zan L, Fa W, Wang S (2006) Novel photodegradable low-density polyethylene—TiO2 nanocomposite film. Environ Sci Technol 40:1681–1685

Zhao X, Li Z, Chen Y, Shi L, Zhu Y (2008) Enhancement of photocatalytic degradation of polyethylene plastic with CuPc modified TiO2 photocatalyst under solar light irradiation. Appl Surf Sci 254:1825–1829

Biological and Thermochemical Strategies for Building Biorefinery Platform

Anjireddy Bhavanam ⓘ**, Amit Kumar** ⓘ**, Neeraj** ⓘ**, and G. N. Nikhil** ⓘ

Abstract Disposal of municipal solid waste (MSW) in urban areas is a big issue nowadays in most countries. The mismanagement of MSW can cause adverse environmental impacts, public health risks, and other socio-economic problems. India, the second most populated country globally, faces the problem of waste management and simultaneously grave energy crisis. The pressing need for the development of alternatives gave several different technological solutions. This chapter examines the most recent technical approaches, namely biological and thermo-chemical strategies, used to treat MSW while also capturing energy and other value-added products. These strategies assist in building a waste biorefinery, which is an integrative closed loop approach that has recently gained high interest world-wide. Besides, life cycle assessment will highlight which aspects need improvement in order to make these processes more environmentally friendly.

Keywords Fermentation · Pyrolysis · Microbial electrochemical systems · Circular economy

1 Introduction

India has garnered global attention as a result of its fast industrialization, urbanisation, and population growth. However, this growth has led to an increase in waste and

A. Bhavanam
Department of Chemical Engineering, Dr. B.R. Ambedkar National Institute of Technology, Jalandhar, Punjab 144011, India

A. Kumar
Department of Civil Engineering, Malaviya National Institute of Technology, Jaipur, Rajasthan 302017, India

Neeraj · G. N. Nikhil (✉)
Department of Biotechnology, Dr. B.R. Ambedkar National Institute of Technology, Jalandhar, Punjab 144011, India
e-mail: nikhilgn@nitj.ac.in

33

the use of natural resources, which has led to environmental deterioration and pollution. In 2015, urban India created roughly 62 Mt of municipal solid waste (MSW) (450 g/capita/day). As the public becomes more aware of the negative consequences of present waste disposal systems on the environment, accountability is required for a successful waste management system. MSW was collected in 82% of cases, with litter accounting for the remaining 18%. Out of the total waste collected, only 28% is currently being processed, leaving the remaining 72% discarded in the open (Sharma and Jain 2019). However, creating a sustainable waste management situation is complex because of consistent heterogeneity in MSW composition. In the last decade of research, integrated solid waste management has emerged as one of the alternative solutions, with waste biorefinery emerging as a critical component. A waste biorefinery recovers bio-based products and energy from waste as a renewable feedstock. This strategy needs to be an essential aspect of the MSW management hierarchy, and may significantly contribute to the purpose of successful waste management system (Mohan et al. 2016).

The combustion of fossil fuels emits toxic emissions and greenhouse gases (GHGs) (Gurjar et al. 2008). Attempts to reduce these emissions and the societal dependency on current fossil fuels drive the need for low-carbon fuels soon. Biofuels are emerging as an alternative source to achieve these goals (Hao et al. 2018). Biofuels are described as fuels produced directly or indirectly from biological resources using a combination of processes. Plants such as maize, sugarcane, sugar beans, soybeans, cassava, wheat, and barley (first-generation biofuels) or agricultural cellulosic biomass (inedible for food production) or non-edible plant biomass (second-generation biofuels) may be used to produce biofuels (Bardhan et al. 2015). Third-generation biofuels are microalgae products and do not have the disadvantages associated with first and second-generation biofuels (Katiyar et al. 2017). The latest research in third-generation biofuels involves employing low-cost materials, e.g., recycled glycerol (Katiyar et al. 2017) or by-products, e.g., de-oiled algal biomass (Katiyar et al. 2018; Saladini et al. 2016). Bio-products are products that are made mainly with biological components or renewable materials. Generally, renewable biomass undergoes multiple biological and chemical processes to produce bio-products (Bardhan et al. 2015). Agriculture (e.g., crops and crop wastes, dried distillers' grains) and/or food processing (bio-products) are examples of biological sources of inputs (by-products, residues, and off-specification materials). When compared to petroleum-based alternatives, bio-products often result in lower greenhouse gas emissions. Other environmental benefits emanating from the bio-products include a reduction in environmental risk and an increase in biodegradability. Being dependent on renewable feedstocks, these can be considered sustainable products. The bio-product market is expected to grow at a double rate compared to biofuel (Piemonte et al. 2013). In this chapter, biological and thermochemical routes for energy and other mercantile products are discussed to develop a waste biorefinery network. Aspects such as life cycle analysis and future outlook are also highlighted, which are critical in determining sustainability, market potential and the supply chain.

2 Biological Routes for Harnessing the Energy and Value-Added Products

2.1 Anaerobic Digestion

Anaerobic digestion (AD) is the biological process of degradation of complex organic substrates such as food waste, agro-waste, leather waste, paper industry solid waste, dairy farm waste, food processing industry organic waste, etc. The process of biodegradation progresses through hydrolytic, fermentative, acetoclastic, and methanogenic steps. When bioconversion pathways of organic waste move through different AD steps, they produce different valuable products, e.g., hydrogens, ethanol, butanol, propanol, formic acid, acetic acid, butyric acids, propionic acids, methane, etc. Hydrogen is an important energy source because of its carbon-free nature and high energy yield, i.e., 122 kJ/g, approximately 2.75 times higher than hydrocarbon-based fuel. At present, hydrogen production comes from gasification or water electrolysis. So, carbon-free hydrogen production technology needs to be developed based on renewability and sustainability (Dahiya et al. 2020). Dark fermentation, photo-fermentation, photosynthetic or non-photosynthetic algae, and bio-electrochemical routes to biohydrogen production are all types of biohydrogen production that can be done by plants.

2.2 Dark Fermentation

Biohydrogen produced by organic waste degradation by an anaerobic digestion process in an acidogenic phase under dark conditions comes from dark fermentation (Nikhil et al. 2014). In the dark fermentation process, simple sugars such as glucose undergo glycolysis to form pyruvate, which further forms formate through the pyruvate-ferredoxin oxidoreductase pathway or the pyruvate-formate lyase pathway. Then hydrogen production is catalyzed by the enzyme formate: hydrogen lyase, or the reduction of protons (Bundhoo 2019). The enzymes responsible for biohydrogen production are [FeFe]-hydrogenase and [NiFe]-hydrogenase. Depending upon the substrate, different by-products are generated during dark fermentation for biohydrogen production. These by-products are propionic acids, acetic acids, butyric acids, etc. (Fig. 1). Due to the by-product generation yield of hydrogen production, the theoretical yield of 12 mol of H_2/mol of glucose is reduced to 3.47 mol of H_2/mol of glucose (Tian et al. 2019). Microbial species involved in dark fermentative biohydrogen production are *Clostridium* sp., *Enterobacter* species, *E. coli*, *Bacillus* sp., and *Citrobacter* sp. (Das and Basak 2021; Ghimire et al. 2015). The biochemical reactions of hydrogen production through dark fermentation are as follows:

$$2H^+ + 2e^- \leftrightarrow H_2 \tag{1}$$
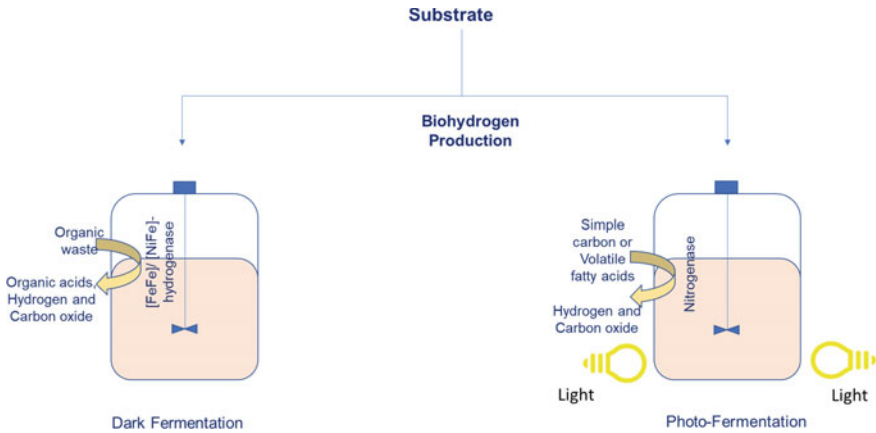
Fig. 1 Schematic representation of biohydrogen production from dark and photo-fermentation

$$C_6H_{12}O_6 + 6H_2O \rightarrow 6CO_2 + 12H_2 \tag{2}$$

$$C_6H_{12}O_6 + 2H_2O \rightarrow 2CH_3COOH + 2CO_2 + 4H_2 \tag{3}$$

$$C_6H_{12}O_6 + 6H_2O \rightarrow 2CH_3CH_2CH_2COOH + 2CO_2 + 2H_2 \tag{4}$$

$$C_6H_{12}O_6 \rightarrow CH_3COOH + CH_3CH_2COOH + CO_2 + H_2 \tag{5}$$
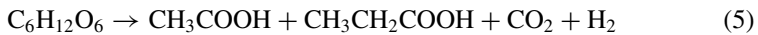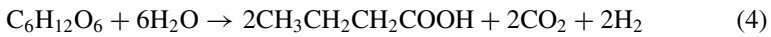
2.3 Photo-Fermentation

Photo-fermentation is a microbial process for biohydrogen production via fermentation of carbon sources and volatile fatty acids such as butyrate, acetate, propionate, formate, etc., in the presence of light (sunlight or artificial light) and the absence of nitrogen and oxygen (Fig. 1) (Tian et al. 2019). Bacteria involved in photo-fermentation are photosynthetic bacteria, e.g., *Rhodobacter*, *Rhodopseudomonas*, *Rhodospirillum*, and *Rhodobium* strains (Ferraren-De Cagalitan and Abundo 2021). The key enzyme responsible for photo-fermentative hydrogen production is the nitro-genase enzyme, and the biochemical reactions of the photo-fermentative hydrogen reaction are shown below.

$$C_6H_{12}O_6 + 6H_2O + light \rightarrow 6CO_2 + 12H_2 \tag{6}$$

$$CH_3COOH + 2H_2O + light \rightarrow 2CO_2 + 4H_2 \tag{7}$$

$$CH_3CH_2CH_2COOH + 6H_2O + light \rightarrow 4CO_2 + 10H_2 \tag{8}$$

$$N_2 + 8H^+ + 8e^- + 16ATP \rightarrow 2NH_3 + H_2 + 16ADP + 16P_i \tag{9}$$

$$8H^+ + 8e^- + 16ATP \rightarrow 4H_2 + 16ADP + 16Pi \tag{10}$$
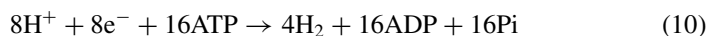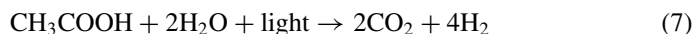
2.4 Bio-Electrochemical Strategies

Bajracharya et al. (2016) describe bioelectrochemical systems (BES) as the most efficient technology for simultaneous remediation of waste with electricity generation, hydrogen production, and value products such as ethanol, acetic acids, butyric acid, propionic acid, butanol, acetone, etc. BES technologies use microorganisms such as electron-respiring exoelectrogens that grow as biofilms on the anode, also called anode. Bioanode oxidizes organic waste into protons, electrons, and CO_2. In abiotic cathode use, a simple reduction reaction occurs in the presence of oxygen. In biocathode, if bacteria are protons, carbon dioxide is converted into methane, volatile fatty acids, alcohol, and other essential products. Venkata Mohan et al. (2016) say that BESs are microbial fuel cells, electrolysis cells, and desalination cells, which are all types of cells.

Microbial Fuel Cell

Microbial fuel cells (MFC) are bioelectrochemical technologies that can convert the chemical energy in organic materials directly into electrical energy with waste treatment (Pareek et al. 2019). In an MFC, electricity is generated due to the oxidation of substrates in an anode chamber by exoelectrogens growing on anodic biofilm release of electrons, protons, and carbon dioxide. Transport of electrons from the anode to the cathode via an external electric circuit and protons via a proton exchange membrane (Fig. 2a). In the presence of oxygen, electrons and protons combine to form water molecules. This process generates electricity during electron transfer and reduction at the cathode. Exoelectrogens can be mixed or pure culture at the anode, e.g., sewage sludge, anaerobic reactor sludge, *Geobacter*, *Pseudomonas*, *Enterobacter*, etc. Some MFC designs also use cathode chambers as anaerobic environments where methanogens can grow with or without syntrophic bacteria to generate methane.
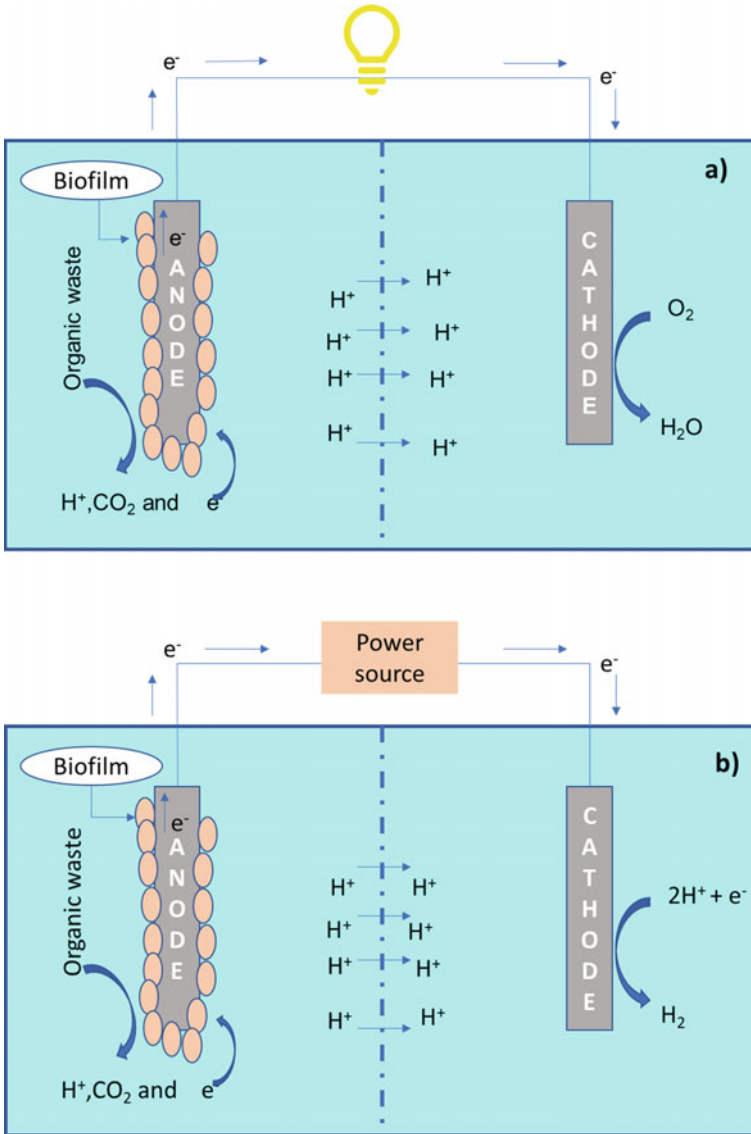
Fig. 2 A graphical representation of **a)** microbial fuel and **b)** microbial electrolysis cell production which can be used for dark and photo-fermentation

Microbial Electrolysis Cell

Degradation of organic matter by microorganisms such as exoelectrogens, which grow as a biofilm on the anode to produce bicarbonate, protons, and electrons. Protons produced at the anode are transferred to the cathode chamber via a

proton exchange membrane, and electrons generated are transferred to the cathode via a small applied voltage (0.1–1 V) (Fig. 2b). At the cathode, protons from the anode chamber are reduced to hydrogen by taking electrons in the presence of electrolytes (Zhen et al. 2017). The electron-respiring or exoelectrogens present in MEC are *Geobacter*, *Shewanella*, *Enterobacter*, *Rhodopseudomonas*, *Desulfuromonas*, *Rhodoferax*, etc. The materials used as the anode are carbon-based materials such as graphite felt, graphite brushes, carbon clothes, ammonia-treated graphite granules, etc. For the cathode, Ni-foam, stainless steel brushes, platinum, titanium tube, carbon cloth, and carbon felt can be used. Anolytes comprise real-field wastewater or synthetic wastewater with pure substrates such as sodium acetate, butyric acid, glucose, propionic acid, etc. Catholytes used are KCl or phosphate buffer (Cardeña et al. 2019) (Table 1).

3 Thermochemical Routes for Harnessing the Energy and Value-Added Products

Thermochemical conversion is more efficient and cost-effective in converting solid waste biomass into biofuels and other value-added products. The various thermochemical conversion (TCC) processes include combustion (incineration), pyrolysis, gasification, and liquefaction. From the combustion/incineration process, only heat is extracted as energy. While pyrolysis and liquefaction processes yield liquid oils (called bio-oils), gaseous fuel (called synthesis gas) is produced from the gasification process. The bio-oil produced from pyrolysis is water-soluble and contains a higher oxygen content than liquefied oils (Huber et al. 2006). This chapter mainly highlights the conversion technologies for second-generation biofuels derived from municipal solid waste materials. Thermochemical technologies are good for waste that can't be separated, like MSW, because they can't be separated.

3.1 *Combustion/Incineration*

Incineration involves solid waste combustion, which reduces volume by 90% and weight by around 70%. With typical MSW as feedstock, the incinerator produces 25% bottom ash, 5% as solid residues in gas cleaning systems, and the rest 70% as flue gases. It is considered the most efficient waste treatment process for volume reduction, requiring less space during landfilling (Tillman 2012; Obe et al. 2017). The first incinerator was built around 100 years ago (1911) in the UK, primarily to maintain hygiene and reduce waste production. Later, in the 1950s and 1960s, as environmental problems and the oil crisis worsened, changes were made to the design of incinerators to improve pollution control and energy recovery (Brunner and Rechberger 2015). The incineration products are broadly classified as bottom

Table 1 Recent studies in which municipal solid waste was utilized for biofuel and other valuable bioproducts

S. No.	Strategy	Type of waste	Product	References
1	Dark-fermentation	Synthetic medium	Lactate driven biohydrogen production	Ohnishi et al. (2022)
2	Anaerobic digestion	Food waste	Methane	Ambaye et al. (2021)
3	Anaerobic digestion	Household food waste	Volatile fatty acids	Strazzera et al. (2021)
4	Dark-fermentation	Organic fraction of municipal solid waste	Biohydrogen production	Alavi-Borazjani et al. (2021)
5	Photo-fermentation	The effluent of dark fermentative cheese whey waste	Biohydrogen	Rao and Basak (2021)
6	Anaerobic digestion	Kitchen waste	Acidogenic hydrogen production, methane, algal biomass, and water treatment and reuse	Sarkar et al. (2021)
7	Microbial fuel cell	Synthetic medium	Energy generation	Shanthi Sravan et al. (2021)
8	Dark-fermentation	Food waste	Bio-hydrogen	Alian et al. (2021)
9	Microbial electrolysis cell	Food waste	Biohydrogen	Huang et al. (2020)
10	Anaerobic digestion	Orange peel	Limonene, VFA and methane	Battista et al. (2020)
11	Microbial fuel cell	Municipal solid waste	Energy generation	Moharir and Tembhurkar (2018)
12	Anaerobic digestion + microbial electrolysis cell	Food waste	Methane	Park et al. (2018)
13	Anaerobic digestion	Food waste	Methane	Demichelis et al. (2017)
14	Anaerobic digestion (acidogenic fermentation)	Food waste	Lactic acid	Tang et al. (2017)

ash, fly ash, and flue gases. This technology mainly concentrates on extracting heat energy from flue gases and further utilizing the other products, bottom ash and fly ash, in various applications in an eco-friendly manner. Various types of incinerators are used. The inability of this process to produce various bio-fuels limits further discussion of it.

3.2 Pyrolysis

Pyrolysis is defined as the thermal degradation of solid waste or any carbonaceous material in the absence of air or an oxidizing agent at a specified heating rate and holding time. Pyrolysis was observed as a pre-stepin the combustion and gasification process. Because of various advantages, this process has been identified as an attractive alternative to incineration for MSW disposal that allows energy recovery by producing bio-oil and biochar (Chen et al. 2016). The pyrolysis process has been identified as one of the most feasible ways of extracting the maximum energy present in biomass into biofuels. The thermal degradation during the pyrolysis process involves cracking long-chain hydrocarbons into small-chain hydrocarbons at temperatures ranging from 300 to 600 °C (Sipra et al. 2018). The initial degradation reactions in the pyrolysis process include depolymerization, hydrolysis, oxidation, dehydration, and decarboxylation (Demirbaş 2000). The products from this process include liquid (heavier hydrocarbons, tar, and water), solid (char or carbon), and gases (CO_2, H_2O, CO, C_2H_2, C_2H_4, C_2H_6, C_6H_6, etc.) (Basu 2010). Typically, the compounds in liquid fuels are classified into five broad categories: hydroxyaldehydes, hydroxyketones, sugars, and dehydrosugars; carboxylic acids; and phenolic compounds.

Based on the heating rate, pyrolysis can be classified into two types: (i) slow pyrolysis and (ii) fast pyrolysis. In the case of slow pyrolysis, the time (t) required to heat the fuel/feed to the pyrolysis temperature is much longer than the characteristic pyrolysis reaction time (t_r) and vice versa in the case of fast pyrolysis (i.e., $t < t_r$). The characteristic pyrolysis reaction time is determined by taking the reciprocal of the rate constant, which is calculated for each reaction step at pyrolysis temperature. The resident time for slow pyrolysis is a minute or more, and for fast pyrolysis it is in the order of seconds or milliseconds (Basu 2010). Fast pyrolysis produces more liquid products compared than slow pyrolysis. Fast pyrolysis offers good advantages and is of particular interest for many researchers because of its bio-oil product, which offers better adaptability in its storage, transport, and use as a source of energy or production of various chemicals (Greenhalf et al. 2013). Various studies have been reported in the literature on converting municipal solid waste into biofuels and value-added products using the fast pyrolysis process. Fast pyrolysis maximizes the yield of liquid fuels, which can be stored, transported, and used for energy production (Greenhalf et al. 2013). Most of the commercial biofuel production industries use fast pyrolysis for bio-oil production. However, from the characterization of bio-oil obtained from fast pyrolysis, it was observed that its quality is low compared to conventional fuels and requires higher temperatures. So, fast catalytic pyrolysis (CFP) is used to increase biofuel quality and decrease energy usage. CFP is more amenable to converting biomass into high-quality biofuel directly. ZSM-5, HZSM-5, HY mesoporous, β- and γ-zeolites, de-silicated ZSM-5, metal impregnated ZSM-5, and other conventional catalysts were primarily used as CFP catalysts alongside metal oxides, spent fluid catalytic cracking catalysts, and other conventional catalysts. Table 2 shows the distribution and yield of bio-oils, which are both solid and gaseous products from

Table 2 Literature review of different feedstocks and pyrolysis type for biofuel and bioproducts synthesis

Feedstock	Pyrolysis type	Catalyst/additives	Reactor type	Process conditions	Products distribution	References
Representative MSW sample	Fast pyrolysis	Zeolite and calcined dolomite	Fixed-bed reactor	Temperature: 200–750 °C Heating rate: 50 °C/min	Bio-oil: 10.88 (dolomite), 36.35 (zeolite) Gases: 56.67 (dolomite), 24.98 (zeolite) Char: 32.44 (dolomite), 38.66 (zeolite) in wt%	Tursunov (2014)
Wheat straw (WS), switchgrass (SG), miscanthus (MS), and beechwood (BW) (0.25–1 mm)	Fast pyrolysis	–	Bubbling fluidized bed reactor	Temperature: 500–525 °C Vapour residence time: <1.5 s	Bio-oil: 34.97 (WS), 57.90 (SG) 63.17 (BW), 46.61 (MS) Gases: 26.99 (WS), 16.57 (SG) 13.03 (BW), 9.13 (MS) Char: 28.05 (WS), 20.03 (SG) 14.43 (BW), 31.37 (MS) in wt%	Greenhalf et al. (2013)
MSW in the form of refuse-derived fuel (RDF)	Fast pyrolysis	–	Fixed bed pyrolysis	Temperature: 400–700 °C Heating rate: 10 K/min	Bio-oil/wax: 30–50 wt% Gases: 18.6–20.1 wt% Char: 49.8–32.3 wt%	Buah et al. (2007)

(continued)

Table 2 (continued)

Feedstock	Pyrolysis type	Catalyst/additives	Reactor type	Process conditions	Products distribution	References
Plastic HDPE grocery bags	Fast pyrolysis	–	Two-zone pyrolysis batch reactor followed by distillation	Upper zone temperature: 420 °C Lower zone temperature: 440 °C	Bio-oil: saturated aliphatic paraffinic hydrogens (96.8%), aliphatic, olefinic hydrogens (2.6%) and aromatic hydrogens (0.6%) in total liquid fraction Gases: 9 wt% Char: 17 wt%	Sharma et al. (2014)
Cornstalk and high-density polyethylene (HDPE)	Catalytic co-pyrolysis	HZSM-5	Pyroprobe 5200, CDS analytical	Temperature: 550 °C Heating rate: 20 °C/ms	Bio-oil–aromatic hydrocarbons yield %: 30–35% Coke: 3–3.5%	Zhang et al. (2015)
Pinewood and low-density polyethylene (LDPE)	Catalytic co-pyrolysis	Phosphorus (P) and phosphorus/nickel (P/Ni) modified ZSM-5	Semi-batch reactor (pyroprobe 5200, CDS analytical)	Temperature: 550 °C Heating rate: 20 °C/ms	Bio-oil/olefins and aromatic hydrocarbons: 52.8–54.1 C% Char/coke: 18.9–15.7 C%	Yao et al. (2015)
MSW	Catalytic pyrolysis	Natural zeolite	Fixed bed vacuum reactor	Temperature: 400 °C	Bio-crude oil: 21.4 wt%	Gandidi et al. (2018)
Waste high-density polyethylene	Fast co-pyrolysis	–	Fluidized bed reactor	Temperature: 600 °C	Bio-oil: alcohols and hydrocarbons to 85.88%	Chen et al. (2016)
Soapstock and waste tires	Catalytic fast co-pyrolysis	HZSM-5	Microwave pyrolysis system	Temperature: 550 °C	Bio-oil yield (wt%): 38.86 wt%	Dai et al. (2017)

the pyrolysis of municipal solid waste components. The reactor configuration and process conditions are also shown.

Co-pyrolysis

Further study on CFP, however, demonstrates that even in the presence of an efficient catalyst, biomass CFP yields a poor yield of aromatic hydrocarbons and significant production of coke (Wang et al. 2012). When compared to conventional fuels like diesel and others, this lowers the quality of liquid fuel. A hydrogen-rich co-reactant (waste plastic) boosts aromatics output and reduces coke formation. Catalytic co-pyrolysis boosts aromatic hydrocarbon yield while reducing the problem of plastic disposal in landfills, which has serious environmental consequences. The H/C ratios can be increased by adding a hydrogen-rich co-reactant in the form of waste polymers. This, in turn, changes the oxygen removal reaction pathway by replacing decarboxylation and decarbonylation with dehydration (Zhang et al. 2016). To establish or commercialize this technology, a substantial amount of research should be conducted to understand the catalytic co-pyrolysis process's reaction kinetics and pathways, which will aid in designing and developing a commercial pyrolysis reactor for the production of biofuels. Table 2 shows the distribution and yield of bio-oils, which are both solid and gaseous products from the pyrolysis of MSW components. The reactor configuration and process conditions are also shown.

3.3 Gasification

Gasification converts biomass, coal or carbonaceous material into a combustible gas containing carbon monoxide, hydrogen, carbon dioxide, and trace amounts of other gases like methane by partial oxidation at high temperatures (> 800 °C). The resulting gas mixture is called Syngas (synthesis gas or synthetic gas). Gasification requires a medium for reaction, which includes gases and supercritical water. The gaseous medium can be air, oxygen, subcritical steam, or a mixture based on the targeted product composition (Basu 2010). Compared to liquid fuels, syngas cannot be seen as the ideal form of product for storage, transport, and application. However, it can serve as a suitable intermediate resource for direct bio-fuels and products using Fischer Tropsch synthesis and other conversion processes like catalytic reforming and syngas fermentation (Chen et al. 2016). Some of the reactions that happen in solid waste gasification systems are shown here (Basu 2010; Arena 2012).

Combustion/Oxidation Reactions

$$C + O_2 \rightarrow CO_2 \quad \Delta H^o_{f(298)} = -394 \text{ kJ/mol} \tag{11}$$

$$CO + 0.5O_2 \rightarrow CO_2 \quad \Delta H^o_{f(298)} = -284 \text{ kJ/mol} \tag{12}$$

$$H_2 + 0.5O_2 \rightarrow H_2O \quad \Delta\mathbf{H^o_{f(298)}} = -242 \text{ kJ/mol} \tag{13}$$

$$C_nH_m + n/2 \, O_2 \leftrightarrow nCO + m/2 \, H_2 \quad \Delta\mathbf{H^o_{f(298)}} < \mathbf{0} \tag{14}$$
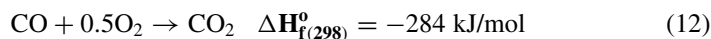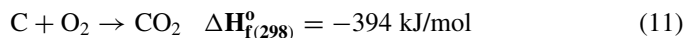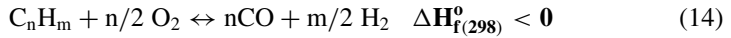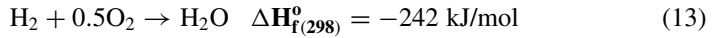
Gasification/Carbon Reactions

$$C + CO_2 \leftrightarrow 2CO \,\, \Delta\mathbf{H^o_{f(298)}} = 172 \text{ kJ/mol (Boudouard reaction)} \tag{15}$$

$$C + H_2O \leftrightarrow CO + H_2 \,\, \Delta\mathbf{H^o_{f(298)}} = 131 \text{ kJ/mol (Water gas reaction)} \tag{16}$$

$$CO + H_2O \leftrightarrow CO_2 + H_2 \,\, \Delta\mathbf{H^o_{f(298)}} = -41.2 \text{ kJ/mol (Water gas shift reaction)} \tag{17}$$

Methanation Reaction

$$C + 2H_2 \leftrightarrow CH_4, \,\, \Delta\mathbf{H^o_{f(298)}} = -74.9 \text{ kJ/mol} \tag{18}$$

Steam Reforming Reaction

$$CH_4 + H_2O \rightarrow CO + 3H_2, \,\, \Delta\mathbf{H^o_{f(298)}} = 205.31 \text{ kJ/mol} \tag{19}$$

$$C_nH_m + nH_2O \leftrightarrow nCO + (n + m/2) \, H_2 \quad \Delta\mathbf{H^o_{f(298)}} > \mathbf{0} \tag{20}$$
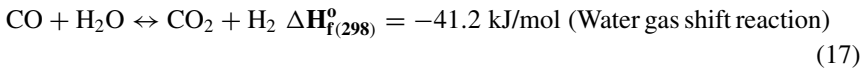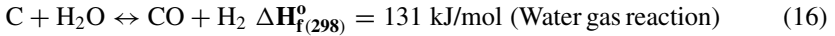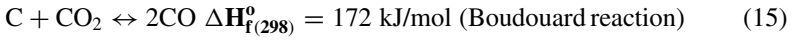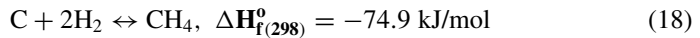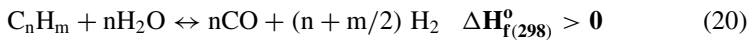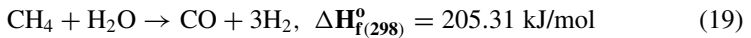
Decomposition Reactions of Tars and Hydrocarbons

$$pC_xH_y \rightarrow qC_nH_m + rH_2 \quad \Delta\mathbf{H^o_{f(298)}} > \mathbf{0} \,\,\, \text{(Dehydrogenation)} \tag{21}$$

$$C_nH_m \rightarrow nC + m/2 \, H_2 \quad \Delta\mathbf{H^o_{f(298)}} > \mathbf{0} \,\,\, \text{(Carbonization)} \tag{22}$$
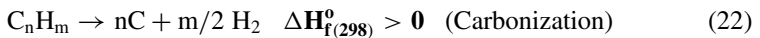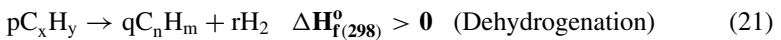
Various gasifiers used for syngas production mainly include fixed/moving, fluidized, and entrained bed systems. Currently, the gasification process uses steam as a gasifying medium to produce H_2-rich syngas, which can be used as a feedstock to produce various biofuels via catalytic chemical synthesis (Sikarwar et al. 2017). He et al. (2009) studied the influence of catalyst, temperature, steam/MSW ratio, and weight hourly space velocity on product composition in catalytic steam gasification of the organic fraction in MSW. In this study, calcined dolomite was used as a catalyst. The gasification is conducted in a bench-scale downstream fixed bed reactor at the temperature range of 750–950 °C, with a steam to MSW ratio of 0.77, for a weight hourly space velocity of 1.29 h^{-1}. The high gasification temperature resulted in more H_2 and CO production, high carbon conversion efficiency (CCE), and dry gas

yield. The tar formed is completely decomposed when the temperature is increased from 850 to 950 °C. At 950 °C, the hydrogen gas in the syngas reached more than 50 mol%. The total syngas produced is in the range of 36–70 mol%, and the char produced contains a high ash content (84%) with negligible hydrogen, nitrogen, and sulfur content. With the increase of the steam to MSW ratio, the potential yield of hydrogen/kg of MSW has reached a maximum of 59.83 mol% at a steam/MSW ratio of 1.04. The effect of weight on hourly space velocity was insignificant on product composition. Wang et al. (2012) studied MSW steam gasification in a two-stage gasifier facility (gasification zone and catalytic zone) with NiO supported on modified dolomite (NiO/MD) and at different steam/MSW ratios (S/M). The selected MSW sample contains five different components: textile (19.95 wt%), wood (11.4 wt%), kitchen garbage (42.37 wt%), plastic (9.57 wt%), and paper (16.71 wt%). The results found that the modified catalyst (NiO/MD) significantly reduced the tar content (0.23 g/Nm^3 of gas produced) at an S/M of 1.23. The hydrogen gas yield and CCE at that S/M ratio are 80 g/kg of MSW and 76.79%, respectively. Hu et al. (2015) the studied gasification of wet MSW (paper—37 wt%, textile—8 wt%, plastics—43 wt%, wood—12 wt%) coupled with carbon dioxide capture in a fixed bed reactor. This study looked at the effects of moisture content, the molar ratio of CaO to carbon in MSW ([Ca]/[C], and reactor temperature on gas composition and H$_2$ yield. The moisture content of selected MSW changes from 10 to 60 wt% by adding different quantities of distilled water. At a moisture content of 40%, a gasification temperature of 750 °C, and a [Ca]/[C] ratio of 0.7, the maximum hydrogen yield of 277.67 mL/g MSW was obtained. Kwak et al. (2006) conducted experiments in a pilot-scale gasification/melting plant using MSW as feedstock at a temperature of around 1200 °C using a double inverse diffusion flame burner. Due to the higher temperature, toxic volatile organic compounds like furan, dioxin, and other organics in the gaseous and liquid phase were effectively destroyed. The obtained syngas' volumetric composition and average heating value are 25–34% CO, 28–38% H$_2$, and 12.765 MJ/Nm^3. The concentration of heavy metals in the melted slag, fly ash, and treated water was much less than the limiting values.

Plasma Gasification

Plasma gasification is a thermal process that uses a high-temperature plasma torch to thermally break down the organic part of municipal solid waste into syngas. The undesirable hydrocarbons in the syngas are broken down into gases by plasma, which acts as a reforming agent. The MSW's inorganic part is transformed into non-leachable, inert slag. This procedure is applicable to a wide range of heterogeneous solid waste because of the high temperature. Agon et al. (2016) conducted experiments on a single-stage plasma gasification system for the conversion of refuse-derived fuel (RDF) prepared from solid waste at a temperature range of 1400 to 1600 K. The syngas heating value, range of carbon conversion efficiency, cold gas efficiency, and mechanical gasification efficiency were observed as 10.9 MJ/Nm^3, 80–100%, 56%, and 95%, respectively.

Supercritical Water Gasification

Supercritical water gasification (SCWG) is a type of biomass gasification in which the medium is supercritical water (374 °C and 22.1 MPa). Supercritical water in this process acts as both a reactant and a medium in gasification. At supercritical conditions, the probability of hydrogen generation (H^+) and hydroxide (OH^-) ions is high, making the environment suitable for undergoing hydrolysis and pyrolysis reactions. Production of hydrogen through SCWG is irrespective of the solid waste's moisture content, making this process superior to other conventional thermochemical routes. The H_2 produced in this process is at high pressure, which means it can be directly sent for storage. This also saves the compression energy costs during its storage (Reddy et al. 2014).

3.4 Liquefaction

Pyrolysis, gasification, and hydrothermal processes can all be used to turn solid biomass into liquid fuel. Hydrothermal liquefaction is a process in which biomass is turned into a liquid by contacting it with water at high temperatures (300–350 °C) and high pressures (12–20 MPa) over a period of time (HTL) (Basu 2010). The main products of HTL are bio-crude, char, water-soluble substances, and gas. By using alkaline catalysts, the char formed in the process will be suppressed, increasing the quality and quantity of bio-oil. If the temperature of this process is higher than the critical point of the water, the gasification process will be dominant. HTL has unique features compared to the other conversion technologies, like higher heating values and the ability to high moisture content feedstocks without drying. Hydrothermal liquefaction is one of the TCC processes which mimics the natural formation of fossil fuel in the presence of water (Zhang et al. 2016). HTL is also called hydrous pyrolysis; it involves the direct liquefaction of biomass in water with a catalyst. At these conditions, water is still in a liquid state and has a range of exotic properties (low viscosity, high solubility). Many researchers have investigated the feasibility of the hydrothermal liquefaction process in converting different types of biomass into bio-crude or bio-oil. The bio-crude obtained from the HTL process can be directly used as an alternative to heavy fuel oil. However, it must be upgraded to remove oxygen and to produce diesel and gasoline range fuels. Catalytic hydrotreating in a process similar to the hydrotreating of petroleum products is used to produce low-sulfur and marketable liquid hydrocarbon products in a process similar to that of petroleum products. The HTL process is less used for MSW components because of its complex composition. Today, a lot of research is being done on how to turn algae into biofuels because it has the ability to make high-quality bio-oils from them.

3.5 Hydrothermal Carbonisation

Hydrothermal carbonization (HTC) is a novel thermal conversion process conducted at a relatively low temperature (180–350 °C) under autogenous pressures that can convert carbohydrates contained in various municipal waste streams into a carbonaceous residue referred to as hydro-char (Berge et al. 2011). This process is used for heterogeneous feedstocks like MSW with high moisture content. The produced hydro-char is stable, carbon-rich and has reduced oxygen content in the solid phase (Escala et al. 2013). The hydro-char produced from the HTC process is further used as a feedstock for the gasification process to convert it into syngas. From the studies on combustion, pyrolysis, and char CO_2-gasification of hydrochar from MSW, it was found that combining the hydrothermal carbonization process with the thermochemical process could be a very good way to both make energy and clean up waste (Lin et al. 2016).

3.6 Hybrid Conversion Technologies

For the complete conversion of lignocellulosic biomass and other complex solid waste, these are converted to high-quality biofuels using hybrid processing technologies, which are observed to be a viable solution. Brown (2007) reported two distinct approaches to hybrid processing.

(i) Rapid pyrolysis, followed by hydrolysis and/or fermentation of the bio-oil that results.
(ii) The gasification of the mixture of carbon monoxide, hydrogen, and carbon dioxide, then the fermentation of the mixture.

In the first case, bio-oil produced from the fast pyrolysis process is further converted into biofuels and chemicals using fermentation. The bio-oil obtained from the pyrolysis process cannot be directly used as feedstock for the fermentation process. The sugars are present in anhydrous form (as levoglucosan), and bio-oil contains a lot of microbial inhibitors. Levoglucosan from cellulose (from biomass) is also retarded by alkali cations in the untreated biomass. With the removal of these cations, the production of levoglucosan is increased by ten times. The levoglucosan can be converted into various chemicals (such as itaconic acid, citric acid) using fungi (*Aspergillus terrus*-K26, *Aspergillus niger*-CBX-209). Furans, phenols, and organic acids are thought to be responsible for the inhibition effect in bio-oil. These can be separated by various detoxification steps like solvent extraction and adsorption on activated carbon. The other parallel approach uses biocatalysts, which are tolerant to the inhibitors (Jarboe et al. 2011). In the latter hybrid processing, the syngas produced from the gasification process is further converted into biofuels using the fermentation technique. Shen et al. (2017) conducted fermentation experiments in a novel horizontal rotating packed bed reactor to produce fuels and chemicals

from syngas obtained from biomass gasification. The mass transfer in this reactor was considerably improved compared to conventional fermentation reactors, which will enhance ethanol production. A *Clostridium carboxidivorans* P7 strain was used in this reactor. From the results, it was observed that 6.7 g/L/day of ethanol was produced. It is 3.3 times more than the amount that can be found in a CSTR under the same circumstances.

4 Life Cycle Analysis

Life cycle analysis (LCA) involves a method of evaluating the environmental performance of any product in terms of its partial or complete life cycle, taking into account the effects produced during its life cycle (Pradhan et al. 2011; Bartolozzi et al. 2018). Initially restricted to industrial products, the ISO 14040 series provides the LCA standard; it is now used in various fields (Finkbeiner et al. 2006). ISO 14040 describes the LCA as "the evaluation and compilation of the inputs, outputs, and potential environmental impacts of a product system throughout its life cycle." Therefore, the LCA is an essential tool for assessing the environmental impacts and resources used in the product life cycle and considering all aspects of the natural environment, resources, and human health (Chau et al. 2015). The environmental impact of a product is looked at every step of its life cycle, from the extraction of resources to the use of the product, to the disposal, reuse, or recycling of the product (Gnansounou and Dauriat 2011; Lecksiwilai et al. 2017).

4.1 Life Cycle Assessment

A life cycle assessment is the formal procedure of evaluating the sustainability of a product or a system. Sustainability includes three aspects: environmental, social, and economic (Allen 2012). However, social and economic aspects are difficult to quantify, so environmental aspects are generally considered while performing the life cycle assessment. Life cycle analysis includes the four steps: (i) goal and scope; (ii) life cycle inventory background data; (iii) life cycle impact assessment; and (iv) interpretation. The primary objective of a study is referred to as the goal and scope of the investigation. Inputs and outputs in processes for the manufacture of accessory materials and process energies and direct emissions such as steam, electricity, fertilizer, diesel, pesticides, and chemicals are included in the life cycle inventory background data. Background data is typically included in worldwide databases, but the process circumstances (e.g., energy structure, energy efficiency, emissions, and so on) can vary. Then, a life cycle impact assessment is performed using the inventory analysis data collected for the unit processes. The inventory data is classified according to its potential impact on the environment. The final step is interpretation. After determining the impacts, the final step is the interpretation of

the results. By interpreting the results, recommendations may be made to reduce the environmental impacts.

Case Studies for Life Cycle Analysis of Biofuels

A review of the case studies concerning the life cycle assessment of biofuels and bio-products shows the wide variety of the four steps involved in the life cycle analysis (Table 3). As far as goals and scope are concerned, these range from evaluating the environmental impact and energy balance to addressing the variability of results and modelling issues (Rocha et al. 2014; Malça and Freire 2011). For inventory analysis, the input materials considered are the crop used for biofuel, herbicides, fertilizers, chemicals employed for biofuel processing, and the fuel used in production. The output emissions include mainly the gases produced from energy production and wastewater. The impact categories considered for the environmental impact assessment are: abiotic depletion potential, global warming potential, human toxicity potential, acidification potential, eutrophication potential, climate change, smog, ozone depletion, indirect land-use change, and GHG emissions. The interpretation of the results shows that the life cycle assessment is usually done to look at health and environmental effects, update the database for inventory analysis, and show how important the main issues and their uncertainty are.

5   Industrial Perspective and Future Scope

Biofuel production has increased dramatically over the last two decades. Only two-thirds of ethanol production is centered in Brazil and the United States. On a global scale, biofuel production and consumption have increased dramatically in recent years. Total biofuel output climbed by 15.7% annually from 16.4 Mtoe (megaton of oil equivalent) in 2004 to 70.8 Mtoe in 2014. According to the International Energy Agency, global biofuel consumption will continue to rise over the next few decades, reaching 720 Mtoe by 2050 (Hao et al. 2018), a tenfold increase over present levels. Simultaneously, the biomass required for biofuel production has shifted significantly from food crops to non-food crops and non-plantation resources. The growing global market for biofuels has sparked questions about their long-term viability. The potential influence of biofuels on food security and agricultural commodity prices, as well as social and environmental aspects such as deforestation, monoculture, water resource depletion, and labor conditions, is also being evaluated (Koçar and Civaş 2013). These concerns are a setback for the growth of the biofuel market, and they need to be looked into and talked about in more detail.

Table 3 Review of case studies concerning the life cycle assessment of biofuels

Goal and scope	Inventory analysis	Impacts assessment	Interpretation	References
Evaluation of significant environmental impacts and energy balance of ethanol	Sugarcane, diesel fuel, urea, herbicide, potassium, natural gas, crude oil, methane, fuel oil, gasoline, bentonite, fuel emissions, gasoline emissions, methane emissions, and ethanol	Abiotic depletion potential, global warming potential, human toxicity potential, acidification potential, and eutrophication potential	To assess the health and environmental impacts of ethanol	Rocha et al. (2014)
Sustainability of perennial crops production for bioenergy and bioproducts	Giant reed, miscanthus, switchgrass, fertilizers, water, energy input	Climate change, energy use, acidification, marine eutrophication, freshwater eutrophication, summer smog, ozone depletion, particulate matter	Providing options for strengthening advantages and preventing disadvantages for future development of these crops in a sustainable context	Fernando et al. (2018)
Evaluation of significant environmental impacts and energy balance of biodiesel	Soya bean, palm oil, biodiesel, glycerol, diesel fuel, electricity, fuel emissions, fertilizers, herbicides, water, palm shells	Abiotic depletion potential, global warming potential, human toxicity potential, acidification potential, and eutrophication potential	To assess the health and environmental impacts of biodiesel	Rocha et al. (2014)
To evaluate the energy life-cycle of soybean biodiesel	Soyabean, electricity, gasoline, propane, natural gas, water, fertilizers, biodiesel, emissions, wastewater	Energy use	Updation of National Renewable Energy Laboratory (NREL) data	Pradhan et al. (2011)

(continued)

Table 3 (continued)

Goal and scope	Inventory analysis	Impacts assessment	Interpretation	References
Life cycle study of biofuel in Europe to check variability and modeling issues	Input energy requirement, emissions	Indirect land-use change, GHG emissions	To emphasize the need for transparency in inputs and assumptions; to demonstrate the importance of main issues and related uncertainty in the life cycle and GHG accounting of biofuel	Malça and Freire (2011)

6 Conclusions

The current fossil-based linear economy has resulted in rapid economic growth, harmful climate change, and the discharge of unprocessed trash into natural environment. Traditionally, waste treatment procedures have been designed to eliminate or minimize the associated contaminants to protect the environment. However, the urgent demand for alternative feedstocks has prompted a shift from waste treatment to waste refining to recover valuable minerals. Through a closed-loop bioprocessing cascade, any waste (solid, liquid, or gaseous) has an inherent net positive energy that may be collected and reused to make biobased products and biofuels, enabling the shift to a circular and low-carbon bioeconomy. Acidogenesis, bioelectrogenesis, photosynthesis, photo-fermentation, and other technologies are required for bioprocesses that use waste as a substrate for manufacturing biobased goods. Besides, thermochemical conversion is also potentially competitive in harnessing energy and bioproducts. A systemized interlinking of these bioprocesses and thermochemical processes aids in the construction of a waste biorefinery. Understanding life cycle analysis is crucial as it makes these processes sustainable and marketable.

References

Agon N, Hrabovský M, Chumak O et al (2016) Plasma gasification of refuse derived fuel in a single-stage system using different gasifying agents. Waste Manage 47:246–255

Alavi-Borazjani SA, Tarelho LA da C, Capela MI (2021) Parametric optimization of the dark fermentation process for enhanced biohydrogen production from the organic fraction of municipal solid waste using Taguchi method. Int J Hydrogen Energy 46:21372–21382. https://doi.org/10.1016/J.IJHYDENE.2021.04.017

Alian M, Saadat S, Rezaeitavabe F (2021) An investigation on the dose-dependent effect of iron shaving on bio-hydrogen production from food waste. Int J Hydrogen Energy 46:19886–19896. https://doi.org/10.1016/J.IJHYDENE.2021.03.121

Allen DT (2012) Sustainable engineering: concepts, design, and case studies

Ambaye TG, Rene ER, Nizami AS et al (2021) Beneficial role of biochar addition on the anaerobic digestion of food waste: a systematic and critical review of the operational parameters and mechanisms. J Environ Manage 290:112537. https://doi.org/10.1016/J.JENVMAN.2021.112537

Arena U (2012) Process and technological aspects of municipal solid waste gasification a review. Waste Manage 32:625–639

Bajracharya S, Sharma M, Mohanakrishna G et al (2016) An overview on emerging bioelectrochemical systems (BESs): technology for sustainable electricity, waste remediation, resource recovery, chemical production and beyond. Renew Energy 98:153–170

Bardhan SK, Gupta S, Gorman ME, Haider MA (2015) Biorenewable chemicals: feedstocks, technologies and the conflict with food production. Renew Sustain Energy Rev 51:506–520

Bartolozzi I, Baldereschi E, Daddi T, Iraldo F (2018) The application of life cycle assessment (LCA) in municipal solid waste management: a comparative study on street sweeping services. J Clean Prod 182:455–465

Basu P (2010) Biomass gasification and pyrolysis: practical design and theory. Academic Press

Battista F, Remelli G, Zanzoni S, Bolzonella D (2020) Valorization of residual orange peels: limonene recovery, volatile fatty acids, and biogas production. ACS Sustain Chem Eng 8:6834–6843. https://doi.org/10.1021/ACSSUSCHEMENG.0C01735

Berge ND, Ro KS, Mao J et al (2011) Hydrothermal carbonization of municipal waste streams. Environ Sci Technol 45:5696–5703

Brown RC (2007) Hybrid thermochemical/biological processing. Appl Biochem Biotechnol 137:947–956

Brunner PH, Rechberger H (2015) Waste to energy—key element for sustainable waste management. Waste Manage 37:3–12

Buah WK, Cunliffe AM, Williams PT (2007) Characterization of products from the pyrolysis of municipal solid waste. Process Saf Environ Prot 85:450–457

Bundhoo ZMA (2019) Potential of bio-hydrogen production from dark fermentation of crop residues: a review. Int J Hydrogen Energy 44:17346–17362

Cardeña R, Cercado B, Buitrón G (2019) Microbial electrolysis cell for biohydrogen production. In: Biohydrogen. Elsevier, pp 159–185

Chau CK, Leung TM, Ng WY (2015) A review on life cycle assessment, life cycle energy assessment and life cycle carbon emissions assessment on buildings. Appl Energy 143:395–413

Chen P, Xie Q, Addy M et al (2016) Utilization of municipal solid and liquid wastes for bioenergy and bioproducts production. Bioresour Technol 215:163–172

Dahiya S, Chatterjee S, Sarkar O, Mohan SV (2020) Renewable hydrogen production by dark-fermentation: current status, challenges and perspectives. Bioresour Technol 124354

Dai L, Fan L, Duan D et al (2017) Microwave-assisted catalytic fast co-pyrolysis of soapstock and waste tire for bio-oil production. J Anal Appl Pyrol 125:304–309

Das SR, Basak N (2021) Molecular biohydrogen production by dark and photo fermentation from wastes containing starch: recent advancement and future perspective. Bioprocess Biosyst Eng 44:1–25

Demichelis F, Pleissner D, Fiore S et al (2017) Investigation of food waste valorization through sequential lactic acid fermentative production and anaerobic digestion of fermentation residues. Bioresour Technol 241:508–516. https://doi.org/10.1016/J.BIORTECH.2017.05.174

Demirbaş A (2000) Mechanisms of liquefaction and pyrolysis reactions of biomass. Energy Convers Manage 41:633–646

Escala M, Zumbuhl T, Koller C et al (2013) Hydrothermal carbonization as an energy-efficient alternative to established drying technologies for sewage sludge: a feasibility study on a laboratory scale. Energy Fuels 27:454–460

Fernando AL, Rettenmaier N, Soldatos P, Panoutsou C (2018) Sustainability of perennial crops production for bioenergy and bioproducts. Elsevier Inc.

Ferraren-De Cagalitan DDT, Abundo MLS (2021) A review of biohydrogen production technology for application towards hydrogen fuel cells. Renew Sustain Energy Rev 151:111413

Finkbeiner M, Inaba A, Tan R et al (2006) The new international standards for life cycle assessment: ISO 14040 and ISO 14044. Int J Life Cycle Assess 11:80–85

Gandidi IM, Susila MD, Mustofa A, Pambudi NA (2018) Thermal–catalytic cracking of real MSW into bio-crude oil. J Energy Inst 91:304–310

Ghimire A, Frunzo L, Pirozzi F et al (2015) A review on dark fermentative biohydrogen production from organic biomass: process parameters and use of by-products. Appl Energy 144:73–95

Gnansounou E, Dauriat A (2011) Life-cycle assessment of biofuels. In: Biofuels. Elsevier, pp 25–50

Greenhalf CE, Nowakowski DJ, Harms AB et al (2013) A comparative study of straw, perennial grasses and hardwoods in terms of fast pyrolysis products. Fuel 108:216–230

Gurjar BR, Butler TM, Lawrence MG, Lelieveld J (2008) Evaluation of emissions and air quality in megacities. Atmos Environ 42:1593–1606

Hao H, Liu Z, Zhao F et al (2018) Biofuel for vehicle use in China: current status, future potential and policy implications. Renew Sustain Energy Rev 82:645–653

He M, Xiao B, Liu S et al (2009) Hydrogen-rich gas from catalytic steam gasification of municipal solid waste (MSW): influence of steam to MSW ratios and weight hourly space velocity on gas production and composition. Int J Hydrogen Energy 34:2174–2183

Hu M, Guo D, Ma C et al (2015) Hydrogen-rich gas production by the gasification of wet MSW (municipal solid waste) coupled with carbon dioxide capture. Energy 90:857–863

Huang J, Feng H, Huang L et al (2020) Continuous hydrogen production from food waste by anaerobic digestion (AD) coupled single-chamber microbial electrolysis cell (MEC) under negative pressure. Waste Manage 103:61–66

Huber GW, Iborra S, Corma A (2006) Synthesis of transportation fuels from biomass: chemistry, catalysts, and engineering. Chem Rev 106:4044–4098

Jarboe LR, Wen Z, Choi D, Brown RC (2011) Hybrid thermochemical processing: fermentation of pyrolysis-derived bio-oil. Appl Microbiol Biotechnol 91:1519–1523

Katiyar R, Gurjar BR, Biswas S et al (2017) Microalgae: an emerging source of energy based bio-products and a solution for environmental issues. Renew Sustain Energy Rev 72:1083–1093

Katiyar R, Bharti RK, Gurjar BR et al (2018) Utilization of de-oiled algal biomass for enhancing vehicular quality biodiesel production from *Chlorella* sp. in mixotrophic cultivation systems. Renew Energy 122:80–88

Koçar G, Civaş N (2013) An overview of biofuels from energy crops: current status and future prospects. Renew Sustain Energy Rev 28:900–916

Kwak T-H, Lee S, Park J-W et al (2006) Gasification of municipal solid waste in a pilot plant and its impact on environment. Korean J Chem Eng 23:954–960

Lecksiwilai N, Gheewala SH, Silalertruksa T, Mungkalasiri J (2017) LCA of biofuels in Thailand using Thai Ecological Scarcity method. J Clean Prod 142:1183–1191

Lin Y, Ma X, Peng X et al (2016) Combustion, pyrolysis and char CO_2-gasification characteristics of hydrothermal carbonization solid fuel from municipal solid wastes. Fuel 181:905–915

Malça J, Freire F (2011) Life-cycle studies of biodiesel in Europe: a review addressing the variability of results and modeling issues. Renew Sustain Energy Rev 15:338–351. https://doi.org/10.1016/j.rser.2010.09.013

Mohan SV, Nikhil GN, Chiranjeevi P et al (2016) Waste biorefinery models towards sustainable circular bioeconomy: critical review and future perspectives. Bioresour Technol 215:2–12

Moharir PV, Tembhurkar AR (2018) Effect of recirculation on bioelectricity generation using microbial fuel cell with food waste leachate as substrate. Int J Hydrogen Energy 43:10061–10069. https://doi.org/10.1016/J.IJHYDENE.2018.04.072

Nikhil GN, Mohan SV, Swamy YV (2014) Behavior of acidogenesis during biohydrogen production with formate and glucose as carbon source: substrate associated dehydrogenase expression. Int J Hydrogen Energy 39:7486–7495

Obe RKD, de Brito J, Lynn CJ, Silva RV (2017) Sustainable construction materials: municipal incinerated bottom ash. Woodhead Publishing

Ohnishi A, Hasegawa Y, Fujimoto N, Suzuki M (2022) Biohydrogen production by mixed culture of *Megasphaera elsdenii* with lactic acid bacteria as lactate-driven dark fermentation. Bioresour Technol 343:126076. https://doi.org/10.1016/J.BIORTECH.2021.126076

Pareek A, Sravan JS, Mohan SV (2019) Exploring chemically reduced graphene oxide electrode for power generation in microbial fuel cell. Mater Sci Energy Technol 2:600–606

Park J, Lee B, Tian D, Jun H (2018) Bioelectrochemical enhancement of methane production from highly concentrated food waste in a combined anaerobic digester and microbial electrolysis cell. Bioresour Technol 247:226–233. https://doi.org/10.1016/J.BIORTECH.2017.09.021

Piemonte V, de Falco M, Basile A (2013) Sustainable development strategies: an overview. In: Sustainable development in chemical engineering innovative technologies, pp 1–24

Pradhan A, Shrestha DS, McAloon A et al (2011) Energy life-cycle assessment of soybean biodiesel revisited. Trans ASABE 54:1031–1039. https://doi.org/10.13031/2013.37088

Rao R, Basak N (2021) Process optimization and mathematical modelling of photo-fermentative hydrogen production from dark fermentative cheese whey effluent by *Rhodobacter sphaeroides* O.U.001 in 2-L cylindrical bioreactor. Biomass Convers Biorefin. https://doi.org/10.1007/s13399-021-01377-1

Reddy SN, Nanda S, Dalai AK, Kozinski JA (2014) Supercritical water gasification of biomass for hydrogen production. Int J Hydrogen Energy 39:6912–6926

Rocha MH, Capaz RS, Lora EES et al (2014) Life cycle assessment (LCA) for biofuels in Brazilian conditions: a meta-analysis. Renew Sustain Energy Rev 37:435–459. https://doi.org/10.1016/j.rser.2014.05.036

Saladini F, Patrizi N, Pulselli FM et al (2016) Guidelines for emergy evaluation of first, second and third generation biofuels. Renew Sustain Energy Rev 66:221–227

Sarkar O, Katakojwala R, Venkata Mohan S (2021) Low carbon hydrogen production from a waste-based biorefinery system and environmental sustainability assessment. Green Chem 23:561–574. https://doi.org/10.1039/d0gc03063e

Shanthi Sravan J, Raunija TSK, Verma A, Venkata Mohan S (2021) Impregnated thermoset pre-pressurized carbon composite electrodes in microbial fuel cell: compositional functionalities influence on ORR with reference to graphite. Fuel 285:119273. https://doi.org/10.1016/J.FUEL.2020.119273

Sharma KD, Jain S (2019) Overview of municipal solid waste generation, composition, and management in India. J Environ Eng 145:04018143

Sharma BK, Moser BR, Vermillion KE et al (2014) Production, characterization and fuel properties of alternative diesel fuel from pyrolysis of waste plastic grocery bags. Fuel Process Technol 122:79–90

Shen Y, Brown RC, Wen Z (2017) Syngas fermentation by Clostridium carboxidivorans P7 in a horizontal rotating packed bed biofilm reactor with enhanced ethanol production. Appl Energy 187:585–594

Sikarwar VS, Zhao M, Fennell PS et al (2017) Progress in biofuel production from gasification. Prog Energy Combust Sci 61:189–248

Sipra AT, Gao N, Sarwar H (2018) Municipal solid waste (MSW) pyrolysis for bio-fuel production: a review of effects of MSW components and catalysts. Fuel Process Technol 175:131–147

Strazzera G, Battista F, Tonanzi B et al (2021) Optimization of short chain volatile fatty acids production from household food waste for biorefinery applications. Environ Technol Innov 23:101562. https://doi.org/10.1016/J.ETI.2021.101562

Tang J, Wang XC, Hu Y et al (2017) Effect of pH on lactic acid production from acidogenic fermentation of food waste with different types of inocula. Bioresour Technol 224:544–552. https://doi.org/10.1016/J.BIORTECH.2016.11.111

Tian H, Li J, Yan M et al (2019) Organic waste to biohydrogen: a critical review from technological development and environmental impact analysis perspective. Appl Energy 256:113961

Tillman DA (2012) Incineration of municipal and hazardous solid wastes. Elsevier

Tursunov O (2014) A comparison of catalysts zeolite and calcined dolomite for gas production from pyrolysis of municipal solid waste (MSW). Ecol Eng 69:237–243

Venkata Mohan S, Nikhil GN, Chiranjeevi P et al (2016) Waste biorefinery models towards sustainable circular bioeconomy: critical review and future perspectives. Bioresour Technol 215. https://doi.org/10.1016/j.biortech.2016.03.130

Wang J, Cheng G, You Y et al (2012) Hydrogen-rich gas production by steam gasification of municipal solid waste (MSW) using NiO supported on modified dolomite. Int J Hydrogen Energy 37:6503–6510

Yao W, Li J, Feng Y et al (2015) Thermally stable phosphorus and nickel modified ZSM-5 zeolites for catalytic co-pyrolysis of biomass and plastics. RSC Adv 5:30485–30494

Zhang B, Zhong Z, Ding K, Song Z (2015) Production of aromatic hydrocarbons from catalytic co-pyrolysis of biomass and high density polyethylene: analytical Py–GC/MS study. Fuel 139:622–628

Zhang X, Lei H, Chen S, Wu J (2016) Catalytic co-pyrolysis of lignocellulosic biomass with polymers: a critical review. Green Chem 18:4145–4169

Zhen G, Lu X, Kumar G et al (2017) Microbial electrolysis cell platform for simultaneous waste biorefinery and clean electrofuels generation: current situation, challenges and future perspectives. Prog Energy Combust Sci 63:119–145

Advanced Oxidation Processes for Wastewater Treatment: Perspective Through Nanomaterials

Rasmeet Singh ⬤**, Gaurav Rattan, Mandeep Singh** ⬤**, Ravi Manne** ⬤**, Simran Kaur Oberoi** ⬤**, and Navneet Kaur**

Abstract The advanced oxidation processes (AOPs) are an important development for wastewater purification systems. AOPs are capable of degrading the complete organic compounds present in wastewater. In the past few decades, main attention has been given on nanomaterials involving AOPs/hybrid AOPs. The idea of this study is to lay out a quick map of wastewater treatment through nanomaterials in correlation with AOPs and hybrid AOPs, along with recent innovations in process intensification for effective removal of organic pollutants. In support of the importance of ·OH radical in AOPs, a special attention has also been given to its mechanistic aspects with photo and nano-photo chemical AOPs.

Keywords Wastewater purification · Advanced oxidation process · Nanomaterials · Process intensification · ·OH radical

R. Singh (✉) · G. Rattan
Dr. S.S. Bhatnagar University Institute of Chemical Engineering and Technology, Panjab University, Chandigarh 160014, India
e-mail: srasmeet9@gmail.com

M. Singh
School of Mechanical and Mechatronic Engineering, University of Technology Sydney, Sydney, NSW 2007, Australia

R. Manne
Chemtex Environmental Lab, Quality Control and Assurance Department, 3082 25th Street, Port Arthur, TX 77642, USA

S. K. Oberoi
Department of Chemical Engineering, SRM Institute of Science and Technology, Kattankulathur, Chennai 603203, India

N. Kaur
Doutta Galla Harmony Village, 20 Zurcas Ln, Shepparton, VIC 3630, Australia

1   Introduction

The world has changed drastically due to chaos created by global warming and climate changes. In all this rigid situation, water scarcity has come up as a serious predicament. Around 80% of industrial wastewater released into water bodies is untreated, disturbing aquatic life, flora and fauna, and human life (Singh et al. 2021). The current infrastructure for the treatment of polluted water has several drawbacks and requires several modifications and intensifications of processes for efficient decontamination of organic pollutants present in wastewater (Obotey Ezugbe and Rathilal 2020; Singh 2021).

For many years, researchers have contributed to the development of advanced oxidation processes for wastewater treatment. Among them, few researchers have used nanoparticles as an effective adsorbent, as well as catalysts in lieu of micrometer-sized particles with AOPs to treat wastewater (Ede et al. 2020; Cardoso et al. 2021). These AOPs give rise to ·OH radicals, helping in degradation of organic pollutants. These radicals come in contact with organic molecules non-selectively. ·OH radicals can be produced through different methods. AOPs are also preferred because they produce less toxic reaction intermediates when interacting with organic contaminants. Instead of artificial sources of light (i.e. ultraviolet, visible, etc.), few AOPs are also capable of operating on natural sources of light (i.e. sunlight) (Wang and Xu 2012). The research so far has shown that nanomaterials can effectively remove/degrade both organic and biological pollutants (Bashambu et al. 2021). Nano-membranes, nano-tubes, and metal-based nanoparticles have been successfully employed for removing harmful compounds like Hg, Ni, CN^-, Zn, Cd, algae, bacteria, nutrients, viruses, and antibiotics (Krzemińska et al. 2015; Nasrollahzadeh et al. 2021; Rao et al. 2021). Improvements have been seen in advanced nanotechnology in wastewater purification. Usually, the large surface/volume ratio of the nanoparticles improves the adsorption capacity of the material.

This article is an important research on the latest developments in the field of improved nanomaterial oxidation processes, the intensification of their processes and the main pathways of the reaction mechanism followed by AOP to generate radicals.

2   AOPs Involving Nanomaterials

AOPs received immense popularity in R&D fields for wastewater purification technologies in the past few decades. Processes such as Fenton, cavitation, ozonation and photocatalytic oxidation have been successfully used to decompose persistent organic pollutants on a small scale. Homogeneous and heterogeneous AOPs are another two classifications overtaking wastewater purification applications. For activation of AOPs, several factors like ultraviolet light, visible light, oxidants, and catalysts are essential. Activation of AOPs is necessary because the hydroxyl radical

(·OH) generating AOPs will then be more reactive towards the organic compounds, that too in conditions where activating oxygen is in abundance. Between numerous industrial pollutants, dyeing, oil and grease, and paper are the most harmful ones because of their substantial use in production processes in various industrial unit operations (Singh 2021). The mixing of organic dyes in water fields reduces the ability to absorb and reflect sunlight and thus increases the toxicity of the water. This ultimately turns out to be a problem for aquatic life. To overcome this problem, effective AOPs can be used to mineralize organic dyes. Many studies have shown that AOP can also be very effective at degrading pigments in the aquatic environment. The sole purpose of AOP is to completely mineralize the harmful compounds (Matafonova and Batoev 2018). Many scientists have used micro-sized catalysts for photocatalytic AOPs in order to achieve maximum degradation of organic pollutants. But only few of them have utilized nanomaterials as nano-photocatalytic agents in AOPs. This article focuses on developing an understanding of the employment of nanomaterials in AOPs used for efficient degradation of organic compounds in wastewater.

2.1 Role of Visible and Ultraviolet Light Influenced Nanomaterials as Photocatalyst

Nanocrystalline TiO_2 is emerging as a photocatalyst for degradation of organic pollutants (Saini et al. 2020). Most of the literature studies have used TiO_2 as a photocatalyst in wastewater treatment, but few of them focus on doped TiO_2 as a nanophotocatalyst for wastewater treatment. Compared to other photocatalysts, TiO_2 has a wide band gap of 3.2_{eV} and acts as a semiconductor in the near ultraviolet range. When ultraviolet light hits the TiO_2 surface, the atoms come into an excited state and generate holes and electron pairs in valence and conduction bands. The hole gets oxidized by absorbing the molecules of surrounding water and forms hydroxyl radical. The formation of hydroxyl radicals is a cyclic process leading to successive reactions on the TiO_2 surface. It has recently been drawn that using visible and sunlight can be much more economical as compared to ultraviolet light. Following the same, Reeves et al. (1992) put forward the utilization of high intensity sunlight for non-biological entities and textile dyes degradation from wastewater. However, only about 5% of the total ultraviolet energy reaches the earth surface which is insufficient for effective photocatalytic degradation of organic pollutants. Most of the dyes and organic pollutants generate toxic intermediates during degradation. These are the basic structures of the parent molecule known as the toxic and carcinogenic components (Kumar and Bansal 2015). Ao et al. (2007) experimented with the decolonization of anthraquinonic acid blue 80 from a thin layer of TiO_2 during photocatalytic oxidation. The results showed that thin layers of TiO_2 synthesized by low-temperature calcination are effective at discoloration in the ultraviolet region. While the Cr ion implanted TiO_2 thin film displayed the shift of light absorption from ultraviolet to visible range. Cr ion-TiO_2 thin film came out as an effective solar photocatalyst in

decolorizing the textile effluent dye. Zhu et al. (2009) studied the degradation of Congo Red on crosslinked chitosan/nano-Cds composite catalysts under the irradiation of visible light. Factors like initial dye concentration, catalyst loading, and pH we studied against the decolorization. Muruganandham and Swaminathan (2006) assessed the performance of TiO_2-P25 (Degussa) photocatalyst for degradation of Reactive Orange 4 under ultraviolet-A irradiated light. Reactive Orange 4 was fully decolorized in 80 min and degraded in 180 min. Yousefi-Mohammadi et al. (2018) used MnCo–Ferrite/TiO_2 composite as a magnetically separable photocatalyst for decolorization of dyes from aqueous solution. The kinetics followed a pseudo-first order model and reusability after five cycles was also observed. Abdellah et al. (2018) used air sparging to enhance the TiO_2/ultraviolet system for photocatalytic decolorization of methyl blue. Complete removal of color was directly proportional to the pH of the solution and inversely proportional to the dye concentration. The air sparging highly contributed to the decolorization when its superficial velocity was increased from 0.42 to 1.96 cm/s. Moreover, increasing superficial velocity also increased the reaction rate. Shehzad et al. (2020) developed $AgFeO_2$/rGO/TiO_2 ternary composite photocatalyst to enhance the decolorization of methylene blue dye under ultraviolet_visible light irradiations. The effect of solution pH, initial dye concentration, and silver ferrite ($AgFeO_2$) loading were intensively investigated. Results showed that by addition of reduced graphene oxide (rGO) and $AgFeO_2$, the properties of TiO_2 were highly improved.

Liu et al. (2012a) prepared a photocatalyst from nanotubes made of polyurethane nanotubes and TiO_2 nanocomposites for photocatalytic decomposition of rhodamine B. The composite acts as a heterogeneous phase catalyst, and hence can be reused further. Liu et al. (2012b) studied Fe/TiO_2 nanocatalysts to remove chloro-phenol from aqueous solution. The prepared nanophotocatalyst showed positive results in terms of de-chlorination and oxidation of 2,4-dichlorophenol under the influence of ultraviolet radiation. Ananda (2014) synthesized a nano Se/ZnO photocatalyst to study the decomposition of indigo carmine dye. The decomposition efficiency of the Se/ZnO photocatalyst was 96%. Zhang et al. (2020) synthesized polypyrrole (PPy) onto TiO_2 nanotube array to study the decolorization of methylene blue through photocatalytic, electrocatalytic, and photo-electrocatalytic degradation. It was observed that PPy acts as an effective sensitizer for TiO_2 nanotube arrays to enhance the decolorization efficiency. The decolorization rate of methylene blue was enhanced under photo-electrocatalytic conditions, compared to the total rate of other two conditions. Karimi-Shamsabadi and Behpour (2021) compared the photocatalytic activities of TiO_2 nanotube supported with Sb_2S_3–TiO_2–SiO_2 and Ag_2S–TiO_2–SiO_2 photocatalysts for photocatalytic degradation of binary mixture of basic blue 41 (BB41) and basic red 46 (BR46) dyes under improved visible light. Comparison showed that Sb_2S_3–TiO_2–SiO_2 TiO_2 nanotube can degrade BB41 and BR46 mixture more efficiently as compared to Ag_2S–TiO_2–SiO_2 TiO_2 nanotube. It was also seen that the ratio of TiO_2, Sb_2S_3, and SiO_2 is an influential parameter for governing the photocatalytic activity of the photocatalysts.

3 Intensification of Wastewater Treatment Processes Based on Nanostructured Materials

Process intensification usually refers to the design and development of new tools and techniques to improve a product's performance over its predecessor. Intensification of operation considerably reduces the overall size of plant, waste generation, and energy consumption. Improvements in present technologies through development of new catalysts or chemical pathways are not subject to process intensification. Process intensification can be divided into two categories: (i) equipment-based and (ii) method-based. Process intensification based on equipment and methods for oxidation of organic pollutants present in wastewater has been deeply researched in the past few years (Bethi et al. 2016). But, very limited research has been done on the effects of process intensification arising from nanostructural materials in wastewater.

Zhang et al. (2013) employed micro-electrolysis hybrid compounds (Fe^0-CNTs) in contaminated water remediation. Fe^0-CNTs showed high efficiency of decomposition of methylene blue. It is enhanced by a moderate reduction in the adsorption band over a long period of time. It indicates the effectiveness in degrading aromatic intermediates. Pinho et al. (2015) tested the removal of phenol from highly concentrated phenol solutions through wet peroxide oxidation using multi-walled carbon nanotubes as a catalyst. The whole setup was carried for $4.5\,gL^{-1}$ phenol concentration, $25\,gL^{-1}$ hydrogen peroxide concentration, $2.5\,gL^{-1}$ catalyst loading, 3.5 pH, and 353 K temperature for 24 h. On employing some carbon nanotubes, a complete phenol and carbon removal was reported. Ribeiro et al. (2017) assessed the intensification of the high-performance magnetic graphite nanocomposite catalyst in the wet catalytic peroxide oxidation of 4-nitrophenol. The Fe_3O_4 nanoparticles were introduced in graphitic structure in the synthesis process of magnetic graphite nanocomposite. In contrast to sole Fe_3O_4, Fe_3O_4/magnetic graphitic nanocomposite greatly enhanced the catalytic activity in catalytic wet peroxide oxidation. The graphitic nanocomposite here provided extra surface area for catalyst and pollutants interaction. The complete withdrawal of 4-Nitrophenol was obtained in 4 h.

Ebrahiminezhad et al. (2018) reported the synthesis of ultra-small zero valent iron nanoparticles from Mediterranean cypress for application of dye removal from aqueous solution. Also in the case of methyl orange, it showed decolorization efficiency of 95% for a 6 h long process. The study also proposed the use of iron nanoclusters as a future method of removing pollutants from the aquatic environment. Karimnezhad et al. (2020) combined Fenton and iron-based immobilized nano-filtration processes for the rejection of amoxicillin. The concentration of hydrogen peroxide, iron-based nanoparticles in membranes and amoxicillin were the main governing factors for removal efficiency. Results also stated that high amoxicillin concentrations can only be effectively removed by polyacrylonitrile/Fenton iron-based catalyst membrane intensification.

Furthermore, to shape up the nanomaterials potential in intensification of oxidation in wastewater, deep analysis has to be done to develop less energy intensive

nanomaterials. Study of clusters of nanoparticles is required to fully uncover the potential of nanoparticles and nanocomposites in process intensification.

4 Mechanism of AOPs

The mechanism of advanced oxidation processes generates highly oxidative and highly reactive hydroxyl radicals when treated with wastewater. Hydroxyl radicals take electrons of surrounding electron rich compounds and hence completely degrade the organic pollutants. Hydroxyl radicals have also shown higher oxidative potential of 2.33 V, making them more preferable than chemical oxidants like H_2O_2 and $KMnO_4$.

4.1 Photochemical Methods

Non-photochemical processes sometimes produce toxic intermediates as compared to initial compounds. Consequently, the complete decomposition of organic pollutants can be achieved by combining ultraviolet radiation and non-photochemical AOP (Vilhunen and Sillanpää 2010). Most UV lamps display energies in the 200–300 nm range. As a result of direct photolysis, the excited molecules absorb ultraviolet energy, creating hydroxyl radicals. Reactions (1)–(7) describes the main routes and role of hydrated electrons and hydrogen radicals in the formation of oxidation products.

$$e^- + O_2 \rightarrow \cdot O_2^- \tag{1}$$

$$h^+ + A^- \rightarrow \cdot A \tag{2}$$

$$h^+ + OH^- \rightarrow \cdot OH \tag{3}$$

$$\cdot OH + RH \rightarrow \cdot RHOH \tag{4}$$

4.1.1 Photo-Fenton System

In this, Fe^{3+} ions and H_2O_2 are disclosed to ultraviolet irradiation. Upon contact, H_2O_2 decomposes beneath photocatalytic activity of Fe^{3+} ions and leads to $\cdot OH$ and Fe^{2+} ions initiation. At pH 3, $Fe(OH)^{2+}$ (Reaction 5) complex was observed (Bethi et al. 2016).

$$Fe^{3+} + H_2O \rightarrow Fe(OH)^{2+} + H^+ \tag{5}$$

$$Fe(OH)^{2+} \leftrightarrow Fe^{3+} + OH^- \tag{6}$$

$$Fe(OH)^{2+}hv \rightarrow Fe^{2+} + (\cdot OH) \tag{7}$$
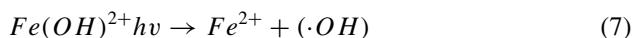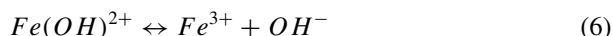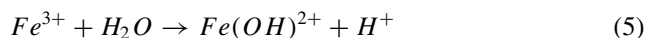
The foremost advantage of this process is that it decomposes both organic and inorganic pollutants (Martins and Quinta-Ferreira 2011). Among various AOPs, Fenton's reaction is considered most effective for removal rate and operating expenses in toxic/refractory industrial wastewater treatment, coffee effluent, distillery wastewater, and etc. (Krzemińska et al. 2015).

4.1.2 O_3/H_2O_2/Ultraviolet System

Among O_3 and UV AOPs, the fusion of O_3, H_2O_2, and UV (O_3/H_2O_2/UV) presents an attractive option for direct and indirect degradation of wide variety of contaminants (Kusic et al. 2006; Wu et al. 2008). However, the research on the potential complicated process is still lacking. The addition of H_2O_2 can improve the decomposition rate of the O_3/ultraviolet process. Improved decomposition rates will directly accelerate the rate of generation of hydroxyl radicals. Also, the use of H_2O_2 can be cost effective for some AOPs, especially when organic pollutants have low energy of absorption when irradiated with ultraviolet light (Lester et al. 2011).

4.1.3 Ultraviolet/TiO_2 Photocatalytic System

In ultraviolet or visible light irradiation, suitable semiconductor compounds may excite photons and generate a pair of electrons in the conduction band and holes in the valence band. In this way, the generated charge carriers initiate the reduction and oxidation reactions (Krzemińska et al. 2015). The factors influencing TiO_2/UV photocatalytic process are initial organic load, pH value, the catalyst concentration, reaction temperature, intensity of light, and ionic species (Krzemińska et al. 2015; Stasinakis 2008). Various studies have proven photocatalytic as an effective treatment process for winery-based and distillery wastewater (Chatzisymeon et al. 2008), and olive-mile wastewater (Rajesh Banu et al. 2008).

4.2 Non-photochemical Methods

This type of AOPs can generate ·OH without utilizing light energy. The mechanism followed to produce hydroxyl radical in non-photochemical AOPs is as follows:

4.2.1 Ozonation

Compared to pure oxygen and air, O_3 is a strong oxidizing agent used in the oxidation of chemicals. It is capable of producing oxidative radicals in contaminated water and degrades the pollutants by attacking ·OH radicals (Gottschalk et al. 2009). Direct ozone oxidation acts as a selective path with reaction rates ranging from 1×10^0 to 10^3 M^{-1} s^{-1}. This leads to the reaction of O_3 with ionized and dissociated organic compounds in spite of neutral ones. Under such conditions, ·OH gets generated from O_3 and initiates the indirect mechanism. Reaction (8) represents the overall reaction for generation of ·OH, involving ozone as an oxidative agent (Deng and Zhao 2015). If other oxidants or irradiations are present, ·OH yields can be highly enhanced.

$$3O_3 + OH^- + H^+ \rightarrow 2(\cdot OH) + 4O_2 \tag{8}$$
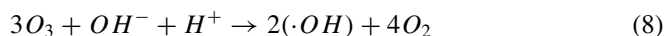
4.2.2 O_3/H_2O_2 Ozonation

Wet peroxide ozonation refers to the fast decomposition of ozone by addition of H_2O_2 to O_3 (Katsoyiannis et al. 2011). This further leads to faster formation of ·OH radical (as shown in Reaction (9)).

$$2O_3 + H_2O_2 \rightarrow 2(\cdot OH) + 3O_2 \tag{9}$$
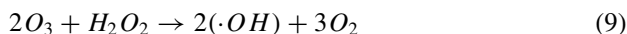
The AOPs with O_3/H_2O_2 enhances the kinetics for ozone decay and speed ups the transformation to ·OH. However, in case of compounds which are less reactive towards ozonation (e.g. p-chlorobenzonic acid), it fails to improve the transformation of micro-pollutants (Acero and Gunten 2001). As tested by Katsoyiannis et al. (2011), the involvement of H_2O_2 significantly reduces the bromate formation in p-chlorobenzonic acid transformation.

4.2.3 H_2O_2/Fe^{2+} System

Catalyzation of H_2O_2 with ferrous sulfate (i.e. Fenton's reagent) is one among the most common processes for advanced oxidation (Fenton 1894). Fenton's reagent is referred to as a catalytic initiation/production of ·OH. This hydroxyl radical results from the chain reaction of Fe^{2+} and H_2O_2. Reaction (10) shows the mechanism for the Fenton/H_2O_2 oxidation process. The interaction of excessive H_2O_2 leads to the oxidation of Fe(II) to Fe(III). As shown in Reactions (11)–(13), hydroxyl radicals are generated through decomposition of H_2O_2 by Fe(III) (Zhang et al. 2005; Neyens and Baeyens 2003).

$$Fe^{2+} + H_2O_2 \rightarrow Fe^{3+} + OH^- + (\cdot OH) \tag{10}$$

$$Fe^{3+} + H_2O_2 \rightarrow H^+ + Fe\text{—}OOH^{2+} \tag{11}$$

$$Fe\text{—}OOH^{2+} \rightarrow HO_2 + Fe^{2+} \tag{12}$$

$$Fe^{2+} + H_2O_2 \rightarrow Fe^{3+} + OH^- + (\cdot OH) \tag{13}$$
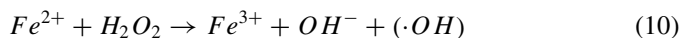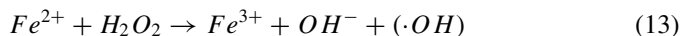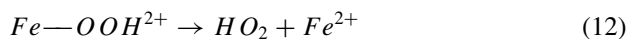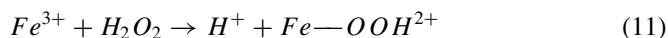
Many studies have been carried out to study Fenton as a catalyst in oxidation of pollutants in wastewater. Several other oxidants have also been employed with Fenton for effective oxidation of pollutants.

4.2.4 Catalytic Ozonation

Apart from the processes like O_3/UV and O_3/H_2O_2, catalytic ozonation is another major widely studied technique to deal with the problem of mineralization of pollutants in wastewater. For degradation of organic pollutants, homogeneous and heterogeneous phase catalysts are employed for improving ozonation reactions. ZnO, Fe_2O_3, MnO_2, TiO_2, Al_2O_3, and TiO_2 are few metal oxides tested for catalytic ozonation. The catalysts when added to ozonation reaction, eases the decomposition of O_3 and forms highly active free radicals. This further leads to efficient mineralization and rapid degradation of the organic pollutants. Moreover, the catalysts also improved the efficiency of O_3 utilization up to some extent (Chen and Wang 2019; Wang and Wang 2019; Ratan and Saini 2019).

5   Conclusion

Catalytic processes like photo-catalysis, Fenton process, catalytic ozonation, photo-electrocatalysts, and anodic oxidation are means to produce free radicals. However, still many disagreements have been noted in the degradation mechanism of pollutants and contaminants. Furthermore, the procedures for catalytic ozonation have proved to be complicated and not fully recognized. The processes reported here have been successfully employed for the removal of harmful contaminants from wastewater. The research of AOPs combined with nanotechnology represents great future opportunities in the field of wastewater purification. The combined techniques of AOPs with nanomaterials are the advanced methods to eliminate pollutants from wastewater or convert them to degradable compounds. To implement AOPs on pilot and commercial scales, techniques like ultrasonic and hydrodynamic cavitation have potential prospects. Nanomaterials/AOPs may become industrialized only after optimization of every effectiveness factor and combination of different hybrid systems together to overcome the potential drawbacks linked with individual processes. For this, more research is required to develop a catalytic material that can be handled

in visible spectra or is solar based. Moreover, the quantity of ·OH generated is an important factor for efficient assessment and accurate comparison of different AOP technologies. It is important to perform the qualitative and quantitative analysis on ·OH to fully explore the degradation mechanisms.

References

Abdellah MH, Nosier SA, El-Shazly AH, Mubarak AA (2018) Photocatalytic decolorization of methylene blue using TiO_2/UV system enhanced by air sparging. Alex Eng J 57(4):3727–3735

Acero J, Von Gunten U (2001) Characterization of Oxidation processes: ozonation and the AOP O_3/H_2O_2. J Am Water Works Assoc 93(10):90–100

Ananda S (2014) Synthesis and characterization of se-doped ZnO nanoparticles by electrochemical method: photodegradation kinetics of indigo carmine dye and study of antimicrobial, antimitotic activities of se-doped ZNO nanoparticles. Chem Sci Int J 4(5):616–637

Ao CH, Leung MKH, Lam RC, Leung DY, Vrijmoed LL, Yam WC, Ng SP (2007) Photocatalytic decolorization of anthraquinonic dye by TiO_2 thin film under UVA and visible-light irradiation. Chem Eng J 129(1–3):153–159

Bashambu L, Singh R, Verma J (2021) Metal/metal oxide nanocomposite membranes for water purification. Mater Today Proc 44:538–545

Bethi B, Sonawane SH, Bhanvase BA, Gumfekar SP (2016) Nanomaterials-based advanced oxidation processes for wastewater treatment: a review. Chem Eng Process Process Intensif 109:178–189

Cardoso I, Cardoso R, da Silva J (2021) Advanced oxidation processes coupled with nanomaterials for water treatment. Nanomaterials 11(8):2045

Chatzisymeon E, Stypas E, Bousios S, Xekoukoulotakis N, Mantzavinos D (2008) Photocatalytic treatment of black table olive processing wastewater. J Hazard Mater 154(1–3):1090–1097

Chen H, Wang J (2019) Catalytic ozonation of sulfamethoxazole over Fe_3O_4/Co_3O_4 composites. Chemosphere 234:14–24

Deng Y, Zhao R (2015) Advanced oxidation processes (AOPs) in wastewater treatment. Curr Pollut Rep 1(3):167–176

Ebrahiminezhad A, Taghizadeh S, Ghasemi Y, Berenjian A (2018) Green synthesized nanoclusters of ultra-small zero valent iron nanoparticles as a novel dye removing material. Sci Total Environ 621:1527–1532

Ede J, Lobaskin V, Vogel U, Lynch I, Halappanavar S, Doak S et al (2020) Translating scientific advances in the AOP framework to decision making for nanomaterials. Nanomaterials 10(6):1229

Fenton H (1894) LXXIII.—Oxidation of tartaric acid in presence of iron. J Chem Soc Trans 65:899–910

Gottschalk C, Libra JA, Saupe A (2009) Ozonation of water and waste water: a practical guide to understanding ozone and its applications. Wiley

Karimi-Shamsabadi M, Behpour M (2021) Comparing photocatalytic activity consisting of Sb_2S_3 and Ag_2S on the TiO_2–SiO_2/TiO_2 nanotube arrays-support for improved visible-light-induced photocatalytic degradation of a binary mixture of basic blue 41 and basic red 46 dyes. Int J Hydrogen Energy 46(53):26989–27013

Karimnezhad H, Navarchian AH, Gheinani TT, Zinadini S (2020) Amoxicillin removal by Fe-based nanoparticles immobilized on polyacrylonitrile membrane: effects of input parameters and optimization by response surface methodology. Chem Eng Process Process Intensif 147:107785

Katsoyiannis IA, Canonica S, von Gunten U (2011) Efficiency and energy requirements for the transformation of organic micropollutants by ozone, O_3/H_2O_2 and UV/H_2O_2. Water Res 45(13):3811–3822

Krzemińska D, Neczaj E, Borowski G (2015) Advanced oxidation processes for food industrial wastewater decontamination. J Ecol Eng 16(2):61–71

Kumar J, Bansal A (2015) CFD simulations of immobilized-titanium dioxide based annular photo-catalytic reactor: model development and experimental validation. Indian J Chem Technol 22:95–104

Kusic H, Koprivanac N, Bozic A (2006) Minimization of organic pollutant content in aqueous solution by means of AOPs: UV- and ozone-based technologies. Chem Eng J 123(3):127–137

Lester Y, Avisar D, Gozlan I, Mamane H (2011) Removal of pharmaceuticals using combination of UV/H_2O_2/O_3 advanced oxidation process. Water Sci Technol 64(11):2230–2238

Liu P, Liu H, Liu G, Yao K, Lv W (2012a) Preparation of TiO_2 nanotubes coated on polyurethane and study of their photocatalytic activity. Appl Surf Sci 258(24):9593–9598

Liu L, Chen F, Yang F, Chen Y, Crittenden J (2012b) Photocatalytic degradation of 2, 4-dichlorophenol using nanoscale Fe/TiO_2. Chem Eng J 181:189–195

Martins R, Quinta-Ferreira R (2011) Remediation of phenolic wastewaters by advanced oxidation processes (AOPs) at ambient conditions: comparative studies. Chem Eng Sci 66(14):3243–3250

Matafonova G, Batoev V (2018) Recent advances in application of UV light-emitting diodes for degrading organic pollutants in water through advanced oxidation processes: a review. Water Res 132:177–189

Muruganandham M, Swaminathan M (2006) Photocatalytic decolourisation and degradation of Reactive Orange 4 by TiO_2-UV process. Dyes Pigm 68(2–3):133–142

Nasrollahzadeh M, Sajjadi M, Iravani S, Varma R (2021) Green-synthesized nanocatalysts and nanomaterials for water treatment: current challenges and future perspectives. J Hazard Mater 401:123401

Neyens E, Baeyens J (2003) A review of classic Fenton's peroxidation as an advanced oxidation technique. J Hazard Mater 98(1–3):33–50

Obotey Ezugbe E, Rathilal S (2020) Membrane technologies in wastewater treatment: a review. Membranes 10(5):89

Pinho MT, Gomes HT, Ribeiro RS, Faria JL, Silva AM (2015) Carbon nanotubes as catalysts for catalytic wet peroxide oxidation of highly concentrated phenol solutions: towards process intensification. Appl Catal B 165:706–714

Rajesh Banu J, Anandan S, Kaliappan S, Yeom I (2008) Treatment of dairy wastewater using anaerobic and solar photocatalytic methods. Sol Energy 82(9):812–819

Rao N, Singh R, Bashambu L (2021) Carbon-based nanomaterials: synthesis and prospective applications. Mater Today Proc 44:608–614

Ratan J, Saini A (2019) Enhancement of photocatalytic activity of self-cleaning cement. Mater Lett 244:178–181

Reeves P, Ohlhausen R, Sloan D, Pamplin K, Scoggins T, Clark C, Hutchinson B, Green D (1992) Photocatalytic destruction of organic dyes in aqueous TiO_2 suspensions using concentrated simulated and natural solar energy. Sol Energy 48(6):413–420

Ribeiro RS, Rodrigues RO, Silva AM, Tavares PB, Carvalho AM, Figueiredo JL, Faria JL, Gomes HT (2017) Hybrid magnetic graphitic nanocomposites towards catalytic wet peroxide oxidation of the liquid effluent from a mechanical biological treatment plant for municipal solid waste. Appl Catal B 219:645–657

Saini A, Arora I, Ratan J (2020) Photo-induced hydrophilicity of microsized-TiO_2 based self-cleaning cement. Mater Lett 260:126888

Shehzad N, Zafar M, Ashfaq M, Razzaq A, Akhter P, Ahmad N, Hafeez A, Azam K, Hussain M, Kim WY (2020) Development of AgFeO$_2$/rGO/TiO_2 ternary composite photocatalysts for enhanced photocatalytic dye decolorization. Curr Comput-Aided Drug Des 10(10):923

Singh R (2021) Municipal solid waste management in the City of Indore—a case study. J Civ Eng Environ Sci 7(1):008–017

Singh R, Singh M, Kumari N, Maharana S, Maharana P (2021) A comprehensive review of polymeric wastewater purification membranes. J Compos Sci 5(6):162

Stasinakis AS (2008) Use of selected advanced oxidation processes (AOPs) for wastewater treatment—a mini review. Global NEST J 10(3):376–385

Vilhunen S, Sillanpää M (2010) Recent developments in photochemical and chemical AOPs in water treatment: a mini-review. Rev Environ Sci Biotechnol 9(4):323–330

Wang S, Wang J (2019) Activation of peroxymonosulfate by sludge-derived biochar for the degradation of triclosan in water and wastewater. Chem Eng J 356:350–358

Wang J, Xu L (2012) Advanced oxidation processes for wastewater treatment: formation of hydroxyl radical and application. Crit Rev Environ Sci Technol 42(3):251–325

Wu J, Yang J, Muruganandham M, Wu C (2008) The oxidation study of 2-propanol using ozone-based advanced oxidation processes. Sep Purif Technol 62(1):39–46

Yousefi-Mohammadi S, Movahedi M, Salavati H (2018) MnCo–ferrite/TiO_2 composite as an efficient magnetically separable photocatalyst for decolorization of dye pollutants in aqueous solution. Surf Interfaces 11:91–97

Zhang H, Choi HJ, Huang CP (2005) Optimization of Fenton process for the treatment of landfill leachate. J Hazard Mater 125(1–3):166–174

Zhang S, Wang D, Zhou L, Zhang X, Fan P, Quan X (2013) Intensified internal electrolysis for degradation of methylene blue as model compound induced by a novel hybrid material: multi-walled carbon nanotubes immobilized on zero-valent iron plates (Fe^0-CNTs). Chem Eng J 217:99–107

Zhang J, Pang Z, Sun Q, Chen X, Zhu Y, Li M, Wang J, Qiu H, Li X, Li Y, Chronakis IS (2020) TiO_2 nanotube array modified with polypyrrole for efficient photoelectrocatalytic decolorization of methylene blue. J Alloys Compd 820:153128

Zhu H, Jiang R, Xiao L, Chang Y, Guan Y, Li X, Zeng G (2009) Photocatalytic decolorization and degradation of Congo Red on innovative crosslinked chitosan/nano-CdS composite catalyst under visible light irradiation. J Hazard Mater 169(1–3):933–940

Coal Gasification in a Circulating Fluidized Bed

Vikrant Sharma and **Ravikant R. Gupta**

Abstract The major concern of today's world is Energy security and environmental protection due to rapidly depleting non-renewable energy sources and increasing greenhouse gases and other pollutants from energy production. A need to focus on efficient and eco-friendly coal utilization technologies is of vital importance as coal is the most abundant and polluting fuel. Coal gasification has been emerging as the most important coal utilization technology. Gasifiers are broadly classified into fluidized, fixed, and entrained bed gasifiers. Fluidized bed gasifiers, especially circulating fluidized bed gasifiers (CFBG), has major advantages over other gasifiers, such as, fuel-flexibility, high heat and mass transfer rates, high efficiency, lower emissions etc. Therefore, this chapter is devoted to impart fundamental understanding of the CFBG. It includes fundamentals of CFBG including hydrodynamics, heat transfer, mass transfer and chemical reactions. Further, various modeling and simulation techniques for CFBG and effect of process parameters, namely, temperature, pressure, air/coal ratio and steam/coal ratiohas been covered.

Keywords Coal gasification · Fluidized bed gasifiers

1 Introduction

Energy is at the core of economic growth and human development. The demand for energy is increasing rapidly with increase in population and industrialization. Currently, approximately 80% of the energy is produced through non-renewable fossil fuels, i.e., coal, crude oil and natural gas, which will not be able to sustain current production rate for more than a few decades (BP 2021). Although renewable sources of energy are growing, their current share in global energy very small and

V. Sharma
Department of Chemical Engineering, Indian Institute of Technology (IIT) Roorkee, Roorkee 247667, Uttarakhand, India

R. R. Gupta (✉)
Department of Chemical Engineering, Banasthali Vidyapith, Tonk 304022, Rajasthan, India
e-mail: ravikantg@banasthali.in

their growth will not be adequate to fulfill energy requirements. Consequently, fossil fuels will continue to play a prominent role over the next few decades. However, utilization of fossil fuels changes the composition of the atmosphere through emissions of greenhouse gases (CO_2 and CH_4), acid gases (SO_x and NO_x), toxic gases (CO) and heavy metals (As, Hg) as well as particulate matter (PM). The increased concentration of greenhouse gases leads to global warming and in turn, rise in sea level, climate change etc. Further, acid gases cause acid rain and rest of the pollutants lead to numerous health problems. Therefore, twin goals of energy security and environmental protection are of vital importance for the world.

Coal is the most abundant fuel and largest source of energy for electricity production. Further, it is relatively inexpensive, widely and equitably distributed, readily available, easy to store and transport and has greater price stability. However, coal and power sectors are also the biggest contributors to anthropogenic greenhouse gas emissions. Global electricity demand is expected to double by 2050 (IEA 2016). Therefore, reduction in emissions to meet climate objectives must start from coal and power sectors. Consequently, clean, efficient, cost-effective and sustainable coal technologies are the need of the hour.

Coal-fired combustion-based power plants can be divided into four type of generation technologies, i.e., are sub-critical, super-critical (SC), ultra-super-critical (USC) and advanced-ultra-super-critical (AUSC). About 75% of the coal-fired power plants use the least-efficient and the cheapest sub-critical technology. The demand of integrated gasification combined cycle (IGCC) is increasing in the market due to higher efficiency (45–50%), lower emissions, fuel-flexibility and poly-generation (IEA 2012; Simpson 2006; Prabhanshu et al. 2016). However, IGCC plants require higher capital and operating costs than subcritical power plants but if carbon capture, utilization and storage (CCUS) is included in the power plant, IGCC plants are the most efficient and have the lowest cost. A gasifier is at the heart of an IGCC plant which converts any carbonaceous solid fuel (e.g. coal, biomass, municipal solid waste, petroleum coke or heavy oil), in sub-stoichiometric environment of air mixed with steam, into synthesis gas (syngas), containing mainly CO, H_2, CH_4, CO_2, H_2O, NH_3, H_2S and N_2 etc. (Basu 2006). The syngas, after thorough cleaning, can be utilized for electricity generation (via IGCC and/or fuel cells) and/or production of various chemicals including gaseous and liquid fuels (via Fischer–Tropsch synthesis).

Commercial gasification has a long history and several gasifiers are commercially available or under development. The gasifiers can be broadly classified, according to the mode of contacting, into fixed/moving, fluidized and entrained bed. Further, they are also classified based on ash discharge (dryor slag), pressure (atmospheric or pressurized) and feed (dry or slurry) (Basu 2006). The basic characteristics of fixed, fluidized and entrained bed gasifiers has been presented in Table 1. The fluidized bed gasifiers offer advantages such as intense mixing, excellent heat and mass transfer, uniform flow and temperature distribution, moderate oxygen and steam demand, high fuel-flexibility, ow fuel preprocessing, low emissions, compact equipment, high efficiency, high degree of controllability, high turn down ratio, in-situ sulfur capture, high throughput and high capacities. However, lower carbon conversion (< 97%), due to low temperature as well as high degree of solid attrition, back-mixing and

Table 1 Basic characteristics of various gasifiers

Gasifiers	Basic characteristics							
	Diameter of particles (mm)	Operating temperature (°C)	Capacity	Oxygen requirement	Steam requirement	Tar content	Fuel-flexibility	Cold gas efficiency (%)
Fixed/moving bed	6–50	500–800	Small	Low	High	High	Low	80–85
Fluidized bed	0.5–6	800–1000	Medium to high	Medium	Medium	Medium	High	85–90
Entrained bed	< 0.5	1200–1500	High	High	Low	Low	High for coal but unsuitable for biomass	80–85

entrainment is a notable disadvantage. The fluidized bed gasifiers can be of two types: Bubbling Fluidized Bed gasifier (BFBG) and Circulating Fluidized Bed Gasifier (CFBG). The CFBG increases the carbon conversion and efficiency by capturing the entrained particles in the cyclone are feeding them back to the gasifier (external circulation). Further, enhanced mixing owing to higher gas and particle velocities and internal circulation leads to higher heat and mass transfer rates, uniformity of temperature, throughput and capacities. Furthermore, CFBG can process a wider range of feedstock and its size and shape without any major modification to the equipment. Therefore, CFBG provide excellent option for a large-scale coal gasification projects in the future (Prabhanshu et al. 2016; Basu 2006).

2   Fundamentals of CFBG

2.1   Hydrodynamics

Fritz Winkler (Germany 1921) produced gaseous products by combustion of coke particles in the crucible and observed the particles lifting by the drag force applied by the gas. Thus, a new process, called Fluidization, was defined wherein solids particles are in a suspended state due to contact with a liquid or gas. A schematic diagram of a CFBG is shown in Fig. 1. A carbonaceous solid fuel is fed into the lower section of fluidized bed gasifier, and fluidized by the gasifying mediums (oxygen, air and/or steam) delivered from the bottom to promote gas–solid reactions. The increase in gas velocity through the solid particles the fixed bed successively comes to fluidized which successively goes through fixed, incipient, bubbling, turbulent, fast and pneumatic fluidization regime.

A typical CFBG consists of a riser, a standpipe, a cyclone, and a loop-seal or non-mechanical valve. The behavior of a CFBG depends on the superficial gas velocity, solids holdup and the solids circulating rate. Axial variation of the solid volume fraction is "S-shaped" due to the effect of solids from the return-pipe (Sharma and Agarwal 2019a). Two different radial regions can be distinguished, the core region, characterized by a dilute gas–solid suspension flowing upwards and the slip velocity close to terminal velocity, and the annular region where a dense film of particles moves downwards on the wall. The flow of particles at the bottom of the riser is chaotic due to back-mixing of solids from the wall. However, the chaotic movement decreases along the length of the riser. Therefore, the radial distribution of solid volume fraction becomes flatter with increasing riser height as well as with decreasing circulation rates. The gas and solid velocities are higher than superficial velocity in the core of the bed and it is considerably lower (even negative) near the wall. Moreover, the average velocity of solid particles traveling upward is higher than those going in the downward direction, making the center leaner in particles. Large fluctuations in axial velocities at the inlet and outlet are observed due to the chaotic motion of solid particles in these regions. More uniform profiles and lesser fluctuations are observed
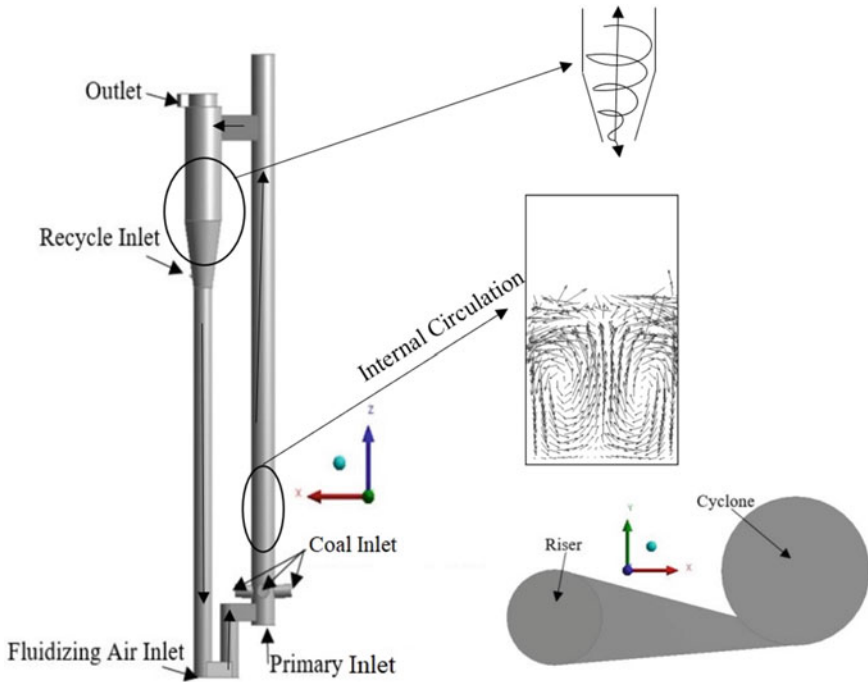
Fig. 1 Schematic of a circulating fluidized bed gasifier

in the mid region of the riser, and distance away from the inlet and exit. The clusters or solid particles move with the high upward gas flow in the core region and fall back near the wall where gas velocity is very small or negative, thus, creating an internal circulation. Internal circulations are composed of many toroidal paths which can split into several smaller to roids with an increase in the superficial velocity. The internal circulation rate (10^2–10^3 kg m^{-2} s^{-1}) is higher for small particles and is many times higher than the external circulation rate. The temperature uniformity and high heat and mass transfer rates in the CFBG is a direct effect of this internal solid circulation.

At the exit of the riser, towards the horizontal connector between riser and cyclone, the vertical movement of gases and solids changes to horizontal. The gas–solid suspension flows into the cyclone tangentially and then spirally flow downward along the cyclone surface under the influence of centrifugal force and gravity. Due to the particle–particle and particle–wall friction and collisions, the particles are decelerated moving downward. The gas flow has a strong rotation in the center of cyclone to join central upward flow towards the exit of the cyclone due to the pressure difference (Luo et al. 2015). The solid phase continues its downward spiral movement under gravity. As the drag force on the particles is mainly not in the vertical direction, entrainment of particles is limited and the solid volume fraction is small. In contrast, in the return-pipe, particles move in a nearly packed bed dominated by

gravity whereas the motion of solid phase in the valve or loop-seal can be assumed to be similar to a typical plug flow or a bubbling bed. Such a packed bed condition in the return-pipe and loop-seal ensures that gas from the riser should not leak to the recycle system. The drag, buoyancy, virtual mass, Basset, Magnus and Staffman lift forces are applied to the particles by the gas. The drag force is the largest and most significant force acting on the particles and is related to the kinetic energy of the fluid and the projected area of the particle (Smoot and Pratt 1979).

The maximum pressure occurs at the distributor because of the introduction of the gasifying agents into dense solid bed. Thereafter, pressure decreases monotonically with increasing height of the gasifier due to transfer energy from gas phase to particles and it is increases when gases are separated from solids in the cyclone and solids flow towards the return-pipe. The higher the particle loading or suspension density, the stronger the pressure gradient. The solids distribute themselves between the riser and return leg so that the pressure drops across the two balance each other. The pressure drop in the riser varies in the range of 200–5000 Pa (Gräbner et al. 2007; Sharma and Agarwal 2020).

2.2 Heat Transfer

As cold coal particles are introduced at the coal inlet, heat transfer plays a crucial role in absorption and dissemination of heat of reactions within and between the phases by circulating hot solids around the loop. The particle temperature increases due to heat evolved during exothermic combustion reactions and decreases with consumption of heat by endothermic gasification reactions. Thereafter, intra- and inter-phase heat transfer occurs through conduction, convection and radiation. Conduction is mode of heat transport within the gas or solid phase. The Biot number (Bi) is a measure of temperature gradient inside a particle and Bi < 1 denotes that the internal heat conduction is much faster than the external heat transfer. The temperature gradient within the particle is usually neglected as Bi < 0.1 for a typical particle in a fluidized bed. As the thermal conductivity of gas is very small, heat conduction deemed to be unimportant. Further, it was observed that the temperature gradient inside the particle is very small and particle–particle conduction is also small owing to small contact area (Wahyudi et al. 2018; Nikrityuk and Meyer 2014; Basu 2006). However, solid clusters moving towards the wall experience unsteady-state heat conduction to and from the wall. Thus, making the gas thermal conductivity and the thickness of the gas layer the most important parameters for bed-to-wall heat transfer. However, due to small thickness of gas layer, the convective heat transfer from gas to wall is very small.

Radiative heat transfer occurs by absorption and emission from the particle. The gas phase is generally transparent, except in the dilute core region, concerning radiative heat transfer. Furthermore, radiative heat transfer is relevant only at elevated temperatures (>1000 °C). Particle radiation effects are the highest close to the coal inlet due to high solid concentration (Gräbner et al. 2007). It is mathematically

complex to include radiation as it depends on the properties of the emitting body as well as on the receiving body and the characteristics of the gas layer between them.

Therefore, convective heat transfer is considered to be the dominant inter-phase heat transfer mechanism in a CFBG due to small particles and high circulation rate of particles. The convective heat transfer rate to the particles is quantified by the heat transfer coefficient or Nusselt number which is primarily a function of Mach number and Reynolds number based on the relative velocity. The time-averaged suspension density is considered to have the most significant influence on the heat transfer coefficient and the heat-transfer coefficient increases with suspension density (Gräbner et al. 2007). The heat-transfer coefficient on the wall decreases along the height of the riser similar to suspension density. The overall heat transfer coefficient increases with bed temperature ($\propto T^{1.5}$) due to reduction of the thermal resistance caused by the increase in thermal conductivity. Gunn's correlation (Gunn 1978) is most widely used to calculate heat transfer coefficient and is applicable for a porosity range of 0.35–1.0 and Reynolds number of up to 10^5 (Yu et al. 2018). The highest temperatures are observed at the bottom of the riser where the highest intensity of combustion reactions is located. Thereafter, most of the reactor has a homogeneous temperature due to high heat transfer rates caused by excellent mixing affected by extensive internal circulation of particles. However, the temperature decreases slightly with increasing riser height because of the heat loss to the environment and the endothermic gasification reactions.

2.3 Mass Transfer

Mass transfers is an important for rates of production and consumption of chemical species in the gasifier. Although it influences both homogeneous and heterogeneous reactions, the mass transfer resistances are much more pronounced for heterogeneous reactions. The heterogeneous chemical reactions between porous coal and gaseous species can be described by seven consecutive steps as follows:

1. *External Mass Transfer*: Transport of reactants from the bulk fluid to the particle surface through the boundary layer.
2. *Internal Mass Transfer*: Transport of reactants from the surface of particles to the pores.
3. *Adsorption*: Adsorption of reactants on active sites.
4. *Surface Reaction*: Surface reaction between adsorbed molecules and/or atoms with each other or with the active sites.
5. *Desorption*: Desorption of products from active sites.
6. *Internal Mass Transfer (Back-Diffusion)*: Transport of the products from the pores to the particle surface.
7. *External Mass Transfer (Back-Diffusion)*: Transport of products from the surface to the bulk gas stream.

The rate-controlling step is usually judged based on temperature. Other important factors are particle shape and size, particle and gas velocity, pressure and coal reactivity. At high temperature mass transfer is believed to control the process as the reaction rate has a stronger temperature dependency than diffusion. In contrast, chemical reaction is rate controlling step at lower temperature. For intermediate temperatures (transitional regime), rates of both chemical reaction and mass transfer are comparable. For the char combustion reaction (highest reaction rate), the limiting temperature for kinetic-controlled region is estimated to be above 600 °C. For fine (< 1 mm) porous particles, where the mass-transfer rates are high due to small diffusion resistance, this limiting temperature (~ 1500 °C) would be even higher (Basu 2006). For all other reactions (considerably slower reaction rate), the limiting temperature for kinetic-controlled region would be significantly higher (1200–1300 °C) than that for combustion reaction. Therefore, in a CFBG (< 100 μm particles, < 1000 °C temperature and high Re), surface reaction should be the rate-controlling step (Nikrityuk and Meyer 2014; Basu 2006; Smoot and Pratt 1979).

2.4   Chemical Reactions

In coal gasification, the organic component of the coal is completely converted to gas and ash when it is subjected to the gasifying agent at a temperature above 700 °C (Berkowitz 1979). However, coal has an infinite number of possible structures and consequently, its chemistry is very complex. The knowledge of the chemistry of gasification is far from complete and reliable kinetic information on coal or char gasification reactions is still lacking as it depends on coal characteristics, operating parameters and catalytic effects of ash constituents. Gasification of coal involves thousands of elementary reactions occurring in series and/or in parallel. However, determining all these reactions and their kinetics as well as incorporating these into a predictive model and getting the results of this model in a practically reasonable time would be a nightmare. Therefore, for simplicity and faster computation, the chemistry is usually modeled using semi-global rate expressions i.e. considering the reaction as single step elementary reaction composite of many reaction steps. The rate constant is generally provided in modified Arrhenius form, due to the universal and easy application in numerical modeling, as:

$$K = AT^n exp\left(-\frac{E}{RT}\right) \tag{1}$$

Ideally, the kinetic parameters i.e. pre-exponential factor or frequency factor (A), temperature-exponent (n) and activation energy (E) should be determined empirically using the pressure and char temperature conditions prevailing in the desired reaction system. A particle of the solid fuel injected into a CFBG is considered to undergo few important elementary reactions, namely, drying, devolatilization, combustion and gasification reactions.

Drying: As the coal particles are dropped into the bed of hot solids, they are immediately heated up and drying occurs where the moisture contained in the coal leaves in the form of steam depending on the operating pressure (Kraft et al. 2017; Liu et al. 2016). Drying can be represented as:

$$\text{Wet Coal} \rightarrow \text{Dry Coal} + H_2O(g) \tag{1}$$

$$H_2O(l) \leftrightarrow H_2O(g) \qquad \Delta H = 2260 \, \text{kJ/kg} \tag{2}$$
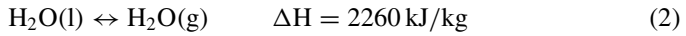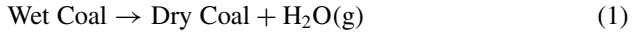
Although drying is a phase transition process, it is generally modeled as a chemical reaction based on the assumption that the simultaneous heat and mass transfer within the particle are infinitely fast. The kinetic parameters for drying can be given as: A = 1.1×10^5 s^{-1}, n = 0 and E = 88.7 kJ/mol (Hassan 2013).

Devolatilization: In devolatilization (called pyrolysis in inert atmosphere), coal is thermally decomposed (above 300 °C), by a sequence of reactions, to form three pseudo compounds i.e. light gases (CO, H_2, CH_4, CO_2, H_2O, NH_3, H_2S etc.), tar (a complex mixture of larger molecules) and char. The particle left after the devolatilization, where most of the non-carbon elements (only < 20% of C but almost all of H, O, N and S) are removed, is a porous solid containing char and ash (Nikrityuk and Meyer 2014). The char can be thought of as a highly disordered graphite (poly crystalline graphite, almost pure carbon above 1600 K), therefore, it is generally considered as graphite. The devolatilization can be represented as:

$$\text{Dry Coal} \rightarrow \text{Char/Ash} + \text{Volatiles} \rightarrow a\text{H}_2 + b\text{CH}_4 + c\text{CO}$$
$$+ d\text{CO}_2 + e\text{H}_2\text{O} + f\text{NH}_3 + g\text{H}_2\text{S} + h\text{Tar} \tag{3}$$
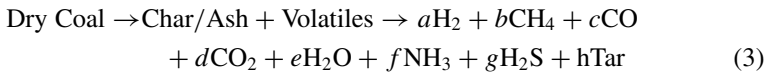
The devolatilization reaction is very fast and generally endothermic having small heat of devolatilization (500 to −3500 kJ/kg; exothermic or endothermic based on the rank of coal) (Kraft et al. 2017). The mechanism of devolatiliazation is essentially free radical mechanism and all the primary reactions are heterogeneous. As temperature increases, the small amount of gases (HO, CO, HS etc.) trapped in the particle pores are released and then, cracking of large organic molecules of coal take place to forms smaller unstable structures. The coal usually undergoes a viscoelastic liquid state, called metaplast, and swelling during devolatilization. However, it is not observed at relatively high temperatures (1000 K or above) due to rapid escape of volatiles and coking of tar. About 75% of all volatile matter (VM) is released by the coal in metaplast stage. After complete devolatilization at about 980 °C (and/or H content < 3%), immobilization and resolidification occurs due to a lack of metaplast and the occurrence of condensation, repolymerization and aromatization reactions (Berkowitz 1979). The volatiles (light gases and tar), during their trip to the surface, are also cracked, condensed and/or repolymerized to form light gases and coke or soot.

The sequence and characteristics of these processes as well as the composition and yield of the product are dependent on fuel properties and operating conditions. Temperature is possibly the most important variable. Increases in the temperature or heating rate leads to increases (almost linearly with temperature) in the yield of volatile products and the extent of devolatilization (generally determined experimentally) can go beyond VM from proximate analysis (Smoot and Pratt 1979). Further, increase in temperature leads to lower tar and higher amount of light gases due to secondary cracking and other reactions of tar.

The increases in pressure decrease volatile yield which increases secondary repolymerization reactions due to increase in residence time. In addition, higher pressures decrease reactivity of the char because of increase in the H/C ratio of released volatile (i.e. higher carbon content char). For the range particle size (74–1000 μm) usual in a CFBG, the effect of particle size is not much on product distribution and the rate of devolatilization (Smoot and Smith 1985). However, increase in particle size has an effect analogous to an increase in pressure. The major difference between devolatilization of two different coals comes in the composition of the volatiles (more tar for bituminous whereas more gases for lignite).

Composition of devolatilization from coals has been reported in several studies (Loison and Chauvin 1964; di Blasi 1993). However, the concentration of each component vary with coal type, temperature, the heating rate and secondary reactions etc. The practical approach to assess devolatilization products (CO, CO_2, H_2, CH_4, H_2O, NH_3, H_2S and Tar (C_xH_y)) and their stoichiometric coefficients is through balancing proximate and ultimate analysis and validating it through experiments. Typical overall volumetric composition of gas from coal pyrolysis is reported as follows: H_2 (55–70%), CH_4 (20–35%), CO (7–22%), CO_2 (2.6%), SO_x (2.6%), O_2 (0.9%) and N_2 (4%) (de Souza-Santos 2010).

Heterogeneous Reactions: In the heterogeneous reactions, the char produced by the devolatilization reacts with the gaseous components. The heterogeneous reactions can be classified into char combustion and gasification reactions.

Gasification Reactions: Major char gasification reactions include steam char gasification (with H_2O), boudouard reaction (CO_2) and methanation reaction (H_2) and yield combustible gases such as H_2, CO and CH_4.

Steam Char Gasification: Steam char gasification or water–gas reaction is the most important reaction of a gasifier as O_2 is depleted rapidly at the inlet and syngas, the desired high heating value product, is mainly generated from this reaction. It can be represented as:

$$C + H_2O \rightarrow CO + H_2 \qquad \Delta H_{1000\,K} = 136 \text{ KJ/mol}; \ \Delta G_{1000\,K} = -7.6 \text{ KJ/mol} \tag{4}$$
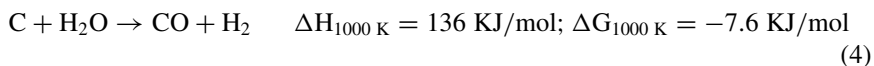
Mechanism of this reaction is proposed to follow three steps i.e. H_2O adsorption and dissociation, CO oxidation and C oxidation. At the conditions found in most

gasifiers, the reaction order is proposed to be first order and the activation energy usually varies between 140 and 235 kJ/mol (Smoot and Pratt 1979).

Boudouard Reaction: The boudouard reaction, char gasification reaction with CO_2, can be represented as follows:

$$C + CO_2 \rightarrow 2CO \quad \Delta H_{1000\,K} = 171 \text{ KJ/mol}; \Delta G_{1000\,K} = -5.3 \text{ KJ/mol} \quad (5)$$

High temperature and low pressure favor forward reaction. The mechanism of this reaction is proposed to follow two steps i.e. CO_2 adsorption and dissociation and C oxidation. The reaction rate is lower than that for steam gasification as the size of the CO_2 molecule is higher than H_2O. Activation energies for this reaction has been reported to vary between 130 and 263 $_{kJ}$/mol and the reaction orders has been reported either 0 (at low temperatures and high CO_2 concentration) or 1 (Smoot and Pratt 1979).

Methanation: The reaction of char with H_2, forming methane, is called the methanation reaction and can be represented as follows:

$$C + 2H_2 \rightarrow CH_4 \quad \Delta H_{1000\,K} = -89.9 \text{ KJ/mol}; \Delta G_{1000\,K} = -19.3 \text{ KJ/mol} \quad (6)$$

The hydrogenation of coal is a very slow reaction and has not been considered as appreciable unless a catalyst is used, especially at temperatures below 500 °C. However, at temperatures of 750–1200 K, elevated pressures and high partial pressures (3–20 mPa) of H_2, this hydrogenation reaction becomes important, increasing the CH_4 content. This reaction is believed to proceed via successive hydrogen additions at the edges of carbon crystallites. The reaction orders varying from 1 to 2 and activation energy between 20 and 200 kJ/mol have been observed (Smoot and Pratt 1979).

Combustion Reactions: The gasification reactions are endothermic i.e. require thermal energy to be supplied either externally or internally. The most of the gasifiers are operated in auto-thermal mode i.e. exothermic combustion reactions balance endothermic gasification reactions and maintain the operating temperature in the gasifier. Thus, the temperature can be controlled by varying the oxygen/steam ratio. The main heterogeneous combustion reactions are the partial and complete combustion of char.

Complete Char Combustion: The complete combustion of char can be represented as:

$$C + O_2 \rightarrow CO_2 \quad \Delta H_{1000\,K} = -394 \text{ KJ/mol}; \Delta G_{1000\,K} = -396 \text{ KJ/mol} \quad (7)$$

Char first oxidizes heterogeneously and carbon monoxide desorbs to the bulk gas. The char combustion reactions are very fast (lower than devolatilization) and highly exothermic even at ambient conditions.

Partial Char Oxidation: The products of complete combustion reactions have no further combustion value whereas from the partial oxidation of char, only 28% of the coal's heating value is released as thermal energy and it can be formulated as:

$$C + 1/2O_2 \rightarrow CO \quad \Delta H_{1000\ K} = -112 \text{ KJ/mol}; \Delta G_{1000\ K} = -200 \text{ KJ/mol} \quad (8)$$

It usually occurs when the oxygen is not sufficient for complete combustion. Some researchers (Liu et al. 2016) considered a combined a combustion reaction resulting in both CO and CO2 as follows:

$$C + (1 - \alpha/2)O_2 \rightarrow \alpha CO + (1 - \alpha)CO_2 \quad (9)$$
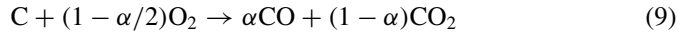
The value α represents the relative conversion of carbon to CO and CO_2 and it is dependent on particle diameter, temperature, fuel properties and oxygen concentration.

Homogeneous Reactions: Similar to heterogeneous reactions, main homogeneous reactions can also be classified into gasification and combustion reactions.

Gasification Reactions: The most important homogenous gasification reactions are the steam methane reforming and water gas shift reactions and these play a vital role in outlet concentration of CO and H_2.

Steam Methane Reforming: Steam methane reforming reaction is frequently used for production of syngas from natural gas in catalytic reactors and can be represented as:

$$CH_4 + H_2O \leftrightarrow CO + 3H_2 \quad \Delta H_{1000\ K} = 225.8 \text{ KJ/mol}; \Delta G_{1000\ K} = -27 \text{ KJ/mol} \tag{10}$$
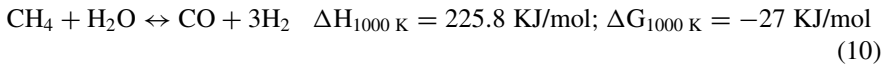
This is a reversible reaction and the forward reaction is favored by low pressure and high temperatures.

Water Gas Shift Reaction: Water gas shift reaction increases the H_2/CO ratio at the outlet of the gasifier and can be represented as:

$$CO + H_2O \leftrightarrow CO_2 + H_2 \quad \Delta H_{1000\ K} = -34.6 \text{ KJ/mol}; \Delta G_{1000\ K} = -3 \text{ KJ/mol} \tag{11}$$
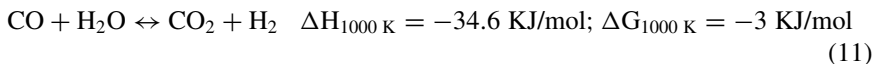
As the heating value of H_2 is higher than that of CO, water gas shift reaction is a highly desirable reaction. This is also a reversible reaction whose equilibrium constant varies (decreases from 1 to 0.5 with increasing temperature) relatively little over a wide range of temperature. As the number of moles on both side of the reaction is same, pressure has a very small effect on the equilibrium constant of water gas shift reaction.

Combustion Reactions: The O_2 present in the gasifier may also react with gas phase species. The main homogeneous combustion reactions are that of CH_4, CO and H_2.

Methane Oxidation: Methane oxidation can be represented as:

$$CH_4 + 2O_2 \rightarrow CO_2 + 2H_2O \qquad \Delta H_{1000\ K} = -802.28 \text{ KJ/mol} \qquad (12)$$

CO Oxidation: CO can react with O_2 to form CO_2 as follows:

$$CO + 1/2\ O_2 \rightarrow CO_2 \qquad \Delta H = -285 \text{ KJ/mol} \qquad (13)$$
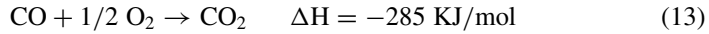
In this reaction, water acts as a catalyst and its concentration is generally included in the rate laws. This catalytic effect may be caused by the enhancement of the water gas shift reaction.

H_2 Oxidation: H_2 is oxidized to H_2O during gasification as follows:

$$H_2 + 1/2\ O2 \rightarrow H_2O \qquad \Delta H = -238 \text{ KJ/mol} \qquad (14)$$
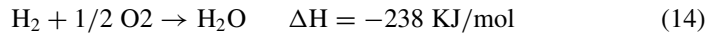
Nitrogen and Sulfur Reactions: Coal contains various nitrogen- and sulfur-containing compounds. Oxides of nitrogen (NOx) can form only above 1540°C, therefore, are negligible in a gasifier (Basu 2006). The NOx emissions are also significantly reduced due to the lack of excess air in the gasifier. Therefore, most of the nitrogen in coal is assumed to be gasified, especially during devolatilization at the same rate as devolatilization, as HCN initially which subsequently converts to NH_3 which is the major nitrogen-containing species in the syngas, especially above fuel/air ratios of 1.3. In the reducing environment of a gasifier, S is primarily (~ 70–90%) converted to H_2S and traces of COS, CS_2, thiophenes and mercaptans can be found. Remaining sulfur is found in the ash (~ 5%) as sulfides and sulphates and retained in the char (1%).

The pyrolysis reactions are completed very rapidly and within a very small distance from the coal inlet, introducing several gaseous species. Thereupon, the devolatilized gases begin to react with char and other gases while penetrating through the bed. Oxygen is consumed completely immediately after its introduction at the inlet due to very fast combustion reactions leading to sudden increase in concentrations of CO, CO_2 and H_2O as well as temperature. The CO produced from devolatilization and partial combustion partially oxidizes to CO_2 until O_2 is available. Thereafter, gasification reactions take place in the reducing environment and consequently, concentration of CO and H_2 increase and that of CO_2 and H_2O decrease along the length of the riser. In addition, the axial profile of concentration of CO follows the axial profile of solid volume fraction. The water gas shift reaction is active throughout the reactor and causes a slight decrease in concentration of CO along the height of the riser. The concentration of H_2 remains nearly constant in most of the reactor. CH_4 is mainly produced by devolatilization and consumed by both combustion and gasification reactions, therefore, somewhere between particle inlet

and distributor, a maxima of methane occurs. Methanation reaction plays a minor role in the production of CH_4 owing to its very small reaction rate, especially at low operating pressures. The concentration of H_2O also exhibits a maximum in the regions of highest devolatilization and combustion intensity i.e. close to the inlet. Thereafter, it decreases as a result of gasification reactions and dilution by the gasification products. The concentration of N_2 decreases monotonically along the riser height due to increasing concentration of other species with increasing conversion of coal. As the solid volume fraction in the core region is very small, homogeneous reactions dominate and radial variation in species concentration is observed. The CH_4, CO and H_2 mainly accumulate near the wall due to higher solids concentration. These local radial gradients disappear, due to excellent mass transfer and mixing, with the height of the reactor (Sharma and Agarwal 2019a, 2020). Transient variations of the concentration of the products species is such that the concentration of H_2 and CO increase and O_2 decreases continuously until steady state.

3 Modeling and Simulation

Coal is a very complex heterogeneous substance whose structure and behavior are highly variable and are not well known as well as the subject of reacting gas–solid systems (e.g. CFBG) is very broad, has multiscale character and involves complex interplay of several simultaneously occurring physical and chemical aspects i.e. hydrodynamics, heat and mass transfer and chemical reactions. Therefore, design and scale-up of CFBGs becomes very challenging. Several experimental studies on CFBGs have been performed (Ju et al. 2010; Chen et al. 2004; Matsuoka et al. 2013; Mahapatro and Mahanta 2020). However, experimental studies are very long, expensive and risky. Modelling and simulation have emerged as an effective, in terms of both time and cost, tool to understand, design, develop and analyze CFBGs. However, simultaneously occurring, complicated and inter-related physical and chemical processes makes the design of a CFBG a non-trivial task.

Several mathematical models have been developed for a CFBG and can broadly be classified as Equilibrium, Black-box and Computational Fluid Dynamic (CFD) models. The equilibrium models provide equilibrium composition and maximum efficiency (theoretically achieved at infinite residence time) for a pre-defined set of species to offer thermodynamic limits as a guide to process design, evaluation and improvement. The equilibrium models can further be classified into stoichiometric and non-stoichiometric approaches. Stoichiometric approach employs equilibrium constants of all the independent elementary reactions. In contrast, non-stoichiometric approach (Li et al. 2001; Sharma and Agarwal 2019b) minimizes the total Gibbs free energy subject to mass balance and non-negativity constraints. Non-stoichiometric approach is excellent in modelling multiple feed streams of unclear or unknown molecular formulation. The two approaches are proved to be essentially equivalent. As the real gasification processes deviate from chemical equilibrium due to effects of hydrodynamics as well as heat and mass transfer, the equilibrium models can

only be recommended for preliminary analysis. The black-box models are based on machine learning and artificial intelligence techniques trained on experimental data. In contrast, CFD models are based on the fundamental laws of conservation of mass, momentum and energy and can provide detailed spatio-temporal profiles of volume fractions, velocities, temperature and species concentration of both the phases. Further, simultaneous and interdependent influence of hydrodynamics, heat and mass transfer and chemical reactions on the performance of a CFBG can be analyzed. Therefore, CFD is becoming increasingly popular as an accurate and inexpensive tool to understand various complex industrial processes with the advancement of computational capacity and speed.

The earliest CFD-type models for CFBGs were semi-empirical one-dimensional models where hydrodynamic description was based on empirical correlations, such as, two phase theory of fluidization, considering gas-rich bubble and particle-rich emulsion phases. Although these models were easy to develop and implement as well as computationally inexpensive, these can only be applied under certain conditions and extrapolation of the results, to different coals, and operating parameters which certainly not give consistently reliable simulation results. With the advancement of computers as well as numerical techniques and algorithms, two- and three-dimensional CFD simulations are becoming popular. The multi-dimensional CFD models can broadly be classified, into Eulerian-Eulerian (EE), Eulerian–Lagrangian (EL) and Direct Numerical Simulation (DNS) models. DNS is the most rigorous method, in which the flow of fluid is solved based on the full Navier–Stokes equations and particles are treated as moving boundaries. DNS allows the prediction of parameters which are impossible to measure through experimental studies. It can also be utilized for the development of closure correlations or sub-models (bridges between micro- and macro-scale modeling). However, the complexity of interface tracking algorithms and their coupling with the momentum, heat transfer and chemical species conservation equations of chemically reacting particles is very challenging, time-consuming and computationally expensive. Therefore, DNS is restricted to small number of particles, low Reynolds numbers ($Re = 20$) and is suitable for particle-liquid systems. Thus, application of DNS models on a large scale CFBG is impossible with the currently available computational resources. The EL models, also referred to as discrete element models (DEM) or discrete particle models (DPM), individual particle is tracked in Lagrangian reference frame and their movement is governed by Newtonian equations of solid mechanics and the fluid is solved by averaged Navier–Stokes equations in Eulerian reference frame. The gas-particle and particle–particle interactions can be coupled in one- (fluid affects particles only), two- (fluid and particles affect each other), three- (fluid and particles affect each other and effect of particles on fluid affect other particles) or four-way (all the aforementioned effects plus particle collisions) coupling. The particle–particle collisions are described by the soft-sphere or hard-sphere approach. In the hard-sphere model, the particle–particle and particle wall collisions are assumed to be instantaneous and expressed by binary collisions i.e. multiple collisions at the same instant cannot be considered. In contrast, in the soft-sphere model, these collisions are expressed by the Hertzian contact theory and the particles are allowed to overlap as well as simultaneous multiple contacts

are possible. As each particle is tracked individually, particle size distribution and properties of single particle can readily be taken into consideration. However, the computation time increases with number of particles, therefore, it is normally limited to a relatively small number of particles ($< 20,000$), small volume fraction ($< 5\%$), and small-scale systems for fundamental research. As number of particles is approximately 10^{10}–10^{12} for typical operating conditions (bed inventory ~ 100,000 kg, mean particle diameter ~ 300 μm, particle density ~ 2500 kg/m^3) in a large scale CFBG, EL models are not feasible. Therefore, some hybrid EL models, such as, dense discrete particle model (DDPM), multi-phase particle-in-cell (MP-PIC) model, direct simulation Monte Carlo method (DSMC), distinct cluster method, etc., has been developed where group of particles (parcels or clusters) are considered as discrete elements and tracked in lieu of individual particles, significantly reducing the computational cost. However, even these models cannot be applied to industrial cases with currently available computational resources. In the EE models, also called the two-fluid method (TFM), both the gas and the solid phases are considered as interpenetrating continua in Eulerian frame and governed by averaged Navier–Stokes equations. As the solid phase is considered as a pseudo-fluid, the transport properties of the solid phase are estimated by the KTGF and the resulting model can be referred to as Euler Granular Multiphase Model (EGMM). Although these models have been successfully applied to large scale multiphase flow processes with a large number of particles and high solid volume fraction with relatively lesser computational resources, homogeneous particle properties can be considered due to increase in computational cost and complexity with increase in solid phases with different properties.

Several 2D models has been developed for CFBGs. However, 2D models may not be appropriate as real system is generally asymmetric, especially in the region close to recycle inlet and in the cyclone. Recent comparative studies on 2D against 3D modelling (Li et al. 2014a) have shown critical differences and therefore, a 3D CFD study is essential for accurate prediction of CFBGs. Despite the clear need for comprehensive 3D models and the rapid advancement in capacity and speed of computers, only a few studies have been published as the computational time is large. Further, most of these studies focus on only one component of a CFBG i.e. riser and exclude the recirculation system. However, the complex and integrated interactions between the components of the CFB are of critical importance to capture the true physics and effective coordination among the components can lead to highly efficient operation. Li et al. (2014b) presented detailed comparison between the hydrodynamics predicted by full-loop and riser-only simulations of a pilot-scale CFB using open-source code MFIX (Multiphase Flow with Interphase exchanges). It was concluded that riser-only simulation can provide reasonably accurate results but is not capable to accurately capture the dynamic response of the CFB and predict the transition between different fluidization regimes. Therefore, the full-loop simulation of a CFB is more realistic and has shown great potential in understanding the complex flow phenomena and especially the possible flow instabilities but it requires higher computational resources and a comprehensive model to represent full spectrum of flow regimes present in a CFB loop. Only a few 3D full-loop CFD simulation studies

of CFBGs have been performed (Liu et al. 2015; Yan et al. 2016; Kraft et al. 2017; Yu et al. 2018; Wahyudi et al. 2018; Sharma and Agarwal 2019a, 2020).

4 Effect of Process Parameters

The performance of a CFBG, i.e., composition and heating value of the syngas, depends on the coal characteristics, temperature, pressure, air/coal (A/C) and steam/coal (S/C) ratios, superficial gas velocity, solid circulation rate and residence time.

4.1 Temperature

The temperature inside CFBG has immense effect on syngas composition and calorific value as the reaction rates increase exponentially with temperature. With the increase in temperature, CO and H_2 concentration increase, due to increasing rate of the endothermic gasification reactions as well as augmented volatile yield and tar reactions, while CO_2, CH_4, H_2O and tar content decrease. As a result, gas yield, carbon conversion, H_2/CO ratio and cold gas efficiency increase but calorific value decreases with increasing temperature because of decrease in hydrocarbons and CH_4 (Sharma and Agarwal 2020). The hydrodynamics of the gasifier is also affected by the temperature. Since interphase momentum transfer coefficient (Kgs) depends on the gas density and viscosity, Kgs, solid holdup and pressure drop decrease with increase in temperature. When the temperature rises, the gas velocity increases and in turn, solid velocities and residence time also change accordingly.

4.2 Pressure

Thermodynamically, high pressure supports reactions with volume contraction whereas volume-increasing reactions are suppressed from Le Chatelier's principle. Consequently, concentration of CO and H_2 decrease while that of CO_2, CH_4 and H_2O increase with increase in pressure. Although, it is not a desirable outcome, there are operational benefits to utilize higher pressures such as smaller equipment, larger capacities and lower capital cost. Additionally, higher pressures are required for the gas turbine, gas clean-up, CO_2 capture and chemical synthesis. As required energy to pressurize the reactants is lesser in comparison to that for product syngas, high pressure is preferred in CFBGs. The yield of volatiles decreases with increasing pressure due to increase in residence time of volatiles within the particles and tar reactions which leads to increased char yield.

4.3   Equivalence Ratio and Air/Coal Ratio

Equivalence ratio (ER) can be defined as the ratio of the amount of oxygen supplied to the stoichiometric amount of oxygen required for complete combustion. In contrast, air/coal (A/C) ratio is the ratio of the mass of air supplied to the mass of coal fed. Both of the operating parameters show similar effect as both, in effect, change the relative concentration of O_2 in the gasifier. The concentration of CO_2 and H_2O increase while that of H_2, CH_4 and CO decrease with increase in ER (or A/C) due to increase in combustion reactions. Therefore, with the increase in ER, carbon conversion and syngas yield increase but calorific value and cold gas efficiency decrease. As a result of enhanced combustion with increasing ER, temperature in the gasifier and at the outlet increases. Further, CO/CO_2 and CH_4/H_2 ratios decrease whereas H_2/CO ratio increases with increasing ER. The tar content in the syngas decreases with increase in ER due to enhanced tar reactions caused by higher temperatures. The larger A/C ratio causes a larger gas velocity that decreases both gaseous and solid residence time. For gasifiers, ER is usually kept between 0.2 and 0.4 but optimum ER, at which concentration of combustible gases is maximum, is suggested to be 0.19–0.43 for fixed bed and 0.2–0.3 for fluidized bed gasifiers and 0.41–0.6 for circulating fluidized bed gasifiers (Liu et al. 2013).

4.4   Steam/Coal Ratio

Steam/coal (S/C) ratio can be defined as the ratio of the mass of steam supplied to the mass of coal fed. The concentration of the H_2 and CO_2 increase with the increase of the S/C ratio while that of CH_4 and CO decrease. The increase of S/C ratio lowers the temperature of the riser which decreases the rate of gasification reactions and in turn, concentration of CO. With the increase in S/C ratio, tar yield and H_2/CO ratio increase and heating value, gas yield and carbon conversion decrease. As the heating value of CO is higher than that of H_2, decrease in CO cannot be compensated by increase in H_2 with increase in the S/C ratio. The decrease in CH_4 is caused by enhanced char-steam reaction, which cannot be overcome be slow methanation reaction (Ju et al. 2010). The increase in CO_2 concentration is mainly because of intensification of water gas shift reaction. With increasing S/C ratio, the temperature in the gasifier decreases due to increase in energy requirement for steam heating and endothermic reactions. Therefore, increased steam requires higher ER to maintain the gasifier temperature. The gas flow increases and consequently, residence time decreases with the increase in S/C ratio.

5 Conclusion

Circulating fluidized bed gasifier (CFBG) offers certain important advantages, such as, fuel-flexibility, excellent heat and mass transfer, high carbon conversion and efficiency, high throughput, lower emissions etc. Therefore, in this chapter, fundamentals of CFBG, i.e., hydrodynamics, heat and mass transfer and typical chemical reactions, modeling and simulation and effect of process parameters, namely, temperature, pressure, air/coal ratio and steam/coal ratio, are discussed. Apart from external circulation owing to cyclone and return-pipe, several internal circulation loops are observed in the riser of CBFG, wherein, particles are entrained from the middle and fall back along the wall of the riser. The convective heat transfer is the most important mode of heat transfer in CFBGs. Mass transfer limitation usually occurs only in the case on rapid combustion reactions. Among thousands of chemical reactions occurring in the CFBG due to complex coal chemistry, drying, devolatilization, steam char gasification, boudourd reaction, methanation, char combustion, steam methane reforming, water gas shift reaction, methane oxidation, CO oxidation, H_2 oxidation, NH_3 and H_2S formation are some of the most important reactions. Equilibrium modeling of CFBGs can be used for preliminary analysis to study thermodynamic limits of the process. In contrast, computational fluid dynamics (CFD) provides comprehensive understanding of the CFBG. Temperature is the most important variable affecting the performance of the gasifier. However, it must be limited by requirement of state of ash and material of construction. Air/coal and steam/coal ratios can be used to vary the relative occurrence of combustion and gasification reactions and in turn, to control temperature and syngas composition.

References

Basu P (2016) Combustion and gasification in fluidized beds. CRC Press, Boca Raton

Berkowitz N (1979) An introduction to coal technology. Academic Press, New York

BP (2021) Statistical review of world energy. https://www.bp.com/en/global/corporate/energy-economics/statistical-review-of-world-energy.html. Last accessed 21 July 2021

Chen G, Andries J, Spliethoff H, Fang M, van de Enden PJ (2004) Biomass gasification integrated with pyrolysis in a circulating fluidised bed. Sol Energy 76:345–349

de Souza-Santos ML (2010) Solid fuels combustion and gasification: modeling. Simulation and equipment operations. CRC Press, Boca Raton

di Blasi C (1993) Modeling and simulation of combustion processes of charring and non-charring solid fuels. Prog Energy Combust Sci 19(1):71–104

Gräbner M, Ogriseck S, Meyer B (2007) Numerical simulation of coal gasification at circulating fluidised bed conditions. Fuel Process Technol 88:948–958

Gunn DJ (1978) Transfer of Heat and Mass to Particles in Fixed and Fluidized Beds. Int J Heat Mass Transf 21:467–476

Hassan MIO (2013) Modelling and simulation of biomass gasification in a circulating fluidized bed reactor. Ph.D. Thesis, Aston University, Birmingham, UK

International Energy Agency (IEA) (2012) Technology roadmap: high-efficiency, low-emissions coal-fired power generation

International Energy Agency (IEA) (2016) Energy technology perspectives: towards sustainable urban energy systems

Ju F, Chen H, Yang H, Wang X, Zhang S, Liu D (2010) Experimental study of a commercial circulated fluidized bed coal gasifier. Fuel Process Technol 91:818–822

Kraft S, Kirnbauer F, Hofbauer H (2017) CPFD simulations of an industrial-sized dual fluidized bed steam gasification system of biomass with 8 MW fuel input. Appl Energy 190:408–420

Li X, Grace JR, Watkinson AP, Lim CJ, ErguÈdenler A (2001) Equilibrium modeling of gasification: a free energy minimization approach and its application to a circulating fluidized bed coal gasifier. Fuel 80:195–207

Li T, Pannala S, Shahnam M (2014a) CFD simulations of circulating fluidized bed risers: Part II—evaluation of differences between 2D and 3D simulations. Powder Technol 254:115–124

Li T, Dietiker J-F, Shadle L (2014b) Comparison of full-loop and riser-only simulations for a pilot-scale circulating fluidized bed riser. Chem Eng Sci 120:10–21

Liu H, Elkamel A, Lohi A, Biglari M (2013) Computational fluid dynamics modeling of biomass gasification in circulating fluidized-bed reactor using the Eulerian-Eulerian approach. Ind Eng Chem Res 52:18162–18174

Liu H, Cattolica RJ, Seiser R, Liao CH (2015) Three-dimensional full-loop simulation of a dual fluidized-bed biomass gasifier. Applied Energy 160:489–501

Liu H, Cattolica RJ, Seiser R (2016) CFD studies on biomass gasification in a pilot-scale dual fluidized-bed system. Int J Hydrogen Energy 41:11974–11989

Loison R, Chauvin F (1964) Pyrolyserapide de charbon. Chim Ind (paris) 91:269–275

Luo K, Wu F, Yang S, Fang M, Fan J (2015) High-fidelity simulation of the 3-D full-loop gas-solid flow characteristics in the circulating fluidized bed. Chem Eng Sci 123:22–38

Mahapatro A, Mahanta P (2020) Gasification studies of low-grade Indian coal and biomass in a lab-scale pressurized circulating fluidized bed. Renewable Energy 150:1151–1159

Matsuoka K, Hosokai S, Kato Y, Kuramoto K, Suzuki Y, Norinaga K, Hayashi JI (2013) Promoting gas production by controlling the interaction of volatiles with char during coal gasification in a circulating fluidized bed gasification reactor. Fuel Process Technol 116:308–316

Nikrityuk PA, Meyer B (2014) Gasification processes: modeling and simulation. Wiley-VCH, Germany

Prabhansu CP, Karmakar MK, Chatterjee PK (2016) Circulating fluidized bed gasification: status, challenges and prospects in Indian perspective. Ind J Sci Technol 9(48):1–14

Sharma V, Agarwal VK (2019a) Numerical simulation of coal gasification in a circulating fluidized bed gasifier. Braz J Chem Eng 36(3):1289–1301

Sharma V, Agarwal VK (2019b) Equilibrium modeling and optimization for gasification of high ash Indian coal by gibbs free energy minimization method. Process Integr Optim Sustain 3(4):487–504

Sharma V, Agarwal VK (2020) Effect of process parameters on circulating fluidized bed coal gasification using 3D full-loop CFD simulation. Can J Chem Eng 98(8):1708–1728

Simpson LA (2006) The suitability of coal gasification in India's energy sector. M.S. Dissertation, The Engineering Systems Division, Massachusetts Institute of Technology, USA

Smoot LD, Pratt DT (1979) Pulverized-coal combustion and gasification: theory and applications for continuous flow processes. Springer, USA

Smoot LD, Smith PJ (1985) Coal combustion and gasification. Springer, USA

Wahyudi H, Pinem MP, Rosyadi I, Chu K (2018) Numerical study of biomass gasification in 3D full-loop circulating fluidized beds using a Eulerian multi fluid model. Int J Technol 2:229–237

Yan L, Lim CJ, Yue G, He B, Grace JR (2016) Simulation of biomass-steam gasification in fluidized bed reactors: model setup, comparisons and preliminary predictions. Bioresour Technol 221:625–635

Yu X, Blanco PH, Makkawi Y, Bridgwater AV (2018) CFD and experimental studies on a circulating fluidised bed reactor for biomass gasification. Chem Eng Process 130:284–295

Carbon Sequestration and Capturing Technologies—A Review

Mohd Aseel Rizwan and Surinder Singh

Abstract Carbon emissions worldwide is an issue of serious concern pertaining to its worrisome effects like global climate change, warming and ozone depletion. The natural and anthropogenic activities like forest fires, fossil fuel burning, respiration, decomposition of flora and fauna, geogenic activities and chemical changes in the rock beds, automotive and industrial exhausts, etc., all lead to an immense amount of CO_2 being produced. CO_2 is a greenhouse gas that traps solar heat and facilitates earth warming up to an extent of 66%. Hence, it is essentially required to reduce carbon emissions and sequester the carbon being produced effectively. Many upcoming and existing technologies are utilized for carbon-capturing such as carbon capture and storage (CCS), carbon sequestration utilizing rocks and hydrates, chemical looping separation, membrane technology, cryogenic carbon capture (CCC), absorption, and adsorption. Each one of these technologies are having its own merits and demerits and carbon capture potential. This review describes these technologies for carbon capture and reducing the carbon emission for the environmental safeguarding and combating the global warming and climate change effects.

Keywords Carbon capture · Greenhouse gas · Cryogenic carbon capture · Climate change · Global warming

1 Introduction

The industrial revolution started way back in the eighteenth century having the aim to develop modern civilization with the accelerated pace of development. The race for development has led us to what we are now witnessing as increased concentrations of Carbon dioxide (CO_2) in the atmosphere which is a greenhouse gas (GHG) and one of the major contributors to global warming. The current energy gap on earth, as well as the recent rise of net climate forcing, are driving global warming. The last

M. A. Rizwan (✉) · S. Singh
Dr. S. S. Bhatnagar University Institute of Chemical Engineering and Technology, Panjab University, Chandigarh 160014, India
e-mail: aseelrizwan6@gmail.com

few years have had the greatest impact on current warming (Hansen and Sato 2020).
CO_2, N_2O, CH_4, and halocarbons are the four certainly major greenhouse gases
(GHGs) produced by human activities, with CO_2 being the major anthropogenic
GHG, accounting for roughly two-thirds of the increase in greenhouse gases (Pan
and Chiang 2012). People of underdeveloped countries are the ones who are suffering
at large. In December 2015, the Paris Agreement, which was essential for the United
Nations Framework Convention on Climate Change (UNFCCC), was embraced. In
November 2016, the treaty came into force. Its primary objective is to work on
worldwide cooperation to mitigate the danger of environmental and climate change
by keeping worldwide average temperature well underneath expanded 2 °C above
pre-modern levels and seeking after endeavors to keep temperature increments to
1.5 °C above pre-industry era levels (Nakao et al. 2019).

According to NOAA's Annual Global Climate Report 2021, the land and ocean
global surface temperature jointly as estimated in Jan 2021 has expanded at a normal
pace of 0.88 °C (1.58 F) which is higher than the 20th-century average and it set's in
the 142-year global record as the fifth warmest June. Also, June 2021 temperature
was above the 20th-century average temperature for the 45th successive June and the
438th successive month. This is the major reason for concern among the research
community as if this rise cannot be curbed soon; we will be going to witness more
disasters that haven't been heard before (NOAA 2021). The monthly temperature
variation of June month is shown in Fig. 1 for the past 141 years.

Since the beginning of the coronavirus pandemic, global emissions decreased
briefly in 2020 due to the decline in transportation usage, industrial and economic
activity. However, the 2020 emissions reductions were insufficient to significantly
reduce the amassing of carbon dioxide in the air, which continues to increase
(Pollution 2021).

There are a few common ways by which CO_2 reach the atmosphere:
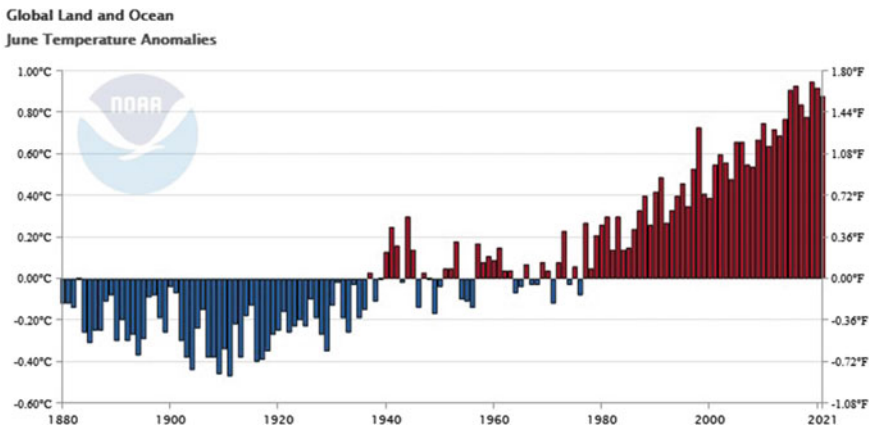
Fig. 1 Monthly temperature June 1880–2021 [*Source* NOAA Global Climate Report 2021 (NOAA
2021)]

- When carbon dioxide is exhaled out of the body, it is a consequence of regular cell function.
- When fossil fuels are burned or flora decomposes, CO_2 is released.
- Because of dying vegetation or chemical changes in the bedrock, significant amounts of this gas can sometimes be found in surface soils.

CO_2 openness can have a scope of wellbeing results on people. Cerebral pains, discombobulation, fretfulness, shivering or tingling sensations, shortness of breath, perspiring, weariness, raised pulse, raised circulatory strain, obviousness, suffocation, and spasms are a portion of the manifestations that may happen (Wisconsin Department of Health Services 2021).

Carbon dioxide is a highly oxidized and thermodynamically stable gas, therefore is a very stable compound, meaning it is not very reactive and can stay in the atmosphere much longer relative to other GHG's as a result contributing to the current warming (Omae 2006). Carbon dioxide is an ozone-harming substance (GHG). A GHG retains and transmits heat. After being warmed by daylight, the earth's territory and sea surfaces ceaselessly emanate warm infrared radiation (heat). Not quite the same as oxygen or nitrogen, which make up most of our air, ozone-depleting substances trap warm and gradually emanate it, like blocks in a chimney after the fire has gone out. Carbon dioxide expansion represents around 66% of the general energy uniqueness that is making the Earth's temperature rise. This becomes one of the major reasons to look for technologies to lower emissions (Lindsey 2020).

Current measurements at Mauna Loa Observatory in Hawaii are worrisome that reveals CO_2 levels in the atmosphere have reached 419 parts per million (ppm) the monthly average for 2021 reaching its highest point in May, the highest amount in years from when accurate monitoring began 63 years ago which is almost reaching 50% higher over the 1750–1800 average, i.e., 278 ppm, that was the pre-industrial level. Earlier in February and March also concentration remained at 417 ppm for several days. The Annual cycle of atmospheric CO_2 level is depicted in Fig. 2. The graph here depicts the annual period of CO_2 levels in the atmosphere. CO_2 levels as observed are shown in black, and the projection for 2021 is shown in red.

The public's desire for clean air is increasing. There are tools to make it happen. As the cooling layer of smog is removed, even more warming is on the way. Then, for states, societies, and all of us, dealing with climate change, would be the most difficult challenge. Heat, food shortages, floods, and other violent effects of the climate emergency will destroy millions of more lives than the pandemic (Smith 2020). To capture CO_2 from the atmosphere: Absorption, adsorption, membrane, chemical looping, hydration, and bio fixation capture technologies have been explored in recent decades. A brief introduction of these technologies has been discussed to get the idea of presently available means and the future scope of research. Carbon Capture Storage (CCS) and cryogenic carbon capture (CCC) via phase change have received special attention among many technologies due to their potential in tackling the excessing carbon problem. The fact is that many technologies are available, but making them cost-effective and easily accessible is one of the biggest hurdles
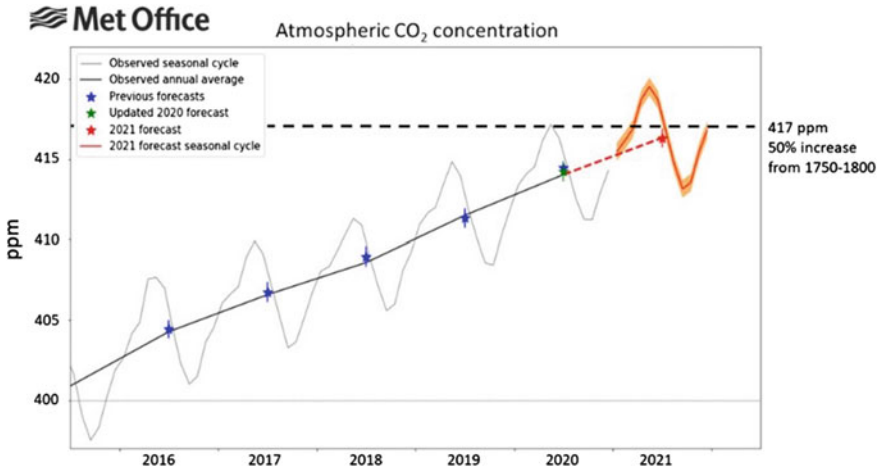
Fig. 2 Annual cycle of atmospheric CO_2 level [*Source* Carbon Brief; https://www.carbonbrief.org/met-office-atmospheric-co2-now-hitting-50-higher-than-pre-industrial-levels (Betts 2021)]

for the research community as well as governments because no industry wants to increase the manufacturing costs for its products (Song and Liu 2019).

2 Carbon Capture Technologies

CO_2 capture, transportation, and storage are critical components of a framework to minimize greenhouse gas emissions. The kind of CO_2 producing plant and fuel used substantially influences the CO_2 capturing technique chosen (Leung 2014).

2.1 Carbon Sequestration

There are 4 major sequestration and storage technologies that has been discussed below.

2.1.1 Carbon Capture and Storage (CCS) or Geologic Sequestration

Scientists have studied the potential of a promising carbon sequestration technology i.e., Carbon Capture and Storage (CCS) or geologic carbon sequestration for lowering carbon emissions. It is a type of carbon-capturing technique that stores carbon dioxide (CO_2) into deep geological formations to keep from escaping into the atmosphere and ruining the environment as a GHG. CO_2 is captured at a major pollution source

(such as a factory or power plant), transported to a storage site (such as a natural gas field), and permanently stored deep below the surface into porous and permeable geologic layers, where for months or even years it will remain isolated (Broecks et al. 2016; Duncan and Morrissey 2011).

The utilization of CCS directly affects the expense of energy delivered and the speed at which the innovation can be fabricated. Since the world keeps on relying intensely upon petroleum derivatives, a proficient strategy for gathering CO_2 from power plants, which is one of the significant CO_2 sources, is significant (Wilberforce 2021). Methods that can be utilized for removing CO_2 from flue gas can be Wet scrubbing, amine scrubbing, chemical adsorption, etc. These capturing techniques are either retrofitted in existing power plants or installed within newly built power stations. Capture technology selection is usually based on several factors, including partial pressure of CO_2 in the gas flow, percentage of CO_2 requisite for recovery, purity of the expected CO_2 product, responsiveness to impurities, and the capture procedure's initial and overall operational expenses, as well as the procedure's environmental impacts (Arora 2019).

The three main capture processes that are currently available for CCS; work in the following ways:

- Post-Combustion: CO_2 is eliminated from the fumes gas after burning by means of particular dissolvable assimilation.
- Pre-ignition: The fuel is pre-treated and changed into a combination of CO_2 and hydrogen, after which the CO_2 is isolated. From that point onward, the hydrogen is scorched to create energy or fuel.
- Oxy-fuel ignition: Instead of air, oxygen is utilized to consume the fuel, bringing about a pipe stream of CO_2 and water fume with no nitrogen. CO_2 might be separated rather essentially from this stream. The oxygen fundamentally required for consuming the fuel is gathered from the air on the spot (IPCC 2005).

The fundamentals and illustration of components of Carbon Capture and Storage technology have been depicted in Fig. 3.

CCS is one of the useful techniques that can be utilized to relieve a worldwide temperature alteration and its impacts on people and other living beings. As of now, most CCS innovations can assimilate around 85–95% of CO_2 produced by a power plant. CO_2 is most efficiently delivered when crushed to a pressure of more than 7.4 MPa and a temperature of more than 31 °C. CO_2 has supercritical qualities under these conditions, i.e., it is a liquid with gas qualities. As a result, CO_2 would often be transported at high pressures in carbon steel pipelines, similar to petroleum gas pipelines, or on ships if it is expected to cross an enormous waterway.

Abandoned oil and gas fields or deep saline formations with a projected minimum depth of 800 m, where the ambient temperature and pressures are high enough to keep the CO_2 in a liquid or supercritical state, are suitable CO_2 storage places. Sadly, most power plants with CCS frameworks would utilize more energy than power plants without the CCS innovation. The vast majority of CCS applications are now uneconomical. The additional equipment required to absorb and compress CO_2
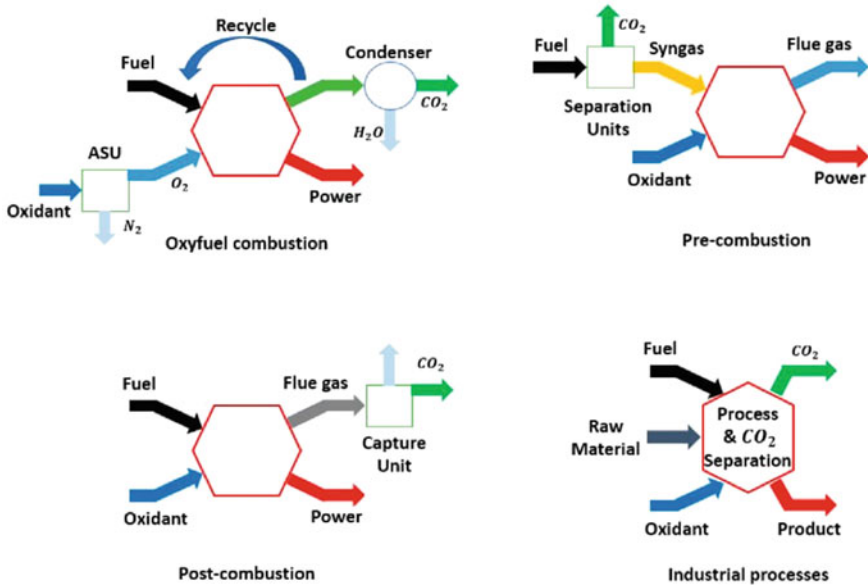
Fig. 3 Illustration of **a** oxy-fuel ignition, **b** pre-ignition capture, **c** post-ignition capture, **d** fossil-fuel-based industrial power generation

consumes a large amount of energy, increasing the fuel requirements of a coal-fired power station by 25–40% and driving up expenses (Wilberforce 2019; CTCN).

One major drawback is that CCS adds four additional costs to a "normal" power station. First and foremost, capture equipment must be set-up. Second, the capturing process must be powered, which adds to the expense of fuel. Finally, transportation infrastructure must be constructed. Last but not least, the CO_2 must be kept. All of this necessitates greater capital expenditure as well as increased operational expenses. Early full business scale CCS projects are required to cost around € 35–€ 50 for every huge load of CO_2 sequestered. Future exploration of the technology gives hope that these difficulties will be dispensed; with in coming a very long time for CO_2 stockpiling (Naucler et al. 2008).

2.1.2 Oceanic Carbon Sequestration (OCS)

It is a technique for equally distributing CO_2 all through the depths of the ocean while minimizing oceanic surface consequences. Direct injection and ocean fertilization (encouraging aquatic creatures to fix CO_2 through photosynthetic fixation) are the two main ways of OCS (Chow 2014). Both methods for increasing oceanic carbon sequestration take advantage of natural ocean phenomena. Enhancing the productivity of ocean biological systems by fertilization is one while another is to directly

inject CO_2 into the ocean's depths. Ocean sequestration is still in its initial development phase when compared to land ecosystems and geological structures (Miller 2005). The global potential of the seas to sequester CO_2 is between 1400 and 20,000 GT, which is the largest among other sedimentary formations. Although the ocean has 39,000 GT of carbon in the form of carbonate and bicarbonate, its absorbing capacity is significantly less. A carbon injection of 1000 GT would already have a severe significant impact on ocean chemistry. Despite these constraints, estimations for ocean storage capacity exceeding 100,000 billion GTC have been given. Once CO_2 is deposited in the ocean, the dissolved CO_2 reacts with the marine water to generate H_2CO_3 (carbonic acid), increasing the acidity and decreasing the pH of the ocean, making it unsuitable for living creatures. Only if alkalinity (e.g., NaOH) was introduced to the marine to neutralize the carbonic acid could make it possible for such figures to be achieved. CO_2 sequestration in the water is indicated not to be an acceptable choice for CO_2 storage because of the negative environmental effects, including potential dangers to marine life and public criticism but research is still finding out the probability of utilizing this technology with minimum environmental effects (Rabiu 2017; Lackner et al. 2010).

2.1.3 Mineral Sequestration

Mineral sequestration, also known as carbonation, is a chemical phenomenon in which CO_2 combines with metal oxides (e.g., calcium and magnesium oxides) to form carbonates. Mineral carbonates, in addition to preserving CO_2 for long periods (decades or even centuries), have numerous applications, particularly in the construction sector as construction materials, and so can be regarded as a utilization alternative (Cuéllar and Franca 2017). For simplicity, it is estimated that 1.6 T of olivine (magnesium iron silicate) is required to sequester 1 T of CO_2 and produce 2.6 T of mineral carbonate, based on the carbonation process stoichiometry. Among the natural minerals, olivine is said to have the largest concentration (57%) of reactive MgO. Pure serpentine, on the other hand, has a MgO concentration of about 44% while natural ores have a MgO concentration of 50%. As a result, it is predicted that to sequester 1 t of CO_2, 1.6–3.7 t of mineral feedstock, capable of producing 2.6–4.7 t of mineral carbonates, is required (Chakraborty and Jo 2018). The sluggish dissolution kinetics and high energy demands associated with mineral processing have always been the main drawbacks of this storage technology. However, recent breakthroughs in research have demonstrated a significant potential for lowering the cost of ex-situ mineral carbonation. Total costs must be decreased from present estimates of \$80–\$100 per t of CO_2 to more affordable amounts, such as \$30 per t (Gayathri 2021).

2.1.4   Biological Sequestration

CO_2 is filtered naturally by plants and microbes. The biological carbon fixation process, which uses photosynthesis, produces a variety of biomolecules such as carbohydrates, proteins, and lipids. In many species of plants and microbes such as bacteria, fungi, yeast, algae, and others, six different photosynthetic routes and some non-photosynthetic pathways to fix atmospheric CO_2 have been documented (What's the Difference Between Geologic and Biologic Carbon Sequestration 2021). The storage of atmospheric carbon in soils, vegetation, woody materials, and aquatic ecosystems is referred to as biologic carbon sequestration. Supporters of biologic sequestration, for example, want to assist to remove CO_2 from the atmosphere by boosting the growth of plants, particularly bigger plants like trees. Carbonates are inorganic and therefore can store carbon for over 70,000 years, but soil organic matter can only store carbon for a few decades. Scientists are investigating ways to speed up the carbonate formation process by incorporating finely crushed silicates into the soil, which would allow carbon to be stored for longer periods of time (Biological Carbon Sequestration 2021).

2.2   Absorption

As a result of its higher productivity and cheaper cost, absorption is the most mature and widely used CO_2 sequestration technology (Leung 2014). Physical and chemical absorption are the two phases in the entire carbon dioxide absorption process. The migration of CO_2 from the gaseous to the liquid phase over contact is referred to as physical absorption. The reaction CO_2 performs while in the liquid phase is then used to illustrate chemical absorption (Karlsson and Svensson 2017). To reduce greenhouse gas emissions, CO_2 should be eliminated, and SO_2 (sulphur dioxide) levels must be kept at very low levels. The most common method of purification is chemical absorption. Absorption techniques function by contacting the gas to be collected (Hoff 2021). Ionic fluid, monoethanolamine, calcium oxide, the engineered activity of lye and microalgae, smelling salts, and molten carbonate fuel cells (MCFCs) are now the most common absorption technologies used to sequester carbon dioxide across the world. In these technologies, the two most efficient ones are ammonia and calcium looping. Ammonia has a high CO_2 absorption rate. The ammonia volatilization problem, on the other hand, invariably leads to complications that are difficult to solve. Calcium looping is an energy-saving procedure that uses inexpensive absorbents. However, the absorbent's absorption capability declines fast during the absorption process. Accordingly, the investigation and advancement of CO_2 separation innovations will consistently be the examination focal point of researchers (Zhang 2021).

2.3 Adsorption

The adherence of a substance or material at an interface between a solid surface and a bathe solution is known as adsorption (Sparks 2005). Because of imbalanced forces, the particles or molecules on the crystal surface have extra surface energy, which prompts adsorption. At the point when certain substances crash into a crystal surface, they are attracted to it by the imbalanced forces and stay there. The adsorption interaction can be carried out into two gatherings dependent on the distinctive adsorption powers: actual adsorption (physical adsorption) and synthetic adsorption (chemical adsorption). Actual adsorption happens due to the interactivity of intermolecular forces (Van Der Waal's forces), as displayed in the adsorption of initiated carbon for gas. Chemical adsorption is adsorption that occurs as a result of chemical bonding. The production and breakdown of chemical bonds are both parts of the chemical adsorption process. Adsorption heat absorption or release is greater, and the activation energy required is correspondingly greater (Hu 2020). Albeit both assimilation and adsorption are reasonable advancements for carbon dioxide evacuation, the absorption innovation's energy cost makes adsorption by utilizing strong adsorbents the favored alternative today. In contrast with synthetic adsorbents (chemical), carbon dioxide adsorption by means of actual adsorbents (physical) (carbonaceous and non-carbonaceous materials) takes almost no energy. The justification for this is on the grounds that no new connections between carbon dioxide and the outside of the adsorbents (surface) are formed, bringing about a lower energy utilization for carbon dioxide recovery with high productivity (Abd 2020).

2.4 Membrane Separation

Membrane separation procedures necessitate the separation of two bulk phases by a third phase, the membrane. The feed is split into two stages in all membrane processes, permeate (materials that pass through the membrane) and retentate (materials that remain after passing through the membrane) (National Research Council 1998). A membrane is employed in the process to separate the target by rejecting undesired contaminants and allowing the others to pass through (Saleh and Gupta 2016). This method has a great deal of guarantee since it can join the phases of filtrate, extraction, and filtration into a solitary unit, and it can be utilized with an organic reactor to make another response partition measure (reaction separation) (Chen et al. 2017). For CO_2-related separations, numerous membrane materials have been explored and developed. Membrane-based separation technology, despite being a novel technique, is an energy-efficient and environmentally beneficial solution that is currently attracting special interest for certain CO_2 removal applications when compared to alternative chemical-based separation processes (Lei 2020).

2.5 Chemical Looping Separation

The essential aspects of chemical looping processes are that it can be utilized for fossil fuel conversion, as well as for the looping cycles' operational qualities and capacity to produce a sequestration-ready CO_2 stream (Cormos and IGCC 2017). The most peculiar emphasis of the circling measure (chemical looping process) of chemical looping combustion (CLC), is that a neat CO_2 stream with heat as its essential yield is obtained. Circling innovations empowered the interaction to be changed to deal with more perplexing feedstocks or produce substitute items, for example, blend gas or hydrogen (Voitic et al. 2018). Chemical looping separation (CLS) makes use of a solid-state oxygen carrier, which is an oxygen transfer substance. The procedure necessitates the use of two reactors. The oxygen carrier is preheated in the presence of air in the first step, at which point it preferentially collects oxygen and leaves a runnel of nitrogen. The oxygen-rich solid carrier is then moved to a second reactor, where it is presented to syngas-delivering coal that has been gasified. The oxygen from the carrier will respond with the syngas ignitable segments, resulting in hot exhaust gases containing high carbon dioxide levels. After that, it must be cleansed before compression and delivery. The procedure is still in its early stages of evolution (Breeze 2015).

2.6 Hydrate-Based Gas Segregation

Pre-combustion capture has a lot of potential with the hydrate-based gas segregation method (HBST), which is also a new procedure. The framework for partition is established by the precise separation of CO_2 content in fuel or fumes gas combination between the solid hydrate crystalline form and the vaporous phase during hydrate solid development (Babu 2015). In this cycle, traditional propellants are converted into a synthesis gas blend of H_2 (60%) and CO_2 (40%) with a little amount of H_2O, N_2, and CO. The vaporous stream typically has a pressing factor (pressure) of 2.5–5.0 MPa and a temperature of around 45 °C. The synthesis gas must first be separated from CO_2 before being conveyed to a gas turbine or an energy unit. Depending on the pressing factor state of the synthesis gas flow, this technology can be used to capture CO_2 directly from it, albeit a cooling framework is still required to lower the temperature of the stream (Sabil 2018).

2.7 Cryogenic Carbon Capture

Cryogenic Carbon Capture (CCC) is carried out under the post-burning procedure that can cut fossil fuel byproducts from fossil-filled power plants by 95–99% while utilizing a large portion of the energy and cost of standard carbon capture advances.
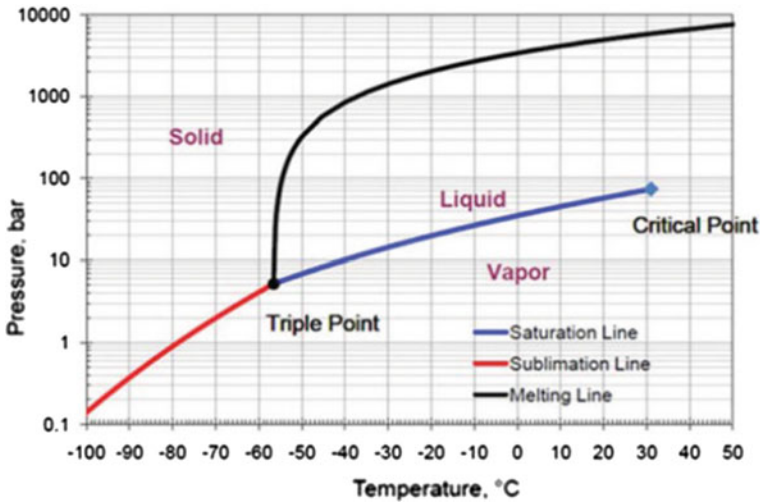
Fig. 4 Phase diagram of CO_2

Different toxins, like SO_X, NO_X, and mercury, are likewise taken out by CCC (Cryogenic Carbon Capture 2021). This method is based on CO_2's phase shift properties, which allow liquid or solid components to be separated from flue gas. Despite the fact that CCC approaches are still in their early stages of development, a number of intriguing methods have been developed. As seen in the phase diagram in Fig. 4, CO_2 can exist in solidified, fluid, and vapor stages relying upon temperature and pressure factors. The temperature and pressure factors at which every one of the three stages of gas exists together is known as the triple point. CO_2 arrives at its triple point at 56.7 °C and 5.1 atm (Rycroft 2019). CCC dries and cools exhaust gas from current frameworks, abjectly compacting it, refrigerating it to the temperature simply over where CO_2 sets. Further, it dilates the gas to cool it much more, compresses it, warms the CO_2, and releases the remaining vent gas by cooling the entering gases and settling a quantity of CO_2 as a solidified material that relies upon a definitive temperature. CO_2 in a fluid stage and a vapor nitrogen stream are the final results. CO_2 capture productivity is to a great extent affected by the pressing factor and temperature towards the finish of the dilate procedure. The procedure gets 99% of CO_2 at -211 °F (-135 °C) and 90% at -184 °F (-120 °C) at 1 atm (Baxter et al. 2009) (Fig. 5).

3 Discussion

There are various ways to reduce ozone harming substance releases from the mechanical region, including energy productivity, fuel trading, combine warmth and power, usage of renewable resources, and the more capable utilization of gas-producing
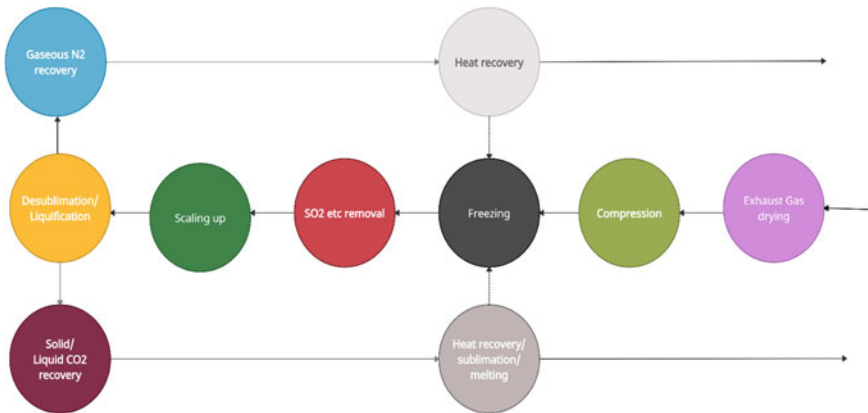
Fig. 5 Cryogenic carbon capture (CCC) process flow (Ammar Ali Abd 2020)

substances and sustainable materials. Various industrial cycles now lack a low-emission option alternative and will require carbon segregation and the ability to reduce releases as time goes on (Industrial and Greenhouse Gas Emissions 2021). Industry discharges from steel, synthetics, and other made items from non-renewable energy source ignition and the concrete formation measure address on normal 29% of the worldwide CO_2 emanations during an ordinary year, with a lot bigger portion of public outflows in non-industrial nations, e.g., 33 and 39% in India and China. To tackle emissions, steps are needed to curb emanations from this sector (Liu et al. 2020). The top five nations that produced the most carbon dioxide in the last accessible information in 2018 are China (10.06 metric giga-tons, GT), the US (5.41 GT), India (2.65 GT), Russia (1.71 GT), and Japan (1.16 GT). When the number of inhabitants in every nation is considered, the rankings change (i.e., per capita discharges) with Saudi (18.48 metric tons, T), Kazakhstan (17.60 T), and Australia (16.92 T) topping the list (Countries and Share of CO_2 Emissions 2020).

As a result, it is necessary to apply cost-effective technologies that are appropriate for the relevant industries in the respective countries. Table 1 summarizes the various capturing and sequestration technologies that have been researched and debated. There is not enough evidence in the literature on marine, oceanic, and biological sequestration to include it in the table. The meanings of the terminologies are well-known, thus there is no need to provide a definition.

4 Conclusion

The future extent of CO_2 removal is now a serious issue among research and the scholarly community while investigation of different innovations to curb CO_2 is going on in the nations. When it comes to long-term CO_2 removal, cryogenic carbon

Table 1 Carbon sequestration and capturing technologies

Carbon capture technologies	Removal efficiency	Advantages of the process	Disadvantages and shortcomings
Carbon capture and storage (CCS)	90% (How Efficient is Carbon Capture and Storage 2021)	CCS has the potential to reduce emissions at the site At point sources, CO_2 is easier to separate Additional pollutants can be eliminated simultaneously CCS has the potential to lower the social cost of carbon (Capture and Storage (CCS) 2021)	The cost is high as CCS adds four additional costs to a "normal" power station including capturing and transportation cost (Naucler et al. 2008)
Absorption	(> 99%) at 5 Nm^3/h and 30–35% at 35 Nm^3/h* (Øia et al. 2017)	Physical is suitable for situations with a high CO_2 partial pressure Because of the flue gas conditions: ambient pressure, low CO_2 concentration, and high volume, chemical is more suitable for a variety of industrial processes (Vega 2018)	Limited gas–liquid contact area, low CO_2 loading, and severe absorbent corrosion (Yu et al. 2012)
Adsorption	Achievable (> 85%) (Clausse et al. 2011)	it requires less energy and has a lower running cost, and it can remove nearly 90% of CO_2 (Krishnaiah 2014)	Because of their very hydrophilic nature, CO_2 adsorption capability is considerably reduced in the presence of moisture in gas, necessitating a high regeneration temperature (typically exceeding 300 °C) (Yu et al. 2012)
Membrane based separation	(> 40–80%) (He 2018)	There is no regeneration step (Bhatta and Lakshminarayana 2014)	Contaminants in the gas stream clogging (Bhatta and Lakshminarayana 2014) During the capture cycle, the deposition of an increasing layer of solid CO_2 on heat exchanger surfaces causes a drop in process efficiency (Barbieri et al. 2011)

Table 1 (continued)

Carbon capture technologies	Removal efficiency	Advantages of the process	Disadvantages and shortcomings
Hydrate-based gas segregation	–	Large gas storage capacity, moderate working conditions, low-cost, ecologically safe materials, and aqueous solution recycling (Li 2021)	energy consumption is high, investment costs are high, and efficiency is low, whereas research on more efficient hydrate-based method is still on the development stage (He 2017)
Chemical looping separation	Membrane-assisted chemical looping reforming (MA-CLR) in an efficient method provides an efficiency of 80% and a capture rate of 90% (Khan 2019)	intrinsic separation of CO_2 from a fuel source, completely eliminating the need for energy-intensive gas–gas separation expenses are some of the advantages (Hu 1187)	The selection and/or manufacture of an appropriate oxygen carrier material is the most difficult part of building a CLC process Full loop process modelling is still a difficult problem to solve (Moheb Shahrestani and Rahimi 2014)
Cryogenic carbon capture (CCC)	99% of CO_2 at − 211 °F (− 135 °C) and 90% at − 184 °F (− 120 °C) at 1 atm (Baxter et al. 2009)	Generation of pure liquid CO_2 ready for shipment Ideal for gas streams with a high pressure Chemical reagents are not required (Bhatta and Lakshminarayana 2014)	Refrigeration has a high energy cost Other pollutants must be removed to avoid freezing and blockage which will cost a lot (Bhatta and Lakshminarayana 2014)

[*] Normal meter cubed per hour gas flow from the absorber

capture (CCC) and carbon capture storage (CCS) have been determined to be the most effective. There is currently research underway to overcome the constraints of these extremely efficient technologies. Though various breakthroughs have been investigated by the research community, implementation of given sequestration and capturing technologies on a large scale is yet to be seen in practice due to various shortcomings such as effectiveness, high cost, and energy demands. Carbon concentration is expanding as time passes with population blast concerns scientific networks. If this rapid expansion of CO_2 into the environment cannot be checked soon, humankind might confront extremely huge climatic fiascos in coming years with more successive pandemics, floods, dry spells, fierce blazes, tornadoes, ice sheets liquefaction, etc. Therefore, it urges the need to bring down the CO_2 emanation straightaway. This can be accomplished by the aggregate dependable help of citizens, arrangements of governments, and explicit restrictions on CO_2 emission on industries along with implementing relevant technologies depending upon the

nation's demographic area. The discussed carbon sequestration technologies alone or in combination can be very helpful to capture CO_2 and contribute towards curbing hazardous effects of climate change.

Conflict of Interest The authors declare no conflict of interest.

References

Abd AA (2020) Carbon dioxide removal through physical adsorption using carbonaceous and non-carbonaceous adsorbents: a review. J Environ Chem Eng 8(5):104–142

Arora V (2019) Separation and sequestration of CO_2 in geological formations. Mater Sci Energy Technol 2(3):647–656

Babu P (2015) A review of the hydrate based gas separation (HBGS) process for carbon dioxide pre combustion capture. Energy 85:261–279

Barbieri G, Brunetti A, Scura F, Drioli E (2011) CO_2 separation by membrane technologies: applications and potentialities. skoge/prost/proceedings.icheap10

Baxter L, Baxter A, Burt S (2009) Cryogenic CO_2 capture as a cost-effective CO_2 capture process. In: 26th Annual International Pittsburgh Coal Conference 2009, p 1. Pittsburgh Coal Conference, Pittsburgh

Betts R (2021) Met office: atmospheric CO_2 now hitting 50% higher than pre-industrial levels, carbon brief-clear on climate, published on 16 March. https://www.carbonbrief.org/met-office-atmospheric-co2-now-hitting-50-higher-than-pre-industrial-levelslast. Accessed: 10 July 2021

Bhatta KG, Lakshminarayana (2014) Progress in hydrotalcite like compounds and metal-based oxides for CO_2 capture: a review. J Cleaner Prod 103:171–196

Biological Carbon Sequestration, https://climatechange.ucdavis.edu/science/carbon-sequestration/biological/. Last accessed: 26 Sept 21

Breeze P (2015) Carbon capture and storage. In: Breeze P (ed) Coal-fired generation. Academic Press, pp 73–86

Broecks KPF, van Rijnsoever FJ, Hekkert MP (2016) Persuasiveness, importance and novelty of arguments about carbon capture and storage. Environ Sci Policy 59:58–66

Carbon Capture and Storage (CCS) Pros and Cons. https://www.treehugger.com/carbon-capture-and-storage-ccs-pros-and-cons-5120005. Last accessed: 24 Sept 21

Chakraborty S, Jo BW (2018) Aqueous-based carbon dioxide sequestration. In: Pacheco-Torgal F, Shi C, Sanchez AP (eds) Woodhead Publishing Series in Civil and structural engineering, carbon dioxide sequestration in cementitious construction materials. Woodhead Publishing, pp 39–64

Chen H, Wang L (2017) Posttreatment strategies for biomass conversion. In: Chen H, Wang L (2017) Technologies for biochemical conversion of biomass. Academic Press, pp 197–217

Chow A (2014) Ocean carbon sequestration by direct injection. In: CO_2 sequestration and valorization. IntechOpen

Clausse M, Merel J, Meunier F (2011) Numerical parametric study on CO_2 capture by indirect thermal swing adsorption. Int J Greenhouse Gas Control 5(5):1206–1213

Climate Technology Centre & Network (CTCN), United Nations Framework Convention on Climate Change (UNFCCC) CO_2 capture technologies

Cryogenic Carbon Capture (2021) Our technology. SES innovation. https://sesinnovation.com/technology/carbon_capture/. Last accessed 14 June 2021

Cormos C-C (2017) IGCC with carbon capture and storage. In: Abraham MA (ed) Encyclopedia of sustainable technologies. Elsevier, pp 327–338

Controlling Industrial Greenhouse Gas Emissions, Regulation, US federal. Centre for Climate and Energy Solutions. https://www.c2es.org/content/regulating-industrial-sector-carbon-emissions/. Accessed 15 July 2021

Cuéllar Franca RM, Azapagic A (2017) Life cycle environmental impacts of carbon capture, storage, and utilization. In: Abraham MA (2017) Encyclopedia of sustainable technologies. Elsevier, pp 447–459

Duncan DW, Morrissey EA (2011) The concept of geologic carbon sequestration. U.S. Geological Survey

Each Countries Share of CO_2 Emissions (2020) Reports & Multimedia, Union of Concerned Scientists, 12 Aug 2020. https://www.ucsusa.org/resources/each-countrys-share-co2-emissions. Accessed 12 July 2021

Gayathri R, Mahboob S, Govindarajan M, Al-Ghanim KA, Ahmed Z, Al-Mulhm N, Vodovnik M, Vijayalakshmi S (2021) A review on biological carbon sequestration: a sustainable solution for a cleaner air environment, less pollution and lower health risks. J King Saud Univ Sci 33(2):101282

He J, Liu Y, Ma Z, Deng S, Zhao R, Zhao L (2017) A literature research on the performance evaluation of hydrate-based CO_2 capture and separation process. Energy Procedia 105:4090–4097

Hu H (2020) Physicochemical technologies for HRPs and risk control. In: High-risk pollutants in wastewater. Elsevier, pp 169–207

Hansen J, Sato M (2020) Global warming acceleration. Green Energy Times, 14 December 2020. https://greenenergytimes.org/2020/12/15/global-warming-acceleration-2/. Last accessed: 22 July 2021

He X (2018) A review of material development in the field of carbon capture and the application of membrane-based processes in power plants and energy-intensive industries. Energ Sustain Soc 8:34

How efficient is carbon capture and storage? https://climate.mit.edu/ask-mit/how-efficient-carbon-capture-andstorage#:~:text=CCS%20projects%20typically%20target%2090,will%20be%20captured%20and%20stored. Last accessed: 24 Sept 2021

Hoff KA (2021) CO_2 Capture—absorption processes. Find expertise—from ocean space to outer space. Sintef.com. https://www.sintef.no/en/expertise/sintef-industry/process-technology/co2-capture-absorption-processes/. Last accessed: 20 June 2021

Hu J (2018) Advanced chemical looping materials for CO_2 utilization: a review. Materials (Basel, Switzerland) 11(7):1187

IPCC (2005) IPCC special report on carbon dioxide capture and storage. In: Metz B, Davidson O, de Coninck HC, Loos M, Meyer LA (eds) Prepared by Working Group III of The intergovernmental panel on climate change. Cambridge University Press, p 442

Karlsson H, Svensson H (2017) Rate of absorption for CO_2 absorption systems using a Wetted Wall column. Energy Procedia 114:2009–2023

Khan MN (2019) Efficiency improvement of chemical looping combustion combined cycle power plants. Energy Technol 7(11)

Krishnaiah D (2014) Carbon dioxide removal by adsorption. J Appl Sci 14:3142–3148

Lackner KS, Alissa Park A-H, Miller BG (2010) Eliminating CO_2 emissions from coal-fired power plants. In: Sioshansi FP (ed) Generating electricity in a carbon-constrained world. Academic Press, pp 127–173

Lei L (2020) Carbon membranes for CO_2 removal: status and perspectives from materials to processes. Chem Eng J 401:126–084

Leung DYC (2014) An overview of current status of carbon dioxide capture and storage technologies. Renew Sustain Energy Rev 39:426–443

Li X-Y (2021) Review on hydrate-based CH4 separation from low-concentration coalbed methane in China. Energy & Fuels 35(10):8494–8509

Lindsey R (2020) Climate change: atmospheric carbon dioxide. NOAA Climate.gov, 14 Aug 2020. https://www.climate.gov/news-features/understanding-climate/climate-change-atmospheric-carbon-dioxidelast. Accessed: 23 July 2021

Liu Z, Ciais P, Deng Z (2020) Near-real-time monitoring of global CO_2 emissions reveals the effects of the COVID-19 pandemic. Nat Commun 11:5172

Miller BG (2005) Emissions control strategies for power plants. In: Miller BG (ed) Sustainable world, coal energy systems. Academic Press, pp 283–392

MohebShahrestani M, Rahimi A (2014) Evolution, fields of research, and future of chemical-looping combustion (CLC) process: a review. Environ Eng Res 19(4):299–308

Nakao S, Yogo K, Goto K, Kai T, Yamada H (2019) Introduction. In: Advanced CO_2 Capture Technologies. SpringerBriefs in Energy, Springer, Cham (2019)

National Research Council (1998) Chemical Industry. Separation technologies for the industries of the future. The National Academies Press, Washington, DC

Naucler T, Campbell W, Ruijs J (2008) Carbon capture and storage: assessing the economics. McKinsey & Company, Climate Change Special Initiative, United Kingdom

NOAA National Centers for Environmental Information, State of the Climate: Global Climate Report for July 2021, published online July 2021, https://www.ncdc.noaa.gov/sotc/global/202106. Last accessed 01 July 2021

Øia LE, Hansena PM, Henriksena M (2017) CO_2 absorption efficiency and heat consumption measured at high gas to liquid ratios in laboratory rig. Energy Procedia 114:1273–1281

Omae I (2006) Aspects of carbon dioxide utilization. Catal Today 115(1–4):33–52

Pan SY, Chiang PC (2012) CO_2 capture by accelerated carbonation of alkaline wastes: a review on its principles and applications. Aerosol Air Qual Res 12(5):770–791

Pollution: Carbon dioxide levels in atmosphere reach record high. PA Media, The Guardian, 7 Apr 2021. https://www.theguardian.com/environment/2021/apr/07/carbon-dioxide-levels-in-atmosphere-reach-record-high. Last accessed: 22 July 2021

Rabiu KO, Han L, Das DB (2017) CO_2 trapping in the context of geological carbon sequestration. In: Abraham MA (ed) Encyclopedia of sustainable technologies. Elsevier, pp 461–475

Rycroft M (2019) Cryogenic carbon capture for clean coal power generation. EE Publishers, 29th July, 2019, https://www.ee.co.za/article/cryogenic-carbon-capture-a-lower-energy-option-for-clean-coal-power-generation.html. Accessed 29 July 2021

Sabil KM (2018) Recent advances on carbon dioxide capture through a hydrate-based gas separation process. Current Opin Green Sustain Chem 11:22–26

Saleh TA, Gupta VK (2016) An overview of membrane science and technology. In: Saleh TA, Gupta VK (2016) Nanomaterial and polymer membranes. Elsevier, pp 1–23

Smith (2020) Global warming acceleration!—Hansen&Sato, Radio Ecoshock, 30 Dec 2020. https://www.ecoshock.org/2020/12/global-warming-acceleration-hansen-sato.html. Last accessed: 12 July 2021

Song C, Liu Q (2019) Cryogenic-based CO_2 capture technologies: state-of-the-art developments and current challenges. Renew Sustain Energy Rev 101:265–278

Sparks DL (2005) SORPTION | metals, encyclopedia of soils in the environment. Elsevier, pp 532–537

Vega F (2018) Solvents for carbon dioxide capture, carbon dioxide chemistry, capture and oil recovery. IntechOpen

Voitic G, Pichler B, Basile A (2018) Hydrogen production. In: Hacker V, Mitsushima S (eds) Fuel cells and hydrogen. Elsevier, pp 215–241

What's the difference between geologic and biologic carbon sequestration? https://www.usgs.gov/faqs/what-s-difference-between-geologic-and-biologic-carbon-sequestration?qt-news_science_products=0#qt-news_science_products. Last accessed 26 Sept 2021

Wilberforce T (2019) Outlook of carbon capture technology and challenges. Sci Total Environ 657:56–72

Wisconsin Department of Health Services (2021) Carbon Di Oxide, Environmental health. Last Revised 3 June 2021. https://www.dhs.wisconsin.gov/chemical/carbondioxide.htm. Accessed: 22 July 2021

Wilberforce T (2021) Progress in carbon capture technologies. Sci Total Environ 761:143–203

Yu C-H, Huang C-H, Tan C-S (2012) A review of CO_2 capture by absorption and adsorption. Aerosol Air Qual Res 12:745–769

Zhang C (2021) Absorption principle and techno-economic analysis of CO_2 absorption technologies: a review. In: International symposium on energy environment and green development. IOP conference. series: earth and environmental science, vol 657, pp 012–045. IOP Publishing

Feasibility Evaluation of Reactive Distillation Process for the Purification of Bioethanol

Ankur Kumar Gupta and Shashikant Yadav

Abstract Overuse of fossil fuels is causing their depletion in reservoirs and increasing the concentration of greenhouse gases in the atmosphere, causing climatic changes and other adverse effects like melting of glaciers. Bioethanol proves to be a promising alternative among biofuels, and the best replacements of fossil fuels because of its better burning property and lesser emissions of harmful gases. Due to the formation of an ethanol–water azeotrope, methods such as extractive distillation are used for its production. Alternative methods are being investigated because of the high cost of production by these methods, as these methods require the cost of additional equipment and solvent. This study focuses on the steady-state design of reactive distillation column for the production of bioethanol. Steady-state simulation is done on DWSIM. For this configuration, purity of ethanol in distillate and purity of ethylene glycol in the bottom product achieved is 99.98 and 96.52% respectively. The result shows the dependence of ethanol purity in distillate and conversion of water, on the position of feed plates when all other parameters are kept constant. Moreover, an applicability curve was drawn for the configuration in order to estimate the applicable region for better performance. Optimization is done using the graphical approach to obtain the optimum reflux ratio which is further used to configure the reactive distillation column. Finally, the temperature profile, conversion rate profile, mass transfer rate profile, liquid and vapor composition profile of the column are studied.

Keywords Bioethanol · Bioethanol purification · Process intensifications · Reactive distillation

A. K. Gupta · S. Yadav (✉)
Department of Chemical Engineering, Dr B R Ambedkar National Institute of Technology, Jalandhar, Punjab, India
e-mail: shashikanty@nitj.ac.in

107

1 Introduction

In the last decade, a lot of attention was given to the production of clean energy for sustainable development (Neeraj 2020; Arora et al. 2019; Yadav and Mehra 2019; Saran et al. 2018). Various methods to obtain clean energy are being adopted by different countries (Bora et al. 2014; Sciences et al. 2014). The rapid industrialization and higher population growth have exponentially increased the total energy consumption. The dependence of humans on fossil fuels plays a vital role in its depletion. This causes the price fluctuation, climatic changes, and adverse environmental impacts (Suali and Sarbatly 2012). The majority of the energy, is produced from fossil fuels, whereas only 10% of it is produced from renewable energy sources (Prakash et al. 2014). Among the human sources of producing greenhouse gasses (GHG) the combustion of fossil fuels (coal and petroleum) for electricity and heat production find their way at the top of the list representing 42% of the carbon dioxide production (International E. Agency, 2017). So, the critical challenge to the present world is to discover new alternate energy sources and to implement them to fight with the present problems and to move towards sustainable development for the betterment of the future generation.

Production of bioethanol emerges as a better option for the replacement of fossil fuels because of its lower GHG emissions, continuous supply of feedstock, ease of cultivation harvesting, and transportation (Grover et al. 2019). Moreover, it has some unique properties which contribute to the improvement of engine efficiency (Han et al. 2014; Ying et al. 2011). One of its major advantages is its compatibility with the engines. It can either be blended with gasoline or can be used as a single compound (Conde-mejía et al. 2016).

A lot of sources of bioethanol are present in the literature (Rathnayake et al. 2018; Maupoey and Maupoey 2017; Onay 2018; Derman et al. 2018; Oliveira et al. 2017). When bioethanol is produced, a lot of water is present in it. Water and ethanol form an azeotropic mixture and cannot be separated completely by the simple distillation process (An et al. 2015). Various methods are available in the literature for the separation of the ethanol–water mixture. Extractive distillation is widely used for large scale production of bioethanol. Various configurations of this process have been discussed in the literature (García-ventura et al. 2016; Errico and Rong 2013). Extractive distillation requires relatively more capital and operating costs as more number of plates are required for separation of ethanol and recovery of solvent (Errico and Rong 2013). Moreover, it consists of two energy intensification processes and the use of specific solvents like glycerol as an entertainer (Conde-mejía et al. 2016).

An alternate way to deal with this problem is the use of a reactive distillation column. Reactive distillation finds its way in the separation of water from bioethanol by achieving efficiency as high as 99.9%. Reactive distillation (RD), as the name implies, refers to the distillation process, which involves two unit operations (reaction and separation) in a single column. This saves both the capital cost and the operating cost of production (Shah et al. 2012; Lutze and Gorak 2013; Melles et al. 2000; Li

et al. 2016). RD is applicable only when the reaction conditions coincide with the separation conditions. In addition to this, the boiling point of each compound of a reaction plays a very crucial role in deciding whether the RD column is feasible or not. In the case of quaternary systems ($aA + bB \rightarrow cC + dD$), the boiling point of reactants should lie between boiling points of the products ($T_c < T_a < T_b < T_d$). In the case of ternary systems ($aA + bB \rightarrow cC$) with a single product, the boiling points of all the compounds should be different ($T_a \neq T_b \neq T_c$) (Muthia et al. 2019; Mäyrä and Leiviskä 2008).

Various parameters are studied in this literature in order to design an optimized reactive distillation column for this process. DWSIM was used for the simulation of the RD column because of its inherently strong and inbuilt thermodynamic database and robust numerical solvers.

2 Chemical Reaction Model

This section discusses the kinetic model, which is used in the simulation as well as different simulation modules and process conditions, which are used to set up the reaction system.

2.1 Chemical Reaction

The reaction system consists of one homogeneous reaction. The water present in bioethanol is reacted with Ethylene Oxide (EO) to form ethylene glycol (EG). In this way, the water present in the feed is consumed in the reaction to give high purity ethanol as a top product and high purity ethylene glycol as the bottom product.

$$C_2H_4O(EO) + H_2O \rightarrow C_2H_6O_2(EG) \Delta H = -80\,kJ\,mol^{-1}$$
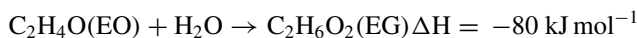
Amount of EO is taken in accordance with the composition and flow rate of feed bioethanol to maintain stoichiometry of the reaction and restrict flow of EO in distillate.

$T_{EO} < T_{H2O} < T_{EG}$, where T_{H2O}, T_{EO}, and T_{GO} are the boiling points of H_2O, EO, EG, respectively.

So, the reactive distillation unit is feasible as boiling points of all the three compounds are different.

2.2 Kinetic and Thermodynamic Model

Rate of reaction can be written as (Ciric and Gu 1994):

$$r = kx_{EO}.x_{H_2O}$$

x_{EO} and x_{H_2O} are the mole fraction of ethylene oxide and water. r is the rate of the reaction. k is the rate constant and is evaluated by Ciric et al. (1994).

$$k = 3.15 \times 10^{12} \exp(-9547/T)$$

In the reaction part, the homogeneous reaction was selected, and activities were chosen as a kinetic basis. Stoichiometric ratios, foreword orders, and rate coefficients were set from the above data. The (Non random two liquid) NRTL model is used to evaluate the activity coefficients to take into account non ideality in liquid solution as this model provides more flexibility in the description of phase equilibria than other activity models because of the extra non-randomness parameters. For vapor pressure, the Antoine model has been used. Heat capacity has been calculated using temperature correlation. K-value has been evaluated using the DECHEMA model. All these models are inbuilt in DWSIM version 5.8. The reference temperature is taken as 298.15 K.

In order to find the conversion of water, its molar flow rate in distillate and bottom were added and denoted as C_f. The formula for conversion of water is given as follow:

$$\text{Conversion} = (C_i - C_f)/C_i$$

where C_i is the molar flow rate of water in the concentrated broth feed.

3 Process Condition and Simulation Module

The reactive distillation column was simulated in this study. Feed flow rates of concentrated broth and ethylene oxide were maintained at 100 and 15 k mol/h, respectively. Pressure in the column was maintained at 450 kPa for the study. This pressure is chosen to maintain proper liquid and gas flow rates throughout the column, to get the best possible results. The composition of ethanol in the broth was taken as 0.85 for simulation. Two streams of feeds were introduced into the column at a stoichiometric ratio at two different trays. In the first case, the numbers of trays were fixed, and the positions of the feed trays were varied to get the data of purity of distillate at different configurations of the feed trays. In the second case, the purity of distillate was fixed at 99.99%, and the numbers of trays were varied. This gave the applicability curve between the number of transfer units (NTU) and the Reflux Ratio (RR).

Optimization is done using the graphical method to find the optimum reflux ratio (RR_{opt}). In this method, RR is plotted against reboiler duty and NTU. The intersection of these curves gives the optimum point corresponding to which RR_{opt} is obtained which is further used to configure the RD column. The optimized configuration was used to obtain temperature, composition, mass transfer rate, vapor composition, and liquid composition profiles for the column.

The steady-state simulations have been performed by the process simulator DWSIM. The column is shown in Fig. 1. A reactive distillation column consists of a rectifying zone, reaction zone, and a stripping zone. The concentrated broth was taken as feed 1, whereas Ethylene oxide was taken as feed 2. Feed 1 was introduced at the higher plate than feed 2 to maintain the counter-current flow in the reaction zone because the boiling point of ethylene oxide is lower than the boiling point of the broth. The overhead vapors were condensed into the liquid using a total condenser, to give distillate consisting of high purity ethanol, and a reflux stream was sent back to the column at the top tray. At the bottom, high purity ethylene glycol was reboiled and was sent back to the column at a boil-up ratio of 12.
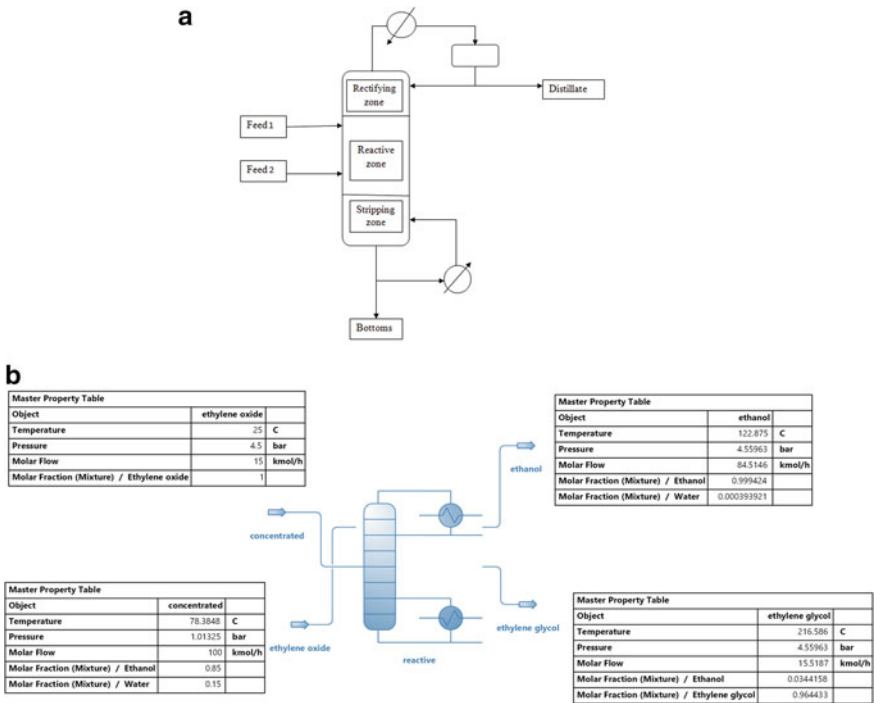
Fig. 1 Schematic representation of a reactive distillation column. **a** zones in a reactive distillation column, **b** using DWSIM simulation

4   Results and Discussion

4.1   Performance of RD Column

The performance of the RD column is decoded in terms of purity of ethanol in distillate and conversion of water in concentrated broth. Feed position is varied, keeping other parameters constant. The effect of this parameter on the purity of ethanol in distillate and conversion of water are discussed in this section.

4.1.1   Effect of Feed Stage Position on the Purity of Ethanol in Distillate

The effect of the position of feed trays on the purity of distillate has been studied. For this, all other parameters, like the number of trays, reflux ratio, were set. The position of feed 2 stage was varied from 18 to 12, and for each position of feed 2 stage, the position of feed 1 stage was varied to the number lesser than the feed 2 stage number. By doing this, a set of configurations was obtained. For each of the configurations, the mole percentage of ethanol in distillate and conversion of water were obtained. In this way, the dependence of purity of ethanol in distillate with respect to the position of feed plate was obtained and shown in Fig. 2. Four different plots were obtained for different feed-2 positions. Y-axis represents the mole percent of ethanol in the distillate, whereas X-axis represents the position of the feed-1 tray. N19, N17, N16, and N15 represent the location of feed-2 as 19th, 17th, 16th, and 15th stages, respectively. As the distance between the two feed trays
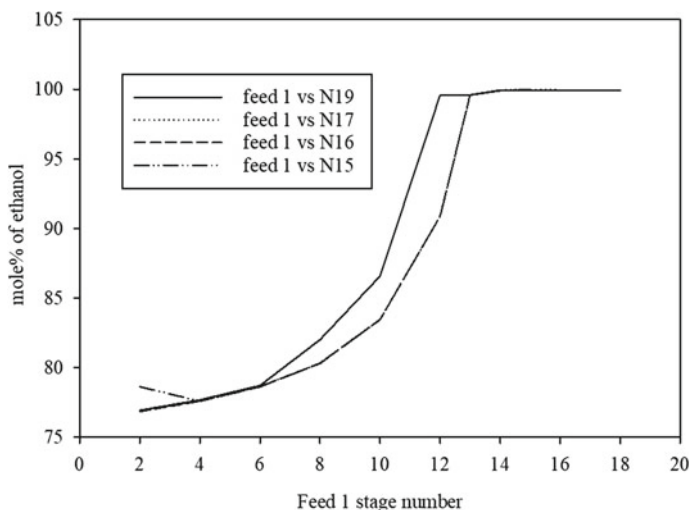
Fig. 2   Effect of position of feed trays on the purity of ethanol in the distillate
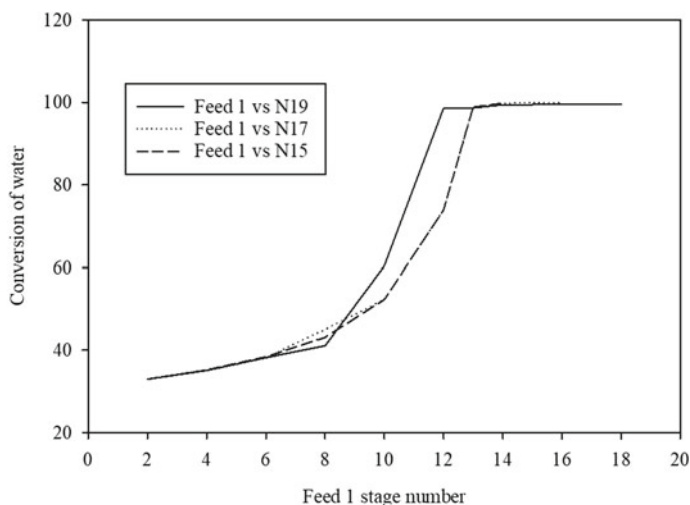
Fig. 3 Effect of position of feed trays on the conversion of water

is increasing, the purity of ethanol in the distillate is decreasing. This is attributed to the reaction which is responsible for the conversion of water. With the increase in distance between the feed trays, the composition of water in the liquid phase over the trays found to decrease resulting in lower reaction rate. Figure 3, showing the effect of conversion of water on feed trays distance. It is found that the conversion of water decrease with the increase in distance between the two feed trays. The highest conversion was achieved when feed-1 and feed-2 were introduced at stage numbers 16 and 17, respectively. The conversion of water, in this case, was 99.96%. Moreover, the purity of ethanol in distillate for this configuration was 99.99%, which is the highest of all configurations.

As the position of feed-2 is changing from 19 to 15 both the graphs are moving downwards. This shows that lower is the position of feed trays better is the separation of ethanol because of better contacting of the two phases as a greater amount of bubbling is occurring at the bottom part.

4.2 Applicability Curve and Selection of Best Possible Configuration

The applicability curve is the plot between RR and NTU. The applicability curve for this process is shown in Fig. 4. Applicability curve is an efficient method of finding the applicability area or an RD column. Purity was set at 99.98%, and NTU was varied. For different values of NTU, RR was obtained.
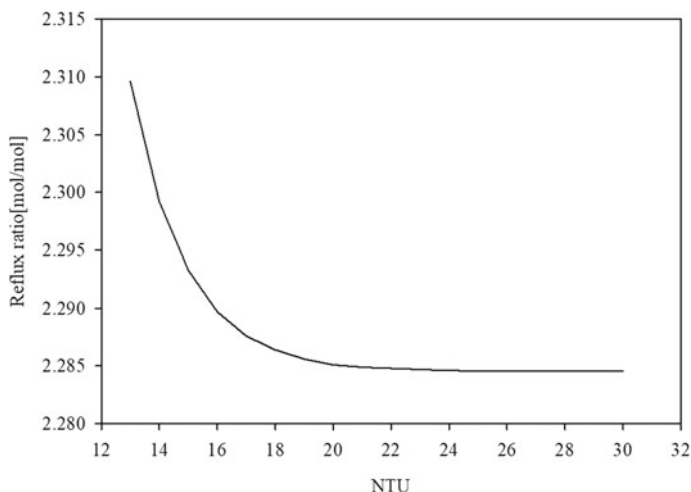
Fig. 4 Applicability curve for RD column for a purity of 99.98%

To choose the best possible configuration of the RD column, a graphical approach is used to optimize the column. The graphical method is the simplest method of optimization which gives a satisfactory result. RR is chosen as the variable to be optimized. RR is a function of NTU and reboiler duty. RR is varied keeping the purity of ethanol in distillate as constant at 99.98% to get NTU and reboiler duty. It is found that the RR is directly proportional to the reboiler duty and decreases with the increase of NTU. A plot is made based on these results as shown in Fig. 5. The point of intersection is the optimum point for the process which is found to be at RR = 2.29 and NTU = 16. Based on these results, the optimized configuration is shown in Table 1. This configuration is used to plot the temperature profile, conversion rate profile, vapor composition profile, liquid composition profile and mass transfer rate profile for the column. Figure 6 shows the temperature profile of the RD column. Change in temperature is occurring between stages 12 and 15. This change in temperature is evident in the fact that the reaction is occurring between these stages. Since, the reaction is exothermic, this resulted in the rise in temperature from stage 12 to stage 15. Figure 7 shows the conversion rates of water and EG at different stages. The conversion rates are found to be the maximum at stage number 13. This also shows that the reaction is occurring between stages 11 and 15. Figure 8 shows that mass transfer rates of ethanol, water, EO, EG at different stages. It is clear from the profile that, most of the mass transfer is occurring in the stages from 11 to 15. The possible reason for this is that the separation is occurring in the stages from 11 to 15. It is evident from the vapor and liquid profile from Figs. 9 and 10 respectively that the composition of ethanol in both liquid and vapor is very high from stage 1 to 11, whereas the composition of EO, water and EG are negligible.
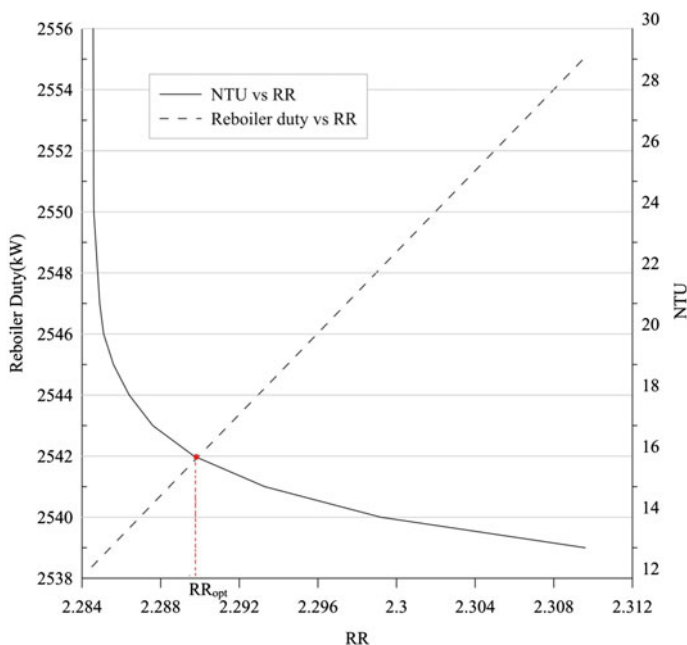
Fig. 5 Optimization plot of RD column for determination of RR_{opt} for the best possible configuration

Table 1 Parameters for best possible configuration

S. No.	Parameters	Values
1	NTU	16
2	Feed 1 stage number	13
3	Feed 2 stage number	14
4	RR	2.29
5	Operating pressure	450 k pa
6	Purity of ethanol in distillate	99.98%
7	Conversion of water	99.91%
8	Purity of EG in bottoms	96.52%

5 Conclusion

In this study, the steady-state design of a reactive distillation column for purification of bioethanol has been presented. Various factors affecting the purity of ethanol are studied. The purity of ethanol and conversion of water in concentrated broth is found to be increased with a decrease in distance between the two feed trays, keeping other parameters constant. Different plots are made to simplify the study. Finally, the best possible configuration was selected based on the graphical approach
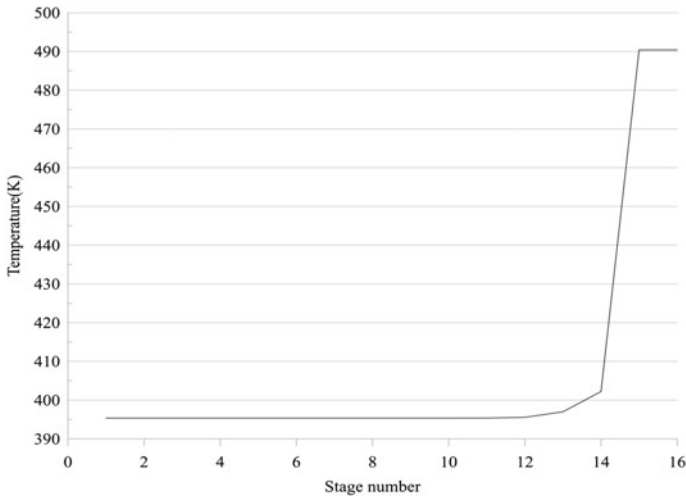
Fig. 6 Temperature profile for the RD column. NTU = 16, feed trays = 13, 14, RR = RR$_{opt}$ = 2.29. Dots represent the temperature at different trays
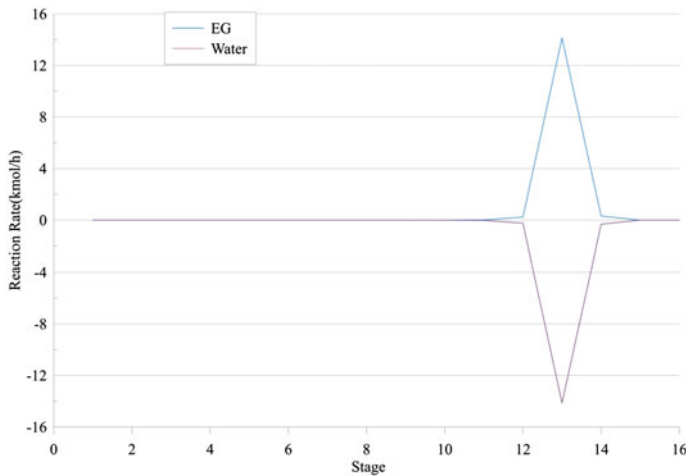
Fig. 7 Conversion rates of water and EG (k mol/h) at different stages inside the RD column. NTU = 16, feed trays = 13, 14, RR = RR$_{opt}$ = 2.29

of optimization. A purity of 99.98% ethanol is achieved in the study using 16 stages with feed 1 and 2 at 13th and 14th tray respectively and optimum reflux ratio of 2.29. Based on the optimized configuration, temperature, conversion, mass transfer rate, vapor composition and liquid composition profiles are obtained to support the study.
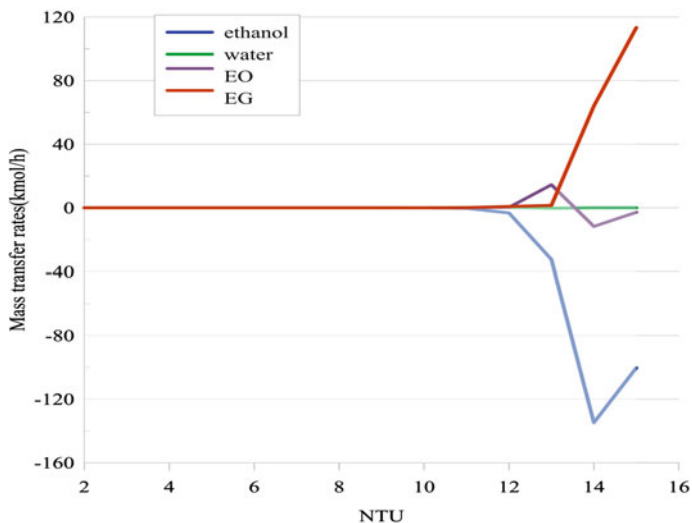
Fig. 8 Mass Transfer rate of ethanol, water, EO and EG in k mol/h at different stages inside the RD column. NTU = 16, feed trays = 13, 14, RR = RR_{opt} = 2.29
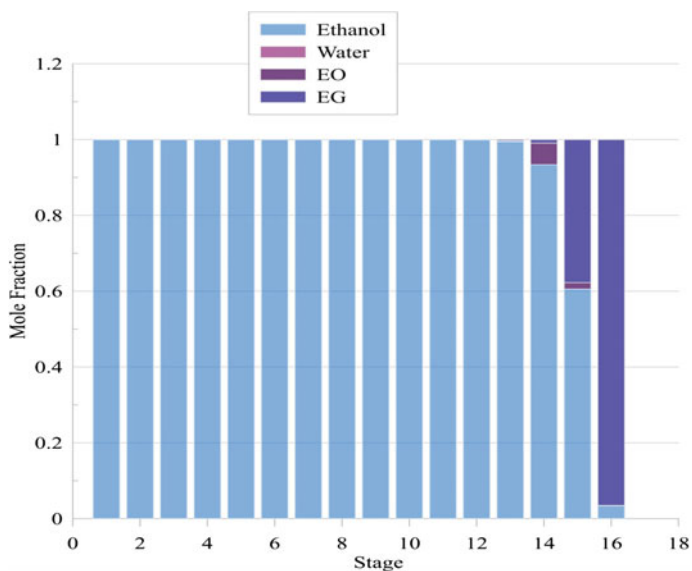
Fig. 9 Vapor composition at different stages of RD column for NTU = 16, feed trays = 13, 14 and RR = RRopt = 2.29
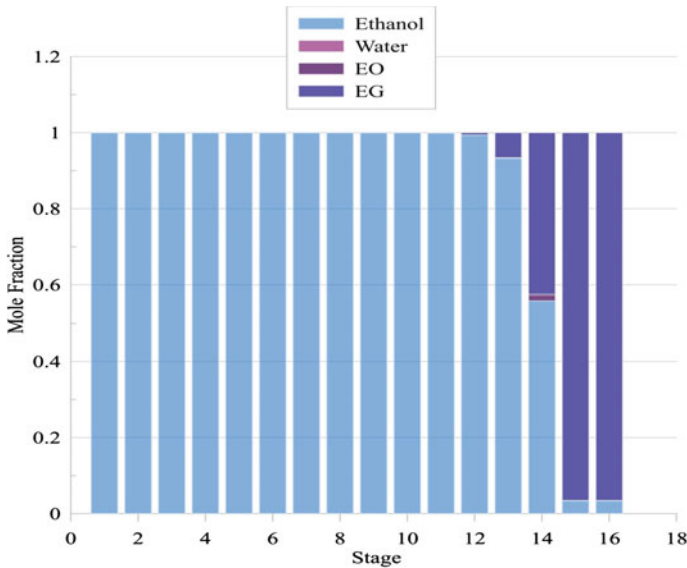
Fig. 10 Liquid composition at different stages of RD column for NTU $= 16$, feed trays $= 13, 14$ and RR $=$ RR$_{opt} = 2.29$

Conflict of Interest

There is no conflict of interest.

References

An Y, Li W, Li Y, Huang S, Ma J, Shen C, Xu C (2015) Design/optimization of energy-saving extractive distillation process by combining preconcentration column and extractive distillation column. Chem Eng Sci 135:166–178. https://doi.org/10.1016/j.ces.2015.05.003

Arora V, Saran RK, Kumar R, Yadav S (2019) Separation and sequestration of CO2 in geological formations. Mater Sci Energy Technol 2:647–656. https://doi.org/10.1016/j.mset.2019.08.006

Bora P, Jyoti L, Boro J, Mausoom M, Deka D (2014) Hybrid biofuels from non-edible oils: a comparative standpoint with corresponding biodiesel. Appl Energy 135:450–460. https://doi.org/10.1016/j.apenergy.2014.08.114

Ciric AR, Gu D (1994) Synthesis of nonequilibrium reactive distillation processes by MINLP optimization, vol 40

Conde-mejía C, Jiménez-gutiérrez A, Gómez- FI (2016) Purification of bioethanol from a fermentation process: alternatives for dehydration. Elsevier Masson SAS. https://doi.org/10.1016/B978-0-444-63428-3.50067-9

Derman E, Abdulla R, Marbawi H, Sabullah MK (2018) Oil palm empty fruit bunches as a promising feedstock for bioethanol production in Malaysia. Renew Energy. https://doi.org/10.1016/j.renene.2018.06.003

Errico M, Rong B (2013) Optimal synthesis and design of extractive distillation systems for bioethanol separation: from simple to complex columns. Elsevier B.V. https://doi.org/10.1016/B978-0-444-63234-0.50063-4

García-ventura UM, Barroso-muñoz FO, Hernández S, Castro-montoya AJ (2016) Chemical engineering and processing: process intensification experimental study of the production of high purity ethanol using a semi-continuous extractive batch dividing wall distillation column. Chem Eng Process Process Intensif 108:74–77. https://doi.org/10.1016/j.cep.2016.07.014

Grover A, Meher LC, Singh R, Singh A, Tiwari S, Dwivedi SK, Bala M (2019) Biofuels for defence use: past, present and future. Def Life Sci 04:3–11

Han S, Hyun S, Sik C (2014) Bioethanol and gasoline premixing effect on combustion and emission characteristics in biodiesel dual-fuel combustion engine. Appl Energy 135:286–298. https://doi.org/10.1016/j.apenergy.2014.08.056

International E. Agency (2017) Statistics

Li H, Meng Y, Li X, Gao X (2016) Chemical engineering research and design a fixed point methodology for the design. Chem Eng Res Des 111:479–491. https://doi.org/10.1016/j.cherd.2016.05.015

Lutze P, Gorak A (2013) Chemical engineering research and design reactive and membrane-assisted distillation: recent developments and perspective. Chem Eng Res Des 91:1978–1997. https://doi.org/10.1016/j.cherd.2013.07.011

Maupoey PF, Maupoey PF (2017) Accepted manuscript. J Clean Prod Prod. https://doi.org/10.1016/j.jclepro.2017.10.284

Mäyrä O, Leiviskä K (2008) Modelling in methanol synthesis

Melles S, Grievink J, Schrans SM (2000) Optimisation of the conceptual design of reactive distillation columns. Chem Eng Sci 55:2089–2097

Muthia R, van der Ham AGJ, Jobson M, Kiss AA (2019) Effect of boiling point rankings and feed locations on the applicability of reactive distillation to quaternary systems. Chem Eng Res Des 145:184–193. https://doi.org/10.1016/j.cherd.2019.03.014

Neeraj SY (2020) Materials science for energy technologies carbon storage by mineral carbonation and industrial applications. Mater Sci Energy Technol 3:494–500. https://doi.org/10.1016/j.mset.2020.03.005

Oliveira J, Almeida MF, Alvim MC, Dias JM, Renew SC (2017) Energy. https://doi.org/10.1016/j.renene.2017.07.052

Onay M (2018) Science direct bioethanol production from nannochloropsis gaditana in municipal Bioethanol production from Nannochloropsis gaditana in municipal wastewater * the heat demand-outdoor assessing the feasibility of using temperature. Energy Procedia 153:253–257. https://doi.org/10.1016/j.egypro.2018.10.032

Prakash J, Hou C, Majumder D, Bundschuh J, Kulp TR, Chen C, Chuang L, Chen CN, Jean J, Yang T, Chen C (2014) The production of biofuel and bioelectricity associated with wastewater treatment by green algae. Energy 78:94–103. https://doi.org/10.1016/j.energy.2014.06.023

Rathnayake M, Chaireongsirikul T, Svangariyaskul A, Lawtrakul L, Toochinda P (2018) Process simulation based life cycle assessment for bioethanol production from cassava, cane molasses, and rice straw. J Clean Prod. https://doi.org/10.1016/j.jclepro.2018.04.152

Saran RK, Arora V, Yadav S (2018) CO2 sequestration by mineral carbonation : a review. Glob NEST J 20:497–503. https://doi.org/10.1016/j.jhazmat.2016.06.060

Sciences N, Stefan J, Postgraduate I (2014) Sustainable development of energy, water and environment systems q. Appl Energy 135:597–599. https://doi.org/10.1016/j.apenergy.2014.09.002

Shah M, Kiss AA, Zondervan E, De Haan AB (2012) Chemical engineering and processing: process intensification a systematic framework for the feasibility and technical evaluation of reactive distillation processes. Chem Eng Process Process Intensif 60:55–64. https://doi.org/10.1016/j.cep.2012.05.007

Suali E, Sarbatly R (2012) Conversion of microalgae to biofuel. Renew Energy Sustain Energy Rev 16:4316–4342. https://doi.org/10.1016/j.rser.2012.03.047

Yadav S, Mehra A (2019) Mathematical modelling and experimental study of carbonation of wollastonite in the aqueous media. J CO2 Util 31:181–191. https://doi.org/10.1016/j.jcou.2019.03.013

Ying Y, Teong K, Nadiah W, Abdullah W, Peng C (2011) Second-generation bioethanol as a sustainable energy source in Malaysia transportation sector: status, potential and future prospects. Renew Sustain Energy Rev 15:4521–4536. https://doi.org/10.1016/j.rser.2011.07.099

A Review of Alternative Sustainable Methods of Ammonia Production

Aditi Bilgaiyan, Riddhi Goel, Sonali Singh, and Anand V. P. Gurumoorthy

Abstract Ammonia (NH_3), one of the most commonly synthesized chemicals worldwide, finds usage in vast applications of industry and commerce. The synthesis of ammonia by Haber–Bosch process is considered as one of the most significant discoveries in the field of Chemistry. Although the Haber process stands unparalleled in terms of the scientific marvel that it is, the rate at which the natural resources are depleting today do raise a question regarding its sustainability. Today, a substantial part of the world's production of ammonia is implemented using hydrogen (H_2) which is produced when natural gas, a fossil fuel, undergoes steam reforming. Carbon dioxide (CO_2) is left behind, which accounts for approximately half the amount of emissions from the whole process. The secondary feedstock, Nitrogen (N_2), is easily separated from air, which is 78% nitrogen. But the generation of the pressure required to react nitrogen and hydrogen in the reactors consumes more fossil fuels, which means more release of CO_2. The emissions continuously add up— Ammonia synthesis results in the consumption of approximately 2% of the world's total energy and produces 1% of its CO_2. The continuous depletion of the naturally occurring resources has led to extensive research to reduce the usage of fossil fuels in the process of ammonia synthesis worldwide. This paper aims to review renewable alternatives to the production of ammonia and its by-products, hydrogen and nitrogen, through methods which are sustainable and show a proven reduction in terms of the emissions emitted and the natural resources utilized.

Keywords Ammonia · Renewable resources · Haber's process · Alternate production · Sustainability · Green hydrogen

A. Bilgaiyan · R. Goel · S. Singh · A. V. P. Gurumoorthy (✉)
School of Chemical Engineering, Vellore Institute of Technology, Vellore, Tamil Nadu 632014, India
e-mail: anand.g@vit.ac.in

1 Introduction

1.1 *Ammonia Production via the Haber's Process*

Ammonia commands huge attention in today's industrial world covering industries such as food, chemicals, pharmaceuticals and energy-related industries. Almost 80% of the ammonia that is industrially produced is used as fertilizer in the agriculture sector worldwide. Apart from this, it is also used for purification of water supplies, for the production of refrigerants and explosives, manufacture of plastics, textiles, pesticides, dyes etc. It is even found in many households and in industrial-strength cleaning solutions. Ammonia is industrially synthesized using Haber's process (also known as the Haber–Bosch process).

Ammonia synthesis by Haber's process has been feeding mankind for more than a century. Production of Ammonia, be it naturally or synthetically, has served as the core of many chemicals. The Haber–Bosch process is arguably the predominant process used for the production of ammonia from nitrogen and hydrogen. Haber–Bosch was the foremost chemical process to utilize the high pressure of a chemical reaction. It combines nitrogen from the atmosphere with hydrogen under incredibly intense pressures and elevated temperatures. An iron catalyst empowers the reaction to be done at a lower temperature than would some way or another be practicable, while the expulsion of ammonia from the cluster when it is formed guarantees that an equilibrium preferring product is obtained. The lower the temperature and the higher the pressure utilized, the more prominent the extent of ammonia yielded in the blend. The process operates at high temperature and intense pressure and makes use of iron as a catalyst. The Haber–Bosch process for the synthesis of NH_3 is economically demanding since it consumes a large amount of energy. The equilibrium reaction is:

$$N_2 + 3H_2 \leftrightarrow 2NH_3$$
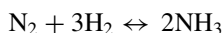
The cycle is exceptionally impervious to technological optimization. Can ammonia be produced at ambient conditions? At ambient conditions, the reaction rate is reduced to such an extent that it can barely be observed. The essential explanation is basically that the N–Ntriple bond, 940 kJ/mol, has to be fragmented before binding with the H atoms. This rate determining step decides the general response rate. Dinitrogen is relied upon to go through dissociative chemisorption on the surface of the catalyst to give N^*. A while later, each N^* reacts with $1.5 \times H_2$ to deliver NH_3. At last, NH_3 leaves the catalyst's surface under the weight of the other nitrogen particles. The devices utilized to sever the triple bond between the Nitrogen atoms can be separated into three ways: (1) reductive catalyst, which supplies electrons to Nitrogen atom (this happens in the Haber–Bosch method); (2) oxidative catalysts that remove electrons from Nitrogen atom; (3) extraordinary conditions, for example, plasma treatment, high voltage and photograph instigated electron elevation:

$$N_2 \rightarrow 2N*$$

$$N_2 - e^- \rightarrow 2N^+$$
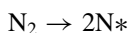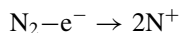
This technique by Modak (2002) devours large quantities of energy, preventing its cost-proficient industrial usage.

1.2 Drawbacks of Haber's Process

As our collective attempts to make industrial processes more environmentally friendly increase manifold, it becomes imperative to acknowledge the drawbacks that come with one of the most widely used processes commercially, Haber–Bosch Process. The commercial synthesis of Ammonia creates serious imbalances in the nitrogen cycle. A group of scientists pondered over the questions of planetary boundaries and their publication clearly shows that while we may have only just slipped past the fringe of the carbon dioxide periphery, the disturbance in the nitrogen cycle was predicted to be around three times more than the secure limit. It was suggested to reduce the fixed nitrogen additions to about a third of what it is currently at. Haber's process functions at high temperatures of 400–500 °C and high pressures of 200–300 atm, which require a lot of energy. To put into perspective, production of nitrogen fertilizers utilizes about 5% of the world's production of natural gas which is analogous to 1–2% of world's yearly energy utilization. This leads to high fossil fuel energy inputs which are not sustainable in the long term scenario. Current research at the Center for Evolutionary Biology and Ecology at the University of Oregon by Dr. J. Fox has found that the communication links between plants and the nitrogen-fixing bacteria are negatively affected by the use of excessive synthetic nitrogen fertilizers leading to damaging effects on soil organic matter and soil organisms. Excess runoff of the nitrogen fertilizer is known to cause ocean dead zones. The expanding use of pesticides as well as N_2 fertilizer into the topsoil and environment brings with it a plethora of significant ecological provocations in the form of emissions of nitrous oxide, groundwater contamination, and surface water eutrophication (University of Oregon 2007). The importance of this enriching process can never be understated; but a question about the enrichment of this planet is long overdue, especially in times like these.

This paper aims to review renewable alternatives to the production of ammonia and its by-products, hydrogen and nitrogen, through methods which are sustainable and show a proven reduction in terms of the emissions emitted and the natural resources utilized.

2   Methods for Ammonia Production

The alternate methods of ammonia production can be broadly classified as: (i) gasification, (ii) electrochemical route, (iii) thermochemical route, and (iv) miscellaneous renewable methodologies. These methods are reviewed in detail below.

2.1   *Ammonia Production from Gasification*

Akbari et al. (2018) proposed black alcohol gasification plant which consists of four significant units: acid gas removal (AGR), the air separation unit (ASU), black liquor vaporizer and synthesis of ammonia. Black liquor which leaves the final evaporator in the mash factory passes into the vaporizer, where it undergoes gasification with O_2 via ASU. The product in the form of raw synthesis gas which generally consists of Carbon monoxide, Carbon dioxide and Hydrogen, and limited quantities of contaminations like (COS)H_2S (carbonyl sulfide). To avoid harming the downstream smelling salts, acidic gases, for example, COS, H_2S and CO_2 are taken out in the corrosive gas evacuation unit before the crude synthesis gas is sent to the alkali blend reactors. The subsequent clean gas includes practically unadulterated H_2, which is shipped off to the alkali combination plant. Other than H_2, N_2 is fundamental for the production of ammonia and is provided via the ASU where air is separated to its essential constituents. The main distinction between the co-gasification cases and black liquor gasification is that the former has a dryer to dry the sludge to a dry state of 80% and a blender to blend black liquor in with the dried slurry.

2.2   *Electrochemical Method*

Synthesis of ammonia by electrochemical means was first experimentally demonstrated in 1998 (Licht et al. 2014). In this method, gaseous H_2 was passed over the anode, which was transformed to protons. The protons produced were electrochemically transferred to a cathode which then reacts with Nitrogen to produce Ammonia by virtue of imposition of voltage. Recently, electrochemical production of NH_3, a substitute to the Haber–Bosch process, has been attracting more attention due to its environmentally friendly approach. A strategy for electrochemical ammonia gas synthesis of including an electrolyte between the negative electrode and the positive electrode that gives H_2 gas to the negative electrode reacts with negatively charged N_2-containing species present in the electrolyte at the negative electrode to form an adsorbed N_2 species, and reacting the H_2 with the adsorbed N_2 species to produce NH_3. Ideally, the H_2 gas is given at the negative electrode by passing the hydrogen

gas through a permeable anode substrate. It is likewise expected to form the negatively charged N_2-containing species in the electrolyte by decreasing the nitrogen gas at the cathode.

Licht et al. (2014) went over an electrochemical method where ammonia can be synthesized by electrolysis of steam, air in a fluid hydroxide suspension of nano-Fe_2O_3. At nearly 200° in an electrolyte with a molar extent of 0.5 NaOH:0.5 KOH, NH_3 is manufactured at 1.3 V under two mA/cm^2 applied at 35% efficiency. Hayes (Nkepang et al. 2019) demonstrated an easy process to synthesize NH_3 from methanol in a single step that uses a low energy cyclotron. A study approaching electrochemical ammonia synthesis in a medium of molten salt modeled using electrochemical impedance spectroscopy was demonstrated by Khalid (Bicer et al. 2020). For the electrochemical synthesis of ammonia, a certain amount of current or potential is supplied to the electrodes which are obtained via the molten salt electrolyte. Nitrogen and hydrogen are right away utilized to carry out electrochemical synthesis of NH_3 at the electrodes. Nitrogen accepts the electrons via an external power supply. Thus, N_2 gas transported through the porous nickel cathode is reduced to nitride and moves to the other electrode where hydrogen is supplied. Hydrogen joins with nitrogen to produce ammonia at anode. The study proposed by Bicer et al. (2017) consisted of a Haber–Bosch plant and an electrolyzer for the synthesis of ammonia. George (Marnellos et al. 2000) studied ammonia synthesis from its elements in a solid state proton conducting reactor at atmospheric pressure. H_2 flowing through the anode was then converted to the protons which was then transferred through solid electrolyte and reached the cathode where nitrogen was passed. More than 78% of hydrogen was then converted to ammonia.

The reaction energy of NH_3 combination is supported at elevated temperatures. Nonetheless, general electrolytes could not be worked in high temperature areas. Profoundly proton-conductive solid state substances operating at elevated temperatures were found in the 1980s. Marnellos and Stoukides (1998) initially showed the electrochemical production of Ammonia from Nitrogen and Hydrogen utilizing a strong proton conductor. Generally, the Solid State Ammonia Synthesis (SSAS) framework is made out of two permeable terminals isolated via a thick strong electrolyte, which encourages particle transport of protons or oxide anions. NH_3 production in solid state electrolytes is generally directed at raised temperatures, due to increased reaction energy as well as significantly supported conductivity of electrolytes. An obvious production rate of up to 10^{-8} mol/(cm^2-s) can be accomplished from Nitrogen and Hydrogen, however this exothermic reaction is not thermodynamically ideal at high temperatures, requiring a compromise for enhancing the ammonia yield. Hydrogen production via natural gas reforming is energy concentrated and results in a large portion of CO_2 discharge. In spite of the fact that NH_3 production from N_2 and H_2O is endothermic and hypothetically sans carbon, the low conductivity of O^{2-} limit NH_3 yield. Contrasted with SSAS, molten electrolytes improve the ionic conductivity and decrease the working temperatures of the products. In liquid alkali metal salts, N^{3-} is settled and performs as an intermediate product from N_2 to NH_3. Besides, protic solvents are avoided, which dispenses with the hydrogen evolution response (HER).

Low-temperature electrochemical NH_3 synthesis in fluid electrolytes has pulled in impressive research potential. From one perspective, NH_3 synthesis at low room temperature could considerably diminish the energy utilization. Then again, H_2O is universally utilized as the proton source rather than H_2, which decreases the cycle cost and represses ozone depleting substance emanation in a general sense. Solid or liquid salt electrolyte-intervened N_2 reduction frameworks contain restricted or zero water atoms, bringing about an inconsequential hydrogen development. In this manner, research on NH_3 blend in strong or liquid salt media basically centers on electrolytes and the framework arrangement to reduce working temperatures and upgrade particle conductivity. In principle, given an exceptionally dynamic electro-impetus, Nitrogen Reduction Reaction (NRR) can continue in a restricted district of negative possibilities without inciting H_2O decrease at any given pH surrounding. Nonetheless, the majority of electro-impetuses have an inadequate action toward Nitrogen Reduction Reaction (NRR). Accordingly, NH_3 must be manufactured at more negative potential as compared to water reduction, where most electrons can support H_2 production.

2.3   Thermochemical Method

The Haber–Bosch method has restrictions because of a negative thermodynamic balance for ammonia production, which brings about low yields per go through the converter. Likewise, synthesizing the hydrogen and nitrogen feedstock for the cycle is an energy intensive cycle. Gálvez (2007) studied ammonia synthesis through a two-step recurring process as another possible alternative in contrast to the Haber–Bosch regular synthesis method (Heidlage et al. 2017). The main heat absorbing process is the preparation of Aluminum Nitride involving carbothermic decrease of Alumina in a dinitrogen environment at over 1500 °C. The secondary heat releasing process is supposed to be the steam-hydrolysis of Aluminum Nitride to deliver Ammonia and change Alumina. Solar thermochemical ammonia synthesis (STAS) demonstrated by Bartel (2016) is an expected course to synthesize ammonia from water, concentrated daylight and air. This process includes chemical looping of a functioning reduction–oxidation pair that recurs between a given metal nitride for example, Aluminum Nitride and its integral metal oxide viz., Alumina to produce ammonia. Thermodynamic cycle examination studied by Ronald (2012) demonstrates that a metal-based solar powered thermochemical Ammonia synthesis carried out at 1500 K or below, along with thermochemical hydrogen synthesis from water can be operated at a net-effectiveness from 23 to 30% (LCV of ammonia compared with an absolute energy input parameter).

Table 1 Comparison of the most acclaimed methods for NH_3 synthesis

Energy source	Process utilized	Energy MJ/t ammonia	Carbon dioxide emissions t/t ammonia	Greenhouse gas index*
Coal	Partial oxidation	42,000	3.8	238
Naphtha	Steam reforming	35,000	2.5	153
Natural gas	Steam reforming	28,000	1.6	100
Heavy fuel oil	Partial oxidation	38,000	3.0	188

* Using natural gas as the base source, GHG Index depicts the relative carbon intensity of various sources of energy
Source Initiating New Projects in the Ammonia Sector (Prince 2007)

2.4 Renewable Methodologies

Increasing world population has put pressure on the food supply chain. Synthetic fertilizers like Urea have helped in increasing the farm productivity by providing essential nutrients like N to the Soil. Urea is produced by reacting Nitrogen and Hydrogen at high pressure and temperature (Abdel-Aal et al. 1999). Nitrogen is sourced from Air whereas Hydrogen is produced by: Natural Gas or naphtha undergoing steam reforming, Heavy Fuel Oil or Coal encountering partial oxidation. Energy consumed for production of urea has improved by about 30% over the years due to improved efficiency of equipment used. Most of this energy is required for steam reforming (an endothermic reaction) and compression of feed stocks to reaction pressure of 200–250 bar. Both steam reforming as well as partial oxidation processes generate CO_2 as a co-product of reaction along with desired Hydrogen. As per one study conducted by IFA, CO_2 produced per MT of NH_3 from various conventional techniques is given in Table 1.

CO_2 is identified as a greenhouse gas and adds to global warming. Globally, production plants of ammonia produced roughly 157 million metric tons (t) of ammonia in 2010, as given in the Institute for Industrial Productivity's Industrial Efficiency Technology Database. This is about 1% of CO_2 emitted worldwide.

Ammonia based synthetic fertilizers will continue to play a significant role in ensuring availability of food to the global population. Attempts are in progress to reduce the CO_2 intensity of this process and hence make it Green.

2.4.1 Alternates Available

Majority of CO_2 in Ammonia manufacturing is produced during Hydrogen production. We can achieve significant reduction in CO_2 emissions by using a greener approach for production of Hydrogen.

Options practical for Hydrogen can be gasification of biomass and electrolysis of water by sustainable means, specifically biomass to ammonia (BtA) and power to ammonia.

Biomass to Ammonia

In this process, Biomass sourced from industrial processes or agricultural waste is gasified to produce a composition of CO, H_2, and CO_2. This mixture is then passed via a synthesis gas reactor to increase the concentration of Hydrogen. Acid gases contained in the mixture are removed in the acid gas removal section. Clean gas is now passed through the Methanation process to produce High Purity Hydrogen.

Just about all carbon in biomass is ultimately transformed to carbon dioxide and the resulting energy efficiency of the BtA (Zhang et al. 2020) is found to be fewer than 50%. A techno-economical study of ammonia synthesis using an integrated gasification of biomass in pulp and paper mills clearly stated that the overall efficiency increased to 55%. A standard natural gas based NH_3 synthesis unit is studied in contrast to a group of unconventional biomass based NH_3 synthesis plants. The outcomes indicated that the exergy efficiency of the biomass based ammonia synthesis and natural gas plants are on average 41.3 and 65.8%. Comparing these with fluidized and moving-bed gasification mechanism, an entrained-flow gasifier (EFG) is currently becoming conventional method for coal-to-ammonia processes in coal gasification and integrated-gasification combined cycles, in which gasification agent is pure oxygen and very high amount of reaction rate is enabled and transformation of biomass to synthesis gas with low CO_2 or CH_4 and nearly no gaseous hydrocarbons or tar due to elevated operating temperatures ranging from 1200 to 1600 °C and pressure of about 1–80 bar. Owing to the higher oxygen demands, a big air separation unit (ASU) is required to be established, which will give N_2 as a by-product that can be used as the origin of N_2 for synthesizing NH_3.

Green Power to Ammonia Production

Alternatively, Electrolyzer can be used for production of Hydrogen by electrolysis of water. Power required for electrolysis is generated by renewable alternatives like solar, wind or hydro. Combining the method of power to ammonia and conventional Haber–Bosch processes (Zhang et al. 2020) helps reduce the usage of fossil fuels or non-renewable resources. The electrolyzer electrochemically parts water into H_2 and O_2. Compared to the moderate temperature electrolysis innovations, specifically polymer electrolyte layers electrolysis and alkaline electrolysis, strong oxide electrolysis (SOE) at high temperature can possibly accomplish a superior coupling with NH_3 production method, because of (1) heat incorporation with ammonia blend to improve system level application, and (2) more electrical effectiveness with steam electrolysis above 650 °C. There have been quite a few papers published, e.g., by Cinti et al. (2017) that evaluated the analysis and design of SOE-combined PtA systems.

Moreover, the economic feasibility and the overall performance of the entire Power to Ammonia process with SOE are inadequately studied from the viewpoint of the process engineering system.

A latest way of cascaded ammonia synthesis (Ishaq and Dincer 2020) was proposed by introducing a clean hydrogen production mechanism. PEM electrolyzer supplies the hydrogen, nitrogen is separated by using PSA from air, and then they encounter compression, after which they are supplied to the cascade of NH_3 production reactors. This method of introducing both the reactors in arrangement prompts an expansion in the NH_3 transformation rate and decrease in the reuse cycles alongside the expense of warming and repressurizing. The examination suitably demonstrates that the scaling of this framework is conceivable in the current commercial NH_3 plants by disposal of the petroleum gas changing and presentation of green power based water electrolysis for the creation of hydrogen and the other reactor establishment in arrangement for cascaded ammonia production to accomplish elevated rates of transformation. In a study on low-carbon based ammonia production and its techno-economic feasibility (Arora et al. 2018), bituminous coal and a eucalyptus-based biomass, present near a CO_2 sequestration plot, were singled out as the two carbonaceous raw materials. A CO_2 removal step is implicitly involved in the synthesis of NH_3 from any carbon-based feedstock; thus, only the Carbon dioxide pressurization towards a supercritical state is necessary before transferring it to the storage location. For the same form of Carbon footprint, the coal-based ammonia method mentioned above is considered to be more economically efficient compared to the biomass-based process. Having said that, one has to consider the fact that the biomass-based method has the prospect to become carbon negative by trapping the biogenic carbon dioxide, which becomes impossible in a coal-based method. On operating a Linde's double column (Sánchez and Martín 2018) for air separation, it gives nitrogen. Hydrogen is synthesized via water splitting. Then, H_2 and O_2 undergo purification to eradicate traces of chemicals, water etc. Next, NH_3 is produced in a packed three bed reactor (Elishav et al. 2020). Both the cooling designs, direct and indirect cooling, were considered. Condensation using the cold air helps in the recovery of ammonia. Power required for electrolysis and compression is acquired from the renewable sources—solar, wind, and photovoltaic energy. The method was simulated by developing substitute models for all the units with added details to the Linde's column, ammonia recovery, electrolyzer, and synthesis reactor. Specifically, the multi-bed reactor is simulated offline to confirm its operation and the conversions. The entire method is drawn up as a mixed-integer nonlinear programming (MINLP) problem. For the production of ammonia, indirect cooling and solar energy are chosen.

In another approach, hydrogen synthesis through traditional methane reforming via steam (Chisalita et al. 2020) along with the gas–liquid CO_2 absorption were studied. Energy and mass balances from process flow modeling is utilized as the basis for the environmental study using Life Cycle Assessment (LCA) tool. System parameters examined in this study are: (i) primary methods include H_2 synthesis, ammonia synthesis, separation of CO_2; (ii) upstream methods include natural gas, nitrogen, and (iii) downstream methods include carbon dioxide compression, transport, storage, and degradation of solvents/oxygen carriers. The outcomes indicate that

the natural gas-based NH_3 production combined with chemical looping H_2 synthesis offers the most observed decrease in Global Warming Potential. All other green ammonia production processes can be attained by supplying H_2 from electrolysis of water to the Haber–Bosch process (possible only when electricity is acquired via renewable energy sources) or from the other low-carbon feed stocks. Xu et al. (2018) invented a mathematical solution to evaluate the feasibility of low-carbon ammonia synthesis paths in China, in which hydropower electrolysis-based ammonia synthesis ranked foremost, accompanied by solar, biomass, wind and nuclear high-temperature electrolysis-based systems. Orhan et al. (2012) studied the synthesis of green H_2 via thermochemical water splitting incorporating renewable (nuclear) energy. The synthesis of hydrogen via the method of water electrolysis established on wind and solar energy was also studied.

Ammonia can be straight away synthesized via air and H_2O (Lan et al. 2014) at surrounding parameters, bypassing the dissociation of N_2 and synthesis stage of hydrogen, but it is necessary to acknowledge that the production of ammonia from water and air at high temperatures may be feasible if the oxidation of NH_3 is steady too. The N_2 is separated from air using Linde's double column in which conversion can be done in high volume. Electrolysis is done in order to separate H_2 from water by splitting it into H_2 and O_2. The little amount of moisture content is removed by condensation. The O_2 obtained can be compressed and stored for further uses. H_2 stream is then sent in a reactor where traces of impurities are removed. In modeling or process optimization various factors are taken into account like thermodynamics; equations are obtained on the basis of chemical equilibria, kinetics of the reactions involved, mass and energy balance of the constituents involved in the process. CHEMCADE can be used to perform simulations of the process. Enough electricity should be generated and stored so as to perform the process; specific units of power need to be stored in order to keep the process going. The final step is the ammonia production which is done by using a synthesis loop. The gases are heated and compressed as per the requirement of the process. Two methods can be used for the same; direct cooling three bed reactor and simpler single chamber reactor. In both the processes the outlet stream is cooled to obtain ammonia.

When we talk about using renewable ways to produce ammonia, there are several other factors which need to be given attention like the cost of consuming renewable energy and power used etc. The cost of storing and scheduling the energy generated by solar or wind sources can be a bit high. Proper calculation and planning needed to be carried out in order to optimize the cost and also the loss of energy. In producing NH_3 through an electrochemical process, water needs to be electrolyzed in order to get H_2 and O_2 is formed as a byproduct and N_2 from air is extracted. This process can take a lot of effort to put in, to combine all these processes and keep in mind the optimization of cost and energy lost. Before installing a plant there are few things to scrutinize like, planning a proper general overview of the plant concept and then working on the modeling challenges. These can become obstacles in the electro- and thermal chemical processes. The process of obtaining N_2 and H_2 renewably, can contribute substantially in reduction of pollution and carbon footprint. After acquiring N_2 and H_2, the elements can be combined to get NH_3.

A pilot scale ammonia synthesis, fueled by wind source, requires the primary energy input from 15 to 107 MJ per functional unit while releasing considerably negligible amount of carbon dioxide, which shows the prospect to notably lessen the non-renewable inputs and greenhouse gas (GHG) releases in contrast to the conventional production method of NH_3. Cinti et al. (2017) showed that the synthesis of NH_3 via energy from the solar/wind sources through solid oxide electrolysis may lead to a reduction of 40% of the energy input in contrast to the natural gas unit and acquire zero emissions of carbon dioxide. Beerbuhl et al. (2015) studied the integrated capacity and lineup arrangement of an adaptable electricity-to-H_2-to-NH_3 plant, relating to its rich potential to include alternative sources of electricity into the synthesis of NH_3. Arora et al. (2018) showed that although the environmental and economic parameters of a geographical location is an important factor for each method, the biomass-to-ammonia methods could acquire attractive reduction in the GHG emissions in contrast to the traditional systems based on fossil fuels. Cinti et al. (2017) described three encouraging NH_3 production pathways in the form of biogas reforming, biomass gasification and water electrolysis (high temperature) by using solar or wind energy, and showed that the path of electrolysis of water is considerably a better choice over the other two when looked at from different viewpoints. Tunå et al. (2014) implemented a techno—economic study of the synthesis of ammonia through grid-based electricity processed from biogas, wind energy and woody biomass, which clearly showed that although the technology based on biomass does consume more energy, it needs low costs as compared to the other processes.

3   Conclusion

As the world moves ahead towards a sustainable future, new technologies emerge simultaneously. Conventionally manufactured by the Haber–Bosch process, ammonia has become a vital part of the industrial sector as well as of domestic usage. The ammonia production industry has seen a revolution in the past few years, as the demand for fertilizers along with industrial and household cleaning products increased. With the growing demand for use of renewable energy, ammonia production has seen various new methods like electrochemical processes, production through gasification and renewable methodologies as discussed above. However none of these processes have been commercialized. They are still at experimental stage or pilot plant stage. Furthermore, it must be emphasized that the Haber–Bosch process remains the most economical and most efficient process to date.

As mentioned earlier, the Haber–Bosch process uses natural gas or other fossil fuels to produce ammonia. The need of the hour is to reduce fossil fuel usage and promote renewable energy for a better future, which has played a key role in developing and studying various alternative methods for the same. The regular method emits large amounts of CO_2, has high energy consumption, resulting in more use and therefore depletion of fossil fuels. Discussing the mentioned alternatives for

ammonia production proves that they are equally efficient but more research needs to be conducted in order to attain efficiency like the novel Haber–Bosch process.

The course of transforming our industries to sustainable production will take time and substantial efforts, not only of industrialists but also of officials and governments. Many governments are extending support to this sector as the focus increasingly shifts towards a sustainable future. Extensive research in the field may possibly result in the alternative methods of production of ammonia to become major contributors in the fertilizer industry and subsequent ammonia products. Ammonia, being a vital part in the process of running the world fertilizer production in large quantities daily across the world, clearly requires a few more energy efficient methods of production to take over in helping us achieve a greener and better future.

References

Abdel-Aal H, Shalabi M, Al-Harbi D, Hakeem T (1999) Simulation of the direct production of synthesis gas from sour natural gas by noncatalytic partial oxidation (NCPO): thermodynamics and stoichiometry. Indus Eng Chem Res 38(3)

Akbari M, Oyedun A, Kumar A (2018) Ammonia production from black liquor gasification and co-gasification with pulp and waste sludges: a techno-economic assessment. Energy 151:133–143

Arora P, Sharma I, Hoadley A, Mahajani S, Ganesh A (2018) Remote, small-scale, 'greener' routes of ammonia production. J Clean Prod 199:177–192

Bartel C (2016) Aluminum nitride hydrolysis enabled by hydroxyl-mediated surface proton hopping. ACS Appl Mater Interfaces 8(28):18550–18559

Beerbühl S, Fröhling M, Schultmann F (2015) Combined scheduling and capacity planning of electricity-based ammonia production to integrate renewable energies. Eur J Oper Res 241(3):851–862

Bicer Y, Dincer I, Vezina G, Raso F (2017) Impact assessment and environmental evaluation of various ammonia production processes. Environ Manage 59:5

Bicer Y, Khalid F, Mohamed M, Al-Breiki M, Ali M (2020) Electrochemical modelling of ammonia synthesis in molten salt medium for renewable fuel production using wind power. Int J Hydrogen Energy 45(60):34938–34948

Chisalita D, Petrescu L, Cormos C (2020) Environmental evaluation of European ammonia production considering various hydrogen supply chains. Renew Sustain Energy Rev 130:109964

Cinti G, Frattini D, Jannelli E, Desideri U, Bidini G (2017) Coupling solid oxide electrolyser (SOE) and ammonia production plant. Appl Energy 192:466–476

Elishav O, Lis B, Miller E, Arent D (2020) Progress and prospective of nitrogen-based alternative fuels. Chem Rev 120:12

Gálvez M (2007) Ammonia production via a two-step Al_2O_3/AlN thermochemical cycle. 1. Thermodynamic, environmental, and economic analyses. Ind Eng Chem Res 46(7):2042–2046

Heidlage M, Kezar E, Snow K, Pfromm P (2017) Thermochemical synthesis of ammonia and syngas from natural gas at atmospheric pressure. Ind Eng Chem Res 56:14014–14024

Ishaq H, Dincer I (2020) Design and simulation of a new cascaded ammonia synthesis system driven by renewables. Sustain Energy Technol Assess 40:100725

Lan R, Alkhazmi K, Amar I, Tao S (2014) Synthesis of ammonia directly from wet air at intermediate temperature. Appl Catal B 152–153:212–217

Licht S, Cui B, Wang B, Li F, Lau J, Liu S (2014) ChemInform abstract: ammonia synthesis by N2 and steam electrolysis in molten hydroxide suspensions of nanoscale Fe_2O3. Chem Inform 45:43

Marnellos G, Zisekas S, Stoukides M (2000) Synthesis of ammonia at atmospheric pressure with the use of solid state proton conductors. J Catal 193:80–87

Marnellos G, Stoukides M (1998) Ammonia synthesis at atmospheric pressure. Science 282(5386):98–100

Modak J (2002) Haber process for ammonia synthesis. Resonance 7:69–77

Nkepang G, Gali H, Houson H, Hedrick A, Hayes B, Causey O, Inman P, Box J, Benton E, Galbraith W, Awasthi V (2019) Production of [13N] ammonia from [13C] methanol on a 7.5 MeV cyclotron using 13C(p, N)13N reaction: detection of myocardial infarction in a mouse model. Appl Radiat Isotopes 150:19–24

Orhan M (2012) Integrated hydrogen production options based on renewable and nuclear energy sources. Renew Sustain Energy Rev 16(8):6059–6082

Prince A (2007) Initiating new projects in the ammonia sector. In: Presented at the IFA Technical Committee Meeting, workshop on energy efficiency and CO_2 reduction prospects in ammonia production. Published online at www.fertilizer.org

Ronald M (2012) Solar thermochemical production of ammonia from water, air and sunlight: thermodynamic and economic analyses. Energy 42(1):251–260

Sánchez A, Martín M (2018) Optimal renewable production of ammonia from water and air. J Clean Prod 178:325–342

Tunå P, Hulteberg C, Ahlgren S (2014) Techno-economic assessment of nonfossil ammonia production. Environ Prog Sustain Energy 33(4):1290–1297

University of Oregon (2007) Pesticides may be hurting rather than helping crop yields. https://www.science20.com/news/pesticides_may_be_hurting_rather_than_helping_crop_yields. Last accessed 05 June 2007

Xu D, Liping L, Ren X, Ren J, Dong L (2018) Route selection for low-carbon ammonia production: a sustainability prioritization framework based-on the combined weights and projection ranking by similarity to referencing vector method. J Clean Prod 193:263–276

Zhang H, Wang L, Herle J, Maréchal F, Desideri U (2020) Techno economic comparison of green ammonia production processes. Appl Energy 249:114135

Experimental Analysis of Spherical Five Hole Flow Analyzer for Subsonic Wind Tunnels

Akhila Rupesh [ID]**, N. Aravind Kumar, Vikas Vijaybahadur Pal, and Shashidhar Rao Pasiyadala**

Abstract In the current ever-growing race for the development of aerodynamic bodies from aerospace vehicles to flying cars there comes also a need for apparatus which can be used to develop them. The wind tunnel is an apparatus that can be used to study the flow parameters around a model by simulating an airflow that is identical to the ambient conditions of the prototype. To make sure that the results are reliable and error is within the limitations, they must be calibrated periodically. Hence there is a requirement for devices that can estimate the required parameters associated with the proper functioning of a wind tunnel. In this paper, a spherical five-hole flow analyzer is devised, fabricated, and experimented with in a subsonic wind tunnel after which the experimental data is studied.

Keywords Spherical five-hole flow analyser · Computational fluid dynamics · Calibration · Wind tunnel

1 Introduction

1.1 Wind Tunnel

A wind tunnel is an aerodynamic tool that is used to study the behavior of fluid flow over a body and determine the forces caused by the flow such as lift and drag acting on that body. There are a large number of wind tunnels depending on the test section size, the fluid used, Mach number, etc., Even though there are different types

A. Rupesh (✉)
Department of Aeronautical Engineering, Mangalore Institute of Technology and Engineering, Moodbidri, Karnataka, India
e-mail: akhilarupesh56@gmail.com

N. Aravind Kumar · V. V. Pal · S. R. Pasiyadala
Department of Aerospace Engineering, Lovely Professional University, Phagwara, Punjab, India

A. Rupesh · N. Aravind Kumar · V. V. Pal · S. R. Pasiyadala
LIPS Research Foundation, Trivandrum, India

of wind tunnels they have a converging section, test section beyond which there is a diffuser section. A typical wind tunnel has an Inlet section followed by a honeycomb mesh, settling chamber, test section, diffuser, and a driver fan. Each section of this apparatus is significant on its own. The air from the atmosphere is sucked in through the inlet, the inlets section has a honeycomb pattern that helps to make the flow less turbulent. The velocity of the flow is increased in the convergent section as the test section should have the maximum velocity. The model is set on the mount to stand in the test section. The flow needs to be axial to the test section and have very little turbulence. The velocity of the flow is lowered in the diffuser section to decrease the losses. Wind tunnels are widely used in automobile, aeronautical and marine industries.

1.2   Calibration of Wind Tunnel

The airflow throughout the test section needs to be steady and axial to the test section so that accurate reading are obtained. Therefore, to assure this test section needs to be calibrated for the fluid speed, flow angularity, Turbulence, velocity distribution, and wake caused in the test section. The model can be tested only if the wind tunnel is calibrated, to obtain reliable data (Kramer and Gerhardt 1984; Muruga Lal Jeyan and Senthil Kumar 2014).

1.3   Instrumentation

In this paper, we have studied the spherical five-hole flow analyzer which is used to determine the fluid velocity and pressure. There is no need to measure force as in the case of turbulence sphere (Yufeng et al. 2021). The spherical five-hole flow analyzer can have either a five-hole probe or a seven-hole probe (Shi et al. 2021). Due to the complexity of the seven-hole probe, the five-hole probe is fabricated. The spherical five-hole flow analyzer consists of an orifice at the stagnation point and another four orifices at $22.5°$ from the stagnation point. All the outer ports are at $45°$ concerning each other. These 5 individual ports are then connected to tubes leading to the manometer. This setup can be used to determine the flow angularity and velocity. The spherical five-hole flow analyzer can also be used to determine the turbulence factor. For this, the stagnation point orifice is connected to one end of the manometer whereas the other orifices are connected to the other end of the manometer. Then from this, the pressure difference is obtained which is then divided by the dynamic pressure to obtain Cp. A graph of Cp v/s the Reynolds Number can be plotted after which the R_e (Reynolds number) analogs to a Coefficient of the pressure of 1.22 is termed as the Critical R_e.

2 Methodology

A Spherical five-hole flow analyzer is drafted and is fabricated with a suitable alloy. CFD analysis is performed to study the variation of various properties along with the instrument (Rupesh et al. 2020). Finally, to verify that this instrument is functional it is fixed in the wind tunnel and tested after which the resultant data is measured and plotted.

2.1 Wind Tunnel

The Apparatus used for the testing of the Pressure was a subsonic suction type wind tunnel available at Lovely Professional University, Punjab. Here a Spherical five-hole flow analyzer is designed by considering the size of the wind tunnel to make sure that the tunnel blockage factor was kept within 5%. Figure 1 shows the apparatus used for testing.

The entire Particulates of the apparatus is mentioned in Table 1
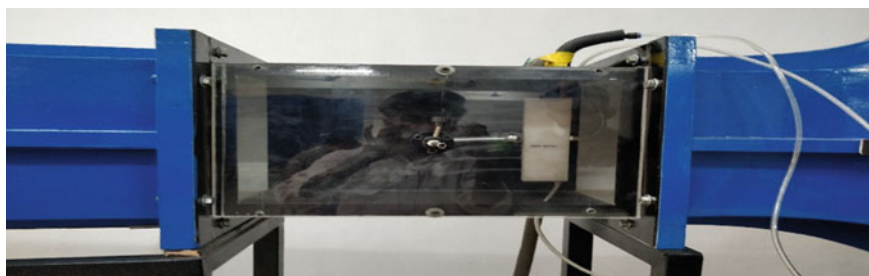
Fig. 1 Spherical five-hole flow analyzer fixed on the test section

Table 1 Wind tunnel specifications

Structural details of wind tunnel	Dimensions and specifications of wind tunnel
Type of the tunnel	Suction type subsonic wind tunnel
Length, breadth and width of test section	1200 mm × 600 mm × 600 mm
Contraction ratio	9:1
Powe supply specifications	3 phase, 440 V and 32 Amps

2.2 Spherical Five-Hole Flow Analyzer

The Spherical five-hole flow analyzer Consists of 5 tubes being at the stagnation point and the other 4 being equally spaced at an angle of 22.5° concerning the axis of the instrument as depicted in Fig. 2. The alloy which is employed here is steel-based with a high composition of Chromium having a grade of 304. Type 304 proves to be resistant to oxidation, corrosion, and durability and can be molded easily as per the requirement (Figs. 2 and 3).

The surface finishes ensuring a smooth surface without any burrs and deformations. Detailed dimensions are specified in Table 2.
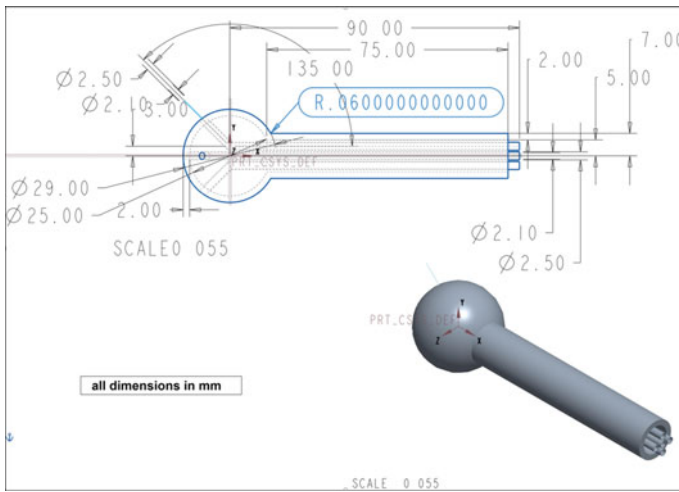
Fig. 2 Schematic design of spherical five-hole flow analyzer
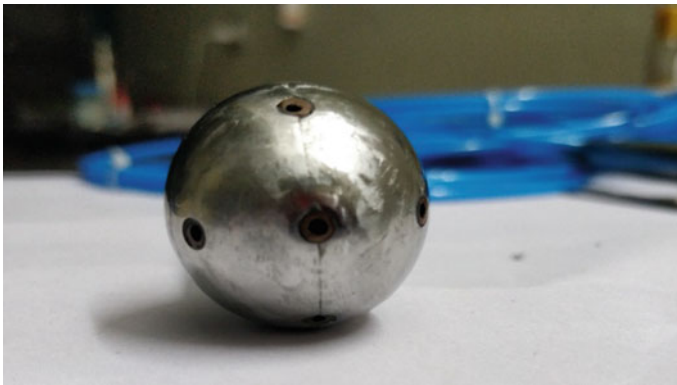
Fig. 3 Spherical five-hole flow analyzer

Table 2 Spherical five hole flow analyzer specifications

Instrument specification	Dimensions of the instrument
Sphere's inner diameter	25 mm
Sphere's outside diameter	29 mm
Pipe's inner diameter	2 mm
Pipe's outside diameter	3 mm
Cylinder pipe length	75 mm
Sphere thickness	2 mm
Angle between central axis and pipe	45°
Angle between both pipes	135°

3 Results and Discussion

3.1 Experimental Testing

The spherical five-hole flow analyzer was mounted on the wind tunnel at 3 different lengths from the start of the test section i.e. at 10, 20, and 30 cm. The ports connected to a pipe were attached to a manometer. It was made sure that the pipes trailing out did not hinder the reading from the instrument. For a given distance the pressure was measured from all five ports at five different velocities. This was repeated multiple times to get a grid of values which were used to plot the graphs shown in Figs. 4, 5 and 6 (Tables 3, 4 and 5).

Several Observations can be made from the graphs. At a given location it is seen that as the velocity is increased the Pressure measured naturally also increases indicating that the ports are working as intended. Also with an increase in velocity the pressure values of each port indicate a different reading. This suggests that there is an angularity in the flow causing the variation in the readings. As there are five ports, two of which are mutually opposite from each other we can analyze along which direction there is a flow angularity. If the two opposite ports indicate the same
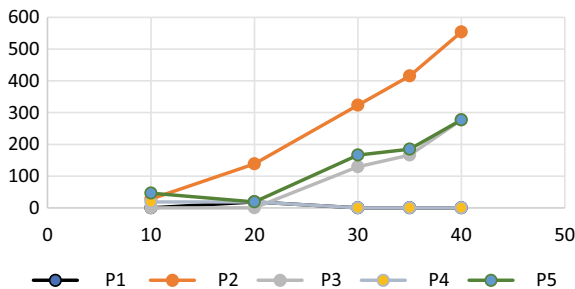
Fig. 4 Pressure versus velocity curve for 10 cm
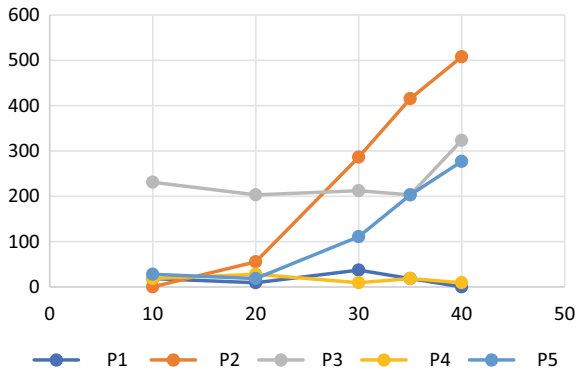
Fig. 5 Pressure versus velocity curve for 20 cm
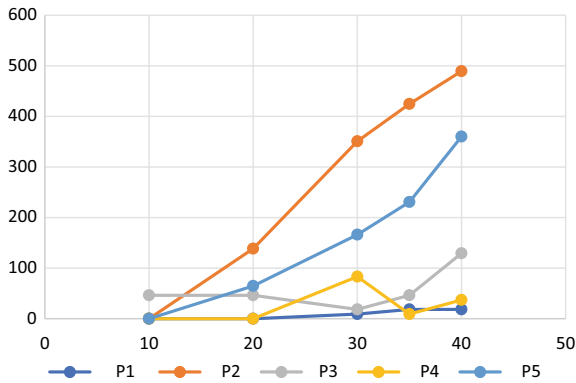
Fig. 6 Pressure versus velocity curve for 30 cm

Table 3 Reading at 10 cm from the test section entry

Velocity	P1	P2	P3	P4	P5
m/s	Pa	Pa	Pa	Pa	Pa
10	0	27.64	0	18.5	46.27
20	18.5	138.56	0	18.5	18.5
30	0	323.15	129.3	0	166.19
35	0	415.44	166.19	0	184.71
40	0	553.88	276.99	0	276.99

pressure reading, this implies that the flow parameters at those ports are the same and in that direction, the flow is straight and symmetric. This can be noticed at several points in the graph. If the readings are not the same then it is evident that there is an angularity in the flow causing the fluctuation in the measured parameters. As the

Table 4 Readings at 20 cm from the test section entry

Velocity	P1	P2	P3	P4	P5
m/s	Pa	Pa	Pa	Pa	Pa
10	18.5	0	230.86	18.5	27.76
20	9.26	55.39	203.21	27.76	18.5
30	37.02	286.26	212.35	9.26	110.79
35	18.5	415.56	203.22	18.5	203.22
40	0	507.85	323.39	9.26	276.99

Table 5 Readings at 30 cm from the test section entry

Velocity	P1	P2	P3	P4	P5
m/s	Pa	Pa	Pa	Pa	Pa
10	0	0	46.27	0	0
20	0	138.56	46.27	0	64.66
30	9.26	350.79	18.5	83.16	166.19
35	18.5	424.69	46.27	9.26	230.74
40	18.5	489.35	129.31	37.02	360.16

velocity increases the inertia of the fluid also increases with an increase Reynolds number thus we see that there is more difference in values at higher velocities. The name nature is seen at various positions of the spherical five-hole flow analyzer.

At the starting point of the test section, the flow is relatively smooth as it comes from the honeycomb section. As the distance from the starting point is increased it is seen that the difference in pressure measurements further rise. This implies that the flow is becoming more turbulent as it flows along the test section.

It is observed that at some points the measured pressure is almost zero which directs that there is flow separation caused by the turbulent flow. Thus this device can successfully determine the nature of the flow in the test section. When the parameters are measured for the entire length of the test section it does not only indicate the nature of the flow, if there are any abrupt changes at a specific location it can indicate there is a local source of disturbance in the test section.

4 Conclusion

A spherical five-hole flow analyzer is designed for a subsonic wind tunnel to examine the flow parameters i.e. velocity distribution & flow angularity. It is made sure that the size of the instrument is following the tunnel blockage factor. To study the flow parameters around the instrument a model was created and was analyzed computationally. Finally, wind tunnel testing was carried out for the fabricated model, and

readings were taken through the manometer at different positions and velocities. From the results, we can conclude that the instrument is capable of determining flow angularity. Also with small changes in the instrument, it can determine the turbulence level.

References

Du Y, Xiong N, Lin J (2021) Analysis of measurement results of dynamic flow quality in probe calibration wind tunnel. In: The 5th international conference on compute and data analysis (ICCDA 2021)

Kramer C, Gerhardt HJ (1984) Wind tunnels for industrial aerodynamics. J Wind Eng Ind Aerodyn 16:225–264

Muruga Lal Jeyan JV, Senthil Kumar M (2014) Performance evaluation of yaw meter with the aid of computational fluid dynamic. Int Rev Mechan Eng 8(2)

Rupesh A, Muruga Lal Jeyan JV, Uthaman S (2020) Design and analysis of five probe flow analyser for subsonic and supersonic wind tunnel calibration. In: IOP conference series: materials science and engineering, vol 01, no 715, pp 1–7. ISSN 1757-899X

Shi L, Feng F, Guo W, Li Y (2021) Research and development of a small-scale icing wind tunnel test system for blade airfoil icing characteristics. Int J Rotat Machin (2021)

Incident Heat Flux Measurements with Efficient Plate Thermometer in the Fire Test Environment

Shagun Agrawal, Deepak Sahu, Bhisham Kumar Dhurandher, Anchal Bahman, Jatinder Kumar Ratan, Kanchan, Nitin Naresh Pandhare, and Om Prakash Verma

Abstract In present study used an effective plate thermometer to investigate the incident heat flux in fire research. Instead of the typical alloys used for manufacturing, the plate thermometer described in the fire resistance design guidelines ISO 834-1 and EN 1363-1 can be fabricated from stainless steel (304L) or nickel metal, keeping the specifications same. The heat flux is observed to be heavily influenced by the density and specific heat of the plate's material, hence metals or alloys with larger specific heat and density can be utilized to create the PT. It's also worth noting that the heat flux is influenced by the insulator's thermal conductivity rather than the material's thermal conductivity. Moreover, emissivity of the material also plays a vital role on the heat flux. Therefore, it is suggested to use the material with lower emissivity for higher incident heat flux.

Keywords Radiation · Heat flux · Material · Plate thermometer

Nomenclature

Variables	Quantities
σ	Stefan–Boltzmann constant (W/m^{2}K^4)
δ	Thickness of plate (m)
ε	Emissivity
c	Specific heat (J/kgK)

S. Agrawal · D. Sahu (✉) · A. Bahman · J. K. Ratan · Kanchan · N. N. Pandhare
Department of Chemical Engineering, Dr. B.R. Ambedkar National Institute of Technology, Jalandhar, Punjab 144011, India
e-mail: sahud@nitj.ac.in

B. K. Dhurandher
School of Mechanical Engineering, VIT, Chennai, India

O. P. Verma
Department of Instrumentation and Control Engineering, Dr. B.R. Ambedkar National Institute of Technology, Jalandhar, Punjab 144011, India

ρ	Density (kg/m^3)
δ'	Thickness of insulator (m)
h	Coefficient of convective heat transfer (W/mK)
K_{plate}	Thermal conductivity of plate (W/m^{2}K)
K_{ins}	Thermal conductivity of plate (W/m^{2}K)
E	Incident heat flux (kW/m^2)
T_∞	Ambient gas temperature (K)
T_s	Temperature of surface (K)

1 Introduction

The amount of heat flux incident on the body's surface can be measured by using a device called plate thermometer. Wickström (1989, 1994) first invented it in the 1980s to monitor fire resistance furnaces temperature, in compliance with the harmonization of European standards ISO 834 (International Organization for Standardization 2020) and EN 1363-1 (European Standards 2020) to test fire furnace.

At high temperature, transfer of heat to the test specimen primarily depends on radiation rather than convection. The temperature measuring device to be fabricated in such a manner that transferring heat due to radiation prevails and at the same time these devices must have fast thermal response and for fast thermal response it can be lower thickness of the plate.

A standard plate thermometer (Wickström 2004) was made of an Inconel 600 steel plate of 100 by 100 mm dimensions. The plate had a thickness of 0.7 mm and an insulation pad (fabric board) of thickness 10 mm was attached at the back to minimize heat losses due to conduction. A thermocouple was attached at the center of the plate, to determine the temperature of the surface, which further helped in determination of heat flux.

The amount of heat exposure was determined by the furnace type. The heat exposure in a floor furnace was larger in a medium-scale furnace (15%) than that in a full-scale furnace, according to Sultan et al. (2003; Sultan 2004). The temperature in the slab was also somewhat higher when medium furnace was being used as compared to full-scale furnace, according to the study. Gustavsson (2017) used a plate thermometer heat flux meter to calculate the radiant heat flux and measure the adiabatic temperature of surface. He was also used the nickel alloy to perform experiments and compared those results with the results obtained from heat flux meter. Wickström (2006) used stainless steel to fabricate plate thermometer (PT) and suggested to modify the plate thermometer to reduce the errors.

In this paper, a theoretical aspect of the incident heat flux using efficient plate thermometer is proposed for evaluating the properties like thermal conductivity, specific heat, density of PT, different material such as stainless steel (304L, 316L), nickel and cobalt, and their effect on the heat flux.

2 Methodology

Theoretical analysis of incident heat flux is carried out using plate thermometer ideas. PTs should be included in all standards related to fire resistance, according to Wickström's (2008), since they harmonize fire resistance testing and offer precise figures for quantitative estimates of heat transport to structures exposed to fire.

The impacts of various insulating plate thicknesses and different building materials on heat flux are explored. The total quantity of heat flux incident on the surface as a result of radiation and convection is calculated.

2.1 Radiation

The quantity of thermal energy that the body absorbs as a result of radiation is (Dutta 2006):

$$\dot{q}_{abs} = \varepsilon E \qquad (1)$$

E is the heat flux incident to the body, and ε is the emissivity of the material. In this paper, emissivity for all the materials is assumed to be constant and same.

According to the Kirchhoff's identity, emissivity ε is equal to the absorptivity. The amount heat reflected by the surface can therefore be written as:

$$\dot{q}_{ref} = (1 - \varepsilon)E \qquad (2)$$

Now, Stefan–Boltzmann stated a law according to which, the heat emitted by the surface is given as:

$$\dot{q}_{emit} = \varepsilon \sigma T_s^4 \qquad (3)$$

where, T_s is the temperature of surface. The total thermal flux by radiation, $\dot{q}_{rad}$, going inside the surface will be:

$$\dot{q}_{rad} = \text{Incident} - (\text{Emitted} + \text{Reflected})$$
$$\dot{q}_{rad} = E - \varepsilon \sigma T_s^4 - (1 - \varepsilon)E$$
$$\dot{q}_{rad} = \varepsilon \left(E - \sigma T_s^4 \right) \qquad (4)$$

2.2 Convection

The amount of heat energy absorbed by the body due to convection is (Wickström 2006):

$$\dot{q}_{conv} = h(T_f - T_\infty) \tag{5}$$

$T\infty$ is the gas temperature at ambient conditions, and h is the coefficient connective heat transfer. This h indicates how well heat will be transferred between the surface and its surroundings. According to the equation, its value is determined by the temperature of the gas and the surface (Wickström 2004):

$$h = 4\left(\frac{T_s - T_\infty}{L}\right)^{\frac{1}{4}}(T_s + T_\infty)^{-0.16} + H \tag{6}$$

This equation is valid for both horizontal and vertical plates.

In this paper, the H factor term is considered to be zero because it is assumed that the air in the room is stagnant and H factor comes into action only when the air in the room is moving.

Therefore, the net transfer of heat by radiation and convection is equal to:

$$\dot{q}_{tot} = \dot{q}_{rad} + \dot{q}_{conv} \tag{7}$$

$$\dot{q}_{tot} = \varepsilon\left(E - \sigma T_s^4\right) + h(T_\infty - T_s) \tag{8}$$

2.3 Plate Thermometer Heat Balance

By applying energy balance at the center of the PT, we get the heat flux incident to PT as:

$$\dot{q}_{tot} = \dot{q}_{lost} + \dot{q}_{store} \tag{9}$$

The temperature shall be monitored using the plate thermometer as shown in Fig. 1.

The sum of the total heat energy lost by conduction from the plate and that by the insulator to the back side of the plate thermometer can be given by the equation:

$$\dot{q}_{lost} = \frac{(T_s - T_\infty)}{R_{th}} \tag{10}$$

Fig. 1 Plate thermometer
(Wickström 1989, 1994)
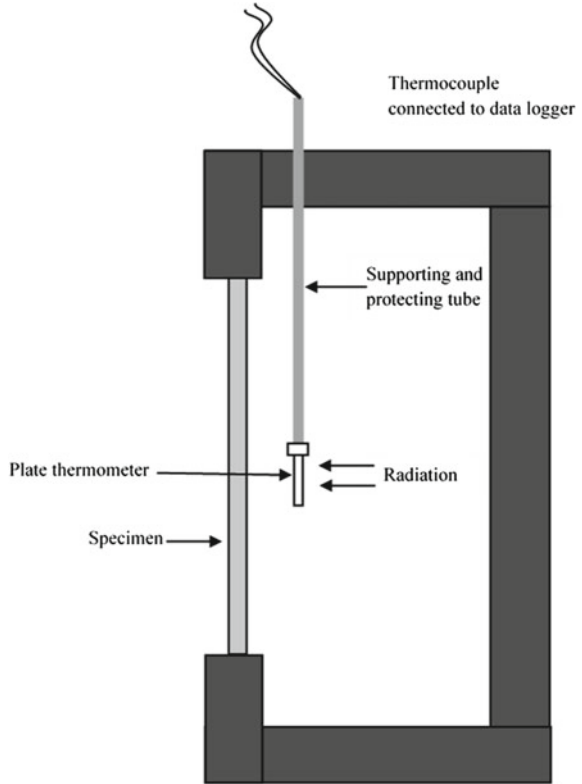
R_{th} is the total heat transfer resistance offered by plate and insulator, and it is equal to:

$$R_{th} = \delta/K_{plate} + \delta'/K_{ins} \quad (11)$$

In this paper, use of polyurethane foam as an insulator has been made and the thermal conductivity of it is supposed to stay the same with temperature.

Net thermal energy stored in plate is given by Holman (1976):

$$\dot{q}_{store} = \rho c \delta \frac{dT}{dt} \quad (12)$$

The temperature gradient between two successive thermocouple temperature records with a time interval of dt is dT. The schematic diagram of the plate thermometer is illustrated in Fig. 2 as per the test standards of fire resistance ISO 834 and EN 1363-1 is for better understanding.

From this, the total heat balance for the PT is given by the equation:
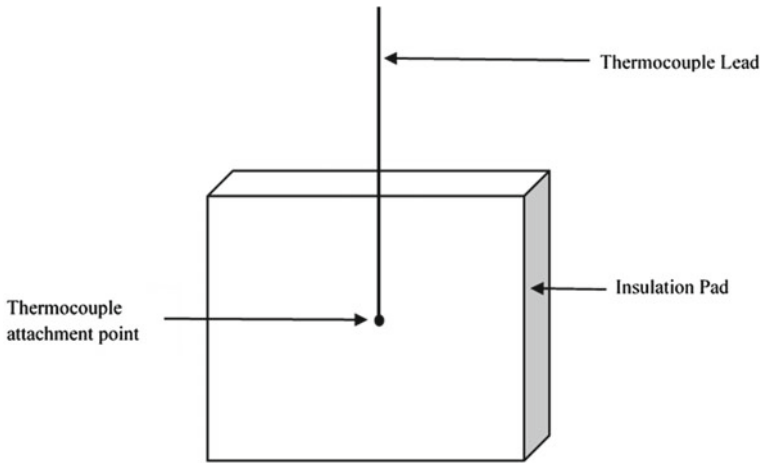
Fig. 2 Standard PT (International Organization for Standardization 2020)

$$\dot{q}_{tot} = \dot{q}_{lost} + \dot{q}_{store}$$
$$\dot{q}_{tot} = \frac{(T_s - T_\infty)}{R_{th}} + \rho c \delta \frac{dT}{dt} \tag{13}$$

Now, equating the equation and we get:

$$E = \frac{\left(R_{th}^{-1} + h\right)(T_s - T_\infty) + \rho c \delta \frac{dT}{dt} + \varepsilon \sigma T_s^4}{\varepsilon} \tag{14}$$

If all the above unknown parameters are known then at particular temperature the value of incident heat flux can therefore be measured using the above Eq. 14.

3 Results and Discussion

For the theoretical calculations data for temperature and heat flux varying with the time is taken from Sahu et al. (2019). All the readings are taken for HFM0, which is at 4 m from the fire. Readings of temperature has been used for performing the theoretical calculations whereas the heat flux readings are used for the comparison between the results. Figure 3 shows the variation of hot gas temperature with time from Sahu et al. (2019) (Table 1).
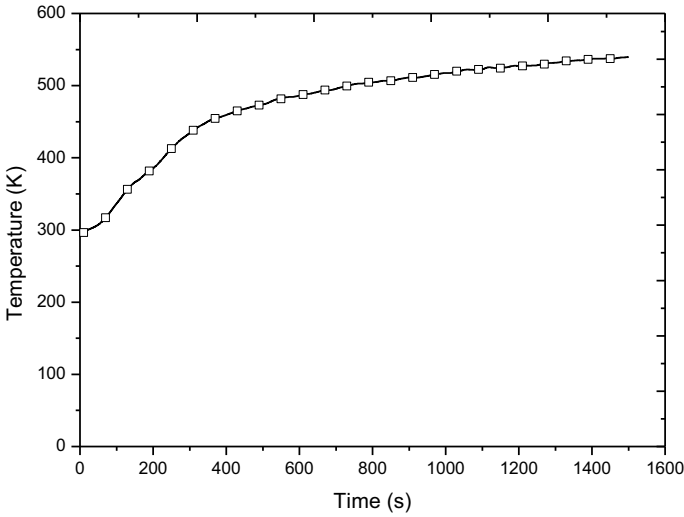
Fig. 3 Variation of temperature with time (Sahu et al. 2019)

Table 1 Details of parameters used for heat flux calculations

Parameter/variable	Variable used in calculations
T_∞	293 K
Emissivity	0.8
K_{ins}	0.024 W/mK
δ'	10 mm
δ	0.7 mm
L	100 mm

3.1 Calculation of Thermal Resistance

The overall thermal resistance varies mostly due to the insulator's thermal resistance. The value of thermal conductivity of insulator is very low in compassion to materials used therefore the value of thermal resistance of insulator becomes significantly high. In this paper, the thermal conductivity of insulator is assumed to be constant with the varying temperature. Overall thermal resistance is calculated using Eq. 11. It's also discovered that the material's thermal conductivity has a minor impact on thermal resistance. If the fluctuation in thermal conductivity of materials with temperature is unknown, it can thus be presumed to be constant.

For Stainless Steel (304L): The following equation is used to calculate the fluctuation of thermal conductivity with changing temperature (Kim 1975).

Table 2 Value of thermal conductivity calculated at different temperature for SS-304L

Temperature (K)	Thermal conductivity (W/mK)
300	12.97
350	13.78
400	14.59
450	15.40
500	16.21

$$k = 8.116 + 1.618 * 10^{-2} T_s \left(\frac{W}{mK} \right)$$

And by using the values of thermal conductivity calculated from the above equation at different temperature, the value of thermal resistance for stainless steel (304L) is calculated (Table 2).

For Stainless Steel (316L): The following equation is used to calculate the fluctuation of thermal conductivity with changing temperature (Kim 1975).

$$k = 9.248 + 1.571 * 10^{-2} T_s \left(\frac{W}{mK} \right)$$

And by using the values of thermal conductivity calculated from the above equation at different temperature, the value of thermal resistance for stainless steel (316L) is calculated.

For Nickel: The value of thermal conductivity of nickel is supposed as a constant value and is equal to 76.2 W/mK.

For Cobalt: The value of thermal conductivity of cobalt is supposed as a constant and is equal to 69.21 W/mK.

The effect of thermal resistance on the heat flux is almost same for all the materials, because the thermal resistance itself doesn't vary much for different materials. Therefore, it can be assumed that heat flux not vary much with the thermal conductivity of material. The higher the value of thermal resistance lesser the heat loss by conduction, therefore, it is observed to use more effective and thicker insulation plate.

3.2 Calculation of Heat Stored

The heat stored in the material is dependent on the specific heat and density of the substance, as shown in Eq. 12. Thickness of plate is same for all.

For Stainless Steel (304L): The variation of density and specific heat with the temperature is calculated using the equation below (Kim 1975).

Table 3 Value of density and specific heat calculated at different temperature for SS-304L

Temperature (K)	Density (kg/m³)	Specific heat (J/kgK)
300	7894.16	509.84
350	7877.14	516.58
400	7859.55	523.32
450	7841.37	530.06
500	7822.62	536.80

$$\rho = 7984.1 - 2.6506 * 10^{-1} T_s - 1.1580 * 10^{-4} T_s^2 \left(\frac{kg}{m^3} \right)$$

$$c = 469.4 + 0.1348 * T_s \left(\frac{J}{kgK} \right)$$

And by using the values of density and specific heat calculated from the above equation at different temperature, the value of amount of heat stored for stainless steel (304L) is obtained (Table 3).

For Stainless Steel (316L): The variation of density and specific heat with the temperature is calculated using the equation below (Kim 1975).

$$\rho = 8084.2 - 4.2086 * 10^{-1} T_s - 3.8942 * 10^{-5} T_s^2 \left(\frac{kg}{m^3} \right)$$

$$c = 458.985 + 0.1328 * T_s \left(\frac{J}{kgK} \right)$$

And by using the values of density and specific heat calculated from the above equation at different temperature, the value of amount of heat stored for stainless steel (316L) is obtained.

For Nickel: The variation of density and specific heat with the temperature is calculated using the equation below NIST/nickel (2021).

$$\rho = 9080 - 0.631 * T_s \left(\frac{kg}{m^3} \right)$$

$$c = 233.287 + 1.41 * T_s - 2.98 * 10^{-3} * T_s^2 + 2.75 * 10^{-6} * T_s^3 - 1.57 * \frac{10^6}{T_s^2} \left(\frac{J}{kgK} \right)$$

And by using the values of density and specific heat calculated from the above equation at different temperature, the value of amount of heat stored for nickel is obtained.

For Cobalt: The variation of specific heat with the temperature is calculated using the equation below NIST/cobalt (2021). For cobalt, the density is considered to remain

unchanged and is equal to 8900 kg/m^3.

$$c = 186.66 + 0.923 * T_s - 9.43 * 10^{-4} * T_s^2 + 4.38 * 10^{-7} * T_s^3 - 2.79 * \frac{10^6}{T_s^2} \left(\frac{J}{kgK} \right)$$

And by using the value of specific heat calculated from the above equation at different temperature, the value of amount of heat stored for cobalt is obtained.

3.3   Variation of h with Temperature

The coefficient of convective heat transfer is measured using Eq. 6. The calculated convective heat transfer coefficient lies between 3.52 and 9.61 W/m^{2}K for the temperature ranging from 296.56 to 539.96 K. The mean value obtained is 8.83 W/m^{2}K.

The surrounding temperature is considered to remain unchanged and the value of coefficient of heat transfer dependent on the surface temperature. As seen in Fig. 4, the coefficient of convective heat transfer lies between 8 and 10 W/m^{2}K when the surface temperature is above 130 °C.
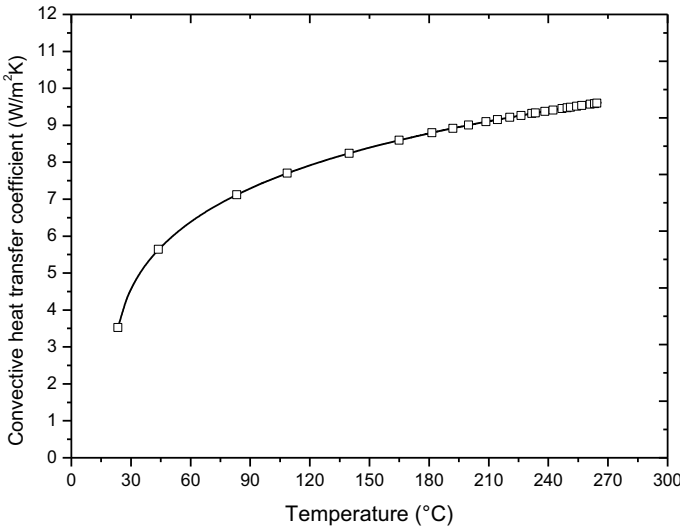
Fig. 4   Variation of coefficient of convective heat transfer with temperature of surface

3.4 Heat Flux for Different Materials

Incident heat flux for different materials has been calculated using Eq. 14. For stainless steel (304L) the incident heat flux's value lies in the range of 1.85–8.78 kW/m^2. The average heat flux for the same is found to be 6.53 ^{kW}/m^2. Similarly, it has been found to be in the range of 1.83–8.78 ^{kW}/m^2 for stainless steel (316L) and an average value of 6.519 ^{kW}/m^2 is acquired. The heat flux incident to nickel's surface is found to be lying between 1.82 and 8.82 ^{kW}/m^2 and an average value of 6.56 ^{kW}/m^2 is calculated. Similarly, for cobalt the incident heat flux is found to be lying between of 1.76 and 8.79 ^{kW}/m^2 and an average value of 6.518 ^{kW}/m^2 is calculated. Table 4 shows the variation of heat flux with temperature for different materials.

Figure 5 shows slightly too almost no difference between the heat fluxes calculated for different materials, because the value of heat flux in the graph is in kW/m^2 and the difference between different materials' heat flux is in watts. In case of surface temperature of 330 K, the heat flux for SS (304L), SS (316L), Ni and Co are 3713, 3667.13, 3717.67 and 3570 W/m^2 respectively. Therefore, the maximum difference between SS (304 L) and Co is 143 watts at particular temperature.

Table 4 Value of incident heat flux calculated at different temperature for different materials

Temperature (K)	E (SS-304L) kW/m^2	E (SS-316L)	E (Ni)	E (Co)
300	1.8482	1.8293	1.8216	1.7587
400	4.9101	4.8791	4.9940	4.8607
500	7.1891	7.1797	7.2498	7.1977
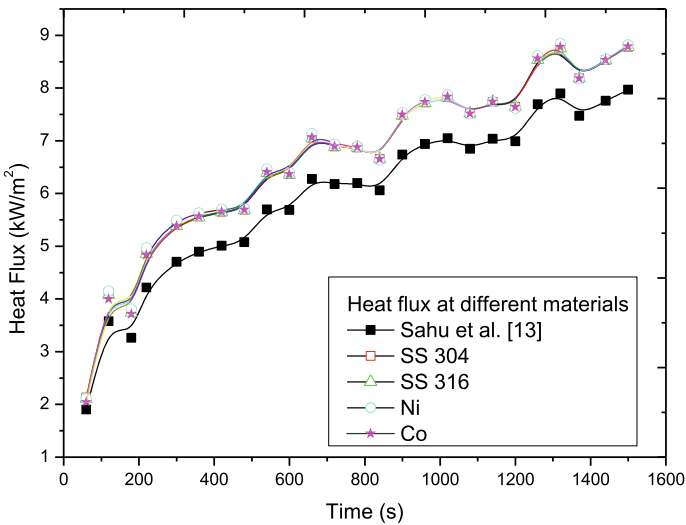
Fig. 5 Comparison between HFM and PT readings

The difference between the average heat flux readings obtained experimentally from HFM and theoretically from the plate thermometer is found to be 0.6384, 0.6737, 0.7184, 0.6730 kW/m^2 for SS (304L), SS (316L), Ni and Co respectively. These readings are obtained for two different temperature monitoring devices. This shows that the heat flux obtained for PT is more.

3.5 Heat Flux Variation with the Thickness of the Insulator

Figure 6 shows the variation of heat flux with thickness of insulation. It has been observed that increasing the thickness of the insulator reduces the heat flux. This is the reason that when the thickness of the insulator is increased, the heat loss via conduction also decreases and therefore the heat flux also decreases. If there heat loss through conduction decreases, it means we're getting closer to our experimental results, or it can be said that there will be minimum error in the theoretical and experimental data. Therefore, it is recommended to use thick insulation plates to avoid the heat loss by conduction. Table 5 shows the heat flux change with thickness of insulation plate for SS-304L. Similar results are obtained for other materials.

The average value of heat flux obtained is 6.5288, 6.2506, 6.1578 kW/m^2 for the thickness 10, 20, 30 mm respectively of the insulation plate.
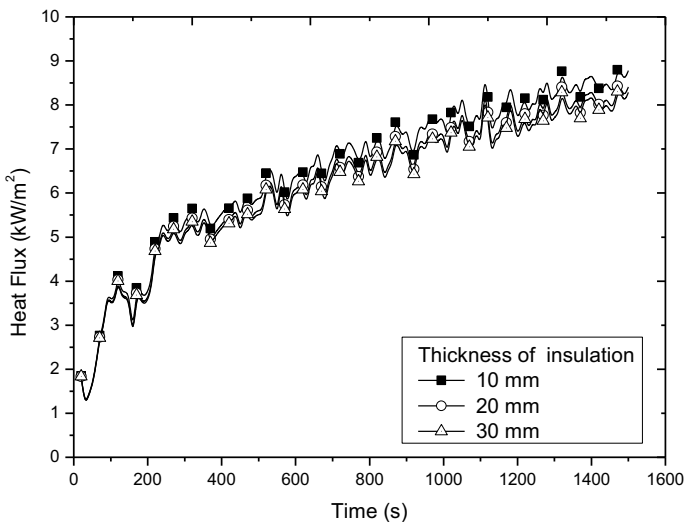
Fig. 6 Heat flux variation with time for different insulator thickness

Table 5 Value of incident heat flux calculated for different thickness of insulator

Temperature (K)	HF (thickness 10 mm)	HF (thickness 20 mm)	HF (thickness 30 mm)
300	1.8482	1.8372	1.8336
400	4.9101	4.7476	4.6935
500	7.1891	6.8873	6.7734

4 Conclusion

A theoretical study has performed to investigate effectiveness of plate thermometer to measure the heat fluxes. The incident heat flux is determined to be mostly dependent on the material's specific heat and density, rather than its thermal conductivity. For the same temperature variation, it is also discovered that the incident heat flux's value is higher in Nickel. So, it is suggested to use Nickel to fabricate plate thermometer instead of standard stainless plate. It is also found that the plate thermometer is a better and economical alternative for heat flux meter and can be used in all the fire resistance furnace testing.

References

Dutta BK (2006) Heat transfer: principles and applications, 1st edn. PHI Learning Pvt. Ltd., New Delhi

European Standards (2020) EN 1363, fire resistance tests—part 1: general requirements. Last reviewed 2020

Gustavsson C (2017) The plate thermometer heat flux meter—an accuracy and calibration study

Holman JP (1976) Heat transfer, 4th edn. McGraw Hill

International Organization for Standardization. ISO 834, fire resistance test, elements of building construction—part 1: general requirements. Last reviewed 2020

Kim CS (1975) Thermo physical properties of stainless steel, Argonne National Laboratory, Argonne, Illinois. Prepared for The U.S. Energy Research And Development Administration, Division of Reactor Research and Development

NIST homepage. https://webbook.nist.gov/nickel. Last accessed 2021/06/02

NIST homepage. https://webbook.nist.gov/cobalt. Last accessed 2021/06/02

Sahu D, Jain S, Gupta A, Kumar S (2019) Experimental studies on different liquid pool fires inside the compartment. Fire Saf J

Sultan MA (2004) A comparison of heat exposure in fire resistance test furnaces controlled by plate thermometers and by shielded thermocouples. In: Interflam, Edinburgh, pp 219–229

Sultan MA, Beni Chou N, Min BY (2003) Heat exposure in fire resistance furnaces: full-scale vs intermediate-scale. In: Fire and materials 2003 international conference, San Francisco, pp 27–29

Wickström U (1989) The plate thermometer—a simple instrument for reaching harmonized fire resistance rests. SP REPORT 1989:03. SP Swedish National Testing and Research Institute, Borås

Wickström U (1994) The plate thermometer—a simple instrument for reaching harmonized fire resistance tests. Fire Technol Second Quart 195–208

Wickström U (2004) Short communication: heat transfer by radiation and convection in fire testing. Fire Mater 28:411–415

Wickström U (2006) Measuring incident radiant heat flux using the plate thermometer. Fire Saf J
Wickström U (2008) Adiabatic surface temperature and the plate thermometer for calculating heat
    transfer and controlling fire resistance furnaces. In: Fire safety science—proceedings of the ninth
    international symposium, pp 1227–1238

Comparison of Experimental and Simulations for Esterification Process for Recovery of Acetic Acid by Reactive Distillation

Mallaiah Mekala, A. V. Raghavendra Rao, and Bhoopal Neerudi

Abstract For the esterification of acetic acid and methanol in a reactive distillation column, modelling and simulation were used. For the reactive distillation process, simulations based on an equilibrium stage-by-stage model were run. The Aspen Plus was used to execute the simulations in reactive distillation using the pseudo homogeneous kinetic model built in our previous study by accounting Indion 180 as a solid catalyst. The impact of various parameters such as the reflux ratio, the number of stages, and the acetic acid supply site on the mixture composition and acetic acid conversion have been investigated. The simulations were also run for the recovery of dilute acetic acid by synthesising methyl acetate, and it was discovered that including our kinetic model resulted in the greatest recovery of acetic acid. Both situations' simulation results are in good accord with the experimental data.

Keywords Reaction · Simulation · Stages · Purity

1 Introduction

Reactive distillation is a unit process that combines reaction and separation in a single column. The column is divided into three zones: rectifying, reactive, and stripping. The reactive zone lies in the centre of the column, with the rectifying zone above it and the stripping zone below it. The catalyst is incorporated into the reactive zone, where it serves as a reactor for the creation of products from reactants. The use of a catalyst speeds up slow processes in the reaction zone, increasing conversion through component separation from the rectifying and stripping phases. As a result, simultaneous elimination of produced products in the reactive zone will

M. Mekala (✉) · A. V. Raghavendra Rao
Department of Chemical Engineering, B V Raju Institute of Technology, Narsapur, Telangana 502313, India
e-mail: mmyadav2001@gmail.com

B. Neerudi
Department of Electrical and Electronics Engineering, B V Raju Institute of Technology, Narsapur, Telangana 502313, India

157

promote equilibrated reaction conversion. Equilibrium limiting reactions, exothermic reactions, and azeotropic mixtures can all benefit from reactive distillation. The key benefits of reactive distillation include increased conversion, lower capital costs, and higher yield. The tests for methyl acetate production in a reactive distillation column were carried out by Agreda et al. (1990). The sulfuric acid catalyst was utilised by the researchers. By conducting experiments with Montz commercial packings in which catalyst particles are placed, Kreul et al. (1998) described the catalytic reactive distillation method. An outstanding overview on the manufacture of methyl acetate using the Amberlyst 15 catalyst in a distillation column with various packings (Bessling et al. 1998). The authors compared the results of the simulation to the experimental data. Popken et al. (2001) investigated the synthesis and hydrolysis of methyl acetate utilising the catalytic structured Katapak-S in a reactive distillation. Amberlyst 15 catalyst particles have filled in structured packings, which play an important function in the reaction's progress to generate the product. To separate the products into pure form, nonreactive packing was employed in the rectifying and stripping stages. Gorak and Hoffmann (2001) used structured packings in both reactive and non-reactive parts of a catalytic distillation to study the production of methyl acetate. They have demonstrated the Multi-performance, Packing's The pressure drop, loading, and separation efficiency of the distillation column were the parameters they looked at.

The recovery of acetic acid from industrial waste streams is a major concern in the petrochemical and fine chemical industries. Recovery of acetic acid from dilute aqueous solutions is a difficult process. If the acetic acid concentration is less than 30% w/w, distillation is not an option for separating the acid from the water. They boil together closely, and the difference in volatility between these components is negligible. As a result, obtaining a pure product necessitates a high level of reflux, which increases the process' energy consumption. Reactive distillation, in which dilute acetic acid reacts with methanol to produce methyl acetate as a valuable product in addition to water, is the best alternative approach.

Neumann and Sasoon (1984) investigated acetic recovery from dilute acetic acid mixtures using a distillation method in a chemo-rectification column. The acidic catalyst was crammed into the column. They looked at kinetics for acetic acid with a concentration of 20–60% by weight, as well as experiments and simulations for the chosen procedure. They discovered that the reactive distillation technique could be used to recover acetic acid from waste streams, and they were able to get an 80% recovery rate.

Xu et al. (1999) reported on the separation of acetic acid from dilute acetic acid using catalytic distillation in the presence of Amberlyst-15 for feed concentrations of 2.5–10 wt%. They were able to convert more than half of the acetic acid into methyl acetate.

Saha et al. (2000) investigated the recovery of dilute acetic acid with n-butanol and isoamyl alcohol in a reaction distillation column utilising Indion 130 as the solid catalyst. The feed to column introduction at various sites, re-flux location, mole ratio, height of the catalytic zone, and total length of the column are the parameters chosen for their investigation.

    The reaction kinetics determine the performance of a reactive distillation (Popken et al. 2000; Mekala et al. 2013; Mekala and Goli 2014). Either the reactions are slow or spontaneous. The role of kinetics in spontaneous reactions is less crucial than in sluggish processes. The reaction kinetics play an important influence in the design of the reactive distillation column in the case of slow reactions. For the simulations of the RD process, we employed the pseudo homogeneous kinetic model described in our previous study (Mekala and Goli 2014).

    The purpose of this study is to evaluate the reactive distillation method for the production of methyl acetate and recovery of dilute acetic acid by reacting it with methanol in an RD column under various operating circumstances and to validate the results through simulation.

2 Mathematical Model

The steady state equilibrium stage wise process contains the mass, energy, summation and equilibrium relations are given below (Peng et al. 2002; Mekala et al. 2017; Taylor and Krishna 2000).

Total Condenser

Molar component balance

$$V_2 y_{i,2} - (D + L_1)x_{i,1} = 0 \tag{1}$$

Total energy balance

$$V_2 H_2^V - (D + L_1)H_1^L - Q_C = 0 \tag{2}$$

Summation

$$\sum_{i=1}^{NC} x_{i,1} = 1 \tag{3}$$

Reboiler

Molar component balance

$$L_{N-1}x_{i,N-1} - V_N y_{i,N} - L_N x_{i,N} = 0 \tag{4}$$

Total energy balance

$$L_{N-1}H_{N-1}^L - V_N H_N^V - L_N H_N^L + Q_R = 0 \tag{5}$$

Summation

$$\sum_{i=1}^{NC} x_{i,N} = 1 \tag{6}$$

$$\sum_{i=1}^{NC} y_{i,N} = 1 \tag{7}$$

Vapour–liquid equilibrium

$$y_{i,N} = K_{i,N} x_{i,N} \tag{8}$$

For jth Stage

Molar component balances

$$L_{j-1} x_{i,j-1} - V_{j+1} y_{i,j+1} - L_j x_{i,j} - V_j y_{i,j} + \varepsilon_j R_{i,j} = 0 \tag{9}$$

For Feed stage

$$L_{j-1} x_{i,j-1} + V_{j+1} y_{i,j+1} + F_j Z_{i,j}^F - L_j x_{i,j} - V_j y_{i,j} + \varepsilon_j R_{i,j} = 0 \tag{10}$$

Total energy balance

$$L_{j-1} H_{j-1}^L + V_{j+1} H_{j+1}^V - L_j H_j^L - V_j H_j^V = 0 \tag{11}$$

For Feed stage

$$L_{j-1} H_{j-1}^L + V_{j+1} H_{j+1}^V + F_j H_j^F - L_j H_j^L - V_j H_j^V = 0 \tag{12}$$

Summation

$$\sum_{i=1}^{NC} x_{i,j} = 1 \tag{13}$$

$$\sum_{i=1}^{NC} y_{i,j} = 1 \tag{14}$$

Vapour–liquid equilibrium

$$y_{i,j} = K_{i,j} x_{i,j} \tag{15}$$

Equations (1)–(15) are used to perform the simulations by Aspen plus.

3   Results and Discussions

3.1   Methyl Acetate Synthesis by Catalytic Reactive Distillation

Figure 1a–d shows the residue curve maps for the ternary mixture of the acetic acid/methanol/methyl acetate, acetic acid/methanol/water, methanol/methyl acetate/water and acetic acid/methyl acetate/water at atmospheric pressure respectively. These residue curves represent the feasible conditions of the methyl acetate formation at atmosphere pressure. These curves represent the design of the reactive distillation at 1 atmosphere pressure and azeotropic composition of the ternary system. From these figures it is observed that there are no ternary azeotropes formed.
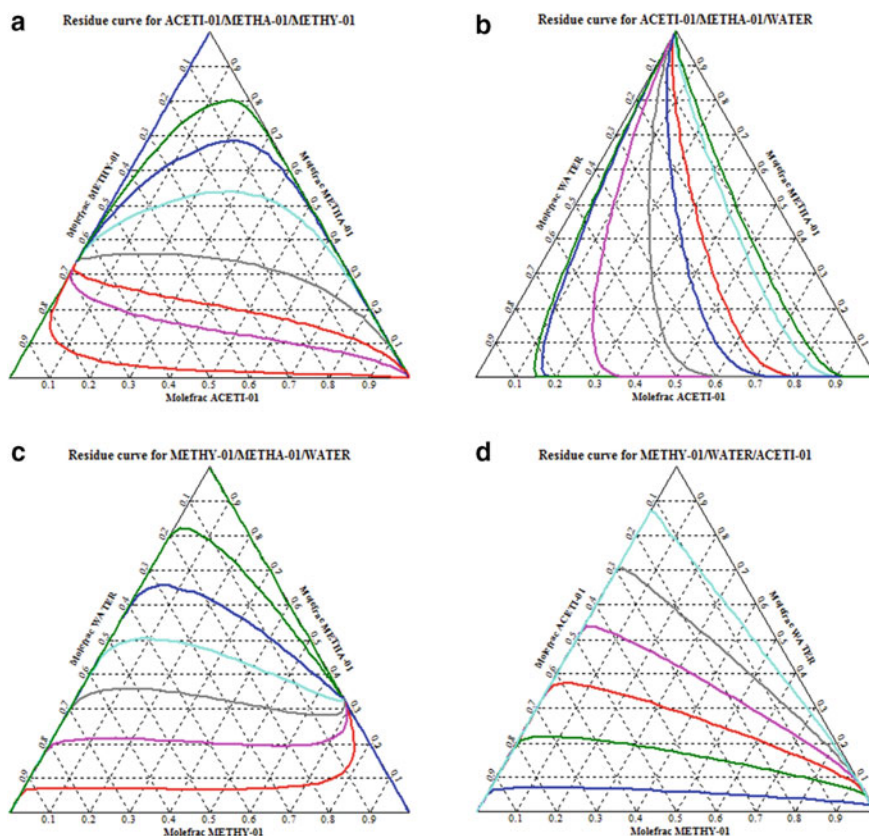
Fig. 1 The ternary mixture curves. **a** Acetic acid/methanol/methyl acetate, **b** acetic acid/methanol/water, **c** methanol/methyl acetate/water and **d** acetic acid/methyl acetate/water

The simulations have carried out for the reactive distillation column by incorporating the developed kinetic rate equation using Aspen Plus.

Figure 2 shows vapor composition profiles for the methyl acetate between reactions of acetic acid with the methanol in a catalytic reactive distillation column. The column is divided into three sections. Rectifying section contains stages of 1–10; reactive section contains stages of 11–20; and stripping section contains stages of 21–30. From Fig. 2, it is observed that 98.5 mol % of methyl acetate and 94.9 mol % water have formed in the distillate and reboiler respectively.

Figure 3 shows the acetic acid conversion with respect to the number of stages. As the number stages increases from 5 to 30, the conversion of acid increases from 1 to 99% by mole. When the number of stages is 30, the maximum conversion is obtained. After 30th stage to 50th stage, the conversion remains same. Hence the optimum stages are found to 30 including condenser and reboiler.
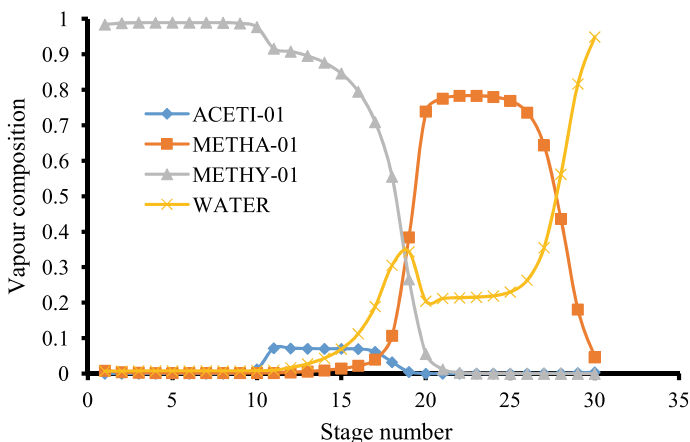
Fig. 2 Vapour composition profiles versus stage number
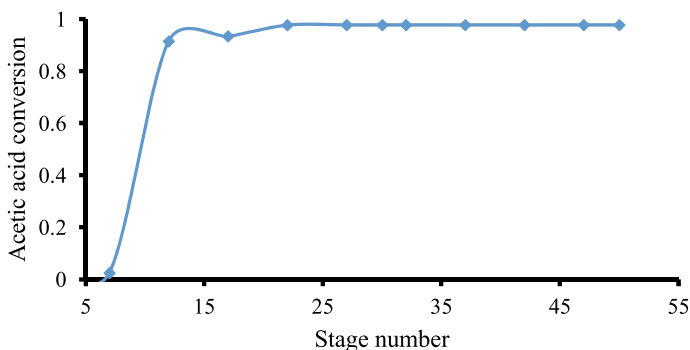
Fig. 3 Conversion of acetic acid with respect to number of stages

3.2 Acetic Acid Recovery by Catalytic Reactive Distillation

The reactive distillation is applied to the dilute acetic acid recovery from the dilute solutions as other case study. The simulations are performed by incorporating our kinetic rate expression in the equilibrium stage model. The simulation results of composition and temperature profiles are compared with the Singh et al. (2006) experimental data. The simulations are performed methanol at flow rates of 10.5 mol/h, acetic acid and water stream at flow rate of 10.5 mol/h, reflux ratio of 4.5, location of methanol is below the reactive zone and acetic acid and water stream above the reactive zone.

Figure 4 shows comparison for the liquid composition along with experimental results for the recovery of the dilute acetic stream by the reaction with the pure methanol. In this process, the model predictions and experimental results are close to each other. standard error and deviation and it is less than 5%. The excess methanol reacting with dilute acetic acid and maximum acetic acid is obtained in the present simulation results compared to Singh et al. (2006) data.

Singh et al. (2006) have reported that the maximum conversion of acetic acid is 79%, but in the present study, the maximum conversion of acetic acid is found to be 99% by using our kinetic model. The present results show that the improvement in composition of methyl acetate when compared to the Singh et al. (2006). It may be attributed to the fact that the activity of the present catalyst (Indion 180) is high when compared to the catalyst proposed by Singh et al. (2006). It may be concluded that Indion 180 catalyst is more efficient for the improvement in the conversion of acetic acid. Hence our simulation results are better compared to the previous results Singh et al. (2006).
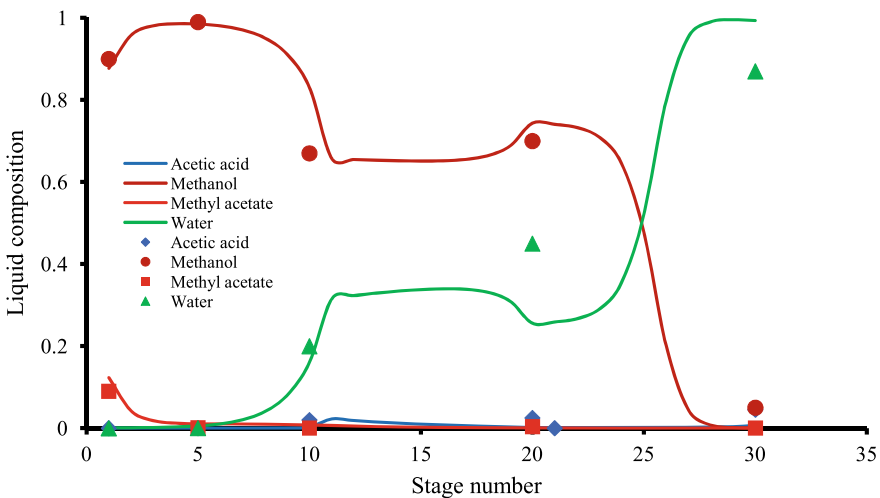
Fig. 4 Composition of liquid mixture versus stage number. Experimental data represented by symbols and simulation results with solid lines (Singh et al. 2006)

Figure 5 shows the comparison of the column temperature between simulation and experimental data acetic recovery from waste water stream. Temperature is gradually decreases last stage (reboiler) to reactive section. In reactive section, column process temperature is almost same. The temperatures decreased from 10th stage to first stage. Whereas in within rectifying section, the temperature more or less constant due to existence of low boiling components of methanol and methyl acetate.

Location of the acetic acid feed stage has much effect on the acetic acid conversion as shown in Fig. 6. Methanol feed location is fixed at 20th stage. When the feed stage location has been changed from 2 to 20; there is variation of the acetic conversion. From the figure it could be observed that, as the feed stage location goes below 11, the acid conversion decreases and becomes very less at 20th stage. It indicates that
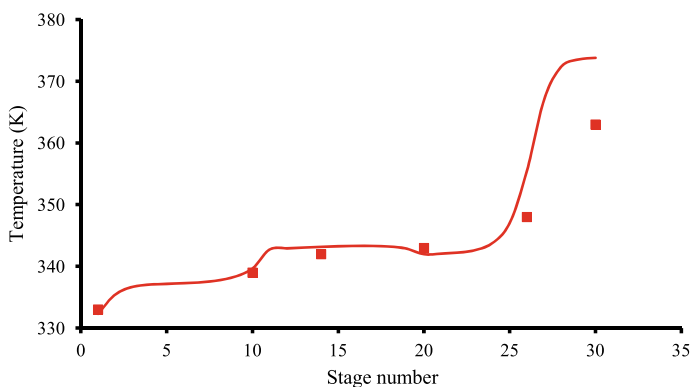
Fig. 5 Temperature profile versus stage number. Experimental data represented by symbols and simulation results with solid lines (Singh et al. 2006)
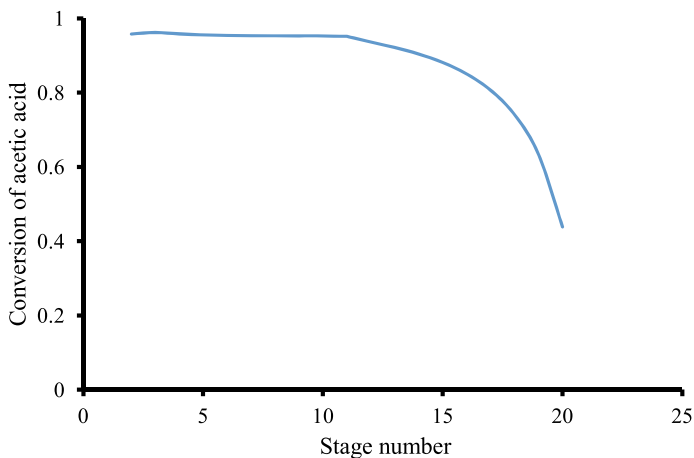
Fig. 6 Conversion of acetic acid versus feed stage from equilibrium stage model (simulation results)
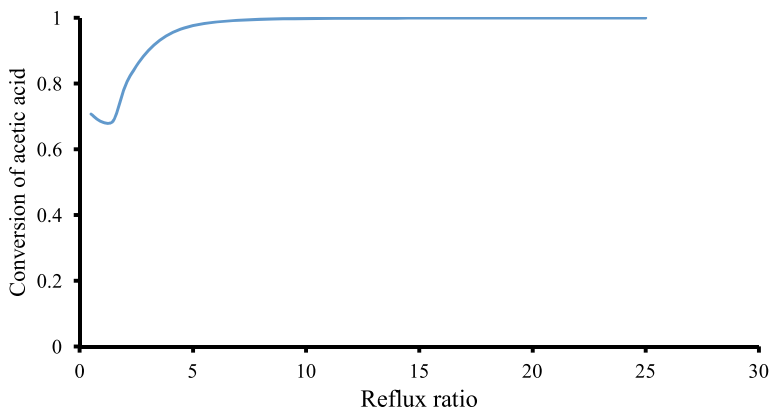
Fig. 7 Conversion of acetic acid as function of reflux ratio from equilibrium stage model (simulation results)

acetic acid feed location is near to reactive zone where it operates as counter current fashion of acid and methanol which increases driving force in the reactive zone.

Figure 7 shows the acetic acid conversion with varying reflux ratio. The conversion increases as increasing reflux ration and reaches maximum when the reflux ratio is of 4.5 and then it is almost constant thereafter. When the reflux ratio below 4.5; the conversion falls to lower values. The reason is that the reaction is kinetically controlled, the performance of the column is depends on reactants concentrations in the reactive zone as well as temperature. If the methanol concentration is more in the reaction zone the saturation temperature is less. The conversion increases for high reflux ratio due to increase in methanol concentration.

4 Conclusions

The experimental results were compared to the models of esterification of concentrated and dilute acetic acid with methanol in a reactive distillation. The influence of stage number and reflux ratio on acetic acid conversion is explored, and it is discovered that acetic acid at stage 11 and methanol at stage 20 with a reflux ratio of 2 gives the highest acetic acid conversion. For the recovery of dilute acetic acid, the model predictions were compared to experimental findings and found to be in good agreement. Reactive distillation is a useful method for recovering acetic acid from a dilute solution, which is difficult to do with traditional distillation. The impact of acetic acid feed stage location on acetic acid conversion is greater, with the greatest conversion found at site 2. In comparison to literature values, the greatest conversion of acetic acid was 99% at a reflux ratio of 4.5.

Conflict of Interest The authors declare that they have no known competing financial interests or personal relationships that could have appeared to influence the work reported in this paper.

References

Agreda VH, Partin LR, Heiss WH (1990) High purity methyl acetate via reactive distillation. Chem Eng Prog 86:40–46

Bessling B, Loning J, Ohligschlager A, Schembecker G, Sundmacher K (1998) Investigation on the synthesis of methyl acetate in a heterogeneous reactive distillation process. Chem Eng Technol 21:393–400

Gorak A, Hoffmann A (2001) Catalytic distillation in structured packings: methyl acetate synthesis. AIChE J 47:1067–1076

Kreul LU, Gorak A, Dittrich C, Barton PI (1998) Dynamic catalytic distillation: advanced simulation and experimental validation. Comput Chem Eng 22:S371–S378

Mekala M, Goli VR (2014) Comparative kinetics of esterification of methanol-acetic acid in the presence of liquid and solid catalysts. Asia-Pac J Chem Eng 9:791–799

Mekala M, Thamida SK, Goli VR (2013) Pore diffusion model to predict the kinetics of heterogeneous catalytic esterification of acetic acid and methanol. Chem Eng Sci 104:565–573

Mekala M, Kola AK, Goli VR (2017) Catalytic reactive distillation for the esterification process: experimental and simulation. Chem Biochem Eng Q 69:293–302

Neumann R, Sasoon Y (1984) Recovery of dilute acetic acid by esterification in a packed chemorectification column. Ind Eng Chem Res Process Des Dev 23:654–659

Peng J, Lextrait S, Edgar TF, Eldridge RB (2002) A comparison of steady state equilibrium and rate based model for packed reactive distillation columns. Ind Eng Chem Res 41:2735–2744

Popken T, Gotze L, Gmehling J (2000) Reaction kinetics and chemical equilibrium of homogeneously and heterogeneously catalyzed acetic acid esterification with methanol and methyl acetate hydrolysis. Ind Eng Chem Res 39:2601–2611

Popken T, Steinigeweg S, Gmehling J (2001) Synthesis and hydrolysis of methyl acetate by reactive distillation using structured catalytic packings: experiments and simulation. Ind Eng Chem Res 40:1566–1574

Saha B, Chopade SP, Mahajani SM (2000) Recovery of dilute acetic acid through esterification in a reactive distillation column. Catal Today 60:147–157

Singh A, Tiwari A, Mahajani SM, Gudi RD (2006) Recovery of acetic acid from aqueous solutions by reactive distillation. Ind Eng Chem Res 45:2017–2025

Taylor R, Krishna R (2000) Modelling reactive distillation. Chem Eng Sci 55:5183–5229

Xu Z, Afacan A, Chuang KT (1999) Removal of acetic acid from water by catalytic distillation. Part 1: experimental studies. Can J Chem Eng 77:676–681

Development and Evaluation of Soft Computing Models for Montana Flume Aeration

K. M. Luxmi, Ashwini Tiwari, N. K. Tiwari, and Subodh Ranjan Vajesnayee

Abstract Montana flume is obtained from Parshall flume by removing diverging section and throat. It is used for measuring flow rate in irrigation canals, spring discharge, etc., and it has an additional benefit that it aerates water flowing through it. Aeration is a process in which oxygen is absorbed from the atmosphere into the water. Dissolved oxygen (DO) indicates water quality, and a minimum of 4 ppm is required to support aquatic life. This study was conducted on two standard Montana flumes of throat width 2.54 cm, 5.08 cm, respectively, and three modified Montana flumes of throat width 7.62 cm. DO was measured using the Azide modification method. Experimental results show that aeration efficiency increases with an increase in discharge per unit width and a decrease in throat width. Adaptive Neuro-Fuzzy Inference System (ANFIS), Multilinear Regression (MLR), and Multi Non-linear Regression (MNLR) were used to develop the model and predict aeration efficiency. The results of ANFIS, MLR, and MNLR are compared using statistical indices like the coefficient of correlation (CC), root mean square error (RMSE) and found that the performance of MNLR was better than ANFIS and MLR.

Keywords Montana flume · Aeration · Dissolved oxygen · Azide modification method · ANFIS · MNLR · MLR

1 Introduction

Montana flume is used for flow measurement in irrigation canals where the small sizes are especially suited to measure farm deliveries. Montana flume is a Parshall flume obtained by deleting diverging section and throat. A definition view of Montana flume is shown in Fig. 1, and a view of the typical model is shown in Fig. 2, respectively. Montana flume is used for free flow conditions as there is no requirement of diverging section for the free-flow condition (https://www.usbr.gov/tsc/techreferences/mands/

K. M. Luxmi (✉) · A. Tiwari · N. K. Tiwari · S. R. Vajesnayee
Department of Civil Engineering, National Institute of Technology, Kurukshetra, Kurukshetra, India
e-mail: burman.luxmi1996@gmail.com

Fig. 1 Definition view of Montana flume
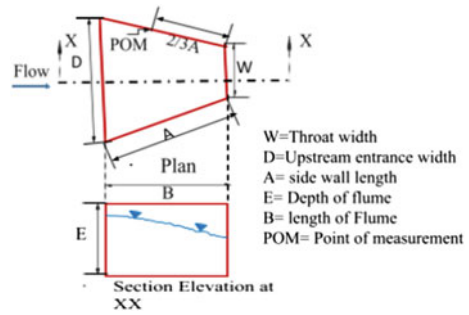
Fig. 2 View of a typical model

wmm/WMM_3rd_2001.pdf). It can clean itself of silt and sand (Parshall 1941). It is also used to measure sewage flow and other liquids carrying solid because of non-clogging characteristics (Zytner et al. 1998). Aeration is a process in which air is entrained into the water through interfacial air circulation. The basis of aeration lies in the fact that every system tends to approach equilibrium. The phenomena of aeration in flumes are expressed by assuming the existence of stationary film of gas and liquids, respectively having an interface (Lewis and Whitman 1924). The oxygen from the gas film is transferred to the water by the slow diffusion process.

Tiwari and Sihag (2020) examined the performance of aeration of the Parshall flume and modified Parshall flume, and used regression analysis to develop the model and predict oxygen transfer. Sangeeta and Tiwari (2019) examined the aeration efficiency of small Parshall flumes using M5P and Adaptive Neuro-Fuzzy Inference System (ANFIS). Dursun (2016) examined the aeration efficiency of Parshall flume and modified Venturi flume and concluded that Parshall and Venturi flumes could be used for aeration of channels with zero or highly low slope. Baylar et al. (2008) studied free overfall jets from triangular sharp-crested weirs system and their effect in air entrainment. Prediction of aeration efficiency was made using ANFIS, MNLR, and MLR; results obtained were compared to determine the best fit model. Tiwari

(2019) studied the effect of hydraulic jump on aeration efficiency. Hydraulic jump causes turbulence in water flow resulting in aeration.

The geometry of the flume affects oxygen transfers; a decrease in throat width and increase in throat length increases aeration efficiency (Dursun 2016). Flow rate also affects oxygen transfer; an increase in discharge increases aeration efficiency (Dursun 2016). Turbulence plays a vital role in oxygen transfer, and thus Reynolds number becomes a significant input parameter (Tiwari and Sihag 2020).

Many researchers worked on different hydraulic structures and used simulation to develop models to predict aeration efficiency. However, there is a lack of knowledge of the aeration performance of the Montana flume. This study aims to determine the aeration efficiency and factors affecting the aeration performance of the Montana flume. The data set obtained from experimental observation is to be modeled using soft computing techniques. The obtained models will be compared to determine the best fit model for the given data set.

2 Materials and Methods

The experiment was conducted in a tilting prismatic rectangular channel in the Hydraulics Laboratory at the Civil engineering department of National Institute of Technology, Kurukshetra. The channel was connected to an aeration cum storage tank. Channel withdraws water from aeration tank using a reciprocating pump. A schematic diagram of the experimental setup is shown in Fig. 3. The maximum flow rate of the channel is 5.2 l/s regulated using a valve. Two standard Montana flumes and three modified Montana flumes made up of timber were used in this study. Dimensions of the Montana flumes and modified Montana flumes are given in Table 1. The aeration tank was filled with clean potable water. An estimated quantity of sodium sulfite and cobalt chloride as catalyst was added to deoxygenate water and
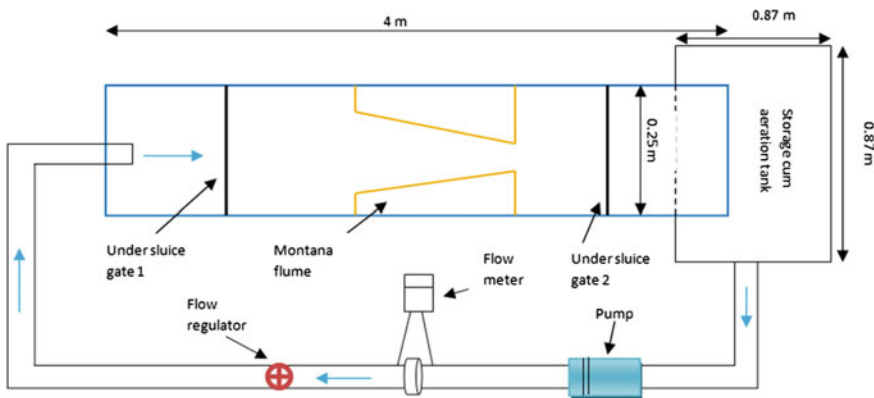
Fig. 3 Schematic diagram of the experimental setup

Table 1 Dimensions of Montana flumes (MFs) and modified Montana flumes (MMFs)

Sr. No.	Model No.	Throat width (W) (cm)	U/S entrance width (D) (cm)	Sidewall length (A) (cm)	Length of the flume (B) (cm)	Depth of flume (E) (cm)
1	MF1	2.54	16.75	36.27	35.56	22.86
2	MF2	5.08	21.35	41.43	40.64	25.4
3	MMF3	7.62	24.28	42	41.16	25.4
4	MMF4	7.62	24.45	42.43	41.58	25.4
5	MMF5	7.62	24.67	43	42.14	25.4

brought the DO content to 1–2 ppm, so that DO content does not reach a saturation level. A water sample was taken to measure the initial DO content of water, and the channel was allowed to run for 90 s, and the final DO was measured. DO of water was measured using the azide modification test (APHA, Awwa, WEF 2005). The water temperature of the tank was measured using a mercury thermometer. This procedure was repeated for different flows in all flumes.

2.1 Adaptive Neuro-Fuzzy Inference System (ANFIS)

ANFIS is a combination of fuzzy logic and neural network, the structure of ANFIS is shown in Fig. 4. There are two types of fuzzy inference system Mamdani and Sugeno; Sugeno is used more often for mathematical analysis (https://in.mathworks.com/). Training data is modeled using a combination of least squares and the backpropagation gradient descent method. The input parameter is related to output by a membership function. A Membership function is a curve that defines how each
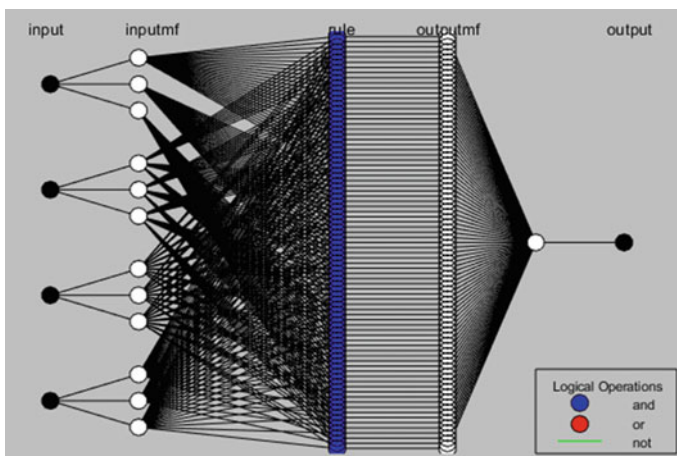
Fig. 4 Structure of ANFIS

input point is mapped to a membership value between 0 and 1. There are two types of FIS generation options available:

- Grid Partitioning: The input variable is uniformly divided to generate a membership function, creating a single Sugeno fuzzy system output. Every input membership function combination has one rule in the fuzzy rule base.
- Subtractive Clustering: This type of FIS is generated by a Sugeno fuzzy system using membership function and rules. The rules are obtained by subtractive clustering of data.

The input parameter is related to output by a membership function.

Membership Function (https://in.mathworks.com/)

Many input membership functions are available, including triangular, trapezoidal, Gaussian, bell shaped, Gaussian combination, sigmoidal, difference between two sigmoid, product of two sigmoid, Z-shaped, Pi-shaped, and S-shaped. There are two output membership functions available one is linear, and another is constant. In the present paper, triangular, trapezoidal, and gbell shaped membership functions are used.

Triangular Membership Function (Trimf)

y = trimf(x, params) gives fuzzy membership values evaluated using the following generalized bell-shaped membership function:

$$f(x; a, b, c) = \max\left(\min\left(\frac{x - a}{b - a}, \frac{c - x}{c - b}\right)\right)$$

x is the input value corresponding to which y (membership value) is obtained; a and c are the feet of the membership function; b is the crest of the membership function.

Trapezoidal Membership Function (Trapmf)

$$y = \text{trapmf}(x, \text{params})$$

$f(x; a, b, c, d) = \max\left(\min\left(\frac{x-a}{b-a}, \frac{c-x}{c-b}\right), 0\right)$ b and c define the shoulder of membership function; a and d defines feet of membership function. When c > b, it gives trapezoidal membership function, when b = c triangular membership function is obtained and when c < b also gives triangular membership function, but the maximum value is less than 1. For every input x, membership value y is calculated.

Generalized Bell-Shaped Membership Function (Gbellmf)

y = gbellmf(x, params) gives fuzzy membership values calculated using the following generalized bell-shaped membership function:

$f(x; a, b, c) = \frac{1}{1+\left\|\frac{x-c}{a}\right\|^{2b}}$ for every input x membership value, y is computed a is the width of membership function; b is the shape of the curve on either side of the central plateau; c is the center of membership function.

2.2   Multi Non-linear Regression (MNLR)

A Multi Non-Linear Regression relation is defined by using aeration efficiency (E20) as a dependable parameter. In contrast, the discharge per unit width (q), depth of flow (Ha), upstream entrance width (D), sidewall length (A) and throat width (W) is considered as an explanatory parameter. The relationship between the dependent variable and the explanatory variable is non-linear, and the equation assumed initially is as follows:

$$E_{20} = p_i q^a D^b A^c W^d \tag{1}$$

where p_i is the constant, a, b, c, d are the function coefficients and can be obtained by reducing the error squares in approximation.

The equation obtained after applying multi non-linear regression to the training data set is as follows:

$$E_{20} = 0.147 \times q^{1.032} \times D^{-0.277} \times A^{-0.264} \times W^{4.961 \times 10^{-2}} \tag{2}$$

2.3   Multiple Linear Regression (MLR)

MLR was used for modeling and establishing a relationship between a dependent variable and independent variables. MLR works on the principle of least square. Multiple linear functions required is as follows:

$$Y = a + b1X1 + b2X2 + b3X3 \tag{3}$$

Here Y is the dependent variable, a, b1, b2, b3 are constants, and X1, X2, X3 are the independent variable. The following equation was obtained after applying linear regression to the training data set:

$$E_{20} = 0.617 + 0.0285 \times q^{0.0121} \times D - 0.02183 \times A \tag{4}$$

3   Results and Discussion

In this study, two standard Montana flume and three modified Montana flume of modified sidewall length, upstream entrance width was tested. In total, 45 observations were taken, out of which 32 were taken as training data and 13 as testing data. Input parameters include discharge per unit width (q in l/s/m), upstream entrance

Table 2 Details of performance evaluation of training and testing data set

Parameters	Training data			Testing data		
	Range	Mean	Std. deviation	Range	Mean	Std. deviation
E_{20}	0.08–0.63	0.3550	0.1361	0.16–0.53	0.3515	0.1345
q (L/ms)	5.34–18.33	12.8044	4.3497	5.34–18.33	12.8044	4.3497
D (cm)	16.75–24.67	22.4413	3.0310	16.75–24.67	22.4413	3.0310
A (cm)	36.27–43.00	41.1316	2.4304	36.27–43.00	41.1316	2.4304
W (cm)	2.54–7.62	6.1913	2.0338	2.54–7.62	6.1913	2.0338

width (D in cm), sidewall length (A in cm), and throat width (W in cm). Aeration efficiency (E_{20}) was taken as output. The details of training and testing data are given in Table 2.

3.1 Result of ANFIS

Sugeno fuzzy inference model is developed having Triangular, Trapezoidal, and Generalized Bell-Shaped membership function. In this study, grid partitioning is used because it gives better results. The output membership function for the data set used was constant as it gave an excellent result compared to the linear function. Furthermore, AND rule is used for modeling, and the optimization method used for the training model was hybrid because it showed the best results. The predicted values of aeration efficiency were plotted against experimental values for both training and testing data, as shown in Fig. 5. The predicted values of E_{20} lie closer to the perfect line indicating good estimation by the developed model. Further, the values of coefficient of correlation (CC) and root mean square error (RMSE) of testing data were 0.8127 and 0.0759, respectively, indicating the developed model is accurate for predicting aeration efficiency.

3.2 Result of MNLR

The predicted values of aeration efficiency were plotted against experimental values for both training and testing data, as shown in Fig. 6. The predicted values of E_{20} lie closer to the perfect line indicating good estimation by the developed model. Further, the values of CC and RMSE of testing data were 0.8337 and 0.0714, respectively, indicating the developed model is accurate for predicting aeration efficiency.
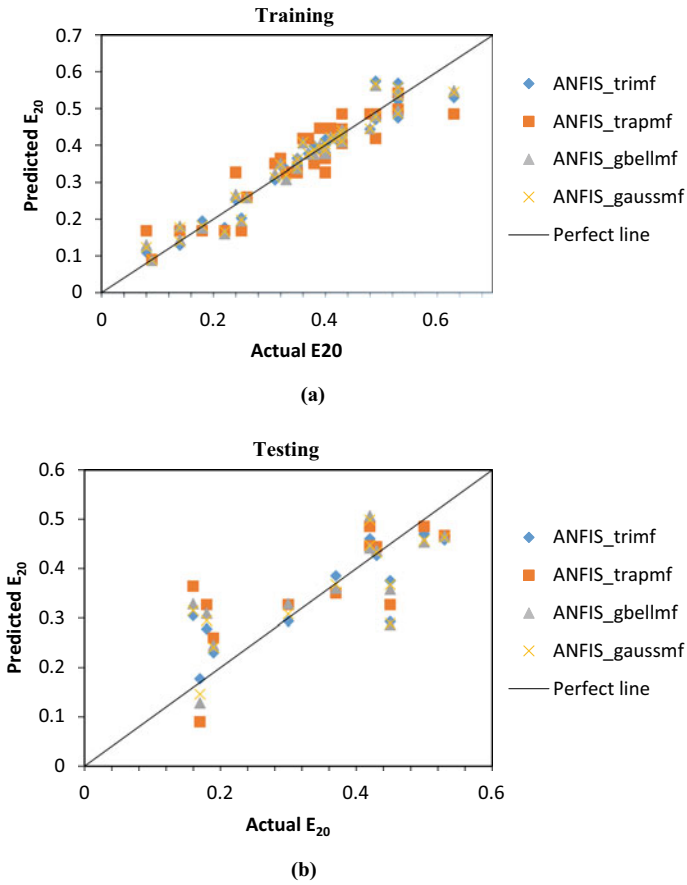
Fig. 5 Performance of ANFIS for training data set (**a**) and testing data set (**b**)
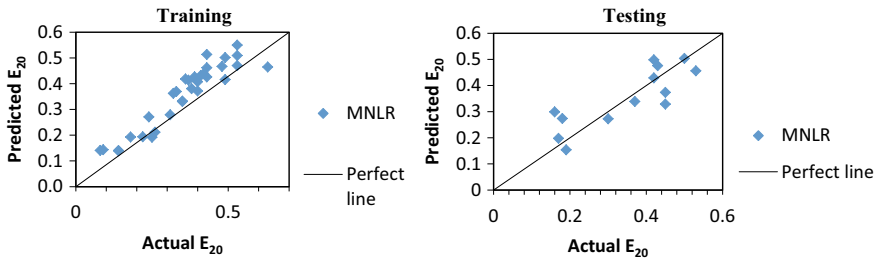
Fig. 6 Performance of MNLR for training data set and testing data set

3.3 Result of MLR

The predicted values of aeration efficiency using MLR were plotted against exper-
imental values for both training and testing data, as shown in Fig. 7. The predicted
values of E_{20} lie closer to the perfect line indicating good estimation by the devel-
oped model. Further, the values of coefficient of correlation (CC) and root mean
square error (RMSE) of testing data were 0.8236 and 0.0734respectively, indicating
the developed model is accurate for predicting aeration efficiency.
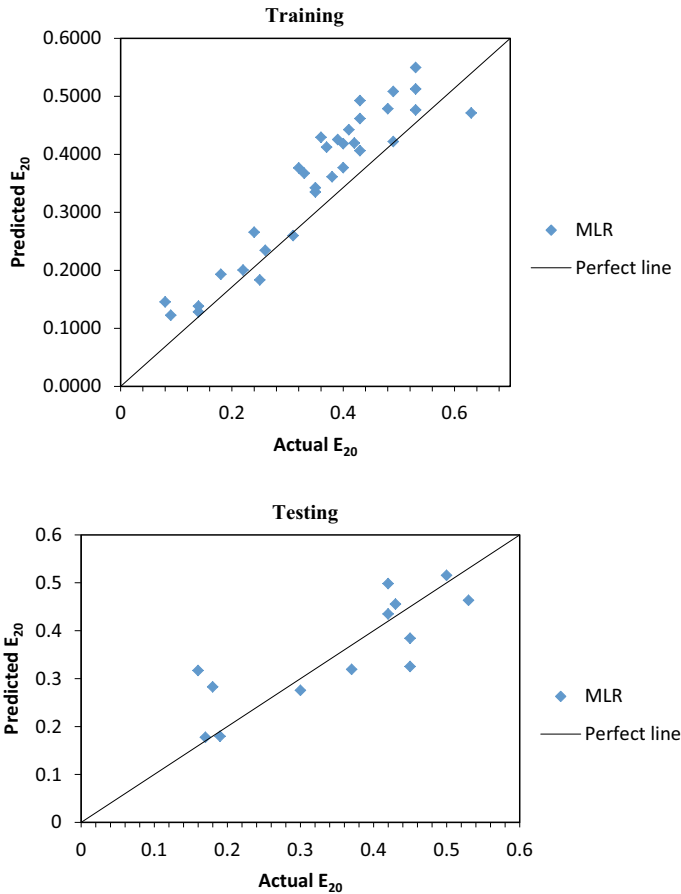
Fig. 7 Performance of MLR for training data set and testing data set

Table 3 Detail of performance evaluation using ANFIS, MLR, and MNLR

Approaches	Training data		Testing data	
	CC	RMSE	CC	RMSE
ANFIS_tri	0.81	0.03	0.81	0.03
ANFIS_trap	0.92	0.05	0.70	0.05
ANFIS_gbell	0.97	0.03	0.74	0.03
MNLR	0.93	0.05	0.83	0.07
MLR	0.94	0.05	0.82	0.07

4 Comparison of Models

It can be seen from Table 3 that aeration efficiency prediction using the MNLR technique yields better results as compared to ANFIS and MLR as it had a higher CC value and lower RMSE value as compared to ANFIS and MLR. The predicted values of aeration efficiency using regression analysis were plotted against experimental values for both training and testing data, as shown in Fig. 8. The predicted values of E_{20} lie closer to the perfect line indicating good estimation by the developed models. Figure 9 reinforces that ANFIS models perform better than the other applied models as RMSE values are least in the ANFIS models. The developed models can be used for predicting the aeration performance of the Montana flume.

The Montana flume accelerates flow by contraction of the sidewall. Turbulence inflow occurs, and the air is entrained into water. Figure 10 shows the variation of aeration efficiency with discharge per unit width. It is clear that aeration efficiency increases by an increase in flow rate. The maximum aeration efficiency of 0.66 is obtained for flume no.4, minimum aeration efficiency of 0.04 for flume no.3, and mean aeration efficiency is 0.37. Since the flow increases but throat thickness is the same, velocity gets accelerated at the throat and other sections as per the continuity equation, increasing aeration due to turbulence in the flow (Tiwari 2019; Tiwari and Sihag 2020).

Figure 11 shows the variation of aeration efficiency with flow rate for different widths, and from observation, it is clear that aeration efficiency increases with a decrease in throat width.

5 Conclusions and Recommendations

This study was conducted on two standard Montana flumes of throat width 2.54 cm, 5.08 cm, respectively, and three modified Montana flumes of throat width 7.62 cm. The following conclusion can be drawn from experimental observation:

- Aeration efficiency increases as discharge per unit width increases.
- Aeration efficiency increases with a decrease in throat width.
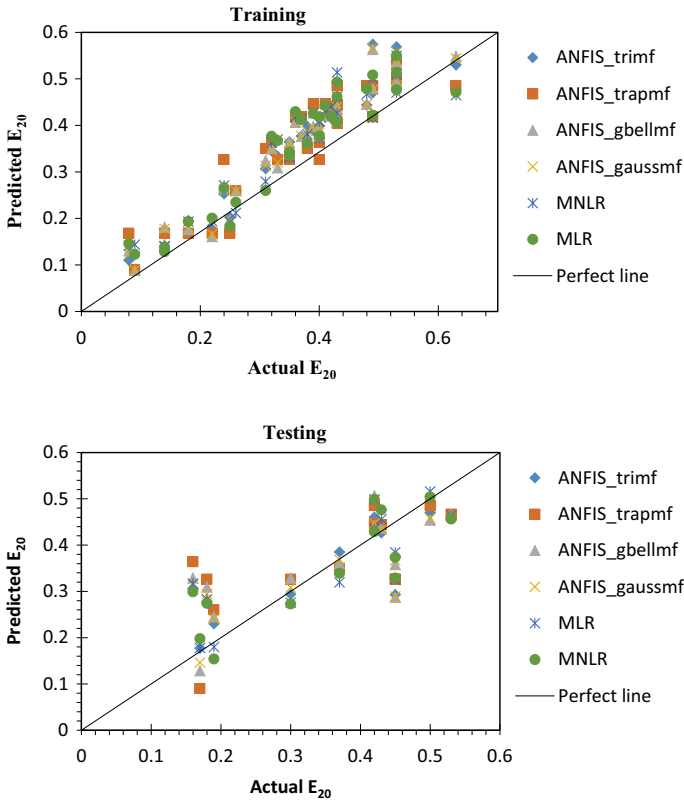
Fig. 8 Performance of models for training data and testing data

- The maximum aeration efficiency is 0.66, which is obtained for flume no. 4.
- The experimental observations obtained were modeled using ANFIS, MLR, and MNLR. An empirical relationship was established using MLR and MNLR with E_{20} as a function of discharge per unit width, upstream entrance width, sidewall length, and throat width. Results show that MNLR works better than MLR and ANFIS as it had a higher CC value and lower RMSE value.

Many researchers on different flumes have studied aeration efficiency, but there is a lack of knowledge of the oxygen transfer efficiency of Montana flume. The present study has been done for small Montana flumes, and future efforts can be made to determine the aeration efficiency of large Montana flumes.
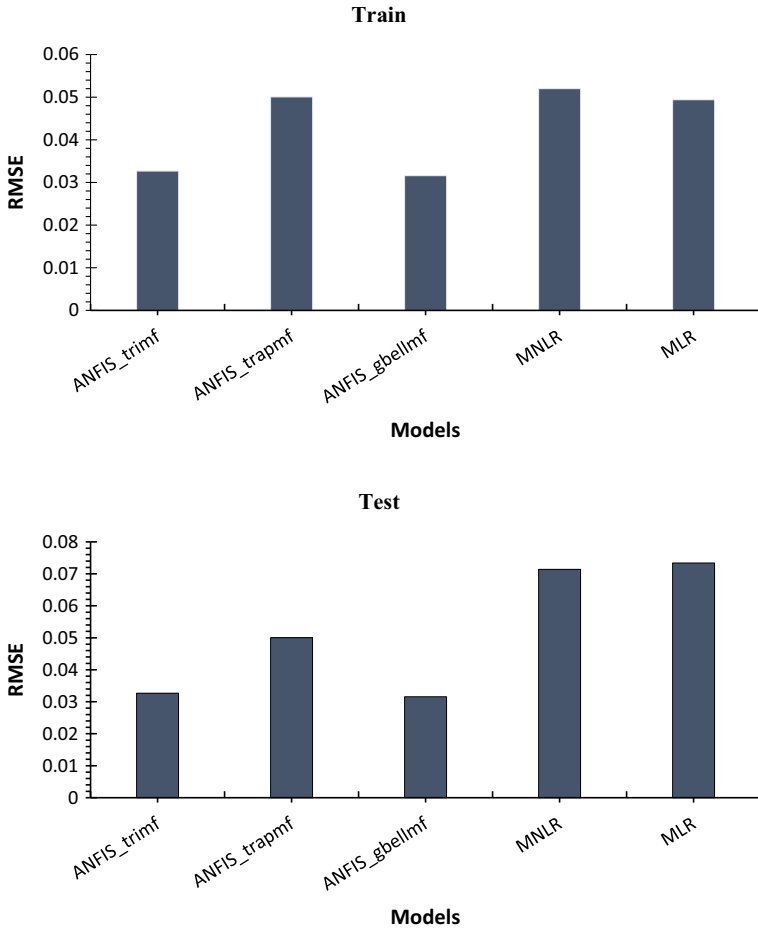
Fig. 9 Performance of soft computing models for Montana flume aeration
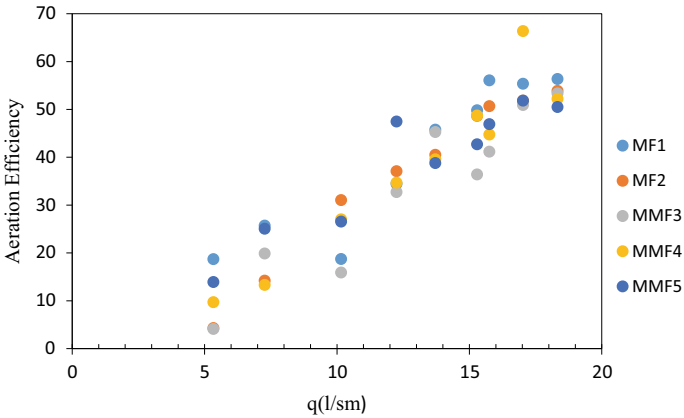
Fig. 10 Aeration efficiency respect to flow
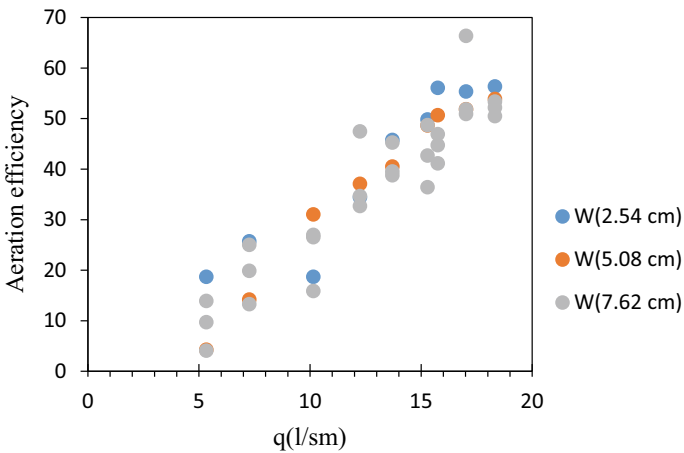
Fig. 11 Aeration efficiency respect to throat width

References

APHA, AWWA, WEF (2005) Standard methods for the examination of water and wastewater, vol 21, pp 258–259

Baylar A, Hanbay D, Ozpolat E (2008) An expert system for predicting aeration performance of weirs by using ANFIS. Expert Syst Appl 35(3):1214–1222

Dursun OF (2016) An experimental investigation of the aeration performance of Parshall flume and Venturi flumes. KSCE J Civ Eng 20(2):943–950

https://in.mathworks.com/. Accessed 2021/09/22

https://www.usbr.gov/tsc/techreferences/mands/wmm/WMM_3rd_2001.pdf. Accessed 2021/09/03

Lewis WK, Whitman WG (1924) Principles of gas absorption. Ind Eng Chem 16(12):1215–1220

Parshall RL (1941) Measuring water in irrigation channels. No. 1683. US Department of Agriculture

Sangeeta, Ranjan S, Tiwari NK (2019) Aeration efficiency evaluation of modified small Parshall flume using M5P and adaptive neuro-fuzzy. In: Sustainable engineering: proceedings of EGRWSE 2018, vol 30, p 243

Tiwari NK (2019) Evaluating hydraulic jump oxygen aeration by experimental observations and data driven techniques. ISH J Hydraul Eng 1–15

Tiwari NK, Sihag P (2020) Prediction of oxygen transfer at modified Parshall flumes using regression models. ISH J Hydraul Eng 26(2):209–220

Zytner RG, Rahmé ZG, Labocha M (1998) Oxygen uptake at Parshall flumes. Can J Civ Eng 25(4):769–776

Physicochemical and Pyrolysis Kinetic Aspects of Biomass Feedstocks: An Overview

Om Prakash Bamboriya, Anil Kumar Varma, Jagjeet Singh Yadav, and Lokendra Singh Thakur

Abstract This chapter focuses on physicochemical properties and kinetics of wood, agricultural, industrial waste, and energy crops for the application of pyrolysis. In the future, biomass could replace fossil fuels as a significant source of renewable energy. Pyrolysis produces valuable energy products, including bio-oil, biochar, and gases under an inert atmosphere and temperatures of 200–600 °C. The physicochemical characteristics are predicted by the lignocellulosic composition, proximal and ultimate analyses, which indicate the potential of biomass for pyrolysis. Reactions progressions depend on kinetics including activation energies and pre-exponential factors. The study of physicochemical and kinetic parameters is crucial for biomass thermal decomposition, design, and optimization of pyrolysis reactor as well as process conditions to obtain the desired product from pyrolysis.

Keywords Physicochemical · Biomass · Pyrolysis · Kinetics · Activation energies

1 Introduction

The over exploitation of fossil fuels impacts the sustainability of non-renewable energy resources and is also responsible for climate change (Feng and Lin 2017; Varma et al. 2020). The United Nations Climate Panel has set a target to reduce GHG emissions by 50–80% by 2050 (Bogner et al. 2008). As we know, fossil fuels are scarce, and rising in price demands the promotion of alternative bio-energy

O. P. Bamboriya · L. S. Thakur (✉)
Department of Chemical Engineering, Ujjain Engineering College, Ujjain, Madhya Pradesh 456010, India
e-mail: lokendrast@rediffmail.com

A. K. Varma
Department of Chemical Engineering, Assam Energy Institute (A Centre of RGIPT, Jais, Amethi), Sivasagar, Assam 785697, India

J. S. Yadav
Department of Petrochemical Engineering, Polytechnic College Ujjain, Ujjain, Madhya Pradesh 456010, India

resources like biomass, solar, wind, hydropower, geothermal and marine. Biomass is a significant contributor to renewable energy sources (Cao et al. 2016; Varma and Mondal 2016a). Biomass is an abundant, renewable, cost-effective, biodegradable, convenient, sustainable, alternative, and carbon–neutral energy source with an annual production of 10^{11}–10^{12} tonnes all over the globe (Demiral and Şensöz 2006). It is possible to take advantage of the ability to convert biomass into energy through thermochemical (direct combustion, gasification, liquefaction, and pyrolysis) and biochemical (fermentation and digestion, anaerobic and aerobic) conversion processes (Wang et al. 2017).

Biomass pyrolysis has emerged as the most desirable thermochemical conversion process by generating energy in three forms (solid, liquid, and gas). In pyrolysis, the thermal breakdown of biomass produces bio-oil, biochar, and non-condensed gases (Varma and Mondal 2016a, b; Thakur et al. 2018). The products distribution of the pyrolysis process depend on biomass characteristics, decomposition mechanism and different operating conditions such as temperature, feed composition (lignocellulose composition), particle size, retention time, moisture content, heating rate, presence of inorganic minerals content as well as the environmental conditions of pyrolysis process (Bamboriya et al. 2019; Varma et al. 2018; Oladeji et al. 2015; White et al. 2011).

Understanding the physicochemical and kinetics aspects of biological materials is essential for the biomass conversion processes (Dhyani and Bhaskar 2018; Cai et al. 2017). Physicochemical characteristics identify the lignocellulosic composition as well as proximate and ultimate composition in the biomass (Santos et al. 2015). Thermogravimetric analysis (TGA) approach is analyse the thermal decomposition mechanisms which is essential for the application of biomass pyrolysis. It is helpful for quantitative and qualitative analysis of energy products. The pyrolysis reaction kinetics is determined through TGA results with the help of kinetic models (Nyakuma et al. 2015; Ceylan and Topçu 2014).

Lignocellulose material is the dry matter of the plant, it mainly consists of hemicellulose, cellulose, lignin, and a limited fraction of moisture, extractive (fatty acids, resins, terpenes, and oils), and mineral matters may also present (White et al. 2011). These compositions depend on the type and grow location of biomass feedstocks (Wang et al. 2017). Biomass feedstocks are generated from the forest, agricultural and industrial sectors. Forest residues and agricultural wastes are the most favorable biomass feedstocks because of their plentiful availability and inexpensive nature (Cai et al. 2017), such as Rice and Wheat straw, Babool seed, Vetiver grass, and many more.

This chapter aims to provide a summary of the physicochemical characteristics and pyrolysis kinetics of biomass and wastes. The pyrolysis kinetics have been analysed by model fitting and model-free method, which are suggested by the Kissinger Akahira Sunose (KAS), Ozawa Flynn Wall (OFW), and Coats Redfern (CR) methods.

2 Physicochemical Characteristics of Biomass

Physicochemical Characterization is essential to determine whether biomass can be adopted as a viable source of energy for pyrolysis process (Parikh et al. 2007). Biomass is evaluated according to its physical and chemical properties to assess its potential as pyrolysis feedstock. The physicochemical characteristics of biomass include lignocellulosic composition, heating value, proximate and ultimate composition.

2.1 *Lignocellulosic Composition*

Biomass is a natural carbohydrate biopolymer constituted of hemicellulose, cellulose, lignin, extractive, and minerals (Bamboriya et al. 2019; Dhyani and Bhaskar 2018; Santos et al. 2015). Table 1 displays the lignocellulosic constituent percentage, temperature range of decomposition, and activation energy. Table 2 summarized the lignocellulosic composition of different biomass.

2.1.1 Cellulose

This is the most prominent lignocellulosic constituent comprise near to 40–50 wt.% of dry wood. It consists of D-glucose molecules in linear homo polysaccharides that are inextricably linked by β-1,4-glycopyranose units; This cellulose network is formed by the repeating units of the cellulose chain, which are the two units of anhydrous glucose (Mohan et al. 2006). The cellulose chains are bound together with intermolecular and intramolecular hydrogen bonds between OH groups and formed a molecular network resembling a crystal. After that, groups of cellulose linkage change in microfibrils, and finally, cellulose fibers are formed. In general, cellulose's molecular weight is approximately 100,000, and the generic structure is like $(C_6H_{10}O_5)_n$ (Saxena et al. 2009).

Table 1 Lignocellulosic composition of biomass, their range of decomposition temperature and activation energy (Feng and Lin 2017; Yang et al. 2007)

Lignocellulose constituents	Composition (wt. %)	Decomposition temperature range (°C)	Activation energy (kJ/mol)
Cellulose	40–50	250–380	145–285
Hemicellulose	20–40	200–380	90–125
Lignin	10–25	180–900	30–39

Table 2 Lignocellulosic composition of different biomass

Biomass	Lignocellulosic composition (wt. %)			References
	Cellulose	Hemicellulose	Lignin	
Azadirachta indica seeds	38.61	24.64	12.89	Mishra and Mohanty (2020)
Phyllanthus emblica	46.11	21.43	10.22	
Parthenium hysterophorus	46.66	26.26	18.83	Lanjewar et al. (2020)
Peanut shell	35.7	18.7	30.2	Varma et al. (2020)
Vetiver grass	39.14	48.57	11.02	Thakur et al. (2018)
Walnut shell	32.19	26.20	36.89	Özsin and Pütün (2017)
Peach stones	29.50	25.10	39.26	
Wood sawdust	32	28	23	Bhatti and Chouhan (2016)
Pine needles	34.5	29.1	31.7	Varma and Mondal (2016a)
Wood saw dust	47.62	39	11.23	Varma and Mondal (2016b)
Sugarcane bagasse	47.6	39	11.2	Varma and Mondal (2016c)
Babool seed	41	24	15	Garg et al. (2016)
Castor beans cake	46.9	4.7	32.3	Santos et al. (2015)
Ramie fabric waste	72.45	14.21	1.03	Zhu (2015)
Hazelnut husk	34.5	20.6	35.1	Ceylan and Topçu (2014)
Wood	35–50	20–30	25–30	Jahirul et al. (2012)
Wheat straw	34.6	21.3	29.3	Naik (2010)
Pinewood	39.0	34.0	12.0	
Rapeseed oil cake	28.6	41.4	5.0	Ucar and Ozkan (2008)

2.1.2 Hemicellulose

It is the second principal lignocellulosic constituent in biomass usually account for 20–40 wt.% of dry wood. In contrast to cellulose, hemicellulose is a heteropolysaccharide consist of different monosaccharide units and lower molecular weight than cellulose (Balat and Kırtay 2010). It is also known as polyose. The monomeric components of hemicellulose are pentose sugar (xylose and arabinose), hexose sugar (glucose, mannose, and galactose), and sugar acid (glucuronic acids and galacturonicacis) (Mohan et al. 2006; Balat and Kırtay 2010).

2.1.3 Lignin

It is the third major lignocellulosic component of biomass. It is a highly branched, substituted, three-dimensional amorphous biopolymer composed of phenyl propane units, primarily p-hydroxy-phenyl, syringyl, and guaacyl, forming bonds with C–O, and C–C. The outermost layer of the fiber consists mainly of lignin, it provides rigid

structure and holds the fibrous cellulosic components (Saxena et al. 2009; Stöcker 2008).

2.1.4 Organic Extractives

Biomass comprises a small amount of low molecular weight organic extractives, miscible in neutral solvents. The extractive includes fats, proteins, phenolics, waxes, simple sugars, alkaloids, gums, starches, saponins, glycosides, and essential oil. Organic extractives are helpful in metabolism and protect against insect attack and microbial destruction (Mohan et al. 2006; Lanjewar et al. 2020).

2.1.5 Inorganic Matter

Biomass consists of small amounts of inorganic substances that end up in ash. Calcium (Ca), magnesium (Mg), potassium (K), and silica (Si) are the most common inorganic elements found in biomass. Other inorganic substances such as sodium (Na) and phosphorus (P) are also found in small amounts in many biomass (Dhyani and Bhaskar 2018; Mohan et al. 2006).

2.2 Proximate Composition

Volatile matter (VM), fixed carbon (FC), moisture (M), and ash (A) present in biomass is determined by proximate analysis. It also provides information about chemical energy stored in biomass. Moisture content varies with the biomass type, and its suitability depends on the conversion process. High moist contents are favourable for the biochemical means, but for thermo-chemical operation, high moisture content adversely affects the processing (Chutia et al. 2013; McKendry 2002). Heat transfer is reduced, and product distribution is affected significantly when biomass has high moist contents (López et al. 2002). In the pyrolysis process, moisture content should be less than 10 wt.% for proper heat transfer (Asadullah et al. 2007). Volatile matter is released during the thermal degradation of biomass in the form of non-condensable and condensable gases (Bamboriya et al. 2019; Chutia et al. 2013). In general, pyrolysis feedstock should have a high VM; high VM biomass is more reactive and easily gasified and thus produces higher bio-oils and syngas. In contrast, the production of biochar is related to high fixed carbon, i.e., the desirable state of VM and FC depends on the energy purpose (McKendry 2002; Graboski and Bain 1979). Another important proximate composition of biomass is ash content, an inorganic residue leftover after combustion because ash is a non-biodegradable material. The high ash contents adversely affect the decomposition rate and responsible for the formation of slag, rust, and fouling (McKendry 2002; Fernandes et al. 2013).

2.3 Ultimate Composition

Ultimate composition gives more comprehensive information of material than proximate composition. It is a quantitative assessment of the various components of biomass, such as carbon (C), hydrogen (H), oxygen (O), sulphur (S), and nitrogen (N) (Varma and Mondal 2016a). Various studies have shown that biomass has a lower C and higher O content than fossil fuels, because of which biomass is less energy efficient than fossil fuels. Low values of N and S content in biomass are environmentally suitable (Parikh et al. 2005).

2.4 Heating Value

The heating value means the energy production per unit mass of biomass during combustion. It is represented by HHV (higher heating value) (Amutio et al. 2012). Since biomass has high O content, it has a low heating value compared to fossil fuels (Varma and Mondal 2016c). A bomb calorimeter is usually used to measure the heating value of solid fuel. In addition, various empirical correlations are used to evaluate the HHV from the proximate and ultimate analysis data. Table 3 shows the proximate and ultimate compositions, as well as HHV for various biomasses.

3 Thermal Analysis and Pyrolysis Kinetics of Biomass

3.1 Thermal Behaviour of Biomass

Thermal degradation of biomass is a critical step to analysing the thermal characteristics of biomass. The thermal degradation behavior of biomass is analysed by thermogravimetric analysis (TGA). TGA provides the information on mass loss over temperature and time (Rana et al. 2013). Many researchers have described the thermal decomposition pattern of different biomass through TGA, such as rice straw (Mishra and Bhaskar 2014), sugarcane bagasse (Varma and Mondal 2016c), wheat straw (Cai and Bi 2009), vetiver grass (Thakur et al. 2018), and many more. The pyrolysis kinetics depends on the thermal stability of biomass (Dhyani and Bhaskar 2018). Pyrolysis process and the distributions of its products are dependent on the lignocellulosic components of the feedstocks. Therefore, knowledge of the thermal degradation behavior of these components is crucial in order to understand pyrolysis of biomass.

Yang et al. (2007) describe the TG and DTG curve for a pure form of lignocellulosic constituents. The thermal decomposition behaviour of hemicellulose, cellulose and lignin biomass components varies widely with each other. Hemicellulose decomposes during the early stages of the process, leading to weight loss in the

Table 3 Proximate and ultimate composition and HHV of different biomasses

Biomass	Proximate composition (wt. %)				Ultimate composition (wt. %)					HHV (MJ/kg)	References
	M	VM	FC	Ash	C	H	O	N	S		
Azadirachta indica	5.68	74.23	16.63	3.46	50.36	7.26	37.78	3.81	0.79	21.25	Mishra and Mohanty (2020)
Phyllanthus emblica	5.26	71.10	18.32	3.32	50.16	6.91	40.31	2.41	0.21	19.24	
Parthenium hysterophos	5.80	74.55	8.82	10.3	44.93	6.43	45.55	2.67	0.42	17.97	Lanjewar et al. (2020)
Peanut shell	5.16	80.24	8.48	6.12	46.86	6.84	44.98	1.03	0.29	18.64	Varma et al. (2020)
Waste milk packets	0.08	97.30	2.53	0.09	82.14	11.3	6.46	0.05	–	–	Singh et al. (2019)
Jatropha de-oil cake	–	–	–	–	53.4	6.81	29.3	0.45	0.12	–	Sharma and Sheth (2018)
Vetiver grass	5.73	80.5	2.84	10.8	42.28	5.54	51.54	0.64	–	15.8	Thakur et al. (2018)
Walnut shell	6.98	76.4	16	0.58	47.5	6.71	45.5	0.21	–	17.83	Özsin and Pütün (2017)
Peach stones	6.68	72.4	19.8	0.86	49.3	6.65	43.7	0.34	–	18.37	
Wood sawdust	5	80.9	12.1	2	55	6	37	–	–	19.2	Bhatti and Chouhan (2016)
Pine needles	5.30	77.5	13.7	3.38	46.4	7.08	46.0	0.45	0.07	19.22	Varma and Mondal (2016a)
Wood saw dust	3.07	80.87	12.68	3.38	46.09	6.62	47.19	0.10	–	18.34	Varma and Mondal (2016b)
Sugarcane bagasse	5.4	80.2	11.3	3.1	44.8	5.87	48.9	0.24	0.06	18.0	Varma and Mondal (2016c)
Babool seeds	12.5	69.1	11	7.3	54.1	6.12	34.5	5.23	–	–	Garg et al. (2016)
Castor bean cake	7.2	65.2	23.3	4.2	48.9	5.5	42.6	2.8	0.12	22.6	Santos et al. (2015)
Ramie fabric waste	4.43	79.9	12.4	2.45	45.9	6.14	47.5	0.42	–	17.65	Zhu (2015)
Hazelnut husk	7.2	73.9	20.9	5.3	42.6	5.5	50.6	1.13	0.14	18.5	Ceylan and Topçu (2014)
Orange waste	5.7	74.6	16.6	3.02	47.0	6.9	44.7	1.3	0.09	–	Lopez-Velazquez et al. (2013)
Sugarcane bagasse	6.7	76.1	6.9	9.6	45.0	6.0	38.8	0.5	0.1	17.6	Carrier et al. (2013)
Wood	2.0	82	17	0.4–1	51.6	6.3	41.5	0.1	–	20	Jahirul et al. (2012)

(continued)

Table 3 (continued)

Biomass	Proximate composition (wt. %)				Ultimate composition (wt. %)					HHV (MJ/kg)	References
	M	VM	FC	Ash	C	H	O	N	S		
Groundnut de-oil cake	5.6	83	6.6	4.8	46.3	7.01	39.4	6.89	0.28	15	Agrawalla et al. (2011)
Wheat straw	6.0	78.3	14.4	1.5	41.6	6.1	52.1	0.14	0.06	20.3	Naik (2010)
Rapeseed oil cake	10.6	67.3	15.8	6.3	45.9	6.2	40.1	6.9	0.88	19.5	Ucar and Ozkan (2008)

220–315 °C temperature range, with a maximum weight loss rate of 0.95 wt.%/°C achieved at 268 °C and at high temperature (900 °C), approximately 20% of solid material was left behind. The decomposition of cellulose is found between 315 and 400 °C, while the highest rate of weight loss is 2.84 wt.%/°C at 355 °C. It is observed that almost all cellulose decomposes at 400 °C, and the remaining residue is only ~6.5%. Compared to cellulose and hemicellulose, lignin has more excellent thermal stability. It decomposes slowly in the 100–900 °C temperature range, and approximately 48 wt.% residues are left (Rastrogi et al. 2016). It is the highest solid residue at higher temperatures compared to cellulose and hemicellulose. These percentages change across the temperature range due to differences in the chemical bonding between these three components and are also responsible for the different thermal behaviour of the biomass (Varma and Mondal 2016a; Dhyani and Bhaskar 2018; Rastrogi et al. 2016).

3.2 Pyrolysis Kinetics of Biomass

The information and knowledge of pyrolysis kinetic parameters are vital for the design and optimization of pyrolysis reactors (Varma et al. 2018; Mishra and Bhaskar 2014). TGA is commonly performed for solid-state biomass. TGA data is used in reaction kinetics prediction (Varma and Mondal 2016a; White et al. 2011). Kinetic studies help to examine the reaction progress and evaluate kinetic parameters. These parameters are essential for design of safe, optimistic, and highly efficient pyrolysis processes (Dhyani and Bhaskar 2018; Ceylan and Topçu 2014; Lopez-Velazquez et al. 2013; Varma and Mondal 2017).

3.2.1 Kinetic Theory

Biomass decomposition can be written in a single step, as shown in Eq. (1) (Lanjewar et al. 2020).

$$\text{Biomass (solid)} \xrightarrow{\text{k(T)}} \text{Char (solid)} + \text{Volatiles (gases and tar)} \tag{1}$$
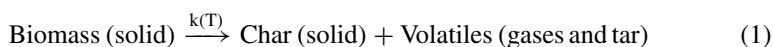
k(T) is a temperature-dependent term that stands for reaction rate constant. As per Arrhenius, k(T) defines as:

$$\text{k(T)} = A e^{-E_a/\text{RT}} \tag{2}$$

This equation includes A, which stands for pre-exponential factor (min^{-1}), E_a for activation energy (kJ/mol), T for temperature (K), and R for gas constant.

The rate of biomass decomposition can be written in the form of k(T) and reaction model f(α),

$$\frac{d\alpha}{dt} = k(T) \, f(\alpha) \tag{3}$$

As a result, conversion will define like this:

$$\alpha = \frac{(m_i - m_\alpha)}{(m_i - m_f)} \tag{4}$$

This equation includes m_i, m_α, and m_f represent mass associated with the initial, at time t, and unreacted samples, respectively.

From Eqs. (2) and (3),

$$\frac{d\alpha}{dt} = A e^{-E_a/RT} f(\alpha) \tag{5}$$

TGA data can be employed for kinetics evaluation using two types of experimental methods (White et al. 2011; Mishra and Mohanty 2020; Varma and Mondal 2016c; Singh et al. 2019).

Isothermal Method

In this method, kinetics is achieved at a constant temperature. In the case of isotheral methods, kinetics is obtained through various experiments conducted at different temperatures (White et al. 2011).

Non-isothermal Method

It is also known as a dynamic method. It is generally preferred for the kinetic analysis of biomass pyrolysis as more than one mass loss curve is used in this method for calculating the kinetic parameters. Results sensitivity and accuracy are better than the isothermal methods, due to this, the non-isothermal methods are widely used (White et al. 2011). Figure 1 displays the various calculation methods for kinetic evaluation of biomass pyrolysis based on TGA data.

There are two types of non-isothermal methods used for calculating kinetics from experimental TGA data: model-free and model-fitting (Thakur et al. 2018). For kinetic analysis, models-fitting kinetic methods are usually suitable because they are simple. For all the proposed model-fitting methods, the reaction rate is correlated with the function of conversion. Inadequacy of linearity in plots and variation in activation energies is the limitations of model-fitting methods. It has been concluded that the applied model cannot portray the actual process behavior when choosing inappropriate models for kinetic parameter calculation corresponds to varying heating rates (White et al. 2011; Sánchez-Jiménez et al. 2013). The model-free method works on isoconversional basis, in which a constant rate of reaction is assumed during biomass thermal degradation, and rate constant and conversion are strongly dependent on
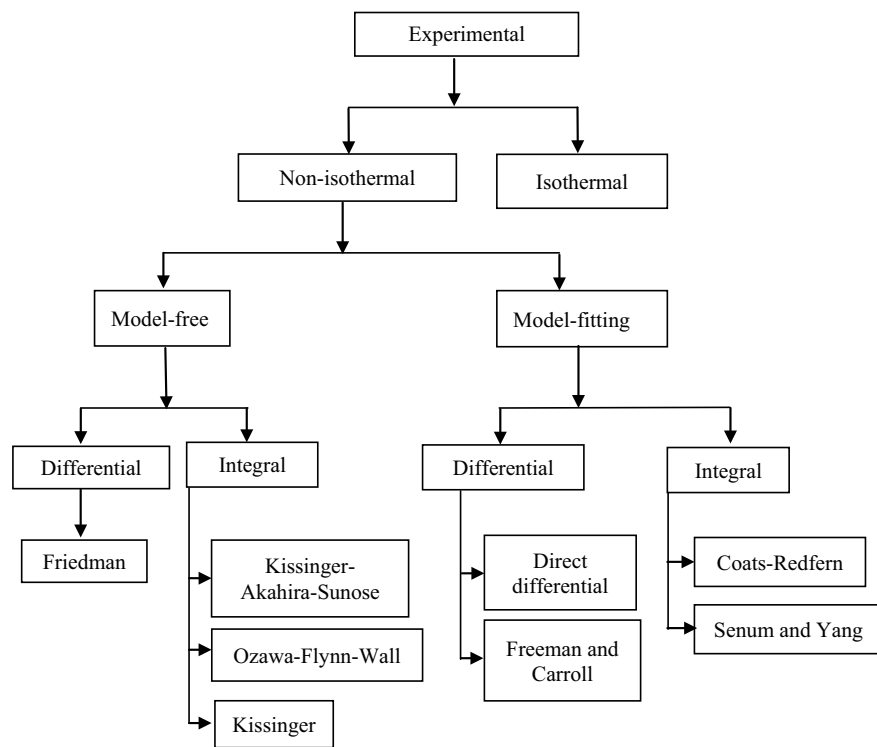
Fig. 1 Summary of different methods for calculating biomass kinetics (White et al. 2011; Sbirrazzuoli et al. 2009)

temperature. The activation energies are calculated by the conversion factor (White et al. 2011; Alwani et al. 2014). The kinetics are analysed by model-free methods using TGA data at various heating rates without considering any hypothesis relating to reaction rate and order (Santos et al. 2015; Slopiecka et al. 2012; Vyazovkin et al. 2011). There are many methods available in the literature to determining the solid-state kinetics from TGA results.

3.2.2 Kinetic Parameter Determine Based on Non-isothermal Methods

For non-isothermal cases, biomass sample temperature at any time t depends on the linear heating rate, which is expressed by Eq. (6) (Lanjewar et al. 2020; Varma and Mondal 2016c; Singh et al. 2019)

$$T = To + \beta t \tag{6}$$

T_o represents for base temperature and β for linear heating rate. From Eq. (6), β can be written as:

$$\beta = \frac{dT}{dt} = \frac{dT}{d\alpha}\frac{d\alpha}{dt} \tag{7}$$

Combining Eqs. (5) and (7), we get Eq. (8)

$$\frac{d\alpha}{dT} = \frac{A}{\beta} f(\alpha)e^{-\frac{E_a}{RT}} \tag{8}$$

Equation (8) shows the mass fraction of biomass reacted with temperature. From Eq. (8)

$$G(\alpha) = \int_0^\alpha \frac{d\alpha}{f(\alpha)} = \int_0^T \frac{A}{\beta}e^{-E_a/RT}dT = \frac{AE_a}{\beta R}\int_x^\infty u^{-2}e^{-u}du = \frac{AE_a}{\beta R}p(x) \tag{9}$$

where the integral G(α) is a conversion-dependent function and x stands for E_a/RT, and p(x) is an integral temperature-dependent function. As shown in Fig. 1, many non-isothermal-based model-fitting and model-free methods are applied to determine the kinetics since each method has its advantages and limitations. However, OFW, KAS, and Coats–Redfern methods are mainly applied for the analysis of pyrolysis kinetics because these methods are simple and provide greater accuracy in the calculation of the kinetic parameters (Wang et al. 2017; Thakur et al. 2018; Ceylan and Topçu 2014; Islam et al. 2015). The detail of the following methods are illustrated below:

Kissinger–Akahira–Sunose (KAS) Method

This model-free method uses algorithms to determine the apparent activation energy for a given model. The KAS method requires a temperature at a particular conversion at a constant β. KAS applies p(x) = $x^{-2}e^{-x}$ approximation in Eq. (9) and take logarithm and rearranging the equation becomes as follows:

$$\ln\left(\frac{\beta}{T^2}\right) = \ln\left[\frac{AE_a}{RG(\alpha)}\right] - \frac{E_a}{RT} \tag{10}$$

$\ln(\beta/T^2)$ versus 1/T plots at a particular value of conversion (0.1–1.0) gives the slope $-E_a/R$ in which the value of R is 8.314 J/mol K (Cao et al. 2016; Lopez-Velazquez et al. 2013).

Ozawa–Flynn–Wall (OFW) Method

This method is also a non-isothermal model-free method. The OFW method uses Doyle's approximation $\log[p(x)] = 2.315 + 0.457x$ in integrating Eq. (9). After substituting and rearranging, the expression becomes as follows:

$$\log(\beta) = \log\left[\frac{AE_a}{RG(\alpha)}\right] - 2.315 - 0.457\left(\frac{E_a}{RT}\right) \tag{11}$$

From Eq. (11), draw a plot between $\log(\beta)$ and $1/T$ at different degrees of conversions give the parallel lines at different conversion values. The slope of each line represents the value of $-E_a/R$ at respective conversion (Varma et al. 2020; Ceylan and Topçu 2014).

Coats–Redfern (CR) Method

This method is widely applied to calculate the pyrolysis kinetics. The CR method evaluated the pre-exponential factor and order of reaction for the pyrolysis process. In contrast, KAS and OFW are sufficient to calculating activation energy (Singh et al. 2019; Mehmood et al. 2017).

For nth order reaction rate, the CR method has been obtained from the Arrhenius expression as follows:

$$\frac{d\alpha}{dt} = K(T)(1 - \alpha)^n \tag{12}$$

From Eqs. (5), (8), and (12)

$$\frac{d\alpha}{(1 - \alpha)^n} = \frac{A}{\beta} e^{-E_a/RT} dT \tag{13}$$

After integrating Eq. (13), which gives the result,

$$\frac{1 - (1 - \alpha)^{1-n}}{1 - n} = \frac{A}{\beta} \int_0^T e^{-E_a/RT} dT \tag{14}$$

The integral term in Eq. (14) has no exact solution. To simplify, we can write the expression by applying Taylor series expansion and eliminating higher-order terms (Ceylan and Topçu 2014).

$$\ln\left[g(\alpha)\right] = -\frac{E_a}{RT} + \ln\left(\frac{AR}{\beta E_a}\right) \tag{15}$$

Table 4 Activation energies of biomasses

Biomass	E_a (kJ/mol)		References
	KAS method	OFW method	
Azadirachta indica seeds	176.66	193.67	Mishra and Mohanty (2020)
Phyllanthus emblica	184.77	195.10	
Parthenium hysterophorus	155.75	163.17	Lanjewar et al. (2020)
Peanut shell	109.94	96.93	Varma et al. (2020)
Waste milk packets	175.36	177.94	Singh et al. (2019)
Vetiver grass	151.23	161.33	Thakur et al. (2018)
Camel grass	84–193	96–192	Mehmood et al. (2017)
Para grass	103–223	117–233	Ahmad et al. (2017)
Pine needle	70.97	79.13	Varma and Mondal (2016a)
Wood sawdust	164.24	173.41	Varma and Mondal (2016b)
Sugar cane bagasse	91.64	104.43	Varma and Mondal (2016c)
Ramie fabric waste	126–167	130–180	Zhu (2015)
Karanj fruit hulls	61.06	68.53	Islam et al. (2015)
Oil palm empty fruit	–	160.21	Nyakuma et al. (2015)
Castor beans presscake	270	263	Santos et al. (2015)
Rice straw	139–282	141–280	Mishra and Bhaskar (2014)
Hazelnut husk	103–164	106–161	Ceylan and Topçu (2014)
Wheat straw	144.05	146.89	Wu et al. (2014)
Cellulose	130.91	134.5	
Orange waste	120–250	–	Lopez-Velazquez et al. (2013)
Poplar wood	104–209	107–209	Slopiecka et al. (2012)
Cardoon stems	224	229	Damartzis et al. (2011)
Cardoon leaves	350	242	
Arbutus unedo	40–125	–	Leroy et al. (2010)
Wheat straw	–	130–175	Cai and Bi (2009)

For the first-order reaction g (α) is expressed $-\ln\left[\frac{(1-\alpha)}{T^2}\right]$ and except for the first-order reaction g(α) is expressed $\frac{1-(1-\alpha)^{1-n}}{(1-n)T^2}$.

Draw a plot between $\ln\left[g(\alpha)\right]$ and 1/T, based on which we get the slope $-E_a/R$ and intercept $\ln\left(\frac{AR}{\beta E_a}\right)$. In other words, we can get E_a and A from these graphical plots (Varma et al. 2020; Cao et al. 2016; Chouhan et al. 2013; Ahmad et al. 2017). Table 4 shows the activation energy of different biomasses.

The pre-exponential factors of biomasses have been reported in the literature. Pre-exponential factors value differ with the types of biomass, degree of conversion, and heating rates, so the values in the literature are given as ranges with unit min^{-1}. The pre-exponential factor is computed by Coats–Redfern method using E_a calculated

by KAS and FWO methods for different biomass are 7.18×10^{10}–2.37×10^{12} for sugarcane bagasse (Varma and Mondal 2016c), 7.61×10^5–2.45×10^{13} for hazelnut husk (Ceylan and Topçu 2014), 7.39×10^{12}–5.13×10^{13} for vetiver grass (Thakur et al. 2018), 1.37×10^{13}–1.54×10^{14} for waste milk packets (Singh et al. 2019), 2.99×10^{12}–7×10^{13} for peanut shell (Varma et al. 2020), 9.56×10^{12}–7.63×10^{13} for *Parthenium hysterophorus* (Lanjewar et al. 2020), 5.62×10^{13}–5.95×10^{13} for waste corn stalks and pyrolusite (Du et al. 2021), 1.60×10^{15}–1.05×10^{20} for *Azadirachta indica* seeds, 6.48×10^{13}–2.90×10^{18} for *Phyllanthus emblica* seeds (Mishra and Mohanty 2020) and so on.

4 Conclusion

An overview of the physicochemical characteristics and pyrolysis kinetics of biomass has been provided in this book chapter. Unlike the bio-chemical conversion process, the thermochemical conversion is much quicker and less complicated. Biomass to energy conversion route by thermochemical means is a favourable choice in many energy applications. Estimation of physicochemical and thermochemical aspect is essential to determine suitability of biomass as a pyrolysis feedstock. The thermochemical route is the best option for energy conversion from biomass. Lignocellulosic biomasses can be converted into biofuels and other valuable chemicals via pyrolysis. In lignocellulosic biomass, there are three principal constituents; hemicellulose, cellulose, and lignin, and their proportions determine the product distribution. Model-free and model-fitting methods for pyrolysis kinetics of biomass can provide the insight of the reaction mechanism that will enable reactors to be designed and optimized on a large scale. Mechanisms of reactions can be explained by considering the kinetic parameters like activation energy and pre-exponential factor. KAS, OFW, Coats Redfern, and many other approaches are available in the literature to determine kinetic parameters for pyrolysis of biomass. This study can help to estimate the kinetic and energy potential of biofuels derived from different biomasses and assesses their potential use as renewable energy.

References

Agrawalla A, Kumar S, Singh RK (2011) Pyrolysis of groundnut de-oiled cake and characterization of the liquid product. Bioresour Technol 102(22):10711–10716

Ahmad MS, Mehmood MA, Al Ayed OS, Ye G, Luo H, Ibrahim M, Rashid U, Nehdi IA, Qadir G (2017) Kinetic analyses and pyrolytic behavior of Para grass (*Urochloa mutica*) for its bioenergy potential. Bioresour Technol 224:708–713

Alwani MS, Abdul Khalil HPS, Sulaiman O, Islam MN, Dungani R (2014) An approach to using agricultural waste fibres in biocomposites application: thermogravimetric analysis and activation energy study. BioResources 9(1):218–230

Amutio M, Lopez G, Aguado R, Artetxe M, Bilbao J, Olazar M (2012) Kinetic study of lignocellulosic biomass oxidative pyrolysis. Fuel 95:305–311

Asadullah M, Anisur Rahman M, Mohsin Ali M, Rahman MS, Motin MA, Sultan MB, Alam MR (2007) Production of bio-oil from fixed bed pyrolysis of bagasse. Fuel 86(16):2514–2520

Balat H, Kırtay E (2010) Hydrogen from biomass—present scenario and future prospects. Int J Hydrogen Energy 35(14):7416–7426

Bamboriya OP, Thakur LS, Parmar H, Varma AK, Hinge VK (2019) A review on mechanism and factors affecting pyrolysis of biomass. Int J Res Adv Technol 7(3):1014–1024

Bhatti B, Chouhan APS (2016) Thermo-gravimetric analysis of wood saw dust for evaluation of kinetics parameter. Indian J Sci Technol 9(44):1–4

Bogner J, Pipatti R, Hashimoto S, Diaz C, Mareckova K, Diaz L, Kjeldsen P et al (2008) Mitigation of global greenhouse gas emissions from waste: conclusions and strategies from the Intergovernmental Panel on Climate Change (IPCC) Fourth Assessment Report. Working Group III (Mitigation). Waste Manag Res 26:11–32

Cai J-M, Bi L-S (2009) Kinetic analysis of wheat straw pyrolysis using isoconversional methods. J Therm Anal Calorim 98(1):325–330

Cai J, He Y, Xi Y, Banks SW, Yang Y, Zhang X, Yang Y, Liu R, Bridgwater AV (2017) Review of physicochemical properties and analytical characterization of lignocellulosic biomass. Renew Sustain Energy Rev 76:309–322

Cao L, Yuan X, Jiang L, Li C, Xiao Z, Huang Z, Chen X, Zeng G, Li H (2016) Thermogravimetric characteristics and kinetics analysis of oil cake and torrefied biomass blends. Fuel 175:129–136

Carrier M, Joubert J-E, Danje S, Hugo T, Görgens J, Knoetze JH (2013) Impact of the lignocellulosic material on fast pyrolysis yields and product quality. Bioresour Technol 150:129–138

Ceylan S, Topçu Y (2014) Pyrolysis kinetics of hazelnut husk using thermogravimetric analysis. Bioresour Technol 156:182–188

Chouhan, Singh AP, Singh N, Sarma AK (2013) A comparative analysis of kinetic parameters from TGDTA of *Jatropha curcas* oil, biodiesel, petroleum diesel and B50 using different methods. Fuel 109:217–224

Chutia RS, Kataki R, Bhaskar T (2013) Thermogravimetric and decomposition kinetic studies of *Mesua ferrea* L. deoiled cake. Bioresour Technol 139:66–72

Damartzis T, Vamvuka D, Sfakiotakis S, Zabaniotou A (2011) Thermal degradation studies and kinetic modeling of cardoon (*Cynara cardunculus*) pyrolysis using thermogravimetric analysis (TGA). Bioresour Technol 102(10):6230–6238

Demiral İ, Şensöz S (2006) Fixed-bed pyrolysis of hazelnut (*Corylus avellana* L.) bagasse: influence of pyrolysis parameters on product yields. Energy Sources Part A Recov Util Environ Effects 28(12):1149–1158

Dhyani V, Bhaskar T (2018) A comprehensive review on the pyrolysis of lignocellulosic biomass. Renew Energy 129:695–716

Du J, Gao L, Yang Y, Chen G, Guo S, Omran M, Chen J, Ruan R (2021) Study on thermochemical characteristics properties and pyrolysis kinetics of the mixtures of waste corn stalk and pyrolusite. Bioresour Technol 324:124660

Feng Q, Lin Y (2017) Integrated processes of anaerobic digestion and pyrolysis for higher bioenergy recovery from lignocellulosic biomass: a brief review. Renew Sustain Energy Rev 77:1272–1287

Fernandes E, Kasper R, Marangoni C, Souza O, Sellin N (2013) Thermochemical characterization of banana leaves as a potential energy source. Energy Convers Manage 75:603–608

Garg R, Anand N, Kumar D (2016) Pyrolysis of babool seeds (*Acacia nilotica*) in a fixed bed reactor and bio-oil characterization. Renew Energy 96:167–171

Graboski M, Bain RL (1979) Properties of biomass relevant to gasification. In: A survey of biomass gasification, vol 2, pp 21–65

Islam MA, Asif M, Hameed BH (2015) Pyrolysis kinetics of raw and hydrothermally carbonized Karanj (*Pongamia pinnata*) fruit hulls via thermogravimetric analysis. Bioresour Technol 179:227–233

Jahirul MI, Rasul MG, Chowdhury AA, Ashwath N (2012) Biofuels production through biomass pyrolysis—a technological review. Energies 5(12):4952–5001

Lanjewar R, Thakur LS, Varma AK, Shankar R, Mondal P (2020) Physicochemical characterization and kinetics study of *Parthenium hysterophorus* for pyrolysis process. Energy Sources Part A Recov Util Environ Effects 1–15

Leroy V, Cancellieri D, Leoni E, Rossi J-L (2010) Kinetic study of forest fuels by TGA: model-free kinetic approach for the prediction of phenomena. Thermochim Acta 497(1–2):1–6

López MCB, Blanco CG, Martínez-Alonso A, Tascón JMD (2002) Composition of gases released during olive stones pyrolysis. J Anal Appl Pyrol 65(2):313–322

Lopez-Velazquez MA, Santes V, Balmaseda J, Torres-Garcia E (2013) Pyrolysis of orange waste: a thermo-kinetic study. J Anal Appl Pyrol 99:170–177

McKendry P (2002) Energy production from biomass (part 1): overview of biomass. Bioresour Technol 83(1):37–46

Mehmood MA, Ye G, Luo H, Liu C, Malik S, Afzal I, Xu J, Ahmad MS (2017) Pyrolysis and kinetic analyses of Camel grass (*Cymbopogon schoenanthus*) for bioenergy. Bioresour Technol 228:18–24

Mishra G, Bhaskar T (2014) Non isothermal model free kinetics for pyrolysis of rice straw. Bioresour Technol 169:614–621

Mishra RK, Mohanty K (2020) Kinetic analysis and pyrolysis behaviour of waste biomass towards its bioenergy potential. Bioresour Technol 311:123480

Mohan D, Pittman CU, Steele PH (2006) Pyrolysis of wood/biomass for bio-oil: a critical review. Energy Fuels 20(3):848–889

Naik S et al (2010) Characterization of Canadian biomass for alternative renewable biofuel. Renew Energy 35(8):1624–1631

Nyakuma BB, Ahmad A, Johari A, Abdullah TAT, Oladokun O, Aminu DY (2015) Non-isothermal kinetic analysis of oil palm empty fruit bunch pellets by thermogravimetric analysis. Chem Eng Trans 45:1327–1332

Oladeji JT, Itabiyi EA, Okekunle PO (2015) A comprehensive review of biomass pyrolysis as a process of renewable energy generation. J Nat Sci Res 5(5):99–105

Özsin G, Pütün AE (2017) Insights into pyrolysis and co-pyrolysis of biomass and polystyrene: thermochemical behaviors, kinetics and evolved gas analysis. Energy Convers Manage 149:675–685

Parikh J, Channiwala SA, Ghosal GK (2005) A correlation for calculating HHV from proximate analysis of solid fuels. Fuel 84(5):487–494

Parikh J, Channiwala SA, Ghosal GK (2007) A correlation for calculating elemental composition from proximate analysis of biomass materials. Fuel 86(12–13):1710–1719

Rana S, Parikh JK, Mohanty P (2013) Thermal degradation and kinetic study for different waste/rejected plastic materials. Korean J Chem Eng 30(3):626–633

Rastrogi A, Jha MK, Sarma AK (2016) A comparative study of kinetics for combustion versus pyrolysis of *Mesua ferrea* husk, soya husk, and *Jatropha curcas* husk using thermogravimmetry and different methods. Energy Sources Part A Recov Util Environ Effects 38(10):1355–1363

Sánchez-Jiménez PE, Pérez-Maqueda LA, Perejón A, Criado JM (2013) Limitations of model-fitting methods for kinetic analysis: polystyrene thermal degradation. Resour Conserv Recycl 74:75–81

Santos NAV, Magriotis ZM, Saczk AA, Fássio GTA, Vieira SS (2015) Kinetic study of pyrolysis of castor beans (*Ricinus communis* L.) presscake: an alternative use for solid waste arising from the biodiesel production. Energy Fuels 29(4):2351–2357

Saxena RC, Adhikari DK, Goyal HB (2009) Biomass-based energy fuel through biochemical routes: a review. Renew Sustain Energy Rev 13(1):167–178

Sbirrazzuoli N, Vincent L, Mija A, Guigo N (2009) Integral, differential and advanced isoconversional methods: complex mechanisms and isothermal predicted conversion–time curves. Chemom Intell Lab Syst 96(2):219–226

Sharma R, Sheth PN (2018) Multi reaction apparent kinetic scheme for the pyrolysis of large size biomass particles using macro-TGA. Energy 151:1007–1017

Singh G, Varma AK, Almas S, Jana A, Mondal P, Seay J (2019) Pyrolysis kinetic study of waste milk packets using thermogravimetric analysis and product characterization. J Mater Cycles Waste Manag 21(6):1350–1360

Slopiecka K, Bartocci P, Fantozzi F (2012) Thermogravimetric analysis and kinetic study of poplar wood pyrolysis. Appl Energy 97:491–497

Stöcker M (2008) Biofuels and biomass-to-liquid fuels in the biorefinery: catalytic conversion of lignocellulosic biomass using porous materials. Angew Chem Int 47(48):9200–9211

Thakur LS, Varma AK, Mondal P (2018) Analysis of thermal behaviour and pyrolytic characteristics of vetiver grass after phytoremediation through thermogravimetric analysis. J Therm Anal Calorim 131(3):3053–3064

Ucar S, Ozkan AR (2008) Characterization of products from the pyrolysis of rapeseed oil cake. Bioresour Technol 99(18):8771–8776

Varma AK, Mondal P (2016a) Physicochemical characterization and kinetic study of pine needle for pyrolysis process. J Therm Anal Calorim 124(1):487–497

Varma AK, Mondal P (2016b) Physicochemical characterization and pyrolysis kinetics of wood sawdust. Energy Sources Part A Recov Util Environ Effects 38(17):2536–2544

Varma AK, Mondal P (2016c) Physicochemical characterization and pyrolysis kinetic study of sugarcane bagasse using thermogravimetric analysis. J Energy Resour Technol 138(5):052205

Varma AK, Mondal P (2017) Pyrolysis of sugarcane bagasse in semi batch reactor: effects of process parameters on product yields and characterization of products. Ind Crops Prod 95:704–717

Varma AK, Shankar R, Mondal P (2018) A review on pyrolysis of biomass and the impacts of operating conditions on product yield, quality, and upgradation. In: Recent advancements in biofuels and bioenergy utilization. Springer, Singapore, pp 227–259

Varma AK, Singh S, Rathore AK, Thakur LS, Shankar R, Mondal P (2020) Investigation of kinetic and thermodynamic parameters for pyrolysis of peanut shell using thermogravimetric analysis. Biomass Convers Biorefin 1–12

Vyazovkin S, Burnham AK, Criado JM, Pérez-Maqueda LA, Popescu C, Sbirrazzuoli N (2011) ICTAC Kinetics Committee recommendations for performing kinetic computations on thermal analysis data. Thermochim Acta 520(1–2):1–19

Wang S, Dai G, Yang H, Luo Z (2017) Lignocellulosic biomass pyrolysis mechanism: a state-of-the-art review. Prog Energy Combust Sci 62:33–86

White JE, Catallo WJ, Legendre BL (2011) Biomass pyrolysis kinetics: a comparative critical review with relevant agricultural residue case studies. J Anal Appl Pyrol 91(1):1–33

Wu ZQ, Wang SZ, Zhao J, Chen L, Meng HY (2014) Pyrolytic behavior and kinetic analysis of wheat straw and lignocellulosic biomass model compound. Adv Mater Res 860:550–554

Yang H, Yan R, Chen H, Lee DH, Zheng C (2007) Characteristics of hemicellulose, cellulose and lignin pyrolysis. Fuel 86(12–13):1781–1788

Zhu F et al (2015) Kinetics of pyrolysis of ramie fabric wastes from thermogravimetric data. J Therm Anal Calorim 119(1):651–657

Air Pollution Modelling for Jharia Region, in India

Ravinutala Shivani and **Sunny Kumar**

Abstract Air pollution is a very big problem to the environment. During coal mining, natural coal fire also contributes to the pollution that causes health problems to humans as well as the environment. The poisonous gases are produced during coal mining because of the presence of oxygen in the environment. The coal oxidation occurs with released heat, which is not dissipated and reacts with oxygen to form this coal fire. The released gases pollute the environment as well as human life. These poisonous gases are carbon monoxide, its by-product, SO_x, and NO_x. In the Jharia coal reserve region, CO, SO_x, NO_x and particulate matter are present in large amounts because of coal fires which are affecting the nearby society's public health. People in Jharia are facing health issues such as tuberculosis and asthma. Here, poisonous gas dispersion in the environment was studied in the Jharia region by a Gaussian dispersion model. The effects of different parameters are also studied for the behaviour of gas dispersion in the environment.

Keywords Air pollution · Modelling · Ammonia · Jharia · Environment

1 Introduction

The Jharia Coal Field is a coal reserve in India that was also related to coal fires. Due to coal fires, this coal field is an involuntary release the huge amounts of greenhouse gases such as CO_2, CH_4, oxides of nitrogen and many others (Mohalik et al. 2016). This region has the best quality of bituminous coal, which has been found to be suitable for coke production (Kumar et al. 2015). The amount of greenhouse gases released increases the amount of pollution into the environment which directly impacts the global climate (Karl and Trenberth 2003; Montzka et al. 2011). Some reports explain that released gases include carbon dioxide, carbon monoxide and methane (108 kg per year) in the Jharia coal field (Shit et al. 2021).

R. Shivani · S. Kumar (✉)
Institute of Chemical Technology, Marathwada Campus, Jalna, India
e-mail: s.kumar@marj.ictmumbai.edu.in

There are various reports published on air pollution in the Jharia coal field. The surrounding atmosphere was analyzed for finding the quantity of suspended particulate matter, respiratory particulate matter, SO_2, NO_2, heavy metals, and polyaromatic hydrocarbons (Saini et al. 2016). The other air pollutants would be produced by topsoil moving, overburden removal, coal mining, deducting size, and wind erosion. The concentrations of particulate matter, sulfur dioxide, and nitrogen oxide were testified which is more than the allowable limits. This excess amount released increases a risk to the residents of the area (Tollefson 2018).

Biswal and Gorai analyzed the coal-fire movements in the Jharia coalfield in the time period 1989–2019 where they reported land surface temperature and loss of coal by the release of gases (Biswal and Gorai 2021). Karanam et al. study the consequences of coal fires in the Jharia region by using satellite images with thermal and microwave remote sensing data (Karanam et al. 2021). Singh et al. analyse the spatio-temporal variation and propagation direction of coal fires in the Jharia region. During 2006–2009, the spatial coverage of surface and subsurface fires observed a decrease of 57.35% and 5.99% respectively, but was enhanced by 137.93% and 74.76% respectively, during 2009–2015 using satellite based night-time land surface temperature imaging (Singh et al. 2021). Saini et al. discussed the environmental impact in the Jharia region which studies the impact of parameters air, water, soil, agricultural land, vegetation, and topography (Saini et al. 2016). Uddin Siddiqui and Kumar Jain were to study the impact of mining ecology near the surroundings of the Jharia region and also to study the land use and land cover changes by matrix union function (Uddin Siddiqui and Kumar Jain 2021). Chatterjee and Paul analyse the coal core samples and coal stem characteristics for quantitative analysis of proximate and petrophysical parameters of coal to assess the potential of coal bed methane (Chatterjee and Paul 2013). Das et al. study the geochemical of the trace material concentrations of V, Cr, Mn, Co, Cu, Zn, and lead isotopic ratios of soil and segments in Chhattisgarh, a specific region (Das et al. 2018). Guttikunda and Jawahar estimate the emission rate of gases present in the atmosphere for thermal power plants during coal production by using a chemical transport model (Guttikunda and Jawahar 2014). Roy et al. study particulate matter from vehicular, liquid petroleum gas, and diesel generator set emissions, as well as residential and commercial activities using a dispersion model in the Jharia region (Roy et al. 2016).

Here, this study will give the release of the CO_2, SO_2, NO_2 and particulate matter into the environment for the Jharia coal field region.

2 Theoretical Model Description

There are various dispersion models which explain the theory of air pollution such as the Lagrangian model, Eulerian model, box model, receptor model, computational fluid dynamics model and Gaussian dispersion model.

A Lagrangian model is used for predicting concentration of pollutants in the air at particular downwind locations based on atmospheric transportation in the air. This

model calls for information on the meteorological, topographical, locational, and time-series data of the emission. This model works with elevated point sources. This model provides pollutant transport in several terrain regions with time-dependent wind speeds. Mesoscale models were used to investigate element of carbon in Mexico and the surrounding area (Doran et al. 2008). A study conducted on the Lagrangian dispersion model (LAPMOD) suggested these models are capable of stimulating the dispersion of inert and radioactive gases over complex terrain (ul Haq et al. 2019).

The Eulerian model predicts air pollution concentrations in urban areas. They are sometimes referred to as grid models. Based on geographic regions or air volume, the model divides them into small squares or volumes called the grid. They are used for long-range transport, air-quality over the entire airshed, and large scales simulations. Fluid dynamics is applied to compute the mixing of a point release into a turbulent air flow moving over a terrain, which is influenced by the emission characteristics, the topography, the wind field, and thermal layering.

A Box model is a model describing the distribution of pollutants in an airshed (geographical region). The assumption is that the pollutants are uniformly distributed in the airshed, and then the model calculates their average concentrations. This model uses the line source.

Receptor model works on the assumption of mass balance. It is dependent on meteorological properties, deposition, and transformations of pollutants in the atmosphere but independent of the emission source. They do not take into account the patterns of dispersion of pollutants when they measure the concentrations. Airborne particles are identified using mass analysis. A recent development in this model was to combine receptors and dispersion models. Using a coupled receptor and dispersion model, they investigated the effect of wind speed on the dispersion of pollutants (Anu et al. 2015a). Other applications of the coupled receptor and dispersion model to estimate the sources of area source emissions include Particulate Matter (PM10, PM2.5), gaseous pollutants, and volatile organic compounds (VOCs) (Anu et al. 2015b).

A Computational fluid dynamics model was used to study the wind flow trajectory and the concentration of contaminants in the computational domain. Pollutants in the atmosphere are described according to their flow characteristics. The model was used to predict particle dispersion in the river, which should help predict the insoluble inert particles in the river. Three-dimensional numerical simulations were carried out for this study. The model has been demonstrated to predict particulate matter emission during the injection of biosolids into soil, allowing the prediction of concentrations of contaminants within those biosolids (Bhat et al. 2011). It is used in urban environments to study the flow characteristics of pollutants present in the atmosphere which are emitted from sources such as vehicles and chemical plants.

Using mathematical models to study the air quality. To predict the behavior characteristics of pollutants in the air influenced by wind speed, emission rate, source, etc. These equations can be elementary or complex, based on the available data.

The Gaussian model (https://link.springer.com/chapter/10.1007/978-1-4757-4465-1_7) was taken to design for air pollution, which has many advantages. A Gaussian

dispersion model can predict the ground-level concentration using a one-dimensional equation. From this model can easily calculate the ground-level concentration and it gives accurate results.

It is suitable for our coal mining region and is based on the meteorological properties of the Jharia coal mining region compared with the features designed for Gaussian dispersion. The models are suitable for the Jharia coal mining region.

The assumptions are homogeneous, uniform atmospheric conditions, steady state flow, and a steady state point source (Veigele and Head 1978). These conditions can help to transport pollutants and dispersion. There are no crosswind barriers present in the Jharia region. Even though the Gaussian model equation doesn't depend on the time, it is used for longer lifetimes of hours to days. For long range transport of these types of pollutants, continental and global transport models need to be employed. This model can be used on the surface, near the surface, or elevated regions of the source.

Ground level concentration due to a ground level source directly downwind of the source

$$q(x, 0, 0) = \frac{Q}{\pi u \sigma_y \sigma_z} \exp(-h_z/(\sigma_z * \sigma_z)) \qquad (1)$$

where q is maximum ground level concentration of emission at point (x, y, z) in $\mu g/m^3$, Q is emission rate in $\mu g/s$, u is average wind speed of stack height in m/s, σy is horizontal dispersion of emission in m, and σz vertical dispersion of emission in m and h_z is effective stack height in m.

3   Result and Discussion

The result and discussion explain about the gas emission from the coal natural fire. Over 70 fires have broken out at eastern India's Jharia coalfields, that cover in excess of 100 square miles and were mined from the late 1800s to the early 2000s. The first coal fire occurred in1916, and subsequent fires have been recorded ever since. A 60-foot flame has been reported at Jharia, according to literature. This coal fire is produced with the help of coal, heat, and oxygen. Oxidation of coal produces heat which is not dissipated, and further it reacts with oxygen to form this coal fire. This result and discussion section includes the Gaussian model, which predicts the concentration of polluted gas and particulate matter for the Jharia region.

Figure 1 explained about nitrogen dioxide concentration in the environment. The NO_2 gas dispersion in the environment was calculated downwind direction by using a Gaussian dispersion model. Figure 1a has calculated the downwind concentration of NO_2 emissions by using a Gaussian dispersion model by keeping the constant wind speed and varying the emission rate from 530 to 950 $\mu g/s$. After tabulating the data, we plotted the graph between the concentration of downwind versus emission rate. Concentration of downwind is linearly changing with the emission rate as plotted in
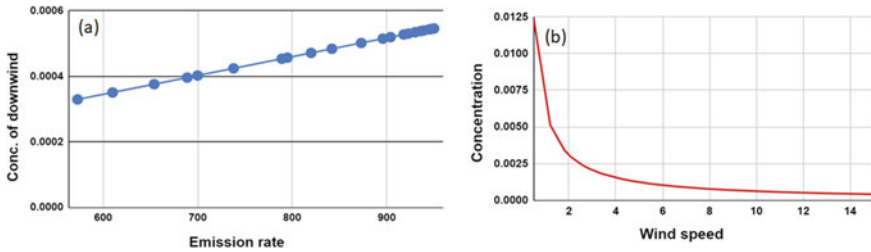
Fig. 1 NO$_2$ concentration in the environment for Jharia region. Plot **a** Constant wind and varying emission rate. Plot **b** Constant emission rate and varying wind speed

Plot (a) and the concentration is varying from 0.000304 to 0.000546 µg/m^3. Figure 1b plotted the graph between the maximum concentration versus wind speed, and the concentration is varying from 0.000935 to 0.123 µg/m^3 (increasing) and 0.000782 to 0.000411 µg/m^3 (decreasing). This study explains the concentration released by keeping the constant emission rate and varying wind speed from 0.5 to 15 m/s. The maximum concentration changes exponentially with the wind speed.

Figure 2 explained about sulphur dioxide concentration in the environment. The SO$_2$ gas dispersion in the environment was calculated downwind direction by using a Gaussian dispersion model. Figure 2a has calculated downwind concentration of SO$_2$ emissions by using a Gaussian dispersion model by keeping the constant wind speed and varying emission rate from 4 to 200 µg/s. After tabulating the data, we plotted the graph between the concentration of downwind versus emission rate (a). The graph of concentration of downwind is linearly changing with the emission rate, and the concentration varies from 0.695 to 34.788 µg/m^3. Figure 2b plotted the graph between the emission rate versus wind speed, and emission rate varying from 0.862 to 25.86 µg/s. This study explains the concentration released by keeping the constant emission rate, and varying wind speed from 0.5 to 15 m/s. The emission rate changes linearly with the wind speed.

Figure 3 explained about the particulate matter (PM) emission rate in the environment. The PM emission rate in the environment was calculated by a Gaussian
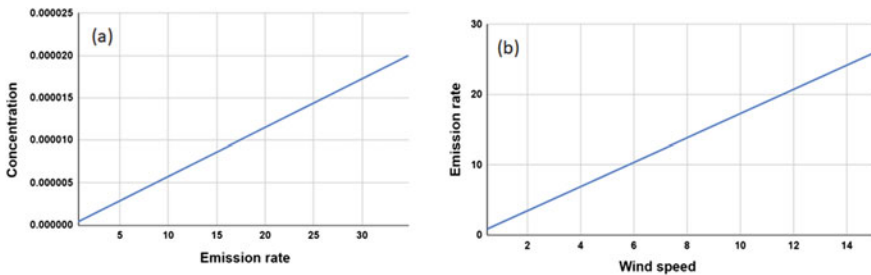
Fig. 2 SO$_2$ concentration in the environment for Jharia region. Plot **a** Constant wind and varying emission rate. Plot **b** Constant emission rate and varying wind speed
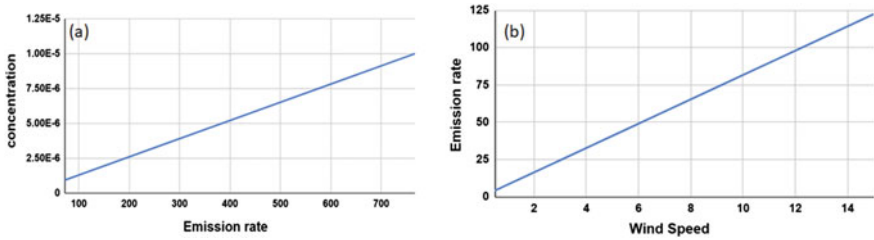
Fig. 3 Particulate matter concentration in the environment for Jharia region. Plot **a** at constant wind and varying emission rate. Plot **b** at constant emission rate and varying wind speed

dispersion model. Figure 3a has calculated the PM emission rate by using a Gaussian dispersion model by keeping constant wind speed and varying the concentration of downwind from 530 to 950 $\mu g/m^3$. After tabulating the data, we plotted the graph between the concentration of downwind versus PM emission rate. The PM emission rate is linearly changing with the concentration of downwind as shown in plot (a) and the emission rate for PM is varying from 4.348 to 17.394 $\mu g/s$. Figure 3b plotted the graph between PM emission rate versus wind speed, and the emission rate for PM is varying from 4.079 to 122.375 $\mu g/s$. This study explains the PM emission rate released by keeping a constant concentration of downwind and varying the wind speed from 0.5 to 15 m/s. The emission rate is linearly changed by the wind speed.

Figure 4 explained about carbon dioxide concentration in the environment. The CO_2 gas dispersion in the environment was calculated downwind direction by using a Gaussian dispersion model. Figure 4a has calculated downwind concentration of CO_2 emissions by using a Gaussian dispersion model by keeping the constant wind speed and varying the emission rate from 250 to 530 $\mu g/s$. After tabulating the data, we plotted the graph between the concentration of downwind versus emission rate. At plot 4 (a), the concentration of downwind is linearly changing with the emission rate and concentration is varying from 43.484 to 92.189 $\mu g/m^3$. Figure 4b plotted the graph between the emission rate versus wind speed, and the emission rate is varying from 2.97 to 89.126 $\mu g/s$. This study explains the concentration released by
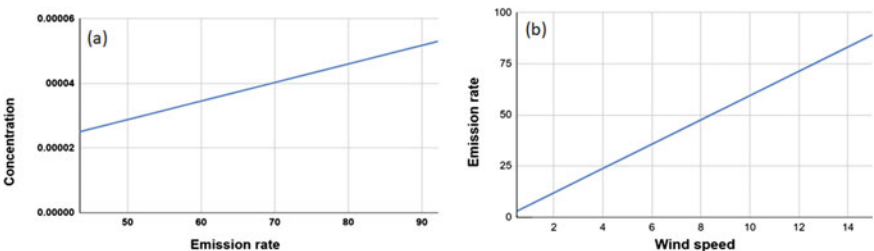
Fig. 4 CO_2 concentration in the environment for Jharia region. Plot **a** Constant wind and varying emission rate. Plot **b** Constant emission rate and varying wind speed

keeping the constant concentration of downwind and varying the wind speed from 0.5 to 15 m/s. The emission rate changes linearly with the wind speed.

The coal mining sector could directly impact the Indian economy, where the Jharia coal region is one of the largest coal mining sites in India (Mohsin et al. 2021). Therefore, the surrounding people get directly benefited by getting employment directly or indirectly (Bhat et al. 2011). Due to natural coal fire, a poisonous gas is being released and is polluting the environment and surrounding society. This poisonous gas is carbon monoxide, and its by-product ammonia is also released in the Jharia region. Instead of this, the reverse effect of the people in Jharia was facing health issues such as tuberculosis and asthma due to coal fires and mining (Li et al. 2015).

Air pollution control measurements require the awareness to the society of the risks involved with air pollution. It should take preventative measures to control sources of air pollution by determining emission sources and taking preventive measures to eliminate them. It is possible to avoid air pollution by using masks and nasal filters. Reducing emission at the source is likely to be the most effective. Pollution control technologies such as mechanical collectors, wet scrubbers, fabric filters, and combustion systems can be implemented in conjunction with cleaner vehicles using cleaner fuels (Cui et al. 2020).

4 Conclusion

We have predicted the maximum downwind concentration of NO_2, SO_2, CO_2 gases present in the atmosphere near the Jharia coal mining region by using a Gaussian dispersion model. We also predicted the emission rate of particulate matter. We then studied the nature of the maximum downwind concentration with respect to emission rate and emission rate with respect to wind speed by using a Gaussian dispersion model. In the case of NO_2, we observed that the maximum concentration of downwind is exponentially changing with the wind speed, but emission rates are linearly changing with the wind speed. This study will help to understand the pollution emission range in the jharia region and impact of the greenhouse gas to the society. In the future, the new technology development will help to prevent the natural coal fire and its impact.

References

Anu N, Rangabhashiyam S, Antony R, Selvaraju N (2015a) Optimization of wind speed on dispersion of pollutants using coupled receptor and dispersion model. Sādhanā 40(Part 5):1657–1666. https://doi.org/10.1007/s12046-015-0396-0

Anu N, Rangabhashiyam S, Rahul A, Selvaraju N (2015b) Evaluation of optimization methods for solving the receptor model for chemical mass balance. J Serb Chem Soc 80(2):253–264. https://doi.org/10.2298/JSC131124052A

Bhat AS, Kumar A, Akbar-Khanjadeh F, Ames A (2011) Application of computational fluid dynamics to dispersion of particulate matter emitted during the injection of biosolids on a farm field. Environ Prog Sustain Energy 30(4). https://doi.org/10.1002/ep.10617

Biswal SS, Gorai AK (2021) Studying the coal fire dynamics in Jharia coalfield, India using time-series analysis of satellite data. Remote Sens Appl Soc Environ 23:100591. https://doi.org/10.1016/j.rsase.2021.100591

Chatterjee R, Paul S (2013) Classification of coal seams for coal bed methane exploitation in central part of Jharia coalfield, India—a statistical approach. Fuel 111:20–29. https://doi.org/10.1016/j.fuel.2013.04.007

Cui L, Zhou J, Peng X, Ruan S, Zhang Y (2020) Analyses of air pollution control measures and co-benefits in the heavily air-polluted Jinan city of China, 2013–2017. Sci Rep 10:5423. https://doi.org/10.1038/s41598-020-62475-0

Das A, Patel SS, Kumar R, Krishna KVSS, Dutta S, Saha MC, Sengupta S, Guha D (2018) Geochemical sources of metal contamination in a coal mining area in Chhattisgarh, India using lead isotopic ratios. Chemosphere. 197:152–164. https://doi.org/10.1016/j.chemosphere.2018.01.016

Doran JC, Fast JD, Barnard JC, Laskin A, Desyaterik Y, Gilles MK (2008) Applications of Lagrangian dispersion modeling to the analysis of changes in the specific absorption of elemental carbon. Atmos Chem Phys 8:1377–1389. https://doi.org/10.5194/acp-8-1377-2008

Gaussian Models | SpringerLink. https://link.springer.com/chapter/10.1007/978-1-4757-4465-1_7. Accessed 21 Aug 2021

Guttikunda SK, Jawahar P (2014) Atmospheric emissions and pollution from the coal-fired thermal power plants in India. Atmos Environ 92:449–460. https://doi.org/10.1016/j.atmosenv.2014.04.057

Karanam V, Motagh M, Garg S, Jain K (2021) Multi-sensor remote sensing analysis of coal fire induced land subsidence in Jharia coalfields, Jharkhand, India. Int J Appl Earth Obs Geoinform 102:102439. https://doi.org/10.1016/j.jag.2021.102439

Karl TR, Trenberth KE (2003) Modern global climate change. Science 302:1719–1723. https://doi.org/10.1126/science.1090228

Kumar H, Mishra S, Mishra MK, Parida A (2015) Petrographical characteristics of bituminous coal from Jharia coalfield India: it's implication on coal bed methane potentiality. Procedia Earth Planet Sci 11:38–48. https://doi.org/10.1016/j.proeps.2015.06.006

Li L, Lei Y, Pan D (2015) Economic and environmental evaluation of coal production in China and policy implications. Nat Hazards 77:1125–1141. https://doi.org/10.1007/s11069-015-1650-9

Manisalidis I, Stavropoulou E, Stavropoulos A, Bezirtzoglou E (2020) Environmental and health impacts of air pollution: a review. Front Public Health 8:14. https://doi.org/10.3389/fpubh.2020.00014

Mohalik NK, Lester E, Lowndes IS, Singh VK (2016) Estimation of greenhouse gas emissions from spontaneous combustion/fire of coal in opencast mines—Indian context. Carbon Manag 7:317–332. https://doi.org/10.1080/17583004.2016.1249216

Mohsin M, Zhu Q, Naseem S, Sarfraz M, Ivascu L (2021) Mining industry impact on environmental sustainability, economic growth, social interaction, and public health: an application of semi-quantitative mathematical approach. Processes 9:972. https://doi.org/10.3390/pr9060972

Montzka SA, Dlugokencky EJ, Butler JH (2011) Non-CO_2 greenhouse gases and climate change. Nature 476:43–50. https://doi.org/10.1038/nature10322

Roy D, Singh G, Yadav P (2016) Identification and elucidation of anthropogenic source contribution in PM10 pollutant: insight gain from dispersion and receptor models. J Environ Sci 48:69–78. https://doi.org/10.1016/j.jes.2015.11.037

Saini V, Gupta RP, Arora MK (2016) Environmental impact studies in coalfields in India: a case study from Jharia coal-field. Renew Sustain Energy Rev 53:1222–1239. https://doi.org/10.1016/j.rser.2015.09.072

Shit PK, Adhikary PP, Sengupta D (eds) (2021) Spatial modeling and assessment of environmental contaminants: risk assessment and remediation. Springer International Publishing. https://doi.org/10.1007/978-3-030-63422-3

Singh N, Chatterjee RS, Kumar D, Panigrahi DC (2021) Spatio-temporal variation and propagation direction of coal fire in Jharia coalfield, India by satellite-based multi-temporal night-time land surface temperature imaging. Int J Min Sci Technol. https://doi.org/10.1016/j.ijmst.2021.07.002

Tollefson J (2018) IPCC says limiting global warming to 1.5 °C will require drastic action. Nature 562:172–173. https://doi.org/10.1038/d41586-018-06876-2

Uddin Siddiqui A, Kumar Jain M (2021) Change analysis in land use land cover due to surface mining in Jharia coalfield through Landsat time series data. Mater Today Proc. https://doi.org/10.1016/j.matpr.2021.04.277

ul Haq A, Nadeem Q, Farooq A, Irfan N, Ahmad M, Rizwan Ali M (2019) Assessment of Lagrangian particle dispersion model "LAPMOD" through short range field tracer test in complex terrain. J Environ Radioact 205–206:34–41. https://doi.org/10.1016/j.jenvrad.2019.04.015

Veigele WJ, Head JH (1978) Derivation of the Gaussian plume model. J Air Pollut Control Assoc 28:1139–1140. https://doi.org/10.1080/00022470.1978.10470720

Kinetic Studies for the Esterification of Propionic Acid with 1-Butanol Process with Ionic Resin Catalyst

Raju Kalakuntala, Mallaiah Mekala, Bhoopal Neerudi, and Srinath Suranani

Abstract The reaction of esterification of propionic acid and n-butanol in a simple isothermal three neck batch reactor was carried out to produce n-butyl propionate and water using the solid acid catalyst. Amberlite was used as the solid catalyst (ion change resin catalyst). The reaction mixture temperature was maintained in the range of 363.15–403.15 K. The reactant mole ratio of propionic acid and n-butanol was in the ranges of 1:1–1:4. The catalyst loading was varied from 1 to 3% by weight based on the reaction mixture volume. The effect of reaction temperature, mole ratio of reactant, catalyst loading, catalyst particle size, stirrer speed on the conversion of propionic acid have been investigated. An experimental results show that reaction is kinetically controlled when compared to internal and external mass transfer effects. A second order kinetic rate equation used to correlate the experimental data and found that it is fitted well with experimental data. The forward reaction rate constants and activation energies were determined from the Arrhenius plot. The heat of reaction has calculated by using Van't Hoff equation.

Keywords Propionic acid · Esterification · Kinetic model · Amberlite · Heat of reaction

1 Introduction

Esterification reaction is a process involved in producing various chemicals such as solvents and flavors. It is mainly used in the production of cosmetic and pharmaceutical products (Yadav and Mehta 1994; Chakrabarti and Sharma 1993; Altiokka and Citak 2003; Erdem and Cebe 2006; Mekala and Goli 2015a). N-butyl propionate is

R. Kalakuntala (✉) · S. Suranani
Department of Chemical Engineering, National Institute of Technology, Warangal 506004, India
e-mail: rajukalakuntala@gmail.com

M. Mekala · B. Neerudi
Department of Chemical Engineering, B V Raju Institute of Technology, Narsapur 502313, India

a good non-volatile organic solvent that can be used as a replacement for volatile organic solvents (Glancy 1988; Sullivan 1995).

In this reaction, H+ ions from propionic acid are combined with alcohol to produce water. The resulting product is n-butyl propionate. The highest converting reactants are determined by equilibrium state of their response. Catalyst is very important for a successful reaction. It helps in accelerating the reaction and reducing the time needed to reach equilibrium state (Mekala et al. 2013; Teo and Saha 2004; Delago et al. 2007; Liu et al. 2006). Heterogeneous or homogeneous catalysts can be used for various reactions. The various catalyst groups include hydrogen Iodide, hydrogen bromide, and sulphuric acid. Heterogeneous catalyst is best compared to homogeneous one because it has advantages such as higher selectivity, less corrosion, and better separation (Mekala and Goli 2015b, c).

They have studied, effects of various sizes of particles on reaction kinetics. They have also tried to determine the amount of catalyst required to trigger the reaction. They discovered that the mass transfer resistance of propionic acid can be neglected. The conversion is increased with decreasing the catalyst size. This liquid phase esterification process is carried out by mixing propionic acid with n-Butanol. It is studied by Liu and Tan. They found no significant internal mass transfer in the operating temperature. The activation energy was also found to be less than 14.1 kcal/mol. In this study, they investigated the effects of the Smopex-103 catalyst on the propionic acid esterification of different alcohols. They subjected the experiments at 60, 70, 75, and 80 °C. The kinetic parameters were studied using the LHHW model. They found that the activation energy for propionic acid was 47.3 kmol/mol. In addition, the kinetic data was correlated with various models. Literature is very limited when it comes to study on esterification of propionic acids with n-butanol. No studies on the effects of Amberlite catalyst are available in the literature. This study aims to study, effects of propionic acid and n-butanol esterification with different parameters in terms of catalyst.

2 Experimental

2.1 Chemicals and Catalyst

Propionic acid of 99.95%w/w purity n-Butanol of 99% w/w purity and were supplied from SD Fine Chemicals Ltd. (Mumbai, India). The resin catalysts used for present reaction system such as Amberlite was supplied by Rohm and Hass, Mumbai.

2.2 Experimental Setup

The reaction between n-Butanol and Propionic acid was conducted in a 500 mL RB three open neck bottle. The reactor was placed inside a heating rota mantle which

has provision of heat and speed control knobs. The stirrer speed was adjusted from 300 to 600 rpm with the help of speed control knob. Vapour losses can be reduced by using a condenser, which is connected to reactor. The thermometer was kept into the reactor for measurement of steady temperature.

2.3 Experimental Procedure
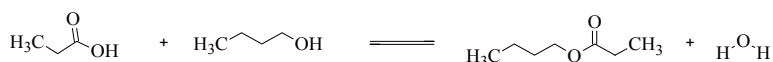
The reactants, propionic acid and n-butanol were measured and charged to the reactor according precalculation of experiment. The heater was on and reaction mixture was heated. When the reaction mixture reaches steady temperature as per the experimental condition, the catalyst was mixed with reactants. The moment catalyst added to reaction mixture considered as zero reaction time. The time interval taken from the zero time onwards. Samples have collected and analyzed for acid concentration with 0.1 N NaOH solution. The reaction is carried out till the system reaches equilibrium.

2.4 Analysis

The concentration of propionic acid (CA) under different time intervals is determined by titration with 0.1 N NaOH. Initially the sample is colour less and upon reaching endpoint it becomes pale pink.

3 Experimental Results

The reaction of n-butanol and propionic acid was carried out isothermal reactor with a temperature of 363.15 K. The experimental conditions were also met with a speed of 300–600 RPM.

The propionic acid conversion is calculated as follows.

$$X_A = 1 - \frac{n_A}{n_{A0}} \tag{1}$$

where X_A is the propionic acid conversion, n_A is the moles of propionic acid and n_{A0} is the initial moles of propionic acid.

Fig. 1 Conversion kinetics of propionic acid at different reaction temperature and at a catalyst concentration of 2% of Amberlite
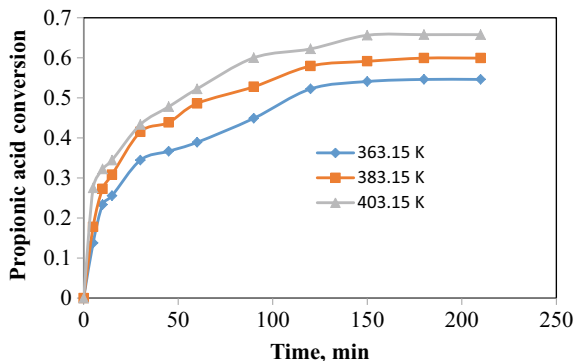
3.1 Effect of Reaction Temperature

The kinetics on propionic acid conversion are shown in Fig. 1. The temperature increases with the increase in propionic acid content. The graph shows the increase in temperature as it affects the propionic acid conversion. This process is initiated by the kinetic control of the reaction.

3.2 Effect of Catalyst Amount

Different catalyst concentrations were studied for different reactions. The results of these experiments were presented in Fig. 2. The conversion of propionic acid to propionic acid increases as the catalyst amount increases. This is evidenced by the kinetics of reaction.

Fig. 2 Conversion kinetics of propionic acid at different catalyst concentration of Amberlite at constant reaction temperature of 383.15 K
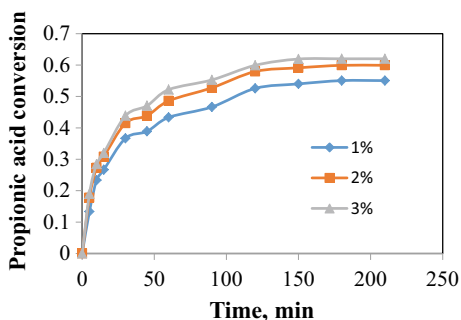
Fig. 3 Conversion of propionic acid at various initial mole ratios of propionic acid and n-butanol
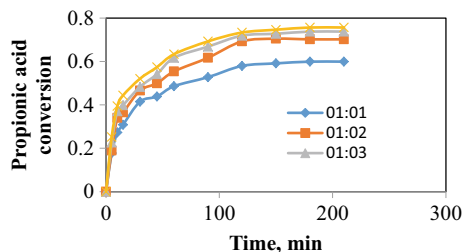
3.3 Effect of Initial Mole Ratio of Propionic Acid to n-Butanol

The reaction rate of propionic acid with n-butanol is influenced by initial molar ratio. It is shown in Fig. 3 that conversion of propionic acid to n-butanol increases. Due to increase in amount of propionic acid to n-butanol, the conversion of propionic acid to n-butanol increased from 60.0 to 75.65%.

3.4 Effect of External Mass Transfer

The experiments conducted at various rpms. The objective of these tests was to find the mass transfer resistance of the propionic acid conversion at these rpms. The other conditions are catalyst concentration, reaction temperature, and catalyst size 2%, reaction temperature: 383.15 K, average catalyst size: 700 µm. In terms of propionic acid conversion, it is not affected by the speed of the stirrer. Since the external mass transfer resistance could be neglected during the esterification reaction, the experiments were conducted at a 300 rpm. These results are also agrees with the reported data as well as our previous results (Mekala et al. 2013; Mekala and Goli 2015b, c).

3.5 Effect of Internal Mass Transfer

The experiments were conducted to determine the internal mass transfer effect of different particle sizes on the conversion of acid. The reaction temperature, the stirrer speed, and the feed molar ratio are controlled by the reaction conditions. The size of catalyst does not affect the propionic acid conversion.

4 The Kinetic Model

The representation of the esterification of reaction for catalysed process is shown below.

$$A + B \overset{k_1}{\underset{k_2}{\leftrightarrow}} C + D \tag{2}$$

$$-r_A = k_1 \left[C_A C_B - \frac{C_C C_D}{K_e} \right] \tag{3}$$

Equation (3) is rearranged in terms of reactant conversion, the rate equation is modified as

$$-r_A = C_{A0} \frac{dX_A}{dt} = k_1 C_{A0}^2 \left[(1 - X_A)(M - X_A) - \frac{X_A^2}{K_e} \right] \tag{4}$$

where $M = C_{B0}/C_{A0}$.

Equation (4) arranged to linear form, the equation is

$$\ln \left[\frac{(1 + M + \eta_2 - 2\eta_1 X_A)(1 + M - \eta_2)}{(1 + M - \eta_2 - 2\eta_1 X_A)(1 + M + \eta_2)} \right] = \eta_2 k_1 C_{A0} t \tag{5}$$

$$\eta_1 = 1 - \frac{1}{K_e} \tag{6}$$

$$\eta_2 = \left[(M + 1)^2 - 4\eta_1 M \right]^{0.5} \tag{7}$$

The Ke values at different temperatures are determined from steady sate data using Eq. (8) as below.

$$K_e = \frac{X_{Ae}^2}{(1 - X_{Ae})^2} \tag{8}$$

where X_{Ae} is equilibrium conversion of propionic acid. The reaction rate constant k_1 value obtained at different temperatures by plotting the LHS of Eq. (5) on y-axis and X-axis. The straight line measurement is a confirmation of the kinetic model's fitness. It shows that the model is well-suited to the system's conditions.

The forward reaction rate constants, k1 are found from slope of straight lines in Fig. 4 at 2% . The forward reaction rate constants evaluated at various temperatures and at different temperatures it is shown in Fig. 5.

$$k_1 = k_{01} \exp\left(\frac{-E_1}{RT} \right) \tag{9}$$

Fig. 4 Adopting Eq. (5) for calculation of reaction rate constants at different temperatures
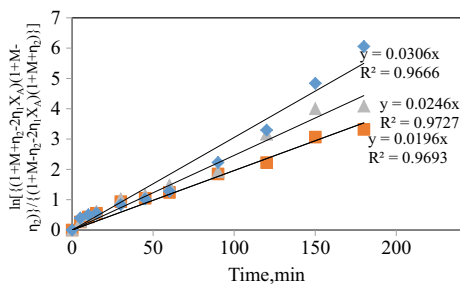
Fig. 5 Forward reaction rate constant (k_1) as function of the temperature
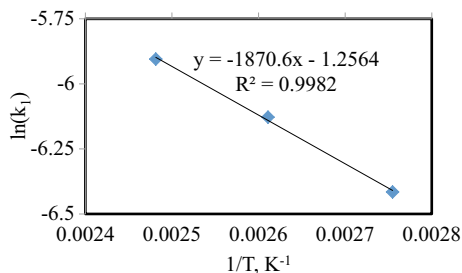
$$k_2 = k_{02} \exp\left(\frac{-E_2}{RT}\right) \tag{10}$$

The temperature dependent reaction rate and forward activation energy are found to be as

$$k_1 = \exp\left[2.612 - \frac{3729.0}{T}\right] \tag{11}$$

The heat of a reaction is calculated from Van't Hoff equation as given below.

$$\ln K_e = \frac{-\Delta H_R}{RT} - \frac{\Delta S_R}{R} \tag{12}$$

The Van't Hoff equation shows the equilibrium constant temperature effect. It is used for analyzing the heat of reaction (Fig. 6).

The equilibrium constant is calculated as the temperature dependence of the ln(Ke). The slope of the line is also calculated and the heat of reaction is evaluated using this figure. The heat of reaction for present reaction is 28.414 kJ/mol indicating an endothermic reaction.

Fig. 6 Temperature
dependency on the
equilibrium constant

$$y = -3418.9x + 9.7691$$
$$R^2 = 0.995$$
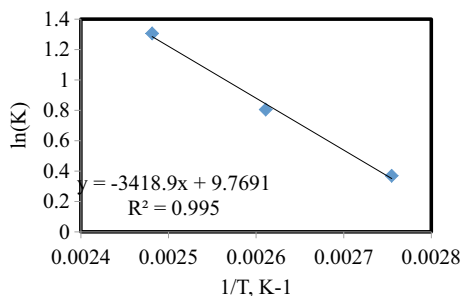
5   Conclusions

An esterification response involving propionic acid and n-butanol has been investigated in various experiments. The experiments revealed that reaction is kinetically-controlled. It is mainly controlled by the mass transfer effects. The kinetic parameters were obtained from the experimental data and were then fitted to the present reaction. The backward and forward reaction rate constants were also found. The reaction temperature was found to be 28.414 kJ/mol with Amberlite catalyst. A complete model of the reaction was then developed.

References

Altiokka MR, Citak A (2003) Kinetics study of esterification of acetic acid with isobutanol in the presence of amberlite catalyst. Appl Catal A Gen 239:141–148. https://doi.org/10.1016/S0926-860X(02)00381-2

Chakrabarti A, Sharma MM (1993) Cationic ion exchange resin as catalysts. React Polym 20:1–45. https://doi.org/10.1016/0923-137(93)90064-M

Delago P, Sanz MT, Beltran S (2007) Kinetic study for esterification of lactic acid with ethanol and hydrolysis of ethyl lactate using an ion-exchange resin catalyst. Chem Eng J 123:111–118. https://doi.org/10.1016/j.cej.2006.09.004

Erdem B, Cebe M (2006) Kinetics of esterification of propionic acid with n-amyl alcohol in the presence of cation exchange resins. Korean J Chem Eng 23:896–901. https://doi.org/10.1007/s11814-006-0005-3

Glancy CW (1988) New solvents for high solids coatings. Mod Paint Coat 35

Liu Y, Lotero E, Goodwin JG Jr (2006) A comparison of the esterification of acetic acid with methanol using heterogeneous versus homogeneous acid catalysis. J Catal 242:278–286. https://doi.org/10.1016/j.jcat.2006.05.026

Mekala M, Goli VR (2015a) Kinetics of esterification of methanol and acetic acid with mineral homogeneous acid catalyst. Chin J Chem Eng 23:100–105. https://doi.org/10.1016/j.cjche.2013.08.002

Mekala M, Goli VR (2015b) Kinetics of esterification of acetic acid and methanol using Amberlyst 36 cation-exchange resin solid catalyst. Prog React Kinet Mech 40:367–382. https://doi.org/10.3184/146867815X14413752286146

Mekala M, Goli VR (2015c) Kinetic study of esterification of acetic acid with methanol over Indion 190 acidic solid catalyst. Kinet Catal 54:419–427. https://doi.org/10.1134/S0023158445040126

Mekala M, Thamida SK, Goli VR (2013) Pore diffusion model to predict the kinetics of heterogeneous catalytic esterification of acetic acid and methanol. Chem Eng Sci 104:565–573. https://doi.org/10.1016/j.ces.2013.09.039

Sullivan DA (1995) Solvent selection in today's regulatory environment. Mod Paint Coat 38

Teo HTR, Saha B (2004) Heterogeneous catalysed esterification of acetic acid with isoamyl alcohol: kinetic studies. J Catal 228:174. https://doi.org/10.1016/j.jcat.2004.08.018

Yadav GD, Mehta PH (1994) Heterogeneous catalysis in esterification reactions: preparation of phenethyl acetate and cyclo-hexyl acetate by using a variety of solid acidic catalysts. Ind Eng Chem Res 33:2198–2208. https://doi.org/10.1021/ie00033a025

Preparation and Characterization of Amine Modified Activated Carbon from Corncobs for Carbon Dioxide Capture

Dipa Das and Liku Swain

Abstract Carbon dioxide adsorption was carried out using a specific bio-adsorbent. The bio-adsorbent was prepared from corncobs. In the present study attempt was made to prepare, characterize and to develop low cost adsorbent. The structure and physical characteristics were outlined and described in details after defining the activated carbon. Moreover, surface modification of the prepared activated carbon was carried out using Methyl diethanol amine (MDEA) solution with impregnation ratio 0.4. Different Characterizations technique like Proximate Analysis, Ultimate Analysis, BET, and Scanning Electron Microscope (SEM) of adsorbents were studied extensively in order to predict the composition, surface area, porosity and surface topography. The experimental work is focused on removal of CO_2 gas using prepared activated carbon and amine impregnated activated carbon. From the experiment it has been seen that the adsorption capacity of Methyl diethanol amine impregnated activated carbon is much more than simple activated carbon. Thus, the given activated carbon prepared from corncob impregnated with MDEA in a ratio 0.4 can be extensively used for the removal of CO_2 from industrial flue gases.

Keywords Adsorption · Activated carbon · Corncob · Impregnation · Methyl diethanol amine

1 Introduction

Carbon dioxide is a greenhouse gas with high global warming potential (Peters et al. 2020). The flue gas from coal based thermal power plants is a major anthropogenic source of this gas. Possible imbalance in the concentration of carbon dioxide in the atmosphere can be avoided in principle by treatment of the flue gas before releasing them to the atmosphere. CO_2 capture and sequestration from point source emissions has been recognized as a potential way to stabilize CO_2 in the atmosphere. By

D. Das (✉) · L. Swain
Department of Chemical Engineering, Indira Gandhi Institute of Technology, Sarang, Dhenkanal, Odisha 759146, India
e-mail: dipadas@igitsarang.ac.in

2035, CO_2 concentration is estimated to reach about 550 ppm which might result in a global temperature rise of 2–3 °C, which will threaten 15–40 species with extinction (Hussain 2012). We largely focus on the efficient capture of CO_2 gas from the gaseous effluents of various industrial operations as it has a major impact on elevation in atmospheric CO_2 levels causing global warming. The goal in reducing CO_2 emissions on an industrial scale is the development of cost-effective techniques for the separation and capture of CO_2 (Gholidoust et al. 2017).

Currently the technologies used by thermal power plants predominantly rely on selective absorption (Fang et al. 2020) of carbon dioxide from the flue gas by treating it with an amine-based liquid (Ping et al. 2020). However chemical absorption technology suffers from low carbon dioxide loading capacity, energy intensiveness, solvent degradation, and equipment corrosion (Yeh et al. 2005; Resnik et al. 2004). Though membrane processes and cryogenic processes are two other technologically futuristic alternatives. But at present cost factor comes in the way of implementing them for carbon capture from large volume of flue gas (Song et al. 2018).

Adsorption is a process in which spontaneous deposition of atoms/molecules of a gas or liquid or dissolved solid on a solid substrate. The deposited material is known as adsorbate while the substrate is called adsorbent. The adsorbate–adsorbent interaction divides the process into two parts, viz., physical adsorption (Vanderwaal forces) and chemical adsorption (covalent bonding due to electrical force in addition to Vanderwaal forces) (Ben-Mansour et al. 2016). The mechanism of chemisorption varies from one material type to other. However, one drawback of chemisorption is the difficulty of regeneration which is overcome by adapting physical sorbents like zeolites and carbonaceous materials needing less energy for regeneration (Parshetti et al. 2015). CO_2 capture by adsorption is also most widely used technique. A widespread and inexpensive natural resource like corncob can be used to prepare activated carbon by chemical activation methods which can be used as solid bio-adsorbents. The adsorption capacity of the bio-adsorbents can be further improved by addition of amines. Amine modified materials have better adsorption capacity and better selectivity for CO_2 as compared to non-modified adsorbents (Das and Meikap 2018, 2019a, b; Das et al. 2015, 2016).

2 Experimental Section

2.1 Preparation of Adsorbent

Corncobs were collected from the local market, and were cut into small pieces of nearly equal size. It was washed with simple tap water to remove dust and other impurities that are bound to the outer surface of the raw material. It was then dried in direct sunlight for 30–40 days as shown in Fig. 1. The dried raw material was then put inside the oven at around 110 °C for 24 h for the complete elimination of the surface bounded moisture and other volatile impurities to ease the process of crushing. It

Fig. 1 Raw material (corncobs)

was then crushed and sieved to a size range of 300–500 μm. H_3PO_4 was used for the chemical activation of the powdered sample. The raw material was impregnated with H_3PO_4 (1:1). The semi liquid form of the material was properly stirred and kept for 24 h. So that H_3PO_4 has enough time for proper soaking on its surface. Then material formed was kept inside the oven at 100 °C for 24 h. H_3PO_4 is used for this experiment because it is a dehydrating agent which decreases carbonization temperature during the process of chemical activation, helps in better charring of carbon and doesn't allow for the formation of ash. The resulting sample was then taken out of the oven and was filled in galvanized pipes then was put inside a muffle furnace. Inside the muffle furnace the sample was heated up to a final carbonization temperature up to 650 °C at the rate of 100 °C min^{-1}under the continuous flow of nitrogen at a flow rate of 120 cm^3 min^{-1} at STP. The entire setup for preparation of activated carbon is shown in Fig. 2. It was kept inside the furnace for one hour at 650 °C in a galvanized iron pipe as shown in Fig. 3. After this it was cooled by constant flowing nitrogen gas and then the muffle furnace was opened. The sample taken out was then washed with 0.5 N HCl for 2–3 times and then with warm distilled water to eliminate various residual organic and mineral material. The sample was finally washed with cold water to make it neutral and then dried for 24 h at 100 °C

Fig. 2 Experimental setup for preparation of AC

Fig. 3 AC in galvanized
pipes

in an oven and then packed in an air tight container. The activated carbon sample
was impregnated with Methyl diethanol amine (MDEA). Impregnation was done in
ratios of 0.4. This process helps in functionalization of unsaturated sites of AC and
we get the AC impregnated in 0.4 as shown in Fig. 4.

Fig. 4 MDEA-AC (0.4)
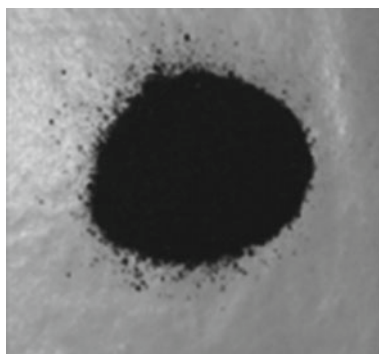
Table 1 Proximate analysis of adsorbents

Sample	Moisture (wt %)	Volatile matter (wt %)	Ash content (wt %)	Fixed carbon (wt %)
Activated carbon	3.36	15.01	1.44	80.21
MDEA-AC (0.4)	3.16	14.62	1.31	79.05

3 Characterization of Adsorbents

3.1 Proximate Analysis

From proximate analysis, it has been observed that the fixed carbon content of the raw precursor is lower as compared to the activated carbon and amine impregnated activated carbon which makes the activated carbon a better adsorbent. The fixed carbon content of activated carbon and Methyl diethanol amine (MDEA-AC) impregnated activated carbon with impregnation ratio 0.4 is found to be 80.21% and 79.05% respectively. Which shows better adsorbent properties for adsorption The Proximate Analysis of the adsorbents are tabulated in Table 1.

3.2 Ultimate Analysis

Ultimate analysis has been done to know the composition of Nitrogen, Oxygen, Sulphur, Hydrogen and Carbon % in the prepared adsorbents. It is observed that the content of Hydrogen, Nitrogen, Oxygen and Sulphur has been lowered due to the activation process. During the preparation and activation of the activated carbon from its raw precursor, normally Nitrogen, Oxygen, Hydrogen leaves the compound making it carbon rich. The nitrogen content of activated carbon and MDEA-AC (0.4) is found to be 1.71% and 4.91% respectively. The nitrogen content of MDEA-AC (0.4) is more due to amine group present in activated carbon surface to enhance the adsorption of carbon dioxide. The Ultimate analysis of the adsorbent is tabulated in Table 2.

Table 2 Ultimate analysis of adsorbents

Sample	Carbon (%)	Hydrogen (%)	Nitrogen (%)	Sulphur (%)	Oxygen (%)
Activated carbon	74.68	5.08	1.71	0.85	17.78
MDEA-AC (0.4)	69.78	5.02	4.91	0.81	19.43
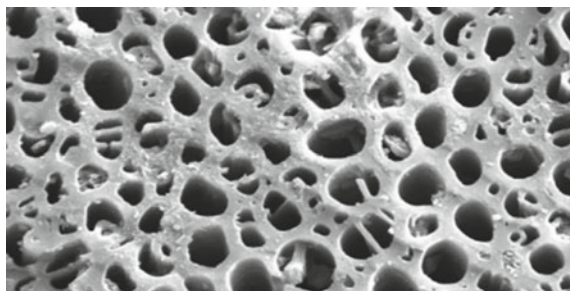
Fig. 5 SEM image of AC
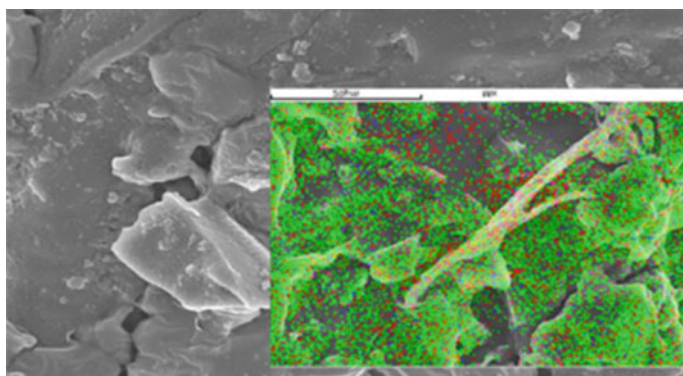
Fig. 6 SEM image of MDEA-AC (0.4)

3.3 Scanning Electron Microscope (SEM)

SEM is used to visualize the porous structure of activated carbon and amine impregnated activated carbon. The SEM images have been shown in Figs. 5 and 6. From the SEM image it has been observed that the porous structure can easily seen in case of activated carbon which is required for adsorption. In case of Methyl diethanol amine impregnated activated carbon the porosity of amine getting blocked due to impregnation of amine solution on the surface of activated carbon.

3.4 BET Analysis

The BET surface area helps in determining the adsorption capacity of the adsorbents. Higher surface area implies more availability of surface for adsorption hence better adsorption capacity. Due to the excess pores developed during the activation of raw precursor of activated carbon, the adsorption of nitrogen is more in case of activated

Table 3 BET analysis of adsorbents

Sample	BETSSA (m^2/g)	V_{tot} (cm^3/g)	V_{micro} (cm^3/g)	A_{micro} (m^2/g)	Avg pore radius (in Angstrom)
Activated carbon	991.976	0.428	0.324	919.51	8.943
MDEA-AC (0.4)	761.011	0.403	0.308	691.31	8.03

carbon. The smallest pores are called micro pores which play an essential role in adsorption. However, there are both micro pores and meso pores on the surface. BET Analysis data is tabulated in Table 3. From the BET analysis of adsorbents, it has been seen that the micropore surface area of activated carbon and MDEA-AC (0.4) were found to be 919.51 m^2/g and 691.31 m^2/g respectively. The volume of the micropore in activated carbon and MDEA-AC (0.4) were found to be 0.324 m^2/g and 0.308 m^2/g respectively. Which shows the better adsorption characteristics. Lower micropore surface area and lower micropore volume of MDEA-AC (0.4) is due to blocking of pore occurs due to impregnation of amine solution on the surface of activated carbon.

4   Results and Discussion

4.1 CO_2 Adsorption Analysis

Figure 7 shows the plot for CO_2 adsorption capacity versus relative pressure for MDEA-AC at impregnation ratios 0.4, and for AC. Figure 8 shows the plot for volume of CO_2 adsorbed versus relative pressure for MDEA-AC at impregnation ratios 0.4, and for AC. The batch adsorption of CO_2 was carried out by using the AutosorbiQ manufactured by Quanta Chrome instruments. CO_2 adsorption was carried out till the relative pressure (P/P$_o$) reached the atmospheric pressure. At around 523 K, the samples were out-gassed for 6 h till it reached atmospheric pressure. After degassing under vacuum, the evaluation of CO_2 adsorption of sorbents at relative pressure (P/P$_o$) was carried out at 298 K. From Fig. 7, it has been observed that MDEA-AC (0.4) has the best adsorption capacity. The reason behind this can be easily explained by the knowledge of amine -CO_2 bonding chemistry. Amine provides the sources for basic sites for the adsorption of acidic CO_2 gas. Amine when present on the activated carbon surface enhances the adsorption capacity and selectivity towards CO_2 due to their basic-acidic characteristics (Lee et al. 2015). As per Lewis theory, amine is a Lewis base and CO_2 is Lewis acid. The presence of lone pair of electrons on the Nitrogen atom in amine group leads to the nucleophilic attack on the acidic CO_2, leading to the formation of carbamate through the carboxyl group (Gholidoust et al. 2017). The

Fig. 7 CO_2 adsorption capacity versus relative pressure for MDEA-AC (0.4) and AC
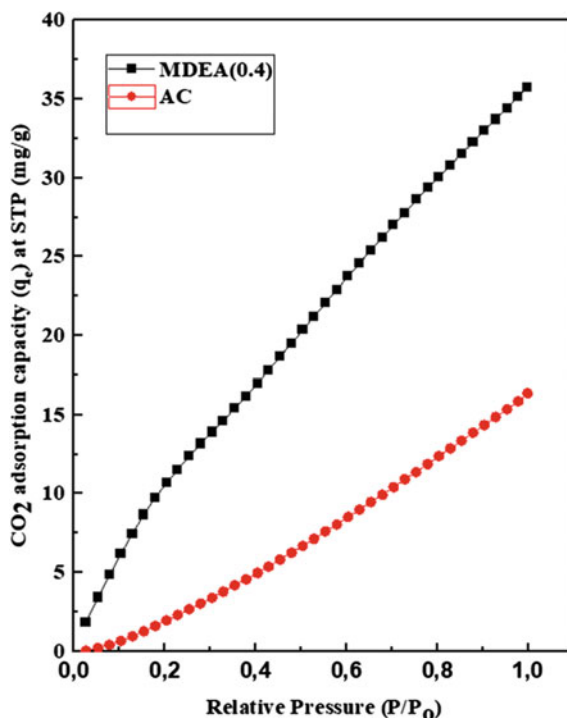
adsorption between the active site of amine and carbon dioxide is the driving force for capture of carbon dioxide by amine-modified carbon materials. It is observed that MDEA impregnated AC has higher efficiency of CO_2 capturing as compared to AC without impregnation due to the phenomenal effects of chemisorption. Moreover, it was found out that with the increase of impregnation ratio the efficiency of CO_2 capturing capacity decreases as amine anchoring decreases the surface area with increases the amine content. From Fig. 7, at atmospheric pressure, the values of CO_2 adsorption capacity for MDEA-AC (0.4) and activated carbon, are found to be 37 mg/g and 15 mg/g respectively. From Fig. 8, it has been observed that the volume of CO_2 adsorbed at atmospheric pressure is highest for MDEA-AC (0.4), i.e., around 18.6 cc/g and for AC it was 7.8 cc/g. In case of unimpregnated AC, the adsorption is physical but in case of MDEA-AC, adsorption is both chemical and physical. From the Carbon dioxide adsorption analysis, it has been found that the adsorption capacity of amine modified activated carbon is much more than simple activated carbon.

Fig. 8 Volume of CO_2 adsorbed versus relative pressure for MDEA-AC (0.4) and AC
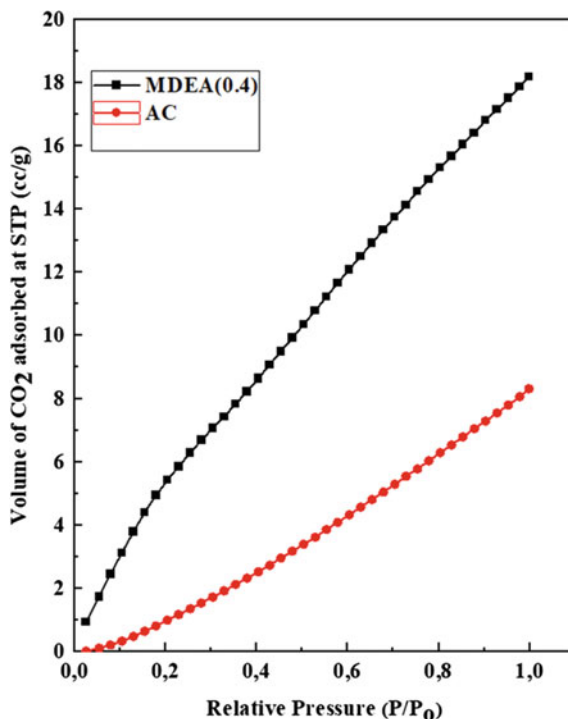
5 Conclusion

Characterization of prepared adsorbents were done by the techniques like Proximate Analysis, Ultimate Analysis, SEM and BET surface area. From the relative pressure versus adsorption capacity for MDEA-AC and AC graph, it has been observed that MDEA-AC (0.4) has maximum CO_2 adsorption capacity i.e. 37 mg/g as compare to un-impregnated AC which is 15 mg/g. From the relative pressure versus volume of CO_2 adsorbed for MDEA-AC and AC graph, MDEA-AC (0.4) has maximum volume of CO_2 adsorption i.e. 18.6 cc/g as compared to un-impregnated AC which is 7.8 cc/g. This tendency can be attributed to the fact that the adsorption capacity of the adsorbent and the selectivity towards CO_2 is enhanced due to the presence of amine on the surface of the activated carbon. From both the graphs, it can be stated that the prepared activated carbon acts as a better adsorbent when impregnated with MDEA solution. From all the above experiments, it can be concluded that MDEA-AC (0.4) acts as a good adsorbent for the removal of CO_2 from industrial flue gas.

References

Ben-Mansour R, Habib MA, Bamidele OE, Basha M, Qasem NAA, Peedikakkal A et al (2016) Carbon capture by physical adsorption: materials, experimental investigations and numerical modeling and simulations—a review. Appl Energy 161:225–255

Das D, Meikap BC (2018) Comparison of adsorption capacity of mono-ethanolamine and di-ethanolamine impregnated activated carbon in a multi-staged fluidized bed reactor for carbon-dioxide capture. Fuel 224:47–56

Das D, Meikap BC (2019a) Removal of CO_2 in a multistage fluidized bed reactor by monoethanol amine impregnated activated carbon. Miner Process Extr Metall Rev 1–7

Das D, Meikap BC (2019b) Removal of CO_2 in a multistage fluidized bed reactor by amine impregnated activated carbon: optimization using response surface methodology. Int J Coal Sci Technol 6(3):445–458

Das D, Samal DP, Meikap BC (2015) Preparation of activated carbon from green coconut shell and its characterization. J Chem Eng Process Technol 6(5):1–7

Das D, Samal DP, Meikap BC (2016) Removal of CO_2 in a multistage fluidized bed reactor by diethanol amine impregnated activated carbon. J Environ Sci Health Part A 51(9):769–775

Fang M, Yi N, Di W, Wang T, Wang Q (2020) Emission and control of flue gas pollutants in CO_2 chemical absorption system—a review. Int J Greenh Gas Control 93:102904

Gholidoust A, Atkinson JD, Hashisho Z (2017) Enhancing CO_2 adsorption via amine-impregnated activated carbon from oil sands coke. Energy Fuel 31(2):1756–1763

Hussain A (2012) Single stage membrane process for CO_2 capture from flue gas by a facilitated transport membrane. Sep Sci Technol 47(13):1857–1865

Lee YC, Lee SM, Hong WG, Huh YS, Park SY, Lee SC, Kimba HJ (2015) Carbon dioxide capture on primary amine groups entrapped in activated carbon at low temperatures. J Ind Eng Chem 23:16–20

Parshetti GK, Chowdhury S, Balasubramanian R (2015) Biomass derived low-cost microporous adsorbents for efficient CO_2 capture. Fuel 148:246–254

Peters GP, Andrew RM, Canadell JG, Friedlingstein P, Jackson RB, Korsbakken JI et al (2020) Carbon dioxide emissions continue to grow amidst slowly emerging climate policies. Nat Clim Change 10(1):3–6

Ping T, Dong Y, Shen S (2020) Energy-efficient CO_2 capture using nonaqueous absorbents of secondary alkanolamines with a 2-butoxyethanol cosolvent. Sustain Chem Eng 8(49):18071–18082

Resnik KP, Yeh JT, Pennline HW (2004) Aqua ammonia process for simultaneous removal of CO_2, SO_2 and NO_x. Int J Environ Technol Manag 4(1):89–104

Song C, Liu Q, Ji N, Deng S, Zhao J, Li Y et al (2018) Alternative pathways for efficient CO_2 capture by hybrid processes—a review. Renew Sustain Energy Rev 82:215–231

Yeh JT, Resnik KP, Rygle K, Pennline HW (2005) Semi-batch absorption and regeneration studies for CO_2 capture by aqueous ammonia. Fuel Process Technol 86(14–15):1533–1546

Electrolyte Role in Electrocoagulation Process for Nitrates Removal from Groundwater

Sanigdha Acharya, Surendra Kumar Sharma, and Vinita Khandegar

Abstract Heedless growth of global population, environment change, and collapsing water framework have all surged for a better water treatment system. Electrochemical technologies have a brighter perspective in this requisite over established water treatment technologies, as they have numerous advantages such as high efficiency, safety, ease of operation, flexibility, and cost-effectiveness. Therefore, the present study envisages nitrate removal from groundwater using the electrochemical technique (electrocoagulation (EC)). The effect of the presence of electrolyte (NaCl and Na_2SO_4) concentration, on current flow, electrolysis, pH of the solution, energy, and operating cost on the nitrate's removal efficiency were assessed. It was observed that NaCl has positive effects on nitrate removal as compared to Na_2SO_4.

Keywords Current · Electrolyte · Electrocoagulation · Efficiency · Nitrates

1 Introduction

Contamination of water resources due to nitrates is a ubiquitous environmental issue. Reports by the Central Ground Water Board of India (CGWB 2010) revealed 100–800 mg/L nitrate concentration in several regions of India, including Delhi. Nitrate is a colorless, odorless, and tasteless anion that has a fatal effect on different creatures when found in concentrations higher than permissible limits in the water. Nitrates presence in water even in a very small amount of (<10 mg/L) may form Methemoglobins in the red blood cells (RBC) causing methemoglobinemia (blue baby syndrome) which can be fatal for neonates (Ghafari et al. 2008). As reported by the World Health Organization (WHO), in 97% of cases observed methemoglobinemia, it occurred in infants under three months old. Hypertension, thyroid disability, cancer,

S. Acharya (✉) · S. K. Sharma · V. Khandegar
University School of Chemical Technology, Guru Gobind Singh Indraprastha University, Dwarka, New Delhi, India
e-mail: sanigdha@ipu.ac.in

V. Khandegar
e-mail: vinita@ipu.ac.in

Table 1 International standard for nitrate concentration in drinking water

Country	Nitrate concentration (mg NO_3^-/L)	References
US	45	USEPA (2017)
Canada	44	Health Canada (2017)
Australia	50	Health Australia (2011)
Malaysia	50	NWQS (2008)
Ontario	45	OME (2006)
India	45	BIS (2012)

and mutagenic health problem are other problems for which nitrates may also be responsible for. Current pieces of evidence advocate nitrate in drinking water can modify human thyroid gland function by hindering thyroidal iodide uptake, leading to altered thyroid hormone concentration and functions. Nitrates can strongly influence aquatic life (Sumino et al. 2006) causing eutrophication in water bodies. Because of the severe effects of nitrate on humans, WHO set 50 mg/L as the acceptable limit of nitrates in drinking water (Kaur and Mehra 2012). In India, the permissible limit of nitrate concentration is 45 mg/L for drinking water (BIS 2012).

Table 1 lists the nitrate concentration limits in drinking water according to some international agencies across the world.

Removal of nitrates from water is a niche research area due to increased groundwater usage for drinking and agricultural purposes. The high solubility and adsorption property of nitrate make its removal a challenging task. Nitrate removal is difficult using techniques such as chemical coagulation, lime softening and oxidation because of its stability and high solubility (Ansari and Parsa 2016). Several physicochemical and biological treatment methods for the removal of nitrates from groundwater and surface water such as filtration, adsorption, flocculation, and membrane separation have been reported in the literature (Reddy and Lin 2000; Keshvardoostchokami et al. 2017). These methods are highly capital intensive with high maintenance costs and the addition of other chemicals. ECtechniques have attracted a lot of attention because of their versatility and environmental compatibility. EC has emerged as a suitable treatment method for nitrate removal because of its high efficiency, flexibility, minimal sludge generation and cost-effectiveness. Furthermore, EC setup occupies a small area, does not produce too much sludge, and there is no need for the addition of chemicals. Equations 1–3. In shows the mechanism floc and sludge generation. In this process, coagulant is generated in situ by the current which leads to the dissolution of the anode and generates hydroxide ions. These hydroxide ions help in the removal of pollutants through the flocculation and sedimentation process.

Oxidation reaction takes place at the anode

$$Al_{(s)} \rightarrow Al^{3+}(aq) + 3e^- \tag{1}$$

Reduction reaction takes place at the cathode

$$3H_2O + 3e^- \rightarrow (3/2)H_2 + 3OH^- \tag{2}$$
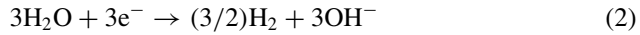
Overall reaction during electrolysis

$$Al^{3+} \rightarrow Al(OH)_n^{(3-n)} \rightarrow Al_2(OH)_2^{4+} \rightarrow Al_3(OH)_4^{5+}$$
$$\rightarrow Al_{13}\text{complex} \rightarrow Al(OH)_3 \tag{3}$$
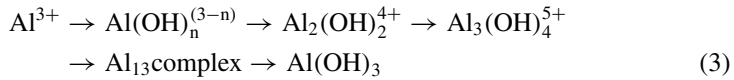
The electrocoagulation process efficiency majorly depends on current density. However, the current density is proportionate to type of electrolyte and its conductivity. Therefore, in the present study, the effect of presence of electrolyte (NaCl and Na_2SO_4) concentration, on current flow, electrolysis time, pH of the solution, energy consumption, and operating cost for nitrates removal from groundwater using aluminum electrodes were assessed.

2 Materials and Method

2.1 Synthetic Nitrate Solution Preparation

A simulated 100 mg/L nitrate solution was prepared in double-distilled water using an appropriate amount of potassium nitrate (Qualikems, India).

2.2 Batch Electrocoagulation Process

Batch EC experiments were conducted in a glass beaker of capacity 500 mL using Aluminum electrodes of dimensions (12.5 cm × 2.5 cm × 0.3 cm). 400 mL of nitrate solution was taken for each experiment and to maintain uniform concentration, agitation was carried by a magnetic stirrer (Labman, India). DC power supply (0–30 V and 0–3 A) (Kitheley, China) was used for the current flow. The electrodes were dipped up to 5 cm and spacing between electrodes was kept at 1 cm in the solution, making the effective area of the electrodes 28.75 cm^2. Figure 1 depicts a schematic diagram for the EC process. In the present study, both NaCl (Qualikems, India) and Na_2SO_4 (Qualikems, India) were tested as supportive electrolytes due to easy availability and low toxicity. Series of experiments were conducted to find the optimum (economically suitable) electrolyte (NaCl or Na_2SO_4) and its concentration (0.01, 0.02, and 0.03 M). The initial values of process variables were; pH (6), spacing between electrodes (1 cm), and stirring speed (300 rpm). Nitrate removal efficiency (NRE) was evaluated using Eq. 4.

$$NRE(\%) = \left[\frac{Y_o - Y_f}{Y_o} \right] \times 100 \tag{4}$$

Fig. 1 Experimental setup of EC
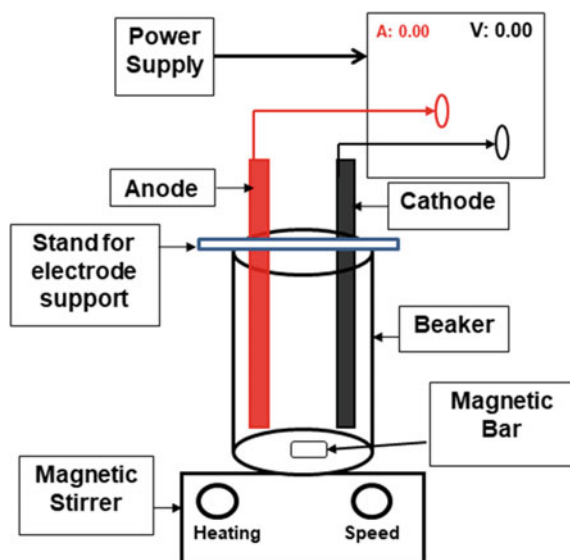
where Y_o and Y_f = Initial and final nitrate concentration at time "t" in mg/L.

In the present study, energy consumption (ENC) and operating cost (OC) were estimated at an industrial electricity price of 0.08 \$/(kWh) as reported by Thakur and Mondal (2017).

3 Results and Discussion

3.1 Effect of Type of Electrolyte

Experiments were performed taking 100 mg/L of nitrate solution in a batch operation. Initially, no electrolyte was added (conductivity: 0.09 mS/cm), and consequently no nitrate removal was observed. Further, experiments were performed using NaCl and Na_2SO_4 at an initial concentration of 0.01 M. Results are shown in Fig. 2. It can be observed from Fig. 2 that higher nitrate removal was achieved in presence of NaCl (95%) as compared to Na_2SO_4 (18%). Further, the concentration of electrolyte (NaCl or Na_2SO_4) was varied from 0.01 to 0.03 M and results are shown in Fig. 3.

It was observed from Fig. 2 that nitrate removal efficiency increased with time for both NaCl and Na_2SO_4. However, as observed from Fig. 3, nitrate removal decreased with increasing Na_2SO_4 concentration from 0.01 to 0.03 $_M$ (66.65–18.59%). This is due to the formation of a shielding layer on the metal electrode surface by SO_4^{2-} ions present in electrolytes. This hinders the localized corrosion of aluminium electrodes, leading to lower current efficiency which lowers the performance of the EC process (Safari et al. 2015). Further, Fig. 3 indicates that adding NaCl has a significant impact
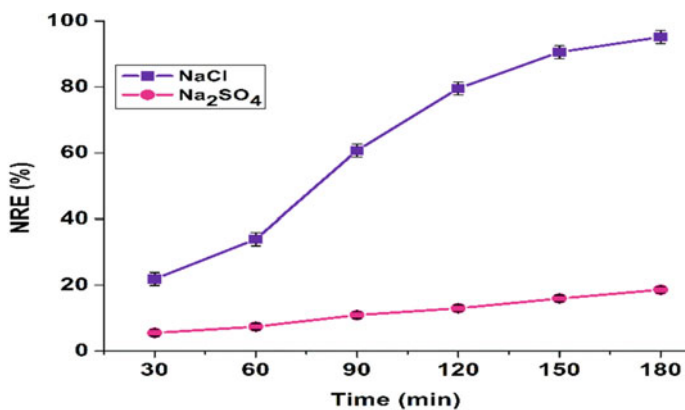
Fig. 2 Effect of electrolyte type
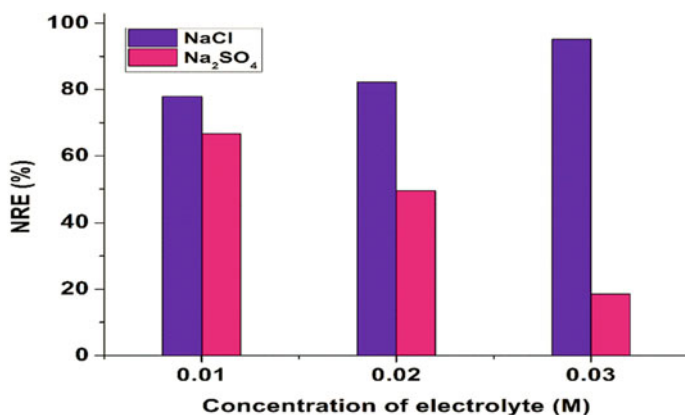
Fig. 3 Effect of electrolyte concentration on NRE (%)

on nitrate removal efficiency. A nitrate removal efficiency of 77% was obtained at the 0.01 M NaCl concentration while 95% removal was obtained at 0.03 M at 180 min. The higher removal achieved at a high concentration (0.03 M) of NaCl ions in the solution is due to an increase in the ionic strength by the addition of electrolyte to the solution. Furthermore, at constant cell voltage (10 V), an increase in electrical conductivity causes increased current flow thereby leading to an increase in nitrate removal efficiency. The results are in agreement with those reported in the literature (Maitlo et al. 2018).
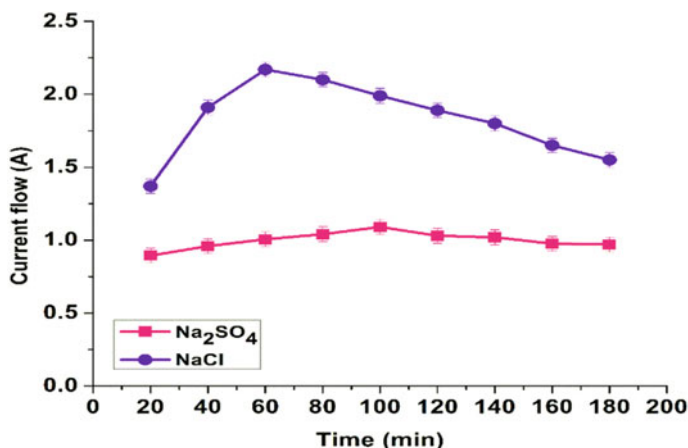
Fig. 4 Effect of electrolyte concentration on current flow (A)

3.2 Effect of Electrolyte on Current Flow

The effect of electrolyte on current flow for removal of nitrate from the solution was investigated. The change in current flow was observed during the electrocoagulation period (20–180 min) at a constant cell voltage 10 V and the results are shown in Fig. 4. Higher current flow was observed using NaCl as compared to Na_2SO_4. A low current flow using Na_2SO_4 leads to low nitrate removal. This is because SO_4^{2-} ions tend to form complexes with Al electrodes and form a passive oxide layer on the electrode surface. This layer diminishes the current flow and current efficiency due to increased potentials between the electrode and as a result, Na_2SO_4 perform poorly as an electrolyte with Al electrodes (Keyikoglu et al. 2019). While in the case of NaCl electrolyte, the high corrosive power of Cl^- ions supports the coagulant dissolution and the presence of chloride ions requires much lower voltage as compared to Na_2SO_4 electrolyte. Results infer that adding NaCl improves the performance of electrocoagulation but diminishes beyond a certain NaCl concentration in the solution. The possible reason is that Cl^- ions from NaCl can remove the passivation layer on aluminium electrodes and subsequently enhance anodic dissolution, which leads to more production of aluminium hydroxide. Nevertheless, sludge formation is there continuously in the solution which causes hindrance in the current flow, consequently forming a passive layer and decreasing the current flow.

3.3 Effect of Electrolyte on Final pH

pH of a solution is an important parameter that influences the performance of the electrocoagulation process (Maitlo et al. 2018). Therefore, series of experiments
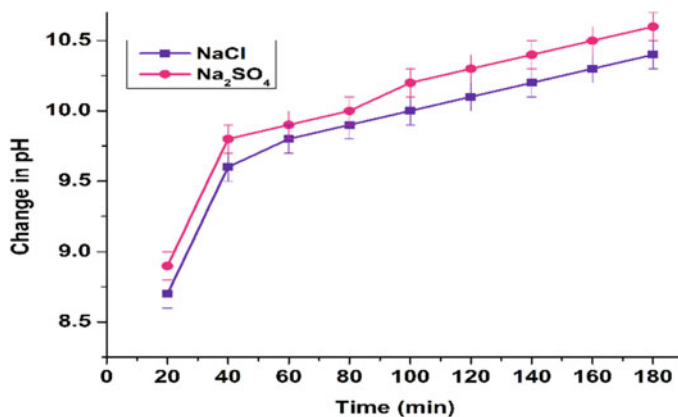
Fig. 5 Effect of electrolyte on final pH

were performed at initial pH 6 in the presence of NaCl and to Na_2SO_4 (0.03 M) from 20 to 180 min. After each run, the change in pH during electrocoagulation was recorded and the results are shown in Fig. 5. It can be noticed from Fig. 5 that the pH of the solution during EC process increases with an increase in the electrolysis time. In general, final pH values were higher than 10 in the presence of both electrolytes at 180 min. Further, a higher change in the final pH value was observed on Na_2SO_4 as compared to NaCl. This is because there is a generation of OH^- in the EC process, which leads to an increase in the pH of the solution. These findings are directly in line with previous studies for nitrate removal using electrocoagulation (Keyikoglu et al. 2019).

3.4   Effect of Electrolyte on ENC and OC

Solution conductivity influences the current efficiency, cell voltage, energy consumption, and overall operating cost. Experiments were performed to investigate the ENC and OC in the presence of NaCl and Na_2SO_4. The results are shown in Fig. 6 and it can be observed that with increasing electrolysis time from 20 to 180 min, ENC linearly increases from 11.3 to 116 kWh/m^3 and 7.3–72 kWh/m^3 for NaCl and Na_2SO_4 respectively. Thus 90 min is preferred to 180 min due to low ENC and OC for NaCl and Na_2SO_4. While comparing the NRE using NaCl and Na_2SO_4, almost 60% removal was achieved in 90 min by NaCl. But only 7% NRE was removed in 90 min using Na_2SO_4. These results revealed that NaCl is a suitable electrolyte as compared to Na_2SO_4. In addition, further, the use of NaCl increases the solution conductivity and is also accompanied by the production of chloride ions that increase the dissolution rate. While in case of Na_2SO_4, high current flow was observed butthe NRE decreased due to the formation of oxide layer by SO_4^{2-} ions.
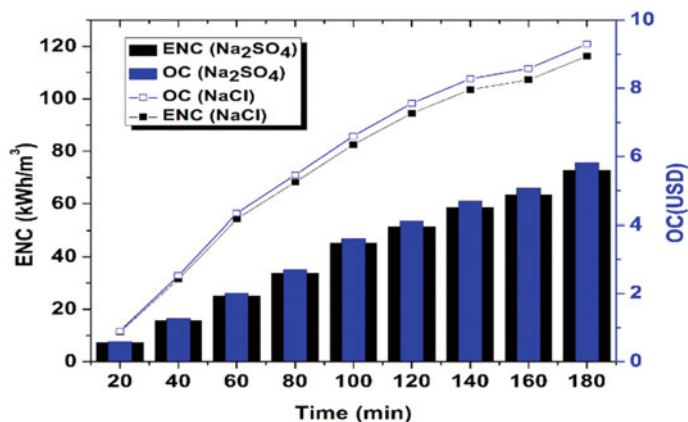
Fig. 6 Effect of electrolyte on ENC and OC

3.5 Effect of Electrolyte on Sludge Generation

Characterization through scanning electron transmission microscopy (SEM) was performed using NaCl and Na_2SO_4 electrolyte at optimum conditions (current $= 1$ A, Voltage $= 10$ V, spacing $= 1$ cm, nitrate concentration $= 100$ mg/L, concentration of NaCl and $Na_2SO_4 = 0.03$ M and time $= 90$ min). After the experiment, performed at optimized conditions, the produced sludge was filtered and dried at room temperature for 24 h. The sludge characterization results are shown in Fig. 7 for NaCl and Na_2SO_4. From Fig. 7 it can be seen that the sludge generated by NaCl shows the sizes of several micrometers in thin shape and could be calcined and can be further used as a low-cost adsorbent in the adsorption process. Further, particles of sludge in the SEM image of Na_2SO_4 were relatively nonuniform in size, which were macrostructures
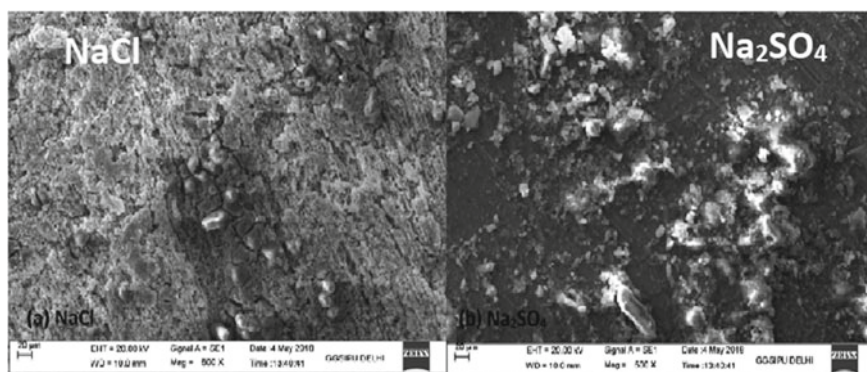
Fig. 7 Effect of electrolyte on sludge generation (**a**) NaCl (**b**) Na_2SO_4

of aluminum hydroxides. Similar results have been reported in the literature (Yadav and Khandegar 2019).

4 Conclusion

Several researchers have reported physicochemical and biological methods for the removal of nitrate from water and wastewater. However, they found critical issues such as the generation of toxic by-products and membrane fouling. The EC method could be a good alternative due to its high efficiency, ambient operating conditions, small equipment size, minimal sludge generation, and rapid start-up. In the present study nitrate concentration (100 mg/L) was prepared and successfully reduced the concentration (45 mg/L) within WHO and BIS drinking water guidelines using EC process in 90 min at 0.03 M of NaCl and in 120 min at 0.01 M of Na_2SO_4 electrolyte. The higher NRE was achieved at 0.03 M of NaCl ions due to the increase in the ionic strength that cause an increase in the current flow at constant cell voltage (10 V). NaCl electrolyte has high corrosive power of Cl^- ions, which supports the electrode dissolution, and the presence of chloride ions required much lower voltage as compared to Na_2SO_4 electrolyte. Further, a higher change in final pH value was observed on Na_2SO_4 as compare to NaCl which leads to high operating costs. Thus 90 min is preferred to 180 min due to low energy consumption and operating cost 2.7 and 5.5 USD/m^3 for NaCl and Na_2SO_4 respectively. Characterization study revealed that the particles of EC sludge produced by Na_2SO_4 electrolyte were relatively nonuniform in size, which were macrostructures of aluminum hydroxides. While the sludge produced by NaCl electrolyte was porous and could be calcined and can be further used as a low-cost adsorbent in the adsorption process. Overall, NaCl was found most suitable electrolyte as compare to Na_2SO_4 for the treatment of groundwater containing nitrate.

References

Ansari MH, Parsa BJ (2016) Removal of nitrate from water by conducting polyaniline via electrically switching ion exchange method in a dual cell reactor: optimizing and modelling. Sep Purif Technol 169:158–170

BIS (2012) Bureau of Indian Standards Specification for drinking water. IS: 10500, New Delhi, India

CGWB (2010) Central Ground Water Board, Ministry of water resources, Government of India. Ground water quality in shallow aquifers of India

Ghafari S, Hasan M, Aroua MK (2008) Bio-electrochemical removal of nitrate from water and wastewater—a review. Bioresour Technol 99:3965–3974

Harsha K, Senthil P, Panda RC (2019) A review on heavy metal pollution, toxicity and remedial measures: current trends and future perspectives. J Mol Liq 290:111197

Health Canada (2017) Guidelines for Canadian drinking water Quality, water and air quality bureau, Health Canada, Ottawa, Ontario

Health Australia (2011) Australian Drinking Water Guidelines National water quality management strategy. National Health and Medical Research Council, Commonwealth of Australia, Canberra

Kaur S, Mehra P (2012) Assessment of Heavy Metals in Summer & Winter Seasons in River Yamuna Segment Flowing through Delhi, India. J Environ Ecol 3:149–165

Keshvardoostchokami M, Babaei S, Piri F, Zamani A (2017) Nitrate removal from aqueous solutions by ZnO nanoparticles and chitosan-polystyrene–Zn nanocomposite: Kinetic, isotherm, batch and fixed-bed studies. Int J Biol Macromol 101:922–930

Keyikoglu R, Can OT, Aygun A, Tek A (2019) Comparison of the effects of various supporting electrolytes on the treatment of a dye solution by electrocoagulation process. Colloids Interface Sci Commun 33:100210

Maitlo HA, Kim JH, An BM, Park JY (2018) Effects of supporting electrolytes in treatment of arsenate-containing wastewater with power generation by aluminumair fuel cell electrocoagulation. J Ind Eng Chem 57:254–262

NWQS (2008) National water quality standards of Malaysia. Ministry of Natural Resources and the Environment

OME (2006) Technical support document for Ontario drinking water standards, objectives and guidelines, Ontario ministry of environment

Reddy KJ, Lin J (2000) Nitrate removal from groundwater using catalytic reduction. Water Res 34:995–1001

Safari M, Rezaee A, Ayati B, Jonidi-Jafari A (2015) Simultaneous removal of nitrate and its intermediates by use of bipolar electrochemistry. Res Chem Intermed 41:1365–1372. https://doi.org/10.1007/s11164-013-1279-9

Sumino T, Isaka K, Ikuta H, Saiki Y, Yokota T (2006) Nitrogen removal from wastewater using simultaneous nitrate reduction and anaerobic ammonium oxidation in single reactor. J Biosci Bioeng 102:346–351

Thakur LS, Mondal P (2017) Simultaneous arsenic and fluoride removal from synthetic and real groundwater by electrocoagulation process: Parametric and cost evaluation. J Environ Manag 190:102–112

USEPA (2017) U.S. Environmental Protection Agency, Assessment Plan for Nitrate and Nitrite (Scoping and Problem Formulation Materials), Washington, DC, EPA/635/R-17/331

Yadav A, Khandegar V (2019) Dataset on statistical reduction of highly water-soluble Cr (VI) into Cr (III) using RSM. Data Br 22:1074–1080

A Review on Titanium Dioxide Based Photocatalytic Cement: Self-cleaning Cement

Anil Saini and Jatinder Kumar Ratan

Abstract In the presence of UV/visible light, Titanium dioxide (TiO_2) generates electrons and holes, which get transferred to its surface and cause the formation of reactive oxygen species (ROS). The ROS react with the available pollutants to decompose them to less harmful products. This characteristic of TiO_2 can be further utilized for clean-up of the environmental pollution of the urban areas. Now a days, TiO_2 based cementitious materials are of great interest as far as the aesthetic durability of masonry structures and reduction in environmental pollution is concerned. TiO_2 based cement, which is widely known as self-cleaning cement, exhibits three distinguished characteristics viz. self-cleaning property, depollution ability, and antimicrobial activity. These characteristics have made the self-cleaning cement a grand topic of concern for sustainable development in the constructional practices. This paper aims to present a comprehensive review on TiO_2-photocatalysisandits mechanism, modification of the structure of TiO_2 for better performance, self-cleaning white cement, its properties & advantages, and application of self-cleaning cement for environmental remediation.

Keywords Photocatalysis · Titanium dioxide · Photocatalytic · Self-cleaning cement · White cement

1 Photocatalysis

Photocatalysis necessitates the use of both light and a catalyst for a reaction to occur. Photocatalysis can be split into two groups based on the phase of the photocatalyst and the medium: homogeneous photocatalysis and heterogeneous photocatalysis (Kutal and Serpone 1993) Fujishima and Honda's work on photocatalysis for hydrogen generation by water splitting in the early 1970's described the photocatalytic process (Fujishima and Honda 1972; Fujishima et al. 2007). The scope of photocatalysis

A. Saini (✉) · J. K. Ratan
Department of Chemical Engineering, Dr BR Ambedkar National Institute of Technology, Jalandhar, Punjab 144011, India
e-mail: anilsingh.saini321@gmail.com

239

was then substantially expanded, with a variety of practical ramifications, such as photodegradation/photooxidation (Bickley et al. 1973). Photocatalytic CO_2 reduction (Inoue et al. 1979), photocatalytic synthesis (Yamagata et al. 1988), photocatalytic gas-phase oxidation (Faust et al. 1989), photocatalytic removal of heavy metals (Butler and Davis 1993), and photoinduced self-cleaning (Wang et al. 1997a). The photocatalytic mechanisms can be described by a Langmuir-Hinshelwood process (Serpone and Emeline 2005).

1.1 Homogeneous Photocatalysis

Homogeneous photocatalysis occurs when the photocatalyst and reaction media are in the same phase. Separating the utilized catalyst in homogeneous photocatalysis is a tough task. Homogeneous photocatalysis is made up of a collection of soluble molecular catalysts that includes a light-absorbing system (photosensitizer), as well as catalytic sites for oxidation and reduction processes (solution). Transition-metal complexes are commonly used as homogeneous photocatalysts because they have the necessary stability and electronic bandgap (Mrowetz et al. 2004). Ozone and the photo-Fenton process (i.e., Fe^{2+} and Fe^{2+}/H_2O_2 systems) are two often employed processes of homogeneous photocatalysis. By using homogenous molecular catalysts, great strides have been made in photo-induced catalytic H_2 synthesis (Hoffmann et al. 1995).

1.2 Heterogeneous Photocatalysis

Heterogeneous photocatalysis occurs when the photocatalyst and reaction media are not in the same phase. Semiconductors can be utilized as photocatalysts because they have a certain electrical structure with a filled valence band and an empty conduction band. Bandgap energy is the energy difference between the conduction and valence bands. The absorption of a photon with ultra-bandgap energy can activate a semiconductor photocatalyst, resulting in the promotion of an electron from the valence band to the conduction band while simultaneously generating a hole in the valence band (Mills et al. 1993). The intensity of incident light and the electrical properties of the semiconductor that prevent electron-hole pairs from recombining, determine the concentration of electron-hole pairs in a semiconductor particle. Light absorption with energy equal to or greater than the bandgap of the semiconductor initiates the excitation of an electron from the valence band to the conduction band. The migration of electrons and holes to the semiconductor surface causes photoinduced electron transfer to adsorbed organic compounds or the solvent. If the species are pre-adsorbed on the surface, the electron transfer mechanism is more efficient (Matthews 1988). The divided electron and hole may take various paths to their destination as shown in Fig. 1. The migration of electrons and holes to the semiconductor surface
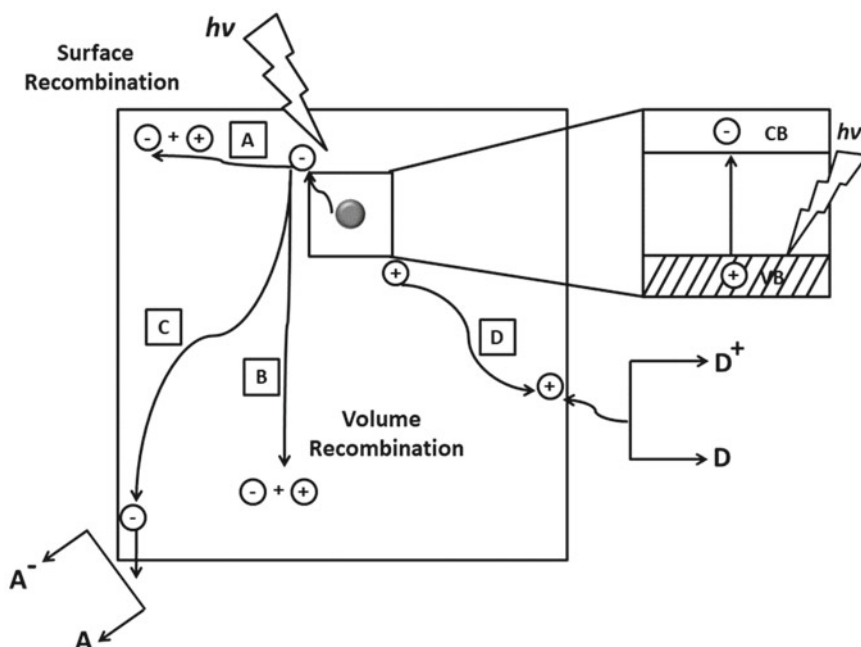
Fig. 1 Schematic photoexcitation in a solid semiconductor (Linsebigler et al. 1995)

is one possibility. The photocatalyst can transfer an electron to an electron acceptor (C), which is commonly molecular oxygen, while at the surface. In turn, the valence band hole can oxidize a donor species (D). These charge transfer mechanisms are influenced by the position of the valence and conduction band edges, as well as the adsorbed species' redox potential. Recombination of electrons and holes competes with charge transfer to adsorbed species. With the release of heat, dispersed electrons and holes can recombine in the volume of the semiconductor particle (B) or on the surface (A) (Linsebigler et al. 1995).

In heterogeneous photocatalytic process, the reaction takes place in the adsorbed phase, and the whole process may be broken down into the following stages:

1. Transfer of reactants from the bulk of the fluid to the catalyst's external surface;
2. Transfer of reactants from the catalyst's exterior surface to its pore structure;
3. Adsorption of at least one of the reactants;
4. Reaction in the adsorbed phase;
5. Desorption of the products;
6. Product transfer from the pore structure to the catalyst surface's outside;
7. Products are transferred from the catalyst's exterior surface to the fluid's bulk.

2   Titanium Dioxide—A Semiconductor Photocatalyst

Among the semiconductor materials that can be used for heterogeneous photocatalysis are ZnO, ZnS, CdS, Fe_2O_3, and TiO_2 etc. The titanium dioxide (TiO_2) is a semiconductor that is most widely applied as a photocatalyst to initiate a series of reductive and oxidative processes on its surface. Aphotocatalyst is fundamentally a substance (photosensitive) that exhibits a solid oxidation impact under the influence of light vitality. It should be nontoxic. Apart from that, it should be highly stable, have a high oxidising power, be inert, and be inexpensive. After studying the extensive research done on photocatalysts, it was discovered that titanium dioxide meets all of the criteria for successful photocatalytic degradation. Titanium dioxide, commonly known as titanium (IV) oxide or titania(TiO_2), is a naturally occurring substance that is utilized in a wide range of applications, including toothpaste, sunscreen, and cosmetics, as well as architectural materials. Because it is white, nontoxic, and affordable, TiO_2 granules were employed as white paints in ancient times (Hashimoto et al. 2005).

2.1   Properties of TiO₂ Photocatalyst

Titanium is found in rutile (highlystable form of titanium dioxide), anatase (defective crystal structure with a longer vertical axis), brookite, ilmenite, leucoxene, perovskite, and sphene, as well as titanates and many iron ores, where it istypically bonded with oxygen in the form of titanium oxides. The main two properties of TiO_2photocatalyst are structural and photocatalytic properties.

2.1.1   Structural Properties

Titanium dioxide crystallizes in three major different structures; anatase (tetragonal), rutile (tetragonal), brookite (rhombohedrical). The properties of different crystal structures of TiO_2 are shown in Table 1 (Matthews 1988). Onlyrutile and anatase playan importantrole in the applications of TiO_2. Rutile is a white pigment with low photocatalytic activity and it is used in paints. Brookite is an uncommon mineral with few uses in regular activities (Beeldens and Gemert 2004). Anatase is chemically stable at room temperature and has proven to be the best photocatalyst material among other semiconductor materials such as ZnO (Husken et al. 2009). The phase thermodynamic stability of one phase to another varies with heat, and the particle sizealso influencesthe phase thermodynamic stability.

Table 1 Crystal Structure of TiO_2 (Xu et al. 2006)

Properties	Rutile	Anatase	Brookite
Structures	Tetragonal crystal lattice	Tetragonal crystal lattice	Orthorhombic crystal lattice
Lattice parameters	a = 4.5941 Å, b = 4.5941 Å and c = 2.9589 Å	a = 3.7842 Å, b = 3.7842 Å and c = 9.5146 Å	a = 9.184 Å, b = 5.447 Å and c = 5.145 Å
Density (gm/cm^3)	4.27	3.90	4.1
Refractive index	2.72	2.52	2.63
Energy bandgap (eV)	3	3.2	–
Permittivity	114	48	78

2.1.2 Photocatalytic Properties

The potential applications of photocatalysis for pollution cleanup have fueled research since 1972 when Fujishima and Honda discovered the photocatalytic capabilities of titanium dioxide (TiO_2) (Fujishima and Honda 1972). Anatase, rutile, and brookite are the three primary crystal polymorphs of titanium dioxide, with rutile being the most common metastable polymorph. The bandgap positions of each polymorph vary as per structure. Anatase has a bandgap of 3.2 eV, which is higher than rutile's bandgap of 3.0 eV (Fujishima et al. 2000a). Their ideal UV wavelength range for promoting a photocatalytic reaction is determined by the bandgap difference. TiO_2 can produce free radicals on its surface when exposed to UV light by boosting electrons to the conduction band. The electron and the accessible hole can react with adsorbed water or oxygen to produce free radicals and singlet oxygen (Carp et al. 2004a). There are several methods for determining a material's photocatalytic activity. Because of its simplicity, the degradation of a dye in aqueous solution under UV radiation is the most often employed approach. The rate of degradation of a suitable organic dye is employed as a measure of activity under these conditions (Fujishima 2006; Tryk et al. 2000). The effective area that will interact and absorb the dye prior to degradation will be determined by physical factors such as particle size and surface area. Aqueous-based approaches have different physical mechanisms than gas-phase reactions. Mass spectrometers are used in more advanced procedures to assess titanium dioxide's photocatalytic activity in the gas phase. A photocatalyst that is efficient in creating radicals as a result of an absorbed photon is an effective photocatalyst for heterogeneous processes in the gas phase (Hoffmann et al. 1995; Tryk et al. 2000; Heller 1995).

Table 2 Photocatalytic reduction and oxidation of TiO_2

Reactions	References	Eq. No.
$TiO_2 + h\nu \rightarrow e_{cb}^- + h_{vb}^+$	Hoffmann et al. (1995)	(1)
$e_{cb}^- + h_{vb}^+ \rightarrow heat$	Hoffmann et al. (1995), Rothenberger et al. (1985)	(2)
$h_{vb}^+ + H_2O \rightarrow OH^\bullet + H^+$	VelLeitner et al. (2002)	(3)
$h_{vb}^+ + OH^- \rightarrow OH^\bullet$	Zhang et al. (2005)	(4)
$e_{cb}^- + O_2 \rightarrow O_2^{\bullet -}$	Buxton et al. (1988)	(5)
$O_2^{\bullet -} + O_2^{\bullet -} + 2H^+ \rightarrow H_2O_2 + O_2$	Zhang et al. (2005)	(6)
$O_2 + H^\bullet(H^+ + e_{cb}^- \rightarrow H^\bullet) \rightarrow HO_2^\bullet$	Zhang et al. (2005), Buxton et al. (1988)	(7)
$HO_2^\bullet + H^+ + e_{cb}^- \rightarrow H_2O_2$	Buszek et al. (2012)	(8)
$H_2O_2 + h\nu \rightarrow 2OH^\bullet$	Jacobson (2005)	(9)
$H_2O_2 + e_{cb}^- \rightarrow OH^\bullet + OH^-$	VelLeitner et al. (2002), Buxton et al. (1988)	(10)

2.2 Mechanism of TiO₂ Photocatalysis

TiO_2 is remarkable in that it has photocatalytic reduction oxidation activity as well as super-hydrophilicity. While the specific reaction mechanism varies on the type of TiO_2 utilized, as well as its mineral composition and manufacturing technique, the following sections provide a basic overview of the reaction mechanism (refer to Table 2). When the titanium dioxide particle is irradiated by UV radiation of wavelength 388 nm, the valence band electrons are transferred to the conduction band and holes are produced in the valence band. After a few tens of picoseconds, the majority of the electron-hole pairs created recombine, and the energy is released as photons, phonons, or both (Serratos and Bronson 1996; Rothenberger et al. 1985). The remaining charges are trapped by coordination defects on the particle's surface and lattice defects within the particle (Ge et al. 2006). The electrons have a very reactive reduction potential, while the holes trapped at the surface have a highly reactive oxidation potential. As a result, the holes and electrons can activate catalytic reactions at the surface, known as photocatalytic reactions (Anpo 2000).

The oxygen radicals $OH^\bullet$, $O_2^\bullet$, $HO_2^\bullet$ produced during the process are known as reactive oxygen species (ROS). The ROSs then react with pollutants to convert it to less objectionable salts, CO_2 and H_2O. The mechanism of TiO_2 photocatalysis is pictorially shown in Fig. 3.

2.3 Kinetics of TiO₂ Photocatalysis

The reaction rate in a photocatalytic system is regulated not only by global "reaction resistances," but also by the concentration of photogenerated electron–hole pairs, which is determined by the intensity of relevant energy radiation applied to the
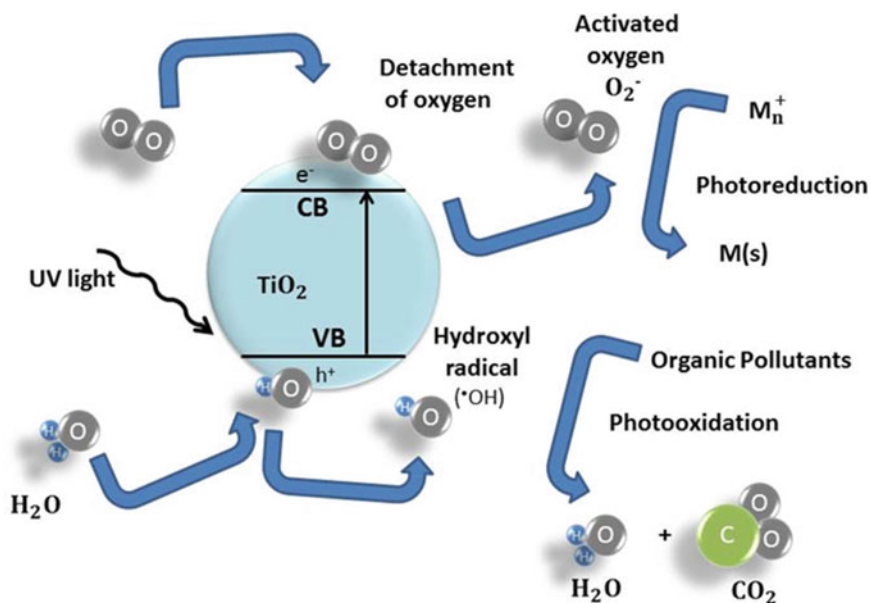
Fig. 3 Photocatalytic reaction mechanism of Titanium dioxide

system and their recombination rate. The photocatalytic reaction rate is determined by various factors such as the semiconductor's electrical, chemical, and morphological properties, the presence of additives in the reacting system, the solution's and solid's donor-acceptor and acid-base properties, the reaction system's temperature and pressure at steady state or when the maximum concentration of electron-hole pairs is reached.

Organic pollutant degradation kinetics on irradiated TiO_2 has been extensively studied, with being proposed as a plausible explanation. The initial reaction rate with the elimination of any single pollutant in this model can be explained using the following equation:

$$r = \frac{-dC_0}{dt} = \frac{kKC_0}{1 + KC_0} \qquad (11)$$

where r represents the rate of reaction that changes with time (t), as a function of the initial concentration of the pollutant (C_0),The Langmuir adsorption constant on the surface of TiO_2 is K. The 'k' is a proportionality constant which provides a measure of the intrinsic reactivity of the photoactivated surface with pollutant. Generally, 'k' is proportional to light intensity (I^Z) in general, where z is a power term. It is also worth noting that 'k' is proportional to the O_2 fraction, which can be expressed as (Kumar et al. 2008):

$$f(O_2) = \frac{K_{O_2}P_{O_2}}{1 + K_{O_2}P_{O_2}} \tag{12}$$

where K_{O_2} is the Langmuir adsorption coefficient for O_2. P_{O_2} is concentration of oxygen. The pollutant and $OH^{\bullet}$ are expected to adsorb exclusively at Ti^{IV} lattice sites, while O_2 is expected to adsorb non-competitively on TiO_2. As a result, the initial rate equation can be expressed as follows (Mills and Morris 1993):

$$r = k_0 \frac{kKC_0}{1 + KC_0} \frac{I^Z K_{O_2}P_{O_2}}{1 + K_{O_2}P_{O_2}} \tag{13}$$

where k_0 is a proportional constant. If the temperature is regarded as a parameter that can affect the reaction rate, the following equation can be written using the Arrhenius equation:

$$r = k_0 \frac{kKC_0}{1 + KC_0} \frac{I^Z K_{O_2}P_{O_2}}{1 + K_{O_2}P_{O_2}} \exp\left(\frac{-E_a}{RT}\right) \tag{14}$$

Instead of mole transformation per unit volume of solution per unit time, the reaction rate should be expressed as mole transformation per unit mass of catalyst per unit time. Such a rate statement is not typical in the open literature dealing with photocatalysis. It is easier to collect intrinsic kinetic data for catalyst analysis and reactor design by distinguishing the kinetic domain from the transport constrained regime. Because the mole transformation doubles when the amount of catalyst is doubled, the reported rate is exclusively dictated by kinetics in the kinetic domain. As a result, the consistency of the rate data, which is reported in mole transformation per unit mass of catalyst per unit time, may easily identify this regime (Mehrotra et al. 2003). The pollutants (external and internal mass transfer) and light transport become dominating in the transport limited regime, which is generated by the agglomeration of solid particles in the fluid phase (Fernandez-Ibanez et al. 2003; O'Shea et al. 1999).

2.4 Methods of Improving the Performance of TiO₂ Photocatalysis

Titanium dioxide photocatalysis has attracted a lot of interest due to its high photo-catalytic efficiency, low cost, lack of toxicity and high stability. TiO_2 has such a large bandgap (3.2 eV), it can only be activated by high-energy UV light with a wavelength of less than 385 nm. This effectively eliminates the use of sunlight as an energy source. To make better use of solar energy, tremendous efforts have been made to expand the useful response of TiO_2 based materials to the visible area, which necessitates the change of the electronic structure of TiO_2. Specific surface area, pore volume,

density, size, pore structure, crystalline phase and bandgap energy are all important aspects in TiO_2 photocatalytic activity (Nakata and Fujishima 2012). Titanium dioxide has larger bandgap energy to create free radicals, and chemical modification has been extensively studied to reduce the bandgap energy. The chemical modification not only lowers the bandgap energy but also changes the photocatalytic activity to visible light active. Moreover, the introduction of the doping concept can change other physical features including surface and shape, which increases the photoactivity of TiO_2 photocatalysts. The recombination of the photo-generated electron and hole is one of the key drawbacks of TiO_2 photocatalysis. This process lowers the quantum yield and wastes energy (Özkan et al. 2004). The following approaches should be considered to increase the efficiency of TiO_2 and decrease the recombination rate:

2.4.1 Doping

Doping TiO_2 to modify the optical response of semiconductor photocatalysts has been a popular method of bandgap engineering. The main objective of doping is to decrease the bandgap or intra-bandgap states are introduced, resulting in the absorption of additional visible light. Photocatalytic systems with increased efficiency may result from doping (Carp et al. 2004b). It is preferable to keep the photocatalyst's crystal structure intact while modifying its electronic structure by doping. Because of the difference in ionic radii and charge states, replacing Ti^{4+} in TiO_2 with a cation is easier than replacing O_2^- with another anion (Mor et al. 2006). Because of their inherent lattice strain, nanomaterials are more tolerant to structural distortion than bulk materials. As a consequence, surface modification of TiO_2 nanoparticles appears to be more advantageous than bulk TiO_2 modification (Burda et al. 2003; Verma and Kumar 2014).

2.4.2 Metal Doping

In the literature, three types of metals have been employed to dope TiO_2: transition metals, noble metals, and rare earth metals. Transition metals such as V, Ni, Fe, Zn, Co, Cr, and Mn have been studied as a dopant with TiO_2 to improve photocatalytic activity and move the wavelength of TiO_2 spectral response towards the visible region (Czoska et al. 2008). The addition of transition metals to TiO_2 can increase photocatalyst activity by decreasing the energy required for electrons and holesgeneration; however, the presence of transition metals in the TiO_2 has been shown to induce thermal instability (Choi et al. 1994). AsTiO_2 photocatalysts cannot absorb visible light and only utilize 3_5% of the solar rays that reach the ground, and the ultraviolet light source is required for its activation. As a result, a modified TiO_2 photocatalytic system that may be used under visible and/or solar light irradiation is highly required. By doping a semiconductor with metal ions, the rate of photoreduction can be increased, a TiO_2 with higher trapping to recombination rate ratio may be created. When metal ions or oxides are doped into TiO_2, the impurity

energy levels produced in the TiO_2 bandgap can enhance the rate of photogenerated electrons and holes recombination and hinder the charge transfer. To achieve effective charge transfer, metal ions should be doped at the photocatalyst's surface. Metal ions can act as recombination centres in the case of high-concentration doping (Joshi et al. 2009). Because of the creation of localised d-states in the TiO_2 bandgap, doping it with transition metal ions has a negative influence on photocatalytic activity. Localized d-states operate as trapping sites for electrons from the conduction band and holes from the valence band (Maruska and Ghosh 1979). The space-charge area narrows as the dopant concentration increases, and the enormous electric field efficiently separates the electron-hole pairs. When the doping concentration is high, the space-charge area narrows, and the depth of light penetration into TiO_2 much surpasses the width of the space-charge layer. As a result, because there is no driving force in the semiconductor to separate photogenerated electron-hole pairs, the rate of recombination rises. There is an optimum dopant ion concentration at which the thickness of the space-charge layer is identical to the depth of light penetration (Xin et al. 2007; Periyasami et al. 2009). Another method for modifying photocatalysts is to add noble metals. Noble metals such as Ag, Pd, Au, Cu, Rh, Pt, and Ni have been shown to significantly improve TiO_2 photocatalysis (Rupa et al. 2009; Papp et al. 1993; Thampi et al. 1987; Adachi et al. 1994). These noble metals have lower Fermi levels than titanium dioxide. In this doping photogenerated electrons can go from the conduction band to noble metal particles on the surface, whereas photogenerated holes in the valence band remain on TiO_2. The electron-hole recombination is significantly decreased, leading to more efficient separation and increased photocatalytic activity (Turner et al. 2008). It has been proposed that a high metal particle concentration lowers photon absorption by TiO_2 and permits metal particles to become electron-hole recombination centres, resulting in decreased efficiency (Sakthivel et al. 2004). At room temperature, copper-doped TiO_2 powder was used to reduce CO_2. The photocatalytic activity of TiO_2 for generating H_2 from aqueous methanol solution was considerably increased by coating with Cu particles, according to the study (Wong and Malati 1986; Wu and Lee 2004). Highly reactive TiO_2 doping with rare earth (Ln(III)) focuses in particular, on the modification and enhancement of the surface, optical and electrical characteristics of TiO_2 by doping Ln(III) by moving the absorption wavelength to the visible range (Saqib et al. 2016). Doping with lanthanide metal ions was reported to decrease the agglomeration in aqueous solutions of TiO_2 particles (Wang et al. 2005).

2.4.3 Non-Metal Doping

Since it was first discovered that non-metal doped TiO_2 powders display visible-light activity in both aqueous and gas phases, many research interests have shifted to the study of non-metal doped TiO_2 that is visible light sensitive. In their study, they first evaluated the influence of dopants (N, S, F, P, and C) on the electronic bandgap structure using theoretical state density calculations. The mixing of the p states of the doped anion (C, S, or N) with the O_2p states in these anion-doped

TiO_2photocatalysts, moves the valence band edge upward, reducing the bandgap energy of TiO_2. Anions, unlike metal cations, are less prone to generate recombination centres and so are more efficient in increasing TiO_2 photocatalytic activity (Meng et al. 2007). A one-pot hydrothermal technique was used to manufacture N-doped TiO_2 hollow spheres utilizing urea as a nitrogen precursor. The photocatalytic activity of the spheres was demonstrated to be greater than that of undopedTiO_2 hollow spheres and commercial Degussa P25 by degrading Reactive Brilliant Red dye under visible light irradiation (Ao et al. 2010). Non-metal fluorine can enhance surface acidity and induce the production of reduced Ti^{3+} ions. Furthermore, charge separation will be enhanced and encouraged in the photoinduced process (Czoska et al. 2008). F-doped TiO_2 was shown to have more photocatalytic activity for the oxidation of acetone into CO_2 than undopedTiO_2 (Yu et al. 2002). C-doped TiO_2 was shown to be five times more active than N-doped TiO_2 in degrading 4-chlorophenol by artificial light (Sakthivel and Kisch 2003). For 500 W tungsten halogen lamp, photocatalytic degradation of Rhodamine B dye employing C-doped TiO_2 photocatalysts, about 59% dye degradation efficiency was found (Ren et al. 2007). Based on TiO_2 photocatalytic activity in visible light, dopants such as carbon, sulphur and phosphorus provide good results (Irie et al. 2003). The impact of photocatalytic and thermal stability of surface modification on Rhodamine B solution was studied. TiO_2 was changed by phosphoric acid post-treatment, which increases the anatase phase and therefore the surface area. P-doped TiO_2 has a high photocatalytic activity due to its wide surface area and strong charge separation, as well as a specific hydroxyl group. P-doped TiO_2 had greater degradation efficiency than normal TiO_2 (Qina et al. 2009). Doping TiO_2photocatalyst with boron using sodium borohydride at 55 °C under hydrothermal conditions resulted in a photocatalyst that was active under visible light. When compared to pure Titanium dioxide, the doped sample showed increased visible absorption and a larger surface area (Xu et al. 2009a). Non-metal doped TiO_2 is highly effective in removing organic compounds from textile effluent.

2.4.4 Co-doping

TiO_2 co-doping might be an effective approach to increase charge separation. TiO_2 has been used as a co-dopant in degrading dye such as Methylene Blue, Reactive Red, Methyl Orange, Direct dye, and others. There are three methods for metal and nonmetal co-doping to occur; (i) metal-nonmetal, (ii) metal-metal, and (iii) nonmetal-nonmetal. When exposed to visible light, Fe and Eudoped TiO_2 exhibited a redshift in its absorption spectra as well as strong photoactivity for the degradation and catalytic oxidation processes of styrene and phenol, respectively (Vasiliu et al. 2009). Co-doping with Cu and N in TiO_2 increased the absorbance to 590 nm and higher photocatalytic activity for the photocatalytic degradation of xylenol orange as compared to pure Cu or N-doped $TiO_2$was observed (Song et al. 2008). Under mild conditions, (C, Ce) codopedTiO_2 was synthesised using a modified sol-gel technique. The photocatalytic activity of codoped TiO_2 with C and Ce for degradation of Reactive Brilliant Red X-3B in visible light was significantly higher than that of pure

C-doped TiO_2, undopedTiO_2, and Degussa P25 because Ce doped TiO_2 reduced the hole and electron recombination rate (Xu et al. 2009b). Si-W co-doped TiO_2codoped with W-Si has a positive impact on photocatalytic efficiency of Methyl Orange dye than undopedTiO_2 when exposed to a mercury lamp. Changes in bandgap energy and co-dopant nanoparticle structure may account for the obtained results (Mragui et al. 2019). Photocatalytic activity of Metal-metal co-doped TiO_2 was improved than non-doped TiO_2 for the degradation of organic compounds from textile effluents. The sol–gel technique was used for metal-non-metal co-doping of nickel oxide—Boron on TiO_2 photocatalyst for the degradation of the organic compound under UV light (Zhao et al. 2004). As a result, metal-nonmetal co-doped TiO_2photocatalyst has been identified as one of the potential agents for textile wastewater treatment. Nonmetal N-F co-doping has also been explored because to its similar structural behaviour under UV-TiO2 photocatalysis. This coupled structure has the benefit of playing a significant role in charge separation due to F-doping, while N-doping improves the behavior of the catalytic phenomena in the visible light zone. Furthermore, it reduces the energy cost of N-F co-doping (Wang et al. 2009). The sol-gel technique was used to create C-N co-doped TiO_2 nanoparticles for photocatalytic treatment of azo dye in textile effluent (Boscaro et al. 2019). As a result, nonmetal-nonmetal co-doped TiO_2 performs better in terms of textile effluent degradation.

2.4.5   Dye Sensitization of Semiconductor

Dye sensitization is a helpful technique for inducing visible light photocatalysis on the surface of wide bandgap semiconductors such as TiO_2, which would otherwise be inert under visible light (Irie et al. 2012; Fujishima et al. 1999). The weak Vander Waals contact between the dye molecule and the surface of the semiconductor causes the physical adsorption of dye. Electron transport between dye molecules and the host semiconductor is facilitated by dye sensitization (Zhao et al. 2005). To sensitize TiO_2particles to visible light, dye such as acid red 44,8-hydroxyquinone (HOQ), methylene blue (MB), reactive red dye 198 (RR 198), eosin-Y, merbromine, $2',7'$-dichlorofluorescein, rhodamine B, and rhodamine 6G have been employed (Rehman et al. 2009; Kumar and Bansal 2010a). When exposed to visible light, these surface-adsorbed dye molecules are activated and inject electrons into the host semiconductor's conduction band (CB) (Fig. 4). Electrons injected by dye molecules rapidly hop across to the surface of titania, where they are scavenged by molecular oxygen, forming superoxide radical $O_2^{\bullet-}$ and hydrogen peroxide radical $OOH^{\bullet}$.

2.4.6   Coupled/composite TiO_2

Coupled titanium dioxide photocatalysts demonstrate very high photocatalytic activity for both liquid and gas phase processes by enhancing charge separation and extending the photoexcitation energy range. Titanium dioxide has been coupled with semiconductors with small bandgaps capable of absorbing visible light, such
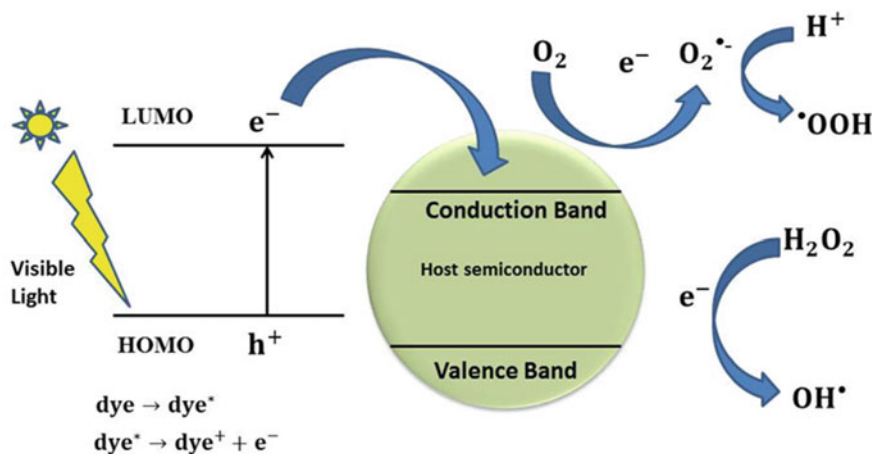
Fig. 4 Visible light activation of semiconductor

asCdS, CdSe, WO_3, Bi_2S_3, and V_2O_5 (Rehman et al. 2009). This method is similar to dye sensitization, except that the sensitizer is a narrow bandgap semiconductor rather than an organic dye. In the presence of visible light, the sensitizer semiconductor absorbs it and injects electrons into the titania CB, which is inactive. These injected electrons can move to the surface of TiO_2 particles and interact with them, resulting in active oxidative species (Fig. 5).
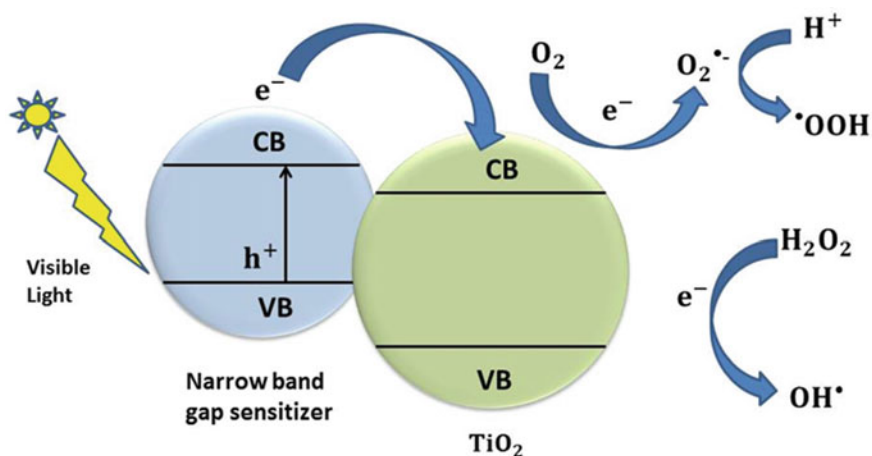
Fig. 5 Visible light activation of Titanium dioxide

2.4.7 Surface Modification by F-doping

Photocatalytic reactions mainly occur on the surface of TiO_2 photocatalysts, TiO_2 surface properties such as surface area, defects, surface acidity, surface functional groups, particle size, and crystalline phase have a major effect on photochemical activity and related mechanisms (Chen et al. 2009). The fluorine (F) was the most actively researched among the inorganic anions as TiO_2 surface modifier. The fluorination of the surface is typical for fluoride-hydroxyl group ligand exchange on TiO_2 surfaces in water (Park et al. 2013). Adsorbing the fluoride (F^-) ions on the surface to alter the surface charge and polarity lead to improved charge carrier transfer and recombination, and enhanced pollutant adsorption (Shayegan et al. 2019). In surface fluorination, adsorption of F^- ions on Ti (titanium) atoms takes place, while in F doping, F^- ions are substituted with O_2^- lattice ions in the crystal structure of TiO_2. Since the photocatalytic reactions are surface reactions, the surface fluorination of TiO_2 can also effectively enhance its photocatalytic performance by modifying the surface charge, surface acidity, surface functional groups and crystalline phase content (Chen et al. 2009; Shayegana et al. 2018; Dozzi and Selli 2013; Mrowetz and Selli 2005; Minero et al. 2000; Park and Choi 2004; Kumar and Bansal 2015).

3 Cement

An ordinary cement is made from a combination of calcium silicate and aluminates, along with minor amounts of gypsum, which hardens when exposed to water.

Manufacturing processes of cement include (i) wet process and (ii) dry process. Ordinary Portland cement is a cementing substance that resembles a natural stone mined near Portland, England. Portland cement is a product made by finely pulverizing clinker generated by calcining to incipient fusion, which is an intimate and correctly balanced blend of argillaceous and calcareous materials. After burning, care must be taken in proportioning the raw materials so that clinker of the suitable constitution may be produced (Jackson 2004; Taylor 1997). Thecalcium oxide (CaO), silicon dioxide (SiO_2), sulphur trioxide (SO_3), aluminium trioxide (Al_2O_3), and ferric oxide (FeO) are the four basic oxides found in ordinary Portland cement (Fe_2O_3). The ordinary Portland cement has been classified as 33 Grade (IS269:1989), 43 Grade (IS8112:1989), and 53 Grade (IS 12669-1987). The oxide composition of cement and its functions are presented in Table 3.

3.1 *Manufacturing Process of Cement*

Cement clinkers are made from raw materials such as limestone, sand, clay, and iron ores, which are crushed and burned. Finally, the cement clinkers are finely pulverized at a high temperature in a kiln to make cement. The manufacturing process of cement

Table 3 Chemical composition of cement (Hashimoto et al. 2005)

Oxide	Composition (%)	Function
CaO	60–65	Controls strength and whiteness. Its deficiency reduces strength and settling time
SiO_2	17–25	Gives strength. Excess of it causes slow settling
Al_2O_3	3.0–8.0	Responsible for quick setting. If in excess, it lowers the strength
Fe_2O_3	0.5–6.0	Gives color and helps in fusion of different ingredients
Na_2O	5.0–1.3	These are residues. If in excess causes efflorescence and cracking
K_2O, P_2O_5	0.1–0.2	
SO_3	1.0–2.0	Makes a cement sound

is divided various into steps, which are explained below (http://iti.northwestern.edu/cement/index.html):

3.1.1 Grinding and Blending

The raw ingredients are ground and mixed before being sent into the kiln, either using the dry method or the wet process. Water aids in the grinding process, but it must be removed before the materials enter the kiln, which costs more energy and time. The wet method is now nearly obsolete because the majority of production plants utilize high-efficiency grinding equipment that allows for dry grinding.

3.1.2 Burning—Cement Clinker Formation

The mixed ingredients are subsequently burned to create cement clinkers in a separate kiln. A variety of fuels, including coal, natural gas, fuel oil, lignite, and others, are used to power the kiln at the bottom (http://iti.northwestern.edu/cement/index.html). This operation needs the highest temperature and energy levels possible. The raw ingredients are loaded into the kiln at the top and gently rotated and pushed ahead so that each reaction may be completed at the proper temperature. There are many reaction zones in the kiln, which are further explained in detail below (http://iti.northwestern.edu/cement/index.html).

Dehydration Zone (up to 450 °C)

In this zone of kiln, the blended raw mixture is dried to remove the moisture from the components. Even if the grinding is done dry, this procedure is required to remove adsorbed moisture.

Calcination Zone (450–900 °C)

The dehydrated mixture is burned at a higher temperature in this zone to produce oxides from solid components. The various oxides formed are calcium oxide, silicon dioxide, sulphur trioxide, aluminium trioxide, and ferric oxide. Calcination is the process of solid matter disintegrating (http://iti.northwestern.edu/cement/index.html).

Solid State Reaction Zone (900–1300 °C)

The reaction begins in the solid state in this zone, forming dicalcium silicate (C_2S), one of the most important mineral components in cement (http://iti.northwestern.edu/cement/index.html). Also generated in this zone are calcium aluminates (C_3A) and calcium ferrites (C_4AF), which are later utilized in a clinkering zone to lower the temperature for the creation of tricalcium silicate (C_3S). Calcium aluminates and ferrites melt at a lower temperature (about 1300 °C) and help to reduce the temperature in the clinkering zone by speeding up the reaction rate. Following solid state reactions takes place in this zone of the kiln

$$2CaO + SiO_2 \rightarrow 2CaO.SiO_2(C_2S) \tag{15}$$

$$3CaO + SiO_2 \rightarrow 3CaO.SiO_2(C_3S) \tag{16}$$

$$3CaO + Al_2O_3 \rightarrow 3CaO.Al_2O_3(C_2A) \tag{17}$$

$$4CaO + Al_2O_3 + Fe_2O_3 \rightarrow 4CaO.Al_2O_3.Fe_2O_3(C_4AF) \tag{18}$$
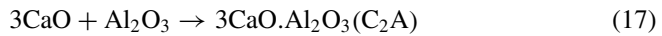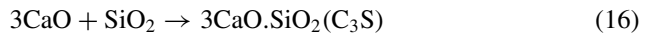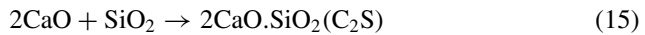
Clinkering Zone (1300–1500 °C)

This is the hottest zone, where tricalcium silicates (C_3S), one of the primary components responsible for concrete strength, are produced. C_3A and C_4AF initially melt, causing the mixture to agglomerate into large nodules bound by a thin layer of liquid (http://iti.northwestern.edu/cement/index.html). C_2S crystals in this liquid combine with CaO to create C_3S. As a result, C_3S crystals develop inside the liquid while the quantity of C_2S drops. When all of the silica is changed to C_3S and C_2S, and the quantity of CaO is decreased to less than 1%, the clinkering process is complete. Finally, cement clinkers are produced, which include all of the cement components but in a solid condition (http://iti.northwestern.edu/cement/index.html).
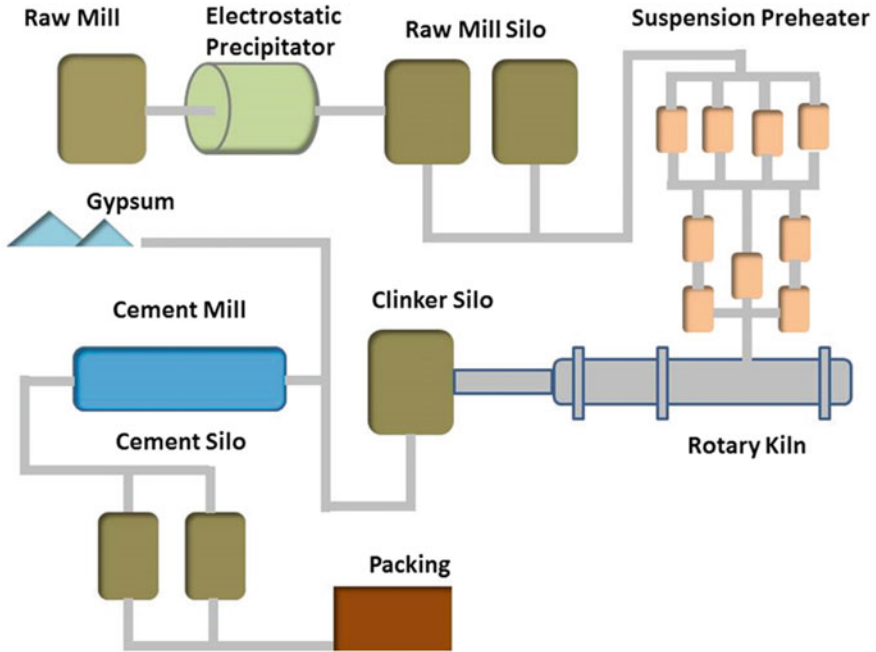
Fig. 6 Manufacturing process of cement

Cooling Zone

To avoid the decomposition of C_3S back into C_2S and CaO and to produce more reactive cement, the clinkers are rapidly cooled, either by blow drying or by utilizing water.

Grinding

The cement clinkers are now crushed into a fine powder to create Portland cement in this procedure. Gypsum (CSH_2) is used in this procedure to prevent cement flash set due to the presence of calcium aluminates and ferrites (http://iti.northwestern.edu/cement/index.html). At this stage, the cement manufacturing process is complete, and it is ready to be bagged and transported. Figure 6 represents the flow sheet of cement manufacturing process in detail.

3.2 Mineral Composition of Cement

Each of the cement minerals contributes to the overall quality and efficiency of the cement. Some constituents participate in the manufacturing process, while the others contribute during cement hydration. Table 4 describes the mineral composition of the ordinary cement with chemical formula.

The characteristics of the various minerals found in cement are discussed in the following section.

3.2.1 Tricalcium Silicate (C_3S)

Half of the cement is made up of C_3S, commonly known as Alite. Alite is the most significant component of all typical cement clinkers, constituting 50–70% of the total cement (Taylor 1997). It interacts fast with water and is the most essential component phase for strength development in typical Portland cement.

3.2.2 Dicalcium Silicate (C_2S)

Belite makes about 15–30% of ordinary Portland cement clinkers. It is dicalcium silicate (Ca_2SiO_4) that has been changed by ionic substitutions and is typically found as the polymorph. It takes a long time to react with water, thus it contributes little to strength during the first 28 $_{days}$, but a lot later on. Belitecomprises about a quarter of the cement composition and is not as reactive as alite. But, C_2S contributes to

Table 4 Mineral composition of ordinary Portland cement (http://iti.northwestern.edu/cement/index.html)

Mineral name	Cement notation	Oxide formula	Chemical formula	Chemical name
Alite	C_3S	$3CaO.SiO_2$	Ca_3SiO_5	Tricalcium silicate
Belite	C_2S	$2CaO.SiO_2$	Ca_2SiO_4	Dicalcium silicate
Aluminate	C_3A	$3CaO.Al_2O_3$	$Ca_3Al_2O_6$	Tricalcium aluminate
Ferrite	C_4AF	$4CaO.Al_2O_3.Fe_2O_3$	Ca_2AlFeO_5	Tetracalcium aluminoferrite
Portlandite	CH	$CaO.H_2O$	$Ca(OH)_2$	Calcium hydroxide
Gypsum	CSH_2	$CaO.SO_3.2H_2O$	$CaSO_4.2H_2O$	Calcium sulfate dihydrate
Lime	C	CaO	CaO	Calcium oxide

the later age strength of cement paste. Under comparable conditions, the strengths obtained from pure alite and pure beliteare almost the same after one year (Taylor 1997; Maa and Shen 2019).

3.2.3 Tricalcium Aluminates (C_3A)

Most typical Portland cement clinkers include 5–10% aluminate. It is tricalcium aluminate ($Ca_3Al_2O_6$), which has been significantly altered in composition and, in some cases, structure by ionic replacements. It interacts quickly with water and can result in an unfavorable rapid setting unless a set-controlling agent, generally gypsum, is applied. As a result, gypsum is added to slow down the hydration of C_3A. These minerals have little to no impact on the cement paste's strength. However, they assist in the creation of the elite by lowering the temperature of a cement kiln in a production facility in the clinkering zone by (1000 °C) (Taylor 1997).

3.2.4 Tetracalciumaluminoferrite (C_4AF)

Ferrite contributes about 5–15% of standard Portland cement clinkers. It is tetracalciumaluminoferrite (Ca_2AlFeO_5), whose composition has been significantly altered by changes in the Al/Fe ratio and ionic replacements. The rate at which it interacts with water appears to be fairly varied, maybe due to variations in composition or other properties, but in general, is high at first and low or extremely low later on (Taylor 1997). This compound has the same contribution as tricalcium aluminates and does not assist in the strength of cement paste. C_4AF are employed as fluxing agents to lower the temperature in the clinkering zone of a concrete production (Pourchez et al. 2009; Gartner and Myers 1993).

3.3 White Cement

The white ordinary Portland cement, generally known as "White Cement," is one of the most significant raw materials used in building construction. Except for whiteness, white cement has the same characteristics as grey common Portland cement. It has a high degree of whiteness and is as durable and robust as grey regular Portland cement. White cement is manufactured from raw ingredients that are lacking colorants like Fe, Mn, Cr, and Ti. White cement is made from pure white chalk and clay that is devoid of iron oxide. The greyish color of cement is caused by iron oxide. As a result, the iron oxides were decreased and restricted to less than 1%. Colored cement can be created by adding 5 to 10% color pigments in white cement before grinding (Hashimoto et al. 2005).

3.3.1 Physical Properties of the White Cement

Fineness of Cement

The fineness of the cement is determined by the size of its particles. The needed fineness of excellent cement is attained in the final stage of the cement production process by grinding the clinker. Because the hydration rate of cement is closely connected to the particle size of cement, the fineness of cement is critical.

Soundness

Soundness refers to the ability of cement to not shrink upon hardening. Good quality cement retains its volume after setting without delayed expansion, which is caused by excessive free lime and magnesia.

Consistency

The ability of cement paste to flow is referred to as consistency. The Vicat Test is used to determine it. In Vicat Test, cement paste of normal consistency is taken in the Vicat Apparatus. The plunger of the device is lowered till it touches the top surface of the cement. Depending on the consistency of the cement, the plunger will penetrate it up to a specific depth (GB/T 1999, 2011).

Strength of Cement

Cement strength is assessed in three ways: compressive, tensile, and flexural. Water-cement ratio, cement-fine aggregate ratio, curing circumstances, specimen size and shape, molding and mixing method, loading conditions, and age are all factors that influence strength (Khuda 2021).

Compressive Strength: It is the most often used strength test. A test specimen (50 mm) is collected and compressed until it fails. The loading procedure must be completed between 20 and 80 s.

Tensile strength: While this test was used in the early days of cement manufacture, it no longer provides meaningful information about the properties of cement.

Flexural strength: Flexural strength is a measurement of tensile strength in bending. The test is carried out in a cement mortar beam $40 \times 40 \times 160$ mm in size, which is loaded at its centre point till failure.

Setting Time

When water is added to cement, it sets and hardens. This time can vary based on several parameters, including cement fineness, cement-water ratio, chemical content, and admixtures. Cement used in construction should have a reasonable beginning setting time and a reasonable final setting time. As a result, two setting times are measured; (a) Initial setting time-when the paste becomes significantly stiffer; (b) Final setting time-being able to withstand some load when the cement hardens.

Heat of Hydration

Hydration is central to cementitious materials. It is the nearly miraculous transformation of a fluid suspension into a rigid solid at room temperature, without the need of heat or other external processing agents, and with minimum bulk volume change (Scrivener and Nonat 2011). When Portland cement is mixed with water, heat is produced. This heat, known as the heat of hydration, is the result of an exothermic chemical interaction between cement and water (Majdi and Abbasb 2017). The presence of C_3S and C_3A in cement, as well as the water-cement ratio, fineness, and curing temperature, all, influence the heat of hydration. The difference between the dry and partially hydrated cement is used to determine the heat of hydration of Portland cement (obtained by comparing these at 7th and 28th days) (Scrivenera et al. 2019).

4 Photocatalysis in Cementitious Materials

A large number of scientific research and patents are focused on titanium dioxide (TiO_2), either on photoinduced degradation mechanisms on diverse chemical compounds and associated kinetics or the manufacture and characterization of TiO_2 nanopowders. Several research groups have explored the interactions of TiO_2 nanoparticles with cementitious materials, with an emphasis on cement pastes or mortars with low water/cement ratios (Diamanti et al. 2008). TiO_2 is typically dry mixed with cement powder before being hydrated with water. TiO_2 is present throughout the produced cement structure when it hardens. TiO_2 is an extremely stable and inert oxide. It has no interaction with any cementitious phase and does not participate in any hydration process. It has been observed that TiO_2 can cause changes in the material's properties. TiO_2 additions may have a direct impact on the strength, sensitivity, and aging processes. Furthermore, organic molecules might be subjected to photoassisted decomposition, which is required for many construction materials. From a material structural standpoint, it serves as pore filler, decreasing porosity and providing some early-stage strength advantages. When water is introduced to hydrate the cement powder, no chemical reactions involving TiO_2 occur.

The newly created chemical environment is predicted to significantly alter titania particle surface chemistry and electrokinetic properties.

In the case of new concrete, the addition of TiO_2 nanopowders to mortar or concrete reduces workability due to their large specific surface area, which increases the quantity of water adsorbed and alters the rheological behavior of the mix by raising viscosity. The results reveal that the concrete containing nano-TiO_2 particles had significantly greater compressive strength than the concrete without nano-TiO_2 particles (Nazari et al. 2010). At early age, the incorporation of nano-TiO_2 powders increased significantly the hydration rate and enhanced the hydration degree of the cementitious materials. During the cement hydration process, TiO_2 was shown to be inert and stable. The fast consumption of free water indicates that hydration processes are accelerated: as a result, dosing TiO_2 nanopowders into cement pastes affects solidification, resulting in a reduction in setting time (Cheng et al. 2012). TiO_2 alters the pore size distribution and overall pore volume in cementitious materials. In addition, as the number of nanoparticles increases, the water content must rise to ensure adequate workability, which adds to increased porosity: therefore, there is a combined impact of pore size reduction and increased porosity in compositions containing large quantities of TiO_2 (Lucasa et al. 2013). Because of the filler effect of the nanoparticles, the compressive strength of hardened concrete is increased: TiO_2 is a non-reactive nano-filler, and the increase in mechanical resistance is due to its large surface area for hydration product nucleation or clinging. Moreover, during the service life of the building, various changes in the microstructure of concrete and mortar occur (Bertolini 2008). Because of the small size effect and the filling impact, nano-titanium dioxide refines the microstructure, making it denser. The addition of TiO_2 slows the growth of $Ca(OH)_2 (CH)$ crystals, resulting in decrease in the size of CH (Calcium Hydroxide). Prior study has also shown that TiO_2 can regulate the development of hydration products and enhance cement hydration (Li et al. 2018). As a result, TiO_2 refines the pore structure of concrete and enhances its resistance to chloride penetration (Zhang and Li 2011). Because of photocatalytic degradation processes, the use of organic admixtures in TiO_2 containing concrete and other cementitious materials may result in organic component degradation, with possible reductions in durability and photoactivity. As a result, the use of organic binders and admixtures in cementitious materials must be limited (Chen and Poon 2009). Moreover, it was reported that the carbonation rate of lime-TiO_2 binary mixes was significantly accelerated owing to a rise in carbon dioxide content caused by photocatalysis (photo-oxidation) of organic pollutants in both laboratories (methyl orange) and outdoor environments. The incorporation of TiO_2 nanoparticles may speed up the carbonation process linked with CO_2 release (Karatasios et al. 2010). However, carbonation-induced changes might have an effect on the photoactivity of the TiO_2 admixture by lowering its efficiency (Diamanti et al. 2008; Chen and Poon 2009).

4.1 Self-cleaning White Cement

Prolonged contact with different air contaminants causes discoloration of cementitious materials (Maury and Debelie 2010). The beauty of buildings, monuments, and other infrastructure exposed to external settings deteriorates with time as a result of this discoloration effect. Aside from visual discoloration, contamination of cement-based surfaces by airborne particles such as algae and fungus can be detrimental to structural integrity (Giannantonio et al. 2009; Gu et al. 1998). Ordinary structures lose their aesthetic durability over time as a result of age and weathering. For example, building surfaces may be contaminated by greasy and sticky deposits, resulting in a high adhesion of ambient dust and tiny particles, causing dirt to accumulate on the surface. The aesthetic properties of buildings are therefore restored by consistent and proper repair, which frequently requires the use of chemicals and energy demanding technologies (Diamanti et al. 2008; Guan 2005). The formation of biogenic acids has been related to microorganisms' essential involvement in the degradation of cementitious materials (Parker 1945). The first development of cementitious materials incorporating TiO_2 photocatalyst was done largely to improve the visual durability of cementitious materials, particularly those based on white cement (Maury and Debelie 2010). Self-cleaning cement is a good answer to this issue. A self-cleaning cement removes pollutants from the air while keeping its surface clean. Self-cleaning cement is a new extraordinary cement that not only maintains itself clean but also removes pollutants from the air. Photocatalytic components, which utilize the energy from UV light to oxidize most organic and certain inorganic molecules, are the key to such properties. The components eliminate air pollutants that would usually cause discoloration of exposed surfaces from the environment, and their residues are rinsed away by rain (Kumar et al. 2005). Although the photoinduced processes of TiO_2 photocatalytic destruction of pollutants and superhydrophilicity are distinct mechanisms, the combined impact of the two results in the self-cleaning effect being maintained (Guan 2005). TiO_2 possesses another uniquephoto-induced phenomenon that alters the wettability of its surface, which it uses to degrade organic contaminants through photocatalysis. The latter is known as 'super hydrophilicity.' The first, photocatalysis, has been researched intensively for decades, but the second, super hydrophilicity, has just recently been found. The property of photocatalyst-based cement to increase wettability when illuminated has a significant impact on the efficiency of self-cleaning activities (Mills et al. 2012). The self-cleaning cement basically depicts three properties such as self-cleaning property, depollution ability and antimicrobial activity.

4.1.1 Self-cleaning Property

Self-cleaning properties are nearly entirely determined by the efficiency with which organic molecules are oxidized. Composite materials mostly derived from atmospheric aerosol pollution are visible stains on building surfaces. Organic binders

like hydrocarbons and fatty acids attach small particles and greasy residues to the building surface (Kawakami et al. 2007). The deposition of organic and mineral particles, the buildup of fly ash, hydrocarbons, and soot from the burning of fossil fuels and biomass, as well as biological development, all contribute to the formation of undesirable stains and color changes (e.g., cyanobacteria, fungi, algae) (Berdahl and Akbari 2008; Ratan and Saini 2019). Fatty acid molecules, for example, have carboxylic groups (–COOH) that allow them to stick to the surface of a building through chemical binding with calcium ions present in concrete; on the other hand, their long chains link with other hydrophobic molecules perpendicular to the surface, resulting in fatty stains that trap many atmospheric particles and dust. The organic binders can be decomposed by the high redox power of the UV-induced oxygen-based radicals generated on the surface of the self-cleaning cement containing the TiO_2. The atmosphere provides the water and oxygen required for the production of OH radicals, but the UV light required for TiO_2 activation is a small fraction of the UV energy present in sunlight that reaches the Earth's surface ($\approx$7 to 8% UV light). When we talk about self-cleaning properties, we're talking about the surface of the cementitious material. Furthermore, the substances that cause dirt and stains are often extremely large organic molecules in the environment that adsorb on the exposed cementitious surface. Because of this, TiO_2 particles in the cementitious binder must be well distributed in small particle agglomerates. The first condition can be satisfied by selecting a titania sample with suitable particle size and surface properties that allow for the development of small agglomerates. Because just solar light and rainwater are required as driving factors, TiO_2's self-cleaning ability is cost effective. Its use might minimize the need for maintenance, which can be difficult and expensive in tall structures (Diamanti et al. 2013). Self-cleaning is considered to be the result of two primary mechanisms: (1) photocatalysis enhanced by superhydrophilicity, (2) superhydrophilicity enhanced by photocatalysis. In this case, the photoexcited electrons might react with the Ti^{4+} cations to produce Ti^{3+} after generating electron-hole pairs as shown in Fig. 7. In the meanwhile, the holes might oxidise the O_2^- anions to produce molecular oxygen. The oxygen atoms are then released, resulting in oxygen vacancies. Water molecules may then occupy the oxygen vacancies, generating a layer of chemisorbed OH groups that tend to make the surface hydrophilic (Husken et al. 2007). Organic binders such as hydrocarbons and fatty acids, which may retain various air particles and dust, adhere small particles and greasy deposits to building surfaces. The high redox power of the photocatalyst's UV-induced electron-hole pair can decompose the soiling chemicals into H_2O, CO_2, and organic molecules (Fujishima et al. 2000b; Schwarz et al. 1997). Furthermore, when water flow, such as natural rainfall, was applied to the surface, the self-cleaning effect of TiO_2 surfaces was shown to be increased. They ascribed these improved water flow phenomena to TiO_2's superhydrophilic feature, i.e., water soaking the molecular level gap between the stain and the superhydrophilic TiO_2 surface (Saini et al. 2020). The adsorption of organic molecules on the surface can cause the surface to change from hydrophilic to hydrophobic; however, photocatalysis can destroy the organic compounds on the surface, restoring hydrophilicity. Photocatalytic decomposition of these organic pollutants can now restore the superhydrophilic characteristic, which
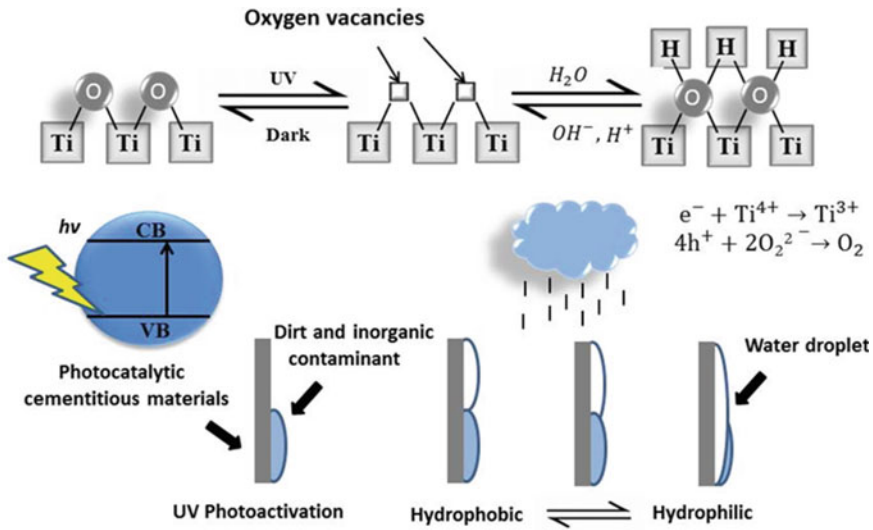
Fig. 7 Mechanism of photoinduced hydrophilicity on TiO$_2$ cement surface under UV irradiation and rainfall (Husken et al. 2007)

will last for a long time (Guan 2005). Figure 7 shows The TiO$_2$photocatalyst can maintain the surface clean only when the photocatalytic sterilization rate is greater than the tainting rate (Wang et al. 1997b). The efficiency of the self-cleaning effect is dependent on the interaction of photocatalysis and photoinduced super hydrophilicity (Husken et al. 2007). Water contact angle measurement and organic dye decomposition are two typical test methods for evaluating photocatalytic surface's self-cleaning ability.

4.1.2 Depolluting Ability

The depolluting ability of the self-cleaning cement is responsible for the degradation of environmental pollutants. The ROS, generated by self-cleaning cement in the presence of sunlight, photo-oxidize the available gaseous pollutants to water, carbon dioxide, and less objectionable by-products. The synergy between the photocatalyst and cement matrix makes it a suitable substrate for photocatalytic oxidation of gaseous pollutants. The porous structure of the hardened cement provides a suitable platform for an efficient contact between the pollutants and photocatalyst, thus facilitating the photo-degradation of the pollutants (Zhang and Banfield 2000; Karapati et al. 2014). Moreover, the basic nature of the cement matrix is particularly apt for degradation of the gaseous pollutants and fixing the by-products of photocatalytic oxidation. The self-cleaning cement has been demonstrated to degrade the various gaseous pollutants such as NO$_x$, SO$_x$, CO, and various VOCs (Kumar and Bansal 2010b). VOCs (volatile organic compounds) are a prominent category of biogenic

and anthropogenic indoor air pollutants that have been linked several health problems (Shayegan et al. 2018). VOCs are not only dangerous chemicals, but they also play a role in damaging by-products such as organic compounds, ozone, and secondary organic aerosols. Several air purification strategies for VOC elimination have been developed to tackle this problem. Photocatalyst oxidation (PCO) is a promising VOCs elimination technique (Cheng et al. 2015). Air pollution caused by nitrogen oxides (NO_x) is a major problem in modern society. They are one of the primary causes of photochemical smog. Acid rain is caused by a combination of dangerous chemicals produced in the atmosphere as a result of sunlight interacting with contaminants already existing; they produce acid rain when combined with sulphur oxides (SO_x) (Bahri and Haghighat 2014). The sum of NO and NO_2 is known as NO_x in atmospheric chemistry. NO is released into the atmosphere directly from a source (e.g. high temperature combustion in transport and industry). The interaction between NO and ozone (O_3), or molecular oxygen produces NO_2 in the atmosphere, which is aided by sunlight (Bahri and Haghighat 2014; Harrison 1992). Further atmospheric reactions can convert NO and NO_2 into nitric acid, HNO_3, peroxyacyl nitrates (PANs), $RC(O)OONO_2$, peroxynitric acid, HNO_4, and other compounds. The sum of all these species and NOx is known as NO_y, total reactive nitrogen (Cotton and Wilkinson 1988; Seinfeld 1998). Nitrogen monoxide (NO) and nitrogen dioxide (NO_2) are the most prevalent nitrogen oxides. Because three fundamental mechanisms that lead to the formation of nitrogen oxides during combustion, three kinds of NO_x have been identified: There are three types of NO_x emissions: quick NO_x, fuel NO_x, and thermal NO_x (Elsom 1987; Charles 2005). To control NO_x emissions, certain approaches have been developed and applied, which are classified as primary and secondary methods (Roy et al. 2009). Photocatalysis with titanium dioxide is an alternate technique for decomposing this species of pollutant. The de-polluting rate of photocatalytic cement, which is made up of cement with around 1–5% anatase TiO_2 nano-particles, was studied (Chen and Chu 2011). The ability of TiO_2 containing cement to remove NO_x reduces with curing age and increases with surface carbonation. As the curing period increases, the hydration products rise, filling the capillary pores and resulting in the formation of diffusion barriers to both reactants and photons (Folli et al. 2010). The porosity and surface roughness of TiO_2 cementitious materials have been shown to impact their air-cleaning performance (Chen and Poon 2009). Pacheo-Torgal et al. said in a study of nanotechnology that TiO_2 cementitious composites with high surface porosity had a greater decrease in NO_x (Ramirez et al. 2010). The degradation mechanism for both organic and inorganic pollutants, such as NO, NO_2, and SO_2, is a multi-step chain of reactions that includes the creation of reaction intermediates. The photocatalytic oxidation of nitrogen monoxide (NO) to nitric acid (HNO_3) over TiO_2 begins with the creation of O_2 and $OH^\bullet$ radicals during the photocatalyst's activation process, which subsequently react with the pollutant gas to produce NO_2 and HNO_3 (Pacheo-Torgal and Jalali 2011; Lim et al. 2000).

4.1.3 Antimicrobial Activity

The antimicrobial ability of the self-cleaning cement prevents the growth of the pathogenic microorganisms on its surface, thus protecting human beings from their ill effects on health. Moreover, the proliferation of microorganisms is also accountable for damage of the constructional materials. Therefore, inducing antimicrobial properties to the constructional materials may enhance their life, strength, and aesthetic durability (Dalton et al. 2002; Bolashikov and Melikov 2009). Several studies have found links between mold development and respiratory illnesses in buildings, particularly wet and water-damaged structures (Wiszniewska et al. 2009). Many studies have already pointed out that when favoring conditions such as high humidity and nutrient content are available, indoor building materials may become important sites of microbial growth (Fung and Hughson 2003). The antibacterial effect of photocatalytic TiO_2 was first discovered by Matsunaga et al. (Verdier et al. 2014). They assessed the photocatalytic oxidation under UV irradiation on a variety of microorganisms including Gram-positive bacteria (Lactobacillus acidophilus), Gram-negative bacterial (Escherichia coli), yeast (Saccharomyces cerevisiae), and green algae (Chlorella vulgaris). There has been a lot of research published on the effect of photocatalyticTiO_2 nanoparticles on microbes including viruses, fungi, and several bacterial species (Matsunaga et al. 1985; Foster et al. 2011). PCO is an innovative technique that uses short-wave ultraviolet radiation (UVC) to remove bacteria from the air and water. Some pathogens are easily killed by following treatment with a TiO_2 coated PCO unit, thus the results are somewhat encouraging (Sordo et al. 2010; Wong et al. 2010; Pal et al. 2007). Even if a wealth of material has been collected revealing the efficiency of the TiO_2 catalyst's biocidal activities, there is a lack of any solid evidences indicating the main species responsible for the photochemical inactivation of the microorganism. TiO_2photocatalyst biocidal activity has been attributed to two main photochemical oxidants: $OH^\bullet$ radical (Krishna et al. 2005; Sjogren and Sierka 1994; Watts et al. 1995; Melian et al. 2000; Bekbolet 1997) and reactive oxygen species (ROS) (Lee et al. 1997; Huang et al. 2000). When TiO_2 is exposed to UV light, electrons from the valence band are transported to the conduction band, leaving a positively charged hole behind. The activated charge carriers react with the oxygen and water molecules in the atmosphere to create reactive oxygen species (ROS) (Maness et al. 1999). The antibacterial activity of TiO_2photocatalyst is always attributed to $OH^\bullet$ radicals and other reactive oxygen species (ROS), which are the driving force behind TiO_2's biocidal effect (Cho et al. 2004; Mukherjee et al. 2011). An initial attack on the bacterium cell wall is the major cause of the basic photocatalytic disinfection mechanism (Allahverdiyev et al. 2011), superoxide anions $\left(O_2^-\right)$ had dual actions on lipid peroxidation, which might improve membrane fluidity while disrupting cell integrity. After the cell wall protection is removed, oxidative damage occurs on the bacteria's plasma membrane, resulting in cell death. It was also determined that cells subjected to TiO_2-UV treatment demonstrate fast cell inactivation at the signaling stages, which impacts a limited range of respiratory components (Carre et al. 2014). The biocidal properties of a photocatalytic cement-based surface can cause microbial death while also keeping the surface sterile. In comparison to air

purification and self-cleaning applications, however, less study has been conducted to examine the antimicrobial impact of photocatalytic cementitious materials.

5   Conclusion

The article showcases the fundamentals of TiO_2-photocatalysis along with an overview of TiO_2 based self-cleaning cement. It provides an overlook about the photocatalysis in cementitious materials, related photoreactions & their mechanism, properties and advantages of self-cleaning cement. Although extensive research has been conducted in the field of self-cleaning cement, its commercial application still needs to be accelerated. Therefore, the researchers all over the world should focus on the existing technological challenges of this area of research such as development of visible-light-active TiO_2, modification of structure of TiO_2 for efficient photocatalysis, restoration of photocatalytic activity of TiO_2 for reuse, and reduction in the cost of formation of self-cleaning cement.

Conflict of Interest   The authors state that they don't have any conflict for interest for this paper.

References

Adachi K, Ohta K, Mizuno T (1994) Photocatalytic reduction of carbon dioxide to hydrocarbon using copper-loaded titanium dioxide. Sol Energ 53:187–190

Allahverdiyev AM, Abamor ES, Bagirova M, Rafailovich M (2011) Antimicrobial effects of TiO_2 and Ag_2O nanoparticles against drugresistant bacteria and leishmania parasites. Future Microbiol 6(8):933–940

Anpo M (2000) Utilization of TiO_2 photocatalysts in green chemistry. Pure Appl Chem 72(7):1265–1270

Ao Y, Xu J, Zhang S et al (2010) A one-pot method to prepare N-doped titania hollow spheres with high photocatalytic activity under visible light. Appl Surf Sci 256:2754–2758

Bahri M, Haghighat F (2014) Plasma-based indoor air cleaning technologies: the state of the art-review. CLEAN-Soil Air Water 42(12):1667–1680

Beeldens A, Van Gemert D (2004) Experimental investigation of efficiency of TiO_2-cement coating for self-cleaning and air purification. In: RILEM international symposium on environment-conscious materials and systems for sustainable development, pp 353–359

Bekbolet M (1997) Photocatalytic bactericidal activity of TiO_2 in aqueous suspensions of *E. coli*. Water Sci Technol 35:95–100

Berdahl P, Akbari H (2008) Evaluation of titanium dioxide as a photocatalyst for removing air pollutants. California Energy Commission. PIER Energy-Related Environmental Research Program CEC-500-2007-112

Bertolini L (2008) Steel corrosion and service life of reinforced concrete structures. Struct Infrastruct Eng 4:123–137

Bickley RI, Munuera G, Stone FS (1973) Photoadsorption and photocatalysis at rutile surfaces. 2. Photocatalytic oxidation of isopropanol. J Catal 31:398–407

Bolashikov ZD, Melikov AK (2009) Methods for air cleaning and protection of building occupants from airborne pathogens. Build Environ 44:1378–1385

Boscaro P, Cacciaguerra T, Cot D, Fajula F, Hulea V, Galarneau A (2019) C, N-doped TiO_2 monoliths with hierarchical macro-/mesoporosity for water treatment under visible light. Microporous Mesoporous Mater 280:37–45

Burda C, Lou Y, Chen X et al (2003) Enhanced nitrogen doping in TiO_2 nanoparticles. Nano Lett 3:1049–1051

Buszek RJ, Torrent-Sucarrat M, Anglada JM, Francisco JS (2012) Effects of a single water molecule on the OH+ H_2O_2 reaction. J Phys Chem A 116(24):5821–5829

Butler EC, Davis AP (1993) Photocatalytic oxidation in aqueous titanium-dioxide suspensions-the influence of dissolved transition-metals. J Photochem Photobiol A 70:273–283

Buxton GV, Greenstock CL, Helman WP, Ross AB (1988) Critical review of rate constants for reactions of hydrated electrons, hydrogen atoms and hydroxyl radicals (·OH/·O- in aqueous solution. J Phys Chem Ref Data 17(2):513–886

Carp O, Huisman CL, Reller A (2004b) Photoinduced reactivity of titanium dioxide. Prog Solid State Chem 32:33–117

Carp O, Huisman CL, Reller A (2004) Photoinduced reactivity of titanium dioxide. Prog Solid State Chem 32(1, 2):33–177

Carre G, Estner M, Gies J-P, Andre P, Hamon E, Ennahar S, Keller V, Keller N, Lett M-C, Horvatovich P (2014) TiO_2 photocatalysis damages lipids and proteins in *Escherichia coli*. Appl Environ Microbiol 80:2573–2581

Charles B (2005) Everything you need to know about NO_x: controlling and minimizing pollutant emissions is critical for meeting air quality regulations. Met Finish 103:18–24

Chen M, Chu J (2011) NO_x photocatalytic degradation on active concrete road surface from experiment to real-scale application. J Clean Prod 19:1266–1272

Chen J, Poon CS (2009) Photocatalytic construction and building materials: from fundamentals to applications. Build Environ 44:1899–1906

Chen Y, Chen F, Zhang J (2009) Effect of surface fluorination on the photocatalytic and photo-induced hydrophilic properties of porous TiO_2 films. Appl Surf Sci 255:6290–6296

Cheng M-D, Miller W, New J, Berdahl P (2012) Understanding the long-term effects of environmental exposure on roof reflectance in California. Constr Build Mater 26:516–526

Cheng Y-H, Lin C-C, Hsu S-C (2015) Comparison of conventional and green building materials in respect of VOC emissions and ozone impact on secondary carbonyl emissions. Build Environ 87:274–282

Cho M, Chung H, Choi W, Yoon J (2004) Linear correlation between inactivation of *E. coli* and OH radical concentration in TiO_2 photocatalytic disinfection. Water Res 38(4):1069–1077

Choi W, Termin A, Hoffmann MR (1994) The role of metal ion dopants in quantumsized TiO_2: correlation between photoreactivity and charge carrier recombination dynamics. J Phys Chem B 98:13669–13679

Cotton FA, Wilkinson G (1988) Advanced inorganic chemistry, 5th edn. Wiley-Interscience, USA

Czoska AM, Livraghi S, Chiesa M, Giamello E, Agnoli S, Granozzi G, Finazzi E, Valentin CD, Pacchioni G (2008) The nature of defects in fluorine-doped TiO_2. J Phys Chem C 112:8951–8956

Dalton JS, Janes PA, Jones NG, Nicholson JA, Hallam KR, Allen GC (2002) Environ Pollut 120:415–422

Diamanti MV, Lollini F, Pedeferri MP, Bertolini L (2008) Mutual interactions between carbonation and titanium dioxide photoactivity in concrete. Build Environ 62:174–181

Diamanti MV, Del Curto B, Ormellese M, Pedeferri MP (2013) Photocatalytic and self-cleaning activity of colored mortars containing TiO_2. Constr Build Mater 46:167–174

Dozzi MV, Selli E (2013) Effects of phase composition and surface area on the photocatalytic paths on fluorinated titania. Catal 206:26–31

Elsom D (1987) Atmospheric pollution, 1st edn. Basil Blackwell, New York

Faust BC, Hoffmann MR, Bahnemann DW (1989) Photocatalytic oxidation of sulfur-dioxide in aqueous suspensions of alpha-Fe_2O_3. J Phys Chem 93:6371–6381

Fernandez-Ibanez P, Blanco J, Malato S, Nieves FJ (2003) Application of the colloidal stability of TiO₂ particles for recovery and reuse in solar photocatalysis. Water Res 37:3180–3188

Folli A, Pochard I, Nonat A, Jakobsen U, Shepherd AM, Macphee DE (2010) Engineering photocatalytic cements: understanding TiO₂ surface chemistry to control and modulate photocatalytic performances. J Am Ceram Soc 93:3360–3369

Foster HA, Ditta IB, Varghese S, Steele A (2011) Photocatalytic disinfection using titanium dioxide: spectrum and mechanism of antimicrobial activity. Appl Microbiol Biotechnol 90(6):1847–1868

Fujishima A, Honda K (1972) Electrochemical photolysis of water at a semiconductor electrode. Nature 238:37

Fujishima A, Rao TN, Tryk DA (2000a) Titanium dioxide photocatalysis. J Photochem Photobiol C Photochem Rev 1(1):1–21

Fujishima A, Rao T, Tryk D (2000b) Titanium dioxide photocatalysis. J Photochem Photobiol c: Photochem Rev 1:1–21

Fujishima A, Zhang X, Tryk DA (2007) Heterogeneous photocatalysis: from water photolysis to applications in environmental cleanup. J Hydrog 32(14):2664–2672

Fujishima AZ (2006) Titanium dioxide photocatalysis: present situation and future approaches. ComptesRendusChim 9(5, 6):750–760

Fujishima A, Hashimoto K, Watanabe T (1999) TiO₂ Photocatalysis: fundamentals and application, 1 edn. BKC, Tokyo

Fung F, Hughson WG (2003) Health effects of indoor fungal bioaerosol exposure. Appl Occup Environ Hyg 18:535–544

Gartner E, Myers D (1993) Influence of Tertiary alkanolamines on Portland cement hydration. J Am Ceram Soc 76:1521–1530

GB/T 1346-2011 (2011) Test methods for water requirement of normal consistency, setting time and soundness of the Portland cement. China Standard Press

GB/T 17671-1999 (1999) Method of testing cements-determination of strength. China Standard Press

Ge M, Azouri A, Xun K, Sattler K, Lichwa J, Ray C (2006) Solar photocatalytic degradation of Atrazine in water by a TiO₂/Ag nanocomposite. ASME 17070:217–220

Giannantonio DJ, Kurth JC, Kurtis KE, Sobecky PA (2009) Effects of concrete properties and nutrients on fungal colonization and fouling. Int Biodeterior Biodegradation 63:252–259

Gu JD, Ford TE, Berke NS, Mitchell R (1998) Biodeterioration of concrete by the fungus Fusarium. Int Biodeterior Biodegradation 41:101–109

Guan K (2005) Relationship between photocatalytic activity, hydrophilicity and selfcleaning effect of TiO₂/SiO₂ films. Surf Coat Technol 191(2):155–160

Harrison RM (1992) Pollution: causes, effects and control, 2nd edn. The Royal Society of Chemistry, Cambridge

Hashimoto K, Irie I, Fujishima A (2005) TiO₂ photocatalysis: a historical overview and future prospects. Jpn J Appl Phys 44:8269–8285

Heller A (1995) Chemistry and applications of photocatalytic oxidation of thin organic films. Acc Chem Res 28(12):503–508

Hoffmann MR, Martin ST, Choi W, Bahnemann DW (1995) Environmental applications of semiconductor photocatalysis. Chem Rev 95(1):69–96

Huang Z, Maness PC, Blake DM, Wolfrum EJ, Smolinksi SL, Jacoby WA (2000) Bactericidal mode of titanium dioxide photocatalysis. J Photochem Photobiol A Chem 130:163–170

Husken G, Hunger M, Brouwers H (2009) Experimental study of photocatalytic concrete products for air purification. Build Environ 44:2463–2474

Husken G, Hunger M, Brouwers H (2007) Comparative study on cementitious products containing titanium dioxide as photo-catalyst. In: Proceedings of international RILEM symposium on photocatalysis, environment and construction materials, pp 147–154

Inoue T, Fujishima A, Konishi S, Honda K (1979) Photoelectrocatalytic reduction of carbon-dioxide in aqueous suspensions of semiconductor powders. Nature 277:637–638

Irie H, Watanabe Y, Hashimoto K (2003) Carbon-doped anatase TiO_2 powders as a visible-light sensitive photocatalyst. Chem Lett 32:772–773

Irie H, Folli A, Pade C, Hansen TB, Marco TD, Macphee DE (2012) TiO_2 photocatalysis in cementitious cement: Insights into self-cleaning and depollution chemistry. Cem Concr Res 42:539–548

Jackson PJ (2004) Portland cement: classification and manufacture. In: Hewlett PC (ed) Lea's chemistry of cement and concrete, 4th edn. Elsevier Science and Technology Books, pp 25–94

Jacobson MZ (2005) Fundamentals of atmospheric modeling. Cambridge University Press

Joshi MM, Labhsetwar NK, Mangrulkar PA et al (2009) Visible light induced photoreduction of methyl orange by N-doped mesoporous titania. Appl Catal A General 357:26–33

Karapati S, Giannakopoulou T, Todorova N, Boukos N, Antiohos S, Papageorgiou D, Chaniotakis E, Dimotikali D, Trapalis C (2014) TiO_2 functionalization for efficient NO_x removal in photoactive cement. Appl Surf Sci 319:29–36

Karatasios I, Katsiotisa MS, Likodimosb V, Kontos AI (2010) Photo-induced carbonation of lime-TiO_2 mortars. Appl Catal B: Environ 95(1, 2):78–86

Kawakami M, Furumura T, Tokushige H (2007) NO_x removal effects and physical properties of cement mortar incorporating titanium dioxide powder. In: Proceedings of international RILEM symposium on photocatalysis, environment and construction materials, pp 163–170

Khuda SN-E (2021) Influence of wetting–drying cycles on compressive and flexural strength of cement mortar and CFRP-mortar bond strength. Constr Build Mater 271:121513

Krishna V, Pumprueg S, Lee S-H, Zhao J, Sigmund W, Koopman B et al (2005) Photocatalytic disinfection with titanium dioxide coated multi-wall carbon nanotubes. Process Saf Environ Prot 83(B4):393–397

Kumar J, Bansal A (2015) CFD simulations of immobilized-titanium dioxide based annular photocatalytic reactor: model development and experimental validation. Indian J Chem Technol 22:95–104

Kumar J, Jana AK, Bansal A, Garg R (2005) Development of correlation between BOD and COD for refinery waste. Indian J Environ Prot 25(5):405

Kumar KV, Porkodi K, Rocha F (2008) Langmuir-Hinshelwood kinetics—a theoretical study. Catal Commun 9:82–84

Kumar J, Bansal A (2010) Photocatalytic degradation of amaranth dye in aqueous solution using sol-gel coated cotton fabric. In: Proceedings of the world congress on engineering and computer science, vol 2, pp 20–22

Kumar J, Bansal A (2010) Photocatalytic degradation of amaranth dye over immobilized nano-crystals of TiO_2. In: International conference on energy and environment, Cambridge, pp 129–133

Kutal C, Serpone N (1993) Division of inorganic chemistry, photosensitive metal-organic systems: mechanistic principles and applications. J Am Chem Soc Washington DC xiii:449

Lee S, Otaki NM, Ohgaki S (1997) Photocatalytic inactivation of phage QB by immobilized titanium dioxide mediated photocatalyst. Water Sci Technol 35:101–106

Li Z, Ding S, Yu X, Han B, Ou J (2018) Multifunctional cementitious composites modified with nano titanium dioxide: a review. Compos Part a: Appl Sci Manuf 111:115–137

Lim TH, Jeong SM, Kim SD, Gyenis J (2000) Photocatalytic decomposition of NO by TiO_2 particles. J Photochem Photobiol 134(3):209–217

Linsebigler A, Lu G, Yates JT (1995) Photocatalysis of TiO_2 surfaces: principles, mechanisms, and selected results. Chem Rev 95:735–758

Lucasa SS, Ferreiraa VM, Barroso de Aguiarb JL (2013) Incorporation of titanium dioxide nanoparticles in mortar—influence of microstructure in the hardened state properties and photocatalytic activity. Cem Concr Res 43:112

Maa S, Shen WLX (2019) Study on the physical and chemical properties of Portland cement with THEED. Constr Build Mater 213:617–626

Majdi HS, Abbasb ZH (2017) Study of heat of hydration of Portland cement used in Iraq. Case Stud Constr Mater 7:154–162

Maness PC, Smolinski S, Blake DM, Huang Z, Wolfrum EJ, Jacoby WA (1999) Bactericidal activity of photocatalytic TiO_2 reaction: toward an understanding of its killin mechanism. Appl Environ Microbiol 65:4094–4098

Maruska HP, Ghosh AK (1979) Transition-metal dopants for extending the response of titanatephotoelectrolysis anodes. Sol Energ Mater 1:237–247

Matsunaga T, Tomoda R, Nakajima T, Wake H (1985) Photoelectrochemical sterilization of microbial cells by semiconductor powders. FEMS Microbiol Lett 29(1,2) 211–214

Matthews RW (1988) Kinetics of photocatalytic oxidation of organic solutes over titanium dioxide. J Catal 111:264–272

Maury A, Debelie N (2010) State of the art of TiO_2 containing cementitious materials: self-cleaning properties. Mater Constr 60:33–50

Mehrotra K, Yablonsky GS, Ray AK (2003) Kinetic studies of photocatalytic degradation in a TiO_2 slurry system: distinguishing working regimes and determining rate dependences. Ind Eng Chem Res 42:2273–2281

Melian JAH, Rodriguez JMD, Suarez AV, Rendon ET, Campo CVD, Arana J, Pena JP (2000) The photocatalytic disinfection of urban waste waters. Chemosphere 41:323–327

Meng N, Leung MKH, Leung DYC et al (2007) A review and recent developments in photocatalytic water-splitting using TiO_2 for hydrogen production. Renew Sustain Energy Rev 11:401–425

Mills A, Morris S (1993) Photomineralization of 4-chlorophenol sensitized by titanium dioxide: a study of the initial kinetics of carbon dioxide photogeneration. J Photochem Photobiol A Chem 71:75–83

Mills A, Davies RH, Worsley D (1993) Water purification by semiconductor photocatalysis. Chem Soc Rev 22:417–426

Mills A, Hill C, Robertson PKJ (2012) Overview of the current ISO tests for photocatalytic materials. J Photochem Photobiol a: Chem 237:7–23

Minero C, Mariella G, Maurino V, Vione D, Pelizzetti E (2000) Photocatalytic transformation of organic compounds in the presence of inorganic Ions. 2. Competitive reactions of phenol and alcohols on a titanium dioxide−fluoride system. Langmuir 16:8964–8972

Mor GK, Varghese OK, Paulose M et al (2006) A review on highly ordered, vertically oriented TiO_2 nanotube arrays: fabrication, material properties and solar energy applications. Solar Energ Mater Solar Cell 90:2011–2075

Mragui AE, Zegaoui O, Daou I (2019) Syntheis, characterization and photocatalytic properties under visible light of doped and co-doped TiO_2 based nanoparticles. Mater Today Proc 13:857–865

Mrowetz M, Selli E (2005) Enhanced photocatalytic formation of hydroxyl radicals on fluorinated TiO_2. Phys Chem Chem Phys 7:1100

Mrowetz M, Balcerski W, Colussi AJ, Hoffmann MR (2004) Oxidative power of nitrogen-doped TiO_2 photocatalysts under visible illumination. J Phys Chem B 108(45):17269–17273

Mukherjee A, Mohammed Sadiq I, Prathna TC, Chandrasekaran N (2011) Antimicrobial activity of aluminium oxide nanoparticles for potential clinical applications. In: Science against microbial pathogens. Communicating current research and technological advances, vol 1, pp 245–251

Nakata K, Fujishima A (2012) TiO_2 photocatalysis: design and applications. J Photochem Photobiol C Photochem Rev 13:169–189

Nazari A, Riahi S, Shamekhi SF, Khademno A (2010) Assessment of the effects of the cement paste composite in presence TiO_2 nanoparticles. J Am Sci 6(4):43–46

O'Shea KE, Pernas E, Saiers J (1999) The influence of mineralization products on the coagulation of TiO_2 photocatalyst. Langmuir 15:2071–2076

Özkan A, Özkan MH, Gürkan R, Akçay M, Sökmen M (2004) Photocatalytic degradation of a textile azo dye, Sirius Gelb GC on TiO_2 or Ag-TiO_2 particles in the absence and presence of UV irradiation: the effects of some inorganic anions on the photocatalysis. J Photochem Photobiol a: Chem 163:29–35

Pacheo-Torgal F, Jalali S (2011) Nanotechnology: advantages and drawbacks in the field of construction and building materials. Constr Build Mater 25:582–590

Pal A, Pehkonen SO, Yu LE, Ray MB (2007) Photocatalytic inactivation of grampositive and gram-negative bacteria using fluorescent light. J Photochem Photobiol A Chem 186:335–341

Papp J, Shen HS, Kershaw R et al (1993) Titanium(IV) oxide photocatalysts with palladium. Chem Mater 5:284–288

Park H, Choi W (2004) Effects of TiO_2 surface fluorination on photocatalytic reactions and photoelectrochemical behaviors. Chem J Phys Chem B 108:4086–4093

Park H, Park Y, Kim W, Choi W (2013) Surface modification of TiO_2 photocatalyst for environmental applications. J Photochem Photobiol C Rev 15:1–20

Parker CD (1945) The corrosion of concrete. Aust J Exp Biol Med Sci 23:81

Periyasami V, Chinnathambi M, Chinnathambi S et al (2009) Photocatalytic activity of iron doped nanocrystallinetitania for the oxidative degradation of 2,4,6-trichlorophenol. Catal Tod 141:220–224

Pourchez J, Grosseau P, Ruot B (2009) Current understanding of cellulose ethers impact on the hydration of C_3A and C_3A-sulphate systems. Cem Concr Res 39(8):664–669

Qina X, Jing L, Tian G, Qu Y, Feng Y (2009) Enhanced photocatalytic activity for degrading Rhodamine B solution of commercial Degussa P25 TiO_2 and its mechanisms. J Hazard Mater 172:1168–1174

Ramirez A, Demeestere K, De Belie N, Mantyla T, Levanen E (2010) Titanium dioxide coated cementitious materials for air purifying purposes: preparation characterization, and toluene removal potential. Build Environ 45:832–838

Ratan JK, Saini A (2019) Enhancement of photocatalytic activity of self-cleaning cement. Mater Lett 244:178–181

Rehman S, Ullah R, Butt AM, Gohar ND (2009) Strategies of making TiO_2 and ZnO visible light active. J Hazard Mater 170:560–569

Ren W, Ai Z, Jia F, Zhang L, Fan X, Zou Z (2007) Low temperature preparation and visible light photocatalytic activity of mesoporous carbon-doped crystalline TiO_2. Appl Catal B Environ 69:138–144

Rothenberger G, Moser J, Graetzel M, Serpone N, Sharma DK (1985) Charge carrier trapping and recombination dynamics in small semiconductor particles. J Am Chem 107:8054–8059

Roy S, Hegde MS, Madras G (2009) Catalysis for NO_x abatement. Appl Energy 86:2283–2297

Rupa AV, Divakar D, Sivakumar T (2009) Titania and noble metals deposited titania catalysts in the photodegradation of tartrazine. Catal Lett 132:259–267

Saini A, Arora I, Ratan JK (2020) Photo-induced hydrophilicity of microsized-TiO_2 based self-cleaning cement. Mater Lett 260:126888

Sakthivel S, Kisch H (2003) Daylight photocatalysis by carbon-modified titanium dioxide. Angrew Chem Int Ed 42:4908–4911

Sakthivel S, Shankar MV, Palanichamy M et al (2004) Enhancement of photocatalytic activity by metal deposition: characterization and photonic efficiency of Pt, Au and Pd deposited on TiO_2 catalyst. Water Res 38:3001–3008

Saqib N, Adnan R, Shah I (2016) A mini-review on rare earth metal-doped TiO_2 for photocatalytic remediation of wastewater. Environ Sci Pollut Res 23:15941–21595

Schwarz PF, Turro NJ, Bossmann SH, Braun AM, Wahab AAA, Dürr H (1997) A new method to determine the generation of hydroxyl radicals in illuminated TiO_2 suspensions. J Phys Chem B 101(36):7127–7134

Scrivener KL, Nonat A (2011) Hydration of cementitious materials, present and future. Cem Concr Res 41:651–665

Scrivenera K, Ouziaa A, Juillandb P, Mohameda AK (2019) Advances in understanding cement hydration mechanisms. Cem Concr Res 124:105823

Seinfeld JH (1998) Atmospheric chemistry and physics: from air pollution to climate change, 1st edn. Wiley, New York

Serpone N, Emeline AV (2005) Modelling heterogeneous photocatalysis by metal-oxide nanostructured semiconductor and insulator materials: factors that affect the activity and selectivity of photocatalysts. Res Chem Intermed 31:391–432

Serratos M, Bronson A (1996) The effect of oxygen partial pressure on the stability of Magneli phases in high temperature corrosive wear. Wear 198(1, 2):267–270

Shayegan Z, Lee C-S, Haghighat F (2018) TiO$_2$photocatalyst for removal of volatile organic compounds in gas phase. A review. Chem Eng J 334:2408–2439

Shayegan Z, Lee C-S, Haghighat F (2019) Effect of surface fluorination of P25-TiO$_2$ coated on nickel substrate for photocatalytic oxidation of methyl ethyl ketone in indoor environments. J Environ Chem Eng 7:103390

Shayegana Z, Haghighata F, Lee CS, Ali Bahloulb MH (2018) Effect of surface fluorination of P25-TiO$_2$ on adsorption of indoor environment volatile organic compounds. Chem Eng J 346:578–589

Sjogren JC, Sierka RA (1994) Inactivation of phage MS2 by iron-aided titanium dioxide photocatalysis. Appl Environ Microbiol 60:344–347

Song K, Zhou J, Bao J et al (2008) Photocatalytic activity of (copper, nitrogen)-codoped titanium dioxide nanoparticles. J Am Ceram Soc 91:1369–1371

Sordo C, Van Grieken R, Marugan J, Fernandez-Ibanez P (2010) Solar photocatalytic disinfection with immobilised TiO$_2$ at pilot-plant scale water science and technology. A J Water Pollut Res 61(2):507–512

Taylor HFW (1997) Cement chemistry, 2nd edn. Academic Press Thomas Telford, London

Thampi KR, Kiwi J, Grätzel M (1987) Methanation and photomethanation of carbon dioxide at room temperature and atmospheric pressure. Nature 327:506–508

The science of concrete. Retrieved from http://iti.northwestern.edu/cement/index.html

Tryk DA, Fujishima A, Honda K (2000) Recent topics in photoelectrochemistry: achievements and future prospects. Electrochim Acta 45(15, 16):2363–2376

Turner M, Golovko VB, Vaughan OPH et al (2008) Selective oxidation with dioxygen by gold nanoparticle catalysts derived from 55-atom clusters. Nature 454:981–983

Vasiliu F, Diamandescu L, Macovei D et al (2009) Fe-and Eu-doped TiO$_2$ photocatalytical materials prepared by high energy ball milling. Top Catal 52:544–556

VelLeitner NK, Berger P, Legube B (2002) Oxidation of amino groups by hydroxyl radicals in relation to the oxidation degree of the α-carbon. Environ Sci Technol 36(14):3083–3089

Verdier T, Coutand M, Bertron A, Roques C (2014) A review of indoor microbial growth across building materials and sampling and analysis methods. Build Environ 80:136–149

Verma P, Kumar J (2014) Degradation and microbiological validation of meropenem antibiotic in aqueous solution using UV, UV/H$_2$O$_2$, UV/TiO$_2$ and UV/TiO$_2$/H$_2$O$_2$ processes. Int J Eng Res Appl 4(7):58–65

Wang R, Hashimoto K, Fujishima A, Chikuni M, Kojima E, Kitamura A, Shimohigoshi M, Watanabe T (1997a) Light-induced amphiphilic surfaces. Nature 388:431–432

Wang R, Hashimoto K, Fujishima A, Chikuni M, Kojima E, Kitamura A, Shimohigoshi M, Watanabe T (1997b) Light-induced amphiphilic surfaces. Nature 388:431–432

Wang RF, Wang FM, An SL, Song JL, Zhang Y (2005) Y/Eu co-doped TiO$_2$: synthesis and photocatalytic activities under UV-light. J Rare Earths 33(2):154–159

Wang H, Wang HL, Jiang WF, Li ZQ (2009) Photocatalytic degradation of 2,4-dinitrophenol (DNP) by multi-walled carbon nanotubes (MWCNTs)/TiO$_2$ composite in aqueous solution under solar irradiation. Water Res 43:204–210

Watts RJ, Kong S, Orr MP, Miller GC, Henry BE (1995) Photocatalytic inactivation of coliform bacteria and viruses in secondary wastewater effluent. Water Res 29:95–100

Wiszniewska M, Walusiak-Skorupa J, Gutarowska B, Krakowiak A, Palczynski C (2009) Is the risk of allergic hypersensitivity to fungi increased by indoor exposure to moulds? Int J Occup Med Environ Health 22:343

Wong WK, Malati MA (1986) Doped TiO$_2$ for solar energy applications. Sol Energ 36:163–168

Wong MS, Sun DS, Chang HH (2010) Bactericidal performance of visible-light responsive titaniaphotocatalyst with silver nanostructures. PLoS ONE 5(4):1–7

Wu NL, Lee MS (2004) Enhanced TiO$_2$ photocatalysis by Cu in hydrogen production from aqueous methanol solution. Int J Hydrol Energy 29:1601–1605

Xin B, Ren Z, Wang P et al (2007) Study on the mechanisms of photoinduced carriers separation and recombination for Fe_3+TiO_2 photocatalysts. Appl Surf Sci 253:4390–4395

Xu T, Song C, Liu Y, Han G (2006) Band structures of TiO_2 doped with N, C and B. J Zhejiang Univ Sci B 7:299–303

Xu J, Ao Y, Chen M et al (2009a) Low-temperature preparation of Boron-doped titania by hydrothermal method and its photocatalytic activity. J Alloy Comp 484:73–79

Xu J, Ao Y, Fu D (2009b) A novel Ce, C-codoped TiO_2 nanoparticles and its photocatalytic activity under visible light. Appl Surf Sci 256:884–888

Yamagata S, Nakabayashi S, Sancier KM, Fujishima A (1988) Photocatalytic oxidation of alcohols on TiO_2. Bull Chem Soc Jpn 61:3429–3434

Yu JC, Yu JG, Ho WK et al (2002) Effects of F-doping on the photocatalytic activity and microstructures of nanocrystalline TiO_2 powder. Chem Mater 14:3808–3816

Zhang H, Banfield JF (2000) Understanding polymorphic phase transformation behavior during growth of nanocrystalline aggregates: insights from TiO_2. J Phys Chem 104B:3481–3487

Zhang MH, Li H (2011) Pore structure and chloride permeability of concrete containing nano-particles for pavement. Constr Build Mater 25:608–616

Zhang SJ, Yu HQ, Zhao Y (2005) Kinetic modeling of the radiolytic degradation of Acid Orange 7 in aqueous solutions. Water Res 39(5):839–846

Zhao W, Ma W, Chen C, Zhao J, Shuai Z (2004) Efficient degradation of toxic organic pollutants with Ni_2O_3/TiO_2-xBx under visible irradiation. J Am Chem Soc 126:4782–4783

Zhao J, Chen C, Ma W (2005) Photocatalytic degradation of organic pollutants under visible light irradiation. Top Catal 35:269–278

A Review on the Valorization of Biorefinery Based Waste Lignin: Exploratory Potential Market Approach

Kaleem Ahmad, Himadri Roy Ghatak, and Sandeep Mohan Ahuja

Abstract The world is facing difficulties to make a bridge between energy production and demand due to the diminishing of fossil fuel reserves. Energy resources are limited and unevenly distributed across the globe. Because of waste to wealth, the lignin from industries may play as a metamorphic gamester in biorefineries to enhance the life cycle assessment as well as to meet the ever-increasing global demand for myriad products. From the perspective of lignin valorization, the production of valuable chemicals, different extraction techniques, structures, global market potential, and SWOT analysis will be spotted and reviewed. Markets that are growing lignin-specified biorefinery are expected from 874.3 USD in 2020 to 1537.1 million USD by the end of 2026. Despite the availability of bountiful lignin as an aromatic substrate, its recalcitrant nature restricts the easy and economical production of valuable products. This review study also aims to understand the latest market trends, strategies, and challenges of lignin and its products globally.

Keywords Lignin · Biorefinery · Lignin products · Market analysis · SWOT analysis

1 Biorefinery

A biorefinery is a complex combination of various feedstocks and vantages that integrates the conversion processes of biomass for the production of fuels, electricity, and value-added chemicals (Demirbas 2009) and which can bring out the maximum economic value of the biomass used while simultaneously reducing the waste material produced (Thomsen 2005). A processing plant for biomass feedstock conversion or extraction in a spectrum of valuable products can be called biorefinery as per the US department of energy (Mussatto and Dragone 2016). As per the definition of IEA (International Energy Agency), sustainable biomass processing into a spectrum

K. Ahmad · H. R. Ghatak (✉) · S. M. Ahuja
Department of Chemical Engineering, Sant Longowal Institute of Engineering and Technology, Longowal, Punjab 148106, India
e-mail: h_r_ghatak@yahoo.com

of value-added marketable products and energy are referred to as biorefinery under the Bioenergy task of 42. In most countries like India, millions of tonnes of stubble are being burnt in the open field during the post-monsoon to create room for winter crops. There is an interest in the utilization of plant-based matter (biomass) as a raw material for the chemical industry (Marcilly 2003; Lynd et al. 2005), as we know the biomass is not a non-renewable energy source, like the fossil fuel resources such as petroleum, coal, and natural gas (Speight 2008). Although, the development of biorefinery works on the basic principle goal as (Kamm 2014):

$$(\text{Biomass})\text{feedstock} - \text{mix} + \text{process} - \text{mix} \rightarrow \text{product} - \text{mix}$$

Many contemplations are being taken to replace the current fossil fuel-based refinery with a sustainable bio-based refinery mainly due to the price hike, shortage of reserves, and pollution (Arevalo-Gallegos et al. 2017). Biomass is like petroleum as very complex compositions, and it may become an alternative way to tackle the critical situation of the declining reserve to production ratio. In a biorefinery, the production of value-added products from agro-residue or agro-commodities is a very old concept. However, the production of high-value low volume (HVLV) and low-value high-volume (LVHV) products from biomass commodities by using a series of unit operations is the main target of a biorefinery (Fernando et al. 2006). Harvesting, storage, pre-treatment of feedstock, enzymatic hydrolysis, and fermentation of sugar to ethanol (Dale and Ong 2012; Chen et al. 2005; Zhang and Cai 2008), has focused on the production of biofuels, electricity, and value-added products. The biorefinery would require a huge investment to establish new infrastructure and emerging technologies to produce biodiesel and products to end-users (Demirbas 2009; Balat 2008; Mohan et al. 2006).

1.1 Feedstocks

Feedstocks refer to the raw material to supply or fuel used in a biorefinery. Researchers discussed various types of biomass in several ways, but Mackendry has defined several types of biomass namely, woody plants, herbaceous plants/grasses (high- and low-moisture contents), and aquatic plants (Mackendry 2002). These biomasses are the feedstock plant material produced through the photosynthesis process which involves a reaction between CO_2 in the air, water, and sunlight, to produce carbohydrates. Speight has subdivided biomass feedstock into primary, secondary, or tertiary (Speight 2008). The primary biomass is directly produced by photosynthesis, by-products after processing from primary feedstock are the secondary biomass while tertiary is the post-consumer residues. Forestry, agriculture (dedicated crops and residues), industries (process residues and leftovers), households (municipal solid waste and wastewaters), and aquaculture (algae and seaweeds) are renewable biomass for biorefinery feedstocks (Cherubini 2010).

1.2 Categorization of Biorefinery

Multiple types of biorefineries have been proposed, developed, and categorized by various researchers. Biorefineries are classified based on feedstocks, intermediates production, conversion processes, and technological steps (Parajuli et al. 2015; Jong and Jungmeier 2015). It can also be divided according to the conversion processes as thermochemical, chemical, biochemical, or a combination of them (Ghatak 2011) and mechanical/physical (Cherubini 2010). Syngas and sugar platform biorefineries fall under the main intermediates production category (Jong and Jungmeier 2015). Dedicated edible crops are used in first-generation biorefineries and non-edible feedstocks are used in second-generation biorefineries (Ozdenkçi et al. 2017). Based on the different feedstock the possibilities of integrated biorefineries are discussed by Moncada et al. (2014). Nizami et al. have discussed and categorized several types of waste biorefineries to get a solution for the disposal of waste from various sources. They categorized wastes as forestry, agricultural, industrial, food, wastewater, plastic waste, and algae-based biorefinery to tackle the waste disposal situations in developing countries (Nizami et al. 2017). Based on feedstocks, biorefineries have been classified as conventional bio-refinery (Arevalo-Gallegos et al. 2017), advanced biorefinery (Parajuli et al. 2015), green biorefinery (Fernando et al. 2006), lignocellulosic biorefinery or lignocellulosic feedstock biorefinery (Zoia et al. 2011; Anwar et al. 2014), and whole crop bio-refiner (Fernando et al. 2006). Classification of biorefineries is not homogenous, although various systems are involved such as type of feedstocks, technologies, and platforms. The classification was briefly discussed based on platforms, products, feedstock, and processes (Cherubini 2010). Several types of biorefineries have been proposed and developed by researchers as discussed in table 1.

2 Lignocellulosic Biorefinery

The term "lignocellulose" was introduced by Edward John Bevan (1856–1921) and Charles Frederick Cross (1855–1935), which is a type of non-food fraction that comes from several diverse types of plants such as wood, grass, and agricultural residues. Lignocellulosic biomass is expected to become one of the most important sources of biomass shortly (Jong and Jungmeier 2015). The biomasses, predominantly derived from corn stover, sorghum stalks, sugarcane bagasse, wheat, rice, barley straw, wood, coconut husk, and rice straw, belong to lignocellulosic biomass. Lignocellulosic biomass is the most abundant renewable carbon resource in the world (Ravindran and Jaiswal 2016) having three basic chemical constituents as hemicellulose, cellulose, and lignin. Agro lignocellulosic biomass contains about 10–20% lignin, hemicellulose 20–30%, and 40–50% cellulose (Iqbal et al. 2011).

A general phenomenon or mechanism of LCF biorefinery is discussed by Fernando et al. (2006).

Table 1 Types of biorefineries concerning system, feedstocks, and end products

S. No.	Types of biorefinery	System based on	Feed stock	End products	Sources
1	Whole crop bio-refinery (WCBR)	Type of feedstock	Entire crops	Syngas, methanol using the Fischer–Tropsch (FT) process	Fernando et al. (2006), Balagurumurthy et al. (2015)
2	Lignocellulosic biorefinery (LCBR)	Type of feedstock	Cellulose-containing biomass and wastes	Fuels (ethanol, methane, and hydrogen), fructose glucose, levulinic and lactic acid	Zoia et al. (2011), Anwar et al. (2014), Barakat et al. (2013)
3	Green biorefinery (GBR)	Type of feedstock	Nature-wet biomasses, such as green grass, alfalfa, clover or immature cereal	biomethane, organic acids and biomaterials	Fernando et al. (2006)
4	Conventional bio-refinery (CBR)	Technology	Based on existing industries, such as the sugar and starch industry	Ethanol	Arevalo-Gallegos et al. (2017)
5	Integrated biorefinery (IBR)	Technology feedstock	All types of biomass	Electricity and bioproducts	Xie et al. (2017)
6	Two-platform concept biorefinery (TPBR)	Technology	Wood	Fischer-Tropsch fuels and bioethanol	Balagurumurthy et al. (2015)
7	Marine biorefinery (MBR)	Type of feedstock	Micro- or macro-algae (seaweeds)	Biofuel and commodity chemicals	Balina et al. (2017)
8	Forest-based biorefinery (FBBR)	Type of feedstock	Forestry	Chemicals, transport fuels, chemicals, pulp and paper	Soderholm and Lundmark (2009)
9	Biogas Biorefinery (BBR)	Technology and feedstock	Agricultural residues and energy crops	Biogas and fertilizers	Lindorfer and Frauz (2015)
10	Thermochemical Biorefinery (TCBR)	Technology	All type of biomass	Biofuels	Xuan et al. (2012)

$$\text{Lignocellulose} + \text{Water (H}_2\text{O)} \rightarrow \text{Lignin} + \text{Cellulose} + \text{Hemicellulose}$$

$$\text{Hemicellulose} + \text{Water (H}_2\text{O)} \rightarrow \text{Xylose (C}_5\text{H}_{10}\text{O}_5)$$

$$\text{Xylose (C}_5\text{H}_{10}\text{O}_5) + \text{Acid catalyst} \rightarrow \text{Furfural (C}_5\text{H}_4\text{O}_2) + \text{Water (H}_2\text{O)}$$

$$\text{Cellulose (C}_6\text{H}_{12}\text{O}_6) + \text{Water (H}_2\text{O)} \rightarrow \text{Glucose (C}_6\text{H}_{12}\text{O}_6)$$
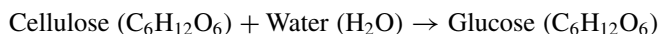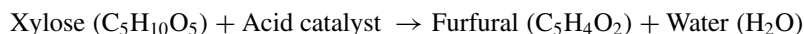
Due to the genetic variability, chemical compositions in various lignocellulosic biomass are not uniformly distributed, it varies among the various sources (Iqbal et al. 2013). Some researchers had reported the composition of rice straw as 18% lignin, 24% hemicellulose and 32% cellulose (Malherbe and Cloete 2002; Perez et al. 2002; Prasad et al. 2007; Kumar et al. 2009) whereas another group reported as 11.2%, 18.0%, and 32.0% respectively (Barakat et al. 2013). Bhutto et al. found 5–24% lignin, 19–23%, hemicellulose, 32–47% cellulose, and 12.4% ash in rice straw (Bhutto et al. 2015). In bagasse, lignin is 21.75%, cellulose 38.37%, and hemicellulose 23.73% (Kanosh et al. 1999) but Bhutto et al. found 18.4, 43.1, and 31.1 in percentage respectively (Bhutto et al. 2015). Harper and Lynch have reported chemical components of wheat straw as 37.7% cellulose, 32.4% hemicellulose, 15.3% lignin, and 11.5% ash determined by gravimetric analysis on a dry basis (Harper and Lynch 1981).

Cellulose is an organic compound and the most abundant organic polymer on the earth. Cellulose in biomass is in both crystalline and amorphous forms, consisting of D-glucose subunits linked to each other by (1,4)-glycosidic bonds (Kumar et al. 2009), having extensive intramolecular and intermolecular H_2 bonding networks (Isikgor and Becer 2015). Content of cellulose in agro cellulosic biomass is about 40–50%, generally used in the production of paperboard, paper, and cellulosic ethanol is at the research stage (Iqbal et al. 2011). Hemicellulose is a low-molecular-weight as compared to cellulose and the second most abundant heterogeneous polymer with a degree of polymerization ranging from 70 to 200 in different biomass. It has a random, amorphous structure and notably consists of glucuronoxylan, glucomannan, and trace amounts of other polysaccharides (Anwar et al. 2014). In agro cellulosic biomass hemicellulose have a contribution of 20–30%, which are being used as films and gels in packaging to maintain the texture, taste, and mouthfeel (Iqbal et al. 2011). A flowsheet of the lignin-specified lignocellulosic biorefinery is shown in the custom animation effect in Fig. 1.
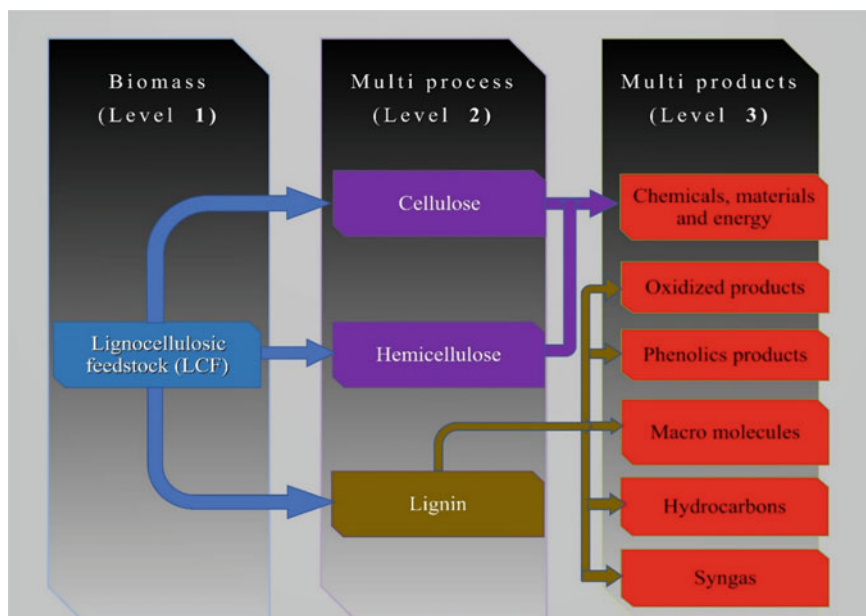
Fig. 1 A schematic diagram of lignin specified LC Biorefinery in custom animation effects

3 Lignin

Lignin is an aromatic and rigid biopolymer (Mielenz 2001) found in most terrestrial plants (Ragauskas et al. 2014) with a molecular weight of 10,000 Da bonded via covalent bonds to xylans (hemicellulose portion). Lignin is a three-dimensional, highly irregular, and insoluble polymer consisting of phenylpropanoid subunits (Isikgor and Becer 2015). Structurally, lignin is an amorphous heteropolymer (Perez et al. 2002) with no chains, unlike cellulose or hemicellulose. Three broad classes of lignin-based on their structure and composition are softwood, hardwood, and grass lignin (Adler 1977).

3.1 Chemistry and Structure

Lignin structure is not unique, derived from three hydroxycinnamyl alcohols such as p-coumaryl alcohol, coniferyl alcohol, and sinapyl alcohol where phenyl propane structural units of lignin can be divided into three types: p-hydroxyphenyl propane (H), guaiacyl propane (G), and syringyl propane (S). The monomers like p-phenyl monomer (H type) are derived from coumaryl alcohol, guaiacyl monomer (G type) is derived from coniferyl alcohol, and syringyl monomer (S type) derived from sinapyl alcohol (Chen 2015). Guaiacyl (G) monomer is generally found in softwood lignin

Table 2 Chemical composition of lignin in the cell wall of plants

Subunits	Bonds between subunits	Polymerization	Polymers	Composition	Bonds between three components
Syringyl (S), Guaiacyl (G), and p-Hydroxyphenyl (H)	Various ether bonds and carbon–carbon bond, mainly O-4 ether bond	4,000	G lignin, GS lignin, and GSH lignin	Amorphous, inhomogeneous, nonlinear three-dimensional polymer	Contain chemical bond with hemicellulose
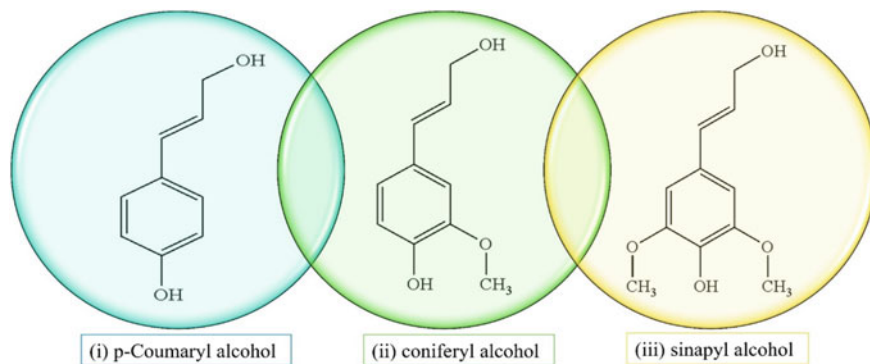
Fig. 2 The precursor of lignin linkages resembled p-coumaryl, coniferyl and sinapyl alcohol

while hardwood lignin consists of both Syringyl (S) and Guaiacyl (G) units (Ahvazi et al. 2016). The presence of guaiacyl propane and syringyl propane is more dominant than p-hydroxyphenyl propane in straw lignin as the ratio varies with plant species (Mathew et al. 2018). The structure and chemical composition of lignin in cell walls of plants is shown in Table 2 (Chen 2014).

Essentially methoxylated derivatives of Benzene (Phenylpropanoid alcohols) are also called Monolignols species as shown in Fig. 2.

3.2 Types

Ingeniously categorization of lignin is very difficult. The extraction process is generally used to separate the lignin from lignocellulosic biomass. Several researchers extracted lignin by chemical, physical, and biochemical approaches (Mosier et al. 2005; Tejado et al. 2007; Minu et al. 2012; Thakur and Thakur 2014). Based on the extraction process the several types of lignin are conventionally named kraft lignin, lignosulfonate lignin, soda lignin, and organosolv lignin (Ludmila et al. 2015). The separation methods can be classified in 1-dissolution of lignin and 2-hydrolysis of

cellulose and hemicellulose, leading to two types of lignin: lignin as a dissolved solution and lignin as an insoluble residue respectively (Chen 2014; Jiang et al. 2010). Softwood, hardwood, and grass lignin are falling under its sources (Khan et al. 2019). Some exemplary types of lignin isolated by insoluble methods are klason and hydrolytic lignin (Xu and Ferdosian 2017). Several types of lignin obtained from various isolation and extraction methods along with their properties, sources, and applications are mentioned in Table 3.

3.3   Lignin from Biorefinery

Various authors have discussed examples of biorefinery where they use cellulose, hemicellulose but left lignin as waste (Arevalo-Gallegos et al. 2017; Dyne et al. 1999). Lignin is the residue after ethanol production in biorefinery from lignocellulosic biomass (Cherubini 2010). Lignin is responsible for the recalcitrant property of lignocellulosic biomass because of the discharge as waste; this is not only a waste of resources but also an environmental pollutant. Lignin is the cheapest raw material to produce aromatic compounds, but the pathway from lignin to aromatics is deceptive, considering the low recovery efficiency (Tuck et al. 2012). The method of isolation of lignin followed by its composition and characteristics varies from various sources of biomass. Past scientists and researchers had shown that lignin from biomass when burnt to generate heat and electricity for process requirements, added revenue to the operation (Wooley et al. 1999), but also caused pollution problems (Hinman et al. 1992). Lignin from biorefinery is a waste residue for lignocellulosic biorefinery after treatment (Hu et al. 2017). Pre-treatment of lignin is more costly than the burning of lignin.

3.4   Status of Lignin from Agro Residue Based Biorefinery

Apart from hemicellulose and cellulose, lignin is a potential raw material in a biorefinery to produce different value-added products. Most of the lignin presents in the cell wall of wood, for lignin the rice is the third most important grain crop in the world after wheat and corn (Binod et al. 2010). The maximum yield of lignin from alfalfa, pine straw, and wheat straw is reported as 34%, 22.65%, and 20.40% respectively (Watkins et al. 2014). Bagasse, wheat, and rice straw are copious agricultural wastes in the world that can have viability as an economical and environment-friendly energy source. 1.0–1.5 kg of rice straw is produced from every kilogram of grain harvested (Molina et al. 2011). Food and Agricultural Organization has estimated in 2014 that in India 43.40-million-hectare areas is under paddy production, which produced 157.20 MMT rice along with 157.20–235.8 MMT paddy straw. The residue left after sugar juice extraction from sugarcane is called sugarcane bagasse. It is an agro-industrial waste, used as the main source of the energy required in sugar mills

Table 3 Types of lignin, properties, sources, extraction or isolation methodology, and its application

S. No.	Type of lignin	Sources	Properties	Avg. molecular wt. (Da)	Method of isolation or extraction	Application	References
1	Organosolv lignin (OSL)	Hardwood and softwood	Low ash content, high ability to be derivatized, high purity, low molecular weight, high hydrophobicity	500–10,800	Dissolved air flotation and precipitation	Creation of new substance, varnishes, additives for paints, good reactivity for industrial applications, biofuels and biomaterials	Kaleinert (1975), McGEE and April (1982), Johansson et al. (1987), Cook et al. (1991), Lawther et al. (1997), Visthal and Kraslawski (2011), Nitos et al. (2018)
2	Milled wood lignin (MWL)	Wood meal	Low ash content	2800–14,200	Aqueous p-dioxane extraction of finely milled wood	Chemicals	Zoia et al. (2011), Ludmila et al. (2015), Higuchi et al. (1967), Crestini et al. (2011)
3	Pyrolytic lignin (PL)	Wood	Highly cross-linked, high homogeneity	620–1320	In form of dry powder from vacuum after washing and drying	Polyurethane foams, chemicals, liquid fuels	Nsimba et al. (2012), Agrwal et al. (2014)

(continued)

Table 3 (continued)

S. No.	Type of lignin	Sources	Properties	Avg. molecular wt. (Da)	Method of isolation or extraction	Application	References
4	Alkali Lignin (AL)/Kraft lignin (KL)	Black Liquor	Hydrophobic, low ash content	200–20,000	Precipitation (pH change) or ultrafiltration	Low molecular weight compounds, surfactants, vanillin, dispersants, emulsifiers, phenol–formaldehyde resins	Gierer (1980), Villar et al. (2001), Smook and Smook (2002), Holladay et al. (2007)
5	Sulphite lignin (SL) or lignosulfonate (LS)	Softwood and hardwood	Good complexing agents and emulsifying agents	1000–140,000	Sulphite pulping processes	Dispersants, agricultural chemicals, binders, carbon black ink, and colloidal suspension	Smook and Smook (2002), Restolho et al. (2009)
6	Steam explosion lignin (SEL)	Hardwood species, annual plants	Low molecular weight, and good solubility in organic solvents	10,700–19,300	Hydrothermal Process	Feedstock for biodiesel and chemicals	Ludmila et al. (2015), Zhang et al. (2007), Ruiz et al. (2008), Wang and Chen (2016)
7	Dilute acid lignin (DAL)	softwood	Contains sugar derivative	5000–10,000	Hydrolysis	Dispersants and polymeric materials	Guo et al. (2013), Visthal and Kraslawski (2011), Ruiz et al. (2008)
8	Soda lignin (SL)	Annual plants	High carboxylic acid content	1000– 15,000	Precipitation, ultrafiltration, alkaline hydrolysis	Production of animal's nutrients, phenolic resins, and polymer synthesis	Visthal and Kraslawski (2011), Gierer (1980)

(Gabov et al. 2017). It has a composition of 43% cellulose, 25–32% hemicellulose, and 21–23% lignin (Rocha et al. 2012). Some researchers reported that lignin in bagasse, wheat straw, and barley straw was 25–30% (Canilha et al. 2012; Andrade and Colodette 2014), 16.3% (Nanda et al. 2013), and 19.4% (Tamaki and Mazza 2010) respectively.

3.5 Isolation of Lignin from Agro Residue Based Biorefinery

As stated previously, various methods were used for lignin extraction and isolation from lignocellulosic biomass. Hydrolyzing or solubilizing cellulose and hemicellulose while keeping lignin as an insoluble residue is an effective method based on isolation mechanisms whereas recovery of lignin from liquor stream by dissolution is another method (Azadi et al. 2012; Suhas et al. 2007). Researchers studied the feasibility of ionic liquids to isolate lignin from woods with microwave heating (Casas et al. 2012) and without microwave heating (Lee et al. 2009). Jin et al. used general alkali- solution and acid-isolation method for the separation of enzymatic hydrolysis lignin (Jin et al. 2011). Lignin extraction by organosolv process under high pressure and temperature is reported (Buranov and Mazza 2008). El Mansouri et al. used alkaline lignin as the starting material for the glyoxalation reactions from rice straw in the form of fine dry powder (Mansouri et al. 2011). The glyoxylate lignin treated with glyoxal and sodium hydroxide for 10 h was found to have better structural properties and suitability for wood adhesives. Guo et al. extracted lignin by solvent extraction method from the residue of bio-ethanol production by using benzyl dioxane, alcohol, and ethanol. They obtained higher lignin yields of 71.55% and 74.14% respectively as compared to conventional alkali-solution and acid-isolation methods. The solvent was added according to different liquid ratios (mass ratio of solvent/raw material): 3:1, 5:1, and 7:1 (Guo et al. 2013).

However, the above-discussed isolation and extraction methods are not easy to apply to biorefinery on an industrial-scale due to the prohibitive cost or complex process. So, an adequate and effective method is necessary for lignin application in the biorefinery.

3.6 Characterization of Lignin and Lignin-Derived Products

Several methods have been employed to analyze lignin such as Nuclear Magnetic Resonance (NMR), Infrared (IR), Ultraviolet-Visible (UV–Vis), and Raman Spectroscopy (RS). NMR has a surpassing resolution than others, providing presented hydrogen protons in lignin (Mousavioun and Doherty 2010). Thermo-Gravimetric Analysis (TGA), Fourier Transform Infrared Spectroscopy (FTIR), and Differential Scanning Calorimetry (DSC) have been applied for thermal and structural characterization of lignin. Air-dried bio-ethanol production residue was analyzed by FTIR

and XRD (Casas et al. 2012). Tejado et al. have analyzed the chemical structure of lignin by using FTIR and Proton Nuclear Magnetic Resonance Spectrometry (H NMR). They found G units with high quantities of non-etherified hydroxyl groups in kraft pine, S units, and less free hydroxyls in soda/AQ flax lignin, whereas both G and S structural units, were found in organosolv hardwood lignin (Tejado et al. 2007). Five lignin samples were characterized after complete esterification with acid anhydrides by FTIR spectroscopy. In FTIR spectra of (HW-KL) hydroxyl groups completely disappeared (Dehne et al. 2016). Stanzione III et al. have synthesized a low viscosity polymer resin by utilization of lignin-derived vanillin and potential bio-based reactants, methacrylic anhydride, and glycidyl methacrylate without by-product (Stanzione et al. 2012). Abdelaty and Kuckling also reported the synthesis of new functional monomers based on lignin-derived vanillin (Abdelaty and Kuckling 2016). Hongzhang has discussed various possible products in near future i.e.; lignin modified phenolic resin adhesive, lignin modified phenolic resin foam insulation board, dye dispersants, concrete water reducing agent, ceramic adhesive, coumaric acid, ferulic acid, vanillin, vanillin acid, and phenol (Hongzhang 2015). Sreekrishnan identified more than 250 chemicals in effluents that were produced at different stages of papermaking (Sreekrishnan 2001). Ragauskas has discussed lignin-based engineered plastics, low-cost carbon fibers, biopolymer fungible fuels, and commodity chemicals, which were produced by coupling with genetic engineering (Ragauskas et al. 2014). Fache reported an alkaline oxidation process for lignin-to vanillin (Fache et al. 2016). Fragues et al. produced a 10% yield of vanillin from the chemical oxidation of Pinus spp Kraft lignin (Fragues et al. 1996).

3.7 Possible Products from Lignin-Based LCBR and Its Application

Most of the industrially produced lignin is being used as burning fuel in industries to meet the electricity requirement. All these industries are required to change their trends of direct use of lignin by burning. They would need to change their methods and processes from burning to value-added products and chemicals to realize the benefits. Today's lignin fuel can be purchased by a few cents per 10 kg but as a value-added chemical or product, the material could be much more valuable and potential. Possible products from lignin are phenol, carbon fiber, binder, soil improvement, solid/liquid fuels, and electric power (Wising and Stuart 2006). Lignin could be a potential additive in the plastic industry to produce engineered plastics, however, deeper knowledge of lignin is required (Kun and Pukánszky 2017). It could be converted by using hydrogenation processes into value-added products such as phenols, aromatics, and olefins, or simply burned as boiler fuel for cost-efficiency of the overall process (Cheng and Wang 2013). There are very few research papers for the use of lignin as a hydrogel in different fields. Larraneta et al. have prepared lignin hydrogels by combining LIG with poly (ethylene glycol) and poly (methyl vinyl ether-co-maleic

acid) through an esterification reaction and used as drug-eluting antimicrobial coatings for medical materials (Larrañeta et al. 2018). Thakur and Thakur have discussed the various potential application of lignin as hydrogel (Thakur and Thakur 2014). The utilization of biorefinery-based waste lignin depends upon the virtue of the inherent functionality and many different plant sources of lignin. The lignin of higher molecular weight from biorefinery may be modified to the low molecular weight which leads to the production of different grades of value-added chemicals and products. Several products that might be interesting to develop for future market utilization in many industries such as pulp and paper, agriculture, and construction are illustrated in Table 4.

Lignin tree is picturized as possible lignin products from LC biorefinery in Fig. 3. The possible lignin-based products are described below:

- **Hydrogel**: A hydrogel is a macromolecular polymer gel constructed of a network of cross-linked polymer chains. Lignin-based hydrogels are used in tissue engineering and regeneration, absorbable sutures (Gibas and Janik 2010), hydrophobic drug delivery systems (Larrañeta et al. 2018). Recently, Thakur et al. have elaborated on different types of hydrogels from different sources-based lignin hydrogels for water purification (Thakur et al. 2017). Suhas et al. have reviewed kinds of literature on different grades of activated carbons and chars from lignin as adsorbents to purify the water over the decades (Suhas et al. 2007).

- **Activated Carbon**: It is also called activated charcoal, a high-porosity material and form of carbon processed to have small, low-volume pores. Hayashi et al. have prepared activated carbon by chemical activation with $ZnCl_2$, H_3PO_4, and some alkali metal compounds. Generally used in solvent for recovering the removal of organic pollutants from drinking water (Hayashi et al. 2000). Mussattoa et al. have produced different types of activated carbon from brewer's spent grain lignin (BSG). They used phosphoric acid (H_3PO_4) at several carbonization temperatures (300, 450, or 600 °C) concerning various acid/lignin ratios, (1, 2, or 3 g/g). They found that activated carbon can be produced with high product yields at high temperatures (Mussatto and Dragone 2016).

- **Lignin Film**: Lignin is an effective and excellent light absorber due to its phenolic structure having the possibility of application in sensing devices and surface coatings. Properties of the films from lignin such as thickness, molecularity, and crystallinity may be remarkable when used in any device (Chatterjee and Saito 2018). Preparation and characterization of lignin films were carried out by Sadeghifar et al. by using Indulin kraft lignin of 6000 g/mol average weight and 1500 g/mol number molecular weight. The study showed 100% protection of UV-B (280–320 nm) and more than 90% of UV-A (320–400 nm) (Sadeghifar et al. 2016). Extracted lignin from spruce, wheat straw, and eucalyptus was fabricated as lignin films (Pereira et al. 2017).

- **Aerogels**: This is a solid of low density, highly porous, and low thermal conductive materials, which is a class of open-cell, mesoporous foams that can be derived from lignin (Karaaslan et al. 2016). Yang and Kang have prepared almost similar density

Table 4 The possible lignin products and their production techniques along with applications

S. No.	Product	Product type	Technique	Application	References
1	Hydrogel	Hydrophilic	Esterification	Hydrophobic drug delivery systems, tissue engineering and regeneration, absorbable sutures, water purification	Larrañeta et al. (2018), Gibas and Janik (2010), Thakur et al. (2017)
2	Activated Carbon	Macromolecules	Microwave-assisted, ultrasound, and UV irradiation method	Food and beverage processing, odour removal, industrial pollution control, removal of organic pollutants from drinking water, gold purification, sewage treatment	Mussatto and Dragone (2016), Suhas et al. (2007), Jin et al. (2011), Hayashi et al. (2000), Meng et al. (2019)
3	Lignin film	Phenolic	Solution-casting method	Surface coatings, composites and transducer in sensing devices	Chatterjee and Saito (2018), Pereira et al. (2017)
4	Aerogels	Hydrophilic	Chemical pulping with biorefinery integrated process	Thermal and acoustic insulators, dielectrics, nano supercapacitor, gas and energy storage materials and scaffolds for tissue engineering	Yang and Kang (2017)

Table 4 (continued)

S. No.	Product	Product type	Technique	Application	References
5	Catechol (1,2-benzenediol)	Phenolic products	Alkalic fusion	Intermediate for the synthesis of pharmaceuticals, perfumes, agrochemicals and other formulations as a building block in the organic synthesis	Jeenpadiphat et al. (2016), Schuler et al. (2017), Barta et al. (2014)
6	Phenols	Phenolic products	Depolymerization	Thermosetting applications, formaldehyde resins, intermediates for industrial synthesis, mouthwash, cleaner and antioxidant activity	Frost (2012), Redman (1923), Faustino et al. (2010)
7	Bitumen	Hydrocarbon	Blending	As a binder in asphalt for roads, runways, parking lots, and foot paths	Perez et al. (2002), Vliet et al. (2016), Boomika et al. (2017)
8	Motor Fuel	Fuel	Hydrogenation	Use as biodiesel	Olsson (2015), Bhat et al. (2015), Huang et al. (2019), Abdullah et al. (2017), Anheden et al. 2017)
9	Guaiacol	Phenolic products	Depolymerization	As a precursor in roasted coffee and vanillin, its derivatives are being used in antiseptic, medicines to cure chest and anaesthetics complains	Hongzhang (2015), Huang et al. (2019)

Table 4 (continued)

S. No.	Product	Product type	Technique	Application	References
10	Carbon Fibre	Macromolecules	Spinning	Materials of aircraft and aerospace, reinforcing material in composite products	Kadla et al. (2002), Luo et al. (2010), Mainka et al. (2015), Souto et al. (2018)
11	Bioplastics	Macromolecules	Membrane separation technology	Furniture, packaging, jewellery, decoration, musical devices, consumer electronics, lawn and garden goods	Yang and Kang (2017)
12	Binder	Macromolecules	High frequency heating	Particle boards, Li-ion batteries, in foundry coke substitute after briquetting anthracite fines	Nirmale et al. (2017), Lu et al. (2017), Mathiasson and Kubát (1994), Lumadue et al. (2012)
13	Vanillin	Oxidized products	Oxidation	Food, beverage, perfumery, and pharmaceutical industries	Fache et al. (2016), da Silva et al. (2009), Araújo et al. (2009), Singh and Ghatak (2017)

Table 4 (continued)

S. No.	Product	Product type	Technique	Application	References
14	Antioxidant	Oxidized products	Delignification, pyrolysis, and hydrolysis	Use in cosmetic, food and pharmaceutical industries as antioxidant	Nanda et al. (2013), Tamaki and Mazza (2010), Azadi et al. (2012), Suhas et al. (2007), Casas et al. (2012), Lee et al. (2009), Jin et al. (2011), Buranov and Mazza (2008), Mansouri et al. (2011), Guo et al. (2013), Mousavioun and Doherty (2010), Dehne et al. (2016), Stanzione et al. (2012), Abdelaty and Kuckling (2016), Hongzhang (2015), Sreekrishnan (2001), Fache et al. (2016), Fragues et al. (1996), Wising and Stuart (2006), Kun and Pukánszky (2017), Cheng and Wang (2013), Larrañeta et al. (2018), Balagurumurthy et al. (2015), Xie et al. (2017), Balina et al. (2017), Soderholm and Lundmark (2009), Lindorfer and Frauz (2015), Xuan et al. (2012), Kaleinert (1975), McGEE and April (1982), Johansson et al. (1987), Cook et al. (1991), Lawther et al. (1997), Visthal and Kraslawski (2011), Nitos et al. (2018), Higuchi et al. (1967), Crestini et al. (2011), Nsimba et al. (2012), Agrwal et al. (2014), Gierer (1980), Villar et al. (2001), Smook and Smook (2002), Holladay et al. (2007), Restolho et al. (2009), Zhang et al. (2007), Ruiz et al. (2008), Wang and Chen (2016), Gibas and Janik (2010), Thakur et al. (2017), Hayashi et al. (2000), Chatterjee and Saito (2018), Sadeghifar et al. (2016), Pereira et al. (2017), Karaaslan et al. (2016), Yang and Kang (2017), Aegerter et al. (2011), Quraishi et al. (2015), Jeenpadiphat et al. (2016), Schuler et al. (2017), Barta et al. (2014), Kloekhorst et al. (2015), Ma et al. (2015), Luo (2017), Frost (2012), Shimzu et al. (1992), Redman (1923), Duan et al. (2019), Rana et al. (2018), Yoshikawa et al. (2013), Farooz et al. (2018), Sun et al. (2017), Vliet et al. (2016), Boomika et al. (2017), Bourzac (2015), Slaghek et al. (2017), Olsson (2015), Bhat et al. (2015), Huang et al. (2019), Abdullah et al. (2017), Anheden (2017), Shen et al. (2010), Feng et al. (2019), Kadla et al. (2002), Luo et al. (2010), Mainka et al. (2015), Souto et al. (2018), Vengal and Srikumar (2005), Tsang et al. (2019), Ochi (2006), Stevens et al. (2010), Nirmale et al. (2017), Lu et al. (2017), Mathiasson and Kubát (1994), Lumadue et al. (2012), Luo et al. (2018), Björsvik and Liguori (2002), da Silva et al. (2009), Araújo et al. (2009), Singh and Ghatak (2017), Pinto et al. (2012), Vinardell et al. (2008), Yearla and Padmsree (2016), Alzagameem et al. (2018)

<div align="right">(continued)</div>

Table 4 (continued)

S. No.	Product	Product type	Technique	Application	References
15	Surfactant	Aliphatic	Enhanced oil recovery	Pharmaceutical, cleaning, household, dispersants and emulsifiers in industries	Vinardell et al. (2008), Yearla and Padmsree (2016), Alzagameem et al. (2018), Alwadani and Fatehi (2018), Manko and Zdziennicka (2015), Rojas et al. (2009), Alvarado and Manrique (2010), Gan et al. (2014)
16	Coating materials	Carboxylate	Enzymatic oxidation	Coatings for the protection of aluminium surfaces, packaging, laminating objects in industries	Holladay et al. (2007), Shim (2010), Dastpak et al. (2018)
17	Adhesive	Macromolecules	Oxidation	Wood panel industry, replacement of phenol in phenol formaldehyde resins in industries	Abdelaty and Kuckling (2016), Yang and Kang (2017), Hemmilä et al. (2013), Kalami et al. (2017)
18	Fuel cell	Fuel	Direct use after pre-treatment	As fuel	Zhao and Zhu (2016), Che et al. (2018)
19	Electricity Generation	Heat	Direct use after pre-treatment	Electricity generation, thermal energy, electricity surplus for selling to the grid	Zhao and Zhu (2016), Weetall et al. (1985), Shewa et al. (2016), Liu and Bao (2017)

Fig. 3 Lignin tree: possible value-added lignin products from LC biorefinery

but different surfaces of Kraft lignin-based-carbon and Organosolv lignin-based-carbon aerogel as 120.56 and 19.20 m^2/g respectively (Yang and Kang 2017). It can be used as a thermal insulator, acoustic insulators, dielectrics, storage for gas and energy materials, etc. (Aegerter et al. 2011). Quraishi et al. have produced hybrid alginate–lignin aerogels by employing pressure on of 4.5 MPa on lignin aqueous alkali solution containing calcium carbonate (Quraishi et al. 2015).

- **Catechol**: It is an organic compound, also known as pyrocatechol or 1,2 dihydroxy benzene, a colorless organic compound and isomer of the three isomeric benzenediols. It is generally used as an intermediate for the synthesis of pharmaceuticals, agrochemicals, and other formulations (Jeenpadiphat et al. 2016). Several methods are discussed to produce catechol from waste lignin by several research groups (Schuler et al. 2017; Barta et al. 2014; Kloekhorst et al. 2015). High yields of catechol can be produced by hydrothermal liquefaction derived by the combination of fast hydrolysis, because of the presence of two hydroxy groups in lignin (Schuler et al. 2017). Variegated metal chlorides ($AlCl_3$, $NiCl_2$, $ZnCl_2$, and $CuCl_2$) were tested to obtain a great extent of monomers after depolymerization of Kraft lignin in ethanol and extracted the highest with $ZnCl_2$ (Ma et al. 2015).

- **Phenol**: An aromatic and crystalline solid is commonly synthesized by cumene using alkylation of benzene (Luo 2017). Several applications are reported by researchers as thermosetting (Frost 2012), intermediates for industrial synthesis (Shimzu et al. 1992), chemical and allied industries (Redman 1923). Phenol-rich bio-oils are produced by a combination of pre-treatment with catalytic conversion of lignin (Duan et al. 2019). Rana et al. have employed hydro thermolysis of Kraft lignin with MoO_3 catalyst in the batch reactor to produce phenolic monomers (Rana et al. 2018). The conversion of phenols from lignin was carried out into two reaction steps. Depolymerization in an autoclave reactor using a silica-alumina

catalyst followed by catalytic cracking of the first step's liquid products in a fixed-bed flow reactor with an iron oxide catalyst was carried out, extracted 6.6–8.6% phenols from lignin (Yoshikawa et al. 2013).

- **Bitumen**: A dense natural or crude oil distillate polycyclic aromatic hydrocarbons is generally used for the causeway, roof sealing. Approximately 90–95% of total road in the world is paved by bitumen which consumes 100 million tons of bitumen annually (Farooz et al. 2018). Drastically decreasing crude oil resources (Sun et al. 2017) can be tackled by fragmental replacement of lignin-derived bitumen. Several attempts are made with associated problems because of overexploitation of fossil resources, asphalt market and environment pioneer are searching for an alternative to reduce the use of fossil sources as well as CO_2 emission (Farooz et al. 2018; Vliet et al. 2016). Lignin was used with plastic as a limited bitumen substitute, reported 15%, and 20% efficient outcomes of lignin and plastic respectively (Boomika et al. 2017) while 5–20% could be improved by Xie et al. (2017). Limitation is adduced because some type of waste lignin needs treatment before being used as bitumen in road paving (Bourzac 2015; Slaghek et al. 2017). Because of the lignin mark-up, some chemical modification, physical testing, and blending attempts with asphalt are required, also beneficial for the reduction of greenhouse gas emission (Vliet et al. 2016) as an environmental concern.

- **Motor Fuels**: Generally, gasoline or diesel are being used for providing power to motor vehicles. Due to higher energy demand, the world needs to unravel the situation of fuel crisis by replacing it with alternate sources of energy from conventional sources. The use of other alternate natural resources such as compressed natural gas, ethanol, biodiesel, propane, and hydrogen are some profitable solutions for the conservation of energy. Motor fuel production from lignin is currently attracting much interest. Olsson presented research work for the preparation of biodiesel from pulp and paper industry-based residual lignin (Olsson 2015). Bhat et al. and Huang et al. extracted a solvent of 50 wt% of lignin oil from the lignin in the first biorefinery by hexane which was further converted to phenols over MoO_3 catalyst under ambient pressure. 6.9 wt%-dry-applewood (Bhat et al. 2015; Huang et al. 2019). Recently, it was remarkably noticed that hydrogenation is one of the most efficient and practicable entelechies for biofuel production from lignin (Abdullah et al. 2017). The altisonant production cost of lignin-based oil as compared with crude is oil three times higher than today's cost (Anheden et al. 2017).

- **Guaiacol**: A natural phenolic, yellowish aromatic oil is generally produced from guaiacum or wood creosote. On large scale alkylation of benzene with propylene and further partial oxidation of phenol were carried out and then guaiacol and its derivatives were obtained by pyrolysis of kraft lignin at 575 °C, 675 °C, and 700 °C (Shen et al. 2010). A potential route was introduced to produce guaiacol and its derivatives from black liquor lignin decomposition by using a novel thermolysis process at scarce temperature and sparing reaction time (Feng et al. 2019).

- **Carbon Fibres**: Composed of carbon atoms, first time used in the 1950s in industries as material parts of aircraft and aerospace materials due to remarkable properties of high modulus and low density (Kadla et al. 2002). Carbon fibers having

10 µm of diameter, strengthened to improve the properties of polymers. Luo reported 40 and 80% yield of carbon fibers through spun lignin on carbonization and the thermo-stabilization process (Luo et al. 2010). Mainka et al. investigated the production of carbon fiber by using hardwood lignin and Souto et al. have reviewed economic viability, sustainability, material importance, market segment, and certain application of lignin-based carbon fiber (Mainka et al. 2015; Souto et al. 2018).

- **Bioplastic**: As our great concern about plastic in day-to-day life, non-degradable generally produced from petroleum with the result that inducement of critical environmental issues (Thakur et al. 2017; Vengal and Srikumar 2005). Adscititious, a sustainable approach is required to extenuate the cost and possible options to reduce pollution from fossil fuels. Bioplastic may be an ideal option in sustainability and conservation of environmental concern (Tsang et al. 2019). Instead of the low mechanical strength of bioplastic (Ochi 2006; Stevens et al. 2010), the use of bioplastic becomes a vital factor to tackle unsustainability and making a circular bio-economy.

- **Binders**: A substance that clasps another material by adhesion or osculant. Due to less toxicity, effective adhesive, and cohesive properties of lignin, the lignin-based binders have objurgated the way of sustainability towards ecological balance. Several reports are published to make a lignin-based binder for various purposes such as in the area of lithium-ion battery (Nirmale et al. 2017; Lu et al. 2017), Particleboards (Mathiasson and Kubát 1994), and foundry coke substitute after briquetting anthracite fines (Lumadue et al. 2012). A pioneer lignin-derived binder material, PAL-NaPAA was synthesized for micro silicon anodes in LIBs via a free radical graft copolymerization, after alkaline hydrolysis of lignin (Luo et al. 2018).

- **Vanillin**: A major flavor of vanilla is vanillin (4-hydroxy-3-methoxy benzaldehyde) having a wide range of applications in industries. It is generally extracted from dried pods of the vanilla plant most widely used in several pharmaceuticals, chemicals, and food industries (Bjørsvik and Liguori 2002). On the commercial level, over 90% of vanillin is produced from chemical/petrochemical sources while technologies have been developed for vanillin production from biowaste lignin (da Silva et al. 2009; Araújo et al. 2009; Singh and Ghatak 2017). Norwegian company Borregaard is merely producing vanillin from lignin by oxidizing emulsifying and lignosulphonate complexing agents (Fache et al. 2016; Pinto et al. 2012).

- **Antioxidant:** A compound that fends damage to cells due to oxidation of free radicals, it can also be called free-radical scavengers. Industrial lignin was exhibited as an antioxidant in its probable application in cosmetics (Vinardell et al. 2008). Dioxane lignin and alkali lignin nanoparticles were examined for their radical scavenging activity and declared to have higher antioxidant activity for further exploitation in the cosmetic and food industries (Yearla and Padmsree 2016). Although, due to the complex discrepant structure of lignin it could not be used as a natural antioxidant yet (Alzagameem et al. 2018).

- **Surfactants**: A compound that can cause interfacial changes between two phases by accumulation on the surface of a liquid (Alwadani and Fatehi 2018). Dispersants for solid-liquid mixtures (Manko and Zdziennicka 2015) and stabilization of liquid-liquid mixtures as emulsifiers (Rojas et al. 2009) were spaciously applied in chemical industries, pharmaceuticals, cleaning, household (Alvarado and Manrique 2010; Gan et al. 2014). A variety of lignin surfactants are possible in the form of anionic, nonionic, cationic, and amphoteric surfactants based on charge disparity (Huang et al. 2019). A few patents are also carried out for the preparation of a surfactant at high temperature and pressure in presence of hydrogen or carbon mono oxide as a reducing agent (Naae et al. 1988; Adam et al. 1998). An expensive chemical surfactant for oil recovery may lead to the development of new lignin-based surfactants in the future (Ganie et al. 2019).
- **Coating Materials**: A substrate that is generally applied to an object's surface for covering or laminating techniques (Shim 2010). Investigation of lignin on stainless steel as an anti-corrosion coating (Dastpak et al. 2018) was studied, while a coating material was synthesized and characterized for great anti-corrosion properties from lignin so far (Haro et al. 2019).
- **Adhesive**: Adhesive is the substance used for binding two separate materials and impeding their dissociation. Since the 1920s, lignin was used as an adhesive with limited industrial applications (Hemmilä et al. 2013). Adhesive from lignin brought the idea in research because the tariff of petroleum-derived adhesive components is continuously increasing (Ghaffar and Fan 2014). Several kinds of literature were subjected to lignin as an adhesive review (Ghaffar and Fan 2014; Rowell 2012; Pizzi 2006). Instead of massive research in this area by several groups (Sarkar and Adhikari 2000; Windsten and Kandelbauer 2008; Zhang et al. 2014), effective application is required to be cured. The simplest way was found an only partial replacement for phenol-formaldehyde (PF) resin from lignin (Hemmilä et al. 2013). Recently, A research group has replaced 100% phenol-formaldehyde (PF) resin from agricultural-based lignin to find a new market for lignin valorization as phenol replacement (Kalami et al. 2017).
- **Fuel cell**: A device that is responsible for the conversion of electrical energy from chemical potential energy, where hydrogen gas (H_2) is mostly used (Appleby 1994) followed by oxygen gas (O_2) as fuel. A research group compared the use of lignin as fuel directly in conventional proton exchange membrane fuel cells (PEMFCs) and direct biomass fuel cells (DBFC). They failed to the direct use of lignin in PEMFCs due to arduous oxidation at low temperature, even not fit in catalytic reaction (Zhao and Zhu 2016). Che et al. have demonstrated the fabrication of polymer electrodes poly (3,4-ethylene dioxythiophene) towards the truly sustainable electrical energy storage can be designed by the use of lignin. They further claimed that they are the first who developed a method to use lignin as fuel in a fuel cell (Che et al. 2018).
- **Electricity Generation:** Conversion of energy to electricity from different existing methods is even direct capture or burning to produce energy is not new. The burning of biomass to electricity on a large scale is economically very difficult to compete with coal and natural gas. 1 kWh of electricity generated from

sulfonated lignin and Kraft Black Liquor by using an anthraquinone mediated fuel cell (Weetall et al. 1985)**.** Shewa et al. used single chamber microbial fuel cells (SCMFCs) to produce electricity from sodium LS (lignosulfonate) under TiO_2-UV photocatalytic process. The maximum current of 6556 ± 360 mAm^{-3} and power density of 1881 ± 103 mWm^{-3} was generated as PrLS feed SCMFCs, operated at 37 ± 1 ^{0}C and achieved a coulombic efficiency of $17.7 \pm 1.2\%$ (Shewa et al. 2016).

3.8 Market Values

Initially, the lignin market faced instability due to the poor soundness of pulping companies and became a source of revenue for biorefineries (Holladay et al. 2007). The primary application of lignin as a fuel in power generation globally, dry lignin has a high calorific value of 26.5 MJ/kg as compared with cellulose and hemicellulose of 16.7 MJ/kg (Bruijnincx et al. 2016). The price of lignin is based on the sources of lignin that have different ranges of fuel or heating value over industrial concern (Holladay et al. 2007). As a sinewy precursor for the production of several aromatic compounds, the lignin market is expected to grow at a rate of 3.42% during the 2018–23 epoch from the current 974.6 million as reported by a website (Dhiman 2019). In power generation, Kraft lignin is an important fuel varying its price from 70 to 150 USD per tonne based on logistic cost, moisture, and ash contents (Bruijnincx et al. 2016). A prediction says that Europe will be a great market shareholder who is currently accounting for 34% of the total market of lignin-based products (Dhiman 2019). A report about lignin from pulping industry states that 50–60 million tons annually extracted as a by-product (https://www.transparencymarketresearch.com/lignin-based-products-market.html) can improve the economy of biorefineries in terms of value-added chemicals and products. Approximately 90% of carbon fiber is being produced from petroleum-derived polyacrylonitrile (PAN) (https://www.transparencymarketresearch.com/lignin-based-products-market.html) extensively used in multiple body parts of aircraft and automotive industries due to its lightweight. By application, the macromolecule is dominating in the lignin market as stimulating product demand by 50% composites used aircraft (Maximize, Market Research 2021). Another report claimed that the kraft lignin market will increase with a 7% CAGR during the forecast period due to the exponential demand for carbon fiber globally (Mordor Intelligence 2021). Lignin road products applied to the road surface ligates the cellulose fibers with trees and plants unlike insoluble in water under solar light. A report stated that these lignin road products are cost-effective and cheaper than petroleum-based road products. The same report predicted that the lignin road products market will increase by more than USD 6.1 billion by the end of 2021 (Technavio 2017).

In the context of vanillin, 16,000 metric tons were expected to be produced with a value of USD 230 million in 2011, 20% synthetic vanillin was expected to come from lignin while remaining produced from crude oil (Frost 2012). As per the Ph.D.

research thesis presented by Wong, the market price is USD 100–200 per kg of vanillin and accounting for 60% of industrial vanillin in the food industry, 33% in the perfume industry while 7% in pharmaceuticals (Timothy 2012). A study showed that the bioplastics will be replaced in place of polymer market almost 80% in Western Europe in this year (Shen et al. 2010) estimated overall fabrication of bioplastics will be around 2.44 million tons in 2022 from natural resources such as lignin, lipids, etc. globally (Johansson et al. 2012). Electricity production of 4335–5981 kWh by combustion of the generated lignin residue was reported as 1.26–1.85 tons of dry lignin generated from one ton of cellulosic ethanol (Liu and Bao 2017). An expected market of lignin and lignin-based products will be USD 874.3 in 2020, while it will increase with 8.3% CAGR and reach 1537.1 million USD by the end of 2026 globally (Market Watch 2021). The evolution of prices of possible value-added products from lignin can be seen by an animation diagram in Fig. 4.

Although, not a single research group has thoroughly studied and explained the dynamics and potential of the lignin market globally as well as nationally. Emerging trends, market threats, restraints, challenges of lignin and lignin products are also not yet reported based on sources, types, and products at the global and regional level. Due to the novel coronavirus (nCOVID-19) outbreak, it may cause the global lignin market to slow or fall into exacerbation.
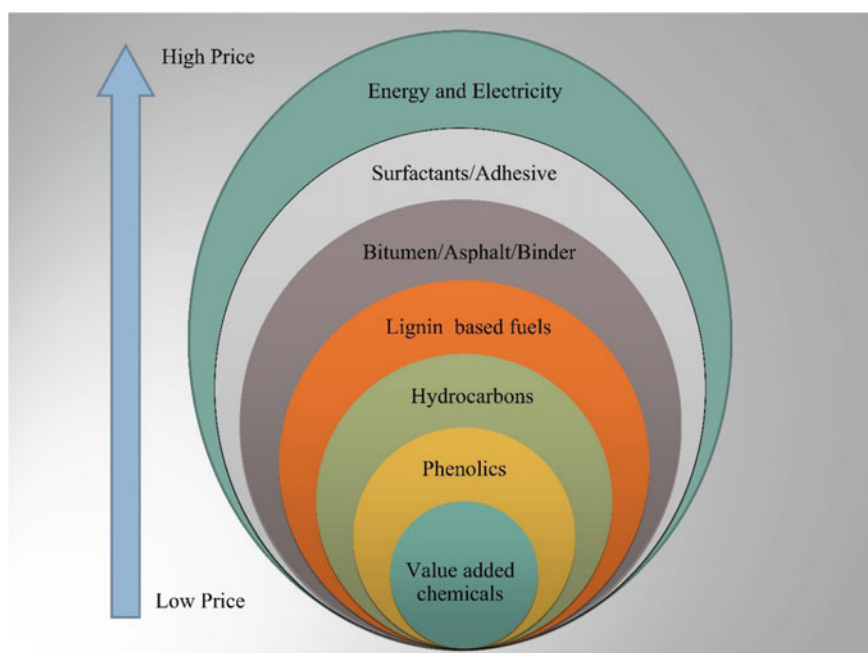
Fig. 4 Price of lignin products from low to high showing by an animation diagram

3.9   SWOT Analysis of Lignin Market Potential

A tool of strategical and tactical planning to elicit internal and external factors of four areas. Strengths and weaknesses are internal factors under the concerned subject while identifying the opportunities and the threats are external factors under the subject's environment (Gurel and Merba 2018). Similarly, in this study SWOT analysis of lignin in the form of market potential and strategic point of view is carried out. The analysis is based on the study and the estimation of several research groups such as (Frost 2012; Market Watch 2021; Gurel and Merba 2018; Lora and Glasser 2002; Stewart 2008; Ten and Vermerris 2015) is tabulated in Table 5. The four important parameters i.e., strengths and weaknesses as internal whereas opportunities and threats as external factors. Lignin market potential has several strengths and weaknesses like abundant availability of lignin with low cost, accounting for 60% of carbon content and adequate experiences are available for lignin conversion into value-added products. The internal weakness is the complex structure of lignin, alteration of energy density, and quality of lignin and lignin products are sometimes costly than existing products. The lignin market has presented promising chances for the development of new and renewable products, reduction of GHGs emissions, evaluation of new techniques, no-waste approach, lignin specified BR market is expected to grow from 874.3 USD in 2020 to reach 1537.1 million USD by the end of 2026. However, competitive utilization of lignin products, fluctuation in petroleum products have shown ample threats, recent novel COVID-19 outbreak is also observing a possible threat to the lignin market globally.

4   Conclusion

Lignin products influx of ergastic for commercial applications in various fields from biorefinery are briefly discussed and reviewed. Abundant availability of lignin in nature fetches possibilities of valuable biopolymer products as well as future precursors for biofuel from lignin despite its recalcitrant. The current review is critically assessing the lignin specified LCBR, types, extraction techniques, and possible lignin product potential because of the valorization of lignin. Possible market potential including strength and opportunities via SWOT analysis is concisely summarized. Even now, there is still a long path to go before valorizing lignin via commercialization of its products could be continued by the evolution of technical and economic methods. The following potentiality of lignin valorization should be regarded as forthcoming studies:

1. More efficient pathways are required for pervasive lignin conversion into valuable products in the biorefinery.
2. Methods are not developed that can assimilate a complete fraction of lignin and further conversion into valuable products.

Table 5 SWOT analysis: pros and cons of lignin market potential

Internal	Strength (+)	Weakness (−)
	• Second most abundant biopolymer accounting 15–30% of the plants in the nature • Alternate of fossil fuel refinery • By products of bio-based industries and a valuable resource for the chemical industry • Raw lignin including uncustomed residue from agriculture and forestry is available almost in all countries • Adequate experiences are available for lignin conversion into value added products • Lignin is a waste in some industry, that could be beneficial for biorefinery as raw material • Ideal substitute for oil-based products • Low-cost material • Easily available • Approximately 60% carbon content	• Complex structure of lignin • Varies properties with location as well as sources of lignin • Different variety based on the sources • Production cost of lignin-based value-added products is costly than existing products • Lignin products utilization is immature with respect to high value creation • Alteration of energy density and quality of lignin • Activities towards the biorefinery concept in countries like India is underdeveloped
External	Opportunity (+)	Threat (−)
	• Development of new products from lignin • Evaluation of new technique with great efficiency • Lignin conversion leads to no waste principle approach • Transformation opportunities for exchanging techniques and system with establishment of more biorefineries in poor countries • May get more significant market value of lignin products in case of cascading approach of feedstock and technology • Possibilities of reduction of CO_2 emission as well as GHGs • Significantly improving the economy of a bio-refinery • Increase the contribution of biomass conversion efficiency • Reduce the dependency of petroleum refinery • Increasing interest for material applications day by day • Innovative integrated biorefineries are established that will build and strengthen the structure of global economy • Market expectation from 874.3 USD in 2020 to reach 1537.1 million USD by the end of 2026	• Less resources of biorefinery equipment's in market • Competitive utilization options of lignin products • Fluctuation in petroleum products • May affect the global lignin market to slow or fall in to exacerbating due to nCOVID-19 outbreak globally

3. More studies and research to understand the recalcitrant structure and characteristics are required to achieve absolute lignin conversion.
4. In view of the great market potential of carbon fiber, it would require more knowledge about structure-characteristics-property relationship.
5. Use of lignin in fuel cell enthralling lignin market but still critical analysis and optimizations are needed.

Conflict of Interest The Authors declare that there is no conflict of interest.

References

Abdelaty M, Kuckling D (2016) Synthesis and characterization of new functional photo cross-linkable smart polymers containing vanillin derivatives. Gels 2(1):3

Abdullah B, Muhammad SAFS, Mahmood NAN (2017) Production of biofuel via hydrogenation of lignin from biomass. In: Ravanchi MT (ed) New advances in hydrogenation processes, pp 289–305

Adam GA (1998) Lignin-based surfactants. US Patent. US2015/0158898 A1

Adler E (1977) Lignin chemistry-past, present and future. Wood Sci Technol 11:169–218

Aegerter MA, Leventis N, Koebel MM (2011) Aerogels handbook. Springer, New York

Agrwal A, Kaushik A, Biswas S (2014) Derivatives and applications of lignin—an insight. Scitech J 1–07:30–36

Ahvazi B, Cloutier E, Wojciechowicz O, Ngo TD (2016) Lignin profiling: a guide for selecting appropriate lignins as precursors in biomaterials development. ACS Sustain Chem Eng 4(10):5090–5105

Alvarado V, Manrique E (2010) Enhanced oil recovery: an update review. Energies 3(9):1529–1575

Alwadani N, Fatehi P (2018) Synthetic and lignin-based surfactants: challenges and opportunities. Carbon Resour Convers 1:126–138

Alzagameem A, Khaldi-Hansen BE, Büchner D, Larkins M, Kamm B, Witzleben S, Schulze M (2018) Lignocellulosic biomass as source for lignin-based environmentally benign antioxidants. Molecules 23:2664

Andrade MF, Colodette JL (2014) Dissolving pulp production from sugar cane bagasse. Ind Crop Prod 52:58–64

Anheden M, Uhlin A, Wolf J, Hedberg M, Berg R, Ankner T, Berglin N, Schenck A, Larsson AL, Guimaraes M, Fiskerud M, Andersson S (2017) Value chain for production of bio-oil from kraft lignin for use as bio-jet fuel, NWBC 2017, Stockholm, 28–30 Mar

Anwar Z, Gulfraz M, Irshad M (2014) Agro-industrial lignocellulosic biomass a key to unlock the future bio-energy: a brief review. J Radiat Res Appl Sc 7(2):163–173

Appleby AJ (1994) Fuel cells and hydrogen fuel. Int Z Hydrogen Energy 19(2):175–180

Araújo JDP, Grande CA, Rodrigues AE (2009) Structured packed bubble column reactor for continuous production of vanillin from kraft lignin oxidation. Catal Today 147:S330–S335

Arevalo-Gallegos A, Ahmad Z, Asgher M, Parra-Saldivar R, Iqbal HMN (2017) Lignocellulose: a sustainable material to produce value-added products with a zero waste approach—a review. Int J Biol Macromol 99:308–318

Azadi P, Inderwildi OR, Farnood R, King DA (2012) Liquid fuels, hydrogen and chemicals from lignin: a critical review. Renew Sustain Energ Rev 21:506–523

Balagurumurthy B, Ohri RSP, Prakash A, Bhaskar T (2015) Thermochemical Biorefinery. In: Bhaskar T, Pandey A (edn) Advances in thermochemical conversion of biomass—introduction, pp 157–174

Balat M (2008) Mechanisms of thermochemical biomass conversion processes. Part 3: reactions of liquefaction. Energ Source Part A 649–659

Balina K, Romagnoli F, Blumberga D (2017) Seaweed biorefinery concept for sustainable use of marine resources. Energ Proc 128:504–511

Barakat A, de Vries H, Rouau X (2013) Dry fractionation process as an important step in current and future lignocellulose biorefineries: a review. Bioresour Technol 134:362–373

Barta K, Warner GR, Beach ES, Anastas PT (2014) Depolymerization of organosolv lignin to aromatic compounds over Cu-doped porous metal oxides. Green Chem 16:191–196

Bhat AH, Dasan YK, Khan I (2015) Extraction of lignin from biomass for biodiesel production. Agr biom potential mater, pp 155–179

Bhutto AW, Harijan K, Qureshi K, Bazmi AA, Bahadori A (2015) Perspectives for the production of ethanol from lignocellulosic feedstock—a case study. J Clean Prod 95:184–193

Binod P, Sindhu R, Singhania RR, Vikram S, Devi L, Nagalakshmi S, Pandey A (2010) Bioethanol production from rice straw: an overview. Bioresour Technol 101(13):4767–4774

Bjørsvik H-R, Liguori L (2002) Organic processes to pharmaceutical chemicals based on fine chemicals from lignosulfonates. Org Proc Res Dev 6(3):279–290

Boomika A, Naveen MA, Richard JD, Mythili A, Vetturayasudharsanan R (2017) Experimental study on partial replacement of bitumen with lignin and plastic. SSRG Int J Civ Eng Special Issue 9–14

Bourzac K (2015) Inner workings: paving with plants. Proc Natl Acad Sci USA 112(38):11743–11744

Bruijnincx P, Weckhuysen B, Gruter G-J, Engelen-Smeets E (2016) Lignin valorisation: the importance of a full value chain approach. Utrecht Univ 22

Buranov AU, Mazza G (2008) Lignin in straw of herbaceous crops. Ind Crop Prod 28(3):237–259

Canilha L, Chandel AK, Milessi TSS, Antunes FAF, Freitas WLC, Felipe MGA, Da Silva SS (2012) Bioconversion of sugarcane biomass into ethanol: an overview about composition, pretreatment methods, detoxification of hydrolysates, enzymatic saccharification, and ethanol fermentation. J Biomed Biotechnol

Casas A, Oliet M, Alonso MV, Rodríguez F (2012) Dissolution of Pinus radiata and Eucalyptus globulus woods in ionic liquids under microwave radiation: lignin regeneration and characterization. Sep Purif Technol 97:115–122

Chatterjee S, Saito T (2018) Lignin-derived advanced carbon materials. Chem Sus Chem 8:23

Che C, Vagin M, Wijeratne K, Zhao D, Warczak M, Jonsson MP, Crispin X (2018) Conducting polymer electrocatalysts for proton-coupled electron transfer reactions: toward organic fuel cells with forest fuels. Adv Sustain Syst 1800021

Chen H (2015) Lignocellulose biorefinery engineering, CB22 3HJ. Woodhead Publishing Limited is an imprint of Elsevier, Cambridge

Chen S, Wen Z, Liao W, Liu C, Kincaid RL, Harrison JH, Stevens DJ (2005) Studies into using manure in a biorefinery concept. Appl Biochem Biotechnol 121–124:999–1015

Chen H (2014) Biotechnology of lignocellulose. Theory Pract

Cheng H, Wang L (2013) Lignocelluloses feedstock biorefinery as petrorefinery substitutes, biomass now—sustainable growth and use. Miodrag Darko Matovic, IntechOpen

Cherubini F (2010) The biorefinery concept: using biomass instead of oil for producing energy and chemicals. Energ Convers Manage 51(7):1412–1421

Cook et al (1991) Organosolv Lignin modified phenolic resins and method for their preparation. United States Patent, 5010156

Crestini C, Melone F, Sette M, Saladino R (2011) Milled wood lignin: a linear oligomer. Biomacromol 12:3928–3935

da Silva EAB, Zabkova M, Araujo JD, Cateto CA, Barreiro MF, Belgacem MN, Rodriques AE (2009) An integrated process to produce vanillin and lignin-based polyurethanes from kraft lignin. Chem Eng Res Des 87:1276–1292

Dale BE, Ong RG (2012) Energy, wealth, and human development: why and how biomass pretreatment research must improve. Biotechnol Prog 28(4):893–898

Dastpak A, Yliniemi K, Monteiro MCO, Höhn S, Virtanen S, Lundström M, Wilson BP (2018) From waste to valuable resource: lignin as a sustainable anti-corrosion coating. Coatings 8:454

Dehne L, Vila, Babarro C, Saake B, Schwarz KU (2016) Influence of lignin source and esterification on properties of lignin-polyethylene blends. Ind Crop Prod 86:320–328

Demirbas A (2009) Biorefineries: current activities and future developments. Energ Convers Manage 50(11):2782–2801

Dhiman G (2019) Lignin biorefinery: an effective biomass conversion to value added product. TT Consultants patent

Duan D, Lei H, Wang Y, Ruan R, Liu Y, Ding L, Zhang Y, Liu L (2019) Renewable phenol production from lignin with acid pretreatment and ex-situ catalytic pyrolysis. J Clean Prod 231:331–340

Van Dyne, DL., Blasé, MG., Clements, LD., A strategy for returning agriculture and rural America to long-term full employment using biomass refineries. p. 114–123. In: J. Janick (ed.), Perspectives on new crops and new uses. ASHS Press, Alexandria, VA (1999).

El Mansouri N-E, Yuan QL, Huang F (2011) Study of chemical modification of alkaline lignin by the glyoxylation reaction. Mater Sci 6(4):4523–4536

Fache M, Boutevin B, Caillol S (2016) Vanillin production from lignin and its use as a renewable chemical. ACS Sustain Chem Eng 4(1):35–46

Farooz N, Sofi QF, Mir MS (2018) Lignin as partial replacement for bitumen. In: Conference on recent innovations in emerging technology and science, 6–7 Apr 2018. ISSN: 2320-2882 by JB Institute of Technology, Dehradun & IJCRT

Faustino H, Gil N, Baptista C, Duarte AP (2010) Antioxidant activity of lignin phenolic compounds extracted from kraft and sulphite black liquors. Molecules 15:9308–9322

Feng P, Wang H, Lin H, Zheng Y (2019) Selective production of guaiacol from black liquor: effect of solvents. Carbon Resour Convers

Fernando S, Adhikari S, Chandrapal C, Murali N (2006) Biorefineries: current status, challenges, and future direction. Energ Fuel 4:1727–1737

Fragues C, Mathis A, Silva J, Rodrigues A (1996) Kinetics of vanillin oxidation. Chem Engg Tech 9–2:127–136

Frost S (2012) High-value opportunities for lignin: Unlocking its potential. Frost and Sullivan, Santa Clara. Available at: http://www.frost.com/sublib/display-marketinsight-top.do?id¼269017995

Gabov K, Hemming J, Fardim P (2017) Sugarcane bagasse valorization by fractionation using a water-based hydrotropic process. Ind Crop Prod 108:495–504

Gan C, Wang H, Zhao Z, Yin B (2014) Sugar-based ester quaternary ammonium compounds and their surfactant properties. J Surf Deterg 17(3):465–470

Ganie K, Manan MA, Ibrahim A, Idris AK (2019) An experimental approach to formulate lignin-based surfactant for enhanced oil recovery. Int J Chem Eng 6

Ghaffar SH, Fan M (2014) Lignin in straw and its applications as an adhesive. Int J Adhes Adhes 48(2014):92–101

Ghatak HR (2011) Biorefineries from the perspective of sustainability: feedstocks, products, and processes. Renew Sustain Energ Rev 15:4042–4052

Gibas I, Janik H (2010) Review: synthetic polymer hydrogels for biomedical applications. Chem Chem Technol 4:4

Gierer J (1980) Chemical aspects of kraft pulping. Wood Sci Technol 14:241–266

Guo G, Li S, Wang L, Ren S, Fang G (2013) Separation and characterization of lignin from bio-ethanol production residue. Bioresour Technol 135:738–741

Gurel E, Merba TAT (2018) SWOT analysis: a theoretical review. J Int Social Res 10:51

Haro JC, Magagnin L, Turri S, Griffini G (2019) Lignin-based anticorrosion coatings for the protection of aluminum surfaces. ACS Sustain Chem Eng 7:6213–6222

Harper SHT, Lynch JM (1981) The chemical components and decomposition of wheat straw leaves, internodes and nodes. J Sci Food Agric 32–11

Hayashi J, Kazehaya A, Muroyama K, Watkinson AP (2000) Preparation of activated carbon from lignin by chemical activation. Carbon 38:1873–1878

Hemmilä V, Trischler J, Sandberg D (2013) Lignin—an adhesive raw material of the future or waste of research energy? In: Brischke C, Meyer L (eds) Proceedings of 9th meeting of the Northern European network for wood science and engineering (WSE), Hannover, Germany, 11–12 Sept, pp 98–103

Higuchi T, Itu Y, Shimada M, Kawamura I (1967) Chemical properties of milled wood lignin of grasses. Phytochem 6:1551–1556

Hinman ND, Schell DJ, Riley J, Bergeron PW, Walter PJ (1992) Preliminary estimate of the cost of ethanol production for ssf technology. Appl Biochem Biotechnol 34–35(1):639–649

Holladay JE, White JF, Bozell JJ, Johnson D (2007) Top value-added chemicals from biomass volume ii—results of screening for potential candidates from biorefinery lignin. Pacific Northwest Natl Lab II(October):87

Hongzhang C (2015) Lignocellulose biorefinery engineering, principles and applications. eBook ISBN: 9780081001455

Hu J, Zhang Q, Lee DJ (2017) Kraft lignin biorefinery: a proposal. Bioresour Technol 8–10

Huang J, Fu S, Gan L (2019) Lignin chemicals and their applications. In: Huang J, Fu S, Gan L (eds) Lignin chemistry and their applications. Chemical Industry Press. Elsevier, pp 79–134

Iqbal HMN, Ahmed I, Zia MA, Irfan M (2011) Purification and characterization of the kinetic parameters of cellulase produced from wheat straw by Trichoderma viride under SSF and its detergent compatibility. Adv Biosci Biotechnol 2(3):149–156

Iqbal HMN, Kyazze G, Keshavarz T (2013) Advances in the valorization of lignocellulosic materials by biotechnology: an overview. Bio Resources 8(2):3157–3176

Isikgor FH, Becer CR (2015) Lignocellulosic biomass: a sustainable platform for the production of bio-based chemicals and polymers. Polym Chem 6(25):4497–4559

Jeenpadiphat S, Mongkolpichayarak I, Tungasmita DN (2016) Catechol production from lignin by Al-doped mesoporous silica catalytic cracking. J Anal Appl Pyrol 121:318–328

Jiang G, Nowakowski DJ, Bridgwater AV (2010) A systematic study of the kinetics of lignin pyrolysis. Thermochim Acta 498:61–66

Jin Y, Ruan X, Cheng X, Lü Q (2011) Liquefaction of lignin by polyethylene glycol and glycerol. Bioresour Technol 102(3):3581–3583

Johansson AJ, Aaltonen O, Ylinen P (1987) Organosolv pulping—methods and pulp properties. Biomass 13:45–65

Johansson C, Bras J, Mondragon I, Nechita P, Plackett D, Simon P, Svetec DG, Virtanen S, Baschetti MG, Breen C (2012) Renewable fibers and bio-based materials for packaging applications-a review of recent developments. Bio Resources 7:2506–2552

Jong ED, Jungmeier G (2015) Biorefinery concepts in comparison to petrochemical refineries. In: Pandey A et al (eds) Industrial biorefineries and white biotechnology, pp 3–33

Kadla JF, Kubo S, Venditti RA, Gilbert RD, Compere AL, Griffith W (2002) Lignin-based carbon fibers for composite fiber applications. Carbon 40:2913–3292

Kalami S, Arefmanesh M, Master E, Nejad M (2017) Replacing 100% of phenol in phenolic adhesive formulations with lignin. J Appl Polym Sci

Kaleinert TN (1975) Ethanol-water delignification of sizable pieces of wood disintegration into stringlike fiber bundles. Holzforschung 29:108–110

Kamm B (2014) Biorefineries: their scenarios and challenges. Pure Appl Chem 86(5):821–831

Kanosh AL, Essam SA, Zeinat AN (1999) Biodegradation and utilization of bagasse with Trichoderma reesie. Polym Degrad 63:273–278

Karaaslan MA, Kadla JF, Ko FK (2016) Lignin-based aerogels. Lignin in polymer composites, pp 67–93

Khan TA, Lee J, Kim HJ (2019) Lignin-based adhesives and coatings. In: Arriffin A (ed) Lignocellulose for future bioeconomy, Elsevier, UK, pp 153–206

Kloekhorst A, Shen Y, Yie Y, Fang M, Heeres HJ (2015) Catalytic hydrodeoxygenation and hydrocracking of Alcell® lignin in alcohol/formic acid mixtures using a Ru/C catalyst. Biomass Bioenerg 80:147–161

Kumar P, Barrett DM, Delwiche MJ, Stroeve P (2009) Methods for pretreatment of lignocellulosic biomass for efficient hydrolysis and biofuel production. Ind Eng Chem Res 48(8):3713–3729

Kun D, Pukánszky B (2017) Polymer/lignin blends: interactions, properties, applications. Eur Polym J 93:618–641

Larrañeta E, Imizcoz M, Toh JX, Irwin J, Ripolin A, Perminova A, Dominguez-Robles J, Rodriguez A, Donnelly RF (2018) Synthesis and characterization of lignin hydrogels for potential applications as drug eluting antimicrobial coatings for medical materials. ACS Sustain Chem Eng

Lawther JM, Sun RC, Banks WB (1997) Isolation and characterization of organosolv lignin under alkaline condition from wheat straw. Int J Polym Anal Charact 3(2):159–175

Lee SH, Doherty TV, Linhardt RJ, Dordick JS (2009) Ionic liquid-mediated selective extraction of lignin from wood leading to enhanced enzymatic cellulose hydrolysis. Biotechnol Bioeng 102(5):1368–1376

Lindorfer H, Frauz B (2015) Biogas biorefineries. In: Pandey A, Höfer R, Taherzadeh M, Nampoothiri KM, Larroche C (eds) Industrial biorefineries & white biotechnology. Elsevier, Amsterdam, pp 271–294

Liu G, Bao J (2017) Evaluation of electricity generation from lignin residue and biogas in cellulosic ethanol production. Bioresour Technol

Lora JH, Glasser WG (2002) Recent industrial applications of lignin: a sustainable alternative to non-renewable materials. J Polym Environ 10:39

Lu Y, Lu Y-C, Hu H-Q, Xie F-J, Wei X-Y, Fan X (2017) Structural characterization of lignin and its degradation products with spectroscopic methods. J Spectrosc

Ludmila H, Michal J, Andrea S, Slovak HA (2015) Lignin, potential products and their market value. Wood Res 60(6):973–986

Lumadue MR, Cannon FS, Brown NR (2012) Lignin as both fuel and fusing binder in briquetted anthracite fines for foundry coke substitute. Fuel 97:869–875

Luo L, Voet E, Huppes G (2010) Biorefining of lignocellulosic feedstock-technical, economic and environmental considerations. Bioresour Technol 101:5023–5032

Luo A-O (2017) Chemicals from lignin, Encyclopedia of sustainable technologies, 1st edn., pp 573–585

Luo C, Du L, Wu W, Xu H, Zhang G, Li S, Wang C, Lu Z, Deng Y (2018) Novel lignin-derived water-soluble binder for micro silicon anode in lithium-ion batteries. ACS Sustain Chem Eng

Lynd LR., Wyman C, College MLD, Hampshire N, Johnson D, Proforma RL (2005) Strategic biorefinery analysis: analysis of biorefineries. National Renewable Energy Laboratory (NREL), pp 403–465

Ma R, Xu Y, Zhang X (2015) Catalytic oxidation of biorefinery lignin to value-added chemicals to support sustainable biofuel production. Chem Sus Chem 7:1–29

Mackendry P (2002) Energy production from biomass (part 2): conversion technologies. Bioresour Technol 83:47–54

Mainka H, Täger O, Körner E, Hilfert L, Busse S, Edelmann FT, Herrmann AS (2015) Lignin—an alternative precursor for sustainable and cost-effective automotive carbon fiber. J Mater Res Technol 160–114

Malherbe S, Cloete TE (2002) Lignocellulose biodegradation: fundamentals and applications. Rev Environ Sci Biotechnol 1(2):105–114

Manko D, Zdziennicka A (2015) Sugar-based surfactants as alternative to synthetic ones. Ann UMCS, Chem 70(1):161–168

Marcilly C (2003) Present status and future trends in catalysis for refining and petrochemicals. J Catal 216(1–2):47–62

Market Watch, https://www.marketwatch.com/press-release/lignin-and-lignin-based-products-market-2020-with-top-countries-data-overview-cost-structure-analysis-growth-opportunities-and-forecast-to-2026-2020-02-04. Last accessed 4 Feb 2021

Mathew AK, Abraham A, Mallapureddy KK, Sukumaran RK (2018) Waste biorefinery: potential and perspectives. In: ed. Lignocellulosic biorefinery wastes, or resources. Elsevier

Mathiasson A, Kubát DG (1994) Lignin as binder in particle boards using high frequency heating. Holz Als Roh-Und Werkstoff 52:9–18

Maximize, Market research, https://www.maximizemarketresearch.com/market-report/lignin-market/13321/. Last accessed 13 Feb 2021

McGEE JK, April GC (1982) Chemicals from renewable resources: hemicellulose behavior during organosolv delignification of southern yellow pine. Chem Eng Comm 19:1–3

Meng L-Y, Ma M-G, Ji X-X (2019) Preparation of lignin-based carbon materials and its application as a sorbent. Mater 12:1111

Mielenz JR (2001) Ethanol production from biomass: technology and commercialization status. Curr Opin Microbiol 4(3):324–329

Minu K, Kurian, Jiby K, Kishore VVN (2012) Isolation and purification of lignin and silica from the black liquor generated during the production of bioethanol from rice straw. Biomass Bioenerg 39(SI):210–217

Mohan D, Pittman CU, Steele P (2006) Pyrolysis of wood/biomass for bio-oil: a critical review. Energ Fuels 20:848–889

Molina J, Sikora M, Garud N, Flowers JM, Rubinstein S, Reynolds A, Purugganan MD (2011) Molecular evidence for a single evolutionary origin of domesticated rice. Proc Natl Acad Sci 108(20):8351–8356

Moncada J, Johnny A, Tamayo, Carlos A, Cardona A (2014) Integrating first, second and third generation biorefineries: incorporating microalgae into the sugarcane biorefinery. Chem Eng Sci 118:126–140

Mordor Intelligence (2021) Kraft lignin products market—growth, trends, and forecast (2020–2025)

Mosier N, Hendrickson R, Ho N, Sedlak M, Ladisch MR (2005) Optimization of pH controlled liquid hot water pretreatment of corn stover. Bioresour Technol 96(18):1986–1993

Mousavioun P, Doherty WOS (2010) Chemical and thermal properties of fractionated bagasse soda lignin. Ind Crops Prod 31:52–58

Mussatto SI, Dragone GM (2016) Biomass pretreatment, biorefineries and potential products for a bioeconomy development. In: Biomass fractionation technologies for a lignocellulosic feedstock based biorefinery, 1st edn., pp 1–22

Naae DG, Whittington EL, Ledoux AW (1988) Surfactants from lignin. United States Patent. 4,739,040

Nanda S, Mohanty P, Pant KK, Naik S, Kozinski JA et al (2013) Characterization of north american lignocellulosic biomass and biochars in terms of their candidacy for alternate renewable fuels. Bioenerg Res 6:663–677

Nirmale TC, Kale BB, Varma AJ (2017) A review on cellulose and lignin based binders and electrodes: small steps towards a sustainable lithium ion battery. Int J Biol Macromol

Nitos C, Rova U, Christakopoulos P (2018) Organosolv fractionation of softwood biomass for biofuel and biorefinery applications. Energies 11:50

Nizami AS, Rehan M, Waqas M, Naqvi M, Ouda OKM, Shahzad K, Pant D (2017) Waste biorefineries: enabling circular economies in developing countries. Bioresour Technol 241:1101–1117

Nsimba RY, Mullen CA, West NM, Boateng AA (2012) Structure–property characteristics of pyrolytic lignins derived from fast pyrolysis of a lignin rich biomass extract. ACS Sustain Chem Eng 1:260–267

Ochi S (2006) Development of high strength biodegradable composites using Manila hemp fiber and starch-based biodegradable resin. Compos Part A Appl Sci Manuf 37:1879–1883

Olsson M (2015) Preparation of lignin die. Experimental and statistical study of the biodiesel preparation process from a pulp- and paper industry residual product. Ph.d. Thesis (Karlstads universitet 651 88 Karlstad), pp 1–41

Ozdenkçi K, Blasio C, Muddassar HR, Melin K, Oinas P, Koskinen J, Järvinen M (2017) A novel biorefinery integration concept for lignocellulosic biomass. Energ Convers Manage 149:974–987

Parajuli R, Dalgaard T, Jørgensen U, Adamsen APS, Knudsen MT, Birkved M, Gylling M, Schjoerring JK (2015) Biorefining in the prevailing energy and materials crisis: a review of sustainable pathways for biorefinery value chains and sustainability assessment methodologies. Renew Sustain Energ Rev 43:244–263

Pereira A, Hoeger IC, Ferrer A, Rencoret J, Rio JCD, Kurus K, Rahikainen J, Kellock M, Gutierrez A, Rojas OJ (2017) lignin films from spruce, eucalyptus, and wheat straw studied with electroacoustic and optical sensors: effect of composition and electrostatic screening on enzyme binding. Biomacromolecules 18(4):1322–1332

Perez J, Muñoz-Dorado J, De La Rubia T, Martínez J (2002) Biodegradation and biological treatments of cellulose, hemicellulose and lignin: an overview. Int Microbiol 5(2):53–63

Pinto PCR, Borges da Silva EA, Rodrigues AE (2012) In: Baskar C, Baskar S, Dhillon RS (eds) Biomass conversion: the interface of biotechnology, chemistry and materials science. Springer Berlin Heidelberg, Berlin, pp 381–420

Pizzi A (2006) Recent development in eco-efficient bio-based adhesives for wood bonding: opportunities and issues. J Adhes Sci Technol 20:829–846

Prasad S, Singh A, Joshi HC (2007) Ethanol as an alternative fuel from agricultural, industrial and urban residues. Resour, Conser Recycl 50(1):1–39

Quraishi S, Martins M, Barros AA, Gurikov P, Raman SP, Smirnova I, Duarte AR, Reis RL (2015) Novel non-cytotoxic alginate–lignin hybrid aerogels as scaffolds for tissue engineering. J Supercrit Fluid 105:1–8

Ragauskas AJ, Beckham GT, Biddy MJ, Chandra R, Chen F, Davis MF, Wyman CE (2014) Lignin valorization: improving lignin processing in the biorefinery. Science 344(6185):1246843–1246843

Rana M, Islam MN, Agarwal A, Taki G, Park S-J, Dong S, Jo Y-T, Park J-H (2018) Production of phenol-rich monomers from kraft lignin hydrothermolysates in basic-subcritical water over MoO3/SBA-15 catalyst. Energ Fuel 32(11):11564–11575

Ravindran R, Jaiswal AK (2016) Exploitation of food industry waste for high-value products. Trends Biotechnol 34(1):58–69

Redman LV (1923) New applications of phenol resins in the chemical and allied industries. Ind Eng Chem 677

Restolho JA, Prates A, Pinho MN, Afonso MD (2009) Sugars and lignosulphonates recovery from eucalyptus spent sulphite liquor by membrane processes. Biomass Bioenerg 33:1558–1566

Rocha GJM, Martin C, da Silva VFN, Gomez EO, Goncalves AR (2012) Mass balance of pilot-scale pretreatment of sugarcane bagasse by steam explosion followed by alkaline delignification. Bioresour Technol 111:447–452

Rojas OJ, Stubenrauch C, Lucia L, Habibi Y (2009) Interfacial properties of sugarbased surfactants. In: Hayes D, Kitamoto D, Solaiman D, Ashby R (eds) Bio-based surfactants and detergents: synthesis, properties and applications, AOCS Press, Urbana, pp 457–480

Rowell RM (2012) Handbook of wood chemistry and wood composites. CRC Press, Bio-based Adhesives

Ruiz E, Cara C, Manzanares P, Ballesteros M, Castro E (2008) Evaluation of steam explosion pre-treatment for enzymatic hydrolysis of sunflower stalks. Enzyme Microb Technol 42:160–166

Sadeghifar H, Venditti R, Jur J, Gorga RE, Pawlak JJ (2016) Cellulose-lignin biodegradable and flexible UV protection film. ACS Sustain Chem Eng 5(1):625–631

Sarkar S, Adhikari B (2000) Lignin-modified phenolic resin: synthesis optimization, adhesive strength, and thermal stability. J Adhes Sci Technol 14(9):1179–1193

Schuler J, Hornung U, Kruse A, Dahmen N, Sauer J (2017) Hydrothermal liquefaction of lignin. J Biomater Nano 8:96–108

Shen DK, Gu S, Luo KH, Wang SR, Fang MX (2010) The pyrolytic degradation of wood-derived lignin from pulping process. Biores Technol 101(15):6136–6146

Shewa WA, Lalman JA, Chaganti SR (2016) Heath, DD,: Electricity production from lignin photocatalytic degradation byproducts. Energy 111:774–784

Shim E (2010) Coating and laminating processes and techniques for textiles. In: Smith WC (ed) Smart textile coatings and laminates. Woodhead Publishing Limited, pp 10–41

Shimzu M, Yoshihito W, Hideo O, Takahi H, Katsuomi T (1992) Synthesis of alkyl substituted p-benzoquinones from the corresponding phenols using molecular oxygen catalyzed by copper(II) chloride-amine hydrochloride systems. Bull Chem Soc Jpn 65:1522–1526

Singh S, Ghatak HR (2017) Vanillin formation by electrooxidation of lignin on stainless steel anode: kinetics and byproducts. J Wood Chem Technol 37(6):407–422

Slaghek TM, van Vliet D, Giezen C, Haaksman IK (2017) US patent application no. 15/125, 268

Smook GA (2002) Kraft pulping. In: Smook GA (ed) Handbook for pulp and paper technologists. Angus Wilde Publications, Vancouver, pp 75–85

Soderholm P, Lundmark R (2009) The development of forest-based biorefineries: implications for market behavior and policy. Forest Prod J 59:1–2

Souto F, Calado V, Pereira Jr N (2018) Lignin-based carbon fiber: a current overview. Mater Res Express

Speight, JG.: Synthetic fuels handbook: Properties, process and performance. The McGraw-Hill Companies, inc. (2008).

Sreekrishnan MATR (2001) Aquatic toxicity from pulp and peper mill effluenes a review. Adv Environ Res 5(2):175–196

Stanzione III, JF, Sadler JM, La Scala JJ, Reno KH, Wool RP (2012) Vanillin-based resin for use in composite applications. Green Chem 14(8):2346

Stevens ES, Klamczynski A, Glenn GM (2010) Starch-lignin foams. Express Polym Lett 4:311–320

Stewart D (2008) Lignin as a base material for materials applications: chemistry, application and economics. Ind Crop Prod 27(2):202–207

Suhas PJM, Carrott MML, Carrott R (2007) Lignin from natural adsorbent to activated carbon: a review. Bioresour Technol 98:2301–2312

Sun D, Lu T, Xiao F, Zhu X, Sun G (2017) Formulation and aging resistance of modified bio-asphalt containing high percentage of waste cooking oil residues. J Clean Prod 161:1203–1214

Tamaki Y, Mazza G (2010) Measurement of structural carbohydrates, lignins, and micro-components of straw and shives: effects of extractives, particle size and crop species. Ind Crop Prod 31:534–541

Technavio (2017) Global lignin products market 2017–21. Retrieved from: https://www.technavio.com/report/global-lignin-products-market?tnplus

Tejado A, Peňa C, Labidi J, Echeverria JM, Mondragon I (2007) Physico chemical characterization of lignins from different sources for use in phenol-formaldehyde resin synthesis. Bioresour Technol 98(8):1655–1663

Ten E, Vermerris W (2015) Recent developments in polymers derived from industrial lignin. J Appl Polym Sci

Thakur S, Chaudhary J, Kumar V, Thakur VK (2017) Progress in pectin based hydrogels for water purification: trends and challenges. J Environ Manage 238:210–223. https://www.sciencedirect.com/science/journal/03014797/238/supp/C

Thakur VK, Thakur MK (2014) Recent trends in hydrogels based on psyllium polysaccharide: a review. J Clean Prod 82(1):1–15

Thomsen MH (2005) Complex media from processing of agricultural crops for microbial fermentation. Appl Microbiol Biotechnol 68(5):598–606

Timothy WJ (2012) Technological, commercial, organizational and social uncertainties of a novel process for vanillin production from lignin. Simon Fraser University, Canada

Transparency: Market Research, https://www.transparencymarketresearch.com/lignin-based-products-market.html

Tsang YF, Kumar V, Samadar P, Yang Y, Lee J, Ok YS, Songf H, Kim K-H, Kwon EE, Jeon YJ (2019) Production of bioplastic through food waste valorization. Environ Int 127:625–644

Tuck CO, Pérez E, Horváth IT, Sheldon RA, Poliakoff M (2012) Valorization of biomass: deriving more value from waste. Science 337:695

Vengal JC, Srikumar M (2005) Processing and study of novel lignin-starch and lignin-gelatin biodegradable polymeric films. Trends Biomater Artif Organs 18:237–241

Villar JC, Caperos A, Garcia-Ochoa F (2001) Oxidation of hardwood kraft-lignin to phenolic derivatives with oxygen as oxidant. Wood Sci Tech 35:245–255

Vinardell MP, Ugartondo V, Mitjans M (2008) Potential applications of antioxidant lignins from different sources. Ind Crop Prod 27:220–223

Visthal A, Kraslawski A (2011) Challenges in industrial application of technical lignins. BioResources 6(3):3547–3568

van Vliet D, Slaghek T, Giezen C, Haaksman I (2016) Lignin as a green alternative for bitumen. In: Proceeding of the 6th eurasphalt and eurobitume congress. Prague, Czech Republic, 1–3 June

Wang G, Chen H (2016) Enhanced lignin extraction process from steam exploded corn stalk. Sep Purif Technol 157:93–101

Watkins D, Nuruddin M, Hosur M, Tcherbi-Narteh A, Jeelani S (2014) Extraction and characterization of lignin from different biomass resources. J Mater Res Technol 4(1):26–32

Weetall HH, Forsyth BD, Hertl WA (1985) A direct fuel cell for the production of electricity from lignin. Hertl Biotechnol Bioeng 27:972–979

Windsten P, Kandelbauer A (2008) Adhesion improvement of lignocellulosic products by enzymatic pre-treatment. Biotechnol Adv 26:379–386

Wising U, Stuart P (2006) Identifying the Canadian forest biorefinery. Pulp Pap Canada 107(6):25–30

Wooley R, Ruth M, Sheehan J, Ibsen K, Majdeski H, Galvez A (1999) Lignocellulosic biomass to ethanol process design and economics utilizing co-current dilute acid prehydrolysis and enzymatic hydrolysis current and futuristic scenarios. Biotechnology Center for Fuels and Chemicals, NREL/TP-580-26157

Xie S, Li Q, Karki P, Zhou P, Yuan JS (2017) Lignin as renewable and superior asphalt binder modifier. ACS Sustain Chem Eng 2017(5):2817–2823

Xu C, Ferdosian F (2017) Conversion of lignin into bio-based chemicals and materials. Springer

Xuan TD, Sakanishi K, Nakagoshi N, Fujimoto S (2012) Biorefinery: concepts, current status, and development trends. Int J Biom Renew 1–8

Yang BS, Kang K-Y (2017) Preparation of lignin-based carbon aerogels as biomaterials for nano-supercapacitor. J Korean Phys Soc 71:478–482

Yearla SR, Padmsree K (2016) Preparation and characterisation of lignin nanoparticles: evaluation of their potential as antioxidants and UV protectants. J Exp Nanosci 11(4):289–302

Yoshikawa T, Yagi T, Shinohara S, Fukunaga T, Nakasaka Y, Tago T, Masuda T (2013) Production of phenols from lignin via depolymerization and catalytic cracking. Fuel Process Technol 108:69–75

Zhang QZ, Cai WM (2008) Enzymatic hydrolysis of alkali-pretreated rice straw by Trichoderma reesei ZM4-F3. Biomass Bioenerg 32(12):1130–2113

Zhang M, Xu Y, Li K (2007) Removal of residual lignin of ethanol-based organosolv pulp by an alkali extraction process. J Appl Poly Sci. 106:630–636

Zhang X, Zhang Q, Long J, Xu Y, Wang T, Ma L, Li Y (2014) Phenolics production through catalytic depolymerization of alkali lignin with metal chlorides. BioResources 9:3347–3360

Zhao X, Zhu YZ (2016) Efficient conversion of lignin to electricity using a novel direct biomass fuel cell mediated by polyoxometalates at low temperatures. Chem Sus Chem 9:197–207

Zoia L, King AWT, Argyropoulos S (2011) Molecular weight distributions and linkages in lignocellulosic materials derivatized from ionic liquid media. J Agric Food Chem 59:829–838

Chelating Poly (Amidoxime) and Poly (Hydroxamic Acid) Derived from Co-Polymers of Butyl Acrylate, Acrylonitrile and Cinnamic Acid Used as Metal Ion Sorbents: A Brief Review

Suresh Kumar and Shveta Sharma

Abstract Chelating network polymers are those which form stable complexes with metal ions and exhibit considerable selectivity particularly towards heavy metal ions. The working principal of these networks is similar to those of cation exchanger resins. Tendency to form stable complexes and high selectivity render these polymers useful for water based technologies including purification, separation, enrichment and detoxification. Chelating polymers based on poly(acrylonitrile)[poly(AN)] have been in use since long and most widely used among those are poly(amidoxime) based. Nitrile group in poly(AN) can be conveniently modified to chelating amidoxime functional group by post polymer reactions. A number of polymers thus can be synthesized as single or binary monomer mixtures with acrylonitrile as one component. Another chelating polymer, poly (hydroxamic acid) with high affinity for iron (III) and copper (II) has been synthesized from poly (acrylamide) and poly (acrylate) by reacting it with hydroxylamine in basic aqueous solution. The polymer thus obtained becomes a co-polymer and containing hydroxamic acid groups and unreacted amide and ester groups. Synthesis of such materials opens the ways to explore their multifaceted role and to widen the spectrum of their application including those involving separation, recovery or removal of metal ions. In this piece of information an effort has been made to conduct literature survey on past studies carried on chelating poly (amidoxime) and poly (hydroxamic acid) derived particularly from acrylonitrile, butyl acrylate and cinnamic acid polymers to review their role in metal ion sorption.

Keywords Chelate · Co-polymer · Sorption · Post polymer reaction

S. Kumar (✉) · S. Sharma
Department of Chemistry, Govt. P.G. College, Una, Himachal Pradesh 174303, India
e-mail: sureshchemistry2013@gmail.com

311

1   Introduction

Polymer based chelating networks consist of various cation active anchor groups covalently bonded to the polymer molecules. These anchor groups are uniformly distributed over the entire polymer matrix and perform specific functions. In present case the term '**network**' is particularly used to express cross-linked polymers. Interaction with metal ions occurs by way of co-ordination, chelation, sorption and *ion exchange* processes or combination of these. Chelation is a wider term that includes formation of stable *ring type complexes* by all those polymers which contain functional groups with more than one donor atoms to interact with metal ions. Thus these polymers can be broadly grouped into three categories viz. Polymer based cation exchangers, immobile polymeric supports and polymer based sorbents for extraction or separation of dissolved metal ions from solutions. An important characteristic of these polymers is their insolubility that makes these environmentally stable and compatible and easy to recover after use by simple process like filtration. These are increasingly used in column chromatographic techniques, demineralization of water, detoxification of industrial waste water, water purification in general and other recent separation techniques.

   The working principal of these chelating networks is similar to those of cation exchange resins. Selectivity of these polymers for a particular ion can be enhanced by incorporating chelating groups such as *amidoxim*e and *hydroxamic acids* into their structure. Polymers such as poly(acrylonitrile)[poly(AN)], poly(acrylamide)[poly(AAm), poly(ethyl acrylate)[poly(EA)], poly(butyl acrylate)[poly(BuA] and poly(cinnamic acid)[poly(CiA)] have functional groups those can be easily transformed by post polymer reactions to cation active moieties. Their co-polymers also serve as important precursors for developing such chelating groups on polymer chains in different combinations. Further, their graft co-polymers with naturally occurring polymeric backbones such as cellulose and starch are other excellent materials for such functional group modifications. Synthesis of such materials opens the ways to explore their multifaceted role and to widen the spectrum of their application including those involving separation, recovery or removal of metal ions. Thus in present work efforts have been made to conduct literature survey on past studies carried on chelating poly (amidoxime) and poly (hydroxamic acid) derived particularly from polymers (including graft and co-polymers) based on acrylonitrile, butyl acrylate and cinnamic acid to review their role in metal ion sorption and to discover the fields where there are ample scopes for further research.

2   Literature Survey

Chelating polymers based on poly(AN) have been in use since long and most widely used among those are poly(amidoxime) based. Nitrile group in poly(AN) can be conveniently modified to chelating amidoxime functional group by post polymer

reactions. A number of polymers thus can be synthesized as single or binary monomer mixtures with acrylonitrile as one component. A co-polymer of acrylonitrile (AN) and acrylamide (AAm) [poly (AN-co-AAm)] prepared by chemical initiation method using sodium bisulphite and potassium persulphate redox system and later chemically modified to poly (amidoxime) with hydroxylamine, has been used as achelating sorbent for recovery of toxic heavy metal ions present in aqueous solutions (Jamil et al. 2015). A co-polymer of ternary monomer mixtures has been prepared for use as improved binder for lithium ions based batteries. This polymer derived from poly (acrylic acid-acrylonitrile-butylacrylate)-polystyrene system has exhibited enhanced efficiency as a binder having minute particle size, rigid polymer base, large adhesion power, and smaller contact angle features when compared to unmodified poly (acrylonitrile-butylacrylate) binder (Nguyen and Eun-Suok 2015). Maleic anhydride and acrylonitrile (AN) have been copolymerized by an aqueous-phase precipitation co-polymerization process induced by Na_2SO_3-$K_2S_2O_8$ initiator system and the co-polymers thus obtained have been further utilized to synthesize ultra-filtration hollow fiber membranes (UHFMs) by applying a dry-wet phase inversion technique, the immobilization potential of poly (ethylene glycol) [PEG] on the surface of membrane has been further improved by the reacting of anhydride group with PEG (Nie et al. 2004). A novel chelating resin for selective sorption of Ag (1) from a mixture with other divalent ions like Mg (II), Zn (II), Cd (II), and Ni (II), has been developed from beads based on chloromethylated poly (styrene-divinylbenzene) (CMPS) initially modified by reacting it with dicyandiamide (DCDA) and later by functionalization of nitrile group to amidoxime group (NH_2-C=NOH) by treating with hydroxylamine hydrochloride under basic medium (Wang et al. 2012). Another chelating polymer, poly (hydroxamic acid) with high affinity for Fe (III) and Cu (II) has been synthesized from poly (AAm) by reacting it at room temperature with hydroxylamine in alkaline solution (pH > 12). The polymer thus obtained becomes a co-polymer that contains 70% hydroxamic acid groups (–CONHOH), 25% unreacted amide groups and less than 5% carboxylic acid (–COOH) groups. Preliminary investigation studies reveal that this polymer has inhibitory action on the activity of urease enzyme both in cross-linked and linear forms (Domb et al. 1988). Chelating behaviour of poly(amidoxime-*co*-hydroxamic acid) and poly(N-methyl amidoxime-*co*-N-methyl hydroxamic acid) have been reported by many workers. These polymers, when subjected to batch equilibration process as a function of pH, counter-ion and contact time, have shown high sorption preferences for some trivalent lanthanoid ions such as La(III), Nd(III), Sm(III), Gd(III), and Tb(III) (Alakhras et al. 2005). A novel polymer with amidoxime and hydroxamic acid moieties on same backbone [poly (amidoxime-*co*-hydroxamic acid)] has been used for extraction of uranium from seawater. Poly (amidoxime-co-hydroxamic acid) fibre has been synthesized by the amidoximation of poly (AN). The resultant polymer has reported substantial sorption of uraniumfrom uranium-tricarbonato complex containing solutions and has been found efficient to retain 12.5% uranium present in seawater within 2 s contact time. Poly (amidoxime-co-hydroxamic acid) fibre also has the advantage of being weaved into a cloth with chelating properties (Vernon and Shah

1983). An active packaging material has been prepared from polypropylene-graft-poly(acrylic acid) and polypropylene-graft-poly(hydroxamic acid) based chelating films using laminated photografting technique. This material has surface immobilized metal chelating ligands that make thermodynamically more stable co-ordination compounds with transition metal ions and has been found to exhibit high affinity for Fe (III) (Lin et al. 2016). Kausar, A., has presented a literature survey on types, essential aspects and applications of poly (AN) based nanocomposite materials those can be drawn into fibres. The poly (AN)-carbon nanotubes, poly (AN)-graphene, and poly (AN)-inorganic nanoparticle based nanocomposite fibres with improved characteristics have been credited to interfacial bonding between nanofiller and nitrile groups (Kausar 2019). Poly(acrylonitrile) post functionalized with diethylenetriamine (DTA), produced amine containing resins those have been applied for removal of Fe(III), Pb(II), Hg(II), Zn(II)and Ag(I) found in aqueous media. From the sorption studies of the resins for these ions it can be concluded that high sorption occurs at larger pH values. For metal ions such as Zn(II) and Fe(III), the highest observed sorption values on PAN-DTA150 have been reported to be 1.38 and 1.42 mmol g^{-1}, respectively (Kiani et al. 2011). Chaudhary, B. K., and Farrell, J., have reported chemical modification of poly (AN) fibers to develop cost-effective sorbents for arsenic removal. These fibers have been chemically transformed and cross-linked to more usable form by using a mixture of sodium hydroxide (NaOH) and hydrazine hydrate (Chaudhary and Farrell 2014). For first time an advanced modified poly (AN) membrane embedded with diazoresin-ethylenediaminetetraacetic acid (DR-EDTA) layer has been designed and synthesized. Membrane shows high adsorption capacity particularly for heavy metal ions. The diazoresin-ethylenediaminetetraacetic acid (DR-EDTA) moiety has been found to effectively partition the metal ions like Cu (II), Pb(II), Hg(II) present in wastewater (Zhang et al. 2018). A nanofiber based on phosphorylated poly(AN) [P-PAN] developed by electro spinning process and later modified by chemical grafting, has been observed as a good substrate for metal ion sorption as it exhibits large capacity for adsorption of ions like Pb(II), Cu(II), Ag(I), and Cd(II). Functional groups containing donor atoms such as phosphorous nitrogen and oxygen play the key role in heavy metal ions complexation (Zhao et al. 2015). Ion-exchange adsorbers have been reported to be extensively applied for removal of hazardous fission products and separation of radioisotopes from aqueous waste before being disposed of to the environment. Inorganic exchangers have their own advantages and disadvantages; these are resistant to radiolytic hazards and are selective for other products of radioactive fission, on the other hand these are expensive and are not eco-friendly. Another group of adsorbers include 'Composite inorganic-organic' ion exchangers. In these, inorganic ion exchangers have been modified with organic binding material such as poly (AN), for preparation of particles of bigger size and higher granular strength. Three different sorbents derived from inorganic materials based on granular hexacyanoferrate ion exchanger, have been prepared to remove Cobalt and Caesium ions found in waste water bodies that contain different detergents as complexing agents. Thermal stability and radiation studies reveal that these materials are suitable for environment-responsive treatment of waste (Nilchi et al. 2007). A novel ultrafiltration (UF) nanocomposite membranes based on poly (AN) [PAN]

have been prepared for preferential adsorption of copper ions [Cu(II)] present in aqueous media. These membranes contain goethite nanoparticles (NPs). The highest removal of Cu (II) ions that has been achieved by these membranes is 49.1% and the highest water-permeability has been observed to be 285 LMH/bar (Zahed et al. 2019). A review has been presented on chelating polymer based adsorbents for preferential adsorption of boron found in waste water bodies (Nasef et al. 2014). Silica supported poly(acrylonitrile) has been synthesized and further functionalized to metal ion sorbent, polyacryl(amidoxime), that has been used for recovery of Ga(III) from water (Lu, et al. 2019). The recent developments in the field of polymeric materials based on chelating poly(amidoxime) and poly(hydroxamic acid) include grafted and cross-linked polymer networks with ***ionogenic*** groups those can effectively and selectively partition ions from the surrounding medium. Cellulose provides an excellent such material that can be conveniently grafted with suitable vinyl monomers like acrylonitrile, acrylamide, ethyl acrylate and butyl acrylate. The functional groups in these polymers get readily converted into amidoxime and hydroxamic moieties by post polymer reactions. There have been much earlier developments in the field of grafting of Acrylic acid (AAc) onto cellulose and use of the graft co-polymers thus obtained as ion exchangers and water sorbing agents have been invariably reported (Loría-Bastarrachea et al. 2002). Polymers of acrylonitrile (AN) have been known as an efficient ion exchanger and water adsorbate materials. Dessouic et al. have transformed the filter paper into chelating filter paper by treating the cell-g-poly(AN) with hydroxylamine (Dessouki et al. 1999). The graft co-polymers of AN with cellulose and its derivatives have been reported for their ion exchange properties. There are much earlier developments in the field of grafting of AN onto cellulose, and it is reported that there is a decrease in the water uptake properties of the graft co-polymer compared to native cellulose due to hydrophobic nature of AN (Rao and Kapur 1969). AN, MMA and vinyl pyridine have been grafted onto Rayon by Voinova and his co-workers using Fe(II)–$H_2 O_2$ as initiator and have also reported effect of reducing agents over grafting efficiency. All these polymers have potential groups those can be modified to impart chelating behaviour (Voinova et al. 1981). Pre-radiation technique has been used by Hebeish and his co-workers for grafting of AN, and mixture of some another vinyl monomers onto cotton fabrics (Hebeish and Mehta 1967). Teflon-FEP films have been modified with meth acrylic acid and 4-VP with the use of gamma rays to develop polar membranes for separation processes (Kaur et al. 2010). 1,2 dimethyl poly (5vinyl pyridinium sulphate) and quaternary salts of vinylpryidine grafted cellulose has been reported as ion exchangers (Mazov et al. 1973). Sayed and Hegazy have used LDPF-g-poly (AAc-*co*-4VP) membranes for waste water treatment (Hegazy et al. 1997). Ghanshyam and co-workers have pioneered in synthesizing a large number of graft co-polymers and hydrogels based on natural occurring cellulose with potential applications in metal ion sorption and ion exchange processes (Chauhan et al. 2000a, b, 2002, 2005b; Singh et al. 2007). Starch is carboxymethylated to carboxymethyl starch (CMS), that has been later modified by way of radical grafting with acrylonitrile using ammonium persulphate and N,N,N,N-tetramethylethylenediamine as initiator-accelerator mixture. The process has been repeated to synthesize networks using ethylene glycol dimethacrylate and

N,N-methylenebisacrylamide as cross linkers. Networks thus obtained have been functionalized to amidoxime using hydroxylamine. Sorption behaviour of Fe(II) was thoroughly investigated on the modified polymer (Chauhan et al. 2006). Cellulose grafted with methyl methacrylate using benzoyl peroxide has been used as such polymeric support for metal ion sorption (Chauhan et al. 2005c). Radiation induced grafting of 1-vinyl-2-pyrrolidone (N-VP) onto naturally occurring cellulose, obtained from huge pine needles waste, has been carried out at various intervals of time. Grafting parameters have been optimized. At optimum grafting conditions N-VP has also been graft copolymerized onto some cellulosics such ascyanoethyl cellulose, cellulose phosphate, hydroxypropyl cellulose, and deoxyhydrazino cellulose. Some select graft co-polymers were investigated for Cu(II), Fe(II) and iodine sorption (Chauhan et al. 2005a). Another class of adsorbents for metal ion removal is based upon Corn Stalk, that can be conveniently modified to acquire the desired properties by incorporating groups such as cyano, amino, amidoxime and carboxylic. This group of adsorbents includes graft co-polymers of corn stalk with other monomers that contain potential functional groups for further transformation such as corn stalk-graft-polyacrylamide [CS-*g*-PAM], corn stalk-graft-polyacrylonitrile [CS-*g*-PAN], carboxyl corn stalk-graft-poly(methyl acrylate) [CO CS-*g*-PMA] and amidoxime corn stalk-graft-polyacrylonitrile [AO CS-*g*-PAN]. These polymers have been found to exhibit high preference for Hg (II). Amidoximated, [AO CS-*g*-PAN] has shown highest adsorption capacity for Hg(II) equal to 8.06 mmol g^{-1} (Wang et al. 2016). A wide range chelating polymers of the type poly(amidoxime-hydroxamic acid) have been prepared from graft co-polymers of cellulose with suitable monomers by oximation of the amenable functional groups (Jiao, et al. 2017). Poly(methyl acrylate) [PMA] grafted onto sago starch serves an excellent precursor for the development of chelating poly(hydroxamic acid) based polymers for metal ion sorption. The PMA grafted co-polymer has been prepared by a free-radical copolymerization technique chemically induced by ceric ammonium nitrateinitiator (CAN). Ester group of PMA-grafted co-polymer was further functionalized into chelating hydroxamic acid group (–CONHOH) by reacting the graft co-polymer with hydroxylamine hydrochloride in highly alkaline solution. Characterization of functionalized poly (hydroxamic acid) has been done by FT-IR, DSC, and TG analysis. Presence of hydroxamic acid group (–CONHOH) after functionalization is confirmed from vibrational spectra. The metal ion chelating properties of the synthesized polymer have been finally explored for some metal ions. Polymer exhibited excellent binding preferences for chromium, copper, iron and nickel. The metal ion holding powers of the chelating polymer have been found pH dependent of metal ion solution. The synthesized polymer has exhibited the following selectivity order toward metal ions sorption: Cu (II) > Fe(III) > Cr(III) > Ni(II) > Co(II) > Zn(II) > Cd(II) > As(III) > Pb(II) (Lutfor et al. 2001). Rahman and co-workers have developed a graft co-polymer of kenaf cellulose and poly(AN) by free radical process that was later converted to chelating poly (amidoxime) ligand by amidoximation reaction. The functionalized polymer with amidoxime groups was subjected to sorption of various transition metal ions under different pH of solution. Metal-ligand complex was detected by observing the change

in optical properties of solution. Reflectance spectra of metal-ligand complex exhibited maximum absorbance between 97 and 99.9% at pH 6. Reflectance spectra have been found to increase with increase in concentration of Cu(II) ions resulting into a broad peak at 700 nm observed due to formation of charge transfer complex (CT-complex) involving π-π transition. Polymer has shown excellent adsorption capacity for copper, equal to 326.6 mg g^{-1}. Further, adsorption capacity of the synthesized polymer has also been found to be substantially good for other transition metal ions. Another important feature of the said polymer is its reusability that has been studied by observing seven cycles of sorption-desorption process and for each cycle the sorption and extraction efficiency is recorded (Lutfor et al. 2016). Other monomer of interest for present study is cinnamic acid. At low temperatures, cinnamic acid has been reported to retard ceric ion (CeIV) induced polymerization of acrylonitrile. It has been observed that the polymerization process is induced by Ce (IV) ions, and is essentially terminated by the free radical derived from cinnamic acid by the interaction with Ce(IV) (Patnaik, et al. 1980). An attempt has been made to synthesizecinnamic acid based liquid crystalline star materials bearing mesogens. Polysiloxanes derived from these materials are known to exhibit smectic C phases. These are also capable of being photo chemically cross-linked through the cinnamate group (Ruder et al. 1999). Esters of cinnamic acid have been prepared by reacting it with epoxidized soybean oil and reaction has been catalysed by triphenyl phosphine. Esters thus prepared have been subjected to polymerization with UV light or by chemical initiation using benzoyl tert-butyl peroxide. Epoxidized cinnamate esters can also be homopolymerized by free-radical initiation into a soft and insoluble polymer and co-polymerized with methyl methacrylate, styrene and vinyl acetate. All the polymers thus obtained served as useful precursors for development of chelating networks for metal ion sorption processes (Esen and Küsefoğlu 2003). Side chains in cinnamic acid can be oxidized with some selected oxidants to secondary carboxylic groups to further enhance its metal ion holding capacity. A mixture of imidazolium dichromate, oxalic acid and 60% acetic acid has been used for this purpose. The reaction of above reagents with cinnamic has also been found to inhibit the polymerization of acrylonitrile (Vanangamudi et al. 2007). Poly (cinnamic acid) has also been used to synthesize polymer based fluorescent brighteners such as cinnamic acid-triazene. These compounds have been synthesized via three-step condensation process involving substitution of one of amino compounds of traditional fluorescent brighteners by cinnamic acid followed by polymerization reaction with styrene by Liu (2012). Synthesis of such materials opens the ways to explore their multifaceted role and to widen the spectrum of their application including those involving separation, recovery or removal of metal ions. Graft co-polymers of cinnamic acid onto vinylidne fluoride prepared using benzoyl peroxide as radical initiator have been used to synthesize microporous membranes with improved pore size distribution (Zhang et al. 2012). A novel polymer, N-cinnamoyl chitosan (NCC) has been prepared by reacting chitosan with cinnamic acid. From Thermogravimetric analysis and studies of activation energies of thermal degradation (calculated using Arrhenius equation) of NCC and chitosan polymers, it has been observed that the NCC polymerhas lower thermal stability in comparison to native chitosan polymer (Prashanth

and Tharanathan 2007). Cinnamic acid based monomers are useful chemicals which are obtained from biomass. These polymers contain aromatic rings at β position in addition to α, β-unsaturated carbonyl groups. They have both polystyrene and polyacrylate structures and their homopolymers serve important resource for further modifications to impart chelating properties to these polymers. Poly(acrylate)groups on these can be converted to poly (hydroxamic acid). Besides, these polymers have also been found to show high heat resistance comparable to other plastic materials (Imada et al. 2019). Naturally occurring phenylpropanoids contain a large number of cinnamic acid monomers in native and derivatized forms like esters, aldehydes, nitriles and amides. All these groups are amenable to modifications to amidoxime and hydroxamic acid groups. Further, these polymers can be conveniently subjected to radical induced copolymerization processes with styrene and other related monomers such as acrylates (methyl, ethyl and butyl acrylate). The resulting co-polymers can be further subjected to polymer analogous reactions to modify the potential functional groups and aromatic rings to impart chelating properties (Terao et al. 2018).

3   Methodology

From the literature survey conducted on chelating polymers, it has been established that most of these belong to two broad categories one of which is *amidoxime based* (NH_2-C = NOH) and the other is *hydroxamic acid* (–CONHOH) based. Amidoxime based polymers have been obtained from stock polymers (homopolymer, co-polymer and graft co-polymers) containing potential functional groups such as nitrile (–CN) and amides (–CONH$_2$) and those based on hydroxamic acids are obtained from stock polymers containing ester groups (–COOR) as these groups are amenable to polymer analogous reaction. Synthesis of both involves a common scheme. Hydroxyl amine used for present synthesis has been received as hydroxylamine hydrochloride ($NH_2OH.HCl$), thus initial step of synthesis involves preparation of potassium salt of hydroxylamine (NH_2OK) that is done by reacting hydroxylamine hydrochloride and potassium hydroxide (KOH) in required molar ratio in methanol. The reaction scheme is given below:

$$NH_2OH.HCl + 2KOH \longrightarrow NH_2O^-K^+ + 2H_2O$$
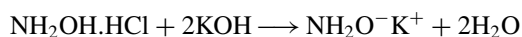
The stock polymer(SP) is then refluxed with the above solution in methanol medium for 4–6 h at 60–70 °C followed by filtration and equilibration with dilute hydrochloric acid. Following reactions take place:

SP----- $(CH_2\text{-}CH\text{-})_n$ + (i) $NH_2O^-K^+$ (ii)HCl $\longrightarrow$ SP-----$[(CH_2\text{-}CH)_{n\text{-}m}\text{- co- }(CH_2\text{-}CH)_m]$

        CN   CN $NH_2\text{-}C=NOH$

    SP-poly (AN)   **SP-poly (AN-co-Amidoxime)**

SP----- $(CH_2\text{-}CH\text{-})_n$ + (i) $NH_2O^-K^+$ (ii)HCl $\longrightarrow$ SP-----$[(CH_2\text{-}CH)_{n\text{-}m}\text{- co- }(CH_2\text{-}CH)_m]$

        $COOC_2H_5$ $COOC_2H_5$ $O=C\text{-}NHOH$

    SP-poly (EA)   **SP-poly (EA-co-Hydroxamic acid)**
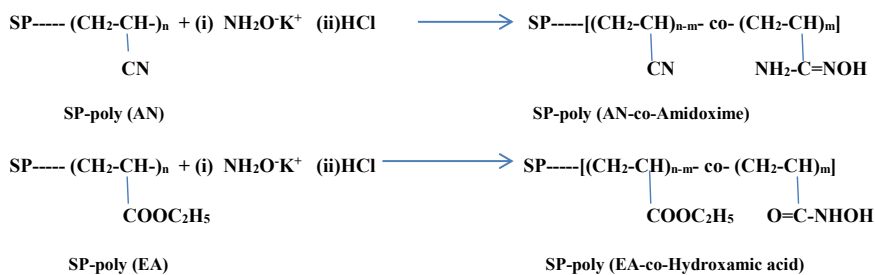
As reported earlier, reactions in polymers never occur to 100% thus the resulting polymer becomes a co-polymer of parent and functionalized polymer with degree on conversion equal to m.

4 Results and Discussion

Both amidoxime and hydroxamic acid groups are bi-dentate chelating ligands with O: and N: as donor atoms and are known to form a stable complexes with metal ions (a dark blood red coloured chelate if metal ions are Fe (III), a chemical test for conversion of nitrile to amidoxime). Stability of these chelates depends upon nature of metal ion, nature of stock polymer, degree of polymer conversion and pH of the solutions under investigations. The plausible mechanism for chelate formation by amidoxime is presented below:

            NH_2 NH_2

----C   + M^{+n} $\longrightarrow$ ----- C $M \quad]^{+n\text{-}1} + H^+$

            NOH   NO

     Poly (Amidoxime)   **Metal ion**   **Metal-Amidoxime Chelate**
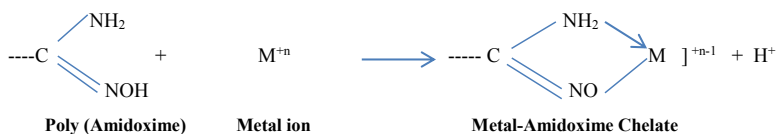
A similar mechanism can be evolved for hydroxamic acid.

5 Conclusions

After having gone through the relevant literature on chelating polymers based upon poly(amidoxime) and poly(hydroxamic acid), it can be concluded that a large number of such polymers were prepared in the past and thoroughly investigated for metal ion sorption properties. Most of researches done in past on these materials have now been used in recent technologies based on purification, separation and enrichment processes. Some recently developed materials based on graft co-polymers and their functionalized chelating poly(amidoxime) and poly(hydroxamic acid) derivatives

have shown a diversified spectrum of applications, and have been proved excellent materials for future technologies. Synthesis of such materials opens the ways to explore their multifaceted role and to widen the spectrum of their application including those involving separation, recovery or removal of metal ions.

References

Alakhras FA, Dari KA, Mubarak MS (2005) Synthesis and chelating properties of some poly (amidoxime-hydroxamic acid) resins toward some trivalent lanthanide metal ions. J Appl Polym Sci 97(2):691–696

Chaudhary BK, Farrell J (2014) Preparation and characterization of homopolymer polyacrylonitrile-based fibrous sorbents for arsenic removal. Environ Eng Sci 31(11):593–601

Chauhan GS, Mahajan S, Guleria LK (2000a) Polymers from renewable resources: sorption of Cu^{2+} ions by cellulose graft copolymers. Desalination 130(1):85–88

Chauhan GS et al (2000b) Evaluation of optimum grafting parameters and the effect of ceric ion initiated grafting of methyl methacrylate on to jute fibre on the kinetics of thermal degradation and swelling behaviour. Polym Degradat Stabil 69(3):261–265

Chauhan GS, Bhatt SS, Kumar S, Lal H (2002) Synthesis and characterization of graft copolymers of hydroxyethyl cellulose with acrylamide and some comonomers. J Polym Mater 19:403–412

Chauhan GS, Singh B, Kumar S (2005a) Synthesis and characterization of N-vinyl pyrrolidone and cellulosics based functional graft copolymers for use as metal ions and iodine sorbents. J Appl Polym Sci 98(1):373–382

Chauhan GS et al (2005b) Synthesis and characterization of reactive graft copolymers of poly (butyl acrylate) and cellulose. Polym Polym Compos 13(5):467–478

Chauhan GS et al (2005c) Graft copolymers of poly (methyl methacrylate) on cellulose and their use as supports in metal ion sorption. Polym Polym Compos 13(1):105–116

Chauhan GS, Jaswal SC, Verma M (2006) Post functionalization of carboxymethylated starch and acrylonitrile based networks through amidoximation for use as ion sorbents. Carbohydr Polym 66(4):435–443

Dessouki AM et al (1999) Chemical reactive filter paper prepared by radiation-induced graft polymerization—I. Radiat Phys Chem 54(6):627–635

Domb AJ, Cravalho EG, Langer R (1988) The synthesis of poly (hydroxamic acid) from poly (acrylamide). J Polym Sci, Part a: Polym Chem 26(10):2623–2630

Esen H, Küsefoğlu SH (2003) Photolytic and free-radical polymerization of cinnamate esters of epoxidized plant oil triglycerides. J Appl Polym Sci 89(14):3882–3888

Hebeish A, Mehta PC (1967) Grafting of acrylonitrile on cellulosic materials by tetravalent cerium1. Text Res J 37(10):911–913

Hegazy E-SA et al (1997) Anionic/cationic membranes obtained by a radiation grafting method for use in waste water treatment. Polym Int 43(4):321–332

Imada M et al (2019) Unique acrylic resins with aromatic side chains by homopolymerization of cinnamic monomers. Commun Chem 2(1):1–9

Jamil SNAM, Khairuddin M, Daik R (2015) Preparation of acrylonitrile/acrylamide copolymer beads via a redox method and their adsorption properties after chemical modification. e-Polymers 15(1):45–54

Jiao C et al (2017) Synthesis of a poly (amidoxime-hydroxamic acid) cellulose derivative and its application in heavy metal ion removal. RSC Adv 7(44):27787–27795

Kaur I et al (2010) Gamma-radiation-induced grafting of binary mixture of methacrylic acid and 4-vinyl pyridine onto Teflon-FEP film as an effective polar membrane for separation processes. Nuclear Instrum Methods Phys Rese Sect B: Beam Interact Mater Atoms 268(10):1642–1652

Kausar A (2019) Polyacrylonitrile-based nanocomposite fibers: a review of current developments. J Plast Film Sheeting 35(3):295–316

Kiani GR, Sheikhloie H, Arsalani N (2011) Heavy metal ion removal from aqueous solutions by functionalized polyacrylonitrile. Desalination 269(1–3):266–270

Lin Z, Decker EA, Goddard JM (2016) Preparation of metal chelating active packaging materials by laminated photografting. J Coat Technol Res 13(2):395–404

Liu J (2012) A study of the optical properties of triazene-cinnamic acid polymeric fluorescent brighteners. Appl Mech Mater 184. Trans Tech Publications Ltd.

Loría-Bastarrachea MI, Carrillo-Escalante HJ, Aguilar-Vega MJ (2002) Grafting of poly (acrylic acid) onto cellulosic microfibers and continuous cellulose filaments and characterization. J Appl Polym Sci 83(2):386–393

Lu Siming et al (2019) Amidoxime functionalization of a poly (acrylonitrile)/silica composite for the sorption of Ga (III)—application to the treatment of Bayer liquor. Chem Eng J 368:459–473

Lutfor MR et al (2001) Synthesis and characterization of poly (hydroxamic acid) chelating resin from poly (methyl acrylate)-grafted sago starch. J Appl Polym Sci 79(7):1256–1264

Rahman ML et al (2016) Efficient removal of transition metal ions using poly (amidoxime) ligand from polymer grafted kenaf cellulose. RSC Adv 6(1):745–757

Mazov MY et al (1973) Synthesis of graft polymers of cellulose with quaternary salts of 2-methyl-5-vinylpyridine. Fibre Chem 4(3):272–275

Nasef MM, Nallappan M, Ujang Z (2014) Polymer-based chelating adsorbents for the selective removal of boron from water and wastewater: a review. React Funct Polym 85:54–68

Nguyen MHT, Oh E-S (2015) Improvement of the characteristics of poly (acrylonitrile–butylacrylate) water-dispersed binder for lithium-ion batteries by the addition of acrylic acid and polystyrene seed. J Electroanal Chem 739:111–114

Nie F-Q et al (2004) Acrylonitrile-based copolymers containing reactive groups: synthesis and preparation of ultrafiltration membranes. J Membr Sci 230(1–2):1–11

Nilchi A et al (2007) Preparations of PAN-based adsorbers for separation of cesium and cobalt from radioactive wastes. Appl Radiat Isot 65(5):482–487

Patnaik SN et al (1980) Retardation of cerium (IV)-initiated polymerization of acrylonitrile by cinnamic acid. J Macromol Sci: Part A-Chem 14(6):899–906

Prashanth KVH, Tharanathan RN (2007) Chitin/chitosan: modifications and their unlimited application potential—an overview. Trends Food Sci Technol 18(3):117–131

Rao SR, Kapur SL (1969) Grafting of acrylonitrile onto cellulose initiated by ceric ion. J Appl Polym Sci 13(12):2649–2656

Ruder SM, Allen SD, Alsobrook JA (1999) Synthesis of liquid crystalline star materials bearing mesogens derived from cinnamic acid. Abstracts of papers of the American chemical society, vol 217, 1155 16th st., NW, Washington, DC 20036 USA: Amer Chemical Soc

Singh B et al (2007) Synthesis, characterization and swelling responses of pH sensitive psyllium and polyacrylamide based hydrogels for the use in drug delivery (I). Carbohydr Polym 67(2):190–200

Terao Y, Satoh K, Kamigaito M (2018) Controlled radical copolymerization of cinnamic derivatives as renewable vinyl monomers with both acrylic and styrenic substituents: reactivity, regioselectivity, properties, and functions. Biomacromol 20(1):192–203

Vanangamudi G et al (2007) Kinetics of oxidation of some substituted cinnamic acids by imidazolium dichromate in the presence of oxalic acid. Asian J Chem 19(2):1341

Vernon F, Shah T (1983) The extraction of uranium from seawater by poly (amidoxime)/poly (hydroxamic acid) resins and fibre. Reactive Polym Ion Exchan Sorbents 1(4):301–308

Voinova GU, Morin BP, Br IP (1981) USOVA and ZA ROGOVIN. Cell Chem Technol 15:269

Wang Y et al (2012) Preparation of a novel chelating resin containing amidoxime–guanidine group and its recovery properties for silver ions in aqueous solution. Chem Eng J 209:394–400

Wang Y-T et al (2016) Preparation of corn stalk-based adsorbents and their specific application in metal ions adsorption. Chem Pap 70(9):1171–1184

Zahed SSH, Khanlari S, Mohammadi T (2019) Hydrous metal oxide incorporated polyacrylonitrile-based nanocomposite membranes for Cu (II) ions removal. Separ Purif Technol 213:151–161

Zhang X, Meng H, Di Y (2012) Synthesis and characterization of cinnamic acid-grafted poly (Vinylidene Fluoride) microporous membranes. Energy Procedia 17:1850–1857

Zhang X et al (2018) Advanced modified polyacrylonitrile membrane with enhanced adsorption property for heavy metal ions. Sci Rep 8(1):1–9

Zhao R et al (2015) Preparation of phosphorylated polyacrylonitrile-based nanofiber mat and its application for heavy metal ion removal. Chem Eng J 268:290–299

Stabilization of Expansive Soil with Thermal Power Plant Waste (Fly Ash and Coal Bottom Ash)—A Review

Omkar Prakash Navagire, Shashi Kant Sharma ⓘ, and Dadi Rambabu ⓘ

Abstract Soil Stabilization is a replacement of the additives materials chemically or mechanically which is improve the soil properties than the natural Soil. Generally, Cement, Lime, GGBS, Fly ash, and Coal bottom ash, etc. are used for the Stabilization of Soil. Out of these materials, Fly ash and Coal bottom ash are obtained from the thermal power plant. In India, 226.13 million tons of Fly ash and Coal bottom ash are generated per annum from thermal plants. Contrary, Fly ash and Coal bottom ash contains pozzolanic properties which improve the strength properties of Soil. So, these materials are used in construction work, and ground improvement techniques. The percentage of improvement in the properties are observed by review is according to some reviewers says 30% of Fly ash and CBA gives Maximum Dry Density values. And the maximum UCS value is obtained at 30% Fly ash and Coal bottom ash greater than the conventional limit. The CBR value is increased greater than the Natural soil which is suitable for pavement design or construction. Normally the studies focus on the use of either fly ash or coal bottom ash individually. This review intends to find out the effect of these two materials either individually or in combination with other materials, like fibers, cement, lime, etc. on expansive soils. Hence the focus would be to find out the maximum beneficial utilization of these materials in expansive soils.

Keywords Black cotton soil · Expansive soil · Soil Stabilization · Fly ash · Coal bottom ash

O. P. Navagire (✉) · S. K. Sharma · D. Rambabu
DR B R Ambedkar National Institute of Technology, Jalandhar, Punjab, India
e-mail: omkarpn.gg.19@nitj.ac.in

S. K. Sharma
e-mail: sharmask@nitj.ac.in

D. Rambabu
e-mail: dadir.ce.19@nitj.ac.in

1 Introduction

Soil is the sedimentation of parent rock by the physical and chemical weathering or disintegration. Generally, the soil is classified into two main parts organic soil and inorganic soil, organic soil contains more than 65% of organic parameters or minerals (like plants residue, skeletons or shells, and small organisms), and inorganic soil derived from parent rock by physical and chemical weathering. In India, both types of soils are deposited in different forms, Alluvial soil, black soil, red and yellow soil, laterite soil, mountain soil, forest soil marine soil. Out of these approximately 51.8 million hectares of the land area surround by Expansive soil (mostly Black Cotton soil). Expansive soils, which are also called swell-shrink soil, tend to shrink and swell with variation in moisture content. As a result of this variation in the soil, significant distress occurs in the soil, which is subsequently followed by damage to the overlying structures. During periods of greater moisture, like monsoons, these soils imbibe the water, and swell; subsequently, they become soft and their water holding capacity diminishes. As opposed to this, in drier seasons, like summers, these soils lose the moisture held in them due to evaporation, resulting in their becoming harder. Generally found in semi-arid and arid regions of the globe, these types of soils are regarded as potential natural hazards—if not treated, these can cause extensive damage to the structures built upon them, as well causing a loss in human life. Soils whose composition includes the presence of montmorillonite, in general, display these kinds of properties. Tallied in billions of dollars annually worldwide, these soils have caused extensive damage to civil engineering structures. To overcome these drawbacks some researchers' approach to soft subgrades stabilization removes the loose soil, and replaces it with strong materials like crushed particles of rock. The high cost of replacement caused highway contractors to estimate alternative methods of highway construction on soft subgrades. One approach is to use the chemical to stabilize the soft subgrade. Instead of using the chemical product, fly ash and bottom ash are some of the residues that offer more economical alternatives for a wide range of soil stabilization applications (Table 1; Fig. 1).

2 Industrial Waste Materials (Fly Ash and Coal Bottom Ash)

In India, the thermal power plant is the largest source of electrical power, and about ¾th part of the electricity consumed in India is produced by thermal power plants. Approximately 75 Thermal power plants generate electricity at the present condition in India and during the power generation in plants coal combustion, large amounts of waste ash are created along with hazardous carbon dioxide and other gases. The fine particle of ash that rises with the flue gases is called as Fly ash while the heavier ash that settles down in the bottom is called Coal bottom ash. These refer to the part of the non-combustible residues of Coal combustion. These are very harmful

Table 1 Properties of expansive soil (Katti 1979)

Description	Range of value (%)
Specific gravity	2.7–2.9
Liquid limit (%)	40–100
Plastic limit (%)	20–50
Plasticity index (%)	20–50
Shrinkage limit (%)	8–18
Maximum dry density (t/m^3)	1.3–1.7
Optimum moisture content (%)	18–30
Soil group symbol (I.S)	CH
Degree of shrinkage (wet volume)	40–50
Volumetric shrinkage (dry volume)	200–300
Size of shrinkage cracks (%) (in summer)	10 cm (wide), 3 m (deep)
Volumetric expansion (rainy season)	60% (in horizontal) 30% (in vertical)
Free swell index (%)	70–300

Fig. 1 Black cotton soil

to the environment and living things. The disposal of fly ash and coal bottom ash is a big problem. So, the constructions field utilizes industrial waste materials in the construction work due to the presence of lime and silica in them. The European Coal Combustion Products Association Calculate the use of Coal bottom ash in the construction work at 46% and the use of fly ash at 43%. Coal bottom ash applications

(a)   (b)
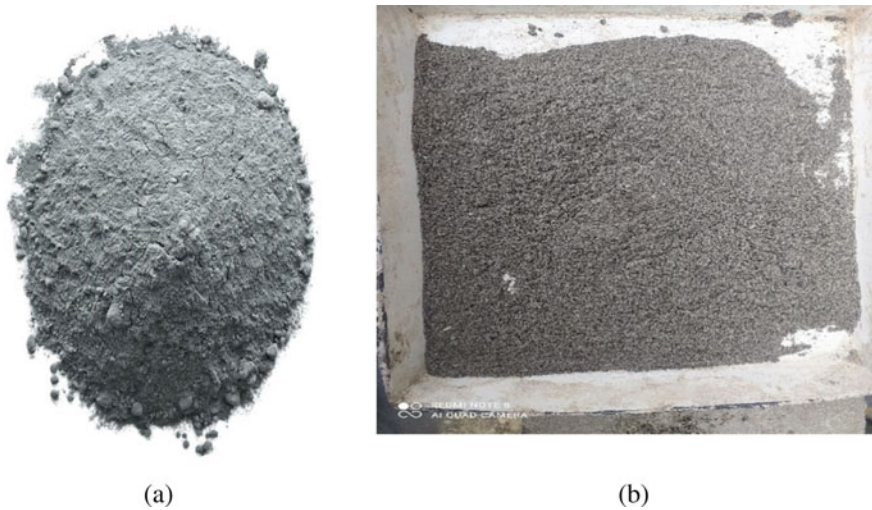
Fig. 2 **a** Fly ash and **b** coal bottom ash

come in filler material for structural applications and embankments, aggregate in road
bases, pavement, sub-bases, and lightweight concrete, in the production of cement.
The chemical makeup of fly ash and bottom ash varies significantly and is dependent
on the source and composition of the coal being burned.

This paper reviews the stabilization of expensive soil with thermal power plant
waste (Fly ash and Coal bottom ash) by evaluating their engineering properties, like
maximum dry density, Compressive strength, and California bearing ratio (Fig. 2).

3 Review of Research Paper

Engineering properties of soils are very essential parameters to be analyzed the
suitability of the soil for sub-base formation of roads, tunnels, stability of the slopes,
etc.

3.1 Compaction Tests

Compaction means the removal of air voids. This test was used to find out the
maximum dry density (MDD) soil at Optimum Moisture Content (OMC) of the
Soil-mix. The OMC of the soil shows that the particular water content at which the
soil should be compacted to achieve the Maximum dry density of the Soil. If the
compacting effort applied is less, the OMC increases, and the value can again be

found experimentally/estimated. In the field compaction test, the compacting moisture content is first controlled at OMC and the adequacy of rolling or compaction is controlled by checking the dry density achieved and comparing it with the maximum dry density. Thus, compaction test results (OMC and maximum dry density) are used in the field control test in the compaction projects. Compaction, in general in considered most useful in the preparation of subgrade and other pavement layers and construction of embankments to increase stability and to decrease settlement. There is also a soil classification method based on the maximum dry density in the standard (proctor compaction test lower values indicating weaker soil).

　　Hakari and Puranik (2012), investigated the behavior of black cotton soil with fly ash by the observation of results of standard proctor test the variation of Dry density and moisture content value varying with the addition of Dry Fly Ash in Black Cotton Soil. The Optimum values of Maximum Dry Density and Optimum moisture content on 30–40% Fly ash. Fly ash is a suitable stabilizer to improve the properties of Black Cotton Soil. Devi et al. studied the Stabilization of soil with Coal Bottom Ash at different percentages. The result of the standard compaction test gives the MDD and OMC. MDD increases at 30% CBA 14.12% as compared to natural soil. The MDD and OMC at 30% CBA is 2.46 g/cc and 10% respectively (Devi et al. 2018). Ramlakhan et al. (2013) investigated the black cotton stabilization with fly ash content, the result of the compaction test show that the moisture content of Soil-fly ash combination increases with increases the percentage of Fly ash in a soil sample and the maximum dry density of the Soil-Fly ash combination is decreases with increases the Fly ash. Sudhakaran et al. (2018), investigated the soil stabilization of Black cotton soil with Coal bottom ash, the result of the compaction test shows that the Maximum Dry Density increases with the increased Bottom ash content in Soil, and OMC decreases with the addition of BA in soil up to 30% BA beyond 30% of CBA increases water content. The addition of excess amount coal bottom ash in soil then decreasing the MDD because bottom ash having low specific gravity compared to black cotton soil. Decreasing water content shows that black cotton soil can be stabilized with lower water content. Increasing MDD gives the information of suitability of soil-BA mixture for stabilization. Osinubi (2000), investigated the soil stabilization of black cotton soil with CBA at a different percentage, maximum Dry Density found at Soil-30% CBA combination beyond that MDD falls. Patil (Patil 2020), studied the soil stabilization soil with the fly ash. Maximum dry density increases the increasing the fly ash in the soil. The value of MDD and OMC is varying with the CBA addition in soil. Murmu et al. (2020), studied the soil stabilization of black cotton soil with fly ash, the results of the compaction test show that the addition of fly ash in Black cotton soil MDD decreasing up to a certain limit and then slightly increases and OMC increases up to 10% fly ash and then falls. Reddy et al. (2018), studied the behavior of black cotton soil stabilized with fly ash, the results of the compaction test show that the MDD of the Soil-Fly ash mixture increases with the increased fly ash in the mixture. The MDD increases 30% and OMC 14% greater than the natural soil. Mohanty (2018), studied soil stabilization of Black cotton soil with coal bottom ash, MDD and OMC obtained from compaction test on the Black

cotton soil-fly ash mixture. The MDD improve from 19 to 21 kN/m^3. OMC decreases 14–7%.

3.2 Unconfined Compressive Strength

The Unconfined compressive strength test is one of the methods to find the strength parameters of the soil, test performs to find the compressive strength of the soil sample. The sample of soil and additives size is 38 mm diameter and 76 mm long as per the IS 2720, part 10. The following review paper gives an idea about the compressive strength of black cotton soil and stabilizing agent.

Hakari and Puranik (2012), studied the soil stabilization material used for study Black cotton soil and Fly ash. The UCS test performs on soil-fly ash combination, UCS strength of the combination increases with increases the curing period of sample. The maximum value of the UCS test comes on 28 days. The strength of the UCS sample increases with the addition of fly ash in the soil. Devi et al. (2018), studied expansive soil stabilized with coal bottom ash at a different percentage. UCS test is used to calculate the Undrained Shear Strength. UCS test is given the strength of the soil by the addition of 30% of Coal bottom ash the value of UCS is more than the conventional value of the natural soil UCS. Ramlakhan et al. (2013) investigated the soil stabilization of black cotton soil with coal bottom ash is pointed. Compressive strength obtained from UCS test of soil-CBA mixture at different curing periods the maximum 90 days. The strength of the Soil-CBA mixture improves the addition of coal bottom ash in the soil. Maximum UCS value comes at 30% coal bottom ash and it reduces to 40% addition of coal bottom ash. Patel and Mahiyar (2014), studied expansive soil stabilized by the coal bottom ash. The UCS value of the Soil increasing with increasing Coal bottom ash percentage in the expansive soil. Jose et al. (2018) investigated the study of black cotton soil stabilized with fly ash, Study various strength parameters of soil. The UCS value of black cotton soil is increasing with increasing coal bottom ash in the soil with different curing periods. Maximum UCS value of Soil-Fly ash comes on 28 Days on Soil + 20%Fly ash mix. The UCS value of mix increases Day by Day due to the pozzolanic reactivity of Fly ash. Mahadevi (2017) investigated the Soil stabilization of black cotton soil with fly ash, analyzed of strength parameter of soil + %fly ash. The UCS value of Soil + Fly ash increases with increasing the percentage of fly ash. 30% of fly ash gives the maximum value of the UCS test. Patil (2020) investigated, black cotton soil stabilized with the fly ash, suitability of fly ash in the civil construction world is based on strength parameters of the Soil + Fly ash mix. The strength of the Black soil increases with the increase Fly ash in the soil. The maximum value of UCS is found on 15% of fly ash. The fly ash improves the strength of black cotton soil so fly ash is utilized in civil construction work.

3.3 California Bearing Ratio (CBR)

The CBR test of a soil mix was conducted in the laboratory as per IS 2720 (part XXI) 1979. CBR test gives the thickness of pavement and bearing capacity of the soil. Following review, the paper performs a CBR test on various combinations to find the bearing capacity of soil and thickness of pavement.

Hakari and Puranik (2012), investigated the soil stabilization investigation of black cotton soil, and fly ash is used to stabilize the black cotton soil. Black cotton soil having a low CBR value and it is not suitable for pavement and road construction, Stabilization of expansive soil with fly ash improves the bearing capacity of the soil as compared to the natural soil. CBR value increases of Soil + Fly ash mix with the increasing the Fly ash up to 30% and decreasing CBR value further addition of Fly ash in the mix. CBR increases due to the addition of Fly ash it is suitable for pavement design, it can be used in a wide range. Devi et al. (2018), studied expansive soil stabilize with the waste of thermal power plant is Coal bottom ash, Coal bottom ash is not widely used as compared to the Fly ash. Coal bottom ash is used as a stabilizing agent to stabilize the Black cotton soil. CBR test conducts on treated and untreated soil samples and it gives the bearing capacity of the soil. The maximum value of CBR is coming on Soil + 30CBA mix, the CBR value is greater than the Conventional value of Expansive soil. Ramlakhan et al. (2013), study represented the Soil stabilization of Expansive soil with Fly ash. The CBR test performs to study of bearing capacity of Soil + Fly ash mix and the maximum CBR value comes at 40% addition of Fly ash in the soil. The CBR value is suitable for subgrade soil. Ramlakhan et al. (2013) studied expansive soil stabilized by the Coal bottom ash at different percentages is 0–30% Coal bottom ash. The CBR test gives the thickness of pavement it is used to design thickness of pavement. This study soaked and unsoaked perform to find the bearing capacity of soil + Coal bottom ash mix, curing period is 7 days to calculate CBR value. CBR value is the increase 39.45% ion unsoaked condition of mix and 29.98% increases in soaked condition. The maximum value is found at 30% of Coal bottom ash. Osinubi (2000), studied soil stabilization of Black cotton soil with CBA. CBA is used as a stabilizing agent which improves the properties and bearing capacity of expansive soil. The CBR test performs on the different percentages of CBA, the maximum value of CBR is comes on Soil + 5%CBA mix. The value of CBR is increased from 9 to 130%. Patel and Mahiyar (2014) investigated the soil stabilization of black cotton soil with Fly ash. The CBR value of Combination Black cotton soil and Fly ash is varying with varying the percentage of fly ash. The value of soaked CBR value of mix Soil + Fly ash is varying with the increases the percentage Fly ash content. The maximum value of CBR is coming on 20% of Fly ash content. CBR value improves greater than the conventional value of the natural soil.

4 Conclusions

Expansive soil is problematic soil in the construction of roads, tunnels, embankments, slope stability these problems occur due to low bearing capacity, and high shrink and swells properties of soil. Expansive soil stabilization with Industrial waste Fly ash and Coal bottom ash is already done by some authors based on this study it can be concluded.

- The geotechnical properties of expansive soil improve by the addition of Fly ash and Coal bottom ash. MMD of Soil-mix is increasing with increasing the Fly ash and coal bottom ash. At 30% of Fly ash and Coal bottom ash improve the maximum Dry density of the mix. And OMC of expansive soil reduces up to a certain limit.
- The compressive strength also increases with increases in the FA and CBA content in the mix. The value increases with increases the curing period of the soil sample at 90Days of curing some reviewers say maximum compressive strength is found.
- CBR value also increases greater than the conventional value of the natural soil. That indicates the Soil can be used for road works or other civil works. The maximum value of CBR was observed at 30% CBA content.
- The FA (15–20%) and CBA (25–30%) are suitable Stabilizing agents for the stabilization of Black cotton soil.

References

Cadersa AS, Seeborun AK, Chan Chim Yuk A (2014) Use of coal bottom ash as mechanical stabiliser in subgrade soil. J Eng (UK) 2014. https://doi.org/10.1155/2014/184607

Devi CR, Surendhar S, Vijaya Kumar P, Sivaraja M (2018) Bottom ASH as an additive material for stabilization of expansive soil. Int J Eng Tech 4:174–180

Fauzi A, Nazmi WM, Fauzi UJ (2010) Subgrades stabilization of Kuantan clay using fly ash and bottom ash. Int Conf Geotech Transp Eng Geotropika 2010:1–4

Güllü H (2014) Factorial experimental approach for effective dosage rate of stabilizer: application for fine-grained soil treated with bottom ash. Soils Found 54:462–477. https://doi.org/10.1016/j.sandf.2014.04.017

Güllü H (2015) Unconfined compressive strength and freeze–thaw resistance of fine-grained soil stabilised with bottom ash, lime and superplasticiser. Road Mater Pavement Des 16:608–634. https://doi.org/10.1080/14680629.2015.1021369

Gupta A, Arora VK, Biswas S (2017) Contaminated dredged soil stabilization using cement and bottom ash for use as highway subgrade fill. Int J Geo-Eng 8. https://doi.org/10.1186/s40703-017-0057-8

Hakari UD, Puranik SC (2012) Stabilisation of black cotton soils using Fly ash, Hubballi-Dharwad municipal corporation area, Karnataka. India Glob J Res Eng Civ Struct Eng 12:21–29

Hastuty IP, Jeriko BS (2017) A study of the effectiveness of the use of cement and bottom ash towards the stability of clay in terms of UCT value. Procedia Eng 171:484–491. https://doi.org/10.1016/j.proeng.2017.01.360

Hauashdh A, Radin Mohamed RMS, Jailani J, Abd Rahman J (2020) Stabilization of peat soil using fly ash, bottom ash and portland cement: soil improvement and coal ash waste reduction approach. IOP Conf Ser Earth Environ Sci 498. https://doi.org/10.1088/1755-1315/498/1/012011

Heebink LV, Hassett DJ (2001) Coal fly ash trace element mobility in soil stabilization

Jorat ME, Marto A, Namazi E, Amin MFM (2011) Engineering characteristics of kaolin mixed with various percentages of bottom ash. Electron J Geotech Eng 16 H:841–850

Jose S, Rodrigues A, John J, Venu D (2018) A study on strength characteristics of bacterial concrete, pp 2939–2942

Katti RK (1979) First IGC annual lecture-search t(Jr solution to problems in black cotton soil. Indian Geotech J 9:1–80

Kim HK, Lee HK (2015) Coal bottom ash in field of civil engineering: a review of advanced applications and environmental considerations. KSCE J Civ Eng 19:1802–1818. https://doi.org/10.1007/s12205-015-0282-7

Kolathayar S, Prasannan S, Sharma AK (2020) Strength tests and model experiments on soil reinforced with areca and PVA fibers. Lect Notes Civ Eng 85:147–153. https://doi.org/10.1007/978-981-15-6086-6_12

Kumar D, Kumar N, Gupta A (2014) Geotechnical properties of fly ash and bottom ash mixtures in different proportions. Int J Sci Res 3:1487–1494

López López E, Vega-Zamanillo Á, Calzada Pérez MA, Hernández-Sanz A (2015) Bearing capacity of bottom ash and its mixture with soils. Soils Found 55:529–535. https://doi.org/10.1016/j.sandf.2015.04.005

Mahadevi, R.: Experimental investigation for stabilization of black cotton soil by using lime and brickdust waste. Int J Recent Trends Eng Res 3:11–19 (2017). https://doi.org/10.23883/ijrter.2017.3424.lg17q

Mehta KS, Sonecha RJ, Daxini PD, Ratanpara PB, Gaikwad KS (2014) Analysis of engineering properties of black cotton soil and stabilization using by lime. J Eng Res Appl 4:2248–962225. www.ijera.com

Mohanty S (2018) Stabilization of expansive soil using industrial waste: fly ash. Civ Eng Res J 3. https://doi.org/10.19080/cerj.2018.03.555606

Murmu AL, Dhole N, Patel A (2020) Stabilisation of black cotton soil for subgrade application using fly ash geopolymer. Road Mater Pavement Des 21:867–885. https://doi.org/10.1080/14680629.2018.1530131

Osinubi KJ (2000) Stabilisation of tropical black clay with cement and pulverised coal bottom ash admixture. Proc Sess Geo-Denver 2000 Adv Unsaturated Geotech GSP 99:287, 289–302. https://doi.org/10.1061/40510(287)20

Oza JB, Gundaliya PJ (2013) Study of black cotton soil characteristics with cement waste dust and lime. Procedia Eng 51:110–118. https://doi.org/10.1016/j.proeng.2013.01.017

Pant A, Datta M, Ramana GV (2019) Bottom ash as a backfill material in reinforced soil structures. Geotext Geomembranes 47:514–521. https://doi.org/10.1016/j.geotexmem.2019.01.018

Patel P, Mahiyar HK (2014) An experimental study of black cotton soil, stabilized with rice husk ash, fly ash and lime. Int J Eng Res Technol 4:660–665

Patil RJ (2020) Experimental investigation of black cotton soil by lime and fly-ash stabilization, pp 83–89

Ramlakhan B, Kumar SA, Arora TR (2013) Effect of lime and fly ash on engineering properties of black cotton soil. Int J Emerg Technol Adv Eng 3:535–541

Reddy CS, Mohanty S, Shaik R (2018) Physical, chemical and geotechnical characterization of fly ash, bottom ash and municipal solid waste from Telangana State in India. Int J Geo-Eng 9:1–23. https://doi.org/10.1186/s40703-018-0093-z

Sharma V, Singh S (2020) Modeling for the use of waste materials (bottom ash and fly ash) in soil stabilization. Mater Today Proc 33:1610–1614. https://doi.org/10.1016/j.matpr.2020.05.569

Sudhakaran SP, Sharma AK, Kolathayar S (2018) Soil stabilization using bottom ash and areca fiber: experimental investigations and reliability analysis. J Mater Civ Eng 30:04018169. https://doi.org/10.1061/(asce)mt.1943-5533.0002326

Thomas MDA (2007) Optimizing the use of fly ash in concrete. Portl Cem Assoc 24

Synthesis, Properties and Photo Catalytic Application of Cadmium Based Quantum Dots: A Review

Sandeep Singh, Sangeeta Garg, and Amit D. Saran

Abstract Recent development of novel particles at nanoscale and worldwide financial worth of nanoparticles attracted all zones of society in last few decades towards nanotechnology. As nanoparticles show unique properties at each size level, leave numerous zones of this field either unexplored or underexplored. A lot different kinds of nanoparticles risen in past decades as like Carbon Nano Tubes (CNTs), Quantum Dots (QDs), ceramics, colloidal nanoparticles etc. Semiconductor nanoparticles or QDs are among the most unforeseen developments in this developing field. QDs of few nanometer range shows strange properties as they have tunable band gap which depends on various factors. Tunable optical and electronic properties of semiconductor QDs resulted in widespread application in chemical, pharmaceutical, biomedical as well as in environmental fields. In recent years QDs made siginificant progress in molecular imaging or bioimaging, in chemical analysis as chemosensors, as an alternative of traditional organic dyes, in drug delivery, in heavy metal detection, in cancer detection and treatment, in dye removal as photocatalyst, in catalytic hydrogen production, as photovoltaic devices, etc. Despite the wide applications of QDs, its own toxicity limited its applications in human health and restricts potential of in vivo studies upto some extent. A review for better understanding of QD's behaviour by knowing its limitations alongside advantages will help in enhancing efficiency in its applied area as well as will also circumvent the problem of QDs toxicity.

Keywords Quantum dots (QDs) · Tunable band gap · Photocatayst

1 Introduction

The size gap between the bulk and atomic levels is filled by nanostructured materials, attracting the researchers with totally new possibilities for applications in optical,

S. Singh · S. Garg · A. D. Saran (✉)
Department of Chemical Engineering, Dr. B.R. Ambedkar National Institute of Technology, Jalandhar, Punjab 144011, India
e-mail: saranad@nitj.ac.in

chemical, mechanical, biological and electronics fields. In seminal talk on nanostructured materials in 1959, Richard Feynman said that "there's plenty of room at the bottom", from his words one can visualize the theoretical possibilities which can born by transforming bulk matter to atomic and molecular levels (Khan and Saeed 2019; Bahadar et al. 2016; Ferreira et al. 2013). Transformation of the matter as well as of ongoing macro processes to nano level, generates new world of potentials and benefits impacting not only almost all the segments of industries (chemical, production, electronic, energy, biotechnology, etc.) but also on our each area of society (Jeevanandam et al. 2018). Due to the shining potential of nano structures, the presence of nano scale particles is confirmed in our surroundings, and will increase much more in coming years exponentially. For size relevance of nano scale materials, about 1 million of particles from 3 g of 100 nm spherical size nanoparticles can be distributed among every human being throughout the world (Kumar and Kumbhat 2016; Jeevanandam et al. 2016).

Nanostructured materials are classified on basis of number of dimensions of the material, which lies outside the nano range i.e. less than 100 nm (Njuguna et al. 2014). Thus, nanostructured materials are broadly categorized as Zero Dimensional nanomaterials (0D) or Dots/QDs: whose all dimensions lies within nano range; One Dimensional nanomaterials (1D) i.e. Quantum wires, nanorods, nanotubes: whose one dimension lies outside the nano range; Two Dimensional nanomaterials (2D) i.e. nanofilms, layers at nanoscale, nanocoatings, Quantum wells: whose two dimensions lies outside the nano range; Three Dimensional nanomaterials (3D): whose dimensions are not confined to the nanorange as like nanopowders, nanowires in bundles, nanoparticles in dispersed form, or multi nanolayers (Boverhof et al. 2015; Donaldson and Poland 2013; Sharma et al. 2016).

As most of the classifications of nanomaterials is done on basis of size and dimensions only. The factor of size or dimensions of material in range from 0.1 to 100 nm plays a vital role in field of nanotechnology. At nanoscale, surface area of material with respect to its volume becomes very large (Rao and Geckeler 2011). This results in discretion of energy states in case of semiconductor nanomaterials. Separation of the energy states leads to the distinct electronic, optical, mechanical and chemical properties. The properties of materials at nanoscale becomes size as well as shape dependent (Guisbiers et al. 2012). With each unit change in dimension of nanoparticle, the properties varies with greater effect (Zhang and Saltzman 2013). This change in properties due to size and shape variation at nanoscale is due to quantum confinement effect or Quantum effect. This effect leads to the emergence of new nanomaterials at lower nanoscale called as QDs (Sahai et al. 2017).

QDs are the semiconductor materials having dimensions in nano range less than 10 nm. The quantum dot is an assembly of atoms of specific material that has few nanometer dimensions, sometimes it is also termed as a virtual atom. From last decade, QDs have gained much attention as better substitute to other nanomaterials due to large ability of absorbing light of particular wavelength, tuneable energy band gap as per its quantum size and elemental composition, better chemical stability, its ability to carry charge, photonic stability, higher mechanical strength, opto-electronics distinction, etc. (Jeevanandam et al. 2018; Mourdikoudis et al. 2018)

These strengths of semiconductor QDs resulted in widespread application in chemical, pharmaceutical, biomedical as well as in environmental fields (Cotta 2020).So far, several materials have been widely reported for their photocatalytic activity, including TiO2, ZnO, ZnS, and CdS. (Kumar 2015; Verma and Kumar 2014; Kumar and Bansal 2010a; Saini et al. 2020; Yu and Liu 2021; Wen et al. 2015; Senasua and Hemaviboolb 2018). The semiconductor QDs are made mainly from atoms of group II and VI elements (e.g. CdSe and CdTe) or group III and V elements (e.g. InP and InAs) (Dorfs et al. 2011; Hardman 2006; Colvin 2003; Service RF. 2004). Cd based QDs have received a lot of attention among the II–VI group of semiconductor QDs because of their suitable bandgap and ability to create electron–hole pairs (charge carriers) quickly when exposed to sunlight compared to other photocatalysts (Murali et al. 2014). In today's scenario, an important challenge is designing and manipulation of these QDs as per the application required to as much maximum efficiency as possible. Thus improvement of existing and creation of new integrated QDs for unique size dependent properties requires much more effort of researchers at present before working on application part directly (Ray et al. 2009a).

This reviews deals with the synthesis, properties, and applications of QDs for better understanding their behaviour by also knowing its drawbacks along with advantages. This will not only aid in improving efficiency of QDs in its applied area but also will make us aware about the toxicity of QDs in applied area.

2 Synthesis

Methods used for the synthesis of QDs are mainly classified into two approaches named as top-down and bottom-up approach. In top down approach, a bulk material is thinned or etched to form QDs to achieve particle size diameter of 10 nm (Valizadeh et al. 2012). Desired shapes and sizes can be accomplished by precise investigations on quantum confinement effects. Etching or thinning of the particles is done by laser beams to fabricate to zero dimensional QDs (Edvinsson 2018). This can be achieved by various techniques as like dry etching, wet etching, reactive ion etching (RIE), focused ion beam (FIB) and lithography (Fornari 2011; Namdaria et al. 2017; Shinde and Pillai 2013; Ray et al. 2009b). Particles fabricated with these techniques are of 8–15 nm reported for both lab and commercial synthesis (Namdaria et al. 2017). In top down approach as in etching and lithographic processes major drawbacks are due to incorporation of impurities, structural and surface imperfections in fabricated QDs. These drawbacks restricts the use of these processes in synthesis of QDs up to some extent (Gates et al. 2005).

The other approach called as bottom-up approach or self-assembly approach have been used to synthesize the QDs. Self-assembly methods includes wet-chemical and vapour-phase methods. Micro-emulsion, sol–gel technique, reaction and electro chemistry, hot solution decomposition are some methods placed in the class of wet chemical methods (Biswas et al. 2012). Wet chemical methods are also known as

precipitation method, involves the nucleation and limited growth of particles. Molecular beam epitaxy (MBE), vapour deposition, aggregation techniques falls under the class of Vapor—phase methods. Controlling factors like temperature, stabilizers, water to surfactant ratios, amount of solvent, concentration of precursors, QDs of desired shape, size and composition can be synthesized (Biswas et al. 2012; Ghassan et al. 2019).

3 Properties

3.1 Band Gap

Band gap is nothing but minimum energy required to keep electrons in conduction band and a holes in valence band apart from each other (Alivisatos 1996). As soon as electron absorbs the energy to overcome the energy barrier called band gap it jumps from conduction to valence band, and they may form an exciton (an electron–hole pair). This exciton behaves like a proton where hole acts as a nucleus (Yoffe 1993, 2001).

In case of QDs there is a relation between band gap and its size, due to quantum confinement effect. Confinement means to limit the movement in a confined space (Bera and Qian 2008). Due to the nanoscale dimensions of QDs electrons are restricted inside very small dot region as like electrons are confined in an atom in atomic space. Likewise in semiconductors electrons are confined in conduction band and holes in valence band. As the size of QDs is decreased the band gap increases. When size is decreased below 6 nm the band gap increases significantly (Jang et al. 2003; Steckel et al. 2006). Band gap not only depends on the size of the quantum dot but shape factor also plays an important role. In shape factor, ratio of volume to the surface area plays a vital role which revise the quantity of atoms on surface as well as cohesive energy each time the ratio is altered. This dependence of band gap on size can be explained by molecular orbital theory and mass approximation models. In simple way, as the size of the particle reaches at nano level, the overlapping of energy levels gets decreased, resulting in formation of thin conduction and valence bands. This in turn give rise to energy band gap in both the bands (Bhargava 1996; Bera et al. 2010; Wang and Herron 1991). This explains the widening of band gaps at nano scale as compared to bulk semiconductors. Due to narrow and size dependent band gap, Cadmium based QDs are efficient in visible as well as in some part of UV spectrum. CdS QDs are more efficient in range of 400–430 nm and CdSe QDs in range of 550–580 nm depending on the particle size. The size and shape of quantum dot to be synthesised can be decided as per required band gap.

3.2 Luminescence

There are number of ways by which electrons and holes get excited to form an exciton by absorbing some external energy. Sources of external energy can be simple sunlight, an electric field, electrons from laser beam, thermal energy, etc. the energy required to overcome the energy barrier called band gap is defined by the electronic structure of the considered particle which depends on shape and size of the particle (Hines and Sionnest 1996). The excited electrons may merge with holes present in valence bands and attains stability releasing some amount of energy. After releasing energy they again reaches to ground state. Energy emitted can be in form of either photons or electrons. This energy emitted in form of photons is a source of QDs important property luminescence (Richter 2004). There can be number of causes for luminescence as like band edge emission, emission of photon due to some defect, it can be intrinsic defect (composition impurity in particle) or extrinsic defect (external factors: high energy irradiation, temperature), even some activators are used in some cases aids in luminescence phenomenon. There is predominant effect of particle size on photoluminescence property and on excitation wavelength. The absorption peak energy decreases as the size of nanoparticles was increased, which is explained by quantum confinement effect. As the size of the QDs was decreased from 35 to 5 nm, the peak absorption energy increased from 4.6 to approximately 6.2 eV. Whereas the photoluminescence showed unpredictable behaviour, reporting minimum at particle size of 17 nm (Singh et al. 1549; Xu et al. 2018). Photoluminescence also depends on the wavelength of the excitation energy. With variation in excitation wavelength from 300 to 470 nm, the photoluminescence peak shifts from blue to red region of longer wavelength (Sharma et al. 2019).

3.3 Quantum Yield

Many applications of quantum dot as like in lasers, lighting devices, displays, bioanalysis, as sensors are based on tuning of band gap as well as their ability of releasing energy called as luminescence. The discovery of nanomaterials made search of efficient and highly luminescent materials fruitful upto much extent, but still much more to go in this field (Wong et al. 2020).

The QDs by absorbing the energy converts that into photons. As this conversion is not 100%, two different terms come into existence named quantum yield and quantum energy efficiency. Quantum yield is defined as number of photons emitted by absorbing some certain number of photons by any material. As the quantum dot here acts as a wavelength converting mean, therefore even if numbers of both emitted and absorbed are same but quantum energy efficiency will be less than 100% as excitation energy will be more than the cumulative energy of the photos emitted of longer wavelength. Main focus of researchers is on synthesizing materials delivering high quantum yield. Most important factor in case of QDs regarding

luminescence property is to control the number of photons it emits per area and in what unit time. Both the absorption of excitation energy and quantum yield are important characteristics to be focused. Since if material of high quantum yield is designed in such a way that its tendency to absorb light is low then it will yield poor luminescent property (Li and Li 2017; Serpone 1997; Kudo and Miseki 2009). The composition of QDs and precursor's ratios are also considered as predominant factor to increase the Quantum Yield of QDs (Qu and Peng 2009). The quantum yield of QDs was decreased with increase in the size of particle from 1.4 to 2 nm. Coating of semiconductor of wider band energy barrier over the quantum dot also aided in improving the quantum yield (Wu et al. 2007). Reported quantum yield of bare QDs is about 20% however with coating of same quantum dot with material increased quantum yield to 80% (Hao et al. 2019).

4 Applications

4.1 Photocatalytic Degradation

The waste effluent discharged by the industries in natural water bodies makes them a major source of water pollution and indirectly cause other forms of pollution too as soil pollution. Ability to oxidise the hazardous pollutants for degradation at cost of very low energy consumption has shifted the attention of researchers towards QDs (Sajjadi et al. 2017). Many mechanisms are in support of photo catalytic activity shown by QDs. This can be achieved by H^+, $O_2^{\cdot}$, e^- and OH^- species. Many researchers reported the ability to degrade stable toxic organic dyes by different QDs with more than 80% efficiency in less than 100 min in different environments. To enhance the photo catalytic activity of QDs, QDs are now a days tested at various size levels of different shapes to obtain maximum quantum yield. Other factors influencing directly the photo catalytic activity of QDs are specific area and charge separation (electron hole pair recombination). This charge separation can be achieved by synthesising shells of another metal semiconductor over the core, or by attachment of some metal oxide layers over the synthesised QDs. This not only increases the quantum yield, better disperse ability in aqueous phases and also makes the structure of QDs stable in toxic environments of very high pH (Jouyandeh et al. 2021; Huang et al. 2020; Matea et al. 2017).

Mechanism of photocatalytic degradation

The h^+ and $^{\cdot}O_2$ are the main active species responsible for photocatalysis. Macromolecules of organic pollutants are degraded to simple products by these active species. Understanding the mechanism of photo activity, by absorption of photons by QDs the electron hole pairs gets separated. Absorption of photons cause excitation of electrons from valence band (VB) to conduction band (CB) (Linsebigler and Yates 1995) (Fig. 1).
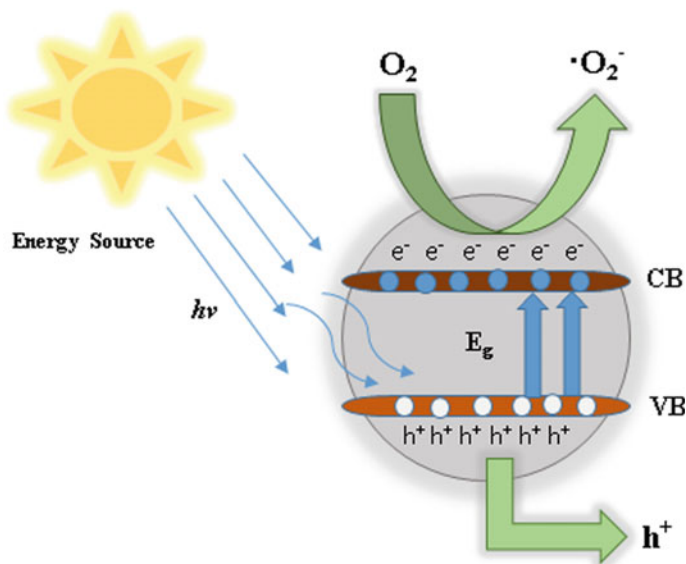
Fig. 1 Schematic mechanism of photo degradation of QDs

$$QD + hv \rightarrow e^-(CB) + h^+(VB) \tag{1}$$
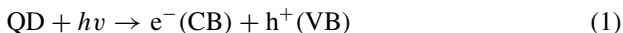
These induced electrons migrate on the surface of the catalyst and take part on oxidation reduction reactions with water and oxygen mainly. $\cdot O_2^-$ active species were formed by reaction of oxygen molecules and electron migrated at the surface of photo catalyst.

$$e^-(CB) + O_2(ads.) \rightarrow \cdot O_2^- \tag{2}$$
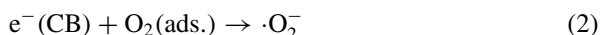
These active species formed is mainly responsible for the degradation of methylene blue molecule to simple non-toxic degradable chemical compounds.

$$O_2^-/h^+ + \text{pollutant} \rightarrow \text{degradation products} \tag{3}$$
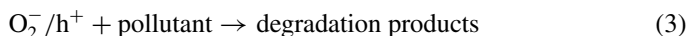
Active sites as well as formation of active species influence rate of degradation and percentage degradation both. These both factors depends on the catalyst concentration used for degradation, concentration of pollutant in water (in ppm), and pH value of testing aqueous phase (Hisatomi et al. 2014; Chen et al. 2010; Chen and Mao 2007).

From table no 1., it can be figured out very clearly the tendency of cadmium based QDs to act as photo catalyst with good percentage degradation and capability of degrading much stable and toxic dyes. Factors like method of synthesising these

Table 1 Comparative study of cadmium based photo catalyst QDs for degradation of organic compounds

References	Catalyst	Size	Pollutant	Percentage degradation	Time
Cao et al. (2020)	CdSe	5 nm	Malachite green (MG)	94.28% (Visible) 86.5% (Uv)	60 min
Gajendiran et al. (2020)	CdS	4–10 nm	Indigo carmine (IC) and Congo red (CR)	82% (IG) 65% (CR)	180 min
Qureshi et al. (2020)	CdS-Bi$_2$S$_3$	1 um	Methyl orange (MO) Methyl green (MG)	60% (MO) 100% (MG)	120 min
Khan et al. (2020)	CdS	2–5 nm	Ponceau BS dye	94.6%	55 min
Ma et al. (2020)	rGO-CdS	6–7 nm	Rhodamine-B	40% (pure CdS) 9 times more (with rGO)	60 min
Bhuvaneswari et al. (2020)	CdS	7 nm	Methyl orange (MO)	95%	30 min
Bhuvaneswari et al. (2020)	gZnS/CdS	7.1 nm	Methylene blue	93%	120 min
Vidhya et al. 2020)	SnO$_2$	42 nm	Methylene blue	98%	120 min
Santra et al. (2020)	CdS	15 nm	Rose bengal (RB)	96%	90 min
Prasad et al. 2020)	Carbon aerogel – CdS	60 nm	Methylene blue	43.27%	180 min
Men et al. (2019)	CdSe	8–9 nm	Tetracycline	73.1%	80 min
Sridevi et al. 2002)	Fe/CdSe	1.2 nm	Methylene blue	79%	150 min
Patidar et al. (2019)	CdSe-rGO	20 nm	Methylene blue	70%	210 min
Thirugnanam et al. (2017)	CdSe	4 nm	Brillent green	81.9%	90 min
Ma et al. (2017)	CdSe/Al$_2$TiO$_5$	5–10 nm	Methylene blue	98%	90 min

QDs, concentration of QDs, structural parameters, doping, excitation source and absorption time affects the degradation rate as well as irradiation time (Table 2).

From table no 2., it can be concluded that the performance of CdS QDs can be altered with shape and structure of materials used for photocatalysis. But reviewing above work, some drawbacks were faced as like high energy consumption during synthesis, large particle size, high irradiation time, etc. moreover from table it can be

Table 2 Comparative study of particle shape and size and degradation irradiation time of CdS QDs

References	CdS photocatalyst	Particle size	Dye	Irradiation time
Jamble et al. (2018)	Dentrites	26–31 nm	Methylene blue	220 min
Dey and Das (2020)	Nanoparticles	8.5 nm	Methyl orange	300 min
Shende et al. (2018)	Nano-films	26 nm	MB. CR and IC	6 h
Srinivasan (2019)	Nanostrutures	80–160 nm	Reactive orange	180 min
Chakrabortya et al. (2019)	Nanosflakes	22 nm	Rhodamine B	180–300 min
Gajendiran et al. (2020)	QDs	4–10 nm	CR and IC	180 min
Esmaili and Yangjeh (2011)	Nanoparticles	4–8 nm	Methylene blue	180 min

figured out that for complete degradation of by photocatalyst it requires about 6 h. even with use of mercury, xenon, helium lamps for degradation.

With alteration in properties of QDs, this field of photo catalytic degradation has much scope as to attain lower irradiation time and in synthesising most efficient materials knowing the parameters affecting the efficiency. Reviewing the literature one can conclude that QDs has shown a promising photoactivity better than other nanomaterials in past history.

One reason of today's deep root research interest of researchers in nanoscience, nanotechnology and nanomaterials is size tunable optical properties shown at lower nano scale. With better optical, mechanical and electrical properties of semiconductor nanomaterials has already replaced much of the nano scale materials used in various applications in past times. Other fields were QDs came into existence are electroluminescene, renewable energy, bioimaging, drug delivery, in metal detection etc. (The Royal Society the Royal Academy of Engineering (2004).

4.2   Other Applications

The QDs were used as electrochemical based sensors for detection of neutravidin, glucose and as electrochemical signal transducers. In past QDs scope in biotechnology resulted in bio imaging, cellular imaging, bio sensing, and in drug delivery applications (Ali and Abdoos 2021). The applications of QDs in cancer diagnosis and treatment due to their excellent photo-physical properties making them capable to be used as probes in cellular and in vivo image studies. Many researchers focused on diagnosis of tumors (ovarian cancer, breast cancer, prostate cancer and pancreatic cancer) in early stages and their treatment as well. QDs application in environmental field as in detection of heavy metals in water (Peng and Li 2010; Zou et al. 2015; Jin et al. 2011). The detection of mercury, copper, silver heavy metal ions by chemically modified QDs making them very specific to be used as probes. Combination of

adsorption and photo degradation process has much better capability in dye degradation (Kumar and Bansal 2010b; Kumar 2010). By virtue of these properties QDs plays a vital role in field of food security and drug testing fields. The photo luminescence properties of QDs were also utilized effectively for applications in sensing fields (Zhou et al. 2018; Mansuriya and Altintas 2020). CdSe QDs were used as photo catalyst and surface absorbent for dye removal with UV irradiation, thus quantifying QDs in waste water treatment too (Mahmoodi et al. 2018).

5 Conclusion and Future Scope

In concluding words, as it's been noticed that researchers have attained noticeable achievements in understanding the structure, applications, performance and behaviour of QDs by knowing the factors varying their properties. This is so as the QDs exhibit considerably numerous optical, electronic and physical properties as compared to nano bulk materials. The 'bottom to up' approaches are widely used to explore new methods to generate QDs. Despite this huge contribution, there is still a lot to explore about the applications of QDs in large scale solid state optical and biological fields. As there is a lot of QD's field which is not ploughed yet. Enhancement in preparation techniques and investigating their properties at different scale, shape and surface chemistry as per application is required to be explored more deeply. Although experiments at the laboratory level have been reported to be successful, scaling up the synthesis and retaining the properties of QDs is not trivial (Hardman 2006; Namdaria et al. 2017). Continued research and development on QDs will lead to greater quantum efficiency, improved device fabrication, and novel materials that extend the emission range into the near-IR region. The research at nanoscale is expected to be a major research and development sector in the twenty-first century (Namdaria et al. 2017). This encourages the researchers to continue their exploration by coating these materials with inorganic shells, biomolecules or polymers to modify their properties considering the toxicity as well, from the scientific and engineering community.

Conflict of Interest On behalf of all authors, the corresponding author states that there is no conflict of interest.

References

Ali M, Abdoos F (2021) A critical review on quantum dots: from synthesis toward applications in electrochemical biosensors for determination of disease-related biomolecules. Talanta 224:121828
Alivisatos (1996) Semiconductor clusters, nanocrystals, and quantum dots. Science 271:933–937

Bahadar H, Maqbool F, Niaz K (2016) Toxicity of nanoparticles and an overview of current experimental models. Iran Biomed J 20:1–11

Bera D, Qian L (2008) Phosphor quantum dots. Wiley, WestSussex

Bera D, Qian L, Tseng T, Holloway P (2010) Quantum dots and their multimodal applications: a review. Materials 3:2260–2345

Bhargava RN (1996) Doped nanocrystalline materials–physics and applications. J Lumin 70:85–94

Bhuvaneswari K,Vaitheeswari V, Maiyalagan T, Pazhanivel T (2020) Glutathione capped inverted core-shell quantum dots as an efficient photocatalyst for degradation of organic dyes. Mater Sci Semicond Process 106:104760

Biswas A, Ilker S. Bayer B, Alexandru S (2012) Advances in top–down and bottom–up surface nanofabrication: techniques, applications and future prospects. Adv Colloid Interface Sci 170:2–27

Boverhof D, Bramante C, Butala J (2015) Comparative assessment of nanomaterial definitions and safety evaluation considerations Regulatory. Toxicol Pharmacol 73(1):137–150

Cao K, Chen M, Hang F, Cheng Y, Deng G (2020) The biosynthesis of cadmium selenide quantum dots by Rhodotorula mucilaginosa PA-1 for photocatalysis. Biochem Eng J 156:107497

Chakrabortya S, Sau S, Pal M (2019) Impact of morphology on the electrical and photocatalytic property of Cds nanostructures. Mater Today Proc 18:5481–5487

Chen X, Mao S (2007) Titanium dioxide nanomaterials: synthesis, properties, modifications, and applications. Chem Rev 107(7):2891–2959

Chen X, Shen S, Guo L, Mao S (2010) Semiconductor-based photocatalytic hydrogen generation. Chem Rev 110(11):6503–6570

Colvin V (2003) The potential environmental impact of engineerednanomaterials. Nat Biotechnol 21:1166–1170

Cotta M (2020) Quantum dots and their applications: what lies ahead? ACS Appl Nano Mater 3(6):4920–4924

Dey P, Das R (2020) Enhanced photocatalytic degradation of methyl orange dye on interaction with synthesized ligand free CdS nanocrystals under visible light illumination. Spectrochim Acta A Mol Biomol Spectrosc 231:118122

Donaldson K, Poland C (2013) Nanotoxicity: challenging the myth of nano-specific toxicity. Biotechnol 24:724–734

Dorfs D, Krahne R, Falqui A, Manna L (2011) Quantum dots: synthesis and characterization. Nanosci Nanotechnol 1(2):17–60

Edvinsson T (2018) Optical quantum confinement and photocatalytic properties in two-, one- and zero-dimensional nanostructures. R Soc Open Sci 5(9):180387

Esmaili M, Yangjeh A (2011) Microwave-sssisted preparation of CdS nanoparticles in a halide-free ionic liquid and their photocatalytic activities. Chin J Catal 32:933–938

Ferreira A, Cemlyn-Jones J, Robalo C (2013) Nanoparticles, nanotechnology and pulmonary nanotoxicology. Pneumol 19:28–37

Fornari R (2011) Bulk crystal growth of semiconductors: an overview comprehensive. Semicond Sci Technol 3:1–35

Gajendiran J, Senthil V, Parthasaradhi S (2020) Ionic liquid assisted wet chemical synthesis CdS quantum dots and their structural, morphological, optical, electrochemical, photocatalytic, antibacterial and hemocompatibility characterization. Optik 213:164638

Gates BD, Xu Q, Stewart M, Ryan D (2005) New approaches to nanofabrication: molding, printing, and other techniques. Chem Rev 105(4):1171–1196

Ghassan A, Mijan N, Yap H (2019) Nanomaterials: an overview of nanorods synthesis and optimization. In: Nanorods and nanocomposites, pp 845–850

Guisbiers G, Rosales S, Deepak F (2012) Nanomaterial properties: size and shape dependencies

Hao J, Liu H, Miao J, Lu R, Zhou Z, Zhao B (2019) A facile route to synthesize CdSe/ZnS thick-shell quantum dots with precisely controlled green emission properties: towards QDs based LED applications. Sci Rep 9:12048

Hardman R (2006) A toxicologic review of quantum dots: toxicity depends on physicochemical and environmental factors. Environ Health Perspect 114(2):164–172

Hines M, Sionnest P (1996) Synthesis and characterization of strongly luminescing ZnS-capped CdSe nanocrystals. J Phys Chem 100(2):468–471

Hisatomi T, Kubota J, Domen K (2014) Recent advances in semiconductors for photocatalytic and photoelectrochemical water splitting. Chem Soc Rev 43:7520–7535

Huang L, Martinez Z, Johnson M, Luther J, Beard J (2020) Transforming energy using quantum dots energy and environmental science

Jamble S, Karuna P, Rohidas B (2018) Studies on growth mechanism and physical properties of hydrothermally synthesized CdS with novel hierarchical superstructures and their photocatalytic activity. J Phys Chem Solids 114:109–120

Jang E, Jun S, Pu L (2003) High quality CdSeS nanocrystals synthesized by facile single injectionprocess and their electroluminescence. Chem Comm 2964–2965

Jeevanandam J, Chan Y, Michael K (2016) Biosynthesis of metal and metal oxide nanoparticles. J Chembioeng 3(2):55–67

Jeevanandam J, Barhoum A, Chan Y, Dufresne A (2018) Review on nanoparticles and nanostructured materials: history, sources, toxicity and regulations. J Nanotechnol 9:1050–1074

Jin S, Hu Y, Gu Z, Liu L, Wu H (2011) Application of quantum dots in biological imaging. J Nanomater 834139:13

Jouyandeh M, Khadem S, Habibzadeh S, Esmaeili A, Abida O (2021) Quantum dots for photocatalysis: synthesis and environmental applications. Green Chem 23:4931–4954

Khan Y, Ahmad A, Ahmad N, Mir F (2020) Biogenic synthesis of a green tea stabilized PPy/SWCNT/CdS nanocomposite and its substantial applications, photocatalytic degradation and rheological behaviour. Nanoscale Adv 2:1634–1645

Khan I, Saeed K (2019) Nanoparticles: properties, applications and toxicities. Arab J Chem 12(7):908–931

Kudo A, Miseki Y (2009) Heterogeneous photocatalyst materials for water splitting. Chem Soc Rev 38:253–278

Kumar J (2010) Photocatalytic degradation of amaranth dye over immobilized nano-crystals of TiO$_2$, recent advances in energy and environment, pp 129–133

Kumar J (2015) Bansal A: CFD simulations of immobilized-titanium dioxide based annular photocatalytic reactor: model development and experimental validation. Indian J Chem Technol 22:95–104

Kumar J, Bansal A (2010) Photocatalytic degradation of amaranth dye over immobilized nano-crystals of TiO$_2$. In: International conference on energy and environment, Cambridge, pp 129–133

Kumar J, Bansal A (2010b) Photocatalytic degradation of amaranth dye in aqueous solution using sol-gel coated cotton fabric. In: Proceedings of the world congress on engineering and computer science, p 2

Kumar N, Kumbhat S (2016) Essentials in nanoscience and nanotechnology. In: Carbon-based nanomaterials, pp 189–236

Li R, Li C (2017) Photocatalytic water splittingon semiconductor-basedphotocatalysts. Adv Catal 60

Linsebigler A, Yates J (1995) Photocatalysis on TiO2 surfaces: principles, mechanisms, and selected results. Chem Rev 95(3):735–758

Ma C, Wu D, Yao X (2017) Enhanced visible-light photocatalytic decomposition of organic dye over CdSe/Al$_2$TiO$_5$ heterojunction photocatalysts. J Alloy Compd 712:486–493

Ma L, Ai X, Lu Y (2020) Development of a new synthetic strategy for highly reduced graphene oxide-CdS quantum-dot nanocomposites and their photocatalytic activity. J Alloys Compd 282:154406

Mahmoodi M, Karimi B, Mazarji M, Moghtaderi H (2018) Cadmium selenide quantum dot-zinc oxide composite: synthesis, characterization, dye removal ability with UV irradiation, and

antibacterial activity as a safe and high-performance photocatalyst. J Photochem Photobiol B 188:19–27

Mansuriya B, Altintas Z (2020) Applications of graphene quantum dots in biomedical sensors. Sensors 20(4):1072

Matea C, Mocan T, Tabaran F, Pop T (2017) Quantum dots in imaging, drug delivery and sensor applications. Int J Nanomedicine 12:5421–5431

Men Q, Wang T, Yang Y (2019) In-suit preparation of CdSe quantum dots/porous channel biochar for improving photocatalytic activity for degradation of tetracycline. J Taiwan Inst Chem Eng 99:180–192

Mourdikoudis S, Pallares R, Thanh N (2018) Characterization techniques for nanoparticles: comparison and complementarity upon studying nanoparticle properties. Nanoscale 27:12871–12934

Murali G, Reddy DA, Giribabu G, Vijayalakshmi RP (2014) Growth and characterization of rose-flower-like CdS microstructures. Ceram Int 40(8):11813–11817

Namdaria P, Negahdarib B, Eatemadib A (2017) Synthesis, properties and biomedical applications of carbon-based quantum dots: an updated review. Biomed Pharmacother 87:209–222

Nanoscience and nanotechnologies: opportunities and uncertainties, Nanoscience and nanotechnologies. The Royal Society & the Royal Academy of Engineering (2004)

Njuguna J, Ansari F, Sachse S, Zhu H (2014) Nanomaterials, nanofillers, and nanocomposites: types and properties. In: Health and environmental safety of nanomaterials, pp 3–27

Patidar D, Yadav A, Paul D, Sharma A (2019) Nanohybrids cadmium selenide-reduced graphene oxide for improving photo-degradation of methylene blue. Physica E Low-Dimension Syst Nanostruct 114:113560

Peng C, Li Y (2010) Application of quantum dots-based biotechnology in cancer diagnosis: current status and future perspectives. J Nanomater 676839:11

Prasad S, Shanmugam P, Bhuvaneswari K (2020) Rod-shaped carbon aerogel-assisted CdS nanocomposite for the removal of methylene blue dye and colorless phenol. Curr Comput Aided Drug Des 10(4):300

Qu L, Peng X (2009) Control of photoluminescence properties of CdSe nanocrystals in growth. J Am Chem Soc 124(9):2049–2055

Qureshi F, Nawaz M, Rehman S, Shahzad S (2020) Synthesis and characterization of cadmium-bismuth microspheres for the catalytic and photocatalytic degradation of organic pollutants, with antibacterial, antioxidant and cytotoxicity assay. J Photochem Photobiol B Biol 202:111723

Rao J, Geckeler K (2011) Polymer nanoparticles: preparation techniques and size-control parameters. Prog Polym Sci 36:887–913

Ray P, Yu H, Fu P (2009a) Toxicity and environmental risks of nanomaterials: challenges and future needs. J Environ Sci Health C Environ Carcinog Ecotoxicol Rev 27(1):1–35

Ray S, Saha A, Jana N, Sarkar R (2009b) Fluorescent carbon nanoparticles: synthesis, characterization, and bioimaging application. J Phys Chem C 113(43):18546–18551

Richter M (2004) Electrochemiluminescence (ECL). Chem Rev 104(6):3003–3036

Sahai S, Rai S, Shrivastav R, Dass S (2017) Quantum dots sensitization for photoelectrochemical generation of hydrogen: a review. 68(1):19–27

Saini A, Arora I, Kumar J (2020) Photo-induced hydrophilicity of microsized-TiO_2 based self-cleaning cement. Mater Lett 260:126888

Sajjadi S, Khataee A, Kamali Z (2017) Sonocatalytic degradation of methylene blue by a novel graphene quantum dotsanchored CdSe nanocatalyst. Ultrason Sonochem

Santra A, Brandao P, Mondal G, Bera P (2020) Monomeric and dimeric cadmium (II) complexes of S-alkyl/aryl dithiocarbazate as single-source precursors for cadmium sulfide nanoparticles: an experimental, theoretical interpretation in the stability of precursor and visible light dye degradation study. Inorg Chim Acta 501(1):119315

Senasua T, Hemaviboolb K (2018) Nanan S: Hydrothermally grown CdS nanoparticles for photodegradation of anionic azo dyes under UV-visible light irradiation. RSC Adv 8:22592–22605

Serpone N (1997) An overview of semiconductor photocatalysis. Photochem Photobiol A Chem 104:1–12

Service RF. (2004) Nanotechnology grows up. Science 304:1732–1734

Sharma D, Kanchi S, Bisetty K, Nuthalapati VN (2016) Perspective on analytical sciences and nanotechnology. Adv Environ Anal Appl Nanomater 1:1–34

Sharma S, Beyer J, Gloaguen R, Heitmann J (2019) Non-quenching photoluminescence emission up to at least 865 K upon near-UV excitation in a single crystal of orange-red emitting SmPO$_4$. Phys. Chem Chem Phys 21:25669–25677

Shende D, Rane Y, Raghuwanshi M (2018) Visible-light-driven photocatalytic activity of mixed phase CdS-flakes. Optik 161:284–292

Shinde D, Pillai V (2013) Electrochemical resolution of multiple redox events for graphene quantum dots. Chem Int Ed 52(9):2482–2485

Singh K, Ahmed T, Gautam P, Sadhu A (2021) Recent advances in two-dimensional quantum dots and their applications. Nanomaterials 11(6):1549

Sridevi D, Sundaravadivel E, Kanagaraj P (2002) Influence of Fe doping on structural, physicochemical and biological properties of CdSe nanoparticles. Mater Sci Semicond Process 101:67–75

Srinivasan N (2019) Fabrication and photocatalytic properties of Multi-Morphological CdS NSs prepared by the thermolysis of heterocyclic dithiocarbamate Cadmium complexes as precursors. Dye Pigment 162:786–796

Steckel J, Snee P, Coe-Sullivan S, Zimmer J (2006) Color-saturated green-emitting QD-LEDs. Angew Chem Int Ed 45:5796–5799

Thirugnanam N, Song H, Wu Y (2017) Photocatalytic degradation of Brilliant Green dye using CdSe quantum dots hybridized with graphene oxide under sunlight irradiation. Chin J Catal 38(12):2150–2159

Valizadeh A, Samiei M, Farkhani M (2012) Quantum dots: synthesis, bioapplications, and toxicity. Nanoscale Res Lett 7(1)

Verma P, Kumar J (2014) Degradation and microbiological validation of meropenem antibiotic in aqueous solution using UV, UV/H$_2$O$_2$, UV/TiO$_2$ and UV/TiO$_2$/H$_2$O$_2$ processes. Int J Eng Res Appl 4(7):58–65

Vidhya M, Pandi R, Archana R, Sadayandi K, Sagadevan S (2020) Comparison of sunlight-driven photocatalytic activity of semiconductor metal oxides of tin oxide and cadmium oxide nanoparticles. Optik 217:164878

Wang Y, Herron N (1991) Nanometer-sized semiconductor clusters–materials synthesis, quantum-size effects, and photophysical properties. J Phys Chem 95:525–532

Wen J, Li X, Liu W (2015) Photocatalysis fundamentals and surface modification of TiO$_2$ nanomaterials. Chin J Catal 36(12):2049–2070

Wong K, Bunzli J, Tanner P (2020) Quantum yield and brightness. J Lumin 224:117256

Wu Y, Lim C, Fu S, Zeng X (2007) Surface modifications of ZnO quantum dots for bio-imaging. Nanotechnology 18:215604

Xu Q, Cai W, Li W, Sreeprasad T, He Z, Ong W (2018) Two-dimensional quantum dots: fundamentals, photoluminescence mechanism and their energy and environmental applications. Mater Today Energy 10:222–240

Yoffe (1993) Low-dimensional systems–quantum-size effects and electronic-properties of semiconductor microcrystallites (zero-dimensional systems) and some quasi-2-dimensionalsystems. Adv Phys 42:173–266

Yoffe (2001) Semiconductor quantum dots and related systems: Electronic, optical, luminescenceand related properties of low dimensional systems. Adv Phys 50:1–208

Yu H, Liu J (2021) Li X: Fabrication of ZnO/ZnS/ZnSe nanosheets for enhanced photocatalytic activity under simulated solar light. J Mater Sci Mater Electron 32:20082–20092

Zhang J, Saltzman M (2013) Engineering biodegradable nanoparticles for drug and gene delivery. Chem Eng Prog 109:25–30

Zhou J, Zou X, Song S, Chen G (2018) Quantum dots applied to methodology on detection of pesticide and veterinary drug residues. J Agric Food Chem 66(6):1307–1319

Zou L, Gu Z, Sun M (2015) Review of the application of quantumdots in the heavy-metal detection. Toxicol Environ Chem 97:3–4, 477–490

In-Silico Identification of Potential Phytochemicals Against Human Protease Activated Receptor-2 (PAR2) Involved in Rheumatoid Arthritis

Apoorva Vashisth, Khushboo Choudhury, Navjyoti Chakraborty, Ram Singh Purty, and Sayan Chatterjee

Abstract The extensive use of synthetic drug molecules has paved way to the new era of drug resistance and drug-associated toxicity and are highly expensive to the manufacturers which is ultimately passed on to be borne by the patients. The occurrence of drug resistance and drug-associated toxicity have led to reduced sales or even put some drugs out of the market. The use of phytochemicals has been reported as an alternative to synthetic drugs. Protease activated receptor 2 (PAR2) has been established as a promising target in many diseases including rheumatoid arthritis. The activation of PAR-2 molecule is carried out by tryptase by cleaving its N terminal chain after binding with it. The disease progression in rheumatoid arthritis can thus be inhibited by plant protease inhibitors as a therapeutic agent. In this work, we report a few serine protease inhibitors of plant origin such as At_KPI1, At_Serpin1 and BTICMe as phytochemicals with therapeutic potential for prevention or as an antagonist against progression of the disease. The results are indicative and may be used for clinical studies on dose dependent therapy via ex vivo or in vivo methods.

Keywords In silico screening · Protease activated receptor 2 (PAR2) · Molecular docking · Rheumatoid arthritis · Serine protease inhibitors · Protein–protein interaction

1 Introduction

Rheumatoid arthritis (RA) is characterized by inflammation along with extra-articular involvement primarily led by autoimmune responses. Irregular production of inflammatory regulators (which includes tumour necrosis factor α, interleukins such as 1, 6, and 8, and others subsequent to an exposure towards any antigenic pathogen), is followed by activation of endothelial cells and synovial cell hyperplasia and ultimately cartilage degradation (Shapouri-Moghaddam et al. 2018). This

A. Vashisth · K. Choudhury · N. Chakraborty · R. S. Purty · S. Chatterjee (✉)
University School of Biotechnology, Guru Gobind Singh Indraprastha University, Sec-16C, Dwarka, New Delhi 110078, India
e-mail: sayan@ipu.ac.in

considerably contributes to the state of disability, sometimes also resulting in premature death and an increase in socio-economic burdens. The basis of a cure for RA, like many other diseases, is diagnosis at an early stage in order to prevent the progression of the disease to the advanced stage where joint degradation reaches an irreversible stage (Combe 2009). Due to the absence of any promising cure for RA, the objective of the treatment strategy remains to expedite diagnosis in order to achieve a low disease activity state (LDAS). To be able to completely suppress the activity, rheumatologists need to continuously and accurately monitor the progression of the disease and simultaneously keep modifying the treatment regime accordingly. However, the entire remission of the disease with everlasting long-term effects is pretty challenging to achieve (Nagpal et al. 2011). The current study is aimed to discover new potential pharmacological interventions for the optimization of treatment of RA regimes.

The direct involvement of PAR2 in RA was first elucidated by Ferrell et al. using a comparative analysis of Protease Activated Receptor-2 deficient homozygote (Par2−/−) mice with Protease Activated Receptor-2 heterozygote (Par2+/−) mice. It was found that the heterozygote showed intermediate phenotypes when comparisons were drawn with mutant homozygotes and wild-type individuals. The results of synovial tissue biopsies of RA patients have shown a notable increase in the concentration of PAR2. Amplified PAR2 expression on CD14 + monocytes (along with other cells of RA synovium), complemented with enhanced TNF-α production, translating to pro-inflammatory phenotype, all provide promising evidence of the significant role of PAR2 in RA (Palmer et al. 2002). However, to decipher the precise pathways of involvement of PAR2 in the activation of inflammatory mediators and progression of RA and the corresponding synovial pathology, various studies have yet to be conducted. The popular PAR2 binding molecule for activation of PAR2 is reported to be tryptase. Protease activated receptor 2 (PAR2) expressed by fibroblasts may be activated by serine proteases, such as the mast cell mediator tryptase (Bagher et al. 2018).

The cumulative evidence of involvement of PAR2 in nociception along with its role in inflammation and joint erosion during rheumatoid arthritis makes it a prospective therapeutic target. And due to no available targets of PAR2 in the therapeutic treatment of RA, makes it even more important to exploit the available options and consider it a viable treatment option for RA (Kumar et al. 2018).

2 Material and Methods

2.1 Data Mining of PAR2 Structural File/information

A thermostabilised human protease-activated receptor-2 (PAR2) crystal structure is reported to be present in ternary complex with Fab3949 and AZ7188 at a 4.0-angstrom resolution in the PDB structure database.

2.2 Preparation of PAR2 as a Target Molecule for Drug-Interactions

Further, the structure was prepared for subsequent analysis via PDB Tools (Rodrigues et al. 2018). The active chain of PAR2 was cleaved off from the accessory structures not involved in the direct interactions, based on the structural information of PAR2 given in the PDB structure database (Rose et al. 2021).The interacting A chain was cleaved off from non-interacting H and L chains. The chain A of 5NJ6 was taken as our PAR2 structure file for all further structural analysis denoted as 5NJ6_A.

2.3 Data Mining of Serine Protease Inhibitors (SPIs) Against PAR2 and SPI Library Construction

The literature review was done to find out the Serine Protease Inhibitors (SPIs) against PAR2 naturally occurring in different plant species, characterized into different categories based on their mode of action. The biochemical nature of the SPIs was determined through NCBI database. SPI library construction was done using the PDB structure database (Purty et al. 2017).

2.4 Molecular Modeling of SPIs

SPIs in the library, for which structures were not available in the PDB database, molecular modeling was carried out using template-based homology modeling through Swiss Model (Meena et al. 2015; Waterhouse et al. 2018) and their respective models were obtained and viewed in ChimeraX (Pettersen et al. 2021).

2.5 Data Mining for the Protease Activator of PAR2: Tryptase

Through literature review (Swedberg 2011), PAR2 activator protease was determined. Crystal structure of human tryptase with potent non-peptide inhibitor was searched for in the PDB database.

2.6 Preparation of PAR2 Protease Activator: Tryptase, as a Positive Control Molecule for Drug Interactions

Further, tryptase structure was prepared for subsequent analysis via PDB Tools. The active chain of the tryptase was cleaved off from the accessory structures not involved in the direct interactions with PAR2, based on its structural information given in the PDB structure database.

2.7 Molecular Docking of PAR2 with Its Known Activator Protease

SAXS profile for PAR2 was computed to calculate the approximate distribution of pairwise atomic distances of the macromolecule (i.e., the pair-distribution function), using FoXS SAXS profile computational tool (Schneidman-Duhovny et al. 2016). The profiles were calculated as per the Debye Formula. Subsequently these were fitted to the experimental data. Appropriate adjustments of the parameters were made for a refined fit. These included hydration layer density (c2) and excluded volume (c1). The fit score is computed by minimizing the χ function with respect to c, c1, and c2. The PAR2 structure in PDB format, along with its respective chain Id would be used as input to generate its SAXS profile.

2.8 Receptor—Activator (PAR2—protease Activator) Docking

FoXSDOCK web server was used to carry out protein–protein docking. The input to the server was the PDB structure files of both the interacting entities, along with their respective chain IDs and the SAXS profile of the receptor which determined the scattering intensity of the interaction to the greater extent.

2.9 Protein-Inhibitor Interactions of PAR2 and SPI Library

The PDB files of PAR2 and SPIs, along with their respective chain IDs and the SAXS profile of the receptor was required as the inputs to the webserver, FoXSDOCK, to perform molecular docking of receptor and ligands (SPIs).
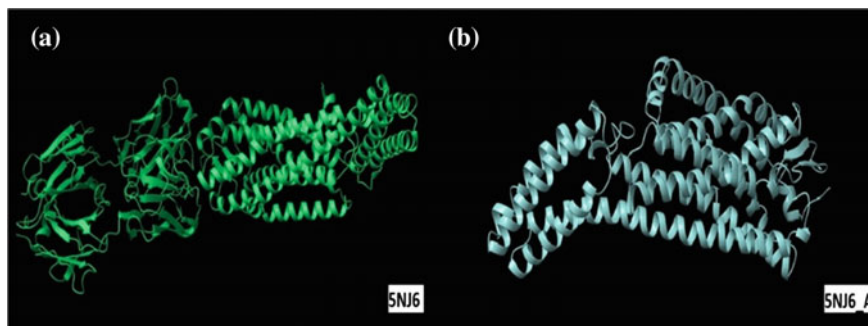
Fig. 1 Structure of **a** PAR2 (5NJ6) and **b** PAR2_A (5NJ6_A)

3 Results

3.1 Data Mining of PAR2 Structural File/information

PAR2 crystallography structures have been reported by many researchers (Cheng et al. 2017; Paula et al. 2019). Among these, the most popular and well-characterized structure used by researchers is PDB Id—5NJ6 (Fig. 1a). The structure has a co-crystal of PAR-2 denoted as the A-chain along with two other molecules namely Fab3949 and AZ7188 as H and L chains respectively. The structure file of 5NJ6 was retrieved from RCSB PDB database. As reported by McCulloch et al. (2018), the structure file contains PAR2 molecule as chain A with two non-interacting chains of Fab3949 (H chain) and AZ7188 (L chain).

3.2 Preparation of PAR2 as a Target Molecule for Drug Interactions

The interacting A chain was cleaved off from non-interacting H and L chains. The chain A of 5NJ6 was taken as our PAR2 structure file for all further structural analysis. The PAR2 (5NJ6_A) structure (Fig. 1b) displays characteristic structural features of the protease activated receptors such as intertwined alpha helices which constitutes the active core of the molecule along with two small segments of beta sheet at one of its end.
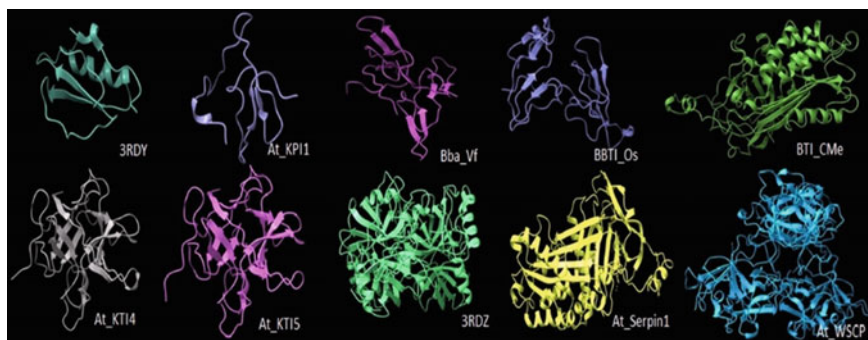
Fig. 2 Molecular models of SPIs

3.3 Construction of Library of Serine Protease Inhibitors Against PAR2

A list of naturally occurring 10 serine protease inhibitors (SPIs), in different species of plants were populated in the library. They were categorized into different classes based on their mechanism of action. Out of these 10 SPIs the structure of Atserpin1 (PDB Id; 3LE2) was available and thus retrieved from the PDB database.

3.4 Molecular Modeling of SPIs

For the SPIs whose structures were not found in the PDB database, their models were constructed through Template based homology modelling via Swiss-Model through its online server. These 9 models were built using their respective protein sequence files (Fig. 2).

3.5 Structural Classification of Tryptase as a Protease Activator of PAR2

The structure of Tryptase (Fig. 3a) was retrieved from the PDB database. All the four chains A, B, C, D are characterized by small segments of alpha helices, beta sheets running parallel and anti-parallel at their core with multiple loop structures loosely surrounding the catalytic site.
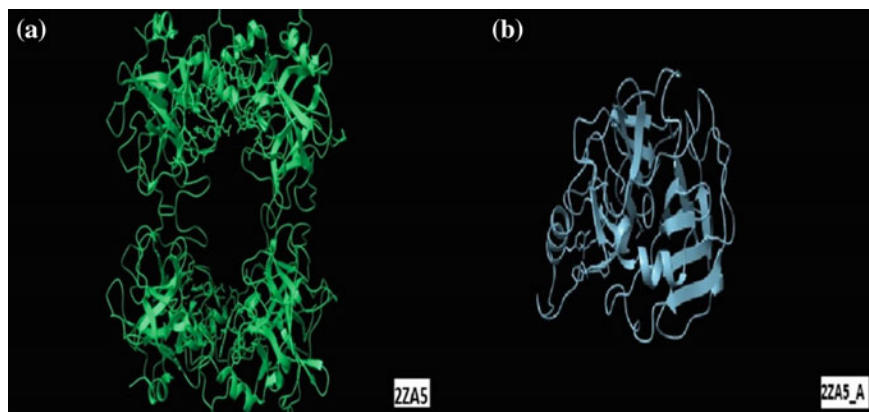
Fig. 3 Structure of **a** Tryptase (2ZA5) and **b** Tryptase_A (2ZA5_A)

3.6 Preparation of Tryptase as a Positive Control Molecule for Drug Interaction

Four chains of Tryptase namely A, B, C, D were cleaved off from each other to be used separately for further analysis (Fig. 3b). Since all the four chains interact differently with the receptor owing to their structural and functional differences, it is important to analyse the interactions of all the four chains independently as a catalytic chain.

3.7 Molecular Docking of PAR2 and Tryptase

Computing small-angle X-ray scattering (SAXS) profile. The SAXS profile for PAR2 (5NJ6_A) was generated to be used for further molecular docking analysis (Fig. 4). Small Angle X-Ray Scattering profile is useful in defining the ambient environment where the reaction between the receptor and substrate takes place. Since the receptor molecule PAR2 primarily contributes to defining the ambient reaction conditions, SAXS profile, for 5NJ6_A was calculated and used as an input for the further docking analysis.

PAR2 Tryptase docking. Chain A of PAR2 molecule (5NJ6_A) was docked with four different chains of tryptase i.e. A, B, C, D, using their structural co-ordinates along with SAXS profile of chain A of PAR2 molecule (Table 1). The following dock scores were obtained and based on the highest affinity of chain A of tryptase (2ZA5_A) with PAR2 (5NJ6_A), it was selected to be used as a benchmark for further docking analysis of the SPIs.
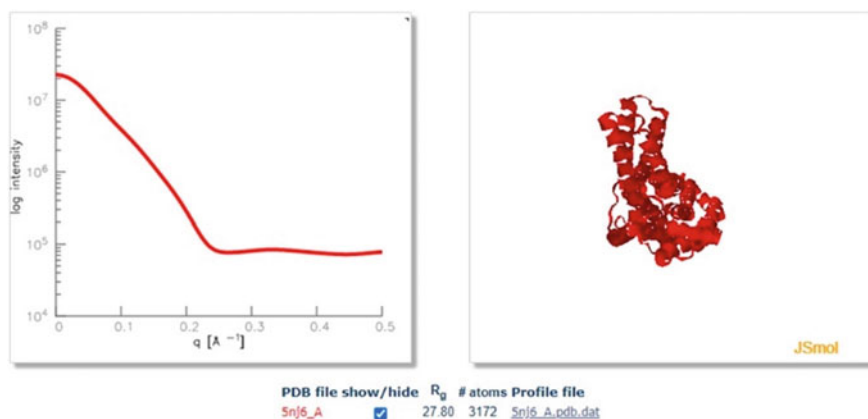
Fig. 4 SAXS profile of 5NJ6_A

Table 1 Tryptase individual chain Docking Scores

Tryptase (2ZA5)	Docking scores
2ZA5_A	−5.057
2ZA5_B	−4.641
2ZA5_C	−4.134
2ZA5_D	−4.412

3.8 Interactions of PAR2 and SPIs

PAR2- SPIs. The dock scores of PAR2 (5NJ6_A) and SPIs were obtained and plotted in a line chart along with the docking scores of 2ZA5_A as a benchmark for comparative analysis of relative affinities of SPIs and Tryptase (2ZA5_A) for PAR2 (5NJ6_A) (Table 2; Fig. 5).

The SPIs with the higher negative docking scores than Tryptase (2ZA5_A) were selected as comparatively more potent than the activator tryptase molecule (Verma et al. 2021) Three out of ten SPIs namely, At_KPI1, At_Serpin1 and BTICMe showed docking scores greater than 5.057 (in negative scale), signifying their greater affinity for PAR2. These 3 SPIs demonstrated effective inhibition of the activation of PAR2 and may serve as competitive inhibitors for Tryptase, which is the primary serine protease involved in PAR2 activation. Thus, we may propose that these SPIs can serve as potential therapeutic agents to arrest the progression of RA.

Table 2 SPI Docking scores

SPIs	Docking scores
3rdy	−4.525
3rdz	−4.805
At_KPI1	−5.304
At_KTI5	−4.075
At_KTI4	−4.744
At_Serpin1	−5.541
At_WSCP	−4.414
BBA_Vfaba	−4.746
BBTI_Os	−4.92
BTICMe	−6.385
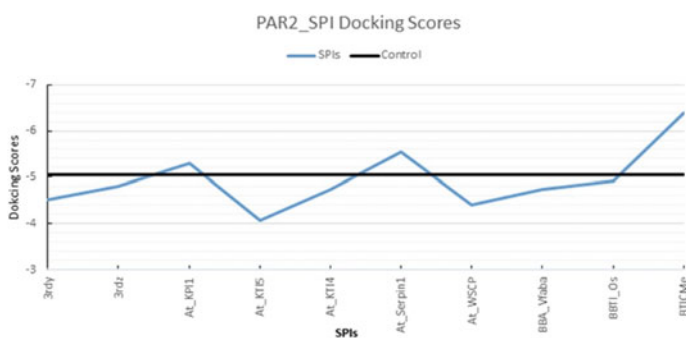
Fig.5 PAR2_SPI docking scores

4 Conclusion

The activation of PAR-2 molecule by tryptase by cleaving its N terminal chain can be inhibited by plant protease inhibitors. These molecules may thus be proposed as natural therapeutic agents against progression of rheumatoid arthritis. In this study we are reporting At_KPI1, At_Serpin1 and BTICMe as phytochemicals with therapeutic potential for prevention or as an antagonist against progression of the disease. The results are indicative and may be used for clinical studies on dose dependent therapy via ex vivo or in vivo methods.

Competing Interests The authors declare that there are no conflicts of interest.

References

Bagher M, Larsson-Callerfelt AK, Rosmark O, Hallgren O, Bjermer L, Westergren-Thorsson G (2018) Mast cells and mast cell tryptase enhance migration of human lung fibroblasts through protease-activated receptor 2. Cell Commun Signal 16(1):1–3

Cheng RK, Fiez-Vandal C, Schlenker O, Edman K, Aggeler B, Brown DG, Brown GA, Cooke RM, Dumelin CE, Doré AS (2017) Structural insight into allosteric modulation of protease-activated receptor 2. Nature 545(7652):112–115

Combe B (2009) Progression in early rheumatoid arthritis. Best Pract Res Clin Rheumatol 23(1):59–69

De Paula VS, Sgourakis NG, Francischetti IM, Almeida FC, Monteiro RQ, Valente AP (2019) NMR structure determination of Ixolaris and factor X (a) interaction reveals a noncanonical mechanism of Kunitz inhibition. Blood J Am Soc Hematol 134(8):699–708

Kumar S, Chatterjee S, Kumar S (2018) Dual anti-cholinesterase activity of Ajoene by in silico and in vitro studies. Pharmacognosy Res 10(2)

McCulloch K, McGrath S, Huesa C, Dunning L, Litherland G, Crilly A, Hultin L, Ferrell WR, Lockhart JC, Goodyear CS (2018) Rheumatic disease: protease-activated receptor-2 in synovial joint pathobiology. Front Endocrinol 9:257

Meena SS, Chatterjee S, Aggarwal KK (2015) Structural modelling of a-subunit of ringhy-droxylating dioxygenases (RHDs) from microbial sources. Int J Curr Microbiol App Sci 4:740–752

Nagpal N, Munjal N, Chatterjee S (2011) Analysis of annotation strategies for hypothetical proteins: a case study of Neisseria. J Nat Sci Biol Med 2(3)

Palmer G, Guerne P-A, Mezin F, Maret M, Guicheux J, Goldring MB, Gabay C (2002) Production of interleukin (IL)-1 receptor antagonist by human articular chondrocytes. Arthritis Res Ther 4(1):1–38

Pettersen EF, Goddard TD, Huang CC, Meng EC, Couch GS, Croll TI, Morris JH, Ferrin TE (2021) UCSF ChimeraX: structure visualization for researchers, educators, and developers. Protein Sci 30(1):70–82

Purty R, Sachar M, Chatterjee S (2017) Structural and expression analysis of salinity stress responsive phosphoserine phosphatase from Brassica juncea L. J. Proteomics Bioinform 10:119–127

Rodrigues JP, Teixeira JM, Trellet M, Bonvin AM (2018) pdb-tools: a swiss army knife for molecular structures. F1000Research 7

Rose Y, Duarte JM, Lowe R, Segura J, Bi C, Bhikadiya C, Chen L, Rose AS, Bittrich S, Burley SK (2021) RCSB Protein data bank: architectural advances towards integrated searching and efficient access to macromolecular structure data from the PDB archive. J Mol Biol 433(11):166704

Schneidman-Duhovny D, Hammel M, Tainer JA, Sali A (2016) FoXS, FoXSDock and MultiFoXS: single-state and multi-state structural modeling of proteins and their complexes based on SAXS profiles. Nucleic Acids Res 44(W1):W424–W429

Shapouri-Moghaddam A, Mohammadian S, Vazini H, Taghadosi M, Esmaeili SA, Mardani F, Seifi B, Mohammadi A, Afshari JT, Sahebkar A (2018) Macrophage plasticity, polarization, and function in health and disease. J Cell Physiol 233(9):6425–6440

Swedberg JE (2011) Rational design of serine protease inhibitors. Queensland University of Technology

Verma SK, Kaur S, Tevetia A, Chatterjee S, Sharma PC (2021) Structural characterization and functional annotation of microbial proteases mined from solid tannery waste metagenome. Biologia 76(6):1829–1842

Waterhouse A, Bertoni M, Bienert S, Studer G, Tauriello G, Gumienny R, Heer FT, de Beer TAP, Rempfer C, Bordoli L (2018) SWISS-MODEL: homology modelling of protein structures and complexes. Nucleic Acids Res 46(W1):W296–W303

Crop Residues: A Potential Bioenergy Resource

Maninder Kaur and **Sandeep Dhundhara**

Abstract Most of the population in India relies on agriculture and livestock for their livelihood as the country is bestowed by the nature with a variety of geographical regions vacillating from high mountains to wetlands, myriads rivers to plains, thus making most land fertile and suitable for a variety of food crops. The crop residues like rice straw, leaves, roots, bagasse, etc. that remain in fields after harvesting and processing are proving to be a major concern as these residues are frequently burnt by the farmers in the open fields causing environmental pollution leading to serious health problems. On the other hand, the share of bioenergy in power generation is significantly low as compared to the other available resources in the total energy mix of the country. The biomass can provide reliable and consistent power supply to the end-user in comparison with solar and wind energy resources, therefore, preferred as a renewable energy resource over other resources. Due to dependency on the season, the solar and wind energy resources fluctuate over short and large time frames. Thus, provides unreliable and inconsistent supply to end-user however biomass seems to be a feasible alternative to fossil fuels. So, the solar, wind, and biomass due to their different characteristics provide an opportunity for hybrid utilization of these resources to compensate for their individual drawbacks. Hybridization of these resources helps to utilize the biomass efficiently and provides electricity to end-users reliably and consistently. Hence, biomass-based hybrid power plants are tremendously promising energy systems in near future. Biogas production through anaerobic digestion from such crop residues can offer great potential for replacement of the fossil fuel for our energy requirements.

Keywords Anaerobic digestion · Crop residues · Biogas · Energy mix · Biomass

M. Kaur (✉)
Dr. S.S.B. University Institute of Chemical Engineering and Technology, Panjab University, Chandigarh 160014, India
e-mail: maninderkaur2780@gmail.com

S. Dhundhara
College of Agricultural Engineering & Technology (COAE&T), CCS Haryana Agricultural University, Hisar 125001, Haryana, India

1 Introduction

The socio-economic development of any country is highly reliant on the availability of electrical energy. For this, the installed capacity of power needs to be raised at the same pace as that of rapid urbanization, and an increase in population. As per reports from UNDESA (United Nations Department of Economic and Social Affairs), the world population will be raised to 9.7 billion by the year 2050, so this will employ extra pressure on the agriculture and energy sector. The power sector leads in the consumption of fossil fuels mainly in developing countries such as India, where most of the growing load demand is fulfilled by coal-based power plants. The installed capacity of 121 GW power plants in India consumes 503 million tons of coal which emitted a large amount of GHGs in the year 2010–11 (Guttikunda and Jawahar 2014). The GHGs emission resulted in 20 million asthma cases and approximate 80,000–115,000 premature deaths on exposure to $PM_{2.5}$ pollutions alone which costs wastage of the public and Government in crores. The open field burning of residues in the field stimulates the existing pollution due to coal-based power plants resulting in the emission of various air pollutants including GHGs (Lohan et al. 2018).

Therefore, renewable energy has gained more attention as promising means of increased energy security and provides multiple environmental benefits, and also plays a crucial role to replace fossil fuels based conventional energy resources. The sustainable utilization of crop residue in a biomass-based hybrid power plant through the biochemical conversion pathway of anaerobic digestion is very significant in current scenario.

1.1 Biofuels Classification

Due to the increased concerns about GHGs emissions and energy, biofuels have attracted a lot of attention these days. The renewable energy sources will approximately grow to 15% of the world energy market by 2035 as reported by "International Energy Outlook" And liquid biofuels such as biodiesel, bioethanol will cover about 29% of world energy demand. The accelerated reliance on biofuels is associated with the abundance availability of biomass for biofuel production. Thus, bioenergy is a key contributor to provide sustainable energy for developing industrialization and developing nations. Biofuels are classified as liquid, gaseous, and solids fuels that are produced from biomass. Biofuels utilize unprocessed biomasses like wood chips, pellets, fuel woods, etc. are referred to as solid fuels or primary fuels. Biomasses after processing and transformations get converted into liquids and gaseous biofuels also known as secondary biofuels (Dahman et al. 2019). Fig. 1 represents the biofuels classification according to the biomass source used for biofuel production.

First-generation biofuel utilizes edible biomasses which are meant for food purposes like carbohydrate-rich crops such as wheat and corn fermented into bioethanol, lipid-rich crops such as soya for biodiesel, and both carbohydrate and
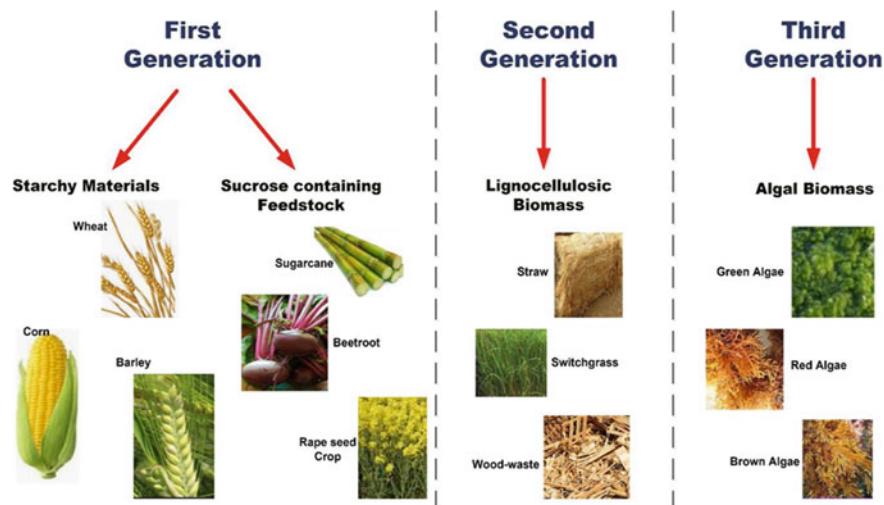
Fig. 1 Biofuel classification

lipid-rich crop for methane production. However, the increase in the cost of production, energy spent in cultivation, and inefficient utilization of resources limits the use of first-generation biofuel. The augmented biofuels demand from first-generation biomass has been reflected in the US Energy Independence and Security Act of 2007 which sets the target of 21 billion gallons of biofuels such as biobutanol by 2022. Biofuels produced from edible products such as sugars, starch, and vegetable oil are not advisable as they may cause food scarcity in developing countries like India (Dahman et al. 2019).

The second-generation biofuel production is based on more effective renewable alternatives by utilizing non-edible lignocellulosic biomass of crop residues such as straw, stalks, sorghum, stover, etc. The use of lignocellulosic biomass for biofuel production has the advantage as available in abundance worldwide. Crop residues correspond to the waste that remains in the fields after food extraction without any extra land required for their production (Balat and Balat 2010). The fermentation of these residues in the soil, open field burning, manure management, etc. results in approximately 47% of global methane emissions. The biogas production through anaerobic digestion of crop residue could be one of the sustainable options to remove the crop residue from the fields and capture the methane as a renewable energy resource simultaneously (Ohman et al. 2006).

The utilization of lignocellulosic biomass for biofuel generation has the advantage as available in abundance worldwide. Crop residues correspond to the waste that remains in the fields after food extraction without any extra land requirement for their production (Balat and Balat 2010). The fermentation of these residues in the soil, open field burning, manure management, etc. results in approximately 47% of global methane emissions. The biogas production through anaerobic digestion of

crop residue could be one of the sustainable options to remove the crop residue from the fields and capture the methane as a renewable energy resource simultaneously (Ohman et al. 2006).

Among the biofuel production from second-generation (biodiesel, bioethanol, biogas, etc.) by biochemical conversion pathway, the biogas production through anaerobic digestion of lignocellulosic biomass could be one of the sustainable options for increasing the renewable resources share in the energy sector of the country. As bioethanol can be derived from the fermentation of cellulose, however, both hemicellulose and cellulose can be utilized to produce methane. Secondly, methane can be mixed with the natural gas grid once purified and compressed, which can be further used for various applications such as electricity production, heat, or as vehicle fuel. Finally, the digestate obtained from the anaerobic digestion process being rich in nitrogen and phosphorous can be utilized as fertilizer for agricultural plants (Kleinert and Barth 2008).

Microalgae, the third generation of biofuels is another viable alternative renewable energy source that can be used to produce biomethane, bioethanol, and biodiesel (Frigon and Guiot 2010). However, the large areas, high initial cost, and huge amount of water required for cultivation remain a major disadvantage that limits third-generation biofuel commercialization (Nigam and Singh 2010).

1.2 Anaerobic Digestion

Anaerobic digestion, a biochemical process comprising the conversion of complex organic matter present in biomass into a valuable product such as biogas in the absence of oxygen. Methane, the main component of biogas is the highly combustible component that can be used as the energy source for cooking, lighting, and heating. The anaerobic digestion process optimization requires the understanding of different biological processes along with associated chemical reactions. Mainly, the process involves four key phases namely; hydrolysis, acidogenesis, acetogenesis, and methanogenesis:

In the first step of hydrolysis, the complex organic matter is directly utilized by the bacteria to decompose it into soluble molecules with the effect of hydrolytic enzymes (Azapagic and Stichnothe 2011). The organic matter gets converted into monosaccharides (simple sugars), fatty acids, amino acids, and peptides in this process. The hydrolysis of carbohydrates is a fast process that takes only a few hours however, the hydrolysis of lipids and proteins takes few days thus making the degradation of lignocellulosic biomass slow and incomplete. The hydrolysis process can be chemically explained as follows:

$$n\mathrm{H_2O} + (\mathrm{C_6H_{10}O_5})_n \rightarrow n\mathrm{C_6H_{12}O_6} + n\mathrm{H_2} \tag{1}$$
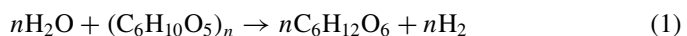
The breaking of β-1,4-glycosidic linkages as shown in Eq. (1) is an essential step for cellulose ($C_6H_{10}O_5$) conversion as it opens the possibility of catalytic transformation.

Acidogenesis is also known as the fermentation process that results in volatile fatty acids after attack by acidogenesis bacteria. Then, acidogenic bacteria convert the hydrolysis product into CO_2 and H_2. The most significant organic acid CH_3COOH is produced in this stage which is further used as a substrate by microorganisms (Appels et al. 2011). The following Eqs. (2)–(4) represent the sequence of reactions taking place in the acidogenic stage of the anaerobic digestion process:

$$C_6H_{12}O_6 \leftrightarrow 2CO_2 + 2CH_3CH_2OH \tag{2}$$

$$2H_2 + C_6H_{12}O_6 \leftrightarrow 2CH_3CH_2COOH + 2H_2O \tag{3}$$

$$C_6H_{12}O_6 \rightarrow 3CH_3COOH \tag{4}$$

Acetogenesis is also known as the dehydrogenation stage of the anaerobic digestion process. The volatile fatty acids produced in the acidogenesis are broken down into CH_3COOH, H_2, and CO_2 in this stage. As some amount of H_2O is still available from the previous stages so the conversion of the volatile fatty acids is possible (Appels et al. 2011; Anukam et al. 2019). Equations (5) to (7) represent the chemical reactions taking place in this stage.

$$3H_2O + CH_3CH_2COO^- \leftrightarrow CH_3COO^- + H^+ + 3H_2 + HCO_3^- \tag{5}$$

$$C_6H_{12}O_6 + 2H_2O \leftrightarrow 2CO_2 + 4H_2 + 2CH_3COOH \tag{6}$$

$$CH_3CH_2OH + 2H_2O \leftrightarrow H^+ + 3H_2 + CH_3COO^- \tag{7}$$
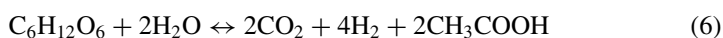
However, there is no clear distinction between acidogenic and acetogenic reactions as H_2 and $CH3COO^-$ produced in both types of reactions, which act as a substrate for methanogenic bacteria.

Methanogenesis, results in the breaking down of the acetic acid and volatile fatty acids molecules into methane (CH_4), carbon dioxide (CO_2) (Li et al. 2019). The bacteria responsible for the conversion in this process are known as methanogens. Although methanogens grow slowly and are extremely sensitive to environmental changes but can easily absorb and digest the substrate. The chemical reactions Eqs. (8)–(10) represent the conditions taking place in this stage of the anaerobic digestion process.

$$CH_3COOH \rightarrow CO_2 + CH_4 \tag{8}$$

$$CO_2 + 4H_2 \rightarrow 2H_2O + CH_4 \tag{9}$$

$$CO_2 + 2CH_3CH_2OH \rightarrow CH_4 + 2CH_3COOH \tag{10}$$
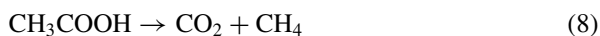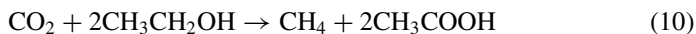
The two groups in which methane-producing bacteria can be divided are Acetophilic and hydrogenophilic. Acetophilic has based the production of methane by decarboxylation of acetate as represented by Eq. (10) whereas in hydrogenophilic group methane production takes place by reduction of CO_2 and H_2 as represented in Eq. (9).

1.3 Pretreatment of Crop Residues

Lignocelluloses have a complex organic polymer structure composed of physical and chemical associations among hemicelluloses, cellulose, and lignin which are difficult to be decomposed by anaerobic bacteria to produce biogas. Cellulose is the most abundant component of lignocellulose biomass represents 35–40% of dry matter while hemicellulose and lignin represent 25–40% and 10–20% of total dry matter of biomass.

Thus, lignocellulose is one of the most abundantly available biopolymers, having various structural and compositional characteristics which provide recalcitrance to its biological degradation thereby reducing biofuel conversion efficiency. Pretreatment of biomass is an essential step to break the outer layer of lignin, thereby decreasing the crystallinity of cellulose and aggregate the obtainability of carbohydrates. The various methods of pretreatment of lignocellulose like physical, biological, and chemical are used to produce second-generation bioethanol.

1.3.1 Physical Pretreatment

Physical pretreatment of residue involves size reduction using ball mill, grinding, chipping, mechanical extrusion, and irradiation. Milling or mechanical grinding can be done through the knife, ball milling, hammer, colloid mill, etc. The size of biomass can be reduced to 5–30 mm through chipping however, with the help of ball milling and grinding the size of particles may be reduced to 0.2 mm. However, the specific kind of biomass, duration of milling, and types of milling are the main factors that affect the degree of polymerization, disruption in the crystalline structure, and surface area enhancement of lignocellulosic biomass. The physical pretreatment reduces the particle size and enhances the surface area of biomass for enzymes accessibility (Kratky and Jirout 2011).

Mechanical Pretreatment

The results of mechanical pretreatment of lignocellulosic biomass are diverse as reported by various researchers, suggesting that the effect on methane production depends upon the methods used (cutting, chopping, milling, grinding). For instance, it has been observed that biogas production enhanced by 22% as the size of sisal fiber particles reduced from 10 to 2 mm (Mshandete et al. 2016). Similarly, the mechanical pretreatment of barley and wheat straw resulted in an increase of methane potential by 54% and 83.5% with a reduction in particle size to 0.5 cm and 0.2 cm, respectively (Menardo et al. 2012). However, the hydrolysis of sweet corn and ensiled maize mixture was not affected by the reduction in particle size ranging between 2 mm and 5 mm (Ficara and Malpei 2011). Therefore, it becomes more effective if combined with other pretreatment methods such as liquid hot water pretreatment, chemical pretreatment method, etc.

Microwave Irradiation

The enhancement in the digestibility of residue can be observed by the use of irradiation techniques such as microwave irradiation, gamma rays, ultrasound, and electronic beam to increase the enzymatic hydrolysis of lignocellulosic biomass. Irradiation pretreatment leads to cleavage of β-1,4-glucan bonds thus reducing the crystallinity of cellulose (Takacs et al. 2000; Chandra et al. 2012). Microwave irradiation has several advantages such as easy operation, minimum generation of inhibitors, and high heating capability in short duration. Studies using the microwave irradiation technique of physical pretreatment show that it is more effective with mild alkali reagents. Wheat straw pretreatment at 150 °C using microwave radiation resulted into methane enhancement by 28% in comparison with untreated wheat straw (Jackowiak et al. 2011).

Ultrasound Pretreatment

Ultrasound pretreatment is a relatively new technique used for pretreatment in which waves produce both chemical and physical effects on the morphology of biomass. Prolonged saponification has no additional effect in terms of sugar release and delignification after a certain limit (Kumar and Sharma 2017). For cellulosic feedstock accessibility of cellulose enzymes to cellulose increases with ultrasound irradiation by disrupting the cell wall. Ultrasound pretreatment can enhance sugar yield in the hydrolysis process by changing the surface morphology of lignocelluloses material. Further, it has been observed that combined use of NaOH and Ultrasonic irradiation pretreatment effectively disrupts the intermolecular hydrogen bonding of bagasse resulting in the extraction of more than 90% of glucose yield within the duration of 70 h (Velmurugan and Muthukumar 2012).

Steam Explosion Method

Steam explosion pretreatment, involves mechanical forces as well as chemical effects. The biomass is subjected to high temperature (160–260 °C) with sufficient pressure

of 1–7 MPa ranging from few seconds to minutes resulting in hydrolysis of hemicel-luloses. Wheat straw pretreatment by this method of the steam explosion at 180 °C for 25 min showed 31% enhancement in biogas production (Bauer et al. 2010). Another study reported that pretreatment of bulrush represents 24% enhancement in methane yield at steam pressure 1.72 mPa with 8.14 min of residence time (Wang et al. 2010). However, the steam explosion method on paper tube residuals represents no change in biogas production and has shown the negative effect of a pretreatment when the time was increased from 10 to 30 min in the case of paper tube residuals. The steam explosion method limits the complete disruption of the LCC's and thus formation of inhibitors and unwanted degradation of the cellulose takes place (Kumar et al. 2009).

Liquid Hot Water

The liquid hot water method of pretreatment involves cooking of biomass in hot water without using any chemicals or catalysts. Water at high pressure easily breach into the biomass and it hydrates the cellulose and takes out hemicellulose along with some part of lignin. Corn fiber (de-starched) after the liquid hot water pretreatment at 160 °C for 20 min dissolved 75% of the xylans (Dien et al. 2006). Further, it has observed that liquid hot water pretreatment dissolved hemicellulose completely at the higher temperature of 220 °C with partial removal of lignin within 2 min (Sreenath et al. 1999).

1.3.2   Chemical Pretreatment

Chemical pretreatment of biomass includes alkaline pretreatment, ionic pretreatment acidic pretreatment, and wet oxidation. The concentration of chemical used, time, and temperature of pretreatment significantly affects the effectiveness of the chemical pretreatment method on delignification of crop residues. Various chemical pretreat-ment methods reported in the literature depending on the nature of the chemical used are as follows:

Acidic Pretreatment

Acids are commonly used to increase the enzymatic hydrolysis of biomass. Acid pretreatment can be carried out either at high temperature (120–170 °C) for a short duration (1–5 min) of time or at low temperature (about 25 °C) for a long duration of time (hours, days). Sulphuric acid is the most commonly used acid for pretreatment, while hydrochloric acid has also been used in various studies (Kumar et al. 2009; Taherzadeh and Karimi 2008). Chemical pretreatment of corn cob using 2%(w/w) H_2SO_4 at 121 °C for 1 h resulted in 17% delignification with the increase in cellulose from 35.9 to 54.78% (Ayeni et al. 2015). The production of inhibitory products mainly furfural, derived from hemicellulose degradation and corrosion of reactors limits its use.

Alkaline Pretreatment

Alkali pretreatment alters the crystalline structure of biomass and enhances enzymatic hydrolysis without producing inhibitors as was observed in the case of acid pretreatment. Calcium hydroxide, sodium hydroxide, ammonia, and potassium hydroxide are the most commonly used alkalis used for the chemical pretreatment of biomass. Sodium hydroxide (NaOH) is the most common alkali reagent used for chemical pretreatment. Alkaline pretreatment dosages ranging between 1–30 g NaOH per 100 gm substrate at a temperature ranging between 10–200 °C and time for the pretreatment varying from few minutes to days are reported in the literature. Also, it can be used for various lignocellulosic biomasses like wheat straw, rice husk, corn stover, sunflower stalks.

Wheat straw pretreatment with 4% NaOH (g/g TS) increased the methane production to 166 L/kg VS from 78 L/kg VS at a temperature of 37 °C for five days (Chandra et al. 2012). And 2% NaOH pretreated corn stover for 3 days at 20 °C increased the biogas production by 72.9% and decreases the digestion time by 34.6%. KOH has effectiveness nearly equal to NaOH for pretreatment to increase biogas production (Zheng et al. 2010). NaOH and KOH pretreatment of the rice husk resulted into 50% increment in the biogas yield (Dong et al. 2009). Alkaline pretreatment results in swelling of fibers increasing the surface area and pore size thus facilitating the diffusion of hydrolytic enzymes.

Ionic Pretreatment

Ionic liquid pretreatment also referred to as "green solvents", is an effective technique to increase the proper utilization of lignocellulosic biomass (Dadi et al. 2006; Samayam and Schall 2010). Ionic liquids are salts in liquid form and generally made up of ions and short-lived ions pair. NMMO (N-methyl morpholine-N-oxide monohydrate) mainly used ionic liquid for the pretreatment to increase the yield of biogas. Wheat straw treatment with 85% NMMO for 7 h at 900 °C increased the methane yield by 47% along with increased porosity of treated straw (Purwandari et al. 2013). A significant increase in the production of biogas was reported after pretreatment of rice straw with NMMO at 130 °C for one hour (Teghammar et al. 2011). Pretreatment of an empty bunch of oil palm fruit with 85% NMMO for 3 h at 120 °C and reported 48% enhancement of methane (Purwandari et al. 2013). Ionic liquids were found to be efficient in lignin removal as reported that 40% of lignin removal of wood takes place after this pretreatment (Lee et al. 2009).

Ionic liquids pretreatment has advantages like minimal effect on the environment due to their low volatility and it can be reused after pretreatment. However, the high cost of ionic liquids makes the method expensive (Nguyen et al. 2010). Moreover, the application of ionic liquid for pretreatment to produce biofuels needs to be tested in order to validate the ability of the microorganism to attack the organic matter in presence of these solvents (Brodeur et al. 2011).

Wet Oxidation

The wet oxidation method of pretreatment utilizes oxidizing agents such as air, hydrogen peroxide, and oxygen along with water at high temperatures (above 120 °C) and high pressure. The crystalline structure of cellulose (Panagiotou and Olsson 2006). The high risk of formation of inhibitors such as aromatic compounds and furfural, cost of reagents are some major drawbacks which restrict its use for pretreatment.

Among various chemical pretreatment methods, alkaline pretreatment seems to be the most economic and effective in disrupting the crystalline structure of biomass without producing inhibitors.

1.3.3 Biological Pretreatment

In comparison with chemical and physical methods of pretreatment, biological pretreatment is considered to be an economical, easy, and environment-friendly pretreatment method. Biological pretreatment makes use of white-rot fungi, brown rot fungi, and soft fungi which mainly degrade lignin and hemicelluloses with a lesser amount of cellulose. A significant increase in methane production has been observed after the pretreatment of bagasse with acid combined with enzymatic pretreatment (Badshah et al. 2012). The white-rot fungi such as Phanerochaetechrysosporium, Pleurotusostreatus, Coriolus Versicolor, and Ceriporiopsissubvermispora have been used for pretreatment of various biomass feedstock for biofuel production through solid-state or liquid state fermentation. The degradation process of biomass through biological pretreatment is extremely slow therefore, not favored method among industries. Several studies on biological pretreatment combined chemical and physical pretreatment have proven to be more effective than biological pretreatment alone. Further, studies show that performing fermentation and saccharification processes at high-substrate concentration results in an increase in the concentration of inhibitors. Pretreatment with enzymes has been suggested to prevent the production of such inhibitors.

1.4 Prominent Factors Affecting Biogas Production

The main factors affecting bacterial activity are the pH, COD, total alkalinity, micronutrients compounds (Yadvika et al. 2003). All these parameters are dependent upon the process parameters such as temperature, pH value, carbon to nitrogen ratio, hydraulic retention time, etc.

Carbon to Nitrogen Ratio

Carbon is the main constituent present in organic wastes which are digested by bacteria to convert it into methane and carbon dioxide. The inadequate amount of

nitrogen content slows down the microbial growth rate thus affecting the conversion of substrate into biogas (Wilkie and Colleran 1986). The C:N ratio of the biomasses varied widely between ratios 32:1 to 82:1, the high C:N ratio in the anaerobic digestion process leads to VFAs accumulation and lower pH, leading to inhibition. The optimum ratio of C:N to produce maximum biogas has been observed to vary from 25:1 to 30:1 (Ghatak and Mahanta 2014). Straw has high carbon content in comparison to nitrogen consequently having a high C:N ratio. Therefore, straw needs to be digested with organic matter rich in nitrogen (Yong et al. 2015).

Straw in co-digestion with food waste in ratio 1:5 resulted into C:N ratio of 31:1 which resulted in enhancement of methane production by 150% in comparison with straw and food waste only (Yong et al. 2015). Co-digestion of rice straw, food waste, and pig manure in ratio 1:0.4:1.6 resulted into 72% increase in methane production (Ye et al. 2013). In a study, the co-digestion of oat straw with cow manure in ratio 1:2 resulted in biogas enhancement by 26.64% and also stated that the addition of cow manure above this ratio resulted in inhibition (Zhao et al. 2018).

Temperature

Temperature of digester has a strong influence not only on the quality but also on the quantity of biogas production. Anaerobic digestion mainly takes place at either mesophilic temperature or thermophilic temperature. The change of temperature from 25 to 35 °C resulted in 24% enhancement of biogas (Lianhua et al. 2010). Further, a study reported the highest biogas production at 50 °C then followed by 60 and 40 °C respectively (Sambo et al. 1995). The positive effect of thermophilic conditions affects adversely if it is raised from 55 to 60 °C owing to suppression of bacteria due to high temperature. Moreover, if the digester operating at thermophilic conditions, it requires more technological efforts for insulation and high energy input therefore such conditions generally prove to be uneconomical.

pH Value

pH is an important variable strongly impacting the degradation of organic matter through anaerobic digestion. The pH value ranging between 6.25–7.50 has been reported to be most optimum for effective biogas production (Ghatak and Mahanta 2014). Methanogenic bacteria are very sensitive to pH value and do not thrive below 6.5.

Hydraulic Retention Time and Organic Loading Rate

Hydraulic retention time is the period for which a given quantity of substrate remains in the digester for methanogenesis bacterial attack. HRT is a temperature-sensitive parameter and usually varies between 20 and 120 days. HRT in India varies between 40–60 days and about 100 days for colder countries. Optimal HRT must allow 75% degradation of the substrate (Castillo et al. 1995). However, longer HRT requires installation of large dimensions which consequently results in high operating and construction costs.

Organic Loading Rate represents the quantity of raw materials fed per day per unit volume of the digester capacity. OLR has a significant effect on the biogas production of straw. Methane production increases with diminished OLR owing to the accumulation of VFA and lowering of pH as OLR has been increased from 2.80 kg SV m-3d-1to 6.97 kg SV m-3d-1 (Kaparaju et al. 2009). Total solids concentration is not affected by an increase in the retention time of solids (Pohl et al. 2012). The various studies concluded that overfeeding the plant will adversely affect performance as acids will accumulate and bacteria cannot survive in the acidic situation on the other hand if it is underfed even then production will be low due to alkaline solution.

Dilution/Solid Concentration

The concentration of total solids in the feedstock is one of the main parameters considered for the effectiveness of the anaerobic digestion process. The total solid content of the substrate is less than 10–20% TS result into wet anaerobic digestion system and total solid content of substrate greater than 20–40% leads to dry anaerobic digestion system. Wet anaerobic digestion takes little time to start up but at the same time, it tends to float more foam. On the other hand, dry anaerobic digestion takes a long time to produce the optimum content of methane, but the digestion process is stable.

However, wet anaerobic digestion under thermophilic conditions was found to be more effective in enhancing methane production than dry anaerobic digestion under the same conditions (Lianhua et al. 2010). As high temperature and high total solid concentration, both factors may induce the accumulation of acids thus adversely affecting biogas production. However, according to the findings of TERI, fresh cattle waste consists of approximately 80% of water and 20% total solids (TS). For optimum gas production through anaerobic digestion the appropriate dilution is required as if the slurry is too diluted then the solid particles will settle down in the digester and if it is too thick then the particles hamper the flow of gas formed at the lower part of the digester. In either case, the gas production will be less than the optimum value.

Co-Digestion/Inoculum

The anaerobic digesters are initially seeded with bacteria to improve the start-up process of digestion. Usually, the animal or municipal organic matter or digested sludge from active biogas plants are taken as inoculum. It has been reported that when both S/I and total solid content were high, the reduced amount of available microorganisms relative to substrate led to the failure of the digestion process (Liew et al. 2011).

2 Biomass Potential in India

India produces a large number of crops such as wheat, sugarcane, rice, corn, etc. as result most of the population relies on livestock and agriculture for their livelihood.

The agriculture sector in India contributes to 17.32% of Gross Domestic Product (GDP) with 48.9% employability as per reports from National Sample Survey Office (NSSO). India has the second-largest cultivated area (159.7 million ha or 394.6 million acres) in the world after the United State of America and the irrigated crop area in the country amounts to 82.6 million ha.

The country has seen tremendous growth in crop production which has been increased from 476 MT in 2003–04 to 511 MT in the year 2017–18. Total 511 MT of crop residue generated in India out of which 145 MT are available as surplus crop residue which can be utilized to generate electricity (Ravindra et al. 2018; Bellarby et al. 2008). Rice and wheat together contribute to a maximum of 63% of primary crop residue in India. Wheat straw is mainly used as fodder by the farmers, but rice straw due to its high silica content and low digestibility is not considered suitable for the health of livestock. Therefore, rice straw is frequently burnt by farmers in the open fields. Overall, around 15.9% of the residue is burned in the fields owing to the small window of rabbi and Kharif cropping pattern system, weeds removal, etc., thereby causing the increase in GHGs emissions, resulting in severe air pollution. Indian agriculture sector contributes to nearly 12% of the world's total GHGs emissions (Bellarby et al. 2008; Maraseni and Qu 2016; Cardoen et al. 2015a, b; Thambi et al. 2018; Central Electricity Authority (CEA) 2020). The uncontrolled burning of crop residues leads to severe atmospheric pollutants such as carbon dioxide, particulate matter, carbon monoxide, sulfur dioxide, and nitrogen oxide, methane, polycyclic aromatic hydrocarbons, volatile organic compound, elemental carbons, etc. Thus, declining air quality due to the burning of biomass in the open fields and its dispersion in the surrounding areas are of great concern to the Government as it has an adverse impact on human health. Rice straw and bagasse being lignocellulosic materials rich in organic matter can be utilized in a sustainable way to produce biogas in the anaerobic digestion process.

The total crop residue saving energy potential is about 7236.2 PJ/Year with 100% collection efficiency and 3618.1 PJ/Year with 50% collection efficiency of residue as reported for open burning for the year 2017 (Ravindra et al. 2018). Further, it has been estimated that this can produce 120 TWh of electricity amounting to be 10% of total power production in India.

3   Contribution of Bioenergy in Total Energy Mix

The energy demand in India is going to accelerate as expected to have emerged as the fastest-growing economy in the future globally. Consequently, the predicted installed capacity has to be raised to in the same stride. Although, India has shown immense progress in the renewable energy sector during the last few years but still nearly 27 million houses do not have access to electricity, and many people still using biomass as the heating source for daily cooking purposes (Central Electricity Authority (CEA) 2020). The enhancement of renewable energy resources shares to 40% by the year 2022 in power production will help the country to surpass the Paris
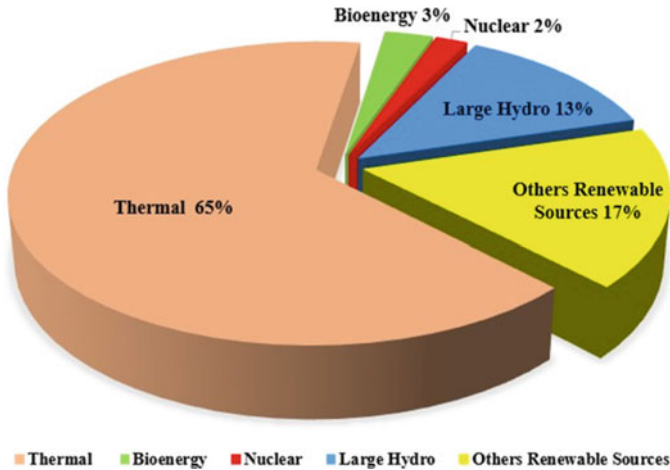
Fig. 2 Contribution of different energy resources

Agreement on environment change. The further enhancement of 45% by renewable energy contribution in the power sector may help to reduce the emissions significantly. At present coal-based power plants contributes to a maximum of around 56% of total demand being followed by renewable energy from solar, wind with 17% of total contributions by different energy resources. And the share of bioenergy is just about 3% as of March 2020 (CEA 2020) represented in Fig. 2 (Central Electricity Authority (CEA) 2020).

The renewable energy sector in India has reflected incredible growth during the period 2011–2020 as can be seen in Fig. 3. The grid-connected renewable installed capacity has increased from 19.974 to 77.004 GW (CEA 2020) during the last decade and the grid-interactive bioenergy contribution has accelerated from 2.6 to 10.339 GW during the same interval. In the last decade, the country's energy sector has observed average annual growths of renewable energy and bioenergy reaching to 5.7 and 0.75 GW, respectively. However, in order to fulfill the commitments made under the Paris Agreement on climate change the share of renewable energy resources has to be enhanced to 12.92 GW/year from the existing share of 5.9 GW/Year (Central Electricity Authority (CEA) 2020; Bisht and Thakur 2019).

The bagasse-based co-generation power plants lead the bioenergy sector in India. The Indian state Uttar Pradesh which is tops in sugarcane production has also stood first in total installed bioenergy capacity with the contribution of 2.13 GW being followed by Maharashtra and Karnataka with installed capacities of 2.08 and 1.62 GW, respectively. These three states have set targets for the year 2022 to enhance their capacities to 3.5, 2.47, and 1.42 GW respectively, from existing installed capacities. The south, north, east, west, and north-eastern regions of India have set targets of 3.18, 2.89, 0.5, 2.5, and 0.014 GW respectively as bioenergy potential in the energy mix by the year 2022. The two regions eastern and southern have accomplished their targets set for the year 2022 (Central Electricity Authority (CEA) 2020; Bisht and
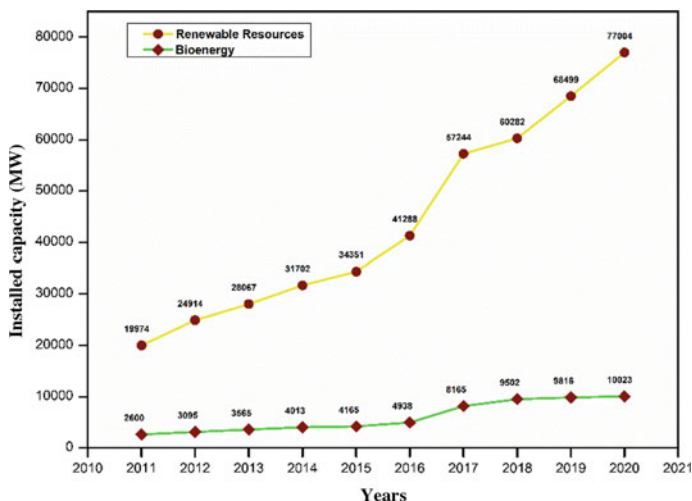
Fig. 3 Bioenergy contribution and other renewable energy resources contribution in total energy mix during one decade

Thakur 2019). The agrarian state of India, Punjab has a bioenergy potential of about 3300 MW out of which the state has installed a capacity of 322 MW as of the year 2018.

4 Biomass to Electricity Generation

Crop residues can be converted into energy through thermochemical conversion techniques and biochemical conversion techniques. Thermochemical conversion techniques of biomass involve combustion, gasification, and pyrolysis whereas the biochemical conversion pathway includes anaerobic digestion and fermentation as seen in Fig. 4. In the first method of combustion, biomass can be directly fired to generate steam which in turn runs the turbine for electricity generation. Biomass gasification results in incomplete combustion of biomass resulting into the release of harmful gases such as carbon monoxide, traces of methane, and hydrogen. The resulting gas produced after gasification is also known as producer gas which is used to run an internal combustion engine to generate electricity.

Pyrolysis is another method for power production based on slow and fast pyrolysis. Slow pyrolysis takes time to complete the process and produces more char along with organic gases which can be utilized for firing the boiler to produce steam and subsequent power production. However, in fast pyrolysis organic matter is heated at the temperature of 450–600 °C in absence of air to produce syngas in seconds (Woods and Hall 1994). The syngas is further utilized for power production. It has been
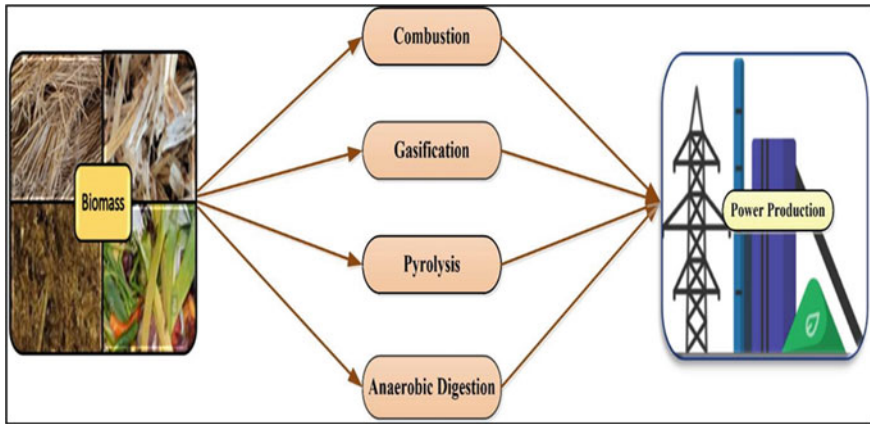
Fig. 4 Different methods to convert biomass into bioenergy for power production

observed that gasification plants work efficiently till 2 MW capacity and pyrolysis plants work beyond 2 MW capacity.

Biogas production through anaerobic digestion can be efficiently utilized in small size rural and off-grid locations. The rising competition of waste disposal methods may improve its economic usefulness. Anaerobic digesters are used both at small-scale and large-scale levels. Industrial applications mainly process large amounts of feedstock. This would require a well-developed logistical system for feedstock collection and effluent disposal. Overall, power production from anaerobic digestion is quite well established as a technology, though the economics of this route is still evolving. The slurry remained in the digester after biogas production can be utilized as fertilizer in the field.

Hybrid Power System

Indian power sector mostly relies on coal-based thermal power plants. However, coal deposits in the country are confined in north-eastern and eastern regions. Power generation capacity expansion through the thermal route via coal would also require increased transportation of coal (Singh 2016). High losses occurring during transmission and distribution of electricity add difficulty to remote villages electrification, so power shortages are major issues in India, where fossil fuel-powered plants suffer from supply shortages. Therefore, decentralized power generation through microgrids based on renewable energy resources available locally is the best option for reliable electrification of these villages.

Although solar and wind power had gained significant momentum in the last few years in the energy sector. Solar photovoltaic energy system along with battery storage system has observed to be favorable among the counties which have most of the sunny days in a year such as India to provide electricity to the off-grid locations, commercial buildings, and residential loads. However, the extra cost involved due to the requirement of battery storage and low conversion efficiency has led to substantial

growth in wind power generation. But the stochastic nature of wind and solar energy raised concern about the reliability of power to the end-user.

However, abundantly available biomass can complement the intermittent nature of solar and wind energy resources thereby reducing GHGs emissions. Biomass-based microgrids system can help the world to reduce the dependency on non-renewable energy and to become fossil-free by 2050 especially in agriculture rich countries like India. For instance, the thermodynamic study of solar-biomass power generation systems represents that cost of electricity has been reduced to 74.94 \$/MWh for hybrid systems along with the reduction in CO_2 emission to 0.62 T/MWh (Sarkis and Zare 2018). The increase in fuel efficiency has been observed from 15 to 32% of solar energy in solar-biomass hybrid power plants without energy storage (Srinivas and Reddy 2014). The PV-Biomass-based microgrid system was found to be capable of full-fill the load demand of a village with more than 80% reduction in GHGs emission (Kaur et al. 2020). In another study, a biomass-based microgrid system with the battery as a backup system was found to provide the load demand of an educational institute in Bhopal, India at an economical cost of energy of 15.064 Rs/kWh with excess electricity generation (Singh and Baredar 2016).

5 Conclusion

In the last few years solar energy, wind energy has originated as emerging renewable resources and presented competition to fossil fuels in terms of cost also. But the irregular nature of these resources provides a hindrance to the existence of a standalone solar wind-based energy system. Renewable energy resources based hybrid energy system requires diesel generator or other energy storage devices as the backup to full-fill load demand. The use of diesel generators in hybrid power systems not only raises the cost of the system but also adds to the GHGs emissions. The biomass can provide a reliable and consistent power supply to the end-user in comparison with solar and wind energy resources, therefore, preferred as a renewable energy resource over other resources. The intermittent nature of solar and wind energy resources can be adequately complemented by the biomass power plant. So, solar, wind, and biomass due to their different characteristics can compensate for their individual drawbacks. Hybridization of these resources helps to utilize the biomass efficiently and provides electricity to end-users reliably and consistently. Hence, biomass-based hybrid power plants are extremely promising energy systems. As biomass not only avoids ecological and social damage but also helps to mitigate pollution being a carbon–neutral process.

So, among the renewable energy sources options, biomass seems to be a more reliable source of energy that can help the world to reach their long-term energy strategy to become fossil-free by 2050 especially in agriculture-rich countries like India.

References

Anukam A, Mohammadi A, Nqvi M, Granström K (2019) A review of the chemistry of anaerobic digestion: methods of accelerating and optimizing process efficiency. Process 7(8). https://doi.org/10.3390/pr7080504

Appels L, Lauwers J, Degrève J, Helsen L, Lievens B, Willems K (2011) Anaerobic digestion in global bio-energy production: potential and research challenges. Renew Sustain Energy Rev 15:4295

Ayeni AO, Adeeyo OA, Oresegun OM, Oladimeji TE (2015) Compositional analysis of lignocellulosic materials: evaluation of an economically viable method suitable for woody and non-woody biomass. Am J Eng Res 4(4):14–19

Azapagic A, Stichnothe H (2011) Lifecycle sustainability assessment of biofuels. In: Luque R, Campelo J, Clarks J (eds) Handbook of biofuels production-processes and technologies. Woodhead Publishing, Cambridge

Badshah M, Lam DM, Liu J, Mattiasson B (2012) Use of automatic methane potential test system for evaluating the biomethane potential of sugarcane bagasse after different treatments. Biores Technol 114:262–269

Balat M, Balat H (2010) Progress in biodiesel processing. Appl Energy 87(6):1815–1835

Bauer A, Leonhart BC, Bosch P, Amon B, Friedl A, Amom T (2010) Analysis of methane yields from energy crops and agricultural by-products and estimation of energy potential from sustainable crop rotation systems in EU-27. Clean Technol Environ 12:153–161

Bisht AS, Thakur N (2019) Small scale biomass gasification plants for electricity generation in India: resources, installation, technical aspects, sustainability criteria & policy. Renew Energy Focus 28:112–126

Bellarby J, Foereid B, Hastings AFSJ, Smith P (2008) Cool farming: climate impacts of agriculture and mitigation potential. Greenpeace Int 44. https://www.eprints.lancs.ac.uk/68831/1/11111/pdf

Brodeur G, Yau E, Badal K, Collier J, Ramachandran KB, Subramanian Ramakrishanan S (2011) Chemical and physiochemical pretreatment of lignocellulosic biomass: a review. Enzyme Res. https://doi.org/10.4061/2011/787532

Cardoen D, Joshi P, Sarma P, Pant D (2015a) Agriculture biomass in India: Part 1 estimation and characterization. Resour Conserv Recycl 102:39–48

Cardoen D, Joshi P, Diels L, Sarma P, Pant D (2015b) Agriculture biomass in India: Part 2. Post-harvest losses, cost and environment impacts. Resour Conserv Recycl 101:143–153

Castillo RT, Luengo PL, Alveraz JM (1995) Temperature effect on anaerobic of bedding manure in one phase system at different inoculums concentration. Agric Ecosyst Environ 54:55–66

Central Electricity Authority (CEA), Government of India, Installed generation capacity in India. http://www.cea.nic.in

Chandra R, Takeuchi H, Hasegawa T (2012) Hydrothermal pretreatment of rice straw biomass: a potential and promising method for enhanced methane production. Appl Energy 94:129–140

Dahman Y, Syed K, Begum S, Roy P, Mohtaseb B (2019) Biofuels: their characteristics and analysis. Biomass, biopolymer-based materials, and bioenergy. Elsevier Ltd.

Dadi AP, Schall CA, Varanasi S (2006) Enhancement of cellulose saccharification kinetics using an ionic liquid pretreatment step. Biotechnol Bioeng 95(4):904–910

Dien BS, Li XL, Iten LB, Jordan DB, Nichols NN, O'Bryan PJ, Cotta MA (2006) Enzymatic saccharification of hot-water pretreated corn fiber for production of monosaccharides. Enzyme Microb Technol 39(5):1137–1144

Dong Y, Zheng Y, Zhang RH (2009) Alkali pretreatment of rice straw for increasing the biodegradability. American Society of Agricultural and Biological Engineers, Reno, Nevada, 095685

Ficara E, Malpei F (2011) Maize mono-digestion efficiency: results from laboratory tests. Water Sci Technol 64(10):2029–2037

Frigon JC, Guiot SR (2010) Biomethane production from starch and lignocellulosic crops: a comparative review. Biofuels Bioprod Biorefin 4(4):447–458

Ghatak M, Mahanta P (2014) Kinetic assessment of biogas production from lignocellulosic biomasses. Int J Adv Technol 3(5):244–249

Guttikunda SK, Jawahar P (2014) Atmospheric emissions and pollution from coal-fired thermal power plants in India. Atmos Environ 92:449–460

Jackowiak D, Bassard D, Pauss A, Ribeiro T (2011) Optimization of a microwave pretreatment of wheat straw for methane production. Biores Technol 102(12):6750–6756

Kaparaju P, Serrano M, Angelidaki I (2009) Effect of reactor configuration on biogas production from wheat straw hydrolysate. Biores Technol 100:6317–6632

Kaur M, Dhundhara S, Verma YP, Chauhan S (2020) Techno-economic analysis of photovoltaic-biomass-based microgrid system for reliable rural electrification. Int Trans Electric Energy Syst. e12347. https://doi.org/10.1002/2050-7038.12347

Kleinert M, Barth T (2008) Towards a lignocellulosic biorefinery: direct one step conversion of lignin to hydrogen enriched biofuel. Energy Fuels 22(2):1371–1379

Kratky L, Jirout T (2011) Biomass size reduction machines for enhancing biogas production. Chem Eng Technol 34:391–399

Kumar AK, Sharma S (2017) Recent updates on different methods of pretreatment of lignocellulosic feedstocks: a review. Bioresour Bioprocess 4:7. https://doi.org/10.1186/s40643-017-0137-9

Kumar R, Mago G, Balan V, Wyman CE (2009) Physical and chemical pretreatment of corn stover and poplar solids resulting from leading pretreatment technologies. Biores Technol 100(17):3948–3962

Lee SH, Doherty TV, Linhardt RJ, Dordick JS (2009) Ionic liquid-mediated selective extraction of lignin from wood leading to enhanced enzymatic cellulose hydrolysis. Biotechnol Bioeng 102(5):1368–1376

Li Y, Chen Y, Wu J (2019) Enhancement of methane production in anaerobic digestion process: a review. Appl Energy 240:120–137

Lianhua I, Dong I, Yongming S, Longlong M, Zhenhong Y, Xiaoying K (2010) Effect of temperature and solid concentration on anaerobic digestion of rice straw in South China. Int J Hydrogen Energy 35:7261–7266

Liew LN, Shi J, Li Y (2011) Enhancing the solid-state anaerobic digestion of fallen leaves through simultaneous alkaline treatment. Biores Technol 102:8828–8834

Lohan SK, Jat HS, Yadav AK, Sidhu HS, Jat ML, Choudhary M, Peter JK, Sharma PC (2018) Burning issues of paddy residue management in north-west states of India. Renew Sustain Energy Rev 81:693–706

Maraseni TN, Qu J (2016) An international comparison of agricultural nitrous oxide emissions. J Clean Prod 135:1256–1266

Menardo S, Airoldi G, Balsari P (2012) The effect of particle size and thermal pretreatment on the methane yield of four agricultural by-products. Biores Technol 104:708–714

Mshandete A, Bjornsson L, Kivaisi AK, Rubindamayugi MST, Mattiasson B (2016) Effect of particle size on biogas yield from sisal fibre waste. Renew Energy 31(14):2385–2392

Nguyen TAD, Kim KR, Han JS, Cho HY, Kim JW, Park SM, Park JC, Sim JS (2010) Pretreatment of rice straw with ammonia and ionic liquid for lignocellulose conversion to fermentable sugars. Biores Technol 101(19):7432–7438. https://doi.org/10.1016/j.biortech.2010.04.053

Nigam PS, Singh A (2010) Production of liquid biofuels from resources. Prog Energy Combust Sci 37(1):52–68

Ohman M, Boman C, Hedman H, Eklund R (2006) Residential combustion performance of Pelletized hydrolysis residue from lignocellulosic ethanol production. Energy Fuels 20(3):1298–1304

Panagiotou G, Olsson L (2006) Effect of compounds released during pretreatment of wheat straw on Microbial Growth and Enzymatic hydrolysis rate. Biotechnol Bioeng 96(2):250–258

Pohl M, Mumme J, Heeg K, Nettmann E (2012) Thermo and mesophilic anaerobic digestion of wheat straw by upflow anaerobic solid-state process. Biores Technol 124:321–327

Purwandari FA, Sanjaya AP, Millati R, Cahyanto MN, Horváth IS, Niklasson C (2013) Pretreatment of oil palm empty fruit bunch (OPEFB) by N-methylmorpholine-N-oxide (NMMO) for biogas production: structural changes and digestion improvement. Bioresour Technol 128:461–466

Ravindra K, Singh T, Mor S (2018) Emissions of air pollutants from primary crop residue burning in India and their mitigation strategy for cleaner emissions. J Cleaner Prod. https://doi.org/10.1016/j.clepro.2018.10.031

Samayam IP, Schall CA (2010) Saccharification of ionic liquid pretreated biomass with commercial enzyme mixtures. Biores Technol 101(10):3561–3566

Sambo AS, Garba B, Danshehu BG (1995) Effect of some operating parameters on biogas production rate. Renew Energy 6(3):343–344

Sarkis RB, Zare V (2018) Proposal and analysis of two novel integrated configurations for hybrid solar-biomass power generation systems: thermodynamic and economic evaluation. Energy Conserv Manage 160:411–425

Singh J (2016) A roadmap for production of sustainable, consistent and reliable electric power from agriculture biomass. Energy Policy 92:246–254

Singh A, Baredar P (2016) Techno-economic assessment of a solar PV, fuel cell, and biomass gasifier hybrid energy system. Energy Rep 2:254–260

Sreenath HK, Koegel RG, Moldes AB, Jeffries TW, Straub RJ (1999) Enzymic saccharification of alfalfa fibre after liquid hot water pretreatment. Process Biochem 35:33–41

Srinivas T, Reddy BV (2014) Hybrid solar-biomass power plant without energy storage. Case Stud Therm Eng 2:75–81

Taherzadeh MJ, Karimi K (2008) Pretreatment of lignocellulosic waste to improve ethanol and biogas production: a review. Int J Mol Sci 9(9):1621–1651

Takacs E, Wojnarovits L, Foldvary C, Hargittai P, Bosra J, Sajo I (2000) Effect of combined gamma-radiation and alkali treatment on cotton-cellulose. Radiat Phys Chem 57(3–6):399–403

Teghammar A, Karimi K, Horvath IS, Taherzadeh MJ (2011) Enhanced biogas production from rice straw, triticale straw and softwood spruce by NMMO pretreatment. Biomass Bioenergy 36:116–120

Thambi S, Bhatacharya A, Fricko O (2018) India's energy and emission outlook: results from India energy model. Energy, Climate Change and Overseas Engagement Division. NITI Aayog, India

Velmurugan R, Muthukumar K (2012) Ultrasound-assisted alkaline pretreatment of sugarcane bagasse for fermentable sugar production: optimization through response surface methodology. Biores Technol 112:293–299. https://doi.org/10.1016/j.biortech.2012.01.168

Wang J, Yue ZB, Chen TH, Peng SC, Yu HQ, Chen HZ (2010) Anaerobic digestibility and fiber composition of bulrush in response to steam explosion. Biores Technol 101:661–673

Wilkie A, Colleran E (1986) Pilot scale digestion of pig slurry supernatant using an upflow anaerobic filter. Environ Technol Lett 7:65–76

Woods J, Hall DO (1994) Bioenergy conversion technologies. Bioenergy for development—Technical and environmental dimensions. FAO, Environment and energy paper, Rome

Yadvika S, Sreekrishnan TR, Sangeeta K, Vineet R (2003) Enhancement of biogas production from solid substrates using different techniques: a review. Biores Technol 95:1–10

Ye J, Li D, Sun Y, Wang G, Yuan Z, Zhen F, Wang Y (2013) Improved biogas production from rice straw by co-digestion with kitchen waste and pig manure. Waste Manage 33:2653–2658

Yong Z, Dong Y, Zhang X, Tan T (2015) Anaerobic co-digestion of food waste and straw for biogas production. Renew Energy 78:527–530

Zhao Y, Sun F, Yu J, Cai Y, Luo X, Cui Z, Hu Y, Wang X (2018) Co-digestion of oat straw and cow manure during anaerobic digestion: Simulative and inhibitory effects on fermentation. Bioresour Technol. https://doi.org/10.1016/j.biortech.2018.08.040

Zheng M, Li L, Li X, Xiong J, Mei T, Chen G (2010) The effect of alkaline pretreatment parameters on anaerobic bio gasification of corn stover. Energy Source Part A 32:918

Kinetics Analysis of Solid State Reaction for the Synthesis of Lithium Orthosilicate

N. S. Ghuge, D. Mandal, M. C. Jadeja, and B. K. Chougule

Abstract Lithium orthosilicate is a candidate material for carbon dioxide adsorption and for the International Thermonuclear Experimental Reactor (ITER) DEMO and future fusion reactor. Solid State Reaction Process (SSRP) is one of the methods for the synthesis of lithium orthosilicate using silicon dioxide and lithium carbonate. In the present study, reaction kinetics of lithium orthosilicate synthesis by SSRP using lithium carbonate and silicon dioxide were studied using non isothermal Thermo-Gravimetric and Differential Thermal Analysis (TG–DTA). TG–DTA data analyzed using different methods for the prediction of kinetic triplet viz. pre-exponential factor (A), activation energy (E) and model for solid state reactions (f(α)). The lithium orthosilicate synthesis reaction of lithium carbonate and silicon-dioxide is controlled by nucleation mechanism for the synthesis of lithium orthosilicate and the best suitable reaction model for this reaction is Avrami–Erofeyev nucleation (A4). The average activation energy and pre-exponential factor calculated using various methods were 568 kJ/mol and 6.45×10^{28} min^{-1} respectively.

Keywords Solid state reaction · Thermo gravimetric and differential thermal analysis (TG–DTA) · Lithium orthosilicate

1 Introduction

Lithium orthosilicate has many industrial applications viz., catalyst for biodiesel production, novel CO_2 adsorbent and equilibrium shift agent in steam reforming process. It has been observed that lithium orthosilicate has highest absorption capacity of about 36% at high temperature. It is one of the promising materials for carbon capturing technology (Wang et al. 2012; Amorim et al. 2016; Kenji et al.

N. S. Ghuge (✉) · D. Mandal · M. C. Jadeja · B. K. Chougule
Alkali Material and Metal Division, Bhabha Atomic Research Centre, Trombay, Mumbai, 400085, India
e-mail: gnagesh@barc.gov.in

N. S. Ghuge
Homi Bhabha National Institute, Mumbai 400094, India

2008). Lithium orthosilicate is also one of the suitable ceramic breeder materials and will be used for production of tritium as fuel for ITER fusion reactor programme (Carella and Hernandez 2002). Mandal et al. (2010, 2011, 2012, 2015) has developed a SSRP process for the making of pebbles of ceramic solid breeder materials viz., lithium orthosilicate and lithium titanate. The process consists of several unit operations; viz., (i) mixing, (ii) classification, (iii) calcination, (iv) grinding, (v) extrusion, (vi) spherodization and (vii) sintering. Mandal et al. synthesized lithium orthosilicate using lithium carbonate and silicon dioxide as raw materials. The calcination is one of the most important steps to produce single phase lithium orthosilicate powder. The single phase lithium orthosilicate was synthesized at 800 °C for 6 h operating condition (Mandal et al. 2015). Other similar studies have also been reported (Mandal et al. 2020, 2016). Previously, Ghuge and Mandal (2017), 2013), Mandal (2014) studied the reaction kinetics of lithium carbonate with titanium dioxide for the synthesis of lithium titanate by Thermo Gravimetric-Differential Thermal Analysis (TG–DTA) techniques. The similar work was repeated by Sonak et al. using different technique (Sonak 2015). Recently, Yasnó et al. (2021) studied non-isothermal reaction mechanism and kinetic analysis for the synthesis of monoclinic lithium zirconate using TG–DTA, estimated kinetics parameter.

Till date kinetics of solid state reaction between lithium carbonate and silicon dioxide for the synthesis of lithium orthosilicate were not studied and reported. The objective of this paper is to study of reaction kinetics of lithium carbonate and silicon dioxide reaction for the synthesis of lithium orthosilicate using different techniques. TG–DTA analysis of homogenous mixture of lithium carbonate and silicon dioxide were carried out at different heating rate. The different methods were adopted for estimation of kinetic parameter viz. activation energy, pre exponential factor and solid state reaction model. The knowledge of reaction kinetics will be used for optimization of process parameter and designing of reactor for the continuous production of lithium orthosilicate.

2   Materials and Methods

99.9% pure Li_2CO_3 (SD Fine Chem. Make) and 99.9% pure SiO_2 (Loba Chemie. make) were used as raw materials. The purity of raw materials was checked using ICPMS instrument. Lithium carbonate and silicon dioxide were mixed using helical turbo mixer for 2.5 h in stoichiometric ratio. The mixing quality was checked using ICPMS instrument. TG–DTA experiments were carried out using homogeneous mixture at 5, 10 and 15 K/min heating rate. Nitrogen gas at 40 ml/min flow rate was used for all these experiments. STA 449 Jupiter F3 model of TG–DTA instrument made by Netzsch was used for these experiments.

3 Kinetic Models for Solid State Reactions

The rate law of solid state reaction can be written as (Eq. 1).

$$\frac{d(\alpha)}{dt} = kf(\alpha) \tag{1}$$

- k is the reaction rate constant and can be expressed as $k = A \exp^{(-Ea/RT)}$
- $f(\alpha)$ is the solid-state reaction model and α is the conversion

Equation (1) may be written in integral form as shown in Eq. (2) and g(α) is integral form solid state reaction model.

$$g(\alpha) = kt \tag{2}$$

The solid–solid reaction is limited by nucleation, phase boundary formation and diffusion mechanism. Based on different assumption and mechanism of reaction, various solid state reaction models are reported in literature (Khawam and Flanagan 2006; Akashi et al. 1998). Table 1 shows various solid state reaction models equation f(α) and integral form g(α) g(α) of same.

Table 1 Algebraic expression for various reaction mechanisms (Khawam and Flanagan 2006)

Reaction mechanism	f(α)	g(α)
Nucleation models		
Avarami-Erofe'ev (A2)	$2(1-\alpha)[-\ln(1-\alpha)]^{1/2}$	$[-\ln(1-\alpha)]^{1/2}$
Avarami-Erofe'ev (A3)	$3(1-\alpha)[-\ln(1-\alpha)]^{2/3}$	$[-\ln(1-\alpha)]^{1/3}$
Avarami-Erofe'ev (A4)	$3(1-\alpha)[-\ln(1-\alpha)]^{3/4}$	$[-\ln(1-\alpha)]^{1/4}$
Power Law (P2)	$2\alpha^{1/2}$	$\alpha^{1/2}$
Power Law (P3)	$3\alpha^{2/3}$	$\alpha^{1/3}$
Power Law (P4)	$4\alpha^{3/4}$	$\alpha^{1/4}$
Phase boundary formation model		
Contracting area (R2)	$2(1-\alpha)^{1/2}$	$1-(1-\alpha)^{1/2}$
Contracting volume (R3)	$3(1-\alpha)^{2/3}$	$1-(1-\alpha)^{1/3}$
Diffusion model		
1D Diffusion (D1)	$1/2\alpha$	α^2
2D Diffusion (D2)	$-[1/\ln(1-\alpha)]$	$(1-\alpha)\ln(1-\alpha)+\alpha$
3D Diffusion (D3)	$\frac{3/2(1-\alpha)^{2/3}}{[1-(1-\alpha)]^{2/3}}$	$[1-(1-\alpha)^{1/3}]^2$
Reaction order model	$(1-\alpha)^n$	Integral form

4 Non-isothermal Analysis of Kinetic Parameters

TG–DTA is non-isothermal study and it provides weight loss with temperature at different heating rate. Equations 1 and 2 cannot be used to predict kinetic parameter. The following equations converted in non-isothermal form is used for estimation of kinetic parameter (Khawam and Flanagan 2006; Akashi et al. 1998). The conversion (α) from TG–DTA can be calculated by using Eq. (3).

$$\alpha = \frac{M_i - M_t.}{M_i - M_f} \tag{3}$$

In Eq. (3), M_i is the initial mass of sample, M_t is the mass of sample at time t, T is the temperature; M_f is the final mass of sample. The data obtained by TG–DTA is non-isothermal and Eq. (2) may be written as shown in Eq. (4)

$$\frac{d[g(\alpha)]}{dt} = k \tag{4}$$

$$k = A \exp^{(-Ea/RT)} \tag{5}$$

Equation (6) may be obtained from Eqs. (4) and (5).

$$\frac{d[g(\alpha)]}{dt} = A \exp^{(-Ea/RT)} \tag{6}$$

Multiplying by $\frac{dt}{dT}$ on both sides of Eq. (6), we get,

$$\frac{d[g(\alpha)]}{dt} \frac{dt}{dT} = A \exp^{(-Ea/RT)} \frac{dt}{dT} \tag{7}$$

Assuming $\frac{dt}{dT} = \frac{1}{\beta}$. Equation (7) can be rewritten as

$$d[g(\alpha)] = \frac{A}{\beta} \exp^{(-Ea/RT)} dT \tag{8}$$

Equation (8) doesn't have exact solution. The following methods are reported for estimation of kinetic parameter and model.

Table 2 Model free methods for the kinetic parameters estimation

Method name and reference	Equation	Eq. No.
Flynn–Wall–Ozawa Method (Khawam and Flanagan 2005; Flynn and Wall 1966)	$\ln \beta = \ln(\frac{AEa}{Rg(\alpha)}) - 5.331 - 1.052 \frac{Ea}{RT}$	(9)
Kissinger–Akahira–Sunose Method (Flynn and Wall 1966; Ozawa 1965; Kissinger 1957; Akahira and Sunose 1971; Coats and Redfern 1964)	$\ln \frac{\beta}{T^2} = \ln(\frac{AR}{Ea}) - \frac{Ea}{RT} + \ln\left(\frac{\mathrm{d}f(\alpha)}{\mathrm{d}\alpha}\right)$	(10)
Kissinger method (Kissinger 1957)	$\ln \frac{\beta}{Tp^2} = \ln(\frac{AR}{Ea}) - \frac{Ea}{RTp}$	(11)
Augis and Bennett's Method (Augis and Bennett 1978)	$\ln \frac{\beta}{(Tp-To)} = \ln(A) - \frac{Ea}{RTp}$	(12)
Boswell Method (Boswell 1989)	$\ln \frac{\beta}{Tp} = \ln(A) - \frac{Ea}{RTp}$	(13)

4.1 Estimation of Kinetic Parameters Using Model Free Method

The following model free techniques equations given in Table 2 were used for calculation of activation energy without knowledge of best suitable of solid-state reaction model. In all the methods, graph of LHS term of equations is plotted against 1000/T and the slope obtained from the graph gives the activation energy. The preexponential factor has been calculated after prediction of best suitable model of solid-state reaction.

4.2 Methods for Determination Solid State Reaction Model and Reaction Mechanism

Activation energy can be calculated from all above model free methods. The following techniques were used for determination of suitable reaction model. In all the following methods average of activation energy calculated from above method can be used for prediction of best suitable solid state reaction model.

4.2.1 Malek Method Based on Y(A) and Z(A) Curve

Malek et al. (1992) has proposed following two function $y(\alpha)$ and $z(\alpha)$ to predict solid state model for reaction. In this method, $y(\alpha)$ and $z(\alpha)$ are plotted against α. The values of α at peak value of $y(\alpha)$ and $z(\alpha)$ for each model has been denoted by α_m and α_p^∞ respectively. The theoretical values α_m and α_p^∞ for different solid state reaction modelare previously reported in literature. Theoretical values of α_m and α_p^∞ are used for prediction of solid state reaction model in comparison with calculated values from experimental data. But in this literature, values are not available for A4,

Table 3 Theoretical calculated values of α_p^∞ and α_m for different solid state reaction model

Models	α_p^∞	α_m
Avarami-Erofe'ev (A2)	0.38	0.62
Avarami-Erofe'ev (A3)	0.5	0.62
Avarami-Erofe'ev (A4)	0.52	0.62
Power law (P2)	1	0
Power law (P3)	1	0
Power law (P4)	1	0
Contracting area (R2)	0	0.73
Contracting volume (R3)	0	0.7
1D Diffusion (D1)	0	0
2D Diffusion (D2)	0	0.81
3D Diffusion (D3)	0	0.78
Chemical reaction first order (F1)	0	0.61
Chemical reaction second order (F2)	0	0.5
Chemical reaction third order (F3)	0	0.4

F2, F3, P2, P3, P4 model. The values of A4, F2, F3, P2, P3, P4 models were calculated in present work by using method reported in literature. The following Eqs. (14) and (15) are used to estimate the theoretical values α_m and α_p^∞ for all models (Malek 1992; Vyazovkin et al. 2011). Table 3 shows theoretical calculated values of α_p^∞ and α_m for different solid state reaction model.

$$y(\alpha) = f(\alpha) \tag{14}$$

$$z(\alpha) = f(\alpha) * g(\alpha) \tag{15}$$

The experimental y(α) and z(α) data will be generated from TG–DTA data. α_m and α_p^∞ observed from experimental data were used to predict solid state reaction model in comparison with theoretical values noted in Table 3.

$$y(\alpha) = \frac{d\alpha}{dt} \exp\left(\frac{Ea}{RT}\right)) \tag{16}$$

$$z(\alpha) = \frac{d\alpha}{dt} \exp\left(\frac{Ea}{RT}\right).\pi(x) \tag{17}$$

$\pi(x)$ can be obtained from Eq. (18)

$$\pi(x) = \frac{x^3 + 18x^2 + 86x + 96}{x^4 + 20x^3 + 240x + 120} \tag{18}$$

whereas $x = Ea/RT$.

5 Result and Discussion

5.1 Kinetic Analysis

All above method described are for the prediction of kinetic triplet viz. activation energy, pre-exponential factor and solid state reaction model.

5.1.1 Estimation of Kinetic Parameter Using Model Free Techniques

Figure 1 shows variation ln (β) against 1000/T for Flynn Wall Ozawa method and Fig. 2 shows variation ln (β/T² β/T²) against 1000/T for Kissinger–Akahira–Sunose method (KAS). Graph of LHS term is plotted against 1000/T for Eqs. (9) and (10) at various values of α and the slope obtained from the graph gives the activation energy. The activation energy estimated in the range 0.3–0.7 of conversion value (α). The tail of values neglected because it may create error in calculation. Figure 3 shows the variation of activation energy with conversion value (α). It is observed that the activation energy increases with conversion. This is due to resistance of product layer for diffusion path of lithium carbonate. The pre exponential factor was determined from intercept of graph after prediction of solid state reaction model. The activation energy calculated from FWO and KAS methods at different conversion value (α) are different. The average activation energy calculated from FWO and KAS method is about 448 and 488 kJ/mol respectively. Figure 3 shows that activation energy initially increases with conversion that is due to increase in product layer thickness. As product layer increases it's create resistance to diffusion of Li compound
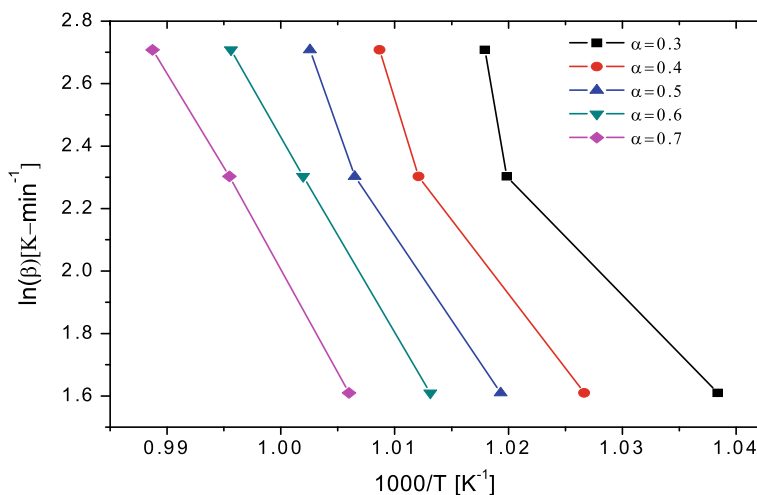
Fig. 1 Variation in ln (β) against 1000/T for evaluation of activation energy by FWO method
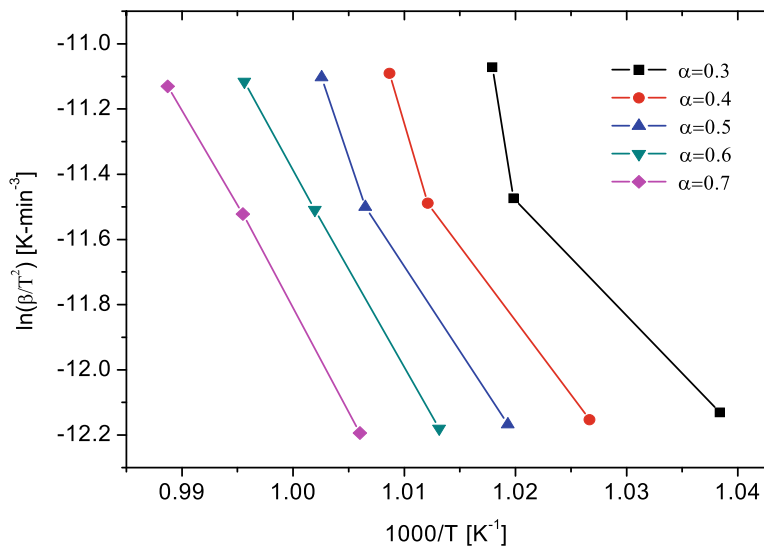
Fig. 2 Variation in $\ln(\beta/T^2)$ against 1000/T for evaluation of activation energy by KAS method
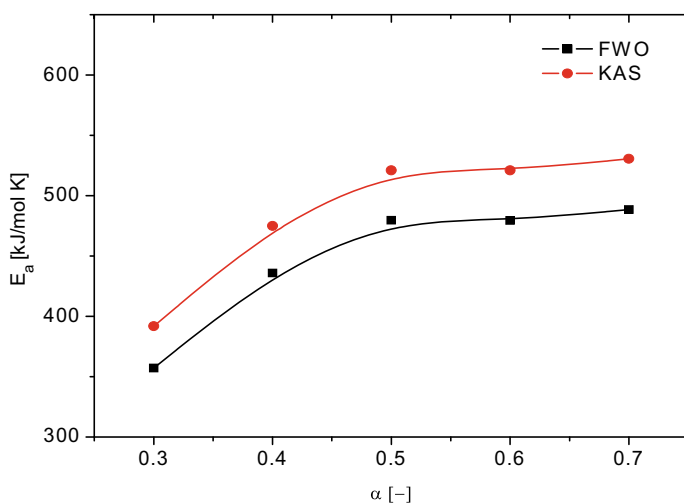
Fig. 3 Variation in activation energy with conversion value (α) for FWO and KAS method

which resulting increase in activation energy. Rate of product layer formation stabilize after specific conversion hence activation energy also become constant over the conversion.

Kissinger method (Eq. 11), Augis & Bennett method (Eq. 12) and Boswell Method (Eq. 12) are based on DTA data i.e. peak temperature and onset temperature of crystallization. Table 4 shows data obtained from DTA analysis at different heating rate.

Table 4 DTA Data obtained from TG–DTA Experiments at different heating rate

β (K/min)	Peak temperature Tp(K)	Onset temperature T0 (K)
5	990	800
10	1000	805
15	1005	810

Figure 4 shows variation RHS term of Eqs. (11)–(13) against $1000/T_p$ for Kissinger method, Augis & Bennett and Boswell method. Graph of RHS term of equations is plotted against $1000/T_p$ and the slope obtained from the graph gives the activation energy and intercept gives pre-exponential factor.

The activation energy and pre-exponential factor calculated from all methods are reported in Table 5.
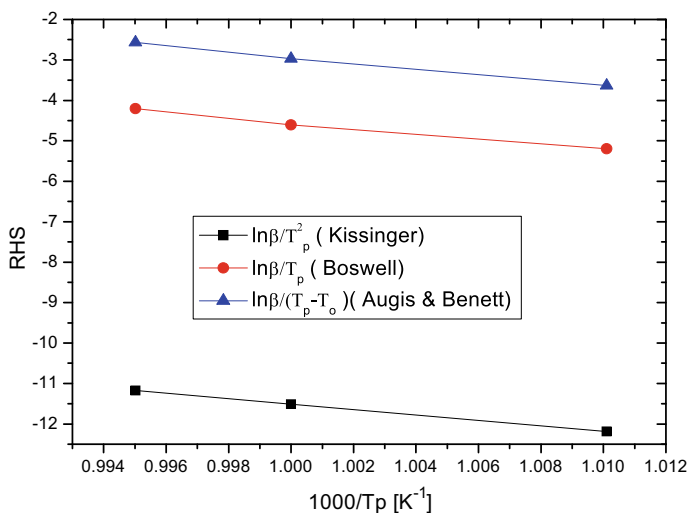
Fig. 4 Variation RHS term of Eqs. (11)–(13) against $1000/T_p$ for Kissinger method, Augis & Bennett and Boswell method

Table 5 Tabulated results of activation energy and pre-exponential factor

	FWO	KAS	Kissinger	Augis&Bennet	Boswell
E_a (kJ/mol K)	448	488	635	631	643
Pre Exponential Factor	5.8×10^{28}	3.6×10^{23}	3.4×10^{26}	1.9×10^{29}	-

5.1.2 Determination Solid State Reaction Model and Reaction Mechanism

The average activation energy from above methods is 568 kJ/mol and it is used for theprediction ofreaction model. Malek method is based on $y(\alpha)$ and $z(\alpha)$ function for prediction of solid-state reaction model. Experimental values $y(\alpha)$ and $z(\alpha)$ at different α were calculated from TG–DTA data using Eqs. (3), (16)–(18). Figure 5 shows variation for $y(\alpha)$ with α for obtaining value of α_m for reaction lithium carbonate and silicon dioxide. Figure 6 shows variation for $z(\alpha)$ with α for obtaining value of α_p^∞ for the reaction of lithium carbonate and silicon dioxide. The values of α_p^∞ and α_m are 0.52 and 0.62 respectively and matched theoretical values of Avarami-Erofe'ev (A4) model noted in Table 3.

Avrami–Erofeyev nucleation model developed on assumptions that in the solid state reaction loss of reactants may take place in-between product crystal growth or one product crystal and reactant crystal. This result lowers the kinetics of reaction which becomes limiting step. This is mainly due to particle size silicon dioxide powder which is much lower than lithium carbonate. It assumed that fraction of lithium carbonate and silicon dioxide was not uniformly mixed in some micro zone which cannot be analyzed which considered as dead spot zone. In this zone one of the reactant trapped in other reactant or product layer which needs more path of diffusion. Hence, reaction kinetics is limited by Avrami–Erofeyev nucleation mechanism.
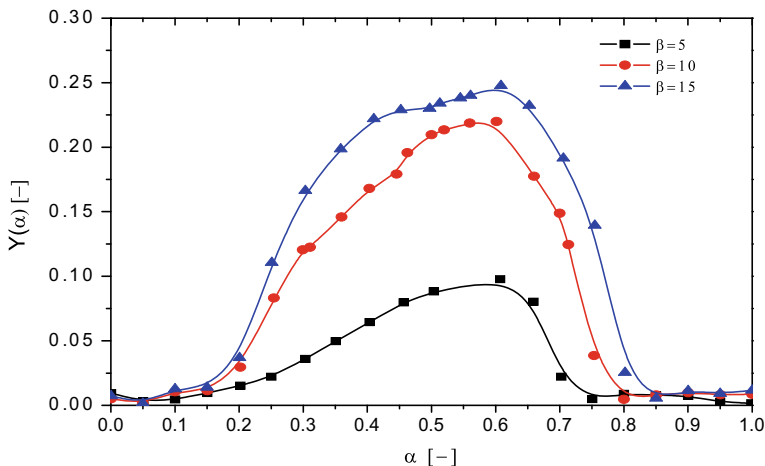
Fig. 5 Variation for $y(\alpha)$ with α for obtaining value of α_m for reaction lithium carbonate and silicon dioxide
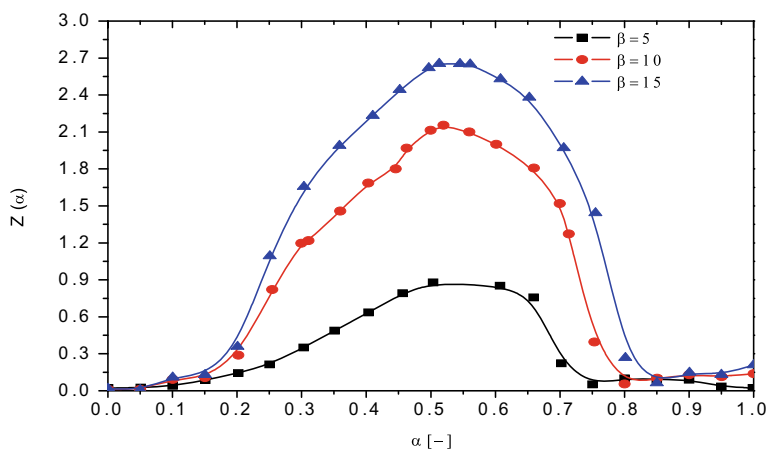
Fig. 6 Variation for z(α) with α for obtaining value of α_p^{∞} for reaction lithium carbonate and silicon dioxide

6 Conclusion

The reaction kinetics for the synthesis of lithium orthosilicate by solid state reaction using lithium carbonate and silicon dioxide as raw materials was investigated in the present study. It was observed that the synthesis of lithium orthosilicate by solid state reaction follows nucleation mechanism and the best suitable model for this reaction is Avrami–Erofeyev nucleation (A4). Avrami–Erofeyev nucleation model developed on assumptions that in the solid state reaction loss of reactants may take place in-between product crystal growth or one product crystal and reactant crystal. The activation energy and pre- exponential factor calculated from various methods are given Table 5. The average activation energy and pre-exponential factor calculated from various methods is about 568 kJ/mol and 6.45×10^{28} min^{-1}.

Declaration of Interests The authors declare that they have no known competing financial interests or personal relationships that could have appeared to influence the work reported in this paper.

References

Akahira T, Sunose T (1971) Joint convention of four electrical institutes. Res Rep Chiba Inst Technol (Sci Technol) 16:22–31

Akashi T, Nanko M, Maruyama T, Shiraishi Y, Tanabe J (1998) Solid-state reaction kinetics of LaCrO from the oxides and determination of La 3+ diffusion coefficient. J Electrochem Soc 145(6):2090–2094

Amorim SM, Domenico MD, Dantas TLP, José HJ, Moreira RFPM (2016) Lithium orthosilicate for CO2 capture with high regeneration capacity: kinetic study and modelling of carbonation and decarbonation reactions. Chem Eng J 283:388–396

Augis JA, Bennett JE (1978) Calculation of the Avrami parameters for heterogeneous solid state reactions using a modification of the Kissinger method. J Therm Anal 13:283–293

Boswell PG (1989) On the calculation of activation energies using a modified Kissinger method. J Therm Anal Calorim 18:353–358

Carella E, Hernandez T (2002) Ceramics for fusion reactors: the role of the lithium orthosilicate as breeder. Phys B: Condens Matter 407:4431–4435

Coats AW, Redfern JP (1964) Kinetic parameters from thermogravimetric data. Nature (London) 201:68–90

Flynn JH, Wall LA (1966) A quick direct method for determination of activation energy form thermogravimetric data. J Poly Science B, Poly Lett 4:323–328

Ghuge NS, Mandal D (2013) Kinetics study of solid state reaction for synthesis of lithium titanate by using TG-DTA. CHEMCON-2013

Ghugeand NS, Mandal D (2017) Synthesis of LiDyO$_2$ by solid-state reaction process and study of reaction kinetics by using TG-DTA and XRD techniques. Indian Chem Eng 59:2101–2116

Kenji E, Takehiko M, Masahiro K (2008) Effect of equilibrium-shift in the case of using lithium silicate pellets in ethanol steam reforming. Int J Hydrogen Energy 33:6612–6618

Khawam A, Flanagan DR (2005) Complementary use of model-free and modelistic methods in the analysis of solid-state kinetics. J Phys Chem B 109:10073–17080

Khawam A, Flanagan DR (2006) Solid-state kinetic models: basics and mathematical fundamentals. J Phys Chem B 110:17315–17328

Kissinger HE (1957) Reaction kinetics in differential thermal analysis. Anal Chem 29:1702–1706

Malek J (1992) The kinetic-analysis of nonisothermal data. Thermochim Acta 200:257–269

Mandal D (2014) Reaction kinetics for the synthesis of lithium-titanate (Li$_2$TiO$_3$) by solid state reaction. ARPN J Sci Tech 4(2):59–66

Mandal D, Shenoi MRK, Ghosh SK (2010) Synthesis & fabrication of lithium-titanate pebbles for ITER breeding blanket by solid state reaction & spherodization. Fusion Eng Design 85:819–823

Mandal D, Jadeja MC, Ghuge NS, Sen D, Mazumder S (2016) Effect of excess lithium on sintering behaviour of lithium-titanate pebbles: Modifications of microstructure and pore morphology. Fusion Eng Des 112(15):520–526

Mandal D, Sen D, Mazumder S, Shenoi MRK, Ramnathan S, Sathiyamoorthy D (2011) Sintering behaviour of lithium-titanate pebbles: modifications of microstructure and pore morphology. Wiley, Hoboken, vol 32, no 2, pp 165–170

Mandal D, Sathiyamoorthy D, Rao VG (2012) Preparation and characterization of lithium–titanate pebbles by solid-state reaction extrusion and spherodization techniques for fusion reactor. Fusion Eng Design 87:7–12

Mandal D, Jadeja MC, Chougule BK (2015) Synthesis of lithium orthosilicate and fabrication of pebbles by the solid-state reaction process. IICHE 1–15

Mandal D, Ghuge NS, Jadeja MC (2020) Development and demonstration of a semi-automatic system for the bulk production of lithium titanate (Li$_2$TiO$_3$) pebbles by solid state reaction process (SSRP). Fus Eng Des 159:111871

Ozawa T (1965) A new method of analyzing thermogravimetric data. Bull ChemSocJpn 38:1881–1886

Sonak S, Jain U, Sahu AK, Kumar S, Krishnamurth N (2015) Thermogravimetric analysis and kinetic study of formation of lithium titanate by solid state route. J Nuclear Mater 457:88–93

Vyazovkin S, Burnham AK, Criado JM, Parez-Maqueda LA, Popescu C, Sbirrazzuoli N (2011) ICTAC Kinetics Committee recommendations for performing kinetic computations on thermal analysis data. Thermochim Acta 520:1–19

Wang J-X, Chen K-T, Wu, Jhong-Syuan, Wang P-H, Chen C-C (2012) Production of biodiesel through transesterification of soybean oil using lithium orthosilicate solid catalyst. Fuel Process Technol 104:167–173

Yasnó JP, Conconi S, Visintin A (2021) Non-isothermal reaction mechanism and kinetic analysis for the synthesis of monoclinic lithium zirconate (m-Li2ZrO3) during solid-state reaction. J Anal Sci Technol 12:15. https://doi.org/10.1186/s40543-021-00267-5

An Assessment of GHG Emission Reduction by Using Renewable Energy and Energy Efficient Processes

Kosha Navnit Vaishnav and Ritesh Ramesh Palkar

Abstract Nowadays, consumer prefers product and services from companies which adhere the principle of sustainability and operation with Sustainable Commitments. The main objective of this study is the reduction of GHG emission by the use of Renewable Energy and Energy Efficient processes and equipment. Detailed assessment of an energy profile and GHG emission is to be carried out from different micro, small and medium scale industries and lack of data monitoring found to be a major drawback. Energy efficiency interventions based on techno-economic analysis of the prevailing electricity tariff, fuel cost and conservation of operating hours includes improved performance, better insulation, reduction in the consumption of resources such as water, fuel and energy, efficient operation and better energy management with proper monitoring system. Renewable energy interventions result in potential saving of 10–12% of electrical energy by replacing the conventional pumps with the solar water pump as it gives remarkable savings with average payback period of 3–9 months according to the study. According to the Solar supplier/vendors, investing in this asset have their own pros and cons with investment classes and payback period with the inclusion of technical specifications, warranty/guaranty periods, maintenance and service, quality assurance plan and special offers/intensives. Some suggestions for the same such as CAPEX Model, OPEX Model and Off-site Model are given by solar suppliers and vendors. This could be the step towards the low carbon pathway and efficient use of renewable energy to get the maximum possible benefit from the same.

Keywords Renewable energy · Solar pumps · Energy efficient processes · GHG emission · Low carbon pathway

K. N. Vaishnav (✉) · R. R. Palkar
Department of Chemical Engineering, Faculty of Technology, Marwadi University, Rajkot, Gujarat, India
e-mail: kosha.vaishnav111303@marwadiuniversity.ac.in

R. R. Palkar
e-mail: ritesh.palkar@marwadieducation.edu.in

1   Introduction

The consumer nowadays prefers product and services from companies that adhere to the principle of sustainability and operation. The objective of this study is the reduction of Green House Gases (GHG) emission by the use of Renewable Energy and Energy Efficient processes and equipment. A detailed assessment of Green House Gases (GHG) emission from about 100 member industries of **NIA (Naroda Industries Association, Ahmedabad, Gujarat, India)** including micro, small and medium scale was carried out. The assessment showed about 28, 59, 13% (GHG) emission from micro, small, and medium scale industries respectively. This emission results into approx. 144,250 MT of CO_2 and it further requires millions of trees for balancing the amount of CO_2 in the atmosphere, which is not feasible. Therefore, energy efficiency and renewable energy pathway come into the picture for the adaptation to decrease the amount of GHG emission (Fig. 1).

1.1   Energy Efficiency and Renewable Energy Pathway

In accordance with the study (Evans et al. 2009) we can explain the application of energy efficient processes and use of renewable energy.

Energy we are producing from solar, wind, geo-thermal sources, biomass, etc. are to be considered as renewable energy. Aim to reduce the GHG can be satisfied by
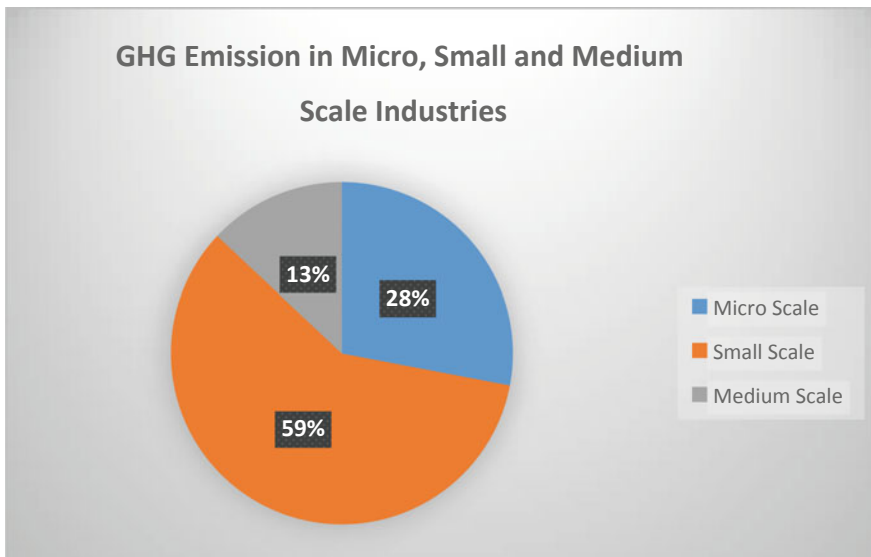
Fig. 1   GHG emission data for micro, small and medium scale industries

using renewable energy as this energy source is carbon-free and not emitting GHG. Apart from switching the use of energy source, other important parameter is to make the processes energy efficient. Energy efficiency usually works in the background but it has a huge impact on GHG reduction. This is one of the powerful tools for the reduction of GHG emission.

2 Background Work

In the beginning of the study, a detailed survey on the basis of energy consumption, in all the industries was performed. From this survey and analysis, the conclusion was arrived that highest consumption of energy is observed in Ceramics and Chemical sector (Dyes and Dye Intermediate). During this assessment, the major drawback was found from the industries is lack of data monitoring. Industries have no records or monitoring of data in terms of resource consumption like fuel (i.e., wood or coal). There is total 200 chemical units from almost 900 industries of Naroda Industrial Association (NIA), among which data collection in 60 units was successfully completed and from which detailed energy assessment is being carried out in 8 Dyes and Dye Intermediate industries selected by NIA. The assessment showed that to balance the GHG emission from 8 industries, 56 million Trees needs to be planted. Selection of units was based on size of the unit (micro, small and medium), types of process, energy consumption and potential scope for clean energy transition, total Green House Gases emission and willingness to participate in the study to understand the present energy efficiency scenario. Into this, lack of data monitoring was the major problem for data collection.

The common and high energy consuming utilities and its key observations from selected units are summarized in Table 1.

Table 1 High energy consuming utilities and its key observations

Utilities	Observations and findings
Boiler	• Poor insulation and less efficiency • Steam traps having improper working and no condensate recovery • Lack of maintenance and parameter controlling • Improper fuel feeding
Dryer	• Poor operating conditions • No waste heat recovery unit available in dryer and no temperature control for hot air
Cooling tower	• Formation of Algae • No temperature controls available • Less efficient cooling tower • Improper designing of the tower

3   Practical Applications

Based on these observation, findings and analysis, some of the common energy saving intervention has been shortlisted in terms of thermal as well as electrical energy. The focus is given on Energy Efficiency Intervention with less than 1-year payback and 5-years for Renewable Energy interventions.

Energy Efficiency Intervention which are based on techno-economic analysis on the prevailing electricity tariff, fuel cost and conservation of operating hours includes:

- Improvement in cooling tower performance through better temperature control, interlocking the cooling tower fan with water temperature, changing fan blades with FRP (Fiber-reinforced plastic)
- Providing insulation on heating lines and hot water storage tanks, repairing and maintaining the existing insulation
- Controlling temperature across air dryer for uniform heating and drying of material
- Installation of condensate recovery system for reducing water and fuel energy consumption.
- Efficient compressor operation by reducing the set pressure to required operational pressure, changing the motor torn belts, providing auto-moisture drain system, restructuring the compressed air network considering pressure vessel
- Installing energy efficient motors and star rated pumps, avoiding rewinding of motors more than 3 times.
- Regular maintenance of steam traps
- Exploring the possibility of utilizing waste heat generated from boiler and dryer
- Better energy management and monitoring system and adopting good practice for up-keep of equipment and utilities

Here, one thing is to be highlighted that out of 8 units where the detailed energy assessment was carried out, 6 units has a potential for solar rooftop installation having a capacity of 125–150 KW. This renewable energy intervention results in potential saving of 10–12% of electrical energy. Some industry experts also suggested replacing the conventional pumps with the solar water pump. Based on the energy audit, the suggestion for energy efficiency are categories from low hanging measures like insulation, installation of temperature sensors etc. and core technology transfer or modification of existing technology like waste heat recovery. Replacement of conventional pumps with solar water pumping gives remarkable savings with average payback period of 3–9 months.

The investment of these measures is mentioned in Table 2 with the total cost saving due to potential energy saving.

Table 2 Data summary of suggestions, investments and total cost saving

Suggestion	Investment (INR)	Total cost saving due to potential energy saving (INR)
Minor retrofits Controlling operating parameters	1, 20,000	4, 00,000
Low to medium cost installation Insulation Interlocking system Waste heat recovery etc	26, 62,000	13, 21,000
Line modification Cross cutting technology	1, 60,000	1, 23,600
Solar water pumping solution Off—grid solar rooftop having a potential of 20–25 kW p	53, 55,200	8, 20,200

3.1 Case Studies

Here we have the results of an energy audit conducted in some of the industries. From this case studies, we can justify the importance of the positive response from the industries and implementation of the suggestions. These case studies included replacement of old torn belts of compressors, reuse of hot air of exhaust in dryer, temperature interlock for thermic fluid network, installation of the cooling tower fan energy saver, waste heat recovery unit for dryer, etc. are mentioned here to make other industries aware regarding this and to take an initiative for making their processing efficient. We have found from these case studies that if we consider the investment of money in different investment classes such as real estate, debt funds, gold and solar, highest returns and lowest risks is observed in solar.

Case studies are listed in Tables 3, 4, 5 and 6.

To understand the potential for Renewable energy implementation, detailed analysis of the technology of solar module with its structural facilities, its optimum design and engineering specifications of the system has to be specified.

Table 3 Case study 1: Replacement of old torn belts of compressors

Power consumption after belt Replacement	kW	4.5
Number of belts	Number	4
Reduction in cycle time (@0.75 h/batch)	H/day	3.0
Average batches for drying	Batches/year	1200
Annual energy saving	kWh/year	3600
Annual energy saving	INR/year	21,000
Total investment	INR	10,000
Payback period	Months	5.0

Table 4 Case study 2: reuse of hot air of exhaust in dryer

Thermal energy saving	k Cal/day	288,750
Fuel (wood) saving	Kg/day	150
Financial saving (on basis of wood)	INR/day	525
Investment	INR	5000
Equivalent saving in gas	SCM/day	31.4
Annual saving	INR	130,000
Payback period	Months	Less than a month

Table 5 Case study 3: Installation of the cooling tower fan energy saver

Cooling tower fan power	kW	5.5
Operating hours	h	24
Annual energy saving	kWh	3366
Annual saving	INR	26,900
Investment	INR	16,000
Payback Period	Months	7

Table 6 Case study 4: Waste heat recovery unit for dryer

Annual fuel saving	SCM	3560
Annual thermal saving	k Cal	3,27,52,000
Annual saving	INR	1,35,000
Investment	INR	1,25,000
Payback period	Months	11.1

From one of the solar vendor/suppliers, the concept with pros and cons of investing in this asset has been discussed with their investment classes and payback period which also includes basic technical specifications, warranty/guaranty period, maintenance and service, payment terms, quality assurance plan and their special offers/incentives. One of the vendors further explained the general assumptions and energy saving values for the very 1st year of solar generation i.e., INR 10, 87, 500 by generating 1, 45, 000 kWh energy annually by solar panels with the capacity of 100 kW. Calculation of payback period i.e., approximately 4 years has also showed.

All the calculations are mentioned in the table below.

3.2 General Assumption

See Table 7.

Table 7 General Assumptions for the calculation

Project capacity	kW	100
System price per Watt	INR	45
Project cost	INR	45,00,000
Subsidy from Govt	%	0%
1st year solar generation	kWh	1,45,000
Tariff	INR /kWh	7.5
Total O and M cost per year	INR	45,000
Tenor on tariff	Years	20
Insurance cost—% of total cost	%	0.10%
D/E ratio	%	100%
Equity	100%	45,00,000
Dept	%	0%
Tax rate	%	25%
Accelerated depreciation rate	%	40%

Cash flow calculations for 10 years

See Tables 8 and 9.

Payback period

EIRR (Economic internal rate of return)	27.35%
Payback period	4 years

Table 8 Cash flow calculation data for 1–5 years

Year	–	1	2	3	4	5
Solar through power generation	kWh	1, 45,000	1, 43,500	1, 42,115	1, 40,693	1, 39,286
Energy saving from utility	INR	10,87,500	10, 98,158	11, 08,919	11,19,787	11,30,761
Total revenue (A)	INR	10,87,500	10,98,158	11,08,919	11,19,787	11,30,761
O & M cost	INR	45,000	47,250	49,613	52,093	4,698
Insurance cost	INR	4,500	4,500	4,500	4,500	4,500
Total cost (B)	INR	49,500	51,750	54,113	56,593	59,198
Net annual saving (A-B)	INR	10,38,000	10,46,408	10,54,807	10,63,194	10,71,563
Depreciation	INR	18,00,000	10,80,000	3,24,000	2,59,200	2,07,360

Table 9 Cash flow calculation data for 5–10 years

Year	–	6	7	8	9	10
Solar through power generation	kWh	1, 37,894	1, 36,515	1, 35,149	1, 33,798	1, 32,460
Energy saving from utility	INR	11,41,842	11,53,032	11,64,332	11,75,742	11,87,265
Total revenue (A)	INR	11,41,842	11,53,032	11,64,332	11,75,742	11,87,265
O and M cost	INR	57,433	60,304	63,320	66,485	69,810
Insurance cost	INR	4,500	4,500	4,500	4,500	4,500
Total cost (B)	INR	61,933	64,804	67,820	70,9858	74,310
Net annual saving (A-B)	INR	10,79,910	10,88,228	10,96,512	11,04,757	11,12,955
Depreciation	INR	1,65,888	1,32,710	1,06,168	84,935	67,948

Operating cost of generation

Year	1	2	3	4	5	6	7	8	9	10
Cost/kWh	0.34	0.36	0.38	0.40	0.43	0.45	0.47	0.50	0.53	0.56

From the example explained by one of the solar vendors to further describe this technology of installing a solar panel generating 1 kW of energy which requires 100 square feet of area, approximately 1500 unit of solar energy can be produced from this panel annually with a payback period of approximately 4–5 years.

4   Conclusion

As the main objective of this study is the reduction of Green House Gases (GHG) emission, the efficient use and implementation of the Energy Efficient processes &equipment and use of Renewable Energy is required. From the selected ceramics and chemical industries, high energy consuming utilities and higher GHG gases emission were observed and some of the common energy saving intervention has been shortlisted in terms of thermal as well as electrical energy. The major focus was on Energy Efficiency Intervention with less than 1-year payback and 5-years for Renewable Energy interventions. Renewable energy interventions result in potential saving of 10–12% of electrical energy by replacing the conventional pumps with the solar water pump as it gives remarkable savings with average payback period of 3–9 months according to the study. We have found from this study that if we consider the investment of money in different investment classes such as real estate, debt funds, gold and solar, highest returns and lowest risks is observed in solar. All the calculations with general observations and assumptions, technical specifications, cash flow calculation along with payback period and operating cost calculation has

been shown and we concluded that for the very 1st year of solar generation i.e., INR 10, 87, 500 by generating 1, 45, 000 kWh energy annually by solar panels with the capacity of 100 kW can be achieved with the payback period of approximately 4 years.

Major benefit of installing solar panels is that generally tariff of electricity increases with time but once an invested in the solar power, the cost of the energy remains constant. Also, there will be decrease in depreciation and operational maintenance cost in solar installation. One year of free technical service is offered by some of the solar vendors and companies if the industry is willing to install their solar system. Training to the concerned person of the industry is also offered by the solar vendors and companies which will ultimately reduce the operational and maintenance cost of the industry and later on it will reduce the Annual Maintenance Cost of the system.

Few solar vendors suggested that in-house Solar PV plant can be owned and operated by the industrial firm (CAPEX model) or by a 3rd party which owns and operates the plant and sells solar power produced back to the firm (OPEX model). It is feasible for big industries with very high load requirements to get installed captive solar power plants within their facilities. If industry cannot afford both CAPEX and OPEX model then there is another way i.e., Off-site model in which developer installs and maintains large scale solar parks at a location away from your site and wheels electricity to the industry using the state-owned transmission network.

For the financial support, there is an Environmental Protection Measures Scheme of Gujarat Industrial Policies (2015) where in any existing MSME can avail financial assistance in tune of 35% of the project cost with ceiling of 35 lakhs which results in process optimization and water and energy saving. While any existing MSME can avail financial assistance in tune of 25% of the project cost with the ceiling of 35 lakhs when they upgrade their existing end of pipe treatment with any innovative technology.

The question arises over here is about the technical feasibility of the solar panel. Being a chemical industry, emission of many harmful chemicals and off gases from various chemical reactions takes place which could further damage the solar panels. Techno-economic feasibility of the solar panels has to be evaluated which includes the investment cost and maintenance cost of the solar panels with its life span.

Basically, from this whole analysis, studies and assessment we can conclude that by implementing solar technology to reduce the GHG emission, could be the step towards the low carbon pathway and efficient use of renewable energy to get the maximum possible benefit from the same.

References

Environmental Protection Measures Scheme of Gujarat Industrial Policies 2015

Evans A, Strezov V, Evans TJ (2009) Assessment of sustainability indicators for renewable energy technologies. Renew Sustain Energy Rev 13(5):1082–1088

Industrial data, Findings, Case Studies from Naroda Industrial Association (NIA), Naroda GIDC, Ahmedabad, Gujarat

Removal of Fluoride Using Nanoparticles of Fe_2O_3 with Al_2O_3 and Activated Sugarcane Bagasse

Prema Malali, Sujata S. Kulkarni, Geeta Bellad, and Sharanabasava V. Ganachari

Abstract A combination of Fe_2O_3 nanoparticles with Al_2O_3 nanoparticles produced using low-combustion methods and activated sugar cane bagasse was used for the adsorption of fluoride from water, and the results were promising. In order to optimize pH, dose of mixed adsorbent, and contact duration, experiments were carried out on a small scale in the lab. When a hybrid adsorbent was used in conjunction with first order kinetic reaction, a regression analysis was carried out using GeoGebra, and the R_2 value was shown to be absolutely accurate. According to the findings of the study, a combination of Fe–Al nanoparticles and activated sugar cane bagasse is effective in adsorbing fluoride ions from water.

Keywords Fluoride · Nanoparticles · Synthetic water · Activated carbon · Iron and aluminum oxide

1 Introduction

Fluoride is present in sedimentary and igneous rocks that leach out to contaminate water. Fluorosis, which occurs when the fluoride concentration in water exceeds the tolerance limit, is irreversible. The only way to prevent fluorosis is to maintain the optimum quantity of fluoride in drinking water. Currently, available methods for removing fluoride from water are broadly classified into three categories based

P. Malali (✉) · G. Bellad
School of Civil Engineering, KLE Technological University, Hubballi, Karnataka 580031, India
e-mail: prema@kletech.ac.in

S. V. Ganachari
Department of Chemistry, School of Advanced Sciences, KLE Technological University, Hubballi, Karnataka 580031, India

S. S. Kulkarni
Indian Institute of Technology, Gandhinagar, Palaj Gandhinagar, Gujarat, India

on the fluoride removal mechanism like precipitation, adsorption, and membrane-based methods. Adsorption is widely recognized as an ideal and appropriate technique because of its simplicity and the availability of a wide range of adsorbents for defluoridation. Surface area is a crucial factor that influences adsorption to a significant extent. The higher the surface area of the adsorbent, the higher will be its adsorbing capacity. It is most important to identify the materials with a higher surface area. Nanomaterials that provide ample surface area have been the subject of active research worldwide in many fields. Numerous studies have shown that nanoparticles can effectively remove pollutants from water. However, to achieve an appropriate treatment, excess powder material needs to be added to water on a large scale, which proves to be uneconomical. Researchers have been attempting to minimize the cost by combining the nanoparticles with low-cost adsorbents. Fatemech et al. (2020) studied the adsorption of fluoride ions from synthetic wastewater using active oak shell/Fe_3O_4 in a batch system. The experiments showed 97.4% highest adsorption efficiency of fluoride at pH 3. Adeno et al. (2012) investigated the removal of fluoride from water using nanoscale aluminum oxide hydroxide. Almeelbi and their team used nanoscale zero-valent iron (nZVI) of size 16 nm as an adsorbent in batch scale to remove phosphate. They showed that nano ZVI (16 nm) was 13.9 times more efficient than micro ZVI (¡10 m) in removing phosphate. Fataei et al. (2013) reported 100% efficient removal of nitrate from drinking water in laboratory-scale using Iron and sand nanoparticles for a contact time of 60 min. Rytwo (2012) observed a 100% reduction in TSS and turbidity at a polymer/clay nanocomposite ratio of 70 mg/g. Rout et al. (2015) utilized Bermuda grass along with Iron oxide nanocomposite to achieve 97% of fluoride removal at pH 4. The present work aims at exploring the possibility of utilizing the nanoparticles of Fe and Al oxides with activated sugarcane bagasse.

2 Materials and Methods

2.1 Materials

To make activated carbon, sugarcane bagasse was purchased from a local market in Hubballi. It was cleaned with distilled water and sun-dried. Dried bagasse was combined with concentrated Sulphuric acid (0.05 N) and soaked for 2 h followed by heating in oven for 24 h at 150 °C. The heated material was rinsed with distilled water to remove excess acid and then steeped in a 1% sodium bicarbonate solution. The material was then dried in an oven for 24 h at 105 °C. The metal oxide was produced using a Low-temperature solution combustion technique (Ganachari et al. 2012). FAS, Oxalic acid, Al_2O_3 were procured from the laboratory. The Fe–Al metal oxide was prepared using a Low-temperature solution combustion technique. In this process, 1_N solution of FAS, Oxalic acid, Al_2O_3 of 50 ml each was prepared. These three solutions were homogeneously mixed using a magnetic stirrer, and the solution

was filtered using filter paper. The residue was air-dried for 24 h before being oven-dried for 4 h at 80 °C. To make the stock solution, dissolve 0.221 g of sodium fluoride in 1 L of distilled water. Distilled water was used to dilute 100 ml of stock fluoride solution to 1000 ml. Synthetic water of different concentrations varying from 2 to 20 mg/1 of fluoride is prepared (Association et al. 1912).

2.2 Characterization of Materials

The materials prepared were sent for particle characterizations FTIR Spectrophotometer, (Make: Perkin-Elmer, Model-Spectrum 100), X-ray Powder Diffractometer (Make: Bruker Model: D2 PHASER), Scanning Electron Microscope (SEM) (Make: JEOL Model: JSM6360 and to testing laboratory located in Shivaji University, Kolhapur, India.

Figure 1a, b represent the surface chemistry of the synthesized activated carbon and Aluminum Ferrite characterized using Fourier Transform Infrablack Spectroscopy (FTIR), respectively. Figure 1a showed that the 3833.38, 3737.48, 2925.60, 1602.48, 1228.78, 1046.67, 823.12, 752.17, and 620.55 cm^{-1} peaks are in correspondence to O–H, O–H, C–H, C=C, C–O stretch, C–N stretch, C=C bending, C=C bending and C–Br stretching respectively. According to Fig. 1b, the 2926.85 cm^{-1} peak corresponds to C–H bending, C–H bending, C=C stretching, C=C stretching, C=C, C–H stretching, N–O stretching, C–H bending, C–H bending, C=C, C=C, C–H stretching, C=C, C–H stretching, C–Br stretching, C-H bending, C–H bending, C=C, C=. The peaks were in the range of 3833–2925 cm^{-1}, which corresponded to the O–H stretching mode of hydroxyl groups and absorbed water, which indicates sugarcane bagasse activated carbon impregnated with sulphuric acid (0.05 N). The findings revealed the presence of an aromatic molecule. The most powerful vibration in the spectrum was caused by the C=O stretching vibration, which was the most intense in the spectrum (Arilasita et al 2020).

A scanning electron microscope was used to examine the surface morphology of the (a) activated carbon and (b) aluminium ferrite ($AlFe_2O_4$) samples. The secondary electron images are obtained at various magnifications in order to investigate the morphology of materials using a scanning electron microscope. Figure 2a, b above depict the SEM microstructures of activated carbon and Aluminum Ferrite, respectively. The surface morphology and particles size of the samples seem to be non-uniform with to some extent larger flakes like (a) homogeneously arranged smaller particles with agglomeration in the synthesized samples (b). From the initial explanations of the SEM images, one can observe that the grain size is slightly affected by the higher temperature with chemical concentration.

XRD analysis of sugarcane bagasse activated carbon and Aluminum Ferrite ($AlFe_2O_4$) as depicted in Fig. 3a, b, respectively. The XRD spectra of the activated carbon indicated that all those chars are amorphous. This was denoted by the presence of multiple peaks at the $2\theta = 25°$, $2\theta = 42°$, and $2\theta = 50°$ for the sample (a) became stronger after the impregnation process with Sulphuric acid (0.05 N) and
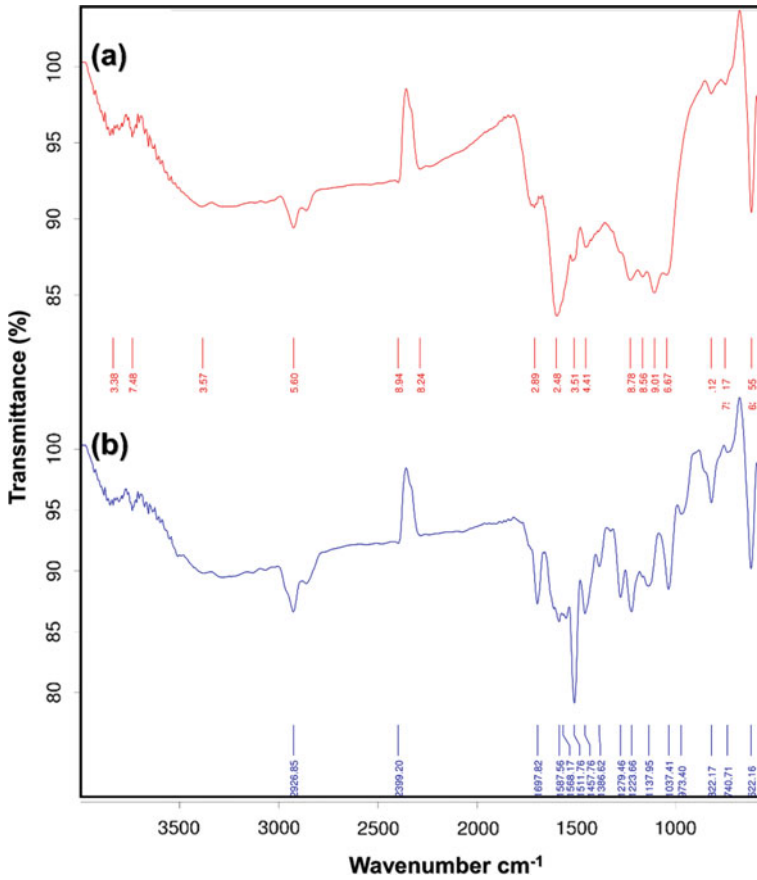
Fig. 1 FTIR image of **a** activated carbon (bagasse) and **b** Aluminum Ferrite (AlFe$_2$O$_4$)
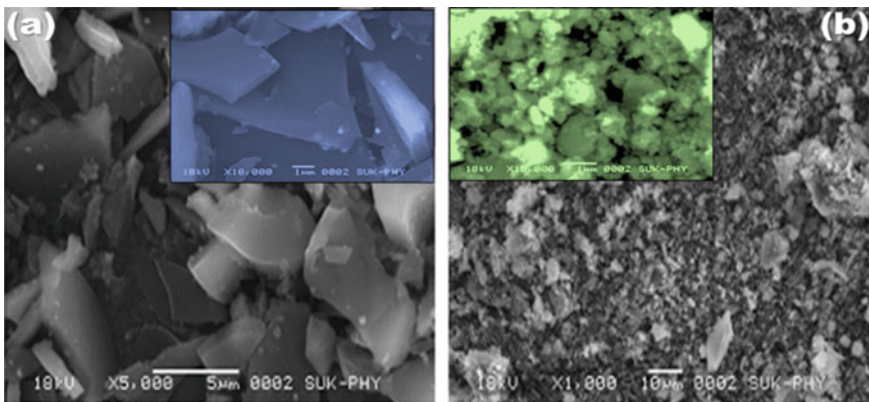
Fig. 2 SEM images of **a** activated carbon (bagasse) and **b** Aluminum Ferrite (AlFe$_2$O$_4$)
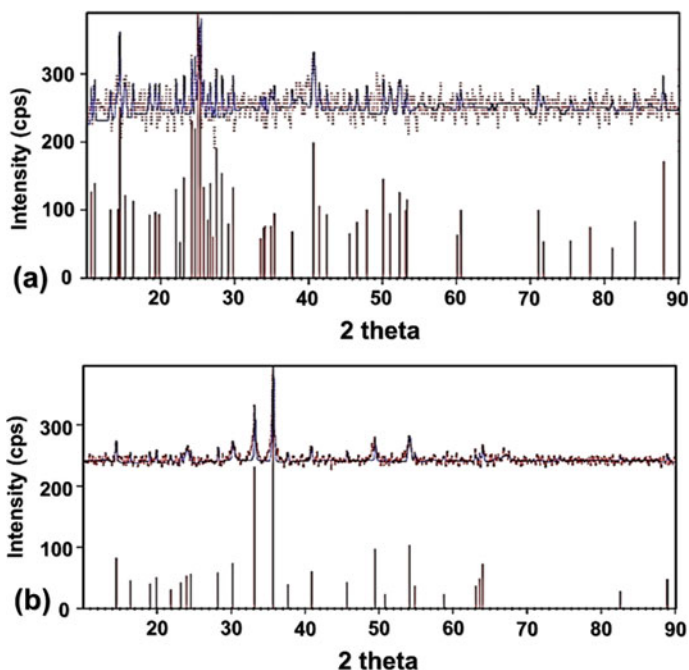
Fig. 3 XRD pattern of **a** activated carbon (bagasse) and **b** Aluminum Ferrite ($AlFe_2O_4$)

sugarcane bagasse which described that the carbon tends to crystallize at an elevated temperature. Figure 3b depicts the X-ray diffraction pattern of the Aluminum Ferrite ($AlFe_2O_4$) ferrites, which confirms the formation of cubic spinel structure in single phase without the presence of any impurity peaks. The strongest reflection occurs from the $2 = 35°$ plane, which corresponds to the spinel phase and is the most intense. It is evident that the development of cubic spinel structure in single phase is indicated by the peaks indexed to $2 = 24°$, $2 = 30°$, $2 = 33°$, $2 = 35°$, $2 = 49°$ and $2 = 54°$ of a cubic unit cell, all planes are the allowed planes, and all planes are the allowed planes of a cubic unit cell.

2.3 Methodology

Batch tests were designed to determine the effect of pH, contact time, and media dosage on the fluoride removal from water. Initially activated carbon in varying dosages (2–15 g/L) was exposed to solutions containing initial fluoride concentration varying from 2, 5, 10, 15, and 20 mg/L, along with the pH varied from 2, 4, 6, 8, 10. The size of the water sample taken of the experiment each time was 200 ml. The analysis for fluoride content was done using a spectrophotometer at 570 nm

as defined by American Public Health Association (Association et al. 1912). The filtrate was analyzed every 15 min for 1 h. In the above process, contact time, pH, and the dosage of activated carbon were optimized. Similarly, the dosage of metal oxide was varied from 0.02 to 0.07 g/L, and various parameters were optimized for metal oxide.

3 Results and Discussion

The absorption technique was employed to remove fluoride from synthetic water in conjunction with activated carbon and iron and aluminum metal oxide as adsorbents. Batch experiments were conducted in the laboratory for the removal of fluoride. The contact time, pH, and dose of adsorbents were optimized for activated carbon and nano metal oxide in this study.

3.1 Optimization of Parameters for Activated Carbon

Optimization of pH. The experiments were carried out in 500 ml Erlenmeyer flasks containing 200 ml of fluoride water sample with initial fluoride concentration 2 mg/L, adsorbent dose of 2 g/L, and pH ranging from 2 to 12. After 30 min of contact with the fluoride solution, the residual fluoride was determined. In Fig. 4, it can be seen that the percentage elimination of fluoride increases up to pH 8 and then declines with each subsequent increase in pH greater than 8. This might be explained by the fact that the surface charge of the adsorbent has changed. In conditions when the pH was low, the fluoride anions were drawn to the positively charged surface of the

Fig. 4 Optimization of pH for activated carbon
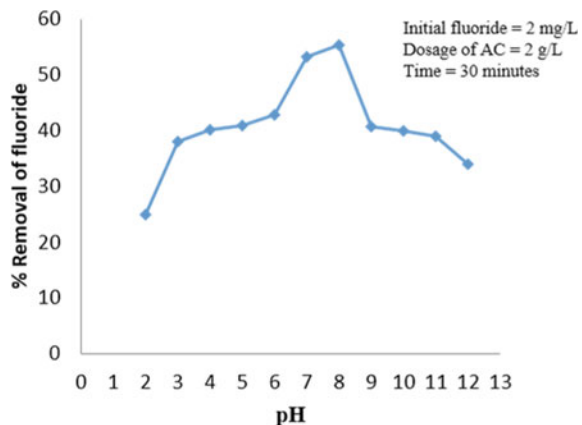
Fig. 5 Optimization of contact time for activated carbon
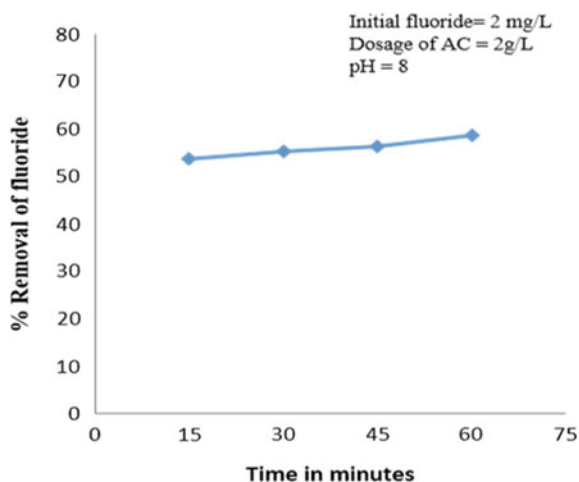
water. In highly alkaline circumstances, negatively charged OH$^-$ ions competed with fluoride ions for space on the adsorbent surface, resulting in a loss of efficiency.

Optimization of contact time. Batch experiments on adsorption were carried out by changing contact duration (15–60 min) at an optimum pH of 8, starting fluoride concentration of 2 mg/L, the adsorbent dosage of 2 g/L, and the fluoride adsorption efficiencies were displayed. Upon closer inspection of Fig. 5, it appears that the percentage removal of fluoride increases with increasing contact time and that there is no substantial fluoride removal between 30 and 60 min of contact time. As a result, the optimal contact time is thirty minutes.

Optimization of dosage. The experiments were conducted by varying doses (2–15 g/L) at optimized pH 8 and contact time of 30 min to analyze the residual fluoride. Similar tests were performed for other initial fluoride concentrations ranging from 5 to 20 mg/L. Figure 6 depicts the outcomes of the study. For all starting fluoride concentrations, it has been shown that increasing the adsorbent dosage results in a rise in the percentage removal of fluoride. The optimal dose was 13 g/L of the compound. Higher adsorbent dose increases adsorption due to the increased surface area and availability of additional adsorption sites.

3.2 Optimization of Parameters for Metal Oxide.

Optimization of pH. Adsorption experiments were performed in a 500 ml Erlenmeyer flask containing a 200 ml fluoride water sample, and initial fluoride concentration of 5 mg/L and adsorbent dose of 0.05 g/L were used with pH ranging from 2 to 12. The residual fluoride was analyzed after a contact time of 30 min. The results are shown plotted in Fig. 7. Upon examination of Fig. 7, it is clear that the fluoride

Fig. 6 Optimization of dosage
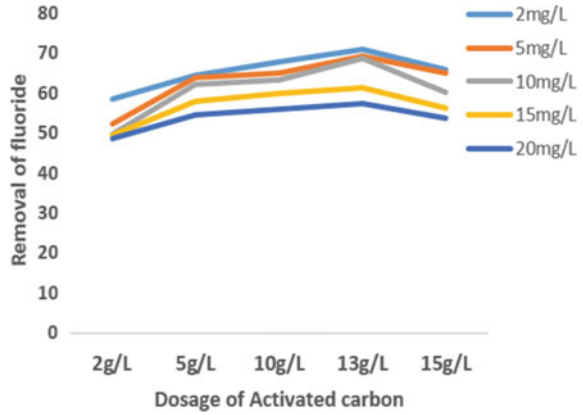
Fig. 7 Optimization of pH for metal oxide
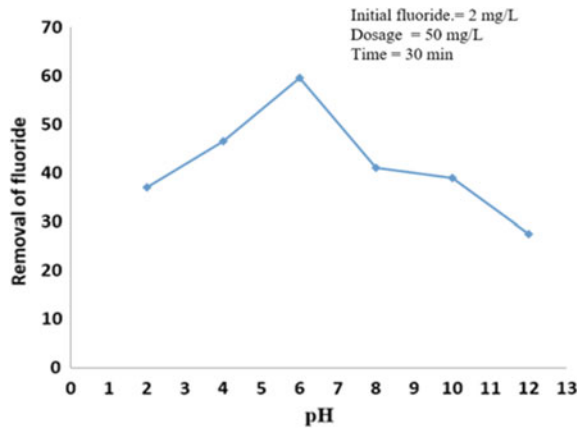
adsorption increases with increasing pH, reaching a maximum of 60% at pH 6, and subsequently declines with further increases in pH. According to specific theories, the production of weekly ionized fluoric acid under very acidic conditions (pH 6) might be the cause of this phenomenon.

Optimization of contact time. Variations in contact duration (15–45 min) at optimal pH 6, starting fluoride concentration (2 mg/L), and adsorbent dosage (0.05 g/L) were used in the tests, which were done in triplicate. Figure 8 depicts the removal efficiencies as a function of time. The proportion of fluoride removed rises as the amount of time spent in contact with the fluoride increases.

Optimization of dosage of metal oxide. The batch adsorption tests were carried out by adjusting the adsorbent dose (0.02–0.07 g/L) and the contact period (45 min) at the optimal pH 6 and the optimum temperature. In the same way, experiments were conducted with varied starting fluoride concentrations, ranging from 5 to

Fig. 8 Optimization of contact time for metal oxide
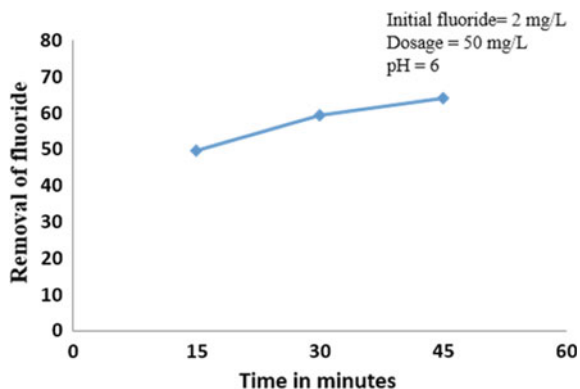
Fig. 9 Optimization of dosage of metal oxide
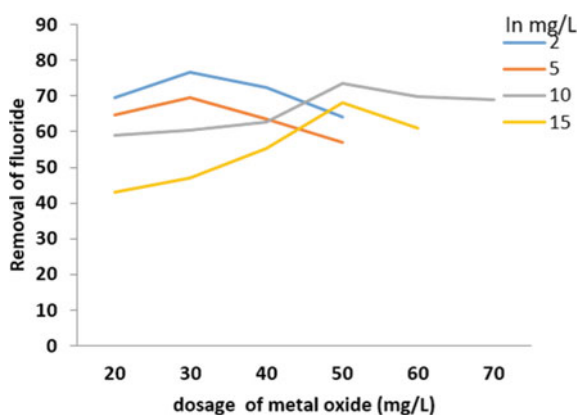
15 mg/L. The removal efficiencies are plotted in Fig. 9. The fluoride removal efficiency increases up to a certain level and then gradually decreases. The optimized metal oxide dosage for a lower fluoride concentra tion is 0.03 g/L, and a higher concentration is 0.05 g/L. The increase in fluoride adsorption due to the increase in dosage is because of the large number of active sites available for adsorption. After reaching a certain point, the percentage of removed fluoride gradually decreases.
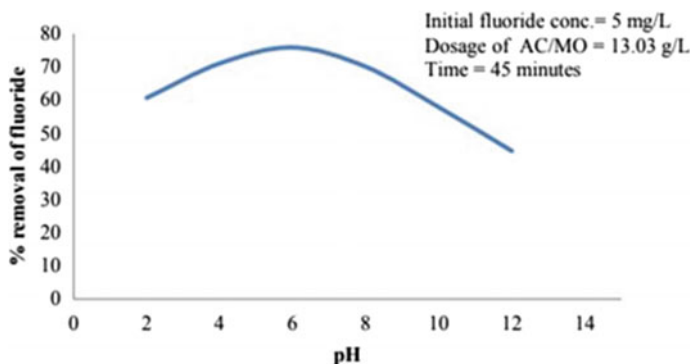
Fig. 10 Optimization of pH for the mixture of metal oxide and activated carbon

4   Optimization of Parameters for the Mixture of Metal Oxide and Activated Carbon

4.1   Optimization of pH

In this phase, experiments were conducted for initial fluoride concentration of 5 mg/L, adsorbent dosage 13.03 g/L, contact time 30 min and pH varied from 2 to 12. Figure 10 reveals that the percentage removal of fluoride increases initially and reaches maximum value at pH 6, thereafter decreases gradually as the pH further increases to 12. When pH is raised above 6, the adsorption of fluoride increases, reaching a maximum of 76% at pH 6, and then begins to decline with each subsequent increase in pH above 6.

4.2   Optimization of Contact Time

In this phase, experiments were carried out at an initial fluoride concentration of 5 mg/L, adsorbent dose of 13.05 g/L, optimum pH 6, and contact time varied from 0 to 45 min. Figure 11 shows that the percentage removal of fluoride increases with an increase in contact time. There is no remarkable increase in fluoride removal efficiency from 45 to 60 min. So, the optimized contact time was 45 min. The fluoride adsorption capacity of the mixture of both metal oxides and activated sugarcane bagasse was higher compared to the removal efficiencies of activated sugarcane bagasse and the metal oxides. This behavior may be attributed to the synergistic effect of both the adsorbents in the mixture.

The filtrate was tested for the concentration of Fe particles to verify the suitability of using nanoparticles for water treatment. The concentration of iron was found to
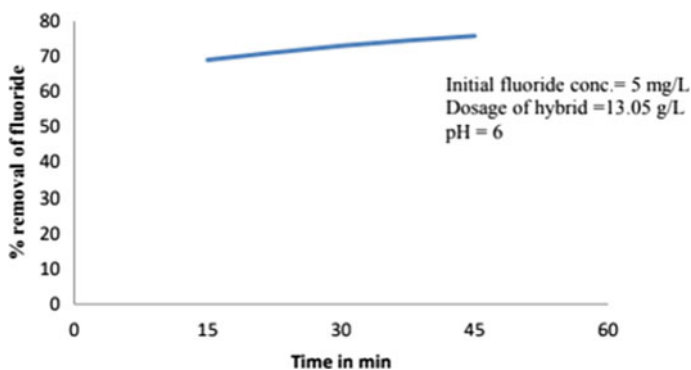
Fig. 11 Optimization of contact time for the mixture of metal oxide and activated carbon

be 0.091 mg/L which is within the tolerable limit of Fe content in drinking water 0.3 mg/L (IS10500 2012).

5 Conclusion

Based on batch studies conducted for fluoride adsorption using a mixture of nanoparticles of iron and aluminum oxides and activated sugarcane bagasse, we found that the optimal condition for the maximum fluoride removal using activated sugarcane bagasse was pH 8, contact time 30 min, and dosage 13 g/L for the initial fluoride concentration ranging from 5 to 20 mg/L. The maximum removal efficiency of 70–75% of fluoride using Fe and Al oxides nanoparticles occurred at optimized pH 6 and contact time 45 min. The optimized dosage of metal oxide nanoparticles was 0.03 g/L for an initial fluoride concentration of 5 mg/L and 0.05 g/L for a higher fluoride concentration. The mixture of activated sugarcane bagasse and metal oxides efficiently reduced fluoride content up to 72–80% in the pH range of 6–8 with an optimum contact time of 45 min at the optimized adsorbent dosage. Finally, it can be concluded that the mixture of nanoparticles of iron and aluminum metal oxides can be utilized as adsorbents for water treatment.

References

Almeelbi T, Bezbaruah A (2012) Aqueous phosphate removal using nanoscale zero-valent iron. In: Nanotechnology for sustainable development. Springer, Cham, pp 197–210.

Arilasita R, Utari, Purnama B (2020) The effect of annealing on the crys-talline structure of CoBi0.1Fe1.9O4 nanoparticles. In: AIP conference proceedings 2296, 020128

American Public Health Association et al (1912) Standard methods for the examination of water and wastewater, vol 2. American Public Health Association

Fataei E et al (2013) Nitrate removal from drinking water in laboratory-scale using iron and sand nanoparticles. Int J Biosci 3(10):256–261

Ganachari SV et al (2012) Large scale synthesis and characterization of $\Gamma-Fe_2O_3$ nanoparticles by self-propagating low temperature combustion method. Int J Sci Res 1(2):77–79

IS10500, B. I. S (2012) Indian standard drinking water–specification (second revision). Bureau of Indian Standards (BIS), New Delhi

Rout TK et al (2015) Study the removal of fluoride from aqueous medium by using nanocomposites. J Encapsul Adsorpt Sci 5(01):38

Rytwo G (2012) The use of clay polymer nanocomposites in wastewater pretreatment. Sci World J 2012

Takmil F et al (2020) Nano-magnetically modified activated carbon prepared by oak shell for treatment of wastewater containing fluoride ion. Adv Powder Technol 31(8):3236–3245

In Silico Characterization and Structural Modeling of Proteins Involved in Arsenic Tolerance of Hyper Accumulating Fern *Pteris Vittata*

Rahul Deogam, Nikhil Kumar Pipil, Navjyoti Chakraborty ⬤**,**
Sayan Chatterjee ⬤**, and Ram Singh Purty** ⬤

Abstract Arsenic is known as the king of poisons due to its toxic nature and is used as pesticide and fertilizers. Accumulation of arsenic in plants causes toxic reactions, negative impact on growth and productivity. Increment in arsenic uptake is directly proportional to oxidative stress resulting in the production of reactive oxygen species. However, few plants have developed mechanism for tolerance by expressing genes or proteins such as antioxidants enzymes, arsenite oxidase, that playing some beneficial role in detoxification against arsenic effect. *Pteris vittata* is one such example of plants which can tolerate both forms of Arsenic i.e., arsenate (+5) and arsenite (+3). Tolerance to arsenic in *P. vittata* is due to the activity of three genes i.e., Glyceraledhyde 3-phosphate dehydrogenase C1 (*PvGAPC1*), Organic cation/carnitine transporter 4 (*PvOCT4*), and Glutathione S transferase (*PvGSTF1*). Knowing the importance of these genes in arsenic tolerance, in the present investigation we have characterized and predicted the tertiary structure of these proteins using computational approaches. Further to understand the mechanism of arsenic tolerance, we have compared the 3D structure of PvGAPC1, PvOCT4 and PvGSTF1 with its counterpart predicted from arsenic sensitive *Oryza sativa* and *Arabidopsis thaliana*. Thus, crop improvement techniques using these genes of *Pteris vittata* be utilized for developing arsenic tolerance in important cultivated crops.

Keywords *Pteris vittate* · Fern · Abiotic stress · Phytoremediation · Multiple sequence alignment · Homology modelling · Computational approach

R. Deogam
Agricultural and Food Engineering, IIT Kharagpur, Kharagpur, West Bengal 721302, India

N. K. Pipil · N. Chakraborty · S. Chatterjee · R. S. Purty (✉)
University School of Biotechnology, Guru Gobind Singh Indraprastha University, Sec-16C, Dwarka, New Delhi 110078, India
e-mail: rspurty@ipu.ac.in

1 Introduction

Arsenic is well known metalloid found in the environment in four different forms. Out of these four, two are considered as toxic i.e., Arsenate (+5) and Arsenite (+3). Arseniteis more toxic than Arsenate. Arsenic occurs as both organic and inorganic compounds forms, out of the two forms, inorganic forms are more toxic (Mandal and Suzuki 2002). Arsenic is highly soluble in water therefore it is responsible for groundwater contamination in many parts of the world (Shankar and Shanker 2014; Purty et al. 2020; Shaji et al. 2020). Contaminated water and soil are sources of exposure of Arsenic to humans. In humans Arsenic toxicity is cause of some serious health related issues like cancer, liver and kidney related diseases (Chakraborti et al. 2016; Engwa et al. 2019; Shah et al. 2020). Detoxification of ground water is important because large number of people worldwide uses it for various activities such as drinking, irrigation etc. There are many techniques which can be employed for detoxification.

Bioremediation is considered as one of the best methods of remediation. Many bacteria and plants can tolerate high concentrations of Arsenic (Brown et al. 2018). These bacteria and plants can be used for remediation purposes. Bacteria can reduce or oxidise Arsenic so that it can tolerate high concentration. In the arsenate reduction, Arsenate (+5) is reduced to Arsenite (+3) and extrude it out of the bacterial cell (Ghosh et al. 2015). In this process, bacteria use the enzyme Arsenate reductase. Some bacteria oxidise Arsenite to Arsenate and use this Arsenate as terminal electron acceptor. In anaerobic condition, bacteria use Arsenate as an energy source. Methylation is also used by bacteria to cope up with high concentration of Arsenic but it is not considered as remediation method as methylation produce compounds that are toxic to nature (Chakrabarty 2015).

In plants, the process of arsenic degradation is known as phytoremediation. Some plants can hyper accumulate Arsenic therefore tolerate high concentration of Arsenic. There are many plants that can hyper accumulate Arsenic (Popov et al. 2021). A well-known example is a fern *Pteris vittata.* Unprecedently *P. vittata* and related species can tolerate a high concentration of Arsenic as well as accumulate Arsenic in their fronds above normal concentration (Cai et al. 2019). Most plants can accumulate below 1 mg/kg but *P. vittata* can accumulate 10,000 mg/kg dry weight (Chakrabarty 2015). In *Pteris vittata* arsenic tolerance is majorly contributed by three proteins i.e., Glyceraledhyde 3-phosphate dehydrogenase C1 (PvGAPC1), Organic cation/carnitine transporter 4 (PvOCT4), and Glutathione S transferase (PvGSTF1). In the presence of arsenic, reduction in the growth of *P. vittata* gametophyte was reported when the expression of these three genes was suppressed using RNAi technology (Cai et al. 2019).

In *P. vittata,* arsenate enters the cell through phosphate transporter (PvPht1;3),where it is directly reduced to arsenite with the enzyme Arsenate reductase (PvAcr2), then transported to vacuoles via PvACR3 or converted to 1-arseno-3-phosphoglyerate (1-As-3-PG) by PvGAPC1 (Ma et al. 2001).The transmembrane protein PvOCT4, is involved in transporting of 1-As-3-PG to vesicles. Once inside

the vesicle 1-As-3-PG is hydrolysed and converted into Arsenate. Arsenate inside the vesicle get reduced to Arsenite by Arsenate reductase by Glutathione S transferase PvGSTF1 or PvACR2. After the formation of Arsenite vesicle fuse with vacuole, Arsenite transferred to vacuole for long time storage (Cai et al. 2019).

Therefore, knowing the importance of these three proteins i.e., PvGAPC1, PvOCT4 and PvGSTF1, in arsenic tolerance in hyper accumulating fern *Pteris vittata*, present investigation was carried to characterize and predict secondary and tertiary structure and compared the structures with its counterpart predicted from arsenic sensitive *Oryza sativa* and *Arabidopsis thaliana* using a computational approach.

2 Material and Methods

2.1 Sequence and Phylogenetic Tree Analysis

In the present investigation, protein sequence of PvGAPC1, PvOCT4 and PvGSTF1 was analyzed. ProtParam tool was used for analysis of sequence, molecular weight, amino acid composition and pI value calculation (Gasteiger et al. 2005). NCBI server was used for BLAST search (Altschul et al. 1990). The hits obtained was used for multiple sequence alignment using MEGA X and visualized by Jalview software (Kumar et al. 2018; Edgar 2004; Waterhouse et al. 2009). The phylogenetic trees analysis was generated in MEGA X program applying neighbor joining algorithm (Saitou and Nei 1987).

2.2 Subcellular Localization and Domain Analysis

Localization of proteins was predicted using COMPARTMENTS subcellular localization database and Cell eFP Browser (Binder et al. 2014; Winter et al. 2007). Domain analysis was performed using the Simple Molecular Architecture Research Tool and Pfam database (Schultz et al. 1998; Mistry et al. 2021).

2.3 Prediction of Secondary Structure and Tertiary Structure

In the present study, SOPMA was used for the prediction of secondary structure of proteins (Geourjon and Deleage 1995). For tertiary structure, the template for each protein was searched in SWISSMODEL TEMPLATE LIBRARY (SMTL) using the peptide sequence of the desired proteins. The template with highest quality was selected to build the model using SWISSMODEL and I-TASSER (Iterative Threading ASSEmbly Refinement) server (Guex et al. 2009; Zhang 2008). The

protein structures or models obtained was validated using PROCHECK and Verify 3D (Laskowski et al. 1993; Eisenberg et al. 1997).

2.4   Structural Comparison

For structural comparison, all the three predicted tertiary structure of *Pteris vittata* i.e., PvGAPC1, PvOCT4, or PvGSTF1, were saved in PDB format and were compared one-by-one with the target tertiary structure of *Orzya sativa* and *Arabidopsis* using PyMOL, Molecular Graphics System version 2.5.1 (Schrodinger, LLC) (DeLano 2002). The PDB file of OsGAPC1 (3E6A) and AtGAPC1 (6QUQ) were downloaded from Protein Data Bank (Berman et al. 2000). Similarly, PDB file of AtGSTF1 (5A5K) protein was retrieved whereas OsGSTF1 was predicted using Swiss Model. The templates downloaded were used for structural comparison using PyMOL Molecular Graphics System.

3   Results

3.1   Characterization and Structural Modeling PvGAPC1 Protein

Sequence analysis showed that glyceraldehyde 3-phosphate dehydrogenase (PvGAPC1) has 355 amino acids with the predicted molecular mass 38.3 kDa with pI value 7.19. The most frequent amino acids was glycine (9.0%) and valine (9.0%), followed by serine (8.7%), alanine (8.5%) and threonine (7.6%). Both negatively charged residues (Asp + Glu) and positively charged residues (Arg + Lys) constituted 9.8% of the polypeptide. The instability index is computed as 29.37 which confirms the protein as stable.

BLASTP analysis showed that PvGAPC1 protein showed above 70% homology with other plant species which includes *Ginkgo biloba* (Q39769.1), *Apostasia shenzhenica* (PKA55814.1), *Helianthus annuus* (XP_022011534.1), *Carexlittledalei* (KAF3337947.1), *Aeluropus lagopoides* (AEP31954.1) and *Actinidia chinensis* var. chinensis (PSS30165.1), *Dioscorea oppositifolia* (ANA57341.1), *Gossypium raimondii* (XP_012489505.1), *Oryza sativa* Japonica Group (XP_015650130.1), *Camellia sinensis* (XP_028061864.1), *Phyllostachys edulis* (ADB98096.1), *Arabidopsis thaliana* (NP_187062.1). Whereas with GAPC1 protein sequence of *Ectocarpus* sp. (CAB1116843.1) it showed 64.55% similarity. The multiple sequence analysis and phylogenetic tree generated indicated that PvGAPC1 protein is conserved across plant species (Fig. 1).

Subcellular localization of glyceraldehyde 3-phosphate dehydrogenase protein is predicted in cytosol of the cell. SMART predicted the presence of one domain
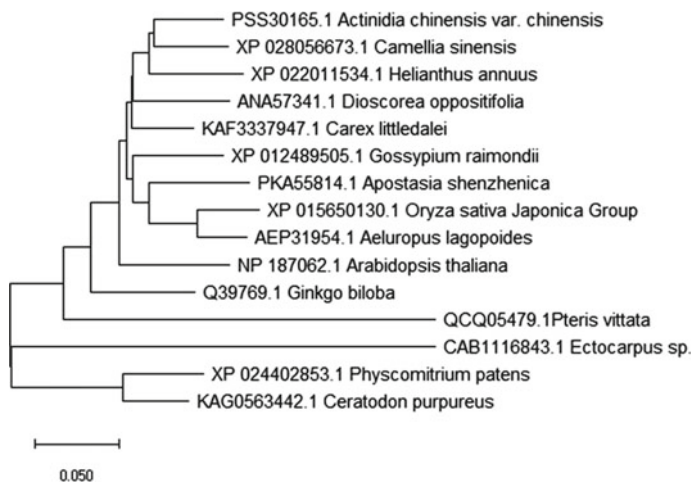
Fig. 1 Neighbor-joining evolutionary tree showing relationship of Glyceraldehyde 3-phosphate dehydrogenase (PvGAPC1) from *Pteris vittata* (QCQ05479.1) with other plant species

Gp_dh_N which start at 21st amino acid and end at 171st amino acid. While Pfam predicted two domain Gp_dh_N and Gp_dh_C from 21st amino acid to 124th amino acid and 176th amino acid to 333th amino acid, respectively.

The secondary structure of glyceraldehyde 3-phosphate dehdrogenase protein showed that the peptide composed of 33.80% alpha helix, 22.66% extended strand, 6.76% beta turn, and 35.77% random coil. Tertiary structure was predicted by homology modelling using the peptide sequence of glyceraldehyde 3-phosphate dehydrogenase (Fig. 2). A total of 50 templates showed sequence similarity to the peptide sequence. The template with greatest QSQE among the list was 6lgk (oxido-reductase, QSQE: 0.96, Resolution: 2.0A). Template 6lgk showed the sequence identity of 63.86% with coverage of 94% which ranged from 20 to 353 with the target peptide sequence.

3.2 Characterization and Structural Modeling PvOCT4 Protein

Sequence analysis showed that organic cation transporter 4 (PvOCT4) has 520 amino acids with the predicted molecular mass 56.7 kDa with pI value 8.24. The most frequent amino acids was leucine (12.7%) and alanine (10.6%), followed by glycine (8.1%), valine (8.5%) and serine (7.3%). Negatively charged residues (Asp + Glu) and positively charged residues (Arg + Lys), constituted 6% and 6.7% of the polypeptide, respectively. The instability index is computed as 38.77 which confirms the protein as stable.
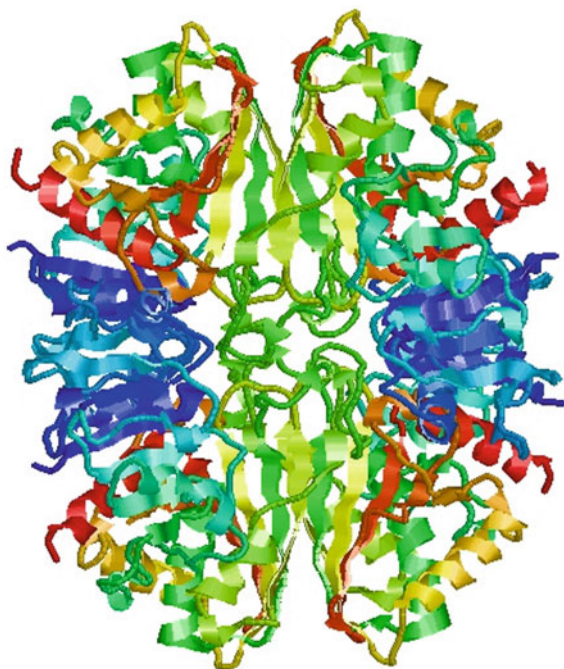
BLASTP analysis showed that PvOCT4 protein showed above 90% homology with other plant species which includes *Camelina sativa* (XP_010509193.1), *Capsella rubella* (XP_006297422.1), *Arabidopsis thaliana* (NP_188702.2), *Brassica napus* (CAF1932029.1). Using the peptide sequences of obtained from BLAST analysis, multiple sequence alignment and phylogenetic tree analysis was performed (Fig. 3). The result showed conservation of organic cation transporter 4 in all the plant species.

The subcellular localization of organic cation transporter 4 was predicted to be in plasma membrane. SMART predicted the presence of 12 transmembrane regions within the protein. Pfam predicted one domain sugar_tr (Sugar transporter) from 98th amino acid to 513rd amino acid. The secondary structure prediction of organic cation transporter 4 protein showed that the peptide composed of 46.16% alpha helix, 18.65% extended strand, 3.46% beta turn, and 31.73% random coil. Using the peptide sequence of PvOCT4 tertiary structure was predicted using the I-TASSER server (Fig. 4). The predicted structure was later used for structural comparison.
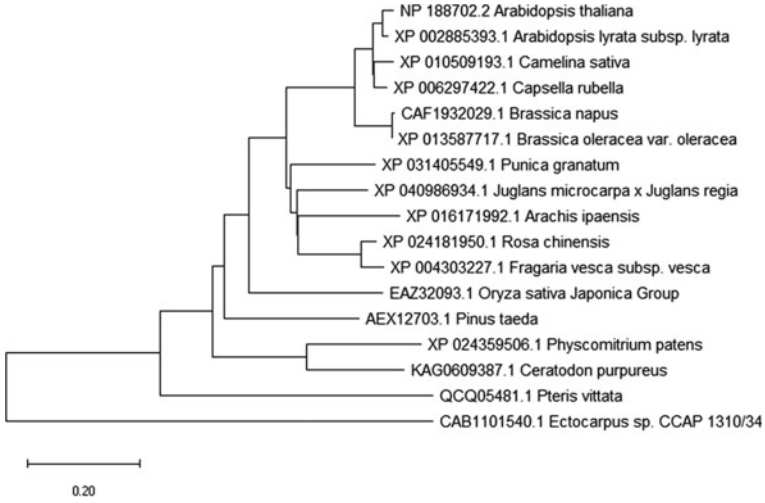
Fig. 3 Neighbor-joining evolutionary tree showing relationship of Organic cation/carnitine transporter 4 (PvOCT4) from *Pteris vittata* (QCQ05481.1) with other plant species

Fig. 4 Tertiary structure prediction of Organic cation/carnitine transporter 4 (PvOCT4) protein of *Pteris vittata*

3.3 Characterization and Structural Modeling PvGSTF1 Protein

Sequence analysis showed that glutathione S-transferase (PvGSTF1) has 217 amino acids with the predicted molecular mass 24.37 kDa with pI value 6.71. The most frequent amino acids was leucine (12.9%) and serine (10.6%), followed by alanine (8.3%) and valine (7.4%). Negatively charged residues (Asp + Glu) and positively charged residues (Arg + Lys), constituted 11.5% and 11% of the polypeptide, respectively. The instability index is computed as39.76 which confirms the protein as stable. The hits obtained from BLAST analysis were used for multiple sequence alignment and phylogenetic tree analysis (Fig. 5). The result showed conservation of glutathione S-transferase (PvGSTF1) in all plant species.

The subcellular localization of glutathione S-transferase protein was predicted to be in endoplasmic reticulum. Pfam predicted two domain, GST_N from 1st amino acid to 77th amino acid and GST_C from 92nd amino acid to 204th amino acid. The secondary structure of glutathione S-transferase protein showed that the peptide consisted of 43.78% alpha helix, 14.29% extended strand, 7.37% beta turn, and 34.56% random coil. Tertiary structure was predicted by homology modelling using the peptide sequence of glutathione S-transferase (Fig. 6). A total of 50 templates showed sequence similarity to the peptide sequence. The template with greatest QSQE among the list was 5f07 (glutathione transferase, QSQE: 0.81, Resolution: 1.5A). The template 5f07 showed highest sequence similiraty of 52.61% and coverage of 97% ranging from 2 to 213 with the target peptide sequence.
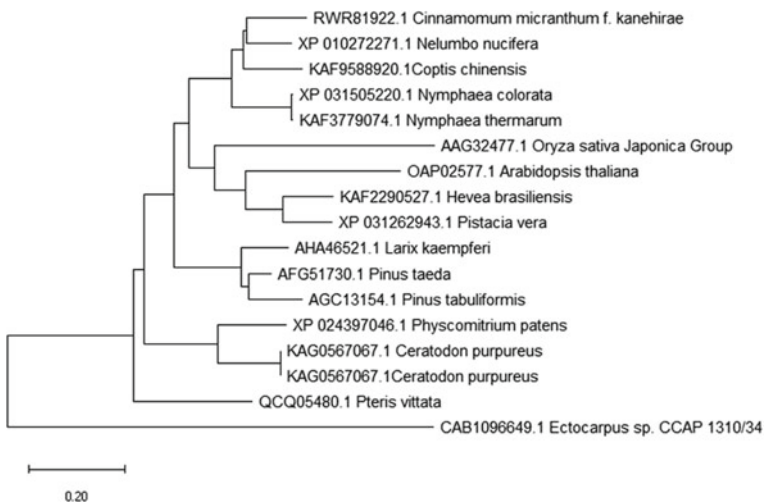
Fig. 5 Neighbor-joining evolutionary tree showing relationship of glutathione S-transferase class phi (PvGSTF1) from *Pteris vittata* (QCQ05480.1) with other plant species

Fig. 6 Tertiary structure prediction of glutathione S-transferase (PvGSTF1) protein of *Pteris vittata*

3.4 Structural Comparison

The proposed tertiary structures of each of the proteins namely, PvGAPC1, PvOCT4 and PvGSTF1 were compared with their corresponding proteins expressed in *Oryza sativa* and *Arabidopsis thaliana* (Fig. 7a–f). The superimposition visually highlighted the difference in the structural motifs of the proteins of *Pteris vittata* with that of the other plants. It is observed that PvGAPC1 contains much less of the structural domains thus having a clear approach path of its binding molecules towards the core of the molecule which holds the major binding sites (Fig. 7a, b). In the case of PvOCT4 protein, superimposition showed high degree of homology with *Oryza sativa* and *Arabidopsis thaliana* (Fig. 7c, d).Similarly, the PvGSTF1 was observed to be a much leaner molecule to allow bigger binding clefts and groves which are important for allowing better binding opportunity to any prospective substrates (Fig. 7e, f).

4 Discussion

Arsenic contamination in land is a major concern for population living in or near the contaminated area. Arsenic in soil majorly present in three forms, first as Arsenite second as Arsenate and third as methylated form (Chakrabarty 2015). There are many plants that can tolerate high concentration of Arsenic present in the soil (Sharma et al. 2021; Porter and Peterson 1975). Basically, they can tolerate high concentration of arsenic via two strategies (Souri et al. 2017). In first strategy, plant does not
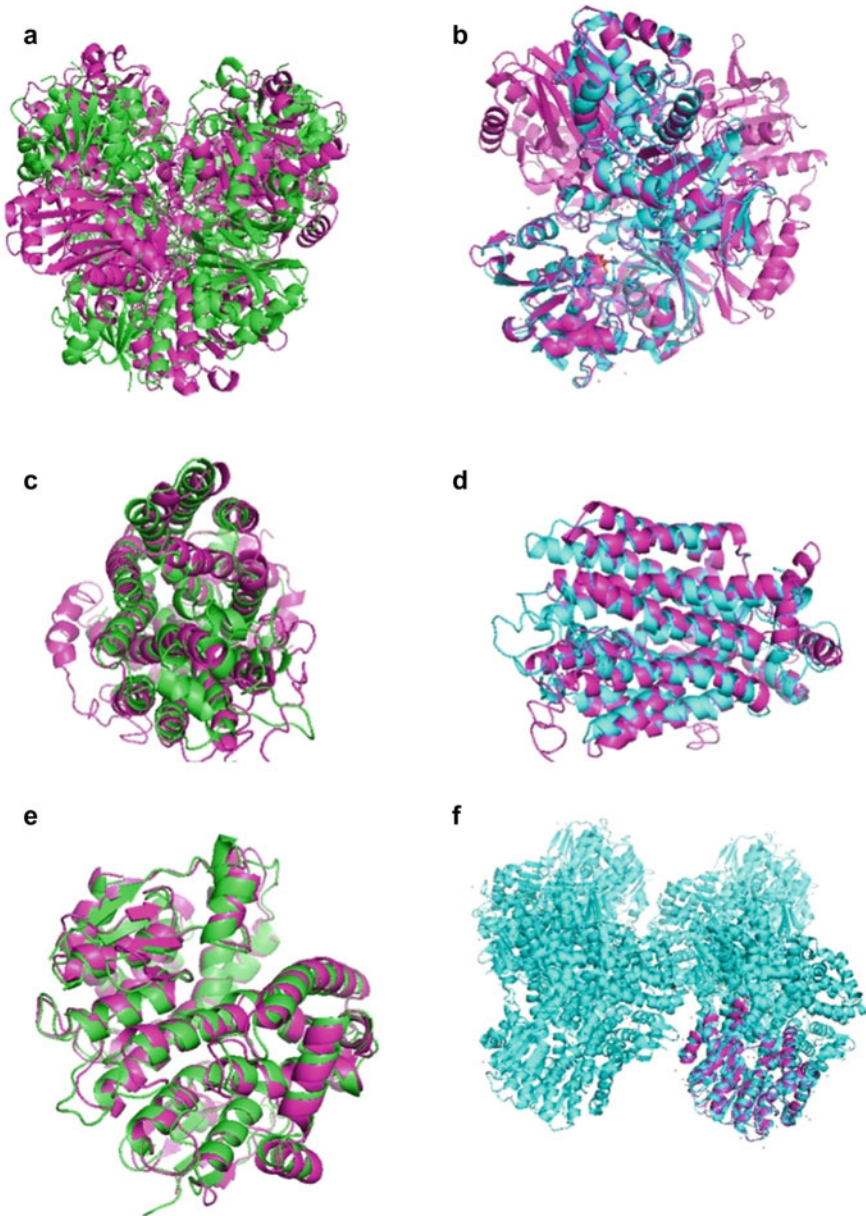
Fig. 7 The superimposition model generated by PyMOL, where protein of *Pteris vittata* is shown in purple is structurally compared with the template of *Oryza sativa* and *Arabidopsis thaliana* in green and blue, respectively. **a** PvGAPC1 versus OsGAPC1 (3E6A), **b** PvGAPC1 versus AtGAPC1 (6QUQ), **c** PvOCT4 versus OsOCT4, **d** PvOCT4 versus AtOCT4, **e** PvGSTF1 versus OsGSTF1 and **f** PvGSTF1 versus AtGSTF1 (5A5K)

take up or restrict the uptake of Arsenic from soil therefore a constant concentration is maintained in cell. In second strategy, plant take up Arsenic from soil and degrade it into less toxic form and accumulate it in upper parts like leaves, fronds and seeds. *Pteris vittata* is an excellent example that can tolerate arsenic by various enzymes and proteins (Cai et al. 2019; Ma et al. 2001). All these proteins are reported to be involved in Arsenic tolerance i.e., PvGAPC1, PvOCT4, or PvGSTF1showed significant sequence similarity with other plants under comparison in the molecular phylogeny analysis. The tertiary structures of these molecules when constructed via template-based homology modelling showed significant and well characterized functional regions as available in other plants. The proposed functional sites were dominated by alpha helices. The interesting finding in this study is that the 3D structures of PvGAPC1 and PvGSTF1 with that of its counterpart from arsenic sensitive *Oryza sativa* and *Arabidopsis thaliana* showed significant difference inspite of having an appreciable sequence homology. This indicates that the overall environment or habitat of the plants plays a major role in expression of the proteins as well as defining the functional domains of these proteins (Xu et al. 2016; Boyce et al. 2020; Purty et al. 2017). The *Pteris vittata*, found mostly in the highlands are a better accumulator of phosphates and other plant nutrients due to comparatively lack of nutrients in their habitat as compared to crop plants like Rice or the model plant like *Arabidopsis*. In soil arsenite is unstable, therefore most plants uptake arsenic as arsenate, it gets oxidized to arsenate by various biochemical processes (Mirza et al. 2014; Finnegan and Chen 2012). Arsenate has similar structure as phosphate therefore it competes with phosphate for its uptake and is actively taken up by plants (Strawn 2018; Tawfik and Viola 2011; Tu and Ma 2003).

5   Conclusion

The treatment of Arsenic contaminated soil and water using microorganisms and plants increasing day by day. Microorganism and plants have shown a great potential to remediate contaminated system. Practical and theoretical knowledge have been applied to develop many bioremediation technologies. Development in genomics and development of new tools in area of genomics and proteomics made it very easy to characterize and analyses new variant that have potential of accumulating and tolerating high concentration of Arsenic. Identification of genes that are involved in Arsenic tolerance have made it easy to develop improved genetically modified new variant of bacteria and plants to enhance the efficacy of Arsenic tolerance. Even after several years of research and development in the field, very little is known about the proteins and genes that are involved in Arsenic tolerance and therefore lies an unlimited scope of research and development.

Competing Interests The authors declare that there are no conflicts of interest.

References

Altschul SF, Gish W, Miller W, Myers EW, Lipman DJ (1990) Basic local alignment search tool. J Mol Biol 215(3):403–410

Berman HM, Westbrook J, Feng Z, Gilliland G, Bhat TN, Weissig H, Shindyalov IN, Bourne PE (2000) The protein data bank. Nucleic Acids Res 28(1):235–242

Binder JX, Pletscher-Frankild S, Tsafou K, Stolte C, O'Donoghue SI, Schneider R, Jensen LJ (2014) Compartments: unification and visualization of protein subcellular localization evidence. Database 2014

Boyce WT, Sokolowski MB, Robinson GE (2020) Genes and environments, development and time. Proc Natl Acad Sci 117(38):23235–23241

Brown E, Mengmeng Z, Taotao F, Juanli W, Junbo N (2018) Mechanisms of bacterial degradation of arsenic. Indian J Microbiol Res 5:436–441

Cai C, Lanman NA, Withers KA, DeLeon AM, Wu Q, Gribskov M, Salt DE, Banks JA (2019) Three genes define a bacterial-like arsenic tolerance mechanism in the arsenic hyperaccumulating fern Pteris vittata. Current Biol 29(10):1625–1633. e1623

Chakrabarty N (2015) Arsenic toxicity: prevention and treatment. CRC Press

Chakraborti D, Rahman MM, Ahamed S, Dutta RN, Pati S, Mukherjee SC (2016) Arsenic ground-water contamination and its health effects in Patna district (capital of Bihar) in the middle Ganga plain, India. Chemosphere 152:520–529

DeLano WL (2002) Pymol: an open-source molecular graphics tool. CCP4 Newslett Protein Crystallogr 40(1):82–92

Edgar RC (2004) MUSCLE: multiple sequence alignment with high accuracy and high throughput. Nucleic Acids Res 32(5):1792–1797

Eisenberg D, Lüthy R, Bowie J (1997) VERIFY3D: assessment of protein models with three-dimensional profiles. In: Methods in enzymology, vol 277. Academic Press, pp 396–404. doi 10.s0076-6879

Engwa GA, Ferdinand PU, Nwalo FN, Unachukwu MN (2019) Mechanism and health effects of heavy metal toxicity in humans. Poisoning Mod World-New Tricks Old Dog 10

Finnegan P, Chen W (2012) Arsenic toxicity: the effects on plant metabolism. Front Physiol 3:182

Gasteiger E, Hoogland C, Gattiker A, Wilkins MR, Appel RD, Bairoch A (2005) Protein identification and analysis tools on the ExPASy server. In: The proteomics protocols handbook, pp 571–607

Geourjon C, Deleage G (1995) SOPMA: significant improvements in protein secondary structure prediction by consensus prediction from multiple alignments. Bioinformatics 11(6):681–684

Ghosh P, Rathinasabapathi B, Teplitski M, Ma LQ (2015) Bacterial ability in AsIII oxidation and AsV reduction: relation to arsenic tolerance, P uptake, and siderophore production. Chemosphere 138:995–1000

Guex N, Peitsch MC, Schwede T (2009) Automated comparative protein structure modeling with SWISS-MODEL and Swiss-Pdb viewer: a historical perspective. Electrophoresis 30(S1):S162–S173

Kumar S, Stecher G, Li M, Knyaz C, Tamura K (2018) MEGA X: molecular evolutionary genetics analysis across computing platforms. Mol Biol Evol 35(6):1547

Laskowski RA, MacArthur MW, Moss DS, Thornton JM (1993) PROCHECK: a program to check the stereochemical quality of protein structures. J Appl Crystallogr 26(2):283–291

Ma LQ, Komar KM, Tu C, Zhang W, Cai Y, Kennelley ED (2001) A fern that hyperaccumulates arsenic. Nature 409(6820):579–579

Mandal BK, Suzuki KT (2002) Arsenic round the world: a review. Talanta 58(1):201–235

Mirza N, Mahmood Q, Maroof Shah M, Pervez A, Sultan S (2014) Plants as useful vectors to reduce environmental toxic arsenic content. The Scientific World Journal 2014

Mistry J, Chuguransky S, Williams L, Qureshi M, Salazar GA, Sonnhammer EL, Tosatto SC, Paladin L, Raj S, Richardson LJ (2021) Pfam: the protein families database in 2021. Nucleic Acids Res 49(D1):D412–D419

Popov M, Zemanová V, Sácký J, Pavlík M, Leonhardt T, Matoušek T, Kaňa A, Pavlíková D, Kotrba P (2021) Arsenic accumulation and speciation in two cultivars of Pteris cretica L. and characterization of arsenate reductase PcACR2 and arsenite transporter PcACR3 genes in the hyperaccumulating cv. Albo-lineata. Ecotoxicol Environ Safety 216:112196

Porter E, Peterson P (1975) Arsenic accumulation by plants on mine waste (United Kingdom). Sci Total Environ 4(4):365–371

Purty R, Sachar M, Chatterjee S (2017) Structural and expression analysis of salinity stress responsive phosphoserine phosphatase from Brassica juncea L. J Proteom Bioinform 10:119–127

Purty RS, Jha AN, Chatterjee S (2020) Presence of heavy metal in water (Yamuna River), soil and vegetables in delhi and to examine the effect of phyto-accumulating capacity of *Eichhornia crassipes*. Plant Cell Biotechnol Mol Biol 21(3–4):22–36

Saitou N, Nei M (1987) The neighbor-joining method: a new method for reconstructing phylogenetic trees. Mol Biol Evol 4(4):406–425

Schultz J, Milpetz F, Bork P, Ponting CP (1998) SMART, a simple modular architecture research tool: identification of signaling domains. Proc Natl Acad Sci 95(11):5857–5864

Shah MT, Suleman M, Abdul Baqi S, Sattar A, Khan N (2020) 1. Determination of heavy metals in drinking water and their adverse effects on human health. A review. Pure Appl Biol (PAB) 9(1):96–104

Shaji E, Santosh M, Sarath K, Prakash P, Deepchand V, Divya B (2020) Arsenic contamination of groundwater: a global synopsis with focus on the Indian Peninsula. Geosci Front 12:101079

Shankar S, Shanker U (2014) Arsenic contamination of groundwater: a review of sources, prevalence, health risks, and strategies for mitigation. Sci World J 2014

Sharma P, Jha AB, Dubey RS (2021) Arsenic toxicity and tolerance mechanisms in crop plants. In: Handbook of plant and crop physiology. CRC Press, pp 831–873

Souri Z, Karimi N, Sandalio LM (2017) Arsenic hyperaccumulation strategies: an overview. Front Cell Dev Biol 5:67

Strawn DG (2018) Review of interactions between phosphorus and arsenic in soils from four case studies. Geochem Trans 19(1):1–13

Tawfik DS, Viola RE (2011) Arsenate replacing phosphate: alternative life chemistries and ion promiscuity. Biochemistry 50(7):1128–1134

Tu C, Ma LQ (2003) Effects of arsenate and phosphate on their accumulation by an arsenic-hyperaccumulator Pteris vittata L. Plant Soil 249(2):373–382

Waterhouse AM, Procter JB, Martin DM, Clamp M, Barton GJ (2009) Jalview Version 2—a multiple sequence alignment editor and analysis workbench. Bioinformatics 25(9):1189–1191

Winter D, Vinegar B, Nahal H, Ammar R, Wilson GV, Provart NJ (2007) An electronic fluorescent pictograph browser for exploring and analyzing large-scale biological data sets. PloS one 2(8):e718

Xu Q, Zhu C, Fan Y, Song Z, Xing S, Liu W, Yan J, Sang T (2016) Population transcriptomics uncovers the regulation of gene expression variation in adaptation to changing environment. Sci Rep 6(1):1–10

Zhang Y (2008) I-TASSER server for protein 3D structure prediction. BMC Bioinform 9(1):1–8

Potential Application of Carbon Nanotubes Membranes in Water and Wastewater Treatment: A Review

Ashish Kumar Pandey and M. Laxmi Deepak Bhatlu

Abstract Affordable and good quality water is one of the significant universal challenges. Due to continuous growth in the world's population, industrial development, social process and immense agriculture use, polluted water becomes more complicated and challenging to remove, alarms water scarcity in several areas, and this challenge is rising at full tilt. Additionally world also facing to supply fresh and good quality water at lower treatment costs. Thus proper wastewater treatment or reuse has become a common necessity to supply good quality water demand. In this regard, carbon nanotubes based membranes, due to their extraordinary properties such as high surface area, high stability, great flexibility, electrochemical, magnetic properties, tunable pore size and antimicrobial activity, provide huge opportunities in wastewater treatment application. Carbon nanotubes membranes show an excellent impact on removing suspended particles, particulate matter, microorganisms, chemical and biological contaminants from wastewater. In this paper potential application of carbon nanotubes membranes for water and waste water treatment are comprehensively reviewed. Furthermore, key challenges and future perspectives for carbon nanotubes membranes are also briefly outlined.

Keywords Nanomaterials · Carbon nanotubes · Membranes · Water treatment

Abbreviations

CNTs   Carbon nanotubes
SWNTs   Single-walled carbon nanotubes

A. K. Pandey (✉)
Department of Chemical Engineering, Institute of Engineering and Technology, Lucknow 226021, India
e-mail: akp0510@gmail.com

M. Laxmi Deepak Bhatlu
Department of Chemical Engineering, Faculty of Engineering, Karpagam Academy of Higher Education, Coimbatore 641023, India

MWCNTs	Multi-walled carbon nanotubes
TFN	Thin-film nanocomposite
MWCNTs-IPDI	Multi-walled carbon nanotubes–isophorone diisocyanate
VA-CNT	Vertically aligned-carbon nanotube
TFC	Thin film composite
MWCNTs-PA	Multi-walled carbon nanotubes-polyamide

1 Introduction

As we know, water is a valuable inherent resource, and its quality is needed for the existence and development of surviving on the earth. But due to speedy urbanization and increasing population, the water demand is growing rapidly. But aquatic resources are bounded and decreasing day by day. Thus insufficiency of aquatic resources calls for effective technologies for water treatment.

According to a recent report (WHO 2019), 1 in 3 people or 2.2 billion individuals around the earth need safe drinkable water. The report also reveals that 785 million (together with 144 million individuals) depend on surface water. At least 2 billion individuals globally make use of drinking water sources polluted with faeces. Polluted water can spread different types of infection such as typhus, flux, diarrhoea, enteric fever and polio. It has been estimated that 485,000 people dies due to diarrhoea each year. In the least developed countries, around twenty-two percent no waste control service and twenty-two percent of health maintenance amenities have no water facility. These reported data represent that water availability and quality are major global challenges for the current century.

Due to populations growth throughout the world causes imposing inaquatic resources for household, manufacturing, and agriculture purposes. The pressure on freshwater resources increased more, which threats to climate change (Shannon et al. 2008; Mulder et al. 2010). Also, the prime origins of wastewater are domestic, farming and factory waste because all these prime origins require fresh quality water but give back polluted water, particularly in factories (Jassby et al. 2018; Deshpande et al. 2020).

Another reason for the freshwater shortage is polluting groundwater resources from anthropogenic activities (Rajasekhar et al. 2018). Water levels throughout the earth are exhausting and being polluted because of miscellaneous factors such as soil erosion, seawater intrusion, inadequate sanitation, pollutant of groundwaters by chemicals, heavy metals, detergents, pesticides, fertilizers, etc. (Kemper 2004; Foley et al. 2005; Ritter et al. 2002; Fawell and Nieuwenhuijsen 2003; Falconer and Humpage 2005).

Several pollutants cannot be separated from conventional wastewater treatment methods. Conventional water remedy techniques are not very effective for the complete removal of the emerging contaminants or pollutants as per water quality level (Qu et al. 2012, 2013). The existing engineering of water treatments has

some down sides including incomplete pollutant removal, huge energy demand and creation of destructive sludge (Ferroudj et al. 2013). Thus appropriate material with immense purification capability, lower value and reusability is required for water purification. For this purpose, nanotechnology gives a scope to develop suitable new materials for efficient water treatment by amending their properties namely hydrophobicity, hydrophilicity, porosity, and mechanical strength. Nanotechnology is an emerging area of nanoscience which involves the engineering of nanosize particles of various materials. Nanomaterials are the smallest structures that possess a dimension of a few nanometers (Chaturvedi et al. 2012). More accurately, nanoparticles are particles that have structural elements sized from less than 100 nm. Nanoparticles have outstanding properties compared with other conventional materials mechanical strength, electrical and magnetic properties owing to higher specific surface area (Dargo et al. 2017; Amin et al. 2014).

A variety of energy-saving, convenient and sustainable nanomaterials have been developed which have extensive demand in water and wastewater treatment because they have the potential to eliminate heavy metals, inorganic anions, organic pollutants, toxins, pathogens etc. (Brumfiel 2003; Theron et al. 2008; Kahrizi et al. 2016; Selvi et al. 2019; Muzammil et al. 2019; Baby et al. 2019). Nanoparticles having high surface area play a vital role in water treatment, but their aggregation restricted its usage, which can be reduced by transforming nanoparticles into nanocomposites (Daer et al. 2015; Ray and Shipley 2015).

From literature, it has been found that carbon nanotubes, because of their extraordinary properties, like high specified surface areas, mechanical flexibility and wide pore volumes, are the most recent contemporary nanomaterials for water and wastewater treatment (Obare and Meyer 2004; Akasaka and Watari 2009; Abdelbasir and Shalan 2019; Raghunath and Perumal 2017; Verma and Balomajumder 2020). The concept of carbon nanotubes was first given in 1991 by Iijima; two years later, the author synthesized SWNTs (Iijima 1991; Iijima and Ichihashi 1993). After that, many scientists and investigators have broadly adapted carbon nanotubes in water and wastewater treatment accomplishments.

CNTs are cylindrical, substantial molecules having the dimension of few nanometres and 20 cm as length enclosed of hybridized carbon atoms in a hexagonal array, which is similar to the graphite's atomic planes. Carbon nanotubes can be categorized as SWCNTs and MWCNTs, where SWCNTs are just fabricated of mono layer of carbon atoms while MWCNTs contain up to dozens of concentric tubes as shown in Fig. 1 (Hirsch and Vostrowsky 2007; Meng et al. 2010).Various research articles are also available in the open literature that deals with properties, synthesis, and preparative CNTs (Eatemadi et al. 2014; Choudhary et al. 2014; Dervishi et al. 2009; Popov 2004; Terrones 2003; Dai et al. 1995).

This paper summarises the potential application of carbon nanotubes membranes for water and wastewater treatment and outlines the key challenges and future perspectives.
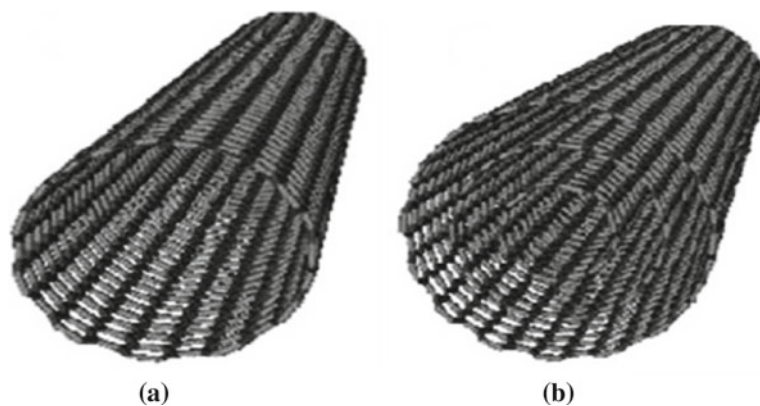
Fig. 1 Schematic structure of **a** SWCNTs and **b** MWCNTs (Eaemadi et al. 2014)

2 CNTs Membranes for Water Treatment

Membrane technologies, together with nanofiltration, ultrafiltration, microfiltration, and reverse osmosis, constitute essential parts of numerous water treatment systems. In recent years advancement in membrane technology, nanofiltration membrane has gained the attention of many researchers. Nanofiltration membranes are cost-effective, highly flexible, and easy to produce.

2.1 CNTs as Filtration Membranes

Filtration technique plays a crucial role in water or wastewater treatment by removing the suspended particles, particulate matter, microorganisms, synthetic and biotic contaminants (Koyuncu et al. 2015; Shon et al. 2013; Benfer et al. 2001). Several researchers also report that filtration membranes with carbon nanotubes are very cost-effective in removing pathogenic microorganisms in a concise period of time due to size barring and extensive filtration (Estevez et al. 2010; Vecitis et al. 2011; Rahaman et al. 2012; Liu et al. 2013; Lilly et al. 2012).

Parham et al. (2013) used carbon nanotubes based ceramic composite for yeast filtration, observed a high filtration capability for yeast and approximately complete removal of heavy metal ions from water. Similarly, Mostafavi et al. (2009) used CNTs based nanofiltration membrane to eliminate the MS2 virus (also known as Bacteriophage MS2, which is icosahedral, positive-sense single-stranded ribonucleic acid virus) from wastewater, which is connected to bacterial viruses that infect the bacterium Escherichia coli and additional components Enterobacteriaceae family. High removal efficiencies were reported.

Silver-based MWCNTs-TFN membrane was developed by interfacial polymerization to remove pseudomonas aeruginosa bacteria from water. It was reported

that 96% of pseudomonas aeruginosa bacteria were removed by a thin-film nanocomposite membrane (Kim et al. 2012).

A Chitosan/Silica-coated carbon nanotube composite membrane was developed by acquiring a simple sol–gel method. Composite membranes exhibited increased mechanical properties and thermal stability (Liu et al. 2016). Integrated carbon nanotubes polymer composite membrane with the help of a polyvinyl alcohol layer to treat oil-contaminated water was constructed. More than 95% removal efficiency was observed. The composite membranes enhanced the acceptability of membrane for practical implementation due to optimum tensile strength, stability and young's modulus (Maphutha et al. 2013). Similarly, MWCNTs/polysulfone blend membranes were developed by considering the phase inversion process. The permeation and morphology effects of the blend membranes were subjected to the contents of MWCNTs used. In addition, as the pressure increased over 95% of rejection was observed (Choi et al. 2006).

Guo et al. (2016) developed nanofibrous filtration membranes by using polyhydroxybutyrate-calcium alginate/carboxyl MWCNTs composite. Membrane enhanced the tensile strength and hydrophilicity, which enhanced the removal of selected contaminants. In addition, 98.20% of the rejection rate for the dye brilliant blue was observed. MWCNTs were cooperated with the help of polyethersulfone to blend membranes by phase inversion process by Celik et al. (2011), suggested that enhancement in MWCNTs content in the membranes enhanced the membrane roughness, porosity, hydrophilicity and pure water flux. Investigation on polyether urethane membranes charged with isophorone diisocyanate grafted with the help of multi-wall carbon nanotubes, MWCNTs-IPDI exhibited remarkable improvement in mechanical properties in polyether urethane membranes by using less amount of MWCNTs-IPDI (Deng et al. 2007).

A nanocomposite membrane was prepared by applying the polymer grafting method in which MWNCTs have cooperated with aromatic polyamide. It was observed that increment in the MWCNTs content enhances the tensile strength, toughness and Young's modulus of nanocomposite membrane. Also, the membrane provided an excess of 90% salt rejection (Shawky et al. 2011). Due to powerful interaction between MWCNTs and polyamide matrix, the nanocomposite membranes constructional compactness leads to higher salt rejection and a higher permeability (Lee et al. 2007).

2.2 Antibiofouling Properties/Characteristics of CNTs Membranes

In water and wastewater treatment, biofouling is a crucial issue; thus in recent years, using VA-CNT membranes various methods have been tried to control biofouling by exploiting the antibacterial properties of CNTs. Generally, CNTs comprise other polymeric materials or nanomaterials to develop nanocomposite membranes to

reduce membrane biofouling. In order to emphasize the antibiofouling properties of VA-CNT membranes, it is advisable to use smaller-diameter CNTs in the membrane. Kang et al. (2008) found that the dimension of CNTs is anessential parameter for affecting their antibacterial properties, which indicated that MWNTs are less harmful to bacteria than SWNTs. Furthermore, the functionalization of CNTs has also influenced the toxicity of bacteria. Functionalization is associated with the dispersal properties and surface phenomenon of CNTs; functionalized carboxylation is seriously dangerous, however, carboxylation builds SWNTs biocompatible and much water-soluble (Wang et al. 2011). Carboxyl multi-walled carbon nanotubes/calcium alginate composite was synthesized by taking polyethylene glycol400 as a pore-forming agent with hydrogel nanofiltration membrane. Composite membrane had 98.62% of removal efficiency and suitable antifouling property (Jie et al. 2015).

An innovatory polyphenol-metal affected nanohybridization method was produced for the motivation of making anti-oil-fouling CNTs membranes to achieve tremendousflux, antifouling and better removal of oil/water. A high water recovery ratio and excellent water permeability was reported (Zhao et al. 2020). For water treatment, investigation on the immobilization of silver nanoparticle-based carbon nanotubes coveredon the surface of a polyacrylonitrile membrane was done. The membrane was used for the separation of Ecoli polluted water. The outcome showed that silver nanoparticle based carbon nanotubes coating remarkably enhanced the membranes antifouling properties and antimicrobial effects (Gunawan et al. 2011). Lee et al. (2016) exhibited immense antibiofouling property of VA-CNT membranes at small cross-flow velocity performance in separate bacterial suspensions, because of its immense antibacterial property, together with a measurable conception of a link between fouling resistance and biofilms of VA-CNT membranes. The results enhanced the accessibility of VA-CNT membranes for water and wastewater treatment even at a minimal cross-flow velocity.

Youngbin et al. (2014) reported the suitability of the VA-CNTs membrane for water treatment. The membrane was fabricated, and their biofouling effects, water flux, and rejection performance were evaluated against commercial ultrafiltration. VA-CNTs membrane showed better salt rejection and biofouling resistance. Additionally, water flux in VA-CNTs membrane approximately three times higher than the ultrafiltration was observed. VA-CNTs membranes having the eminent packing density of CNTs indicated better antibacterial property without leachates. Furthermore, acidified membrane surfaces provide doubled antibacterial properties compared to non-acidified membranes (Lee and Park 2016). SWCNTs and polyvinyl-N-carbazole based nanocomposite membrane exhibited great inactivation of bacteria upon direct contact and reduced biofouling (Ahmed et al. 2012). Moderate antibacterial properties were noticed when the SWCNTs bonded covalently to the TFC membrane (Tiraferri et al. 2011).

3 Applications of CNTs Membranes in Desalination

Usually, work on VA-CNTs membranes is associated with seawater desalination. Desalination is performing a preeminent role in order to provide quality water. Present desalination depends on polymer reverse-osmosis membranes for the removal of fine solids and dissolved salts. Thus significant energy and high pressure required in the desalination process. High water flux and selectivity are key factors in the membrane development process. One promising way of treating water with CNTs demands VA-CNT sequence membranes to eliminate organic pollutants (Lee et al. 2015; Jafari et al. 2015).

Significant manufacturing processes for CNTs membranes and speculate on their performances were reviewed and found that the integrated CNT membrane into the desalination system plays a vital role in wastewater applications (Ahn et al. 2012). Das et al. (2014) extensively studied molecular modelling and experimental characteristics of CNTs membrane construction and functionalization for the desalination applications in both brackish and seawater and suggested that carbon nanotubes membranes had exceptional accomplishments in terms of desalination capacity, permeability, energy savings, scalability etc. Recently development on synthesis and uses of carbon nanotubes membranes in water and wastewater treatment is also reviewed by Ihsanullah (2019) and suggested that carbon nanotubes membranes have the capability to be a leading breakthrough in water treatment, mainly desalination.

Considering the inside pores of CNTs, high closeness and VA-CNT membranes were prepared by using the chemical vapour deposition method. CNTs array were soaked into n-hexane organic solvent, and then the surface was dried at room temperature. Evaporation of solvents diminished the surface to about 5% of its initial area, dominating to a high density, VA-CNT forest membrane (Yu et al. 2009). Trivedi and Alameh (2016) investigated the execution of developed VA-CNT membranes of different densities. Experimental outcomes expressed that permeability of developed VA-CNT membranes increases with the density of the VA-CNTs, while the salt elimination is almost free of the VA-CNT density. An aligned sub-2-nm carbon nanotubes membrane was developed by Holt et al. (2006) considering catalytic chemical vapour deposition process subsequently laser etching to unlock the nanotubes. It was noticed that in spite of having smaller pore sizes, the water permeabilities of above mentioned CNTs membranes were several orders of magnitude more than that of commercial polycarbonate membranes. In the work of Corry (2008), considering the inherent power for ion and water translocation ions features huge energy boundary was proposed that can get over the wider (7,7) and (8,8) nanotubes, and not suitable to get over the narrower tubes ((5,5) and (6,6) "armchair" type tubes). However, water faces no such limitation due to the generation of strong hydrogen bonds and passes the tubes at abundantly high rates. Thus, the production of bug free CNTs membranes with sub-nanometer pores promising future desalination processes.

Aligned CNTs membranes were made to introduce negatively charged category by plasma analysis in which membranes refuse more than 98% of ions (Fornasiero et al. 2008). The charge exclusion technique influenced the ion exclusion. However,

in a greater ionic domain like blackish water and seawater, the effectiveness of the charge exclusion technique may be declined. In recent years, the diameter of carbon nanotubes has fallen to as low as 0.3 nm (Zhao et al. 2004) which almost commence the hydrated radium of sodium ions, ranging from 0.178 to 0.358 nm relying on surroundings states (Tansel et al. 2006; Carrillo et al. 2006).

Controllable ion-selective nanopores based on SWCNTs membranes along with a special arrangement of carbonyl oxygen atoms were examined. The different forms of carbonyl oxygen atoms established the hydration formation of K+ and Na+ within the nanopores, directing to a tunable ionic selectivity (Gong et al. 2010). The heads of CNTs membranes were modified by Majumder et al. (2007), using the electrochemical grafting process of diazonium salts. It was observed that by changing the voltage, the filtration coefficient of the CNTs membranes could be tuned.

Permeability effects through 0.8-nm-diameter carbon nanotubes pores inserted in lipid membranes under advanced experimental conditions studied by Yuhao et al. (2020) and suggested that carbon nanotubes pores impressively removes chloride ions and showed higher permeability as compared to commercial desalination membranes.

Using classic molecular dynamics simulations, extensive work on the rejection of salt from CNTs membranes and water permeability with many dipole moments anchored at their rims were done. The study reveals that CNTs with a small dipole moment at the rim could moderately enhance salt rejection rate and the water flow, while CNTs with a large dipole moment can remarkably improve the salt rejection rate, however, water passage is lowered. Additionally, functional groups with a larger dipole moment on broader CNT rims removed more than 95% of salt with higher water permeability (Hong et al. 2019). Dong et al. (2018) presented a comprehensive conceptual outlined and utilization plan for a superhydrophobic ceramic-based CNTs desalination membrane with exceptional performance and handling stability. In this work, fully covered CNTs membranes presented remarkably better thermal and superhydrophobic stable properties. In addition to these membranes also revealed a stable high flux along with approximately 100% rejection of salt. CNTs based composite membranes were developed by directly approaching membrane distillation with different operating processes. Composite membranes were also structurally identified, which strengthened performance when associated with unmixed self-supporting CNTs and achieved higher permeability with 95% salt removal (Dumee et al. 2010). Aani et al. (2018) studied thin-film nanocomposite membranes amended with polydopamine layered metals/carbon-nanostructures for the desalination process and suggested that fabricated membranes exhibited higher permeability than the thin-film composite membrane. A TFC membrane and advanced MWCNT-PA composite dismissal surface were prepared by interfacial polymerization method below negative pressure. This advanced layering evidently increased the water flux and antifouling characteristics without affecting the desalination rate in reverse osmosis. Additionally, enhancement in density of water channels in hydrophilicity of membrane surface and polyamide rejection layer could successfully enhance the thin-film composite membrane performance (Sun et al. 2019).

A TFN membrane containing graphene oxide nanosheets (Yin et al. 2016) and porous MCM-41 silica nanoparticles (Yin et al. 2012) was manufactured using an in-situ interfacial polymerization method. Both studies based on removal of salt and water permeability membrane performances were evaluated, and results indicated that incorporation of graphene oxide nanosheets and MCM-41 porous silica nanoparticles was distributed adequately in the polyamide thin film layer and enhanced membrane performances.

4　Key Challenges and Future Perspective

The common aspect which was shared by many countries is to generate better quality water by removing extensive contaminants at the lowest cost. The cost of carbon nanotubes is relatively high compared to other nanomaterials. Thus CNTs can be utilized many times for water and wastewater treatment, which is finally the important key to saving the cost.

The desalination process based on the preliminary design of the carbon nanotubes associated filter accomplishes the process variables optimization. In this regard, electrochemically employ CNTs membranes having several benefits such as high porosity, specific area, and hydrophobic nature, which help to remove chemical and biological pollution and ion rejection from seawater.

CNTs membranes effectively consider treating the quality and quantity of water-related challenges. However, the risk related to CNTs nanoparticles cannot be overlooked. Some studies also reported the toxicity of carbon nanotubes, which are adverse to environmental and individual health, and it should be further regulated and investigated.

The studies show that high water flux with CNTs pore has attracted attention to produce CNT membrane for desalination process with higher permeability and salt rejections. CNT blended polymeric membranes exhibit higher water permeability and better antifouling ability. However many challenges remain, such as proper synthesis of the CNT membranes with uniform pore size distributions, accurate control of CNTs regarding alignment, tip introduction and functionalization. Cost is an additional concern in the preparation of CNTs membranes.

Extensive research and technical study on CNTs membranes still required at lab scale and commercial scale because a comparison between these scales would come up with better results on the implementation of membranes in water and wastewater treatment. Additional water and wastewater treatment units should be expanded to meet the requirement for quality water.

5 Conclusion

In a current scenario, successful treatment of water and wastewater is main prerequisite for many countries because water resources are limited and decreasing day by day. Thus inadequacy of water resources calls for effective technologies with better efficiency at lowest cost required for water treatment. Among several technologies, carbon nanotubes based membrane is one of the leading applicable alternatives for wastewater treatment. CNTs membranes express an excellent effect on the separation of wastewater pollutants. The literature communicated that the execution of CNTs membrane is thrice of the conventional membranes. CNTs membranes have been used for eliminating ions and bacteria from water. It has also been found that the inherent properties of CNTs as well as the fabrication of the membrane are the important feature for their appropriateness in many wastewater treatments.

CNTs membranes have also confirmed distinctly fruitful for eliminating heavy metals, dyes, ions and bacteria from wastewater. Furthermore, membranes reduce the membrane fouling. The mechanical properties of CNTs restrict any distortion on the filter of CNTs membrane. Proper formation of CNTs based nanocomposite membranes improves the performance of multifunctional nanocomposites membranes. The CNTs membranes can be further modified by the application of coating operation to enhance its efficiency in the wastewater treatment. Previous and present studies show that extraordinary breakthroughs have been made towards CNTs and porous graphene membranes in water treatment and desalination process.

Conflict of Interests The authors declare that there is no conflict of interests regarding the publication of this manuscript.

References

Aani SA, Haroutounian A, Wright CJ, Hilala N (2018) Thin film nanocomposite (TFN) membranes modified with polydopamine coated metals/carbon-nanostructures for desalination applications. Desalination 427(1):60–67

Abdelbasir SM, Shalan AE (2019) An overview of nanomaterials for industrial wastewater treatment. Korean J Chem Eng 36(8):1209–1225

Ahmed F, Santos CM, Vergara RAMV, Tria MCR, Advincula R, Rodrigues DF (2012) Antimicrobial applications of electroactive PVK-SWNT nanocomposites. Environ Sci Technol 46(3):1804–1810

Ahn CH, Baek Y, Lee C, Kim SO, Kim S, Lee S, Kim SH, Bae SS, Park J, Yoon J (2012) Carbon nanotube-based membranes: fabrication and application to desalination. J Ind Eng Chem 18:1551–1559

Akasaka T, Watari F (2009) Capture of bacteria by flexible carbon nanotubes. Acta Biomater 5:607–612

Amin MT, Alazba AA, Manzoor U (2014) A review of removal of pollutants from water/wastewater using different types of nanomaterials. Adv Mater Sci Eng 825910

Baby R, Saifullah B, Hussein MZ (2019) Carbon nanomaterials for the treatment of heavy metal-contaminated water and environmental remediation. Nanoscale Res Lett 14:341

Benfer S, Popp U, Richter H, Siewert C, Tomandl G (2001) Development and characterization of ceramic nanofiltration membranes. Sep Purif Technol 22:231–237

Brumfiel G (2003) Nanotechnology: a little knowledge. Nature 424:246–248

Carrillo TM, San RML, Hernandez CJ, Saint MH, Ortega BI (2006) Ion hydration in nanopores and the molecular basis of selectivity. Biophys Chem 124(3):243–250

Celik E, Park H, Choi H, Choi H (2011) Carbon nanotube blended polyether-sulfone membranes for fouling control in water treatment. Water Res 45(1):274–282

Chaturvedi S, Dave PN, Shah NK (2012) Applications of nanocatalyst in new era. J Saudi Chem Soc 16:307–325

Choi JH, Jegal J, Kim WN (2006) Fabrication and characterization of multi-walled carbon nanotubes/polymer blend membranes. J Membr Sci 284(1):406–415

Choudhary N, Hwang S, Choi W (2014) Carbon nanomaterials: a review. In: Handbook of nanomaterials properties. Springer, USA, pp 709–769

Corry B (2008) Designing carbon nanotube membranes for efficient water desalination. J Phys Chem B 112(5):1427–1434

Daer S, Kharraz J, Giwa A, Hasan SW (2015) Recent applications of nanomaterials in water desalination: a critical review and future opportunities. Desalination 367:37–48

Dai H, Wong EW, Lu YZ, Fan S, Lieber CM (1995) Synthesis and characterization of carbide nanorods. Nature 375:769–772

Dargo H, Ayaliew A, Kassa H (2017) Synthesis paradigm and applications of silver nanoparticles (AgNPs), a review. Sustain Mater Technol 13:18–23

Das R, Ali ME, Hamid SBA, Ramakrishna S, Chowdhury ZZ (2014) Carbon nanotube membranes for water purification: a bright future in water desalination. Desalination 336:97–109

Deng J, Zhang X, Wang K, Zou H, Zhang Q, Fu Q (2007) Synthesis and properties of poly (ether urethane) membranes filled with isophorone diisocyanate-grafted carbon nanotubes. J Membr Sci 288:261–267

Dervishi E, Li Z, Xu Y, Saini V, Biris AR, Lupu D, Biris AS (2009) Carbon nanotubes: synthesis, properties, and applications. Part Sci Technol 27(2):107–125

Deshpande B, Agrawal P, Yenkie M, Dhoble S (2020) Prospective of nanotechnology in degradation of waste water: a new challenges. Nano-struct Nano-objects 22:100442

Dong Y, Ma L, Tang CY, Yang F, Quan X, Jassby D, Zaworotko MJ, Guiver MD (2018) Stable super-hydrophobic ceramic-based carbon nanotube composite desalination membranes. Nano Letter 18(9):5514–5521

Dumee L, Sears K, Schü J, Finn N, Duke M, Gray S (2010) Carbon nanotube based composite membranes for water desalination by membrane distillation. Desalin Water Treat 17:72–79

Eatemadi A, Daraee H, Karimkhanloo H, Kouhi M, Zarghami N, Akbarzadeh A, Abasi M, Hani-fehpour Y, Joo SW (2014) Carbon nanotubes: properties, synthesis, purification, and medical applications. Nanoscale Res Lett 9

Estevez AS, Schnoor MH, Kang S, Elimelech M (2010) SWNT-MWNT hybrid filter attains high viral removal and bacterial inactivation. Langmuir 26(24):19153–19158

Falconer R, Humpage AR (2005) Health risk assessment of cyanobacterial (blue-green algal) toxins in drinking water. Int J Environ Res Public Health 2(1):43–50

Fawell J, Nieuwenhuijsen MJ (2003) Contaminants in drinking water. Br Med Bull 68:199–208

Ferroudj N, Nzimoto J, Davidson A, Talbot D, Briot E, Dupuis V, Abramson S (2013) Maghemite nanoparticles and maghemite/silica nanocomposite microspheres as magnetic Fenton catalysts for the removal of water pollutants. Appl Catal B 136:9–18

Foley JA, DeFries R, Asner GP, Barford C, Bonan G, Carpenter SR, Cha FS (2005) Global consequences of land use. Science 309:570–574

Fornasiero F, Park HG, Holt JK, Stadermann M, Grigoropoulos CP, Noy A (2008) Ion exclusion by sub-2-nm carbon nanotube pores. Proc Natl Acad Sci USA 105(45):17250–17255

Gong XJ, Li JC, Xu K, Wang JF, Yang H (2010) A controllable molecular sieve for Na$^+$ and K$^+$ ions. J Am Chem Soc 132(6):1873–1877

Gunawan P, Guan C, Song X, Zhang QS, Leong SJ, Tang C, Chen Y, Chan-Park MB (2011) Hollow fiber membrane decorated with Ag/ MWNTs: toward effective water disinfection and biofouling control. ACS Nano 5:10033–10040

Guo J, Zhang Q, Cai Z, Zhao K (2016) Preparation and dye filtration property of electrospun poly-hydroxybutyrate–calcium alginate/carbon nanotubes composite nanofibrous filtration membrane. Sep Purif Technol 161:69–79

Hirsch A, Vostrowsky O (2007) Functionalization of carbon Nanotubes. Functional organic materials. Wiley-VCH Verlag GmbH & Co. KGaA, pp 1–57

Holt JK, Park HG, Wang YM, Stadermann M, Artyukhin AB, Grigoropoulos CP (2006) Fast mass transport through sub-2-nanometer carbon nanotubes. Science 312:1034–1037

Hong Y, Zhang J, Zhu C, Zeng XC, Francisco JS (2019) Water desalination through rim functionalized carbon nanotubes. J Mater Chem A7:3583–3591

Ihsanullah (2019) Carbon nanotube membranes for water purification: developments, challenges, and prospects for the future. Separat Purif Technol 209:307–337

Iijima S (1991) Helical microtubules of graphitic carbon. Nature 354:56–58

Iijima S, Ichihashi T (1993) Single-shell carbon nanotubes of 1-nm diameter. Nature 363:603–605

Jafari A, Mahvi AH, Nasseri S, Rashidi A, Nabizadeh R, Rezaee R (2015) Ultrafiltration of natural organic matter from water by vertically aligned carbon nanotube membrane. J Environ Health Sci Eng 13:51

Jassby D, Cath TY, Buisson H (2018) The role of nanotechnology in industrial water treatment. Nat Nanotechnol 13:670–672

Jie G, Kongyin Z, Xinxin Z, Zhijiang C, Min C, Tian C, Junfu W (2015) Preparation and characterization of carboxyl multi-walled carbon nanotubes/calcium alginate composite hydrogel nano-filtration membrane. Mater Lett 157:112–115

Kahrizi H, Bafkar A, Farasati M (2016) Effect of nanotechnology on heavy metal removal from aqueous solution. J Central South Univ 23:2526–2535

Kang S, Herzberg M, Rodrigues DF, Elimelech M (2008) Antibacterial effects of carbon nanotubes: size does matter. Langmuir 24:6409–6413

Kemper KE (2004) Groundwater-from development to management. Hydrogeol J 12(1):3–5

Kim ES, Hwang G, Gamal EDM, Liu Y (2012) Development of nanosilver and multi-walled carbon nanotubes thin-film nanocomposite membrane for enhanced water treatment. J Membr Sci 394:37–48

Koyuncu I, Sengur R, Turken T, Guclu S, Pasaoglu M (2015) Advances in water treatment by microfiltration, ultrafiltration, and nanofiltration. In: Advances in membrane technologies for water treatment. Woodhead Publishing, Oxford, pp 83–128

Lee KJ, Park HD (2016) The effect of morphologies of carbon nanotube-based membranes and their leachates on antibacterial property. Desalin Water Treat 57:7562–7573

Lee SY, Kim HJ, Patel R, Im SJ, Kim JH, Min BR (2007) Silver nanoparticles immobilized on thin film composite polyamide membrane: characterization, nanofiltration, antifouling properties. Polym Adv Technol 18(7):562–568

Lee B, Baek Y, Lee M, Jeong DH, Lee HH, Yoon J, Kim YH (2015) A carbon nanotube wall membrane for water treatment. Nat Commun 6:7109

Lee KJ, Cha E, Park HD (2016) High antibiofouling property of vertically aligned carbon nanotube membranes at a low cross-flow velocity operation in different bacterial solutions. Desalin Water Treat 57:23505–23515

Lilly M, Dong X, McCoy E, Yang L (2012) Inactivation of Bacillus anthracis spores by single-walled carbon nanotubes coupled with oxidizing antimicrobial chemicals. Environ Sci Technol 46:13417–13424

Liu H, Gong C, Wang J, Liu X, Liu H, Cheng F, Wang G, Zheng G, Qin C, Wen S (2016) Chitosan/silica coated carbon nanotubes composite proton exchange membranes for fuel cell applications. Carbohyd Polym 136:1379–1385

Liu SY, Zheng X, Yang Y, Liu J, Li J (20113) The removal and inhibitory effect of CNTs on model viruses. Mater Sci Forum 743–744:402–408

Majumder M, Zhan X, Andrews R, Hinds BJ (2007) Voltage gated carbon nanotube membranes. Langmuir 23(16):8624–8631

Maphutha S, Moothi K, Meyyappan M, Iyuke SE (2013) A carbon nanotube-infused polysulfone membrane with polyvinyl alcohol layer for treating oil-containing waste water. Sci Rep 3:1509

Meng H, Xue M, Xia T, Zhao YL, Tamanoi F, Stoddart JF, Zink J, Nel AE (2010) Autonomous in vitro anticancer drug release from meso-porous silica nanoparticles by pH-sensitive nanovalves. J Am Chem Soc 132:12690–12697

Mostafavi S, Mehrnia M, Rashidi A (2009) Preparation of nanofilter from carbon nanotubes for application in virus removal from water. Desalination 238:271–280

Mulder K, Hagens N, Fisher B (2010) Burning water: a comparative analysis of the energy return on water invested. Ambio 39(1):30–39

Muzammil A, Miandad R, Waqas M, Gehany F, Barakat MA (2019) Remediation of wastewater using various nanomaterials. Arab J Chem 12:4897–4919

Obare SO, Meyer GJ (2004) Nanostructured materials for environmental remediation of organic contaminants in water. J Environ Sci Health Part A 39(10):2549–2582

Parham H, Bates S, Xia Y, Zhu Y (2013) A highly efficient and versatile carbon nanotube/ceramic composite filter. Carbon 54:215–223

Popov VN (2004) Carbon nanotubes: properties and application. Mater Sci Eng R Rep 43(3):61–102

Qu X, Brame J, Li Q, Alvarez PJ (2012) Nanotechnology for a safe and sustainable water supply: enabling integrated water treatment and reuse. Acc Chem Res 46(3):834–843

Qu X, Alvarez PJ, Li Q (2013) Applications of nanotechnology in water and wastewater treatment. Water Res 47(12):3931–3946

Raghunath A, Perumal E (2017) Metal oxide nanoparticles as antimicrobial agents: a promise for the future. Int J Antimicrob Agents 49:137–152

Rahaman MS, Vecitis CD, Elimelech M (2012) Electrochemical carbon-nanotubes filter performance toward virus removal and inactivation in the presence of natural organic matter. Environ Sci Technol 46(3):1556–1564

Rajasekhar B, Nambi IM, Govindarajan SK (2018) Human health risk assessment of ground water contaminated with petroleum PAHs using Monte Carlo simulations: a case study of an Indian metropolitan city. J Environ Manage 205:183–191

Ray PZ, Shipley HJ (2015) Inorganic nano-adsorbents for the removal of heavy metals and arsenic: a review. RSC Adv 5:29885–29907

Ritter L, Solomon K, Sibley P, Hall K, Keen P, Mattu G, Linton B (2002) Sources, pathways, and relative risks of contaminants in surface water and groundwater: a perspective prepared for the Walkerton inquiry. J Toxicol Environ Health Part A 65(1):1–142

Selvi A, Rajasekar A, Theerthagiri J, Ananthaselvam A, Sathishkumar K, Madhavan J, Rahman PKSM (2019) Integrated remediation processes toward heavy metal removal/recovery from various environments—a review. Front Environ Sci 7:66

Shannon MA, Bohn PW, Elimelech M, Georgiadis JG, Marıas BJ, Mayes AM (2008) Science and technology for water purification in the coming decades. Nature 452:301–310

Shawky HA, Chae SR, Lin S, Wiesner MR (2011) Synthesis and characterization of a carbon nanotube/polymer nanocomposite membrane for water treatment. Desalination 272(1):46–50

Shon HK, Phuntsho S, Chaudhary DS, Vigneswaran S, Cho J (2013) Nanofiltration for water and wastewater treatment—a mini review. Drink Water Eng Sci 6:47–53

Sun H, Lia D, Liu B, Yao J (2019) Enhancing the permeability of TFC membranes based on incorporating polyamide matrix into MWCNTs framework. Appl Surf Sci 496:143680

Tansel B, Sager J, Rector T, Garland J, Strayer RF, Levine LF (2006) Significance of hydrated radius and hydration shells on ionic permeability during nanofiltration in dead end and cross flow modes. Separat Purif Technol 51(1):40–47

Terrones M (2003) Science and technology of the twenty-first century: synthesis, properties, and applications of carbon nanotubes. Annu Rev Mater Res 33(1):419–501

Theron J, Walker JA, Cloete TE (2008) Nanotechnology and water treatment: applications and emerging opportunities. Crit Rev Microbiol 34:43–69

Tiraferri A, Vecitis CD, Elimelech M (2011) Covalent binding of single-walled carbon nanotubes to polyamide membranes for antimicrobial surface properties. ACS Appl Mater Interfaces 3(8):2869–2877

Trivedi S, Alameh K (2016) Effect of vertically aligned carbon nanotube density on the water flux and salt rejection in desalination membranes. Springer plus 5:1158

Vecitis CD, Schnoor MH, Rahaman MS, Schiffman JD, Elimelech M (2011) Electrochemical multiwalled carbon nanotubes filter for viral and bacterial removal and inactivation. Environ Sci Technol 45(8):3672–3679

Verma B, Balomajumder C (2020) Surface modification of one-dimensional Carbon Nanotubes: a review for the management of heavy metals in wastewater. Environ Technol Innov 17:100596

Wang R, Mikoryak C, Li S, Bushdiecker D, Musselman IH, Pantano P, Draper RK (2011) Cytotoxicity screening of single-walled carbon nanotubes: detection and removal of cytotoxic contaminants from carboxylated carbon nanotubes. Mol Pharm 8:1351–1361

WHO/UNICEF Report on progress on household drinking water, sanitation and hygiene (2019) https://data.unicef.org/resources/progress-drinking-water-sanitation-hygiene-2019/

Yin J, Kim ES, Yang J, Deng B (2012) Fabrication of a novel thin-film nanocomposite (TFN) membrane containing MCM-41 silica nanoparticles (NPs) for water purification. J Membr Sci 423–424:238–246

Yin J, Zhu GC, Deng B (2016) Graphene oxide (GO) enhanced polyamide (PA) thin-film nanocomposite (TFN) membrane for water purification. Desalination 379:93–101

Youngbin B, Cholin K, Dong KS, Taewoo K, Jeong SL, Yong HK, Kyung HA, Sang SB, Sang CL, Jaelim L, Kyunghyuk L, Jeyong Y (2014) High performance and antifouling vertically aligned carbon nanotube membrane for water purification. J Membr Sci 460:171–177

Yu M, Funke HH, Falconer JL, Noble RD (2009) High density, vertically-aligned carbon nanotube membranes. Nano Lett 9(1):225–229

Yuhao L, Zhongwu L, Fikret A, Jana Q, Xi C, Yun CY, Cheng Z, Yunfei C, Tuan AP, Aleksandr N (2020) Water-ion permselectivity of narrow-diameter carbon nanotubes. Sci Adv 6:1–9

Zhao X, Liu Y, Inoue S, Suzuki T, Jones RO, Ando Y (2004) Smallest carbon nanotube is 3 Å in diameter. Phys Rev Lett 92(12):125502

Zhao X, Cheng L, Jia N, Wang R, Liu L, Gao C (2020) Polyphenol-metal manipulated nanohybridization of CNT membranes with FeOOH nanorods for high-flux, antifouling and self-cleaning oil/water separation. J Memb Sci 600:117857

Remediation of Crude Oil Contaminated Kaolin Clay

Saqib Showkat Wani, Pardeep Singh, and Heena Malhotra

Abstract Crude oil-contamination is observed in soils that often come in contact with leakage of petroleum or their derivatives. An experimental study was carried out on the combined effect of Ground Granulated Blast Furnace Slag (GGBS) and Cement on kaolin clay contaminated by crude oil. The crude oil percentage of 10% was considered as the maximum level of contamination. The Ground Granulated Blast Furnace Slag and Cement were added in the ratio of 2:1 in percentages of 5, 10, and 15%. A series of tests were performed to investigate consistency limits, shear strength parameters, and unconfined compressive strength of stabilized crude oil contaminated kaolin clay. The results of the investigation made clear that consistency limits declined while the stabilizer percentage was increased. Direct Shear parameters both increased with stabilizer percentage but the increase was more seen in cohesion (c) with the peak value of 85 kN/m^2 at the stabilizer percentage of 15%. Maximum values of UCS were observed at 15% stabilizer percentage for both cured and uncured samples. However, the peak UCS values for 0, 7, and 14 days cured samples were observed to be equal to 300, 450, and 750 kN/m^2 respectively. The study reveals the effectiveness of using this combination of binders to stabilize crude oil contaminated clay and at the same time reducing the burden on the environment by making proper use of waste material i.e., Ground Granulated Blast Furnace Slag. Thus stabilization/solidification (S/S) remediation technique that utilizes Ground Granulated Blast Furnace Slag and Cement to treat contaminated kaolin clay was found to be effective.

S. S. Wani (✉) · P. Singh · H. Malhotra
Department of Civil Engineering, GNDEC, Ludhiana 141006, Punjab, India
e-mail: ersaqibshowkatwani@gmail.com

P. Singh
e-mail: Pardeepsjoia@gndec.ac.in

H. Malhotra
e-mail: malhotraheena@gndec.ac.in

S. S. Wani
Department of Civil Engineering, St. Andrews Institute of Technology and Management, Gurugram, Haryana, India

1 Introduction

The major components of the biosphere are mostly contaminated by human activities, the soil being the major component of the environment gets polluted by various contaminants exposed to the soil through various contaminants like petroleum products or its derivatives like crude oil, diesel, petrol, gasoline, etc. as they contain the polycyclic aromatic hydrocarbons and if they are exposed to soil, it has been found that it alters its geotechnical properties (Safehian et al. 2018) as the pore fluid of soil is changed from naturally occurring water to petroleum product. Among geotechnical engineers, the interaction of these petroleum hydrocarbons with the soil and its impact on the basic soil properties has been the prime focus of various researchers. The petroleum hydrocarbons and their derivatives get exposed to the soil through various factors like tanker accidents, breakage of pipelines, and spillage during the transit facilities, leakage from storing units, etc. and cause enormous damage to the mechanical properties of soil and may penetrate the soil layer and can contaminate the groundwater. The typical example of previously mentioned reasons of contamination can be cited by the way the soil got contaminated during the gulf crisis in 1991 and had serious implications on the soil (Ai-Sanad and Ismael 1997).

Among the petroleum hydrocarbons, crude oil spillage cases have been reported more than the other derivatives of hydrocarbons. As per the estimate among the total global production of crude oil, 10% of it interacts with the environment and causes a potential threat to the environment and specifically soil. Wide research has been done in case of contamination of soil by oil (Safehian et al. 2018; Ai-Sanad and Ismael 1997; Khosravi et al. 2013; Khamehchiyan et al. 2007).

Abousnina et al. (2015) stated that when the contaminant that's light crude oil was mixed with the clay sample, reduction in shear strength parameters was found. Ostovar et al. (2020) conducted a series of tests on oil exposed sandy soils and found a reduction in direct shear parameters i.e. (c) and (φ)and stated crude oil has the potential to reduce the bearing capacity. Rahman et al. (2010) stated that oil contamination has adverse effects on soil properties. Kermani and Ebadi (2012) observed that the increase in Atterberg's limits, maximum dry density, and compression index while a declining trend was observed in cohesion and omc of the soil when contaminated.

Thus for geotechnical engineers, remediating the soil that's restoring the soil to its original form has been the priority and the remediation technique to be implemented depends upon the type of contaminant, There are various methods of remediating the soil like bioremediation, phytoaugmentation, electrokinetic remediation, thermal remediation, etc. (Lim et al. 2016). Concetta Tomei and Daugulis (2013) stated that bioremediation is quite effective when it comes to decontaminating the soil rather than the physical/chemical processes. Molina-Barahona et al. (2004) stated

that decontaminating the soil by biostimulation or crop residues is one of the cheap, cost-effective, and sustainable approaches for soil that got contaminated with diesel.

Stabilization/solidification is a remediation technique categorized under the heading of physical/chemical treatment for contaminated soils. Fox (1996) stated that the s/s remediation technique is cost-effective as it encapsulates or immobilizes the contaminant around the clay particle and converts them into stable and solidified mass by the chain of reactions with the help of additives and pozzolanic binders. Sörengård et al. (2019) discussed the remediation of soil by the S/S technique and found effective results with this treatment. Akinwumi et al. (2016) stabilized the soil by the S/S remediation technique and used cement as a solidifier and concluded that stabilization by cement improved its overall parameters and specifically the strength of the soil through the set of reactions. Tajudin et al. (2016) concluded that OPC incorporated with a different set of binders proves to be a cost-effective and environmentally sustainable S/S remediation technique for decontaminating the soil.

Geotechnical experts have been curious about remediating the crude oil contaminated soil or restoring it to its original state thus adding further knowledge about the behavior of contaminated samples with different stabilizers and expanding the utilization of S/S remediation technique involving the use of ggbs and cement in remediating the crude oil contaminated fine grained soil specifically kaolin clay has not been analyzed yet. The ultimate objective of the investigation presented here is to analyze the combined effect of Cement and Ground Granulated Blast Furnace Slag (GGBS) on the consistency limits, strength parameters and effect of curing on crude oil contaminated stabilized samples has also been the core objective of this research.

2 Material and Methods

2.1 Collection of Representative Fine Grained Clay Sample

The fine-grained clay sample chosen for research is Kaolin clay and was procured from a local seller from city of Ludhiana namely J. minerals. The geotechnical properties of virgin kaolin claylike relative density, Consistency limits, strength parameters (ucs), and shear strength parameters were determined in accordance with (IS: 2720 (Part 13) 1986; IS: 2720 (Part 5) 2006; IS: 2720 (Part III/sec 1) 2002; IS 2720 (Part 10) 2006). The composition of clay is given in Table 1. The summary of uncontaminated or virgin soil parameters is given in Table 2.

Table 1 Chemical composition of kaolin clay (Khosravi et al. 2013)

Chemical constituents	SiO_2	Al_2O_3	CaO	Fe_2O_3	MgO	K_2O	Other
Quantity (%)	66.55	27.33	1.79	0.59	0.50	0.34	2.94

Table 2 Summary of virgin kaolin clay properties

Clay type	L.L. (%)	P.L. (%)	P.I. (%)	G	MDD (g/cc)	OMC (%)	UCS (kN/m^2)	C (kN/m^2)	$\Phi(^o)$
CI	44%	24%	20%	2.60	1.71	20	118	50	22.9

Table 3 Characteristics of crude oil (Kermani and Ebadi 2012)

Parameter	Unit	Value
Viscosity	g/ms	40.2
Bulk Density γ (at 25 °C)	g/cc	0.895
Gravity (15.56 °C)	–	26.6
Flashpoint	°C	44.1
Sp. Gravity (at 25 °C)	–	0.89

2.2 Crude Oil

The crude oil was obtained from refinery based in Bathinda city of Punjab. The chemical properties of crude oil are listed in Table 3.

2.3 Ground Granulated Blast Furnace Slag and Cement

The Ground Granulated Blast Furnace Slag (GGBS) was obtained from Gujarat based seller namely Guru Corporations Ahmadabad. Since it's the waste material produced from the iron industry thus incorporating it in s/s remediation will reduce some burden on the environment. The properties of GGBS are enlisted in Tables 4 and 5.

The cement used was of Grade 43 OPC (Ordinary Portland Cement) and was procured from a local seller available in Ludhiana. The proportion of GGBS and Cement used was 2:1 for S/S remediation of crude oil contaminated soil samples. The physical and chemical properties of OPC are enlisted below in Table 6a, b respectively.

Table 4 Physical parameters of GGBS

Physical parameters	Value
Fineness	386.45 m^2/kg
Residue (90 μ)	0.86
Residue (45 μ)	4.12

Table 5 Chemical composition of GGBS

Chemical constituents	Quantity (%)
Total loss of ignition (% by Mass)	Nil
Insoluble residue (% by Mass)	0.35
Sulphuric anhydride (% by Mass)	0.45
Magnesia (MgO) (% by Mass)	8.2
Silicon oxide (SiO_2)(% by Mass)	34.12
Aluminium oxide (Al_2O_3)(% by Mass)	18.95
Ferric oxide (Fe_2O_3) (% by Mass)	0.23
Sulphur (% by Mass)	0.76
Calcium oxide (CaO) (% by Mass)	35.46

Table 6 a Summary of chemical properties of OPC (Shukla et al. 2019). **b** Physical Properties of OPC

S. No.	Chemical component	Component %
1	LOI	1.90
2	SO_3	2.36
3	K_2O	0.53
4	Na_2O	0.28
5	MgO	1.76
6	CaO	62.85
7	Fe_2O_3	3.92
8	Al_2O_3	5.42
9	SiO_2	20.98
S. No.	Physical properties (OPC)	Value
1	Specific gravity	3.14
2	Setting time (initial)	75 min
3	Setting time (final)	255 min
4	Color	Gray
5	Consistency (normal)	32%

2.4 Preparation of Oil Contaminated Soil Sample

The crude oil of 10% by the dry weight of soil sample is taken and manually mixed with the oven-dried fine-grained soil sample and was kept in an airtight containers for the curing of at least 7 days at a temperature of 30 °C so that the sample comes in equilibrium. Then various Laboratory tests were performed on crude oil contaminated soil samples and the summary of the properties of kaolin clay contaminated by crude oil is presented in Table 7.

Table 7 Summary of 10% crude oil contaminated kaolin clay

L.L. (%)	P.L. (%)	P.I. (%)	MDD (g/cc)	OMC (%)	C (kN/m^2)	Φ (°)	UCS (kN/m^2)
51	30	21	1.64	17	42	16.18	93

2.5 Methodology

Preparation of GGBS and Cement (2:1) Stabilized Samples

The crude oil contaminated kaolin clay samples are further mixed and remediated with varying percentages of GGBS and Cement (2:1) ranging from 5 to 15% by the weight of representative soil samples taken (Table 8).

Curing of Stabilized Samples for UCS Testing

The different percentages of stabilized UCS samples are then placed in polythene bags to safeguard against the loss of moisture and are placed for curing of 0, 7, and 14 days and UCS tests are performed for these stabilized samples at regular intervals of 0, 7 and 14 days (Table 9).

Table 8 Program of experimental testing

% GGBS and Cement to be added to contaminated kaolin clay (2:1)	Soil Parameters under investigation	Tests executed
Initial amount added shall be 5% by dry weight of kaolin sample and shall also be added with increments of 5% till the value reaches 15%	Atterberg limits	Casagrande and thread test
	Compaction characteristics	Light compaction test
	Cohesion (c) and Angle of internal friction (φ)	Shear test
	Compressive strength	Compressive strength test

[*] GGBS is first activated by alkali activator NaOH 10 Molar in concentration
[**] Shear strength parameters are tested after 28 days of curing of stabilized samples.

Table 9 UCS testing program of cured samples

% of GGBS and Cement (2:1)	Parameter under investigation	Curing period (days)
5%	Unconfined compressive strength	0, 7, 14
10%	Unconfined compressive strength	0, 7, 14
15%	Unconfined compressive strength	0, 7, 14
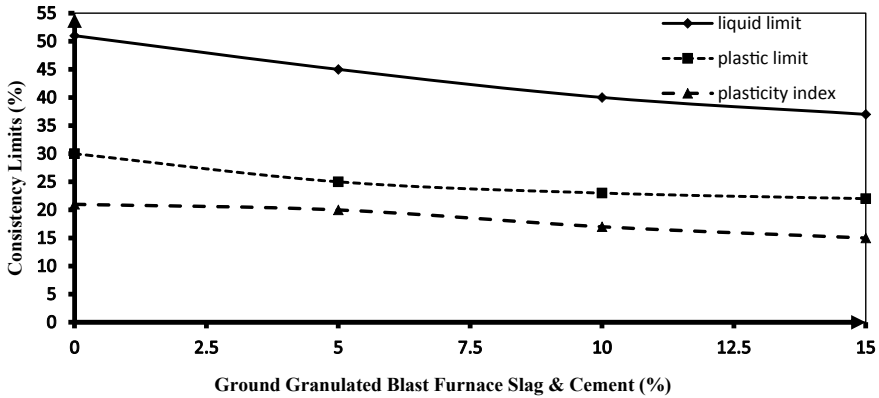
Fig. 1 Variation of consistency limits with stabilizer percentage

3 Results and Discussions

3.1 Atterberg's Limits

The results of remediated crude oil contaminated kaolin clay on consistency limits are shown in Fig. 1. The consistency limits like L.L., P.L., P.I., were seen to follow the declining trend with an increase in the percentage of stabilizers from 0 to 15%. The reason being the chain of reaction occurring between stabilizer and clay particles and the series of interactions which occur possibly are pozzolanic reactions, ion exchange, and agglomeration. The attractive force that's developed develops the flocculated clay structure and hence produces negative effect on the Atterberg's limits.

3.2 Compaction Characteristics

The increasing trend was observed in dry density (maximum) of our stabilized kaolin clay samples with the percentage increase in stabilizers and the reason behind the increase is when these cementitious or pozzolanic compounds react with clay particles they attract the clay particles together and consequently result in denser packing and thus our dry density is increased. When it comes to optimum moisture content (OMC), an increasing pattern was observed with the percentage increase in stabilizer and the increase could be explained because pozzolanic reactions require more water for the occurrence, and thus causing the OMC to increase (Figs. 2 and 3).
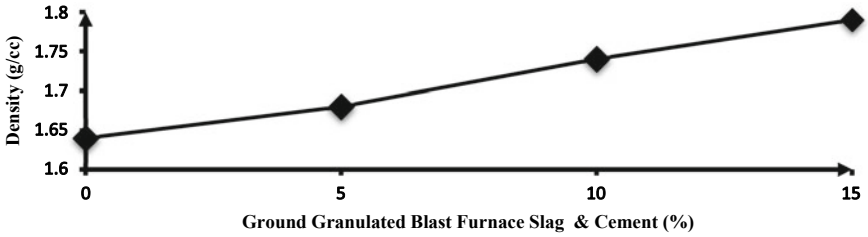
Fig. 2 Variation of dry density with stabilizer percentage
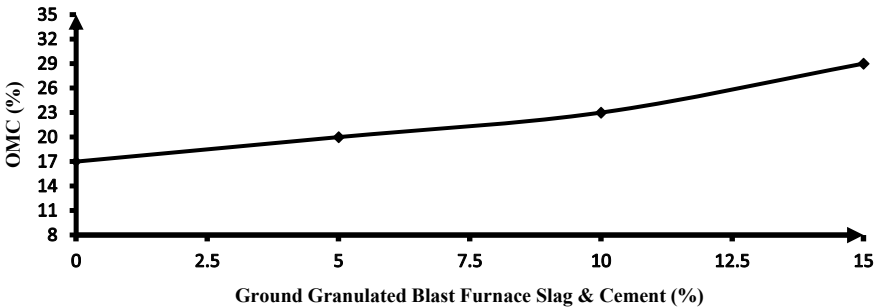
Fig. 3 Variation of OMC with stabilizer percentage

3.3 Shear Strength Parameters

Ground Granulated Blast Furnace Slag (GGBS) and Cement being the cementitious or pozzolanic products they bind or cement the clay particles with each other and result in the formation of products with an increased level of affinity towards each other thus increasing the cohesion (c) value and cohesion (c) was seen to follow the continuous increasing pattern with the stabilizer percentage increase. As far as the angle of internal friction (φ) is considered which is solely dependent on the particle size since the S/S remediation technique results in the formation of flocs and hence our angle of internal friction (φ) increases with the percentage increase in the binder and then attained almost constant value at 10 and 15% of GGBS and Cement (Fig. 4).

3.4 UCS Test of Uncured and Cured Samples

An increase in UCS of the representative kaolin clay samples was detected while the percentage of stabilizers was elevated for uncured samples while the continuous increasing trend was observed in samples cured at 7 and 14 days. The increase is attributed to the fact that the chain of the pozzolanic reactions takes place between the binder and clay particles and this reaction occurs quickly in presence of the alkali
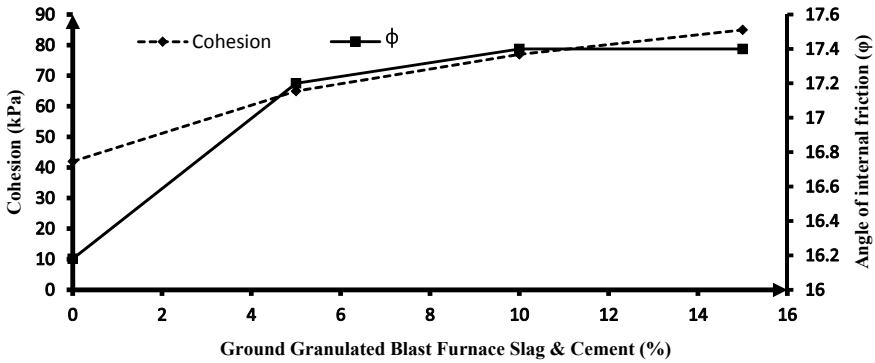
Fig. 4 Variation of cohesion and angle of internal friction with stabilizer percentage
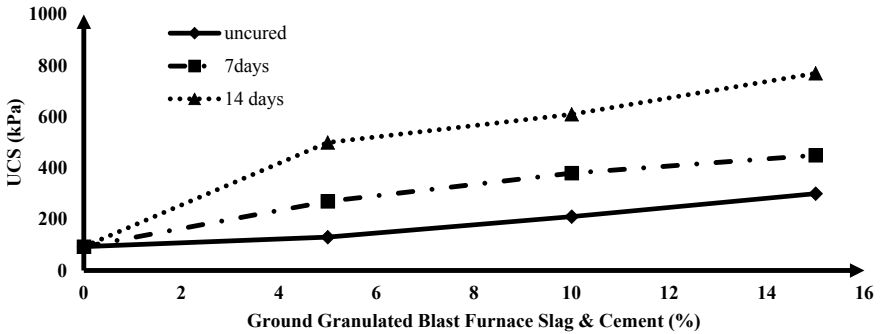
Fig. 5 Graphical relation of influence of curing on UCS

activator sodium hydroxide. The long-term gain in unconfined compressive strength due to curing can be attributed to the formation of more stable compounds that coat and solidify the oil-contaminated clay particle. The results are shown in Fig. 5.

4 Conclusion

Atrial investigation was executed on crude oil-contaminated samples remediated by Ground Granulated Blast Furnace Slag (GGBS) and Cement in varying percentages of 5, 10, and 15%, and the corresponding effect on Atterberg's limits, compaction parameters, direct shear parameters, and unconfined compressive strength (UCS) of crude oil contaminated kaolin clay samples were observed and also the curing effect of stabilizers on UCS of contaminated soil samples were observed. It was found that Atterberg's limits showed a decreasing trend and the liquid limit showed

a 27.5% decrease and the plastic limit showed a decrease by 26.67% at a stabilizer percentage of 15% and the corresponding plasticity of soil specimen showed a percentage decrease of 28.57% at stabilizer percentage of 15%.

MDD of the stabilized soil specimen showed the increase with the peak value of 1.79 g/cc at stabilizer percentage of 15% from the base value of MDD that was 1.64 g/cc at 0% addition of stabilizer and our corresponding OMC increased consistently with the increase in stabilizer percentage with its peak value of 29% at 15% stabilizer percentage.

Cohesion (C) of the stabilized contaminated samples substantially increased by 102% at the stabilizer percentage of 15%. While as the angle of shearing resistance (φ) increased by 7.4% at the stabilizer percentage of 10% and then attained the constant value and remained unchanged even at the 15% stabilizer percentage.

UCS of the uncured samples attained the peak value of 300 kN/m^2 at the stabilizer percentage of 15% or the percentage increase for uncured samples at 15% stabilizer percentage was observed to be equal to 222.5%. While as that for 7 days cured samples the percentage increase was found to be equal to 383.8% at a stabilizer percentage of 15%. For the samples cured for 14 days, the percentage increase in unconfined compressive strength was found to be equal to 727.95% that is roughly equal to 2.5 times the peak strength of uncured samples at a 15% stabilizer percentage.

References

Abousnina RM, Manalo A, Shiau J, Lokuge W (2015) Effects of light crude oil contamination on the physical and mechanical properties of fine sand. Soil Sediment Contam 24:833–845. https://doi.org/10.1080/15320383.2015.1058338

Ai-Sanad HA, Ismael NF (1997) Aging effects on oil-contaminated Kuwaiti Sand. J Geotech Geoenviron Eng 123:290–293.https://doi.org/10.1061/(ASCE)1090-0241

Akinwumi II, Booth CA, Diwa D, Mills P (2016) Cement stabilisation of crude-oil-contaminated soil. Proc Inst Civ Eng Geotech Eng 169:336–345. https://doi.org/10.1680/jgeen.15.00108

Concetta Tomei M, Daugulis AJ (2013) Ex situ bioremediation of contaminated soils: an overview of conventional and innovative technologies. Crit Rev Environ Sci Technol 43:2107–2139. https://doi.org/10.1080/10643389.2012.672056

Fox RD (1996) Physical/chemical treatment of organically contaminated soils and sediments. J Air Waste Manag Assoc 46:391–413. https://doi.org/10.1080/10473289.1996.10467473

Guru Corporations Ahmedabad, Gujarat, India. https://www.refractoryproduct.com. Last accessed 12 Oct 2021

IS: 2720(Part III/sec 1) (2002) Indian standard methods of test for soils Part III determination of specific gravity. New Delhi

IS 2720 (Part 10) (2006) Indian standard methods of test for soils part 10 determination of unconfined compressive strength. Bureau of Indian Standards, New Delhi

IS : 2720 (Part 5) (2006) Indian standard methods of test for soils part 5 determination of liquid and plastic limit. Bureau of Indian Standards, New Delhi

IS : 2720 (Part 13) (1986) Indian standard methods of test for soils part 5 determination of shear strength. New Delhi

Kermani M, Ebadi T (2012) The effect of oil contamination on the geotechnical properties of fine-grained soils. Soil Sediment Contam 21:655–671. https://doi.org/10.1080/15320383.2012.672486

Khamehchiyan M, Hossein Charkhabi A, Tajik M (2007) Effects of crude oil contamination on geotechnical properties of clayey and sandy soils. Eng Geol 89:220–229. https://doi.org/10.1016/j.enggeo.2006.10.009

Khosravi E, Ghasemzadeh H, Sabour MR, Yazdani H (2013) Geotechnical properties of gas oil-contaminated kaolinite. Eng Geol 166:11–16. https://doi.org/10.1016/j.enggeo.2013.08.004

Lim MW, Lau E, Von Poh PE (2016) A comprehensive guide of remediation technologies for oil contaminated soil—present works and future directions. https://doi.org/10.1016/j.marpolbul.2016.04.023

Molina-Barahona L, Rodríguez-Vázquez R, Hernández-Velasco M, Vega-Jarquín C, Zapata-Pérez O, Mendoza-Cantú A, Albores A (2004) Diesel removal from contaminated soils by biostimulation and supplementation with crop residues. Appl Soil Ecol 27:165–175. https://doi.org/10.1016/j.apsoil.2004.04.002

Ostovar M, Ghiassi R, Mehdizadeh MJ (2020) Soil and sediment contamination : an international effects of crude oil on geotechnical specification of sandy soils effects of crude oil on geotechnical specification of sandy soils. Soil Sediment Contam Int J 00:1–16. https://doi.org/10.1080/15320383.2020.1792410

Rahman ZA, Hamzah U, Taha MR et al (2010) Influence of oil contamination on geotechnical properties of basaltic residual soil. Am J Appl Sci 7:954–961

Safehian H, Rajabi AM, Ghasemzadeh H (2018) Effect of diesel-contamination on geotechnical properties of illite soil. Eng Geol 241:55–63. https://doi.org/10.1016/j.enggeo.2018.04.020

Shukla A, Gupta N, Kishore K (2019) Experimental investigation on the effect of steel fiber embedded in marble dust based concrete. Mater Today Proc 26:2938–2945. https://doi.org/10.1016/j.matpr.2020.02.607

Sörengård M, Kleja DB, Ahrens L (2019) Stabilization and solidification remediation of soil contaminated with poly- and perfluoroalkyl substances (PFASs). J Hazard Mater 367:639–646. https://doi.org/10.1016/j.jhazmat.2019.01.005

Tajudin SAA, Azmi MAM, Nabila ATA (2016) Stabilization/solidification remediation method for contaminated soil: a review. In: IOP conference series: materials science and engineering, vol 136. https://doi.org/10.1088/1757-899X/136/1/012043

Cost and Global Warming Optimization Through Landfill Reuse and Integrated Waste Management for Kolkata

Sayan Banerjee, Shristi Gupta, Samran Banerjee , and Amit Dutta

Abstract Issues on climate change, global warming, GHG emission, pollution hazards etc. are of huge concern in relation with municipal solid waste management of Indian cities. Kolkata, a metropolitan city of India with 11 million population has incremental trend of waste generation with enormous inefficiency not only in waste processing level but also having disposal problem in engineered manner to the exhausted landfill site Dhapa with its 30 years long legacy waste. Reusing this land area through landfill mining proclaims an opportunity to recover valuable mined waste (60%) along with a space to be converted into an engineered landfill site. This paper objectifies landfill reuse of a depleted non-engineered landfill through Bio-mining followed by implementation of an integrated waste management linear programming model considering transfer station, sorting station, thermal and biological processing units as well as an engineered landfill site to optimize the economic aspect and global warming hazard. The model has been solved using LINGO optimization software. As a solution, plausible reduction in total waste management cost is 43% and landfilling cost by 48%. Vehicle optimization enhances the cost minimization possibility by 70% which is substantial. Direct greenhouse gasses like CO_2 and CH_4 have been analysed. Viable reduction in Methane emission is 87% achievable which leads to a substantial reduction in GWP in relation to CO_2-eq. by 65%. This sustainable methodological analysis can be elucidated as a generic multi-objective strategy to empower not only the economic sector but also the atmospheric and pollution aspects along with circularity.

Keywords Integrated solid waste management · Global warming · Cost optimization

S. Banerjee (✉) · S. Gupta
Meghnad Saha Institute of Technology, Kolkata, India
e-mail: banerjee.2@iitj.ac.in

S. Banerjee · A. Dutta
Jadavpur University, Kolkata, India
e-mail: amit.dutta@jadavpuruniversity.in

1 Introduction

Expeditious urban sprawling, economic development and enormous growth rate in population is instigating the solid waste generation of developing countries. The scarcity in proper waste management is arising because of the unplanned growth in population. Lack of reuse and recycling of the solid waste composition has taken place due to limited economy and infrastructure, restraint in the land area for safe disposal and lack of public awareness lead to ineffective Solid Waste Management (SWM) system of various cities in India. The municipal bodies in India allocate 75–95% of the financial budgets towards the collection and transportation of waste generated, although the collection efficiency of Municipal Solid Waste (MSW) ranges from 70 to 90% in megacities whereas 50% for smaller towns (Annepu 2012; Ghose et al. 2006; Krook et al. 2012; Sharholy et al. 2008; Siddiqui et al. 2006). The amount of per capita waste generation has an annual increase rate of 1 to 1.33% in the last few decades. The major fraction in MSW is the biodegradable fractions (50–60%) and inert (30–50%) in the urban areas. So the government has set up a limit for minimization of the wastes going to landfill by at least 75% through processing of MSW using appropriate methods and technologies. There are various plausible treatment processes for MSW with material and energy recovery option. The most extensive are thermal processing through mass burn incinerator, RDF based plants, pyrolysis and gasification. Whereas for bio-chemical conversion, there are composting, vermicomposting, bio-methanation is available. Which conversion technique is to be chosen solely depends on the characteristics of MSW, desirable form of energy, environmental standards and norms, economic configurations and factors specific to project area (Singh et al. 2011). Improper and inefficient waste management system leads to heap up of wastes that create certain problems in society.

Open dumping of waste materials cause unhygienic condition due to biodegradable portion of waste which gets rot and decompose under uncontrolled condition. Information regarding waste generation of different cities depends upon the living standard and population of that particular city as per capita waste generation is varies for every city. MSW generation per capita in India ranges from approximately 0.17 kg per person per day in small towns to approximately 0.62 kg per person per day in cities (Kurian et al. 2003b). The average waste composition in India contains approximately 52.32% biodegradable waste, 13.8% paper, 7.89% rubber, 1.49% metal, 0.93% glass, 1% rags and rest are inert (KEIP 2007a). So the method of composting of wastes will be more preferred in Indian cities as biodegradable waste is majorly present and incineration may not be much profitable because wastes possess less calorific value. India holds second position when it comes to population. So it is very obvious that country with more population will generate more waste. For metropolitan cities, the average waste generation is 6000–7000 TPD (Ortner et al. 2014) and average population is about 3 crore. But if we see this for one of the smart cities of India like Indore the average waste generation is 1115 TPD. One of the worst conditioned landfill site in India is Ghazipur landfill site where garbage dump is now 65 m tall which is just 8 m less than that of Qu tub Miner's height. In present scenario, there

is an exclusion of sorting plant, incineration plant and composting plant in most of the disposal sites in India. The inert as well as biodegradable fraction are disposed as open dumping without being processed. Due to low calorific valued waste present in the biodegradable waste composition, sorting is necessary before any thermal processing and it is causing inefficient waste to energy (WTE) project which is in huge demand worldwide.

2 Literature Analysis

2.1 Global Scenario of Landfill Reuse and Landfill Mining

Generation of immense amount of MSW end up with open dumping in non-engineered landfills if untreated in proper manner, leads to consumption of massive land area with enormous pollution hazards, GHG emission, leachate generation, toxic metal contamination and so on. These huge land areas are being exhausted with these years long aged commingled MSW, termed as legacy waste, are of utmost concern to be treated thus to recover not only the land area but also loads of valuable resources escaping into the MSW followed by remediation of contaminated landfill site. Landfill mining is one such procedure being followed globally since 1953 (Savage et al. 1993). Annual generation of 2 billion MT of MSW worldwide left 33% waste to not being managed in an environmentally safe and sound strategy. Global situations of meteoric growing competition for valuable resources, price hike for raw materials, devastating natural reservoirs for valuable resources and increasing environmental discrepancies are the leading cause of enhanced landfill mining strategy (Kumar et al. 2017). Recovery of landfill volume was achieved in Thomson landfill, Connecticut, USA in 1989, Groundwater contamination reduction and landfill space reclamation were executed in Hopewell landfill, Pennsylvania, USA in 1991 (Guerriero 1996). Landfill reclamation through waste mining and recovery were accomplished in Veneendal and Born landfills of Netherlands (Kurian et al. 2003a; Paul et al. 2014; Zee et al. 2004). Study on Landfill rehabilitation study including reclaiming, treatment, and reassembly of excavated material in Schöneiche landfill of Germany was executed in 1995 (Bockreis and Knapp 2011). Indian landfill mining were studied in Kodungaiyur and Perungudi landfills for recovery of compost and cover materials (NEERI 2005).

2.2 Integrated Solid Waste Management and Recent Trends

To minimize all the adverse impacts of this inefficient waste handling and control system, there is a need of proper effective waste management norms which can be done in an integrated manner. Integrated Solid Waste Management system is thus

widely applicable for an economical and environmentally sustainable approach to meet the needs of public health and welfare of society. An effective waste management system comprises one or more of the following options which includes collection and transportation of waste, resource recovery through sorting and recycling, recovery of waste materials (such as compost) or energy recovery through biological, thermal or other processing, waste transformation i.e. reduction of volume, toxicity or other physical/chemical properties of waste for safe and acceptable final disposal meeting the environmental and sustainable needs. For an extensive analysis on different aspect of SWM, a necessary modelling is required to predict the effect of a proposed system with integrated approach. Difficulties in domestic waste management, increased waste quantities, decreasing land space, waste prevention and recycling goals demands involvement of integrated solid waste management techniques. Cost control, sustainable environment and recycling of waste are some of the major consideration behind model implementation. Recent trends on ISWM modelling are exhibiting as such development of a Multi Integer Linear Programming Model considering waste composition, rate and environmental impacts (Daskalopoulos et al. 1998), a proposed model for economic and optimized management of MSW for Middle Eastern country Egypt (Badran and El-Haggar 2006), a decision model defining recycling, processing and disposal units for MSW management (Costi et al. 2004), investigation of quantitative air pollutants, waste collection system followed by comparison study (Vilms et al. 2015) and modelling on MSW management for Indian cities in LINDO (Chattopadhyay et al. 2018). However, no such studies have been appeared to estimate the economy and pollution both by reusing exhausted land area considering integrated system.

3 Interpretation on Study Area

3.1 Existing Municipal Solid Waste Management in Kolkata

The Solid Waste Management (SWM) system of Kolkata is under control of Kolkata Municipal Corporation (KMC) with a regular generation of municipal solid waste (MSW) of around 4000–4350 MT/day. The municipal area covered under KMC was 187.33 km^2 along with 15 no. of boroughs and 141 electoral wards till 2015. After that one borough has been incorporated within the municipal area with 3 wards from Joka and 2 wards from other two boroughs. Apart from that the number of ward has been increased up to 144 and it leads to 200.71 km^2 municipal covered area of Kolkata. Our study solely based on the waste generation from all the 16 no. of boroughs. It has a total population of 11 million including floating population which is around 4 million and the population of the slums and also the urban poor (about 2 million). The generation rate of MSW in Kolkata is around 600 g per capita per day (gpcd) for the residential population and around 250 gpcd for the floating population.

Waste Composition and Segregation

Due to increasing rate of biodegradable portion, the average physical composition of MSW shows 64.84% (on wet wt. basis) of compostable fraction out of the total garbage generated, whereas 17.55% (on wet wt. basis) of recyclable fractions are especially due to rising uses of plastic and paper. Rest of the 17.61% (on wet wt. basis) of waste (garbage fraction only) are inert and other material. The recyclables present in the garbage generated are paper (5.25%), plastics (7.25%), glass (1.06%), metals (0.18%) and rubber (3.81%). Very small fraction of recyclable garbage is recycled by generators and informal sectors like rag pickers (around 10%) at open vats and disposal sites. Garbage of other materials consist of rubber (3.81%), rags (3.83%), wood (0.65%), coconut shell (3.13%), inert (8.96%) and others (1.04%). From composition analysis, among the total 100 MT of commingled MSW, at source including landfill site recyclable portion is 12.8 MT. Rest of the mixed waste is dumped into the open dumpsite Dhapa.

Landfilling

In the existing system, around 4500 MT of waste is dumped openly per day to the major landfill site Dhapa which is operated by KMC and lies within the ward no 57 and 58 of the KMC administrative boundaries, the eastern part of Kolkata. Almost the entire area is situated within a protected wetland area called east Kolkata wetland. The inefficiency in the operation of Dhapa landfill is due to the absence of earth cover, liner system and leachate as well as gas collection system. From physical composition analysis, out of 100 MT of MSW, 87.2 MT of mixed MSW is directly disposed to Dhapa landfill site prior minimal segregation by informal sectors and at household level in existing condition. With the growing population and consecutive waste generation, the life of the Dhapa landfill site has shattered with passing years. Besides, around 100–150 MT of waste is disposed per day at Garden Reach landfill site with a gross landfill area of 3.52 ha (Chattopadhyay et al. 2009b; CPCB 2012).

Major Disparities and Remedial Actions

The waste collected by both departmental vehicles and hired vehicles are disposed to Dhapa landfill without any segregation of bio-degradable and inert. The bio-degradable organic fraction generates foul gasses like CO_2, CH_4, and H_2S and pollute the environment as well as harmful for the human health. The Greenhouse gas emission is taking place in uncontrollable manner due to open dumping with being treated properly. There is also absence of any sorting or segregation system. Hence the fraction of recyclable present in the waste is very less. Handpick recycling takes place by some informal sectors i.e. rag pickers. Government proposed two-bin system for segregation at household level. But due to less promotion of awareness and improper management, it did not take place for longer time. Due to presence of more than 60% of bio-degradable organic fraction which are of low calorific valued and high moisture content, the energy generation from the mixed waste is inefficient. Proper segregation will give separate proportion of bio-degradable, inert and recyclable. In the present scenario, there is absence of any incinerator based plant/Refuse Derived fuel (RDF)

plant however a composting plant has been established in the year 2000. But it has not been fully functional since 2003 due to presence of high inert content in the unsegregated waste. A composting plant can generate compost from bio-degradable waste which will reduce pollution and generate revenue. Same is applicable for the incineration plant which will help in generation of energy by thermal processing of high calorific valued inorganics. The Dhapa landfill has been exhausted due to the legacy waste of last 30 years. So there is a need of engineered landfill consist of liner, proper cover, biological and thermal processing plant along with sorting system.

4 Implementation Approach

4.1 Integrated Municipal Solid Waste Management

In accordance with the Solid Waste Management Rule, 2016, KMC requires setting up a dynamic and economical Integrated SWM system in Kolkata city. Due to improper MSW management system, the rate of pollution generation is on growing trend worldwide and causing a subsequent disruption of environmental and economic sustainability. An appropriate municipal solid waste management consists of sorting and segregation of wastes at source, recycling, waste treatment through incineration, composting, biomethanation, pyrolysis, gasification, anaerobic digestion and safe disposal of wastes to engineered landfill to retain a sustainable environment. Integrated Solid Waste Management (ISWM) will help to segregate the compositions from the mixed waste. Those segregated waste will be treated in their respective treatment process like biological process for the bio-degradable organic fractions will lead to methane entrapment as biogas and will be used as fuel. Apart from that, compost made from this process can be sold to generate revenue. Incineration or other thermal processing will decrease the inert portion and will lead to generate energy which can be further used to generate electricity. From pollution perspective, Greenhouse Gas emission will get reduced due to very less disposal of waste as disposable waste will contain only the inert portion. Thus by implementation of ISWM, sustainable and economically viable waste management system can be achieved.

4.2 Landfill Reclamation and Reuse Potential at Dhapa Landfill

Reclamation of land area and valuable resources from old landfill site is commonly known as landfill mining which has been popularizing worldwide since 1953 (Savage et al. 1993). Successful implementation of landfill mining as a medium of expansions of landfill capacity and curbing high land acquisition cost have been reported by US Environmental Protection Agency (USEPA) through reclamation projects at

municipal landfill sites across the USA as well as in Netherlands, Canada and UK. An assessment study of extracted aged waste from three test pit location for analyzing the suitability of material as a landfill cover (Khan 1994). Analysis of twenty five years long legacy waste in Dhapa suggests that more than 60% landfill recovery possibility is there. So, implementation of Bio-mining in the exhausted landfill, followed by reclaiming the total acquired land area for the sole purpose of constructing a new engineered landfill site is one of the prime aim of this model study.

5 Methodology

5.1 Linear Program Modelling and Major Assumptions

For getting the optimized solution in case of cost and pollution generating from various processing units and landfill site, a cost optimization mathematical model has been developed taking into considerations of rate of waste generation, their composition, mode of transportation, reuse and recycling, revenues generating from waste processing, waste disposal to safe landfill sites. The model includes some major constraints like waste flows and mass balance, processing plants capacity, recycle amount, engineered landfill capacity, capacity of transport vehicle, number of trips, and pollution generation from different elements of waste management. The basic objective function is a cost optimization function where the pollution generation from greenhouse gases have been incorporated for pollution impact study along with economic aspects. The linear programming model integrating different functional elements can be solved using LINGO optimization software. The model is strictly based upon some assumptions i.e. two bin system at source, borough centers as waste generation points, a central sorting system for waste recycling, zone wise borough distribution, usage of thermal and biological processing followed by engineered landfill sites, maximum and minimum number of trips for waste transportation, maximum and minimum waste fraction limit for vehicles collecting waste from each borough however excluding the environmental costs of processing units and landfill sites followed by waste collection cost. One of our major assumption consist as the Dhapa landfill site is exhausted with its legacy waste, so landfill mining is required here and landfill reclamation will take place as an option to construct an engineered landfill site. The landfill includes a transfer station which is located at UttarpanchannaGram (22°32′02″ N, 88°23′50″ E), near Science City region of east Kolkata (Paul et al. 2015, 2019). The central sorter and all the processing units will be situated at the transfer station and the processed rejects, inert and ash will be collected by TATA LPT 2518 Heavy Duty trucks whereas the silts/rubbish and inert are transported directly to the landfill site by TATAT LPT 2518 trucks. In this model, the waste is initially collected by departmental and hired vehicles from the borough and silts are collected by hired vehicles only. Then the garbage is transported to transfer station from 16 boroughs

and the silts are transported directly to the landfill site. Certain percentage of recycling is done at the borough by rag pickers. The garbage at the transfer station are first go through central sorter where the sorting process takes place by various process and equipments include conveyor belt, trommel screen, air separator, magnetic separator, crusher along with manual sorting etc. From central sorter, recyclable are sent for recycling process and the bio-degradable and non-biodegradables are sent for further processing whereas the inert from the sorter are sent directly to the landfill site. The bio-degradable organic fraction are sent for biological process where windrow composting or anaerobic digestion will take place to make compost from the waste and methane entrapment takes place as biogas which is further used as fuel to generate revenue. Apart from that, non-biodegradable fraction are burnt in the thermal processing to generate energy from the waste. Biological and thermal processing units are consist of pre-sorter which help in further sorting operation of waste to get segregated for better treatment quality. The process rejects generated from both biological process and thermal process are sent directly to the landfill site (see Fig. 1).

Objective Function and Linear Programming Equations

The basic objective function is a cost optimization function considering total SWM cost (SWcost), Landfilling cost (LFcost), total Transportation cost (TRcost), Incentive cost (INCVcost), sorting cost (SORcost), incineration cost (INCNcost), composting cost (COMPcost), Fuel cost (FLcost), Fixed and Idle cost (FXDcost and IDLcost), and cost from revenue generation (RRECYcost, RINCcost and RCOMPcost). Total SWM cost is calculated by the addition of total Transportation cost, landfilling cost, incentive cost, sorting cost, incineration cost and composting cost.
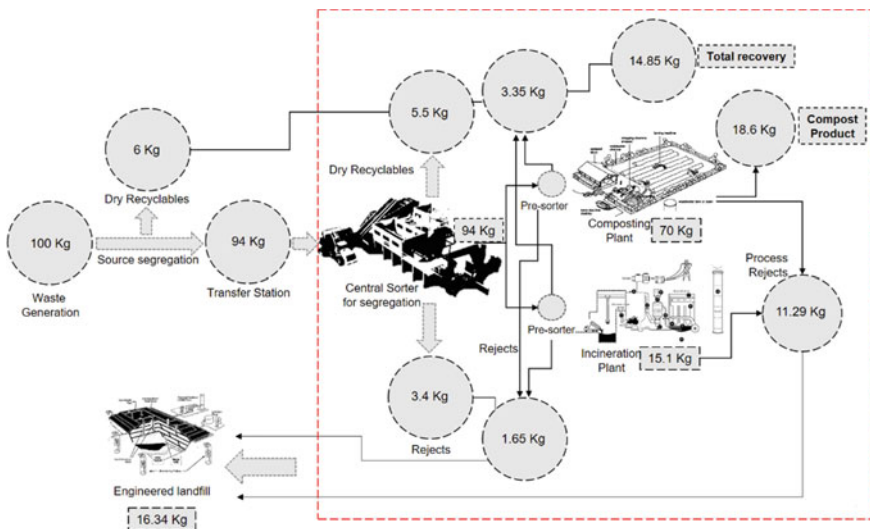
Fig. 1 Material balance flow chart of integrated waste management model

Revenue generated from recyclables, by selling cost and energy generated from incineration has been incorporated in the calculation of waste management cost. The model has been developed by generating linear programming equations using LINGO optimization software. Then the model has been validated from 2007 dataset (Savage et al. 1993) and multi-objective optimization has been done for reduction of both cost and pollution.

5.2   Calculation and Analysis

This paper represents an estimation of probable cost of different ISWM segment followed by optimization and calculating direct GHGs (CO_2 and CH_4) with subsequent minimization. In the existing SWM system of Kolkata, transport sector and landfill site contribute towards the generation of GHGs e.g. CO_2, CH_4 etc. Although, in case of proposed ISWM system, incinerator plant and composting plant play the major role for the potential GHG generation. Minimizing the potential GHG reduces the risk of future climate change problem as well as global warming effects. Various input data regarding cost, pollution have been incorporated as follows.

Transport Sector

In addition to waste disposal, waste transportation is an extensive aspect of both incurring cost and generating air pollution. Transportation cost includes fuel cost, incentive and fixed cost. Different set of input data regarding this cost have been contemplated considering present diesel price, vehicle condition, fuel consumption and distance of different boroughs from transfer station and landfill site. The major potential GHG generates from this sector is CO_2. Other pollutants to be considered here are CO, NO_x and SO_2. The emission is considered from six types of departmental vehicles i.e. Dumper placer Type-1, Dumper placer Type-2, Tipper truck, Compactor Type-1, Compactor Type-2 and Compactor Type-3 along with the hired vehicles which transport the wastes from boroughs to Dhapa landfill in KMC area for the existing system. Although a heavy duty LPT truck has been incorporated for the proposed system which will transfer the process rejects coming from the processing units as well as the silt/rubbish from the transfer stations considered to the disposal. The CO_2 gas generation rate (gm/MT/trip) is calculated indirectly assuming a weighted average emission factors (gm/km) for CO for different departmental and hired vehicles. The estimate depends on the total fuel consumption and % carbon (87%).

Landfill Sector

The garbage generated is 90% of the total waste and rest of the 10% is inert silt or rubbish in the Kolkata waste generation system. Due to high percentage of biodegradable fraction i.e. organic content and less portion of recyclable materials as well as presence of inert materials leads to low energy content of the commingled waste at landfill site (Chattopadhyay et al. 2009b). Reusing the reclaimed land area after

landfill mining suggests that maximum landfill capacity of 5000 MT/day may be operated in an engineered manner. Assumed cost of landfilling including land cost is 197.5 Rs/MT. This disposed garbage generates gaseous pollutants like CH_4 (47.7%), CO_2 (47%), H_2S (0.01%) v/v along with some small amount of toxic VOCs. The presence of high moisture content causes CH_4 generation. The average gas generation rate is taken as 150 m^3/MT of total waste (Chattopadhyay et al. 2018). In the current study, the rate of CH_4 and CO_2 generation (w/w) for the existing system has been considered as 46.82 kg of CH_4/MT of waste and 126.87 kg of CO_2/MT of waste respectively. In case of proposed system, due to high inert content and engineered landfill, the gas generation is considered as nil.

Thermal Processing

As, there is no incinerator/RDF based plant available in Kolkata for the existing scenario, there will not be any gas generation for this case. Operational cost of incinerator is considered to be 689 Rs/MT, although revenue earned from the pre-sorted recyclables are 50 Rs/MT. In pollution aspect for the proposed system, other than the major gas i.e. CO_2 generated from the incinerators burning MSW can also produce NO_2 and SO_2, a number of pollutants in the flue gas in varying concentration like CO, PM containing heavy metal compounds and dioxins due to incomplete or partial combustion. The rate of CO_2 gas generation (w/w) from the incinerator is considered as 888.3 kg of CO_2/MT of waste.

Biological Processing

More than 60% of MSW is biodegradable with high moisture content that highly enables its biological processing either aerobically or anaerobically. For this model study, aerobic composting through windrow has been acquired. Due to irregular operational activity and smaller capacity of the existing composting plant in Kolkata, the gas generation for the existing system from composting is taken as to be nil. For proposed system with 5000 MT/day capacity of composting plant, as windrow composting method has been considered, due to microbial activities during the composting process, the major gases generated from windrow composting are CO_2, CH_4, N_2O and NH_3. N_2O after oxidation is converted to NO_2. The GHG gas generation rate from windrow composting of MSW is considered as 206.88 kg of CO_2/MT of waste, 9.098 kg of CH_4/MT of waste. Operational cost of composting facility is presumed to be 269 Rs/MT and selling price of compost is fed as 3000 Rs/MT.

6 Result and Discussion

6.1 Cost Optimization

In the existing SWM system, the total SWM cost is 2507238 Rs/day. Around 77% of total garbage fraction is carried by departmental vehicles and the rest 23% garbage is

carried by hired vehicle and all the silts are carried by hired vehicle only. Maximum amount of waste is generated from Borough 10 i.e. around 550 MT/day and movable compactor D5 carries maximum fraction (34.15%) of garbage. So the Compactor Type-2 contributes in generating maximum fuel cost which is around 181,833.1 Rs/day. As there is absence of any sorting station, incineration and composting plant, so the processing cost of sorting, incineration and composting are not included. But due to open dumping, the landfilling cost is as high as 427,499 Rs/day. The cost optimization linear programming model was initially validated with 2007 KMC datasets which gave 7.5% cost reduction possibility. After implementation of the cost optimization model with integrated waste management system over the existing scenario, the total SWM cost has been minimized by 43%. Although due to incorporation of transfer station at a distance 7 km from the Dhapa landfill site along with heavy duty truck for transporting silt, rejects and ashes to proposed engineered landfill Dhapa, total transportation cost along with incentive and fuel cost have been increased by 18, 7 and 9% respectively. Due to presence of incineration and composting plant, open dumping fraction has been reduced which ultimately results in reduction of landfilling cost by 48%. Around 35.58% of total garbage is carried by Compactor Type-2 which results in maximum transportation cost among all the departmental vehicles i.e. 591,389.4 Rs/day. Due to processing of bio-degradable fraction at the compost plant and processing of non-biodegradable fraction at the incineration plant, revenue is generating which is not present in the existing scenario. Revenue from composting is maximum i.e. 2,319,356 Rs/day as the production of compost will be 773 MT/day. Apart from that, revenue will also be generated from sorter plant and thermal processing which is around 105,199 Rs/day and 436,130 Rs/day (see Fig. 2).

Effect of Vehicle Optimization

Further, vehicle optimization has been done where number of each types of departmental vehicles has been reduced. 70% cost reduction is possible due to implementation of vehicle optimization. The percentage of optimized departmental vehicles are Dumper placer Type-1 (31%), Dumper placer Type-2 (78%), Tipper Truck (46%), Compactor Type-1 (46%) and Compactor Type-2 (26%) with no reduction in number of Compactor Type-3 keeping the garbage carrying quantity constraint by different vehicles from different boroughs. By making the number of vehicles optimum, around 16% transportation cost, 57% fixed idle cost and 42% fixed running cost minimization has been achieved. As the number of vehicles has been decreased, so to carry equal amount of waste, the number of trip must be increase. So the fuel cost and incentive cost has been increased by 9 and 72% respectively. The maximum percentage of transportation cost reduction has been seen in Dumper placer Type-2 (73.2%) due to 78% vehicle optimization but fuel cost has been increased by 2.8% (see Fig. 2).
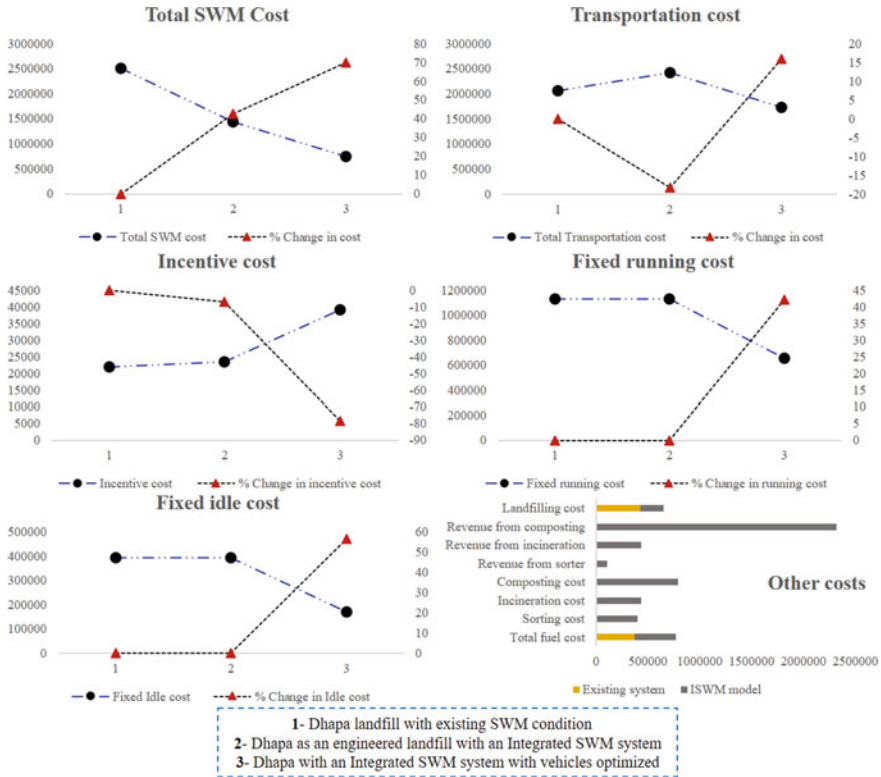
Fig. 2 Comparative analysis of different cost of SWM and their percentage change

6.2 GWP Minimization

The contribution towards GHG emission from transport sector of the present SWM system of Kolkata is especially originated by CO_2 emission (4716 MT/year). Incorporation of ISWM system however, leads to a smaller increase (6%) of CO_2 emission from only departmental vehicles but with a 12% decrease in hired vehicles (see Fig. 3). The CH_4 generation for existing system of Kolkata is contributed only from landfill site Dhapa which has drastically decreased by the conversion of non-engineered to engineered landfill site. The only small amount of CH_4 is generating from the compost processing whereas the value for landfill site is considered as nil. It has been possible to reduce the CH_4 emission up to around 87% which is substantial. Although overall emission of gases contributing GWP have increased in proposed system by around 51% by wt. due to 98% by wt. emission of CO_2 from the incinerator and composting plant. But overall GWP reduction (CO_2e) in case of proposed ISWM system is calculated as around 65% as CO_2-eq which is considerable amount. This overall reduction of GHG has possible by that substantial reduction of CH_4 in proposed ISWM condition (see Fig. 4).
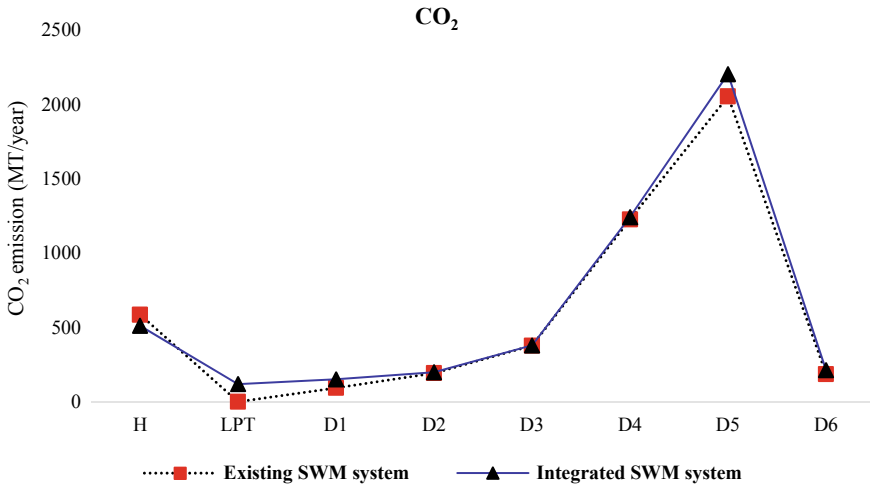
Fig. 3 Comparative study of Carbon dioxide (CO_2) emission in both SWM system
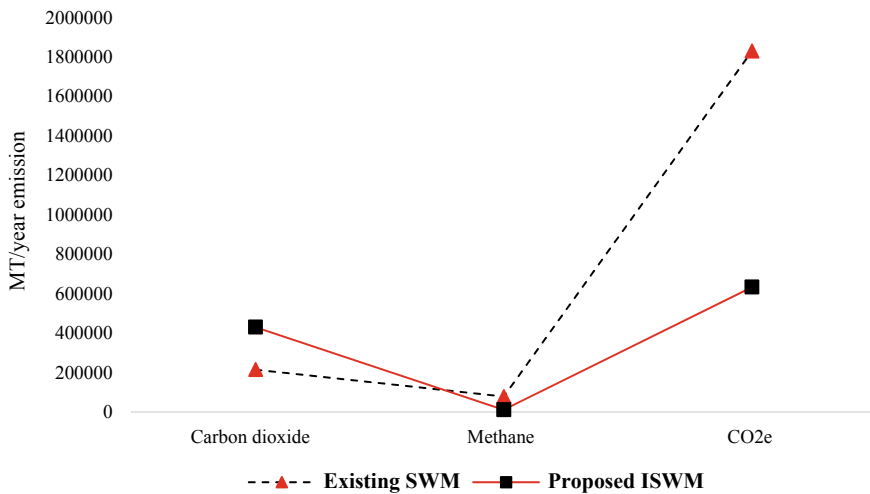
Fig. 4 Comparative analysis of Carbon footprint (CO_2e) in both SWM system

7 Conclusion

Rapid urbanization, economic development and massive rate of population growth are increasing the management process complex and in turns enhancing the quantity of solid waste for developing countries like India. Due to unplanned urbanization and heavy population demand, most of the Indian cities are experiencing such scarcity in a proper waste management venture. Previously, due to small population demand,

the waste was simply acquired in nature. But waste management now a day have been very crucial for the mega cities due to lack of proper planning of route selection, waste collection system, improper waste management, lack of proper Material Recovery Facilities (MRF), absence of proper processing facilities and open uncontrolled dumping of MSW is leading to consequent pollution generation both in air, water and soil. Generation of toxic gases, GHGs from vehicles, landfills are causing global warming which not only causes the destruction of resources but also the social and environmental sustainability. To meet the need of a sustainable environment, SWM rule 2016 implies the requirement of an Integrated SWM system to minimize the economic and pollution aspect in a sustainable manner. Thermal and biological processing play a very significant role in this aspect to manage the MSW wisely. Proper segregation of solid waste prior to the processing leads to simultaneous generation of valuable recyclables and secondary resources for industrial activities. Resource extraction should be mandatory for any integrated waste management plant for revenue generation and pollution minimization. Thermal processing leads to generation of electricity. However, biological processing enhances the production of compost if treated aerobically or methane entrapment through anaerobic digestion which in turn generate revenues. The most important aspect is minimization of landfill waste quantity to be disposed by consequent landfill area savings. Hence, this cost effective methodology conclusively delivers an optimized solution for MSW management of any metropolitan Indian city not only to manage the waste economically but also sustainably with less polluted solution towards circularity.

Conflict of Interest   Sayan Banerjee, Shristi Gupta, Samran Banerjee and Amit Dutta declare that they have no conflict of interest during this work.

References

Annepu RK (2012) Sustainable solid waste management in India (Master's Thesis). Columbia University Earth Engineering Center, New York

Badran M, El-Haggar S (2006) Optimization of municipal solid waste management in port said-Egypt‖. Waste Manage 26:534–545. https://doi.org/10.1016/j.wasman.2005.05.005

Bockreis A, Knapp J (2011) Landfill mining—Deponien als Rohstoffquelle. Österreichische Wasserund Abfallwirtschaft 63:70–75

Chattopadhyay S, Dutta A, Ray S (2018) Integrated solid waste management in a metropolitan city. A Thesis by Subhasish Chattopadhyay, pp 164–221

Chattopadhyay S, Dutta A, Ray S (2009b) Municipal solid waste management in Kolkata, India—a review. Int J Integr Waste Manage Sci Technol. Waste Manage 29(4):1449–1458

Costi P, Minciardi R, Robba M, Rovatti M, Sacile R (2004) An environmentally sustainable decision model for urban solid waste management. Waste Manage 24(3):277–295

CPCB (Central Pollution Control Board) (2012) Status report on municipal solid waste management. CPCB, Govt. of India, New Delhi

Daskalopoulos E, Badr O, Probert SD (1998) An integrated approach to municipal solid waste management. Resour Conserv Recycl 24:33–50

Ghose MK, Dikshit AK, Sharma SK (2006) A GIS based transportation model for solid waste disposal—a case study on Asansol municipality. Waste Manage 26:1287–1293. https://doi.org/10.1016/j.wasman.2005.09.022

Guerriero JR (1996) Status of landfill reclamation and its applicability to solid waste management. American Society of Mechanical Engineers, New York

Joshi R, Ahmed S (2016) Status and challenges of municipal solid waste management in India: a review. Cogent Environ Sci 2:1139434. https://doi.org/10.1080/23311843.2016.1139434

KEIP (Kolkata Environmental Improvement Project) (2007a) Outline strategy for solid waste management, KMC-study of solid waste management disposal and public private partnership options. Kolkata Municipal Corporation, India

Khan RR (1994) Environmental management of municipal solid wastes. Indian J Environ Prot 14(1):26–30

Krook J, Svensson N, Eklund M (2012) Landfill mining: a critical review of two decades of research. Waste Manage 32(3):513–520

Kumar S, Smith SR, Fowler G, Velis C, Kumar SJ, Arya S, Rena KR, Cheeseman C (2017) Challenges and opportunities associated with waste management in India. R Soc Open Sci 4:160764. https://doi.org/10.1098/rsos.160764

Kurian J, Nagendran R, Planivelu K, Thanasekaran K (2003b) Dumpsite rehabilitation and Landfill Mining. Technology, Asian Regional Research Programme on Environmental Technology, Chennai, India. http://www.swlf.ait.ac.th/data/pdfs/DRLM1.pdf

Kurian J, Esakku S, Palanivelu K, Selvam A (2003a) Studies on landfill mining at solid waste dumpsites in India. Ninth International Waste Management and Landfill Symposium, October, Margherita di Pula, Cagliari, Sardinia, Italy

NEERI (National Environmental Engineering Research Institute) (2005) Comprehensive characterization of municipal solid waste at Calcutta, India

Ortner M, Bockreis A, Knapp J (2014) Landfill mining: objectives and assessment challenges. Waste Resour Manage 167(2):51–61. https://doi.org/10.1680/warm.13.00012

Paul K, Dutta A, Krishna AP (2014) A Comprehensive study on landfill site selection for Kolkata City, India. J Air Waste Manag Assoc 64(7):846–861. https://doi.org/10.1080/10962247.2014.896834

Paul K, Dutta A, Krishna AP (2015) A comprehensive study on solid waste vehicle routing and tracking—a case study on Kolkata City. KSCE J Civ Eng 20(1):137–144. https://doi.org/10.1007/s12205-015-0214-6

Paul K, Chattopadhyay S, Dutta A, Krishna AP, Ray S (2019) A comprehensive optimisation model for integrated solid waste management system—a case study on Kolkata city, India. Environ Eng Res 24(2):220–237. https://doi.org/10.4491/eer.2018.132

Savage GM, Gloueke CG, Von Stein EL (1993) Landfill mining: past and present. Biocycle 34:58–61

Sharholy M, Ahmed K, Mahmood G, Trivedi RC (2008) Municipal solid waste management in Indian cities: a review. Waste Manage 28:459–476. https://doi.org/10.1016/j.wasman.2007.02.008

Siddiqui TZ, Siddiqui FZ, Khan E (2006) Sustainable development through integrated municipal solid waste management (MSWM) approach—a case study of Aligarh District. In: Proceedings of national conference of advanced in mechanical engineering (AIME-2006), pp 1168–1175, JamiaMilliaIslamia, New Delhi, India

Singh RP, Tyagi VV, Allen T, Ibrahim MH, Kothari R (2011) An overview for exploring the possibilities of energy generation from municipal solid waste (MSW) in Indian scenario. Renew Sustain Energy Rev 15:4797–4808. https://doi.org/10.1016/j.rser.2011.07.071

Van Der Zee DJ, Achterkamp MC, De Visser BJ (2004) Assessing the market opportunities of landfill mining. Waste Manage 24(8):795

Vilms M, Voronova V, Loigu E (2015) Proceedings Sardinia 2015. In: 15th international waste management and landfill symposium. CISA Publisher, S. Margherita di Pula, Cagliari, Italy

Evaluation of Abrasive Wear of Bio-waste Based Silica/Carbon Particulate Epoxy Composites

S. Ojha, V. Pranay, G. Raghavendra, G. Sumithra, P. Divya, B. Anji Reddy, B. Aswani Kumar, and Harsha Vardhan

Abstract In the current perspective of ecological contamination, utilization of biowaste is essential in the recent trends. Among the different bio-waste, Rice husk (RH) is one of the plentiful materials presently having significantly less utilization and more as a landfilling material. This bio-waste, after ample storage, decomposes and creates environmental pollution. Bio silica and biocarbon have had many applications in the recent past. Extraction of biosilica and biocarbon from Rice husk by pyrolysis process and calcination process has many applications in the composite industry. In the present study, an effort has been made to extract silica and carbon from rice husk and reinforce them as a filler material in polymer composites and test the tribological properties of the fabricated composites. The composites are made-up by hand layup technique with filler percentages 2, 4 and 6 wt.%. A Pin on disc equipment is used to investigate the abrasive wear behaviour of silica-based and carbon-based polymer composites. The samples were tested at different loading conditions and different RPMs by keeping the total sliding distance constant and measuring the abrasive wear and coefficient of friction of the fabricated composites.

Keywords Carbon · Silica · Rice husk · Abrasive wear

S. Ojha · V. Pranay · G. Sumithra · P. Divya
Department of Mechanical Engineering, KITS, Warangal, Telangana, India

G. Raghavendra (✉)
Department of Mechanical Engineering, NIT, Warangal 506004, Telangana, India
e-mail: raghavendra.gujjala@nitw.ac.in

B. Anji Reddy
Chemical Engineering, Dr. B R Ambedkar NIT, Jalandhar 144011, Punjab, India

B. Aswani Kumar
Mechanical/Biomedical Engineering, Munster Technological University, Cork, Ireland

H. Vardhan
Mechanical Engineering, PVKK Institute of Technology, Ananthapuramu, Andhra Pradesh, India

1 Introduction

Tribology is the combination of friction, lubrication, and wear principles which includes its studies and applications. Wear is caused by tribological interactions between the solid, the interface material, and the environment, which results in material loss. Annual direct and indirect losses caused by attrition in various industries in the United States account for about 12% of GDP (Gahr and Heinz 1987). So, considering the loss of due to wear, research in this area becomes essential.

The abrasive wear is one of the vital aspects of the tribological behaviour of the composite. The abrasive wear of natural fibre reinforced polymer composites is a critical factor in maximizing their use in various applications. There are several techniques to improve the tribological nature of clean polymer composites in general. Making composites by embedding fibres in polymers is a popular process (Unal et al. 2014; Zhang et al. 2015; Lv et al. 2015).

The adding of PTFE to polymers like polyphenylene sulphide (PPS), polyvinylchloride (PVC), polyacrylate (PA), polyoxymethylene (POM), and polyamide reduced the rate of wear (PA) (Yamaguchi 1990). Bolvari et al. (1997) testified that the PTFE reinforced PPS decreased the wear of polymer astoundingly. Because of incorporating various fillers such as natural, inorganic, and metallic particulates in both full scale and nano levels with polymer, polymer composites' mechanical and tribological behaviour is significantly improved. Friedrich et al. (2005) examined the effect of particle size and filler content on wear analysis.

In addition, agricultural residues in 2013 exceeded 5 billion magnesium, of which 47% of the remaining residues came from the Asian continent, followed by America (29%), Europe (16%), Africa (6%) and Oceania. (21%). So, waste disposal is a central problem for the environment. The biggest challenge today is to find novel ways to use this waste. Between 2003 and 2020, Cherubin et al. (2018) residues were reported, such as leaf litter, straw, rice husk, sawdust, forest waste, leaves, weeds, and other rejected crops' by-products, an increase of about 33%, accounting for total products Percentage.

At the same time, natural fibre has the advantages of economy and environmental friendliness. Rice husk is an agricultural residue used as a natural fibre to develop biocomposite materials. The significant elements of rice husk are amorphous silica and amorphous carbon, which make it highly desirable (Shigetaka et al. 2005; Yamaguchi et al. 2006). Generally, RH is the outer shell that protects seeds or grains. It is made of rigid material, is insoluble in water, abrasive, and has a high cellulose-silica structure. The outer part of the hull is composed of silica covered with a stratum, and the innermost layer contains a small amount of silica.

The tribological behaviour of silica and carbon extracted from RH-reinforced epoxy composites was investigated (Ojha et al. 2021). The tribological nature of RH reinforced epoxy composites was analyzed (Majhi et al. 2012). The majority of research is focused on the tribological behaviour of silica and carbon-based polymer composites.

The study of the bio char for bio energy and composite of this research focuses on the production and characterization of the pyrolytic products (biochar, bio-oil and syngas) for potential bioenergy application.The application of biochar wastewater treating and biochar and bioenergy glass fibre composite material (Dahal 2018).

The use of biodegradable waste from agricultural waste to create ecological constituents with durable properties with tunable properties is fictitious. Thermal stability, hydrophobic characteristics, and mechanical strength were all outstanding in the forged bio-carbon blocks. The compressive strength of these bio-carbon blocks existed around 6.0–7.5 N/mm^2, which is 5–6 times greater than that of commonly used polystyrene packing materials (Joshi et al. 2020).

Carbon block prepared from the agricultural waste of wood apple shell particles at different temperatures (400, 600 °C) and thermoset polymer composite fabrication was studied. The composites were analyzed using spectroscopy. The results showed that the strength of the polymer composites increased as the filler % increased to some different loading at flexural and tensile properties (Ojha et al. 2016).

Comparative investigation of the biodegradability of filler (wood apple-coconut) reinforcement polymer composite susceptible to peripheral outbreaks like solid particle corrosion. Coconut shells are obtained at 78.19 MPa and 15 wt% filler content per wooden apple shell. The wood apple particle compound shows better corrosion and mechanical properties than the coconut particle compound (Ojha et al. 2014).

In this study, calcination and carbonization, silica and novel hard porous carbon material are derived from rice husk. Using Pin-on-disc apparatus, the tribological characteristics for silica and carbon rice husk composite were investigated.

2 Experimental Details

The resin used as the matrix material is Epoxy LY 556. The following are the materials which were employed here.

- Rice husk (RH)
- Silica (SiO$_2$)
- Carbon
- Epoxy resin (LY 556)
- Hardener (HY 951)
- Injection syringe.

2.1 Synthesis of Silica and Biocarbon from Rice Husk

The calcination process is used to extract silica from the rice husk, and the carbonization process is used to remove biocarbon from rice husks in an inactive state. Firstly, the rice stalks were washed with water to eliminate impurities and debris from the
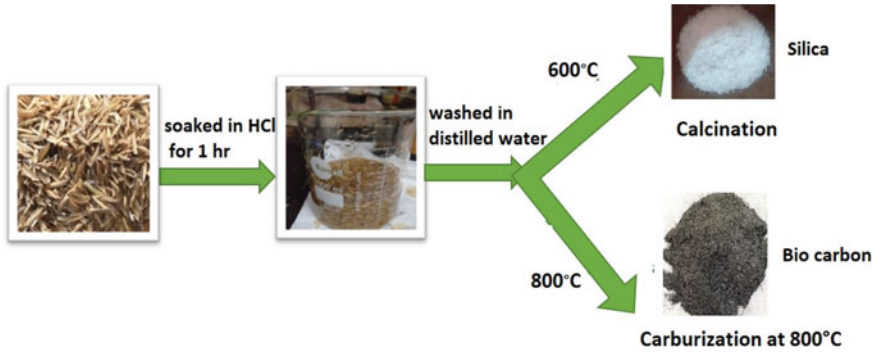
Fig. 1 Fabrication of silica and biocarbon from Rice husk

rice husks. Follow up with 1 N HCl for one hour, rinse with finely ground water to dissolve HCl in rice husks, and moisture content is removed by means of oven which were dried for 24 h. Dried rice husks are heated in a furnace at 600 °C at a rate of 6 °C per minute. After reaching a temperature of 600 °C for the carbon, the silica samples were immersed in this temperature for one hour before cooling.

In the same way, rice husk is carburized at 800 °C in a tubular furnace while an inert atmosphere is maintained to produce biocarbon. Figure 1 depicts the process of making silica and biocarbon from rice husk.

2.2 Composite Fabrication

Different amounts of silica (2, 4 and 6 wt%) were added to epoxy and hardener in ratio of 10:1. The combination was agitated for 10 min with a glass stirrer and put into a syringe mould to obtain a uniform distribution of nano-silica particles. Care was taken in this attempt to make sure no epoxy escapes from mould. The size of the samples is 25 mm long and 10 mm wide. Samples were stored in curing moulds at room temperature for 24 h followed by removing the samples. The cured composites were then tested. Similarly, raw rice and biocarbon composite were prepared. The preparation of samples can be seen in Fig. 2.

2.3 Sliding Wear Behavior

The sliding wear occurs when two interacting surfaces have relative motion between them. Sliding wear is quantified as wear rate, i.e., material loss per unit sliding distance. The effect of the tribological parameters for sliding wear like the sliding distance, sliding velocity and applied pressure on the wear behaviour is reported.

Fig. 2 Method for the preparation of pin sample

Pin on disc tribometer shown in Fig. 3 is generally used to test a material's sliding wear behaviour. The pin and the disc materials are selected based on the potential application of the material to be tested. The pin used in the experimentation generally

Fig. 3 Top view of the pin on disc tribometer with showing counter surface and pin holder

has lower hardness as compared to that of the disc material. This reduces the damage to the disc, and the disc can be reused after polishing its surface. The wear rate of the sample is determined by weighing it before and after the experiment. The volume loss was analyzed using the weight loss of the sample during the investigation, and the volume loss per unit sliding distance was reported using Eq. 1.

$$wearrate = \frac{Wi - Wf}{L \times \rho} \tag{1}$$

W_i and W_f are weights of the sample before and after the experimentation, ρ is the density and L is the slide distance. The sliding wear of a material can be reduced by either improving the lubrication between the interacting surfaces or by increasing the material's wear resistance. The current focus is on reviewing the work done by researchers to improve the materials' wear resistance. The pinon disc shown in Fig. 3.

3   Results and Discussions

Figure 4 shows the effect of filler percentage on the abrasive wear of the natural rice husk/epoxy with the sliding velocity at constants of 400 rpm, load 10 N and time 5 min. It is observed that due to reinforcement addition, the abrasive wear resistance the composites are enhanced. The better wear resistance is seen in the 4 wt% filler addition. Beyond 4 wt%, the wear resistance starts degradation. This may be to poor interface and wettability problems that occurred due to higher filler loading.

Figure 5 shows the effect of biocarbon filler percentage on the abrasive wear of the composites with the sliding velocity at constant 400 rpm, load 10 N and time 5 min. It is observed that biocarbon filler increasing the wear resistance properties.
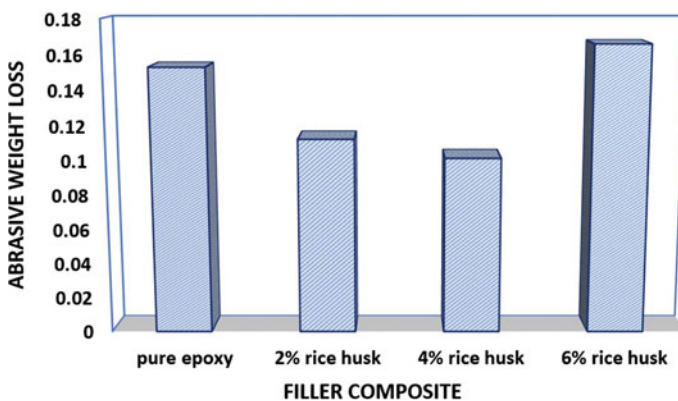
Fig. 4   Abrasive wear of the rice husk filled epoxy composites
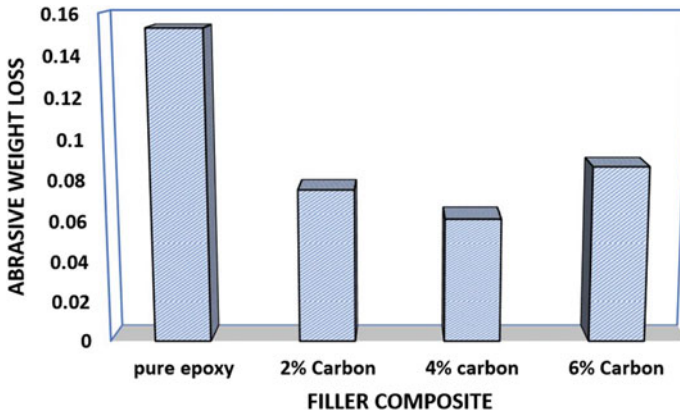
Fig. 5 Abrasive wear of the biocarbon filled epoxy composites

When matched to other composites, 4 wt% biocarbon composite has better wear resistance.

Figure 6 shows the effect of nano-silica filler percentage on the abrasive wear of the composites with the sliding velocity at constant 400 rpm, load 10 N and time 5 min. It is observed that the addition of nano silica with neat polymer enhances the wear resistance. 4 wt% silica composite shows better wear resistance than another composite. Among all the various filler composites, the better wear resistance is observed with 4 wt% nano-silica composite.
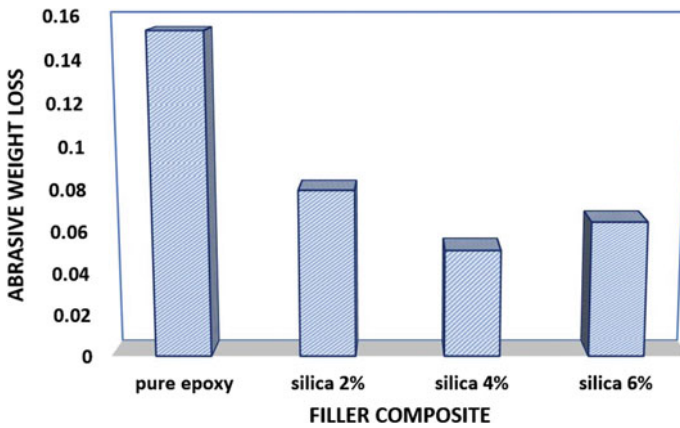
Fig. 6 Abrasive wear of the nano-silica filled epoxy composites

4 Conclusions

In the present investigation Rice husk is used to extract silica and biocarbon and fabricated composites. The wear analysis was conducted. The pure epoxy shows higher wear rate when compared to other composites. The 4 wt% silica composites shows better wear resistance when compared to all other composites. The 4 wt% biocarbon composites shows better resistance in carbon composites. from experimental analysis it can be concluded that the wear resistance of the composite is increased with increase of filler loading.

It was observed that abrasive wear resistance is enhanced with raw rice husk, biocarbon and nano-silica filler with neat polymer. Among all the varying weight percentages of filler 4 wt%, nano-silica filler composite gives better wear resistance than other composites.

References

Bolvari A, Glenn S, Janssen R, Ellis C (1997) Wear and friction of aramid fiber and polytetrafluoroethylene filled composites. Wear 203:697–702

Cherubin MR, Oliveira DMDS, Feigl BJ, Pimentel LG, Lisboa IP, Gmach MR, Varanda LL, Morais MC, Satiro LS, Popin GV (2018) Crop residue harvest for bioenergy production and its implications on soil functioning and plant growth: a review. Scientia Agricola 75:255–272

Dahal RK (2018) A study on biochar for bioenergy and composite applications

Friedrich K, Zhang Z, Schlarb AK (2005) Effects of various fillers on the sliding wear of polymer composites. Compos Sci Technol 65(15–16):2329–2343

Gahr Z, Heinz K (1987) Microstructure and wear of materials. Elsevier

Joshi K, Meher MK, Poluri KM (2020) Fabrication and characterization of bioblocks from agricultural waste using fungal mycelium for renewable and sustainable applications. ACS Appl Bio Mater 3(4):1884–1892

Lv M, Zheng F, Wang Q, Wang T, Liang Y (2015) Friction and wear behaviors of carbon and aramid fibers reinforced polyimide composites in simulated space environment. Tribol Int 92:246–254

Majhi S, Samantarai SP, Acharya SK (2012) Tribological behavior of modified rice husk filled epoxy composite. Int J Sci Eng Res 3(6):180–184

Ojha S, Raghavendra G, Acharya SK (2014) A comparative investigation of bio waste filler (wood apple-coconut) reinforced polymer composites. Polym Compos 35(1):180–185

Ojha S, Acharya SK, Raghavendra G (2016) A novel approach to utilize waste carbon as reinforcement in thermoset composite. Proc Instit Mechan Eng J Process Mechan Eng 230(4):263–273

Ojha S, Pranay V, Raghavendra G, Gara D (2021) Experimental evaluation and comparison of silica/biocarbon particulate-epoxy composites for high-strength applications. In: Proceedings of the institution of mechanical engineers, Part L

Shigetaka W, Weerasak M, Zhemchai H (2005) Survey of the research on the utilization of rice husk and rice husk silica. In: Proceedings of 1st workshop on the utilization of rice husk and rice husk silica, pp 6–14

Unal H, Saylan T, Mimaroglu A (2014) Thermal, mechanical and tribological performance of polymer composites rubbed against polymer composites in application in electrical contact breakers. Proc Instit Mechan Eng Part J J Eng Tribol 228(6):608–615

Yamaguchi Y (1990) Tribology of plastic materials: their characteristics and applications to sliding components, vol 16. Elsevier

Yamaguchi T, Sekiguchi T, Toyoshima H, Kohira E, Shikano SH, Hokkirigawa K (2006) Friction and wear properties of new hard porous carbon materials made from Rice Chaff. In: Proceedings of 3rd Asia international conference on tribology, pp 379–380

Zhang X, Pei X, Wang Q, Wang T (2015) Friction and wear of potassium titanate whisker filled carbon fabric/phenolic polymer composites. J Tribol 137(1):011605

Analysis and Comparison of Mechanical Properties of a Specimen by Using FEA

G. Sumithra, B. Saikumar, Sk. Yunas, T. Srikanth, and K. Raja Narender Reddy

Abstract FEA has become popular with fast digital computers because it is very useful and supportive practice in every design. One of the useful tests to quantify the performance of isotropic materials such as steel is tensile test. Finite Element Analysis (FEA) can pretend stiffness and strength visualizations of an element and forecast the probable behavior under operational conditions. In this project the specimen was developed in CATIA software as per ASTM Standards. Later on, by using software package ANSYS 19.2 is used to perform FEA. The determination of this project is to evaluate the mechanical properties of specimen geometry for different materials. By using static and dynamics analysis, loads and velocity from one side or biaxial sides are subjected with different materials. The materials used in this are PLA (Poly lactic acid or Polylactide) and ABS (Acrylonitrile butadiene styrene). The obtained results were deformation, maximum principal stress and strain, those results were compared so that strength of the specimen for a particular material can be evaluated.

Keywords FEA · CATIA · ANSYS · Polylactide (PLA) · ABS (Acrylonitrile butadiene styrene)

1 Introduction

Material testing will done to recognize the physical appearance and performance of material. Recently the developments are increasing in the use of numerical analysis this is due to the growing demand of limited boundary conditions and design space. It is used to encourage designers to use FEA for analyzing complicated structures and able to solve a large number of a simultaneous equations in a short time with various test conditions and various loads can be applied easily. The tensile test properties were measured during for the development of new materials and process can be compared. It is very helpful because of its flexibility and ability to calculate stress,

G. Sumithra (✉) · B. Saikumar · Sk. Yunas · T. Srikanth · K. Raja Narender Reddy
Kakatiya Institute of Technology and Science, Warangal 506015, India
e-mail: gst.me@kitsw.ac.in

481

strain and deformation at anywhere in the sample. Finite element analysis has become popular with the rapid digital computers because it is very supportive practice in every design. The first model is created in the CATIA with the given dimensions. And the data is transferred to FEA software to analysis it. By the ANSYS we get results like displacements, total deformation, and equivalent stress by applying boundary conditions.

2 Literature Review

Dolgov et al. (2018) showed in his paper that in what way stress state in coating subtract boundary and can effect the mechanical failure of the plasma sprayed coating and especially this struggle to deformation. The purpose is distribution of coated test specimen under tensile stress was considered by FEM. The study was approved that alloy coating sprayed by plasma spraying on steel.

Ashik et al. (2017) evaluated the mechanical features of hybrid composites made of bi- directional jute and glass fiber. Al-Mosawi et al. (2016) shows the trials they determine about the elasticity, flexural strength using static procedures as per ASTM guidelines.

Mahmood et al. (2019) main motivation of this study to simulate numerical results with experiment. This will reduce both the cost and the time required for the experiment tests and preventing manual calculations and avoid excessive design of parts. Anoosha et al. (2018) and Chen et al. (2013) showed the study models of the tensile test samples to assess the effect of changing laboratory conditions and numerical analysis factors on increasing the accuracy of results compare to the experimental results and reduce time and effort by using ANSYS.

Sonzogni and Cardona their point is to introduce an exploratory investigation and a numerical simulation was done on the specimens of SAE 1045 steel by using tensile test. The tentative process was considered specifically for determination of the boundaries associated in exponential plastic strengthening law were given. The finite element model is momentarily introduced for conduct of the incompressible plastic flow to overwhelm the recognized volumetric locking in the mathematical performance is deliberated. It ought to be stated that this FEM formulation is an elective way to deal with present procedures which deals with huge plastic distortion.

3 Standards and Geometry Selection

Standards: The standards are a significant piece of our society, filling in as directions to measure on capacity, quantity, content, extent, value and quality. Some standards appear as an genuine item. The most common standards are AISI, ASTM/ASME, ANSI, DIN, ISO, BS EN, ANSI, JIS, AFNOR, AS.

- Among these standards, ASTM standard specimen were considered for our project as it was used worldwide. The material was selected based upon the application

for the project from the letters specified below, like A, B, C, D, E, F, G. Form that D specimen was selected as it is applicable for plastic materials.

Specimen Selection

- **D includes Miscellaneous Materials**—it contains the standard specimen as per the application. Standards Range for D is ranging from D1-8378. From above reference paper we have chosen "**D638-14 Test Method for Tensile Properties of Plastics**" as our specimen in this project.

ASTM-D638

ASTM D638 is the most plastics strength type of standard specifications which protects the tensile properties of both reinforced and unreinforced plastics. This test technique utilizes standard dog bone shaped/dumbbell examples having thickness of 4 mm. The **ASTM D638** standard estimates the capacity of reinforced and non-reinforced plastics to withstand tensile forces. It is a fundamental test in our current reality where plastic packaging leads the market, since this test can predict the defensive capabilities of the material to tensile forces, which are very normal during shipping and handling just as in different circumstances.

3.1 Dimensions of ASTM D638 Specimen

See Fig. 1.
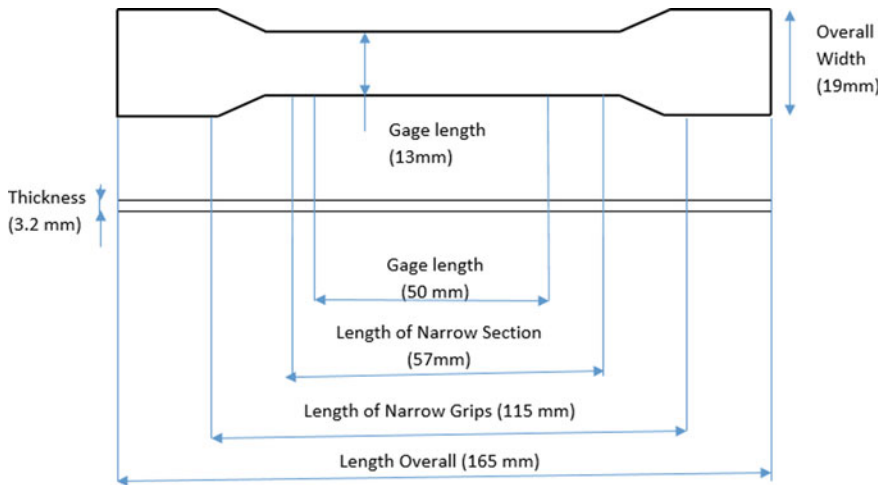
Fig. 1 Dimensions of ASTM D638-Dog bone test specimen

4 Design of Specimen in CATIA

CATIA: Computer Aided Three Dimensional Interactive Application (CATIA). It is designing software, is a multi-stage s/w valuable for CAD, CAE, CAM, created by French company Dassult Systems. It was promoted by IBM Company. It was first named as CATI (Conception assisted tridimensional interactive). Later it was named as CATIA in 1981.

4.1 Specimen Designed in CATIA

See Figs. 2, 3 and 4.

5 ANSYS

ANSYS is Analysis Systems, used for analyzing of the components. In this the model which done in any modeling software like CATIA, CREO, SOLID WORKS, AUTO-CAD etc., the geometry is imported into ANSYS workbench that are meshed or divided into number of same equal parts with small pieces the divided parts are known as elements. This software is generally used to know the behavior of the elements and then this are used to solve them. In this the results are generally compared with the graphical method or tabulate method.

- ANSYS is generally not consider for environment condition of the material which is modelled. This are used to reduce over time and make as quick as possible, the strength can be determined for any metal or any material as well as the break
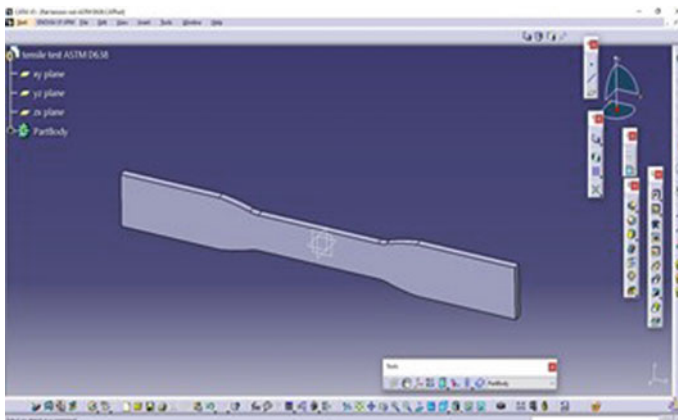
Fig. 2 Isometric view of the specimen ASTM D638
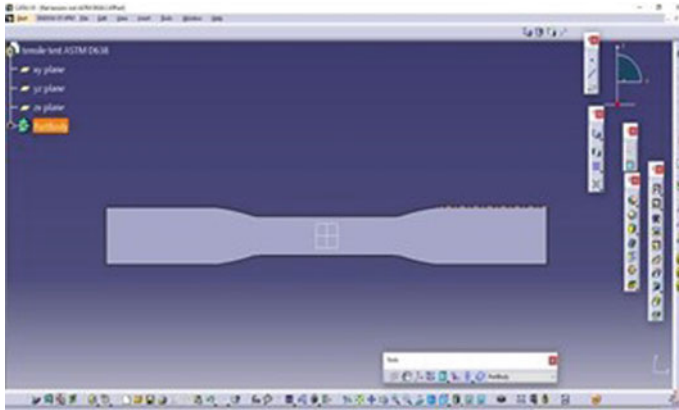
Fig. 3 Front view of the specimen ASTM D638

Fig. 4 Top view of the specimen ASTM D638

down can also be known by applying the forces and some other pressure on the model.

- Following steps are used to solve problem: To solve a problem analytically we need to define the following such as

  (a) **Build Geometry**: A model is said to be constructed in any modeling software and imported or inserted the geometry to work plane system in ANSYS.
  (b) **Define material properties**: A model is applied by the required materials or metals by considering there mechanical and thermal properties.
  (c) **Generate mesh**: In this the model is said to be broken or divided in to small number of elements where there we can find the solution at our required position.

(d) **Apply Boundary conditions**: Once the meshing is done and then we have to select the profile where we have to apply the boundary conditions on the model.

(e) **Obtain solution**: The step generally used to obtain the solution of the given model like total deformation, strain and stress of the model.

Generate the results: After the solution is said to be done we can make the result or compare the result by the following way like graphical method, tabular method and contour plots.

5.1 Materials Used in ANSYS

The following are the materials used in ANSYS.

- PLA
- ABS

PLA: PLA is known as Polylactide. It is one of the biodegradable polymer resulting from lactic acid. It is very simple used in 3D printing and the great outcomes it transports. It involves a minor extrusion temperature. It does not experience huge bends while printing and it holds fast well to the platform and not needed a hotness base. It does not emit an awful smell or poisonous fumes during printing. The melting of it is 175 °C, which gives great surface quality. The material is displayed in yellow color and tensile strength is 51 MPa.

ABS: ABS is known as Acrylonitrile butadiene styrene. It is also a thermoplastic that is tremendously resistant to impact, abrasion and chemical elements. Hibbert et al. (2019) and Vidakis et al. (2016) showed the utilized material in 3D printing which has great mechanical properties, long assistance life and scope of utilizing FDM technologies. The parts made by it can with stand cyclical loads and temperature changes. This material isn't biodegradable and ecosystem. Melting point is 205 °C, which has the fine surface quality. The material is displayed in blue color and tensile strength is 41–45 MPa.

5.2 Explicit Dynamics Analysis Done on Specimen

Steps involved in Explicit Dynamics for ABS Material

- Imported the stp file which is designed in CATIA software.
- **Assigning materials**: In this step required material is assigned (ABS material is assigned).
- **Meshing**: In this the geometry is subjected to mesh and obtained nodes are 370 and elements 144 (Figs. 5, 6 and 7).
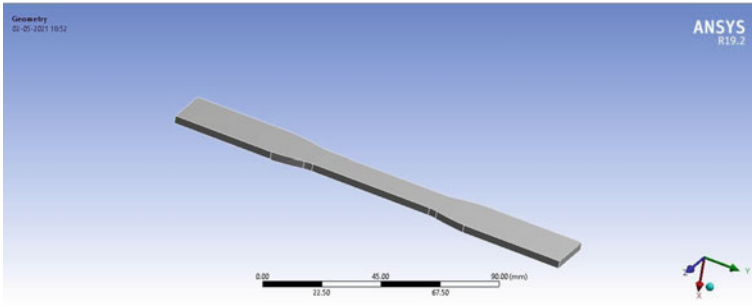
Fig. 5 Specimen imported into ANSYS
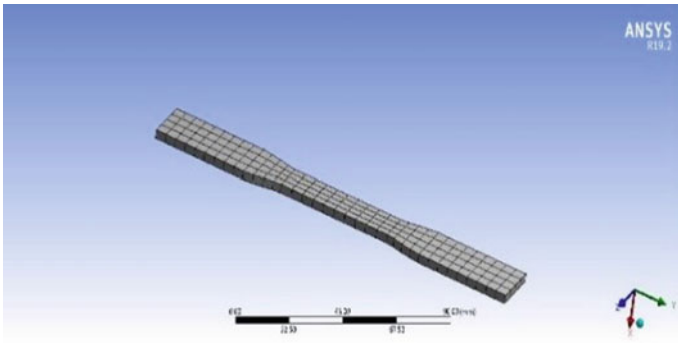
Fig. 6 Meshing
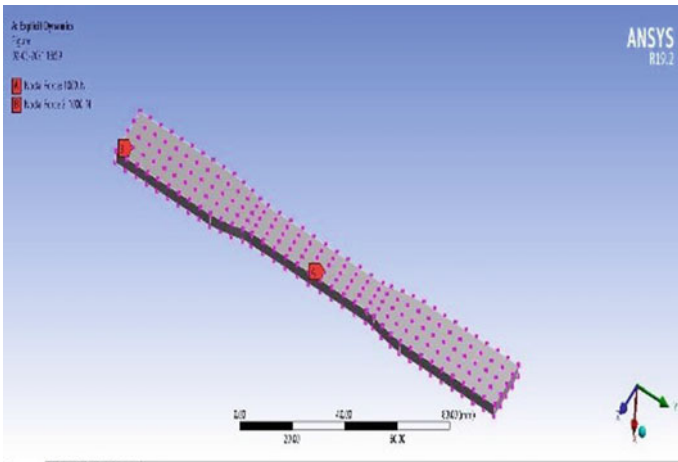
Fig. 7 Nodal forces applied on the specimen

By creating nodes on the specimen it divides into two parts, nodal forces are applied on it varying from 1000 to 5000 N in Y-direction.

Solving: In this step the following results were obtained for ABS Material of Nodal force of 1000 N (Figs. 8, 9 and 10).

- ABS Material for 2000 N (Figs. 11, 12 and 13)

- ABS material l3000 N (Figs. 14, 15 and 16)

- ABS material at 4000 N (Figs. 17, 18 and 19)

- ABS material for 5000 N (Figs. 20, 21 and 22)

In similar process the explicit dynamic analysis is done for PLA material.
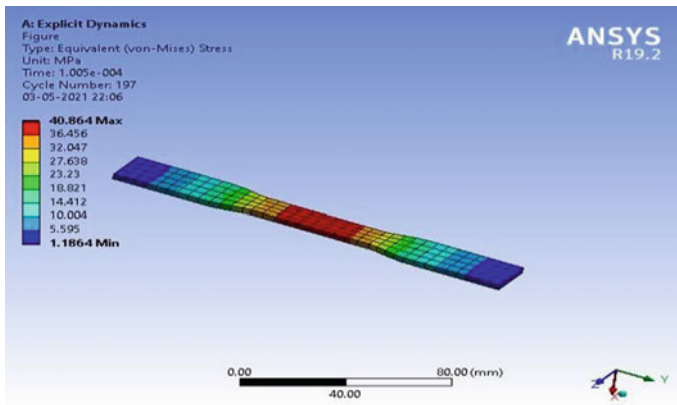
Fig. 8 Max deformation at 0.658 mm for ABS Material at 1000 N
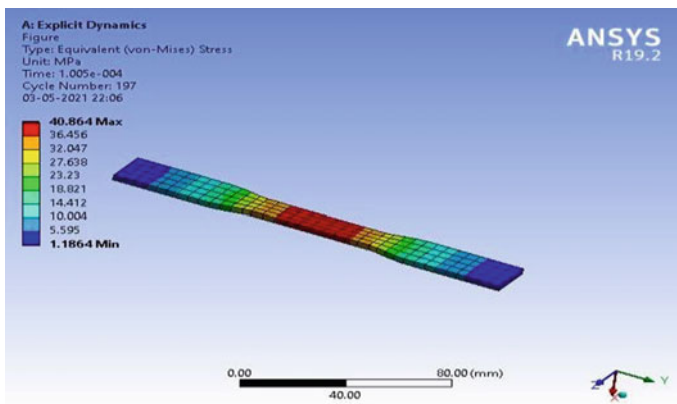
Fig. 9 Max. stress at 42.701 MPa for ABS material at 1000 N
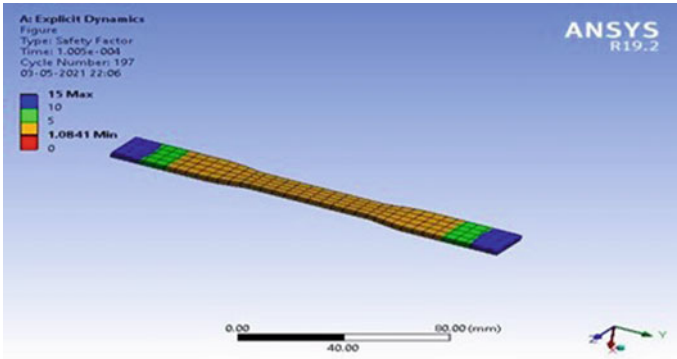
Fig. 10 Safety factor is 1.4 for ABS material at 1000 N
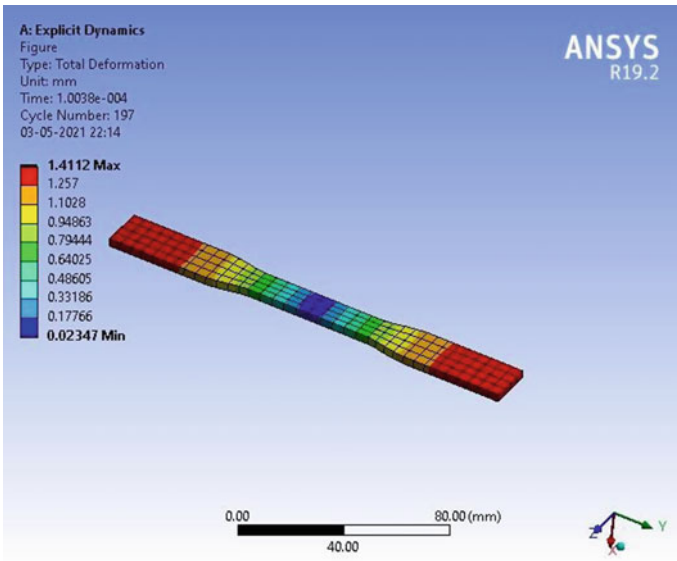
Fig. 11 Max deformation is at 1.32 mm for ABS material at 2000 N

Following are the results for different loads of PLA material.

- PLA material for 1000 N (Figs. 23, 24 and 25)

- PLA material for 2000 N (Figs. 26, 27 and 28)

- PLA material for 3000 N (Figs. 29, 30 and 31)

- PLA material for 4000 N (Figs. 32, 33 and 34)

- PLA material for 5000 N (Figs. 35, 36 and 37)
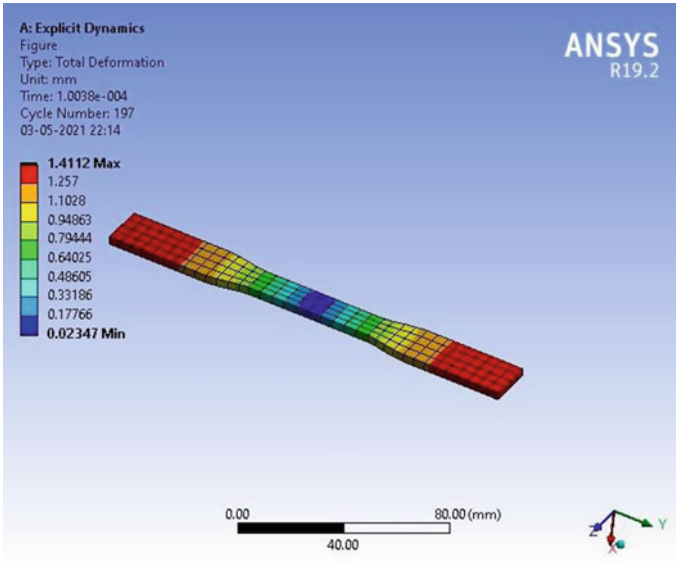
Fig. 12 Max Equivalent stress at 85.36 MPa for ABS material at 2000 N
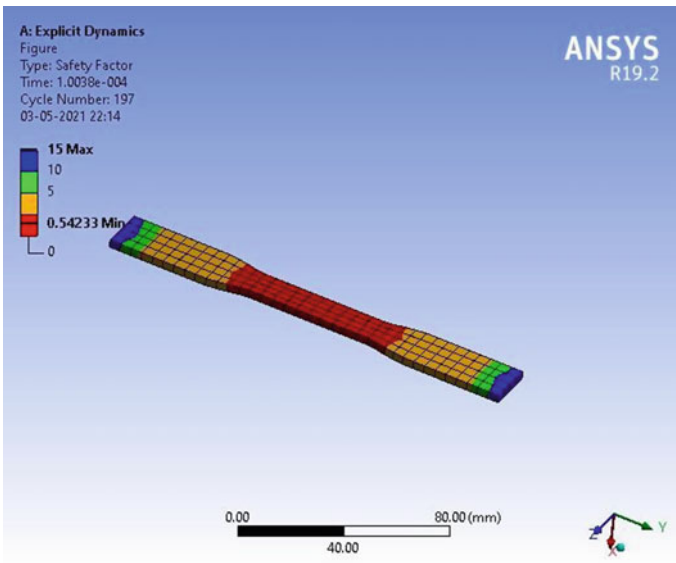
Fig. 13 Safety at 0.54 for ABS material at 2000 N
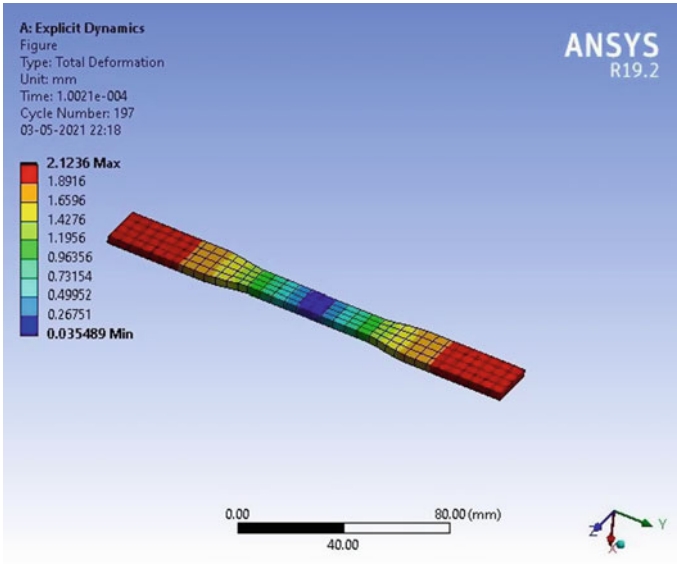
Fig. 14 Max deformation is at 2 mm for ABS material at 3000 N
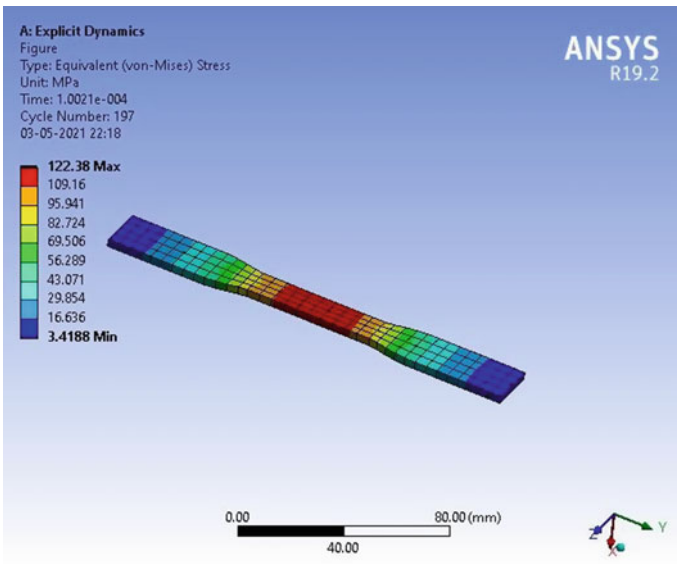
Fig. 15 Max equivalent stress at 129.36 MPa for ABS material at 3000 N
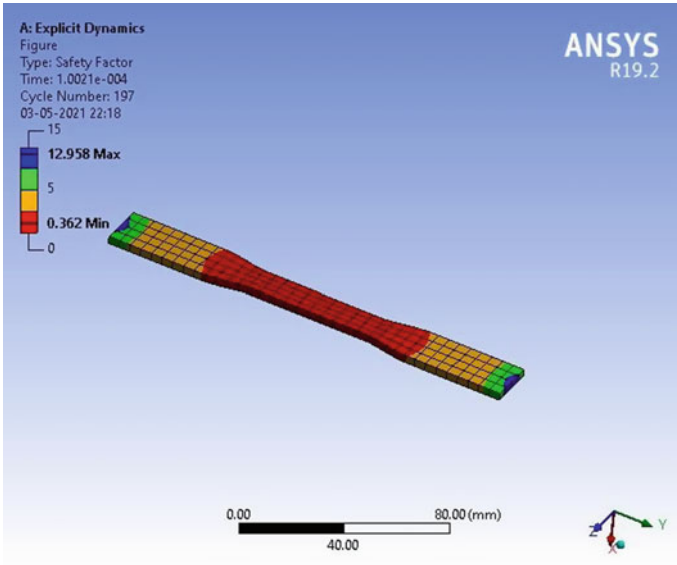
Fig. 16 Safety at 0.46 for ABS material at 3000 N
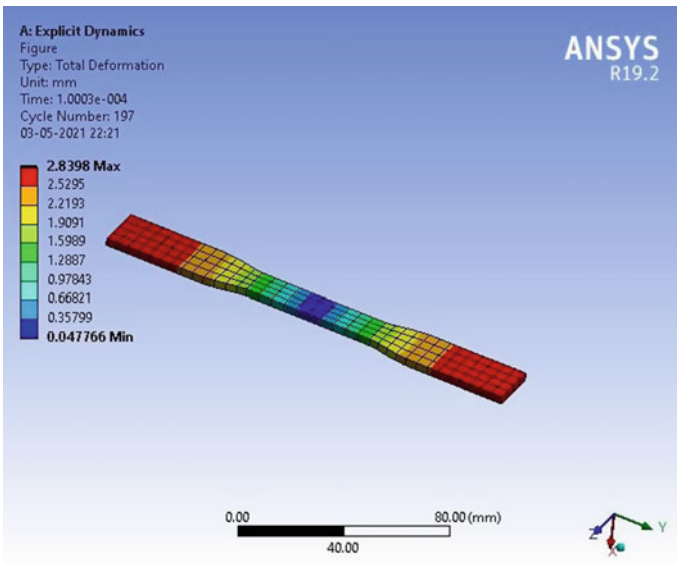
Fig. 17 Max deformation is 2.67 mm for ABS material at 4000 N
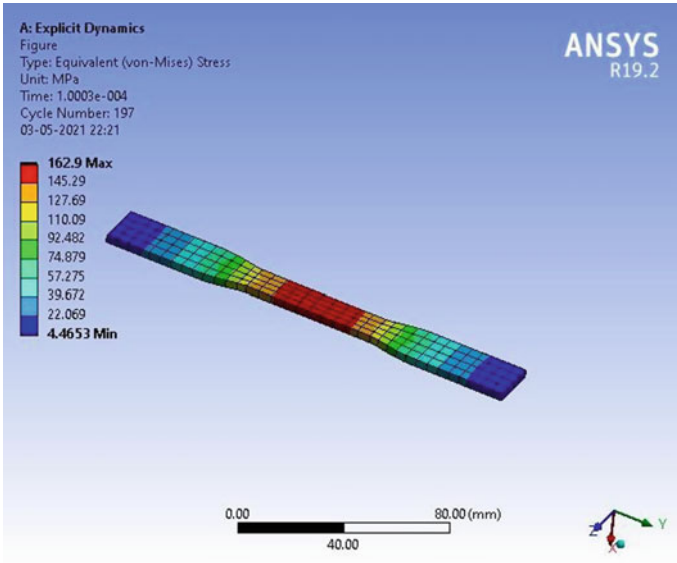
Fig. 18 Max equivalent stress is 172.31 MPa for ABS material at 4000 N
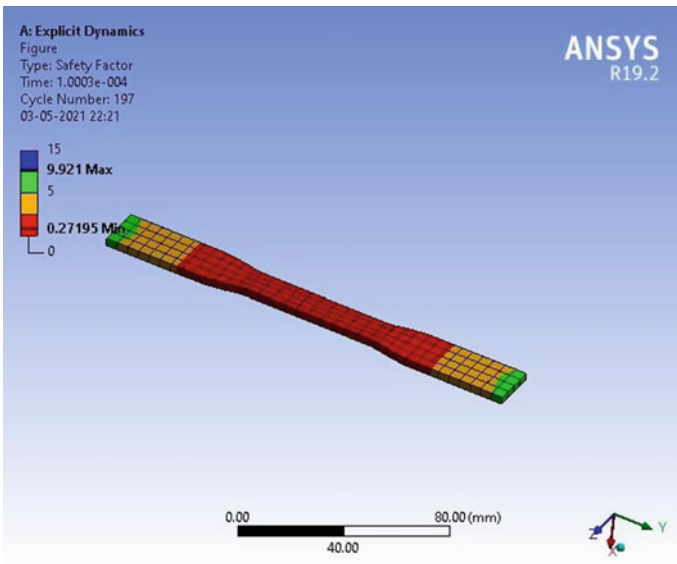
Fig. 19 Safety at 0.34 for ABS material at 4000 N
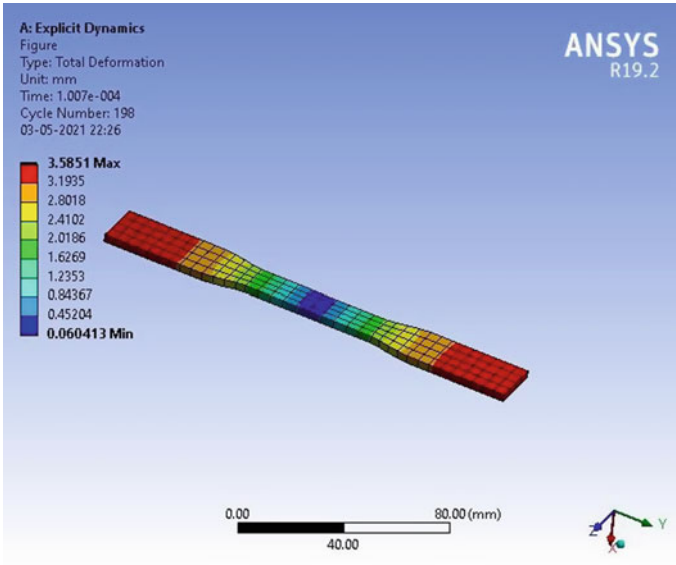
Fig. 20 Max deformation is 3.35 mm for ABS material at 5000 N
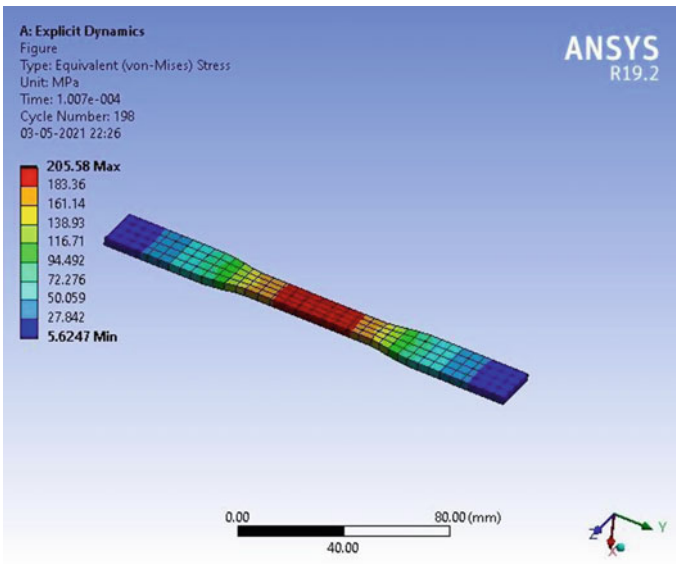
Fig. 21 Max equivalent stress is 215 MPa for ABS material at 5000 N
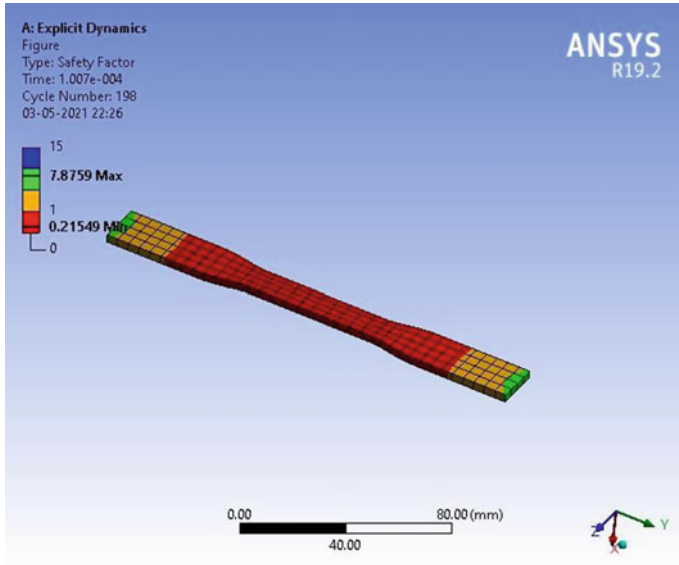
Fig. 22 Safety factor is 0.27 for ABS material at 5000 N
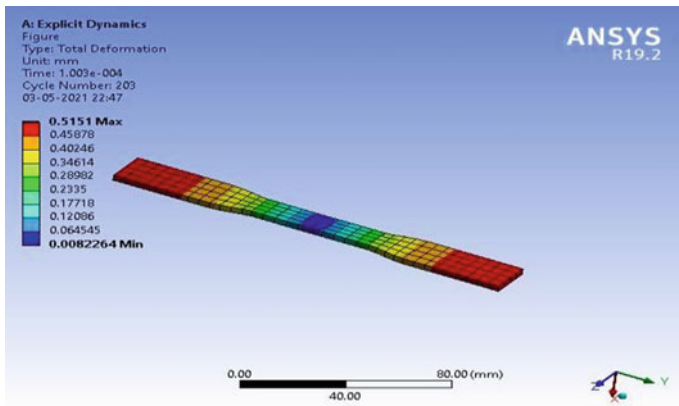
Fig. 23 Max deformation is 0.55 mm for PLA material at 1000 N
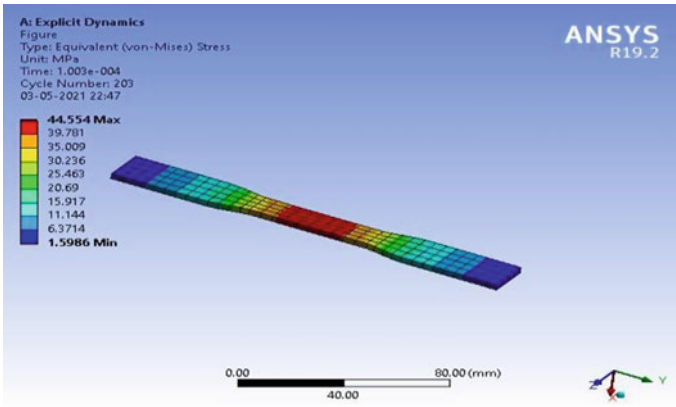
Fig. 24 Max equivalent stress is 43.0 MPa for PLA material at 1000 N
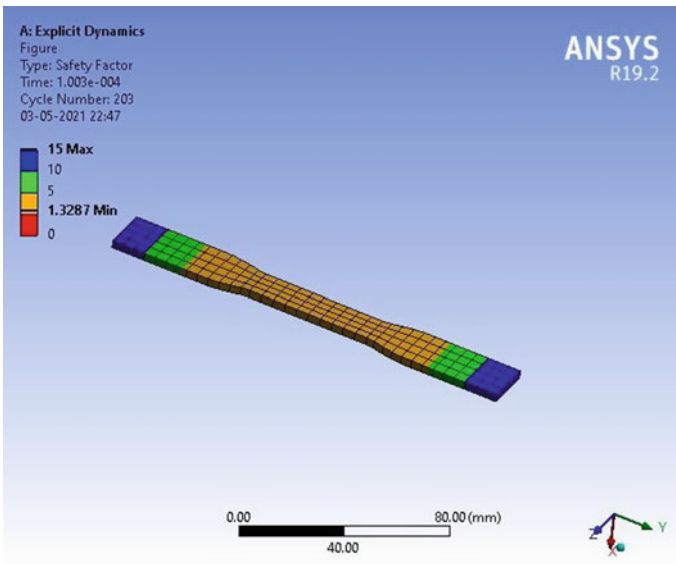
Fig. 25 Safety factor is 1.39 for PLA material at 1000 N
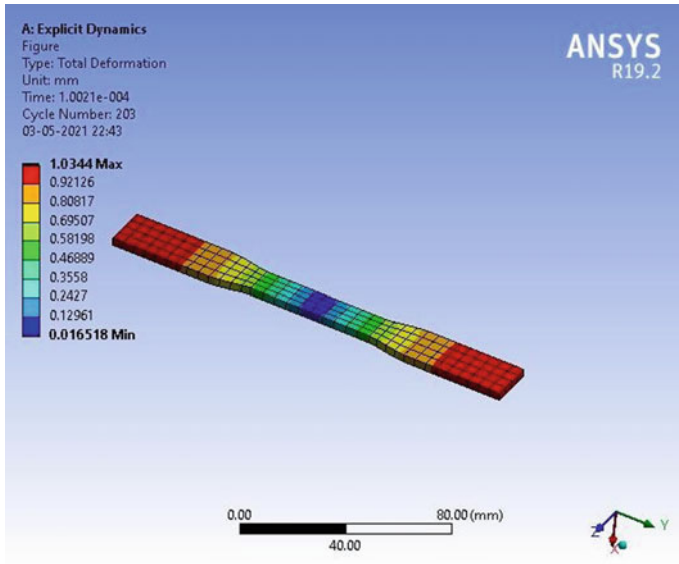
Fig. 26 Max deformation is 1.12 mm for PLA material at 2000 N
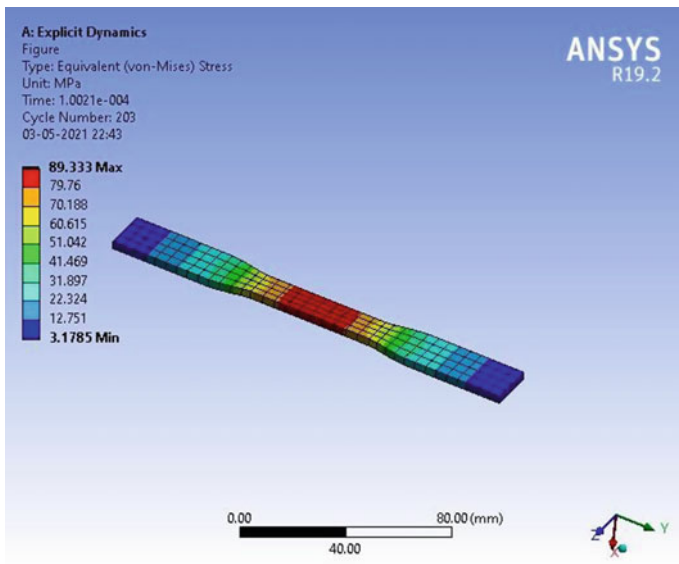
Fig. 27 Max Equivalent stress is 86.01 MPa for PLA material at 2000 N
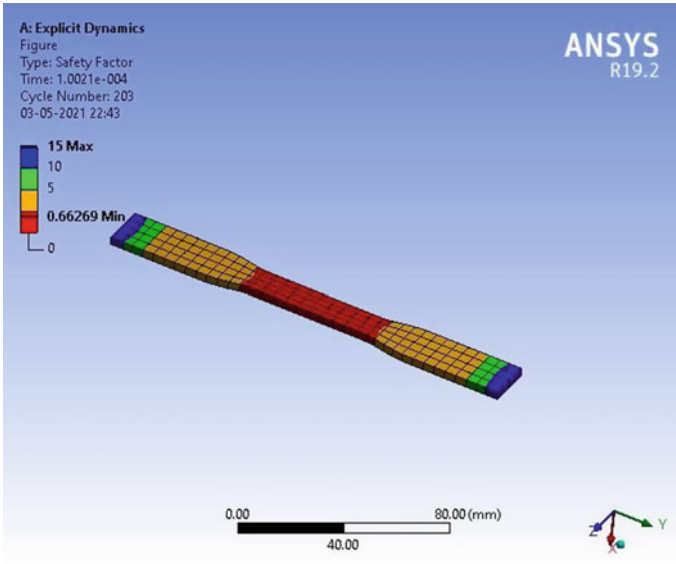
Fig. 28 Safety factor is 0.69 for PLA material at 2000 N
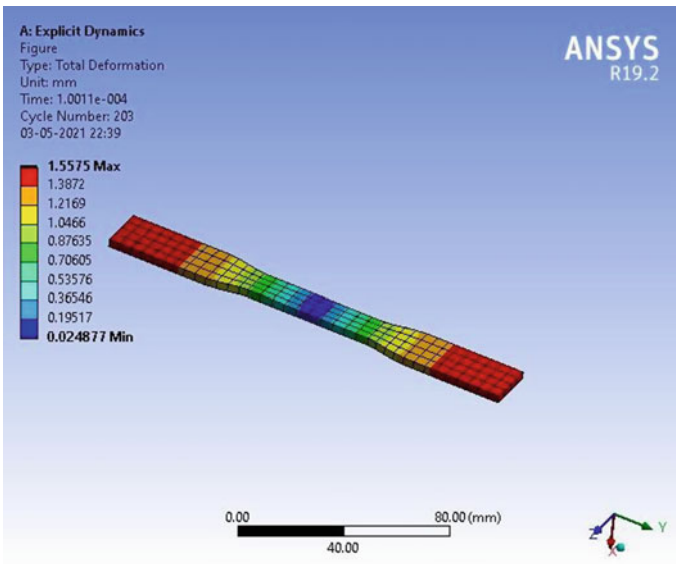
Fig. 29 Max deformation is 1.68 mm for PLA material at 3000 N
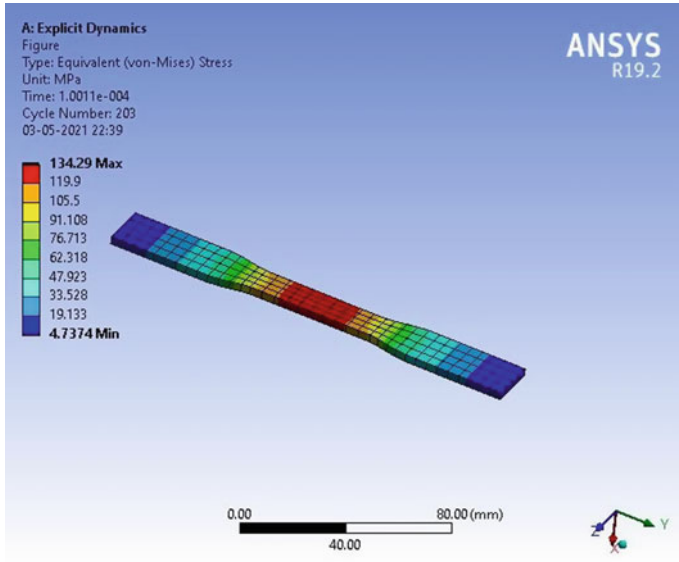
Fig. 30 Max equivalent stress is 128.9 MPa for PLA material at 3000 N
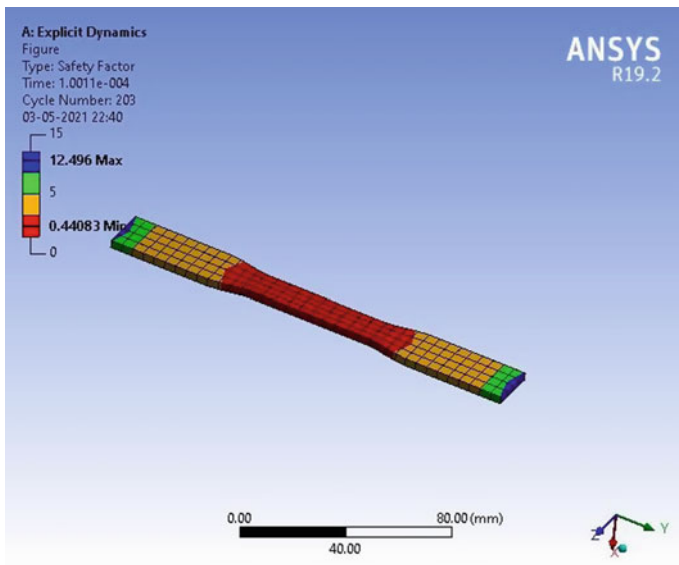
Fig. 31 Safety factor is 0.46 for PLA material at 3000 N
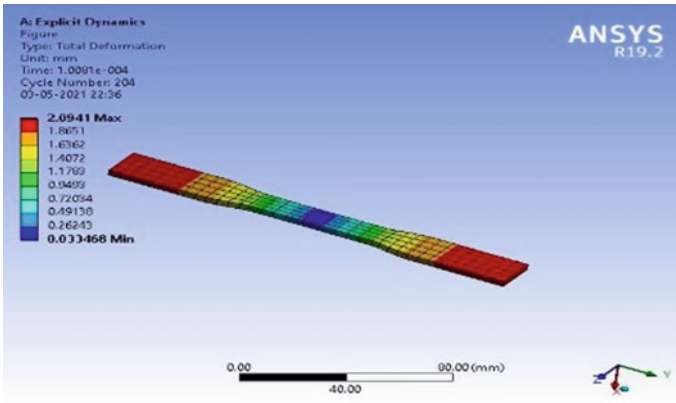
Fig. 32 Max deformation is 2.25 mm for PLA material at 4000 N
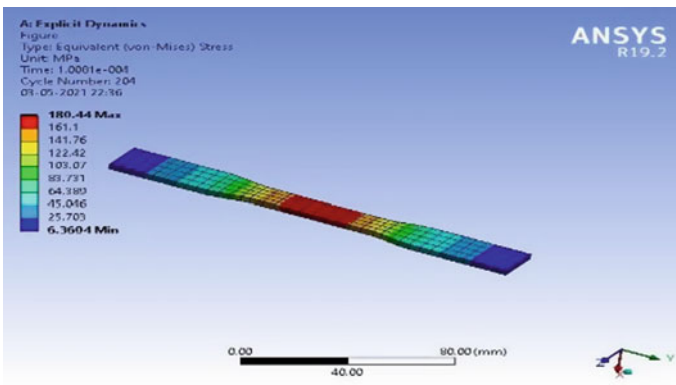
Fig. 33 Max equivalent stress is 171.62 Mpa for PLA material at 4000 N
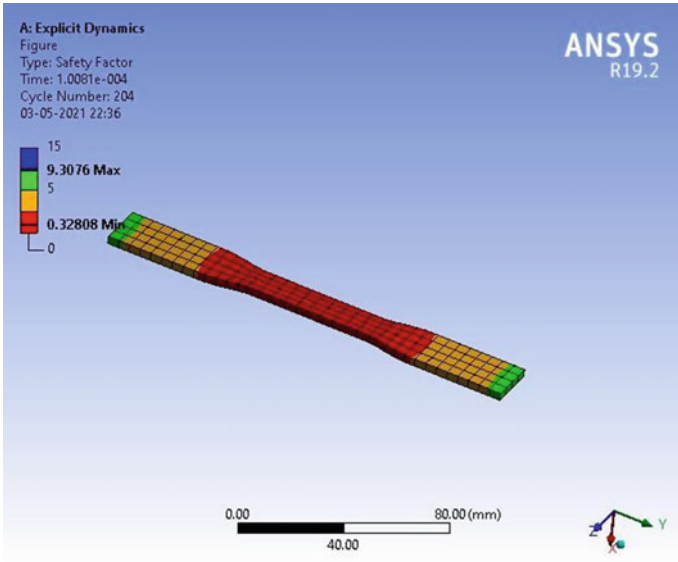
Fig. 34 Safety factor is 0.349 for PLA material at 4000 N
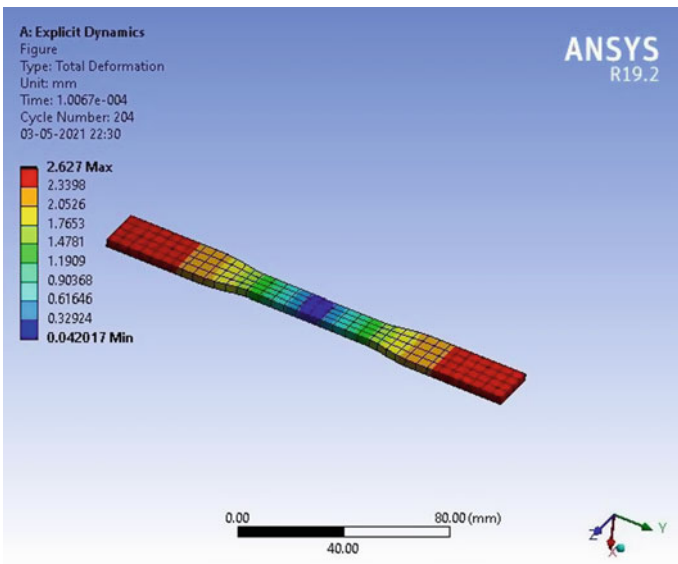
Fig. 35 Max deformation is 3.011 mm for PLA material at 5000 N
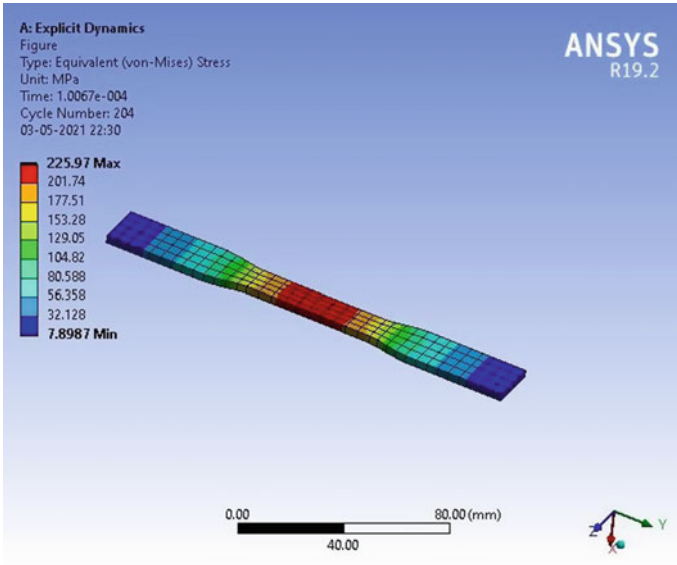
Fig. 36 Max equivalent stress is 193.48 MPa for PLA material at 5000 N
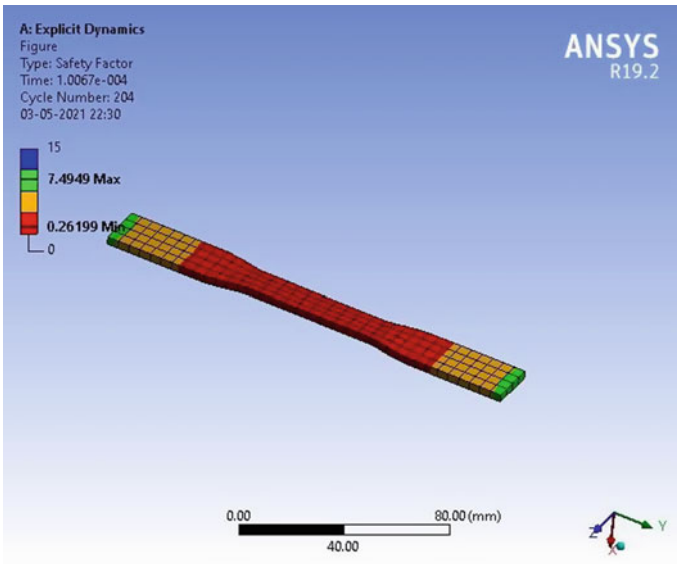
Fig. 37 Safety factor is 0.309 for PLA material at 5000 N

6 Results and Conclusion

Deformation (mm)

Load in N	ABS	PLA
1000	0.70302	0.5151
2000	1.4112	1.0344
3000	2.1236	1.5575
4000	2.8398	2.0941
5000	3.5851	2.627

Stress (MPa)

Load in N	ABS	PLA
1000	40.864	44.554
2000	81.685	89.333
3000	122.38	134.29
4000	162.9	180.44
5000	205.58	225.97

Factor of Safety (FOS)

Load in N	ABS	PLA
1000	1.084	1.32
2000	0.542	0.66
3000	0.362	0.44
4000	0.27	0.32
5000	0.21	0.26

7 Conclusion

- From above tables we can say that, deformations is less for PLA, stress is more for PLA material and safety factor is more for PLA. We can conclude that as per yield strength, PLA is strong compared to other materials.
- Both PLA and ABS are thermoplastics. PLA is more grounded and harder than ABS, yet helpless hotness opposition properties implies PLA is for the most part a specialist material. ABS is more vulnerable and less unbending, yet additionally harder and lighter, making it a superior plastic for prototyping applications.

- PLA is a thermoplastic having higher strength and stiffness greater than ABS. PLA is the humblest material to 3D print the components effectively as it is having low melting temperature and minimal warping,. As it is having low melting point likewise makes it lose basically all stiffness and strength at temperatures over 50 °C. As PLA is strong compared to ABS, the parts can be 3D printed using PLA material and used in Engineering, medical and other applications.

References

Al-Mosawi AI et al (2016) Ansys modeling for estimation Tensile and flexural strength of green composite. 2(1):1–7. http://www.ajournals.com/journals/acms

Anoosha NM et al (2018) Tensile test & FEM analysis of ABS material using FDM technique, vol 7, no 6

Ashik KP et al (2017) Evaluation of tensile, flexural and Impact strength of natural and glass fibre reinforced hybrid composites. Renew Bio Resour 5:1

Azra UE et al (2018) Design of a mild steel specimen using FEA and tensile test data. Sci Direct 5(1):2605–2608

Chen BY et al (2013) Numerical analysis of size effects on open hole tensile composite laminates. Compos Part A 47:52–62. https://doi.org/10.1016/j.compositesa.2012.12.001

Dolgov NA, Tonchev N (2018) Modeling and finite element analysis of tensile testing for the coated specimens. Year IV 4:122–125

Hibbert K et al (2019) The effects of build parameters and strain rate on the mechanical properties of FDM 3D-printed acrylonitrile butadiene styrene. J Organ Polym Mater 9:1–27

https://www.astm.org/Standards/D638

Kumar K et al (2014) Use of miniature tensile specimen for measurement of mechanical properties. 1877–7058 © 2014 the Authors. Elsevier Ltd.

Mahmood AS et al (2019) Comparative study on mechanical properties of steel by numerical analysis and experimental test. REVISTA, AUS, 26 July 2019

Vidakis N et al (2016) Fused deposition modeling parts tensile strength characteristics. Acad J Manuf Eng 14(2)

Use of Multi-Criteria Decision-Making Techniques for Selecting Waste-to-Energy Technologies

Himanshu Sadhya, M. Mansoor Ahammed, and Irshad N. Shaikh

Abstract Waste-to-energy technologies can have a significant role in reducing the burden of waste generated on municipal authorities and municipal solid waste management problems. The selection of the best waste-to-energy technology from different alternatives available is a challenging task, which poses the problem of multi-criteria decision-making (MCDM). A comparison of different multi-criteria decision-making techniques for ranking waste-to-energy technologies is attempted. Further, sensitivity analysis on the weights of the decision criteria is also carried out. Four MCDM methods namely AHP, PROMETHEE, VIKOR, and TOPSIS were used to rank the five selected waste-to-energy technology alternatives i.e. anaerobic digestion, incineration, pyrolysis, gasification, and landfills with gas recovery based on six criteria namely global warming potential, capital cost, operation and maintenance cost, revenue return, moisture content and need for segregation. A questionnaire-based survey was conducted and responses were obtained from 20 experts familiar with waste-to-energy technologies. All the four MCDM techniques gave anaerobic digestion as the best waste-to-energy approach followed by landfills with gas recovery with a reasonably higher score compared with the other waste-to-energy technologies. The ranks provided by AHP and PROMETHEE were the same while the ranking given by TOPSIS and VIKOR were different from other MCDM techniques. Sensitivity analysis of the AHP data showed that the most sensitive criterion was revenue return followed by operation and maintenance cost and capital cost. Scores obtained from TOPSIS were more distinct compared to the other three MCDM methods. Therefore, the decision-maker can see the level of preference amongst the evaluated alternatives, and hence TOPSIS would be the most suited method for the selection of waste-to-energy technology since it provides distinct scores for the alternatives.

Keywords MCDM · TOPSIS · AHP · PROMETHEE · Waste-to-energy · SWM

H. Sadhya · M. Mansoor Ahammed · I. N. Shaikh (✉)
Department of Civil Engineering, Sardar Vallabhbhai National Institute of Technology, Surat, Gujarat, India
e-mail: shaikhirshad1990@gmail.com

505

1   Introduction

Worldwide urban population is expanding at a rate (i.e. 1.5%) quicker than that of the aggregate population (Ouda et al. 2016; Kumar and Samadder 2017) Presently, over half of the total population lives in urban regions, so the worldwide ascent of municipal solid waste (MSW) generation is fundamental because of the population rise, urbanization, and monetary advancement. At present, the rate at which per capita MSW is generated in developed nations is more than that of the developing nations due to its dependence relies upon the financial and social prosperity of a nation (Kumar and Samadder 2017). Gradually, the general populations of developing nations are adopting the way of life of developed countries because of globalization, resulting in extensive amounts of waste. In this way, the expansion in the rate of generation of MSW is predominantly because of changing consumption models, food habits, and expectations for everyday comforts of the urban population (Khan et al. 2016).

Toward the finish of this century, the worldwide energy need is relied upon to be around six-fold of that of the present need. Grave environmental issues can be caused by MSW; in this manner, its utilization as a potential sustainable power source would effectively meet expanded power needs and also the disposal of waste (Kumar and Samadder 2017). It is the need of the hour to understand the capabilities of waste-to-energy (WTE) as a choice for sustainable solid waste management (Kumar and Samadder 2017). WTE is a procedure to harness the energy from waste materials as useable heat, electricity, or fuel (Zhao et al. 2016). WTE advancements are considered as one of the most reasonable choices for taking care of waste-related issues.

Among the different waste-to-energy technologies, anaerobic digestion, incineration, gasification, pyrolysis, and landfills with gas recovery are the few most frequently used technologies. Advanced waste-to-energy technologies like plasma Arc gasification, hydrothermal carbonization (HTC), microwave pyrolysis, hydrothermal liquefaction (HTL) are also available but, those are associated with higher costs, hence, not considered in the present study. To simplify and facilitate the decision process, several mathematical methods have been suggested. Here, the basics of multi-criteria techniques, which have been applied in decision processes, are presented. Analytic hierarchy process (AHP), Technique for Order of Preference by Similarity to Ideal Solution (TOPSIS), VIekriterijumsko KOmpromisno Rangiranje (VIKOR), Preference ranking organization method for enrichment evaluation (PROMETHEE) methods are some of the multi-criteria techniques in decision processes. These methods are based on resolving complex problems into the hierarchy, where the goal is on tops the hierarchy, while criteria along with sub-criteria, and alternatives belong to the lower level.

The technique used to decide how one variable will affect another needy variable under a given arrangement of conditions is characterized as sensitivity analysis. Utilization of sensitivity analysis will rely upon one or more than one info factor within the particular limits. It is otherwise called the what–if investigation. Any action or framework can be checked by sensitivity analysis. From family vacation's

arranging in light of the factors to the corporate levels choices; all can be possible through sensitivity analysis. Sensitivity Analysis assists in breaking down how reactive the yield is, by adapting in single data input while keeping every other source of info steady. Sensitivity Analysis created by Triantaphyllou and Sanchez (1997), additionally distinguishes the scope of weights for which the ranking won't be influenced. Sensitivity analysis is among the techniques that assist decision-makers with multiple answers for an issue. Fitting understanding of the related issues to the model under reference.

Many nations have understood the capability of the waste-to-energy exercise and began utilizing waste to create power. Outstanding cases of the utilization of waste-to-energy procedures all through history have been in the USA, Japan, and Germany. In the USA in 1990, municipal solid waste was used to produce energy to meet the expected consumption of 394 trillion BTUs. As per the Japanese Ministry of Health and Welfare (MHW), there have been 102 operational incineration plants for power creation since late 1991, which are all still operational. Furthermore, in Germany, there were numerous working waste-to-energy plants in the '90s (Wolpert 1994).

China is a newcomer in WTE adaption, with seven plants in the act and an expected yearly limit of 1.6 million metric tons every year. An aggregate of 154 WTE systems have been built or being constructed, totaling an ability of 16.5 million t (Moya et al. 2017). Waste management exercises in India are still in their incipient stage. As of Nov. 2016, five municipal solid wastes (MSW) to energy plants with a cumulative of 66.5 MW are presently operational/under preliminary keep running in the nation. Ministry of Urban Development (MoUD) has gotten 53 propositions from 22 states with the potential to create 405.3 MW of power under the Swachh Bharat Mission (SBM) which are at present under different phases of development or offering.

In the present study, a comparison of different multi-criteria decision-making techniques for ranking waste-to-energy technologies is attempted. Further, sensitivity analysis was used on the weights of the decision criteria. Four MCDM methods namely AHP, PROMETHEE, VIKOR, and TOPSIS were used to rank the five selected waste-to-energy technology alternatives i.e. incineration, pyrolysis, anaerobic digestion, gasification, and landfills with gas recovery based on six criteria namely global warming potential, capital cost, operation and maintenance cost, revenue return, moisture content and need for segregation. A questionnaire-based survey was conducted and responses were obtained from 20 experts familiar with waste-to-energy technologies.

2   Methodology

2.1   Date Collection and Analysis by Various MCDM Techniques

Figure 1 presents the stream diagram of the approach embraced for the present study. The available technologies for waste-to-energy technologies were reviewed to assess their possible applicability for municipal solid waste. Priority was given to technologies that are specifically suitable for municipal solid waste, with distinct characteristics such as low cost, easy installation, low operation and maintenance cost, low dependency on electricity or chemicals, high revenue rate, low need for segregation of waste, low global warming potential, and accessibility. Based on the review, five WTE technologies were selected. The selected alternatives were incineration, gasification, anaerobic digestion, pyrolysis, and landfills gas recovery.

Attributes/criteria are extremely crucial to the MCDM technique as an important role has been played in the process of decision-making. A review of the literature gave an idea regarding various criteria that should be considered for waste-to-energy technologies. Selection of criteria for ranking of waste-to-energy alternative is a pain-taking task. It requires in-depth knowledge about how particular waste-to-energy
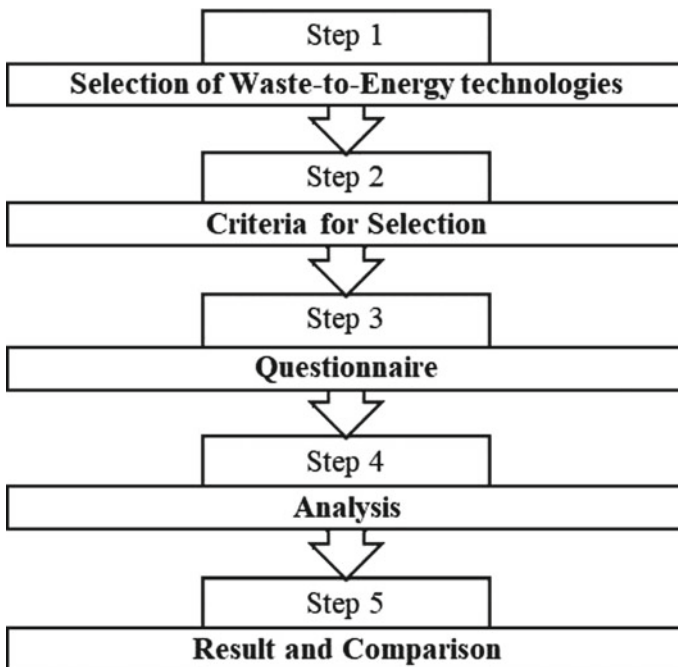
Fig. 1 Flow diagram of the methodology employed

works and how much energy it can harness; what form of energy can be extracted for given waste characteristics, the sole objective of the project proponent, etc. As some criteria are interrelated and it will be a cumbersome task if we take all the criteria at the same time for analysis purposes. So, for simplicity point of view, we have reduced the no. criteria to make it easier for analysis. Capital cost, operation and maintenance cost, rate of revenue, moisture content, need for segregation, and global warming potential is the selected criteria for the present study. A short description of the selected criteria is presented here.

2.2   Fixing the Criteria and Modeling of Hierarchy

Capital expenses are settled, one-time costs brought about on the buy of land, structures, development, and hardware utilized as a part of the creation of products or in the rendering of administrations/services. Capital expenses incorporate costs for substantial products like trademarks and programming improvement. Capital expenses are hard and fast; in this way autonomous of the level of yield.

The Operation and Maintenance (O and M) cost of a Component is the cost related to working and keeping up that Component. O and M costs have for some time been an unsure yet notable part of the cost of energy from Waste-to-vitality technologies. The expenses of operation and maintenance depend on the chosen technology.

Return on revenue (ROR) is a measure of organization productivity that is figured by partitioning net income by profit. The most critical income of the WTE plant is income from the waste disposal charge, called entryway expense or gate fee. Gate fee is the installment that the WTE plant gathers per ton of waste got. The gate expense relies upon economic situations, working costs, measure of power that could be sold, and the cost of aggressive techniques for disposal of waste. Income from the disposal of waste ought to guarantee productivity. Trading of electric power into the conveyance grid guarantees a steady purchaser of power, while the heat is being sold, e.g. to neighboring industries. The high-valued heat (198 °C) energy from the WTE plant could accomplish a higher cost. This cost couldn't be precisely decided since it involves a contract between the maker and the purchaser.

Weight reduction (expressed in percentage) of the solid waste sample upon dried at a temperature of 100–105 °C. The percentage of moisture contained in a solid waste sample can be figured on basis of dry or wet mass. Moisture content impacts the heat of ignition and in addition to the biological processing of matter; organic. It relies upon organic matter content, climate, kind of source, and so forth. The reported moisture contents of 58 and 36% for the wet and dry months individually demonstrate the possibilities of bio-synthetic change for the wet month and thermo-chemical transformation for the dry month (Kuleape et al. 2014).

Segregation of waste is incorporated into law since it is substantially less demanding to recycle. Successful isolation of waste implies that less waste goes to landfills which makes it less expensive and fit for individuals and the environment as well. It is additionally essential to isolate for general wellbeing (EMS 2017). It

is easier to process segregated waste because it is having a higher calorific value than unsorted waste. Segregate waste emits fewer pollutants than unsorted waste on processing; so, it is environmentally viable as well. Sorting hazardous and toxic waste from non-hazardous and non-toxic also helps in reducing the chances of any catastrophic event.

A relative measure to the account of how much heat a greenhouse gas traps in the atmosphere is Called Global warming potential (GWP). A GWP is computed over a particular period, usually 20, 100, or 500 years. Particularly, it is a quantum of energy that 1 t of gas can mop up emissions in a given timeframe, concerning the discharges of 1 t of carbon dioxide (CO_2). More the GWP the earth gets heated up over that period. GWPs depend on the heat energy absorbing capacity of gas in respect to that of carbon dioxide (CO_2). By allocating a GWP value, it enables policy planners to analyze the effects of emissions and decreases of various gases. Figure 2 presents the first stage of the hierarchy as the topmost goal of the project; the second stage presents the criteria based on which project is to be accessed, and the third stage represents the adaption options.

Once the criteria/attributes and alternatives for waste-to-energy technologies were finalized, the technical survey questionnaire was prepared in both online and offline mode to evaluate the selected alternatives by obtaining the opinions of experts. Two different questionnaires were prepared in this study. The questionnaire I am used for AHP, in which participants analyze the correlative significance of the decision choices of pair-wise concerning criteria and the goal on Saaty scale of 0–9. Questionnaire II was designed for TOPSIS, in which participants prioritize the alternatives with respect to criteria on a cardinal scale of 0–100. The data set obtained from the survey questionnaire I and II were utilized for the analysis. The questionnaire was sent to more than 30 experts with knowledge and experience in the field of waste-to-energy technology. A total of 20 experts responded. The sample space used
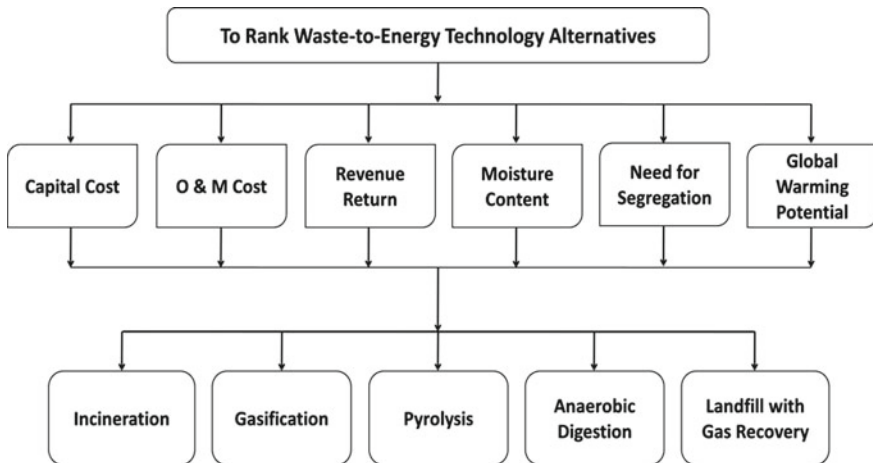
Fig. 2 Analytical hierarchy of decisions

for this study includes faculty, research scholars of academic institutions, and environmental consultants working on waste-to-energy systems; broadly categorized into two: Academician and Industry personnel. The expert selection requires major attention and care because they should have good experience and thorough knowledge in the field of waste-to-energy alternatives.

For taking the final and aggregated decision, researchers have recommended using geometric mean instead of arithmetic mean for aggregation between factors (Forman and Peniwati 1998). Therefore, in the present study, the geometric mean of experts' opinion for aggregation of the result was used. The multi-criteria decision-making techniques were used in the present study for ranking different waste-to-energy technology alternatives to select suitable technology as per the given criteria.

2.3 Multi-criteria Decision-Making Techniques

The multi-criteria decision-making techniques were used in the present study for ranking different waste-to-energy technology alternatives for the selection of suitable technology as per the given criteria.

Analytic Hierarchy Process (AHP)

Arrangement and investigation of complex decisions is made by using analytic hierarchy process (AHP). The relative significance of elements at each stage could be obtained, a pair-wise differentiation matrix is arrived at using Saaty 1–9 preference scale. Pairwise balancing matrices yield both eigenvector and maximum Eigenvalue (λ_{max}). The following steps demonstrate the stepwise procedure of AHP:

Step 1: Construct the structural hierarchy based on the goal, criteria, and alternatives. With the help of the questionnaire, the participants weigh up the relative significance of the decision choices pairwise regarding criteria and goals. Based on a common criterion, any two elements can be compared in pairs. Saaty's preference scale for comparison is used to demonstrate the significance of one element over another.

Step 2: Construct the pair-wise comparison matrix from the comparisons generated at step 1 based on various criteria. The diagonal elements of the matrix are 1. The basis in the *i*th row is superior to the basis in the *j*th column if the strength of element a_{ij} is more than 1; or else the basis in the *j*th column is superior to in the *i*th row. Where a_{ij} denotes the comparative significance of attribute *i* regarding attribute *j*. In the matrix, $a_{ij} = 1$ when i = j and $a_{ji} = 1/a_{ij}$.

The opinions of each expert should be sorted out separately and take geometric mean to aggregate the results.

Step 3: Determine priority vector, the standardized Eigenvector of the matrix. For obtaining the Eigenvector as well as maximum Eigenvalue (λ_{max}), the pairwise comparison matrix obtained in Step 2 is squared first. Then sum the total of the rows of the square matrix and finally normalize it by dividing the row sum by the

row totals. This process must be iterated until the Eigenvector result doesn't change from the previous iteration. Determining the Eigenvector computes the corresponding ranking of the options under each criterion.

Step 4: Pairwise comparison matrices gives both eigenvector and the maximum Eigenvalue (λ_{max}) (Saaty 1980, 2008). The last step is to get the consistency index (CI) as well as consistency ratio (CR) and is calculated by the following equations:

$$CI = (\lambda_{max} - n)/(n - 1) \tag{1}$$

where λ_{max} is the highest Eigenvalue of the pairwise comparison matrix of size n

$$CR = \left({CI}/{RI} \right) \tag{2}$$

RI indicates the degree of matrix and randomly produced consistency index, respectively (Karim and Karmaker 2016). Random consistency index (RI) for matrix size n is obtained from Saaty (2008). Saaty suggested that the value of CR should be less than 0.1. If the CR value is more than 0.1 the expert's opinions may be inconsistent and the result is said to be not reliable.

Preference Ranking Organization Method for Enrichment Evaluation (PROMETHEE)

Preference Ranking Organization Method for Enrichment Evaluation (PROMETHEE) method, where the options are investigated on the different criteria. It needs added details on the relative significance of the option (weights). PROMETHEE does not yet provide any conventional guidelines on how weights can be elicited. It assumes that the decision-maker can weigh the criteria correctly, at the minimum when the number of options is not too large (Macharis et al. 2004). For a large number of criteria, Macharis et al. (2004) suggested finding weights as stated in several methods: trade-off, direct rating, pairwise comparisons, point allocation, and so on. In the present study, the latter method (AHP) is used to evaluate the weight of each criterion.

Step 1: Evaluation of Normalized Decision Matrix (rij).

For increasing criterion: If a higher value of aij is always denoted better accomplishment of alternative Ai, then

$$ri.j = \frac{a_{imax} - a_{ij}}{a_{imax} - a_{imin}} \tag{3}$$

For decreasing criterion: If a smaller value of aij denotes better accomplishment of alternative Ai, then

$$ri.j = \frac{a_{ij} - a_{imax}}{a_{imax} - a_{imin}} \tag{4}$$

Step 2: Evaluate Preference for all pairs of alternatives. Let A1, A2, A3, …, Am be MALTERNATIVES and g1, g2, g3, …, gn be n cardinal criteria and let yij be the criteria value of the ith alternative Ai with respect to the jth criterion gj.

Pj(Ai, Ak) denotes the liking function on criterion gj, which equals to p (yij − ykj).

Step 3: To get the aggregated preference function S (Ai, Ak), the preference function on each criterion was formulated following the formula.

$$S(Ai, \ Ak) = \sum_{j=1}^{n} w_j p_j(A_i, A_k) \tag{5}$$

where, wj represent the weight of the criterion gj.

Step 4: Rank the options from the best one to the worst one, the outgoing and incoming flow for each alternative is given as follows:

The outgoing flow of alternative Ai is defined as

$$\Phi + (Ai) = \sum_{A_k \in A} S(A_i - A_k) \tag{6}$$

The incoming flow of alternative Ai is defined as

$$\Phi - (Ai) = \sum_{A_k \in A} S(A_k - A_i) \tag{7}$$

Based on the outgoing flow and incoming flow, the net flow (Ai) is defined by Eq. (8) represents the aggregate preference degree of alternative Ai and Aj.

$$(Ai) = \Phi + (Ai) - \Phi - (Ai) \tag{8}$$

Alternative can be ranked from the best to the worst one by the net flow. If (Ai) = (Aj), the alternative Ai is indifferent to Aj. If (Ai) > (Aj), then the alternative Ai is preferential to Aj (Zhaoxu and Min 2010).

VIekriterijumsko KOmpromisno Rangiranje (VIKOR)

VIekriterijumsko KOmpromisno Rangiranje (VIKOR) method was used to resolve decision problems with disputing and non-commensurable criteria, considering that compromise is tolerable for contradictory resolution, the result should be the closest to the ideal is a desire of decision-maker, and the alternatives are evaluated as stated in all earlier criteria (Opricovic and Tzeng 2004).

Step 1: Evaluate the best (fi*) and the worst (fi)-values of all concerned functions, i = 1, 2, …, n; fi* = max(fij, j = 1, …, j), fi- = min(fij, j = 1, …, j), if the ith function is benefit; fi* = min(fij, j = 1, …, j), fi- = max(fij, j = 1, …, j), if the ith function is cost.

Step 2: Determine Sj and Rj, j = 1,2, …, j, as follows:

$$Sj = \sum_{i=1}^{n} \frac{w_i\left(f_i^* - f_{ij}\right)}{f_i^* - f_i^-}, \, i = 1, 2, \ldots n \tag{9}$$

Weighted as well as normalized Manhattan distance;

$$Rj = \frac{max_j\left(f_i^* - f_{ij}\right)}{\left(f_i^* - f_i^-\right)}, i = 1, 2, \ldots n \tag{10}$$

where, wi are the rank of criteria, conveying the decision maker's desire.

Step 3: Find out Qj, j = 1, 2, …, J, as follows:

$$Qj = \nu(Sj - S*)/(S- - S*) + (1 - \nu)(Rj - R*)/(R- - R*) \tag{11}$$

where S* = min(Sj, j = 1, …, j), S- = max(Sj, j = 1, …, j), R* = min(Rj, j = 1, …, j), R- = max(Rj, j = 1, …, j); and ν is established as a weight for the approach of maximum group benefit, whereas $1 - \nu$ is the rank of the discrete regret. These schemes could be settled by $\nu = 0.5$, and here ν is modified as = (n + 1)/2n (from $\nu + 0.5(n - 1)/n = 1$) as the criterion (1 of n) related to R assumed in S, too.

Technique for Order Preference by Similarity to Ideal Solution (TOPSIS)

Technique for Order Preference by Similarity to Ideal Solution (TOPSIS) endeavors to demonstrate the best option that at the same time has the shortest distance from the positive ideal solution (PIS) and the farthest distance from the negative ideal solution (NIS). The PIS is a solution that attempts to maximize the profit option and minimize the cost criteria, while NIS is just the contrary of the previous one. The PIS is made out of all the great qualities feasible of criteria, though the NIS contains every single most noticeably awful value achievable of criteria. In the TOPSIS technique, specific scores that each option gets from every one of the criteria are considered in the evolution of a decision matrix as well as normalized decision matrix. By considering the rates of all the attributes, PIS and NIS are found. Considering the distance coefficient of each option, the priority order of the options is found.

Step 1: Formulate a normalized decision matrix of beneficial as well as non-beneficial criteria.

$$rij = \frac{x_{ij}}{\sqrt{\sum_{i=1}^{m}\left(x_{ij}\right)^2}}, i = 1, 2, \ldots m; \, j = 1, 2, \ldots n \tag{12}$$

where xij is original while rij is the normalized rank of the decision matrix, respectively.

Step 2: Formulate the ranked normalized decision matrix by multiplying the weights wi of evaluation criteria with the normalized decision matrix rij. The ranked normalized value Pij is determined as:

$$Pij = wi * rij, i = 1, 2, \ldots, m \text{ and } j = 1, 2, \ldots, n$$

Step 3: Decide the PIS and NIS as follows:

$$PIS = (p1+, \ p2+, \ldots, pm+)$$
$$NIS = (p1-, \ p2-, \ldots, pm-) \tag{13}$$

where,

$Pj+ = (maxi(Pij), \ j \in J1; \ mini(Pij), \ j \in J2)$

$Pj- = (mini(Pij), j \in J1; \ maxi(Pij), \ j \in J2)$

where, J1 and J2 represent the criteria benefit and cost, respectively.

Step 4: Determine the separation distances from the PIS and the NIS of each alternative Ai, respectively as follows:

$$dij+ = \sqrt{\sum_{j=1}^{n} \left(d_{ij}^{+}\right)^2} \tag{14}$$

$$dij- = \sqrt{\sum_{j=1}^{n} \left(d_{ij}^{-}\right)^2} \tag{15}$$

where,

$dij+ = Pj + -Pij, \ \text{with } i = 1, 2, \ldots, m.$

$dij- = Pj\text{-} - Pij, \ \text{with } i = 1, 2, \ldots, m.$

Step 5: Determine the corresponding closeness coefficient Ri* considering PIS for each option as given by:

$$Ri* = \frac{d_i^{-}}{d_i^{+} + d_i^{-}}, i = 1, 2, \ldots\ldots, m \tag{16}$$

Step 6: Depending on the decrease in values of the closeness coefficient, alternatives are weighted from most valuable to worst. The alternative with the highest closeness coefficient (Ri*) is chosen (Karim and Karmaker 2016).

2.4 Sensitivity Analysis

The sensitivity of AHP data to the criteria weights were studied in detail (Trianta-phyllou and Sanchez 1997). The original parameter weights after AHP analysis was taken for the sensitivity analysis. Each criterion weight was substituted separately to observe how the analysis results and pattern of ranking would be affected.

In this method, the variation of ranking pattern is determined with changes in each criteria weightage taking one criterion at a time. In this study, the original criteria weights were taken from AHP analysis.

Let w_k, k = 1, 2, 3,…, n be the weight being disturbed first, w_k* be the new weight after the initial variation ratio of γ_k, then w_k* = γ_k w_k, the disturbance to wk will make other weights to change in such a way that some of the weights is equal to unity. The unitary ranks for parameters 1, 2, k, and n after w_k is urged on interference are w_1', w_2', wk′, and wn′ respectively. The unitary variation ratio of w_k after disturbance is denoted by βk.

Where,

$$\beta k = \frac{w_k'}{w_k}$$

Therefore, we get

$$\gamma k = \frac{\beta_k - \beta_k w_k}{1 - \beta_k w_k}$$

In general, wn′ can be expressed as follows:

$$\mathrm{Wn}' = \frac{w_n}{w_1 + w_2 + \cdots w_k^* + \cdots w_n} = \frac{w_n}{1 + (\gamma_k - 1) w_k} \tag{17}$$

The selected values of unitary variation ratios (βk) in this study are 0.01, 0.02, 0.05, 0.1, 0.2, 0.5, 1.0, 1.5, 2.0, 2.5, 3.0, 3.5, 4.0 and 4.5 as recommended by Legendre (2005). The criteria weights under these variations βk were recalculated and the weighted score of alternatives was obtained. By plotting the graph of βk versus weighted score the changing trend of rankings of the alternative was studied.

2.5 Comparison of the Ranking

The ranking obtained by different MCDM Techniques was compared with the help of non-parametric statistical parameters such as Kendall's coefficient of concordance and Spearmen rank correlation coefficient, Kendall's coefficient of concordance represents the uniformity of rankings generated by all the MCDM methods used

for the study whereas Spearman rank correlation coefficient represents the degree of association between two MCDM methods rankings.

Kendall's coefficient of concordance (ζ): It is an estimate of the variance of the row sum of ranks divided by the maximum possible value the variance can take and proposed by Maurice G. Kendall and Bernard Babington Smith (Legendre 2005). Equation (2) for ζ is given by:

$$\zeta = \frac{\sum_{i=1}^{m}\left(S_i - \frac{\sum_{i=1}^{m} S_i}{m}\right)^2}{\frac{1}{12}\left(p^2\left(m^3 - m\right)\right)} \tag{18}$$

where S_i is the sum of rank assigned to ith alternative across all p MCDM methods and m is the total number of alternatives. The value of ζ ranges from 0 to 1, where 1 represents perfect rank correlation.

Spearman rank correlation coefficient (ρ): It is a statistical estimate of the strength of a monotonic relationship between paired data (Legendre 2005). Equation (3) gives the value of ρ and the value may vary from −1 to 1 where 1 represents the best correlation.

$$\rho = 1 - \frac{6\sum K_i^2}{m\left(m^2 - 1\right)} \tag{19}$$

Here $K_i = X_i - Y_i$, where X_i and Y_i be the ranks generated by pair of MCDM methods for the same alternative and m is the total number of alternatives.

3 Results and Discussion

3.1 Data Analysis for Questionnaire

The response sheet of the questionnaire I was utilized as a part of the present investigation, conflicting suppositions were excluded by checking the consistency of expert's opinion, to get the reliable outcomes by taking geometric mean (Forman and Peniwati 1998). The weightage of every attribute in accomplishing the objective is presented in Fig. 3. High weightage for a specific attribute shows that the criterion was more crucial in the assessment of the suitable waste-to-energy innovation. As it can be seen that weightage of the criteria needs for segregation, capital cost along with operation and maintenance cost scored high, and it can be reasoned that need for segregation was more important followed by capital cost as well as operation and maintenance cost whereas global warming potential was least crucial in deciding the suitable waste-to-energy process. The final preference of the choices is profoundly
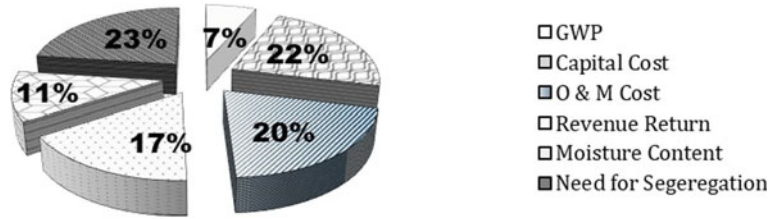
Fig. 3 Priority of each criterion towards goal

subject to the weights of the criteria because even little changes in the criteria weights can cause critical changes in the final ranking of the decision (Li et al. 2013).

Figure 4 represents that the anaerobic digestion scored well in all the selected criteria except the need for segregation since anaerobic digestion requires biodegradable waste only which requires segregation from another inorganic as well toxic or hazardous waste. Anaerobic digestion scored highest in global warming potential, capital cost, and moisture content while compared to other alternatives because it provides excellent treatment for waste with low capital costs, minimal effect of moisture content, and no chemical requirements. Landfills with gas recovery scored highest in operation and maintenance cost and need for segregation; meaning it has a minimum requirement for extra work which further reduces the operation and maintenance cost compared with other technologies.
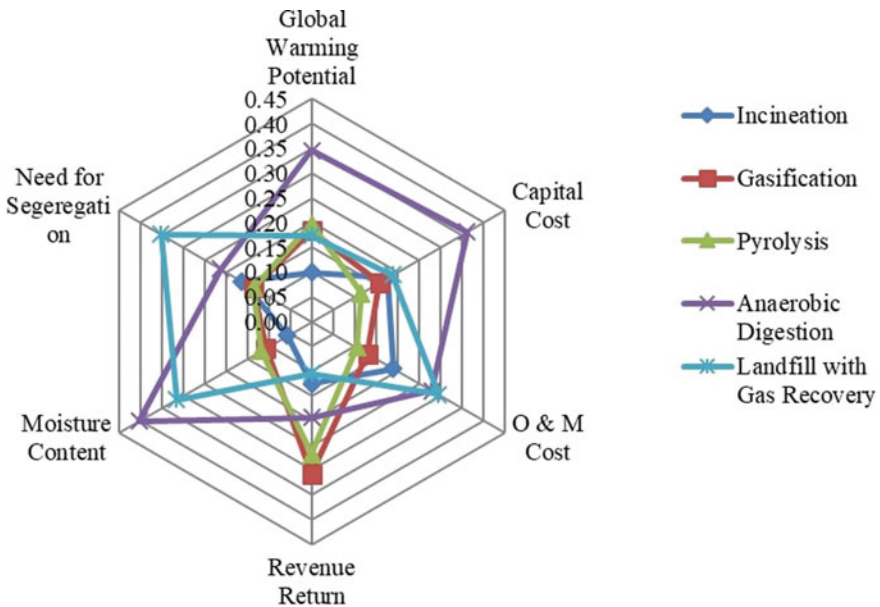
Fig. 4 Weights of each alternative for waste-to-energy technology with each criterion by AHP

Table 1 Overall score and ranking of the alternatives by AHP

Alternatives	Experts from Industry' score	Rank	Academician' score	Rank	Combined score	Rank
Incineration	0.277	1	0.131	5	0.151	4
Gasification	0.112	5	0.168	3	0.170	3
Pyrolysis	0.164	4	0.133	4	0.148	5
Anaerobic digestion	0.205	3	0.308	1	0.288	1
Landfill with gas recovery	0.242	2	0.261	2	0.243	2

3.2 Ranking Using AHP

The ranking of the alternatives using the Analytic Hierarchy Process (AHP) was obtained by multiplying the preference vector matrix of alternatives for each criterion with criteria weightage and the results are presented in Table 1.

A pairwise comparison matrix was constructed for alternatives for criterion. It can be concluded that anaerobic digestion is the most suitable alternative followed by landfill with gas recovery and gasification for waste-to-energy technology. Landfill with gas recovery scored high with respect to the need for segregation criteria which was one among the highest weightage criterion as per expert opinion-making it a preferable alternative in comparison to other alternatives. It can be noted that the overall score for the first ranked alternative anaerobic digestion (0.288) is having a slight difference compared with the second-ranked alternative Landfill with gas recovery (0.243).

However, 4th ranked incineration (0.151) and 5th ranked pyrolysis (0.148) are not having much higher differences as compared with others. This is because some of the criteria weightage obtained were very close to each other, as the need for segregation and capital cost criteria are having very little variation. Therefore a small variation in the criteria weights will affect the ranking. Kalbar et al. (2015) reported that five MCDM methods generated a similar ranking for the selection of wastewater treatment alternatives when equal criteria weights were used. Many researchers have done similar work for selecting waste-to-energy techniques using AHP (Soltani et al. 2016; Karagiannidis and Perkoulidis 2009; Rahman et al. 2017). Since the experts' opinions about criteria are represented in the form of exact numbers, AHP is currently one of the most commonly employed approaches for ranking various options.

3.3 Ranking Using PROMETHEE

The decision matrix and preference vector for criteria derived from AHP were used for the PROMETHEE analysis. At first, the PROMETHEE method weighs up pairs

Table 2 Ranking of the alternatives based on net outranking flow

Alternative	Leaving flow	Entering flow	Net flow	Rank
Incineration	−0.1641	0.1641	−0.3282	4
Gasification	−0.0986	0.0986	−0.1971	3
Pyrolysis	−0.1834	0.1834	−0.3667	5
Anaerobic digestion	0.2883	−0.2883	0.5766	1
Landfill with gas recovery	0.1578	−0.1578	0.3155	2

of options on each criterion. The normalized decision matrix for PROMETHEE was evaluated by Eqs. 3 and 4. In this method, to express the difference in priority between pairs of alternatives on each criterion preference function is used.

The aggregated priority function is determined by summing up the values across the alternative's combination by Eq. 5. Hence, preference functions outlined the differences in preference from the point of the decision maker's view and its value ranges lie 0–1. The leaving flow and entering flow values are found out by using Eqs. 6 and 7. The net flow is the summation of leaving flow and entering flow. Based on the decreasing order of net flow the ranking of the options is done presented in Table 2.

3.4 Ranking Using VIKOR

The VIKOR technique investigates a settled solution that would be acknowledged by the decision-makers since it gives a viable solution that is nearest to the perfect, and a settled solution gives an understanding set up by mutual acceptance (Opricovic and Tzeng 2004). Table 3 shows ranking using VIKOR. The data obtained from the questionnaire I was utilized for the VIKOR analysis.

The weightage of the alternatives depends on three scalar quantities S_j (concordance), R_j (disapproval), and Q_j (incorporates both S_j and R_j i.e., more reliable). Weightage the alternatives, sorted by the values S_j, R_j, and Q_j in the decreasing order. Table 3 shows the scalar values S_j, R_j, and Q_j by assuming weights of most of the criteria strategy or largest group utility value [0,1] $v = 0.5$. An alternative

Table 3 Ranking order by S_j, R_j, and Q_j

Rank	1	2	3	4	5
By S_j	Anaerobic digestion	Landfill with gas recovery	Gasification	Incineration	Pyrolysis
By R_j	Anaerobic digestion	Landfill with gas recovery	Incineration	Pyrolysis	Gasification
By Q_j	Anaerobic digestion	Landfill with gas recovery	Incineration	Gasification	Pyrolysis

is proposed as a compromise solution, which is the best ranked by the measure Q (minimum) if the two conditions acceptable advantage and acceptable stability in decision making are satisfied. In this case $Q(A^{(2)}) - Q(A^{(1)}) = 0.290$, which is $\geq$ 0.250 Therefore acceptable advantage condition is satisfied. Since the alternative $A^{(1)}$ i.e., Anaerobic digestion is also best ranked by S and R. Therefore, the settled solution is said to be stable within a decision-making process. The correct alternative is anaerobic digestion followed by landfills with gas recovery and incineration and the least ranked one is pyrolysis (Table 3).

3.5 Ranking Using TOPSIS

The response of questionnaires I and II was used for the analysis using TOPSIS. The selected alternative should have the shortest Euclidian distance from the PIS and the farthest from the NIS is the basic concept of the TOPSIS method (Hwang and Yoon 1981). The geometric mean of the experts' opinion was taken for the further analysis process. Table 4 presents the ranking of the alternatives based on the relative closeness value. Anaerobic digestion scored highest (0.669) followed by landfill with gas recovery (0.634) and pyrolysis (0.393).

Global warming potential (GWP), capital cost (CC), operation and maintenance cost (OMC), moisture content (MC), and need for segregation (NFS) were considered to be cost type and revenue return (RR) criteria were benefit type. The deviation from positive and negative ideal solution was determined for each criterion, Euclidian distance of each alternative from the PIS, d_{ij}^{+}, and separation of each alternative from the NIS, d_{ij}^{-} were determined by Eqs. 14 and 15 respectively. The ranking of the alternatives was calculated according to relative closeness value R_i^{*} by Eq. 16 and the best alternatives are those that have a higher value of R_i^{*}.

Table 4 Ranking of the alternative based on relative closeness value in TOPSIS

Ranking of the alternative based on relative coefficient						
Criteria	Si*	Si′	Si* + Si′	Si′/(Si* + Si′)	Rank	Best
Incineration	0.129	0.014	0.143	0.101	5	0.669
Gasification	0.100	0.050	0.150	0.333	4	
Pyrolysis	0.090	0.058	0.148	0.393	3	
Anaerobic digestion	0.054	0.109	0.163	0.669	1	
Landfill with gas recovery	0.057	0.099	0.156	0.634	2	

3.6 Comparison of Ranking

A comparative study of the generated ranking pattern of waste-to-energy alternatives was conducted for the four selected MCDM methods. Table 5 presents the scores and ranks obtained from four different MCDM methods. It can be seen that only AHP and PROMETHEE methods gave similar results. However; all four techniques gave anaerobic digestion as the best alternative.

The least preferred alternative was either pyrolysis or incineration in different MCDM Methods. Tscheikner-Gratl et al. (2017) stated that for consistency checking and for increasing the reliability of the results, application of several MCDM methods is encouraged other than using only one method. A similar comparison has been reported in the literature. For example, Tscheikner-Gratl et al. (2017) used five commonly used MCDM techniques such as ELECTRE, WSM, PROMETHEE, AHP, and TOPSIS for ranking and found that the results of the different methods were not similar. Similarly, Kalbar et al. (2015) in a study for ranking of the wastewater treatment alternatives by taking equal and unequal weightage for all criteria showed that it was difficult to get similar ranking using different MCDM methods for situations in which an equal set of criteria weights. Kolios et al. (2016) applied six different MCDM methods for the selection of wind turbines and concluded that most methods agree on identifying the set with the highest score.

The degree of association of rankings generated by a pair of MCDM methods was determined by Spearmen's rank correlation coefficient (ρ) value. The results are presented in Table 5 and it can be concluded that AHP and PROMETHEE generated a similar ranking pattern for all five alternatives (Anaerobic Digestion > Landfill with Gas Recovery > Gasification > Incineration > Pyrolysis). The Spearman's ρ value for these two methods is 1.0, which indicates similarly in the ranking pattern generated by these two MCDM methods. TOPSIS generated another set of rankings comparatively different from AHP, VIKOR, and PROMETHEE. TOPSIS ranking pattern is somewhat different from VIKOR and PROMETHEE indicated by a small value of $\rho = 0.6$ and 0.7 respectively, except the first and second-ranked alternatives.

Table 5 Score and rank obtained for different MCDM techniques

MCDM technique	AHP		TOPSIS		VIKOR		PROMETHEE	
WTE technology	Score	Rank	Score	Rank	Score	Rank	Score	Rank
Incineration	0.151	4	0.099	5	0.807	3	−0.328	4
Gasification	0.170	3	0.365	4	0.910	4	−0.197	3
Pyrolysis	0.148	5	0.457	3	0.995	5	−0.367	5
Anaerobic digestion	0.288	1	0.760	1	0.000	1	0.577	1
Landfill with gas recovery	0.243	2	0.619	2	0.290	2	0.316	2

The Kendall's coefficient of concordance (ζ) value by Eq. 18, for all the four methods, was 0.85 which suggests that there exists more than a partial agreement between rankings generated by these four MCDM methods. It can be easily seen from Table 6 that scores obtained from TOPSIS are more distinct compared to the other three MCDM methods. Therefore decision-makers can see the level of preference amongst the evaluated alternative hence TOPSIS is the most suited method for the selection of waste-to-energy technology since it provides distinct scores for the alternatives.

3.7 Sensitivity Analysis

Figure 5 shows weighted score of AHP under different unitary variation ratios for weight GWP. This technique of sensitivity analysis is used for the assessment of the variation of ranking pattern with change in each criterion weightage by taking one at a time. In the present study, the initial weights for the six criteria were taken from the AHP analysis. Similarly, if the interference was imposed on other ranks, the variations of the results under different unitary variation ratios for w_2, w_3, w_4, w_5, and w_6 were determined and the results are shown in Fig. 5. The criteria weights were: Global Warming Potential (w_1) = 0.0656, Capital cost (w_2) = 0.2227, O and M cost (w_3) = 0.2046, Revenue return (w_4) = 0.1660, Moisture content (w_5) = 0.1120, Need for segregation (w_6) = 0.2292. The unitary variation ratios have been designed first varying from β_1 = 0.01, 0.02, 0.05, 0.1, 0.5, 1.0, 1.5, 2.0, 2.5, 3.0, 3.5 etc., till the weightage becomes maximum value (close to 1). Global warming potential (w_1) was the rank being urged a disturbance first. Then the weights under each of these strategies were re-determined, and the weighted score value under these strategies was also recalculated. Revenue return and need for segregation criteria showed larger variation as compared to other criteria. Figure 5d demonstrates that all the five alternatives are empathetic to the variation of revenue return (w_4). After imposing a disturbance of β_4 = 4.0, the first ranked AD was replaced by coagulation as the most preferred one. From Fig. 4d it is clear that variation of revenue return criteria (w_4) had imposed a greater impact on all the alternatives and their ranking got reversed completely. It shows that all the five alternatives are sensitive to changes in revenue return (w_4) because their weighted score values begin to change once a small disturbance is imposed at about β_4 = 0.05. Gasification got the first rank after imposing disturbance of β_4 = 4.0 because gasification is having a good or higher revenue return compared to other technologies and they got more weightage among decision-maker opinions. We can see that the alternatives Anaerobic digestion, Incineration, and Landfill with gas recovery follow decreasing trends (at about β_4 = 2.5) as unitary variation increases, whereas others follow an increasing trend for weighted score values as unitary variation increases. After imposing a disturbance of β_4 = 4.5 the first ranked alternative anaerobic digestion became the third one in preference order. As compared with the other criteria, In this study nearly all the criteria except GWP, Capital cost, and Moisture content begin to change at around β = 0.5 − 1.5.

Table 6 Spearman's coefficient (ρ) for various MCDM techniques by pairwise comparison

MCDM Technique	AHP–TOPSIS	AHP–VIKOR	AHP–PROMETHEE	TOPSIS–VIKOR	TOPSIS–PROMETHEE	VIKOR–PROMETHEE
Spearman's coefficient	0.70	0.90	1.00	0.60	0.70	0.90
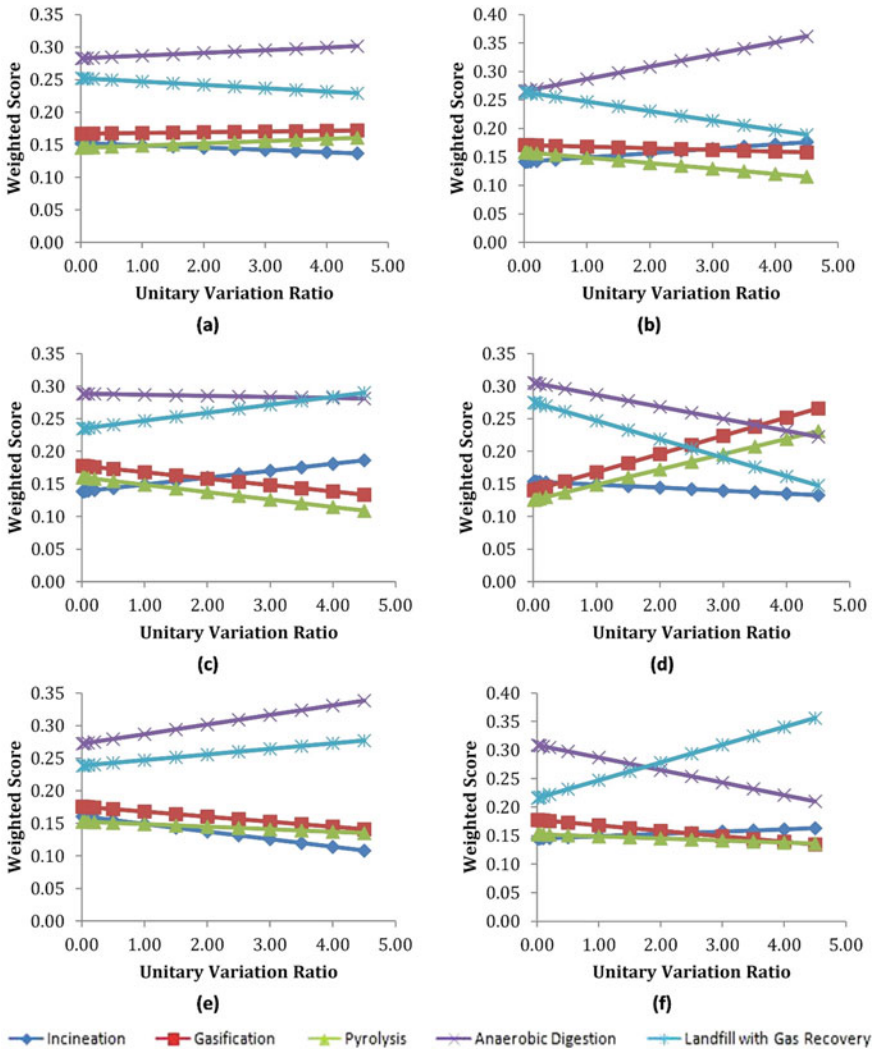
Fig. 5 A weighted score of AHP under different unitary variation ratios for weight global warming potential (**a**), capital cost (**b**), operation and maintenance cost (**c**), revenue return (**d**), moisture content (**e**), and need for segregation (**f**)

4 Conclusions

Four different MCDM techniques AHP, TOPSIS, PROMETHEE, and VIKOR were used in the present study to rank the alternatives for waste-to-energy solutions from five technologies namely incineration, pyrolysis, landfill with gas recovery gasification, and anaerobic digestion based on six criteria i.e., global warming potential,

capital cost, operational and maintenance cost, revenue return, moisture content and need for segregation respectively. Out of the six criteria, the need for segregation and capital cost scored higher weightage whereas moisture content and global warming potential had lower weights. All the four MCDM techniques gave anaerobic digestion as the best waste-to-energy technology with a reasonably higher score compared with the other alternatives. Since TOPSIS does not provide weight elicitation for the criteria and consistency checking of expert's opinion, criteria weightage was taken from AHP and was used for TOPSIS ranking. It is found that the ranks provided by different MCDM techniques were not the same. Comparison of the rankings generated by the four MCDM techniques by using Kendall's coefficient of concordance (ζ) suggested that there existed more than a partial agreement between rankings generated by these four MCDM techniques. Sensitivity analysis of the AHP data showed that the most sensitive criterion was revenue return followed by operation and maintenance cost and capital cost. The study can be further extended by incorporating quantitative information and life cycle assessment (LCA) for the weightage of quantitative criteria such as global warming potential, capital cost, and operation and maintenance cost. Other methods of MCDM like ELECTRE can also be used to compare the results.

References

EMS (2016) Why should I segregate my waste properly? Retrieved September 23, 2017, from Environmental Monitoring Solutions

Forman E, Peniwati K (1998) Aggregating individual judgments and priorities with the analytic hierarchy process. Eur J Oper Res 108(1):165–169

Hwang CL, Yoon K (1981) Methods for multiple attribute decision making. Multiple attribute decision making. Springer, Berlin, pp 58–191

Kalbar P, Karmarkar S, Asolekar SR (2015) Selection of wastewater treatment alternative: significance of choosing MCDM method. Environ Eng Manag J 14(5):1011–1020

Karagiannidis A, Perkoulidis G (2009) A multi-criteria ranking of different technologies for the anaerobic digestion for energy recovery of the organic fraction of municipal solid wastes. Biores Technol 100(8):2355–2360

Karim R, Karmaker C (2016) Machine selection by AHP and TOPSIS method. Am J Indus Eng 4(1):7–13

Khan D, Kumar A, Samadder S (2016) Impact of socioeconomic status on municipal solid waste generation rate. Waste Manage 49:15–25

Kolios AJ, Mytilinou V, Lozano-Minguez E, Salonitis K (2016) A comparative study of multi-criteria decision-making methods under stochastic inputs. Energies 9(7):566

Kuleape R, Cobbina SJ, Dampare SB, Duwiejuah AB, Amoako EE, Asare W (2014) Assessment of the energy recovery potentials of solid waste generated in Akosombo, Ghana. Afr J Environ Sci Technol 8(5):297–305

Kumar A, Samadder S (2017) An empirical model for prediction of household solid waste generation rate—a case study of Dhanbad, India. Waste Manage 68:3–15

Legendre P (2005) Species associations: the Kendall coefficient of concordance revisited. J Agric Biol Environ Stat 10(2):226–245

Li P, Qian H, Wu J, Chen J (2013) Sensitivity analysis of TOPSIS method in water quality assessment: I. Sensitivity to the parameter weights. Environ Monit Assess 185(3):2453–2461

Macharis C, Springael J, De Brucker K, Verbeke A (2004) PROMETHEE and AHP: the design of operational synergies in multicriteria analysis—strengthening PROMETHEE with ideas of AHP. Eur J Oper Res 153(2):307–317

Moya D, Aldás C, López G, Kaparaju P (2017) Municipal solid waste as a valuable renewable energy resource: a worldwide opportunity of energy recovery by using waste-to-energy Technologies. Energy Procedia 134:286–295

Opricovic S, Tzeng G-H (2004) Compromise solution by MCDM methods: a comparative analysis of VIKOR and TOPSIS. Eur J Oper Res 156:445–455

Ouda O, Raza S, Nizami A, Rehan M, Al-Waked R, Korres N (2016) Waste to energy potential: a case study of Saudi Arabia. Renew Sustain Energy Rev 61:328–340

Rahman SM, Azeem A, Ahammed F (2017) Selection of an appropriate waste-to-energy conversion technology for Dhaka City, Bangladesh. Int J Sustain Eng 10(2):99–104

Saaty TL (1980) The analytical Hierarchy process, planning, priority. Resource Allocation, New York

Saaty TL (2008) Decision making with the analytic hierarchy process. Int J Serv Sci 1:83–98

Soltani A, Hewage K, Reza B, Sadiq R (2016) Multiple stakeholders in multi-criteria decision-making in the context of municipal solid waste management: a review. Waste Manage 35:318–328

Triantaphyllou E, Sanchez A (1997) A sensitivity analysis approach for some deterministic multi-criteria decision-making methods. Decis Sci 28(1):151–194

Tscheikner-Gratl F, Egger P, Rauch W, Kleidorfer M (2017) Comparison of multi-criteria decision support methods for integrated rehabilitation prioritization. Water (switzerland) 9(2):8

Wolpert VM (1994) Incineration of municipal solid waste combined with energy production–Latest developments. Renew Energy 5:782–785

Zhao XG, Jiang G-W, Li A, Wang L (2016) Economic analysis of the waste-to-energy industry in China. Waste Manage 48:604–618

Zhaoxu S, Min H (2010) Multi-criteria decision making based on PROMETHEE method. In: 2010 International conference on computing, control and industrial engineering, pp 416–418

Environmental Impact of Application of Ozone Bleaching for Production of Pulp from Agro Based Fibrous Materials—An Innovative Approach

Arvind Sharma, Gunjan Dhiman, Priti S. Lal, and M. K. Gupta

Abstract The pulp and paper sector is facing various issues due to environmental regulatory pressure and expanding market demand, and it is searching for novel solutions to improve product quality and process performance while reducing environmental effects during pulp bleaching. Oxygen delignified wheat straw pulp of kappa number 9.5 was subjected to conventional $CEopH_1H_2$, elemental chlorine free (ECF) i.e. $D_0E_pD_1$ and ozone bleaching sequences at different consistencies to get a final pulp ISO brightness of $85 \pm 2\%$ and evaluation of the physical strength properties of the pulp. The effect of green bleaching was also compared with the conventional and ECF bleaching of wheat straw pulp for their pulp characteristics and physical strength properties. The effect of ozone bleaching of wheat straw pulp on bleach effluent characteristics and their load has also been studied and compared with conventional ECF bleaching system used in agro based mills. The present lab study is helpful in understanding the effect of ozone bleaching on agro based raw material pulp in terms of pulp quality. Less consumption of bleaching chemicals with no effluent load demonstrates that ozone is indeed the bleaching chemical of the future for sustainable growth of the Indian pulp and paper industry.

Keywords Wheat straw pulp · Conventional · ECF · Ozone bleaching · Physical strength properties · Effluent characteristics

1 Introduction

Bleaching of agro pulp has become an environmental issue due to more stringent laws against pollution generated by Indian pulp and paper industries and the release of adsorbable organic halides (AOX). Chlorine based pulp bleaching generates chlorinated organic compounds which accelerate degradation of acute or even chronic toxins and can induce genetic changes in exposed organisms (Métais 2010; Nordén 2006). The recent trend in bleaching is to shift to elemental chlorine free (ECF)

A. Sharma (✉) · G. Dhiman · P. S. Lal · M. K. Gupta
Central Pulp and Paper Research Institute, Saharanpur, India
e-mail: arvind17sharma@yahoo.com

bleaching, i.e. replacing elemental chorine with chlorine dioxide. Chlorine dioxide is a strong oxidant. It has 19 valence electrons, thus, consisting of free radicals. The sensitivity of free radicals present in chlorine dioxide bleaching chemical probably also accounts for its high reactivity as an oxidizing agent used for pulp bleaching. It is specific in reacting with lignin structures of pulp by which lignin gets oxidized. ECF bleaching is more selective which preserves the strength of pulp and at the same time provides high brightness stability with lower effluent load in comparison to the conventional $CEpH_1H_2$ bleaching sequence. The promotion of ECF and total chlorine-free (TCF) bleaching techniques has focused on reducing AOX and total organic chlorides (TOCl) in bleach effluents (McDonough et al. 1985; Chirat and Lachenal 1997; Kawakami and Pikka 2000; Moldenius and Nutt 1995). TCF bleaching techniques considerably decrease the bleach effluent load which provides the scope to make a closed cycle loop system of water. Actually, TCF bleaching process is the culmination of various technologies i.e. oxygen, ozone, hydrogen peroxide, and different other peroxygens. Ozone (O_3) is a very high oxidizing potential agent for bleaching of pulp (Rice and Netzer 1982). Worldwide, since 1990s, it has been used as a bleaching chemical on a commercial scale. Globally, around 25 paper mills were using ozone gas as a bleaching chemical to bleach their pulp (Hannuksela et al. 2004). Ozone is very effective delignifying agent for bleaching wood and non-wood chemical pulps. It can be used by ECF and TCF bleaching sequences at different consistency levels (Liebergott and Lierop 1978; Gellman 1988; Schwarzl 1991; Sixta et al. 1991; Nutt et al. 1993; Lindstrom and Norden 1990). To produce 1 kg ozone gas, 8.3 kg oxygen and 10 kwh power is required. In addition, ozone is a highly viable bleaching chemical which is one and half times less expensive than chlorine dioxide. Only 5–6 kg of ozone is required to bleach 1 ton pulp because ozone is 106 times more reactive to lignin than to carbohydrates (Wyk et al. 2017). During ozone bleaching intermediate radical formations takes place which vigorously attack on carbohydrates that reduces the pulp viscosity (Ragnar 2000; Tripathi et al. 2019). Ozone is an emerging green bleaching practice and favoring on-site chemicals production. TCF based ozone bleaching process is an option to reducing the effluent load as the filtrate from the ozone stage and further extraction stage can be circulated back to the recovery boiler. Ozone is an efficient bleaching agent for the bleaching of wood and non-wood pulps. Ozone can delignify both the wood and non wood chemical pulp when used at low, medium- and high-pulp consistencies in ECF and TCF bleaching. The present study investigated the effects of ozone bleaching on agro wheat straw pulp using conventional ($CEopH_1H_2$), and ECF (D_0EpD_1) bleaching sequences, under optimum process parameters. It was also compared with the TCF bleaching sequence i.e., AZEOP (pressurized) under variable process conditions i.e. pH, fixed ozone dose, ambient temperature, lower to higher consistencies i.e., 5, 12, and 35% and fixed rpm 240 to get a final pulp ISO brightness of $85 \pm 2\%$. The bleached pulp properties, physical strength properties and effluent characteristics were evaluated for all bleaching sequences. For a closure loop system and to mitigate bleach plant effluent load, it is essential to adopt the ECF and TCF bleaching technologies. The implementation of ozone based technologies considerably reduces the generation of hazardous effluent and provides a greener

process for bleaching. It will also help the pulp makers to meet the environmental regulation water norms on the discharge of bleach effluent.

2 Experimental

2.1 Material and Methods

Agro based wheat straw pulp after oxygen delignification stage was received from the pulp and paper mill and stored in the refrigerator at 4 °C for carrying out conventional $CEopH_1H_2$, elemental chlorine free D_0EpD_1 and ozone bleaching AZ(EOP) experiments in the lab to get a target ISO brightness $85 \pm 2\%$. The following standard methods were used to characterize wheat straw pulp, and bleached pulps for various parameters: Kappa number TAPPI T 236-OS-76; Pulp viscosity SCAN-C-15: 65 and Pulp brightness ISO 2470-1-2016(E). 60 g/m^2 bleached pulp hand sheets were prepared using a sheet former. The bleached pulp sheets were pressed, and air dried in atmospheric conditions at 27 ± 1 °C and a relative humidity of $65 \pm 2\%$. The mechanical strength properties were measured using the standard test method i.e. bulk (ISO 534:1988E), burst index (ISO 2758), tensile index (ISO 1924), tear Index (ISO 1974 and P.C. number – CPPRI test method. The Post color (P.C.) number is defined as the brightness reversion of bleached pulp (Giertz 1945) and is calculated by brightness before and after aging. The aging of bleached pulp was determined by putting the pulp sheet in an oven at 105 °C for 4 h as per TAPPI UM200. The post colour number of bleached pulp was calculated as per Eq. 1:

$$\text{P.C. number} = \left(\frac{(1 - R2)^2}{2R2} - \frac{(1 - R1)^2}{2R1} \right) * 100 \tag{1}$$

where R_1 is the brightness before the aging test and R_2 is the brightness afterward.

Methods and Bleaching Conditions

Conventional and ECF bleaching sequences were applied to wheat straw pulp in the laboratory, i.e., $CEopH_1H_2$ and D_0EpD_1 respectively. Bleaching conditions are as follows.

Chlorination (C) Stage

The bleaching experiments were carried out in the laboratory-using batch vessels immersed in a constant temperature bath. The bleaching sequences employed by $CEopH_1H_2$ and $D_0E_pD_1$ were used for oxygen delignification of wheat straw mill pulp. The bleach filtrates were collected for tests. The steps are as follows: Chlorination bleach liquor was used to generate chlorine gas inside the container in which pulp was added. The gas was produced as a result of a decrease in pH < 2 which was kept at around 1.5. After retention time, this pulp was washed and subjected

to a alkali extraction stage reinforcement with a hydrogen peroxide stage. All the conditions, except the chlorine dose for the above-mentioned experiments, were kept constant.

Extraction Followed by Hydrogen Peroxide Stage

Chlorinated lignin derivatives are to be extracted out of the pulp by addition of alkali and hydrogen peroxide chemicals. The alkali and hydrogen peroxide chemical charges were applied at 2.5 and 1% respectively with 2 kg/cm^2 of oxygen pressure. After giving a certain amount of retention time, the pulp was washed.

Hypo Chlorite H_1 and H_2 Stages

The extracted wheat straw pulp is mixed with hypo liquor (40–50 gpl) and the pH was maintained above 9–10. All the process conditions were maintained as in the Fig. 1.

Chlorine Dioxide Stage

Chlorine dioxide bleaching chemical, 40–50 gpl strength, was prepared in the lab using sodium chlorite, acetic acid, and sodium acetate. This solution was added to pulp. The pulp inlet pH of 2–3 was maintained in the D_0 stage, whereas 3–4 in the case of D_1 stage. Chlorine dioxide D_0 and D_1 stages were performed in the polyethylene bags using a water bath. The bleaching chemical of chlorine dioxide was used as D in D_0 and D_1 bleaching stages at 2 and 1%, respectively (Fig. 2).

Bleaching Stage	C	Eop	H_1	H_2
Time - min	45	60	120	120
Temperature- ^{0}C	Ambient	90	80	80
Chemical –kg/O.D. metric ton bleached pulp	23	20	7	2
pH	<2.0	11-12	9-10	9-10
Pulp consistency	3	8	8	8
Pulp brightness %(ISO)	57.2	77.1	81.4	85.1
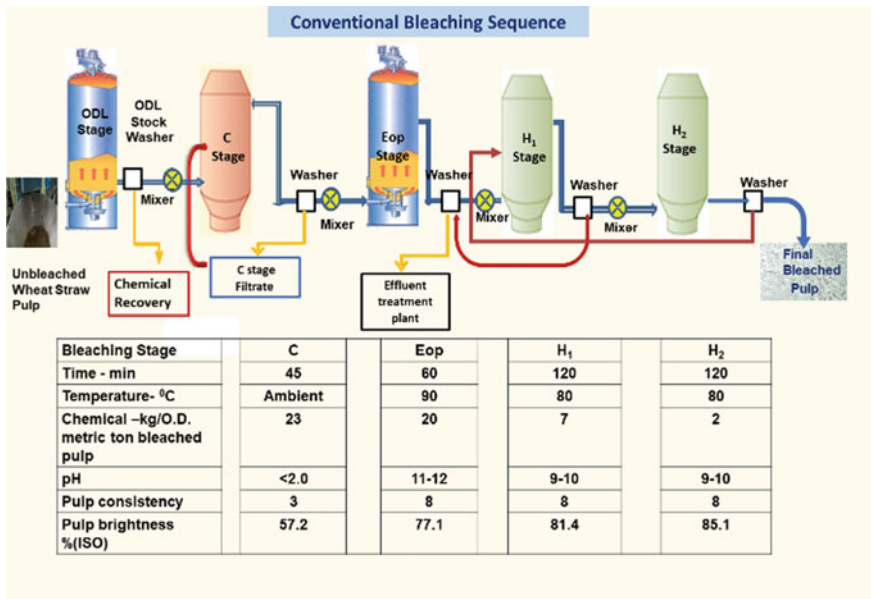
Fig. 1 Graphical representation of conventional bleaching sequence i.e., CEopH$_1$H$_2$
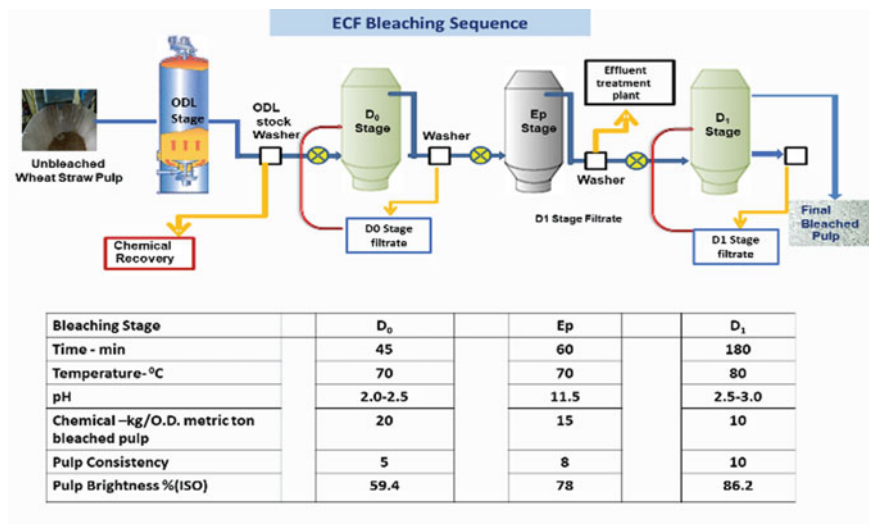
Fig. 2 Graphical representation of ECF bleaching sequence i.e., D_0EpD_1

Bleaching Stage	D_0		Ep		D_1
Time - min	45		60		180
Temperature-°C	70		70		80
pH	2.0-2.5		11.5		2.5-3.0
Chemical –kg/O.D. metric ton bleached pulp	20		15		10
Pulp Consistency	5		8		10
Pulp Brightness %(ISO)	59.4		78		86.2

Total Chlorine Free Bleaching

The oxygen delignified wheat straw pulp was bleached using AZ(EOP) under optimized bleaching conditions. The AZ(EOP) bleaching sequence was carried out at three different pulp consistencies of 5, 12, and 35% as follows.

Acid Stage (A)

Prior to ozone treatment, the pulp was thoroughly mixed with water and sulfuric acid then preheated to the desired temperature in a microwave oven and placed into a temperature-controlled heating bath to maintain a pulp consistency of 5% for 45 min. After the completion of the desired reaction time, about 300 mL of liquor was squeezed out from the pulp for pH analyses. The acid treated pulp was taken for further bleaching experiments.

Ozone Strength Determination

The strength of ozone was determined using the following steps; Take 200 ml of KI solution and 100 ml 4 N H_2SO_4 solution are added in impinger glass bottle with bubbling the sampled air at low flow rate; a second impinger glass bottle is joined in series as a guard detector for ozone transfer and reaction in the bottle; ozone generator at a flow rate 5LPM gas pass in acidified KI solution for 1 min immediately titrating against standard solution of freshly prepared 0.1 N $Na_2S_2O_3$ using 0.5 ml of the starch indicator until solution pale yellow color become colorless.

Ozone concentration in gpl $= 24 \times$ volume of $Na_2S_2O_3$ in ml
$\times$ 0.1 Normality of $Na_2S_2O_3$ divided by initial volume of ozone gas in liter

Ozone Stage

Ozone experiments were performed in a quantum reactor with a 250 g oven dried mixed pulp sample maintaining pulp consistencies of 5, 12, and 35% at pH 2.0–2.5 and an ozone reaction time of 5.0 min with a 10 min retention time. Each pulp sample was acidified to pH 2.5 with 4 N H_2SO_4 and placed into the mixer bowl then supplied with the required amount of ozone injected into the bowl through the ozone generator. The ozone concentration in the stream was measured with the titration method as unreacted ozone from the pulp was collected in a 5% KI solution, after which the residual ozone concentration was determined. The ozone consumed by the pulp was calculated as the difference between applied and residual ozone. At the end of the reaction, the unwashed ozone treated pulp was washed with water for a further bleaching stage.

EOP Stage

Figure 3 depicts the pressurized extraction (EOP) stage of AZ treated pulp in a quantum reactor under various conditions. The desired charges of oxygen, hydrogen peroxide and sodium hydroxide were added into the reactor after the desired temperature was reached. The initial pH of the pulp slurry was taken. After completion of reaction time, the reactor pressure was released, the pulp was transferred to the pulp discharger and 200 mL of liquor was squeezed out from the pulp for pH and residual peroxide analyses.

Bleaching Stage	A	Z	EOP
Time - min	60	10	120
Temperature- °C	85	35-40	110
pH	2.0	2.5-3.0	11-11.5
Chemical –kg/O.D. metric ton bleached pulp	5	4.5	NaOH- 20 kg H2O2- 15 kg
Pulp Consistency	5.0	5,12,35	8
Pulp Brightness %(ISO)	46.0	68.1,69.1, 72.4	81.6,82.4, 85.2
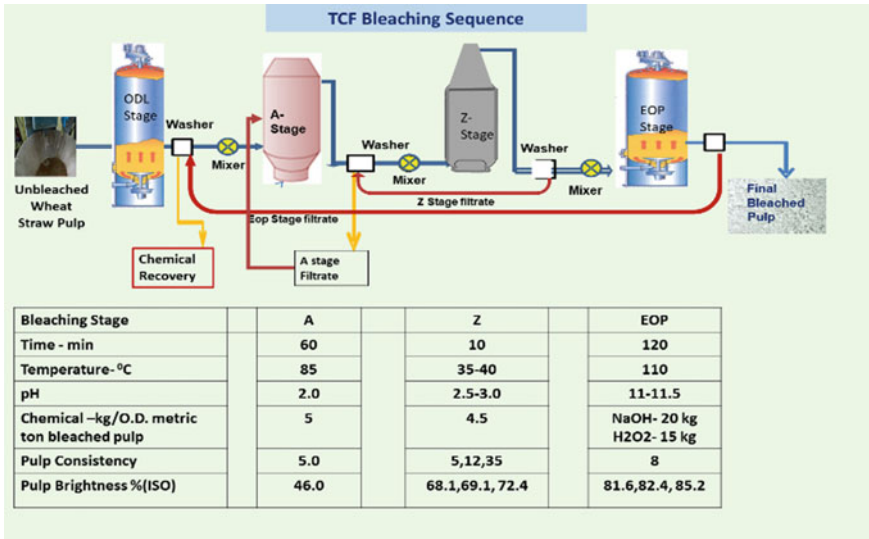
Fig. 3 Graphical representation of TCF bleaching sequence i.e., (AZEOP)

3   Results and Discussions

Table 1 showed the initial characteristics of wheat straw pulp, viz brightness, kappa number, viscosity, and some physical strength properties. Oxygen delignification is an intermediate step applied to unbleached pulp before bleaching to reduce kappa number (Suchy and Dimitris 2002). Maintaining a low kappa number during bleaching of pulp is beneficial for both the economics and the environment (Lal et al. 2020; Pryke 1991). In the oxygen delignification stage, the degree of delignification reaches 40–60%, i.e. kappa number reduction (Rudie 2012). The physical strength properties of wheat straw pulp, i.e. the tensile and tear indices were found to be 40.5 Nm/g and 6.1 mNm^2/g.

A detailed study on the bleaching sequences comparison of wheat straw pulp was carried out as shown in Fig. 4. The results of conventional, ECF and TCF bleaching showed that the final ISO brightness of $CEopH_1H_2$ and D_0EpD_1 bleached pulp is 86.0 and 86.5% respectively. The pulp viscosity of D_0EpD_1 bleached is 552 cc/gm and (13.7%) more compared to $CEopH_1H_2$ bleached pulp, i.e., 476 cc/gm. Chlorine dioxide is more selective towards lignin compared to other bleaching agents;

Table 1 Results of characterization of oxygen delignified wheat straw pulp

Parameters	Unit	Results
Pulp brightness	(%)ISO	47
Kappa number	–	9
Pulp viscosity	cm^3/gm	780
Freeness	ml, CSF	485
Tear index	mN m^2/g	6.1
Tensile index	Nm/g	40.5
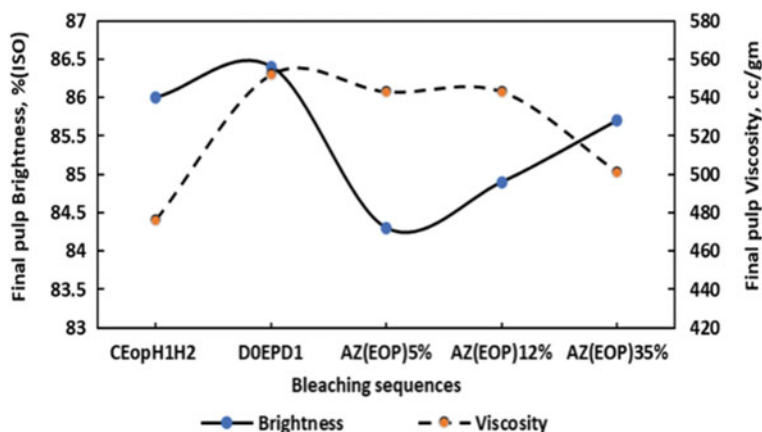
Fig. 4 Effect of different bleaching sequences on brightness and viscosity of final bleach pulp

it can brighten pulp without degrading cellulose. In the $CEopH_1H_2$, chemical used is less selective than chlorine dioxide; hence the viscosity drop is more than in ECF bleaching (Reeve 1987).

The post color number in $CEopH_1H_2$ is 1.53 higher compared to D_0EpD_1 bleached pulp. Post color number of D_0EpD_1 pulp was found to be 0.13, 0.21, and 0.32 points more than AZ(EOP) pulp, when AZ(EOP) bleaching was done at consistency of 5, 12, 35% respectively. Brightness reversion was higher in case of chlorine based bleaching due to destruction of quinine chromophores and generation modified quinones group. Similarly, high PC number was found in conventional and ECF bleaching in comparison to that found in TCF bleaching (Varadha et al. 2007). Acid pretreatment of wheat straw pulp by AZ(EOP) sequence showed minimizing soda carry over and improving performance by lowering bleaching chemical consumption was mentioned in the earlier published research work of Varadha et al. (2007). The removal of hexenuronic acid (HexA) by acid pretreatment and the lowering of bleach chemical demand were discussed in several recent studies. Hexenuronic acids were formed when unsaturated sugars produced from hemicelluloses undergo alkaline degradation during pulping. Bleaching reagents such as chlorine, chlorine dioxide, ozone, and hydrogen peroxide were quickly consumed by these molecules. According to Lindholm (1990a), HexA contributes around 20–60% of the total kappa number for industrial hardwood kraft pulp.

During the ozone stage, pulp viscosity drops by 7.7% at high consistencies of 35%, i.e. 501 cc/gm. The viscosity of pulp was found to on higher side i.e. 543 cc/gm when ozone bleaching was done at lower consistency (5%). As per the earlier research work done by Lindholm (1990a), it was concluded that the reaction product flows more freely in lower consistency than in high consistency bleaching. This may be one of the reasons that contribute to the lower carbohydrate degradation at low consistency bleaching than in high consistency bleaching. The final pulp brightness of the AZ(EOP) bleaching sequence was achieved at 84.3, 84.9, and 85.7% (ISO) at 5, 12, and 35% pulp consistency respectively. The value of post color number varied from 0.12 to 0.40 as shown in Fig. 5. During ozone treatment, ozone breaks the conjugated carbon bonds present in lignin which do not let the pulp become yellow. Ozone stage followed by EOP sequence (pressurized oxygen was used) at high temperature was the final stage of a bleaching sequence AZ(EOP). AZ(EOP) bleaching sequence showed significantly low brightness reversion compared to other bleaching sequences (Gierer and Imsgard 1977; Lindholm 1990b). The purpose of pressurized H_2O_2 addition in AZ(EOP) bleaching sequences was to enhance the lignin removal and brightness gain and to prevent viscosity loss. It is well known that p-quionoid in bleached pulp was mainly responsible for brightness reversion. Hüls (1999) explained that chlorine dioxide creates new p-quionoid structures which enhances the chance of color reversion. Wennerström (2002) also stated that the final pressurized peroxide stage obtained maximum brightness stability. The new quionoid structures formed in the D_0 stage were destroyed in the subsequent peroxide stage at a high temperature (95 °C). Conversely, the chlorine dioxide bleaching stage was not able to remove all the quionoid structures generated (Gierer and Imsgard 1977).
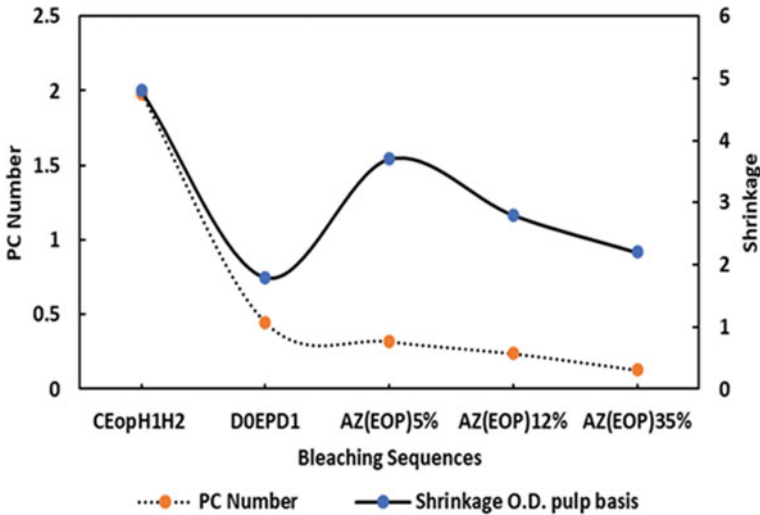
Fig. 5 Effect of different bleaching sequence on PC number and pulp shrinkage of final bleach pulp

Figure 6 showed that the $D_0E_PD_1$ bleached pulp of wheat straw showed an improvement in tear index (5.17%) and tensile index (3.55%) over $CE_{OP}H_1H_2$ bleached pulp. wheat straw pulp at 5, 12, and 35% pulp consistencies showed a tensile index of 28.6, 37.5, and 35.0 Nm/g and a tear index of 6.16, 6.09, and 5.6 mNm^2/g respectively. The decrease in mechanical strength properties was due to less fiber swelling and relative bonding area. The other reason for the decrease in mechanical strength properties may be the extra degradation of low molecular weight carbohydrates after acid and ozone treatments, which adversely affects the inter-fibrillar bonding of the fiber-fiber, fiber-fines and fines-fines (Clark 1981). Zou et al. (2002), demonstrated that hemicelluloses, specifically xylan, can act as protective factors against cellulose degradation and loss of strength and viscosity.

Figure 7 reveals that the increase in COD after the AZ(EOP) bleaching sequence is more than $CE_{op}H_1H_2$, $D_0E_pD_1$ bleaching sequences, which indicates that removal of xylan and lignin after Z stage is more as compared to other bleaching stages. The
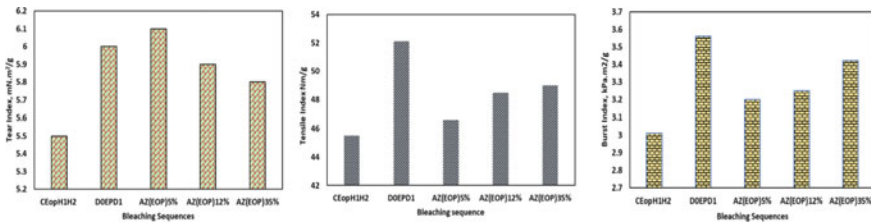
Fig. 6 Effect of physical strength properties i.e. tear, tensile, and burst index, on final bleach pulp
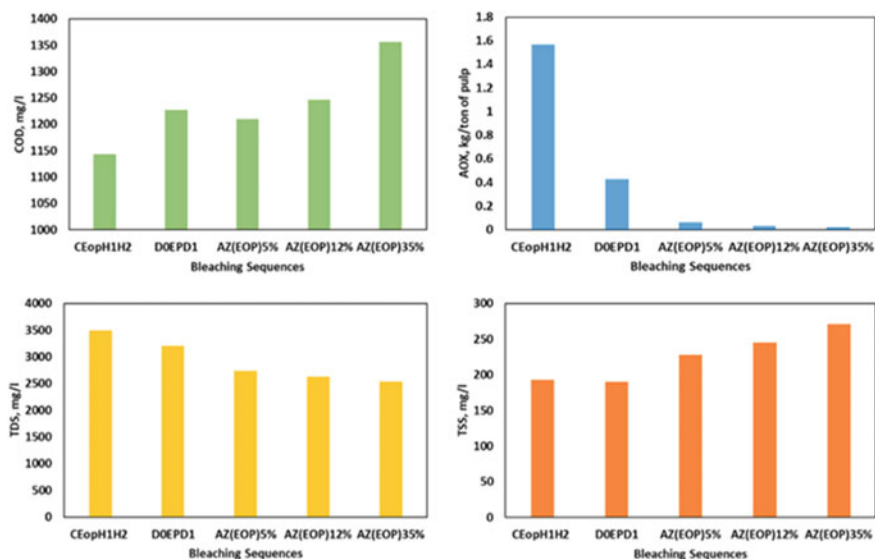
Fig. 7 Effect of bleach effluent characteristics collected in different bleaching stages i.e., TSS, TDS, COD, and AOX of different bleaching sequences

increase in COD of bleached effluents is quite obvious in the case of total chlorine free bleaching, since, the hydrolytic action of ozone leads to the weakening of the carbohydrate bonds in the pulp and its dissolution into the media. Thus, the concentration of lignin and hydrolyzed xylan in the effluent increased markedly, which further added to the color and organic load in effluents (Vidal et al. 1997; Ragnar et al. 2005). The discharge norms of COD as per the industry specific standards notified under the environmental (protection) rules, 1986 is 250 mg/l. The values achieved for COD after different bleaching sequences are higher than 250 mg/l but after the treatment of the bleaching effluent it is easily possible to achieve this range.

The AOX generation was found to be highest in case of $CEopH_1H_2$ sequence i.e. around 1.5 kg/ton of pulp. As per the industry specific standards notified under the environmental (protection) rules, 1986 the upper limit mentioned for small pulp and paper mills for AOX is 2 kg/ton of pulp. The AOX generation was reduced to 0.4 kg/ton of pulp by changing the bleaching sequence to D_0EpD_1 from $CEopH_1H_2$ sequence. As per the industry specific standards notified under the environmental (protection) rules, 1986 the upper limit mentioned for large scale pulp and paper mills for AOX is 1_{kg}/ton of pulp. The D_0EpD_1 sequence provides lower value of AOX generation but even with AOX in the range of 0.4–0.5 kg/ton of pulp it is not feasible for the pulp mill to reuse the water. The above mentioned sequences directly or indirectly require the chlorine based chemicals. Therefore, there is an urgent need of bleaching sequence that is far from the chlorine usage directly or indirectly. The bleaching sequence AZ(EOP) generates AOX in the range of 0.05–0.02 kg/ton of

pulp at different consistency. The lower amount of AOX generated in AZ(EOP) (TCF) provides the scope of water reusage or closed loop system.

4 Conclusion

- The AZ(EOP) bleaching sequence provides a way to achieve pulp brightness of $85 \pm 1\%$ (ISO) at variable pulp consistencies without using a chlorine based bleaching agent.
- The $CE_{OP}H_1H_2$ bleaching sequence showed ISO brightness (86%) and lowest viscosity (490 cc/g). The maximum ISO brightness was achieved by $D_0E_PD_1$ bleaching sequence i.e. 86.5. In case of AZ(EOP) bleaching as the consistency was increased from 5 to 35%, the brightness increased by 1.4 point.
- The AOX generation in AZ(EOP) was found to be lowest at different bleaching consistency in comparison to conventional and ECF bleaching. The AOX generated by AZ(EOP) sequence was found as 0.05 kg/ton of pulp at 5% consistency which was 97% lower than that obtained by conventional bleaching.
- The AZ(EOP) bleaching sequence can be considered as green bleaching processes because the water used in this sequence can be reused.
- The $D_0E_PD_1$ bleaching sequence improved the tear index and tensile index by 5.17 and 3.55% than that obtained by $CE_{OP}H_1H_2$ bleaching sequence. The tensile index obtained after execution the AZ(EOP) bleaching sequence is found to be increased from 28.6 to 35 (22.6% improvement) Nm/g as the consistency was increased from 5 to 35%. Whereas in case of tear index it was vice-versa.
- Green bleaching technology is now on and a pioneering effort will continue to develop processes, especially for agro based raw materials for Indian paper mills.

References

Chirat C, Lachenal D (1997) Effect of hydroxyl radicals on cellulose and pulp and their occurrence during ozone bleaching. Npprj 51(2):147–154

Clark JA (1981) Fibrillation and fiber bonding. In: Pulp technology and treatment for paper. Miller Freeman Publications, San Francisco, pp 160–180

Hüls D (1999) Hydrogen peroxide bleaching in second extraction stage. Information Sheet

Gellman I (1988) Environment effect of paper industry wastewaters—an overview. Wat Sci Tech 20:59–65

Gierer J, Imsgard F (1977) The reactions of lignin with oxygen and hydrogen peroxide in alkaline media. Svensk Papperstidn 80(16):510–517

Giertz HW (1945) Yellowing of pulp. Svenskpapperstidn 48(13):317–321

Hannuksela T, Holmbom B, Lachenal D (2004) Effect of sorbed galactoglucomannans and galactomannans on pulp and paper handsheet properties, especially strength properties. Npprj 19(2):237–244

Kawakami C, Pikka O (2000) Ahlstrom MC ozone bleach technology application to ECF bleach with acid hydrolysis. Japan Tappi 54(7):933–942

Lal PS, Sharma A, Gupta MK, Thapliyal BP, Agrawal P (2020) Response of ozone bleaching on wheat straw and bagasse mixed agro-residue pulp. Paper 23(1)

Liebergott N, Van Lierop B (1978) The use of ozone bleaching and brightening wood pulps. Part 1—chemical pulps, oxygen, ozone and peroxide pulping and bleaching seminar. New Orleans, Louisiana, pp 90–106

Lindholm CA (1990a) Effect of pulp consistency and pH in ozone bleaching. Npprj 5(1):22–27

Lindholm CA (1990b) Effect of alkaline extraction of ozone-bleached pulp on brightness and bleachability. JPPS 16(6):190–195

Lindstrom LA, Norden S (1990) Efficient postoxygen washing—crucial for low bleach plant emissions. Appita 43(5):373–376

McDonough TJ, Berry RM, Betts JL, du Manoir JR, Reeve DW, Turnbull JK (1985) CONFERENCE international pulp bleaching, pp 18–21

Métais A (2010) Proceedings of the TAPPSA National Conference, Durban, South Africa

Moldenius S, Nutt W (1995) Pulp quality and economics of ECF vs. TCF. CONFERENCE International non-chlorine bleaching, Amelia Island, Florida

Nordén S (2006) Eco-friendly bleaching with ZeTrac. IPPTA, Chennai, India

Nutt WE, Griggs BF, Eachus SW, Pikulin MA (1993) Developing an ozone bleaching process. Tappi 76(3):115–123

Pryke DC (1991) Chlorine dioxide substitution. Bleaching: A Tappi press anthology of published papers, pp 253–263

Ragnar M (2000) On the importance of radical formation in ozone bleaching. Doctor Thesis Royal Institute of Technology, Department of Pulp and Paper, Hem. Stockholm, Sweden

Ragnar M, Dahllof H, Lundgren S (2005) Towards environmentally sustainable bleaching of kraft pulp, evaluating the possible role of ozone. Appita 58(6):475–480

Reeve DW (1987) Chlorine dioxide bleaching. Bleach plant operations seminar. Tappinotes, Atlanta, Tappi, pp 67–71

Rice RG, Netzer A (1982) Handbook of ozone technology and applications, vol 1. Ann Arbor Science, Michigan

Rudie AW (2012) The bleaching of pulp. Oxygen delignification. Peter W. Hart

Schwarzl K (1991) Workshop on emerging pulping and chlorine-free bleaching technologies. North Carolina State University, Raleigh, NC, pp 18–20

Sixta H, Gotzinger G, Schrittwieser A, Hendel P (1991) Workshop on emerging pulping and chlorine-free bleaching technologies. North Carolina State University, Raleigh, NC, pp 18–20

Suchy M, Argyropoulos DS (2002) Catalysis and activation of oxygen and peroxide delignification of chemical pulp. Tappi 1(2):1–18

Tripathi SK, Bhardwaj NK, Ghatak HR (2019) Improvement in selectivity of ozone bleaching using DTPA as carbohydrate protector for wheat straw pulp. Npprj 34(3):271–279

Varadha R, Kumar S, Mishra P, Mishra OP, Bajpai P, Tripathi S, Bajpai PK (2007) Hot chlorine dioxide versus conventional D Stage in ECF bleaching of kraft pulps. IPPTA 19(1):87–90

Vidal T, Torres AL, Colom JF, Siles J (1997) Xylanase bleaching of eucalyptus kraft pulp—an economical ECF process. Appita 50(2):144–148

Wennerström M (2002) Decreasing brightness reversion with powerful ozone bleaching. In: International pulp bleaching conference, Portland, USA, pp 265–270

Wyk VB, Madhvan N, Metais A (2017) Ozone bleaching: appropriate strategy for sustainable growth of the pulp and paper industry. In: Proceeding Paperex, pp 74–82

Zou H, Genco JM, Van HA, Cole B, Fort R (2002) Effect of hemicelluloses content in kraft brown stock on oxygen delignification. In: Fall technical conference and trade fair, San Diego, pp 8–111

Perception Towards Infection Control Measures Among Health Care Providers Working in Selected Hospitals of Goa

Shashi L. Yadav, Vedant Bhardwaj, Debasis Patnaik, and Carol Noronha

Abstract Hospitals engage in various types of procedures /devices for early recovery of clients. The majority of Healthcare-Associated Infections [HAIs] manifest after 48 h of admission to the hospital. Central line-associated bloodstream infections [CLABSIs] catheter-associated UTIs [CAUTIs] and ventilator-associated pneumonia [VAP] is a hospital-associated infection that affect the outcome of clients. The objective of this paper is to assess perception towards infection control measures among HealthCare Providers working in selected hospitals of Goa. Exploratory, descriptive design was used to identify whether the health units were following norms as per the Indian Public Health Standards [2013] according to the doctors and nurses working in the selected health units of Goa. 508 participants met the inclusion criteria. A five-point Likert scale was used for the structured questionnaire. This paper used probit models to establish the relationship between socio-demographic variables and the perception of healthcare workers on the three considered parameters. The majority 81.27% of the selected HCP were from public-run hospitals. While 76.25% of them were nurses, doctors remained at 23.75% only. Based on three selected parameters, privately owned hospitals revealed to have better performance than the public run hospitals in Goa. During analysis, it was established that most of the variables did not play a significant role in explaining HCPs' satisfaction perception on infection control measures. Shortage of staff, heavy workload, lack of adequate equipment, and PPE cost-cutting on health hygiene, inadequate use of standard precautions led to HAIs resulting in high morbidity and mortality among hospital admitted clients.

S. L. Yadav (✉)
Department of Economics, K.K BIRLA, Goa Campus, India
e-mail: sshashi_63@yahoo.com

V. Bhardwaj
Department of Economics, Madrid, Spain

D. Patnaik
Department of Economics and Finance, K.K BIRLA, Goa Campus, India
e-mail: marikesh@goa.bits-pilani.ac.in

C. Noronha
Institute of Nursing Education, Goa, India

1   Introduction

Healthcare associated infection [HAI] also known as nosocomial infections are
usually transmitted via healthcare workers, clients, hospital equipment, or interven-
tional procedures. The bloodstream, lungs, urinary tract, and surgical wounds are the
most common sites for infection (Bassetti et al. 2018). The majority of HAIs mani-
fest after 48 h of admission. Invasion with microorganisms multiply and produce
clinical symptoms (Control in Healthcare Facilities, National Centre for Disease
Control 2020) infecting about 90% clients compromised immune systems (Stubble-
field 2017) leading to urinary tract infection in 3%, wound infection in 1.7% and
multiple infections in 0.6%, thus increasing the health cost (Rubinstein et al. 1982).
Central line-associated bloodstream infections [CLABSIs] (Stamm 1991), catheter-
associated UTIs [CAUTIs] (Chastre and Fagon 2002) and ventilator associated pneu-
monia [VAP] (Lolans et al. 2006) are hospital-associated infections that affect the
outcome of clients. Acinetobacter (gram-negative) coccobacillus as an infectious
agent is of clinical [ex. bedridden clients, mechanical ventilation, Haemodialysis
etc.] importance in healthcare institutions (Fournier and Richet 2006). It leads to the
surfacing of strains that are hostile to available commercial antibiotics (Suchitra and
Lakshmidevi 2009). An Indian study revealed total expenses incurred by clients with
surgical site infections [SSIs] was Rs 29,000 [average] as compared to Rs 16,000
[average] incurred by non-infected patients (Jemal 2018). Among health profes-
sionals, 51 [56.0%], had poor practice and 40 [43.0%] had good practice of hand
washing (Kupfer et al. 2019). The study also revealed that the awareness regarding
the Hospital Infection Control Committee was poor among the hospital staff [nurses,
technicians, medical and nursing students] as only 41.7% [N = 120] were aware
of the presence of such a committee (Rosinki et al. 2019). Regardless of the type
of infection, hospital must constituteHospital Infection Control Practices Advisory
Committee and enable the health professionals to adhere to standard precaution
guidelines (Alhmidi et al. 2019). A study showed that 37% of HCP hands were
contaminated after doffing contaminated gloves, but the contamination varied during
the removal of contaminated gloves based on the doffing technique (Chen et al. 2020).

Year 2019 has caused a global pandemic which has continued to be a major public
health issue ever since its emergence [COVID-19] from China (Ministry of Health and
Family Welfare Directorate General of Health Services [Emergency Medical Relief]
2019). To prevent and control transmission of these infections personal protective
equipment (PPEs) is required to be used by healthcare workers to safeguard the health
of others and self by minimizing the exposure to a biological agent (Ward 2020).
Results from a national survey conducted by the French union of private radiolo-
gists revealed that 77% of these radiologists have received and examined clients who
have/or are suspected of having infection. Of the sample, 80% stated that they did

not have sufficient personal protective equipment [PPE] for themselves and technicians (Safe Management of Wastes from Health-Care Activities 2020). Reports of biomedical waste management by nurses in three hospitals indicated that in Hospital I, 86.2% [maximum] participants were found following partially correct practices but in Hospital II, 38.7% of nurses were following correct biomedical waste management practices. 60% nurses were following practices that were partially correct while 74.3% nurses were found following correct practices in Hospital III and 25.1% were found following partially correct practices. However Indian medical students [81–96%] and interns indicated inadequate compliance to BMW management (Kaur 2011).

2 Methodology

2.1 Research Design and Methods

An exploratory, quantitative and descriptive design was used to identify whether the health units were following norms as per the Indian Public Health Standards according to the doctors and nurses working in the selected health units of Goa.

2.2 Data Collection Procedure

Government hospitals were selected because of their provisioning in providing low cost healthcare. A cross-sectional, descriptive study was conducted between May 2017 and May 2018. Primary data was collected from HCPs selected from north and south district of Goa to assess the HCPs' perception towards the quality of infection control measures being carried out at their workplace. A five-point Likert scale was used for this study. Only doctors and nurses willing to participate in the study and who were available at the time of data collection were included. The participants were provided with instructions in a letter addressed to them along with a set of questionnaire. Respondents were aware about the nature and scope of the research under study. Each participant was handed over a questionnaire during a specific time. A feasible slot during the non-busy shift time was provided by the authorities. Every respondent was met by the investigator and requested to complete the questionnaire without discussing the questionnaire items with their colleagues, and to complete the same as soon as possible and hand over to the person kept in charge to collect the envelope which would be later collected by the investigator on the date and time specified to them. Each HCP spent 10–15 min filling up the questionnaire. All the distributed questionnaires were completed and returned after a week's time.

Ethical clearance was obtained from Director, Directorate of Health Services, Goa and Medical Superintendent of a private hospital. Further permission was obtained

from respective Head of Department of the hospitals under study. Initially, a sampling frame of HCPs available in each hospital was prepared. A simple random technique was used to obtain a sample of 700 HCPs However, a total of 508 participated in the study. A structured questionnaire was designed in English. The content of the questionnaire was divided into two sections. Section 1 consisted of socio-demographic variables and Section 2 consisted of questions on the perception of HCPs towards infection prevention and control in their hospitals on three dimensions.

3 Data Analysis

The Excel (Microsoft Office version 2003)/SPSS/STATA computer program was used to analyse the data, with the assistance of a statistician.

This paper uses probit models to establish the relationship between socio-demographic variables and the perception of healthcare workers on the considered parameters which included the constitution of Infection Control Committee, maintenance of standard precautions (hand hygiene, cough etiquette, use of PPE, and prevention of needle stick injury) and waste segregation [Disposable items, blood, body fluids. Secretions and excretions clinical waste in accordance with hospital policy].

Analysis is conducted by estimating models denoted by Eqs. (1–3). The dependent variables Y_1, Y_2 and Y_3, represents whether the healthcare provider is satisfied with Infection Control committee, Standard Precautions maintained in hospitals and Waste Segregation. If the healthcare provider is satisfied the score is equal to "1" and if not satisfied the score is "0".

$$
\begin{aligned}
Y_{1i}^* &= X_i'\beta + \epsilon_1 \\
Y_{1i} &= 1, \quad if\, Y_{1i}^* > 0 \\
Y_{1i} &= 0, \quad if\, Y_{1i}^* = 0
\end{aligned}
\tag{1}
$$

$$
\begin{aligned}
Y_{2i}^* &= X_i'\beta + \epsilon_2 \\
Y_{2i} &= 1, \quad if\, Y_{1i}^* > 0 \\
Y_{2i} &= 0, \quad if\, Y_{1i}^* = 0
\end{aligned}
\tag{2}
$$

$$
\begin{aligned}
Y_{3i}^* &= X_i'\beta + \epsilon_3 \\
Y_{3i} &= 1, \quad if\, Y_{1i}^* > 0 \\
Y_{3i} &= 0, \quad if\, Y_{1i}^* = 0
\end{aligned}
\tag{3}
$$

Source: (IBM User 2005).

In the above equations, Xi is a vector of individual-level characteristics, β is a vector of parameters, and ε_{1i} is the error term that is normally distributed. The above probit equations are estimated by the maximum likelihood method.

4 Results

The majority 81.27% of the selected HCP were from public run hospitals. While 76.25% of them were nurses, doctors remained at 23.75% only. Highest 43.30% had experience of less than five and 7.38% were the lowest i.e. > 15–20 years. 69.83% of the respondents were found to be working in the ward; remaining 30.17% had to manage OPD/Casualty/Emergency. Regarding income, 39.30% earned <Rs 25,000 while 28.99% earned >50,000/month (Table 1)

Table 2 gives the marginal effect estimates for the probit analysis done to study the impact of individual-level variables on their satisfaction level on the considered parameters in ward prevention of infection and control. Compared to males, females were significantly more satisfied [12.7%] with the maintenance of standard precautions in the wards. HCPs' assessment with regards to experience 10–15yrs [12.1%] was found to be significant and negatively associated with satisfaction regarding maintenance of standard precautions. Income between Rs 25,000–50,000/month has a significant positive association [10%] with satisfaction in terms of waste segregation. Whereas income >50.000 also has a slightly higher significant positive association [11.5%] and [18.8%] with satisfaction in relation to standard precautions and waste segregation in hospital. Respondents posted in selected wards [Indoor] of the hospital had a significant positive association [8.66%] with satisfaction pertaining to waste segregation. Doctors [14.6%] had a significant negative association as regards to satisfaction on maintenance of standard precautions when dealing with infection prevention and control measures. Table 2 also displays the hospital type (private) to be statistically significant in determining satisfaction with measures to prevent infection and control in various hospitals.

Based on three selected parameters, private owned hospitals appear to have better performance than the public run hospitals in Goa. Healthcare providers at Primary Health Centres [PHCs], Community Health Centre [CHC], Sub- District hospital [SDH] and District hospital [DH] are [−42.8%, −52%, -−39.9% and −63.9% respectively], significantly less likely to be satisfied with reference to constitution of infection control committee.

HCPs at CHCs, SDH and DH [−33.2%, −10% and −47.9%] are significantly less likely to be satisfied with components of maintenance of standard precautions. HCPs of PHCs, CHCs, SDHs and DHs are significantly less satisfied [−9%, −32.9%, − 21.7% and −51.8%)] concerning hospital waste segregations.

During analysis considering the effect of other variables it is established that most of the variables do not play a significant role in explaining HCPs satisfaction perception on infection control measures. Income per month has a significant role in explaining the satisfaction level for maintenance of standard precautions and

Table 1 Provides the summary statistics for all the independent and dependent variables considered in the below mentioned analysis

Independent variables	
Gender	
Male	18.41%
Female	81.59%
Education level	
Diploma	42.08%
Graduate	28.38%
Postgraduate and above	29.54%
Years of experience	
<5	43.30%
>5–10	23.88%
>10–15	15.73%
>15–20	7.38%
>20	9.71%
Income	
<25,000	39.30%
25,001–50,000	31.71%
>50,000	28.99%
Working field	
OPD/Casualty/Emergency	30.17%
Indoor	69.83%
Medical staff	
Nurses	76.25%
Doctors	23.75%
Hospital type	
Primary Health Centre (PHC)	10.04%
Community Health Centre (CHC)	12.93%
Sub District Hospital (SDH)	35.91%
District Hospital (DH)	22.39%
Private Hospital	18.73%

(*Primary source* Shashi Lata Yadav, May 2016 to December 2018, Goa State)

hospital waste segregations. HCPs working indoors are more satisfied than the HCPs working in the outpatient department with hospital waste segregation procedures. Compare to nurses, doctors are dissatisfied with component related to constitution of infection control committee and maintenance of standard precautions. HCPs of all centres/hospital were dissatisfied with the three main components of infection prevention and control measures.

Table 2 Satisfaction of healthcare providers based on their socio-demographic variables

	Infection control committee	Standard precautions	Waste segregation
Gender			
Male	(Reference)		
Female	0.00138	0.127[a]	0.0348
	(0.0604)	(0.0610)	(0.0554)
Education			
Diploma	(Reference)		
Graduate	−0.0755	0.0289	0.0101
	(0.0520)	(0.0470)	(0.0453)
Post graduate and above	−0.0514	−0.0699	−0.0385
	(0.0496)	(0.0493)	(0.0462)
Experience			
<5	(Reference)		
>5–10	−0.0481	−0.0371	−0.00846
	(0.0511)	(0.0501)	(0.0457)
>10–15	−0.0777	−0.121[a]	−0.0839
	(0.0584)	(0.0593)	(0.0544)
> 15–20	−0.0498	0.0827	−0.0526
	(0.0800)	(0.0709)	(0.0719)
> 20	0.0661	0.0454	−0.0130
	(0.0734)	(0.0703)	(0.0698)
Income			
<25,000	(Reference)		
25,001–50,000	−0.0497	0.0285	0.100[a]
	(0.0524)	(0.0525)	(0.0500)
> 50,000	0.0671	0.115[a]	0.188[b]
	(0.0621)	(0.0589)	(0.0560)
Area			
OPD/Casualty/Emergency	(Reference)		
Indoor	0.0305	0.0785[c]	0.0866[a]
	(0.0453)	(0.0459)	(0.0432)
Medical staff			
Nurses	(Reference)		
Doctors	−0.156[a]	−0.146[b]	−0.0430
	(0.0625)	(0.0558)	(0.0572)

Table 2 (continued)

	Infection control committee	Standard precautions	Waste segregation
Hospital type			
Private Hospital	(Reference)		
Primary Health Centre	-0.428^{b}	-0.107^{c}	-0.0912^{a}
	(0.0671)	(0.0607)	(0.0436)
Community Health Centre	-0.520^{b}	-0.332^{b}	-0.329^{b}
	(0.0741)	(0.0771)	(0.0701)
Sub District hospital	-0.399^{b}	-0.100^{a}	-0.217^{b}
	(0.0542)	(0.0491)	(0.0445)
District hospital	-0.639^{b}	-0.479^{b}	-0.518^{b}
	(0.0415)	(0.0471)	(0.0394)
Observations	508	508	508
AIC			

Standard sserrors in parentheses (Primary source: Shashi Lata Yadav, May 2016 to December 2018, Goa State)

[a] $p < 0.05$, [b] $p < 0.01$, [c] $p < 0.10$

5 Conclusion

Hospital acquired infections are a major safety concern for the admitted clients as majority of HAIs are forty-eight hrs post admission. HCPs are responsible to conform to best evidence based practices to prevent nosocomial infections. Majority of the HCPs in public run hospitals were directly dealing with indoor clients and as per probit analysis had a significant positive association with satisfaction concerning waste segregation which explains that to some extent hospital has been following waste segregation practices and BMW management. Compare to private hospital, public run hospital are required to perform better in reference to constitution of infection control committee to bring about awareness and revert any disaster during state or global pandemic. The present study also highlighted the need to safeguard the health of HCPs and the clients in hospitals pertaining to maintenance of standard precautions by having sufficient PPE.

References

Alhmidi H, Gonzalez-Orta M, Cadnum JL, Mana TS, Jencson AL, Wilson BM et al (2019) Contamination of health care personnel during removal of contaminated gloves. Am J Infect Control 47(7):850–852 (2019) Available from: https://doi.org/10.1016/j.ajic.2018.12.003

Bassetti M, Righi E, Vena A, Graziano E, Russo A, Peghin M (2018) Risk stratification and treatment of ICU-acquired pneumonia caused by multidrug- resistant/extensively drug-resistant/pandrug-resistant bacteria. CurrOpinCrit Care 24(5):385–393 (2018). (https://www.healthline.com/health/hospital-acquired-nosocomial-fections)

Chastre J, Fagon JY (2002) Ventilator-associated pneumonia. Am J RespirCrit Care Med 165(7):867–903

Chen N, Zhou M, Dong X, Qu J, Gong F, Han Y et al (2020) Epidemiological and clinical characteristics of 99 cases of 2019 novel coronavirus pneumonia in Wuhan, China: a descriptive study. Lancet 395(10223):507–13 (2020). https://doi.org/10.1016/S0140-6736(20)30211-7

Control in Healthcare Facilities, National Centre for Disease Control (2020) Directorate general of health services of health and family welfare, Government of India, pp 1–230. Available from: https://www.mohfw.gov.in/pdf/National%20Guidelines%20for%20IPC%20in%20HCF%20-%20final%281%29.pdf

Fournier PE, Richet H (2006) The epidemiology and control of Acinetobacterbaumannii in health care facilities. Clin Infect Dis 42:692

Jemal S (2018) Knowledge and practices of hand washing among health professionals in Dubti Referral Hospital, Dubti, Afar, Northeast Ethiopia. Adv Prev Med 1–7 (2018). Available from: https://doi.org/10.1155/2018/5290797

Kaur SA (2011) Comparative study on knowledge and practices of nurses regarding biomedical waste management in select government hospitals. Nurs Midwifery Res J 7(3):1–11. Available from: http://medind.nic.in/nad/t11/i3/nadt11i3p130.pdf

Kupfer TR, Wyles KJ, Watson F, La Ragione RM, Chambersand MA, Macdona AS (2019) Determinants of hand hygiene behaviour based on the theory of interpersonal behaviour. J Infect Prev 20(5):232–237 (2019) Available from: https://doi.org/10.1177/175717741984628

Lolans K, Rice TW, Munoz-Price LS, Quinn JP (2006) Multicity outbreak of carbapenem-resistant Acinetobacterbaumannii isolates producing the carbapenemase OXA-40. Antimicrob Agents Chemother 50:2941

Ministry of Health and Family Welfare Directorate General of Health Services [Emergency Medical Relief] (2019) Novel coronavirus disease 2019 (covid-19): guidelines on rational use of personal protective equipment. Available from: https://www.mohfw.gov.in/pdf/GuidelinesonrationaluseofPersonalProtectiveEquipment.pdf

Rosinki J, Rozanska A, Jarynowski A, Wojkowska-Mach J (2019) Polish society of hospital infection team (WHAT IS THIS?). Factors shaping attitude of medical staff towards acceptance of the standard precautions. Int J Environ Res Public Health 16:1050 (2019)

Rubinstein E, Green M, Modan M, Amit P, Bernstein L, Rubinstein A (1982) The effects of nosocomial infections on the length and costs of hospital stay. J Antimicro Chem 9(suppl_A):93–100 (1982). Available from: https://doi.org/10.1093/jac/9.suppl_A.93

Safe Management of Wastes from Health-Care Activities (2020) Handling, storage, and transportation of health-care waste, pp 1–6. Available from: https://www.who.int/water_sanitation_health/medicalwaste/061to076.pdf?ua=1

Stamm WE (1991) Catheter-associated urinary tract infections: epidemiology, pathogenesis, and prevention. Am J Med 91(3):S65–S71

Stubblefield H (2017) What are nosocomial infections? June 6, 2017. Available from: https://www.healthline.com/health/hospital-acquired-nosocomial-infections

Suchitra JB, Lakshmidevi N (2009) Surgical site infections: assessing risk factors, outcomes and antimicrobial sensitivity patterns, African J Microbio Res 3(4):175–179. http://www.academicjournals.org/ajmr

IBM USER (2005) Review of linear estimation. http://www.columbia.edu/~so33/SusDev/Lecture_9.pdf

Ward P (2020) Radiographers speak on PPE and COVID-19 infection control. French survey pinpoints PPE shortages, financial pressures. April 28, 2020. Available from: https://www.auntminnieeurope.com/index.aspx?sec=log&itemID=618712

Assessment of Catalytic Biodiesel Production: A Mini-Review

Deeptanshu Sharma, Arnav Gupta, Lavisha Bashambu, Rasmeet Singh[iD], and Surinder Singh

Abstract The Rapid and sustained increase in the world's energy demands has meant that humanity's dependence on fossil fuels is ever-increasing and so are its greenhouse gas emissions. Such is the scenario that unless drastic changes are to the way mankind powers its society, limiting global temperature increase to below 2 °C will not be possible. Biodiesel, whose adoption would require minimal changes to our existing infrastructure presents a viable alternative to petroleum-based fuels. With broad feedstock flexibility such as its ability to be sourced from waste vegetable oils and fats and numerous production techniques, biodiesel production can be ramped up fairly quickly depending upon local conditions to optimize for resource utilization and minimal waste generation. The introduction of newer, more efficient catalysts as well as their recovery techniques and the development of new techniques to extract oil from microalgae mean that biodiesel production will remain one of the most promising areas of inquiry in the energy sector.

Keywords Biodiesel · Homogeneous · Heterogeneous · Catalyst · Transesterification

1 Introduction

The use of conventional fossil fuels has been increasing, a trend which is not sustainable and has led to depletion of fossil fuel reserves. Most of the transportation industry and other energy intensive industries utilize fossil fuels. Although this number has been decreasing recently with the introduction of electrical vehicles, the need for renewable sources is still present. Biodiesel is a combustion fuel similar to petrol/diesel in its combustion properties and is more environment friendly than both petrol and diesel. It is a long chain of methyl or ethyl ester of fatty acid and can be made from various feed stocks such as vegetable oil (fresh or recycled from

D. Sharma (✉) · A. Gupta · L. Bashambu · R. Singh · S. Singh
Dr. S.S. Bhatnagar University Institute of Chemical Engineering and Technology, Panjab University, Chandigarh 160 014, India
e-mail: deeptanshusharma.ds@gmail.com

waste) oil and even animal fats (Al-Zuhair 2007). Biodiesel can be produced from any of these feed stocks with varying yields depending on the availability and quality of feed stock. As waste oils and fats can be used as a feedstock for biodiesel production, biodiesel production not only reduces the waste generated but also provides an eco-friendly alternative to petroleum and diesel. While the original diesel engine developed by Rudolph Diesel was demonstrated to work well with vegetable oil, rapid developments in the petroleum industry led to the adoption of petrol and diesel as the dominant fuel and further development of biofuels did not receive much attention. Now with increasing environmental concerns, use of biofuels has garnered renewed interest. Even with incentives provided by the governments in the form of tax credits and subsidies, biodiesel still has to compete with petro diesel to enable its widespread adoption. While a number of factors such as cost of feedstock, production, purification, distribution and storage play a role in determining the economics of biodiesel, the most important factor is feedstock, which forms about 80% of the cost. Here is where the flexibility of feedstock can play a definitive role as biodiesel can be produced from a wide variety of waste fats and oils. Since the production is not reliant on a particular type of oil, local conditions such as availability of waste oils as well as vegetable oils can drive down the costs considerably. Optimal resource utilization will be a key factor in determining the future of biofuels as they look to compete with petro-fuels (Chisti 2007).

The following review critically analyses the whole biodiesel production chain and not just the production process. This review has analysed various feedstocks and their potential for large scale use in sustainable biodiesel production as well as various methods of biodiesel production laying special focus on their scalability and how they stack up against more conventional methods of biodiesel production. A lot of attention is paid to the transesterification process which remains the favoured method for producing biodiesel. Both the homogeneous and heterogeneous catalytic processes are analyzed with effects of feedstock properties and catalysts on the overall process. The paper discusses the promising advances made towards making this process more commercially viable.

2 Biodiesel Production

There are many steps involved in biodiesel production and each has been analysed in the review. The whole biodiesel production process can be divided into 3 key steps (i.e. feedstock production, feedstock processing, and biodiesel production).

2.1 Biodiesel Feedstock Production

Biodiesel can be produced from extracts from various sources such as vegetable oil, waste cooking oil and animal fats as well as from other unconventional sources

such as oil producing microalgae (Al-Zuhair 2007). The choice of feedstock has profound impact on the quality and cost of the final biodiesel product. The choice of feedstock is further limited by geography and availability of suitable oil-bearing wastes which can be transported and processed effectively. At present, rapeseed is popularly used in Europe, soybean is used in Brazil and USA while coconut and palm are utilized in temperate Asiatic regions. Use of edible oils as biodiesel feedstock presents an issue as these oils are also used for primary consumption and their use for purposes other than that might negatively affect the food chain and drive up the price of food commodities. Although crops producing inedible vegetable oils can also be used, they still would contribute to the massive deforestation and subsequent loss of biodiversity resulting from the need to grow these crops on a massive scale. Europe has already seen extensive discussions and proposals to limit the arable land available for growing biofuel feedstocks.

Another source is by-products from industrial food processing sources such waste cooking oil, waste poultry fats, tallow and fish oils etc. which are often cheaper than raw oil. A lot of research has been focused on using microalgae as feedstock as they could help overcome the above-mentioned constraints faced by vegetable oil crops. Micro-algae do not only have 49–132 times shorter time to harvest when compared with common crops, they pack about 30% more oil per biomass weight (Chisti 2007). They can be grown in harsher environments where they won't compete for land with food crops and can even be used for wastewater treatment efforts such as removal of nitrogen and phosphorous from effluents (Hodaifa et al. 2008).

2.2 Feedstock Processing

2.2.1 Oil Extraction

The oil extraction often involves two steps-mechanical extraction of oil and subsequent solvent extraction for enhanced recovery. The seeds are first cleaned and then pressed mechanically at 40–50 °C to maximize oil collection. The collected oil is filtered and sent for further processing. The oil seed cake obtained as the by-product can be sent for solvent extraction or used as protein rich fodder. For large scale production of oil, solvent extraction is almost always used as the enhanced recovery offsets the additional cost of the process. This oil recovered from this process depends on the type of seeds used, temperature and the solvent used for the process. For more efficient contacting, the pressed oilseeds are flaked and leached with solvent at around 80 °C. The solvent-oil mixture is separated by injecting steam and then condensing the vapors. The solvent often used is n-hexane as it gives the best yields. Toxicity of the solvent and the air and water pollution caused by this process has prompted more research into greener solvents or other extraction methods such as enzymatic extraction method which uses bio-enzymes for extraction of oil and does not produce volatile organic matter and is thus environment friendly.

The efficient extraction of oil from microalgae is still in its early stages but process as described in can be used where the algal biomass is dried in sunlight and grinded to a fine powder (Grima et al. 2003). This dried mass is then separated into different sizes and then the oil is separated by solvent extraction process. The resultant mixture settles into two distinct layers over 24 h and can be separated easily. Due to the high water content in the algal biomass, sun drying is not always effective and other methods such as spray drying and lyophilization might need to be utilized although they would drive up the cost of the oil. Ethanol-Hexane is the preferred choice of solvent as it gives the maximum yield but the choice can be varied depending upon the type of microalgae and the nature of lipids extracted. Overall, this method still has ways to go before it can be economically viable and produce biofuels at a cost competitive with petroleum fuels.

2.2.2   Feed Pre-treatment

The oil extracted from the feedstock needs to be treated before it can converted into biodiesel. The type of pre-treatment depends on the methods used for biodiesel conversion as well as the properties of the feedstock. For the most prominent method, transesterification, the oil needs to degummed, free from moisture and Free Fatty Acids (FFA) for optimal conversion to biodiesel. The degumming process removes phosphatides from the oil.

Degumming of oil is necessary because the presence of phosphatides causes the oil to retain water and gives it a muddy appearance. Acid degumming uses acid to remove insoluble phosphatides which are not in hydrated state from the oil while water degumming involves mixing of water with oil to remove the hydrated phosphatides using centrifugation where the phosphatides are removed with water and the treated oil is sent for further processing.

The next step involves the removal of Free Fatty Acids (FFAs) from the oil. Different types of fatty acids are present in different types of oil but it is seen that FFAs with even number of carbon atoms make up a large portion of the total fatty acid content. FFAs and other oxidized acids must be removed as they negatively affect the transesterification yields as well as the shelf life of biodiesel. Removal of acids is necessary as the FFA can react with the catalyst to form soap which occurs at a much faster rate than the transesterification reaction. The saponification reaction also causes problems later into the process as it forms emulsions and makes purification of biodiesel more difficult. Feeds with FFA content of more than 1% are treated to neutralize the acid and this can help increase the overall yield of the process.

Water content in the oil depends on the source and extraction process used. Waste oils and animal fats depending upon, the source and the treatment process used can have varying amount of water content in them where as oils from other plant-based sources have water content of around 1–5% w/w. Presence of water in the reactor causes suppression of the transesterification reaction and instead leads to the hydrolysis reaction causing soap formation when alkali catalysts are used. The yield of the transesterification reaction may slip below 90% if the moisture content

in the reaction is more than 0.5% (Canakci and Gerpen 1999). The saponification side reaction due to water also uses up some of the catalyst thereby reducing the efficiency of the process and increasing the cost of production as the catalyst will have to be continuously replaced. The oil is dehydrated by low pressure distillation which removes water and keeps the overall water content below 0.06%. Apart from water, depending upon the source of oil, additional treatments such as filtration and centrifugation might be required to removal the solids in the oil. Presence of chlorides might also be a cause of concern as they can lead to corrosion of the piping and equipment over time.

Factors such as the quality of the feedstock and the processes employed for their treatment play an important role in deciding the cost of the final biodiesel product which has to ultimately compete with the economics of petro-diesel.

2.3 Biodiesel Production

Most widely used method for the production of biodiesel production is the transesterification of oils with alcohol. The reaction produces esters and glycerol which need to be separated. The methods is also known as alcoholises of triglycerides (oil) as the alcohol part in the triglyceride is replaced with that from another short chained alcohol where the alcohol plays a role similar to that played by water in hydrolysis.

The two components of the reaction—oil and alcohol are immiscible in each other i.e., they do not mix to form a single phase which leads to poor contacting inside the reactor which leads to long reaction times. Therefore, various kinds of catalysts are employed to enhance the surface contact between the phases leading to vastly improved reaction times. The selection of proper catalyst is essential for improving the yield of biodiesel production as well as lowering the cost of production.

2.3.1 Homogeneous Catalytic Transesterification

Homogeneous catalytic transesterification involves the use of catalyst which is liquid state during the reaction which is same as that of reactants. The catalyst used can be either an acid or base which needs to be separated from the reaction mixture at the end of the process. Usually either methanol or ethanol is used for the production of biodiesel. The biodiesel produced when methanol is used is called Fatty Acid Methyl Ester (FAME) while that produced when ethanol is used is called Fatty Acid Ethyl Ester (FAEE). Use of methanol is more widespread as it undergoes transesterification at a quicker rate and is also cheaper than ethanol. However there are concerns regarding the use of methanol owing to its toxicity as well as the fact that methanol itself is derived by reforming natural gas, which undercuts the goal of biodiesel as a replacement for fossil fuels. Ethanol is non-toxic and can also be produced sustainably from waste biomass and thus help reduce dependence on fossil fuels. FAEE biodiesel has better cetane number than FAME biodiesel and also has
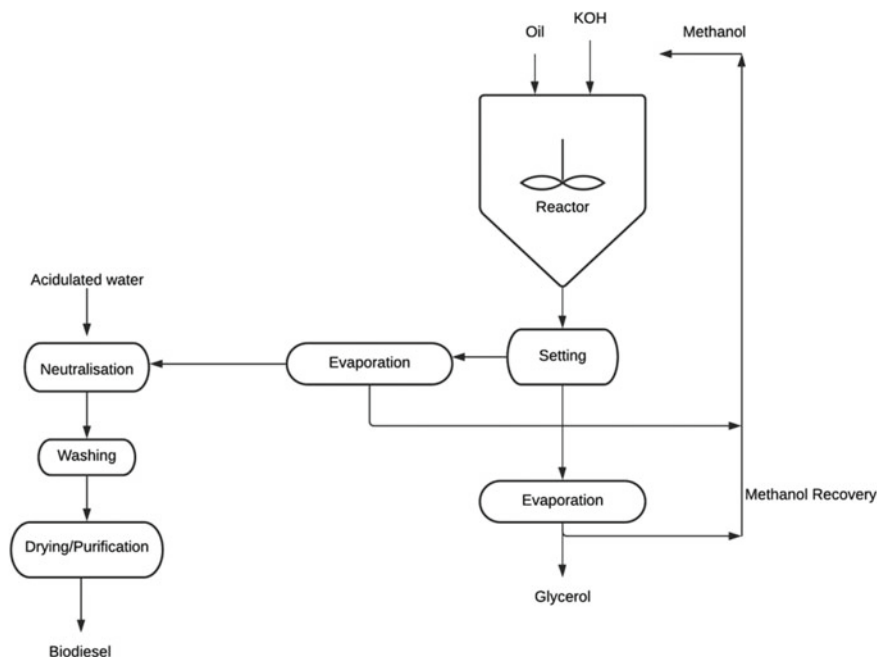
Fig. 1 Typical biodiesel production process with alkaline catalysis (Lotero et al. 2006)

slightly better heat content. However, factors such as lower reactivity of ethanol, higher energy requirements for FAEE biodiesel production as well as difficulty in separation of ester and glycerol mean that methanol is still the preferred short chain alcohol for biodiesel production.

Base Catalysed Homogeneous Transesterification

This type of process uses a catalyst which is alkaline in nature such as alkali metal hydroxides or alkoxides. The reaction as shown in the Fig. 1 gives a mixture of esters, glycerol, unreacted oil (mainly triglycerides) and alcohol as well as the catalyst which all need to be separated.

After reaction, the mixture is allowed to settle for almost 8 h where the ester-triglyceride mixture floats above the heavier glycerol-alcohol mixture and is separated. Stoichiometric molar ratio of oil to alcohol required for the process is 1:3 but since the reaction is reversible, ratios of 1:6 are used to drive the reaction equilibrium forward. The reaction conditions such as temperature and pressure are also mild with the reaction taking place at or slightly above atmospheric pressures and 50–70 °C (Lotero et al. 2006).

The base catalysed reaction is an order of magnitude faster than the acid catalysed one which allows for the production of higher amount of biodiesel at a site. The

concentration of the catalyst required is also low, typically between 0.5 and 2% w/w is enough for the reaction which means that the corrosion of equipment is not as severe as seen in the acid catalysed reaction systems. Since the molar ratios of oil to alcohol required for this process is significantly less than that required for the acid catalysed reactions, a lot of cost saving is achieved due to lower separation costs for the whole process.

The base catalysed homogeneous route although seems to be ideal for volume production of biodiesel, it does suffer some limitations. The reaction is very sensitive to the presence of fatty acids and water in the oil. Presence of either or both of them beyond very low amounts carries significant penalties for the process in the form of reduced yield of biodiesel, lower rate of reaction and loss of catalyst. As explained before, this is mainly due to saponification side reaction which takes precedence over the desired transesterification reaction. Pre-treatment steps to avoid these undesired reactions drive the cost of the overall process.

Acid Catalysed Homogeneous Transesterification

Another way of producing biodiesel is through the use of homogeneous acid catalysts such as hydrochloric acid and sulphuric acid. The acid catalysed reactions are much slower than the base catalysed reactions and also require higher temperature for optimum yield. The oil to alcohol molar ratios required are also much larger with maximum yield obtained for 1:20 which drives up the cost of the process as it requires larger reactors as well as the separation and pumping costs are also much higher.

Where this method can be economical is when the oil has high free fatty acid content as saponification does not take place when acid catalysts are employed for biodiesel production. This allows for greater flexibility in feedstock and saves cost of pre-treatment operations. This method however, just like the base catalysed method, is still susceptible to the presence of moisture in the oil with the process suffering lowered reaction yield from water content as low as 0.1% (Cerveró et al. 2008).

2.3.2 Heterogeneous Catalysis

Heterogeneous Catalysis has been gaining popularity as the catalysts used can be regenerated and do not cause corrosion. In addition, such catalysts are easy to separate from the product, lack sensitivity to free fatty acids, and do not produce any side products such as soap.

Base Heterogeneous Catalysis

A heterogeneous base catalyst is generally a divalent metal oxide which has high covalent character which further benefits in transesterification. Solid base catalysts are known to have higher catalytic activity than their acid counter-part (Renganathan

et al. 2008). Such base catalysts are often of the types such as hydrotalcites, metal oxides, metallic salt, supported base catalyst and zeolites Few of the commonly used heterogeneous catalysts are CaO, MgO, SrO, KNO_3/Al_2O_3, K_2CO_3/Al_2O_3 (Gama et al. 2015, 2010), KF/Al_2O_3, Li/CaO, KF/ZnO, basic hydrotalcite of Mg/Al, Li/Al, anion exchange resins and base zeolites (Wan et al. 2009; Veljkovic et al. 2009). Among the alkali earth metal oxide calcium oxide is reported to have the high yields as high as 98% FAME (Fatty Acid Methyl Esters) yield is achieved during its first reaction cycle. Calcium oxide (CaO) also has a long life as a catalyst. However, the reactivity such a catalyst changes with temperature and can be determined with aid of its calcinations temperature. Another popular option among alkali earth metal oxide includes magnesium oxide (MgO), strontium oxide based catalyst, carbon group based catalyst, and catalysts with boron group elements such as aluminiumetc.

Usually, the mechanism involving base catalysed transesterification process involves three major stages, along with one pre stage. The pre stage involves reaction of base with alcohol, which results in a protonated catalyst and alkoxide. After the pre stage, the first stage takes places in which the carbonyl group of triglyceride is attacked by alkoxide, generating a tetrahedral intermediate (Taft et al. 1947; Meher et al. 2006). During the second stage alkyl ester is formed along the corresponding anion of diglyceride. Finally, In the Third stage the protonated catalyst gets deprotonated and thus, regenerates, starting another catalytic cycle. Figure 2 shows the mechanism for base catalysed transesterification process.

Acid Heterogeneous Catalysis

Acid catalysts undoubtedly have slower rate of reaction as compared to base catalyst, a rate that is as low as four thousand times that for base homogeneous catalysts (Sani et al. 2014). These catalysts are suitable for feed stocks with high free fatty acid content as these catalysts have higher tolerance for free fatty acids and water than base catalysts. Industrially, Acid heterogeneous catalysts are used more than acid homogeneous catalysts. This usage is due to the fact that there are active sites with different strengths of Lewis acidity, making it more effect. Various types of acid heterogeneous catalysts are used comprising of sulphonate saccarides, tungsten oxides, sulphonated zicronia (Helwani et al. 2009). Using these catalysts, Yields varying from 84 to 97% were obtained. While Muthu et al. (2010) obtained a biodiesel yield of 95% with Neem Oil, using a 9:1 methanol to oil and sulphonate zicronia as heterogeneous acid catalyst, a yield around 84% was obtained by using sulfated zirconia catalyst with sea mango oil (Cerberaodollam) (Kansedo et al. 2009). The mechanism of acid catalysed transesterification reaction is shown below in Fig. 3.

2.3.3 Bio Catalysis

The need of bio catalysis rose from the problems related to saponification in transesterification process especially with oils with high free fatty acid content. Enzymes
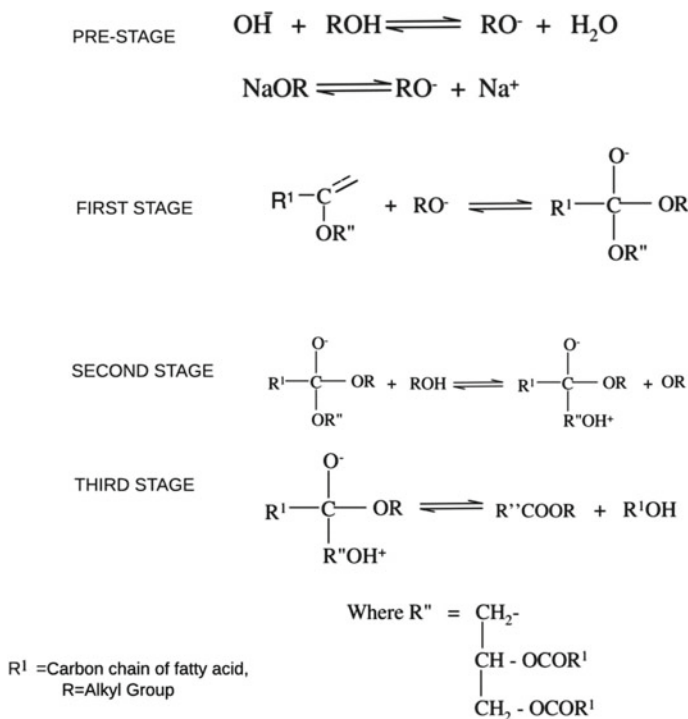
Fig. 2 Mechanism for base catalysed transesterification process. Reprinted with permission form (Meher et al. 2006). Copyright © 2004 Published by Elsevier Ltd
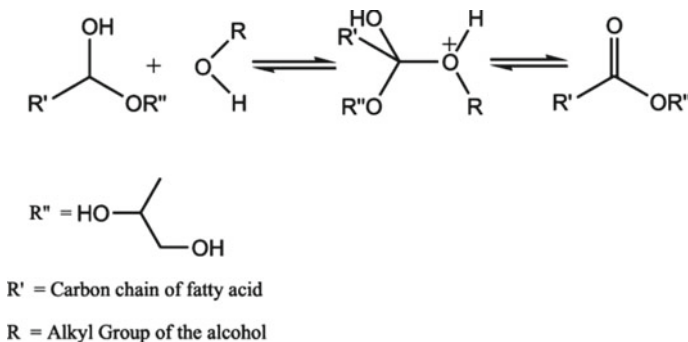
Fig. 3 Mechanism of acid catalysed transesterification. Reprinted with permission form (Ullah et al. 2016). Copyright © 2015 Energy Institute. Published by Elsevier Ltd

are used as catalysts in these processes. Using different enzyme immobilization techniques, Enzymes are immobilized on solid support, thus making them available for reuse. Nano-biocatalysts are also being utilized for enzyme immobilization. Serralha et al. (1998) prepared amino functionalized magnetic nanoparticles for enzyme immobilization. Currently, Lipases are used widely as an enzyme in these transesterification processes, a popularity that can be explained due to the fact that lipases are cost effective and that they are able to catalyse both transesterification of triglycerides (TG) and hydrolysis in moderate conditions and are therefore considered for the production of biodiesel (Miao et al. 2018). They can also catalyse reactions at moderate pressure and temperature because of their special characteristics. Although lipases as a biocatalyst for transesterification are costly than chemical catalysts, they yield more pure products because of their specific reaction, leaving less by products than chemical catalysts (Singh 2021; Singh et al. 2021). Few alcohols such as methanol can decrease activity of the enzyme which can be overcome by multi-step addition of methanol. A yield around 93% was obtained using Candida sp. lipase (immobilized) with vegetable oil feedstock and methanol (Nie et al. 2006).

3   Conclusion

Energy assumes prime importance in day-to-day activities of the twenty-first century and with depleting conventional resources, now is the time to make large investments in renewable sources of energy. Biodiesel is a well-established way to fulfil this demand.

Field of biodiesel production is garnering renewed attention from research groups and the goal of making large scale production economically feasible closer to reality. Developments of new stable catalysts, which result in higher yields as well as new catalyst recovery methods are making it evident that if this pace continues, the industry will realize a boom of cheaper catalyst solutions, a change that will make biodiesel one of the best ways to power our vehicles and will soon replace petroleum-based fuels.

As discussed, even today, there are various options such as heterogeneous catalysts and bio-catalysts which offer high yields (up to 97%) and can be regenerated. The early problem of feedstock with varying amount of free fatty acid is non-existent with catalyst which can work effectively even under high free fatty acid concentration in feed stocks.

References

Al-Zuhair S (2007) Production of biodiesel: possibilities and challenges. Biofuel Bioprod Biorefin 1(1):57–66

Canakci M, Van Gerpen J (1999) Biodiesel production viaacid catalysis. Transactions of the ASABE 42(5):1203

Cerveró JM, Coca J, Luque S (2008) Production of biodiesel from vegetable oils. Grasas Aceites 59(1):76–83

Chisti Y (2007) Biodiesel from microalgae. Biotechnol Adv 25(3):294–306

Gama PE, Gil RA, Lachter ER (2010) Biodiesel production by in situ transesterification of sunflower seeds by homogeneous and heterogeneous catalysis. Quim Nova 33(9):1859–1862

Gama PE, Lachter ER, San Gil RA, Coelho AV, Sidi IA, Poubel RL, Faro AD Jr, de Souza AL (2015) Characterization and catalytic activity of K_2CO_3/Al_2O_3 in the transesterification of sunflower oil in conventional and microwave heating. Quim Nova 38(2):185–190

Grima EM, Belarbi EH, Fernández FA, Medina AR, Chisti Y (2003) Recovery of microalgal biomass and metabolites: process options and economics. Biotechnol Adv 20(7–8):491–515

Helwani Z, Othman MR, Aziz N, Kim J, Fernando WJ (2009) Solid heterogeneous catalysts for transesterification of triglycerides with methanol: a review. Appl Catal A 363(1–2):1

Hodaifa G, Martínez ME, Sánchez S (2008) Use of industrial wastewater from olive-oil extraction for biomass production of Scenedesmus obliquus. Bioresour Technol 99(5):1111–1117

Kansedo J, Lee KT, Bhatia S (2009) Cerberaodollam (sea mango) oil as a promising non-edible feedstock for biodiesel production. Fuel 88(6):1148–1150

Lotero E, Goodwin JG Jr, Bruce DA, Suwannakarn K, Liu Y, Lopez DE (2006) The catalysis of biodiesel synthesis. Catalysis 19:41–83

Meher LC, Sagar DV, Naik SN (2006) Technical aspects of biodiesel production by transesterification—a review. Renew Sustain Energy Rev 10(3):248–268

Miao C, Yang L, Wang Z, Luo W, Li H, Lv P, Yuan Z (2018) Lipase immobilization on amino-silane modified superparamagnetic Fe_3O_4 nanoparticles as biocatalyst for biodiesel production. Fuel 224:774–782

Muthu H, SathyaSelvabala V, Varathachary TK, KiruphaSelvaraj D, Nandagopal J, Subramanian S (2010) Synthesis of biodiesel from neem oil using sulfated zirconia via tranesterification. Braz J 27(4):601–608

Nie K, Xie F, Wang F, Tan T (2006) Lipase catalyzedmethanolysis to produce biodiesel: optimization of the biodiesel production. J Mol Catal 43(1–4):142–147

Renganathan SV, Narashimhan SL, Muthukumar K (2008) An overview of enzymatic production of biodiesel. Bioresour Technol 99:3975–3981

Sani YM, Daud WM, Aziz AA (2014) Activity of solid acid catalysts for biodiesel production: a critical review. Appl Catal A 470:140–161

Serralha FN, Lopes JM, Lemos F, Prazeres DM, Aires-Barros MR, Cabral JM, Ribeiro FR (1998) Zeolites as supports for an enzymatic alcoholysis reaction. J Mol Catal 4(5–6):303–311

Singh R, Singh M, Kumari N, Maharana S, Maharana P (2021) A comprehensive review of polymeric wastewater purification membranes. J Compos Sci 5(6):162

Singh R (2021) Advancements in energy storage through graphene. In: Patnaik A, Kozeschnik E, Kukshal V (eds) Advances in materials processing and manufacturing applications. iCADMA 2020. Lecture notes in mechanical engineering. Springer, Singapore

Taft RW Jr, Newman MS, Verhoek FH (1947) J Am ChemSoc 72:4511

Ullah F, Dong L, Bano A, Peng Q, Huang J (2016) Current advances in catalysis toward sustainable biodiesel production. J Energy Inst 89(2):282–292

Veljkovic VB, Stamenkovic OS, Todorovic ZB, Lazic ML, Skala DU (2009) Kinetics of sunflower oil methanolysiscatalyzed by calcium oxide. Fuel 88:554–1562

Wan T, Yu P, Wang S, Luo Y (2009) Application of sodium aluminate as a heterogeneous base catalyst for biodiesel production from soybean oil. Energy Fuels 23(2):1089–1092

Analysis of Fire and Explosion Hazard of LPG Tanker Truck Accident: A Case Study

Aditya Paliwal, Aayush Ajay Desai, Deepak Sahu,
and Bhisham Kumar Dhurandher

Abstract There have been a lot of casualties because of fire and explosions moreover there have been huge economic as well as environmental problems due to these explosions. Two accidents took place, one after the other, in Wenling city, the eastern Chinese province of Zhejiang, China. Where a speeding truck transporting Liquefied Petroleum Gas (LPG) leans towards the right while exiting the highway and hit the guardrail which broke and disintegrated the body of the truck and the LPG leaked causing an explosion. In the explosion, the fragments of the truck and semitrailer flew out towards nearby buildings and factories triggering another explosion. This incident caused huge loss to human life along with damaging the proximate buildings and factories. The objective is to understand and analyse the LPG explosion and its impact. To achieve the objective ALOHA is used to model and then simulate the explosion.

Keywords LPG Tanker explosion · BLEVE · Jet fire · Threat zone · Aloha

1 Introduction

Fire and explosion have always had a significant area of research all over the world. Fire can cause huge losses to the property as well as can even lead to fatalities so it has become important to understand the behaviour of fire under different circumstances (Dhurandher et al. 2017). Several authors and researchers have extensively

A. Paliwal (✉) · A. A. Desai · B. K. Dhurandher
School of Mechanical Engineering, Vellore Institute of Technology, Chennai Campus, India
e-mail: aditya.paliwal2018@vitstudent.ac.in

A. A. Desai
e-mail: desaiaayush@gmail.com

B. K. Dhurandher
e-mail: bhishamkumar.d@vit.ac.in

D. Sahu
Department of Chemical Engineering, National Institute of Technology, Jalandhar, India

studied the phenomenon of fire and explosion under various scenarios (Sahu et al. 2017; Dhurandher et al. 2017; Rasbashr 1979). Liquefied Petroleum Gas also well known as 'LPG', term is used to describe two Natural Gas Liquids: propane and butane, or a mix of the two. LPG. is extracted through pressurization from natural gas processing and oil refining. LPG remains in the gaseous state at normal room temperature and pressure. On applying modest pressure and cooling it down the gas can be liquefied. For the storage of the gas, the tank pressure needed is near twice the pressure of a normal truck tyre which makes it fairly safe to handle (Brook 2005). LPG is colourless, odourless and non-toxic, and corrosive but is highly flammable. It has auto-ignition temperatures ranging from 410 to 580 °C. The lower and upper combustibility limits are 1.8 and 9.8% respectively (v/v of gas in air). Whereas the heating value is found to be ~50 MJ/kg. Generally, liquid LPG is stored in steel vessels that range from small BBQ bottles to large gas cylinders and large storage tanks (Kowalewicz and Wojtyniak 2005). LPG is held under a variety of environments, from completely refrigerated (at a pressure similar to atmospheric) to pressurized at room temperature (vapor pressure up to 1 MPa). The rapid crack formation, weld failure, or mechanical impact can result in containment loss under any storage conditions. Overfilling of containers in pressurized storage can cause failure if the device temperature rises due to the hydraulic pressure exerted by the expanding liquid as a result of normal environmental changes. When a pressurized device is exposed to a burn, the vapour pressure rises quickly (Casal et al. 2001).

A small LPG cylinder failure might have a lot of consequences (Bariha et al. 2021). It is important to work out the protected range for fire and blast of risky hazardous chemicals during an accident. One of the viable techniques for avoidance is the investigation of the outcomes of accidents utilizing hazard evaluation strategies and climatic dispersion models. It has an incredible significance to decide the span of harm during an accident brought about by poisonous and unsafe gases. For this reason, software modelling techniques is utilized like the ALOHA programming (Koohpae 2018). The ALOHA programming utilizes Gaussian modelling just as dispersion modelling. ALOHA computes the chemical cloud dispersion based on the toxicological/actual attributes of the released material, climatic conditions, and specific circumstances of the release (Terzioglu and Iskender 2021).

The purpose of this paper is to analyse and review the existing information on the fire hazard of instantaneous releases of LPG. Throughout the paper, S.I units are used. The sudden failure of a ground-level vessel containing LPG, destruction of inventory to the atmosphere, and the burning of this created flammable cloud.

2 Accident Details and Accident-Cause Analysis

On June 13, 2020, an accident involving an LPG truck took place in Shenhai Expressway Wenling West Exit, China (NBC 2020). The accident tank semi-trailer has an inner diameter of 2525 mm and the tank volume was around 61.9m^3 and the design pressure is 1.61/−0.1 MPa. The length of the truck was measured to be

13,230 mm (13.2 m), with a maximum filling volume of 26,000 kg, the nominal thickness of the cylinder was 10.0 mm, and the nominal thickness of the head was 8.0 mm. The tank body collided with the end of the concrete guardrail of the ramp overpass, and the tank body was broken and disintegrated. The liquefied petroleum gas in the tank quickly leaked, vaporized, and spreads. LPG diverged to form dense white smoke nearby that got deflagrated by the sparks from passing vehicles. This finally led to the explosion of the bubble. The tank fragments and semi-trailer that flew out (because of the initial blast) caused another accident by hitting nearby buildings. The second explosion, causing the collapse of more than 200 surrounding houses, wind turbine factories, carton factories, and other factories. Most of the houses in the nearby villages had their glass broken, and some houses were almost destroyed. Some buildings were blown to the ground, also some had their roof ripped off, littered with a lot of blackened masonry cement on the road. Most of the three-story factory buildings of Taizhou Jiayi Mechanical and Electrical Co., Ltd. near the accident site collapsed. A mushroom-like cloud rose at the scene and the sound was violent. The tank truck explosion caused loss significant loss to the property and also fatalities were reported life (Zhejiang Provincial Department of Emergency Management 2020) (Figs. 1 and 2).
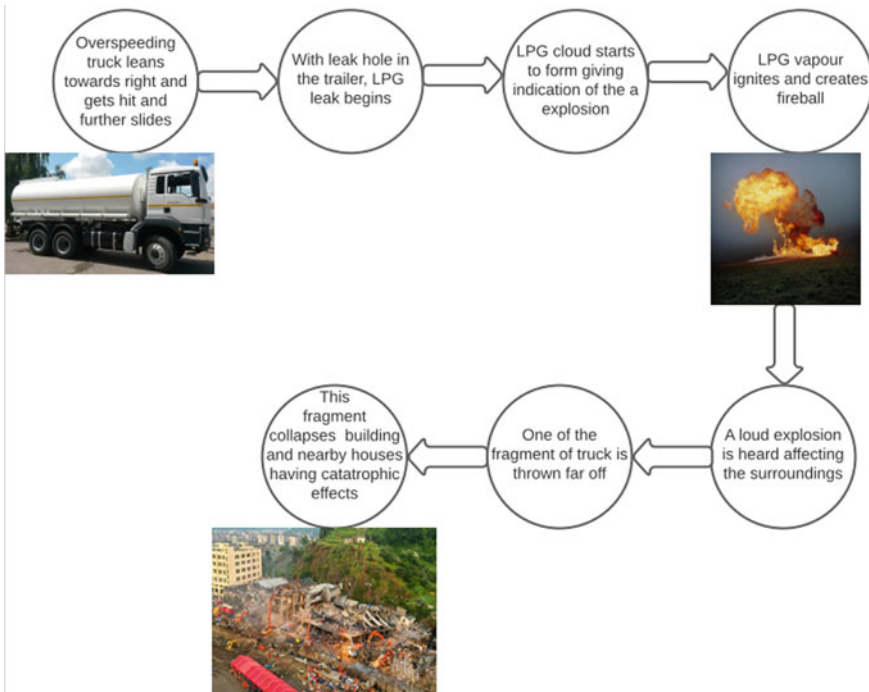
Fig. 1 Sequence of fire breaking and explosion of LPG carrying truck
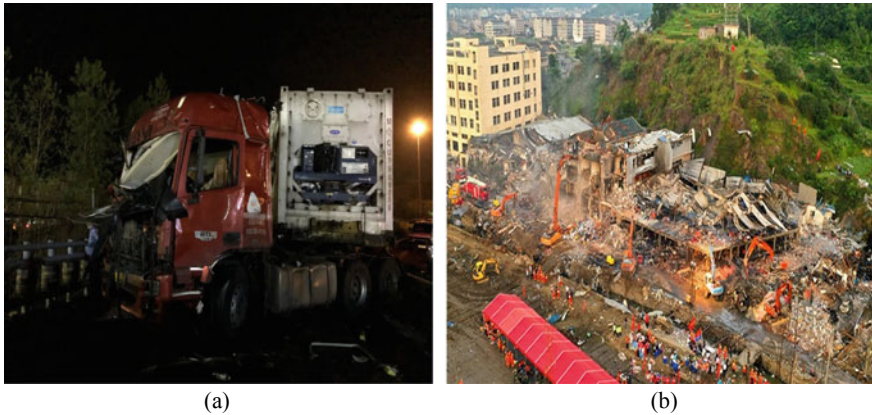
Fig. 2 The photographs showing. **a** The crushed front section of the container truck, **b** Damage caused by the explosion and the parts that flew out (Mirror 2020)

3 Research Methodology

An immense amount of energy and blast over-pressure is generated in Tank truck explosion which carries LPG as fuel. The explosion could cause a significant impact on the properties nearby and can result in casualties. In this present work, the ALOHA (Areal Locations of Hazardous Atmospheres) computer model has been chosen to simulate the scales of impact (threat zones) in the event of an LPG tank truck explosion (Koohpae 2018). The model is used to simulate the scale of threat zones and dispersion when LPG is released from the tanker truck after an accident.

3.1 ALOHA

ALOHA (Areal Locations of Hazardous Atmospheres) is a computer program developed jointly by National Oceanic and Atmospheric Administration (NOAA) and the Environmental Protection Agency (EPA) (Tseng et al. 2012). ALOHA is especially used by people responding to chemical releases, as well as for emergency planning and training. ALOHA models key hazards—toxicity, flammability, thermal radiation (heat), and overpressure (explosion blast force)—related to chemical releases that result in toxic gas dispersions, fires, and/or explosions (Jiang et al. 2014). The ALOHA software is free to use. Aloha enables one to model the explosion site and thus lending a hand for its simulation. Aloha makes hazard modelling easier and is also widely used to plan and react to a chemical emergency (Polorecka et al. 2021). The software enables us to estimate the threat zones that were made by the real-time explosion (already happened) and the potential ones that could happen. Through aloha, we can also model flammable and toxic clouds, BLEVEs (boiling

liquid expanding vapor explosion), pool and jet fires along with vapor cloud explosion. The software gives an option to use different models such as the Gaussian model along with the heavy gas dispersion model and source strength. As it can predict the scale of the explosion and the area that will be affected thus it can help in saving human lives. In order to inculcate the above mentioned steps one needs to go through a series of procedures.

Initially one needs to input the chemical data from the ALOHA library and can also add any new chemical to the datasheet. After that, we need to input the atmospheric conditions such as wind speed, cloudiness, humidity present in the air Fig. 3a. In addition, we need to specify the source strength i.e., the source whether it is direct, puddle, tank, or gas pipeline explosion. After selecting the source we need to mention

Fig. 3 Procedure **a** Atmospheric conditions dialogue box in aloha software. **b** Type of tank failure
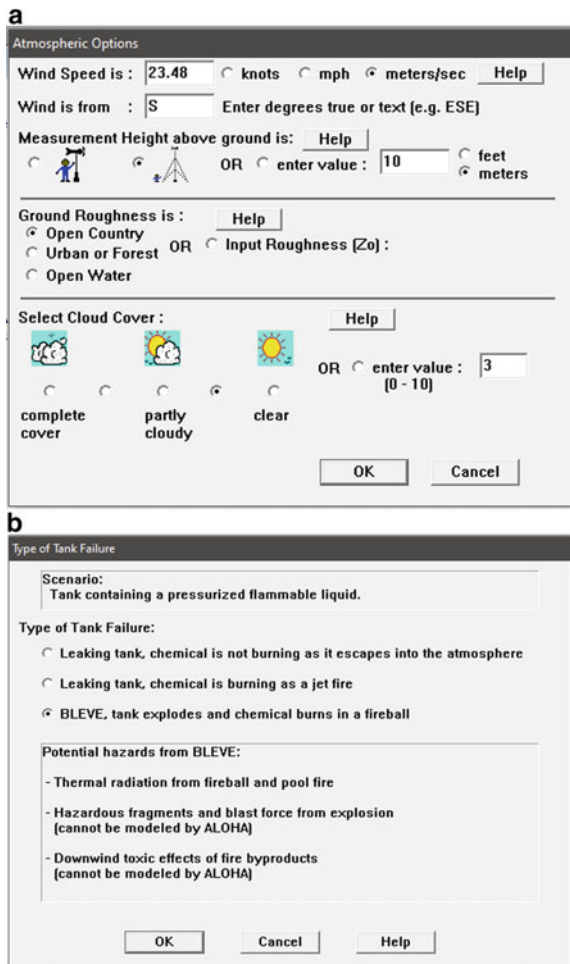
the dimension of the source such as volume, area, and later on select the type of tank failure Fig. 3b.

Depending on the type of tank failure one chooses, the required data needs to be inputted such as opening diameter and position of the leak. Depending on the substance and event, the source strength graph shows the chemical's release rate, burn rate. ALOHA may also provide graphs such as the overpressure threat zone, concentration over time, and so on. Furthermore, the ALOHA software is simple to use and requires few inputs.

Around Working with few assumptions such as low wind speed, stable atmospheric conditions, and not allowing the user to incorporate the effects of chemical mixtures and hazardous fragments are few shortcomings of the software (Venart 1998).

On June 13, 2020, 1641 h ST, Wind speed was 23.48 m/second from South direction at 10 m in Wenling city, China having excellent accident visibility. The temperature at the time was 26 °C and the humidity was equal to 87 percent. To transport LPG in a tanker truck, its properties are to be kept in mind which are mentioned below. Moreover, to ensure safe transport the LPG is kept in liquid form in pressurizedreservoirs at ambient temperature (Abbas et al. 2016).

3.2 Table Properties of Liquified Petroleum Gas (LPG) (Yousufuddin and Mehdi 2008).

Boiling point (°C)	−44
Molecular weight (kg/Kmol)	44.1
Density at 15° C kg/l	0.507
Research octane number	100
Stoichiometric air fuel ratio (kg/kg)	15.6
Flame speed (m/s)	48
Upper flammability limits in air (% vol)	74.5
Lower flammability limits in air (% vol)	4.1
Lower flammability limits in air (% vol)	46.365

3.3 Table: Specification of the Tanker Truck (Zhejiang Provincial Department of Emergency Management 2020).

Tank diameter	2.5 m
Tank length	13.2 m
Tank volume	61.9 cubic meters
Tank contains	Liquid
Internal storage temperature	26 °C
Chemical mass in tank	25,360 kg
Tank fullness	83% full

4 Results and Discussions

4.1 BLEVE

Whenever a flammable liquid that is being carried in a vessel goes above its normal boiling point and is also put under pressure a catastrophic happens known as boiling liquid expanding vapor explosion (BLEVE) (Shaluf 2007). During the failure of the vessel containing flammable liquid, the pressure immediately drops to atmospheric pressure levels and the hot flammable liquid rapidly boils and generates a huge quantity of vapor (Samvatsar et al. 2014). Few circumstances wherein bleve is caused are –The vessel may fail as a result of the present relief valves malfunctioning and also Depressurization and explosion in an instant (Lebel et al. 2013). Figure 4 shows the threat zone of thermal radiation of the fireball caused due to explosion. The area and the effects of radiation in the specified range can be inferred from the graph itself. The percentage of Tank Mass consumed in Fireball was 100%, with the Fireball Diameter reaching 170 m and the burn duration was 11 s.

4.2 Jet Fire

A turbulent diffusion flame also referred to as a jet or spray fire, is caused by the burning of a fuel that is constantly discharged with considerable momentum in one or more directions. Jet fires can occur when gaseous, flashing liquid (two phases), or pure liquid stocks are released (Colella et al. 2020). When a flammable material (usually a pressurized gas or a two-phase mixture) is released in a jet, one of two things can happen: either the jet is quickly ignited by an electrostatic spark or another
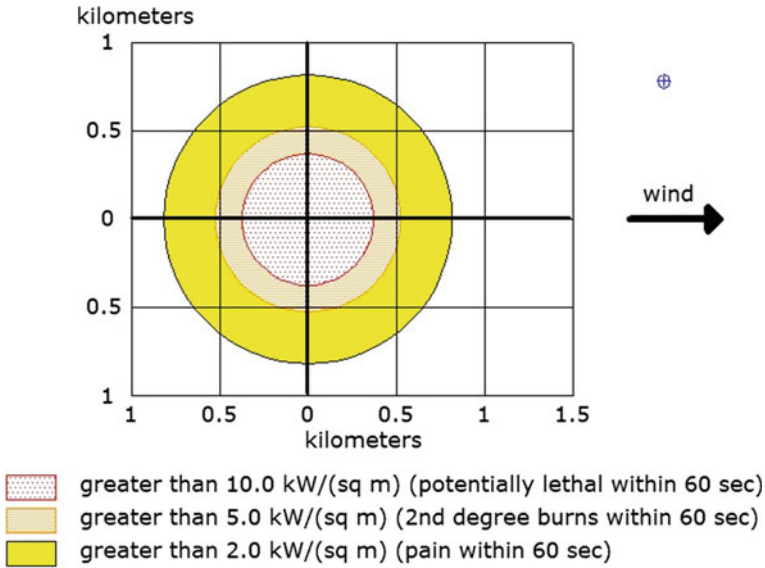
Fig. 4 BLEVE of flammable liquid in a horizontal cylindrical tank

ignition source, or a vapor cloud is formed, the fire flashes back to the leak source, and a jet fire is finally started (Foroughia et al. 2019). High heat fluxes to impinged or absorbed items can result in structural collapse or vessel/pipework failure, with further escalation conceivable. The fuel mix, release circumstances, release rate, release geometry, direction, and ambient wind conditions all influence the characteristics of jet flames. The release rate and capacity of the source influence the length of the jet fire. The length of the flame is directly proportional to the flow rate. To simulate a jet fire model, the aloha software will be used wherein the input of data such as area/size of the leak, the quantity of leaked fuel and the rate at which fuel leak was will be added and a model will be prepared. The solid flame model is used in the ALOHA code for an upward vertical jet release (Gómez-Mares et al. 2012). Figure 5 shows Jet fire thermal radiation because of the difference in hole diameter also called leak diameter. The hole opening is assumed to be around 1.4 m from the tank bottom. For Fig. 5 the hole diameter is taken as 0.02 m and the radiation flux is observed.

4.3   Overpressure Threat Zone

Overpressure is a key danger linked with every explosion. The rapid emergence of a pressure wave after an explosion is referred as overpressure, sometimes known as a blast wave (Kerampran et al. 2016). The energy released in the first explosion causes this pressure wave; the larger the initial explosion, the more destructive the pressure
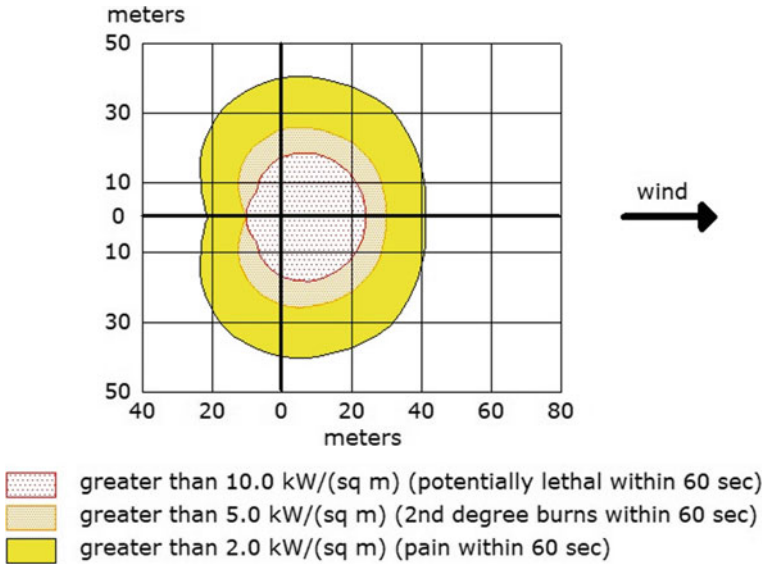
Fig. 5 Threat zone of jet fire of flammable liquid with hole diameter 0.02 m

wave. Pressure waves move at the speed of sound and are virtually instantaneous. Concern Levels of Overpressure an Overpressure Level of Concern (LOC) is a pressure threshold from a blast wave that is generally the pressure over which a hazard exists.

Figure 6 graph shows the formation of the overpressure threat zone's area formation and the damages that can happen within the area affected, for hole diameter (leak diameter) 0.02 m. Two congestion levels can be used in ALOHA. The levels are congested and uncongested. The most precise estimates made on ALOHA do use volume blockage ratio (the volume of the cloud occupied by obstacles divided by the total volume of the cloud). The overpressure threat zone is as high as 44 m towards the downwind direction and can destroythe buildings. However, serious injury can take place up to25 m towards the downwind direction.

4.4 Toxic Threat Zone

A toxic LOC specifies the amount (threshold concentration) of exposure to an airborne chemical that might cause harm to individuals if inhaled over a specified period (exposure duration) (Phanindra et al. 2020).

Figure 7 illustrates the ALOHA software-generated threat zones for the hazardous region of a vapor cloud for LPG if it was not ignited. For a hole of diameter 0.02 m, the maximum sustained release rate is 336 kg/min with a total amount of 15,429 kg being released. The AEGL of each zone represents different severities. The AEGL 3
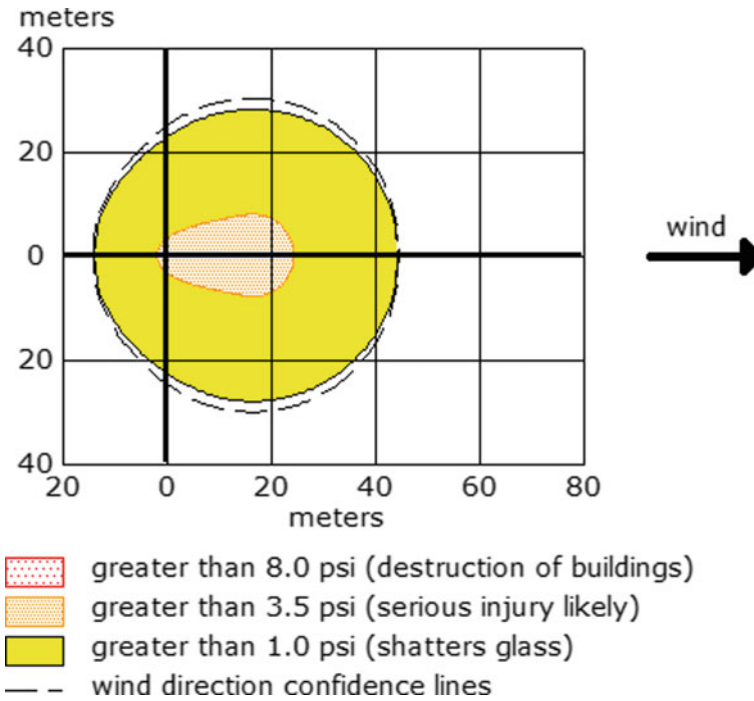
Fig. 6 Overpressure threat zone due to vapour cloud explosion

includes vulnerable individualswho may suffer life-threatening health consequences or even death. The AEGL 2 includes long-term negative health consequences. The AEGL 1 includes discomfort and displeasure (Mohammad Al-Sarawi 2017).

5 Conclusion

There happen to be a lot of explosions including LPG especially with tanker trucks transporting huge amounts of liquefied gas. One such incident happened in China which caused a lot of damage and even affected the surrounding area and buildings hugely. In the paper, we have used Aloha software, with the help of which simulation of the actual accident site is possible with almost similar scenarios as on the day of the accident. Keeping in mind the explosion and scenarios created that day, calculations for the BLEVE was done accordingly. The BLEVE explosion graph shows that the explosion would cause degree 2 burns within 60 s with energy released greater than 5.0 kW/ (sq. m) within a circle of 0.52 km i.e., 520 m radius from point of explosion. And also potentially lethal burns (may lead to death of an individual) within 60 s with energy released greater than 10.0 kW/ (sq. m) within a circle of 4 km i.e. 400 m radius from point of explosion. Along with that, graphs and data of Jet fire,
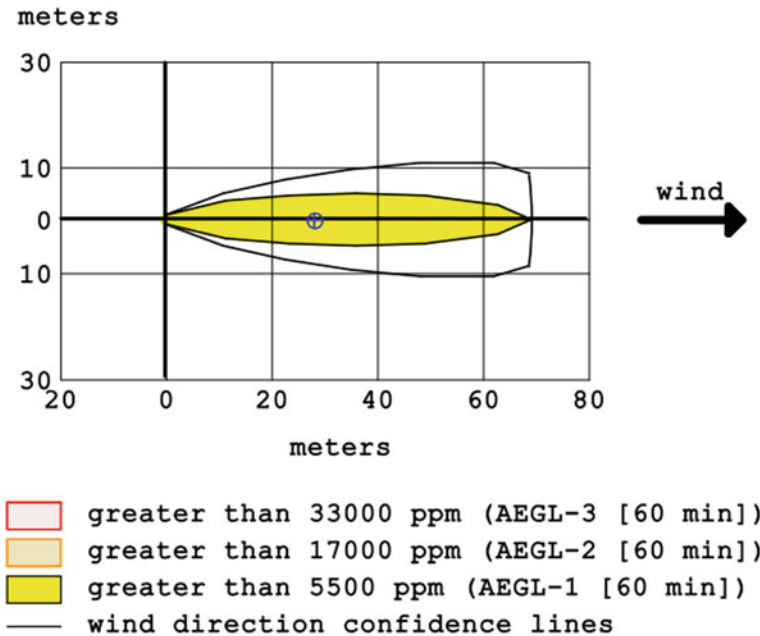
Fig. 7 Threat zone for hazardous region with hole diameter 0.02 m

overpressure threat zone, and toxic threat zone were generated using the software, with leak diameters of 0.02 m, indicating the radiation flux and its intensity in a given area range and the intensity of burns that can happen accordingly. From the jet fire graph and data, one can deduce that the higher the leak diameter, the higher will be the radiation range and intensity over an area. In addition, considering the leak diameter of 0.02 m, we can infere that distance is related to concentration in an indirect manner; the higher the concentration, the shorter the distance travelled in reference to the toxic threat zone. This also helps in understanding the safe distance from these accidents such that physical harm can be avoided and more human life loss as well economic damages could be minimized.

References

Abbas SK, Samad STA, Khalifa KKD (2016) LPG storage tank and pipe line report (May). https://doi.org/10.13140/RG.2.1.3112.0244

Bariha N, Srivastava VC, Mishra IM (2021) Incident analysis of various sections of a liquefied petroleum gas (LPG) bottling plant. Indian Chem Eng 63(1):50–61. https://doi.org/10.1080/00194506.2019.1690591

Brook P (2005) LPG storage systems, atmospheric versus pressurized. Gastech Conf Proc

Casal J, Arnaldos J, Montiel H (2001) Modeling and Understanding Bleves. Handb Hazard Mater Spills Technol 22.1–22.27

Colella F, Ibarreta A, Hart RJ, Morrison T, Watson HAJ, Yen M (2020) OTC-30802-MS jet fire consequence analysis review of experimental data. (May):4–7

Dhurandher BK, Kumar R, Dhiman AK, Sharma PK (2017) An investigation on compartment fires with plywood cribs. Fire Mater 41(3):209–224. https://doi.org/10.1002/fam.2379

Dhurandher BK, Kumar R, Dhiman AK (2017) An experimental study on crib fires in a closed compartment. Thermal Sci 21(3):1431–1441. https://doi.org/10.2298/TSCI141206156D

Foroughia V, Cavinib A, Palaciosc A, Albóa K, Àguedaa A, Pastora E, Casald J (2019) Domino effect by jet fire impingement in pipelines. Chem Eng Trans 77. http://hdl.handle.net/2117/185016

Gómez-Mares M, Muñoz M, Palacios A (2012) Jet fires: a 'minor' fire hazard joaquim casal. Chem Eng Trans 26:13–20. https://doi.org/10.3303/CET1226003

Jiang XJ et al (2014) Application of aloha in emergency response for Hazardous chemicals accidents. Appl Mech Mater 631–632:1080–1085. https://doi.org/10.4028/www.scientific.net/AMM.631-632.1080

Kerampran S, Arrigoni M, Locking P (2016) Blast waves propagation and their mitigation HAL Id : hal-01714103 (January) 2018

Koohpae A (2018) Modelling the consequences of explosion, fire and gas leakage in domestic cylinders containing LPG'. Annal Med Health Sci Res 83–88. Available at: https://www.amhsr.org/articles/modelling-the-consequences-of-explosion-fire-and-gas-leakage-in-domestic-cylinders-containing-lpg.pdf.

Koohpae A (2018) Modelling the consequences of explosion, fire and gas leakage in domestic cylinders containing lpg. Ann Med Health Sci Res 83–88

Kowalewicz A, Wojtyniak M (2005) Alternative fuels and their application to combustion engines. Proc Inst Mech Eng Part D J Automob Eng 219(1):103–125. https://doi.org/10.1243/095440705X6399

Lebel LS, Brousseau P, Erhardt L, Andrews WS (2013) Measurements of the temperature inside an explosive fireball. In: Proceeding of the 27th international symptoms of ballast Ballist vol. 1, pp 707–710

Mirror (2020) https://m.jiemian.com/article/4523728_qq.html. Accessed 14 June 2020

Mohammad Al-Sarawi N (2017) Evaluation of accidental atmospheric releases of chlorine and butane from a mobile source using ALOHA and MARPLOT. Am J Environ Prot 6(6):144, https://doi.org/10.11648/j.ajep.20170606.12

NBC (2020) 18 dead and dozens injured as tanker truck explodes on highway in China, 14 Mar 2020

Phanindra KH, Rao MS, Sivapirakasam SP, Cheepu M (2020) Consequence modeling of Ethyl Acetate storage tank. In: IOP Conference Series: Materials Science and Engineering, vol. 998(1). https://doi.org/10.1088/1757-899X/998/1/012069

Polorecka M, Kubas J, Danihelka P, Petrlova K, Stofkova KR, Buganova K (2021) Use of software on modeling hazardous substance release as a support tool for crisis management. Sustainability 13(1):1–16. https://doi.org/10.3390/su13010438

Rasbashr DJ (1979/801) Review of explosion and fire hazard of liquefied petroleum gas. Fire Saf J 2:223–236. https://doi.org/10.1016/0379-7112(79)90022-5

Sahu D, Kumar S, Jain S, Gupta (2017) Full scale experimental and numerical studies on effect of ventilation in an enclosure diesel pool fire. Building Simul 10(3):351–364. https://doi.org/10.1007/S12273-016-0328-X

Samvatsar A, Jain NK, Patel P (2014) Analysis of BLEVE mechanism and anti BLEVE system in pressurized tank. Int J Eng Res Technol 3(1):2380–2384

Shaluf IM (2007) An overview on BLEVE. Disaster Prev Manag An Int J 16(5):740–754. https://doi.org/10.1108/09653560710837037

Terzioglu L, Iskender H (2021) Modeling the consequences of gas leakage and explosion fire in liquefied petroleum gas storage tank in Istanbul technical university, Maslak campus. Process Saf Prog (March). https://doi.org/10.1002/prs.12263

Tseng JM, Su TS, Kuo CY (2012) Consequence evaluation of toxic chemical releases by ALOHA. Procedia Eng 45:384–389. https://doi.org/10.1016/j.proeng.2012.08.175

Venart JES (1998) Boiling liquid expanding vapor explosions (BLEVE): possible failure mechanisms. ASTM Spec Tech Publ 1336(147):112–132. https://doi.org/10.1520/stp12189s

Yousufuddin S, Mehdi SN (2008) Performance and emission characteristics of LPG-fuelled variable compression ratio SI engine. Turkish J Eng Environ Sci 32(1):7–12. https://doi.org/10.3906/zoo-1212-31

Zhejiang Provincial Department of Emergency Management (2020) "6.13"Liquefied petroleum gas transportation in Wenling section of Shenhai expressway investigation team for major explosion accidents of tank trucks, Dec 2020

Zhejiang Provincial Department of Emergency Management (2020) "6.13" Liquefied Petroleum Gas in Wenling Section of Shenhai Expressway Major Explosion accident of transport tanker Investigation report, 2020

A Review on the Divergent Pathways Used in the Purification of Biodiesel

Amritha Baskar and Adhithiya Venkatachalapati Thulasiraman

Abstract Proper cleaning of Bio-Diesel (BD) has to be obligatory after the extraction of BD because it can be a partial replacement to the current fuel for transportation, heating, manufacturing and much more. To purify the BD the inceptive activity involves a mixing unit that utilises Methanol, plant seed oil/animal Fat and sulphuric acid to ensure proper blending. The following step deals with an injection of some more amount of methanol along with catalyst (Potassium Hydroxide/Sodium Hydroxide) to warrant irreversibility. The culminating progression involves the engendering of both oil-soluble (biodiesel) and Water-Soluble (Glycerine) compounds. The manufactured BD needs purification because it might contain both water and impurities which can cause adverse effects when used directly in vehicles. Technologies used for purifying involves Dry-washing (DW) and Wet washing (WW). Although when it comes to the DW it incorporates Magnesol (ML), Ion Trading Resins (ITR), Sawdust (SD) and Bentonites (BT). In the current discovery, it has been observed that DW has an upper hand over all other conventional mechanisms for scrubbing out the remnants that appear in BD. Certain demerits thrive us towards membrane separation approach.

Keywords Biodiesel · Dry-washing · Magnesol · Ion trading resin · Magnesol

1 Instigation of Biodiesel

BD is a renewable source of energy that can be acquired from viands, non-eatable and discarded oils. Due to the sudden fall in the oil and gas reserves, the exigency for churning out BD came into subsistence. The necessity for unconventional extraction of a combustible commodity should confer with biodegradability and minimal toxicity. This paper concentrates not only on the wiping of BD using the DW approach to narrow down the proportion of light alcohol, glycerol and other filth but also

A. Baskar · A. V. Thulasiraman (✉)
Department of Petroleum Engineering, AMET (Deemed to be University), Kanathur, Chennai, Tamilnadu, India
e-mail: adhithiya.vt@ametuniv.ac.in

on the generation of biodiesel using chemicals/protein catalysis/super-critical spirit techniques.

2   Traits of Biodiesel

BD is a cleaner-burning substitute in comparison with petroleum-based fuels (PBF). The use of BD offers convenience due to its effortless availability, transferability, and favourable combustion efficiency, sky-scraping cetane number and drop in sulphur and benzene content.

It is having a flashpoint significantly higher than hydrocarbon-based fuels (El-Kasaby and Nemit-Allah 2013; Gomes et al. 2013; El-Kassaby and Nemit-Allah 2013; Shuit et al. 2012).

The viscosity of BD is quite exorbitant to that of PBF. BD being a non-depleted fuel produced from non-edible oil, animal fat and catalyst may amortize the ejection of GHG (Carbon dioxide, Methane and Flourine) to the sky. The outcome of igniting during the mass production of BD will have a diminished fraction of carbon monoxide, sulphur oxide and thus shorten the pollution level. It is the only fuel that can be employed in traditional diesel locomotive engines with no interchange. BD can be utilised exclusively or diversely in any ratio with PBF. The universal mixture of BD is "B20" (BD 20% and PBF 80%) (Casas et al. 2011). The principal pitfall of BD as PBF is its outrageous viscosity, soaring cloud and pour point, extreme nitrogen oxide ejection and excessive engine wear (Leung et al. 2010).

3   Roads for Acquiring Biodiesel

The operation of BD manufacture is generally implemented by catalysed Trans-esterification (CTE) with the residence of alcohol that is lighter (Methanol) in nature. A catalyst is employed to not only boost the reaction rate but also to stimulate the solubility of alcohol and output. Examples of catalysts used in CTE include Alkalies (NaOH, KOH, $Na-C_2H_5O^-$ and $K-C_2H_5O^-$) and Acids (H_2SO_4, $R-S(=O)_2-OH$ and HCl). Base CTE materialises briskly than Acid CTE. Researchers have accomplished objectives of procuring BD using coffee grounds, Jatropha curcas, Alligator fat and lipids from single-celled organisms as a raw material Proper cleaning of biodiesel (BD) has to be obligatory after the extraction of BD using a three-stage process. The inceptive activity involves usage of a mixing unit that allows using methanol, plant seed oil/animal Fat and sulfuric acid to ensure proper blending. The following step deals with the injection of some more amount of methanol along with catalyst (Potassium Hydroxide/Sodium Hydroxide) to warrant

$$\text{Triglyceride} + 3 \text{ Moles of Alcohol} \xrightleftharpoons{\text{Catalyst}} 3 \text{ Moles of Alkyl esters} + \text{Glycerol}$$
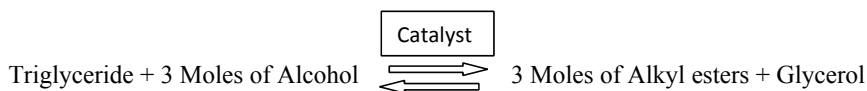
Fig. 1 Transesterification process of Biodiesel

irreversibility. The culminating progression involves the engendering of both oil-soluble elements (biodiesel) and Water Soluble compounds (Glycerine). The manufactured BD needs purification because it might have both water and certain impurities which can cause adverse effects when used directly into vehicles for transportation. Technologies used for purifying involves Dry-washing (DW) and Wet washing (WW). Although when it comes to the DW path it incorporates Magnesol (ML), Ion Trading Resins (ITR), Sawdust (SD) and Bentonites (BT).

In the current discovery, it has been proved that DW has an upper hand over all other Traditional mechanisms for scrubbing out the remnants that appear in BD (Patil and Deng 2009; Kusy 1982; Xue 2013; Özener et al. 2014; Palash et al. 2013; Ayhan 2010; Ferella et al. 2010; Balat and Balat 2008; Bhatti et al. 2008; Fazal et al. 2011) (Fig. 1).

4 Cleansing of Biodiesel

The spawned BD has dirt that reconcile out as a glycerol film including the un-sieved glycerine, methanol and particulates (Atadashi et al. 2012). Expulsion of filth from the reacted crude BD is imperative due to the perilous reverberations on the ignition framework available in cars. Raw materials used to manufacture BD should be dehumidified to manage the dampness content of BD. Possibility of altering the stability due to the existence of free-fatty acid during transesterification response. The scum is purified using Wet washing (WW)/Dry Washing (DW)/Membrane Separation (MS) depending upon the composition of BD reliable option is chosen (Fazal et al. 2011).

4.1 *Wet Washing (WW)*

WW Technique is extensively used to not only draw out production chemicals but also to wipe out polluting substances from BD. This method can be subdivided into distilled water wash, tap water wash and bubble wash (Atadashi 2007). The scum (Soap, Catalyst, glycerol and residual alcohol) is removed from the BD by making them settle at the bottom-most part of the tank. This activity entails the insertion of water into crude BD and stirring it softly to prevent the inception of emulsion. This approach is duplicated several times until colourless wash water (CWW) is earned. CWW is a sign that signifies the total elimination of grime. However, the inclusion

of supplemental water might lead to multiple drawbacks that include piling up of cost and manufacturing schedule. It has been newly mentioned that WW is one of the habitual procedures that is accomplished with an excellent degree of accuracy due to the eminent water solubility of both glycerol and methanol (Talebian-Kiakalaieh et al. 2013; Yaakob et al. 2013; Bondioli 2004; Demirbas and Demirbas 2011; Sani et al. 2013).

4.2 Dry Washing (DW)

DW strategy is exercised to filter out the dirt existing in BD. This is accomplished using a variety of elements such as silicates (ML), ITR and activated (clay, carbon and fibre), etc. These elements are also called adsorbents that embrace binding sites and robust predilection for polar compounds such as methanol, glycerine, glycerides, metals and soap. This procedure was conventionally implemented at a temperature of 149°F and the time taken to finalise this technique was between 20 and 30 min. Detachment of soap and glycerine from BD was implemented by the amalgamation of six methodologies that are as follows:-

These techniques are filtration, physical adsorption, ion exchange and soap pullout by glycerine disposition. The virtue of DW over the unadventurous WW system are as follows:-

  I. The DW approach lessens processing time. Dry washed BD can be primed for use within few hours and eloquently prompt to generate than Wet washed propellant.

 II. The DW method lowers the cost (Talebian-Kiakalaieh et al. 2013). Moreover, to the towering increase of water cost and noteworthy rate of water expulsion equipment, dumping of sewage water is often the sole sizable cost of mass production.

III. Environmental firms are strenuously pursuing unlawful discarding of pollutant water. Penalties and forthcoming shutdown for those shattering the rules and regulations.

IV. A smaller area is essential for conducting DW strategy. Settling is the pivotal tool to productively remove water. Countless large wash tanks and extra water settling tanks are needed in the WW technique.

 V. The quality of fuel acquired is high. The entire surface area required is minimal.

VI. DW technology creates premium quality BD. Since water is not added in the DW technique. It's practicable to attain <500 ppm aqua content in line with ASTM D6751. On the contrary WW, the process has water content >1000 ppm making it overpriced, problematic and consumes a lot of time for effectual removal (Yaakob et al. 2013; Bondioli 2004; Demirbas and Demirbas 2011; Sani et al. 2013).

4.2.1 Magnesol (ML) Dry Washing Technique (DWT)

ML can not only be used as compost, but also as an animal food supplement. It also grips fuel supply possibilities. It was endowed that there was no remarkable change in density, kinematic viscosity, cetane number and saponification number. Removal of both soap and glycerine is possible via adsorption (Yaakob et al. 2013).

4.2.2 Sawdust (SD) DWT

SD from a trudge mill was analysed for its soap downgrading properties. They investigated SD with raw BD accommodating soap and methanol of 0.2% and 4% respectively (Bondioli 2004). They managed to find after many trials that if <14.9 g of BD was cleansed per gram of SD. One key merit of using SD for detaching both soap and Glycerine from BD is not to remove methanol from BD at the initial stage of the refining technique.

4.2.3 Ion Trading Resin (ITR) DWT

When ITR is ingested in the BD the activity of ion trading gets activated and a molecule of hydrogen is captivated by the pollutants that exist in BD. This strong temptation usually proceeds in a particle of hydrogen being traded with a molecule of impurity. The filth is now coupled to the resin in the spot of hydrogen. Substantial reduction of soap and glycerine can be executed using ITR. ITR have a mild consequence on the methanol proportion of BD. ITR not only put forward cost gain in withdrawing water and glycerine but also in eliminating the salt, soap and catalysts from BD (Atadashi 2007; Talebian-Kiakalaieh et al. 2013; Yaakob et al. 2013; Bondioli 2004; Demirbas and Demirbas 2011).

4.2.4 Bentonites (BS) DWT

BS had a pragmatic effect on the value of acid and in the separation of soap, methanol and glycerol from BD. Highly purged impurity was Methanol of about 98% using BS. Other pollutants such as soap and glycerol had approximately 24–40% and 15–20% respectively. (23) The outcome acquired from BS were marginally ancillary than ML.

5 Fortunes of Cleansing Techniques

The topmost priority of filtering BD is to guarantee the spawning of clean BD that can be traditionally utilised on Diesel Engines. The advancement in straining methods

has to lead to a substantial improvement in the quality of BD. DW has a greater competitive edge over WW activity (Atadashi 2007; Talebian-Kiakalaieh et al. 2013; Yaakob et al. 2013; Bondioli 2004).

6　Drawbacks of Cleansing Techniques

WW is not only expensive to implement, but also dispense a vast quantity of unprofitable water. On the Contrary DW, the process has complications when it comes to the regeneration of consumed adsorbent and the philosophy of its chemistry.

7　Conclusions and Recommendations

DW using ITR and ML lead the way to manufacture distilled BD legacy. There is a certain downside of DW that thrive us to look for alternative options such as MS. MS not only needs a minimal portion of vitality but also fosters near to zero unproductive water. MS was launched to mass-produce BD with <0.01% glycerol mixture and this value was noticeably beneath the one disclosed by EN14214 and ASTMD6751. So Further investigation should be carefully manifested on MS to acquire premium fuels.

References

Atadashi IM (2007) Design and construction of a pilot plant for the production of biodiesel from cottonseed oil

Atadashi IM, Aroua MK, Aziz ARA, Sulaiman NMN (2012) The effects of water on biodiesel production and refining technologies: a review. Renew Sustain Energy Rev 16(5):3456–3470

Ayhan D (2010) Use of algae as biofuel sources. Energ Convers Manag 51(12):2738–2749

Balat M, Balat H (2008) A critical review of bio-diesel as a vehicular fuel. Energy Convers Manage 49(10):2727–2741

Bhatti HN, Hanifa MA, Qasim M, Ataur R (2008) Biodiesel production from waste tallow. Fuel 87(13–14):2961–2966

Bondioli P (2004) The preparation of fatty acid esters employing catalytic reactions. Top Catal 27:77–89

Casas A, Ramos MJ, Perez A (2011) New trends in biodiesel production: chemical interesterification of sunflower oil with methyl acetate. Biomass Bioenerg 35(5):1702–1709

Demirbas A, Demirbas MF (2011) Importance of algae oil as a source of biodiesel. Energy Convers Manage 52(1):163–170

El-Kasaby M, Nemit-Allah MA (2013) Experimental investigations of ignition delay period and performance of a diesel engine operated with Jatropha oil biodiesel. Alex Eng J 52(2):141–149

El-Kassaby M, Nemit-Allah MA (2013) Studying the effect of compression ratio on an engine fueled with waste oil produced biodiesel/diesel fuel. Alex Eng J 52(1):1–11

Fazal MA, Haseeb ASMA, Masjuki HH (2011) Biodiesel feasibility study: an evaluation of material compatibility; performance; emission and engine durability. Renew Sustain Energy Rev 15(2):1314–1324

Ferella F, Celso GMD, Michelis ID, Stanisci V, Veglio F (2010) Optimization of the transesterification reaction in biodiesel production. Fuel 89(1):36–42

Gomes MCS, Arroyo PA, Pereira NC (2013) Influence of acidified water addition on the biodiesel and glycerol separation through membrane technology. J Membr Sci 431:28–36

Kusy PF (1982) Transesterification of vegetable oils. Am Soc Agricul Eng 127–137

Leung DYC, Wu X, Leung MKH (2010) A review on biodiesel production using catalyzed transesterification. Appl Energy 87(4):1083–1095

Özener O, Yüksek L, Ergenç AT, Özkan M (2014) Effects of soybean biodiesel on a DI diesel engine performance, emission and combustion characteristics. Fuel 115:875–883

Palash SM, Kalam MA, Masjuki HH, Masum BM, Rizwanul Fattah IM, Mofijur M (2013) Impacts of biodiesel combustion on NOx emissions and their reduction approaches. Renew Sustain Energy Rev 23:473–490

Patil PD, Deng S (2009) Optimization of biodiesel production from edible and non-edible vegetable oils. Fuel 88:1302–1306

Sani YM, Daud WMAW, Aziz ARA (2013) Solid acid catalyzed biodiesel production from microalgal oil the dual advantage. J Environ Chem Eng 1(3):113–121

Shuit SH, Ong YT, Lee KT, Subhash B, Tan SH (2012) Membrane technology as a promising alternative in biodiesel production: a review. Biotechnol Adv 30:1364–1380

Talebian-Kiakalaieh A, Amin NAS, Mazaheri H (2013) Overview of the production of biodiesel from waste cooking oil. Renew Sustain Energy Rev 18:184–193

Xue J (2013) Combustion characteristics, engine performances and emissions of waste edible oil biodiesel in the diesel engine. Renew Sustain Energy Rev 23:350–365

Yaakob Z, Mohammad M, Alherbawi M, Alam Z, Sopian K (2013) Overview of the production of biodiesel from waste cooking oil. Renew Sustain Energy Rev 18:184–193

Fenton Assisted Ultrafiltration for Removal of COD of Reactive Black 5 Dye from Synthetic Wastewater

Hrushikesh Patil, Vignesh Shanmugam, and Kumudini Marathe

Abstract Fenton assisted polymeric membrane separation is one of the current research areas. In the current study, the incorporation of Fe_2O_3 nanoparticles in the PES matrix during membrane fabrication by phase inversion and the addition of H_2O_2 dosage in wastewater provides a synergistic effect of Fenton and membrane separation of Reactive black 5. Attempts were made to incorporate both phenomena in the Dead-End membrane filtration unit. The operating variables for combination process were H_2O_2 dosage (0–30 mM), Reactive Black 5 concentration (100-1000 ppm), membrane with different Fe_2O_3 nanoparticles (0–1.5%), trans-membrane pressure (100–400 kPa), pH (3–9). The significant variables accomplished for this study were 71%COD and 80% dye removalunder optimized conditions such TMP(200 kPa), dye concentration(250 ppm), pH(3),Hydrogen peroxide concentration (10 mM). The membrane fouling with or without Fenton effect experimentation was investigated by resistance fitting model. The surface morphology of the virgin and the fouled membrane was determined by scanning electron microscopy. The membrane was effectively reused five times with a satisfactory performance under optimal conditions. Backwashing of the membrane with acid–alkali treatment operation was found to be a better strategy to maintain membrane stability and its utility. The recycling nature of Fenton aided membrane could be a better option for the ultrafiltration of waste-water.

Keywords Fenton-effect · Phase-inversion · Membrane separation · SEM

H. Patil · V. Shanmugam · K. Marathe (✉)
Chemical Engineering Department, Institute of Chemical Technology, Mumbai 400019, India
e-mail: kv.marathe@ictmumbai.edu.in

H. Patil
e-mail: ce15hg.patil@pg.ictmumbai.edu.in

Symbol

α	Specific cake resistance(M/Kg)
A	Area of the membrane (m2)
b	full width at half maximum (FWHM)
C_b	Bulk concentration
C_p	Dye concentration in permeate (ppm)
C_R	Dye concentration in the feed(ppm)
dV	Differential volume in litre
dt	Differential time in seconds
Dc	Crystalline size (Nm)
k	Shape factor
h	Diffraction angle
J	Permeate flux (m^3/m^2.sec)
J_0	Pure water flux (m3/m2.sec)
l	Wavelength(Nm)
l	Thickness of the membrane (μm)
λ	Modified fouling index
m	Cake density(Kg/m^2)
Q_w	Volumetric flow rate(m^3/sec)
ΔP	Transmembrane pressure (kPa)
r	Rejection factor
R	Rejection (%)
Rm	Membrane resistance (m-1)
Rc	Cake resistance (m)
t	Sampling time h
V	Volume collected during filtration (L)
VT	Membrane volume in a wet state (m^3)
W1	Weight of membrane in the dry state (kg)
W2	Weight of membrane in a wet state (kg)
ρw	Density of water (kg/m^3)
ρmd	Density of membrane in a dry state (kg/m^3)
ε	Porosity of membrane (%)
μ	Viscosity of membrane (m^2/sec

Abbreviations

Al_2O_3	Alumina
$CaCl_2$	Calcium chloride
CA	Cellulose acetate
$Co\text{-}Fe_2O_3$	Cobalt doped iron oxide
DMAc	Dimethylacetamide

DMF   Dimethylformamide
EDX   Energy dispersive analyzer
Fe_2O_3 Iron oxide (III)
Fe_3O_4 iron oxide (III)
FeO   Iron oxide (II)
FWHM   Full width at half maximum
MWCO   Molecular weight cut off
NaCl   Sodium chloride
NMPN   Methyl-2-pyrrolidone
PAN   Polyacrylonitrile
PEG   Polyethylene glycol
PEI   Polyetherimide
PES   Polyethersulphone
PS   Polysulfide
PP   Polypropylene
PVC   Polyvinyl chloride
PVDF   Polyvinylidene fluoride
RB5   Reactive black 5
SEM   Scanning electron microscopy
TiO_2 Titanium oxide
TMP   Transmembrane pressure
XPS   X-Ray photoelectron microscopy
XRD   X-Ray diffraction
ZnO   Zinc oxide
ZrO_2 Zirconium oxide

1 Introduction

Technological advances have increased the demand for water for industry and for survival. With the increase in water demand, humans have been trying to tap every possible water resource available in nature, from using ground water table below the surface and to the seawater, but sadly people are unable to quench their needs sufficiently (Low et al. 2015). The only solution is to reuse, reduce and recycle the water for a better living for the next generation. Chemical industries, pharmaceutical, and tanning industries, etc., generate lot of effluents. Of all the industries textile dyeing industries are large consumers of water up to 1900 million cubic meters per year and 75% of this is generated as waste effluent (Sójka-Ledakowicz et al. 1998; Chidambaram et al. 2015). Treating this water will suffice our water shortage adversely. Membrane separation has been a promising way of filtering the undesired particles from the effluent as they don't require any chemical additives and are operated iso-thermally under low temperature and lower energy consumption compared to that of another thermal process (Ng et al. 2013). Membranes are semi-permeable

barriers in which one or more species can pass through and others get retained. These barriers are often thin porous polymeric, ceramic or metallic films or even liquids or gasses.

In order to increase the efficiency of the membrane, polymeric membranes are being doped with nanoparticles, which bring about a synergistic effect of both the materials. Nanomaterials due to its flexible properties have found its application in wide areas of science including membrane separation. Incorporating nanoparticles in the polymeric membrane has reportedly increased its permeability, selectivity, mechanical and anti-fouling properties (Ng et al. 2013; Homayoonfal et al. 2013). It has been reported that depending upon the type of the nanoparticles used, different properties of the polymeric membrane are enhanced such as mechanical strength, crystallinity, visco-elastic properties, structure change, thermal stability, hydrophilicity, anti-fouling properties and performance (Xu et al. 2009).

Anti-microbial properties were incorporated in polyethyleneimine to form thin-film composite membrane with copper (Ben-Sasson et al. 2014). Magnetic iron nanoparticles were incorporated in Polyethersulphone membrane capsules for controlled release of nitrates in water (Emami et al. 2017). Addition of magnetic nanoparticles positively affected the pore formation in the membrane capsules and increased the performance of the membrane. Similarly, graphene oxide particles were doped in polyimide membranes to increase its permeability (Hu et al. 2018). It was reported that graphene oxide nanosheets increased the hydrophilicity of the membrane drastically thus increasing its water flux to much greater extent of 242 LMH/MPa and 90% salt rejection.

Polypropylene hollow fibre membranes were subjected to surface modification by ammonia plasma treatment, to incorporate hydrophilicity to the membrane (Yu et al. 2015). Concentration polarization was mitigated in the polyether-sulphone forward osmosis membrane by addition of Zn_2GeO_4 nanowires in the polymeric membrane (Kwak et al. 2001). Incorporating Zn_2GeO_4 increased the performance of the membrane and decreased the permeate flux decline rate, but played very less role in reducing the concentration polarization of the membrane. Similarly, TiO_2 nanoparticles were incorporated in aromatic polyamide reverse osmosis membranes (Kwak et al. 2001). Fe_2O_3 nanoparticles were incorporated in polyvinylchloride (PVC) membranes to increase the properties and separation characteristics of the membrane. Commercially purchased Fe_2O_3 were used to prepare mixed Fe_2O_3/PVC ultra-filtration membranes using phase inversion methods. Membranes containing different weight ratio of PVC and Fe_2O_3 were fabricated and compared for its performance. Addition of Fe_2O_3 also incorporated hydrophilic nature in the membrane, causing increased flux which was verified by contact angle measurement (Demirel et al. 2017).

Membranes are being used for reactive separation as well. Photo-catalytic membrane reactors are available with TiO_2 impregnated membranes for wastewater treatment (Mozia 2010). Though this process seems very attractive, the major drawbacks are mass transfer limitation during the reaction, dissolved salts precipitation on the catalyst surface hindering the reaction and most importantly, complete removal of dispersed TiO_2 particles from the solution. The simple solution was to

impregnate the TiO_2 on a membrane (Kim et al. 2003; Lee and Park 2013), thus making the separation of catalyst easy and making it reaction efficient.

1.1 Fenton Mechanism and Combined Fenton Based Polymeric Membrane Separation Approach

The researchers have investigated the effect of iron oxide on membrane separation, but we are going to deal with iron oxide as a catalyst to Fenton reaction, aiding the membrane separation. Similar to photo-catalytic reactions, in Fenton reactions, iron radicals act as a catalyst in initiating hydrogen peroxide to form ions and in oxidizing the organic molecules (Clarizia et al. 2017; Bae et al. 2013; Byrne et al. 2018; Karale et al. 2014; Sychev and Isak 1995; Expósito et al. 2018; Liang et al. 2017; Chen et al. 2016). The Fe^{2+} ions when introduced to H_2O_2, react to form OH radicals and Fe^{3+} ions. The generated Fe^{3+} ions can be reduced by the excess of H_2O_2 and more radicals will be generated. Thus, the Fe^{2+} ions are continuously being regenerated by the cyclic reactions and H_2O_2 is being continuously consumed. The ions which are being produced in the reaction (O_2H, H^+, OH^-, OH) are highly unstable and reactive radicals that attack the organic molecules and reduce them successively into CO_2 and H_2O. The above mechanism is being illustrated in the Eqs. (1–7).

$$Fe^{2+} + H_2O_2 \rightarrow Fe^{3+} + OH^- + OH^{\cdot} \tag{1}$$

$$Fe^{3+} + H_2O_2 \rightarrow Fe^{2+} + O_2H^{\cdot} + H^+ \tag{2}$$

$$Fe^{2+} + OH^{\cdot} \rightarrow Fe^{3+} + OH^- \tag{3}$$

$$Fe^{2+} + O_2H^{\cdot} \rightarrow Fe^{3+} + HO_2^- \tag{4}$$

$$Fe^{3+} + O_2H^{\cdot} \rightarrow Fe^{2+} + O_2 + H^+ \tag{5}$$

$$O_2H^{\cdot} + O_2H^{\cdot} \rightarrow H_2O_2 + O_2 \tag{6}$$

$$OH^{\cdot} + OH^{\cdot} \rightarrow H_2O_2 \tag{7}$$
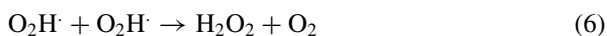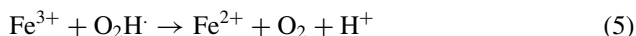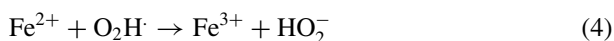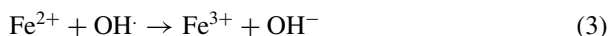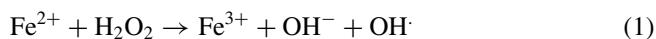
Numerous researches have been done on the kinetic effects of the Fenton process with various precursors and additives (Babuponnusami and Muthukumar 2014; Durán et al. 2015; Blanco et al. 2014; Cabrera Reina et al. 2017; Hama Aziz et al. 2018; Yang et al. 2018; Liu et al. 2011). The important functional group in azo dyes used for textile dyeing as well consists of at least azo group binding with at least one

aromatic ring leading to textile coloration. The discharge of dying effluents cause respiratory problems and inhibit supply of fresh water and sunlight for all aquatic life causing serious environmental damage. The breakdown of such toxic dyes is essential with cost effective water treatment technique for aquatic as well human-being (Liu et al. 2011). Our previous study for reactive black 5 degradations showed that without H_2O_2, 1% Fe_2O_3 blended PES membrane provides better performance as compared to other fabricated reactive membranes in terms of dye removal (98%) and more stabilized flux (60.02*10^{-7} m^3/m^2.sec). The optimized variables under same findings were RB5 concentration (100 ppm), 200 kPa trans-membrane pressure under acidic pH = 3 for 1 h filtration time (Patil et al. 2020). Hence same reactive membrane was employed to investigate the effect of different RB5 concentration, pH, H_2O_2 on dye removal and COD removal efficiency. The further study also makes an impact on membrane fouling, membrane reusability, membrane stability under operating condition. Thus, it is essential to investigate the effect of Fenton's reaction in membrane separation with membranes impregnated with iron catalysts.

2 Materials and Methods

Commercial grade Polyethersulfone (PES 3000P) as the base polymer for the manufacture of membranes was sold by M/s Prakash Chemicals Pvt. Ltd, India. PES in powder form was always stored in the oven at 50 °C to avoid humidity before use. Polyethylene glycol (PEG) 10,000 Da was supplied by M/s Alfa Aesar, USA Ferric chloride hexahydrate was sold by M/s S.D Fine Chemicals Pvt. Ltd, India. Commercial solvents like 35% ammonia solution and ethanol 95% purity were supplied by M/s S.D. Fine Chemicals Pvt Ltd, India. The solvent N-Methyl-2-pyrrolidone (NMP) was obtained from M/s Thomas Baker Pvt. Ltd, India. Reactive Black 5 dye (M.W 0.991 kg/mole) received as a gift sample from the textile industry was used as a pollutant for the study of the efficacy of the in-house fabricated membranes. The supply of all chemicals was ensured free from contamination prior to use. Polyester nonwoven fabric with a thickness of 100 μm was obtained from Advanced Specialty Pvt Ltd., India. The pH of the synthetic RB5 solution and the backwashing of the reactive membranes were performed with 0.1 N sulfuric acid and 0.1 N sodium hydroxide solutions.

2.1 Composition of Fe₂O₃ Blended PES Membranes

The α-Fe_2O_3 nanoparticles were synthesized by the co-precipitation method using ferric chloride hexa-hydrate and ammonium hydroxide as precursors of the same method reported in the literature (Lassoued et al. 2017). The precipitate is formed under high stirring at pH 11 and calcinated at 600^0C for 4 h and pulverized. The

same method was used with suitable modification of ultrasound effect to avoid agglomeration of nanoparticles (Lassoued et al. 2017; Patil et al. 2020).

The synthesized nanoparticles were blended with the solvent NMP, sonicated for 1 h and then stirred with a calculated ratio of PES and PEG powder. Table 1 showed the casting solution of different composition was blended for 6 h to achieve homogeneity and membranes were fabricated using the phase inversion method as reported in literature (Demirel et al. 2017; Patil et al. 2020).

2.2 Membrane Filtration Experiment Set up

The fabricated membranes were cut into the appropriate size of 4 cm diameter and fitted into the dead-end filtration setup. In the filtration setup, the feed is forced to pass through the membrane under constant pressure conditions. The feed containing the amount of Reactive Black 5 (RB5) dye in aqueous solution added to maintain the specific dosage, desired concentration and to initiate the Fenton reaction, Hydrogen peroxide of pre-determined dosage was added into the solution. Maintaining a constant pressure, the permeate volume was collected over a period of time and was analyzed for color and COD rejection. In dead-end filtration, the effluent or feed is passed through the membrane under controlled pressure, which is schematically represented in Fig. 1. Based on pure water filtration experiments, 1% Fe_2O_3 blended PES membrane shows maximum water flux over other membranes and it had been chosen for further different concentrations of RB5 separation studies.

After the membrane was kept in the setup, de-ionized water was filled till volume of membrane reactor. The operating pressure was maintained using pressure knob of nitrogen cylinderat 200 kPa and the permeate water flux was evaluated at the end of 1 h operation and the stabilized flux was determined.

$$J = \frac{V}{A.t} \qquad (8)$$

The water as well as solute flux of the membrane was calculated using Eq. (8), where J, V, A denotes the flux in (m^3/m^2.sec) the volume collected in time t, the effective area of the membrane (m^2) respectively (Demirel et al. 2017; Patil et al. 2020). All membrane filtration experiments were performed three times to maintain consistency of results for dye removal. Rejection efficiency (R) was evaluated using Eq. (9) formula where C_P and C_R are the concentrations of permeate and retentate in terms of COD and Color values respectively (Babuponnusami and Muthukumar 2014; Liu et al. 2011). The concentration of the solution was determined by using UV spectrophotometry with a fixed wavelength of 598 nm.

$$R\% = \left(1 - \frac{C_P}{C_R}\right)*100 \qquad (9)$$

Table 1 Composition of the in-house fabricated virgin PES and Fe_2O_3 blended PES membranes and their properties

Membrane code	PES (%)	PEG (%)	Fe_2O_3 (%)	Pure water flux $(m^3/m^2.sec)*10^7$	Permeate flux $(m^3/m^2.sec)*10^7$	% FRR
M1	16	5	0	37.5	20.83	90
M2	16	5	0.5	47.77	30.66	85
M3	16	5	1	80.94	60.02	75
M4	16	5	1.5	23.86	15.58	70
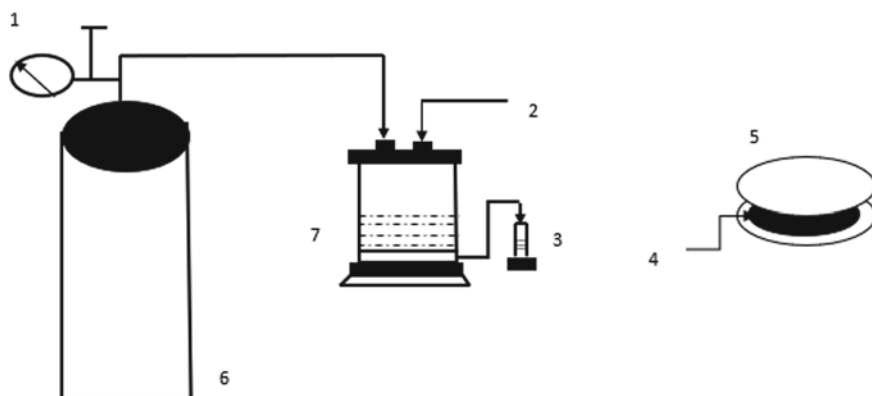
Fig. 1 Schematic of the lab-scale dead-end filtration setup **1** pressure regulator **2** feed solution **3** permeate **4** membrane **5** membrane holders **6** nitrogen cylinder **7** dead-end membrane cell

2.3 Evaluation of Membrane Resistance and Membrane Fouling Index

The pure water flux of the membrane is used to obtain the membrane resistance (R_m) of the membrane as in Eq. 7, where J_o is pure water flux of the membrane, A is the area of the membrane dV is the volume of permeate collected at time interval dt.

$$J_0 = \frac{1}{A}\frac{dV}{dt} = \frac{\triangle P}{\mu R_m} \tag{10}$$

Similarly, feed solution containing a fixed concentration of reactive black 5 (RB5) in de-ionized water was filled in the feed reservoir and the permeate flux was quantified for a specific interval of time throughout 1 h under constant pressure. After 1 h, the remaining sample from the reservoir (retentate), the collected permeate and the prepared feed were subjected to analysis (Patil et al. 2020; Cai et al. 2019).

$$J = \frac{\triangle P}{\mu (R_m + R_c)} \tag{11}$$

where R_c is the cake resistance. Since R_c is proportional to the mass of the solid deposited on the surface. α being a specific cake resistance of the material and m be the cake density in (kg/m^2), R_c can be expressed as

$$R_c = \alpha.m = \frac{\alpha.C_b.r.V}{A} \tag{12}$$

where C_b is the bulk concentration, V being the cumulative permeate volume. The membrane rejection factor r can be expressed as follows

$$r = 1 - \frac{C_P}{C_b} \tag{13}$$

C_p being the permeate concentration. Since rejection close to 100%, the effective concentration C is determined with experimentally obtained rejection factor. Thus, applying Eq. (6) in Eqs. (5) and (4) and (3), it is expressed as

$$\frac{t}{V} = \frac{\mu.R_m}{\triangle P.A} + \left[\frac{\mu.\alpha.C}{\triangle P.2.A^2} \right].V \tag{14}$$

In a plot of t/V versus V, the data commonly exhibiting a linear relationship has a slope (λ), which is also known as the 'Modified Fouling Index'.

$$\lambda = \frac{\mu.\alpha.C}{\Delta P.2.A^2} \tag{15}$$

On the same hand, to carry over the Fenton degradation process in the membrane setup, hydrogen peroxide was added to the feed reservoir and well mixed before enclosing the setup. Then 1 h of flux experiment, the retentate, permeate and feed with and without hydrogen peroxide were used for further analysis.

2.4 Membrane and Nanoparticle Characterization

The particle size distribution (PSD) of the Fe_2O_3 nanoparticles was measured with the Malvern Mastersizer 2000, which operates on the principle of laser detection and can measure particles in the size range of 0.02–2000 μm. The X-ray diffraction patterns of the prepared Fe_2O_3 nanoparticles were obtained from Bruker D8 Advance at 40 kV, 40 mA powder X-ray diffractometer. The morphology of the prepared materials was examined with scanning electron microscopy (SEM). The structure and elemental composition analysis of membrane was performed with an EDAX JEOL JSM 6380la. The membrane and nanoparticle analysis were provided in supplementary file of previous work (Patil et al. 2020**).** The front and cross-section of the membrane were inspected by scanning electron microscopy. The phase inversion parameters such as rate of polymer precipitation and type of additive, nanoparticle or solvents has a significant role in determining the surface-morphology and performance of membranes. The color change in reactive black 5 samples by self-developed PES membranes was observed using LMSP UV1900 Labman UV-Visdual beam spectrophotometer at 598 nm.

3 Results and Discussion

Since the membrane is a catalytic membrane, it should initiate a Fenton reaction in presence of hydrogen peroxide in the membrane. Constant pressure experiment at 200 kPa in the dead-end filtration setup was done using 100–1000 ppm of RB5 and 0–30 mM of H_2O_2 in the feed solution using 1 wt% Fe_2O_3/PES Membrane under pH (3–9). The experiment resulted in a 98% color removal for 100 ppm RB5 dye as compared to normal membrane separation (100 ppm, 200 kPa, pH3, 10 mM H_2O_2 or without H_2O_2). It was observed that the decline in membrane flux is 23.16% for membrane separation without reaction or hydrogen peroxide where the flux decline is 24% for membrane separation with reaction or hydrogen peroxide dosage. Though it was observed that a slight increase in the permeate dye flux, the specific cake resistance α remains approximately the same as about $4.0*10^{15}$ m/kg. To check permeate flux behavior, normalized flux or relative flux was considered for comparison of permeate flux under different operating conditions of membrane filtration.

3.1 Effect of pH on COD Removal of RB5

In Fig. 2, the effect of pH was studied by varying pH value in the solution within the range 3–9, 0.00164 mol/L of [Fe^{3+}], 100–1000 mg/L of RB5 dye solution, 10 mM [H_2O_2], pH (3–9). filtration time of 60 min and 30 °C. As a result of the rise in pH, membrane filtration system also shows lowering efficiency of COD of removal. Fenton assisted membrane system shows lesser efficiency as compared to the Fenton system. In contrast, iron (II) ions are unstable above pH 4 and easily form iron (III) ions, which tend to form iron (III)-hydrogen complexes. At pH above 4, Hydrogen peroxide is also unstable, it can break down to form oxygen and water in a basic solution and lose its oxidation capacity. Therefore, hydrogen peroxide and ferrous

Fig. 2 Effect of pH on COD removal of different dye concentration under operating condition (RB5-100-1000 ppm, pH (3–9), TMP (200 kPa), Filtration time-1 h, H_2O_2 Concentration (10 mM)
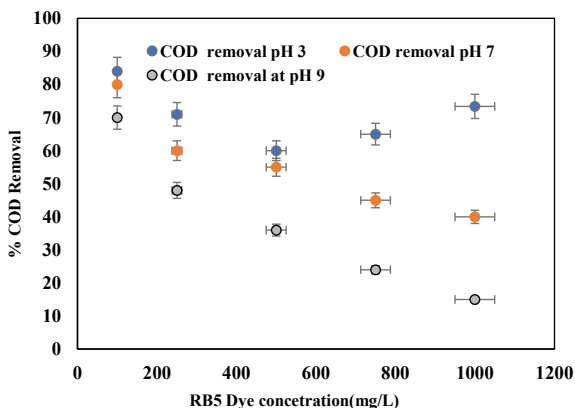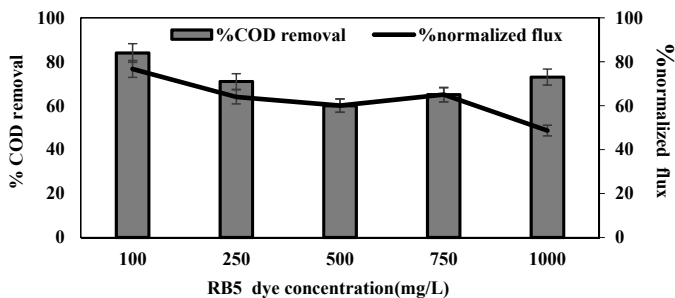
Fig. 3 Effect of Feed concentration on COD removal of different dye concentration under operating condition (RB5-100–1000 ppm, pH (3), TMP (200 kPa), Filtration time 1 h, H_2O_2 Concentration (10 mM))

ions have difficulty in establishing an effective redox system, and their decolorization is also less effective. Hence, the optimum pH for Fenton assisted membrane filtration with 71% COD degradation was 3 (Liu et al. 2011; Sahunin et al. 2006).

3.2 Effect of Feed Concentration on COD Degradation Efficiency

In Fig. 3, the effect of feed concentration of dye was studied by varying feed concentration within 100–1000 ppm. Other parameters were fixed at 0.00164 mol/L of $[Fe^{3+}]$, 10 mM $[H_2O_2]$, pH = 3, and filtration time of 1 h and temperature 30°C. As the feed concentration increases, the COD concentration also increases, the membrane pore gets blocked due to the formation of protective cake layer over the membrane surface. Thus, surface area available for degradation decreases and it results into lower COD removal efficiency. The bulk concentration needs more OH ions for more degradation as the level of Fe ion concentration in membranes were kept constant. Hence, the optimum concentration for Fenton assisted membrane filtration regarding COD degradation was 250 ppm.

3.3 Effect of Trans-Membrane Pressure on COD Degradation Efficiency

In Fig. 4, the effect of trans-membrane pressure was studied by varying trans-membrane pressure within the range 100–400 kPa, 0.00164 mol/L of $[Fe^{3+}]$, 10 mM $[H_2O_2]$, pH = 3, feed concentration 250 ppm, filtration time of 1 h and 30 °C. Trans-membrane pressure acts as a driving force for membrane separation. The varying collapsing of molecules with an increase in TMP increases filtration runs
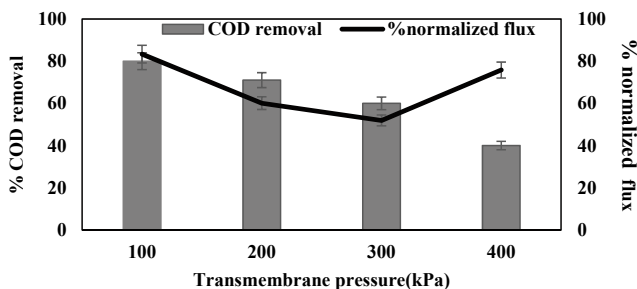
Fig. 4 Effect of Trans-membrane pressure on COD removal under operating condition (RB5-250 ppm, pH (3), TMP (100–400 kPa), Filtration time 1 h, H_2O_2 Concentration (10 mM))

within a short period but also causes fouling of membrane to more extent. Fouling of membrane also shows lowering COD efficiency. Above the TMP of 200 kPa, the minimum COD degradation was achieved.

3.4 Effect of H_2O_2 on COD Degradation Efficiency

In Fig. 5, the effect of H_2O_2 was studied by varying H_2O_2 dosage within the range 0–30 mM, 0.00164 mol/L of $[Fe^{3+}]$, pH = 3, feed concentration 250 ppm, filtration time of 1 h and 30 °C temperature. With the rise in H_2O_2, more OH ion is available for degradation, the reaction takes place in a short period after the end of filtration COD efficiency decreases. The un-reacted H_2O_2 will act as a scavenger of •OH and produces a less potent per hydroxyl radical, resulting in less dye decolorization. Hence the optimum H_2O_2 concentration for degradation of dyes was 10 mM H_2O_2.

Fig. 5 Effect of H_2O_2 concentration on COD removal under operating condition (RB5-250 ppm, pH (3), TMP (200 kPa), Filtration time 1 h, H_2O_2 Concentration (0 mM-30 mM)
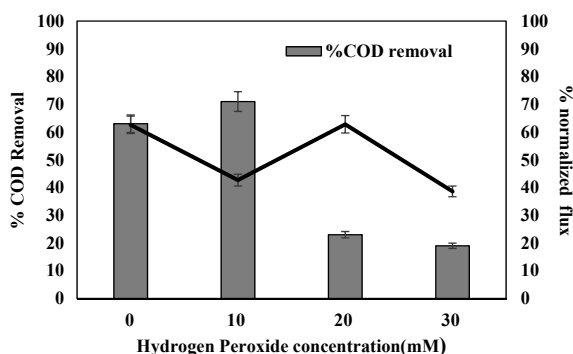
3.5 Membrane Recyclability and Fouling Studies

Fe_2O_3 blended PES membrane had negatively charged polymeric group and positively charged ferric ion from iron oxide source. The membrane itself is a source of Fe ion in such system. Hence, the optimized M3 membrane keeps the Fe ions concentration constant. Fenton like system provides OH-ions selectively for degradation. Reactive black-5 has negatively charged group along with the azo group. The consumption of ferric ions/ ferrous ion produced is the driving factor for such systems to attack complex structured dyes. The rate of fouling depends upon factors like operating feed concentration, trans-membrane pressure, hydrogen peroxide concentration and pH. FRR is flux recovery ratio which is an indication of measuring antifouling characteristics of the membrane. The specific cake resistance observed under best operating condition was found to be $8.0923*10^{14}$(m/kg).

It is very important to know the lifetime of the membrane and the reusability of the membrane, for its effective application to the intended purpose. It is well known that membranes get fouled and are subjected to alkaline or acid backwash treatment for unblocking the pores and making it fully effective**.** Membrane fabrication and its recycle studies for pollutant separation were restricted to use membranes till maximum five cycles for better performance in terms of stabilized flux and pollutant removal (Patil et al. 2020; Warsinger et al. 2018**).** Since the fabricated membranes were small and fragile. Since these membranes were intended to make for dead-end filtration setup, backwashing was a problem. Even though subjected to backwashing, they were highly prone to tear and wear because of the applied pressure. Because of these, the membranes, which used for normal filtration were not used for recycling studies.

It was surprisingly noticed that membranes when subjected to dye water separation of RB5 along with hydrogen peroxide, the amount of pore blockage was minimum. The surface of the membrane was cleaned with a flowing jet of de-ionized water to remove the deposited cake layer and was subjected to a dead-end filtration experiment with de-ionized water. During the experiment, it was noticed that initially, the permeate flux was lower than the initial and then it increased steadily to the original value. It is noticeable that the membrane gave a steady flux of $138*10^{-7} m^3/m^2$. s. The main reason for this astonishing activity of the membrane is found to be the anti-pore blockage due to the reaction. Since the Fe_2O_3 is present throughout the membrane matrix in and out the pores of the membrane, the reaction is happening in every corner of the membrane from Fig. 6. Since the reaction is happening, any foulants blocking the pores of the membrane susceptible to the oxidation reaction. Hence, they break down and flow through the membrane making it blockage free. After five continuous cycles, it can be observed that the permeate flux decreases, which marks the life of the membrane under optimal conditions. This is due to the damage caused to the membrane due to the reaction and the presence of hydrogen peroxide.

Fig. 6 Top morphology of M3 membrane (1 wt% F$_2$O$_3$-PES) virgin and fouled membrane where a, b, shows the top surface morphology

(a)   (b)
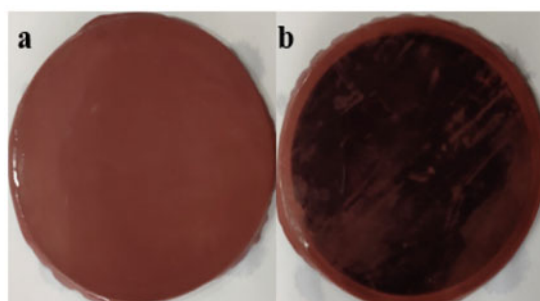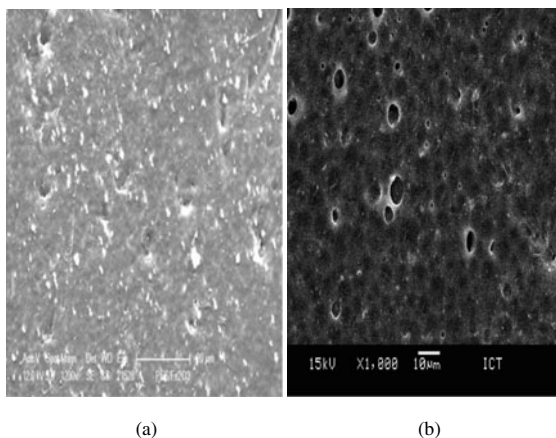
4 Conclusions

PES/Fe$_2$O$_3$ fabricated membranes were highly hydrophilic due to which they provided higher water flux than normal PES membranes. The dye removal test performed on the membrane showed that they were highly effective in the presence of reaction assisted membrane separation. The reaction reduced the flux decline by 23%. When the effect of feed, trans-membrane pressure, the dosage of hydrogen peroxide was studied, it was concluded that the effect of dye concentration had a significant effect on the membrane, increase in trans-membrane pressure resulted in more permeate flux as well as reduced membrane resistance and low dosage of hydrogen peroxide of 10 mM proved to be the optimum concentration of accelerated Fenton reaction. The optimized conditions recommended for such system are feed concentration(100-250 ppm), TMP (100–200 kPa), pH 3, time duration 1 h, hydrogen peroxide concentration (10 mM). The best result for COD removal for 250 ppm dye solution was found to 71% with dye removal %80. The recyclability of reactive membrane (M3-1%Fe$_2$O$_3$mixed PES membrane) was found to be more

active up to five cycles of filtration in terms of flux and COD removal under optimal condition.

Conflict of Interest and Authorship Conformation Form

Please check the following as appropriate:

- All authors have participated in (a) conception and design, or analysis and interpretation of the data; (b) drafting the article or revising it critically for important intellectual content; and (c) approval of the final version.
- This manuscript has not been submitted to, nor is under review at, another journal or other publishing venue.
- The authors have no affiliation with any organization with a direct or indirect financial interest in the subject matter discussed in the manuscript
- The following authors have affiliations with organizations with direct or indirect financial interest in the subject matter discussed in the manuscript:

References

Babuponnusami A, Muthukumar K (2014) A review on fenton and improvements to the Fenton process for wastewater treatment. J Environ Chem Eng 2:557–572. https://doi.org/10.1016/j.jece.2013.10.011

Bae S, Kim D, Lee W (2013) Degradation of diclofenac by pyrite catalyzed Fenton oxidation. Appl Catal B Environ 134–135:93–102. https://doi.org/10.1016/j.apcatb.2012.12.031

Ben-Sasson M, Zodrow KR, Genggeng Q, Kang Y, Giannelis EP, Elimelech M (2014) Surface functionalization of thin-film composite membranes with copper nanoparticles for antimicrobial surface properties. Environ Sci Technol 48(1):384–393. https://doi.org/10.1021/es404232s

Blanco J, Torrades F, Morón M, Brouta-Agnésa M, García-Montaño J (2014) Photo-Fenton and sequencing batch reactor coupled to photo-Fenton processes for textile wastewater reclamation: feasibility of reuse in dyeing processes. Chem Eng J 240:469–475. https://doi.org/10.1016/j.cej.2013.10.101

Byrne C, Subramanian G, Pillai SC (2018) Recent advances in photocatalysis for environmental applications. J Environ Chem Eng 6(3):3531–3555. https://doi.org/10.1016/j.jece.2017.07.080

Cabrera Reina A, Miralles-Cuevas S, Casas López JL, Sánchez Pérez JA (2017) Pyrimethanil degradation by photo-Fenton process: Influence of iron and irradiance level on treatment cost. Sci Total Environ 605–606:230–237. https://doi.org/10.1016/j.scitotenv.2017.06.217

Cai BJ, Baudin I, Ng HY (2019) A modified fouling index (MFI40) and fouling predicting approach for ultrafiltration of secondary effluents. J Water Reuse Desalin 9:67–82. https://doi.org/10.2166/wrd.2018.020

Chen S, Zhang H, Li S (2016) Investigation of mechanism involved in TiO_2 and photo-fenton photocatalytic degradation of emerging contaminant sucralose in aqueous media. Procedia Environ Sci 31:753–757. https://doi.org/10.1016/j.proenv.2016.02.064

Chidambaram T, Oren Y, Noel M (2015) Fouling of nanofiltration membranes by dyes during brine recovery from textile dye bath wastewater. Chem Eng J 262:156–168. https://doi.org/10.1016/j.cej.2014.09.062

Clarizia L, Russo D, Di Somma I, Marotta R, Andreozzi R (2017) Homogeneous photo-Fenton processes at near neutral pH: a review. Appl Catal B Environ 209:358–371. https://doi.org/10.1016/j.apcatb.2017.03.011

Demirel E, Zhang B, Papakyriakou M, Xia S, Chen Y (2017) Fe_2O_3 nanocomposite PVC membrane with enhanced properties and separation performance. J Memb Sci 529:170–184. https://doi.org/10.1016/j.memsci.2017.01.051

Durán A, Monteagudo JM, Gil J, Expósito AJ, San Martín I (2015) Solar-photo-Fenton treatment of wastewater from the beverage industry: Intensification with ferrioxalate. Chem Eng J 270:612–620. https://doi.org/10.1016/j.cej.2015.02.069

Emami N, Razmjou A, Noorisafa F, Korayem AH, Zarrabi A, Ji C (2017) Fabrication of smart magnetic nanocomposite asymmetric membrane capsules for the controlled release of nitrate. Environ Nanotechnol Monit Manag 8:233–243. https://doi.org/10.1016/j.enmm.2017.09.001

Expósito AJ, Monteagudo JM, Durán A, San Martín I, González L (2018) Study of the intensification of solar photo-Fenton degradation of carbamazepine with ferrioxalate complexes and ultrasound. J Hazard Mater 342:597–605. https://doi.org/10.1016/j.jhazmat.2017.08.069

Hama Aziz KH, Miessner H, Mueller S (2018) Comparative study on 2,4-dichlorophenoxyacetic acid and 2,4-dichlorophenol removal from aqueous solutions via ozonation, photocatalysis and non-thermal plasma using a planar falling film reactor. J Hazard Mater 343:107–115. https://doi.org/10.1016/j.jhazmat.2017.09.025

Homayoonfal M, Mehrnia MR, Mojtahedi YM, Ismail AF (2013) Effect of metal and metal oxide nanoparticle impregnation route on structure and liquid filtration performance of polymeric nanocomposite membranes: a comprehensive review. Desalin Water Treat 51:3295–3316. https://doi.org/10.1080/19443994.2012.749055

Hu R, Zhang R, He Y, Zhao G, Zhu H (2018) Graphene oxide-in-polymer nanofiltration membranes with enhanced permeability by interfacial polymerization. J Memb Sci 564:813–819. https://doi.org/10.1016/j.memsci.2018.07.087

Karale RS, Manu B, Shrihari S (2014) Fenton and photo-fenton oxidation processes for degradation of 3-aminopyridine from water. APCBEE Proc 9:25–29. https://doi.org/10.1016/j.apcbee.2014.01.005

Kim SH, Kwak SY, Sohn BH, Park TH (2003) Design of TiO_2 nanoparticle self-assembled aromatic polyamide thin-film-composite (TFC) membrane as an approach to solve biofouling problem. J Memb Sci 211:157–165. https://doi.org/10.1016/S0376-7388(02)00418-0

Kwak SY, Kim SH, Kim SS (2001) Hybrid organic/inorganic reverse osmosis (RO) membrane for bactericidal anti-fouling. 1. Preparation and characterization of TiO_2 nanoparticle self-assembled aromatic polyamide thin-film-composite (TFC) membrane. Environ Sci Technol 35:2388–2394. https://doi.org/10.1021/es0017099

Lassoued A, Dkhil B, Gadri A, Ammar S (2017) Control of the shape and size of iron oxide (α-Fe_2O_3) nanoparticles synthesized through the chemical precipitation method. Results Phys 7:3007–3015. https://doi.org/10.1016/j.rinp.2017.07.066

Lee SY, Park SJ (2013) TiO_2 photocatalyst for water treatment applications. J Ind Eng Chem 19:1761–1769. https://doi.org/10.1016/j.jiec.2013.07.012

Liang C, Liu Y, Li K (2017) Heterogeneous photo-Fenton degradation of organic pollutants with amorphous Fe-Zn-oxide/hydrochar under visible light irradiation. Sep Purif Technol 188:105–111. https://doi.org/10.1016/j.seppur.2017.07.027

Liu X, Qiu M, Huang C (2011) Degradation of the reactive black 5 by fenton and fenton-like system. Procedia Eng 15:4835–4840. https://doi.org/10.1016/j.proeng.2011.08.902

Low ZX, Liu Q, Shamsaei E, Zhang X, Wang H (2015) Preparation and characterization of thin-film composite membrane with nanowire-modified support for forward osmosis process. Membranes (basel). 5:136–149. https://doi.org/10.3390/membranes5010136

Mozia S (2010) Photocatalytic membrane reactors (PMRs) in water and wastewater treatment a review. Sep Purif Technol 73:71–91. https://doi.org/10.1016/j.seppur.2010.03.021

Ng LY, Mohammad AW, Leo CP, Hilal N (2013) Polymeric membranes incorporated with metal/metal oxide nanoparticles: A comprehensive review. Desalination 308:15–33. https://doi.org/10.1016/j.desal.2010.11.033

Patil H, Shanmugam V, Marathe K (2020) Studies in synthesis and modification of PES membrane and its application for removal of reactive black 5 dye. Indian Chem Eng. ,0:1–9. (Accepted and Article in press) https://doi.org/10.1080/00194506.2020.1822761

Sahunin C, Kaewboran J, Hunsom M (2006) Treatment of textile dyeing wastewater by photo oxidation using UV/H2O2/Fe2+ reagents. Sci Asia 32:181–186. https://doi.org/10.2306/scienceasia1513-1874.2006.32.181

Sójka-Ledakowicz J, Koprowski T, Machnowski W, Knudsen HH (1998) Membrane filtration of textile dyehouse wastewater for technological water reuse. Desalination 119:1–9. https://doi.org/10.1016/S0011-9164(98)00078-2

Sychev AY, Isak VG (1995) Iron compounds and the mechanisms of the homogeneous catalysis of the activation of O_2 and H_2O_2 and of the oxidation of organic substrates. Russ Chem Rev 64:1105. https://doi.org/10.1070/rc1995v064n12abeh000195

Warsinger DM, Chakraborty S, Tow EW (2018) A review of polymeric membranes and processes for potable water reuse. Prog Polym Sci 81:209–237. https://doi.org/10.1016/j.progpolymsci.2018.01.004

Xu ZL, Yu LY, Han LF (2009) Polymer-nano inorganic particles composite membranes: A brief overview. Front Chem Eng China 3:318–329

Yang T, Peng J, Zheng Y (2018) Enhanced photocatalytic ozonation degradation of organic pollutants by ZnO modified TiO_2 nanocomposites. Appl Catal B Environ 221:223–234. https://doi.org/10.1016/j.apcatb.2017.09.025

Yu HY, Hu MX, Xu ZK, Wang JL, Wang SY (2015) Surface modification of polypropylene microporous membranes to improve their antifouling property in MBR: NH3 plasma treatment. Sep Purif Technol 45:8–15. https://doi.org/10.1016/j.seppur.2005.01.012

Synthesis of Biodegradable Composite Films from Polyvinyl Alcohol (PVA)/Amla Leaf Fibre (ALF) for Packaging Application

Pankaj Kumar Shrimal, Sangeeta Garg, and ArdhenduSekhar Giri

Abstract In this study, the effect of fibre loading and different surface modification method on the properties of polyvinyl alcohol (PVA)/amla leaf fibre (ALF) were observed. The surface modification of amla leaf fibre was done by alkali treatment (AT) with sodium hydroxide (NaOH) and by graft copolymerization (GC) method using myristic acid (MA) separately. The highest grafting yield was achieved 31.59% at 180 ˚C. The crystallinity index of ALFreduced from 0.79 to 0.17 after graft copolymerization with myristic acid. The composite films were separately prepared from ALF, treated amla leaf fibre (TALF), and grafted amla leaf fibre (GALF) with different composition of loading (5, 10, 15% (w/w)) by solution casting method. Surface modification of fibre showed the enhancement in the mechanical properties of composite film. With 5% loading of ALF, TALF, and GALF the tensile strength of composite films were 32.94, 36.76, and 41.11 MPa, respectively and increased to 34.39, 39.15, and 45.12 MPa with 10% loading in the composite films. However the films containing GALF showed the maximum tensile strength of 45.12 MPa among all the films. The water uptake (%) of the film containing 5% loading of ALF was 134% and it decreased by 47.02% in composite film of GALF. ALF containing composite films showed the faster biodegradation rate as compare to rest of the composite films.

Keywords Amla leaf fibre · Grafting copolymerization · Alkali treatment · Composite films · Mechanical properties

P. K. Shrimal · S. Garg (✉)
Department of Chemical Engineering, Dr. B. R. Ambedkar National Institute of Technology, Jalandhar, Punjab 14400, India
e-mail: gargs@nitj.ac.in

A. Giri
Department of Chemical Engineering, Indian Institute of Science Education and Research, Bhopal, Madhya Pradesh 462066, India

1 Introduction

The plastics are the important class of material for industrial and domestic applications. Plastics are cheap, durable, good mechanical strength, chemically stable, and light weight material these edges gives the good suitability for various industrial and domestic application such as packaging, electronics, biomedical, automobile, agriculture, and pharmaceutical (Zhang et al. 2021; Wu et al. 2021; Saba and Jawaid 2018). The globally plastic waste generation is more than 340 million ton and around approximately 46% waste is from packaging sector. Whereas, more than 90% of total plastics were collected in environment and less than 5% plastic material has been recycled. The estimated market size of plastic packaging will increased with 5% compound growth annual rate (CGAR) between the 2016 and 2022 and reach to nearly 400 billion USD by 2022. The use of petroleum based plastics creates huge environmental pollution and adversely affects the aquatic and wildlife habitat, human society, and natural resources because of its non-degradable behavior(Wu et al. 2021; Kamdem et al. 2019; Beikzadeh et al. 2020; Norcino et al. 2020; Mukherjee et al. 2019). So this serious issue drag the attention of the researchers to design the biodegradable polymers.

Several studies have been reported the development of biodegradable films with renewable sources, abundance of presence and cheaper in cost. Hence, natural cellulosic fibres are the magnificent material to use for the development of biodegradable polymers (Majeed et al. 2013; Ray et al. 2019; Gironès et al. 2012).

Many researchers have used the various natural cellulosic content as a reinforced material such as date palm leaf (Ray et al. 2019), jackfruit waste flour (Ooi et al. 2011), barley husk (Mittal et al. 2020), apple pomance (Gaikwad et al. 2016), rice straw (Mukherjee et al. 2019), sugarcane bagasse (Mandal and Chakrabarty 2014), and kenaf (Pua et al. 2013) for formation of composite film. Amla (emblicaofficinalis) leaf fibre is obtained from the amla tree. Amla leafs are having versatile utilization in the herbal medicines, waste water treatment, and health treatment. Amla leaf fibre is a lignocellulose fibre which contains cellulose, hemicellulose, and lignin content in it (Mishra and Mohanty 2018; Singh et al. 2019; Padmapriya et al. 2015). Whereas, the researchers also done surface modification of natural cellulosic fibres (NCF) by various methods such as graft copolymerization (Mittal et al. 2016), mercerization (Kaith et al. 2008), and cold plasma discharge (Popescu et al. 2011) to improve its mechanical properties. The graft copolymerization is the magnificent technique among several techniques for surface modification of NCF to enhance its mechanical properties (Mittal et al. 2016; Kohli et al. 2017).

The PVA is the synthetic biodegradable polymer and used in packaging application, so it's an appropriate matrix for formation of biodegradable composite film with fibre due to its carboxyl and hydroxyl group, which help to form hydrogen bond with NCF. It has water soluble and thermo plasticity property, due to this it has good film forming property by solution castingmethod (Ooi et al. 2011; Pua et al. 2013; Mittal et al. 2016; Yee et al. 2011). Apart from this, the presence of hydroxyl group makes composite films less resistive towards water barrier property. So to enhance

its water barrier property the surface modification of NCF (such as ALF) with graft copolymerization by long chain of fatty acids has been done in this study. In literature, no study has been reported till date on the graft copolymerization of ALF by myristic acid using redox initiator (potassium per sulphate (KPS) and ferrous ammonium sulphate (FAS)). Also, comparison of properties after incorporation of alkali treated ALF and grafted copolymerized ALF in PVA matrix was not explored yet.

The motive of the present study was to prepare surface modified fibre of ALF by graft copolymerization with myristic acid (MA) and alkali treatment by sodium hydroxide separately. XRD characterization was performed for understand its crystalline behavior. The composite films were developed by reinforcement of ALF on the PVA matrix. The different loading composition (5, 10, 15% (w/w)) of ALF was taken for the preparation of composite films. The separate films were prepared with ALF, TALF, and GALF, and also analyzed it's physico-chemical properties such as water uptake (%), water vapour transmission rate (WVTR), biodegradability, and mechanical properties.

2   Materials and Methodology

2.1   Materials

Amla leaf (AL) was obtained from the local market, Jalandhar, Punjab, India. Acetic acid, dimethyl sulfoxide (DMSO), polyvinyl alcohol (PVA), ferrous ammonium sulphate (FAS), and sodium hydroxide (NaOH) was purchased from the s.d. fine-chem Ltd., Mumbai, Maharashtra, India. Potassium per sulphate (KPS) is procured from the lobachemie Pvt. Ltd., Mumbai, Maharashtra, India. Ethanol was obtained from chongyu hi-tech chemicals, China. Myristic acid (MA) was purchased from sisco research laboratories Pvt. Ltd., Mumbai, Maharashtra, India.

2.2   Alkali Treatment of ALF

Moderately grinded the AL by grinding mixer (Model HL 7600, phillips, Gurugram, Haryana, India), washed with distilled water to remove the dirt from the surface of ALF and dried in a hot air oven at 75 °C for 22–24 h. The ALF were soaked in a 5% NaOH solution for 3 h at room temperature, then washed well in cold water, dipped in a 5% acetic acid solution to remove any excess NaOH from the fibre surfaces, and then washed in cold water before drying at 50 °C for 24 h (Ibrahim et al. 2014). This alkali treatment makes fibres fragile and removes the hemicellulose, waxes, and lignin. The treated amla leaf fibre (TALF) were grinded in fine size (mesh size 120). The alkali treatment process was shown in Scheme 1.

Amla leaf collected from amla tree and moderately grinded

↓

Washed with distilled water and dried at 75 ˚C for 22-24 h.

↓

Fibre were soaked into 5% NaOH solution for 3 h at room temperature

↓

Thoroughly washed with distilled water and soaked into 5% acetic acid for 3h

↓

Give final water wash and dried for 24h at 50˚C

↓

This treated fibre finally grinded into the size of 120 mesh
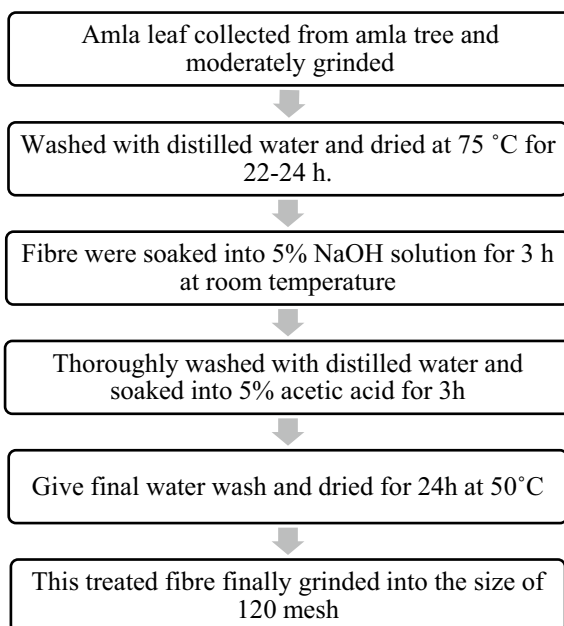
2.3 Grafting of ALF

A solvent medium was prepared with DMSO/water (3:1) for graft copolymerization of AL. To make fibre more fragile and to activate the reactive sites of ALF, it was soaked for overnight in solvent medium. In the reaction media the myristic acid was added gently in the presence of FAS and KPS mixture. The amount of FAS and KPS mixture was kept constant in the specific ratio of (1:1). Under continuous stirring the reaction mixture were heated to 55 ˚C for 135 min. Using ethanol as a solvent the grafted copolymer was extracted by soxhlet extractor. The sample was dried in hot air oven at 55 ˚C for 24 h (Mittal et al. 2016, 2019; Kohli et al. 2017). The grafting process was shown in Scheme 2.

Calculation for graft yield was done by:

$$\text{Percentage graft yield} = \frac{W_g - W_i}{W_i} \times 100 \qquad (1)$$

where W_g and W_i is the weight of the grafted ALF and weight of the initial ALF, respectively.

| Amla leaf fibres were grinded into the size of 120 mesh |

⬇

| A solvet medium was prepared with DMSO and water (3:1) |

⬇

| Fibres were soaked into solvent for overnight |

⬇

| In the reaction media the myristic acid was gently added in the presence of FAS and KPS. |

⬇

| Under the continuous stirring condition of reaction media at 55 ˚C for 135 m |

⬇

| Washed with ethanol and separate out the mother liquor and grafted fibre with help of centrifuge |

⬇

| Dried for 24h at 55 ˚C |

Scheme 2 Grafting process of amla leaf

2.4 Preparation of Composite Films

Composite films were developed by casting method. The homogeneous aqueous solution of PVA was prepared by dissolving PVA in distilled water at 80 ˚C for 60 min to obtain (10% w/w) solution under continuous stirring at 800 rpm (rounds per minute). Loading composition 5, 10, 15% of ALF was reinforced in PVA solution. This mixture continuously stirred at 800 rpm for 40 min at 70 ˚C to prepare homogeneous solution and glycerol was used as a plasticizer. Thereafter, solution was poured into petri plates and put it into hot air oven for drying at 40 ˚C for 24 h. The fully dried films was peeled off from the petri plates. During formation of composite films the composition of ALF was varied, as listed in Table 1.

2.5 X-Ray Diffraction (XRD) Analysis

X-Ray diffraction patterns of the ALF, TALF, and GALF samples were recorded in the 2Θ range of 10–35˚. The X-ray diffractometer (X'PERT-PRO PW3064, Philips Japan) equipped with monochromatic radiation of CuKα ($\lambda = 1.54$ Å). The crystallinity percentage and crystallinity index was done by Chauhan and Kaith (2012):

Table 1 Composition of PVA, ALF, TALF, and GALF for preparation of composite films

S. No.	Sample	Weight (%)			
		PVA	ALF	TALF	GALF
1	PVA	10			
2	PVA/5 ALF	10	5		
3	PVA/10 ALF	10	10		
4	PVA/15 ALF	10	15		
5	PVA/5 TALF	10		5	
6	PVA/10 TALF	10		10	
7	PVA/15 TALF	10		15	
8	PVA/5 GALF	10			5
9	PVA/10 GALF	10			10
10	PVA/15 GALF	10			15

$$\text{Crystallinity } (\%) = \frac{I_{24}}{I_{24} + I_{15}} \times 100 \tag{2}$$

$$\text{Crystallinity index} = \frac{I_{24} - I_{15}}{I_{24}} \tag{3}$$

2.6 Mechanical Properties

The tensile strength and percent elongation (%E) of the films were done by universal testing machine (UTM) (Ashian Engineers Company India, New Delhi, India) at a cross head speed of 50 mm/min at a room temperature. The ASTM D638 method was used for determination of tensile strength. The mechanical testing was performed on all the film samples.

2.7 Water Uptake (%)

The films (25 × 25 mm) was taken as per the ASTM D570-98 for evaluation of water uptake (%). In the hot air oven, specimens were dried for 24 h at 40 °C and weighed (W_i). Then at a room temperature, specimens were immersed in distilled water. After 24 h, the specimens were drawn and weighted (W_f). Before weighing the specimens the excess water was removed on the surface by cotton balls or cloth. The procedure was repeated for 6 days. The calculation of water uptake (%) was done by:

$$\text{Water uptake } (\%) = \frac{W_f - W_i}{W_i} \times 100 \tag{4}$$

Here, W_i and W_f are the initial weight of sample (dry) and final weight of sample after 24 h.

2.8 Water Vapor Transmission Rate (WVTR) and Water Vapor Permeability (WVP)

The WVTR and WVP of composite films were done using ASTM 1995 method (Mittal et al. 2016; Zhong et al. 2009). The samples of films were cut into sizesso as to cover the top of the glass bottle. The glass bottle was filled with 4 g Fused Calcium Chloride(CaCl$_2$). Then glass bottle was covered with samples and glass bottle were sealed with parafilm. After weighing, the bottles were placed into desiccator containing distilled water under controlled atmosphere. Followed the 24 h interval cycle for weighing the specimen until the saturation was achieved. The net movement of water vapor through the films was determined by the increase in weight of glass bottle with respect to time. The calculation of WVTR and WVP was done by:

$$WVTR = \frac{\Delta W}{\Delta t \ \times A} \times 100 \tag{5}$$

$$WVP = \frac{WVTR}{\Delta P} \times 100 \tag{6}$$

where, ΔP is the difference of water vapor pressure between both sides of the films, L is the thickness of film (m), A is the exposed area by film (m^2), and $\Delta W/\Delta t$ is the weight gain per unit time during transfer of water vapor.

2.9 Biodegradationtest

To calculate the biodegradation of the films, soli burial test was done. Weight loss of films were carried out by soil buried method. The sample size of (3 cm $\times$ 10 cm) was buried in soil at a dip of 10 cm in soil filled pots. The sewage water was sprinkled on soil for maintaining the microbial and moisture conditions. The samples were taken out from soil at every 7 days, then washed with distilled water and dried at 40 ˚C for 24 h. The weight loss can be calculated by:

Table 2 Evaluation of grafting yield of ALF

S. No.	Reaction time (min)	Reaction temperature (°C)	DMSO content (ml)	Myristic acid concentration (mol/L × 10⁻³)	Grafting yield of ALF
1	135	55	75	11.09	17.92
2	150	55	75	11.09	23.26
3	165	55	75	11.09	26.81
4	180	55	75	11.09	31.59
5	195	55	75	11.09	29.30

$$\text{Weight loss } (\%) = \frac{W_i - W_f}{W_f} \times 100 \tag{7}$$

Here, W_i and W_f are the initial and final weight of the sample, respectively.

3 Results and Discussion

3.1 Grafting of ALF

ALF was graft copolymerized by using myristic acid (concentration of 11.09 mol/L $\times$ 10⁻³). DMSO content and reaction temperature was kept constant. Whereas, the reaction time varies from 135 to 195 min. The results are shown in the Table 2. It was observed that graft yield varied from 17.92% to 31.59% with increase in reaction time from 135 to 180 min. So the specimen with grafting 31.59% was taken for the further studies and termed as GALF (grafted amla leaf fibre).

3.2 X-Ray Diffraction (XRD)

Studies of X-ray diffraction were done to examine the changes of crystalline and amorphous regions of ALF after surface modification of fibre. ALF diffractogram Fig. 1 showed crystalline peaks at a degree of 15.21 with intensity of 483.21 due to cellulosic content present in the fibres. However GALF diffractogram showed peaks at a degree of 15.16 with intensity counts of 371.54. It is observed that values of d-spacing at the wavelength 1.54 Å of ALF was 5.82, while for GALF it increased to 5.85, which emphasized that grafting of ALF lead to amorphous structure. Grafting of ALF with myristic acid showed in the reduction in crystallinity (%) of ALF from 83.28 to 54.76% as shown in Table 3. The crystallinity of ALF depends on the orientation of cellulosic content. Due to grafting the orientation were changed and
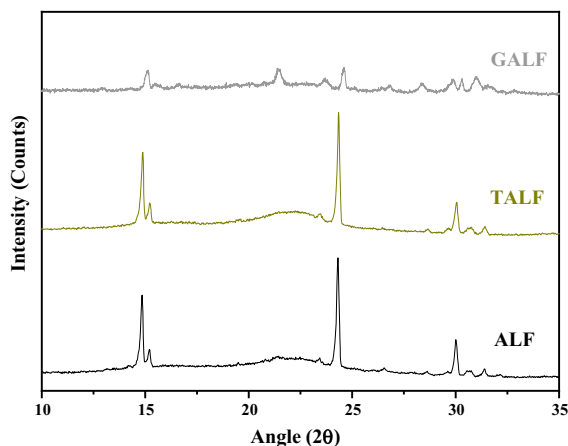
Fig. 1 XRD of ALF, TALF, and GALF

Table 3 Crystallinity (%) and crystallinity index (CI) of ALF, TALF, and GALF

Types of fibre	2 Θ Scale		Crystallinity (%)	Crystallinity index
	I_{15}	I_{24}		
ALF	483.21	2409.75	83.28	0.79
TALF	554.91	2520.30	81.95	0.77
GALF	371.54	449.88	54.76	0.17

this change in orientation is responsible for the lower crystallinity of fibre (Chauhan and Kaith 2012; Mandal et al. 2016; Anjum et al. 2006).

3.3 Mechanical Properties

Effects of loading and modification of fibre on the properties of the films.

3.3.1 Mechanical Properties

Table 2, showed the tensile strength and elongation % of films reinforced with ALF, TALF, and GALF in PVA matrix. The tensile strength of PVA film was 29.8 MPa. Result showed that with the reinforcement of 5% and 10% fibre in the PVA matrix, the tensile strength increased. The tensile strength increased upto 10% of loading of fibre in films due to interaction of OH bonds between and PVA matrix. However, the loading beyond the 10% of fibre in the composite films showed the decreasing

Table 4 Tensile strength (MPa) and elongation (%) of composite films

Composite film	Tensile Strength		Elongation	
	MPa	Relative to PVA (%)	%	Relative to PVA (%)
PVA	29.8	100	275	100
PVA/5 ALF	32.94	110.53	245	89.09
PVA/10 ALF	34.39	115.40	232	84.36
PVA/15 ALF	33.27	111.64	210	76.36
PVA/5 TALF	36.76	123.35	239	86.90
PVA/10 TALF	39.15	131.37	228	82.90
PVA/15 TALF	37.86	127.04	207	75.27
PVA/5 GALF	41.11	137.95	204	74.18
PVA/10GALF	45.12	151.40	190	69.09
PVA/15 GALF	42.23	141.71	171	62.18

trend of tensile strength. The decrement because of higher amount of fibre reinforcement was due to the predominance of aggregation. The elongation (%) of the films decreasedwith increase in the loading of fibre from 5 to 15% in the PVA matrix due to stiffness occured in the composite films.

The loading of TALF from 5 to 10% in composite films increased the tensile strength of the films by 131.37% as compare to PVA film. The alkali treatment of ALF by NaOH made fibres fragile and reduced the fibre diameter and thereby improved its aspect ratio (length/diameter) by changing its orientation of highly packed crystalline cellulose and forming an amorphous region. Further addition of fibre upto 15% caused decrement in tensile strength. Whereas, 13.38% elongation (%) decreased with addition of TALF from 5 to 15% fibre in the composite films due to less molecular mobility in polymer chain.

The surface modification of ALF by graft copolymerization from myristic acid helped to enhance its surface area and amorphous behavior, which was responsible for the good surface adhesion between grafted ALF and PVA matrix. It enhanced the tensile strength of film by 151.40% as compare to PVA film with loading of GALF from 5 to 10% in the composite film. With further increment in GALF content decreased the tensile strength due to less inter chain force of attraction between fibre and matrix. The highest 16.18% reduction in elongation (%) was seen in 5–15% GALF reinforced composite films. This reduction is due to the tight packing between fibres and matrix (Table 4).

3.4 Water Uptake (%)

Water uptake (%) of composite films is shown in Fig. 2. The water uptake (%) was increased with increase in loading of fibre, and time duration of immersion. The PVA
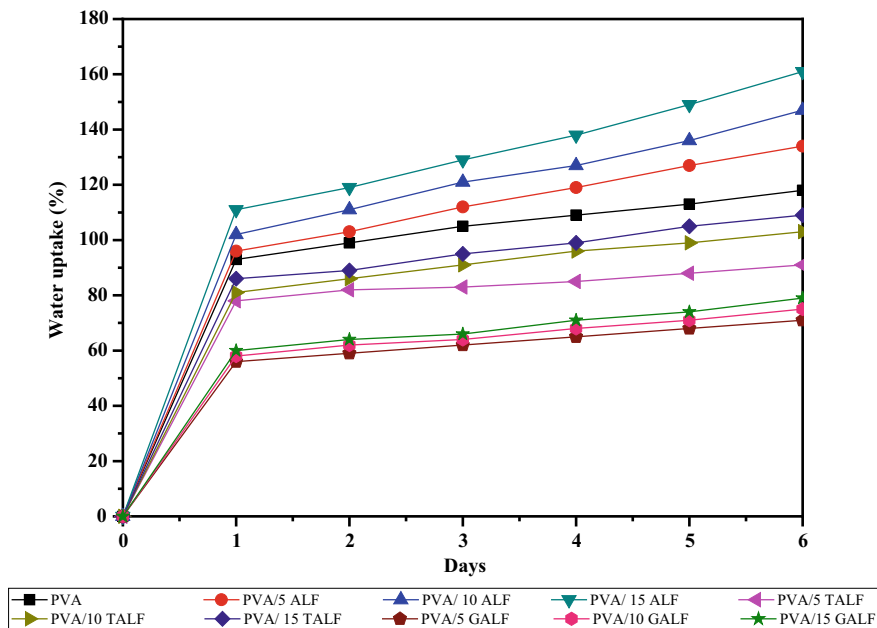
Fig. 2 Water uptake (%) of composite film samples

film showed the water uptake of 118% in 6 days. With 5% loading of ALF, fibre in PVA matrix, the water uptake (%) increased to 134% due to increased in hydroxy groups. It further increased to 161% with fibre loading of 15% in composite film. However, with the loading of 5% TALF and GALF in composite film, water uptake (%) increased to 91% and 71%, respectively. which was less than the film loaded with ALF fibre. The surface modification of fibre with alkali and graft copolymerization reduced the hydrophilicity of the composite films well as the water uptake (%).

3.5 Water Vapor Transmission Rate (WVTR) and Water Vapor Permeability (WVP)

The penetration of water vapor was measured by WVTR and WVP as shown in Fig. 3a, b. The WVTR and WVP was highest value observed for PVA film among all the composite films that was 4.70 (g/h m^2)and 9.33 (10^{-7} g m/m^2 h pa), respectively. The ALF reinforced composite films showed the increment in WVTR with increase in loading of fibre. This is due to the hygroscopic behavior of the ALF. The WVTR value decreased in TALF and GALF reinforced composite films as compare to ALF reinforced composite films. The lowest value of WVTR was 5% GALF content composite film that was 2.64 (g/h m^2). This decreased was due to the increment
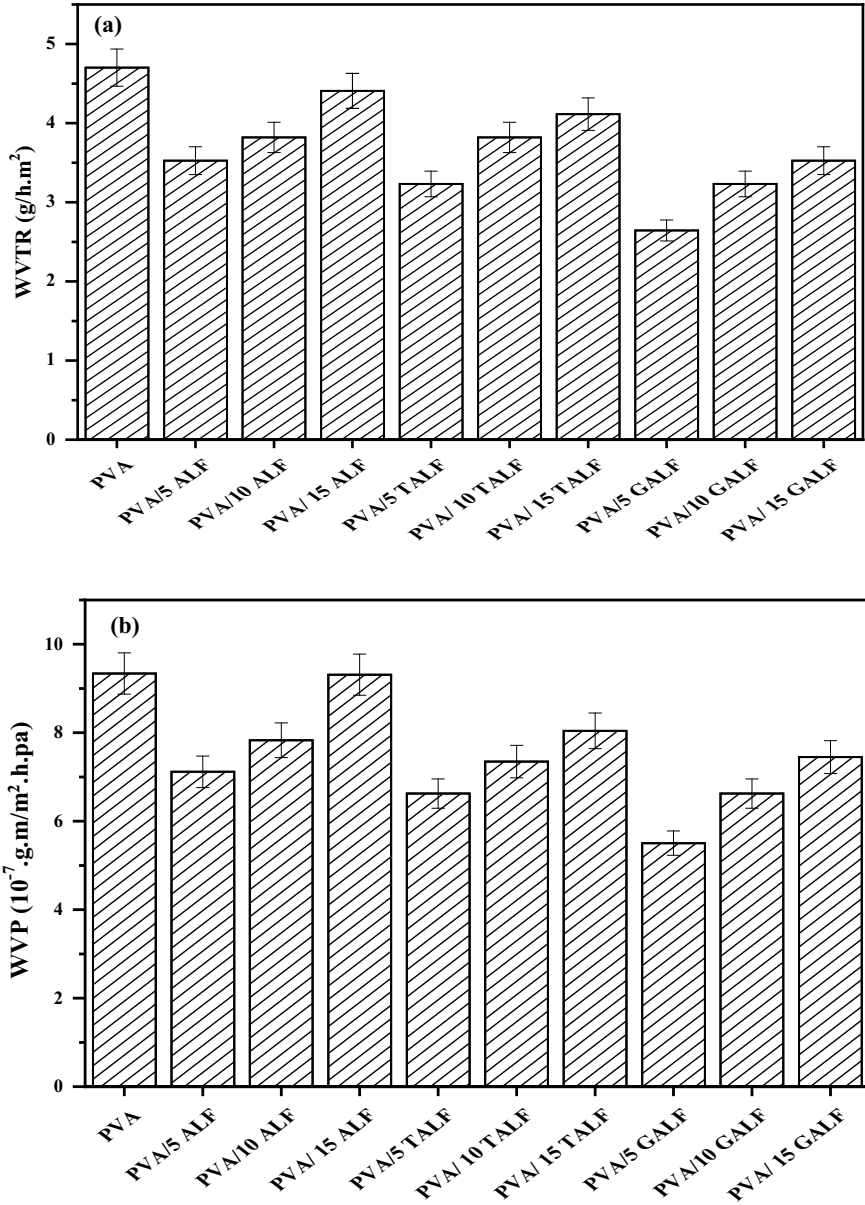
Fig. 3 **a** WVTR of composite films, and **b** WVP of composite films

in hydrophobic nature of composite films. The films showed the same trend in the values of WVP experiment.

3.6 Biodegradation Test

The soil buried test was performed under the natural conditions, for study of the degradation rate of composite films. The Fig. 4 showed the observation of weight loss (%) of composite samples. The PVA/15 ALF show the highest degradation rate was 13.4% in 28 days. The weight loss was increased with increased in loading of fibre in the composite films. The hydrophilicity increased with increase in the loading of ALF in the composite films which responsible for increase in moisture on the composite films. The degradation rate was decreased for the TALF and GALF loaded composite films. The degradation rate for PVA/15TALF and PVA/15GALF was 12.6 and 8.4% in 28 days, respectively. However, grafted ALF composite films showed lower degradation rate because of enhancement in hydrophobic property of composite film. The breakdown of films by presence of microbes on the surface was increased with increased in swelling of the films due to hydrophilic behavior of the film (Mittal et al. 2016).
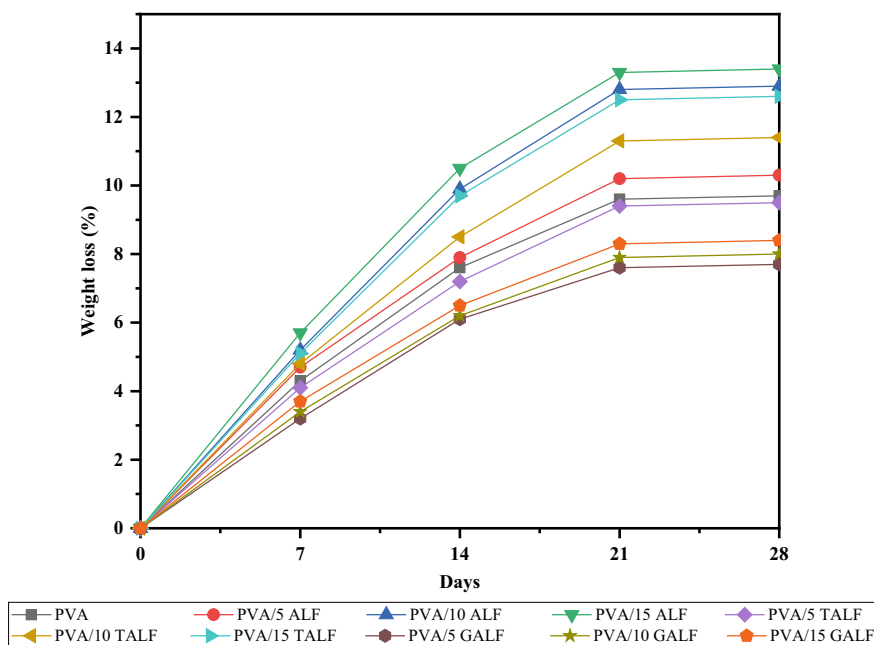
Fig. 4 The weight loss of composite films by soil burial biodegradation

4   Conclusion

Amla leaf fibre (ALF) was treated with alkali and graft copolymerization techniques. Reinforcement of ALF, TALF, and GALF on various properties of composite films was observed. The surface treatment of fibre showed the increase in amorphous part of fibre as shown by XRD analysis. Tensile strength of the composite films increased with the addition of ALF, TALF and GALF fibre in the matrix. Water uptake (%) of films reinforced with GALFfibre is less as compared to films containing ALF fibre due to reduction in OH group and less interaction with water. Biodegradation of the films increased with the incorporation of fibre in PVA matrix. The GALF reinforced composite films can be the suitable sample for further studies due to their magnificent mechanical and physico-chemical properties.

Conflict of Interest   On behalf of all authors the corresponding authors states that there is no conflict of interest.

References

Anjum N, Gupta B, Riquet AM (2006) Surface designing of polypropylene by critical monitoring of the grafting conditions: structural investigations. J Appl Polym Sci 101:772–778

Beikzadeh S, Khezerlou A, Jafari SM (2020) Seed mucilages as the functional ingredients for biodegradable films and edible coatings in the food industry. Adv Colloid Interface Sci 280:102164

Chauhan A, Kaith B (2012) Accreditation of novel roselle grafted fiber reinforced bio-composites. J Eng Fiber Fabr 7:66–75

Gaikwad KK, Lee JY, Lee YS (2016) Development of polyvinyl alcohol and apple pomace bio-composite film with antioxidant properties for active food packaging application. J Food Sci Technol 53:1608–1619

Gironès J, López JP, Mutjé P (2012) Natural fiber-reinforced thermoplastic starch composites obtained by melt processing. Compos Sci Technol 72:858–863

Ibrahim H, Farag M, Megahed H, Mehanny S (2014) Characteristics of starch-based biodegradable composites reinforced with date palm and flax fibers. Carbohydr Polym 101:11–19

Kaith BS, Singha AS, Kumar S, Kalia S (2008) Mercerization of flax fiber improves the mechanical properties of fiber-reinforced composites. Int J Polym Mater Polym Biomater 57:54–72

Kamdem DP, Shen Z, Nabinejad, O (2019) Development of biodegradable composite chitosan-based films incorporated with xylan and carvacrol for food packaging application. Food Packag Shelf Life 21:100344

Kohli D, Garg S, Jana AK, Maiti M (2017) Synthesis of graft copolymers for green composite films and optimization of reaction parameters using Taguchi (L16) Orthogonal Array. Indian Chem Eng 59:136–158

Majeed K, Jawaid M, Hassan A (2013) Potential materials for food packaging from nanoclay/natural fibres filled hybrid composites. Mater Des 46:391–410

Mandal A, Chakrabarty D (2014) Studies on the mechanical, thermal, morphological and barrier properties of nanocomposites based on poly(vinyl alcohol) and nanocellulose from sugarcane bagasse. J Ind Eng Chem 20:462–473

Mandal DK, Bhunia H, Bajpai PK (2016) Radiation-induced grafting of acrylic acid onto polypropylene film and its biodegradability. Radiat Phys Chem 123:37–45

Mishra RK, Mohanty K (2018) Characterization of non-edible lignocellulosic biomass in terms of their candidacy towards alternative renewable fuels. Biomass Convers Biorefinery 8:799–812

Mittal A, Garg S, Kohli D (2016) Effect of cross linking of PVA/starch and reinforcement of modified barley husk on the properties of composite films. Carbohydr Polym 151:926–938

Mittal A, Garg S, Bajpai S (2020) Fabrication and characteristics of poly (vinyl alcohol)-starch-cellulosic material based biodegradable composite film for packaging application. Mater Today Proc 21:1577–1582

Mittal A, Garg S, Bajpai S (2019) The influence of fatty acid chain length on the chemical, physical and morphological properties of the grafted barley husk for application in biocomposites. Polym Test 78

Mukherjee A, Datta D, Halder G (2019) Synthesis and characterisation of rice-straw-based grafted polymer composite by free radical copolymerisation. Indian Chem Eng 61:105–119

Norcino LB, Mendes JF, Natarelli CVL (2020) Pectin films loaded with copaiba oil nanoemulsions for potential use as bio-based active packaging. Food Hydrocoll 106:105862

Ooi ZX, Ismail H, Abu Bakar A (2009) Effects of jackfruit waste flour on the properties of polyvinyl alcohol film. J Vinyl Addit Technol 21:129–133

Ooi ZX, Ismail H, Abu Bakar A, Aziz NA (2011) Effects of jackfruit waste flour on the properties of poly(vinyl alcohol) film. J Vinyl Addit Technol 17:198–208

Padmapriya R, Saranya T, Thirunalasundari T (2015) Phyllanthus emblica-a biopotential for hard water treatment. Int J Pure App Biosci 3:291–295

Popescu MC, Totolin M, Tibirna CM (2011) Grafting of softwood kraft pulps fibers with fatty acids under cold plasma conditions. Int J Biol Macromol 48:326–335

Pua FL, Sapuan SM, Zainudin ES, Adib MZ (2013) Effect of fibre surface modification on properties of Kenaf/Poly(vinyl alcohol) composite film. J Biobased Mater Bioenergy 7:95–101

Ray R, Narayan Das S, Das A (2019) Mechanical, thermal, moisture absorption and biodegradation behaviour of date palm leaf reinforced PVA/starch hybrid composites. Mater Today Proc 41:376–381

Saba N, Jawaid M (2018) A review on thermomechanical properties of polymers and fibers reinforced polymer composites. J Ind Eng Chem 67:1–11

Singh AK, Singh S, Saroj PL (2019) Aonla (Emblica officinalis) in India: a review of its improvement, production and diversified uses. Indian J Agric Sci 89:1773–1781

Wu F, Misra M, Mohanty AK (2021) Progress in polymer science challenges and new opportunities on barrier performance of biodegradable polymers for sustainable packaging. Prog Polym Sci 117:101395

Yee TW, Rahman WAWA, Sin LT (2011) Properties and morphology of poly(vinyl alcohol) blends with sago pith bio-filler as biodegradable composites. J Vinyl Addit Technol 17:184–189

Zhang F, Zhao Y, Wang D (2021) Current technologies for plastic waste treatment: a review. J Clean Prod 282:124523

A Critical Appraisal of Biomedical Waste Management in Uttar Pradesh

Praveen Kumar Tiwari, Surendra Kumar Pandey, Rohit Kushwaha, Sonam, Kapil Malviya, Markandeya, Sheo Prasad Shukla, and Devendra Mohan

Abstract Bio-medical waste is the waste generated from hospitals, including infectious waste, and has a high potential for causing injury and infections to humans as well as to the environment. Effective bio-medical waste management is the requisite parameter for a healthy and unpolluted environment. It is a social and legal responsibility of the medical community and common people to participate in the proper hygienic waste disposal actively and lead the environment free from various infectious diseases. BMW is precarious in the constitution and is different from general municipal waste; hence, it requires a unique approach and handling to avoid environmental and human health risks. The government of India made a statutory requirement for appropriate handling and disposal of bio-medical waste with the publication of gazette notification in July 1998 and further making required changes in it. This article explains various components, techniques for remediation, and consequences of improper disposal of BMW and provisions of BMW management in India. It also gives a brief overview of bio-medical waste management of hospitals in Uttar Pradesh.

Keywords Bio-medical waste · Hospital waste disposal · Bio-waste management · Hazardous · Health risk · Uttar Pradesh

P. K. Tiwari (✉) · S. K. Pandey
Department of Forensic Medicine, Institute of Medical Science, Banaras Hindu University, Varanasi 221005, India
e-mail: praveenpurple@gmail.com

R. Kushwaha · Sonam · Markandeya · D. Mohan (✉)
Department of Civil Engineering, Indian Institute of Technology (Banaras Hindu University), Varanasi 221005, India
e-mail: devendra.civ@iitbhu.ac.in

K. Malviya
Department of Civil Engineering, Maulana Azad National Institute of Technology, Bhopal 462022, India

S. P. Shukla
Rajkiya Engineering College, Banda 210201, India

Abbreviations

BMW	Bio-medical waste
INCLEN	International clinical epidemiology network
CPCB	Central pollution control board
SPCB	State pollution control board
MOEFCC	Ministry of environment, forest and climate change
BMWM	Bio-medical waste management
SSPG	Shri Shiv Prasad Gupt Divisional District Hospital
SSH	Sir Sundarlal Hospital
PPE	Personal protective equipment

1 Introduction

There are different types of pollutants and waste produced by different human activities. The waste produced is basically classified as dangerous/hazardous and non-dangerous/non-hazardous. The various waste such as Industrial, Household, Agricultural, and Sewage pollutes water, air, and soil, making it toxic for living beings and the environment. The proper disposal of waste produced from any resource plays a crucial role in a contamination-free community and environment. The responsible authority should have proper planning and must be concerned regarding waste disposal management techniques.

Out of the many kinds of waste produced, the biomedical waste (BMW) is a serious threat to the human and environment as with enhance in health facilities, the amount of waste generated from different healthcare providers is a big concern. BMW is a specific type of waste produced from hospitals, nursing homes, or any small medical setup and different medical and animal research organizations, which has a high potential for causing injury and infections to humans and the environment.

On 27 July 1998, the Ministry of Environment and Forests (known presently as the Ministry of Environment, Forests and Climate Change) and notified a rule, i.e., Bio-Medical Waste (Management and Handling) Rules, 1998 under Environment (Protection) Act, 1986 to protect the environment and community from the BMWs. According to this rule, any waste generated at the time of diagnosis, immunization, human or animal treatment, or research is defined as Bio-Medical Waste. BMW, which are infectious, are produced from different hospitals, nursing homes, animals and pets clinics, mortuary, medical collages, slaughter homes, blood banks, research labs, biotechnology institutions, and diagnostic laboratories (MoEF 1998). According to WHO, 85% of bio-medical waste are non-hazardous and can easily be treated with household waste and only 15% are infectious waste which consists of different kind of harmful microorganism and pathogens capable of causing life-threatening infectious diseases such as HIV, Hepatitis B, and C, etc. and requires proper management and standard disposal method (Devi et al. 2019).

According to the International Clinical Epidemiology Network (INCLEN) 2014, a study conducted in 20 states of India reported that more than 80% of primary, 60% of secondary, and 54% tertiary health care centers do not follow a standard and reliable waste management techniques (Devi et al. 2019).

Another survey conducted in Bangalore city revealed that the solid waste generated in the government hospitals varied from ½ to 4 kg per bed per day whereas ½ to 2 kg per bed in private hospitals and nearly about ½ to 1 kg per bed in nursing's home. Out of total waste generated in India, 40–50% are infectious, and proper segregation among infectious and non-infectious is done in 30% of wastes (Singh et al. 2001).

The infectious waste produced needed to be segregated from non-hazardous waste and requires proper handling, treatment, and disposal. Safe procedures and effective waste disposal will protect the health care workers, patients, and the community to stay fit and healthy.

2 Components of BMW

According to WHO, there are eight different components of BMW which include waste such as general waste, radioactive, pathological, chemical, sharps, pharmaceuticals, infectious to highly infectious waste, and pressure containers. However, According to the Ministry of Environment and Forest, "Bio-Medical Waste (Handling and Management) Rules 2016" has described four different colour code for disposal of bio-medical waste in India (MoHFW 2016). Table 1 lists the different types of biomedical waste generated in hospitals and suitable treatment methods and disposal methods.

3 What Makes BMW Hazardous?

Waste generated from hospitals consists of hazardous and non-hazardous waste. Nonhazardous waste includes fruit peels, food remnants, paper cartons, wash water, packaging material, etc., whereas the hazardous waste is potentially toxic and infectious (Hegde et al. 2007).The characteristic which makes it hazardous are as follows:

A.   **Infection and Pathological Wastes**

These agents can contaminate food and water and enter the inside body through any cut or abrasion, or inhalation.

B.   **Injurious wastes**

Instruments such as needles, syringes, and scalpels can cause physical injury, leading to transmission of severe infections such as HIV, Hepatitis B and C Virus. There are many cases of transmission of these lethal infections via biomedical waste (Park 2015).

C.   **Cytotoxic or Genotoxic wastes**

These are the drugs specially used in oncology or radiotherapy with a high mutagenic or cytotoxic effect. The main pathway of exposure is via inhalation in the form of dust or aerosol, absorption through the skin, or circumstantial intermixing of food with cytotoxic drugs or chemicals or waste (Park 2015).

Table 1 Categories of bio-medical waste (MoHFW 2016)

Waste category (type)	Colour code	Prescribed treatment	Final disposal
Human anatomical waste (human tissues, organs, body parts, fetus below viability period (as per Medical Termination of Pregnancy Act 1971, amended from time to time)) *Soiled waste* (items contaminated with blood, body fluids like dressings, plaster casts, cotton swabs, discarded linen, mattresses, routine mask and gown, and bags containing residual or discarded blood and blood components) *Expired or discarded medicines* (Pharmaceutical waste like antibiotics, cytotoxic drugs including all items contaminated with cytotoxic drugs along with glass or plastic ampoules, vials etc.) *Microbiology, biotechnology and other clinical laboratory waste* (Blood bags, laboratory cultures, stocks or specimens of micro-organisms, live or attenuated vaccines, human and animal cell cultures used in research, industrial laboratories, production of biological, residual toxins, dishes and devices used for cultures)	Yellow non-chlorinated plastic bag/bin Yellow non-chlorinated plastic bag/bin Yellow non-chlorinated plastic bag/bin Yellow non-chlorinated autoclave/ microwave/ hydroclave safe plastic bag/bin	Incineration Incineration Incineration at temperature > 1200 °C or to common bio-medical waste treatment facility or hazardous waste treatment, storage and disposal facility for incineration at > 12000 °C Or Encapsulation or Plasma Pyrolysis at > 12000 °C Pre-treatment to sterilize/disinfect on-site as per WHO Guidelines*; thereafter incineration	Ash disposal in municipal landfill Ash disposal in municipal landfill Ash disposal in municipal landfill Ash disposal in municipal landfill Ash disposal in municipal landfill

Table 1 (continued)

Waste category (type)	Colour code	Prescribed treatment	Final disposal
Contaminated (recyclable) waste (disposable items other than sharps like tubing, bottles, intravenous tubes and sets, catheters, urine bags, syringes (without needles and fixed needle syringes), vaccutainers (with their needle cut) and gloves)	Red coloured non-chlorinated bag/bin	Autoclaving or micro-waving/hydroclaving followed by shredding or mutilation or combination of sterilization and shredding	Registered or authorised recyclers
Metallic waste sharps (needles, syringes with fixed needles, needles from needle tip cutter or burner, scalpel, blades)	White translucent puncture proof, leak proof, tamper proof containers	Autoclaving or Dry Heat Sterilization followed by shredding or mutilation or encapsulation in metal container or cement concrete; combination of shredding cum autoclaving; and sent for final disposal to iron foundries (having consent to operate from the State Pollution Control Boards or Pollution Control Committees) or sanitary landfill or designated concrete waste sharp pit	Iron foundries or sanitary landfill or designated concrete waste sharp pit
Glass waste (intact and broken) (Broken/discarded and contaminated glass including medicine vials and ampoules except those contaminated with cytotoxic wastes)	Blue puncture proof and leak proof boxes or containers	Disinfection (by soaking the washed glass waste after cleaning with detergent and Sodium Hypochlorite treatment) or through autoclaving or microwaving or hydroclaving and then sent for recycling	Recycler
Liquid waste		Pre-treatment with disinfectant/ 1–2% hypochlorite solution	Discharge in drains or ETP

D.   **Chemicals and pharmaceuticals or toxins wastes**

These are specific substances used in patient treatment and management. They are toxin, corrosive, reactive, inflammable in nature. If the exposure is regular in a small quantity, then it may lead to chronic exposure and injury. Disinfectants used for housekeeping purposes are major chemicals of this group and highly reactive and toxic (Devi et al. 2019).

E.   **Radioactive wastes**

It may lead to many serious diseases, including genetic problems, which depend on the amount and kind of exposure (Park 2015).

4   Abating the Hazards

Improper management and handling of bio-medical waste from clinics, hospitals, and other health facilities may pose several problems to health care workers and handlers of the waste. When BMW is disposed of without proper planning, both the general public and the environment is at risk. Figure 1 summarizes some of the problems caused by improper handling and disposal of BMW.

The final goal of bio-medical waste management is to prevent such problems. There are many successful techniques for the treatment and disposal of different BMWs.

A.   **Onsite Treatment**: Treatment methods include autoclaving, microwaving, and chemical treatments.

(1)   *Autoclaving*: These are instruments used to sterilize medical equipment under high pressure and temperature. Autoclaves are used in the killing of microorganisms on medical equipment. Some reusable equipment is sterilized in autoclaves. Large-density autoclaves are used for treating BMW before dumping the waste into traditional landfills. This method is

Improper handling of bio-medical waste

Environmental
- *Water Pollution*
E.g. contamination of drinking water source.

- *Soil Pollution*
E.g. non-degradable bio-waste used as landfill

- *Air Pollution*
E.g. improper burning emits dioxin and furans etc.

- *Public Sensitivity*
Psychological effect (unaesthetic and offensive)

Health
- *Physical* – Sharps
- *Chemical* – Toxicity, corrosivity etc.
- *Infections:* parasitic, skin, lung, candida, meningitis.
Diseases from improperly disposed waste with trace of vaccines: bacteremia, reproductory, HIV, hepatitis, hemorrhagic, difficile.

Fig. 1 Impacts of improper handling of bio-medical wastes (adopted and modified from Singh et al. 2013)

helpful in the onsite waste treatment of infectious waste (Kalpana et al. 2016).

(2) *Microwaving*: Microwave radiation is used in the remediation of waste. Generally, the wet waste is treated using this method. The frequency used is 2450 MHz, and wavelength of 12.24 nm (Park 2015).

(3) *Chemical treatment*: This method is usually used to kill or deactivate pathogens and microorganisms. This method is highly suitable for liquid waste treatment such as urine, blood, or any body fluid or secretion. The specificity of chemical to be used depends on the type of waste, the kind of microorganism, and its cellular composition (Park 2015; Kalpana et al. 2016).

B. **Offsite treatment**: treatment methods include incinerator, plasma torch technology, land disposal, inertization (Park 2015).

(1) *Incineration*: This method is a highly used method for BMW treatment for those wastes that are not renewable or can be disposed of in outer landfills. This method applies high temperature, leading to the dry oxidation of waste and reducing organic and combustible waste to inorganic non-combustible form. The drawback of this method includes high investment and operating costs and releases toxic gases, ashes, and soot particles into the atmosphere (Park 2015).

(2) *Inertization*: This method includes mixing 65% of pharmaceutical waste/toxic waste with 15% cement, 15% lime, and 5% water substance before disposing it to prevent contamination with groundwater or surface water. The main disadvantage of this method is as it is not applicable for infectious waste (Park 2015).

(3) *Land Disposal*: Specifically engineered and designed sanitary landfills are used for dumping BMW, preventing the contamination of humans, animals, and the environment compared to open landfills (Park 2015).

5 Consequences of Unsupervised Open Burning of BMW

The unsupervised and open burning of solid BMW creates many problems as they emit toxic air pollutants and ash residue, which constitute the release of dioxins and furans in the environment. The toxic ash has a high potential to percolate and pollute groundwater. According to the US environment agency, medical waste is the third largest known source of dioxin release and 10% mercury emission. Dioxins have played an essential role in many problems such as cancer, immune system disorders, diabetes, skin problems, endocrine dysfunction, congenital disabilities, and improper sexual maturity. The compound containing chlorine and cadmium must not be burned as they release dioxins which are carcinogenic in nature. Mercury is neurotoxic that can cross the blood–brain barrier and placenta, and also air-borne mercury is dangerous for the environment and aquatic life (Gautam et al. 2010).

6   Provisions for BMW Management in India

Bio-Medical Waste (Management and Handling) Rules 1998 under Environment (Protection) Act 1986 deals with the generation, collection, segregation, quantification, receiving, storing, treating, and handling of bio-medical waste.

Schedule I states the safe, secure, and ventilated place for storage of BMW and segregation of wastes in color bags and containers. No intermixing of BMW with municipal solid wastes. BMW shall be segregated into containers/bags according to Schedule II (Singh et al. 2001). Onsite treatment of laboratory wastes, microbiological wastes, blood samples, and other body fluid samples with disinfectant as prescribed by WHO Immunization of all healthcare workers involved in handling BMW. Chlorinated plastic wastes shall not be incinerated. Liquid waste does not require bags. Microbiology and biotechnology wastes, if disinfected, need not be put in bags. Schedule III states the label for BMW on bags/containers. Schedule IV states that the proper label of the day, the month should be mentioned on the bags. Schedule V deals with the standard for BMW treatment and disposal (MoEF 1998; MoHFW 2016).

7   Recent Amendments in BMW Rules 1998

In 2011 Ministry of Environment and Forest notified the Draft BMW (Management and Handling) Rules 2011, which stipulated the occupier to obtain authorization, irrespective of the number of beds. BMW was divided into eight categories, and the operator's duties were listed (MoFE 2011).

On March 28, 2016 amendment was made to improve the collection, segregation, treatment, and disposal of bio-medical waste, and it applies to all the person who generates, collect, receive, store, transport, treat or handle BMW in any form (MoHFW 2016).

On March 28, 2018 amendment was made stating that the chlorinating plastic bags (excluding blood bags) and gloves will not be used after 27 March 2019. Establishment of bar code system according to the guideline issued by Central Pollution Control Board (CPCB) by 27 March 2019 On February 19, 2019,the amendment was made stating that all bedded health care centers will have to maintain the biomedical waste register and update on day to day basis and also have to display the monthly record on its website according to the Schedule I specifying BMW generated in terms of category and color-coding. The annual report of bedded health care center (any no. of bed) will be made available on its website within the period of 2 years from the date of publication of BMW Management (Amendment) Rule 2018 (MoE 2018).
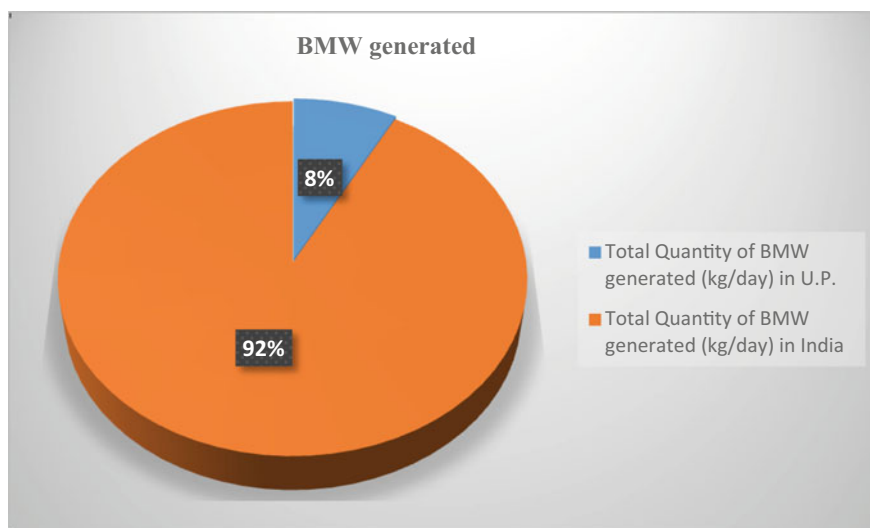
Fig. 2 Quantity of BMW generated in UP w.r.t India

8 Status of Uttar Pradesh in BMWM as Per BMWM Rules 2016 for the Year 2018

As per the annual report submitted by the State pollution control board (SPCB)/Pollution control committee (PCC) of Union Territories for the year 2018 to the Central Pollution Control Board (MOEFCC), the status of UP in BMWM is represented by different pie charts (CPCB 2016). Percentage of bio-medical waste generated and its treatment in the U.P. is shown through pie charts in Figs. 2 and 3, respectively. Figure 4 and 5 represents the health care facilities and BMW treatment facilities in U.P. respectively. Figure 6 shows the mode of treatment of the BMW in U.P.

9 Case Study on BMWM of Some Hospitals in Uttar Pradesh

1. According to the U.P. Solid Waste Management Monitoring Committee constituted by the National Green Tribunal (NGT) order, inspected following government hospital in Varanasi (UPSWMMC 2019).

   - Shri Shiv Prasad Gupt Divisional District Hospital (SSPG), KabeerChaura, Varanasi
   - Sir Sundarlal Hospital, (SSH) Institute of Medical Science (IMS), Banaras Hindu University, (BHU)
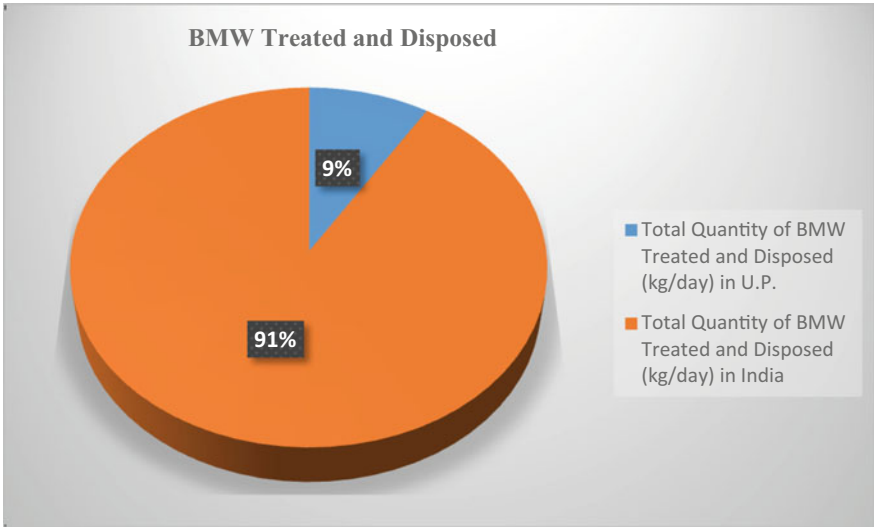
Fig. 3 BMW treated and disposed of in UP w.r.t India
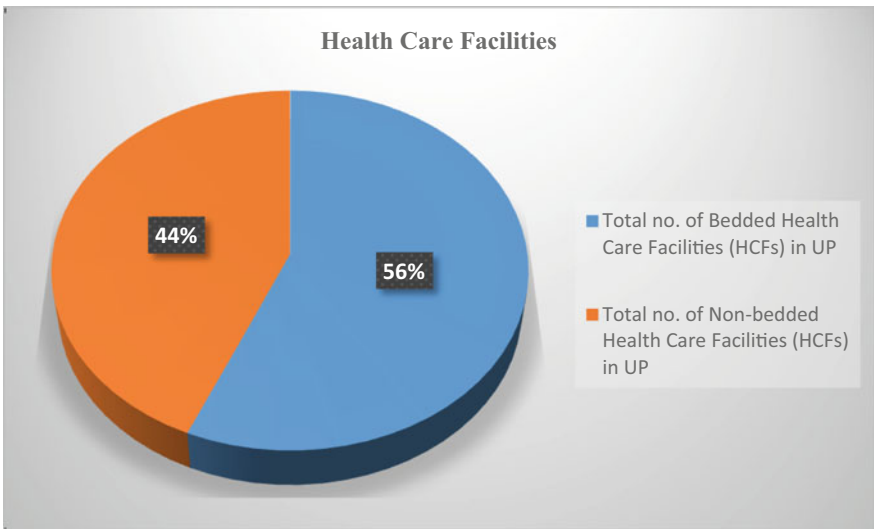
Fig. 4 Health care Facilities in UP listed as per BMWM rule 2016

BMW Treatment Facilities in UP

- No. of HCFs having Captive Treatment Facilities
- No of Captive Incinerators Operated by HCFs
- CBWTFs Operational

26%

26%

48%
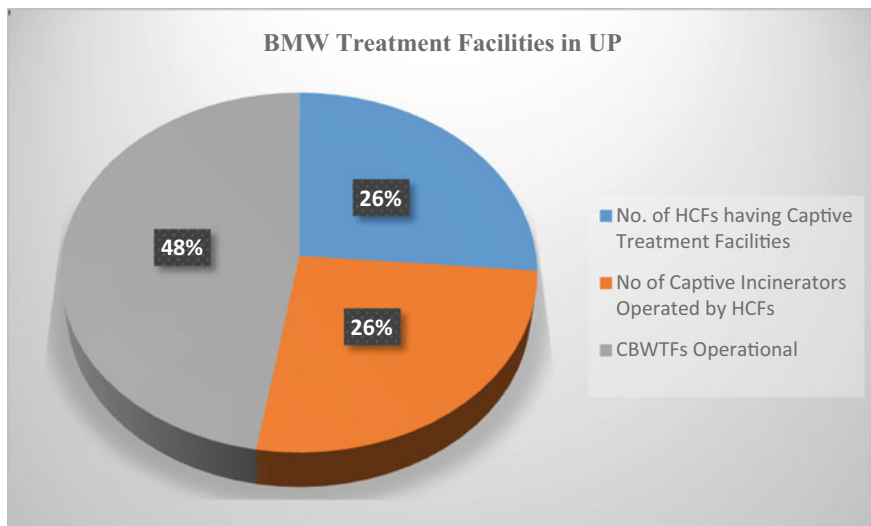
Fig. 5 Different types of BMW treatment facilities used by HCFs in UP

Total BMW treated by various modes

- Total BMW treated by captive treatment facilities by HCF in Kg/day in UP
- Total BMW treated by CBWTFs kg/day) in UP

12%

88%
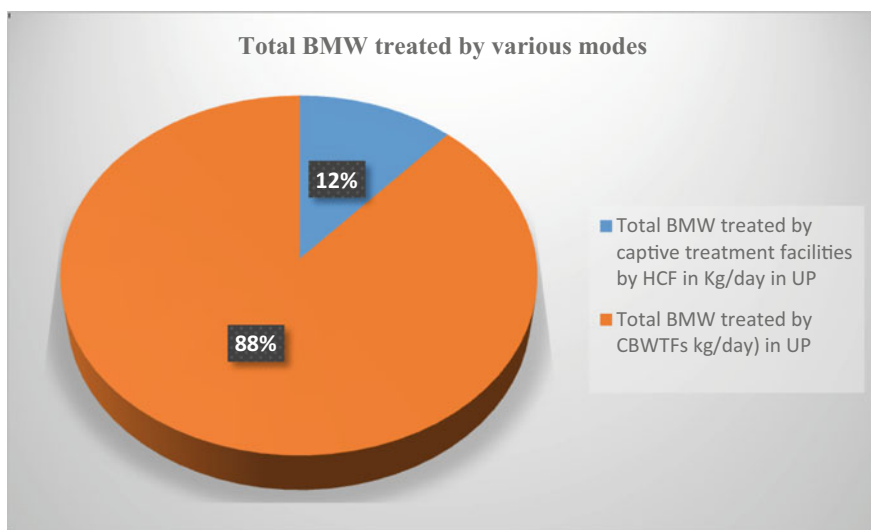
Fig. 6 Various modes of BMW treatment in UP

Keeping the facts and conditions for dealing with BMW following Bio-Medical Waste Management Rule 2016, the report follows observation and recommendations for both the government hospitals in Varanasi.

- At SSPG hospital, the amount BMW generated was approx. 150–200 kg per day, but both hospital authorities have maintained no records concerning collection, reception, transportation, and biomedical waste treatment as mandated under BMW rules 2016 (UPSWMMC 2019).
- BMW are not segregated into separate containers having any color coding and labeling. Medicine and blood sample collection containers needles were openly dumped near the municipal solid waste container.
- A temporary BMW waste storage area was seen, and untreated BMW was kept stored beyond 48 h.
- Unsupervised open burning of BMW was done, and no ETP and STP were found installed.
- The hospital has no valid consent under Water and Air Act.
- A considerable quantity of Sharps and infectious waste was lying in an open area.
- Intermixing of General waste with BMW was noticed in hospital premises.
- Lack of awareness and personal protective equipment (PPE) understanding among various hospital authorities and staff sections were noticed.
- Insight of above observations for non-compliance of BMW rule provision: Environmental compensation has been imposed against SSPG Gov. hospital and SSH, IMS, BHU.
- It is recommended that the Medical Council of India should include BMW rules in the curriculum for medical education and administration of medical colleges and hospitals (MoE 2018).

2. The case study was conducted in ChhatrapatiShahujiMaharaj Medical University (CSMMU) Lucknow to analyze the current status of BMW management (Gupta et al. 2008).

- The methodology used for the study was a general survey and personal observation of handling of BMW at different sections and wards of the hospital and interviewing the personnel engaged in BMWM.
- The highest quantity of waste was generated in the surgical ward, i.e., 70 kg/day, and the total of BMW generated was 239 kg/per day, including 112 kg infectious and 127 kg noninfectious waste per day, which was not segregated in their specific category according to BMW Act.
- The hospital lacked the facility of BMW collection, segregation such as color-coded bags and buckets, and they also lacked the critical operating facility for BMWM although they had autoclave, hydroclave, and needle cotter, but they were not functional. The liquid waste was disposed of in the municipal sewer system, and the organs were thrown open with the other municipal garbage.

3. Study done, and data were collected on BMWM in three government apex hospitals at Agra, namely Sarojini Naidu Medical College, Lady Lyell Maternity Hospital, and District Hospital for the period of one year by using the method as personal observation of waste treatment and disposal and employing questionnaires for assessing the knowledge, attitude and practice of working personnel (Sharma and Chauhan 2008).

   - The result showed that a maximum number of the waste handler in three centers were not aware and had not used personal protective clothing during handling, treatment, and disposal of BMW.
   - The waste was openly disposed of and burned in the hospital premises, and there were no proper treatment and disposal of liquid waste.
   - All three hospitals lacked basic and advanced equipment and techniques for the proper disposal of BMW.

4. This study was done in 660 bedded, tertiary care hospital of Bareilly, Uttar Pradesh. Data were collected for three months from all 30 places generating waste in the hospital premises and interviewing the waste handlers regarding the knowledge, facility, and safety measures taken during the waste management (Singh et al. 2014).

   - The waste produced at tertiary care hospital was 1.32 kg/bed/day and had 13 supervisors, out of which nine had attended special training of waste management and were educated. 80% male and 38.64% female waste handlers were aware of the hazards of hospital waste handling.
   - Segregation of hazardous and non-hazardous waste was adequately managed, and 63.33 places in the hospital have color-coded bins, although the hospital lacked waste treatment and disposal techniques and equipment within the hospital premises.

5. This study was conducted at the Vivekananda Polyclinic, one of the premier health care providers at Lucknow. Data was collected by interviewing medical authorities, doctors, paramedical staff, environmental engineers of the State Pollution Control Board, random patients, and visitors to the polyclinic (Gupta et al. 2009).

   - Polyclinic has all the facilities and has set an excellent example of BMWM for the viewpoint of compliance with the prescribed provision.
   - Polyclinic was well equipped with advanced techniques required for onsite treatment and disposal of BMW.
   - The polyclinic needed additional capacity and staff building to provide state-of-the-art facility and ongoing training to developa model BMWM system in the polyclinic. Creating awareness among other stakeholders regarding BMWM is also required.

6. The study was conducted at ChhatrapatiShivajiShubharti Hospital, Meerut, for five-month. Data was collected by providing sets of questions assessing

the knowledge about BMWM, and awareness was recorded by making direct observations at the workplace (Pandey et al. 2016).

- Segregation of waste was done onsite of production in different color-coded bags as per hospital protocol. 90% of Health Care Personnel were aware of the segregation, 30–35% did not practice, which may lead to intermixing waste.
- Training courses and awareness programs were required to be carried out about BMWM.

7. This study was conducted at the Institute Of Medical Science BHU, assessing the professional behavior of doctors in India about BMWM (Mohapatra et al. 2012).

- Data was collected by the predesigned questionnaire containing sets of nine-question emailed to 557 contacts randomly using respondent-sampling techniques.
- Remnant knowledge was significantly poor ($p < 0.001$) in postgraduates (35.5%) than medical graduates (75%). It was observed that BMW segregation has a significant association ($p < 0.001$) with higher knowledge. One-third of respondents were not aware of the bio-hazardous waste symbol.
- Regular training sessions and workshops of medicos must be made essential for effective BMW management.

8. The study was conducted among hospitals (bed capacity > 100) at Allahabad city, assessing knowledge, attitude, and practice of doctors (75), nurses (60), laboratory technicians (78), and sanitary staff (70) about BMWM (Mathur et al. 2011).

- The interview and observation of all the health care personnel were made by providing sets of questionnaires and a checklist.
- In the study, it was found that sanitary staff has the slightest knowledge regarding the BMWM than others.
- Doctors were least aware of the color coding and waste segregation as compared to laboratory technicians and nurses.
- The Sanitary staff was ignorant on all accounts regarding BMWM practices.

9. The study was conducted at Balrampur Hospital, Lucknow. Data were collected from hospital authorities, doctors, staff, and patients and self-check. The waste collectors were interviewed to assess their knowledge and awareness about BMW. An estimated 50–70 kg/day waste is generated from this hospital (Gupta and Boojh 2006).

- The hospital severely lacks waste segregation, and infectious and non-infectious waste are intermixed together during the collection at hospital premises.
- All kinds of waste are collected in a common bin and dumped along with municipal waste at the city site.

- The hospital does not have any equipment techniques for the onsite disposal of infectious waste.
- The open and accessible dumping makes the waste collectors and the environment susceptible to a severe health hazard.
- All the infectious, pathological and microbiological waste are dumped into municipal sewage without any pretreatment, ultimately polluting the Gomati River and affecting the aquatic ecosystem.

10 Conclusion

With the detailed description given on the bio-medical waste management in hospitals of Uttar Pradesh, it can be concluded that there is a lack of awareness and knowledge among the hospital authorities and staff regarding the hazardous and lethal health complications caused by the improper practice of waste disposal. Hospitals should be appropriately equipped with the necessary facilities to carefully dispose of the waste carefully and health care staff and persons handling the bio-medical waste should be properly trained. Implementing the bio-medical waste management act on a severe note must be established, and the regulatory bodies must keep a check regarding waste disposal on the health care providers. It is also equally important to make people aware of the importance of proper bio-medical waste disposal methods and their harmful impacts on the environment and human health if not disposed of properly.

Conflicts of Interest There are no conflicts of interest.

References

CPCB (2016) Annual report on biomedical waste management as per biomedical waste management rules index. https://cpcb.nic.in/uploads/Projects/Bio-Medical-Waste/AR_BMWM_2018.pdf

Devi A, Ravindra K, Kaur M, Kumar R (2019) Evaluation of biomedical waste management practices in public and private sector of health care facilities in India. Environ Sci Pollut Res 26:26082–26089. https://doi.org/10.1007/s11356-019-05785-9

Gautam V, Thapar R, Sharma M (2010) Biomedical waste management: incineration vs. environmental safety. Ind J Med Microbiol 28:191. https://doi.org/10.4103/0255-0857.66465

Gupta S, Boojh R (2006) Report: biomedical waste management practices at Balrampur Hospital, Lucknow, India. Waste Manag Res 24:584–591. https://doi.org/10.1177/0734242X06068342

Gupta S, Boojh R, Mishra A, Verma S, Agarwal N (2008) Biomedical waste management practices at Chhatrapati Shahuji Maharaj medical University, Lucknow: a case study. Res Environ Life Sci 1:77–80

Gupta S, Boojh R, Mishra A, Chandra H (2009) Rules and management of biomedical waste at Vivekananda Polyclinic: a case study. Waste Manag 29:812–819. https://doi.org/10.1016/j.wasman.2008.06.009

Hegde V, Kulkarni R, Ajantha G (2007) Biomedical waste management. J Oral Maxillofac Pathol 11:5. https://doi.org/10.4103/0973-029x.33955

Kalpana VN, Sathya Prabhu D, Vinodhini S (2016) Biomedical waste and its management. J Chem Pharm Res 8:670–676

Mathur V, Hassan M, Dwivedi S, Misra R (2011) Knowledge, attitude, and practices about biomedical waste management among healthcare personnel: a cross-sectional study. Indian J Commun Med 36:143. https://doi.org/10.4103/0970-0218.84135

MoE (2018) The bio-medical waste management (amendment) rules. http://www.indiaenvironmentportal.org.in/content/453336/the-bio-medical-waste-management-amendment-rules-2018/

MoEF (1998) The bio-medical waste (management and handling) rules. https://hspcb.gov.in/BMW%20Rules.pdf

MoFE (2011) Draft bio-medical waste (management & handling) rules. http://www.indiaenvironmentportal.org.in/content/337411/draft-bio-medical-waste-management-handling-rules-2011/

Mohapatra A, Gupta MK, Shivalli S, Mishra C, Mohapatra S (2012) Biomedical waste management practices of Doctors: an online snapshot. Natl J Community Med 3:227–231

MoHFW (2016) Bio medical waste management rules—2016. Department of Health Research. Government of India. https://dhr.gov.in/document/guidelines/bio-medical-waste-management-rules-2016

Pandey A, Ahuja S, Madan M, Asthana AK (2016) Bio-medical waste managment in a tertiary care hospital: an overview. J Clin Diagn Res 10. https://doi.org/10.7860/JCDR/2016/22595.8822

Park K (2015) Park's textbook of preventive and social medicine, 23rd edn. Bhaton Publication, India

Sharma S, Chauhan SVS (2008) Assessment of bio-medical waste management in three apex government hospitals of Agra. J Environ Biol 29:159–162

Singh Z, Bhalwar R, Jayaram J, Tilak VW (2001) An introduction to essentials of bio-medical waste management. Med J Armed Forces India 57:144–147. https://doi.org/10.1016/S0377-1237(01)80136-2

Singh A, Kumari R, Wakhlu A (2013) Biomedical waste management practices at King George's Medical University, Lucknow, vol 7, pp 93–100

Singh A, Agrawal A, Agrawal VK, Saxsena SK, Agrawal AK, Singh H (2014) Evaluation of biomedical waste management practices in a tertiary care hospital of Rohilkhand region in Uttar Pradesh, India. Int J Med Sci Public Heal 3:1187

UPSWMMC (2019) U.P. solid waste management, monitoring committee. https://drive.google.com/file/d/1V_-aBNnsaqyoN2nYgOB8udM3tK18hDzd/view

Legacy Waste Characterization: Bio-mining Solution for Landfills and Resource Recovery Towards Circularity

Tanmoy Bir, Samran Banerjee 🄳**, and Amit Dutta**

Abstract Bio-mining or Landfill mining is an effective and eco-friendly process which involves the stabilisation of old legacy waste in landfill through recovery of valuable resources. In accordance with circularity, it involves reuse, recycle and recovery aiming to build up a sustainable resource in order to give protection through the elimination of waste which also enable the society to become more autonomous and pollution free. The objective of this paper is to deal with the plausible characterization and recovery of mined legacy waste through average compositional analysis of past 25 years data and their possible recycling and processing options. Plastics assumed to be remain by an amount 80% in landfill, metal and glass remained by an amount 75% and for inert it is assumed that the inert turned into soil like material under the action of weathering by an amount 5%. A possible material balance flowchart and composition analysis is prepared. Expected soil: waste ratio is found to be 40:60. Under co-processing, around 7.3% of combustible material will be send as RDF to Cement Industry/Power Plants. Recyclables will be transferred to authorized recycling plants. The residual amount came as approximately 7% (5–10% as per CPCB) which suggested a maximum recovery option. Recovered non-combustible, C&D waste, inert (30.3%) will further be transferred to low lying areas such as filling of basement/plinth structures, in bedding of road construction etc. Revenue generation from compost product, anaerobic digester, power generation through WTE and recycling products will enhance the economy to meet the sustainable circularity solution.

Keywords Bio-mining · Resource recovery · Circular economy

T. Bir (✉) · S. Banerjee · A. Dutta
Department of Civil Engineering, Jadavpur University, Kolkata, India
e-mail: tanmoybir5@gmail.com

A. Dutta
e-mail: amit.dutta@jadavpuruniversity.in

1 Introduction

Landfilling is a cost effective final solution to store the solid waste generating from different households and industrial activities (Krook et al. 2012). Municipal Solid Waste (MSW) contains various valuable resources which are escaping globally due to lack of effective segregation at source, further disposing into open land. South Asian developing countries like India, Pakistan, Bangladesh, Afghanistan, and Sri Lanka, as well as smaller nations including Nepal and Bhutan are facing prodigious waste management problem in terms of control measure in waste generation, treatment followed by disposal into non-engineered landfills, causing massive pollution hazards and contribution towards resource diminution. Global development as such industrial growth, population surcharge, urban sprawling, demand of raw materials and resource depletion are effectuating to find out viable treatment options as an alternative solution to resource replenishment. Recycling and recovery are the necessary action to be taken for segregating out different valuable resource substitute from different components of solid waste (Halada et al. 2009; Kapur 2006). Landfill mining (LFM) or precisely bio-mining is one such strategical eco-friendly treatment option for non-engineered landfills. In South Asian countries, with an approximate waste generation of 70 million MT per year, with per capita generation of 0.12–5.1 kg per day and an average of 0.45 kg/capita/day. India accounts for 1210 MMT CO_2-eq greenhouse gas (GHG) emission out of which 1.1% methane emission occurs from the landfill sites out of the total GHG emission (World Bank 2012). The theory behind implementing landfill mining is solely dependent on the circularity concept which derives the protection through the elimination of waste through recovery, recycling and reuse of mined waste thus to build up an alternative sustainable resource management system. Bio-mining consists of waste extraction, treatment through stabilizing, separation of extracted materials and conversion for alternate resource. The sole purpose of Bio-mining lies in the context of landfill reclamation, landfill space conservation, land reuse, potential contaminant minimization, omission of point source causing groundwater pollution, energy and resource recovery, cost reduction in waste management and site re-development (Cossu et al. 1996).

1.1 Global Outline of Bio-mining and Landfill Recovery

Israel, a Middle Eastern country adopted landfill mining strategy initially in 1953 in search of fine waste material to be used as a soil amendment (Savage et al. 1993). USA initiated landfill mining to obtain alternative fuel for thermal processing and energy recovery potential from Waste to Energy projects (Cossu et al. 1996; Hogland et al. 1995). Sardinia landfill in Italy and Filborna landfill in Sweden were contemplated the mining operation for the reduction in risk due to installations and shortage of landfill space caused by urban sprawling in 1994 (Cossu et al. 1996; Krüse 2015). In accordance with landfill reuse, site re-development and resource recovery, important

role for adopting Bio-mining treatment is of utmost concern for pollution reduction in simultaneous manner (Krüse 2015). The term Enhanced Landfill Mining (ELFM) has been delineated with the aim of resource and energy recovery from the old landfills with legacy waste accumulation. ELFM has procured wide acceptance in the Flanders region in Belgium (Bosmans et al. 2013; Geysen et al. 2009; Jones et al. 2012; Quaghebeur et al. 2013; Passel et al. 2013). Austria, Belgium, Netherlands, USA these are some of the OECD (Organization for Economic Co-operation and Development) global region where various landfill mining projects have been proposed with optimum results. Halbenrain landfill in Austria strategized ELFM for combined landfill space-resource recovery followed by material extraction. After physio-chemical characterization, 64.5% Refuse Derived Fuel (RDF), 2D and 3D plastics, 3% ferrous metal and 15.5% as high as refused material were obtained (Lopez et al. 2018). In Belgium, around 27.3% of non-ferrous metals were recovered among which 80% of copper and aluminum scraps were estimated. Eastern and Central European regional countries like Estonia and Lithuania procured landfill mining at Torma landfill and Alytus landfill respectively. The model proposed in this case study estimated the entire chain of landfill deterioration process, mining, and maintenance in the aftercare period followed by the options of waste recovery and installation of renewable energy resources (Buĉinkas et al. 2018). Many states of the USA including Florida, New York, Pennsylvania, Massachusetts, New Hampshire, and Delaware, as well as in Ontario, Canada conducted several pilot and full-scale studies (Guerriero 1996). In Chester landfill and Edinburg landfill of New York were acquired landfill mining project with sole objective of 50,000 MT of mined waste reclamation for using as landfill cover. A soil: waste ratio of 20:80 and 75:25 were found as a result for Chester and Edinburg landfills respectively. This aforementioned feasibility solution supports the utmost need to identify site specific conditions and reclamation-recovery options before full scale implementation (Guerriero 1996).

1.2 Indian Landfills and Bio-mining Operation

Landfill mining in India was commenced on 1989 in Deonar dumpsite of Mumbai for the sole aim of compost material recovery from the aged waste of density 0.96 MT/m^3 (Kurian et al. 2003a; Ortner et al. 2014; Scheu and Bhattacharyya 1997). Physical characteristics obtained as 0.4% of soft plastic, 0.9% glass, 1.1% rags, 0.4% metals, 0.6% rubber and leather, 0.6% coconut and wooden matters post mining and excavation. Screening of waste fractions were estimated as 63.5% finer portion having size less than 8 mm with 14.5% biodegradable portion and 31.5% of inert having size more than 25 mm. The chemical characteristics of finer fraction contained pH 7.2, Organic carbon 5.8%, Nitrogen 0.5%, Sulphur 0.4%, Calcium carbonate ($CaCO_3$) 12.6%, Soluble aluminum 1000 ppm, Soluble manganese 270 ppm, Soluble iron 4800 ppm etc. through laboratory analysis. A pilot scale field study on landfill mining activity in India were conducted (Kurian et al. 2003) in two landfill sites named Kodungaiyur and Perungudi located in Chennai. The bio-earth acquired from the Kodungaiyur

landfill site was reported as around 65–70% which was comparable to different landfill sites around the world e.g., Edinburg (NY), Horicon, Chester (USA), Burghof (Germany), Cagliari (Italy) and Deonar (Mumbai). Kodungaiyur landfill reported 4% combustibles and 28% non-combustibles whereas 40% combustibles for Perungudi landfill with 20% non-combustibles. The chemical analysis showed that the concentration of heavy metal in leachate was higher than concentration in fine fractions obtained from both landfill sites. This study only incorporated the qualitative characterization of finer portion of the excavated waste without contemplating different reuse methodologies and Bio-mining components followed by their impact study. An investigation on finer fraction characterization had done on aged MSW through landfill mining from three dumpsites named Okhla (Delhi), Jawahar Nagar (Telangana) and Kadapa (Andhra Pradesh) landfills in India. Composition of mined waste was determined through Grain Size Distribution analysis which revealed that 8% w.r.t dry basis and 43% w.r.t wet basis in case of Delhi landfill, for Hyderabad landfill 2% w.r.t dry basis and 25% w.r.t wet basis and in Kadapa landfill the finer fraction was 12% w.r.t dry basis and 35% w.r.t wet basis. From the compositional analysis, it was found that maximum soil-like material was found from the oldest aged landfill site among the three above-mentioned landfill sites named Kadapa. The concentration of inert waste (especially construction and demolition waste) while was found to be almost negligible in the landfill of Hyderabad. The percentage of paper was found to be almost negligible in all the landfills due to consideration of old aged waste (Somani et al. 2018).

2 Methodology

In Developing countries like India, indiscriminate generation as well as inefficient disposal of solid waste results accumulation of solid waste over years. The changing of life pattern of community, industrial development generation of solid waste is continuously increasing. This huge amount of waste is practiced to dispose in open dumps over years becomes the potential point source of pollution. Considering this adverse situation National Green Tribunal promulgated a veridiction to maintain the provision in SWM rule 2016 named Clause J of Schedule1. The philosophy behind bio-mining is based on the circular economy concept, which entails recovery, recycling, and reuse to create a sustainable resource to protect the elimination of waste, as well as enabling society to become more autonomous, sustainable, and following environmental resource issues as well as the transition from the linear economy concept of waste management which follows the typical "take-make-dispose" step-by-step process. This means that raw resources are collected, then turned into useful goods before being thrown as wastes. In the perspective of the major landfill of Kolkata, Dhapa, which receives a huge amount of municipal solid waste (4000–4500 MT/d) operating since 1987 and the capacity of the landfill, has transgressed the threshold limit with waste carrying load 25 MT/m^2 which may cause subsidence failure. The entire study in this work is based on approximation because bio-mining

is still not implemented in Kolkata but is proposed to be operated per NGT guidelines (National Green Tribunal). Although extensive work based on bio-mining is not done across India (Kurian et al. 2003), conducted a field study in Chennai to determine the composition of mined waste from legacy waste. Because sufficient data is not available, the estimation must rely on various literature works based on landfill mining, as landfill mining operations continue in various countries around the world, including Europe, the United States, and Asia, such as China. By gathering various composition data of excavated sample of waste from a literature survey and used that to perform an approximate compositional analysis of an excavated sample of proposed bio-mining work that must be carried out for the Dhapa landfill.

2.1 Study Area

Dhapa landfill of Kolkata have been chosen as a study site because it receives a large amount of waste and has been in operation since 1987 with exhausted condition. The topographical feature of Dhapa Landfill is that it is situated in Kolkata (latitude 22° 34′ N, Longitude 88° 24′ E), the largest metropolitan city in eastern India, located on the eastern bank of River Hooghly and is 30 km away from the Bay of Bengal with an average elevation of 17 feet (5.1816 m) above the mean sea level. For an approximate estimation of waste obtained from bio-mining of legacy waste for Dhapa landfill, the waste composition of the previous 25 years and their percentage in the case of Dhapa landfill are required. The current "dumping area" is approximately 35 ha in size. It consists of two unlined dumpsites separated by 500 m—one closed dump of 12.14 ha and one active dump of 23 ha. The active dumpsite, which began operations in 1987, is expected to remain operational for another two to three years (2020–21). The disposal of a massive amount of waste began in 1987, resulting in a massive waste mountain that has already surpassed the 50-ft threshold value. Since the waste composition produced in Kolkata is not uniform, we take the average value for uniformity.

2.2 MSW Composition Survey of Kolkata

The average composition of waste generated in Kolkata over 25 years consists of chiefly organic waste (50.17%), followed by Paper, Plastic, Metals and Glass by an amount of 3.47, 4, 0.365, 0.925% respectively which are recyclable in nature. There are also other components of waste which includes Inert, Rubber/leather, Rags, Wood, Coconut Shell, Others such as Construction and Demolition Waste by an amount 29.2, 2.58, 2.51, 0.65, 5.27 and 0.605%. However, all wastes are not entirely disposed of in the waste dump. Some waste is recycled or separated by a certain amount at the point of origin and the remainder is disposed of to waste disposal. It's estimated that around 80% of paper is recycled at source, 70% of plastic

is recycled at source, glass and metals is recycled by 80% at source and textile waste such as Rubber/Leather is recycled by 60% at source. Rest of the amount is disposed in landfill. The portion of recyclable waste which is recycled at source are almost intact or undegraded in nature. But rest of those which is disposed in landfill is either degraded or mostly deteriorated in nature. The main aim of bio-mining is to recover those materials from legacy waste with maximum efficiency so that it can be valorized to the market as a raw material in the various processing plant as well as manufacturing plant.

The final waste disposed in landfill over years or precisely legacy waste can be broadly categorized as decomposable waste which includes food waste or organic waste (50.17%), Paper (0.957%), Wood (0.65%) Coconut Shell (5.27%) Rags (1.87%) and non-decomposable waste Inert (28.77%), Rubber/Leather (0.942%), Plastic (1.2%), Glass (0.185%), Metal (0.072%) and Others including Construction and Demolition waste (3.785%). From the above composition, it can be shown that if 100 tons is considered as a total waste of approximately 91,909 tons of waste, i.e. more than 90% or indirectly less than 10% is recycled in the landfill. If bio-mining can be carried out, the efficiency of recovery from waste disposed of by inefficiency of segregation in the point source will be increased by recycling recyclable material.

2.3 Landfill Waste Degradation

From the composition of legacy waste described above, it is easily recognized that more than 50% of MSW is organic in nature. So, over a year, a large portion of the organic fraction degrades due to the development of several distinct phases. Aerobic, Anaerobic, and Non-Methanogenic are the primary phases. (Acetogenic). Methanogenic and Anaerobic (a non-steady phase). Anaerobic, Methanogenic, and Anaerobic. During compositional analysis, the degradable matter such as food waste, rags, paper, wood, coconut shell are assumed that the degradation pattern follows IPCC model i.e., first-order kinetic decay rate model (see Fig. 1).

For estimating the various amount of decomposable waste this first-order decay rate constant k is used according to the categorization of decomposable waste according to their rate of degradation such as rapidly degradable which is food waste, moderately degradable which is a coconut shell, slowly degrading waste which includes rags as well as paper, wooden matter valid for a tropical country like India. The value of k is taken for rapidly degradable waste 0.085, for slowly degradable waste k value is taken 0.045 and for moderately degradable waste k value is taken 0.045 (Pipatti et al. 2006). Because food waste is mostly carbon, in the first stage of degradation, i.e., in aerobic conditions, carbon is reduced and easily converted to CO_2, resulting in rapid degradation of food waste. The average percentage of food waste remaining over 25 years using the above equation comes 38.4864% nearest round figure 40% for simplification in calculation. Fungal decay of wood and wood products occurs even in the presence of oxygen (Blanchette et al. 1990);
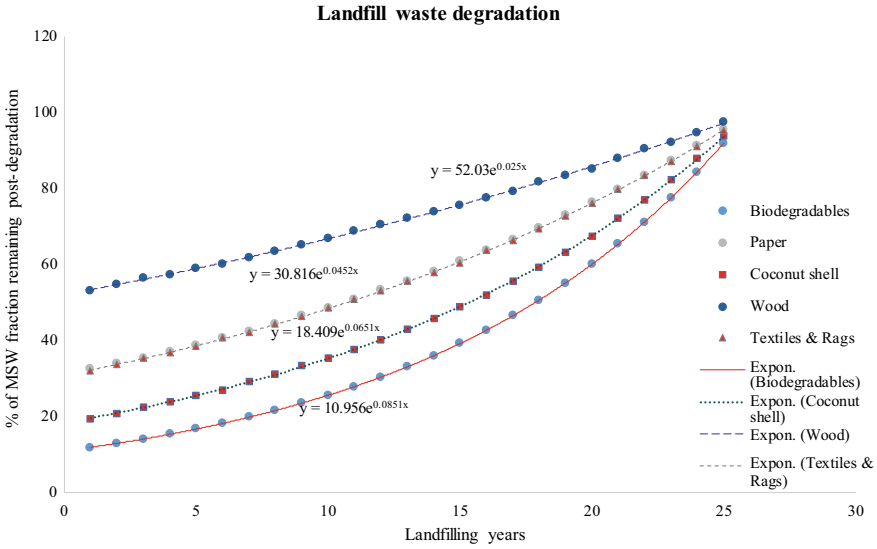
Fig. 1 Exponential degradation of landfill legacy waste for 25 years in Dhapa landfill, Kolkata

thus, any biodegradation of the wood and paper specimen during burial in anaerobic landfills is prone to bacterial activity rather than fungal interaction. Bacteria are known to degrade wood quite slowly than fungi (Blanchette et al. 1990). That is why degradation of wood is considered as slow degradation and for that decay rate constant is taken 0.045. The average % remain after 25 years degradation in landfill is 73.44%. Through pyrolysis or incineration, coconut shell waste can be used as a fuel substitute. The coconut shell contains a high concentration of lignin, cellulose, and hemicellulose, which can degrade in aerobic and acetogenic phases, converting it to a moderately degradable waste. The remaining portion of the coconut shell can be used as an efficient biofuel source (Said et al. 2015). Because coconut shell has a high lignin content, the chemical change under aerobic conditions takes a longer time to degrade than food waste. As a result, degradation of coconut shell can be classified as moderate and the decay rate constant is considered as 0.065. Using these the average % remain of coconut shell over 25 years is 47.672%. Rags are a type of textile waste that contains a lot of cellulose. The degradation rate of cellulose and cellulosic material substrates is primarily determined by the microorganisms used. The two primary groups of microorganisms responsible for the enzymatic degradation of cellulose are microscopic organisms and growths. The degradation of the cellulose textures continues from the surface to the inside in the presence of microorganisms. In the presence of growths, after the restoration of the fingernail skin, the creatures infiltrate through the optional divider into a lumen where they develop (Desai and Pandey 1971). Jute is the main component of rags that deteriorates very slowly due to chemical reactions that consequence in the degradation of chemical composition, which takes a very long time. As a result, rags are classified as slowly degrading

waste, and the decay rate constant is applied to this type of waste. Considering the above discussions k value is taken 0.045 and the average amount of waste remain over 25 years in landfill comes out 58.3972, for the sake of simplicity it is considered in round figure 60%. Paper, which is formed biosynthetically from cellulose, hemicelluloses, and lignin of plant cells, is also susceptible to maturing because it is made from natural substances. Zou et al. (1994) investigated the long-term quality of various paper evaluations by incorporating rapid maturing interaction. It was discovered that most compound responses rise when the temperature rises, and these substance changes influence the actual properties of paper materials. The compound interference of the materials and the impact coming from external factors determine the paper's durability, whereas the paper's sturdiness is dependent on the physical and mechanical properties of the predominant raw materials, added substances, and pollution by particles from the climate, the action of light, mugginess, and microorganisms. As a result of these considerations, paper waste can be classified as slowly degradable waste, with the decay rate constant set at 0.045 for slowly biodegradable waste, and the average solid waste remaining after degradation calculated using the IPCC model equation over 25 years 58.7%.

2.4 Non-biodegradables and Landfill Degradation

Non-decomposable materials such as plastic glass, metal, rubber, and inert may be difficult to degrade as biodegradable. However, it can be assumed that non-biodegradable waste deteriorates due to weathering in old dump waste. Some glass is broken during disposal, and the paper weathers into smaller fractions. Similarly, metal, rubber, and plastic can weather and turn into finer fractions and earthy material. After bioremediation, excavation and screening with the appropriate screen size must be performed during bio-mining to recover the unweathered fraction for resource recovery. Plastic waste in landfills is one of the major waste streams that can be reused. In any case, because of contamination, for example, heavy metals or destructive mixtures, and primary changes caused by the landfilling cycle, it is unlikely to meet the requirements for conventional reusing (Canopoli et al. 2018). Polyethylene (PE) and polypropylene (PP) are the most common thermoplastics in the MSW. In an oxygen-consuming and anaerobic environment, photo degradation and thermo-oxidative deterioration are the most common causes of deterioration for PE and PP (Andrady 2011; Gijsman et al. 1999; Webb et al. 2013). Plastic may not be easily decomposed or may take a long time to break down in the case of old dump waste. Because there is no scope for field data availability, we must depend on various literature studies which was based on field data analysis. Kurian et al. (2003) evaluated landfill mining in three Indian dumpsites, notably Perungudi, Kodungaiyur, and Deonar, and noticed that the composition of plastic waste in excavated samples was 11, 1.9, and 1.5%, respectively. Metal scrap in the old waste dump is comprised of a variety of elements, including ferrous and non-ferrous metals like copper, aluminum, tin, and so forth. Erosion or oxidation caused by exposure in an outdoor environment

such as rainfall, sunlight, and so on is the principal cause of metal refuse deterioration in aged landfill sites. Scrap metal refers to metal that has already been disposed of in landfills. According to existing literatures surveys, it is assumed that nearly 75% of scrap metal can be recovered from old landfills in non-weathered conditions (Law et al. 2014; Savage et al. 1993). Construction and demolition waste, sand, stone, aggregates, and other inert materials make up the majority of inert material. The degradation of inert is a very long process, and the principal reason of degradation is mechanical erosion caused by sunlight, wind, rainfall, and so on, but the degradation rate is very low, resulting in a recovery rate of waste from landfill of nearly 90–95% recovery and around 5% degradation turning into soil-like material (World Resource Foundation). The mining of waste is appropriate for waste which is 15 years old, whereas the waste in the Dhapa landfill is 25 years old, so bio-mining can be used efficiently in this landfill.

2.5 Material Balancing of Different Components of Bio-mining

For the preparation of plausible material balance flow chart which is the modified version of material balance flow chart of crude dumping of existing SWM system in Kolkata derived from the futuristic operation of bio-mining, certain assumption and factors based on secondary research have been inculcated as such paper waste is recovered by around 60% (As per IPCC model), plastic recovery rate is 80% (Law et al. 2014; Savage et al. 1993), metal and glass recycling is being done on a 75% basis (Savage et al. 1993; Law et al. 2014), Inert is assumed to be mixed with bio earth by 5% i.e. 5% partial degradation may be assumed. (World Resource Foundation), Rubber leather is assumed to remain 100%, rags as 58%, wooden matter as 73%, Coconut shell as 48%, and food waste as 40% remain as a residue in the legacy waste as per the IPCC model (Pipatti et al. 2006). Based on the above assumptions the expected composition of material that can be recovered after excavation of legacy waste consists of food waste (21.83%), Coconut shell (2.74%), Paper (0.62%), Rags (1.577%), Wood (0.175%), Plastic (0.261%), Metal (0.06%), Glass (0.046%), Inert (30.182%), Rubber/Leather (1.22%). Among plastic waste, around 80% is HDPE in nature which can be recycled considerably as a bulky waste and rest 20% can goes for incineration. The % of HDPE in recovered material is 0.209% (see Fig. 2).

3 Result and Discussions

The average percentage of combustible and non-combustible waste is around 3.23 and 33.41%. Rags, wood, R/Leather, and an undegraded portion of plastic generate the
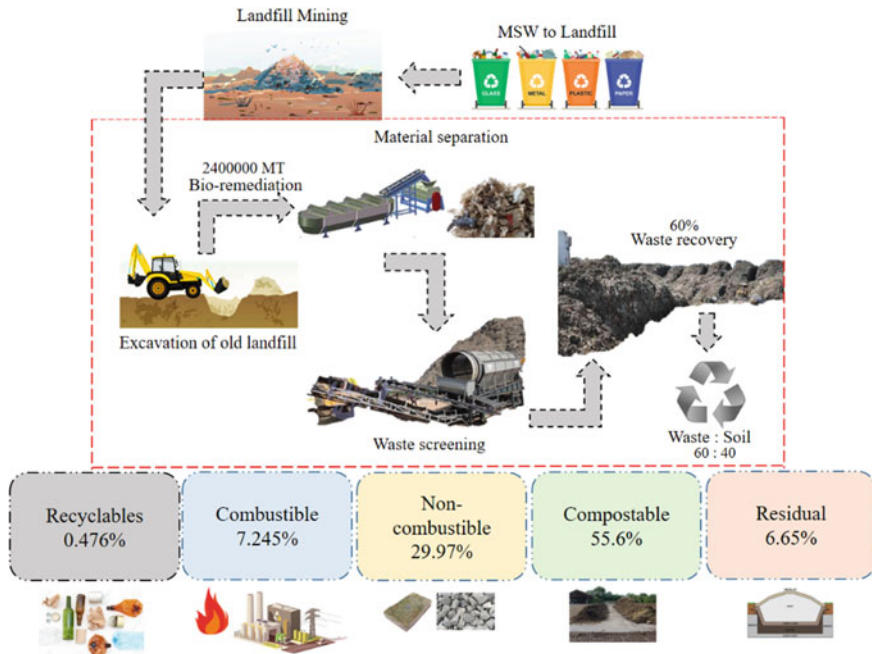
Fig. 2 Material balance flow chart of bio-mining process of Dhapa landfill, Kolkata

combustible material, while coconut shell, paper, metal, and inert make up the non-combustible material. Because of inadequate degradation of non-combustible waste, the percentage of non-combustible material is higher than combustible. In the current study, the age of waste in the Dhapa landfill is assumed to be 25 years. So, over the last 25 years, waste has been continuously disposed of, and degradation has occurred, resulting in a slight variation in percent composition between combustible and non-combustible waste. However, due to the lack of sufficient information, we can rely on CPCB guideline 2019 (CPCB 2019) as current reference. We compare the standard of combustible material composition standard as per CPCB guidelines (CPCB 2019) that the permissible composition of recovered combustible waste is within 5–10% through density separation, and our estimation of the recover combustible material is 3.23% or around 4%. For soil-like fraction findings, we must determine the percent degradation of waste in a landfill over the last 25 years. The soli-like fraction obtained from screening according to the CPCB manual (CPCB 2019), i.e., 4–6 mm for screening of finer fractions that are available. The percentage of soil-like material is 39.14%, which is close to 40%. The soil like fraction or finer fraction consists of Food waste (32.757%), Coconut shell (2.981%), paper (0.416%), Rags (1.142%), Wood (0.264%), Inert (1.58%) etc. The possible material balance flow chart show the various recycling or processing option of the composition that can be reused for different purposes. Under co-processing, around 7.3% of combustible material
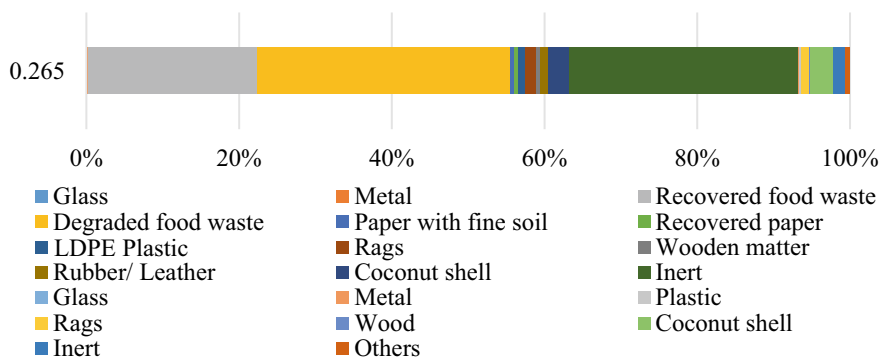
Fig. 3 Waste recovery of different bio-mining components

will be send as RDF to Cement Industry/Power Plants. Recyclables will be transferred to authorized recycling plants. The residual amount came as approximately 7% (5–10% as per CPCB) which suggested a maximum recovery option. Recovered non-combustible, C&D waste, inert (30.3%) will further be transferred to low lying areas such as filling of basement/plinth structures, in bedding of road construction etc. Revenue generation from compost product, anaerobic digester, power generation through WTE and recycling products will enhance the economy to meet the sustainable circularity solution (see Fig. 3). Based on the material balance flow chart the amount of components is estimated under the consideration of actual amount of legacy waste in Dhapa landfill over 25 years which is approximately 40 lakh t and average density of waste 0.85 MT/m^3. It's recommended that before initiation of bio-mining the huge volume of waste must be remediate using bio-culture (CPCB 2019) which cause the reduction of volume of legacy waste by 40 for ease of excavation, loadings and other operations. Before that bulky waste e.g., coconut shell, piece of rag, clothes or other textile waste, broken glass, metal scrap, or other unweathered portion of inert material mainly construction and demolition waste must be removed manually.

3.1 Bio-mining Components and Quantity Estimation

The total amount of recyclable material is 10,080 MT, which includes 1440 MT of metal, 36.24 MT of glass, and 5016 MT of HDPE plastic. According to the graphical representation HDPE makes up the majority of the recyclable material, while metal and glass make up a minor portion. The approximate amount of combustible waste is 178,104 MT, which is nearly 7.421% of total waste, which is in the range of 5–10% according to Central Pollution Control Board guideline (CPCB 2019), which refers to the accuracy of estimation procedure. According to CPCB, density separation can recover up to 5–10% of combustible material. Among the combustible

materials recovered, coconut shell contains a large amount, chiefly 66,000 MT, and other materials such as wood 17,160 MT, light plastic 15,048 MT, rags 38,040 MT, rubber/leather 26,976 MT, and paper 14,880 MT, suggesting that more RDF can be obtained from coconut shell. The approximate estimation for non-combustible material is 726,480 MT, of which 724,800 MT is inert material, 1200 MT is glass, and 480 MT is metal in the form of a finer fraction. As a result, metal can be separated through proper screening using a magnetic separator, overhead magnets, head pulley magnets, and so on. As a result, a large amount of inert soil-like material can be used as landfill material or landscaping material. Compostable material yields approximately 1,321,200 MT, which consists primarily of degraded food waste and the remaining portion of food waste that can be converted into compostable material via windrow composting, though it must meet the FCO standard for compost, which is 524,400 and 786,720 MT, respectively, and paper in compostable material yields 10.080 MT in residual material, which should be kept to a minimum in comparison to the total waste to be bio-mined. The total amount of residual waste is estimated to be 164,616 MT. Which consists of 6240 MT of plastic, 38,400 MT of inert material, 27,600 MT of rags, 71,616 MT of degraded coconut shell, 6240 MT of degraded wood, and 14,520 MT of other waste, including inert material, construction and demolition waste?

3.2 Possible Recycling Options of Recovered Materials

HDPE plastic can be recovered at a rate of 0.209% of total legacy waste. Prior to that, bulky plastic waste is supposed to be recovered by an amount of 80% and to remain intact in a landfill. Light plastic which is partially broken or deteriorated can be recovered at a rate of 0.627% of total legacy waste. Al-Salem et al. (2009) suggested that plastic products are the main components obtained from the recovery of excavated material, and they're used as raw material for renewable plastics or chemically cracked up to oil, carbon coke, waste to energy through incineration, which can be helpful for electricity production through pyrolysis, gasification, incineration, and so on, feed stock for petrochemical plants etc. For paper of old landfill waste which is almost rotten, can be used for the preparation of pore-forming agents in light bricks (Quaghebeur et al. 2013). For recycling options of metal especially for non-ferrous metal such as Al foils can be used as raw material for Food processing industry Brass can be used as raw material for preparation of metallic instruments, Cu wires can be used a straw material for electrical instruments, Pb alloy as Additives in paints, Stainless steel as a raw material in in Various metals e.g., engineering instruments, blending in the steel industry to prepare alloys (Lucas et al. 2019).

4 Bio-mining—A New Aspect Towards Circularity

The 'circular economy' model of waste management that includes not only waste management, but also reuse, recycling, and responsible manufacturing, could help to develop new industries and jobs while lowering emissions and increasing the efficient use of natural resources (including energy, water and materials). Bio-mining follows the basic philosophy of circular economy through maximum recovery of reusable material. Efficiency of bio-mining depends upon the soil to waste ratio as well as the depth of excavation. Deeper the excavation and minimum soil to waste ratio implies the maximum efficiency of bio-mining. Maximum recovery of waste material which includes various components such as recyclable, combustible, non-combustible will signify resource recovery with maximum efficiency. In our study the soil to waste ratio is 40:60 which may be proved efficient operation of bio-mining. The hypothetical waste recovered from the excavation of legacy waste consists of recyclable material by an amount 10,080 MT out of which HDPE plastic is in maximum. If we consider rate of overall cost of recyclable material including collection, hauling, processing 0.24 ₹/MT the overall cost for recyclable material 2419.2 ₹. The amount of combustible material recovered from excavation of legacy waste is 178,104 MT. The combustible waste is supposed to be incinerated, or preparation for RDF or for co-processing. The cost of combustible material for these processing options is 68.42 lakhs considering the rate of processing for combustible material 38.42 ₹/MT. The non-combustible materials include metal, inert and fine fraction of glass can be reused as land filling material or manufacturing of building material or paving blocks incurred 443.5 lakhs considering the rate of processing 61.06 ₹ /MT. The amount of compostable material from excavation of legacy waste 1,321,200 MT, which consists primarily of degraded food waste and the remaining portion of food waste that can be converted into compostable material via windrow composting, though it must meet the FCO standard for compost, the processing cost for compostable material for preparation of compost is 1645.1 lakhs considering the rate of processing 124.52 ₹/MT. The overall cost for hypothetical bio-mining comes out 289.88 Cr. In case of revenue, it is expected that the revenue generated from recyclable material as well as compostable material. The revenue generated from recyclable material is 46,872 Rs. considering the rate of revenue 4.65 (₹/MT). In case of revenue generated from compostable material is comparatively higher than the material for recycle because the rate of revenue is more than recycle of material i.e., 250.5 (₹/MT). The Revenue generation from selling of compostable material is 998.2 lakhs. In particular in case of compostable material the revenue generated is less than cost for processing because 70% reduction of waste during preparation of compost. The total revenue expected to be generated from this bio-mining is 9.93 Cr. The overall expenses for bio-mining are 279.95 Cr. The feasibility of project in terms of cost is validated in accordance with the range 400–700 ₹ /m^3 (CPCB 2019).

5   Conclusion

Age old Municipal Solid Waste or Legacy waste management is a critical issue in developing country like India because of high population density as well as scarcity of available space for creation of new disposal ground and also proper infrastructure for proper minimization at source facility. The long term assemblage of Legacy waste in disposal ground imparts hazardous effect to the entire ecosystem around the dumpsite. Bio-mining has been proved a most suitable ex-situ legacy waste management system in which thorough excavation of waste dump is executed for efficient resource recovery of valuable materials such as glass, metal (ferrous and non-ferrous), wood, putricible material; like organic waste for preparation of compost. Through implementation of bio-mining huge amount of legacy waste gets cleared off due to which carrying capacity of dumpsite get enhanced for further receiving of solid waste which is the possible remediation measure of scarcity of availability of landfill in densely populated country like India. In context of bio-mining it implements the basic philosophy of circular economy model which employs sustainable waste management through reuse, recycle, recovery which is transition from linear economy i.e. take-make-waste and accountable production of materials could support the development of industries and jobs, reducing emission and increasing efficient use of natural resources which can fulfill needs of raw materials for small scale industry such as small manufacturing industry, glass industry, plastic industry etc. which can be beneficial with respect to their financial and infrastructural condition (Towards Circular Economy 2021).

Conflict of Interest Tanmoy Bir, Samran Banerjee and Amit Dutta declares that they have no conflict of interest during this work.

References

Al-Salem S, Lettieri P, Baeyens J (2009) Recycling and recovery routes of plastic solid waste (PSW): a review. Waste Manage 29:2625–2643. https://doi.org/10.1016/j.wasman.2009.06.004
Andrady AL (2011) Microplastics in the marine environment. Mar Pollut Bull 62:1596–1605
Blanchette R, Nilsson T, Daniel G, Abad AR (1990). Biological Degradation of Wood. https://doi.org/10.1021/ba-1990-0225.ch006
Bosmans A, Vanderreydt I, Geysen D, Helsen L (2013) The crucial role of Waste-to-Energy technologies in enhanced landfill mining: a technology review. J Clean Prod 55:10–23
Buĉinkas A, Kriipsalu M, Denfas G (2018) Proposal for feasibility assessment model for landfill mining and its implementation for energy generation scenarios. Sustainability 10(8). https://doi.org/10.3390/su10082882

Canopoli L, Fidalgo B, Coulon F, Wagland ST (2018) Physico-chemical properties of excavated plastic from landfill mining and current recycling routes. Waste Manag 76:55–67

Cossu R, Hogland W, Salerni E (1996) Landfill mining in Europe and USA. ISWA Year Book, pp 107–114. International Solid Waste Association

CPCB (2019) Guidelines for disposal of legacy waste. Central Pollution Control Board, Ministry of Environment, Forest and Climate Change, New Delhi

Desai AJ, Pandey SN (1971) Microbial degradation of cellulose textiles. J Sci Ind Res 30:598–606

Geysen D, Jones P, Van Acker K, Van Passel S, Crabs M, Eyckmans J, Roos J (2009) Enhanced landfill mining—a future perspective of landfilling

Gijsman P, Meijers G, Vitarelli G (1999) Comparison of the UV-degradation chemistry of polypropylene, polyethylene, polyamide 6 and polybutylene terephthalate. Polym Degrad Stab 65:433–441

Guerriero JR (1996) Status of landfill reclamation and its applicability to solid waste management. American Society of Mechanical Engineers, New York

Halada K, Ijima K, Shimada M, Katagiri N (2009) A possibility of urban mining in Japan. J Jpn Inst Metals 73:151–160

Hogland KHW, Jagodzinski K, Meijer JE (1995) Landfill mining tests in Sweden. In: Proceedings of Sardinia 95, Fifth International Landfill Symposium, Cagliari, Italy

Jones PT, Geysen D, Tielemans Y, Pontikes Y, Blanpain B, Mishra B, Apelian D (2012) Closing material loops: the enhanced landfill mining concept. JOM 64(7):743

Kapur A (2006) The future of the red metal: discards, energy, water, residues and depletion. Progr Indus Ecol Int J 3:209–236

Krook J, Svensson N, Eklund M (2012) Landfill mining: a critical review of two decades of research. Waste Manage 32(3):513–520

Krüse T (2015) Landfill mining. Masters thesis

Kurian J, Esakku S, Palanivelu K, Selvam A (2003a) Studies on landfill mining at solid waste dumpsites in India. In: Ninth international waste management and landfill symposium, Margherita di Pula, Cagliari, Sardinia

Kurian J, Esakku S, Palanivelu K, Selvam A (2003b) Studies on landfill mining at solid waste dump-sites in India. In: Proceedings of 9th international waste management and landfill symposium, S. Margherita di Pula, Cagliari, Italy, CISA, Environmental Sanitary Engineering Centre

Law KL, Morét-Ferguson SE, Goodwin DS, Zettler ER, DeForce E, Kukulka T, Proskurowski G (2014) Distribution of surface plastic debris in the Eastern Pacific Ocean from an 11-year data set. Environ Sci Technol 48(9):4732–4738. https://doi.org/10.1021/es4053076

Lopez CG, Küppers B, Clausen A, Pretz T (2018) Landfill mining: a case study regarding sampling, processing and characterization of excavated waste from an Austrian landfill. Detritus 2:29–45. https://doi.org/10.31025/2611-4135/2018.13664

Lucas HG, López CG, Parrodi HCJ, Vollprecht D, Raulf K, Pomberger R, Pretz T, Freidrich B (2019) Quality assessment of non-ferrous metals recovered by means of landfill mining: a case study in Belgium. Detritus 8:79–90. https://doi.org/10.31025/2611-4135/2019.13879

Ortner M, Bockreis A, Knapp J (2014) Landfill mining: objectives and assessment challenges. Waste Resour Manage 167(2):51–61. https://doi.org/10.1680/warm.13.00012

Pipatti R, Sharma C, Alves MYJWS, Gao Q, Koch GHSG, Cabrera M, Mareckova K, Oonk H, Scheehle E, Smith A, Svardal P, Vieira SMM (2006) Waste generation, composition and management data. Chapter 2. IPCC Guidelines for National Greenhouse Gas Inventories. Waste, vol 5

Quaghebeur M, Laenen B, Geysen D, Nielsen P, Pontikes Y, Van Gerven T, Spooren J (2013) Characterization of landfilled materials: screening of the enhanced landfill mining potential. J Clean Prod 55:72–83

Said M, John G, Mhilu C, Manyele S (2015) The study of kinetic properties and analytical pyrolysis of coconut shells. J Renew Energy. https://doi.org/10.1155/2015/307329

Savage GM, Gloueke CG, Von Stein EL (1993) Landfill mining: past and present. Biocycle 34:58–61

Scheu M, Bhattacharyya (1997) Reuse of decomposed waste in lessons from India in solid waste management. Department of International Development, UK Government

Somani M, Datta M, Ramana GV, Sreekrishnan TR (2018) Investigations on fine fraction of aged municipal solid waste recovered through landfill mining: case study of three dumpsites from India. Waste Manage Res 1–12. https://doi.org/10.1177/073424X18782393

Towards Circular Economy (2021) What to do with legacy waste in India, 3 Mar 2021. https://downtoearth.org.in

Van Passel S, Dubois M, Eyckmans J, De Gheldere S, Ang F, Jones PT, Van Acker K (2013) The economics of enhanced landfill mining: private and societal performance drivers. J Clean Prod 55:92–102

Webb HK, Arnott J, Crawford RJ, Ivanova EP (2013) Plastic degradation and its environmental implications with special reference to poly (ethylene terephthalate). Polym 5:1–18

World Bank (2012) What a waste—a global review of solid waste management. In: Hoornweg D, Bhada-Tata P (eds) Urban Development Series. World Bank, Washington, DC

Zou X, Gurnagul N, Uesaka T, Bouchard J (1994) Accelerated aging of papers of pure cellulose: mechanism of cellulose degradation and paper embrittlement. Polym Degrad Stab 43(3):393–402. https://doi.org/10.1016/0141-3910(94)90011-6

Hydrogen Utilisation via Ammonia Borane Dehydrogenation and Regeneration: A Review

Shubham Giri and Ankit Kumar Tripathi

Abstract The recent era has noticed hydrogen energy as a sustainable option for meeting the world's energy requirements. Due to its diverse production source has become a clean and green option for transportation and energy storage. However, its complex storage limits the development and utilization of hydrogen energy. Ammonia borane (AB) has attracted attention to be considered an efficient hydrogen storage material due to its stability, exothermicity, non-toxicity, environmentally friendly, and high hydrogen intrinsic capacity of up to 19.6 wt.%. The thermolysis phenomenon is used for the efficient release of hydrogen gas. The left-out residue needs to be recycled again to maximize the production while considering the economic feasibility of the whole process. Thus, dehydrogenation and regeneration of the AB from the spent fuel play a vital role in deciding its effectiveness. This review paper examines and discusses the various dehydrogenation and regeneration routes of AB.

Keywords Thermolysis · Dehydrogenation · Regeneration

1 Introduction

The developed countries are moving towards accessing inexpensive sources of energy that are infinite and inexhaustible. The scarcity of fossil fuel energy has made it very difficult to satisfy the requirements of the human population, and an increase in environmental pollution has become a severe threat to human development (Manoharan et al. 2019; Midilli et al. 2005; Geng et al. 2019). In the modern era, promoting hydrogen as an alternative to fossil fuels and natural gas is one of the most burgeoning topics in sustainable development. Nearly 65% of the refined petroleum fuel is

S. Giri
National Institute of Technology, Rourkela, India

A. K. Tripathi (✉)
Graduate School of Engineering and Science, University of the Ryukyus, Nishihara, Japan
e-mail: ankittripathi467@gmail.com

exhausted to meet the transportation needs (Stephens et al. 2007). Moreover, these fossil fuels are needed to be imported and exported, thus adds up to an additional cost. Therefore, it is the need of the hour to make our way towards the realization of the hydrogen economy and pave our way towards cleaner energy technologies. Since in recent years, the energy crisis has led humankind to look towards other alternative energy technologies, and hydrogen has been one such source that has attracted our attention. It can be obtained through different routes, such as reforming gases, petroleum, methanol, natural gas, and biogas (Kaiwen et al. 2018).

Hydrogen, now mainly used as a chemical for up-grading fossil-based energy carriers, will in the future increasingly become an energy carrier itself (Jain 2009; Midilli and Dincer 2008; Veziroğlu and Şahın 2019; Nicoletti et al. 2015; Elam 2003; Conte et al. 2009). The Chemical elements in the universe are dominated mainly by hydrogen. Due to its diverse production source becomes a clean and green option for transportation and energy storage (Moradi and Groth 2019).

It will reduce harmful emissions like CO_2, catering to global warming, SOx, and NOx, and prevent the harmful particulates responsible for air pollution. For around a decade, some nations have already paced up to build a successful transportation infrastructure based upon hydrogen. The emissions accounting for the greenhouse gases are between 20 and 100 kg CO_2-equivalent per kg of hydrogen delivered to the vehicles.

Since dihydrogen is very difficult to liquefy and has shallow energy content per unit volume, it possesses storage threat and is difficult to transport. These features limit its use on a broader scale. So, the technologies that involve storing the higher hydrogen content at high pressure and low-temperature conditions suit up the best for the storage (Yu et al. 2017; He et al. 2016). AB is one such source that can meet the requirements (Yu et al. 2017; He et al. 2016; Chandra and Xu 2006; Demirci 2017) as a hydrogen storage carrier, where dehydrogenation can be carried out effectively. Two American research groups, first by Schlesinger (Schaeffer et al. 1951; Schlesinger et al. 1938; Burg and Schlesinger 1937) and second by Shore and Parry (1958, 1955, 1964), carried out the work whose result led to emerging ammonia borane. Schlesinger long sought to synthesize it, and Shore and Parry reported the successful synthesis of ammonia borane.

We must look towards having a means by which hydrogen can be utilized as a fuel carrier with a high volumetric and storage capacity and can be released as per the required demands. Ammonia Borane (H_3N-BH_3, AB) is thus an ideal compound. The hydrogen liberation from AB provides an alternate and economical way to be further used widely as a source of energy production. Ammonia borane (NH_3BH_3, AB) is the simplest B–N hydride, with a low molecular weight of 30.7 g (mol^{-1}) and a very high capacity to store hydrogen (19.6 wt.%). Due to its unique features, such as higher stability, non-toxicity is advantageous in hydrogen storage as a unique material (Kumar et al. 2019). Traditional methods have used porous substances and organic compounds to help adsorb the hydrogen via the principle of van der Waals forces. Still, they are pretty weak, and the result obtained is not so significant to meet the requirements (Bonaccorso et al. 2015; Ren et al. 2017). Other storage techniques involving chemical hydrogen storage involve using alloys, hydrides having

the excellent capability to store high hydrogen content and thus serve as an excellent source for hydrogen utilization (Møller et al. 2017; Li et al. 2019).

To efficiently release hydrogen from ammonia borane, various methods have been adopted, like polymer-supported Pt films (Semiz 2021a), NiRu nanoparticles catalysts (Abay and Rakap 2020), intrazeolite cobalt(0) nanoclusters catalyst (Rakap and Özkar 2010), hydrogen generation via electrochemical methods from AB (Inoue et al. 2012), etc. Using suitable catalysts with varying concentrations and activity can effectively control the hydrogen generation rate from the hydrolysis of AB. For AB to become the efficient material in hydrogen generation, it should be good in the yield and economic aspects. Therefore, the regeneration of AB from spent fuel should be focused upon (Summerscales and Gordon 2013). For AB to serve as a potential source contributor in the hydrogen economy, several energy-efficient methodologies for the regeneration of NH_3BH_3 production has been adopted, like regeneration from BNH-waste products, by direct Reaction with Hydrazine and Liquid Ammonia, a self-contained based on the Catalytic Hydrodechlorination of BCl_3, from reductive dechlorination of BCl_3 to regenerate ammonia borane (Hajari et al. 2021; Hausdorf 2008; Sutton et al. 2011; Reller and Mertens 2012). For a system to be energy-efficient, it is needed to utilize the spent fuel as much as possible. The release of hydrogen is followed by the formation of the spent fuel containing heterogeneous solid BNHx materials that have polymeric nature, and other volatile compounds such as borazine are also released. It is highly flammable and may result in the poisoning of the hydrogen fuel cell if not removed efficiently. Using suitable techniques, this study of dehydrogenation and the efficient Ammonia Borane source's efficient regeneration ensures its regeneration from the dehydrogenated spent fuel materials.

1.1 Hydrogen

Hydrogen is one of the most abundant elements in the universe (Armaroli and Balzani 2011). Hydrogen can be generated from water, biomass, natural gas, coal, etc. Today, hydrogen is mainly produced from natural gas via steam methane reforming (Turner 2004). Liquid hydrogen can be used to move up the wind turbines, but significant energy losses occur due to heat conduction. Thus it is advisable to use the batteries for the power supply to make it more efficient. Utilizing the chemical energy using hydrogen fuel cells is also being practiced these days as it lets the direct conversion of chemical to electrical energy, thus avoiding unnecessary energy losses and it has the highest energy conversion efficiency (~ 60%) when compared with the other energy-producing sources like coal-fired (~ 40%), wind power (~ 50%), solar cell (~ 20), nuclear power (~ 33%), diesel power(~ 35%), and steam gas power (~ 40%).

There are numerous methodologies for the production of hydrogen viz. electrochemical, thermochemical, photochemical, photocatalytic, and photoelectrochemical processes (Kim et al. 2008; Petrov et al. 2011; Pregger et al. 2009; Baghchehsaraee et al. 2010; Voldsund et al. 2016), but these H_2 production technologies face various issues like low efficiency of conversion, storage threat, and

handling (Levin and Chahine 2010). Production of H_2 from agricultural or other waste streams contributes to the production capacity with no net or lower greenhouse gas, increasing flexibility and improving the economics of distributed and semi-centralized reforming.

1.2 Ammonia Borane

The first-ever attempt for the synthesis of ammonia borane took place in 1923. AB has been a considerable hydrogen storage material Li et al. (2014). Previous methods did not successfully synthesize ammonia borane as a diammoniate of diborane, which became difficult to differentiate from AB (Schlesinger et al. 1938; Burg and Schlesinger 1937). Many papers between 1939 and 1948 stated that the diborane structure's diammoniate was NH_3BH_3 (Shore and Parry 1958a). Still, a paper from Parry's in 1958 says that the structure of the diammoniate of diborane is $[NH_3BH_2NH_3][BH_4]$ (Shore and Parry 1958a, b; Schultz and Parry 1958; Parry et al. 1958a; Ramachandran and Kulkarni 2017; Choi et al. 2015; Hu et al. 1977; Heldebrant et al. 2008). NH_3BH_3 was isolated and extensive study was done by them on the generation of AB, particularly with the—NH_4X and MBH_4 metathesis reaction in suitable solvents, through decomposition of diammoniate of borane and in L$\cdot$BH$_3$, we can displace L by ammonia. The synthesis of Ammonia Borane from sodium borohydride and ammonium sulphate takes place under ambient conditions in tetrahydrofuran (THF) at 1 M concentration which uses water as the promoter (Ramachandran and Kulkarni 2017), gives a very high purity (> 99%). Ammonia borane synthesized from diborane and ammonia utilizes a low-temperature process. The synthesized solid AB products have been studied to characterize hydrogen release upon thermal dehydrogenation (Choi et al. 2015) described below by the reaction.

$$LiBH_4 + NH_4Cl \rightarrow NH_4^+ + BH_4^- + LiC \tag{1}$$

$$NH_4 + +BH_{4^-} \rightarrow H_3N - BH_3 + H_2 \tag{2}$$

The general metathesis reaction in the generation of pure AB (Hu et al. 1977; Heldebrant et al. 2008; Kantürk Figen et al. 2013; Ramachandran and Kulkarni 2016; Petit et al. 2016; Semiz 2021b). For dehydrogenation of AB, we can use various catalysts for a higher hydrogen generation rate (Hasenbeck et al. 2020).

2 Ammonia Borane Dehydrogenation

The safe, stable, non-toxic nature and, in addition, lower molecular mass and high solubility make AB an efficient storage for hydrogen (Zhao et al. 2019; Semiz 2020;

Liu et al. 2020; Sevim and Kaplan 2021; Du et al. 2020). In many methods of dehydrogenation, there required a catalyst to achieve a higher generation rate. Therefore, we can use a suitable catalyst with different activities and concentrations to control the hydrogen generation rate. Many metals because of their low price are extensively used like Cu (Li et al. 2020; Furukawa et al. 2019), Co (Xu et al. 2020; Özkar 2020), Ni (Kobayashi and Sunada 2019), Fe (Cui et al. 2018), their oxides (Brooks et al. 2019), bimetallic structures(Miao et al. 2019; Lara et al. 2019). These metals did not perform last long their performances kept on decreasing after each use. Whereas the metals such as Pt (Uzundurukan and Devrim 2019; Xu et al. 2019), Ru (Qiu et al. 2020; Cheng et al. 2020; Liu et al. 2019a; Mao et al. 2020), Pd (Jia et al. 2019; Liu et al. 2019b; Lin et al. 2019; Wen et al. 2020), and Rh (Chen et al. 2020; Sun et al. 2019; Liu et al. 2017) have higher utilization power, but they are costlier than the previous ones. So, it is important to decrease the utilization cost of these metals, which can be done if we can increase the catalytic activity that less amount of catalyst would require for the hydrogen generation.

2.1 Different Methods Used for Dehydrogenation

AB Dehydrogenation via Polymer Supported Platinum (Pt) Film

Using Pt as a catalyst supported on a polynomial substrate can achieve a higher hydrogen generation rate. With the Sputtering technique, we alloy Pt with aluminum, and after the use of NaOH, it was dealloyed. As the sputtering method is used, so the loading of Pt on substrate becomes a positive function of sputtering time. The increase is not strictly linear due to the AB diffusion issue in the interior coating of the catalyst. But after some time rate does not increase even if sputtering time increases.

With the help of surface morphology, many pores and coigns that were less than 100 nm were shown, which can improve the reaction rate by increasing surface area and rate of diffusion of NH_3BH_3 in Pt film (Semiz 2021a). Ammonia borane reaction is carried out in a flask in a tube having water in it. With the water displacement technique, we use to measure the volume of hydrogen which was generated. Using the 50 and 400 W sputtering power of Pt and Al, we can achieve the highest hydrogen generation rate (Semiz 2021a). We can achieve higher durability with similar utility by using an asymmetric membrane as a substrate and having a sputtering power of Al to be 300 W (Semiz 2021a). The solvent composition also affects the rate of hydrogen generation. A higher generation rate of hydrogen (122.3 L H_2 $min^{-1\,g^{-1}}$ catalyst) was achieved when we prepared AB in methanol than water, where the rate of hydrogen generation is achieved only 90.1 L H_2 $min^{-1\,g^{-1}}$ catalyst.

The difference in temperature also affects the rate, a positive function relation is with hydrogen generation, and the temperature was found. The increase in the rate in methanol solution is because of a higher dissociation constant concerning temperature. Because of this release of proton increases which increases the dehydrogenation of the ammonia borane. From the Arrhenius plot, we can calculate

the activation energy. The catalyst having a reliable washing step will conserve its catalytic activity (Semiz 2021a).

AB Dydrogenation via NiRu Nanoparticles as Catalysts

Bimetallic nanocatalysts are recently used in generating hydrogen from boron compounds since the second element added to the first metal brings highly increased catalytic activity to the catalyst due to synergistic effect (Ramachandran and Gagare 2007). We try to synthesize metal nanoparticles by combining cheaper first-row transition elements (like Ni and Co) with the expensive but much more efficient second-row transition element metals (like Ru and Pt) to obtain a cost-effective and more utilizable catalyst. NiRu@PVP nanoparticles are highly effective nanocatalysts to liberate hydrogen gas from ammonia borane by hydrolysis. A well-established strategy efficiently synthesized Ni-Ru@PVP nanoparticles. They provided promising kinetic results to be employed as very efficient catalysts for hydrogen evolution from this significant chemical hydrogen storage material of AB (Abay and Rakap 2020). Synthesis of Ni0.5Ru0.5@PVP nanoparticles can be quickly done from the co-reduction of Ni and Ru salts by the alcohol reduction method. Ni0.5Ru0.5@PVP nanoparticles are determined to be highly efficient nanocatalysts to liberate hydrogen from AB by hydrolysis. The mean TOF value of Ni0.5Ru0.5@PVP nanoparticles in hydrogen liberation from AB is 300 min^{-1}. Provided energy of activation for Ni0.5Ru0.5@PVP nanoparticles in the hydrolysis of AB is 46.8 ± 1.2 kJ mol^{-1} (Abay and Rakap 2020).

Despite this various bimetallic catalysts based upon Ni and Co supported SiO_2 (Ni–M/SiO_2 and Co–M/SiO_2 where M can be Ge, Zn. Ga, Sn) whose potential to act as a catalyst during the dehydrogenation was examined in distilled water/methanol. Compared with the monometallic Ni/SiO_2 and Co/SiO_2, the catalytic activity of Co–Ge/SiO_2 and Ni–Zn/SiO_2 were found to be better (Xu et al. 2020) giving higher hydrogen generation rate.

Dedydrogenation via Hydrolysis of AB Using Intrazeolite Cobalt(0) Nanoclusters as the Catalyst

For an efficient hydrogen release from ammonia borane, we can use a highly active Intrazeolite cobalt(0) nanoclusters catalyst in the hydrolysis of ammonia borane. According to the kinetic study, the hydrolysis of ammonia borane is zero-order for substrate concentration and first-order for catalytic concentration (Rakap and Özkar 2010). The hydrolysis of ammonia borane depends upon the catalytic concentration, substrate concentration, and temperature. We can vary and regulate the cobalt content by changing the slurry's cobalt(II) ion. It is observed that the maximum catalytic activity is obtained when we used intrazeolite cobalt(0) nanoclusters having 0.40 wt% Co. Even after successive runs, the catalyst has good utilization power; it retains 69% of its initial activity in its fifth run; hence, it is an isolable and re-dispersible catalyst in ammonia borane hydrolysis. Therefore due to its catalytic activity and lifetime, this catalyst can be better used in hydrogen generation using AB (Rakap and Özkar 2010).

Hydrogen Generation via Electrochemical Methanolysis of AB

High purity hydrogen independent of AB concentration was produced using methanolysis, and we can regenerate AB using methanolysis product (Heldebrant et al. 2008), which differs in hydrolysis product. Herewith we generate hydrogen via electrochemical methanolysis of AB.

The electrolysis setup had compartment cells separated via filter glass, containing a disk of Pt, Pt plate, Ni plate. A solution of 2 M LiClO$_4$ contained in dry methanol is present in it. AB having different concentrations is dissolved in an electrolyte solution and is used here. With the help of mass spectroscopy and gas chromatography, we can detect hydrogen production in both electrodes and potentiostatic electrolyzes. We can quantitively determine the production of hydrogen with the help of the volumetric method (Heldebrant et al. 2008).

Equation giving AB to hydrogen:

$$\text{Conversion } [\%] = (100 \, nH_2)/(3nNH_3BH_3) \quad (3)$$

where, nH_2 = amount of hydrogen produced [mmol], nNH_3BH_3 = amount of AB [mmol].

The hydrogen production rate increased by 20% when sodium methoxide was added, indicating less catalysis effect on methanolysis by methoxide.

In electrochemical oxidation of AB, hydrogen production can occur by potentiostatic electrolyzes and cyclic voltammograms of AB on Pt anode, which has a 2 M methanol solution of LiClO$_4$. In particular, hydrogen formed at both of the electrodes and < 100% current density at Pt anode present (Inoue et al. 2012).

Dedydrogenation via Hydrolysis by the Use of Limited Water Supply

This concept is generally studied and used when the molar ratio of water to AB is 1.28, 2.57, and 4.50. Hydrogen generation is significantly affected by the rate of injection and water dosage. H$_2$O/AB = 1.28, the case where water is a limiting agent, the production of hydrogen is less than its stoichiometrically. A 100% conversion efficiency of AB reached when H$_2$O/AB = 4.50. Generation of hydrogen takes place via hydrolysis of AB with limited water in Co^{2+}/IR-120 catalyst presence that presents in solid composite form. When H$_2$O/AB = 1.28 and 2.57 by mol, the AB conversion efficiency is less than as predicted by stoichiometry as water evaporation occurs before the hydrolysis, which accounts for the massive loss of exothermic heat. So we should use twice the amount of water than stoichiometric needed, which will be sufficient incomplete AB hydrolysis. The capacity of hydrogen storage reaches 5.33 wt% via the use of a limited water supply (Chou et al. 2012).

Hydrogen Generation via TiO$_2$-Supported RuCo Catalysts from AB

Since hydrogen being dangerous is stored cryogenically or in compressed form, having higher pressure and lower temperature. The strategies adopted usually are expensive (Abe et al. 2019). Thus the need arises to produce a higher yield, higher

release rate, and safer mode that can be achieved by hydrolysis of AB using appropriate catalysts (Zhan et al. 2016; Bhunya et al. 2016). Where sodium borohydride hydrolysis releases four equivalents hydrogen (Eq. 1), the hydrolysis of ammonia borane releases three equivalents of hydrogen (Eq. 2) (Chandra and Xu 2006).

$$NABH_4 + 2H_2O \rightarrow Na + +BO_{2^-} + 4H_2 \qquad \Delta H = -217 \text{ KJ/mol} \qquad (4)$$

$$NH_3BH_3 + 2H_2O \rightarrow NH_4^+ + BO_{2^-} + 3H_2 \qquad \Delta H = -156 \text{ KJ/mol} \qquad (5)$$
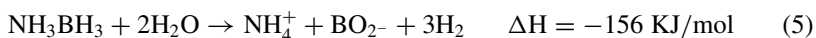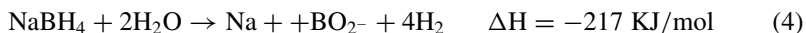
For accelerating dehydrogenation, various catalysts for AB hydrolysis, in which more active is Ru-based catalysts but the higher cost of it create problems in many applications. However, it can be solved using doped non-non-noble metal (such as Co (Li et al. 2015; Wei et al. 2019; Rachiero et al. 2011), Cu (Guo et al. 2019; Coşkuner Filiz et al. 2018; Li and Li 2020), Ni (Chen et al. 2011a, 2012), and Fe (Cao et al. 2014) in the catalysts that can improve the efficiency of Ru. For better dehydrogenation results, catalysts in the nano form performed well due to increased surface area; however, stability is also a concern during the process (Zhang et al. 2021).

Using CPT of Ru_3^+ and Co_2^+, the fabrication of this catalyst was done on TiO_2 nanoparticles surface, which have 40 nm diameter and 64 m^2/g surface area. TiO_2 substrate, based on its availability, stability, and low cost, is better than any other catalyst in supporting metal species. These give better results in hydrolysis of AB in the presence of Co and Ru and are more efficient when alkaline conditions such as NaOH have a higher concentration than 0.5 M (Parry et al. 1958b).

3   AB Regeneration

As AB is an efficient hydrogen storage material, it becomes good the regeneration of AB should be energy efficient and economical in its aspect. An excellent strategy for regeneration should be employed that should give higher yield, be high energy efficient, and be applied to a variety of spent fuel. Dehydrogenation of AB by the thermolysis yield ceramic boron nitride is hard for regeneration; therefore, we can use the route in which incomplete release of H_2 takes place as this is not much difficult as a temperature of 1400 °C and above is required for the entire generation. AB is solid, so for the regeneration of this material, we can add solvent or use off-board treatment.

3.1 Mechanism of AB Regeneration

The dihydrogen has a shallow energy content per unit volume and is very difficult to liquefy (Asadnia and Mehrpooya 2017). Therefore methods involving better hydrogen holding carriers such as amine boranes are needed to be used. After the liberation of the hydrogen, the dehydrogenated spent fuel left behind is required to be recycled. The regeneration of Amine Borane is ensured by taking the thermodynamic parameters of the chemical changes into account. The different synthesis mechanism routes of Ammonia Borane synthesis, such as the Schlesinger process involving the AB from borohydride, require more significant energy consumption and is not very economical while considering the regeneration aspects of AB (Summerscales and Gordon 2013). During the dehydrogenation process of Amine Borane, it is the complete removal of hydrogen (Boron Nitride via thermolysis is produced) (Babenko et al. 2017), which leads to difficulty in the regeneration from the spent fuel.

Thus, for the purpose to regenerate AB, it becomes necessary that some amount of hydrogen is left in the spent fuel, and complete removal/dehydrogenation must be prevented, which can be achieved by controlling the temperature and not carrying the dehydrogenation at very elevated temperatures (1300–1400 °C) (Sutton et al. 2011). Therefore, the approach lies in preventing the production of Boron Nitride type of solid that is hydrogen deprived and supporting the path for producing the B-N-Hx compounds such as aminodiborane, borazine, polyaminoborane, polyborazylene (PB), etc. after the release of 2–2.5 equivalents of hydrogen and have ample boron hydrogen (B–H) and nitrogen hydrogen (N–H) bonds present in the byproducts that can, in turn, regenerate the desired compounds from the spent fuel.

The polyborazylene (PB) thus formed adds an advantage as it has comparatively less energy of formation than the other byproducts formed and is soluble, which confers the recyclability. The properties of AB, such as physical form, melting point, etc., require an apt solvent addition or a proper regeneration treatment system. Such techniques are discussed further regarding the previous research reported for the AB regeneration like Ramachandran et al. studied and carried out the transition metal-catalyzed methanolysis of AB and studied the subsequent regeneration of AB (Ramachandran and Gagare 2007). Sutton et al. used sulfur-based reagent Orthobenzene dithiol (BDT) for the regeneration process of AB from the PB to prevent the formation of B–O bonds that were found to be more stable (Sutton et al. 2011). BDT consisted of B–S bonds that were less stable as compared to the Boron oxygen bonds. It also facilitated the formation of BH_3 fragments by using the BDT, as due to the Sulphur hydrogen bond, the breakdown of the PB was ensured (Sutton et al. 2011). The (BDT)B–H formed were recycled back to AB using Sn–H reagent, but it accounted for the more cost and was not very economical (Sutton et al. 2011). So, a lighter reductant was used by Sutton et al. for the process. Hydrazine is such a lightweight compound that was used for the reduction process as it was able to decompose into hydric hydrogen, nitrogen gas, and a couple of protons (Sutton et al. 2011). THF was used as a solvent for the study of N_2H_4 (Sutton et al. 2011).

Hydrazine converted the PB into BH_3 units, majorly Hydrazine borane (N_2H_4–BH_3, HzB), and some amounts of AB were also produced that were analyzed 11B NMR (Sutton et al. 2011). The reaction between PB and N_2H_4 in the presence of liquid ammonia was carried out at 40 °C for 24 h resulted in the quantitative conversion of PB into BH_3 entities (Sutton et al. 2011).

Multi-step regeneration of Ammonia Borane has three steps: digestion, reduction, and ammoniation, which initially involves the addition of H^+ using a digestion agent HX, adding of H^- by the use of MH agent, and later addition of Ammonia, i.e., ammoniation, respectively (Asadnia and Mehrpooya 2017). The digestion step involves the protonation of the BNHx compounds produced by applying strong acids, alcohols, amines, and thiols. It has been studied that carrying out the digestion process of borates with alcohols is relatively tricky due to its thermodynamic stability. Therefore, for reducing the borates, those digestion processes are preferred that involve the production of weaker BX bonds. Hajari et al. carried out the regeneration of AB from the spent fuel using through digestion mediated B-O-C path, and considerable regeneration of AB (71%) yield was obtained (Hajari et al. 2021).

The reduction step includes the reduction of the digested products by the use of transition metal hydrides; however, over drop must be prevented while the ammoniation process consists of the straightforward and high-yielding regeneration step by the displacement of Lewis base borane compounds such as THF-BH_3 with NH_3 (Chen et al. 2011b) to regenerate AB.

Figure 1 illustrates the mechanism for one-pot regeneration of AB. Upon the dehydrogenation, it liberates > 2 equivalents of H_2 forms the BNHx as the spent fuel, and N_2 is released. Nitrogen reacts with hydrogen according to Haber's process

Fig. 1 Mechanism for one-pot regeneration of AB
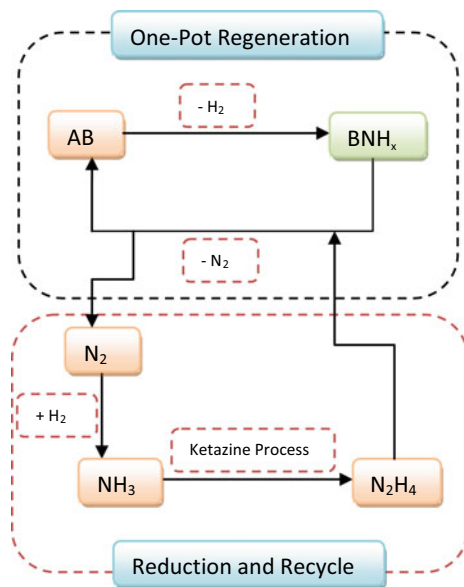
(Baltrusaitis 2017) to form the NH_3. The formed ammonia undergoing Bayer ketazine process (Baumann et al. 2005) includes the hydrazine, which reacts with BNHx to form the AB, and the cycle goes on to regenerate the AB in a single step.

3.2 AB Regeneration via BNH-Waste Products

When hydrogen releases from the ammonia borane, it forms a polymeric waste product. Thus it becomes necessary to carry out an effective procedure for its regeneration. It must involve a recycling strategy that can consume the BNH waste and hydrogen. The primary step consists of the hydrodechlorination of $BCl_3 \cdot$ base adduct in excess base with molecular hydrogen. Generally, a recoverable reactant is used as the base (Hausdorf 2008). Different BNH products are formed when thermal dehydrogenation of ammonia takes place. These are strongly affected by the conditions required for the release of hydrogen (Parry et al. 1958b; Baumann et al. 2005). The following equation will describe the mechanism.

$$BH_3NH_3 \rightarrow BNHx + (3 - (x/2))H_2 \tag{6}$$

$$BNHx + 4HCl \rightarrow BCl_3 + NH_4Cl + (x/2)H_2 \tag{7}$$
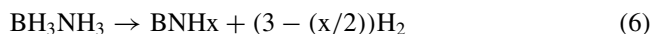
The first process is to treat BNH waste with bronsted acid like HCl in an organic solvent. BNHx (Here x described that it vary with composition) in reaction with HCl converts into BCl_3 and NH_4Cl. The borane having hydride step is energy exhaustive and needs to be monitored. For the second process, an energy-efficient procedure for the BCl_3-hydrodechlorination can be achieved in the presence of hydrogen, and an excess NMe_3 at 200 °C and 2000 bar dehydrodechlorination takes place, which yields 25% BH_3NMe_3. The reaction will be:

$$BCl_3 \cdot NR_3 + 3H_2 + 3NR_3 \rightarrow BH_3 \cdot NR_3 + 3NR_3 \cdot HCl \tag{8}$$
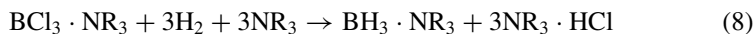
The NR_3 base used here is an auxiliary reactant that tries to influence the thermodynamic property of the reaction. Here, the base NR_3 is recovered.

$$NR_3 \cdot HCl \rightarrow NR_3 + HCl \tag{9}$$
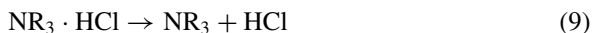
In the process of diborane production, the product mixture is fed with fresh BCl_3.

$$BCl_3 + BH_3 \cdot NR_3 \rightarrow 1/2\,B_2H_6 + BCl_3 \cdot NR_3 \tag{10}$$
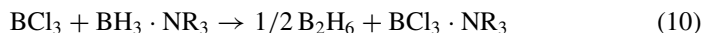
From thermal decomposition of NH_4Cl, ammonia can be recovered that had been produced earlier, or base exchange reaction can also be carried for the recovery of ammonia.

$$NH_4Cl + NR_3 \rightarrow NH_3 + NR_3 \cdot HCl \qquad (11)$$
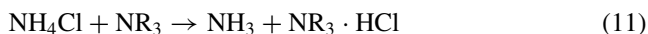
Liquid NR_3 or slurries of NH_4Cl in an organic solvent could be used. The reaction can be made forward if we remove gaseous ammonia from the solution. From the thermal decomposition of $NR_3 \cdot HCl$, we can recover NR_3 and HCl. The last process is to convert ammonia into AB by diborane reaction in the Et_2O to regenerate the AB. The advantage of this concept is that the hydrodechlorination can be carried out several times. The introduction of the weaker base makes the process more economically feasible by lowering the energy requirements. The only difficulty in this process is to ensure the BNH-waste total conversion conditions into BCl_3 and NH_4Cl.

3.3   AB Regeneration from Spent Fuel via BCl₃ Catalytic Hydrodechlorination Route

The low dehydrogenation temperature and exothermic release of hydrogen due to hydridic and protic hydrogen in ammonia borane make it too tricky for direct rehydrogenation/regeneration of AB from spent fuel (Reller and Mertens 2012). In addition to the traditional recycling procedure, Sutton et al. proposed a regeneration route that used hydrazine as a reducing agent (Sutton et al. 2011). The recycling process regenerated the AB from even highly dehydrogenated AB, i.e., using polyborazylene (PB). In the case of highly dehydrogenated species viz. borazine, PB, and cross-linked PB, it was preferred to use $AlCl_3/HCl/CS_2$ as a solvent at 40 bar HCl pressure and 808 °C temperature to form BCl_3 in good yield ~ 90% and ammonium chloride. In the second process, the hydrodehalogenation of BCl3 is required, for which triethylamine is used as an auxiliary reactant forming a BN adduct resulting in Et_3NBCl_3 formation. The third step uses inexpensive hydrogenation catalyst Ni for effective hydrogenation to create Ni borides in the presence of Et_3NBH_3. The last and final step for the AB, the recoverable exchange base in the borane adduct for ammonia, takes place (Reller and Mertens 2012). The reactions of the steps are as follows (Reller and Mertens 2012). Advantages of hydrazine that have been used here can be used for one-pot regeneration synthesis. But must take excellent care as hydrazine is highly unstable and toxic, making it unfit for industrial use (Reller and Mertens 2012).

$$\text{BNH waste} + AlCl_3/HCl/CS_2 \rightarrow BCl_3 + NH_4Cl \qquad (12)$$

$$NH_4Cl \rightarrow NH_3 + HCl \qquad (13)$$

$$BCl_3 + NEt_3 \rightarrow Et_3NBCl_3 \tag{14}$$

$$Et_3NBCl_3 + NiBx/H_2 \rightarrow Et_3NBH_3 + HCl \tag{15}$$

$$Et_3NBH_3 + NH_3 \rightarrow BH_3NH_3 + Et_3N \tag{16}$$
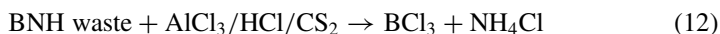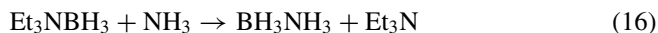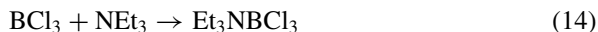
3.4 Effective AB Regeneration via Reductive Dechlorination of BCl₃ Route

Primitive adopted regenerative strategies possess a great challenge like the non-recyclability of a reductant, limiting their success for industrial use (Babenko et al. 2017). Mertens and Reller have suggested a new strategy that used HCl–AlCl₃–CS₂ compound digesting t Hydrogen-depleted AB with 90% yield of BCl_3 and 60% yield using the reduction and the base-exchange steps via H_2–Ni_3B–Et_3N (Reller and Mertens 2012). But the low product, high-temperature ammonia reaction does not make it suitable to carry out. Therefore, adopted a new strategy that made in recycle of reductive dechlorination of BCl_3 easier. It used Bu_3SnH reagent as a reducing reagent to inhibit the unwanted Cl–M products.

In the initial stage, the NH_3 is to be passed to the soda-lime column for effective purification so that the reaction between Bu_3SnH and BCl_3 using helper ligand Et_2PhN at a temperature of 60 °C takes place to yield $Et_2PhN·BH_3$ (Tan et al. 2015). After that, Et_2PhN formed is replaced by the NH_3 produces the AB of about 5% due to base-exchange reaction. The reactions are as follows.

$$6Bu_3SnH + 2BCl_3 \rightarrow B_2H_6 + 6Bu_3SnCl \tag{17}$$

$$B_2H_6 + 2Et_2PhN \rightarrow Et_2PhNBH_3 \tag{18}$$

$$Et_2PhNBH_3 + NH_3 \rightarrow Et_2PhN + NH_3BH_3 \tag{19}$$
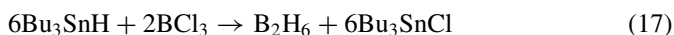
This two-step process helps improve the overall efficiency of this recycling process, and as a result, an all-around good yield of 89% AB is (Tan et al. 2015).

4 Conclusion

Since we discussed various methodologies and routes for the effective dehydrogenation and regeneration of AB viz. generating the hydrogen via polymer-supported

Pt films, using NiRu nanoparticles catalysts, using nanoclusters catalyst intrazeolite cobalt(0) for carrying out the AB hydrolysis, electrochemical methods, from hydrolysis of AB, from AB hydrolysis catalyzed by TiO_2-supported RuCo catalysts and Ni and Co-based bimetallic catalysts, these methods were discussed and their preparation been briefly described. The mechanism, along with the reaction for the same, was thoroughly discussed. For AB to become an efficient material for hydrogen storage, different regeneration routes have also been described. BNH-waste products, based on BCl3 catalytic hydrochlorination and reductive dechlorination of BCl3 used for efficient AB regeneration. It demonstrates how effectively AB can be regenerated with a higher yield and good yield efficiency. However, more emphasis and research on the economic aspects of the methods mentioned above are also required.

References

Abay B, Rakap M (2020) Hydrogen generation from ammonia borane by NiRu nanoparticles catalysts. Inorg Nano-Metal Chem. https://doi.org/10.1080/24701556.2020.1815776

Abe JO, Popoola API, Ajenifuja E, Popoola OM (2019) Hydrogen energy, economy and storage: review and recommendation. Int J Hydrogen Energy 44(29):15072–15086. https://doi.org/10.1016/J.IJHYDENE.2019.04.068

Armaroli N, Balzani V (2011) The hydrogen issue. ChemSusChem 4(1). https://doi.org/10.1002/cssc.201000182

Asadnia M, Mehrpooya M (2017) A novel hydrogen liquefaction process configuration with combined mixed refrigerant systems. Int J Hydr Energy 42(23). https://doi.org/10.1016/j.ijhydene.2017.04.260

Babenko V et al (2017) Time dependent decomposition of ammonia borane for the controlled production of 2D hexagonal boron nitride. Sci Rep 7(1). https://doi.org/10.1038/s41598-017-14663-8

Baghchehsaraee B, Nakhla G, Karamanev D, Margaritis A (2010) Fermentative hydrogen production by diverse microflora. Int J Hydr Energy 35(10). https://doi.org/10.1016/j.ijhydene.2009.08.072

Baltrusaitis J (2017) Sustainable ammonia production. ACS Sustain Chem Eng 5(11). https://doi.org/10.1021/acssuschemeng.7b03719

Baumann J, Baitalow F, Wolf G (2005) Thermal decomposition of polymeric aminoborane (H2BNH2)x under hydrogen release. Thermochim Acta 430(1–2):9–14. https://doi.org/10.1016/J.TCA.2004.12.002

Bhunya S, Malakar T, Ganguly G, Paul A (2016) Combining protons and hydrides by homogeneous catalysis for controlling the release of hydrogen from ammonia–borane: present status and challenges. ACS Catal 6(11). https://doi.org/10.1021/acscatal.6b01704

Bonaccorso F et al (2015) Graphene, related two-dimensional crystals, and hybrid systems for energy conversion and storage. Science 347(6217). https://doi.org/10.1126/science.1246501

Brooks RM, Maafa IM, Al-Enizi AM, El-Halwany MM, Ubaidullah M, Yousef A (2019) Electrospun Bimetallic NiCr Nanoparticles@Carbon nanofibers as an efficient catalyst for hydrogen generation from ammonia borane. Nanomaterials 9(8). https://doi.org/10.3390/nano9081082

Burg AB, Schlesinger HI (1937) Hydrides of Boron. VII. evidence of the transitory existence of borine (BH_3): borine carbonyl and borine trimethylammine. J Am Chem Soc 59(5). https://doi.org/10.1021/ja01284a002

Cao N, Su J, Hong X, Luo W, Cheng G (2014) In situ facile synthesis of Ru-based core-shell nanoparticles supported on carbon black and their high catalytic activity in the dehydrogenation of amine-boranes. Chem Asian J 9(2). https://doi.org/10.1002/asia.201301171

Chandra M, Xu Q (2006a) A high-performance hydrogen generation system: transition metal-catalyzed dissociation and hydrolysis of ammonia–borane. J Power Sources 156(2):190–194. https://doi.org/10.1016/J.JPOWSOUR.2005.05.043

Chandra M, Xu Q (2006b) Dissociation and hydrolysis of ammonia-borane with solid acids and carbon dioxide: an efficient hydrogen generation system. J Power Sources 159(2):855–860. https://doi.org/10.1016/J.JPOWSOUR.2005.12.033

Chen G, Desinan S, Nechache R, Rosei R, Rosei F, Ma D (2011a) Bifunctional catalytic/magnetic Ni@Ru core–shell nanoparticles. Chem Commun 47(22). https://doi.org/10.1039/c1cc10619h

Chen X, Bao X, Zhao J-C, Shore SG (2011b) Experimental and computational study of the formation mechanism of the diammoniate of diborane: the role of dihydrogen bonds. J Am Chem Soc 133(36). https://doi.org/10.1021/ja203648w

Chen G, Desinan S, Rosei R, Rosei F, Ma D (2012) Synthesis of Ni-Ru alloy nanoparticles and their high catalytic activity in dehydrogenation of ammonia borane. Chem Eur J 18(25). https://doi.org/10.1002/chem.201200292

Chen Y, Chen Q, Fan G (2020) Smart construction of oxidized-Ti3C2TX stabilized Rh nanoparticles for remarkable improving the catalytic performance for ammonia borane hydrolysis. Int J Hydr Energy 45(53). https://doi.org/10.1016/j.ijhydene.2020.07.255

Cheng W, Zhao X, Luo W, Zhang Y, Wang Y, Fan G (2020) Bagasse-derived carbon-supported Ru nanoparticles as catalyst for efficient dehydrogenation of ammonia borane. ChemNanoMat 6(8). https://doi.org/10.1002/cnma.202000215

Choi HY et al (2015) Low-temperature synthesis of ammonia borane using diborane and ammonia. Int J Hydr Energy 40(35). https://doi.org/10.1016/j.ijhydene.2015.03.100

Chou C-C, Lee D-J, Chen B-H (2012) Hydrogen production from hydrolysis of ammonia borane with limited water supply. Int J Hydr Energy 37(20). https://doi.org/10.1016/j.ijhydene.2012.05.108

Conte M, di Mario F, Iacobazzi A, Mattucci A, Moreno A, Ronchetti M (2009) Hydrogen as future energy carrier: the ENEA point of view on technology and application prospects. Energies 2(1). https://doi.org/10.3390/en20100150

Coşkuner Filiz B, Kantürk Figen A, Pişkin S (2018) The remarkable role of metal promoters on the catalytic activity of Co-Cu based nanoparticles for boosting hydrogen evolution: ammonia borane hydrolysis. Appl Catal B: Environ 238:365–380. https://doi.org/10.1016/J.APCATB.2018.07.031

Cui L, Cao X, Sun X, Yang W, Liu J (2018) A bunch-like copper oxide nanowire array as an efficient, durable, and economical catalyst for the methanolysis of ammonia borane. ChemCatChem 10(4). https://doi.org/10.1002/cctc.201701317

Demirci UB (2017) Impact of H.I. Schlesinger's discoveries upon the course of modern chemistry on B−(N−)H hydrogen carriers. Int J Hydrogen Energy 42(33):21048–21062. https://doi.org/10.1016/J.IJHYDENE.2017.07.066

Du J, Hou J, Li B, Qin R, Xu C, Liu H (2020) Support-free 3D hierarchical nanoporous Cu@Cu2O for fast tandem ammonia borane dehydrogenation and nitroarenes hydrogenation under mild conditions. J Alloys Compound 815. https://doi.org/10.1016/j.jallcom.2019.152372

Elam C (2003) Realizing the hydrogen future: the International Energy Agency's efforts to advance hydrogen energy technologies. Int J Hydr Energy 28(6). https://doi.org/10.1016/S0360-3199(02)00147-7

Furukawa S, Nishimura G, Takayama T, Komatsu T (2019) Highly active Ni- and Co-based bimetallic catalysts for hydrogen production from ammonia-borane. Front Chem 7. https://doi.org/10.3389/fchem.2019.00138

Geng S, Yang W, Yu YS (2019) Building MoS2/S-doped g-C3N4 layered heterojunction electrocatalysts for efficient hydrogen evolution reaction. J Catal 375. https://doi.org/10.1016/j.jcat.2019.06.026

Guo K, Ding Y, Luo J, Gu M, Yu Z (2019) NiCu bimetallic nanoparticles on silica support for catalytic hydrolysis of ammonia borane: composition-dependent activity and support size effect. ACS Appl Energy Mater 2(8). https://doi.org/10.1021/acsaem.9b00997

Hajari A, Roy B, Kumar V, Bishnoi A, Sharma P (2021) Regeneration of supported ammonia borane to achieve higher yield. ChemistrySelect 6(6). https://doi.org/10.1002/slct.202004833

Hasenbeck M, Becker J, Gellrich U (2020) Efficient organocatalytic dehydrogenation of ammonia borane. Angewandte Chemie Int Ed 59(4). https://doi.org/10.1002/anie.201910636

Hausdorf S (2008) A procedure for the regeneration of ammonia borane from BNH-waste products. Int J Hydr Energy 33(2). https://doi.org/10.1016/j.ijhydene.2007.10.035

He T, Pachfule P, Wu H, Xu Q, Chen P (2016) Hydrogen carriers. Nat Rev Mater 1(12). https://doi.org/10.1038/natrevmats.2016.59

Heldebrant DJ, Karkamkar A, Linehan JC, Autrey T (2008) Synthesis of ammonia borane for hydrogen storage applications. Energy Environ. Sci 1(1). https://doi.org/10.1039/b808865a

Hu MG, van Paasschen JM, Geanangel RA (1977) New synthetic approaches to ammonia-borane and its deuterated derivatives. J Inorg Nucl Chem 39(12):2147–2150. https://doi.org/10.1016/0022-1902(77)80383-7

Inoue H, Yamazaki T, Kitamura T, Shimada M, Chiku M, Higuchi E (2012) Electrochemical hydrogen production system from ammonia borane in methanol solution. Electrochimica Acta 82. https://doi.org/10.1016/j.electacta.2012.05.091

Jain IP (2009) Hydrogen the fuel for 21st century. Int J Hydrogen Energy 34(17):7368–7378. https://doi.org/10.1016/J.IJHYDENE.2009.05.093

Jia H, Liu S, Zheng G-P, Zheng X-C, Wang X-Y, Liu P (2019) Collagen-graphene oxide magnetic hybrids anchoring Pd(0) catalysts for efficient H2 generation from ammonia borane. Int J Hydr Energy 44(49). https://doi.org/10.1016/j.ijhydene.2019.08.159

Kaiwen L, Bin Y, Tao Z (2018) Economic analysis of hydrogen production from steam reforming process: a literature review. Energy Sour Part B: Econ Plan Policy 13(2). https://doi.org/10.1080/15567249.2017.1387619

Kantürk Figen A, Pişkin MB, Coşkuner B, Imamoğlu V (2013) Synthesis, structural characterization, and hydrolysis of Ammonia Borane (NH3BH3) as a hydrogen storage carrier. Int J Hydr Energy 38(36):16215–16228. https://doi.org/10.1016/J.IJHYDENE.2013.10.033

Kim J-M et al (2008) Decomposition of hydrogen iodide on Pt/C-based catalysts for hydrogen production. Int J Hydr Energy 33(19). https://doi.org/10.1016/j.ijhydene.2008.05.092

Kobayashi Y, Sunada Y (2019) A four coordinated Iron(II)-digermyl complex as an effective precursor for the catalytic dehydrogenation of ammonia borane. Catalysts 10(1). https://doi.org/10.3390/catal10010029

Kumar R, Karkamkar A, Bowden M, Autrey T (2019) Solid-state hydrogen rich boron–nitrogen compounds for energy storage. Chem Soc Rev 48(21). https://doi.org/10.1039/C9CS00442D

Lara P, Philippot K, Suárez A (2019) Phosphane-decorated platinum nanoparticles as efficient catalysts for H_2 generation from ammonia borane and methanol. ChemCatChem 11(2). https://doi.org/10.1002/cctc.201801702

Levin DB, Chahine R (2010) Challenges for renewable hydrogen production from biomass. Int J Hydr Energy 35(10). https://doi.org/10.1016/j.ijhydene.2009.08.067

Li Y, Li S (2020) Low-cost CuFeCo@MIL-101 as an efficient catalyst for catalytic hydrolysis of ammonia borane. Int J Hydrogen Energy 45(17):10433–10441. https://doi.org/10.1016/J.IJHYDENE.2019.06.075

Li H, Yang Q, Chen X, Shore SG (2014) Ammonia borane, past as prolog. J Organomet Chem 751. https://doi.org/10.1016/j.jorganchem.2013.08.044

Li X, Zeng C, Fan G (2015) Magnetic RuCo nanoparticles supported on two-dimensional titanium carbide as highly active catalysts for the hydrolysis of ammonia borane. Int J Hydrogen Energy 40(30):9217–9224. https://doi.org/10.1016/J.IJHYDENE.2015.05.168

Li L, Huang Y, An C, Wang Y (2019) Lightweight hydrides nanocomposites for hydrogen storage: challenges, progress and prospects. Sci China Mater 62(11). https://doi.org/10.1007/s40843-019-9556-1

Li J, Ren X, Lv H, Wang Y, Li Y, Liu B (2020) Highly efficient hydrogen production from hydrolysis of ammonia borane over nanostructured Cu@CuCoOx supported on graphene oxide. J Hazard Mater 391. https://doi.org/10.1016/j.jhazmat.2020.122199

Lin H et al (2019) Facile and eco-friendly synthesis of porous carbon nanosheets as ideal platform for stabilizing rhodium nanoparticles in efficient hydrolysis of ammonia borane. Int J Hydr Energy 44(39). https://doi.org/10.1016/j.ijhydene.2019.06.072

Liu P, Gu X, Kang K, Zhang H, Cheng J, Su H (2017) Highly efficient catalytic hydrogen evolution from ammonia borane using the synergistic effect of crystallinity and size of noble-metal-free nanoparticles supported by porous metal–organic frameworks. ACS Appl Mater Interf 9(12). https://doi.org/10.1021/acsami.7b01161

Liu Y, Yong X, Liu Z, Chen Z, Kang Z, Lu S (2019a) Unified catalyst for efficient and stable hydrogen production by both the electrolysis of water and the hydrolysis of ammonia borane. Adv Sustain Syst 3(5). https://doi.org/10.1002/adsu.201800161

Liu S, Chen X, Wu Z-J, Zheng X-C, Peng Z-K, Liu P (2019b) Chitosan-reduced graphene oxide hybrids encapsulated Pd(0) nanocatalysts for H2 generation from ammonia borane Int J Hydr Energy 44(42). https://doi.org/10.1016/j.ijhydene.2019.07.088

Liu M, Zhou L, Luo X, Wan C, Xu L (2020) Recent advances in noble metal catalysts for hydrogen production from ammonia borane. Catalysts 10(7). https://doi.org/10.3390/catal10070788

Manoharan Y et al (2019) Hydrogen fuel cell vehicles; Current status and future prospect. Appl Sci 9(11). https://doi.org/10.3390/app9112296

Mao M, Chen Q, Wu J, Fan G (2020) Anchoring and space-confinement effects to synthesize ultrasmall Pd nanoparticles for efficient ammonia borane hydrolysis. Int J Hydr Energy 45(51). https://doi.org/10.1016/j.ijhydene.2020.07.097

Miao H, Ma K, Zhu H, Yin K, Zhang Y, Cui Y (2019) Ammonia borane dehydrogenation and selective hydrogenation of functionalized nitroarene over a porous nickel–cobalt bimetallic catalyst. RSC Adv 9(26). https://doi.org/10.1039/C9RA01551E

Midilli A, Dincer I (2008) Hydrogen as a renewable and sustainable solution in reducing global fossil fuel consumption. Int J Hydrogen Energy 33(16):4209–4222. https://doi.org/10.1016/J.IJHYDENE.2008.05.024

Midilli A, Ay M, Dincer I, Rosen MA (2005) On hydrogen and hydrogen energy strategies. Renew Sustain Energy Rev 9(3). https://doi.org/10.1016/j.rser.2004.05.003

Møller KT, Jensen TR, Akiba E, wen Li H (2017) Hydrogen—a sustainable energy carrier. Progr Nat Sci Mater Int 27(1):34–40. https://doi.org/10.1016/J.PNSC.2016.12.014

Moradi R, Groth KM (2019) Hydrogen storage and delivery: review of the state of the art technologies and risk and reliability analysis. Int J Hydrogen Energy 44(23):12254–12269. https://doi.org/10.1016/J.IJHYDENE.2019.03.041

Nicoletti G, Arcuri N, Nicoletti G, Bruno R (2015) A technical and environmental comparison between hydrogen and some fossil fuels. Energy Convers Manage 89:205–213. https://doi.org/10.1016/J.ENCONMAN.2014.09.057

Özkar S (2020) Transition metal nanoparticle catalysts in releasing hydrogen from the methanolysis of ammonia borane. Int J Hydr Energy 45(14). https://doi.org/10.1016/j.ijhydene.2019.04.125

Parry RW, Shore SG (1958) Chemical evidence for the structure of the 'diammoniate of diborane.' IV. The reaction of sodium with lewis acids in liquid ammonia. J Am Chem Soc 80(1). https://doi.org/10.1021/ja01534a005

Parry RW, Kodama G, Schultz DR (1958a) Molecular weight measurements in liquid ammonia. The molecular weights of the methylamine-boranes, the 'Diammoniate of Diborane'. Ammonia-boron trifluoride and other substances. J Am Chem Soc 80(1). https://doi.org/10.1021/ja01534a007

Parry RW, Schultz DR, Girardot PR (1958b) The preparation and properties of hexamminecobalt(iii) borohydride, hexamminechromium(iii) borohydride and ammonium borhydride. J Am Chem Soc 80(1). https://doi.org/10.1021/ja01534a001

Petit JF, Miele P, Demirci UB (2016) Ammonia borane H3NBH3 for solid-state chemical hydrogen storage: different samples with different thermal behaviors. Int J Hydrogen Energy 41(34):15462–15470. https://doi.org/10.1016/J.IJHYDENE.2016.06.097

Petrov K, Baykara SZ, Ebrasu D, Gulin M, Veziroglu A (2011) An assessment of electrolytic hydrogen production from H2S in Black Sea waters. Int J Hydr Energy 36(15). https://doi.org/10.1016/j.ijhydene.2011.04.022

Pregger T, Graf D, Krewitt W, Sattler C, Roeb M, Möller S (2009) Prospects of solar thermal hydrogen production processes. Int J Hydr Energy 34(10). https://doi.org/10.1016/j.ijhydene.2009.03.025

Qiu X et al (2020) Hydrolytic dehydrogenation of $NH_3\,BH_3$ catalyzed by ruthenium nanoparticles supported on magnesium–aluminum layered double-hydroxides. RSC Adv 10(17). https://doi.org/10.1039/D0RA01720E

Rachiero GP, Demirci UB, Miele P (2011) Bimetallic RuCo and RuCu catalysts supported on γ-Al_2O_3. A comparative study of their activity in hydrolysis of ammonia-borane. Int J Hydrogen Energy 36(12):7051–7065. https://doi.org/10.1016/J.IJHYDENE.2011.03.009

Rakap M, Özkar S (2010) Hydrogen generation from the hydrolysis of ammonia-borane using intrazeolite cobalt(0) nanoclusters catalyst. Int J Hydr Energy 35(8). https://doi.org/10.1016/j.ijhydene.2010.01.138

Ramachandran PV, Gagare PD (2007) Preparation of ammonia borane in high yield and purity, methanolysis, and regeneration. Inorg Chem 46(19). https://doi.org/10.1021/ic700772a

Ramachandran PV, Kulkarni AS (2016) The role of ammonia in promoting ammonia borane synthesis. Dalton Trans 45(41). https://doi.org/10.1039/C6DT02925F

Ramachandran PV, Kulkarni AS (2017) Water-promoted, safe and scalable preparation of ammonia borane. Int J Hydrogen Energy 42(2):1451–1455. https://doi.org/10.1016/J.IJHYDENE.2016.06.231

Reller C, Mertens FORL (2012) A self-contained regeneration scheme for spent ammonia borane based on the catalytic Hydrodechlorination of BCl_3, Angewandte Chemie Int Ed 51(47). https://doi.org/10.1002/anie.201201134

Ren J, Musyoka NM, Langmi HW, Mathe M, Liao S (2017) Current research trends and perspectives on materials-based hydrogen storage solutions: a critical review. Int J Hydrogen Energy 42(1):289–311. https://doi.org/10.1016/J.IJHYDENE.2016.11.195

Schaeffer GW, Schaeffer R, Schlesinger HI (1951) The preparation of Borazole and its reactions with boron halides. J Am Chem Soc 73(4). https://doi.org/10.1021/ja01148a059

Schlesinger HI, Burg AB (1938) Hydrides of Boron. VIII. The structure of the diammoniate of diborane and its relation to the structure of diborane. J Am Chem Soc 60(2). https://doi.org/10.1021/ja01269a020

Schultz DR, Parry RW (1958) Chemical evidence for the structure of the 'Diammoniate of Diborane' I. Evidence for the borohydride ion and for the Dihydro-diammineboron(III) cation. J Am Chem Soc 80(1). https://doi.org/10.1021/ja01534a002

Semiz L (2020) Hydrogen generation from ammonia borane by chemically dealloyed platinum nanoparticles. React Kinet Mechan Catal 129(1). https://doi.org/10.1007/s11144-019-01700-y

Semiz L (2021) Hydrogen generation from ammonia borane by polymer supported platinum films. Chem Phys Lett 767. https://doi.org/10.1016/j.cplett.2021.138365

Semiz L (2021) Dehydrogenation of ammonia borane by dealloyed ruthenium catalysts. Inorg Nano-Metal Chem 51(1). https://doi.org/10.1080/24701556.2020.1749853

Sevim M, Kaplan F (2021) Ketjen black supported monodisperse nickel–platinum alloy nanoparticles for the efficient catalyst in the hydrolytic dehydrogenation of ammonia borane. Appl Org Chem 35(2). https://doi.org/10.1002/aoc.6095

Shore SG, Boddeker KW (1964) Large scale synthesis of $H_2B(NH_3)_2 + BH_4$- and H_3NBH_3. Inorg Chem 3(6). https://doi.org/10.1021/ic50016a038

Shore SG, Parry RW (1955) The crystalline compound ammonia-borane, $^1H_3NBH_3$. J Am Chem Soc 77(22). https://doi.org/10.1021/ja01627a103

Shore SG, Parry RW (1958a) Chemical evidence for the structure of the 'Diammoniate of Diborane' II. The preparation of ammonia-borane. J Am Chem Soc 80(1). https://doi.org/10.1021/ja01534a003

Shore SG, Parry RW (1958b) Chemical evidence for the structure of the 'Diammoniate of Diborane' III. The reactions of borohydride salts with lithium halides and aluminum chloride. J Am Chem Soc 80(1). https://doi.org/10.1021/ja01534a004

Stephens FH, Pons V, Tom Baker R (2007) Ammonia–borane: the hydrogen source par excellence? Dalton Trans 25. https://doi.org/10.1039/B703053C

Summerscales OT, Gordon JC (2013) Regeneration of ammonia borane from spent fuel materials. Dalton Trans 42(28). https://doi.org/10.1039/c3dt50475a

Sun Q et al (2019) Zeolite-encaged single-atom rhodium catalysts: highly-efficient hydrogen generation and shape-selective tandem hydrogenation of nitroarenes. Angewandte Chemie Int Ed 58(51). https://doi.org/10.1002/anie.201912367

Sutton AD et al (2011) Regeneration of ammonia borane spent fuel by direct reaction with hydrazine and liquid ammonia. Science 331(6023). https://doi.org/10.1126/science.1199003

Tan Y, Zhang L, Chen X, Yu X (2015) Reductive dechlorination of BCl_3 for efficient ammonia borane regeneration. Dalton Trans 44(2). https://doi.org/10.1039/C4DT01592D

Turner JA (2004) Sustainable hydrogen production. Science 305(5686). https://doi.org/10.1126/science.1103197

Uzundurukan A, Devrim Y (2019) Carbon nanotube-graphene hybrid supported platinum as an effective catalyst for hydrogen generation from hydrolysis of ammonia borane. Int J Hydr Energy 44(49). https://doi.org/10.1016/j.ijhydene.2019.08.153

Veziroğlu TN, Şahın S (2019) 21st Century's energy: hydrogen energy system. Altern Energy Ecol (ISJAEE) 4–6. https://doi.org/10.15518/isjaee.2019.04-06.014-027

Voldsund M, Jordal K, Anantharaman R (2016) Hydrogen production with CO2 capture. Int J Hydr Energy 41(9). https://doi.org/10.1016/j.ijhydene.2016.01.009

Wei Z et al (2019) Cobalt-ruthenium nanoalloys parceled in porous nitrogen-doped graphene as highly efficient difunctional catalysts for hydrogen evolution reaction and hydrolysis of ammonia borane. ACS Sustain Chem Eng 7(7). https://doi.org/10.1021/acssuschemeng.8b06745

Wen Z, Wu J, Fan G (2020) Facile fabrication of rhodium/nanodiamond hybrid as advanced catalyst toward hydrogen production from ammonia–borane. Catalysts 10(9). https://doi.org/10.3390/catal10091037

Xu C, Wang H, Wang Q, Wang Y, Zhang Y, Fan G (2019) Ruthenium coordinated with triphenylphosphine-hyper-crosslinked polymer: an efficient catalyst for hydrogen evolution reaction and hydrolysis of ammonia borane. Appl Surf Sci 466. https://doi.org/10.1016/j.apsusc.2018.10.051

Xu S-H, Wang J-F, Guo J-P, Zhang W-Y, de Souza AAU, He D-N (2020) Activating Co nanoparticles on P-doped carbon nitride via enhancing Mott-Schottky effect by constructing interfacial chemical bonding for the efficient dehydrogenation of ammonia-borane. Appl Surf Sci 533. https://doi.org/10.1016/j.apsusc.2020.146999

Yu X, Tang Z, Sun D, Ouyang L, Zhu M (2017) Recent advances and remaining challenges of nanostructured materials for hydrogen storage applications. Prog Mater Sci 88:1–48. https://doi.org/10.1016/J.PMATSCI.2017.03.001

Zhan W-W, Zhu Q-L, Xu Q (2016) Dehydrogenation of ammonia borane by metal nanoparticle catalysts. ACS Catal 6(10). https://doi.org/10.1021/acscatal.6b02209

Zhang J, Li J, Yang L, Li R, Zhang F, Dong H (2021) Efficient hydrogen production from ammonia borane hydrolysis catalyzed by TiO2-supported RuCo catalysts. Int J Hydr Energy 46(5). https://doi.org/10.1016/j.ijhydene.2020.10.234

Zhao W, Wang R, Wang Y, Feng J, Li C, Chen G (2019) Effect of LDH composition on the catalytic activity of Ru/LDH for the hydrolytic dehydrogenation of ammonia borane. Int J Hydr Energy 44(29). https://doi.org/10.1016/j.ijhydene.2019.04.052

Water Conservation Strategies and Opportunities for Sustainability of Pulp and Paper Sector—An Overview of Recent Trends

Nitin Endlay, Mohd Salim, Amitabh Raj Tripathi, Abhishek Tyagi, and M. K. Gupta

Abstract Water is an integral medium for pulp and paper making. Though the Indian Paper Industry is traditionally considered to be a water intensive industry, but actually around 90% of the water consumed is discharged as waste water implying industry is not a water guzzler actually. Today with increasing water scarcity, dwindling ground water resources, increasing environmental awareness and efforts to improve river water quality through minimization of industrial discharge into the river, introduction of new regulatory norms on fresh water consumption and wastewater discharge as well as stringent pollution norms in offing, the onus has come upon pulp and paper mills to adopt appropriate strategies and approach, state of art technologies, equipments and treatment systems to achieve the environmental compliance. In this context CPPRI has provided assistance and guidance to pulp and paper mills in water conservation/optimization of fresh water consumption and have helped several pulp and paper mills specially in river Ganga Basin and river Hindon sub-basin in reducing fresh water consumption, waste water discharge and pollution load leading to overall improvement in environmental status and sustainability. Adoption of "Bare Minimum Technologies (BMT)" including energy efficient as well as clean and green technologies like continuous digesters, improved pulp washing systems, oxygen delignification, elemental chlorine free bleaching, fiber recovery system, modifications in showers on paper machine, upgradation of existing ETP up to tertiary treatment system, adoption of chemical recovery system (for agro based mills), strategies and identification of areas for reuse and recycling of back water and treated effluent etc. as well as optimization of various key process operation variables have been key factor in reducing the water foot print of many pulp and paper mills in recent times. In addition, studies are under progress at CPPRI on evaluation of potential of membrane filtration system in reducing pollution load specially Total Dissolved Solids (TDS), Color and Lignin (a major bottleneck in reuse/recycling of treated effluent). The treated water quality achieved is suitable for reuse/recycle in various operations of pulp and paper making which can facilitate reduction in water

N. Endlay (✉) · M. Salim · A. R. Tripathi · A. Tyagi · M. K. Gupta
Environmental Management Division, Central Pulp and Paper Research Institute, Saharanpur, Uttar Pradesh 247001, India
e-mail: endlay.nitin@cppri.res.in

footprint of pulp and paper mills to a greater extent. The present paper highlights a few such trends or success stories of pulp and paper sector which has helped in significant water conservation.

Keywords Bare minimum technologies · Oxygen delignification · Elemental chlorine free bleaching · Membrane filtration

1 Introduction

Water is an integral medium for pulp and paper making. From raw material cleaning to manufacture of finished paper water is used for various purpose like raw material/pulp washing, pulp dilution, chemical preparation, pulp transportation, wire and felt cleaning, vacuum pulp sealing, gland cooling, etc. Thus almost all the steps in paper making as indicated in Fig 1 are carried out with use of water or back water/recycled water. However, it is to be noted that only 8–10% of the total fresh water actually consumed for paper making while the rest is discharged as waste water which is treated in Effluent Treatment Plant so as to meet the discharge norms prior to discharge in any receiving body or reuse/recycle for paper making.

The general characteristics of Effluent/Wastewater generated from different process operations in pulp and paper making are given in Table 1.

In recent times, with increased emphasis by regulatory authorities on reducing the fresh water consumption and consequently waste water discharge, enforcement of stringent norms under **Charter for "Water Recycling and Pollution Prevention in Pulp and Paper Industries in Ganga River Basin"** (Tables 2 and 3) and likely revision of national norms on the same lines, regular monitoring of Grossly Polluting Industries by State and Central Pollution Control Board on periodical basis, increased restriction on drawl of ground water by Central Ground Water Authority (CGWA), the traditionally water intensive industry like pulp and paper industry have a great challenge at hand to sustain themselves through meeting environmental compliance.

To meet the challenge, the pulp and paper mills need to adopt appropriate strategies which include multi disciplinary approach like at source reduction of pollution load through adoption of appropriate technologies, resource conservation (fiber, water, chemicals etc.), process optimization, incorporation of fiber recovery systems, ETP upgaradtion/modification for increased reuse and recycling of back water and treated effluent etc.

In recent times, CPPRI has assisted many pulp and paper mills in implementation of various strategies/technologies to address the imminent issues affecting their environmental sustainability. This paper highlights some of such strategies/approaches adopted by pulp and paper mills in various areas of paper making as mentioned under to become environmental compliant and sustainable.
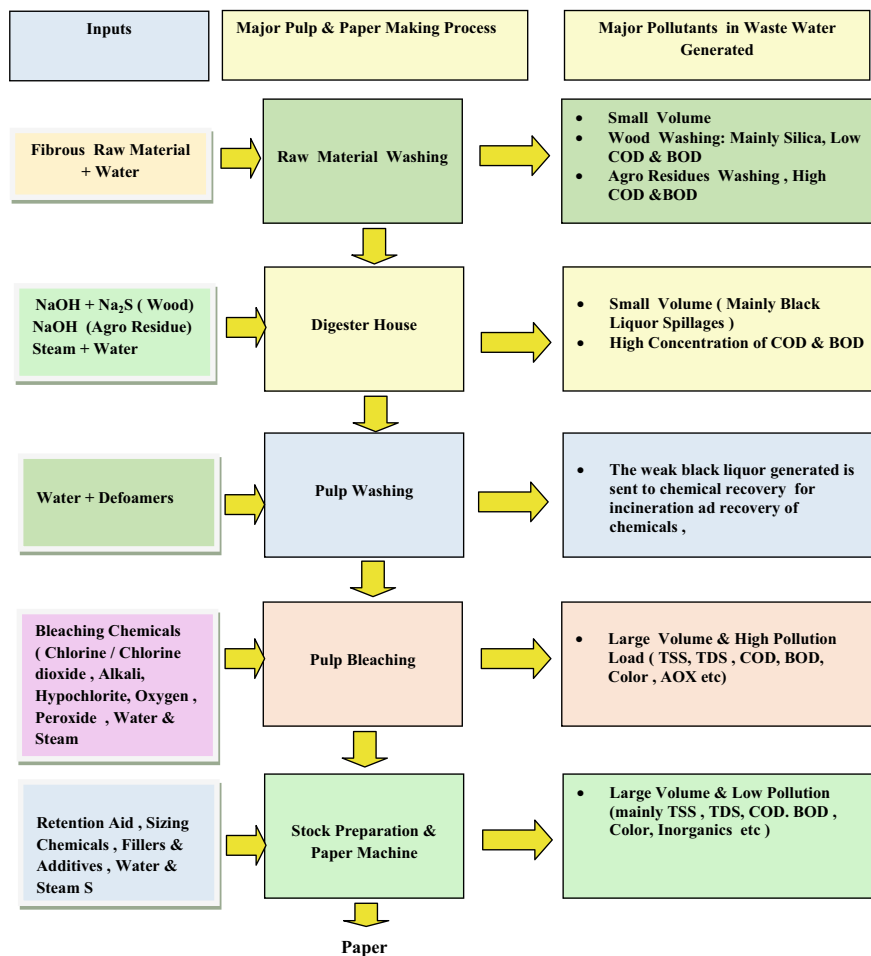
Fig. 1 Major water consuming process operations and sources of effluent generation in a pulp and paper mill

Table 1 General characteristics of effluent/wastewater generated from process operations

Sections	TSS, mg/l	TDS, mg/l	COD, mg/l	BOD, mg/l
Raw material washings (wheat straw/bagasse)	1500–2000	3500–4500	3000–4000	2000–2500
Pulping and bleaching section	100–300	1500–2000	700–1200	200–400
Paper machine	800–1000	1000–1500	500–800	300–500
Chemical recovery	200–500	1500–2000	400–600	200–300
Combined effluent	800–1500	1500–2500	1500–2000	500–800

Table 2 Fresh water consumption and waste water discharge norms under charter (Likely to be enforced on national level soon)

Category	Fresh water consumption, $m^3/tone_{paper}$	Waste water discharge, $m^3/tone_{paper}$
A1: Wood based—bleached grades of papers, paperboards and Newsprint	**50**	**40**
A1: Wood based—unbleached grades of papers and paperboards	**25**	**20**
B1: Agro based—bleached grades of papers, paperboards and newsprint	50	40
B2: Agro based—unbleached grades of papers and paperboards	25	20
C1: RCF based—bleached grades of papers, paperboards and newsprint	15	10
C2: RCF based—unbleached grades of papers and paperboard	10	6
D: RCF and market pulp based specialty paper mills	50	40

Table 3 Discharge norms under charter (likely to be enforced on national level soon)

Parameter	Unit	Category	
		Integrated pulp and paper mills producing chemical pulp	RCF based mills
pH	–	6.5–8.5	6.5–8.5
Total suspended solids (TSS)	mg/l	<30	<30
Total dissolved solids (TDS)	mg/l	<1800	<1600
Chemical oxygen demand (COD)	mg/l	<200	<150
Biochemical oxygen demand (BOD)	mg/l	<20	<20
Colour	PCU	<250	<150
AOX	mg/l	<8	–
SAR	–	<10	<8

2 Adoption of Continuous Digester for Agro Residues Pulping

Pulping process converts raw material (wood/agro residues) into a fibrous mass called pulp. The production of pulp is commercially accomplished by a mechanical or chemical pulping process or a combination of both methods (Rahman et al. 2020). The agro based pulp and paper mills have traditionally used batch digesters for

Fig. 2 Continuous digesters in agro based paper mills

paper making. Due to lower space requirements, less labor and lower energy costs, continuous digesters have become the dominant design in the realm of kraft as well as soda cooking (Pikka and Andrade 2015). The recent trend is use of continuous digester for pulping (Fig. 2) which produces pulp of improved quality, lower kappa no by 2–3 points leading to less bleaching chemical consumption in subsequent bleaching stage along with advantage of more energy efficiency and less gaseous emissions.

3 Adoption of New Generation Pulp Washers for Pulp Washing

Pulp washing is an important process the efficiency of which impacts the quantity of bleach chemical requirement in subsequent bleaching stages as well as chemical recovery system efficiency. In recent times some agro based pulp and paper mills have switched over to new generation pulp washers like Twin roll press (Fig. 3) which is not only efficient from traditional brown stock washers from water consumption point of view but also helps in reducing COD carryover (black liquor) to subsequent bleaching stages which helps in reducing the pollution load. These improved chemistries allow better washing, reduced chemical and biological oxygen demand (COD and BOD) in effluent and cleaner pulp (Alberto et al. 2015).

A comparative general analysis of Brown Stock Washer and Twin Roll Press is indicated in Table 4.

Fig. 3 New generation twin roll press for pulp washing

Table 4 COD carryover and impact on black liquor solids with conventional BSW/Twin roll press

Particulars	Unit	BSW	Twin roll press
COD carryover	kg/Ton pulp	12	8
Black liquor solids (agro residues)	% w/w	10	12
Black liquor solids (Wood)	% w/w	13	16
Wash liquor at dilution factor 2.5	m^3/Ton	9.8	4.8
Outlet consistency	%	12	28

Note All figures are average values

4 Adoption of Oxygen Delignification (ODL) Before Bleaching

Molecular oxygen in alkaline medium allows prolonged delignification with preservation of pulp yield. It shows good performance in presence of carbohydrate stabilizers such as (MgSO$_4$) (Mukherjee and Bandyopadhyay 1993). Incorporation of ODL prior to pulp bleaching (Fig. 4) has helped the pulp and paper mills in reducing the kappa no (indicator of lignin content in the pulp) of the pulp by 30–35% leading to reduction in pollution load including COD, BOD. ODL decreases the formation of chloro-organics such as absorbable organic halide (AOX) in bleach plant effluents. ODL also decreases BOD, COD and color of the effluents (Thomas et al. 2007). It also improves pulp properties like brightness, tear strength, tensile strength, breaking length, bursting strength etc. as well as improvement in machine runnability through reduction in paper breaks.

A comparative study of impact of incorporation of oxygen delignification on chemical consumption, and pollution load prior to conventional chlorine based bleaching is summarized in Table 5.

Fig. 4 ODL reactor and ODL press

Table 5 Impact of oxygen delignification on pollution load generation

Chemical consumption and pollution load in conventional chlorine based bleaching sequence (without ODL)		Chemical consumption and pollution load in conventional chlorine based bleaching sequence (with ODL)	
Chlorine as elemental	48–50 kg/T	Chlorine as elemental	25–28 kg/T
Chlorine as hypo	12–15 kg/T	Chlorine as hypo	8–9 kg/T
Caustic	35 kg/T	Caustic	26–28 kg/T
COD	2600 mg/l	COD	1800 mg/l
BOD	847 mg/l	BOD	700 mg/l
AOX	13 mg/l	AOX	6.5 mg/l

Note All figures are average values

5   Optimization of Fresh Water Consumption in Paper Machine Showers Through Change in Nozzle Diameter

Paper machine is one of the major fresh water consumption area in pulp and paper mills. In general the mills have been using shower of nozzle diameter around 1.2–1.5 mm. Reduction of shower nozzle Dia up to 0.75 mm has helped the mills to reduce the fresh water consumption by over 50% as indicated in Table 6.

Table 6 Reduction in fresh water consumption by change in nozzle diameter

Particulars	Nozzle dia 1.5 mm	Nozzle dia 0.75 mm
No. of shower	6	6
No. of nozzle in each shower	30	30
Nozzle discharge capacity, LPM	5.4	2.7
Operating time, hr	24	24
Total fresh water consumption, m^3/day	1400	700

6 Adoption of Poly Disc Filter for Increased Reuse of Paper Machine Back Water

With increased awareness about need for fiber recovery in terms of resource conservation, as well as reduction in pollution load, the mills earlier installed fiber recovery systems like save all and dissolved air flotation units. In recent times Poly Disc Filters (PDF) (Fig. 5) have received increased interest in context of its high fiber recovery efficiency as well treated backwater quality leading to increased reuse/recycling of paper machine back water into paper machine and ultimately translating into reduced fresh water consumption. A case study as indicated in Table 7 of a paper machine of 300 tpd production capacity which has recently introduced PDF in its closed loop indicates high performance of the system in terms of TSS reduction due to which the mill is able to reuse/recycle significant amount of back water.

7 Adoption of Chemical Recovery System in Agro Based Mills

One of the major environmental issue with agro based mills was the absence of Chemical Recovery System for black liquor management (Fig. 6) which resulted in generation/discharge of high organic load. Making Chemical Recovery mandatory for agro based paper mills have forced the low capacity agro based mills to either switch over to waste paper or undertake capacity expansion to appropriate capacity so that installation of chemical recovery system is techno-economically feasible. The chemical recovery is a very important operation in pulp and paper making process. The chemical recovery process employs treatment of the residual liquor generate after pulping of cellulosic raw material, efficient generation of steam and electrical power from the fuel value of black liquor, and effective conversion into fresh cooking liquor and regeneration of lime from lime mud (Jain 2020). An estimated average

Fig. 5 Poly disc filter for fiber recovery in paper machine

Table 7 Reduction in fresh water consumption by PDF

Particulars	PDF inlet	PDF outlet		
		Cloudy water	Clear water	Super clear water
Volume, m^3/hr	150	75	45	30
TSS, mg/l	3000–4000	400–500	100–200	50–100
Reuse of PDF filtrate	–	Mixed with feed water	– Disc filter showers – Consistency dilution	Low pressure showers
Fresh water saving, m^3/hr	–	–	45	30
Total fresh water Saving, m^3/day	–	–	**1800**	

Fig. 6 Chemical recovery system for black liquor incineration

Table 8 Reduction in pollution load through chemical recovery

S. No.	Parameters	Average reduction in pollution load (kg/ton of paper)	
		Mills without chemical recovery plant	Mills with chemical recovery plant
1	COD	800–1000	60–80
2	BOD	450–550	24–32

reduction in pollution load due to chemical recovery installation is summarized in Table 8.

8 Biomethanation in Agro Based Paper Mills

Anaerobic treatment processes are more suitable for the treatment of high strength wastewater such as pulp and paper mills. Also, anaerobic microorganisms are more efficient than aerobics in order to degrade chlorinated organic compounds (Singar-avelu and Gudo 2016). High strength streams generated during cleaning of raw materials evaporation of black liquor i.e. evaporator condensate and weak washings of pulp have also been found as good sources of high rate biomethanation since these streams contain easily degradable constituents like organic acids, methanol etc. (Panwar et al. 2002).

   The application of biomethanation technology (Fig. 7) in treatment of washings of agro residues is also being increasingly implemented in pulp and paper mills in the country. The advantage of biomethanation is reduction in pollution load along with cogeneration of biogas which can be used as a fuel and can offer payback over a period. The biomethantion as a pretreatment step reduces the pollution load to conventional ETP leading to reduced chemical and energy consumption along with

Fig. 7 Biomethanation plant
at an agro based mill

improved treated water quality which can be reused/recycled again for raw material washing as well as other areas. A comparative reduction in pollution load of wheat straw washing at an agro based pulp and paper mill is summarized in Table 9.

Similarly, the mill are also benefitted by significant reduction in chemical in conventional ETP after commissioning of biomethanation plant as indicated in a case study depicted in Table 10

Table 9 Comparative reduction in pollution load through ETP (with and without biomethanation)

Pollution reduction with conventional ETP (activated sludge process without biomethanation) (%)		Reduction with conventional ETP (activated sludge process with biomethanation) (%)	
TSS	75–80	TSS	90–95
COD	80–85	COD	90–95
BOD	85–90	BOD	95–98
Color	70–80	Color	90–94

Table 10 Comparative reduction in chemical consumption in ETP (with and without biomethanation)

Chemical consumption in conventional ETP without biomethanation (gm/m^3)		Chemical consumption in conventional ETP with biomethanation (gm/m^3)	
Coagulant	500–800	Coagulant	5–10
Flocculent	90–100	Flocculent	1–5

9 Best Practices Versus Pollution Reduction

As indicated above the adoption of in-house approach/best practices and new technologies have translated into significant reduction in fresh water consumption through optimum water consumption, improved back water and treated effluent quality making increased reuse/recycling feasible. The range of reduction of fresh water consumption achieved by the mills through adoption of process wise appropriate strategies/technologies is summarized in Tables 11 and 12.

A comparative fresh water savings adoption of best practices compared to conventional practices adopted in pulp and paper making is indicated in Table 12.

10 Cost of Technologies Implemented

The cost of the technological interventions for reducing the fresh water consumption/waste water discharge or facilitate reuse/recycled of back water/treated effluent is indicated in Table 13. The Return on Investment (RoI) as well as operational cost vary from mill to mill and also depends on scale of production, raw material used and grades of paper produced. As discussed with various pulp and paper mills, in general the pay varies from 3 to 7 years for these technologies in context of direct or indirect savings involving energy conservation, recovery of paper making fiber, water conservation, recovery of chemicals. Recovery of biogas, reduced chemical and energy consumption in ETP etc.

Table 11 Best practices adopted by mill for reduction in fresh water consumption

Section	Water consumption, m^3/t_{paper}	
	Best practices	Fresh water reduction, m^3/ton_{paper}
Raw material preparation (agro residues)	– Installation of separate clarifier for wet washings and 100% reuse of overflow – Use of treated water/black liquor foul condensate as make up water to wet washings	5–10
Pulp washing	– Use of oxygen delignification (ODL) back water in BSW shower – Use of high consistency washers/presses	3–4
Pulp bleaching	– Use of oxygen delignification (ODL) – Use of elemental chlorine free bleaching – Use of high consistency washers/presses	15–18
Paper machine showers	– Reduction in nozzle size of showers – Installation of poly disc filter (PDF) for treatment of back water so as to reuse it in paper machine LP showers	12–16
Sealing and cooling	– Installation of cooling tower followed by micro filtration for making it suitable for reuse	5 – 7
Boiler make up water	– Increase in steam condensate recovery	3–4
Chemical recovery	– Use of black liquor secondary condensate in mud washing and thickening	5–10
Miscellaneous	– Spillage control etc	3–5
Total reduction in fresh water consumption, m^3/ton_{paper}		**51–74**

11 Conclusions

Water is a scarce resource and needs to be conserved. The Indian Pulp and Paper industry, a traditionally water consuming industry has come a long way to reduce its fresh water footprint through adoption of various strategies and approach to reduce fresh water consumption as well as adopt **Bare Minimum Technologies (BMT)/Best Practicable Technologies (BPT)**. The recent trends for adoption of continuous digester, new generation pulp washers, oxygen delignification system, poly disc filters, UASB reactor, screw press for sludge dewatering, chemical recovery system

Table 12 Section wise fresh water consumption in wood/agro based integrated paper mills

Section	Water consumption, m^3/t_{paper}	
	With conventional practices	With best practices
Raw material preparation (agro residues)	5–10	Nil
Cooking	Nil	Nil
Pulp washing	8–10	5–6
Pulp bleaching	25–30	10–12
Chemical preparation	2–5	2–5
Paper machine showers	30–40	18–24
Sealing and cooling	10–15	5–8
Boiler make up water	6–8	3–4
Chemical recovery	5–10	Nil
Spillage etc. to ETP	3–5	Nil
Total	94–133	43–59

Table 13 Cost of technologies adopted by pulp and paper mills for water conservation

Technology implemented	Capacity, TPD	Capital investment INR million
Continuous digester	200–400	750–1500
New generation pulp washing system with twin roll press	250–450	1000–2000
Oxygen delignification (ODL)	150–450	300
New generation pulp bleaching system with twin roll press	250–450	1000–2000
Poly disc filter at paper machine	1500–3000 m^3/day (white water) and 3–6 TPD fibre recovery	500–100
Conventional chemical recovery system	400–6000 BLDS/day	1000–2000
UASB reactor	20,000–5000 m^3/day	50–100

etc. have helped the pulp and paper mills in meeting the environmental challenges, ensure their sustainability as well as improve their competitiveness. The successful case studies drafted with active support from CPPRI are now being replicated in other

mills. The success provides a road map to help the industry in becoming an environmentally friendly industry rather than a polluting industry. However there is a need to develop indigenous technologies/equipments which suits our raw material and scale of operation but are also economically feasible in terms of capital investment and operational cost even for mills with medium/small scale of operation.

References

CPCB Charter for 'Water Recycling and Pollution Prevention in Pulp and Paper Industries' (Specific Ganga River Basin States), 2014–2016. Central Pollution Control Board (CPCB), New Delhi.

dos Santos CA, Hämäläinen H, Lamonato A, Dorronsoro RS (2015) 7th international colloquium on eucalyptus pulp, Vitória, Espirito Santo, Brazil

Jain R (2020) An Efficient agro based integrated chemical recovery plant at M/s Bindals Papers Mills Ltd. IPPTA 32(E3):38–44. ISSN: 0379-5462

Mukherjee D, Bandyopadhyay N (1993) Oxygen delignification technology for improved product quality and pollution abatement in pulp and paper industry. IPPTA J 5(2):27–36

Panwar S, Gupta MK, Endlay N, Mathur RM, Kulkarni AG (2002) Bioenergy generation from pulp and paper mill waste through high rate biomethanation. IPPTA J 14(4)

Pikka O, de Andrade MA (2015) New developments in pulping technology. In: Proceedings of the 7th ICEP—international colloquium on eucalyptus pulp, Vitória, Brazil

Rahman M, Avelin A, Kyprianidis K (2020) A review on the modeling, control and diagnostics of continuous pulp digesters. Processes. https://doi.org/10.3390/pr8101231

Singaravelu M, Gudo AJA (2016) Biomethanation of paper mill liquid effluent through UASB reactor. In: International conference on advances in electrical, electronics, information, communication and bio-informatics (AEEICB16)

Thomas R, Singh SP, Subrahmanyam SV (2007) A study on oxygen delignification of melocanna baccifera (muli bamboo) kraft pulp. Bioresour Technol 2(3):430–441

Sequestering of Heavy Metal Ions from Aqueous Stream by Raw and Modified Lignocellulosic Materials

Shravan Kumar, Rahul, Apoorva Verma, Ira Singhal, Prateek Mishra, Shubhang Shukla, and Manish Singh Rajput

Abstract Heavy metals pollution in aqueous stream is the biggest threat to the environment today. These wastes are released by direct or indirect ways into the aqueous streams through industrial activities. Therefore, removal of heavy metals in an ecofriendly and cost effective manner became an important concern for protecting the environment. After several experiments it has been shown that the conventional methods don't show much efficiency in the heavy metal removal. Biosorption is a type of adsorption and the most efficient method used for the heavy metal removal by using low cost adsorbents which are cost effective and ecofriendly in nature. This review we have reported the removal or sequestering of heavy metals by biosorption using the low cost adsorbents which include the agricultural wastes or lignocellulosic materials that serve as potential biosorbents and show much more efficiency than conventional methods. Here we highlight the different raw and modified lignocellulosic materials with their adsorption capacity used for the heavy metal removal, effects regarding biosorption, sorption isotherms and kinetics. Chemically modified lignocellulosic materials have higher adsorption capacity than unmodified lignocellulosic materials. We have also explained the desorption of metal and recovery of lignocellulosic materials therefore this method is a renewable process. It is observable from different articles that biosorption from raw and modified lignocellulosic materials are most often studied for the heavy metals removal or sequestering.

Keywords Biosorption · Lignocellulose materials · Heavy metals · Mechanism · Kinetics

S. Kumar (✉)
Chemical Engineering Department, Indian Institute of Technology, Assam, India
e-mail: hbti.shravan@gmail.com

Rahul
Chemical Engineering Department, Jaipur National University, Jaipur, India

A. Verma · I. Singhal · P. Mishra · S. Shukla · M. S. Rajput
Department of Biotechnology, Dr. Ambedkar Institute of Technology for Handicapped, Kanpur, India

1 Introduction

Environmental pollution is one of the prime challenges that the entire world is facing today. Although, rapid industrialization and urbanization have boosted the living conditions, they have severely impacted the environment due to excess release of pollutants. These pollutants can be organic or inorganic. Organic pollutants such as pesticides, insecticides, food processing wastes are biodegradable whereas some are inorganic like heavy metal which cannot be degraded. The second category which includes the inorganic pollutants like heavy metal which remain indefinitely in our environment and imposes threat to living organisms by passing through the food chain (Hansda et al. 2016). Release of these chemicals into the air, water and soil contaminates them and affects all the living organisms in adverse ways (Hansda et al. 2016).

Metals can be further divided into three broad categories-

(a)   Essential and non- toxic, example (Ca and Mg)
(b)   Essential and harmful above threshold limit, example (Fe, Mn, Zn, Cu, Co, Ni andMo)
(c)   Toxic, example (Mg and Cd)

Heavy metals can be defined as metals with relatively high densities, high atomic weights or high atomic number that can be toxic or poisonous at very low as well as very high concentrations. Therefore heavy metals have optimal range of intake for the human body. Any change in the concentration can cause serious health problems (Fu and Wang 2011). Several man made or natural sources can cause heavy metal pollutants to reach the environment. The natural sources may include volcanic eruptions, weathering of metal containing rocks, while anthropogenic sources like mining, industrial emission, smelting, agricultural activities, electroplating etc. Combustion of fossil fuels also contribute to environmental pollution by the release of heavy metals, such as cadmium (Cd), to the environment (Srivastava et al. 2015). Elements having atomic weight between 63.5 and 200.6 and a specific gravity greater than 5.0 are described as heavy metals. These heavy metals tend to accumulate in living organisms causing serious damage (Fu and Wang 2011).

These heavy metals pollutants are a big problem as they cause serious health issues. Heavy intake of copper leads to serious toxicological issues such as cramps, vomiting and even death. Excessive nickel might cause serious lung and kidney problems. Mercury is a serious neurotoxin which damages the nervous system. It's higher concentration can impair pulmonary function and causes kidney damage. U.S. environmental protection agency has classified cadmium as a human carcinogen. Exposure to cadmium leads to kidney dysfunction and exposure to high levels can lead to death (Fu and Wang 2011). Lead poses danger to central nervous system as well as kidney, reproductive system and liver. Lead poisoning causes anemia, insomnia irritability, weakness of muscles, headache, dizziness, renal damages and hallucination. Generally Chromium exists in two oxidation states in the environment i.e. Cr(III) and Cr(VI). Cr(VI) is found to be more toxic than Cr(III). Cr(VI) upon accumulation

causes several health problems including skin irritation and lung carcinoma (Ahalya et al. 2005).

Heavy metals can be removed or sequestered by using abiotic or biotic methods. The abiotic methods include conventional processes like chemical precipitation, adsorption, membrane filtration, reverse osmosis, floatation etc. But these methods have limitations such as high cost due to production of toxic secondary sludge, low efficiency, high operational condition. The biotic methods involve bioremediation, biosorption, bioaccumulation. This method is advantageous due to maximum efficiency, low cost, reduced production of biological waste, low operative methods in an eco-friendly manner (Hansda et al. 2016). Adsorption is most effective method for heavy metal removal among various other technologies. It can be done by using various adsorbents such as seaweeds, molds, yeasts and agricultural waste. Agricultural waste especially cellulosic materials have good biosorption capacity due to their structure which includes lignin, lipids etc. The adsorption capacity and kinetics studies can be carried out by several isotherm and kinetics models. For example, for removal of lead and cadmium cotton waste is used and wheat bran is used for removal of chromium. Vibrio fischeri bioluminescence inhibition assay (VFBIA) is used for monitoring toxicity due to less test duration and high sensitivity.

This review article comes up with the current techniques used to isolate or remove the heavy metals from the aqueous stream by using raw and modified lignocelluloses materials (agricultural waste) as biosorbents. This review paper is aimed at providing information about biosorption, adsorption surfaces, methods involved in biosorption etc.

2 Heavy Metals and Their Toxicity

Heavy metals generally defined as the metals that have high relative densities, atomic weights and atomic numbers. Commonly, a density of around 5 g/cm^3 or more is used to define heavy metals. Generally, their atomic number is found to be greater than 20. They are toxic at low concentrations. Some of them are essential elements like iron, zinc, cobalt. Some heavy metals are harmless, e.g., silver, indium. Some of them are highly poisonous like cadmium, mercury, lead. Along with being relatively dense, they have lower reactivity than lighter metals and form very few soluble sulphides and hydroxides.

Pollution caused by heavy metal is one of the crucial need of concern for a long time now. These metal ions do not degrade and are retained as it is in the environment. They are extremely hazardous as they easily assemble in the atmosphere and pass through the food chain inflicting serious damage to living organisms. The major cause for the environmental pollution by heavy metals is the industrial effluents being released into water bodies. Some of these industries include electrolysis, electroplating, mining, electro-osmosis, energy and fuel, fertilizers, leather, pesticides, iron and steel etc.

Some of these heavy metals are described below:

(a) **Cadmium (Cd)**

The industrial discharge acts as a major source for the entry of cadmium into the environment. Studies show that Itai caused by chronic cadmium toxicity (Horiguchi et al. 1994).

(b) **Mercury (Hg)**

Above the permissible limit, mercury causes degeneration of the intestinal tract, kidney failure and death gradually. Low toxic metallic mercury can be converted to highly toxic methyl mercury (CH_3Hg^+) by the use ofcertain bacterial actions which helps in the conversion of Methyl mercury (CH_3Hg^+) passes through food chain, tissues which are soft fattyaccumulated in the body like liver and kidneys and leading to blindness, kidney damage and mental degeneration. Minamata disease is the main cause that took place in Japan (Harris et al. 2003).

(c) **Copper (Cu)**

Excessive ingestion of copper leads to vomiting, tremors, nausea, diarrhea and even death. Wilson's disease can be caused by the heavy collection of copper in liver. According to WHO, the tolerable limit for copper in drinking water is 2.0 ppm.

(d) **Chromium (Cr)**

Chromium in hexavalent form is highly toxic in nature and its trivalent form is comparatively less toxic. Chromium when exposes causes cancers of respiratory tract Skin irritation, failure of kidney and liver and premature oxidative death of the cells of the blood (Tewari et al. 2005; Bhattacharyya and Gupta 2006; Dayan and Paine 2001).

(e) **Lead (Pb)**

Level of lead when exposes to even trace affects the functioning of the body's major organs and organ system (Bashir et al. 2019). Cell's various processes like signaling of the cell, folding of protein, etc. affects lead poisoning (Feng and Guo 2012).

(f) **Zinc (Zn)**

Increased zinc exposure may result in the impairment of growth and reproduction. Zinc toxicity may lead to vomiting, bloody urine, kidney failure, metal fume fever, liver degeneration and anemia (Zhang et al. 2014). According to WHO the allowable limit of Zn in potable water is 5 ppm (Table 1).

3 Biosorption: An Effective Alternative

Biosorption is a process of sequestration of heavy metal through the functional group present on the surface of biosorbent. It is a fast and an unconventional process. In

Table 1 The maximum contaminant level (MCL) standards (Abdel et al. 2016)

Heavy metal	Toxicity	MCL (mg L^{-1})
Arsenic	Irritation of respiratory system, liver and kidney damage, loss of appetite, nausea and vomiting etc	0.020
Cadmium	Lung, liver and kidney damage; irritation of respiratory system	0.06
Mercury	Irritation of respiratory system; lung, liver kidney damage, and loss of hearing and muscle coordination	0.01 (vapor)
Nickel	Lung, liver and kidney damage	0.1
Chromium	Lung damage and irritation or respiratory system	0.050
Lead	Lung and liver damage; loss of appetite, nausea	0.15

recent ages, biosorption has major advantages over conventional methods for the sequestering and elimination of heavy metals. This is because of it's low cost, less chemical or biological sludge, high efficiency, metal selectivity, short operation time, absence of requirements for nutrient, eco-friendly and reconstruction of biosorbents (Hansda et al. 2016). Biosorption process involves two phases. A solid phase which is a sorbent in case of adsorbent and biosorbent in case of biological material and a liquid phase solvent which includes adsorbate which is generally a metal ion or mostly water having dissolved species to be sorbent. These adsorbents have high affinity towards adsorbate species which is later attracted and bind with each other through different mechanisms and it continues till the equilibrium is maintained between adsorbate species and the liquid remaining in the solution. It can include mechanisms like absorbtion, ion exchange, surface complexation and precipitation (Abbas et al. 2014).

3.1 Biosorbents

The first task for biosorption process is to choose the biosorbent by considering the availability of biomaterial which is inexpensive, has high selectivity for heavy metals and has elevated metal binding capacity. Biosorbents are natural ion exchange materials which have both basic and acidic groups. The biomass living or dead, both material can be used as a biosorbent. On an average biosorbents have been classified into (i) nonliving biomass like lignocellulosic materials (lignin, crab shell, bark etc.), (ii) microbial biomass (fungi, bacteria and yeast) (iii) algal biomass (Fu and Wang 2011).

Cost effective biosorbents such as agricultural waste (fruit peels, tea leaves, potato peels, saw dust, eggshell, coffee husk etc.), moss peat, yeast, molds, seaweeds, industrial wastes are good biosorbents can be used for the heavy metals elimination from aqueous solution.

3.1.1 Types of Biosorbents

(A) **Microbial Biomass**

Microorganisms like bacteria, fungi, yeast act as good biosorbents. These show high efficiency and aid in faster removal of heavy metals from the solution, thus bringing the concentration of heavy metals from ppm to ppb level.

Bacterial biomass is used as biosorbent due to smaller size, number of surface binding sites, can grow in controlled conditions, resistance against wide range of environmental conditions, and specificity. Heavy metal generally binds with cell wall of bacteria and exhibits biosorbtion. The concentration range of bacteria in which it has high efficiency is 0.23–0.90 mmol/g (Abbas et al. 2014).

Fungi are the industrial fermentation waste biomass which act as good biosorbents; this is due to high percentage of cell wall material, it's metal binding properties, eco-friendly environment, and availability in large quantities. Both dead and the living fungal cells can act as biosorbents for the elimination of heavy metal. The concentration range of fungi in which it shows maximum efficiency is 0.012 to1.979 mmol/g (Abbas et al. 2014).

(B) **Algal Biomass**

Algal biomass is the most promising biosorbent due to it's high biosorbtion capacity and it's availability in large quantities. These produce large biomass than microbial biomass because they are autotrophic and produce less toxic substances. The concentration range for green algae is 0.066 to 1.20 mmol/g and for brown algae is 0.65 to 1.21 mmol/g (Abbas et al. 2014).

(C) **Non Living Biomass or Lignocellulosic Materials**

Agricultural wastes (rice bran, saw dust of various plants, orange peels, waste tea leaves, bark of the trees, rice husk, black gram, wheat brans, shells, sugarcane bagasse, coffee beans etc.) and by products are titled as lignocellulosic materials. Cellulose, lignin and hemicellulose are the major parts of these materials. Metal ions are strongly attracted towards them because of the presence of hydroxyl groups in metal ions. These materials are rich in functional group like carboxyl, esters, alcohols, acetamide on the surface of these materials. Cellulose based biosorbents are more resourceful for biosorption of heavy metals. Agricultural wastes materials are ecofriendly as well as economic due to their chemical composition, easy obtainability; are renewable and cost effective (Sud et al. 2008). These materials show high binding affinity towards metals and good regeneration properties (Bashir et al. 2019). Biosorbents can be modified physically or chemically to increase their biosorptive properties. Agricultural wastes or lignocellulosic material are promising biosorbents for the sequestering of heavy metals. Raw or modified lignocellulosic materials are used as biosorbent for the heavy metal sequestering aqueous stream.

3.1.2 Selection Criteria for Biosorbents

After several studies and research it shows that selection of biosorbent depends on the origin, availability of material, cost effectiveness, easily renewable, high biosorption capacity, high efficiency, easy desorption and ecofriendly nature. The bisorbents should be less toxic that is negligible leaching into aqueous system (Lata et al. 2015). Biosorbents can be collected naturally from the environment or specially modified by the treatments. Selected biosorbent should have broad range of temperature, pH, rapid kinetics of adsorption and desorption for the selective elimination of heavy metal. There should be high surface to volume ratio of biomass we choose. Biosorbent should have superior capability to detoxify the heavy metals. Presence of certain groups like hydroxylate and carboxylate on the surface of biosorbent shows principle binding sites for Pb^{+2} ions (Bashir et al. 2019).

3.2 Biosorption Due to Microbial and Algal Biomass

Using microbial and algal biomass for biosorption shows strong metal binding and biosorption capacities. They have high selectivity for dilute solution of metal ions. In this, the cell wall of microbial biomass is negatively charged due to the functional groups like hydroxyl, carboxylic acids, amine and phenolic group which are present and which bind with positively charged heavy metal., Using bacteria biomass, biosorption can be done in two stages, the first stage involves interaction between the metal ions and the functional group present onto the cell surface and the next stage shows the deposition of metal species in large concentration (Abbas et al. 2014). Using algal biomass, biosorption can take place either by complexation between functional groups or metal ions or by ion exchange mechanisms. It is on the composition of algal cell wall that the process of biosorption depends (Abbas et al. 2014). Using fungal biomass interactions can occur through ion exchange, complexation and physical adsorbtion. Microoragnisms which have high surface-volume ratio shows high efficiency towards heavy metal removal (Srivastava et al. 2015).

4 Lignocellulosic Material

Lignocellulosic materials are from horticultural or plant squanders are generally concentrated because of their inexhaustible nature, enormous creation and extraordinary nearby accessibility. Malik et al. (2017) investigated minimal expense sorbents from different parts of plant like husks, straws, leaves, stems, barks, grasses, bodies, fibers and seeds characteristic item strips and pulps, stalks, shells, bagasse, woods, and other lignocellulosic or agricultural based materials, for instance oaks, corn cob or natural product stones that can be used as biosorbents (Malik et al. 2017).

The specific physicochemical property decides the character of a sorbent with property of each specific materials.

Sorption of metals by these heterogeneous materials is an unpredictable cycle influenced not simply by the standard framework, yet moreover by other discretionary instruments and blends of distinct wonders which includes adsorption on surface pores, chemisorption, entrapment in entomb and intra-fibrillary vessels, adsorption by actual forces and spaces of the basic polysaccharides organization, dissemination along the cell divider and layers, metal lessening and surface precipitation (Lata et al. 2015; Malik et al. 2017). The participation between metals and specific sorbent materials can be done by rule segment as expected and checked by blend of various spectroscopic techniques and conventional systems like titration, compound obstructing of useful gatherings and similar appearance of cations from adsorbent (Abdolali et al. 2014a).

The adequacy of each and every sorbent unimaginably related upon the functioning state like temperature, pH, sorbent particle size, contact time or starting metal core interest. Thus, an escalated report to determine the ideal biosorption conditions essential for each pair of sorbent metal. Large numbers of those examinations can determine the composition, where the ideal case for each and particular pair of lignocellulosic materials were represented. The rule supporting this area can be discover in studies circulated in lofty diaries, serving the scientists with invigorating the facts about potential and promising biosorbents fitting for a given approach (Lata et al. 2015; Abdolali et al. 2014a; Miretzky and Cirelli 2010; Michalak et al. 2013). In recent reviews, the presentation of various kinds of lignocellulosic adsorbents is by and large conveyed as greatest sorption limit (qmax) and the proficiency examination between materials utilized depends on these qualities. By the by, extra important information is required to consider for each specific metal of sorption proficiency between sorbents as a result of differentiations in atom sizes of sorbent, sorbent estimations and additional preliminary states used in every work.

An enormous portion of flow research on lignocellulosic materials shows metal biosorption has centered on the expulsion of heavy metal cations, like Pb^{+2}, Cd^{+2}, Zn^{+2} and Cu^{+2} (Vanholme et al. 2010), yet other harmful metals like Ni^{+2}, Al^{+2}, Hg^{+2}, Fe^{+2}, chromium and metalloids (arsenic, molybdenum, selenium and vanadium) have been additionally concentrated as target poisons in sorption measures (Volesky 2003).

These days nonetheless, there is attraction in sorption measures that utilizes low cost lignocellulosic materials as biosorbents for the recuperation of valuable metals (Nilanjana Das 2010). The recuperation of important metals by biosorption opens a difficult and energizing new situation in sorption concentrates a long ways past the customary for treatment of water since the recuperated metal material is relied upon to possess a natural financial worth.

In spite of using biomass as biosorbent for the metallic sorption has been consider as an eco-friendly approach and offers a group of probably blessings towards common place technology; a big element of the examinations had been targeted round artificial solutions. From an electroplating wastewater, several agriculture waste adsorbents like olive stones and fruit shell of gulmohar had been explored for the evacuation of

Cr(VI) what's more, from wastewater in a battery industry, coconut shell, rice agrowastes, neem leaves, and hyacinth pulls were utilized for evacuating Pb(II) (Prasad and Abdullah 2010; Liu et al. 2016).

4.1 Structure and Chemical Composition

Lignocellulosic materials have been raised as a huge wellspring of synthetics and substances for several petitions and extremely critical factor for fossil resources to lower the social and financial dependent in the framework arrangement. Materials are typically conveyed through joining CO_2 and water (driven by sun oriented force) by the photosynthesis collaboration. In this exceptional situation, lignocellulosic biomass is the infinite and bio renewable biomass on earth (Zhou et al. 2011).

The critical pieces of these substances are cellulose, lignin and hemicelluloses; besides cellulose and hemicellulose are seen as polysaccharides. The construction of cellulose relies upon sub-atomic equation. Numerous glucose units are associated through glycosidic linkage and particular chains generally interface with each other by using hydrogen bond. The substance has wildly employed in the business paper. Hemicellulose is any other critical polysaccharide ordinarily have in lignocellulosic biomass with an extra diverse construction and linkages than cellulose. Hemicellulose is made out of heteropolymers moreover, possibly contain xyloglucan, glucomannans, xylan, and galactoglucomannans in factor proportions relying upon the sort of biomass (Escudero et al. 2013).

With respect to weighty the sorption of metal by crude, unchanged lignocellulosic biomass, lignin has been essential key part. Lignin have three-dimensional construction made up of phenolic polymers that contains three units of phenylpropanoid that are: p-coumaryl alcohol, coniferyl alcohol and sinapylalcohol. The substance goes about as cell stick, adding the individual filaments to the plant tissue and giving solidarity to it. The bounty in electron-giver dynamic destinations that are given in the polyphenol and polyhydroxy utilitarian gathering of lignin offers a stand-out packaging for the collaboration and restricting of cationic hefty metals (Miretzky and Cirelli 2010). Abdolali et al. investigated the substance arrangement of some essential lignocellulosic materials concentrated in metal sorption measure (Abdolali et al. 2014a). For the most part, lignocellulosic sorbents are (30–35%) shaped of cellulose, (15–25%) lignin, (20–40%) hemicellulose and unassuming water quantity, trash, cyclic hydrocarbons and extractives. The compound structure in lignocellulosic materials are in distinct rate to be determined by the plant and besides as for parts of plant that is leaves includes lower level of cellulose (15–25%) and lignin (5–10%) anyway more elevated level of (70–80%) hemicellulose, while in nuts and stones, the cellulose content is lower than lignin and furthermore hemicellulose (30–40%). Pujol et al., define an arrangement of about 25% complete lignin and 23% of polysaccharides in depleted espresso squanders. They also reported an overall creation relying upon the atom size while portraying the different parts of grape

stalks (GS) (Abdolali et al. 2014b; Pujol et al. 2013). The rule components of ligno-cellulosic materials carry a verity of utilitarian gathering that assume a critical part in metal biosorption. It have being accounted for that acetamido gatherings, carbonyl, amino, phenolic, underlying polysaccharides, sulphydryl, amido, carboxyl gatherings, liquor and esters, available in lignocellulosic materials have partiality for metal complexation. Particle trade between sure cations and sodium, calcium, potassium and magnesium available in the sorbent, recognized as a critical component in a few investigations. These two systems, alongside chelation, are the chief instruments in lignocellulosic sorbents for metal sorption (Lata et al. 2015; Sarin et al. 2006).

4.2   Characterization

Characterization of lignocellulosic substrates can be performed by several instruments such as X-ray diffraction (XRD), scanning electron microscopy (SEM) scanning electron microscopy coupled with energy-dispersive X-ray spectroscopy (SEM–EDX) and transmission electron microscopy coupled with energy-dispersive X-ray spectroscopy (TEM–EDX) (Sarin et al. 2006; Krishnani et al. 2008).

5   Biosorption using Lignocellulosic Materials

Removal or sequestering of heavy metal using agricultural waste or lignocellulosic material as biosorbent shows much more effective technology in recent studies. Biosorption can take place either by the method of ion exchange at low pH or hydrogen ions are replaced by metal ions or with electrostatic interaction or complex formation at higher pH by the uptake of metal ions through the donation of electron pairs (Lata et al. 2015). Therefore this technique bring out the detoxification of heavy metals because of their high affinity, high selectivity of metals by lignocellulosic material, low cost, abundant availability, feasibility and ecofriendly nature. The major advantage is that there is no loss of biosorbent, we can easily recycle these materials to reduce wastes. This technique is developed considering the sustainable method of waste management (Lata et al. 2015) (Table 2).

5.1   Comparison of Adsorption Capacity of Different Lignocellulosic Materials

Various studies have been done for the detection of the adsorbtion capacity of materials which are highly lignocellulosic. It shows that there is a wide range of differences in the capacity of the adsorption of the heavy metal. This adsorption capacity is based

Table 2 Some example of lignocellulosic material for metal removal (Srivastava et al. 2015)

Lignocellulosic materials	Metal purposed	Results	Biosorption capacity	References
Oat biomass	Cr^{+3}, Cr^{+4}	90–100%	NA	Gardea-Torresdey et al. (2000)
Raw rice bran	Cr^{+6}, Ni^{+2}	50%	NA	Oliveira et al. (2005)
Abies sachalinesis and *peciaglehnii*	Ag^{+2}, Cd^{+2}, Cu^{+2}, $Zn^{+2,}$ Ni^{+2}, Mn^{+2}	60%	10.1–14.2	Seki et al. (1997)
Bagasse fly ash	Cr^{+4}, Cd^{+2}, Ni^{+2}	96–98%		Gupta et al. (2003)
Rice straw, soya bean hulls, sugar crane bagasse	Pb^{+2}, $Cd^{+2,}Cu^{+2}$, Zn^{+2}, Ni^{+2}	98%	NA	Johns et al. (1998)
Waste tea leaves	$Pb^{+2,}$ Zn^{+2}, Ni^{+2}, Fe^{+2}	73–92%	73	Ahluwalia and Goyal (2005)
Papaya wood	Cd^{+2}, Cu^{+2}, Zn^{+2}	65–98%	13.45–19.88	Saeed et al. (2005)
Low cost sorbents (bark, dead biomass, chitin, moss)	Pb^{+2}, Cd^{+2}, Cr^{+4}, Hg^{+2}	Good results		Bailey et al. (1999)

on the uptake of metal ions by biological material or removal efficiency of biosorbent from metal ions (Table 3).

6 Biosorption Due to Modified Lignocellulosic Materials

Biosorbents are modified through physical and chemical method to increase the biosorption capacity or biosorptive properties for the elimination of heavy metal.

Physical modification involves heat treatment which denature the cell wall protein and remove the surface impurities for the activity of metal binding site. It also involves thermal and microwave treatment which increases the surface area and permeability resulting in elevated biosorption capacity. At last, treatment of biosorbent with plasma results in enhancing the surface chemical properties without disturbing other properties of biosorbent (Srivastava et al. 2015).

Chemical modification involves the treatment of acid or base and impregnation of metal or metal oxide. In acid treatment adsorbent are treated with acids like citric acid, nitric acid, hydrochloric acid and carboxylic acid like malic acid, tartaric acid which results in protonation thus providing positive surface charge density which establishes strong electrostatic interaction with negatively charged ions. In base treatment adsorbent are treated with base like sodium hydroxide, calcium hydroxide, sodium bicarbonate and ammonium hydroxide thus providing negative surface charge density which attracts with positively charged species. At last due to metal/metal oxide

Table 3 Difference between different adsorption capacities of lignocellulosic materials (Lata et al. 2015)

Metal ion	Biosorbent	Biosorption capacity	References
Cd^{+2}	Cortex banana waste	67.2	Kelly et al. (2012)
	Saw dust	26.73	Naiya et al. (2009a)
Pb^{+2}	*T.aestivium*	90.09	Ali et al. (2011)
	Banana peels	2.18	Anwar et al. (2010)
Cr^{+4}	Wheat bran	310.58	Singh et al. (2009)
	Rice straw	3.15	Gao et al. (2008)
Cu^{+2}	Rose petal waste	124.12	Manzoor et al. (2013)
	Olive solid waste	3.81	Chouchene et al. (2014)
Ni^{+2}	Orange peels	62.30	Gonen and Serin (2012)
	Sweet potato peels	0.509	Kakalnga et al. (2012)
Zn^{+2}	Orange waste	43.16	Marin et al. (2010)
	Neem bark	13.29	Naiya et al. (2009b)
Fe^{+3}	Water bamboo husk	4.7	Asberry et al. (2014)
Hg^{+1}	Sugarcane bagasse	35.71	Asberry et al. (2014)
Co^{+2}	*P.longifolia* leaf powder	3.99	Koramzadeh et al. (2013)

impregnation, adsorbent have high surface to volume ratio. Zinc oxychloride can be used for metal impregnation (Srivastava et al. 2015) (Table 4).

After several studies it was showed that modified lignocellulosic materials have much more advantages than unmodified lignocellulosic materials which can be reuse in a better way and having high biomass loading and minimum choking in continuous flow system.

Table 4 Some example of modified lignocellulosic materials (Lata et al. 2015)

Modified lignocellulosic materials	Metal uptake	References
Orange peel with nitric acid (HNO_3)	Cd^{+2}, Cu^{+2}, Cd^{+2}	Lasheen et al. (2012)
Raw biomass with HCL	Cr^{+4}	Rehman et al. (2012)
Pine cone powder with NaOH	Pb^{+2}	Kumar and Bandyopadhyay (2006)
T.aesitivum with urea	Cd^{+2}	Farooq et al. (2011)
C.*reticulata* with H_2SO_4 and EDTA	Zn^{+2}, Cu^{+2}	Boota et al. (2009)
Orange peels with NaOH and $CaCl_2$	Cu^{+2}, Pb^{+2}, Zn^{+2}	Memoon et al. (2007)
Saw dust with NaOH	Cd^{+2}	Mendieta et al. (2012)
Green tomato with formaldehyde	Mn^{+2}, Fe^{+3}	Qaiser et al. (2009)

7 Mechanism of Sequestering

It is basic study of binding of heavy metals on the adsorbent surface and to explore the component drew in with confining/restricting of metal particles/particles with lignocellulosic materials. The certifiable system of biosorption isn't totally seen at this point since it is found to be affected by various factor including (a) kinds of lignocellulosic material, (b) Chemistry of arrangement, (c) normal/natural conditions, and so forth (Lata et al. 2015).

The interaction of biosorption incorporates a strong stage (sorbent) and a fluid stage (dissolvable) containing a broke down animal type to be sorbed. Due to high specificity of the sorbent for the metal molecule, several mechanism steps are involved in sequestration of heavy metals like complexation, particle trade, chelation, and ion exchange. The metal particles are entangled in intrafibrillar vessels and spaces of the underlying polysaccharides network due to focus slope and dissemination through cell divider and layer (Garg et al. 2007).

Lignin and cellulose are the fundamental constituents of agricultural waste materials. Different components like hemicellulose, extractives, lipids, basic sugars, starches, proteins, water, hydrocarbons, ash and some other compounds contain a variety of functional group present in the binding process. Cellulose a crystalline homo-polymer of glucose which has $\beta_1 \rightarrow 4$ glycosidic linkage and aggregates via both intra-molecular and intermolecular hydrogen bonds. Hemicellulose is a heteropolymer of mostly xylose with $\beta \rightarrow 4$ glycosidic linkage with other

substances of acetyl feruoyl and glycouronyl group (Belfort 1980). Lignin is covalently connected with xylans in hardwood and galacto glucomannans in softwoods. It is a three dimensional polymer of aromatic compounds. Acetamido groups, carbonyl, phenolic, primary polysaccharides, amido, amino, sulphydryl carboxyl groups alcohols and esters are some of the many functional groups present in biomass molecules (Rangabhashiyam et al. 2014). These groups have the affinity for metal complexation. Some biosorbents are non-particular and are not specific and attach to a wide range of metals without specificitys, while others show specificity to certain kinds of metals based on their chemical composition. The presence of different functional groups and their complexation with heavy metals during biosorption process has been chronicled by various researchers using spectroscopic methods (Belfort 1980; Langmuir 1918).

8 Biosorption Models: Kinetics and Isotherms

8.1 Biosorption Isotherms

The isotherms of biosorption explain the relation between the concentration of biosorbent and the quantity of it adsorbed by the unit mass of the biosorbent by keeping constant temperature at equilibrium. This is essential for designing the biosorption systems. The isotherm models gives data and facts about the removal capacity of biosorbents. These isotherm models are essential for determining the biosorption parameters and to compare the different biosorbents using different operating conditions.

(A) **Single Component Isotherm Models**

Short expression and mono component adsorption of ionic metals are given by these models. These are simple mathematical relationships model which is used to describe different experimental behavior over a large number of experiments under various circumstances. The models is used for the outcomes which is able to predict metal binding with low as well as high concentrations (Langmuir 1918; Said et al. 2018).

Some important models are as follows:

(a) **Langmuir Model**

In 1918, Irving Langmuir gave the Langmuir model. It assumes that under isothermal condition an adsorbate shows the property of ideal gas. This model is valid for single layer adsorption. The basis of this model is a continuous monolayer of adsorbate molecules occupying a solid homogeneous surface (Langmuir 1918; Benzaoui et al. 2018). In this model adsorption energy is constant.

The Langmuir isotherm model works on certain assumptions.

These are:

(i)   The surface of adsorbent is uniform, i.e., uniformity of the surface
(ii)   No interactions between the adsorbed molecules
(iii) Molecules get adsorbed at defined sorption sites
(iv)   One adsorbate will occupy only one site on surface of adsorbent.

The Langmuir isotherm equation is given as:

$$q_e = \frac{Q_m b C_e}{1 + b C_e}$$

This equation is expressed in linear form as:

$$\frac{C_e}{q_e} = \frac{1}{b Q_m} + \frac{C_e}{Q_m}$$

Here, q_e is thesorbate amount that adsorb the sorbent per unit mass at equilibrium.

Q_m is the maximum consumption of sorbate per unit mass of sorbent.

C_e is sorbate concentration in solution.

b is Langmuir constant.

(b)   **Freundlich Model**

This model was given by Freundlich and this model describes the process of adsorption by the following equation (Freundlich and Heller 1939).

$$q_e = K C_e^{\frac{1}{n}}$$

Here, K and n are Freundlich constants.

K is related to capacity of adsorption.

Equation of linear form is given as:

$$\ln q_e = \ln K + \frac{1}{n} ln C_e$$

(c)   **Temkin Model**

The adsorption process are examined by Temkin (Temkin and Pyzhev 1940). This isotherm passes a factor that is used to understand the interaction of adsorbent–adsorbate. If low and large value of concentrations are neglected, then this model follow heat of adsorption decreases linearly rather than logarithmic with coverage.

It is given by the equation:

$$q_e = \frac{RT}{b}\ln(K_T C_e)$$

Here, q_e is the amount of sorbate adsorbed per unit mass of sorbent at equilibrium.
Here, b is Temkin constant.
K_T is Temkin constant related to binding.
C_e is the concentration of sorbate in solution.
The linear form of equation is given as:

$$q_e = B_1 \ln K_t + B_1 \ln C_e$$

Here, $B_1 = \frac{RT}{b}$.
R = 8.314 kJ/mol.K (Universal Gas Constant).
Absolute temperature is T in (K).

(d) Toth Model

This model is used in a heterogeneous system. In order to reduce the error experimental data and predicted data, the Langmuir model are modified in term of another empirical model that is called as Toth model. It is given by the equation (Toth 1971) where b and n is Toth isotherm constant (mg g^{-1}).

$$q_e = \frac{Q_m b C_e}{(1 + (b C_e)t)^{\frac{1}{t}}}$$

(e) Redlich–Peterson Model

The Redlich-Peterson isotherm is associated Langmuir and Freundlich isotherms. Therefore, adsorption process assumes the mix response of Langmuir and Freundlich model. It does not show the monolayer adsorption process. Heterogeneous systems are well described by Toth model. This model proves to be effective when pollutants are present at high concentration (Ayawei et al., 2017).

This model is given by the equation:

$$q_e = \frac{A_R C_e}{1 + B_R C_e^{m_R}}$$

Here, A_R, B_R and m_R are the model parameters.

Here, q_e is the sorbate amount adsorbed per unit mass of sorbent at equilibrium.
    Q_m is the maximum sorbate uptake per unit mass of sorbent.
    C_e is the sorbate concentration in solution.

8.2   Kinetic Models

Adsorption kinetics in wastewater treatment is of great significance. It helps us to know about the reaction pathways and mechanisms of adsorption. The kinetic models such as pseudo-first order and pseudo-second order models and inter particle diffusion are fitted to experimental data to find out optimum operating condition using coefficient of determination or by non linear regression analysis. This is used to observe the rate controlling step of sorption mechanism. The kinetic models describe the uptake of solute in which turn controls the time of residence adsorbate at the interface. The residence time is the total time a particular amount of material spends in the reservoir information about the kinetics of metal uptake helps us to provide the best suited condition for batch metal removal process (Said et al. 2018). Some of the models given to outline the adsorption kinetic process are as follows:

(A)   **Pseudo First Order Kinetic Model**

The equation of Lagergren rate is one of the most popular rate sorption equations used to describe the process of adsorption of solid liquid interaction (Kumar et al. 2019). It is expressed as

$$\frac{dq_t}{dt} = K_1(q_e - q_t)$$

It's linear form is expressed as

$$\ln(q_e - q_t) = lnq_e - K_1t$$

(B)   **Pseudo Second Order Kinetic Model**

It is based on certain assumptions (Deng and Wang 2012):

(i)   Adsorption monolayer is considered.
(ii) The energy of adsorption is same for each adsorbent.
(iii) Adsorption occurs on defined sites.
(iv) There is no interaction between adsorbed pollutants.

This model is expressed as:

$$\frac{dq_t}{dt} = K_s\left(q_{eq} - q_t\right)$$

Here, K_s is the adsorption rate constant.
q_{eq} is the of pollutant amount adsorbed on the surface of adsorbent.
The equation of linear form is given as

$$\frac{t}{q_t} = \frac{1}{K_s q_{eq}^2} + \frac{t}{q_{eq}}$$

(C)   **Weber And Morris Intra Particle Diffusion Model**

It is given by the equation (Mallampati et al. 2015):

$$q_t = k_{id}t^{\frac{1}{2}} + C$$

Here, q_t is the adsorbed amount at time t.

k_{id} is the rate constant.

C is the intercept value. This brings idea of the thickness of boundary layer, i.e., the greater the boundary, the larger the effect.

9   Factors Affecting Biosorption

(a)   **Effect of Temperature**

The temperature ranges between 25 and 30 °C. The bisorption process is affected. The temperature is a significant as far as thermodynamic sorption is concerned. Generally, two types of adsorption process is observed like endothermal and exothermic with decrease and increase in temperature respectively (Abbas et al. 2014). Increased temperatures may sometimes aid in biosorption but increase in temperatures can cause permanent damage to microbial cells, thereby decreasing the adsorption of metals (Ahalya et al. 2005; Abbas et al. 2014; Said et al. 2018).

(b)   **Effect of Biomass Concentration**

Adsorption of heavy metal is affected by the concentration of biomass. At a given concentration, low cell density adsorbed more metal ions than high cell density. High biomass concentration restricts the access of metal ions to the binding sites at biomass of low concentration, the biosorption of metals improve. Higher concentration of biomass leads to decreased biosorption due to interference between binding sites. If biomass concentration is high then it do not allow to access the binding site to the adsorbate (Abbas et al. 2014; Liu et al. 2013).

(c)   **Characteristics of Biomass**

The source of biomass used in sorption process can be considered as a significant parameters like plant source, freely-suspended cells, immobilized preparations, living biofilms etc. Physical and chemical treatment of adsorbent resultant to enhanced the adsorption capacity of adsorbent. Often affects the biosorption characteristics. Chemical treatment improves capacity of bisorption, as seen in some fungal biomass by treating them with alkali. Biosorption is also influenced by growth, nutrition and age of biomass because of change in the size of the cell, composition of wall etc. (Abbas et al. 2014; Said et al. 2018).

(d)   **Initial Concentration of Metal Ion**

The concentration of metal ion at initial rate provides a electromotive force to conquer all transferred mass resistances in the biosorption process. By increasing metal concentration, metal intake increases at given concentration of biomass. In order to overcome the mass transfer resistance, the initial concentration of adsorbate impart a significant driving force. With increased in initial concentration of adsorbate concentration causes to increased in uptake of adsorbent. Optimum percentage of adsorbate sequestration can be carried out at low initial concentration. Metal removal can be taken at low initial metal concentration (Abbas et al. 2014; Wan et al. 2014).

(e)   **Effect of PH**

pH of adsorption solution is considered as a important parameters to affect the uptake capacity of adsorbent. Since pH of adsorption solution causes to change the chemistry of metal ion and functional group present of adsorbent. Generally, biomass posses with the weekly basic or acidic functional group which polarity get change on tuning the pH of adsorbate solution. The changing in the polarity of adsorbent surface and chemistry of metal ion with change in pH of adsorbate solution causes to develop electrostatic attraction or repulsion force between adsorbent and adsorbate. So it is the essential biosorption process parameter. It also influences activity of functional groups and the competition of metal ions for the sorption sites. Generally, cations and protons compete for sites of binding which leads to reduction of heavy metal biosorption like Cd, Cu, Ni Zn, Co at low pH.

Generally, metal uptake is reduced at low pH. This is because of the competition between cations and protons for binding sites. This is due to negative ligands liable to positively charged metal ions with increase in attraction sites. Metal uptake gradually increases from pH 3–4.

The biosorption increases drastically beyond pH 6 because of the metal hydroxide formation and their competition effect on their active site of biomass. An optimal pH is essential to achieve an increased rate of biosorption, this capacity decreases further with increase in pH values (Abbas et al. 2014; Said et al. 2018; Wan et al. 2014; Ogbodu et al. 2015) (Table 5).

10   Desorption of Metals and Recovery of Lignocellulosic Materials

Generally, desorption of metal ion from the adsorbent is decided by the adsorption mechanism. Salt can be used to desorb the metal from adsorbent if adsorption mechanism is ion exchange. If adsorption mechanism is complexation and ion exchange then acid can be used to desorb high efficiency of metal ion from adsorbent. Another application of desorbing specialist is to recover biomass by elution of the stacked metal. The guidelines for picking the effective desorbing specialist are: (i) high metal

Table 5 Summary of some of biosorbents materials with their adsorption capacity and heavy metals removed

Biosorbent	Metal ion	Adsorption capacity q_{max} (mg g^{-1})	Temperature	Adsorbent dose	pH	References
Hamimelon	Pb(II)	7.89	25	0.1 g	5.0	Ozdes et al.
	Ni(II)	9.45	25	0.1 g	5.0	(2014)
Soy protein	Zn(II)	254.95	20	2.5 g	5.5	Ajmal et al.
	Cd(II)	120.83	20	2.5 g	5.5	(2003)
	Cu(II)	115.01	20	2.5 g	5.5	
Tea wastes	Pb(II)	33.49	25	0.1 g	5.0	Gupta and
	Cd(II)	16.87	25	0.1 g	5.0	Nayak (2012)
	Cu(II)	21.02	25	0.1 g	5.0	
Parkiza biglobosa biomass	Cd(II)	16.69	27	10 mg	6.0	Kaikake et al.
	Pb(II)	69.44	27	10 mg	6.0	(2007)
	Ni(II)	143.06	27	10 mg	6.0	
Pine bark (Pinusbrutina)	Cr(VI)	140.86	25	5 g		Martínez et al. (2006)

focus should be produced by little volume of the eluent in the subsequent arrangement, (ii) the underlying properties of the biomass should not be impacted, and (iii) the eluent should be economically.

As of now, most of the desorbing specialist applicable for metal and sorbent recuperation rely upon solid mineral acids (HNO_3, HCl, H_2SO_4), salts (NaCl, $CaCl_2$, KCl, KNO_3), bases ($NaHCO_3$, KOH, Na_2CO_3, NaOH, K_2CO_3), short-chain natural acids (CH_3COOH, HCOOH)), chelating specialists (diethylenediamine-pentacetic (DTPA), ethylenediaminetetraacetic (EDTA), nitrilotriacetic (NTA)) or support arrangement (phosphate, bicarbonate) (Ranjan et al. 2009).

Acids are the most widely used desorption specialist for recovering metal-loaded lignocellulosic biomass. The best desorbing solution for Cu(II) and Cr(VI) stacked onto business espresso squanders was found to be an acidic arrangement with (pH 2.0). During desorbing Cd(II) (83.9%) was obtained from rice husk in both bunch and section modes, for Cu(II) (99.4%), Cd(II) (98.5%) and Zn(II) (99.3%) from papaya wood, a 0.1 MHCl arrangement was found to be successful (Amin et al. 2006; Escudero et al. 2006). As(V) from coconut coir substance Gupta and Nayak used a 0.1 M HNO_3 arrangement to desorb 98.2% Cd(II) stacked onto orange strip powder with Fe_3O_4. To successfully desorb Cd(II) stacked onto espresso beans higher focuses than 0.01_M of HNO_3 and HCl were expected. With the use of 0.05_M HNO_3 Lead (II) loaded *Ficus religiosa* was recovered. In order to desorb U(VI) from citrus squander material, HCl and EDTA arrangements were utilized. 0.1 EDTA (94.7%) trailed by 0.1 HCl (89.71%) yielded the best desorption results. Martinez et al., likewise tested HCl and EDTA to recuperate Cu, Pb, Ni and Cd from grape tail and olive stones squanders, the previous being the best (Gupta and Nayak 2012; Kaikake et al. 2007; Qaiser et al. 2009; Martínez et al. 2006).

In order to remove metal particles/particles from biomass basic arrangements were effectively tested as desorbing specialists. Note that 0.5 M sodium citrate could take out lead(II) loaded on bounce side-effects. Elution of arsenic-loaded rice and rice husk stuffed sections was achieved by using arrangements of 10% NaOH and 1 M KOH separately (Amin et al. 2006; Ranjan et al. 2009). The significant desorption amount of metal ion from the adsorbent is to be considered as economical adsorption process and process is recyclable. Thus it can be suggested that adsorbent used in adsorption process is an excellent remediation technology for sequestration of heavy metal (Abbas et al. 2014; Escudero et al. 2006).

11   Conclusion

In the present study, we have reviewed the presence of toxic heavy metal as well as why it is required to remove from environment. In addition, in this article, we have dealt with the process of biosorption and their significant contribution towards the heavy metal elimination from polluted aqueous streams. This method has been found to be a suitable replacement for the existing biosorption systems. Lignocellulosic material can be used as a low cost biosorbent for removal of heavy metals. A thorough and effective method for selection of low cost biosorbents with high metal binding capacity has been covered. The low cost biosorption used in the system that is beneficial because they are relatively easy to obtain, do not cause pollution, show high affinity for metals and can be recovered after sequestering of metals. It can be used to remove heavy metals over quite a broad range of temperature, pH. This article also reviews the kinetics of adsorption and desorption and models explaining it. Biological biomass can be regenerated for further use. Thus, the process of biosorption has many advantages over conventional methods and it will find great applications in near future.

References

Abbas SH, Ismail IM, Mostafa TM, Abbas HS (2014) Biosorption of heavy metals: a review. J Chem Sci Technol 3(4):74–102

Abdel Raouf MS, Abdul Raheim ARM (2016) Removal of heavy metals from industrial waste water by biomass-based materials: a review. J Pollut Eff & Control 05(01). https://doi.org/10.4172/2375-4397.1000180

Abdolali A, Guo WS, Ngo HH, Chen SS, Nguyen NC, Tung KL (2014) Typical lignocellulosic wastes and by products for biosorption process in water and wastewater treatment: a critical review. Bioresour Technol 160:57–66. https://doi.org/10.1016/j.biortech.2013.12.037

Abdolali A, Ngo HH, Guo WS, Lee DJ, Tung KL, Wang XC (2014) Development and evaluation of a new multi-metal binding biosorbent. Bioresour Technol 160:98–106. https://doi.org/10.1016/j.biortech.2013.12.038

Ahalya N, Kanamadi RD, Ramachandra TV (2005) Biosorption of chromium(VI) from aqueous solutions by the husk of Bengal gram (*Cicer arientinum*) Electronic. J Biotechnol 8:258–264

Ahluwalia SS, Goyal D (2005) Removal of heavy metals from waste tea leaves from aqueous solution. Eng Life Sci 5:158–162

Ajmal M, Rao RAK, Anwar S, Ahmad J, Ahmad R (2003) Adsorption studies on rice husk: removal and recovery of Cd(II) from wastewater. Bioresour Technol 86(2):147–149. https://doi.org/10.1016/S0960-8524(02)00159-1

Ali SZ, Athar M, Salman M, Din MI (2011) Simultaneous removal of Pb(II), Cd(II) and Cu(II) from aqueous solutions by adsorption on *Triticumaestivum*—a green approach. Hydrol Current Res 2:118. https://doi.org/10.4172/2157-7587.1000118

Amin MN, Kaneco S, Kitagawa T, Begum A, Katsumata H, Suzuki T, Ohta K (2006) Removal of arsenic in aqueous solutions by adsorption onto waste rice husk. Ind Eng Chem Res 45(24):8105–8110. https://doi.org/10.1021/ie060344j

Anwar J, Shafique U, Waheed-uz-Zaman A, Salman M, Dar A, Anwar S (2010) Removal of Pb(II) and Cd(II) from water by adsorption on peels of banana. Bioresour Technol 101:1752–1755

Asberry HB, Kuo C, Gung C, Conte ED, Suenc S (2014) Characterization of water bamboo husk biosorbents and their application in heavy metal ion trapping. Microchem J 113:59–63

Ayawei N, Augustus Newton Ebelegi, Donbebe Wankasi (2017) Modelling and interpretation of adsorption isotherms. J Chem 1–11. https://doi.org/10.1155/2017/3039817

Bailey SE, Olin TJ, Bricka RM, Adrian DD (1999) A review of potentially low cost sorbents for heavy metals. Water Res 33:2469–2479

Bashir A, Malik LA, Ahad S, Manzoor T, Bhat MA, Dar GN, Pandith AH (2019) Removal of heavy metal ions from aqueous system by ion-exchange and biosorption methods. Environ Chem Lett 17:729–754. https://doi.org/10.1007/s10311-018-00828-y

Belfort G (1980) Adsorption on carbon: theoretical considerations. Environ Sci Technol 14(8):910–913

Benzaoui T, Selatnia A, Djabali D (2018) Adsorption of copper(II) ions from aqueous solution using bottom ash of expired drugs incineration. Adsorpt Sci Technol 36(1–2):114–129

Bhattacharyya KG, Gupta SS (2006) Adsorption of chromium(VI) from water by clays. Ind Eng Chem Res 45:7232–7240

Boota R, Bhatti HN, Hanif MA (2009) Removal of Cu(II) and Zn(II) using lignocellulosic fiber derived from *Citrus reticulate* (kinnow) waste biomass. Sep Puriff Technol 44:4000–4022

Chouchene A, Jeguirim M, Trouve G (2014) Biosorption performance, combustion behavior and leaching characteristics of olive solid waste during the removal of copper and nickel from aqueous solutions. Clean Technol Environ Policy 16:979–986

Dayan AD, Paine AJ (2001) Mechanisms of chromium toxicity, carcinogenicity and allergenicity: review of the literature from 1985 to 2000. Hum Exp Toxicol 20:439–451. https://doi.org/10.1191/096032701682693062

Deng X, Wang P (2012) Isolation of marine bacteria highly resistant to mercury and their bioaccumulation process. Bioresour Technol 121:342–347

Escudero C, Fiol N, Villaescusa I (2006) Chromium sorption on grape stalks encapsulated in calcium alginate beads. Environ Chem Lett 4:239–242. https://doi.org/10.1007/s10311-006-0055-0419

Escudero C, Fiol N, Villaescusa I, Bollinger JC (2013) Effect of chromium speciation on its sorption mechanism onto grape stalks entrapped into alginate beads. Arbian J Chem. https://doi.org/10.1016/j.arabjc.2013.03.011

Farooq U, Khan MA, Athar M, Konzinski JA (2011) Effect of modification of environmentally friendly biosorbent wheat (*Triticum aestivum*) on biosorptive removal of cadmium(II) ions from aqueus solution. Chem Eng J 171:400–410

Feng N, Guo X (2012) Characterization of adsorptive capacity and mechanisms on adsorption of copper, lead and zinc by modified orange peel. Tran Nonferrous Met Soc China 22:1224–1231

Freundlich H, Heller W (1939) The adsorption of cis- and trans-Azobenzene. J Am Chem Soc 61:2228–2230

Fu F, Wang Q (2011) Removal of heavy metal ions from wastewaters. J Environ Manage 92:407–418

Gao H, Liu Y, Zeng G, Xu W, Li T, Xia W (2008) Characterization of Cr(VI) removal from aqueous solutions by a surplus agricultural waste–rice straw. J Hazard Mater 31:446–452

Gardea-Torresdey JL, Tiemann KJ, Armendáriz V, Bess-Oberto L, Chianelli RR, Rios J, Parsons JG, Gamez G (2000) Characterization of Cr(VI) binding and reduction to Cr(III) by the agricultural by products of Avenamonida (Oat) biomass. J Hazard Mater 80:175–188

Garg UK, Kaur MP, Garg VK, Sud D (2007) Removal of hexavalent chromium from aqueous solution by agricultural waste biomass. J Hazard Mater 140:60–68

Gonen F, Serin DS (2012) Adsorption study of orange peels: removal of Ni(II) ions from aqueous solution. Afr J Biotechnol 11:1250–1258

Gupta VK, Nayak A (2012) Cadmium removal and recovery from aqueous solutions by novel adsorbents prepared from orange peel and Fe_2O_3 nanoparticles. Chem Eng 180:81–90. https://doi.org/10.1016/j.cej.2011.11.006

Gupta VK, Jain CK, Ali I, Sharma M, Saini VK (2003) Removal of cadmium and nickel from wastewater using bagasse fly ash a sugar industry waste. Water Res 37:4038–4044

Hansda A, Kumar V, Anshumali (2016) A comparative review toward potential of microbial cells for heavy metal with emphasis on bisorption and bioaccumulation. World J Microbiol Biotechnol 32(10):170. https://doi.org/10.1007/s11274-016-2117-1

Harris HH, Pickering IJ, George GN (2003) The chemical form of mercury in fish. Science 301(5637):1203. https://doi.org/10.1126/science.1085941

Ho YS, McKay G (1999) Pseudo-second order model for sorption processes. Process Biochem 34:451–465

Horiguchi H, Teranishi H, Niiya K, Aoshima K, Katoh T, Sakurangana N, Kasuya M (1994) Hypoproduction of erythropoietin contributes to anemia in chronic cadmium intoxication: clinical study on Itai-itai disease in Japan. Arch Toxicol 68:632

Johns MM, Marshall WE, Toles CA (1998) Agricultural by products as granular activated carbons for adsorbing dissolved metals and organics. J Chem Technol Biotechnol 71:131–140

Kaikake K, Hoaki K, Sunada H, Dhakal RP, Baba Y (2007) Removal characteristics of metal ions using degreased coffee beans: adsorption equilibrium of cadmium(II). Bioresour Technol 98(15):2787–2791. https://doi.org/10.1016/j.biortech.2006.02.040

Kakalnga SJ, Jabulani XB, Olutoyin OB, Utieyin OO (2012) Screening of agricultural waste for Ni(II) adsorption: kinetics, equilibrium and thermodynamics studies. Int J Phys Sci 7:2525–2538. https://doi.org/10.5897/IJPS12.097

Kelly VK, Cerro LM, Reyna TS, Bandala ER, Sanchez-Salas JL (2012) Biosorption of heavy metals in polluted water, using different waste fruit cortex. J Phys Chem Earth 37:26–29

Koramzadeh E, Nasernejad B, Halladj R (2013) Mercury biosorption from aqueous solutions by sugar crane bagasse. J Taiwan Inst Chem Eng 44:266–269

Krishnani KK, Meng X, Boddu VM (2008) Fixation of heavy metals onto lignocellulosic sorbent prepared from paddy straw. Water Environ Res 80(11):2165–2174

Kumar U, Bandyopadhyay M (2006) Sorption of cadmium from aqueous solution by agricultural waste cashew nut shell. Korean J Chem Eng 29:756–768

Kumar S, Narayanasamy S, Venkatesh RP (2019) Removal of Cr(VI) from synthetic solutions using water caltrop shell as a low-cost biosorbent. Sep Sci Technol 54(17):2783–2799. https://doi.org/10.1080/01496395.2018.1560333

Langmuir I (1918) The adsorption of gases on plane surfaces of glass, mica and platinum. J Am Chem Soc 40:1361–1368

Lasheen MR, Ammar NS, Ibrahim HS (2012) Adsorption/desorption of cd(II), Cu(II) and Pb(II) using chemically modified orange peel: equilibrium and kinetic studies. Solid State Sci 14:202–210

Lata S, Singh PK, Samadder SR (2015) Regeneration of adsorbents and recovery of heavy metals: a review. Int J Environ Sci Technol 12:1461–1478. https://doi.org/10.1007/s13762-014-0714-9

Liu D, Li Z, Li W, Zhong Z, Xu J, Ren J, Ma Z (2013) Adsorption behavior of heavy metal ions from aqueous solution by soy protein hollow microspheres. Ind Eng Chem Res 52:11036–11044

Liu C, Fiol N, Poch J, Villaescusa I (2016) A new technology for the treatment of chromium electroplating wastewater based on biosorption. J Water Process Eng 11:143–151. https://doi.org/10.1016/j.jwpe.2016.05.002

Malik DS, Jain CK, Yadav AK (2017) Removal of heavy metals from emerging cellulosic low cost adsorbents: a review. Appl Water Sci 7:2113–2136. https://doi.org/10.1007/s13201-016-0401-8

Mallampati R, Xuanjun L, Adin A, Valiyaveettil S (2015) Fruit peels as efficient renewable adsorbents for removal of dissolved heavy metals and dyes from water. ACS Sustain Chem Eng 3:1117–1124

Manzoor Q, Nadeem R, Iqbal M, Saeed R, Ansari TM (2013) Organic acids pretreatment effect on *Rosa bourbonia* phyto-biomass for removal of Pb(II) and Cu(II) from aqueous media. Bioresour Technol 132:446–452

Marin ABP, Aguilar MI, Ortuno JF, Meseguer VF, Saez J, Lorenz M (2010) Biosorption of Zn(II) by orange waste in batch and packed bed systems. J Chem Technol Biotechnol 85:1310–1318

Martínez M, Miralles N, Hidalgo S, Fiol N, Villaescusa I, Poch J (2006) Removal of lead(II) and cadmium(II) from aqueous solutions using grape stalk waste. J Hazard Mater 133:203–211. https://doi.org/10.1016/j.jhazmat.2005.10.030

Memoon Q, Mehmoon N, Shah SW, Khuhawar MY, Bhanger MI (2007) Sawdust—a green and economical sorbent for the removal of cadmium(II) ions. J Hazard Mater 139:116–121. https://doi.org/10.1016/j.jhazmat.2006.06.013

Mendieta GA, Olguín MT, Marcos SR (2012) Biosorption properties of green tomato husk (*Physalis philadelphica* Lam) for iron, manganese and iron–manganese from aqueous systems. Desalintion 284:167–174

Michalak I, Chojnacka K, Witek-Krowiak A (2013) State of the art for the biosorption process—a review. Appl Biochem Biotechnol 170:1389. https://doi.org/10.1007/12010-013-0269-0

Miretzky P, Cirelli AF (2010) Cr(VI) and Cr(III) removal from aqueous solution by raw and modified lignocellulosic materials: a review. J Hazard Mater 180(1–3):1–19. https://doi.org/10.1016/j.jhazmat.2010.04.060

Naiya TK, Chowdhury P, Bhattacharya K, Das SK (2009a) Sawdust and neem bark as low cost natural adsorbent for adsorptive removal of Zn(II) and Cd(II) ions from aqueus solutions. Chem Eng J 148:68–79

Naiya TK, Chowdhury P, Bhattacharya K, Das SK (2009) Sawdust and neem bark as low cost natural adsorbent for adsorptive removal of Zn(II) and Cd(II) ions from aqueus solutions. Chem Eng J 148:68–79

Nilanjana Das N (2010) Recovery of precious metals through biosorption—a review. Hydrometallurgy 103:180–189. https://doi.org/10.1016/j.hydromet.2010.03.016

Ogbodu RO, Omorogie MO, Unuabonah EI, Babalola JO (2015) Biosorption of heavy metals from aqueous solutions by Parkia biglobosa biomass: equilibrium, kinetics, and thermodynamic studies. Environ Prog Sustain Energy 34:1694–1704

Oliveira EA, Montanher SF, Andrade AD, Nobrega JA, Rollemberg MC (2005) Equilibrium studies for the sorption of chromium and nickel from aqueous solutions using raw rice bran. Process Biochem 40:3485–3490

Ozdes D, Gundogdu A, Kemer B, Duran C, Kucuk M, Soylak M (2014) Assessment of kinetics, thermodynamics and equilibrium parameters of Cr(VI) biosorption onto Pinusbrutia ten. Can J Chem Eng 92:139–147

Prasad AGD, Abdullah MA (2010) Biosorption of Cr (VI) from synthetic wastewater using the fruit shell of gulmohar (*Delonixregia*): application to electroplating waste water. Bioresources 5(2):838–853

Pujol D, Liu C, Gominho J, Olivella MA, Fiol N, Villaescusa I, Pereira H (2013) The chemical composition of exhausted coffee waste. Ind Crops Prod 50:423–429. https://doi.org/10.1016/j.indcrop.2013.07.056

Qaiser S, Saleemi AR, Umar M (2009) Biosorption of lead from aqueous solution by *Ficus religiosa* leaves: batch and column study. J Hazard Mater 166(2–3):998–1005. https://doi.org/10.1016/j.jhazmat.2008.12.003

Rangabhashiyam S, Anu S, Giri NMS, Selvaraju N (2014) Relevance of isotherm models in biosorption of pollutants by agricultural by products. J Environ Chem Eng 2(1):398–414. https://doi.org/10.1016/j.jece.2014.01.014

Ranjan D, Talat M, Hasan SH (2009) Rice polish: an alternative to conventional adsorbents for treating arsenic. Ind Eng Chem Res 48:10180–10185. https://doi.org/10.1021/ie900877p

Rehman R, Anwar J, Mahmud T, Salman M, Mahboob S (2012) Optimization of operational conditions for batchwise biosorption of Cr(VI) using chemically treated *Alstonia scholaris* leaves as biosorbent. J Chem Soc Pak 34:292–298

Saeed A, Akhter MW, Iqbal M (2005) Removal and recovery of heavy metals from aqueous solution using papaya wood as a new biosorbents. Sep Purif Technol 98:3344–3353

Said KAM, Ismail NZ, Jama RL, Alipah NAM, Sutan NM, Gadung GG, Baini R, Zauzi NSA (2018) Application of Freundlich and Temkin isotherm to study the removal of Pb(II) via adsorption on activated carbon equipped polysulfone membrane. Int J Eng Technol 7(3.18):91–93

Sarin V, Singh TS, Pant KK (2006) Thermodynamic and breakthrough column studies for the selective sorption of chromium from industrial effluent on activated eucalyptus bark. Bioresour Technol 97(16):1986–1993. https://doi.org/10.1016/j.biortech.2005.10.001

Seki K, Saito N, Aoyama M (1997) Removal of heavy metal ions from solutions by coniferous barks. Wood Sci Technol 31:44–447

Singh KK, Hasan SH, Talat M, Singh VK, Gangwar SK (2009) Removal of Cr(VI) from aqueous solutions using wheat bran. Chem Eng J 151:113–121

Srivastava S, Agrawal SB, Mondal MK (2015) A review on progress of heavy metal removal using adsorbents of microbial and plant origin. Environ Sci Pollut Res 22:15386–15415

Sud D, Mahajan G, Kaur MP (2008) Agricultural waste material as potential adsorbent for sequestering heavy metal ions from aqueous solutions—A review. Bioresour Technol 14(99):6017–6027. https://doi.org/10.1016/j.biortech.2007.11.064

Temkin MI, Pyzhev V (1940) Kinetics of ammonia synthesis on promoted iron catalyst. Acta Phys Chim USSR 12:327–356

Tewari N, Vasudevan P, Guha BK (2005) Study on biosorption of Cr(VI) by mucorhiemalis. J Biochem Eng 23:185–192

Toth J (1971) State equation of the solid gas interface layer. Acta Chimica (Academiae Scientiarum) Hungaricae. 69:311–317

Vanholme R, Demedts B, Morreel K, Ralph J, Wout-Boerjan W (2010) Lignin biosynthesis and structure. Plant Physiol 153:895–905

Volesky B (2003) Sorption and biosorption. BV Sorbex, Inc., Montreal, p 316

Wan S, Ma Z, Xue Y, Ma M, Xu S, Qian L, Zhang Q (2014) Sorption of lead(II), cadmium(II), and copper(II) ions from aqueous solutions using tea waste. Ind Eng Chem Res 53:3629–3635

Weber WJ, Morris JC (1963) Kinetics of adsorption of carbon from solution. J Sanitary Eng Div Am Soc Civ Eng 89:31–60

Zhang Y, Chi H, Zhang W, Sun Y, Liang Q, Gu Y (2014) Highly efficient adsorption of copper ions by a PVP-reduced graphene oxide based on a new adsorptions mechanism. Nano Micro Lett 6(1):80–87. https://doi.org/10.5101/nml.v6i1

Zhou CH, Xia X, Lin CX, Tong DS, Beltramini J (2011) Catalytic conversion of lignocellulosic biomass to fine chemicals and fuels. Chem Soc Rev 40(11):5588–5617. https://doi.org/10.1039/C1CS15124J

Synthesis of Iron Nanoparticles Loaded Proton Exchange Membrane for Microbial Fuel Cell Application

M. Mukunda Vani, P. Sirisha, Vijaya Kumar Talari, and S. Sridhar

Abstract Preparation of Iron nanoparticles being the cost-effective method by the process of green synthesis is gaining importance nowadays. Water being a vital source, and in order to attain clean, economical and green method for wastewater treatment, we explore synthesis of nanoparticles using neem extract. These nanoparticles after incorporation into polymeric membrane are further used to treat wastewater using microbial fuel cell and produce electricity. Characterization of the nanoparticles was done using UV–Visible spectroscopy, X-Ray Diffraction (XRD), and Scanning Electron Microscopy (SEM), which confirm the formation and presence of iron nanoparticles of size ranging 100 nm. Experiments on microbial fuel cell with nanoparticle coated membrane has given maximum voltage when compared to other polymeric membranes and was very effective in removal of contaminants from municipal wastewater and producing electricity as by-product. This purified water is well suited for all household and industrial applications.

Keywords Green synthesis of nanoparticles · Characterization · Treatment of wastewater · Electricity generation

1 Introduction

The availability of water in India is limited as it is estimated that only 65% of the population are in a state of utility. If we are able to reuse and recycle the contaminated water then the availability of water with increasing population will certainly be

M. Mukunda Vani (✉) · V. K. Talari
Department of Chemical Engineering, Anurag University, Ghatkesar, Hyderabad, India
e-mail: hodchem@cvsr.ac.in

P. Sirisha
Department of Chemical Engineering, Osmania University, Tarnaka, Hyderabad, India

S. Sridhar
CSIR-Indian Institute of Chemical Technology, Hyderabad, India

balanced. The treatment of wastewater by the potential use of engineered nanomaterial has sparked a great deal of interest (Zeng 2003). Nanoparticles are efficient in removal of pollutants and germs from wastewater. Due to its environmental compatibility, high reactivity and less cost, the most widely studied Nanomaterials for the treatment of wastewater is metallic iron (Kumar and Jee 2013). The synthesis of iron nanoparticles using top-down and bottom-up approaches shows various limitations such as low productivity, high energy consumption, the reducing agent that is sodium borohydride being toxic in nature and expensive (Devatha et al. 2016).

Many research studies have revealed that embedding of nanoparticles into membrane enhances the properties of physical, chemical, mechanical, thermal stability, its structure, morphology, porosity and hydrophilicity (Lau et al. 2015). Comparison to other polymeric membranes, nanoparticles prepared by green methods offer improved performance, long lasting durability and anti-fouling nature. Preparation of iron nanoparticles by neem leaf extract is the best convenient finding compared to other typical methods. Two methods are available to incorporate the nanoparticles in membranes: (i) addition of nanopartilces to membrane (ii) deposition of nanoparticles on the surface of the membrane (Lakhotia et al. 2018).

The conventional technologies for the wastewater treatment plants are the major energy sinks, so they areno longer suitable in current scenario of energy crisis. In this regard, a sustainable technology having a capability to treat wastewater is a Microbial fuel cell (MFC) that in turn works as a producer of energy. It uses the ability of microorganisms to decompose the organic matter present in the wastewater along with the generation of bioelectricity (Sahu 2019).

The electrodes effectiveness of MFC is based on the property of material which includes surface area, electrical conductivity, compatibility, anti-corrosive properties and cost factor. Economic viability and efficiency of microbial fuel cell is influenced by the substrate, which acts as an essential factor for the production of energy from solid and liquid waste (Binh et al. 1998).

The power density of 230 mW m^{-2} was generated in double chambered MFC with wastewater generated from food industries (Mansoorian et al. 2013). An MFC with air–cathode was used to generate power from wastewater of starch industries (Lu et al. 2009). Many studies focus on the different membranes to reduce the cost of MFC by using the ceramic materials and ionic liquids which are better than the conventional membranes (Hernández-Fernández et al. 2015).The power is generated from the domestic wastewater, sewage sludge and cow dung in single chamber MFC (Sonu and Das 2016).

The present study focuses on the green synthesis of iron nanoparticles with neem extract. Characterization of synthesized iron nanoparticles was performed using UV–Visible spectroscopy, X-Ray Diffraction and Scanning Electron Microscopy (SEM). These nanoparticles are further incorporated into polymeric membrane and are used in MFC to evaluate its efficiency for treating municipal waste water which also produced electricity as a byproduct. Upon treatment of municipal wastewater by this biological method ensures application for household (washing, cleaning and watering plants) and industrial purposes.

2 Materials and Methods

2.1 Synthesis of Iron Nanoparticles Using Neem Extract

Polyether sulphone, ferric chloride (FeCl$_3$) and potassium chloride are purchased from Sigma Aldrich Chemical Private Ltd., Bangalore, India and neem leaves are collected from the local region. They are cleaned to remove dust particles with distilled water and dried at ambient temperature. Then the dried Neem leaves are chopped into small pieces with the knife sterilized with ethanol and crushed in mortar and pestle. Approximately, 6 g of Neem leaf powder is added in 100 ml of distilled water which is sterilized and kept for heating for about 10 min at 70–80 °C under constant stirring. The extract is then filtered with vacuum filtration using filter paper. By using the standard sterilized filtration method, the filtrate was collected in a clean and dry conical flask and was stored in a refrigerator.

Neem extract is titrated against 0.1 M of FeCl$_3$ in the ratio 2:1. The change in the color of solution from yellowish to black under continuous titration is the key sign for the identification of nanoparticles (Afsheen et al. 2018), which are further subjected to characterization to know their shape and size. This solution is subjected to centrifugation at 5000 rpm for 10 min. The deposited nanoparticles are washed with distilled water and ethanol. The pellet containing the nanoparticles is kept for drying in a hot air oven overnight at 50 °C for 12 h and subjected for characterization of X-ray diffraction and scanning electron microscopy. Figure 1 shows the preparation of iron nanoparticles from neem leaves.
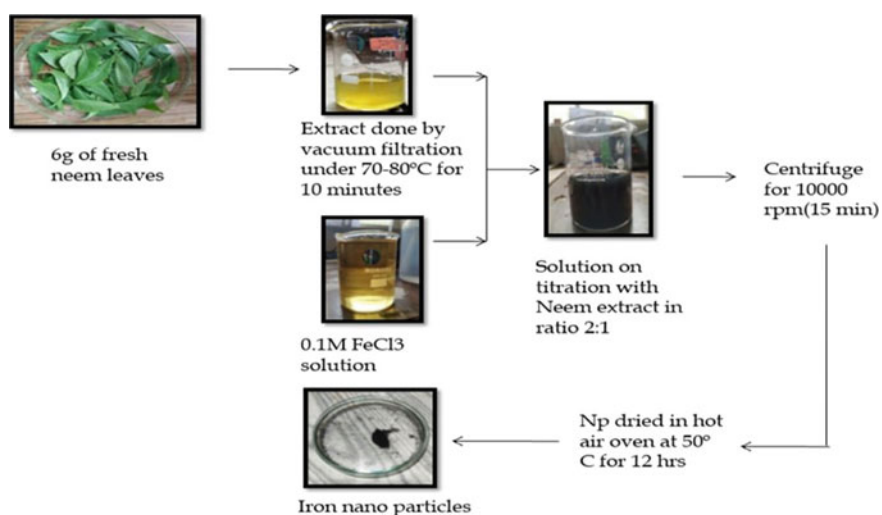
Fig. 1 Green synthesis of iron nanoparticles from Neem leaves

2.2 Incorporating Iron Nanoparticles into Membrane

Iron nanoparticles of 45 mg is added to 20.5 g of *N*-Methyl pyrrolidine (NMP) solvent and the solution kept for sonication for 15 min for uniformly distribution of iron nanoparticles. Then under constant stirring 4.5 g of Polyether sulphone (PES) is added. The resultant polymer solution is de-aerated to remove the gas bubbles. Subsequently the clear solution is poured into the glass plate and kept into vacuum oven for 2 h at 95 °C. Finally the iron nanoparticles are incorporated into polymer electrolyte membrane (Lakhotia et al. 2019).

2.3 Synthesized Membrane into Microbial Fuel Cell

Microbial Fuel Cell (MFC) is defined as biologically electrochemical system which converts the chemical energy in an organic material into electric current through redox reactions. MFC consists of chambers anode and cathode which are physically separated by proton exchange membrane. An electrode of Graphite is used in anode and cathode chamber. These electrodes were connected through external copper wires and the anode chamber was sealed with a no conducting silicone tube. The experimental set up of the microbial cell was shown in Fig. 2 and schematic diagram in Fig. 3. Anode chamber consists of mixture of municipal water of 700 ml and cow dung culture of 70 ml. Cow dung culture consists of organic matter. The mixture of municipal water and cow dung culture is considered as wastewater. Cathode Chamber consists of potassium permanganate of 0.5 g and de-mineralized water of 700 ml. Organic matter is oxidized at the anode by microorganisms and the electrons released during their metabolism pass from the anode towards the cathode through an external electric circuit, where they are transferred to oxygen that acts as an electron acceptor.

Fig. 2 Experimental setup of microbial fuel cell
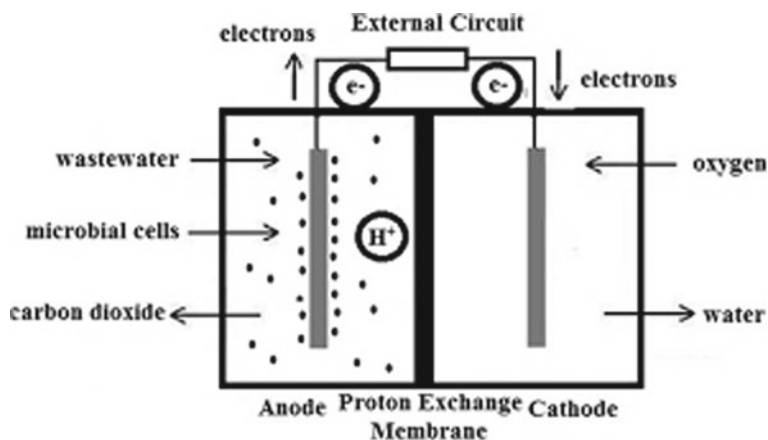
Fig. 3 Schematic diagram of microbial fuel cell

Oxygen is combined with the protons, that crosses a proton exchange membrane which is semi-permeable and forms water (Hernández-Fernández et al. 2015).

- Anode reaction (Oxidation)

$$C_6H_{12}O_6 + 6H_2O \rightarrow 6CO_2 + 24H^+ + 24e^- \tag{1}$$
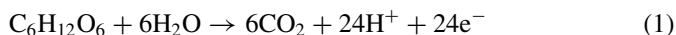
- Cathode reaction (Reduction)

$$6O_2 + 24H^+ + 24e^- \rightarrow 12H_2O \tag{2}$$
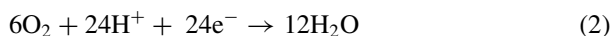
3 Results and discussions

3.1 Characterization of Iron Nanoparticles

The phase of single unit cell with dimensions is identified using XRD. The crystallinity of iron nanoparticless was investigated using XRD (D8 Advance Brukeraxs) by step scan technique with Cu-K_α radiation (1.540 Å, 40 kV, 30 mA). The analysis in XRD is done using the copper radiation K_α for the X-ray generation having a wavelength of 1.54060 A°. XRD peaks observed at 35.74°, 38.5° and 41.37° with planar reflections of 200, 311 and 400 respectively using Azadirachta leaves extract is shown in Fig. 4. In Complete spectrum of $2\theta = 0$–80°, only one peak with high intensity could be seen which implies iron nanoparticles are amorphous in nature.

Scanning electron microscopy (SEM) is used to determine the shape, size and morphology of iron nanoparticles that are prepared by the green synthesis method.
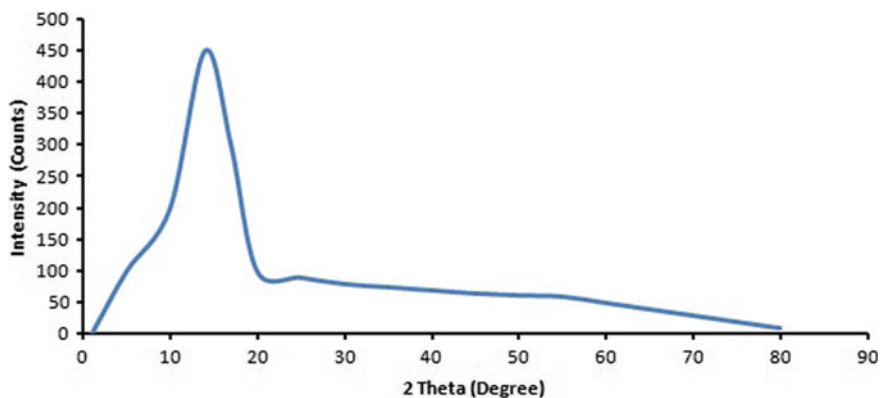
Fig. 4 XRD graph of Iron nanoparticles (intensity vs. 2θ angle)

Fig. 5 SEM image of iron
nanoparticles
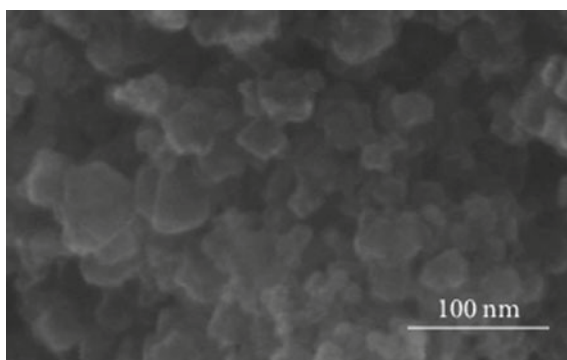
The shapes of the particles are nearly spherical as shown in Fig. 5. They have amorphous structure with diameter around 100 nm and they can be distinguished from each other, which are in agreement with the results of SEM of Afsheen et al. (2018).

UV- visible spectroscopic analysis of iron nanoparticles is carried out using UV–visible spectrometer in the range 200–650 nm and peaks are observed between 212 and 254 nm regions that is due the excitation of surface Plasmon vibrations in the solution of iron nanoparticles, which are identical to the UV–visible spectrum characteristics of metallic iron as shown in Fig. 6.

3.2 Treatment of Wastewater

Various parameters such as total dissolved solids (TDS), electrical conductivity, pH, color and turbidity in the waste water sample collected were found to be 152, 0.17, 5.23, 178 and 22 respectively. Experiments were carried out in Microbial fuel
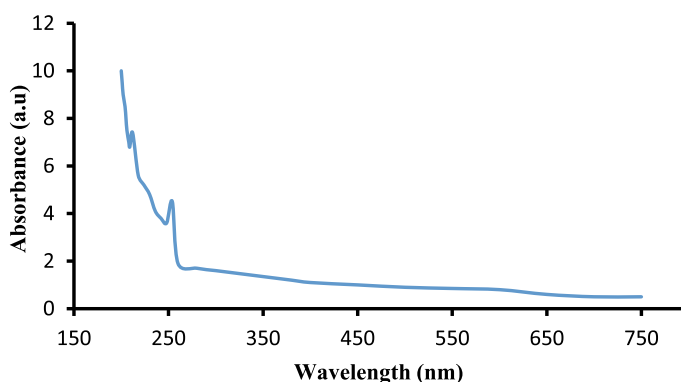
Fig. 6 UV–Visible spectroscopic analysis of iron nanomaterials

Table 1 Various parameters of water in feed and permeate streams

Parameters	Feed	Permeate
pH (mol/L)	5.23	6.14
Electrical conductivity (μS/cm)	0.17	0.09
TDS (ppm)	152	150
Color (ppm)	178	117
Turbidity (NTU)	22	19

cell (MFC) and the permeate was collected after 10 days beyond which there was no significant variation in voltage drop. The above parameters were measured in permeate and found to be 6.14, 0.09, 150, 117 and 19 respectively (Table 1). The pH value increased from 5.23 to 6.14 and whereas electrical conductivity decreases from 0.17 to 0.09. The permeate from microbial fuel cell may be suitable for the domestic use as the pH value close to neutral. TDS in municipal wastewater is slightly reduced from 152 to 150 and color decreases significantly from 178 to 117. Turbidity, which is the measure of clarity of liquid, reduced from 22 to 19. It is found from the results that the performance of microbial fuel cell was improved with the incorporation of iron nanoparticles in proton exchange membrane.

3.3 Voltage Characteristics of Microbial Fuel Cell with Incorporation of Iron Nanoparticles in Proton Exchange Membrane

Proton exchange membrane and graphite electrode combination is found to be appropriate for the treatment of municipal wastewater. The microorganisms release protons and electrons during the oxidation of organic matter in anodic side. These are in turn
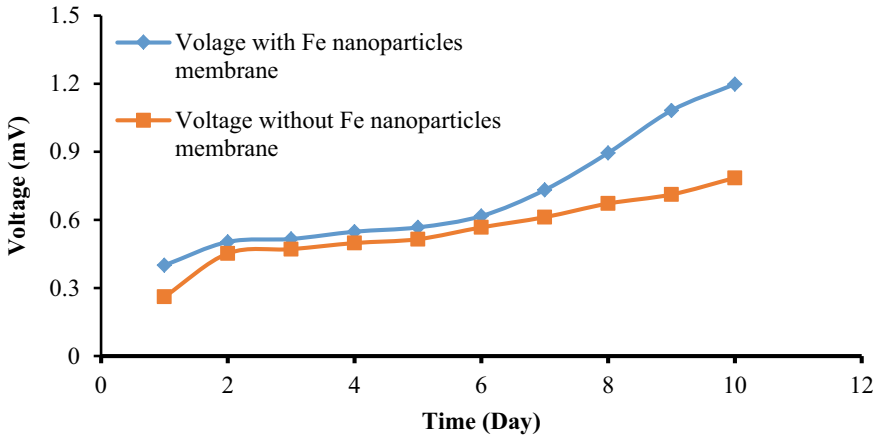
Fig. 7 Voltage of MFC with and without of incorporation of iron nanoparticles in polymer electrolyte membrane

united with electron acceptors in cathode side to produce electricity. Cell voltage of the system was monitored using precision multi meter (DT-830D) which was recorded manually on day basis. The result presented in the Fig. 7 shows that voltage increases with increase in time. At certain point voltage decreases due to reduction in organic compounds, this is raised by adding externally some amount of feed to organisms such as glucose, etc. to sustain in that environment. It was observed that using municipal wastewater and mixed culture showed a maximum voltage of 1.198 mV over 10 days of the experiment which are good agreement with the results obtained by Prakash (Parkash 2016). It was found from the results that the performance of microbial fuel cell was improved with the incorporation of iron nanoparticles in proton exchange membrane than without iron nanoparticles (0.785 mV).

4 Conclusion

Microbial fuel cell is used for power generation from wastewater with an innovative technique. In this study, it was concluded that iron nanoparticles embedded membrane achieved maximum voltage of 1.198 mV for 10 days experiment using municipal wastewater as substrate which showed the increased feasibility of bioenergy generation from wastewater. Pollutants of the contaminated water are significantly reduced, which can be observed from the reduction in electrical conductivity, TDS, color and turbidity values and increase in pH value towards the neutral. Electrodes and membranes which are low cost can be developed without compromising

with the performance of microbial fuel cell. Future research can aim for its operational ease, reduction of cost through construction of materials that are economically viable and enhancement of performance for its successful implementation in full-scale wastewater treatment through self-energy sufficient process.

References

Afsheen S, Tahir MB, Iqbal T, Liaqat A, Abrar M (2018) Green synthesis and characterization of novel iron particles by using different extracts. J Alloy Compd 732:935–944

Binh VT, Purcell ST, Semet V, Feschet F (1998) Nanotips and nanomagnetism. Appl Surf Sci 130:803–814

Devatha CP, Thalla AK, Katte SY (2016) Green synthesis of iron nanoparticles using different leaf extracts for treatment of domestic waste water. J Clean Prod 139:1425–1435

Hernández-Fernández FJ, De Los Ríos AP, Salar-García MJ, Ortiz-Martínez VM, Lozano-Blanco LJ, Godínez C, Quesada-Medina J (2015) Recent progress and perspectives in microbial fuel cells for bioenergy generation and wastewater treatment. Fuel Process Technol 138:284–297

Kumar A, Jee M (2013) Nanotechnology: a review of applications and issues. Int Int J Innov Technol Explor Eng 3(4):1–2

Lakhotia SR, Mukhopadhyay M, Kumari P (2018) Surface-modified nanocomposite membranes. Sep Purif Rev 47(4):288–305

Lakhotia SR, Mukhopadhyay M, Kumari P (2019) Iron oxide (FeO) nanoparticles embedded thin-film nanocomposite nanofiltration (NF) membrane for water treatment. Sep Purif Technol 211:98–107

Lau WJ, Gray S, Matsuura T, Emadzadeh D, Chen JP, Ismail AF (2015) A review on polyamide thin film nanocomposite (TFN) membranes: History, applications, challenges and approaches. Water Res 80:306–324

Lu N, Zhou SG, Zhuang L, Zhang JT, Ni JR (2009) Electricity generation from starch processing wastewater using microbial fuel cell technology. Biochem Eng J 43(3):246–251

Mansoorian HJ, Mahvi AH, Jafari AJ, Amin MM, Rajabizadeh A, Khanjani N (2013) Bioelectricity generation using two chamber microbial fuel cell treating wastewater from food processing. Enzyme Microb Technol 52(6–7):352–357

Parkash A (2016) Characterization of generated voltage, current, power and power density from cow dung using double chambered microbial fuel cell. J Phys Chem Biophys 6(208):2161–0398. https://doi.org/10.4172/2161-0398.1000208

Sahu O (2019) Sustainable and clean treatment of industrial wastewater with microbial fuel cell. Res Eng 100053

Sonu K, Das B (2016) Comparison of the output voltage characteristics pattern for sewage sludge, kitchen waste and cow dung in single chamber single electrode microbial fuel cell. Indian J Sci Technol 9(30)

Zeng L (2003) A method for preparing silica-containing iron (III) oxide adsorbents for arsenic removal. Water Res 37(18):4351–4358

Ferrofluids for Waste-Water Treatment

Abhishek Kumar, Krunal M. Gangawane, and Bomma Ramanjaneyulu

Abstract The availability of high-quality, low-cost water to meet requirements of the human has become a major issue in the twenty-first century. Supply of fresh water systems throughout the globe are failing to keep up with increasing demand, which has also been made worse by human population growth, global warming, and other factors and decreasing water quality in recent years. No amount of emphasis can be placed on the significance of technological innovation in allowing integrated water resource management. Nanotechnology promises to improve water and waste-water treatment efficiency. Due to its unique features, including as very tiny size, high surface-area-to-volume ratio, the surface's potential to be modified, good magnetic characteristics, as well as a high level of biocompatibility, the use of iron oxide nanoparticles has gotten a lot of interest. Iron oxide nanoparticles have been propose as nano absorbents and photo catalysts in various environmental cleanup methods for waste-water treatment. This study described the most recent iron oxide nanoparticles uses in waste-water treatment, as well as the gaps that have hampered their large-scale field usage.

Keywords Ferrofluid · Waste-water · Iron oxide nanomaterials

1 Introduction

Water is essential for public welfare, whether for drinking, residential usage, agricultural production. Improved water and sanitation, as well as improved management of water resources, may contribute to the economic growth of nations and the elimination of poverty in developing countries. Both ancient and new issues beset

A. Kumar · K. M. Gangawane (✉)
Department of Chemical Engineering, National Institute of Technology Rourkela, Rourkela, Odisha 769008, India
e-mail: gangawanek@nitrkl.ac.in

B. Ramanjaneyulu
Department of Chemical Engineering, University of Petroleum and Energy Studies, Dehradun, Uttrakhand 248007, India

our existing water supply. Around 71% of the world's population still lacks better drinking water sources (World Health Organization (WHO), Homepage). Essential water treatment must be implemented immediately in impacted regions (mostly in developing nations), where water and waste-water infrastructure is typically lacking. Human activities are becoming increasingly crucial in worsening water shortage by polluting natural water sources in developing and developed countries. Water treatment and supply chain have increased scrutiny in industrialized nations due to more strict water quality requirements, exacerbated by developing pollutants. The demand is continuously increasing as the world population grows and living standards improve.

Furthermore, global climate change exacerbates the existing inequitable allocation of freshwater, putting the supply in jeopardy. Obtaining water from unusual sources (e.g., storm-water, polluted freshwater, brackish water, waste-water, and seawater) is becoming the new standard, especially in traditionally water-stressed regions, due to increased strain on water supplies. In addition, present water and waste-water treatment technologies are nearing their limits to deliver acceptable water quality to fulfill human and environmental demands.

Some of the vital factors of drinking water according to WHO, 2017 (World Health Organization (WHO), Homepage).

- In 2017, three-quarters of the population of the globe (5.3 billion people) drink from a safe, prudently handle method of distribution drinkable water—one who was there on the premises, accessible whenever it is needed, and it is not polluted by any circumstance.
- 90% worldwide (6.8 billion people) used at least one fundamental service. A free package is better than drinking the water within such a 30-min cycle trip to obtain water.
- 785 million people, particularly 144 million people who rely on surface water, do not have minimum drinking water access.
- At least 2 billion people in the globe drink water that has already been contaminated by pollution.
- Diarrhea, cholera, dysentery, typhoid, and polio can all be spread by contaminated water. Each year, 485,000 people die from diarrhea because of contaminated drinking water.
- By 2025, 50% of the planet population will live in areas of water stress.
- A water supply is not available at 22% of healthcare facilities in least developed countries, sanitation is not available at 21%, and waste management is not available at 22% of these facilities.

Nanotechnology advancements have opened the possibility of a new world to developing water supply systems of the future. Water treatment, circulation, and disposal techniques rely on transport, and interconnected approach is no more viable choices in today's world. Nanotechnology-enabled, highly efficient, flexible, and versatile processes are expected to deliver high-performance, low-cost water and waste-water treatment options that depend less on big infrastructures (Qu et al. 2013). This covers the production and use of different nanomaterials, ranging from

1 to 100 nm in size, as well as the usage of equipment and structures with unusual properties not found in conventional materials (Stone et al. 2004). With its nanotechnology capacities, the waste-water processing system will address critical problems posed by present processing technologies and offer novel treatment process to enable profitable expansion of the water supply to unconventional sources (Wang et al. 2010).

The essential properties of iron oxide nanomaterials are analyzing in this chapter. It shows recent advances in the treatment of waste-water using iron oxide nanoparticles and the gaps that have hindered their use in the field on a broad scale. The importance of recent developments in the application of iron oxide nanomaterials as nano sorbent s is a highlight, followed by a critical assessment of their application as photo catalysts.

Also discussed is the virtual potential of the iron oxide-based immobilization technique for increasing pollution effectiveness in the elimination process. The destiny of iron oxide nanomaterials released into the environment and the related cleanup methodology are also examined. Laurent et al. (2008) and Teja and Koh (2009) provided extensive descriptions of the synthesis process, characteristics, and characterization of iron oxide nanomaterials.

Figure 1 depicts the framework of this chapter (Xu et al. 2012).
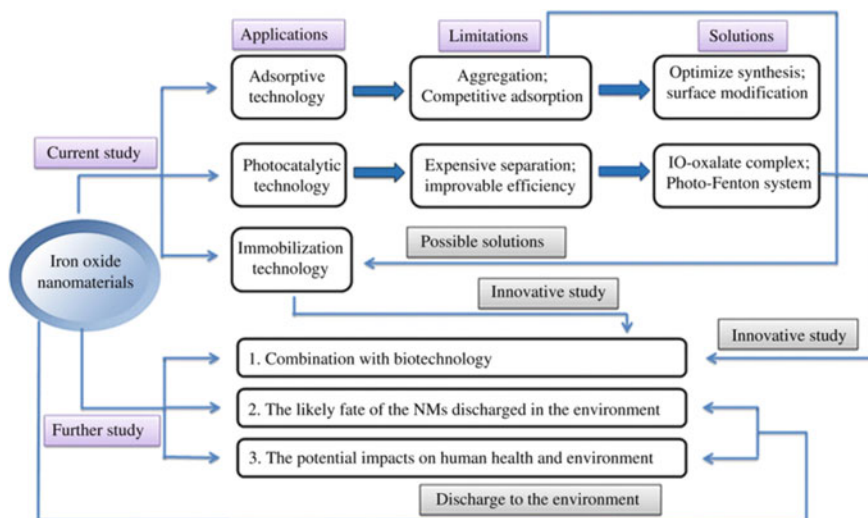
Fig. 1 Depicts the framework of iron oxide nanomaterial for waste-water treatment. Reproduced or reprinted with copyright permission from Ref. Xu et al. (2012)

2 Waste-Water

Waste-water is generated in various ways, including household/domestic, commercial, and industrial operations. Surface and groundwater may enter the waste-water discharge system, increasing the total amount of waste-water to be processed. Domestic waste-water (home and business waste-water) typically contains pollutants such as vegetable materials, grease and scum detergents, and silt, among other things. Elsewhere, industrial effluent has found hazardous compounds and metals, chemical materials, radioactive materials, large amounts of silt, high-temperature waste, or acidic/basic waste. At the same time, waste-water from roadways and parking lots during rainfall may contain oil, gasoline, pesticides, herbicides, and leftover sediments (Feachem et al. 1983; Abedi-Koupai et al. 2006).

3 Types of Contaminants Found in Water and Waste-Water

They are of a certain kind and source of contaminants in water and waste-water have been categorized as inorganic, biological, or organic pollutants. Figure 2 depicts the different forms of pollutants (Gupta et al. 2012). Heavy metals are some of the most pollutants that are poisonous found in water.

and waste-water because they bioaccumulation. Bioaccumulation occurs when a chemical's concentration in an organism exceeds its concentration in the environment. When elements are taken in and stored rather than dismantled or expelled, they accumulate in biological systems (El-Sayed 2020).

Metals with a specific density of 5 g/cm^3 and atomic weights ranging from 63.5 to 200.6 have referred to as "heavy metals" (Beyersmann and Hartwig 2008). While these metals are required for various biochemical and physiological functions at very low concentrations in live organisms, they become hazardous if concentration limits are exceed. Chemicals have been widely used, which has resulted in a rise in a load of undesirable contaminants in accessible waste-water sources all over the world. As a result, social and environmental wellbeing, as well as financial stability, suffer (Chapman et al. 1996).
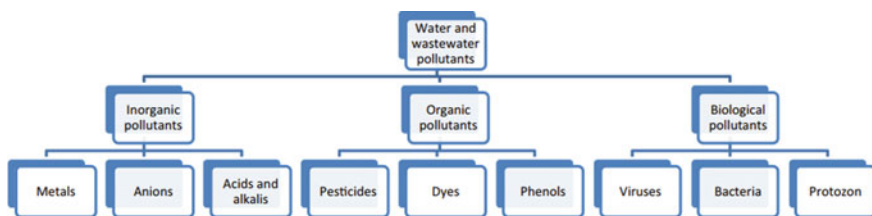
Fig. 2 Contaminant kinds in water and waste-water are categorize according to their chemical composition. Reproduced or reprinted with copyright permission from Ref. El-Sayed (2020)

Organic material is also a significant kind of water pollutant. It has measured in references of total organic carbon (TOC). Dissolved and particulate materials are both included in the TOC. As a result, fluctuations in suspended solids impact total organic carbon, which could be observe in lakes and rivers. Organic carbon in freshwater derives from living organisms and is found in a variety of wastes and sewer water. As a result, the total organic carbon of water is a helpful indicator of pollution levels (Wahaab et al. 2020). The lifespan of marine species and animals is the primary source of organic contaminants in water, including residential sewage, average run-off, and debris. The different combinations of organic compounds in water produce an off-taste and disagreeable odor, preventing it from remedying for industry and household use.

4 Current and Prospective Uses for Treatment of Waste-Water

In the field of nanomaterials, materials having at least one dimension smaller than 100 nm are considered to be such. Regarding the magnitude of the situation, materials frequently exhibit unique size-dependent characteristics that are not present in their larger counterparts. Several of these characteristics have studied for possible use in water and waste-water treatment. Certain applications make advantage of the smooth scaled nanomaterials have characteristics that are depending on their size, which are used in a variety of applications, because of the high surface areas, the material exhibits properties also including rapid degradation, chemical sensitivity, and significant sorption. Others, such as superparamagnetic, confined Surface plasmon resonance (SPR), and the quantum confinement effect, use their discontinuous characteristics. These applications, dependent on nanomaterial functionalities in unit operating processes has addressed further below (Table 1). Most of the following applications are already in the experimental investigation stage. The exception examined in the pilot or field has recorded in the report (Nadeem 2013).

5 Ferrofluid Nanomaterial in Waste-Water Treatment

It has been found that iron-based nanomaterials have great sorption characteristics. This has been shown by their larger surface area, high porosity, and firm magnetic responses, which have resulted in an extraordinary absorption capacity (Hatamie et al. 2016). In nature, there are many minerals such as magnetite (gamma Fe_2O_3), magnetite (Fe_3O_4) and hematite (Fe_2O_3), and iron oxide materials (alpha-Fe_2O_3). Moreover, iron-based magnetic materials focus on different fields such as catalysis, waste disposal, magnetic agents, tissue imaging and magnetic resonance imagery. 10–20 nm nano part has founded to provide maximum efficiency. For such particles,

Table 1 Current and prospective uses for treatment of waste-water

Sr. No.	Application	Nanomaterials	Desirable characteristics of nanomaterials	Modified methods
1.	Adsorption	Carbon nanotubes	Adjustable surface chemistry, large specific surface area, highly assessable adsorption sites, varied micro pollutants interactions, simple reuse	Pre-concentration/detection of pollutants, recalcitrant pollutants adsorption
		Metal oxide on a nanoscale	Large specific surface area, low intra particle diffusion range, higher adsorption sites, compressible without significantly reducing surface area, simple reuse, some are ferromagnetic	Slurry reactors, adsorbent media filters
		Core-shelled nanofibers	Surface chemistry tailored to the shell for adsorption and desorption, a reactive core for breakdown	Nano-adsorbents that are reactive
2.	Membranes technology	Nano-zeolites	Hydrophilicity, molecular Sieve	Nanocomposite membranes with high permeability thin films
		Nano-Ag	Potent and broad-spectrum antibacterial action with little human toxicity	Anti-biofouling Membranes
		Carbon nanotubes	Unaligned carbon nanotubes have antimicrobial properties	Membranes with anti-biofouling properties
			Adjustable aperture, small diameter, atomic smoothness of the inner surface	Membranes made of aligned carbon nanotubes
			Stable mechanical and chemical properties	

(continued)

Table 1 (continued)

Sr. No.	Application	Nanomaterials	Desirable characteristics of nanomaterials	Modified methods
		Aquaporin nano-TiO$_2$	Selectivity and permeability are high	Aquaporin membranes
			High chemical stability, photocatalytic activity, and hydrophilicity	High-performance thin-film nanocomposite membranes, reactive membranes
		Nano-magnetite	Superparamagnetic, tenable surface chemistry	Forward osmosis (F.O.)
3.	Photocatalysis	Nano-TiO$_2$	Photocatalytic activity in UV and possibly visible light range, low human toxicity, high stability, low cost	Solar disinfection systems and photocatalytic reactors
		Fullerene derivatives	High selectivity photocatalytic activity in the sun spectrum	Solar disinfection systems and photocatalytic reactors
4.	Disinfection and microbial control	Nano-Ag	Antimicrobial action that is solid and broad-spectrum, minimal human toxic effects, and simplicity of use	Water disinfection at the point of use, anti-biofouling surface
		Carbon nanotubes	Conductivity, antimicrobial action, and fibres morphology	Water disinfection at the point of use, anti-biofouling surface
		Nano-TiO$_2$	Photocatalytic production of reactive oxygen species, excellent chemical stability, minimal human safety, and cheap cost	From point-of-use disinfecting and decontamination to comprehensive decontamination and disinfecting
5.	Sensing and monitoring	Quantum dots	Broad absorption spectrum, compact, brilliant, and consistent emission that scales with particle size and chemical composition	Optical detection

Table 1 (continued)

Sr. No.	Application	Nanomaterials	Desirable characteristics of nanomaterials	Modified methods
		Noble metal nanoparticles	Surface plasmon resonances are enhanced locally, and conductivity is high	Detection using optics and electrochemistry
		Dye-doped Silica nanoparticles	High sensitivity and stability, as well as silica-rich chemistry that facilitates conjugation.	Optical detection
		Carbon nanotubes	Excellent electrical characteristics, large surface area, muscular mechanical strength, and chemical stability	Preconcentration and electrochemical detection
		Magnetic nanoparticles	Superparamagnetic, tenable surface chemistry	Purification and concentration of samples

a form of magnetism, superparamagnetic behavior, seen in ferromagnetic particles has described (Tijani et al. 2020).

Iron oxide nanoparticles has being studies as efficient adsorbents all around the world. Additionally, certain magnetite oxides and other ferrites, particularly inverse-spinel nickel ferrite, have improved their efficacy ($NiFe_2O_4$). The primary reason for this is studies that its unique tetrahedral and octahedral structure is form by an asymmetrical rotation of Fe^{3+} and Ni^{2+} in the ferromagnetic state. Another explanation for metal ferrites' strong potential for sorption activities is their great porosity, larger surface area, and excellent magnetic force. The amount of magnetic materials spanning from micrometer to nanoscale increases their surface energy and reduces overall stability (Zhao et al. 2013). Researchers have recently used the hydrothermal co-precipitation method to manufacture high-quality inverse-spinel $NiFe_2O_4$ using graphene oxide as the feedstock to address this issue. Using it as a sorbent has yielded cost-effective results, allowing for a more simple separation from heavy metals that have been adsorbed. Heavy metal removal is relate to the magnetic moment of the material from waste-water. The use of a magnet in an aqueous solution containing greasy oil and suspended particles results in a greater magnetic moment, which allows for simpler separation of the waste water. This approach helps avoid high-pressure drops and time-consuming separation procedures like filtering (Baig et al. 2020; Elboughdiri 2020).

Furthermore, the overall cost is reduce because the highly efficient adsorbent may be reuse for non-stop operation. The characteristics and processes of synthesizing iron oxide nanoparticles have extensively investigated. A large amount of

emphasis has been focused on iron-based nanomaterials in recent decades due to its elevated BET surface area, large pore volume, and super magnetic characteristics. As result of this increased attention, a major issue in waste-water treatment has emerged (Fialova et al. 2014). Hazardous heavy metals to provide an example like Cd(II), Pb(II), and Cu(II) are remove from waste-water utilizing graphene and other carob derivatives are examples of this, expanded carbon, and multiwall nanotubes, as well as paramagnetic particles (Fe_2O_3) discovered that graphene and Fe_2O_3 were hopeful candidates for eliminating heavy metals derived from the surrounding environment; with graphene oxide with a decreased reactivity and Fe_2O_3 magnetic properties having greater adsorption effectiveness for all metals analyzed the two additional carbon-based compounds (Paswan et al. 2021). Fe^{3+} and Cd(II) may be remove from waste-water using copper-based oxide nanoparticles. The pH level, a period of time spent in contact, and heavy metal removal is aided by the use of a variety of techniques, including metal concentration. Both metals are effectively remove using a batch adsorption method, according to the findings. The optimal settings were a 20-min adsorption duration and a 250-rpm agitation speed. An initial concentration of Fe^{3+} and Cd(II) ranged from 25 to 250 mg/L, resulting in high metal removal efficiency from waste-water. Furthermore, it was discovered that the adsorbent's selectivity order is Fe^{3+} > Cd(II). As a result, copper and other metel based nanoparticles are efficient adsorbents for the removal of heavy metals from sewage water or waste water. In another investigation, the removal effectiveness of C(VI) using different magnetic nanoparticles was as follows: $MnFe_2O_4$ > $Mg\ Fe_2O_4$ > $Zn\ Fe_2O_4$ > $Cu\ Fe_2O_4$ > $Ni\ Fe_2O_4$ > $Co\ Fe_2O_4$. The effectiveness of utilizing magnetic nanoparticles for removal are determine by pH, the pace at which things shake, and the nanoparticle's magnetic characteristics. The most efficient method for removing 99.5% of Cr(VI) from waste-water was determined to be $MnFe_2O_4$ based ferromagnetic nanoparticles on a magnetic field with an optimal pH of 2 and a shaking rate of 100–400 rpm (Huang et al. 2006).

5.1 Adsorption Process Technologies

The silent features of the adsorption process technologies for the heavy metals (Zn, Cr, Pb, Cd, As, Hg, etc.), and organic pollutants () are discussed in subsequent sub-sections.

5.1.1 Ferromagnetic Nanoparticles as Nanosorbents for Heavy Metals

As a result of its toxicity to plants, animals, and people, as well as its proclivity for accumulation of heavy metals even at small doses, contamination by heavy metals is a major source of concern. As a result, effective heavy metal ion removal techniques are in high demand, attracting a lot of research and practical attention (Chen et al. 2011; Pang et al. 2011a; Iram et al. 2010a). Ferromagnetic nanoparticles (Fe_3O_4)

are the foundation of numerous bench-scale evaluations and related technologies of nanomaterials for waste-water treatment that have been conducted (Stafiej and Pyrzynska 2007), carbon nanotubes (Kobya et al. 2005), activated carbon (Ponder et al. 2000), and zero-valent iron (Chauhan et al. 2019). Iron oxide magnetic nanoparticles, with their capacity to treat vast volumes of waste-water and ease of magnetic separation, appears to be the most critical targets for heavy metal treatment. The iron oxide nanoparticle has the potential to be extremely outstanding (Nassar and Husein 2010). Nassar (Otto et al. 2008) discovered that Fe_3O_4 nanoparticles had a adsorption capacity to the greatest extent possible for Pb(II) ions of 36.0 mg g^{-1}, considerably more significant than previously reported cost-effective adsorbents. The tiny size of Fe_3O_4 nano sorbent s allowed metal ions from the solution to diffuse quickly onto the active sites of the surface of the adsorbent. Fe_3O_4 nano sorbent were indicate as practical and adsorbents that are both cost-efficient and effective in the separation and recovery of metal ions from contaminated wastewater are being developed (Otto et al. 2008).

Ferromagnetic nanoparticles (Fe_3O_4) has shown to efficiently remove various heavy metals in laboratory experiments, including Pb^{2+}, Hg^{2+}, Cd^{2+}, Cu^{2+}, and others. Table 2 summarizes a list of functionalized ferromagnetic nanomaterials and their sorption capacity values. In contrast, on the other side, the ferromagnetic nanoparticles based heavy metal adsorption technique is still in its infancy for widespread use. It is well acknowledge that much more research is need in the realm of nanoparticles, and the transition of ferromagnetic nanoparticles (Fe_3O_4) from the laboratory to field-scale use is fraught with difficulties. More data on the performance and cost of nanoparticles will become accessible as contaminant removal treatment trends continue to grow, providing more knowledge for large-scale industrial applications (Kim et al. 2003).

5.1.2 Ferromagnetic Nanoparticles as Nanosorbent for Organic Contaminants

Adsorption has been long range utilised to manage different type of chemical pollutants in water, and it is a method that works very well for this purpose. The cost, adaptability, efficiency of design/operation, and insensitivity to hazardous contaminants offer several benefits (Rafatullah et al. 2010; Zhang and Fang 2010a). As a result, an efficient and low-cost adsorbent with high permeability to eliminate organic contaminants has been desire. Ferromagnetic nanoparticles are investigate for organic pollutant adsorption, notably for the effective production of severe water samples and rapid separation using a high magnetization. Many tests has carried out to determine ferromagnetic nanoparticles' effectiveness in removing organic contaminants (Luo et al. 2011; Iram et al. 2010b).Fe_3O_4 hollow nanospheres, for example, have been demonstrated to be a suitable sorbent for red dye (having the highest possible adsorption capacity of 90 mg g^{-1}) (Ma et al. 2005). The saturation magnetic induction of developed nanospheres has found to be 42 emu g^{-1}, which is enough for magnetic

Table 2 Heavy metal adsorption using functionalized ferromagnetic nanoparticles

Nanosorbents	Ligands	Heavy metals	Capacity for adsorption	Source
Silica magnetite	– NH2	Cu(II)	For Cu, the adsorbents had a potential of 0.5 mmol/g (II)	Wei et al. (2009)
Iron-nickel oxide with a magnetic field	–	Cr(VI)	For Cr(VI), the produced adsorbent has a highest absorption capacity of 30 mg/g	Yuan et al. (2009)
Montmorillonite-supported MNP	– AlO; –SiO	Cr(VI)	Cr had an adsorption capability of 15.3 mg/g (VI)	Pang et al. (2011b)
PEI-coated Fe3O4 MNPs	– NH2	Cr(VI)	Cr(VI) has a maximum adsorption capacity of 83.3 mg/g	Hu et al. (2007)
δ-FeOOH-coated γ-Fe$_2$O$_3$ MNPs	–	Cr(VI)	Cr(VI) has a maximum adsorption capacity of 83.3 mg/g	Li and Zhang (2006)
Flower-like iron oxides	–	As(V), Cr(VI)	The adsorption capacity of As(V) was 5.3 mg/g	Pradeep (2009)
Hydrous ferric oxide nanoparticles	–	As(V), Cr(VI)	The adsorbent contains 8 mg of arsenic per gram	Ambashta and Sillanpää (2010)
Iron oxide–silica	Si–OH	Pb(II), Hg(II)	For Pb(II) and Hg(II), respectively, the removal effectiveness was 97.34 and 90%	Huang and Chen (2009)
Amino-modified Fe$_3$O$_4$ MNPs	– NH2	Cu(II), Cr(VI)	Cu(II) ions had a maximum adsorption capacity of 12.43 mg/g, while Cr(VI) ions had 11.24 mg/g	White et al. (2009)

(continued)

Table 2 (continued)

Nanosorbents	Ligands	Heavy metals	Capacity for adsorption	Source
m-PAA-Na-coated MNPs	– COO	Cu(II), Pb(II)	Cd(II) (5.0 mg g1), Pb(II) (40.0 mg g1), Ni(II) (27.0 mg g1), and Cu(II) (30.0 mg g1) have adsorption capability	Zeng et al. (2007)
Poly-L-cysteine coated Fe$_2$O$_3$ MNPs	– Si–O; –NH2	Ni(II), Pb(II)	The recovery of the measured elements was nearly all over 50%, with Ni(II) removal effectiveness reaching 89%	Ahmad et al. (2009)

separation with a magnet (critical value of 16.3 emu g^{-1}). These results demonstrated that magnetic nanoparticle technology was a unique, promising, and option for adsorption of selected organic contaminants (Hu et al. 2011).

To improve the target's adsorption capacity, a nanoparticle must be modified and chemically treat. The application of carbon-coated Fe$_3$O$_4$ nanoparticles (Fe$_3$O$_4$/C) to remove trace polycyclic aromatic hydrocarbon is one example in this field. Experimental PAH, recoveries on Fe$_3$O$_4$/C Nano sorbents were substantially higher than those are on pure Fe$_3$O$_4$ nanoparticles, and target compound removal efficiency was above 90% for PHA, FlUA, Pyr, BaA, and BbF. Furthermore, the presence of carboxyl and hydroxyl groups in this technique might alter Fe$_3$O$_4$/C nanoparticles with hydrophilic surfaces. The altered nanoparticles may thus not only disperse stably in solution for actual applications but also reduce irreversible analyte adsorption to address the desorption problem of carbon compounds (Babel and Kurniawan 2003; Cundy et al. 2008). In conclusion, the combined effect of iron oxide NMs' excellent adsorption capability and magnetic characteristics appear to be a viable method to dealing with a range of water and waste-water treatment (Brar et al. 2010; Khan et al. 2019).

5.2 Membranes Process Technologies

Essentially, the purpose of water treatment is to remove pollutants from the water as quickly as possible. Membranes, depending upon the size, provide a physical barrier for these kind of components, enabling for the use of unconventional water sources to be used successfully. In addition to providing a high degree of automation,

reducing unnecessary space and chemical use, the modular architecture allows for customised design as a critical component of water treatment and recycling (Benotti et al. 2009). Membrane fouling increases the power consumption of the process and the degree to which its design and functioning are complicated. It also shortens the lifespan of membranes and membrane modules. The membrane material primarily determines membrane system performance. Incorporating functional nanoparticles into membranes can increase membrane permeability, fouling resistance, mechanical and thermal stability and provide novel pollutant degradation and self-cleaning capabilities (Chong et al. 2010).

5.2.1 Nanofiber Membranes

The technique is a simple, effective, and low-cost method of producing ultra-thin fibers from various materials (polymers, ceramics, and even metals) (Li and Xia 2004). Nanofiber mats with a complex porous structure are formed due to the resultant nanofibers' increased specific surface area and pore volume. Electrospun nanofibers can easily modified in terms of diameter, shape, composition, crystal structures, and spatial orientation for particular purposes. Despite the fact that nanofiber membranes are already in commercial use for air filtration, and their potential for application in water treatment is still largely unexplored (Ge et al. 2011).

5.2.2 Forward Osmosis

The osmotic gradient has applied in forwarding osmosis (FO) to pull water is transferred from a solution with low osmotic pressure to a solution with high osmotic pressure (i.e., the draw solution). To produce pure water, the reduced draw solution has been processed using reverse osmosis or thermal procedures. FO offers two significant benefits over pressure-driven reverse osmosis (RO): it requires less pressure, and the membranes are less prone to fouling. The key to FO is a high-osmolality draw solute that has readily separated from the water. NaCl and ammonia bicarbonate are two chemicals that were now used in draw solutions. To retrieve water from the draw solution, RO or thermal treatment is necessary, both energy-intensive (Liu et al. 2011a).

Due to the simplicity with which magnetic nanoparticles may be separated and reused, they have lately been studied as a possible new type of draw solute. A hydrophilic coating has been applied to aid in the dissolution process and to increase osmotic pressure. When deionized water is utilize as the feed solution, a FO permeates flow of more than $10 \, \text{L} \, \text{m}^2 \, \text{h}^{-1}$ is obtain using 0.065 M poly (ethylene glycol) di-acid-coated magnetic nanoparticles. Moreover, magnetic nanoparticles were utilised to collect dredging dissolved substances from the drawing solution. Magnetic nanoparticles ($Fe_3O_4@SiO_2$) were employed in recent research to convalesce $Al_2(SO_4)_3$ (the draw solute) by flocculation (Liu et al. 2011b; Akhavan and Azimirad 2009).

5.3　Photocatalytic Process Technologies

In recent years, photo catalysis, one of the most sophisticated physico-chemical technologies for photo degradation of organic pollutants (Bandara et al. 2007), has gotten a lot of attention. However, some barriers prevent widespread use of magnetic nano ferroparticles for photo catalysis of harmful chemicals: (a) Separating materials after treatment is time-consuming and expensive since it necessitates the use of human resources, time, and chemicals for precipitation samples, which were centrifuged or decanted at the end of the treatment process, and (b) treatment process quantum yield is low (Feng et al. 2000). These constraints must be consider in the development of nano materials based technology. Decreased photo-catalyst size to increase surface area, integrating photo-catalyst with specific new metal nanoparticles, and boosting hole concentration by doping have all been tried to improve photocatalytic performance (Zhang and Fang 2010b). Enhanced charge separation and charge carrier recombine inhibition, on the other hand, are critical for increasing overall quantum efficiency for interfacial charge transfer (Beydoun et al. 1999; Watson et al. 2002).

5.3.1　Magnetic Nano Ferroparticles Photo-Catalysts

It is possible that magnetic nano ferroparticles will prove to be an effective photo-catalyst for the absorption of visible light in the near future. In comparison to TiO_2, which is capable of absorbing ultraviolet light primarily with wavelengths of 380 nm (covering only 5% of the solar spectrum) as a result of its wide band-gap of 3.2 eV, Fe_2O_3 with a band-gap of 2.2 eV is an interesting n-type semiconducting material and a suitable candidate for photo degradation under visible light conditions (Bandara et al. 2007). Magnetic nano ferroparticles superior photocatalytic activity over TiO_2 may be ascribed to the significant production of electrostatic charge between two electrons and two holes caused by the narrow band-gap illumination (Eq. 1) (Feng et al. 2000).

$$Fe_3O_4 + hv = Fe_3O_4\left(e_{cb}^-, h_{vb}^+\right) \qquad (1)$$
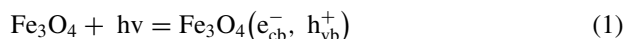
Numerous Fe(III) oxide species have been suggested for degrading organic pollutants and reducing their toxicity through improved photo catalysis, including α-Fe_2O_3, γ-Fe_2O_3, α-FeOOH, β-FeOOH and γ-FeOOH (Khedr et al. 2009). These nanoparticles provide a novel strategy for manipulating the photocatalytic characteristics of magnetic nano ferroparticles, paving the path for safe and effective waste-water treatment nanotechnology. A photo degradation of Congo red (CR) dye ($C_{32}H_{24}N_6 Na_2O_6S_2$) by magnetic nano ferroparticles produced through a thermal evaporation and co-precipitation method is one example. At a size of 100 nm, the highest removal effectiveness was 96%. Additionally, irradiation had no discernible impact depending on the capacity to catalyse decomposition but increased the rate of degradation in the presence of light (Aragaw et al. 2021).
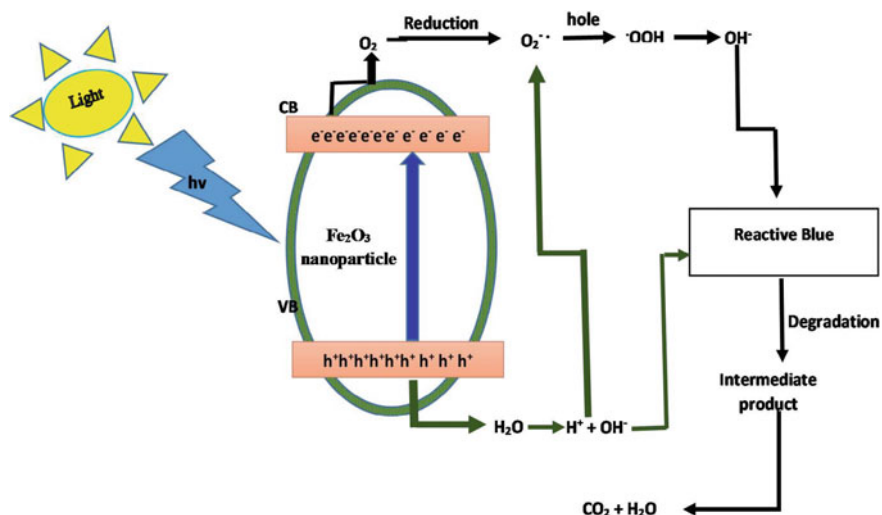
Fig. 3 An illustration of the process by which Fe_2O_3 nanoparticles remove contaminants (in this case, dye). Reproduced or reprinted with copyright permission from Ref.

In specifically, a schematic representation of the degradation of dye utilising Fe_2O_3 nanoparticles, as shown in Fig. 3.

An electron (e) and a hole (h^+) pair are generated when the Fe_2O_3 nanoparticle is irradiated, and the electron is accelerated from the valence band to the conduction band, retaining the h^+ in the bandgap. This hole (h^+) is due to the conversion of water into hydroxyl radicals, which are then responsible for the oxidative destruction of the dye in the solution. Superoxide radicals, on the other hand, are formed when a free electron interacts with a molecule of oxygen. Another radical formed by the superoxide anion radical is hydroxyl radicals. Hydroxyl radical is a powerful oxidising agent that destroys organic molecules in a quasi manner into harmless byproducts (Rothenberger et al. 1985).

Although magnetic nano ferroparticles have extensively used as photo-catalysts, their activity often degrades due to electron–hole charge recombination on the oxide surface, which may occur in nanoseconds (Rothenberger et al. 1985). This issue can addressed by the deposition of a noble metal on a metal oxide accompaniment. For instance, gold/iron oxide aerogels are employ as photo-catalysts under UV light irradiation to degrade Disperse Blue 79 (DB 79) dye in water (Wang 2007).Metallic gold particles, which are think to act as electron accumulation sites when exposed to UV light, may promote the transfer of surface electrons in the photo catalysis system. The improved separation of electrons and holes enables efficient oxidation and reduction processes, thus increasing photocatalytic activity (Liu et al. 2004). At the same time, free hydroxyl radicals near the catalyst surface, which serve as the main oxidative species attacking dye molecules, have been shown to significantly enhance dye degradation. Combining metals with magnetic nano ferroparticles may

enhance the kinetics of oxidation–reduction reactions and it is often use to improve photocatalytic performance (Kim et al. 2003).

Additionally, Fe_2O_3 may be used to sensitize TiO_2 photo-catalysts (Zhang and Lei 2008). Due to the development of the built-in field in the Fe_2O_3–TiO_2 heterojunction, electrons in the valence bands of TiO_2 are push into Fe_2O_3. Charge transfer between the valance bands of Fe_2O_3 and TiO_2 is consider an efficient mechanism for enhancing the composition's photocatalytic activity since as a result, it grows in the period of time during which electrons and holes recombine (Peng et al. 2010; Shinde et al. 2011).

5.4   Disinfection and Microbial Control

Most particles in surface water, including microorganisms, are negatively charged; they repel one another rather than aggregate. Typically, aluminum or ferric ions are use as a coagulant in water treatment processes. The comportment of aluminum remains in treated water, on the other hand, raises health and environmental issues, including neurotoxicity and the possibility of Alzheimer's disease (Rondeau and Sainte-Marie 2001). Additionally, the elimination of microorganisms is concentrated on microbial ecology distribution systems via the addition of chlorine, ozone, or UV treatment, which improves the safety and quality of drinking water. Nonetheless, the disinfection by-products constitute a health hazard, and the expense of ozone or UV treatment negates the process's advantages (Berry et al. 2006).

The purpose of this study was to create an environmentally acceptable material for water treatment. Magnetic iron oxide nanoparticles are produce and described using various water treatment methods (Okoli et al. 2012). Magnetic iron oxide nanoparticles are excellent candidates for creating high-capacity sorbents with improved selectivity/affinity for reducing or removing chemical ions and microorganisms in water. Adsorption using magnetic iron oxide nanoparticles is a rapid and cost-effective method for removing pollutants from water (Pang et al. 2011a). Microorganisms found in water are the focus of several water treatment processes to reduce microbial pollutants in drinking water. Determining the efficacy of magnetic iron oxide nanoparticles in removing microbiological pollutants from surface water is critical to offer a viable alternative to disinfection chemicals or disinfectant aids. Possible methods of microbial reduction include reversible electrostatic forces, van der Waals forces, and irreversible adsorption, which may aid in the formation of bridges between bacteria and the adsorbent. Adsorption occurs as a result of the fluid's conductivity as well as the chemical ion composition of the aqueous solution, among other factors (Pang et al. 2011a).

The findings indicate that magnetic iron oxide nanoparticles may decrease water turbidity even in samples with low turbidity. At 37 C, a 98% decrease in microbial content is detect, and a greater than 90% reduction has seen compared to untreated samples. The approach created using magnetic iron oxide nanoparticles has the potential to improve upon existing techniques significantly. Additionally, the time required

for water treatment was 1 h, which is considerably less than the time required for the current water treatment procedure. Magnetic nanoparticles may be a viable replacement to chemical chelating agents and disinfection assist agents, thus offering a cost-effective and environmentally friendly water treatment solution. Within one hour, at low nephelometric turbidity unit levels (NTU), magnetic iron oxide nanoparticles efficiently decrease the turbidity of surface water (Stevik et al. 2004).

Additionally, there was no significant change in mineral ion concentrations before and after magnetic iron oxide nanoparticles therapy. In treated water, a microbial decrease of more than 90% was founded. Copper and phosphate reduction has accomplished when magnetic iron oxide nanoparticles has used in simulated water, supplementing the usual treatment procedure. The studied treatment technique using magnetic iron oxide nanoparticles did not affect the mineral ion composition, suggesting that it may be used in conjunction with the traditional treatment procedure (Theron et al. 2008).

6 Magnetic Nano Ferroparticles: Limitations and Challenges

Iron oxide nanoparticles have recently recognized as highly capable nano sorbents for removing various pollutants due to their high sorption capacities, rapid removal capabilities, and ease of separation in an aqueous medium. However, their manufacturing expense is the biggest obstacle to their practical use. On the other hand, scientists are still working on reducing the cost of manufacturing to be use in waste-water treatment. The inability to assess the feasibility of these plants on a wide scale has resulted as a consequence.

Consequently, the destiny of these nanomaterials will determine by how quickly they can commercialized in the future. It is also necessary to study the effect of iron oxide-based nanomaterials discharged into aquatic ecosystems. Currently, very little information has known on their disposal in water bodies, which must thoroughly investigated. Identifying the risks in this area will be very useful in determining the impacts of nano toxicity on the environment in this manner. A wide range of experimental techniques must be developed to determine the efficacy of these nanomaterials.

The development of iron oxide-based nanocomposite materials with silica or carbon has altered their physiochemical stability, and their essential magnetic properties have given incredible benefits in their use. One difficulty is identifying the appropriate source for integrating them into creating a nanocomposite capable of increasing the overall adsorption efficiency. Combining iron oxide nanoparticles with activated carbon, for example, improves these materials' overall effectiveness as nano sorbents. Researchers have shown the efficiency with which these nanomaterials may be use in adsorption processes, biomedicine, and catalysis. Another benefit of these materials is that they do not need a carrier to act as catalysts. Iron

oxide nanoparticles coupled with polymers for targeted medication administration are also drawing the attention of many specialists in the area. Numerous researchers are trying to improve the practical output of these nanomaterials to be use as biosensors. In summary, iron oxide nanoparticles have seen rapid development, and their varied and multifunctional applications have the potential to impact a variety of fields, including environmental remediation significantly.

7 Conclusion

Wastewater treatment and reuse is a technique that has a lot of advantages in terms of water balance and management, but it also has a lot of drawbacks. To protect human health and natural ecosystems, immediate research must be undertaken in this area. Nanomaterials offer a lot of promise for removing pollutants because of their unique physical and chemical characteristics. Prioritization of iron oxide nanoparticles and future application prospects have been given to help move the development of iron oxide nanoparticles ahead. Iron oxide nanoparticles would demonstrate their dominance as powerful photocatalysts even when exposed to visible light.

Iron oxide nanoparticles are, in fact, effective Nanosorbents for heavy metals and organic contaminants. The most appealing and effective applications include using iron oxide nanoparticles to absorb heavy metals and organic contaminants. While applications as immobilisation carriers have received little attention, the potential for use as support carriers, such as biosensors and biosorbents, cannot be overlooked. Despite the fact that many instances of success in iron oxide nanoparticles have been aided by their unique chemical and physical characteristics, iron oxide nanoparticle uses in wastewater treatment are still in their infancy. A variety of iron oxide-based wastewater treatment methods have been suggested or are under active development, as shown in this chapter, although many are still in the experimental or pilot stage. Application in vitro and in vivo research using iron oxide nanoparticle may provide challenges. Iron oxide nanoparticle (in various chemical and structural forms) have already shown their versatility and prospective uses in a wide range of environmental fields.

Finally, the utilisation of engineered iron oxide nanoparticle as an in-situ, somewhat non-invasive technique in astewater treatment has sparked a lot of attention recently. However, concerns about the health effects and environmental destiny of these nanomaterials must be addressed before they can be widely used. The study of their destiny and effect on the environment is becoming more essential as a result of the current environmental discharges. Expanding research in this field would be necessitated by the anticipated rise in iron oxide nanoparticle emissions, as well as the rapid industrial development and enormous knowledge gaps in risk assessment and management.

References

Abedi-Koupai J, Mostafazadeh-Fard B, Afyuni M, Bagheri MR (2006) Effect of treated waste-water on soil chemical and physical properties in an arid region. Plant Soil Environ 52(8):335

Ahmad A, Rafatullah M, Sulaiman O, Ibrahim MH, Chii YY, Siddique BM (2009) Removal of Cu (II) and Pb (II) ions from aqueous solutions by adsorption on sawdust of Meranti wood. Desalination 247(1–3):636–646

Akhavan O, Azimirad R (2009) Photocatalytic property of Fe_2O_3 nanograin chains coated by TiO_2 nanolayer in visible light irradiation. Appl Catal A 369(1–2):77–82

Al-Bastaki NM (2004) Performance of advanced methods for treatment of waste-water: UV/TiO2, RO and UF. Chem Eng Process 43(7):935–940

Ambashta RD, Sillanpää M (2010) Water purification using magnetic assistance: a review. J Hazard Mater 180(1–3):38–49

Aragaw TA, Bogale FM, Aragaw BA, Aragaw BA (2021) Iron-based nanoparticles in wastewater treatment: a review on synthesis methods, applications, and removal mechanisms. J Saudi Chem Soc 14:101–280

Babel S, Kurniawan TA (2003) Low-cost adsorbents for heavy metals uptake from contaminated water: a review. J Hazard Mater 97(1–3):219–243

Baig MM, Pervaiz E, Afzal MJ (2020) Catalytic activity and kinetic studies of Core@ Shell nanostructure $NiFe_2O_4$@ TiO_2 for photocatalytic degradation of methyl orange dye. J Chem Soc Pakistan 42:531–541

Bandara J, Klehm U, Kiwi J (2007) Raschig rings-Fe_2O_3 composite photocatalyst activate in the degradation of 4-chlorophenol and Orange II under daylight irradiation. Appl Catal B 76(1–2):73–81

Benotti MJ, Stanford BD, Wert EC, Snyder SA (2009) Evaluation of a photocatalytic reactor membrane pilot system for the removal of pharmaceuticals and endocrine disrupting compounds from water. Water Res 43(6):1513–1522

Berry JW, Phinney JS, Sam DL, Vedder P (2006) Immigrant youth: acculturation, identity, and adaptation. Appl Psychol 55(3):303–332

Beydoun D, Amal R, Low G, McEvoy S (1999) Role of nanoparticles in photocatalysis. J Nanopart Res 1(4):439–458

Beyersmann D, Hartwig A (2008) Carcinogenic metal compounds: recent insight into molecular and cellular mechanisms. Arch Toxicol 8:493–512

Brar SK, Verma M, Tyagi RD, Surampalli RY (2010) Engineered nanoparticles in waste-water and waste-water sludge–evidence and impacts. Waste Manage 30(3):504–520

Chapman ED, Kimstach V, Helmer R. (1996) *-Strategies for water quality assessment

Chauhan A, Sillu D, Agnihotri S (2019) Removal of pharmaceutical contaminants in waste-water using nanomaterials: a comprehensive review. Curr Drug Metab 20(6):483–505

Chen Y, Fay S, Wang Q (2011) The role of marketing in social media: how online consumer reviews evolve. J Interact Mark 25(2):85–94

Chong MN, Jin B, Chow CW, Saint C (2010) Recent developments in photocatalytic water treatment technology: a review. Water Res 44(10):2997–3027

Cundy AB, Hopkinson L, Whitby RL (2008) Use of iron-based technologies in contaminated land and groundwater remediation: A review. Sci Total Environ 400(1–3):42–51

Elboughdiri N (2020) The use of natural zeolite to remove heavy metals Cu(II), Pb(II) and Cd(II), from industrial waste-water. Cogent Eng 7(1):1782623

El-Sayed ME (2020) Nanoadsorbents for water and wastewater remediation. Sci Total Environ 739:139903.

Feachem RG, Bradley DJ, Garelick H, Mara DD (1983) Sanitation and disease: health aspects of excreta and waste-water management. Wiley, New York

Feng W, Nansheng D, Helin H (2000) Degradation mechanism of azo dye CI reactive red 2 by iron powder reduction and photooxidation in aqueous solutions. Chemosphere 41(8):1233–1238

Fialova D, Kremplova M, Melichar L, Kopel P, Hynek D, Adam V, Kizek R (2014) Interaction of heavy metal ions with carbon and iron based particles. Materials 7(3):2242–2256

Ge Q, Su J, Chung TS, Amy G (2011) Hydrophilic superparamagnetic nanoparticles: synthesis, characterization, and performance in forward osmosis processes. Ind Eng Chem Res 50(1):382–388

Gupta VK, Ali I, Saleh TA, Nayak A, Agarwal S (2012) Chemical treatment technologies for waste-water recycling—an overview. Rsc Adv 2(16):6380–6388

Hatamie A, Parham H, Zargar B, Heidari Z (2016) Evaluating magnetic nano-ferrofluid as a novel coagulant for surface water treatment. J Mol Liq 219:694–702

World Health Organization (WHO), Homepage

Hu J, Lo IM, Chen G (2007) Performance and mechanism of chromate (VI) adsorption by δ-FeOOH-coated maghemite (γ-Fe_2O_3) nanoparticles. Sep Purif Technol 58(1):76–82

Hu J, Shao D, Chen C, Sheng G, Ren X, Wang X (2011) Removal of 1-naphthylamine from aqueous solution by multiwall carbon nanotubes/iron oxides/cyclodextrin composite. J Hazard Mater 185(1):463–471

Huang GB, Zhu QY, Siew CK (2006) Extreme learning machine: theory and applications. Neurocomputing 70(1–3):489–501

Huang SH, Chen DH. Rapid removal of heavy metal cations and anions from aqueous solutions by an amino-functionalized magnetic nano-adsorbent. J Hazard Mater 163(1):174–179

Iram M, Guo C, Guan Y, Ishfaq A, Liu H (2010a) Adsorption and magnetic removal of neutral red dye from aqueous solution using Fe_3O_4 hollow nanospheres. J Hazard Mater 181(1–3):1039–1050

Khan NA, Khan SU, Ahmed S, Farooqi IH, Dhingra A, Hussain A, Changani F (2019) Applications of nanotechnology in water and waste-water treatment: a review. Asian J Water Environ Pollut 16(4):81–86

Khedr MH, Halim KA, Soliman NK (2009) Synthesis and photocatalytic activity of nano-sized iron oxides. Mater Lett 63(6–7):598–601

Kim Y, Lee B, Yi J (2003) Preparation of functionalized mesostructured silica containing magnetite (MSM) for the removal of copper ions in aqueous solutions and its magnetic separation. Sep Sci Technol 38(11):2533–2548

Kobya M, Demirbas E, Senturk E, Ince M (2005) Adsorption of heavy metal ions from aqueous solutions by activated carbon prepared from apricot stone. Biores Technol 96(13):1518–1521

Laurent S, Forge D, Port M, Roch A, Robic C, Vander Elst L, Muller RN (2008) Magnetic iron oxide nanoparticles: synthesis, stabilization, vectorization, physicochemical characterizations, and biological applications. Chem Rev 108(6):2064–2110

Li D, Xia Y (2004) Electrospinning of nanofibers: reinventing the wheel? Adv Mater 16(14):1151–1170

Li XQ, Zhang WX (2006) Iron nanoparticles: The core−shell structure and unique properties for Ni (II) sequestration. Langmuir 22(10):4638–4642

Liu SX, Qu ZP, Han XW, Sun CL (2004) A mechanism for enhanced photocatalytic activity of silver-loaded titanium dioxide. Catal Today 93:877–884

Liu S, Yu J, Jaroniec M (2011a) Anatase TiO_2 with dominant high-energy 001 facets: synthesis, properties, and applications. Chem Mater 23(18):4085–4093

Liu Z, Bai H, Lee J, Sun DD (2011b) A low-energy forward osmosis process to produce drinking water. Energy Environ Sci 4(7):2582–2585

Luo LH, Feng QM, Wang WQ, Zhang BL (2011) Fe_3O_4/Rectorite composite: preparation, characterization and absorption properties from contaminant contained in aqueous solution. Adv Mater Res 287:592–598

Ma ZY, Guan YP, Liu XQ, Liu HZ (2005) Preparation and characterization of micron-sized non-porous magnetic polymer microspheres with immobilized metal affinity ligands by modified suspension polymerization. J Appl Polym Sci 96(6):2174–2180

Nadeem U (2013) Magnetic field induced enhanced adsorption efficiency of iron oxide nanoparticles based magnetic ferrofluid: a preliminary investigation. Eur Chem Bull 2(9):629–630

Nassar NN, Husein MM (2010) Ultradispersed particles in heavy oil: Part I, preparation and stabilization of iron oxide/hydroxide. Fuel Process Technol 91(2):164–168

Nawrocki J, Kasprzyk-Hordern B (2010) The efficiency and mechanisms of catalytic ozonation. Appl Catal B 99(1–2):27–42

Okoli C, Sanchez-Dominguez M, Boutonnet M, Jaras S, Civera C, Solans C, Kuttuva GR (2012) Comparison and functionalization study of microemulsion-prepared magnetic iron oxide nanoparticles. Langmuir 28(22):8479–8485

Orge CA, Órfão JJ, Pereira MF, de Farias AM, Neto RC, Fraga MA (2011) Ozonation of model organic compounds catalysed by nanostructured cerium oxides. Appl Catal B 103(1–2):190–199

Otto M, Floyd M, Bajpai S (2008) Nanotechnology for site remediation. Remed j: J Environ Cleanup Costs Technol Tech 19(1):99–108

Pang ZP, Yang N, Vierbuchen T, Ostermeier A, Fuentes DR, Yang TQ, Citri A, Sebastiano V, Marro S, Südhof TC, Wernig M (2011a) Induction of human neuronal cells by defined transcription factors. Nature 476(7359):220–223

Pang Y, Zeng GM, Tang L, Zhang Y, Liu YY, Lei XX, Wu MS, Li Z, Liu C (2011b) Cr (VI) reduction by *Pseudomonas aeruginosa* immobilized in a polyvinyl alcohol/sodium alginate matrix containing multi-walled carbon nanotubes. Biores Technol 102(22):10733–10736

Paswan SK, Kumar P, Singh RK, Shukla SK, Kumar L (2021) Spinel ferrite magnetic nanoparticles: an alternative for wastewater treatment. Pollut Water Manag Resour Strat Scarcity 273–305

Peng Q, Liu Y, Zeng G, Xu W, Yang C, Zhang J (2010) Biosorption of copper (II) by immobilizing Saccharomyces cerevisiae on the surface of chitosan-coated magnetic nanoparticles from aqueous solution. J Hazard Mater 177(1–3):676–682

Ponder SM, Darab JG, Mallouk TE (2000) Remediation of Cr(VI) and Pb(II) aqueous solutions using supported, nanoscale zero-valent iron. Environ Sci Technol 34(12):2564–2569

Pradeep T (2009) Noble metal nanoparticles for water purification: a critical review. Thin Solid Films 517(24):6441–6478

Qu X, Alvarez PJ, Li Q (2013) Applications of nanotechnology in water and waste-water treatment. Water Res 47(12):3931–3946

Rafatullah M, Sulaiman O, Hashim R, Ahmad A (2010) Adsorption of methylene blue on low-cost adsorbents: a review. J Hazard Mater 177(1–3):70–80

Rondeau A, Sainte-Marie B (2001) Variable mate-guarding time and sperm allocation by male snow crabs (*Chionoecetes opilio*) in response to sexual competition, and their impact on the mating success of females. Biol Bull 201(2):204–217

Rothenberger G, Moser J, Graetzel M, Serpone N, Sharma DK (1985) Charge carrier trapping and recombination dynamics in small semiconductor particles. J Am Chem Soc 107(26):8054–8059

Shinde SS, Bhosale CH, Rajpure KY (2011) Photocatalytic oxidation of salicylic acid and 4-chlorophenol in aqueous solutions mediated by modified $AlFe_2O_3$ catalyst under sunlight. J Mol Catal a: Chem 347(1–2):65–72

Stafiej A, Pyrzynska K (2007) Adsorption of heavy metal ions with carbon nanotubes. Sep Purif Technol 58(1):49–52

Stevik TK, Aa K, Ausland G, Hanssen JF (2004) Retention and removal of pathogenic bacteria in waste-water percolating through porous media: a review. Water Res 38(6):1355–1367

Stone V, Nowack B, Baun A, van den Brink N, von der Kammer F, Dusinska M, Handy R, Hankin S, Hassellöv M, Joner E, Fernandes TF (2004) Nanomaterials for environmental studies: classification, reference material issues, and strategies for physico-chemical characterisation. Sci Total Environ 408(7):1745–1754

Teja AS, Koh PY (2009) Synthesis, properties, and applications of magnetic iron oxide nanoparticles. Prog Cryst Growth Charact Mater 55(1–2):22–45

Theron J, Walker JA, Cloete TE (2008) Nanotechnology and water treatment: applications and emerging opportunities. Crit Rev Microbiol 34(1):43–69

Tijani JO, Aminu UA, Bankole MT, Ndamitso MM, Abdulkareem AS (2020) Adsorptive and photocatalytic properties of green synthesized ZnO and $ZnO/NiFe_2O_4$ nanocomposites for Tannery wastewater treatment. Nigerian J Technol Dev 17(4):312–322

Wahaab RA, Mahmoud M, van Lier JB (2020) Toward achieving sustainable management of munic-ipal waste-water sludge in Egypt: the current status and future prospective. Renew Sustain Energy Rev 127:109880

Wang CT (2007) Photocatalytic activity of nanoparticle gold/iron oxide aerogels for azo dye degradation. J Non-Cryst Solids 353(11–12):1126–1133

Wang L, Ma W, Xu L, Chen W, Zhu Y, Xu C, Kotov NA (2010) Nanoparticle-based environmental sensors. Mater Sci Eng R Rep 70(3–6):265–274

Wang S, Shi X. Molecular mechanisms of metal toxicity and carcinogenesis. Molecular and cellular biochemistry 222(1):3–9

Watson S, Beydoun D, Amal R (2002) Synthesis of a novel magnetic photocatalyst by direct deposition of nanosized TiO_2 crystals onto a magnetic core. J Photochem Photobiol A 148(1–3):303–313

Wei L, Yang G, Wang R, Ma W (2009) Selective adsorption and separation of chromium (VI) on the magnetic iron–nickel oxide from waste nickel liquid. J Hazard Mater 64(2–3):1159–1163

Westerhoff P, Moon H, Minakata D, Crittenden J (2009) Oxidation of organics in retentates from reverse osmosis waste-water reuse facilities. Water Res 43(16):3992–3998

White BR, Stackhouse BT, Holcombe JA (2009) Magnetic γ-Fe_2O_3 nanoparticles coated with poly-l-cysteine for chelation of As (III), Cu (II), Cd (II), Ni (II), Pb (II) and Zn (II). J Hazard Mater 161(2–3):848–853

Xu P, Zeng GM, Huang DL, Feng CL, Hu S, Zhao MH, Lai C, Wei Z, Huang C, Xie GX, Liu ZF (2012) Use of iron oxide nanomaterials in waste-water treatment: a review. Sci Total Environ 424:1

Yuan P, Fan M, Yang D, He H, Liu D, Yuan A, Zhu J, Chen T (2009) Montmorillonite-supported magnetite nanoparticles for the removal of hexavalent chromium [Cr (VI)] from aqueous solutions. J Hazard Mater 166(2–3):821–829

Zeng G, Huang D, Huang G, Hu T, Jiang X, Feng C, Chen Y, Tang L, Liu H (2007) Composting of lead-contaminated solid waste with inocula of white-rot fungus. Biores Technol 98(2):320–326

Zhang L, Fang M (2010a) Nanomaterials in pollution trace detection and environmental improve-ment. Nano Toda 5(2):128–142

Zhang L, Fang M (2010b) Nanomaterials in pollution trace detection and environmental improve-ment. Nano Today 5(2):128–142

Zhang X, Lei L (2008) Preparation of photocatalytic Fe_2O_3–TiO_2 coatings in one step by metal organic chemical vapor deposition. Appl Surf Sci 254(80):2406–2412

Zhao H, Dong Y, Wang G, Jiang P, Zhang J, Wu L, Li K (2013) Novel magnetically separable nanomaterials for heterogeneous catalytic ozonation of phenol pollutant: $NiFe_2O_4$ and their performances. Chem Eng J 219:295–302

Thermal Performance Study of Quarterly-Divided Cylindrical Pin Fins Under Natural Convection

Vandana Kumari Jha and **Soubhik Kumar Bhaumik**

Abstract In the present study, a novel design of heat sink with quarterly-divided cylindrical pin fin (QCPF) is proposed which is modified by splitting up the conventional cylindrical pin fin (CPF) design into four equal parts, keeping a gap (one-fifth of fin diameter) between the divided fin pieces. The gap helps in better air circulation as well as enhanced convection coefficient. Flow characteristics and heat transfer performance of QCPF heat sink are compared with CPF heat sink (made with the same amount of material required for construction). The comparative study is carried out for both the circular pin fin and the divided circular pin fin designs based on the rate of heat dissipation, overall average fin temperature and fin efficiency under natural convection. The results are analyzed for a range of Rayleigh number ($2.71 \times 10^4 \leq Ra \leq 1.35 \times 10^5$) defined in terms of pitch between the fins for different values of temperature difference. Flow analysis reveals enhanced air circulation between the gaps and increased surface area for heat transfer that leads to a significant rise in the rate of heat dissipation up to 1.92 times over CPF. Furthermore, divided surfaces of the QCPF increase the heat transfer surface area and efficiency of fin which lies ~3–6 higher in the case of QCPF than in the conventional CPF arrangement. The results establish the superior performance of QCPF compared to CPF design indicating the beneficial role of air circulation in the gaps created, under natural convection.

Keywords Cylindrical pin fin · Quarterly-divided pin fin · Fin efficiency

1 Introduction

The use of fins in heat sink is highly practiced for heat dissipation industrially and at the domestic level through convection and radiation mechanisms (Belhardj et al. 2003; Nakayama 1986; Yamada et al. 2016). Finned structures are applicable in heat exchangers, electronic equipment, refrigeration, etc. Since heat sinks form an

V. K. Jha · S. K. Bhaumik (✉)
IIT (ISM) Dhanbad, Jharkhand 826004, India
e-mail: soubhikge@iitism.ac.in

integral part of the electronic cooling systems, therefore, the designs of fin has got modified and optimized with time, based on their performance for effective removal of heat in order to lower the operating temperature (Jha and Bhaumik 2019a, b; Welling and Wooldridge 1965; Yüncü and Güvenc 2001). Therefore, new designs can be introduced for different industrial applications in order to obtain substantial economic and environmental benefits.

Among the different available fin designs, pin fin heat sink shows excellent thermal performance, and it consists of a large number of pin fins that provide substantial surface area for heat transfer (Horiuchi et al. 2015; Tullius et al. 2011; Naphon and Sookkasem 2007; Yuan et al. 2012). Incorporating a large surface area while improving the thermal performance of the heat sink under natural convection mode, not only reduces the manufacturing cost but also increases the fin efficiency and its reliability. The design of pin fins comes with certain advantages such as easy to manufacture, simple in structure and low thermal resistance. Furthermore, intensifying a heat transfer process leads to the optimization of existing heat sink designs and helps to develop intensified equipment by substantially reducing the equipment volume, floor area, capital cost, and energy consumption, resulting in a smaller, safer, and more energy-efficient process.

A significant amount of research has been carried out earlier on pin fin designs that aim to maximize the surface area (Pandit et al. 2014; Jeng and Tzeng 2007; Khetib et al. 2021). Different shapes or geometry of the pin fin are studied such as tapered, square-shaped, cylindrical, hexagonal, elliptical pin fins to examine their heat dissipation performance (Kirsch and Thole 2017). Arrays of micro pin fins are also investigated over a range of Reynolds number and for different fin spacing (Deshmukh and Warkhedkar 2013). Experimental investigations under natural convection are also carried out by varying the design parameters for pin fins to observe their effect (Dogruoz et al. 2005). Studies imply that an increase in the heat dissipation rate is obtained by deviating the flow that leads to an increase in heat transfer coefficient. Apart from the fin-shape, fin-arrangement is also studied by several researchers establishing that the staggered arrangements are more effective for heat dissipation. Moreover, for pin fin heat sink, application of perforations is explored indicating an increase in Nusselt number. Perforations help in increasing the surface area as well as heat transfer but have a very complex manufacturing technique (Al-Damook et al. 2016a, b2015; Zhou and Catton 2011).

Based on previous works, it can be summarized that pin fins are an inevitable part of heat sink for heat dissipation. Keeping in view the restrictions and challenges faced, it becomes the need of the hour to re-design or adapt the existing conventional pin fin design so as to make the most of the material used in the manufacturing of fins and utilizing maximum surface area. One alternative way to increase the surface area without going into the cumbersome manufacturing process is to divide the pin fin vertically into four equal parts and providing a gap between the fin pieces. This design will help in localizing the boundary layers and better air circulation with superior heat transfer characteristics over conventional pin fins.

In the present work, performance of a novel configuration of quarterly-divided cylindrical pin fins (QCPF) is evaluated and compared with the conventional cylindrical pin fins (CPF) having the same amount of material required for construction. Numerical studies are carried out for both the heat sink configurations, keeping similar operating conditions, for inline arrangements under natural convection. The comparative assessment includes heat dissipation rate, fin efficiency, and flow characteristics or air circulation. Analysis of the results is done for a range of Rayleigh number ($2.71 \times 10^4 \leq Ra \leq 1.35 \times 10^5$) which varies with the temperature difference between surrounding air and base temperature of heat sink, varying from 50 K to 150 K, defined in terms of pitch.

2 Problem Description

In the present study, two different configurations of cylindrical fin pin heat sink, i.e., conventional cylindrical pin fins (CPF) and quarterly-divided cylindrical pin fins (QCPF) are taken up for the comparative assessment. Numerical analysis is carried out by varying parameters such as Ra and pitch of the fins under natural convection environment. Simulations for both the heat sink designs are carried out on 3D-geometries.

2.1 Geometry

The geometric details of the 3-D geometry for both configurations are explained separately as illustrated in Fig. 1. CPF consist of a base plate of dimensions 120 mm ×
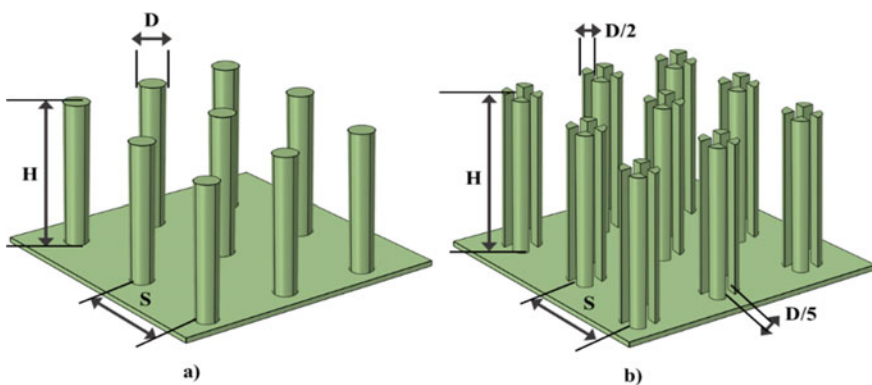
Fig. 1 Schematic showing the geometric details of circular fin pin (CPF) and quarterly-divided pin fin (QCPF) heat sink configurations
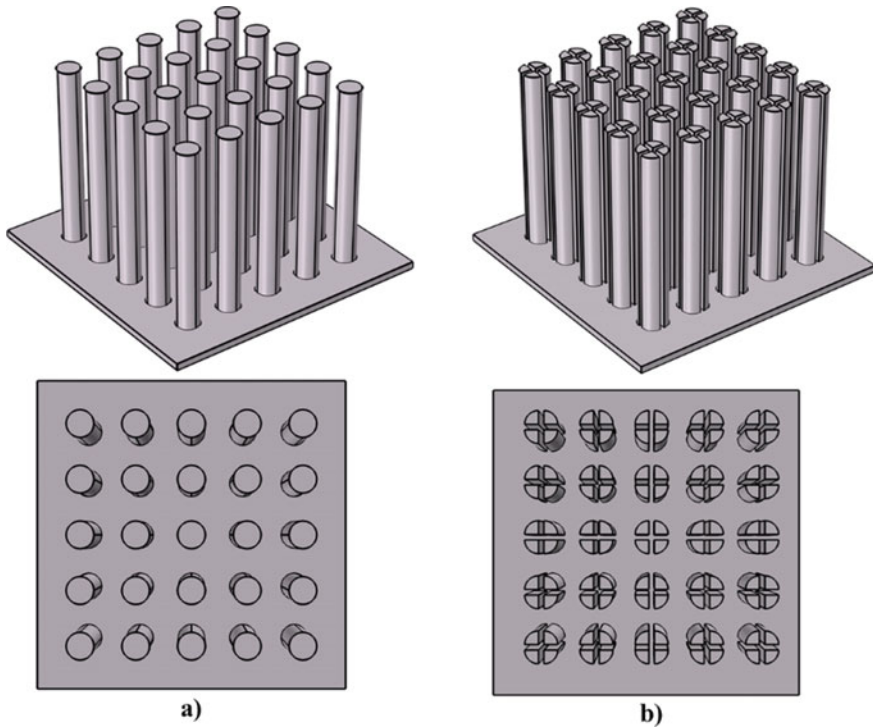
Fig. 2 Schematic of CPF and QCPF heat sink configurations showing the: **a** orthogonal view; **b** top view

120 mm × 3 mm, and 25 cylindrical pin fins of 10 mm diameter (D) and 8 *mm* height (H) attached to the base. Fins are arranged in inline arrangement for both the configurations keeping fin pitch (S) fixed at 20 mm as shown in Fig. 2. For QCPF, the base plate dimensions are kept equal to that of CPF. The quarterly-divided pin fins are obtained by vertically dividing the circular cross-section quarterly into four equal parts, and keeping the fin parts at a distance ($D/5$) of 2 mm from each other. The comparative evaluation of conventional CPF and QCPF heat sink design are studied under similar conditions.

2.2 Comparative Analysis

Heat Flux (Q). For comparative assessment, the rate of heat dissipation or heat flux is considered for the performance study of heat sink which is obtained directly from the numerical results.

Rayleigh Number. Rayleigh number is calculated based on the fin pitch and is given as:

$$Ra = \frac{g\beta(T_b - T_a)S^3}{\nu\alpha} \tag{1}$$

Fin Efficiency. Fin efficiency which is defined as the ratio of actual heat dissipated from the fin to the heat dissipated when the fin is kept at the fin base temperature (T_b) is used to estimate the performance of heat sink designs and is given as:

$$\eta = \frac{Q_f}{h_{f,avg}A_f(T_b - T_a)} \tag{2}$$

3 CFD Modeling

3.1 Geometry and Mesh

The numerical simulations are carried out using a commercial CFD package of COMSOL Multiphysics® 5.4. The computational domain, for CPF configuration, is shown schematically in Fig. 3a along with the boundary conditions. Since heat transfer is taking place both in solid fins as well as in the surrounding fluid domain, therefore conjugate heat transfer model is applied along with the laminar flow model. The conjugate domain consists of solid fin and surrounding fluid domain (air). CPF is considered as the reference geometry for comparison of the novel QCPF heat sink design. The comparative study is carried out for a given range of Rayleigh numbers $(2.71 \times 10^4 \leq Ra \leq 1.35 \times 10^5)$ depending upon the temperature difference between fin base plate and ambient air temperature $(T_a = 298.15)$, *i.e.*, $\Delta T = (T_b - T_a)$. The dimensions of the fluid (air) enclosure are: $(X \times Y \times Z) = (200 \text{ mm} \times 400 \text{ mm} \times 120 \text{ mm})$.

The 3D-geometry is meshed using a physics-controlled mesh sequence that primarily consists of unstructured triangular, tetrahedral and hexahedral elements. The study for mesh refinement is carried out for CPF arrangement corresponding to $Ra = 1.35 \times 10^5$ for a given temperature difference of $\Delta T = (T_b - T_a) = 150\,K$. A negligible variation in the mean Nusselt number is observed beyond *fine* mesh element size which is taken as the optimum mesh size for further simulations. Meshed geometries for CPF and QCPF heat sinks are shown in Fig. 3b–c with *fine* mesh distribution.
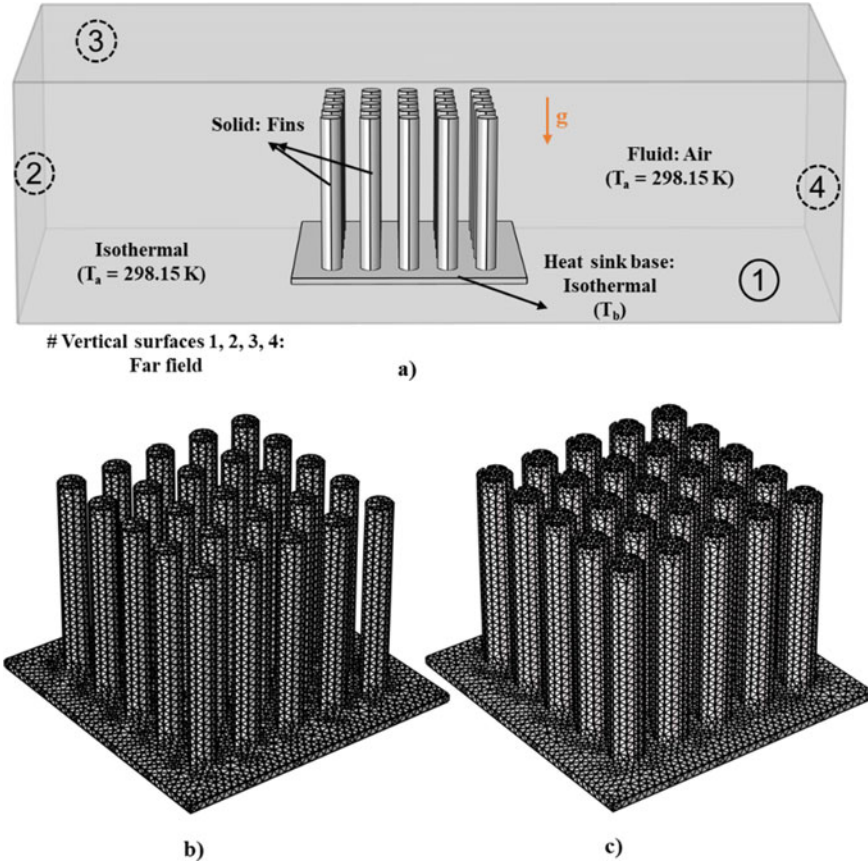
Fig. 3 **a** Schematic showing computational domain along with the boundary conditions for CPF configuration; meshed geometry for **b** CPF; **c** QCPF configurations

3.2 Governing Equations and Boundary Conditions

Air flow inside the fluid domain is supposed to be steady and laminar. Air is supposed to be an incompressible ideal gas with constant thermophysical properties which are measured at film temperature, $T_{film} = (T_b + T_a)/2$. The base of heat sink, in both configurations, is kept at a fixed temperature so as to impose a constant wall temperature boundary condition. For the numerical study, the laminar flow condition is considered in which Ra is varied in the range of $2.71 \times 10^4 \leq Ra \leq 1.35 \times 10^5$. The fin material taken is aluminum which has a high thermal conductivity. Fin material taken is aluminum which has a high thermal conductivity.

The governing equations are:

Continuity equation:

$$\rho\left(\frac{\partial v_x}{\partial x} + \frac{\partial v_y}{\partial y} + \frac{\partial v_z}{\partial z}\right) = 0 \tag{3}$$

Momentum equation:

$$\rho\left(v_x\frac{\partial v_x}{\partial x} + v_y\frac{\partial v_x}{\partial y} + v_z\frac{\partial v_x}{\partial z}\right) = -\frac{\partial p}{\partial x} + \mu\left(\frac{\partial^2 v_x}{\partial x^2} + \frac{\partial^2 v_x}{\partial y^2} + \frac{\partial^2 v_x}{\partial z^2}\right) \tag{4}$$

$$\rho\left(v_x\frac{\partial v_y}{\partial x} + v_y\frac{\partial v_y}{\partial y} + v_z\frac{\partial v_y}{\partial z}\right) = -\frac{\partial p}{\partial y} + \mu\left(\frac{\partial^2 v_y}{\partial x^2} + \frac{\partial^2 v_y}{\partial y^2} + \frac{\partial^2 v_y}{\partial z^2}\right) \tag{5}$$

$$\rho\left(v_x\frac{\partial v_z}{\partial x} + v_y\frac{\partial v_z}{\partial y} + v_z\frac{\partial v_z}{\partial z}\right) = -\frac{\partial p}{\partial z} + \mu\left(\frac{\partial^2 v_z}{\partial x^2} + \frac{\partial^2 v_z}{\partial y^2} + \frac{\partial^2 v_z}{\partial z^2}\right)$$
$$+ \rho_0 g + (\rho - \rho_0)g \tag{6}$$

Energy equation:

Enclosure:

$$v_x\frac{\partial T}{\partial x} + v_y\frac{\partial T}{\partial y} + v_z\frac{\partial T}{\partial z} = \alpha\left(\frac{\partial^2 T}{\partial x^2} + \frac{\partial^2 T}{\partial y^2} + \frac{\partial^2 T}{\partial z^2}\right) \tag{7}$$

Fin:

$$\left(\frac{\partial^2 T}{\partial x^2} + \frac{\partial^2 T}{\partial y^2} + \frac{\partial^2 T}{\partial z^2}\right) = 0 \tag{8}$$

Boundary conditions: Eqs. (3)–(8) are solved in respect to the following boundary conditions:

Heat sink walls: Fin surface and base:

$$v_x = v_y = v_z = 0 \text{ (no slip)} \tag{9a}$$

Fin base:

$$T = T_b \text{ (isothermal)} \tag{9b}$$

Fin-air interface: A coupling surface is applied at the fin-air interface:

$$k_f\frac{\partial T_f}{\partial n}\bigg|_{\text{interface}} = k_{air}\frac{\partial T_{air}}{\partial n}\bigg|_{\text{interface}} \quad \text{(flux continuity)} \tag{9c}$$

$$T_f\big|_{\text{interface}} = T_{air}\big|_{\text{interface}} \text{ (temperature continuity)} \tag{9d}$$

Enclosure: An open boundary condition is imposed on the top surface for air flow. An isothermal boundary condition is applied at the bottom surface which is equal to the ambient temperature. The remaining vertical surfaces are treated as far-field and is assumed that the thermal and velocity fluxes are zero.

4 Results and Discussion

In this section, analysis is carried out based on the comparative results of the two heat sink designs, i.e., CPF and QCPF for a given range of $2.71 \times 10^4 \leq Ra \leq 1.35 \times 10^5$ under laminar flow and constant base temperature conditions. The results are broadly classified into i) flow analysis and ii) heat transfer analysis, and are discussed in detail in the following sections.

4.1 Flow Analysis

Overall flow or velocity profiles for both the CPF and QCPF configurations are depicted in Fig. 4 using 3-D vector or arrow plots. The arrows are colored in total velocity magnitude as shown on the scale provided. It is observed (from the front view) that the flow pattern is more or less symmetrical around the pin fins. The flow of air is more pronounced at the bottom or near the heated plate as observed from the large-sized arrows near the heated plate than away from it since, the hot air or low-density air starts rising up from the heated base plate. Near the top of fins though the air flow is there (of low velocity magnitude), but due to limited scaling factor of vectors, are not clearly visible. In case of QCPF, air velocity is slightly more compared to CPF as made out from the dark red colored arrows. Flow between the gaps created in QCPF helps in creating a more uniform flow around the fins and intensifying the flow of air between the fins. Same velocity profiles can be observed for different *Ra* for both the configurations with slight variation in velocity magnitude. Flow between the fin gaps in QCPF helps in improving the rate of heat dissipation, and is explained in the following heat transfer analysis section.

4.2 Heat Transfer Analysis

The heat transfer characteristics from fins in both the heat sink designs are analyzed based on the rate of heat flux from total fin surface area for different *Ra*, and enhancement factor which is the ratio of rate of heat dissipated from both the designs, and fin efficiency.
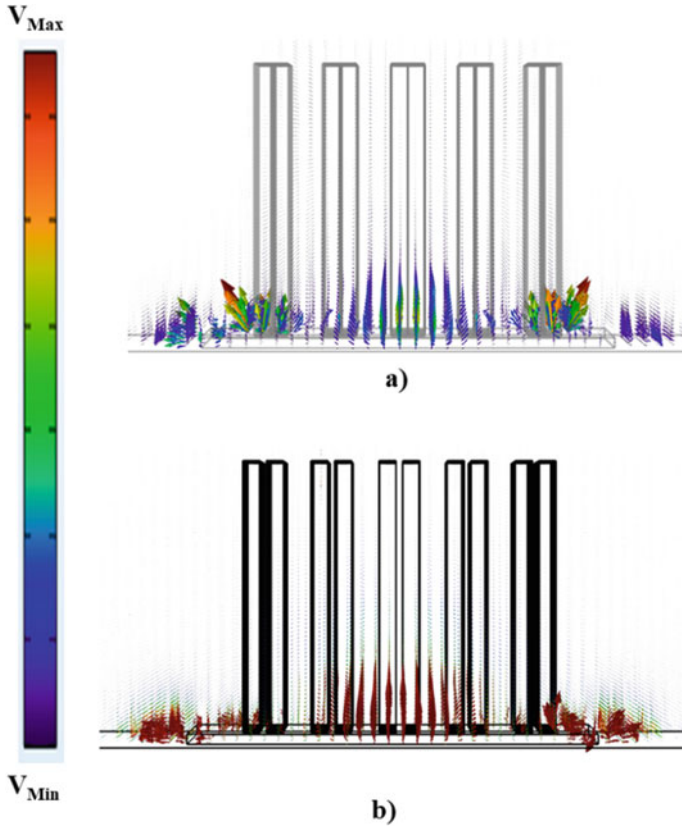
Fig. 4 Arrow plots (3-D vector) showing the flow of air around fins (*front view*) for **a** CPF; **b** QCPF configurations

Heat Dissipation. The plots for heat dissipation rate from the fins, in terms of heat flux, are shown in Fig. 5a as a function Ra for inline arrangements. It can be seen that the rate of convective heat transfer shows an increasing trend with the increase in Ra, which depends upon the temperature difference between fin base and ambient air temperature for both the configurations. However, the rate of heat dissipation is more in case of QCPF and this difference can be attributed to two major factors: (i) increase in fin surface area for heat transfer, and (ii) air flow within the gap regions. Since the cylindrical pin fin gets divided into four parts, the surface area gets increased by 2.2 times. This increase in surface area leads to an overall increases the rate of heat dissipated from the fins. Also, with the increase in air flow circulation within the gaps, the heat transfer coefficient gets increased. At higher Ra, the temperature difference is more, therefore, the flow of air leads to more intensified flow around the fins, thereby increasing the overall heat dissipation rate.
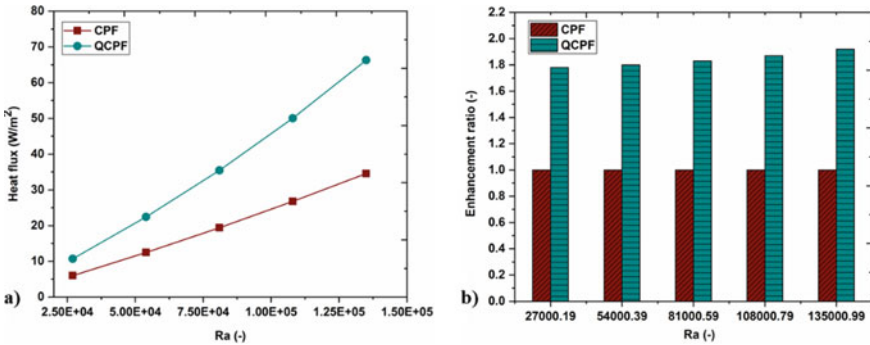
Fig. 5 Plots for CPF and QCPF configurations showing the **a** rate of heat flux with increase in *Ra*; **b** enhancement ratio showing the ratio of heat flux for different *Ra*

The plots for heat transfer enhancement are shown through enhancement ratio (ε)-plots, where $\varepsilon = Q_{QCPF}/Q_{CPF}$. A gradual increase in the trend of enhancement ratio is observed with the increase in *Ra* as shown in Fig. 5b. With the increase in *Ra*, the flow stagnancy gets reduced around the fin surfaces/regions leading to an improved heat transfer characteristics. Therefore, irrespective of temperature difference, QCPF design is more effective than CPF design for the given range of *Ra*.

Average Fin Temperature. The temperature profiles (colored in static temperature) for CPF and QCPF configurations are shown in Fig. 6 along with their base at, $Ra = 1.35 \times 10^5$. It is observed that the average fin temperature is higher in case of QCPF than CPF arrangement. Since, higher rate of heat transfer is obtained when the temperature of the fin gets closer to the temperature of the wall of the heated surface establishing a higher local temperature gradient: ($\Delta T = T_f - T_a$). This helps in more efficient heat dissipation in the surrounding fluid domain. In support of the qualitative temperature plots, a graph is shown in Fig. 7a indicating the average temperature values for both the designs. Average temperature values increase with the increase in *Ra* as the temperature difference increases, which is advantageous for heat dissipation and is also dependent upon the fin material used. The reason behind the differences observed in both the heat sink designs are already discussed in Sect. 4.2.1. Therefore, the homogenizing effect of air flow proves beneficial in case of QCPF design.

Fin efficiency. Values of fin efficiency (η) are used to determine the enhanced performance of QCPF heat sink configuration over CPF design under constant base temperature boundary wall boundary condition. The comparison is carried out for five different temperature differences as shown in Fig. 7b. In case of QCPF, enhancement in overall fin efficiency is seen compared to CPF for the given range of Ra. For CPF, fin efficiency varies from ~68% at $Ra = 2.71 \times 10^4$ to ~92% at $Ra = 1.35 \times 10^5$, whereas in case of QCPF the fin efficiency varies from ~ 74% at $Ra = 2.71 \times 10^4$
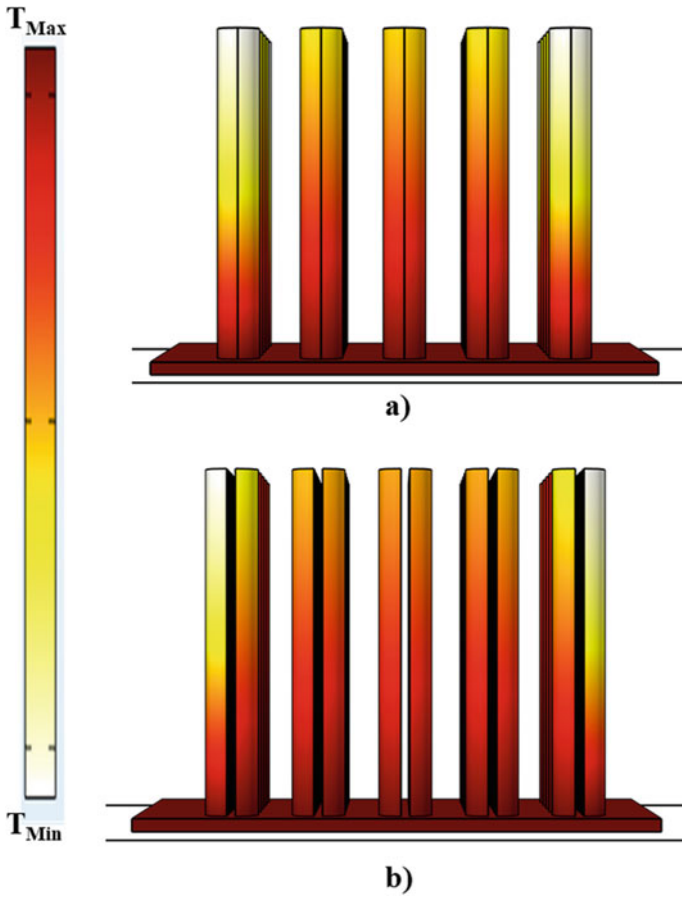
Fig. 6 Surface temperature plots (at $Ra = 1.35 \times 10^5$) showing the static temperature variation for **a** CPF; **b** QCPF configurations
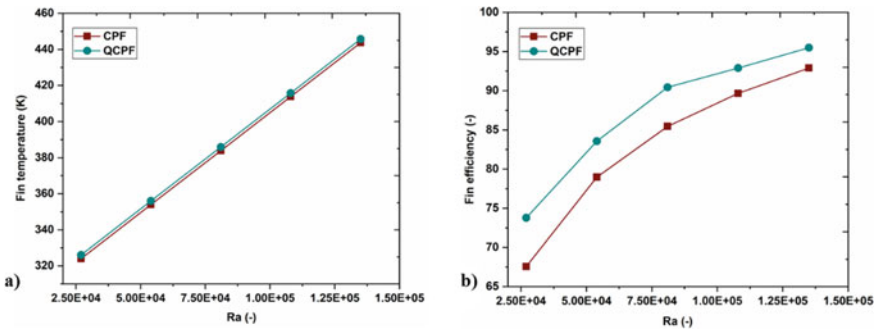
Fig. 7 Plots for CPF and QCPF configurations showing the **a** average fin temperature values for different Ra; **b** fin efficiency

to ~95% at $Ra = 1.35 \times 10^5$. Therefore, QCPF shows more efficient performance over CPF for the given range of Ra.

5 Conclusions

The numerical study of a novel quarterly-divided cylindrical pin fin (QCPF) heat sink is carried out in inline arrangement, which is a modified design of cylindrical pin fin (CPF). The performance of QCPF heat sink design is evaluated for a range of Ra under laminar flow condition ($2.71 \times 10^4 \leq Ra \leq 1.35 \times 10^5$), and is compared to that of conventional CPF design under similar surrounding conditions. The results are analyzed based on flow characteristics, rate of heat flux and fin efficiency. The following conclusions are drawn from the results obtained:

1. Flow feature reveal that air circulation around the fins and fin-gaps is improved, thereby homogenizing the temperature distribution and heat transfer effects in case of QCPF for different Ra.
2. The gap created by splitting the cylindrical pin fin into four equal parts leads to an increase in heat transfer surface area obtained using the same amount of material of construction, as in CPF design.
3. The rate of heat flux increases up to 1.92 times in case of QCPF with the increase in Ra over CPF configuration and is more effective in the given range of Ra.
4. The average fin temperature has higher value, and is closer to the base temperature or heated surface temperature in case of QCPF than CPF configuration.
5. Fin efficiency, in case of QCPF, lies somewhat higher, i.e., $3 - 6\%$ than that in the corresponding CPF arrangement.
6. Above findings establish the potency of QCPF over CPF design through improved air circulation in the gaps under natural convection.

References

Al-Damook A, Kapur N, Summers JL, Thompson HM (2015) An experimental and computational investigation of thermal air flows through perforated pin heat sinks. Appl Therm Eng 89:365–376

Al-Damook A, Kapur N, Summers JL, Thompson HM (2016a) Computational design and optimisation of pin fin heat sinks with rectangular perforations. Appl Therm Eng 105:691–703

Al-Damook A, Summers JL, Kapur N, Thompson HM (2016b) Effect of different perforations shapes on the thermal-hydraulic performance of perforated pinned heat sinks. J Multidisc Eng Sci Techn 3:4466–4474

Belhardj S, Mimouni S, Saidane A, Benzohra M (2003) Using microchannels to cool microprocessors: a transmission-line-matrix study. Microelectron J 34(4):247–253

Deshmukh PA, Warkhedkar RM (2013) Thermal performance of elliptical pin fin heat sink under combined natural and forced convection. Exp Therm Fluid Sci 50:61–68

Dogruoz MB, Urdaneta M, Ortega A (2005) Experiments and modeling of the hydraulic resistance and heat transfer of in-line square pin fin heat sinks with top bypass flow. Int J Heat Mass Transf 48(23–24):5058–5071

Horiuchi K, Nishihara A, Sugimura K (2015) Multi-objective optimization of water-cooled pin fin heatsinks. Int J Heat Mass Tran 81:760–766

Jeng TM, Tzeng SC (2007) Pressure drop and heat transfer of square pin-fin arrays in in-line and staggered arrangements. Int J Heat Mass Transf 50:2364–2375

Jha VK, Bhaumik SK (2019) Novel helically finned heat sink to achieve lower operating temperature and higher fin efficiency. In: Proceedings of the 25th National and 3rd International ISHMT—ASTFE Heat and Mass Transfer Conference, pp. 1091–1096. Begell House, United States

Jha VK, Bhaumik SK (2019a) Enhanced heat dissipation in helically finned heat sink through swirl effects in free convection. Int J Heat Mass Transf 138:889–902

Khetib Y, Sedraoui K, Gari A (2021) Numerical study of the effects of pin geometry and configuration in micro-pin-fin heat sinks for turbulent flows. Case Stud Thermal Eng 27:101243

Kirsch KL, Thole KA (2017) Pressure loss and heat transfer performance for additively and conventionally manufactured pin fin arrays. Int J Heat Mass Transf 108:2502–2513

Nakayama W (1986) Thermal management of electronic equipment: a review of technology and research topics. Appl Mech Rev 39(12):1847–1868

Naphon P, Sookkasem A (2007) Investigation on heat transfer characteristics of tapered cylinder pin fin heat sinks. Energy Convers Manage 48(10):2671–2679

Pandit J, Thompson M, Ekkad SV, Huxtable ST (2014) Effect of pin fin to channel height ratio and pin fin geometry on heat transfer performance for flow in rectangular channels. Int J Heat Mass Transf 77:359–368

Tullius JF, Vajtai R, Bayazitoglu Y (2011) A review of cooling in microchannels. Heat Tran Eng 32(7–8):527–541

Welling JR, Wooldridge CB (1965) Free convection heat transfer coefficients from rectangular vertical fins. J Heat Transfer 87(4):439–444

Yamada Y, Yanase M, Miura D, Chikuba K (2016) Novel heatsink for power semiconductor module using high thermal conductivity graphite. Microelectron Reliab 64:484–488

Yuan W, Zhao J, Tso CP, Wu T, Liu W, Ming T (2012) Numerical simulation of the thermal hydraulic performance of a plate pin fin heat Sink. Appl Therm Eng 48:81–88

Yüncü H, Güvenc A (2001) An experimental Investigation on performance of rectangular fins on a vertical base in free convection heat transfer. Heat Mass Transf 37:409–416

Zhou F, Catton I (2011) Numerical evaluation of flow and heat transfer in plate–pin fin heat sinks with various pin cross-sections. Numer Heat Transfer Part A Appl 60(2):107–128

Chitosan: Derivatives, Properties and Applications

Vineet Kumar Rathore and Jigisha K. Parikh

Abstract Chitosan is biomaterial-derived chitin that is found in abundance in nature. It is one of the main constituents in the shells of crustaceans, insect cuticles, mushrooms, and cell walls of fungi and green algae. The method of synthesis and precursors used to play important role in determining major properties of chitosan like molecular weight, viscosity, and solubility in water. Due to its natural origin, it is having a variety of applications in modern health science, food industry, cosmetics industry, water treatment, etc. In the present work, a review of the derivatives, their properties, and applications of chitosan in several areas like health science, food industry, cosmetics, and water treatment has been carried out. In medical science, it is of particular interest due to its biocompatibility and its possible applications in bone and tissue engineering and dentistry. In the food industry, chitosan can be used as a possible supplement for protein-rich food and also as an alternative for plastic-based packing material. In cosmetics, chitosan-based lotions, creams, and other personal care products are gaining popularity due to their excellent moisture-retaining ability and biocompatibility. In the water treatment industry, chitosan is studied by many research groups as an effective bio-coagulant and bio-flocculent to remove various types of contaminants.

Keywords Chitosan · Derivatives · Applications · Biomaterial

1 Introduction

Most of the commercially available polymers are derived from petroleum-based feedstocks using processing chemistry and pose environmental threats in many ways. One of the possible ways to overcome this problem that has been a topic of interest for the

V. K. Rathore (✉) · J. K. Parikh
Department of Chemical Engineering, Sardar Vallabhbhai National Institute of Technology, Surat, Gujarat 395007, India
e-mail: vkrathore@ched.svnit.ac.in

J. K. Parikh
e-mail: jkp@ched.svnit.ac.in

Fig. 1 Structure of chitosan
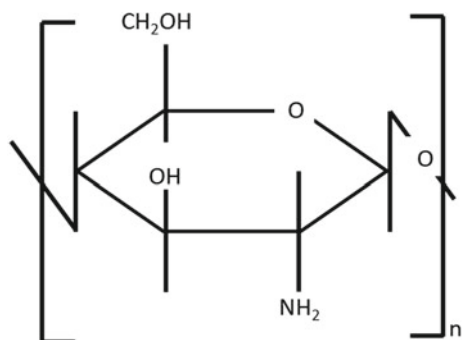
last few decades is the development of novel biological compounds. Such polymeric materials are known as biopolymers and are derived either from living organisms or from renewable sources in a sustainable manner. The major advantage associated with the use of biopolymers is that they are non-toxic and are also biodegradable. A large number of biopolymers are already known to occur in abundance in nature such as cellulose, starch, chitin/chitosan (Fig. 1), and alginates. In 1859, Charles Rouget isolated a novel material by heating chitin powder in an alkaline medium that was soluble in weak acids and was termed chitosan by Felix Hoppe-Seyler in 1894. Chitin as such has very low solubility in water and other solvents and hence it is frequently deacetylated and converted into chitosan. There can be three different types of crystalline forms of chitin in nature depending upon the source. α-Chitin is the most abundantly found form of chitin and is commonly found in shells of crustaceans and cell walls of fungi. It has an orthorhombic crystal structure and composes of antiparallel chains of molecules providing it rigidity. On the other hand, β-chitin has a monoclinic crystal structure and the chain of molecules is arranged in parallel order giving its structure a weak packing. The last form of chitin is γ-chitin which is a combination of these two and has properties of both of its polymorphs (Minke and Blackwell 1978). On the other hand, chitosan is soluble in water and other solvents including acids that make it ideal to be used in various applications. Chitosan can also be converted into many of its derivatives through chemical modifications due to the presence of hydroxyl groups and amino groups in its molecular structure. Due to this property, chitosan has found its application in a wide variety of fields. Currently, chitosan and its derivatives have numerous applications in the form of nanoparticles, beads, resins, sponges, aerogel, solution, foam, membranes, etc.

2 Derivatives

Chitin is one of the most abundantly available natural polysaccharide materials after cellulose (Dutta et al. 2004). It can be obtained from the fungi cell walls, the exoskeleton of crustaceans, and insects. One of the main materials derived from the

deacetylation of chitin is chitosan. Chitosan is obtained by *N*-deacetylation of chitin and is a linear, semicrystalline polysaccharide. It is mainly composed of *N*-acetyl glucosamine and glucosamine units linked by β-(1 → 4) glycosidic bonds (Rinaudo 2006). Chitin and chitosan can be differentiated based on the fraction of glucosamine units present. When the number of N-acetyl glucosamine units is greater than 50%, it is termed chitin and the number of acetamido groups present determines the degree of acetylation (DA). On the other hand, if the fraction of glucosamine units is more than 50% then the polymer is commonly known as chitosan. This fraction of glucosamine units present in the material is known as the degree of deacetylation (DDA) (Fig. 1).

Mathematically, the summation of degree of acetylation and degree of deacetylation is equal to unity (Dornish et al. 2001; VandeVord et al. 2002). When the DDA of chitin is about 50% or greater (depending on the origin of the polymer and processing conditions), it becomes soluble in aqueous acidic media. Generally, in commercially available chitosan DDA ranges from 70 to 95% and has a molecular weight ranging from 10^4 to 10^6 g/mol (Moura et al. 2011). The value of DDA determines the characteristics of chitosan like degree of crystallinity, swelling index, degree of elongation, tensile strength, and viscosity. Based on these properties, chitosan can be transformed into various types of shapes and forms. For example, if the molecular weight of chitosan is low then it leads to low viscosity and vice versa. These low viscosity chitosan can be used in the form of liquid and gels. Furthermore, higher molecular weight and DDA of chitosan also result in its better antimicrobial capability. The presence of three reactive functional groups (Fig. 1) also makes chitosan very versatile for various applications through chemical modification (Vunain et al. 2017).

3 Production

In the area of seafood, shellfish, and other crustaceans processing, large quantities of shell waste are produced. This waste material is rich in chitin and can be further processed into chitosan. In brief, chitin is produced by washing the waste materials obtained from washing the shells of crustaceans, crushing them, soaking in diluted strong acids (to remove the calcium impurities), and then subjecting them to strong alkaline treatment (to remove the other impurities of nitrogen-containing compounds). Finally, carotenoids and other coloring materials are removed by the solvent extraction method. The so obtained chitin material is then deacetylized to produce chitosan. Various techniques like microwave irradiation, enzymes, and the use of strong alkalis (e.g., sodium hydroxide, potassium hydroxide) at high temperatures and pressures, etc. are reported to convert chitin to chitosan. The conversion of chitin to chitosan can be carried in the following steps:

i.   Acid treatment of chitin (decalcification).
ii. Alkaline treatment for deprotonation.
iii. A decolorization process to remove color.
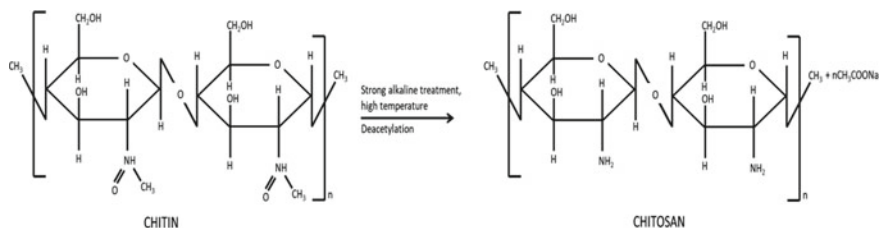
Fig. 2 Conversion of chitin to chitosan

iv. In the last, deacetylation is done with the help of strong alkali under high temperature and pressure or via enzymatic processes (Vunain et al. 2017) (Fig. 2).

Chitin can be N-deacetylated either homogeneously or heterogeneously. Homogenous acetylation of chitin is carried out with NaOH at room temperature and results in the formation of chitosan having more regular distribution of residual acetamide groups. Such chitosan is water-soluble and its DDA ranges from 48 to 55%. On the other hand, in heterogeneous deacetylation, chitosan is obtained by treating chitin in a hot concentrated NaOH solution. The chitosan so obtained is insoluble and has a higher value of DDA (85–93%) as compared to that obtained from the homogenous method. Although both these methods produce chitosan with good DDA yet they are highly energy-intensive and produce chitosan with a high degree of variation in the DDA and molecular weight distribution (Tsigos et al. 2000). To overcome these limitations, more methods are explored by various research groups to increase the efficiency of the conversion of chitin to chitosan. Some of them are as follows:

3.1 Microwave-Assisted Deacetylation

The conversion of molecules structure with the help of microwaves has caught the attention of several research groups due to its shorter reaction time and higher conversion rate. Microwaves are electromagnetic radiations having a high frequency that have shown to highly increase the reaction rates by producing immediate heating and vibrational energy at the molecular level and hence are preferred to achieve the desired conversion in a relatively lesser time. (Lertwattanaseri et al. 2009) claimed to achieve more than 90% DDA in 3 h compared to 21 h needed for conventional alkali treatment. (Kocak et al. 2011) also synthesized chitosan nanoparticles (CHN) based on ionotropic gelation between low molecular weight chitosan and sodium tripolyphosphate (TPP) under microwave irradiation. They reported that the size of the nanoparticles is highly dependent on the reaction time. The microwave irradiation method produced nanoparticles of 183.4 nm size in 60 s and as the microwave exposure time is increased up to 180 s, particle size reduced to 60.6 nm.

3.2 Enzyme Assisted Deacetylation

With the rapid increase in demand for products having very specific properties and lack of control in the thermo-chemical synthesis process of chitosan, enzymatic routes have also drawn the attention of researchers. This type of enzymatic production of chitosan is well reported to be carried out with the help of specific enzymes such as chitosanases, chitinases, and non-specific enzymes like proteases and carbohydrases (Kim and Je 2010). In this method, enzymatic deacetylation is carried out with the help of chitin deacetylases which can be obtained from different biological sources such as fungi and insects (Tsigos et al. 2000). The major advantages of this process are the production of chitosan having higher molecular weight and desired degree of deacetylation. On the other hand, chitooligosaccharides deacetylases are enzymes that can be employed to further modify the structure of the chitosan molecule and get the desired arrangement of the chain (Hirano et al. 2017). Both chitin deacetylases and chitooligosaccharides deacetylases are a group of enzymes catalyzing the hydrolysis of acetamido groups of N–acetyl–D–glucosamine residues in chitin, chitosan, and chitooligosaccharides, respectively (Li et al. 2007; Pacheco et al. 2013). The major advantages of this method are that it produces a homogenous product having a more defined pattern of deacetylation. Moreover, this method is greener than the thermochemical process.

4 Applications

Chitosan finds many applications in the field of biotechnology and health science due to its excellent biocompatibility. This property of chitosan is due to the presence of the homologous nature of chitosan with hyaluronic acid and glycosaminoglycan extracellular matrix molecules (Muzzarelli et al. 1988). Moreover, the ability of chitosan to dissolve in dilute acids and aqueous solutions permits its conversion in various forms like films, gels, fibers, particles, and sponges (Kaur and Dhillon 2014). Moreover, the presence of amino and hydroxyl groups on the ends of the chitosan monomer block makes its molecule very flexible and highly susceptible to chemical modifications.

4.1 Health Science

There are numerous studies available on various search engines reporting the in vivo examination of chitosan-based materials bone repair or regeneration and treatment strategies. In these studies, the usage of chitosan is reported in the modified form along with some types of composites like ceramics, metal alloys, and biological tissues (Table 1). The viability of using chitosan as base material is still not very

Table 1 Some applications of chitosan in the health sector

Form	DDA	Model	Usage	Bone response	Reference
Chitosan coated Ti pins	92.30%	Rabbit, Tibia	Chitosan coated implant and bone graft material	Chitosan coated pins gave a similar response as uncoated coated Ti pins	Bumgardner et al. (2007)
The coating on calcium sulphate pallets	90%	Rabbit, 12 mm radial defect	Coated implant and bone graft material	Chitosan-coated pellets healed the defect whereas noncoated pellets were unable	Cui et al. (2008)
Coating on porous Ti alloy	85–90%	Diabetic sheep, 12 × 5 mm iliac crest defect	The coating on implant and bone graft material	Significant repair of bone in filled-in space as compared to the uncoated place	Li et al. (2015)
Chitosan film	83%	Rat, 5 mm calvarial	Chitosan film with bone	No significant improvement in the bone defect with anion cross-linked chitosan as compared to plain film	Kuo et al. (2006)
Lyophilized membrane	87%	Rat having 8 mm calvarial defect	Chitosan film with bone	Superior bone healing observed with Chitosan membrane than empty control	Ma et al. (2014)
Lyophilized scaffold	Not reported	Rat having 5 mm calvarial defects	Chitosan scaffolds in bone graft	More bone fill than empty defects	D'Mello et al. (2015)
Lyophilized scaffold	88%	Rabbit having 4 mm diameter × 2.5 mm deep tibial defects	Chitosan scaffolds in bone graft	No significant difference between the chitosan-coated implant and empty control observed	Guzmán et al. (2014)

Table 1 (continued)

Form	DDA	Model	Usage	Bone response	Reference
Wet-spun fiber mats	>90%	Rabbit having 2.5 mm diameter tibial defects	Chitosan fibrous membranes in bone	Citric acid ionotropically cross-linked chitosan supported the bone formation	Ghosh et al. (2015)
Electrospun fiber membranes	>95%	Rat 10 mm calvarial defect	Chitosan fibrous membranes in bone	Enhanced bone formation with chitosan membrane versus control	Shin et al. (2005)
Gel	80–82%	Rabbit, trochlear drill holes	Chitosan gel in bones	Supported healing of bone and induced remodeling. Healed bone plate density highly dependent on the molecular weight of chitosan	Guzman-Morales et al. 2014)
Gel	81.80%	Rabbit having osteochondral defect, 14 mm diameter × 2 mm deep	Chitosan gels in bone	Pre-solidified chitosan implants found beneficial for augmented marrow stimulation	Lafantaisie-Favreau et al. (2013)
Solution	110–150 kDa	Rat having femoral osteotomy with stainless steel IM wire fixation	Soluble forms of chitosan	Better healing of bone fractures was observed in mice treated with chitosan	Tan et al. (2014)

clear in these studies as they do not focus on the response of the host tissue. This fundamental information is vital to establish a relation between chitosan-host tissue interaction as well as possible application in clinical use.

4.2 Food Industry

US FDA has approved chitosan and recognized it as a safe dietary fiber, food additive, and functional ingredient for consumers. It is also approved by Japan and South

Korea as a food additive and has been extensively used (Vidanarachchi et al. 2011; Gutiérrez et al. 2017). In the food industry, chitosan is used as a dietary food additive for controlling obesity (Ramya et al. 2012). Chitosan molecule can bind with the fat molecule and forms a mass that is hard to be absorbed in the body and is thus is excreted from the body. As it is not absorbed by the body, it has virtually zero calorific value and can also be used as food for weight loss. The US market is considered as the largest nutraceutical market globally followed by the European market (Germany, France, Netherlands, Sweden, etc.) in the second. China is one of the biggest emerging markets for nutraceuticals by 2030. Commercially, many products available are available under many brand names e.g., Chitoseen™-F, ChitoClear®, MicroChitosan, NutriCology®, etc., and are consumed to reduce fats, cholesterol and as antioxidant agents. It is also claimed that LipoSan Ultra ® is an effective supplement in losing weight naturally and safely (PRIMEX, Iceland). However, the effectiveness of chitosan at blocking fat absorption is a highly debated subject. Further, some other nutraceutical properties of chitosan are also claimed regarding its anti-inflammatory, antibacterial, anti-carcinogenic, and antiulcer bioactivities, etc.

Due to its polymeric structure, chitosan is also been explored by several research groups as potential bio-degradable packaging material. It has a very good capacity to retain the freshness and aroma of the foodstuff. It can be used in place of synthetic packing materials (Miteluț et al. 2015). It is also used for the preservation of beverages as well as clarification and encapsulation of bioactive compounds. One of the drawbacks of chitosan film in packing materials is that it is hydrophilic and hence possesses high permeability towards water vapors. This property can be improved by blending or making multiple films of chitosan with other polymers and fibers.

4.3   Cosmetics

Chitosan has found wide applications in the field of cosmetics both in the areas of skincare and perfumes/fragrances. It is of particular interest in this field as it can be synthesized in the form of various derivatives having specific properties and molecular weight. Most of the chitosan molecules and derivatives have fairly large molecular weight and hence making it difficult to penetrate the skin. This property makes chitosan and its derivatives a good candidate for application in cosmetic products. The carboxymethylchitosans is one such derivative used frequently in cosmetics as an antioxidant, moisture absorption and retention agent, antimicrobial agent, delivery system, and emulsion stabilization. In the case of skincare products, it is used in the manufacturing of moisturizing creams, lotions, and other skin-softening agents. It is attributed to the property of chitosan which allows it to make a natural protective and moisturizing film over the skin. This film helps the skin to stay hydrated and also protects it from adverse environmental conditions. Similar to skincare products, chitosan-containing lip-care products are also widely manufactured and used. Chitosan acts as a good moisturizing agent for the lips and helps them stay soft and

avoids drying (Chen 2008). In the area of perfumes and deodorants also, chitosan-containing products are widely found. Chitosan has a very good ability to inhibit the activity of enzyme-producing bacteria and hence reducing the bad odor. Further, it has excellent skin compatibility as compared to other commonly used synthetic chemicals. Chitosan is also reported to have a higher fragrance adhering capacity hence making it suitable for perfumes (Tzaneva et al. 2017).

4.4 Water Treatment

A large number of papers have been published on the application of this biopolymer for water treatment. The main reason behind the success of this material is the advantages of using this material which is (i) It is low-cost (ii) It has very high pollutant binding capacity (iii) its ability to be used for large kinds of pollutants (iv) its biodegradability makes it easy to dispose of post-application. Further, it is reported to be used in various types of soluble and insoluble forms like beads, gels, films, sponges, fibers, and membranes. It can also be applied through coagulation-, flocculation-, adsorption-, or filtration-based processes. (Crini and Badot 2008) comprehensively discussed the application of various chitosan-based materials for the remediation of dye-contaminated wastewater. They have discussed the effects of various process parameters such as type of linking in the chitosan, synthesis procedure, process conditions, and chemistry of the dye on its removal capacity. Recently, (Desbrières and Guibal 2018; Pakdel and Peighambardoust 2018) also reviewed the application of chitosan-based materials for the wastewater treatment process and have concluded that these are very good for treating wastewater containing metal and organic loadings as well. The capability of chitosan to spontaneously form water-insoluble complexes with anionic polyelectrolytes makes it very effective in the removal of a wide range of pollutants. Further, chitosan is reported to be used as a coagulating agent in the food industry wastewater and also for conditioning of activated sludge that is produced as a result of the biological treatment of waste. This waste is reported to contain significant amounts of protein and can be used as animal feeds. Chitosan being an eco-friendly material, can be a very good possible substitute for the currently available metallic salts and synthetic polyelectrolytes-based materials for the treatment of water containing both particulate and dissolved substances. Despite a large number of applications and benefits like being low-cost and eco-friendly, most of the processes developed are still at laboratory scale and have not found much practical application in the industries. There are only a few products e.g., Pennofloc™ for water clarification, ChitoVan™ for biofiltration are commercially available in the market as concurrent flocculating and adsorbing agents although lesser effective and non-biodegradable and are cheaper.

5   Conclusion

Chitosan-based biomaterials have attracted the large attention of the research community in recent decades due to various properties that are favorable for their application in a variety of fields. They exhibit excellent biocompatibility and can be easily synthesized with the help of conventional methods. Further, the properties can also be customized according to the need when they are synthesized with other novel routes viz. microwave-assisted and with the help of various enzymes. They have been successfully used as active drug delivery agents, dressing materials, and in surgery. They have also been utilized in the food industry as a dietary food additive. Due to its natural origin and no allergic reactions, it is also widely used in the cosmetic industry for making lotions, creams, and other cosmetic products. Moreover, its applications in the field of water treatment have also been successfully established due to its low cost and high ability to bind pollutants.

References

Bumgardner JD, Chesnutt BM, Yuan Y, Yang Y, Appleford M, Oh S, McLaughlin R, Elder SH, Ong JL (2007) The integration of chitosan-coated titanium in bone: an in vivo study in rabbits. Implant Dent 16(1):66–79

Chen YL (2008) Preparation and characterization of water-soluble chitosan gel for skin hydration. M.Sc. Thesis, UniversitiSains Malaysia

Crini G, Badot PM (2008) Application of chitosan, a natural aminopolysaccharide, for dye removal from aqueous solutions by adsorption processes using batch studies: a review of recent literature. Prog Polym Sci 33(4):399–447

Cui X, Zhang B, Wang Y, Gao Y (2008) Effects of chitosan-coated pressed calcium sulfate pellet combined with recombinant human bone morphogenetic protein 2 on restoration of segmental bone defect. J Craniofac Surg 19(2):459–465

de Moura CM, de Moura JM, Soares NM, de Almeida Pinto LA (2011) Evaluation of molar weight and deacetylation degree of chitosan during chitin deacetylation reaction: used to produce biofilm. Chem Eng Process Process Intensif 50(4):351–355

Desbrières J, Guibal E (2018) Chitosan for wastewater treatment. Polym Int 67(1):7–14

D'Mello S, Elangovan S, Hong L, Ross RD, Sumner DR, Salem AK (2015) Incorporation of copper into chitosan scaffolds promotes bone regeneration in rat calvarial defects. J Biomed Mater Res Part B 103(5):1044–1049

Dornish M, Kaplan D, Skaugrud Ø (2001) Standards and guidelines for biopolymers in tissue-engineered medical products: ASTM alginate and chitosan standard guides. Ann N.Y. Acad Sci 944(1):388–397

Dutta PK, Dutta J, Tripathi VS (2004) Chitin and chitosan: Chemistry, properties and applications. J Sci Ind Res 63:20–31

Ghosh P, Rameshbabu AP, Das D, Francis NK, Pawar HS, Subramanian B, Pal S, Dhara S (2015) Covalent cross-links in polyampholytic chitosan fibers enhances bone regeneration in a rabbit model. Colloids Surf B 125:160–169

Gutiérrez TJ (2017) Chitosan applications in textile and food industry. In: Ahmed S, Ikram S (eds) Chitosan—derivatives, composites and applications. Scrivener Publishing LLC, Wiley, pp 185–232

Guzmán R, Nardecchia S, Gutiérrez MC, Ferrer ML, Ramos V, del Monte F, Abarrategi A, López-Lacomba JL (2014) Chitosan scaffolds containing calcium phosphate salts and rhBMP-2: in vitro and in vivo testing for bone tissue regeneration. PloS One 9(2)

Guzman-Morales J, Lafantaisie-Favreau CH, Chen G, Hoemann CD (2014) Subchondral chitosan/blood implant-guided bone plate resorption and woven bone repair is coupled to hyaline cartilage regeneration from microdrill holes in aged rabbit knees. *Osteoarthr. Cartil.*, 22(2), 323–333.

Hirano T, Shiraishi H, Ikejima M, Uehara R, Hakamata W, Nishio T (2017) Chitin oligosaccharide deacetylase from Shewanellabaltica ATCC BAA-1091. Biosci Biotechnol Biochem 81(3):547–550

Kaur S, Dhillon GS (2014) The versatile biopolymer chitosan: potential sources, evaluation of extraction methods and applications. Crit Rev Microbiol 40(2):155–175

Kim S, Je J (2010) Continuous production of chitooligosaccharides by enzymatic hydrolysis. In: Kim S-K (ed) Chitin, chitosan, oligosaccharides and their derivatives: biological activities and applications, pp 185–195. CRC Press

Kocak N, Sahin M, Akin I, Kus M, Yilmaz M (2011) Microwave assisted synthesis of chitosan nanoparticles. J Macromol Sci Part A Pure Appl Chem 48(10):776–779

Kuo SM, Chang SJ, Chen TW, Kuan TC (2006) Guided tissue regeneration for using a chitosan membrane: an experimental study in rats. J Biomed Mater Res Part A 76(2):408–415

Lafantaisie-Favreau CH, Guzmán-Morales J, Sun J, Chen G, Harris A, Smith TD, Carli A, Henderson J, Stanish WD, Hoemann CD (2013) Subchondral pre-solidified chitosan/blood implants elicit reproducible early osteochondral wound-repair responses including neutrophil and stromal cell chemotaxis, bone resorption and repair, enhanced repair tissue integration and delayed matrix deposition. BMC Musculoskelet 14(1):27

Lertwattanaseri T, Ichikawa N, Mizoguchi T, Tanaka Y, Chirachanchai S (2009) Microwave technique for efficient deacetylation of chitin nanowhiskers to a chitosan nanoscaffold. Carbohydr Res 344(3):331–335

Li X, Wang LX, Wang X, Roseman S (2007) The chitin catabolic cascade in the marine bacterium Vibrio cholerae: characterization of a unique chitin oligosaccharide deacetylase. Glycobiology 17(12):1377–1387

Li X, Ma XY, Feng YF, Ma ZS, Wang J, Ma TC, Qi W, Lei W, Wang L (2015) Osseointegration of chitosan coated porous titanium alloy implant by reactive oxygen species-mediated activation of the PI3K/AKT pathway under diabetic conditions. Biomaterials 36:44–54

Ma S, Chen Z, Qiao F, Sun Y, Yang X, Deng X, Cen L, Cai Q, Wu M, Zhang X, Gao P (2014) Guided bone regeneration with tripolyphosphate cross-linked asymmetric chitosan membrane. J Dent 42(12):1603–1612

Minke RAM, Blackwell J (1978) The structure of α-chitin. J Mol Biol 120(2):167–181

Miteluț AC, Tănase EE, Popa VI, Popa ME (2015) Sustainable alternative for food packaging: chitosan biopolymer—a review. AgroLife Sci J 4(2):52–61

Muzzarelli R, Baldassarre V, Conti F, Ferrara P, Biagini G, Gazzanelli G, Vasi V (1988) Biological activity of chitosan: ultrastructural study. Biomaterials 9(3):247–252

Pacheco N, Trombotto S, David L, Shirai K (2013) Activity of chitin deacetylase from Colletotrichumgloeosporioides on chitinous substrates. Carbohydr Polym 96(1):227–232

Pakdel PM, Peighambardoust SJ (2018) Review on recent progress in chitosan-based hydrogels for wastewater treatment application. Carbohydr Polym 201:264–279

Puvvada YS, Vankayalapati S, Sukhavasi S (2012) Extraction of chitin from chitosan from exoskeleton of shrimp for application in the pharmaceutical industry. Int Curr Pharm 1(9):258–263

Ramya R, Venkatesan J, Kim SK, Sudha PN (2012) Biomedical applications of chitosan: an overview. J Biomater Tissue Eng 2(2):100–111

Rinaudo M (2006) Chitin and chitosan: properties and applications. Prog Polym Sci 31(7):603–632

Shin SY, Park HN, Kim KH, Lee MH, Choi YS, Park YJ, Lee YM, Ku Y, Rhyu IC, Han SB, Lee SJ (2005) Biological evaluation of chitosan nanofiber membrane for guided bone regeneration. J Periodontol 76(10):1778–1784

Tan ML, Shao P, Friedhuber AM, van Moorst M, Elahy M, Indumathy S, Dunstan DE, Wei Y, Dass CR (2014) The potential role of free chitosan in bone trauma and bone cancer management. Biomaterials 35(27):7828–7838

Tsigos I, Martinou A, Kafetzopoulos D, Bouriotis V (2000) Chitin deacetylases: new, versatile tools in biotechnology. Trends Biotechnol 18(7):305–312

Tzaneva D, Simitchiev A, Petkova N, Nenov V, Stoyanova A, Denev P (2017) Synthesis of carboxymethyl chitosan and its rheological behaviour in pharmaceutical and cosmetic emulsions. J Appl Pharm Sci 7(10):70–78

VandeVord PJ, Matthew HW, DeSilva SP, Mayton L, Wu B, Wooley PH (2002) Evaluation of the biocompatibility of a chitosan scaffold in mice. J Biomed Mater Res 59(3):585–590

Vidanarachchi JK, Kurukulasuriya MS, Kim SK (2011) Chitin, chitosan, and their oligosaccharides in food industry. In: Kim SK (ed) Chitin, chitosan, oligosaccharides and their derivatives: biological activities and applications. CRC Press, Taylor & Francis Group LLC, Boca Raton, pp 543–560

Vunain E, Mishra AK, Mamba BB (2017) Fundamentals of chitosan for biomedical applications. In: Jennings JA, Bumgardner JD (eds) Chitosan based biomaterials, vol 1, pp 3–30. Woodhead Publishing

Do Millennial Exhibit Environmentally Responsive Consumption Behaviors—A Study on Determinants of Green Purchase Decision?

M. Kirupa Priyadarsini , **T. PraveenKumar** , **B. Aishwarya Lakshmi, S. A. Jyotsna, and A. Swetha**

Abstract The purchase behavior of green products is largely affected by the intention-action gap and skepticism present among consumers. The purpose of this study was to analyze the various factors that affect the purchase behavior of green products among millennials. The practical benefit of this research is that it will assist in the convergence of green marketing and environmental consumer behavior theories. The theory used in the study is the theory of planned behavior. It helps to understand the specific behaviors of consumers as a possibility of a particular behavioral intention. For this purpose, we identified five constructs, namely, Environmental Concerns and Belief (ECB), Eco-Labelling (EL), Green Packaging and Branding (GPB), Green Product, Premium, and Pricing (GPPP), and Consumers Beliefs Towards the Environment (CBTE). These constructs have helped in identifying and analyzing the various factors that affect the purchase behavior of green products among millennials. We analyzed the purchase behavior of green products using a questionnaire approach. For this descriptive study, there were 251 millennials as our respondents who were chosen using the convenience sampling technique. The data was collected through a structured questionnaire via Google form and was analyzed using regression analysis, correlation. It was found that the key factors of green marketing such as Environmental Concerns and Beliefs (ECB), Green Packaging and Branding (GPB), and Green Product, Premium and Pricing (GPPP) have a positive influence on Consumers Beliefs Towards the Environment (CBTE). It implies that by increasing the spending on green packaging and branding there will be a positive effect on consumers' environmental beliefs. On the other hand, Eco-Labelling (EL) has a negative influence on Consumers Beliefs Towards the Environment (CBTE) and this is caused by skepticism present among millennials.

M. K. Priyadarsini (✉) · B. A. Lakshmi · S. A. Jyotsna · A. Swetha
PSG Institute of Management, Coimbatore, India
e-mail: kirupa@psgim.ac.in

T. PraveenKumar
School of Business and Management, Christ (Deemed to be University), Bangalore, India
e-mail: praveenkumar.t@christuniversity.in

Keywords Green products · Purchase behavior · Environmental concerns ·
Consumers environmental beliefs

1 Introduction

Rapid economic expansion in developing countries, such as India, has resulted in
excessive consumption of natural resources. Green consumption is defined as ecolog-
ically responsible behavior that promotes nature and protects the environment. Green
products, also known as sustainable products, are those that help both society and
the environment. It features eco-friendly bags, recycled papers, and energy-efficient
lighting, among other things. This highlights the fact that consumer behavior is
influenced not just by attitudes, but also by cognitive factors such as environmental
concern, environmental beliefs, and antidotes to purchasing green products. However,
little study has been done to investigate the impact of green factors on consumer
purchasing behavior. In today's world, the concept of pro-environmental conduct
is primarily depicted or associated with children. They demonstrate environmental
awareness and support the preservation of natural resources through their actions.
Notably, little research has been done on the factors that influence young customers'
green buy intentions and behavior. As a result, our research develops a model to
investigate the interaction between elements such as premium price, branding, and
environmental beliefs.

2 Theoretical Background and Literature Review

According to traditional consumer behavior theories, such as the idea of planned
behavior, an individual's conduct can be reasonably influenced by his or her behav-
ioral purpose. Researchers have added numerous new psychological variables to the
theory of planned behavior, such as "perceived green value," "environmental aware-
ness," to properly forecast green consumption behavior. The hypothesis of planned
behavior has been investigated in a variety of psychological and sociological research
(Ajzen 1991; Taylor and Todd 1997). This theory has been used to analyze several
green purchase behavior research (Paul et al. 2016).

2.1 Environmental Concerns and Beliefs (ECB)

Environmental concern and belief are defined as the attitude one has towards their
own or other's behavior in terms of the environment (Fransson and Gärling 1999). It
can also be referred to as the feelings of different green issues as felt by consumers
(Zimmer et al. 1994). It is in the vulnerability in the balance of nature, we can see

what decisions can be made to limit the domination of humans in nature (Kropfeld et al. 2018).

The degree to which a consumer has a knowledge of the environmental issues and how much they are eager in initiating a decision to contribute personally to solve those environmental issues is Environmental concerns and beliefs (Dunlap and Jones 2002). Also the degree to how the consumers are worried about the human interventions causing these environmental threats (Kim and Choi 2005; Hassan 2014).

2.2 Eco-labelling (EL)

Eco-labelling is defined as a tool that provides information on the external effects of the production, consumption, and disposal of products on the environment (Bougherara and Combris 2009). Eco-labelling aims to educate consumers about the environmental consequences of their use to enable them to make more environmentally sustainable choices, and another is to encourage manufacturers, states, and other agents to raise their environmental standards for goods and services. Ecolabelling is a method that is constantly being used to communicate environmental information to customers (Delmas et al. 2013). Eco-labelling is defined as a product or service which meets certain environmental standards. That which doesn't affect the quality of the nature that it meets with and that information is readily provided and available to the consumers in their labeling of the product or service by terming their credentials.

2.3 Green Packaging and Branding (GPB)

Green packaging is a form of packaging made entirely of natural plants that can be recycled or reused, is resistant to deterioration, and encourages sustainable growth. It is also safe for the environment, human health, and livestock health over its entire lifecycle (Zhang and Zhao 2012). Green packaging, employs environmentally friendly materials as packaging alternatives, keeping in mind that the goods must be acceptable for human health and the environment while also being better and more efficient (Pauer et al. 2019).

Green packaging is a type of packaging that is made of non-degradable materials so that it doesn't degrade the soil or water or whatever part of the environment that it comes in contact with thus making it a product that we can use without regret. Branding such products to the consumers stating the truth that their product is environmentally safe is termed green branding.

2.4   Green Product, Premium and Price (GPPP)

Green pricing can be referred to as the service that allows the consumers to invest in activities that cause less or no harm to the environment. Green premium is the additional cost paid by choosing the option that supports the environment. Consumers are a little skeptical about buying green products as most provide false information. They do not feel great about buying green products because some of these products are made from recycled material, which is not new. Pricing of products plays an important role in the purchase-related decision-making process of a consumer. Therefore, an additional cost such as the premium will only make the consumers buy less if it's not proved worthy.

2.5   Consumers Beliefs Towards the Environment (CBTE)

In his investigations, researcher said that behavior prediction is directly dependent on the consumer's attitude, which is linked to their knowledge and personal experience (Spruyt et al. 2007). In their investigations, argued that to predict certain behaviors, the attitudes tested must be addressed in a specific environmental situation. In the case of environmental issues, consumers have certain beliefs that, for a long time, are unshaken. Understanding this will help in understanding the purchase intentions and decisions of consumers (Gadenne et al. 2011; Wulf et al. 2003).

2.6   Environmental Concerns Impact on Consumers' Environmental Beliefs

Environmental concern (i.e. mindset) and environmentally friendly conduct have a favorable association (Roberts and Bacon 1997a). In their studies, found that green customers' behavior is influenced by their perceived effectiveness (i.e., attitude) toward environmental conservation (Berger and Corbin 1992).

Consumer attitudes toward the environment and environmental concerns are positively associated, which means that if customers do not make environmentally responsible choices, the severity of the problem in the environment will worsen. Environmental concern, in general, refers to an individual's concern for the environment and their preparedness to solve problems. Therefore the hypothesis, *There is positive relationship between environmental concerns and consumers' environmental beliefs.*

2.7 *Eco-labelling and Its Impact on Consumers'* *Environmental Beliefs*

Eco-labelling is essential for raising consumer awareness and beliefs of the product's environmental impacts and educating consumers about a product's environmental characteristics. Consumers are more likely to appreciate the environmental advantages that an eco-labeled product provides. It is claimed that choosing an eco-labeled product is not driven by the consumer's desire to be socially desirable (Gallardo and Wang 2013; Sörqvist et al. 2016). If the consumer has a positive knowledge in consuming eco-labeled products, then he/she would intend to buy the product. People having environmental concerns would react to eco-labeled products. Hence the Hypothesis *The relationship between Eco-Labelling and Consumers' Environmental Beliefs is positive.*

2.8 *Green Packaging, Branding and Its Impact* *on Environmental Beliefs*

Consumers are unable to differentiate between more and less environmentally friendly package alternatives due to a lack of supply of environmentally friendly packaging options in the marketplace (Bech-Larsen 1996; Thøgersen 1996). They also misinterpret the correlation between their purchasing decision and various environmental consequences (Bech-Larsen 1996). Packaging performs the role of a silent salesman (Singh and Pandey 2018). Backed up this claim, stating that packaging is one of the most important aspects of a product that buyers notice before making a purchasing decision, particularly because the vast majority of purchase decisions (roughly 73%) are made at the point of sale (Connolly and Davison 1996).

Packaging's ability to influence a customer's understanding of how well the product inside looks, sounds, tastes, smells or feels has a significant impact on buying decisions (Underwood et al. 2001). There may be a small group of customers who have strong preferences for green packaging, and there may be a demand for this form of packaging (Bech-Larsen 1996). Green packaging and branding are highly influenced by environmental concerns on their purchase intention (Chamorro et al. 2009; Kalafatis et al. 1999; Roberts and Bacon 1997b). Once it comes to a situation where two products perform identically, additional green values can influence consumer product selection (Ottman and Books 1998). Consumers who have a better understanding of green packaging are more likely to conclude that the use of green packaging may prove to be beneficial (Mishra et al. 2017).

Packaging plays an important role in decision-making on purchasing a product by a consumer. They could change the planned behavior of the consumer. Customers are attracted to the packaging of the product so that it would be helpful to make choices for the consumers. Reducing the harmful impacts of packaging on the environment would concern the choice of the product made by the consumer. Branding would

help in the promotion of the product to the consumers. This way green branding can also add value to the product as well as make it easy to customers to make purchase decisions. The hypothesis formulated is *There exists positive relationship between Green Packaging, Branding and Consumers' Environmental Beliefs.*

2.9 Green Products, Premium, Pricing and Consumers' Environmental Beliefs

Green packaging gives any product potential to 'uniqueness' and its presence in any form influences the consumer towards paying a higher price (Agarwal and Rao 1996; Netemeyer et al. 2004; Wiedmann et al. 2007). According to the theory of value-based pricing, the increased perceived value encourages the buyer to pay a price premium (Kalra and Goodstein 1998). As per the value-based pricing principle, the consumer is more willing to pay a higher price if the perceived value is higher (Kalra and Goodstein 1998). Marketers must improve differentiation and marketing strategies for green products because of the intention-action gap of the consumer. As a consequence, examining the factors that affect consumer preference and decision-making, such as perceptions that shape behavior, is difficult (Smith et al. 2006; Pickett-Baker and Ozaki 2008).

Green buying is more common among people who have a positive attitude toward environmental concerns and eco-social benefits (Cheung et al. 2019). A consumer's purchasing decision on a green product is influenced by the functional value (price) (Finch 2006). Some customers are willing to pay a higher price for environmentally friendly goods. Consumers select green products based on the price paid versus the benefits received (Lin and Huang 2012). The higher the perceived utility of a green product derived from its price, the more likely the buyer is to buy it (Khan and Mohsin 2017).

The Intention-action gap of the customers towards green products makes challenging for the marketers to fix and focus on their target segment. This also makes complex to study consumer behavior towards the environment. Pricing is one main reason to choose green products by the consumer. They would tend to gain maximum benefits out of the price paid to the product. If they are satisfied, the consumer would repeat the purchase action on green products. The additional amount paid for supporting the environment is the green premium should be worthy enough which would encourage the consumer to buy the product. The hypothesis formulated is *There is positive influence of Green Products, Premium, Pricing on Consumers' Environmental Beliefs.*

3 Sample

The study focuses on the millennials of the age 18 years above. These Gen-Z populations are considered to be the eco-warriors of our world, considering their urge to serve the environment. The dedication of millennials to environmental issues has influenced brands to go green. With them jumping on the eco-cart, young consumers are shaping an environmental movement that goes beyond hashtags. In 2015, a report by Nielson found that about 73% of millennials are willing to pay more for sustainable goods. In a report from Forbes in 2019, there was data that 63% of young millennials who have joined the workforce prefer sustainable brands over the ones that are not sustainable. The study includes millennials above the age of 18 years. The sampling method used was crowd sampling, as the questionnaire was made available on Google form. The final sample size was 268 respondents across all demographics (explained in the forthcoming sections).

4 Measures

The data was collected from millennials through an online questionnaire. The questionnaire had 5 constructs namely Environmental Concerns and Beliefs (ECB), Eco-labelling (EL), Green Packaging and Branding (GPB), Green Products, Premium and Pricing (GPPP), and Consumers Beliefs Towards Environment (CBTE). environmental Concerns and Beliefs was measured using 10 questions adopted from Arshad Mahmood (2020), Eco-labelling was measured using 6 questions adopted from Arshad Mahmood (2020), Green Packaging and Branding had 5 questions adopted from Arshad Mahmood (2020), Green Products, Premium and Pricing were measured using 4 questions adopted from Arshad Mahmood (2020) and Consumers Beliefs Towards the Environment was measured using 9 questions adopted from Arshad Mahmood (2020) (Shabbir et al. 2020). All the constructs were measured using a Likert 5-point scale (Strongly disagree to strongly agree). The demographic data were collected from the respondents.

5 Analysis and Interpretation

To assess the direction and magnitude of relationship between the study constructs before assessing the impact, a correlation analysis was carried out. From the values, in Table 1, we could conclude that GPB is highly correlated with all other constructs and also CBTE is highly correlated with ECB.

There is the relationship between Environmental Concerns and Beliefs, Eco-Labelling, Green Packaging and Branding, Green Product, Premium and Price, and Consumers Beliefs Towards the Environment.

Table 1 Relationship between study constructs

Constructs	CBTE	ECB	EL	GPB	GPPP
CBTE	1				
ECB	0.611*	1			
EL	0.360*	0.462*	1		
GPB	0.703*	0.606*	0.476*	1	
GPPP	0.537*	0.559*	0.557*	0.695*	1

Source Primary—*CBTE* consumers beliefs towards the environment, *ECB* environmental concerns and beliefs, *EL* eco-labelling, *GPB* green packaging and branding, *GPPP* green product, premium and price

5.1 Results of Correlation

GPB influences all other constructs highly and positively. This result is because of the consumer's response towards GPB. People are highly attracted by the appearance of the product and in fact, the packaging is said to be a silent salesman by research authors. Increased environmental concerns and beliefs are seen among the consumers when good green packaging and branding are done. And also, when there is attractive green packaging and branding, green products sales have been increased, pricing is easier, and premium pricing adds value to the product. CBTE is having a high correlation with ECB as it is important for a consumer to get knowledge about green products and should have a concern about the environment. This helps to have consumer belief towards the environment. We can also see that EL is having a low correlation with CBTE and ECB.

Eco-labeling has a low correlation with constructs such as CBTE and ECB where the consumers are skeptical about their choice of green products. Consumers are concerned about the trustworthiness of the product even when the required environmental standards are given by eco-labeling. This is because it does not focus on all the environmental concerns and some brands may manipulate the information provided by eco-labeling. So consumers are worried that it might not satisfy their need for making the environment better for the future and so they are not easily convinced about the products sometimes. There is a moderate correlation between GPPP and all other constructs except GPB.

There is a moderate correlation between Green Products, Premium, and Pricing, and Environmental Concerns and Beliefs, Eco-Labelling, and Consumer Beliefs Towards the Environment. This result is because every green product purchased by the consumers has a separate stage during the decision making which is influenced mainly by the consumers' environmental concerns and the knowledge they get through the environmental certifications given to the products. That is what drives the consumers to turn towards green products and how they accept the premium price that is set by the brand for the products which is mainly analyzed by the fact if the environmental factors it covers are proven to be worth it.

5.2 Impact of Environmental Concerns and Beliefs (ECB), Eco-labelling (EL), Green Packaging and Branding (GPB), Green Products, Premium, and Pricing (GPPP) on Consumer Beliefs Towards the Environment (CBTE)

To test if Environmental Concerns and Beliefs (ECB), Eco-Labelling (EL), Green Packaging and Branding (GPB), Green Products, Premium, and Pricing (GPPP) has an impact on Consumer Beliefs Towards the Environment (CBTE), Multiple Linear regression (MLR) was carried out. The Independent constructs were Environmental Concerns and Beliefs (ECB), Eco-Labelling (EL), Green Packaging and Branding (GPB), Green Products, Premium, and Pricing (GPPP). The alternate hypothesis for the same was formulated thus

The independent constructs like Environmental Concerns and Beliefs (ECB), Eco-Labelling (EL), Green Packaging and Branding (GPB), Green Products, Premium, and Pricing (GPPP) do not have an impact on Consumer Beliefs Towards the Environment (CBTE).

Table 2 depicts the results from multiple linear regression. The dependent variable was Consumer Beliefs Towards the Environment (CBTE). The R square value or Coefficient of Determination was 0.55. The F value for the R Square was also found to be significant at a 0.00 level of significance. The R-value was 0.74 and the adjusted R Square was 0.54, the difference between R Square and Adjusted R Square is low. The R square value indicates that 54% variation in the dependent variable which is Consumer Behavior Towards Environment is explained by the independent constructs chosen for the study.

Table 2 Regression results for impact of environmental concerns and beliefs, eco-labelling, green packaging and branding, green products, premium, and pricing on consumer beliefs towards the environment

S. No	Constructs	Coefficients	t	P-value
1	Constant	0.66	3.09	0.002
2	Environmental concerns and beliefs	0.3	5.27	0
3	Eco-labelling	−0.04	−0.83	0.409
4	Green packaging and branding	0.52	8.08	0
5	Green products, premium, and pricing	0.04	0.54	0.587
	R	0.74		
	R Square	**0.55**		
	Adjusted R Square	**0.54**		
	Std. The error of the Estimate	**0.47**		
	Sig.	**0**		

This result support that the model is fit. The regression equation

$$Y = a + bx1$$

can be formulated this Consumer Beliefs Towards the

Environment $= 0.66 + 0.3$(Environmental concerns and belief)
$- 0.04$(Eco-Labelling) $+ 0.52$(Green Packaging and Branding)
$+ 0.04$(Green Products, Premium, and Pricing).

The beta values/regression coefficients of the results indicate that Green Packaging and Branding and Environmental Concerns and Beliefs have the highest impact on Consumer Beliefs Towards the Environment. The sig values for these two constructs were also less than 0.01. This indicates that Environmental Concerns and Beliefs and Green Packaging and Branding influences more on Consumer Beliefs Towards the Environment when compared to other independent variables. Likewise, the higher the Environmental Concerns and Beliefs more is the Consumer Beliefs Towards the Environment.

The beta values/regression coefficient of Green Products, Premium, and Pricing is 0.04 which is closer to zero indicates that it does not influence much on Consumer Beliefs Towards the Environment.

The other construct namely Eco-Labelling is negatively impacting the Consumer Beliefs Towards the Environment. This means it has an inverse impact on the dependent variable. This indicates that the lower the value of Eco-Labelling increases the Consumer Beliefs Towards the Environment.

Green Packaging and Branding have the highest impact on Consumer Beliefs Towards the Environment with a coefficient of 0.52, which indicates that Green Packaging and Branding is attracting the interest of researchers interested in consumer behavior. Packaging acts as a silent salesman and it is the first impression of the product for the consumer which influences their purchase decision.

Environmental Concerns and Beliefs also impact Consumer Beliefs Towards the Environment with a coefficient of 0.3, this indicates that Environmental Concerns and Beliefs influences dependent variable directly. If the consumer's knowledge of environmental concerns and beliefs is poor there will be a decrease in Consumer Beliefs Towards the Environment.

Green Products, Premium, and Pricing do not affect Consumer Beliefs Towards the Environment due to the intention-action gap to buy the green products. It is challenging to segment and target the consumer for the green products. Consumer's choice of synthetic products over green products and their skeptical behavior gave less importance to Green Products, Premium, and Pricing.

Eco-Labelling Hurts Consumer Beliefs About the Environment, which has a coefficient of -0.04. It has a high distrust among the consumers and they don't help in identifying green products. Thus, they have an inverse effect over the Consumer Beliefs Towards the Environment.

6 Implications and Findings

This research offers essential instructions for boosting positive attitudes about green products in society and assisting businesses in developing effective methods to sell their green products. The study suggests that the key factors of green marketing such as Environmental Concerns and Beliefs (ECB), Green Packaging and Branding (GPB), and Green Product, Premium and Pricing (GPPP) have a positive influence on Consumers Beliefs Towards the Environment (CBTE). On the other hand, Eco-Labelling (EL) being an important factor of green marketing has a negative influence on Consumers Beliefs Towards the Environment (CBTE).

From the study, we can infer that majority of the respondents have concerns for and on the environment. They strongly believe that the environment must be saved from the practices of human beings. Also, they deny the fact that humans can alter the environment for themselves. They agree to the fact that exploitation of the natural environment must come to a stop which can be done by following an eco-friendly lifestyle. A large group of respondents believes that mankind is severely abusing the natural environment. Therefore, humans must learn to live in harmony with nature without which survival will become difficult. Various approaches used for promoting green products such as green branding and packaging have a significant and positive influence on consumer belief and consumer behavior towards the environment. The majority of the respondents strongly agree that the packaging of products must be reusable or recyclable. They also prefer products that have bio-degradable packaging, environment-friendly techniques of branding, and safe packaging of products. From the study, the green premium can be identified as one of the important factors of the purchase decision made by millennials. While a fairly great amount of people agree that a green premium is necessary, 9% of the respondents disagree with this fact. This is because most consumers feel that the green premium is not utilized in the right way.

Eco-Labelling of green products is attractive to consumers as it provides adequate information on the label which can be linked to consumers' lifestyles. Despite the numerous efforts taken by various brands, to market their products in an eco-friendly manner, consumers are still skeptical about the various products presented to them. There is a hesitation when it comes to building trust on the eco-brand. This is because many brands have to lead the consumers in the wrong direction by providing false information about their green products and their certifications.

The regression equation $(Y = a + bx1)$ of the study is, Consumer Beliefs Towards the Environment $= 0.66 + 0.3$ Environmental concerns and belief—0.04 Eco-Labelling $+ 0.52$ Green Packaging and Branding $+ 0.04$ Green Products, Premium, and Pricing.

The study implies that businesses start investing more in green packaging and branding to reach and satisfy more consumers. Even though eco-labeling has a negative significance according to the regression equation, businesses can identify ways to reduce the false information provided by other brands. This way they can still keep investing in certifications and labels of their green products without reducing

the ratio of investments. They must also ensure that they do not completely depend or thrive on just the green premium. According to the study, the larger part of the respondents has shown great concern for the environment. Therefore, businesses must start involving in environment-friendly practices.

7 Conclusion

Environmental issues in India are rising at a rapid rate. Being environmentally conscious has become one of the main goals of all businesses, as this way they can appeal to more customers. And as for consumers, especially millennials, they have become very conscious about their consumption pattern. This research explores this pattern and what factors affect the purchase of green products and the interrelationship between the variables of the study. Consumers were set off by five primary variables such as Environmental Concerns and Belief (ECB), Eco-Labelling (EL), Green Packaging and Branding (GPB), Green Product, Premium, and Pricing (GPPP), and Consumers Beliefs Towards the Environment (CBTE). Accordingly, the results show that a high level of investments in green packaging and branding will help businesses reach and satisfy more consumers. This was implied from the study, where the respondents strongly agreed that packaging in an environment-friendly manner is very essential to them. The findings show that Environmental Concerns and Belief (ECB), Green Packaging and Branding (GPB), and Green Product, Premium and Pricing (GPPP) have a significantly positive relationship over Consumers Beliefs Towards the Environment (CBTE). On the other hand, Eco-Labelling hurt Consumers Beliefs About the Environment (CBTE). The various objectives of the study were met by understanding and analyzing the relationship between each variable, and how they affect the purchase decision of millennials. By using a questionnaire, the study was conducted at a descriptive level, by collecting responses from a group of millennials.

Despite the success of the objectives set, there are limitations to this study. While this study aimed to focus on millennials, their degree of skepticism is higher than other age categories, as they are prone to different channels of media, which influences their purchase decisions largely. Media is a large and crucial factor in analyzing the consumption patterns of consumers, it is very unstable. It affects how consumers perceive things thereby affecting the relationship between Green Packaging and Branding (GPB), Green Products, Premium and Pricing (GPPP), and Consumers Beliefs Towards the Environment (CBTE).

The accessibility of green products is another important factor that is very unstable and is yet to be discussed by researchers. Its relationship with consumers' beliefs towards the environment is still a far cry. The age group was fixed from 18 years and above, which restricts the inputs from people below the age of 18. The sample was carefully chosen, but there is scope for further research in this area. This study focused on the areas related to packaging, branding, and pricing majorly. Future studies can explore more about the accessibility of green products and how it affects

the consumers' beliefs towards the environment. The study can be focused more on the demand aspects of the products as well, which will help understand the latter better. Also, future studies can focus on generations X, Y, and Z, while this study focused only on Gen-Z. This study integrated only 5 variables, namely, ECB, EL, GPB, GPPP, and CBTE, and there is still room to involve and integrate other variables related to the demand and complexities in the availability of the green products.

Conflict of Interest The author(s) declare(s) that there is no conflict of interest.

References

Agarwal MK, Rao VR (1996) An empirical comparison of consumer-based measures of brand equity. Mark Lett 7(3):237–247

Ajzen I (1991) The theory of planned behavior. Organ Behav Hum Decis Process 50(2):179–211

Bech-Larsen T (1996) Danish consumers' attitudes to the functional and environmental characteristics of food packaging. J Consum Policy 19(3):339–363

Berger IE, Corbin RM (1992) Perceived consumer effectiveness and faith in others as moderators of environmentally responsible behaviours. J Public Policy Mark 11(2):79–89

Bougherara D, Combris P (2009) Eco-labelled food products: what are consumers paying for? Eur Rev Agric Econ 36(3):321–341

Chamorro A, Rubio S, Miranda FJ (2009) Characteristics of research on green marketing. Bus Strateg Environ 18(4):223–239

Cheung MFY, To WM (2019) An extended model of value-attitude-behavior to explain Chinese consumers' green purchase behavior. J Retail Consum Serv 50:145–153

Connolly A, Davison L (1996) How does design affect decision at point of sale? J Brand Manag 4(2):100–107

Delmas MA, Nairn-Birch N, Balzarova M (2013) Choosing the right eco-label for your product. MIT Sloan Manag Rev 54(4):10

Dunlap R, Jones R (2002) Environmental concern: Conceptual and measurement issues. In: Dunlap R, Michelson W (eds) Handbook of environmental sociology. Greenwood, London

Kalafatis SP, Pollard M, East R, Tsogas MH (1999) Green marketing and Ajzen's theory of planned behaviour: a cross-market examination. J Consum Mark

Underwood RL, Klein NM, Burke RR (2001) Packaging communication: attentional effects of product imagery. J Prod Brand Manag

Pickett-Baker J, Ozaki R (2008) Pro-environmental products: marketing influence on consumer purchase decision. J Consum Mark

Finch JE (2006) The impact of personal consumption values and beliefs on organic food purchase behavior. J Food Prod Mark 11(4):63–76

Fransson N, Gärling T (1999) Environmental concern: Conceptual definitions, measurement methods, and research findings. J Environ Psychol 19(4):369–382

Gadenne D, Sharma B, Kerr D, Smith T (2011) The influence of consumers' environmental beliefs and attitudes on energy saving behaviours. Energy Policy 39(12):7684–7694

Gallardo RK, Wang Q (2013) Willingness to pay for pesticides' environmental features and social desirability bias: the case of apple and pear growers. J Agricult Resour Econ 124–139

Hassan Z (2014) The social labs revolution: a new approach to solving our most complex challenges. Berrett-Koehler Publishers

Kalra A, Goodstein RC (1998) The impact of advertising positioning strategies on consumer price sensitivity. J Mark Res 35(2):210–224

Khan SN, Mohsin M (2017) The power of emotional value: exploring the effects of values on green product consumer choice behavior. J Clean Prod 150:65–74

Kim Y, Choi SM (2005) Antecedents of green purchase behavior: an examination of collectivism, environmental concern, and PCE. ACR North Am Adv

Kropfeld MI, Nepomuceno MV, Dantas DC (2018) The ecological impact of anti-consumption lifestyles and environmental concern. J Publ Policy Mark 37(2):245–259

Lin P-C, Huang Y-H (2012) The influence factors on choice behavior regarding green products based on the theory of consumption values. J Clean Prod 22(1):11–18

Mishra P, Jain T, Motiani M (2017) Have green, pay more: An empirical investigation of consumer's attitude towards green packaging in an emerging economy. In: Essays on sustainability and management, pp 125–150. Springer, Singapore

Netemeyer RG, Brashear-Alejandro T, Boles JS (2004) A cross-national model of job-related outcomes of work role and family role variables: a retail sales context. J Acad Mark Sci 32(1):49–60

Ottman J, Books NB (1998) Green marketing: opportunity for innovation. J Sustain Prod Des 60(7):136–667

Pauer E, Wohner B, Heinrich V, Tacker M (2019) Assessing the environmental sustainability of food packaging: an extended life cycle assessment including packaging-related food losses and waste and circularity assessment. Sustainability 11(3):925

Paul J, Modi A, Patel J (2016) Predicting green product consumption using theory of planned behavior and reasoned action. J Retail Consum Serv 29:123–134

Roberts JA, Bacon DR (1997a) Exploring the subtle relationships between environmental concern and ecologically conscious consumer behavior. J Bus Res 40(1):79–89

Roberts JA, Bacon DR (1997b) Exploring the subtle relationships between environmental concern and ecologically conscious consumer behaviour. J Bus Res 40(1):79–89

Shabbir MS, Sulaiman MABA, Al-Kumaim NH, Mahmood A, Abbas M (2020) Green marketing approaches and their impact on consumer behavior towards the environment—a study from the UAE. Sustainability 12(21):8977

Singh G, Pandey N (2018) The determinants of green packaging that influence buyers' willingness to pay a price premium. Aust Mark J (AMJ) 26(3):221–230

Smith GE, John EH, Nagle TT (2006) A value-based pricing perspective on value communication. Mark Theory Appl 272

Sörqvist P, Marsh JE, Holmgren M, Hulme R, Haga A, Seager PB (2016) Effects of labelling a product eco-friendly and genetically modified: A cross-cultural comparison for estimates of taste, willingness to pay and health consequences. Food Qual Prefer 50:65–70

Spruyt A, Hermans D, De Houwer J, Vandekerckhove J, Eelen P (2007) On the predictive validity of indirect attitude measures: prediction of consumer choice behavior on the basis of affective priming in the picture–picture naming task. J Exp Soc Psychol 43(4):599–610

Taylor S, Todd P (1997) Understanding the determinants of consumer composting behaviour 1. J Appl Soc Psychol 27(7):602–628

Thøgersen J (1996) Recycling and morality: a critical review of the literature. Environ Behav 28(4):536–558

Wiedmann K-P, Hennigs N, Siebels A (2007) Measuring consumers' luxury value perception: a cross-cultural framework. Acad Mark Sci Rev 2007:1

De Wulf K, Odekerken-Schröder G (2003) Assessing the impact of a retailer's relationship efforts on consumers' attitudes and behavior. J Retail Consum Serv 10(2):95–108

Zhang G, Zhao Z (2012) Green packaging management of logistics enterprises. Phys Procedia 24:900–905

Zimmer MR, Stafford TF, Stafford MR (1994) Green issues: dimensions of environmental concern. J Bus Res 30(1):63–74

Screening of Organic Solvents for Separation of Thiophene and Iso-octane: Density Functional Theory and Molecular Dynamic Simulations

Yamini Sudha Sistla and Jai Singh

Abstract Atomistic level understanding of the interactions of thiophene and iso-octane with various organic solvents such as *N*-methylpyrrolidone (NMP), sulfolane, furfural, diethyleneglycol (DEG), 2-aminoethanol (ETA), tetraethyleneglycol (TEG), dimethylformamide (DMF) and cyrene to find an optimum solvent for selective extraction of thiophene, was presented by using DFT and MD simulations. As per the reactivity descriptors computed from Koopmans' theorem based on quantum mechanics, for the eight solvents studied, furfural is most reactive followed by cyrene while sulfolane has the least reactivity. Based on the interaction energies (IE) of solute–solvent systems using DFT, cyrene presented strongest interaction with thiophene followed by TEG, furfural and DEG indicating that cyrene can show good thiophene removal capacity. The difference in the IE values of thiophene and isooctance was considered as a measure of possible sulphur selectivity over hydrocarbon. Among the eight solvents considered, furfural, DEG, TEG and cyrene observed to show good desulfurization selectivity. The favourable positions on solvent molecules for potential interactions with thiophene and isooctane were identified using orbitals, electrostatic potential maps, fukui function maps for electrophilic and nucleophilic attack, match well with the trends in IE values and RDFs from MD simulation. The solute–solvent concentration profiles and radial distribution functions computed using MD simulations evidently show that furfural and cyrene show better capacity and selectivity for Thiophene which are in correspondence with DFT results. The detailed analysis using QM and MM methods, concludes that cyrene, furfural and TEG are the optimum organic solvents for thiophene removal from gasoline using extractive desulfurization method (EDS).

Keywords Extractive desulfurization · Density functional theory · MD simulations

Y. S. Sistla (✉) · J. Singh
Shiv Nadar University, Greater Noida, India
e-mail: Yamini.sistla@snu.edu.in

1 Introduction

Deep Desulfurization of refinery streams such as gasoline, diesel and marine fuel got significant attention these days, thanks to the stricter norms set by environmental boards to cut down the SO_x emissions from burning of petroleum oils. Conventionally, desulfurization of fuel oils such as gasoline, kerosene, and diesel is carried out using Hydrodesulphurization (HDS) (Eleni and Dimitrios 2021; Kumar et al. 2017; Tanimu and Alhoosani 2019). HDS process is carried out by using hydrogen at a partial pressure of 50–200 bar and at temperatures of around 450–650 K by using γ-Al_2O_3 supported molybdenum sulphide or tungsten sulphide catalyst with nickel or cobalt as promoters. However, the HDS process comes with certain challenges such as: (a) requiring severe temperature and pressure conditions (especially diesel desulfurization) which demands lot of energy (b) high temperature and high-pressure conditions to store and use liquid hydrogen (280–330 °C and 3–5 MPa) (c) low activity for polycyclic thiophenic sulphur like benzothiophene (BT), dibenzothiophene (DBT), and their derivatives (d) treating of exhaust gases such as H_2S (Eleni and Dimitrios 2021; Kumar et al. 2017; Tanimu and Alhoosani 2019). To overcome the challenges of HDS, various researchers world-wide, proposed extractive desulphurization (EDS) as a prospective economically and energetically alternative process (Moghadam et al. 2020; Player et al. 2019; Majid et al. 2020; Saha et al. 2019; Ali et al. 2009; Kumar et al. 2014). The EDS process is based on Liquid–Liquid-Extraction (LLE) process, in which, the refinery stream with sulphurous impurities will be brought in contact with a solvent in counter current manner in an extractor column. The extract stream majorly contains "solvent + sulphur" compounds and the raffinate stream will consist majorly of hydrocarbons. Later, the solvent regeneration can be done either by distillation or by crystallization. An efficient EDS process, will ideally produce a raffinate hydrocarbon stream which is free of extractant solvent and sulphurous molecules. Similarly, extractant stream should preferentially comprise of the extractant solvent and the sulfurous compounds along with minimal to insignificant amount of hydrocarbon compounds. Extraction solvents such as organic solvents, ionic liquids, and deep eutectic solvents were reportedly studied by various researchers worldwide for EDS process (Moghadam et al. 2020; Player et al. 2019; Majid et al. 2020; Saha et al. 2019; Ali et al. 2009; Kumar et al. 2014; Shen et al. 2019; Kianpour and Azizian 2014; Cai et al. 2020; Zhang et al. 2009; Gao et al. 2015; Wang et al. 2020; Shah et al. 2019; Zhu et al. 2020; Taha and Lee 2013; Naik et al. 2018; Dehury et al. 2016). Although many researchers reported that ionic liquids and deep eutectic solvents can be used as potential extractant solvents for desulfurization of gasoline and diesel range fuel oils, the commercial acceptability of those solvents is not yet realized. Some bottlenecks associated with usage of ionic liquids as desulfurization solvents are (a) higher cost (b) not very good extraction efficiency (c) regeneration issues. Polar organic solvents such as *N*-Methylpyrrolidone (NMP), dimethylformamide (DMF), Tetraethyleneglycol (TEG) were explored as suitable solvent for the EDS process (Ali et al. 2009; Kumar et al. 2014; Shen et al. 2019). However, these organic solvents suffer from disadvantages

such as high volatility and chance of causing secondary contamination for the oils due to their solubility in hydrocarbons (Ali et al. 2009; Kumar et al. 2014; Shen et al. 2019). Another class of solvents such as poly ethylene glycol (PEG) and etherified PEG were reportedly shown high sulphur extraction efficiency (Kianpour and Azizian 2014; Cai et al. 2020; Zhang et al. 2009). The improved sulphur extraction efficiency was attributed to an active oxygen atom which acts as Lewis base site (Kianpour and Azizian 2014; Cai et al. 2020; Zhang et al. 2009). Therefore, it is imperative to develop hybrid solvent systems to leverage the advantages of low volatile green solvents such as ionic liquids and deep eutectic solvents and the regular organic solvents to enhance the extraction efficiency and also to reduce the operating expenses for the extractive desulfurization of oils. One of the attractive option is to develop mixed solvents with (a) more than two organic solvents, (b) mix of organic and polymeric solvents, (c) mix of organic solvents and ionic liquids/deep eutectic solvents (Majid et al. 2020; Saha et al. 2019; Ali et al. 2009; Kumar et al. 2014; Shen et al. 2019; Kianpour and Azizian 2014; Cai et al. 2020; Zhang et al. 2009).

In order to design efficient solvents for any extraction process, it is critical to study the underlying microscopic level interaction mechanism between solute and solvent resulting from their individual structure–property relationships. Thus, molecular modeling methods can be leveraged to study the process/mechanism which are otherwise difficult to capture from experiments and to significantly reduce the expensive experimental efforts in developing appropriate solvents for liquid–liquid-extraction process with required physical –and chemical properties (Gao et al. 2015). Furthermore, atomistic level understanding of the solute–solvent interactions and solute–solute interactions by using various quantum chemical and molecular mechanics methods is essential for understanding the underlying mechanism of a particular extraction process. (Wang et al. 2020; Shah et al. 2019; Zhu et al. 2020). The MD simulations can capture the experimental phenomena at picosecond level which are actually the governing factors for the experimental phenomena which happen in minutes scale. Various researchers have used MD simulations to screen and develop optimum solvents various gas and liquid separations (Taha and Lee 2013; Naik et al. 2018; Dehury et al. 2016).

Although there are significant studies on the application of molecular simulations of ionic liquids and deep eutectic solvent systems for EDS application (Wang et al. 2020; Shah et al. 2019; Zhu et al. 2020; Taha and Lee 2013; Naik et al. 2018; Dehury et al. 2016), similar fundamental atomistic studies for organic solvents are not ample. Therefore, the present study focuses on application of density functional theory (DFT) and molecular dynamic (MD) simulations for the screening of eight organic solvents such as *N*-methylpyrrolidone (NMP), sulfolane, furfural, diethyleneglycol (DEG), 2-aminoethanol (ETA), tetraethyleneglycol (TEG), dimethylformamide (DMF) and cyrene, to find an optimum solvent for selective extraction of thiophene (sulfurous molecule) from iso-octane (hydrocarbon molecule). The eight organic solvents were chosen based on the compatibility as per polarity, acidity/basicity with respect to thiophene and also based on available literature information. Further, we also have studied the suitability for EDS, of a new organic solvent, Cyrene, which was recently brought into market by Sigma Aldrich.

2 Computational Details

2.1 Interaction Descriptor and Interaction Energy Calculations

Geometry optimization of all the molecules (thiophene, iso-octane and the eight solvent molecules) was performed using a free quantum chemical software package ORCA (Frank 2018). A molecule editor and visualizer software AVOGADRO was used to generate the input files and to analyse the output files (Hanwell et al. 2012). Geometry optimization of all the molecules was initially performed using ab initio method HF (Hartree Fock) with *Pople* basis set 6-311 + G* for calculating Koopmans' theorem-based interaction descriptors (Roothaan 1951; Curtiss et al. 1995). The structures optimized with HF/6-311 + G* were again optimized by DFT functional using Becke's three parameter hybrid method with Lee–Yang–Parr correlation (B3LYP) with dispersion correction in order to account for van der Waals interactions, with the same 6-311 + G* basis set for calculating the solute–solvent interaction energies (Lee et al. 1988; Becke 1993; Frenkel and Smit 2002). The choice of basis set 6-311 + G* was made based on the nature of molecules (organic solvents and solutes) considered in the present study and the nature of interactions (van der Waals and hydrogen bonding) possible between the solvents and solutes considered in the present study. In addition, published literature suggests that the larger basis sets "6-311" are preferred over smaller basis sets for more reliable results. Based on the nature of molecules, we have applied '*s*', and '*p*' polarization (+) function and diffuse function (*) for non-hydrogen atoms only. The current study does not involve any ionic molecules and only contains pure molecules. Therefore, a larger basis set suitable for the molecules studied in the present work was only considered. Each geometry optimization step was followed by vibrational frequency analysis study to confirm that the optimized molecular structure was a stationary point on the potential energy surface by making sure that there were no imaginary/negative vibrational frequencies present. The structures and interaction energies reported in this study correspond to the lowest energy conformation (after considering various conformational structures and complexes) of each individual molecule and pair. The Highest Occupied Molecular Orbital (HOMO), Lowest Unoccupied Molecular Orbital (LUMO), electrostatic potential (ESP) and fukui function maps for electrophilic and nucleophilic attack of the solvent molecules were studied to identify potential solvents which can show more interaction with thiophene molecule. In general, the interaction energy (IE) for weakly bonded systems is calculated as the difference between the energy of whole system and the sum of energies of its sub-units. The IE of each pair was obtained by subtracting the total energy of the isolated 'solute' and isolated solvent molecule from the total energy of the solute–solvent pair, $IE = E_{solute-solvent} - (E_{solute} + E_{solvent})$. Here solute refers to both thiophene and isooctane (Boys and Bernardi 1970; Sistla and Vignesh 2021).

2.2 Solute–Solvent Interactions Using MD Simulations

All the MD simulation calculations were carried out by using Dassault Systems Biovia Material Studio version 2020 software (BIOVIA 2020). In order to model the more realistic LLE phenomena and also to understand the distribution of thiophene in solvent and hydrocarbon phase, MD simulations were run for three solvent–solute systems (1) Furfural-thiophene-isooctane (2) NMP-thiophene-isooctane and (3) Cyrene-thiophene-isooctane (furfural, NMP, and cyrene are mentioned as solvent hereafter). Initially, the molecular structures of solvent, thiophene and isooctane were built and geometry optimized by using DMol3 module of Material Studio. A hybrid functional M06-2X which is superior to B3LYP functional along with DNP basis set, which is equivalent basis set to 6-311 + G* of Gaussian, were used for the geometry optimization. The optimized structures with electrostatic potential (ESP) charges applied for each atom were used for further simulations. By considering a solvent to feed ratio as 5:1 by volume, an amorphous cell was built by loading 88% by weight of solvent molecules, 10.5% by weight of isooctane and 1.5% by weight of thiophene at the density of the solvent. The amorphous cell was initially geometry optimized using Forcite module by using conjugate-gradient method by applying COMPASS III forcefield for the solvent and solute molecules. The resulting optimized structure was then subjected to 150 ps (ps-picosecond) of NVE equilibration runs followed by 250 ps production run to stabilize the energy of the system. The resulting system was then subjected to 250 ps of NVT (T = 298 K) equilibration runs followed by 250 ps production runs. The NVT production runs were followed by a 500 ps of NPT equilibration run at 298 K and 1 atm. Finally the cell was subjected to 2000 ps (2 ns) of NPT production runs. During NVT and NPT simulations, temperature was controlled by Nose–Hoover-Langevin method and pressure was controlled by Berendsen method. For all the simulations, electrostatic interactions were evaluated by using Ewald method with an accuracy of 0.0001 kcal/mol and the van der Waals interactions were evaluated by using Atom based method with a cut off distance of 15.5 Å. Concentration profiles of the solvent and the solutes along the Z-axis, Mean square displacements (MSD) of the solute molecules with respect to time, radial distribution functions between the solute and the solvent were analysed to study the distribution and interactions of the solute in the solvent phase.

3   Results and Discussion

3.1   Interaction Descriptor and Interaction Energy Calculations

3.1.1   Interaction Descriptors of Solute and Solvent Molecules

The energies and regions of Highest Occupied Molecular Orbital (HOMO), Lowest Unoccupied Molecular Orbital (LUMO), ESP partial charges, fukui functions for electrophilic and nucleophilic attack for the optimized stable conformations of the eight solvent molecules are shown in Figs. 1, 2, 3 and 4 respectively. The extraction capacity and selectivity of any targeted solute into a solvent is affected majorly by the favourable solute–solvent interactions which in turn are highly dependent on the physical and chemical properties and activity of the solvents. The electronic properties of the solvents will influence the solvent–solvent interactions as well as solute–solvent interactions. Therefore, it is imperative to apprehend the interaction ability of solvent molecules through some descriptors. Such interaction descriptors include Ionization Potential (IP), Electron Affinity (EA), Electronegativity (χ), Chemical Potential (μ), Global Hardness (η), Global Softness (S), and Electrophilicity index (ω). In the present work, the above mentioned interaction descriptors for various organic solvents were computed using Koopmans' theorem. As per Koopmans' theorem, the ionization potential (IP) can be obtained from the energy of highest occupied molecular orbital (E_{HOMO}) and the electron affinity (EA) can be obtained from the energy of the lowest unoccupied molecular orbital (E_{LUMO}) (Plakhutin 2018; Koopman 1934). The E_{HOMO} and E_{LUMO} values were obtained by using Hartree–Fock (HF) method with *Pople* basis set 6-311 + G* at a fine convergence level. The formulas for the interaction descriptors (Koopmans' theorem) are as given below and the values for all the eight solvents considered in the present work are presented in Table 1.

$$\text{Ionization potential (IP)} = -E_{HOMO} \tag{1}$$

$$\text{Electron Affinity (EA)} = -E_{LUMO} \tag{2}$$

$$\text{Electro Negativity } (\chi) = (IP + EA)/2 \tag{3}$$

$$\text{Chemical Potential}(\mu) = -\chi = -(IP + EA)/2 \tag{4}$$

$$\text{Global Hardness}(\eta) = (IP - EA)/2 \tag{5}$$

$$\text{Global Softness (S)} = 1/(2\eta) \tag{6}$$

LUMO = 1.519eV   LUMO = 1.903eV   LUMO = 1.673eV   LUMO = 1.918eV

12.151eV   13.45eV   11.966eV   12.356eV

HOMO = -10.632eV   HOMO = -11.547eV   HOMO = -10.293eV   HOMO = -10.438eV

(a)   (b)   (c)   (d)

LUMO = 1.600eV   LUMO = 1.461eV   LUMO = 1.895eV   LUMO = 1.802eV

10.967eV   13.015eV   13.487eV   11.936eV

HOMO = -9.367eV   HOMO = -11.554eV   HOMO = -11.592eV   HOMO = -10.134eV

(e)   (f)   (g)   (h)
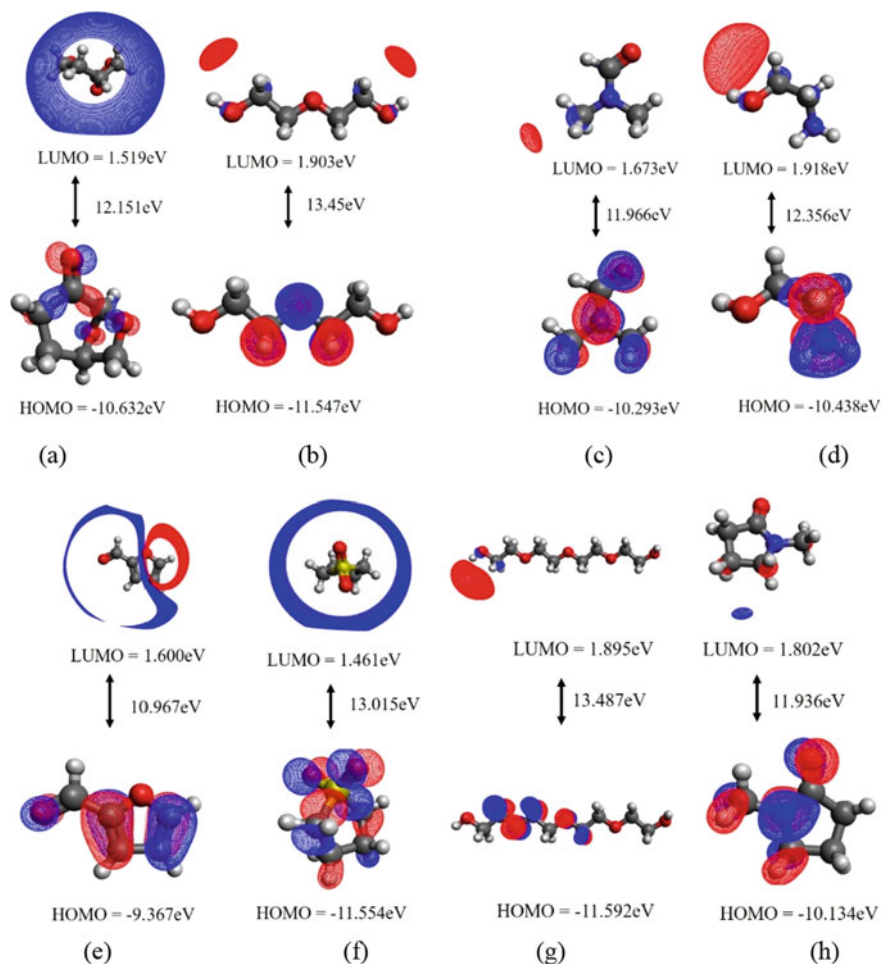
Fig. 1 HOMO and LUMO of the solvents. **a** Cyrene, **b** DEG, **c** DMF, **d** ETA, **e** Furfural, **f** Sulfolane, **g** TEG, **h** NMP (Color codes of atoms: grey—carbon; red—oxygen; white—hydrogen; yellow—sulphur; blue—nitrogen)

$$\text{Electrophilicity Index } (\omega) = \mu^2/2\eta \qquad (7)$$

The IP of a molecule denotes the ability to donate an electron or the energy required to remove one electron from a molecule. Similarly, EA is the ability of a molecule to accept electrons or is the energy released when an electron is added to the molecule. Electronegativity denotes the overall tendency of a molecule to attract electrons. Chemical potential (μ) represents the escaping (donating) tendency of an electron from the molecule. If the μ value is less negative, it is easier for the molecule to lose an electron and more difficult to accept one. The ability to accept
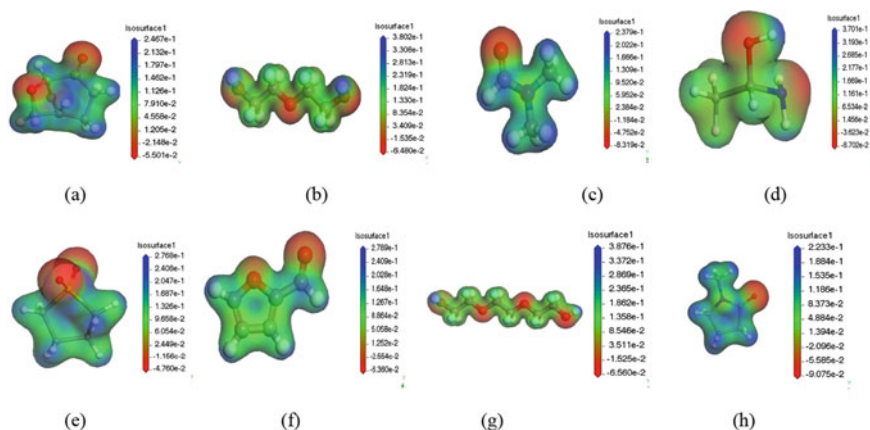
Fig. 2 Electrostatic potential mapped on to electron density iso-surface. **a** Cyrene, **b** DEG, **c** DMF, **d** ETA, **e** Furfural, **f** Sulfolane, **g** TEG, **h** NMP
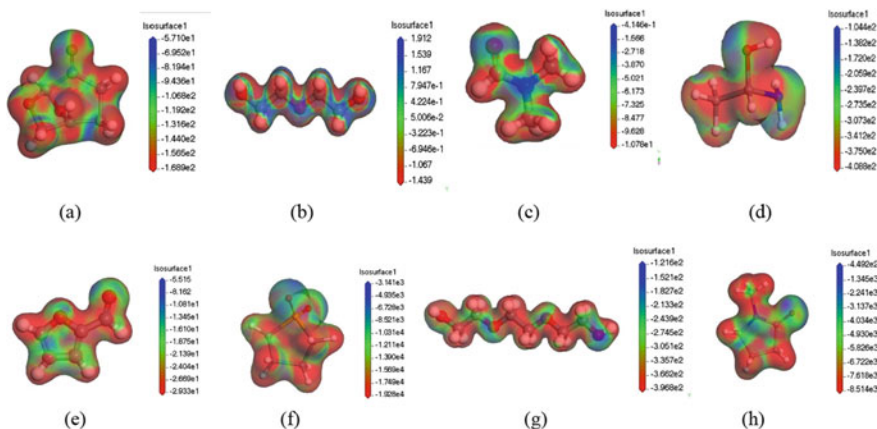
Fig. 3 Fukui function for electrophilic attack mapped on to electron density iso-surface. **a** Cyrene, **b** DEG, **c** DMF, **d** ETA, **e** Furfural, **f** Sulfolane, **g** TEG, **h** NMP

electrons increases (and the ability to lose electrons decreases) with an increase in negative value of chemical potential. Molecules with high softness or low hardness are sensitive to charge transfer indicating high reactivity. Electrophilicity index refers to the overall stabilization energy when a molecule accepts electrons (BIOVIA 2020; Plakhutin 2018; Koopman 1934). Among all the solvents studied, sulfolane has the lowest E_{LUMO} and ETA has the highest E_{LUMO} (Table 1). Whereas, furfural has the lowest E_{HOMO} and TEG has the highest E_{HOMO}. In furfural, the gap between the energies of LUMO and HOMO is small due to which the electron can get easily excited which leads to the lower global hardness for furfural. This indicates that, among the eight solvents studied, furfural is the most reactive solvent (Table 1 and

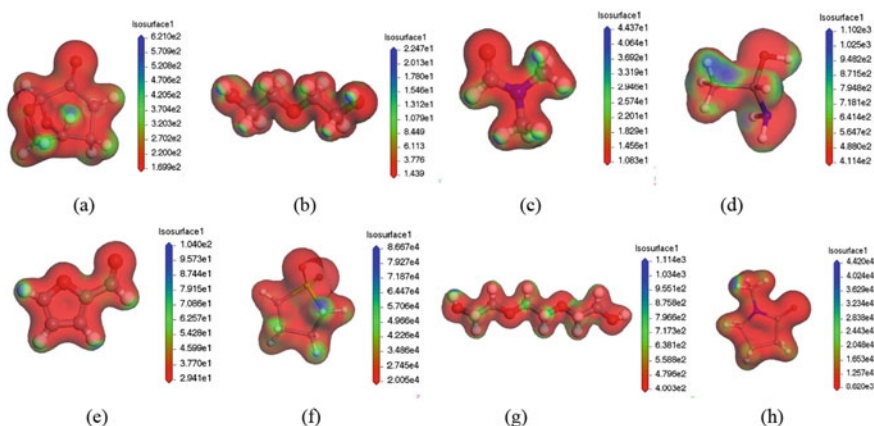**Fig. 4** Fukui function for nucleophilic attack mapped on to electron density iso-surface. **a** Cyrene, **b** DEG, **c** DMF, **d** ETA, **e** Furfural, **f** Sulfolane, **g** TEG, **h** NMP

Fig. 1). In case of solute molecules, thiophene and isooctane have comparable LUMO energies. However, thiophene has lowest IP, that is, it can lose electron easily to other molecules while isooctane has a higher IP. Due to its lower μ value, thiophene has more tendency to lose electron. Thus solvent should be the one which is ready to accept electrons. In other words, thiophene would prefer to interact via those sites on a solvent molecule which are electrophilic or thiophene would react with its hydrogen atom at those sites of solvent molecule which are nucleophilic. Global hardness of thiophene is less than isooctane indicating the high reactivity of thiophene or it can show stronger interactions with solvent. The high IP of isooctane indicates that it can't donate electrons easily. As the isooctane is a saturated stable molecule, it would show weak van der Waals interactions. This would make easier, the process of separating sulfurous molecule such as thiophene from the hydrocarbon such as isooctane.

Fukui functions describe the changes in the electron density of a particular molecule with respect to the loss or gain of electrons. Fukui function calculates the changes in the chemical potential of a system with respect to a perturbation in the external potential at a particular site and thus reflects the reactivity of the molecule. The fukui function for nucleophilic attack (gains electron from a nucleophile) is computed by the equation $f^+(r) = \left(\frac{\partial \rho(r)}{\partial N}\right)_{v(r)}^+$ and the fukui function for electrophilic attack (loses electron to an electrophile) is computed by the equation $f^-(r) = \left(\frac{\partial \rho(r)}{\partial N}\right)_{v(r)}^-$ (Mendez and Gazquez 1994; Faver and Kenneth 2010). The fukui functions for electrophilic attack and nucleophilic attack mapped onto the electron density (at an iso-surface value of 0.2 Ha/e) by applying mulliken fukui charges as shown in Figs. 3 and 4 respectively. The electrostatic potential maps and fukui function for electrophilic attack (Figs. 2 and 3) are in close correspondence. For all the solvents, oxygen and nitrogen atoms are the more susceptible

Table 1 Interaction descriptors of the solutes and solvents considered in the present study

S. No.	Molecule	E_{HOMO} (eV)	E_{LUMO} (eV)	IP (eV)	EA (eV)	Chemical potential (eV)	Global hardness	Electrophilicity index
1	Isooctane	−11.658	1.858	11.658	−1.858	−4.900	6.75	1.77
2	Thiophene	−9.068	1.828	9.068	−1.828	−3.620	5.44	1.20
3	NMP	−10.134	1.802	10.134	−1.802	−4.166	5.96	1.45
4	Cyrene	−10.632	1.519	10.632	−1.519	−4.557	6.07	1.71
5	Furfural	−9.367	1.600	9.367	−1.600	−3.884	5.48	1.37
6	DEG	−11.547	1.903	11.547	−1.903	−4.822	6.72	1.73
7	ETA	−10.438	1.918	10.438	−1.918	−4.260	6.17	1.47
8	TEG	−11.592	1.895	11.592	−1.895	−4.849	6.74	1.74
9	Sulfolane	−11.554	1.461	11.554	−1.461	−5.047	6.51	1.96
10	DMF	−10.293	1.673	10.293	−1.673	−4.310	5.98	1.55

regions for electrophilic attack due to high electron density available at those electronegative atoms. The next favourable regions for interactions are the double bond regions (Figs. 2 and 3). Figure 4 indicate that, the organic solvents considered in the present work have very few regions for possible interaction with a nucleophilic target molecule. Hydrogen atoms of the solvent molecules are the most reactive regions for a nucleophilic attack (Fig. 4).

3.1.2 Interaction Energy of Thiophene and Isooctane with Solvents

The interaction energy (IE) of thiophene and isooctane with various solvents was studied by placing the thiophene/isooctane molecules at different positions around the solvent molecule. The favourable positions were selected based on the analysis of ESP and fukui function maps for electrophilic and nucleophilic attack of solvent molecules. In addition, HOMO of solvent molecule is the preferred site for LUMO of solute and vice versa. The sites for electron acceptance on a thiophene molecule are the hydrogen atoms. Therefore the favourable position is such that the hydrogen of thiophene molecule faces towards oxygen atoms of the solvent molecule or the sulphur atom of thiophene faces toward hydrogen or oxygen atoms of the solvent molecules. The IE values with reference to the solute–solvent complex conformation which gave maximum interaction energy (most stable position identified as per the low IE value for solute molecule around the solvent molecule) are reported in Table 2. The IE of each solute–solvent pair was obtained by subtracting the total energy of the isolated solute and isolated solvent molecule from the total energy of the solute–solvent pair, $IE = E_{solute\text{-}solvent} - (E_{solute} + E_{solvent})$.

Table 2 presents that, all the solvents show van der Waals type of interactions with thiophene and iso-octane. All the solvents evidently showed strong interaction with thiophene and weak interaction with iso-octane. Among the eight solvents studied, cyrene showed strongest interaction with thiophene. However, cyrene also presented strong interaction with isooctane as well compared to other solvents. DMF has shown weakest interactions with both thiophene and iso-octane. When the difference in

Table 2 Solute–solvent interaction energy

Solvent	$IE_{Thiophene}$ (kJ/mol)	$IE_{Isooctane}$ (kJ/mol)	$\Delta IE = IE_{thiophene} - IE_{isooctane}$ (kJ/mol)
Furfural	−33.24	−13.73	−19.51
DEG	−30.89	−11.47	−19.42
Cyrene	−42.33	−23.54	−18.79
Sulfolane	−24.85	−6.96	−17.89
TEG	−34.75	−17.12	−17.63
NMP	−28.31	−11.33	−16.98
ETA	−22.44	−7.90	−14.54
DMF	−16.13	−5.78	−10.36

IE of both the solutes (ΔIE = IE$_{thiophene}$ − IE$_{isooctane}$) is considered as a measure of selectivity of thiophene, Table 2 infers that furfural and DEG can show good thiophene selectivity followed by cyrene. The solvents such as DMF, ETA and NMP have low thiophene extraction capacity as well as selectivity.

The most stable solute–solvent complex configurations for some of the solvents are shown in the Fig. 5. The orientations of the solute and solvent molecules in the stable complex configurations are in close correspondence with the electronic properties of solvents discussed in the Sect. 3.1.1. For example, in the furfural-thiophene complex (Fig. 5a), the HOMO of furfural which is located on the –C=O and the C=C–H region of the ring, interacts with the LUMO of thiophene which is located on the thiophene ring. Also, Fig. 5a shows that =O of furfural interacts with –H of thiophene and –HC of furfural interacts with –S of thiophene which is as per the electrophilic-nucleophilic interactions. i.e., the H of –CH of furfural is susceptible for nucleophilic attack and therefore the thiophene interacts via 'S' in this position. Similarly, the HOMO of isooctane which is located on the hydrogen atoms of branched chain, interacts with the LUMO region of furfural. In the same lines, from Fig. 1, HOMO of DEG is located on the –C–O–C-region. From Figs. 2b, 3b and 4b it can be seen that the –O– is the most reactive site for electrophilic attack and the hydrogens on the –CH are the more reactive sites for nucleophilic attack. The orientation of thiophene with respect to DEG molecule in Fig. 5c proves the hypothesis based on electronic properties of DEG and thiophene. Figure 5d of isooctane-DEG complex shows that the stable orientation of the solute and solvent interactions are also according to their HOMO, LUMO, ESP and fukui maps.
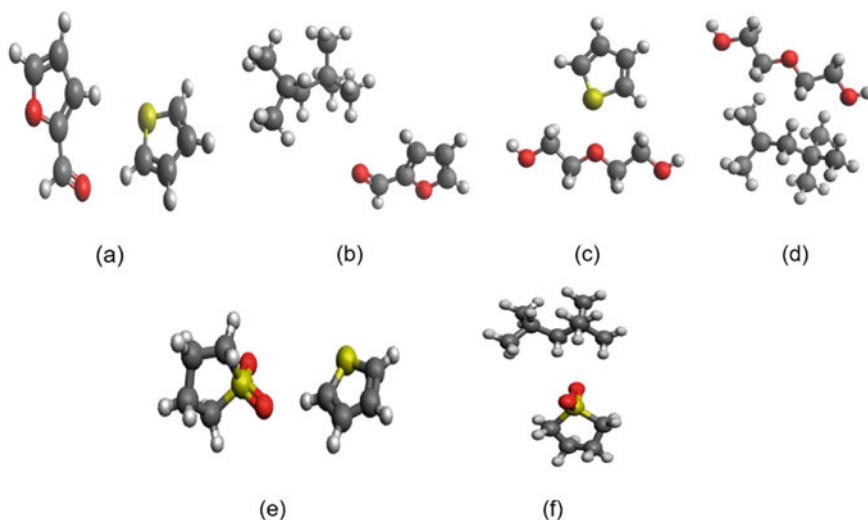
Fig. 5 Stable configurations of interaction. **a** Furfural-thiophene, **b** furfural-isooctane, **c** DEG-thiophene, **d** DEG-isooctane, **e** sulfolane-thiophene, **f** sulfolane-isooctane (color codes of atoms: grey—carbon; red—oxygen; white—hydrogen; yellow—sulphur)

3.2 Solute–Solvent Interaction Studies Using MD Simulations

MD simulations were carried out for three solvent systems (a) Furfural-thiophene-isooctane (b) NMP-thiophene-isooctane (c) Cyrene-thiophene-isooctane. The number of molecules of solvent and solutes for the all the simulations were chosen as per the mixture composition of 88% of solvent 10.5% of isooctane and 1.5% of thiophene by weight. Simulations were carried out as per the details in the Sect. 2.2. The amorphous cell model, concentration profiles, radial distribution function and mean square displacement for the furfural-thiophene-isooctane system are presented in the Fig. 6. The relative concentration profiles in Fig. 6b show that most of the thiophene overlaps into the furfural region (5–15 Å). In the 5–15 Å region, the concentration of iso-octane is very less. Also, the separation of thiophene and isooctane is clear throughout the analysed Z-axis. In the region of 15–25 Å, the concentration of isooctane is high whereas the concentration of thiophene is less and the concentration of furfural is much less. The radial distribution function (RDF) as presented in Fig. 6c indicates that the thiophene molecule is closer towards furfural compared to isooctane. By definition, Radial Distribution Function (RDF), $g(r)$ is the probability of finding an atom or molecule at a distance 'r' from another atom or molecule (Koopman 1934; Anderson et al. 2018; Gupta et al. 2019). Figure 6c infers a high probability for 'S' of thiophene to find an 'O' atom of furfural ($g(r)$ of 1.25 at ~6 Å distance). In addition, a $g(r)$ of 1.2 is available for the 'S' of thiophene to find
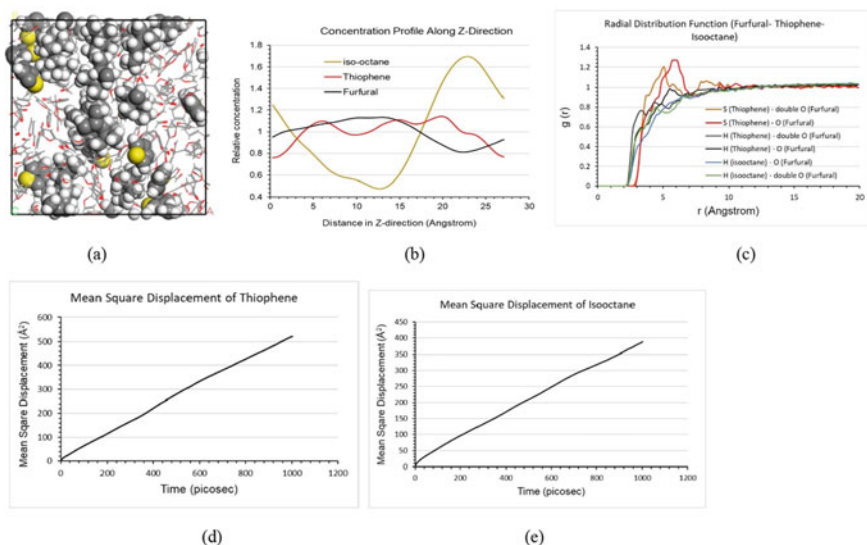
Fig. 6 Furfural-Thiophene-isooctane LLE. **a** Amorphous cell model of Furfural-thiophene-isooctane; **b** concentration profiles; **c** radial distribution functions; **d**–**e** mean square displacements of thiophene and isooctane

a '=O' atom of furfural at a distance of ~5 Å. Furthermore, the $g(r)$ for the 'H' of thiophene to find a '−O' or a '=O' of furfural is significantly less. This phenomena indicates that thiophene preferably interacts via 'S' rather than 'H' with the '=O' or 'O' of furfural. This is in close correspondence with the stable configuration for thiophene-furfural shown in Fig. 5. On the other hand, the RDF between 'H' of isooctane and furfural (Fig. 6c) indicates very week interaction between them ($g(r)$ values less than 1), which is in close correspondence with the observations as discussed in the Sect. 3.1.2. The mean square displacement, MSD (Å^2) versus time (picosec) of thiophene and isooctane are shown in Fig. 6d, e respectively. The increase of MSD with time is related to the diffusivity 'D' by Einstein relationship, based on the centre of mass (COM) motion:

$$D = \frac{1}{6N_\alpha} \lim_{t \to \infty} \frac{d}{dt} \sum_{i=1}^{N_a} \langle |r_i(t) - r_i(0)|^2 \rangle$$

where N_α is the number of diffusive atoms in the system. The term $r_i(t)$ represents the centre of mass position vector of molecule 'i' at time 't' and $r_i(0)$ represents the same at $t = 0$. The diffusivity is obtained by fitting a straight line $y = ax + b$ to the data in the diffusive regime. The diffusivity can then be calculated from slope 'a' as per the equation $D = \frac{a}{6}$. The units of 'a' are Å^2/ps and the units of 'D', which can be converted into m^2/s by using appropriate conversion factor (Mendez and Gazquez 1994; Anderson et al. 2018). The diffusivities of the solute molecules are calculated by fitting the linear data of diffusive regime of the MSD versus time plot. The diffusive regime has been identified by plotting log(MSD) versus log(t) and analysing the slope for $\beta = \frac{\log(MSD)}{\log(t)} \cong 1$. When $\beta < 1$, the molecules are said to be in the sub diffusive regime due to stronger interactions. When $\beta > 1$, the molecules apparently follow ballistic motion because of weak interactions. The diffusive regime is the region in which $\beta = 1$. The values of β inherently depends on the interactions between the molecules being simulated. The diffusion coefficient will be calculated for the diffusive regime of "MSD *vs.* time" plot. The intrinsic diffusivity of thiophene in furfural is 7.91×10^{-10} m^2/sec and of isooctane is 5.81×10^{-10} m^2/s. These diffusivity values clearly indicate that thiophene diffuses more into furfural compared to isooctane.

The amorphous cell model, concentration profiles, radial distribution function and mean square displacement for the NMP-thiophene-isooctane system are shown in the Fig. 7. The relative concentration profiles in Fig. 7b shows that most of the thiophene overlaps into the furfural region (0–15 Å). In the 0–10 Å region, the concentration of isooctane is less than thiophene which starts increasing further. However, the relative concentration of isooctane with respect to NMP is slightly higher compared to that of furfural case (Fig. 5b). The separation of thiophene and isooctane is clear throughout the analysed Z-axis although not to a much significant extent as in case of furfural. In the region of 15–25 Å, the concentration of isooctane is high whereas the concentration of thiophene is less with respect to the relative concentration of NMP. The radial distribution function (RDF) as presented in Fig. 7c indicates that the

Fig. 7 NMP-Thiophene-isooctane LLE. **a** Amorphous cell model of NMP-thiophene-isooctane; **b** concentration profiles; **c** radial distribution functions; **d–e** mean square displacements of thiophene and isooctane
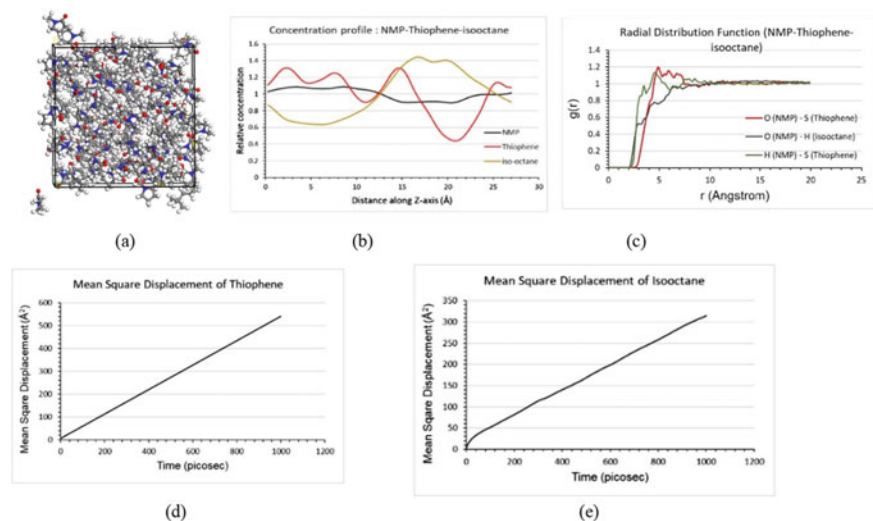
thiophene molecule is closer towards NMP compared to isooctane. Figure 7c infers a high probability for 'S' of thiophene to find an 'O' atom of NMP ($g(r)$ of 1.25 at ~5 Å distance). In addition, a $g(r)$ of 1.15 is available for the for 'S' of thiophene to find a 'H' atom of methyl group of NMP at a distance of ~5 Å. This phenomena indicates that thiophene preferably interacts via 'S' with the '–O' or 'H' of NMP. This is in close correspondence with the favourable positions identified based on the electronic properties of NMP (Figs. 1, 2, 3 and 4). On the other hand, the RDF between 'H' of isooctane and NMP (Fig. 7c) indicates very week interaction between them ($g(r)$ values less than 1), which is in close correspondence with the observations as discussed in the Sect. 3.1. The mean square displacement, MSD (Å^2) versus time (picosec) of thiophene and isooctane are shown in Fig. 7d, e respectively. From the diffusive regime of MSD versus time, the intrinsic diffusivity of thiophene in NMP is 8.91×10^{-10} m^2/s and of isooctane is 4.91×10^{-10} m^2/s. These diffusivity values are close to the case of furfural solvent.
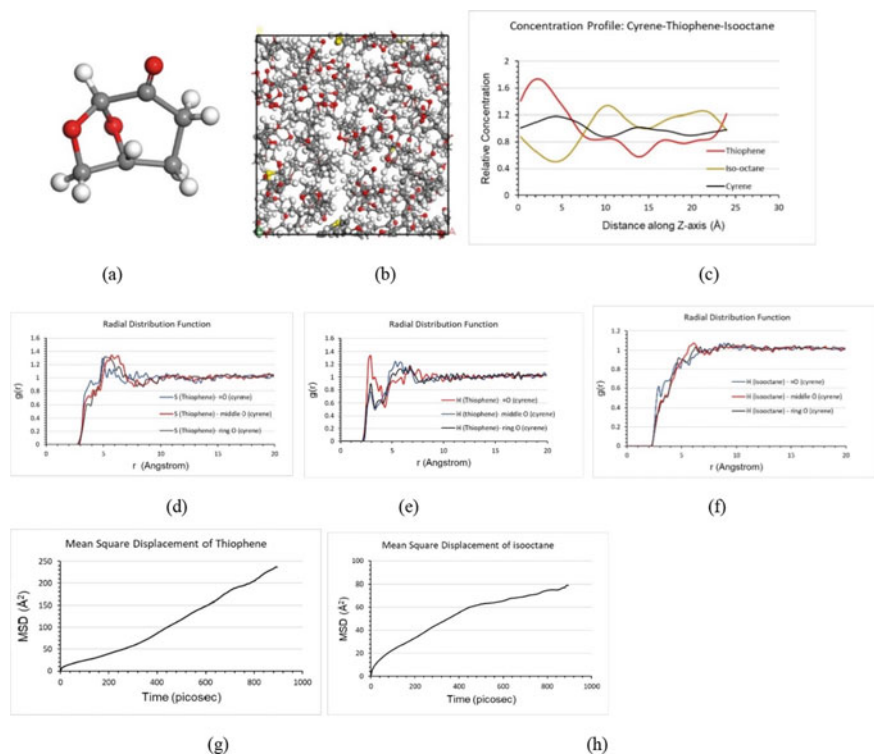
The molecular structure of cyrene, amorphous cell model, concentration profiles, radial distribution function and mean square displacement for the cyrene-thiophene-isooctane system are shown in the Fig. 8. The relative concentration profiles in Fig. 8c indicate a clear separation of thiophene and isooctane throughout the analysed Z-axis although not to a much significant extent as in case of furfural. In the regions of high relative concentration of thiophene, the same for isooctane is low and vice versa. In the 0–8 Å region, the concentration of isooctane is less than thiophene which starts increasing further. However, the relative concentration of isooctane with respect to cyrene is slightly lower compared to that of furfural case (Fig. 5b). In the region of 15–25 Å, the concentration of isooctane is high whereas the concentration of

Fig. 8 Cyrene-thiophene-isooctane LLE. **a** Molecular structure of cyrene; **b** amorphous cell model of cyrene-thiophene-isooctane; **c** concentration profiles; **d–f** radial distribution functions; **g–h** mean square displacements of thiophene and isooctane

thiophene is less. The radial distribution functions (RDF) for thiophene-cyrene and isooctane-cyrene as presented in Fig. 8d–f indicates that the thiophene molecule is closer towards cyrene compared to isooctane. Comparing the RDF between 'S' of thiophene with various oxygen atoms of cyrene (Fig. 8d) and the RDF between 'H' of thiophene with the three types of oxygen atoms of cyrene (Fig. 8e) indicates that, thiophene interacts more favourably through the 'hydrogen, H' of –CH of thiophene ring with the double bond oxygen (=O) of cyrene. This observation is perfectly supported by the fukui function maps for electrophilic attack (Fig. 4), which tells that the thiophene can interact via the electrophilic hydrogen atom. This phenomena is also apparent from Fig. 8e, in which, a high probability for 'H' of thiophene to find a '=O' atom of cyrene ($g(r)$ of 1.37 at ~3 Å distance) exists. However, a $g(r)$ of 1.2 is available for 'S' of thiophene to find the '=O' atom of cyrene at a distance of ~5 Å (Fig. 8d). On the other hand, the RDF between 'H' of isooctane and cyrene (Fig. 8f) indicates a very week interaction between them ($g(r)$ values stabilize at the value 1), which is in close correspondence with the observations as discussed in the Sect. 3.1. The mean square displacement, MSD (Å^2) versus time (picosec) of

thiophene and isooctane are shown in Fig. 8g, h respectively. The intrinsic diffusivity computed from the diffusive regime, of thiophene in cyrene is 5.02×10^{-10} m^2/s and of isooctane is 6.59×10^{-11} m^2/s. These diffusivity values are slightly less than those for the case of furfural and NMP solvents which might be due to strong interactions of cyrene with thiophene (Table 2) hampering free movement of thiophene molecules. Further, cyrene has shown significantly less diffusivity of isooctane compared to those for furfural and NMP.

The MD simulations of thiophene extraction studies in the present work were performed at a temperature of 298 K to gain fundamental understanding about the solute–solvent interactions for thiophene separation from isooctane using various organic solvents. However, experimentally it is proven that the liquid–liquid-extraction efficiency can be enhanced at elevated temperature (50 °C). Therefore, in the future work, we will be performing simulation studies at 323 K for more practical applications. The detailed analysis of molecular modeling studies indicate that, the organic solvents alone may not be able to provide the required separation of thiophene from isooctane or the required extraction of sulfurous compounds from hydrocarbons. However, the present study clearly indicates the importance of "oxygen" based solvents which can show good interactions with sulfurous heterocyclic molecules.

4　Conclusions

Density Functional Theory and Molecular Dynamic Simulation studies were used to study and screen eight organic solvents to identify optimum solvent for extraction of thiophene (sulphurous compound) from iso-octane (hydrocarbon). Eight organic solvents such as *N*-methylpyrrolidone, sulfolane, furfural, diethyleneglycol (DEG), 2-aminoethanol, tetraethyleneglycol (TEG), dimethylformamide and cyrene were chosen for the study to identify optimum solvents for EDS. Quantum mechanics based Koopmans' theorem was used to compute several interaction descriptors. Comparing the interaction descriptors, furfural was identified to be more reactive and sulfolane having the least reactivity. Cyrene, observed to be having reactivity on par with the organic solvents. Interaction energies (IE) of thiophene-solvent and isooctane-solvent complexes were studied by using DFT. The IE values showed that Cyrene has strongest interaction with thiophene followed by TEG, furfural and DEG, indicating that Cyrene can show good thiophene removal capacity. Among the eight solvents considered, furfural, DEG, TEG and Cyrene observed to show good desulfurization selectivity. The favourable positions as per IE values, on solvent molecules for potential interactions with thiophene and isooctane were in close correspondence with the HOMO and LUMO orbitals, electrostatic potential maps and fukui function electrophilic and nucleophilic attack of the respective solvents. Molecular

Dynamic (MD) simulations were performed for Furfural-thiophene-isooctane, NMP-thiophene-isooctane, and Cyrene-thiophene-isooctane systems to study the distribution of Thiophene between solvent and organic phases and interactions. Concentration profiles of the two solutes and three solvent systems using MD simulations evidently show the clear separation of thiophene from isooctane and moving to solvent phase and isooctane separating from solvent phase. Further, furfural and cyrene observed to show better capacity and selectivity for thiophene compared to NMP which was also observed from DFT based IE calculations. Analysis of radial distribution functions (RDF, $g(r)$ versus r) of thiophene and isooctane shows that the probability of interaction between sulphur (of Thiophene) and oxygen (of cyrene/furfural/NMP) is more than the probability of interaction between hydrogen (of isooctane) with the solvents. As a result of detailed analysis using various quantum chemical and molecular mechanical methods, it can be concluded that cyrene, furfural and TEG could be the potential organic solvents for thiophene removal from gasoline.

Conflict of Interest   The authors declare that they have no conflict of interest.

References

Ali SH, Hamad DM, Albusairi BH, Fahim MA (2009) Removal of dibenzothiophenes from fuels by oxy-desulfurization. Energy Fuels 23:5986–5994. https://doi.org/10.1021/ef900683d

Anderson LR, Yang Q, Ediger AM (2018) Comparing gas transport in three polymers via molecular dynamics simulation. Phy Chem Chem Phy 20:22123–22133. https://doi.org/10.1039/C8CP02829J

Becke AD (1993) Density-functional thermo chemistry. III. The role of exact exchange. J Chem Phy 98:5648–5652. https://doi.org/10.1063/1.464913

BIOVIA, Dassault Systèmes (2020) Material Studio 2020. Dassault Systèmes, San Diego

Boys F, Bernardi F (1970) The calculation of small molecular interactions by the differences of separate total energies. Some procedures with reduced errors. Mol Phy 19:553–566. https://doi.org/10.1080/00268977000101561

Cai C, Fan X, Han X, Li J, Vardhan H (2020) Improved desulfurization performance of polyethyleneglycol membrane by incorporating metal organic framework CuBTC. Polymers 12(2):414. https://doi.org/10.3390/polym12020414

Curtiss, L. A., McGrath, M. P., Blaudeau, J.-P., Davis, N. E., Binning R. C. Jr., Radom, L.: Extension of Gaussian-2 theory to molecules containing third-row atoms Ga-Kr. J. Chem. Phy. **103**, 6104-6113 (1995). https://doi.org/10.1063/1.470438

Dehury P, Mahanta U, Banerjee T (2016) Partitioning of butanol between a hydrophobic ionic liquid and aqueous phase: Insights from liquid liquid equilibria measurements and molecular dynamics simulations. Fluid Phase Equilib 425:421–431. https://doi.org/10.1016/j.fluid.2016.06.007

Eleni S, Dimitrios K (2021) Oxidative and extractive desulfurization of petroleum middle distillates, using imidazole ionic liquids. Fuel Commun 7:100011. https://doi.org/10.1016/j.jfueco.2021.100011

Faver J, Kenneth MM Jr (2010) The utility of the HSAB principle via the Fukui function in biological systems. J Chem Theory Comput 6(2):548–559. https://doi.org/10.1021/ct9005085

Frank N (2018) Software update: ORCA program system version: 4. WIREs. Wiley Interdisc Rev Comput Mol Sci 8:e1327. https://doi.org/10.1002/wcms.1327

Frenkel D, Smit B (2002) Understanding molecular simulation: from algorithms to applications, 2nd edn. Academic Press, San Diego

Gao H, Zeng S, Liu X, Nie Y, Zhang X, Zhang S (2015) Extractive desulfurization of fuel using N-butylpyridinium-based ionic liquids. RSC Adv 5:30234–30238. https://doi.org/10.1039/C5R A03762J

Gupta R, Kartha TR, Mallik BS (2019) Solvation structure and dynamics of alkali metal halides in an ionic liquid from classical molecular dynamics simulations. ACS Omega 4:19556–19564. https://doi.org/10.1021/acsomega.9b01672

Hanwell MD, Curtis DE, Lonie DC, Vandermeersch T, Zurek E, Hutchison GR (2012) Avogadro: an advanced semantic chemical editor, visualization and analysis platform. J Cheminform 4:17. https://doi.org/10.1186/1758-2946-4-17

Kianpour E, Azizian S (2014) Polyethylene glycol as a green solvent for effective extractive desulfurization of liquid fuel at ambient conditions. Fuel 137:36–40. https://doi.org/10.1016/j.fuel.2014.07.096

Koopman T (1934) About the assessment of wave functions and Eigen values to the individual electrons of an atom. Physica 1:104–113. http://www.scielo.org.co/scielo.php?script=sci_arttext&pid=S0124-61272013000100002

Kumar S, Srivastava VC, Nanoti SM, Nautiyal B, Siyaram S (2014) Removal of refractory sulfur and aromatic compounds from straight run gas oil using solvent extraction. RSC Adv 4(73):38830–38838. https://doi.org/10.1039/C4RA05841K

Kumar S, Srivastava VC, Nanoti SM (2017) Extractive Desulfurization of gas oils: a perspective review for use in petroleum refineries. Sep Purif Rev 46(4):319–347. https://doi.org/10.1080/15422119.2017.1288633

Lee C, Yang W, Parr RG (1988) Development of the Colle-Salvetti correlation-energy formula into a functional of the electron density. Phy Rev B. 37:785–789. https://doi.org/10.1103/PhysRevB.37.785

Majid MF, Mohd Zaid HF, Kait CF, Jumbri K, Yuan LC, Rajasuriyan S (2020) Futuristic advance and perspective of deep eutectic solvent for extractive desulfurization of fuel oil: a review. J Mol Liq 306:112870. https://doi.org/10.1016/j.molliq.2020.112870

Mendez F, Gazquez JL (1994) Chemical Reactivity of enolate ions: the local hard and soft acids and bases principle viewpoint. J Am Chem Soc 116(20):9298–9301. https://doi.org/10.1021/ja00099a055

Moghadam FR, Kianpour E, Azizian S, Yarie S, Zolfigol MA (2020) Extractive desulfurization of liquid fuel using diamine terminated polyethylene glycol as a very low vapour pressure and green molecular solvent. R Soc Open Sci 7:200803. https://doi.org/10.1098/rsos.200803

Naik PK, Mohan M, Banerjee T, Paul S, Goud VV (2018) Molecular dynamic simulations for the extraction of quinoline from heptane in the presence of a low-cost phosphonium-based deep eutectic solvent. J Phys Chem B 122:4006–4015. https://doi.org/10.1021/acs.jpcb.7b10914

Plakhutin BN (2018) Koopmans' theorem in Hartree-Fock method: a general formulation. J Chem Phy 148:094101. https://doi.org/10.1063/1.5019330

Player LC, Chan B, Lui MY, Masters AF, Maschmeyer T (2019) Toward an understanding of the forces behind extractive desulfurization of fuels with ionic liquids. ACS Sustain Chem Eng 7:4087–4093. https://doi.org/10.1021/acssuschemeng.8b05585

Roothaan CCJ (1951) New developments in molecular orbital theory. Rev Mod Phy 23(2):69–89. https://doi.org/10.1103/RevModPhys.23.69

Saha B, Sengupta S, Selvin R (2019) Comparative studies of extraction ability of organic solvents to extract thiophene from model fuel. Sep Sci Tech 55(6):1123–1132. https://doi.org/10.1080/01496395.2019.1580292

Shah D, Gapeyenko D, Urakpayev A, Torkmahalleh M (2019) Molecular dynamics simulations on extractive desulfurization of fuels by tetrabutylammonium chloride based Deep Eutectic Solvents. J Mol Liq 274:254–260. https://doi.org/10.1016/j.molliq.2018.10.131

Shen X, Li Z, Fang L, Song H, Gan F, Shen Z (2019) Extractive desulfurization from simulated sulfur-rich naphtha. China Pet Process Petrochem Tech 21(3):61–67

Sistla YS, Vignesh S (2021) Molecular understanding of carbon dioxide interactions with ionic liquids. J Mol Liq 325:115612. https://doi.org/10.1016/j.molliq.2020.115162

Taha M, Lee MJ (2013) TES buffer-induced phase separation of aqueous solutions of several water-miscible organic solvents at 298.15 K: phase diagrams and molecular dynamic simulations. J Chem Phys 138:244501. https://doi.org/10.1063/1.4809995

Tanimu A, Alhoosani K (2019) Advanced hydrodesulfurization catalysts: a review of design and synthesis. Energy Fuels 33:2810–2838. https://doi.org/10.1021/acs.energyfuels.9b00354

Wang J, Song Z, Li X, Cheng H, Chen L, Qi Z (2020) Toward Rational functionalization of ionic liquids for enhanced extractive desulfurization: computer-aided solvent design and molecular dynamics simulation. Ind Eng Chem Res 59:2093–2103. https://doi.org/10.1021/acs.iecr.9b05684

Zhang J, Wang P, Ge S (2009) Synthesis and application of polyetheramine as gasoline detergent. China Pet Process Petrochem Tech 7(40):40–43

Zhu S, Cheng H, Dai Y, Gao J, Jiang X (2020) Extractive desulfurization and denitrogenation from fuel oil by a polyether-amine-based solvent. Energy Fuels 34:8186–8194. https://doi.org/10.1021/acs.energyfuels.0c01096

Optimization of *Lactobacillus* and *Aspergillus niger* Biobeads Formation for the Removal of Reactive Yellow Dye from Wastewater

Ayushi Verma, Rama Karn, Richa Pathak, and Pragya Rathore

Abstract Textile industries are one of the most rapidly growing industries. They use synthetic dyes rather than natural dyes for different colouring purposes due to the higher demand rate. Chemical dyes cause severe damage to the environment and aquatic life when they are disposed of in the water bodies. Physical and chemical methods of wastewater treatment produce toxic in the environment and require enormous costs. While biological treatment methods are economical and eco-friendly. For biodegradation of dyes, microbes can be used as free cells or immobilised cells. Immobilisation has certain advantages over free cells, such as producing a higher level of extracellular enzymes and producing a large amount of biomass. Immobilisation of microorganisms also protect the unpleasant external environment of media, and they can be reused in more batch reactions. In this study, *Lactobacillus* and *Aspergillus niger* were used as free cells and immobilised cells (immobilised together and separately) due to their ability to decolourise the dyes. For reactive yellow dye the maximum removal efficiency of 100% has been achieved. The results of this study indicates that biobeads of *Lactobacillus* and *Aspergillus niger* can be used together for decolourisation process to achieve an effective result without the production of toxicity.

Keywords Dye degradation · *Lactobacillus* · *Aspergillus niger* · Immobilisation · Biobeads

A. Verma (✉) · R. Pathak · P. Rathore
Department of Bioscience, Softvision College, Indore, Madhya Pradesh 452010, India
e-mail: drayu18iitr@gmail.com

R. Karn
Department of Biotechnology, Noida Institute of Engineering and Technology, Greater Noida, Uttar Pradesh 201306, India

1 Introduction

Nowadays, synthetic dyes are being extensively used in the printing, textiles, cosmetics, rubber, leather, plastics industries to dyeing their products results in generating a large volume of colored wastewater (Aksu 2005; Aksu et al. 2007; Arumugam and Sivakami 2016). Among all the industries, textile and dyeing industries are highly contributed to water and soil pollution. Colour is applied to the finished products through dyeing or printing, resulting in different wastewaters (Fig. 1). Any synthetic dyes cannot be fixed with 100% efficiency, and thus there is a chance to enter it into the environment as wastewater (Hao et al. 2000). The dye concentrations in the textile processing wastewaters are in the range of 10–200 mg/l. Most of the dyes are more stable and non-biodegradable (Aksu 2005; Bharti et al. 2019; Verma et al. 2019). Dumping of these dyes into the environment results in severe damage since they may notably affect the photosynthetic activity of hydrophytes by reducing light penetration. Some dyes are carcinogenic and mutagenic in nature. Dysfunction of brain, liver, kidney, central nervous system and reproductive system are some lethargic effects of dyes on human being. Thus, removal of dyes from environmental is of great concern (Fazal et al. 2018; Hameed and Ismail 2018; Hao et al. 2000; Karim et al. 2018; Khalaf 2008).

The removal of dye from wastewater can be done using several physical, chemical, and biological methods (Verma et al. 2018). The chemical and physical methods are insufficient, expensive and they are not environment friendly as they can generate unacceptable levels of secondary pollution in sludge (Arumugam and Sivakami 2016). While bioremediation is a cost-effective, clean and practicable alternative means to remediate dye from wastewater (Kuhad et al. 2004; Kulandaivel et al. 2014). Several studies have been carried out to determine the role of the diverse groups of bacteria in the decolourization of different textile dyes Bacterial and fungal cells have been studied to check the capability of industrial dyes. Fungi produces

Fig. 1 Textile wastewater. *Source* Sanghavi and Ranga (2019)

an extracellular enzymates to transform aromatic substances, such as lignin, pesticides or polycyclic aromatic hydrocarbons (PAH). The use of free-cell of fungus for dye removal shows some disadvantages like the mycelium may be more exposed to environmental stresses. Thus, immobilization of fungal and bacterial cell can be a good alternative which involves the immobilization of biomass on different supports (Hameed and Ismail 2018; Lee et al. 2013; Suganya and Revathi 2016).

Immobilized microorganisms are increasingly used for wastewater treatment bioreactors as they offer advantages such as the absence of cell washout, high stability, high cell densities, and multiple reactions. Among the different immobilization techniques, the sol–gel method can be helpful as it permits obtaining materials with required new mechanical and chemical properties, non-toxic to the environment, and does not hinder the activity of microorganisms on decolourization of dyes in the effluent (Sanghavi and Ranga 2019; Tuttolomondo et al. 2014). The aim of present study is removing of reactive yellow dye from textile wastewater, using *Lactobacillus spp.* and *Aspergillus niger*, both as free cells and immobilized cells.

2 Materials and Methods

2.1 Isolation of Bacillus sp.

For isolation of *Lactobacillus* from curd, Rogoa agar was used. The curd sample was serially diluted upto 10^{-8} using sterile distilled water. The serially diluted samples were spread plated on petri dish with de Mann Rogoa agar medium. The plates were incubated at 34 °C for 3 days. Re-streaking of the plates was done almost 7–8 times to obtain a single colony of *Lactobacillus sp.* A single colony of isolated *Lactobacillus sp.* was taken as inoculum to grow in MRS Broth (De Man, Rogosa and Sharpe broth). The flask was kept on an incubator shaker at 150 rpm and room temperature for 2–3 days, after which broth was centrifuged, and the bacterial pellets were stored for further process.

2.2 Characterization of Bacteria

The bacterial colonies were identified by gram staining and a catalase test. Morphological studies of the bacterial isolates were conducted using a light microscope.

2.3 Revival of **A. niger**

Potato Dextrose Agar (PDA) was used for the revival of *Aspergillus niger*. After being autoclaved, media was poured into test tubes and kept in a slanting position. Inoculation was done from the available master strains. All the test tubes were incubated at 22–25 °C for 10 days.

2.4 Preparation of Immobilized Cells (Biobeads)

2.4.1 Immobilisation of *Bacillus sp.* in Alginate Beads

The immobilization of bacterial cell was done by using sodium alginate solution to form biobeads. For this the stored bacterial pellets were resuspended in 10 ml sodium alginate solution. The alginate-bacterial mixture was then added drop by drop in the calcium chloride solution with the help of a syringe. The beads were formed and for hardening purpose kept them in the same solution for 30 min at 4 °C (Table 1).

2.4.2 Immobilisation of *A. niger* in Alginate Beads

One loop of fungus was resuspended in 5 ml sterile water. In this add 10 ml of sodium alginate solution, and mix them to form a homogenous mixture. Then the mixture was added drop by drop in calcium chloride solution using a syringe. To harden the beads kept them in same solution for 30 min at 4 °C (Suganya and Revathi 2016).

2.4.3 Immobilisation of *Bacilli* and *A. niger* (Combined) in Alginate Beads

The equal concentration of fungal and bacteria mixture was added in 10 ml sodium alginate solution, and a homogenous mixture was formed. Add this mixture to the calcium chloride solution drop by drop using a syringe for the formation of beads. To harden the beads kept them in same solution for 30 min at 4 °C (Suganya and Revathi 2016).

2.4.4 Optimization of Sodium Alginate and CaCl$_2$ Concentration to Form Biobeads

For the formation of immobilised microbial beads, different concentrations of calcium chloride and sodium alginate were used. Table 2 shows the different concen-

Table 1 List of different studies for the bioremediation of dye using various microorganisms as free and immobilized cells

Organism name	Immobilised cell	Free cell	Removal efficiency	References
Trametes versicolor		✓	77%	Aksu et al. (2007)
Pseudomonas aeruginosa, Fusarium oxysporum	✓		Bacteria—65.1% Fungus—65.7% Combination—51.4%	Arumugam and Sivakami (2016)
Activated sludge	✓	✓	100%	Hameed and Ismail (2018)
Bacterial consortium		✓	65–90%	Karim et al. (2018)
Aspergillus niger, Spirogyra sp.		✓	88, 85%	Khalaf (2008)
Bacillus sp.	✓		64–100%	Kulandaivel et al. (2014)
Bacillus sp., Escherichia coli, Pseudomonas fluorescens		✓	77, 79, 59%	Sriram et al. (2013)
Microbial consortium	✓		100%	Steffan et al. (2005)
Pseudomonas sp.	✓		75–83%	Tuttolomondo et al. (2014)
Alcaligenes faecalis		✓	87–92%	Bharti et al. (2019)
Microalage		✓	75–80%	Fazal et al. (2018)
Arthrobacter chlorophenolicus	✓		63%	Lee et al. (2013)
Candida tropicalis		✓	90–97%	Li et al. (2015)
Trichoderma asperellum		✓	95%	Shanmugam et al. (2017)

Table 2 Different conditions of calcium chloride and sodium alginate for the formation of beads

Calcium chloride (CaCl$_2$)	Sodium alginate (SA)
2.22 g/100 ml	0.3 g/10 ml
2.22 g/100 ml	0.4 g/10 ml
7 g/100 ml	0.4 g/10 ml 0.5 g/10 ml 0.6 g/10 ml 0.7 g/10 ml

trations of sodium alginate corresponding to the concentrations of calcium chloride (Suganya and Revathi 2016).

2.4.5 Decolorization Experiment

To determine the effectiveness of reactive yellow dye decolourisation by free and immobilised *Lactobacillus* and *A. niger* cells, all the experiment was conducted twice in batch cultures for a total period of 8 days in 250 ml Erlenmeyer flask. The stock solution (1000 mg/L) of reactive yellow dye was prepared. For all the experiments 100 mg/L concentration of dye was used. To allow the growth of microbes in dye solution, growth media were added in the dye solution as external carbon sources to the microorganisms. For *Lactobacillus*, nutrient broth was added and potato dextrose broth was added for *A. niger*. The combination of both the growth media was added for mixture of *Lactobacillus* and *A. niger*. In order to conduct the decolorization experiments, free microbial cells and immobilised biobeads were added in 100 mg/L concentration of dye solution, and all the flasks were incubated at 25 °C under 150 rpm. For 8 days after every 24 h of the experiment, the sample of dye solution was taken and centrifuged at 15,000 rpm for 10 min, and the supernatant was collected. The supernatant was analysed to estimate the removal efficiency of free and immobilised microbial cells. Removal efficiency (%) of microbes for reactive yellow dye was calculated using Eq. (1) (Verma et al. 2018, 2019):

$$R.E. = \frac{C_i - C_f}{C_i} \times 100 \tag{1}$$

where, C_i = initial concentration of dye, 100 mg/L, C_f = final concentration of dye (mg/L).

2.4.6 Spectrophotometer Analysis

During bioremediation studies, samples were collected after 1, 2, 3, 4, 5, 6, 7, and 8 days and absorbance was measured at 420 nm using UV–Visible Spectrophotometer (Spectroquant NOVA 60, Merk).

Calibration Curve

To check the highest absorbance of reactive yellow dye at different wavelengths, UV–Vis spectrophotometer was used. The resultant graph is shown in Fig. 2, which shows that reactive yellow gives the highest absorbance at 420 nm.

For obtaining a standard graph of the dye, different concentrations of dye were used and checked their absorbance at 420 nm and the data is shown in Table 3. The resultant graph is the standard graph shown in Fig. 4. From the standard graph, the

Fig. 2 Absorbance of reactive yellow dye at different wavelengths

Reactive yellow dye
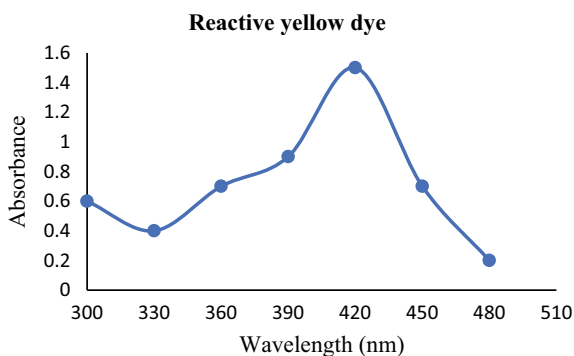
Table 3 Absorbance of dye at different concentrations

Concentration of dye (mg/l)	Absorbance (at 420 nm)
100	1.584
200	2.564
300	3.801
400	5.005

concentration of dye was calculated. From Fig. 4, a linear equation was obtained for the standard curve as follows:

$$y = 1.15x + 0.365 \tag{2}$$

where, y = absorbance of dye; x = concentration of dye.

Extent of dye removal were calculated by the following formula (Eq. 3):

$$x = \frac{y - 0.365}{1.15} \tag{3}$$

3 Results

3.1 Isolation of Single Colony of **Lactobacilli**

A single colony of *Lactobacillus* sp. was isolated using the serial dilution method (Fig. 3). The bacteria were identified by gram staining and catalase test. It was observed that the *Lactobacilli* were gram-positive and catalase-negative (Suganya and Revathi 2016).

Fig. 3 *Lactobacillus sp.*
grown after re-streaking for
7 times
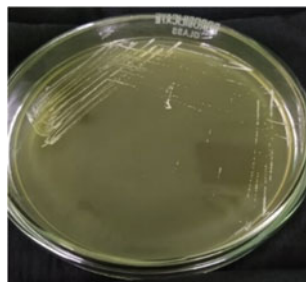
Fig. 4 Revived strain of *A. niger*
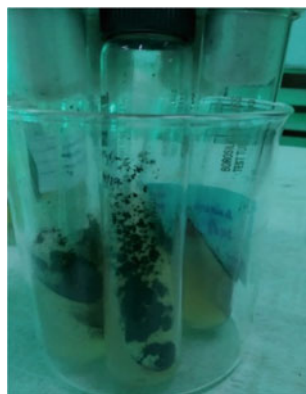
3.2 Revival of A. niger

The fungal strain of *A. niger* was recovered from the PDA slant (Fig. 4).

3.3 Optimization of Sodium Alginate and CaCl$_2$ Concentration to Form Biobeads

Figure 5a–e shows that the beads formed had a central cavity, and they were pliable. Figure 5f depicts the desired structure of beads. Therefore, all the experimental studies for decolourization of dye were carried out using 7 g/100 ml of calcium chloride and 0.7 g/10 ml of sodium alginate.

(a) (b)

(c) (d)

(e) (f)
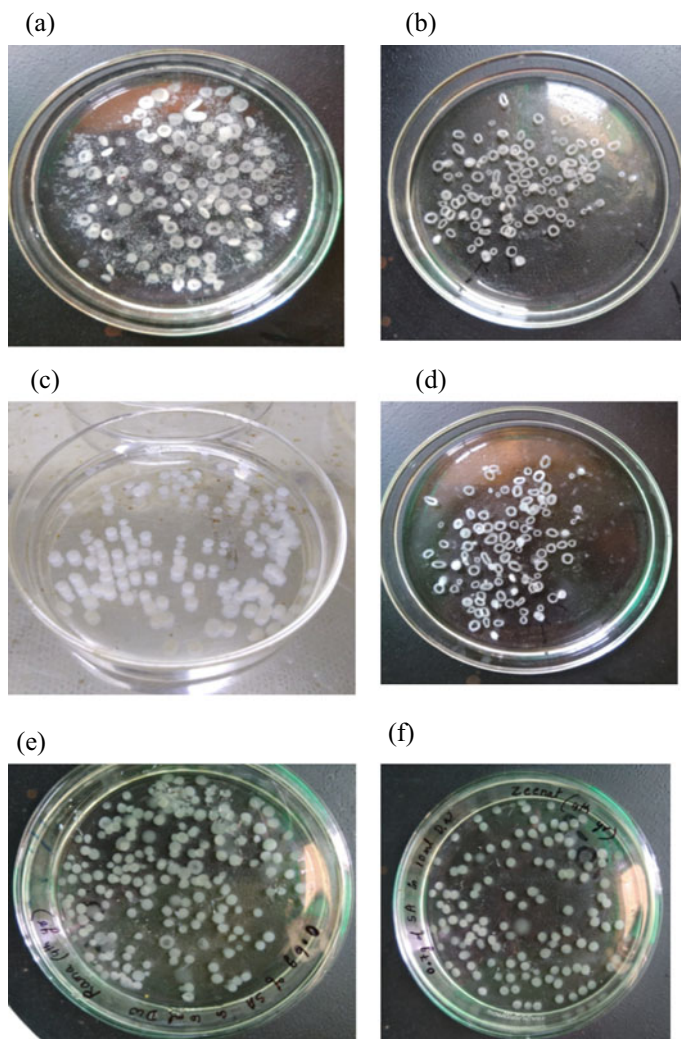
Fig. 5 Immobilized beads of bacterial and fungal cells using different concentration of sodium alginate and calcium chloride **a** SA—0.3 g/10 ml (DW) CaCl$_2$—2.22 g/100 ml (DW); **b** SA—0.4 g/10 ml (DW) CaCl$_2$—2.22 g/100 ml (DW); **c** SA—0.4 g/10 ml (DW) CaCl$_2$—7 g/100 ml (DW); **d** SA—0.5 g/10 ml (DW) CaCl$_2$—7 g/100 ml (DW); **e** SA—0.6 g/10 ml (DW) CaCl$_2$—7 g/100 ml (DW); **f** SA—0.7 g/10 ml (DW) CaCl$_2$—7 g/100 ml (DW)

3.4 Removal of Reactive Yellow Dye

The free and immobilised cells of *Lactobacillus* and *A. niger* were used to remove reactive yellow dye from wastewater. Figure 6 shows the comparative study of the free and immobilised microbial cell removal efficiency for 1–8 days. It was
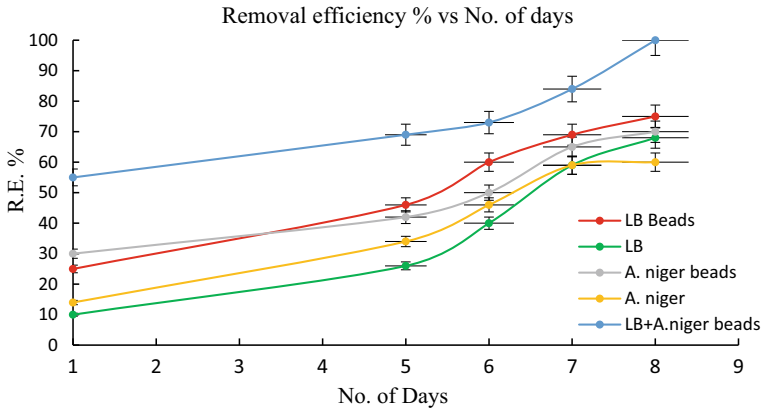
Fig. 6 Graph for removal efficiency of microbial free cell and biobeads for reactive yellow dye

observed that the immobilised biobeads of bacteria and fungus has been achieved as 100% removal efficiency after 8 days. Figure 6 graphs revealed that immobilised bacteria and fungus together work more efficiently than as free cells or immobilised individually (Sanghavi and Ranga 2019).

The *Lactobacillus* bacterium has more potential than fungus in decolourising the dye. Since bacteria adapt to the new environment more rapidly than fungus, their doubling time is shorter than fungus. More the cells, more activity can be seen in a shorter time. Figure 7 shows the dye solutions before and after bioremediation by microorganisms. After bioremediation, the reduction of intensity of the dye was observed. However, some colour was still left in the solution, which could be attributed to the media, biomass and waste products.
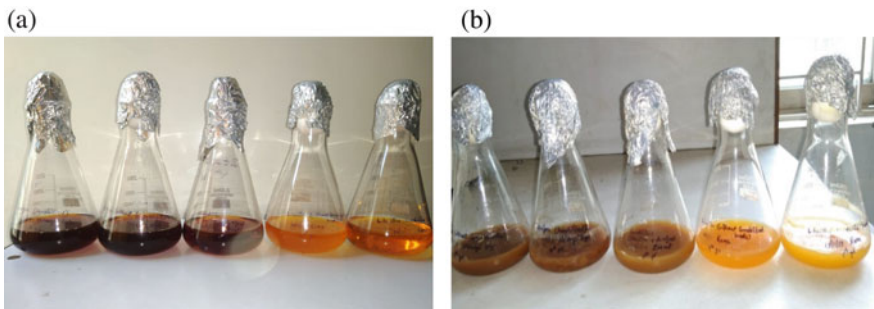
Fig. 7 a Before degradation. From left—*A. niger*, *A. niger* immobilised, *Lactobacillus + A. niger* immobilised, *Lactobacillus* and *Lactobacillus* immobilised. **b** After degradation. From left—*A. niger*, *A. niger* immobilised, *Lactobacillus + A. niger* immobilised. *Lactobacillus* and *Lactobacillus* immobilised

4   Conclusions

Now a day, the use of immobilized cell getting attention in the field of wastewater treatment for decolourization purpose. This method simplifies the separation and recovery of binding agent and immobilized microorganisms. In addition to this, it also makes the application reusable, which decreases the total cost. The immobilized cells are more tolerant to local stress conditions such as changes in pH, temperature and presence of inhibitor compounds (Suganya and Revathi 2016). It has been found that sodium alginate is a suitable matrix material because it is non-toxic and the method of forming biobeads using sodium alginate mild and non-toxic towards the microorganisms. In all experiments, sodium alginate immobilized cells showed maximum colour reduction. Both bacteria and fungus can be used for decolourising the reactive yellow dye from an aqueous solution without losing their capability. It was initially observed that bacteria as free cells function more efficiently than any other combination. As fungus takes more time to reproduce, the result took about four days more than the bacteria alone when put together in the dye solution. After 8 days of experiments 100% removal efficiency has been achieved. It was concluded that immobilised *Lactobacillus* and *Aspergillus niger* together can be used together for the decolourisation purpose without production of toxicity.

References

Aksu Z (2005) Application of biosorption for the removal of organic pollutants: a review. Process Biochem 40(3–4):997–1026

Aksu Z, Kiliç NK, Ertugrul S, Donmez G (2007) Inhibitory effects of chromium (VI) and Remazol Black B on chromium (VI) and dyestuff removals by Trametes versicolor. Enzyme Microb Technol 40(5):1167–1174

Arumugam V, Sivakami R (2016) Treatment of dye industry effluent using immobilized bacteria and fungi isolated from freshwater pond Thiruvarur District, Tamil Nadu, India. Int J Curr Microbiol App Sci 5(6):596–605

Bharti V, Vikrant K, Goswami M, Tiwari H, Sonwani RK, Lee J, Rai BN (2019) Biodegradation of methylene blue dye in a batch and continuous mode using biochar as packing media. Environ Res 171:356–364

Fazal T, Mushtaq A, Rehman F, Khan AU, Rashid N, Farooq W, Xu J (2018) Bioremediation of textile wastewater and successive biodiesel production using microalgae. Renew Sustain Energy Rev 82:3107–3126

Hameed BB, Ismail ZZ (2018) Decolorization, bioremediation and detoxification of reactive red azo dye using non-adapted immobilized mixed cells. Biochem Eng J 137:71–77

Hao OJ, Kim H, Chiang PC (2000) Decolorization of wastewater. Crit Rev Environ Sci Technol 30(4):449–505

Karim ME, Dhar K, Hossain MT (2018) Decolorization of textile reactive dyes by bacterial monoculture and consortium screened from textile dyeing effluent. J Genet Eng Biotechnol 16(2):375–380

Khalaf MA (2008) Biosorption of reactive dye from textile wastewater by non-viable biomass of *Aspergillus niger* and *Spirogyra* sp. Bioresour Technol 99(14):6631–6634

Kuhad RC, Sood N, Tripathi KK, Singh A, Ward OP (2004) Developments in microbial methods for the treatment of dye effluents. Adv Appl Microbiol 56:185–213

Kulandaivel S, Kaleeswari P, Mohanapriya P (2014) Decolorization and adsorption of dyes by consortium of bacteria with agriculture waste. Int J Curr Microbiol Appl Sci 3(12):865–882

Lee SH, Lee SH, Ryu SJ, Kang CS, Suma Y, Kim HS (2013) Effective biochemical decomposition of chlorinated aromatic hydrocarbons with a biocatalyst immobilized on a natural enzyme support. Bioresour Technol 141:89–96

Li H, Tan L, Ning S, He M (2015) Reactor performance and microbial community dynamics during aerobic degradation and detoxification of Acid Red B with activated sludge bioaugmented by a yeast *Candida tropicalis* TL-F1 in MBR. Int Biodeter Biodegrad 104:149–156

Sanghavi LK, Ranga SV (2019) Study of operating parameters for removal of direct yellow 12 dye using *Prosopis juliflora* bark. Int J Res Anal Rev 6(12):869–880

Shanmugam S, Ulaganathan P, Sivasubramanian S, Esakkimuthu S, Krishnaswamy S, Subramaniam S (2017) *Trichoderma asperellum* laccase mediated crystal violet degradation—optimization of experimental conditions and characterization. J Environ Chem Eng 5(1):222–231

Sriram N, Reetha D, Saranraj P (2013) Biological degradation of reactive dyes by using bacteria isolated from dye effluent contaminated soil. Middle East J Sci Res 17(12):1695–1700

Steffan S, Bardi L, Marzona M (2005) Azo dye bioremediation by microbial cultures immobilized in alginate beads. Environ Int 31(2):201–205

Suganya K, Revathi K (2016) Decolorization of reactive dyes by immobilized bacterial cells from textile effluents. Int J Curr Microbiol App Sci 5(1):528–532

Tuttolomondo MV, Alvarez GS, Desimone MF, Diaz LE (2014) Removal of azo dyes from water by sol–gel immobilized *Pseudomonas* sp. J Environ Chem Eng 2(1):131–136

Verma A, Kumar S, Balomajumder C, Kumar S (2018) Efficacy of *Sargassum filipendula* for the removal of Pb^{2+}, Cd^{2+} and Ni^{2+} ions from aqueous solution: a comparative study. Desalin Water Treat 129:216–226

Verma A, Agarwal M, Garg H, Bhati D (2019) Investigation on the removal of direct red dye using *Aspergillus niger*. J Mater Sci Surf Eng 6(6):881–883

Fast Pyrolysis of Coconut Coir in Solar Energy Embedded Fixed Bed Tubular Reactor

Leena Kapoor, Adithya Bontha, Jujjarapu Gnanendra Naidu, Neha Saxena, and Numair Shirqhi Mohammed

Abstract This work investigates the fast pyrolysis of coconut coir by using thermodynamic equilibrium approach using DWSIM software. Peng-Robinson was the chosen thermodynamic model. The real life pyrolizers by virtue are isothermal and function at a steady state. The closest possible reactor setup and environment that can be generated on DWSIM is the RGIBBS reactor since it calculates results based on reduction of overall Gibbs energy. From the simulation process, certain key observations were made in regards with trends of pyrolysis product yields with respect to temperature and pressure. It is observed that at temperatures up to 550 °C the product yields of both Bio-oil and Biogas were increasing, at 550–575 °C maximum yield of bio-oil can be obtained and at temperatures above 575 °C, biogas remains predominant.

Keywords Solar pyrolysis · Fixed bed reactor · Biomass · Bio oil · Bio char

1   Introduction

The growing demand for carbon emission free energy is increasing at an alarming rate across the globe, let alone in India. India for the largest part has been a major energy importing country with 85% of its energy needs being met through imports from oil exporting countries like USA, Saudi Arabia, UAE, etc. Estimates also suggest that to ensure a stable growth of the economy, India needs to increase its primary energy reserves and supply upto 8 folds by from the present stage (Islam et al. 2004). With India being a coal based economy with rapid depletion in the existing coal reserves and inability to explore new mines, growing environmental concerns and other factors, India has now shifted its focus to increase the supply of its primary energy from the renewable sources with extensive budgets being allocated towards development of new technologies to tackle the global energy crisis (Meng et al.

L. Kapoor (✉) · A. Bontha · J. G. Naidu · N. Saxena · N. S. Mohammed
Department of Chemical Engineering, University of Petroleum and Energy Studies, Dehradun, Uttarakhand, India
e-mail: lkapoor@ddn.upes.ac.in

2015). With a population of 1.4 billion, domestic waste is something that is present in extreme abundance, especially plastic and bio wastes. With this motive in mind, extensive technologies have been designed to decompose these wastes to produce fuel grade products. Pyrolysis is one such technology in which we are currently interested. We have been working on pyrolyzing a high carbon feedstock using a zeolite catalyst within a fixed bed reactor to obtain pure fuel grade products without any need for external purifications. The drawback that currently exists is the attainment of the reaction conditions, which becomes highly uneconomical due to its high capital and energy intensities. Hence, in this project we focus on studying techniques that can be used to optimize this process in order to make proposal extremely economical.

Excessive studies are being conducted to select a suitable high carbon feedstock which on one hand would increase the high heating value but on the other hand should also prevent coking, also works are being conducted on selecting a specific catalyst for the pyrolysis fore-mentioned high carbon feedstock to obtain bio-oil with high heating value (Zhao et al. 2006). Research on the international level is focusing on using plant based bio mass like fruit seeds, flowers, stems, fruits etc. due to predominantly high levels of innate carbon. In addition, excessive work on the International level is being conducted to develop in situ pyrolysis reactors where in the pyrolysis and stabilization of the biomass would take place within a single reactor hence further optimizing the energy economy of the entire process. Further in order to optimize the pyrolysis process several solar panel embedded pyrolysis reactors have been designed in order to incorporate the use of solar energy. Currently fixed bed pyrolysis reactors is amongst one of the very few types of reactor that hasn't been experimented with at the moment on both the national and international front. Bangladesh has also been trying to work on studying the prospects of using solar energy accompanied pyrolysis (Zheng et al. 2010). Concluding from the national and international literature review, on one hand pyrolysis of the high carbon biomass followed by the stabilization of bio-oil would require a lot of energy hence the whole concept of ex-situ pyrolysis is put into scrutiny. And on the other hand the simulation studies performed on catalytic pyrolysis of high carbon feedstock in a fixed bed tubular pyrolysis reactor further suggested the most ideal conditions for obtaining high yields to be 500 °C temperature and 1 atm pressure hence forth again a highly energy and capital intense process (Xianjun et al. 2015). Hence in order to obtain alternative fuel on a commercial scale from such energy intensive process would cost a fortune and would therefore seem uneconomical hence there exists a need to study techniques that would optimize the proposed in-situ pyrolysis wherein the production and purification of product would not only take place within a single reactor with maximum yield but also the process becomes extremely economical (Zhang et al. 2013). With this prospect in mind our we decided to go ahead with studying the prospect of incorporating the use of solar energy into our pre proposed fixed bed tubular reactor wherein we would report the potential of solar energy in India and finally propose our unique design for a solar energy embedded fixed bed tubular reactor setup which on necessary approval would be a ground breaking study as a one of its kind solution to revolutionize the whole science of biomass.

As the pyrolysis is one of the most common techniques being used to obtain a fuel grade alternative product from different kinds of biomass like agro and forest residues, domestic household wastes etc. In this case we used coconut coir biomass, a high carbon feedstock that was pyrolyzed in the absence of oxygen and presence of inerts at 1 atm pressure and 500 °C temperatures using zeolite catalysts to obtain bio-oil, bio-fuel, bio crude, char, fuel gases. From the simulations conducted on DWSim for the above system, the fore mentioned conditions was formulated to obtain a maximum yield of approximately 60%. Our typical pyrolysis model includes the fixed bed reactor into which the coconut shell biomass is fed, electric furnace with temperature regulating and controlling devices to control and measure the pyrolysis temperatures and ultimately carry out the pyrolysis process, condenser to cool down high temperature vapors and collect the bio-oil and pyrolysis gas products from the reactor bottom, nitrogen fed into the fixed bed reactor to maintain inert atmosphere which further prevents thermal oxidation of biomass into carbon dioxide, carbon mono oxide, NOx, prevents contamination of gaseous pyrolysis product by the combustion products hence maintaining the calorific value and prevents excess char formation within the reactor (Zhao et al. 2006; Zheng et al. 2010; Xianjun et al. 2015). The fast pyrolysis of biomass results in 74% production of liquid fuel that is bio oil that is why fast pyrolysis is a preferred method of pyrolysis in this study in comparison to slow pyrolysis (Tanneru and Steele 2015).

2 Background

The growing demand of green energy and depletion in conventional fossil fuels calls for an alarming need for an alternative energy source for future generations. In the past few decades there has been a rise in interest of developing bio-oil as an alternative to the current non-renewable sources of energy due to their extensive usage in this industrial age leading to ever depleting energy levels as well as increasing environmental concerns due to ozone layer depletions, elevated pollution levels and global warming prompting the present generation to switch to cleaner resources and conserve existing resources for sustainable development of these resources for the future generations. Out of the existing techniques, fast pyrolysis of high carbon feedstock is our area of interest.

Rigorous literature survey suggests that the pyrolysis bio-oil derived from agricultural wastes like coconut coir is an attractive renewable energy resource due to its high abundance and carbon neutrality (Nematollahi et al. 2016). A High heating value in the range of 25–40 MJ/Kg is sufficient to support smooth functioning of transport, storage etc. hence stands in par with the commercial fuel in the market. Bio-oil can be effectively used in turbines and other heating systems as well as can be added to the refinery feedstock or catalytically upgraded to produce petroleum grade refined fuels. As much as the advantages that the current biomass pyrolysis process tend to possess, the major drawback that negates these advantages is the high capital expenditure and the extensive complexity associated with the system as well

as the paradoxical environmental threat that is associated with the heat generation unit. Hence, we plan to implement a solar embedded fast pyrolysis process in tandem with the existing electrical heating to rectify the existing drawbacks and make the process relatively feasible (Lesage and Graaf 2010). This work thoroughly focuses on studying various aspects of incorporating the use of solar energy to mitigate the existing drawbacks and develop a ground-breaking technology to develop alternative fuel for a greener future.

3   Research Methods

3.1   Design and Classification of Solar Energy Embedded Fast Pyrolysis

Keeping in mind the credibility of pyrolysis as a prominent candidate in a step towards greener future, it also does come with its own set of drawbacks. Two of its most major drawbacks its energy and capital intensity and its contribution towards global warming (a paradox). As much as the product derived from the biomass pyrolysis process can be considered as a promising alternative fuel due to their sustainability and CO_2 neutrality, the drawback exists due to the inexistence of clean techniques to generate massive amount of heat energy that is required to carry out the pyrolysis reactions at around 500 °C. Although there do exist quite a few heating systems, for example, the burning of the fossil fuels being a prominent type which tend to produce CO_2 responsible for pollution or the electrical heaters tend to make the system extremely complex. In the present study, these drawbacks can be eliminated as we plan on combining the use of solar energy with the existing electrical heating system, which would not only make the process eco-friendly but also energy efficient. In this proposed solar embedded pyrolysis system, external parabolic solar heaters would be used for uniform heating (Sivakumar and Mohan 2010).

3.2   Classification of Solar Energy Embedded Fast Pyrolysis

High cost for heat supply has been the major concern for any type of pyrolysis. Providing an external heating source to an extent of 600 °C continuously is expensive, perhaps equivalent to that in a refinery, which is technically impossible to achieve in rural areas and by any chance does not makes the process feasible. Hence, the aim to lower air pollution and pressure on conventional resources remains unchanged. On contrary, the amount of green-house gases released into the atmosphere is hazardous over a longer run (Shen et al. 2016). The proposal of solar embedded pyrolysis should pacify the situation, since the issue with respect to heating is been taken care of. The installation is a one time investment and can be set up parallel to the solar

farms. We could further sub divide the classification into semi solar plant. Where a certain fraction of heat could be externally supplied. The foci of solar radiations achieves extreme temperatures and remains constant for an optimum time span of 5–6 h enough for one cycle of fast pyrolysis. Moreover a backup heating system can make up for cloudy, shady and rainy days. The design is subject to debate, but the results seem to be promising.

3.3 Design of Setup

Reactor design is essentially important when it comes to solar assisted pyrolysis due to its structure (Zakir et al. 2014). The process seems to be complicated due to the addition of solar panels, which require more space and fixed angle of installation, hence the size design and specification of the reactor is dependent on that of the panels. A hypothetical blueprint of continuous solar heating system consisting of sliding solar concentrator and rotating reactor is shown in below. The array of rays refracted from the panels onto the reactor should be sufficient enough to increase the temperature of the reactor upto the desired value for a stretch of approximately 4–5 h, sufficient for a cycle run. One of the major aspects of a pyrolysis system is the design of the Reactor. A rough design of the setup has been made considering the complexity of the system, and an ability to provide uniform heat to the feed. A parabolic solar heater would be used to capture the rays, which then reflect onto the pyrolysis reactor to uniformly raise the temperature of the feed material upto its optimum level.

3.3.1 Energy Input for Heating

High cost for heat supply has been the major concern for any type of pyrolysis. Effectiveness of the pyrolysis is defined as the total quantity of energy required to decompose per unit of produce. Hence, application of solar energy might drastically reduce cost of heating. Hence use of additional energy resources; preferably, renewable sources like solar energy can drastically reduce the energy load of the fast pyrolysis process. Studies suggest that in order to decompose 1 kg of Coconut coir, 15 kg of fuel would be required in one cycle, keeping in mind the low heating values of coconut coir, which means an approximate energy consumption of roughly 80–90 MJ for completion one fast pyrolysis cycle. On the other hand, these figures can be drastically improved by incorporating the use of solar energy as for the fuel requirement for the process can be reduced by roughly 5 kg. Our current focus is only to use both conventional heating and solar heating simultaneously, but if solar heating upto 500 °C can be achieved economically, and then the need for conventional heating systems can be successfully eliminated (Richardson et al. 2015).

3.3.2 Environmental Aspect

It is a well-known fact that existing conventional heating systems using existing energy sources pose a serious threat to the environment. Conventional pyrolysis process itself is a source for greenhouse gases like Carbon monoxide, Carbon dioxide, Methane, and Nitrous oxides. With Coconut coir constituting about 60% of Carbon, 1 kg Coconut coir thereby contributes for roughly 3 kg of Coconut coir along with Sulphur and Nitrogen oxides competitive to the likes of existing fuels. Further, an ideal pilot scale pyrolysis process with a respective amount of coconut coir biomass itself would produce roughly upto 10 kg of GHG emissions in a single cycle for achieving the decomposition temperatures. Hence although the environmental implication with the conventional pyrolysis process is immense, this can to some extent be reduced by incorporating the use of solar energy to an extent that the GHG emissions can be reduced almost two folds per each cycle.

4 Kinetic Modelling

The kinetic study for fast pyrolysis using coconut coir biomass was conducted at different reaction temperatures to effectively depict the order, activation energy and the Arrhenius parameters for the reaction. Following pyrolysis experimental data was taken from the literature highlighted in bold regarding the pyrolysis of coconut coir biomass. In order to determine the kinetic model for, the fractional conversion of f(x) was determined at various extents of reaction using the formula below at four different constant temperatures (600, 700, 800 and 900 °C) and data was tabulated in Tables 1, 2, 3 and 4.

$$\text{Conversion (x)} = (\text{Amount of Sample Taken} - \text{Mass of Unreacted}$$
$$\text{Sample})/\text{Amount of Sample Taken} \tag{1}$$

Table 1 Bio oil yield obtained from fast pyrolysis using 5 g of sample biomass

Residence time (min)	Bio oil yield (wt. %)				
	500 °C	600 °C	700 °C	800 °C	900 °C
5	40	18.6	74.6	74.6	24.4
6	70.8	58.2	75.8	75.8	80
7	69.6	58.8	76.8	76.8	80
8	71.6	64	76.6	76.6	80
9	71.8	68.18	76.8	76.8	80
10	72.8	64.8	76.8	76.8	80
11	72.8	67.8	76.8	76.8	80

Table 2 Conversion function at different temperatures

Time (min)	500 °C	600 °C	700 °C	800 °C	900 °C
5	0.510925623765991	0.205794912979597	0.205794912979597	1.370421011936	0.279713902802604
6	1.231001471671386	0.872273846457381	0.872273846457381	1.418817552542545	1.609437912434341
7	1.190727577757592	0.886731929632611	0.886731929632611	1.461017907311583	1.609437912434341
8	1.256781040082093	1.021651247531981	1.021651247531981	1.452434163362444	1.609437912434341
9	1.265848208044021	1.145075163078451	1.145075163078451	1.461017907311583	1.609437912434341
10	1.301953212686140	1.044124103384041	1.145075163078451	1.461017907311583	1.609437912434341
11	1.301953212686140	1.133203733437731	1.145075163078451	1.461017907311583	1.609437912434341

Table 3 Composition of coconut shell biomass

Component	Percentage (%)
Water solubles	5.25
Hemi-cellulose	0.25
Cellulose	43.44
Lignin	45.84
Ash	2.22

Table 4 Properties taken into consideration for creating compounds in DWSim

Component	CAS-ID	Formula	Molar mass (g/mol)
Cellulose	9004-34-6	$(C_6H_{10}O_5)_n$	162.1406
Lignin	9005-53-2	$C_{81}H_{92}O_{28}$	1513.6

Based on the experimental data we calculated the conversion, conversion percentages, and f(x) conversion function were evaluated at the different temperatures and following plots were made. The plot in Fig. 1 represents the Conversion percentage versus time at different pyrolysis temperatures for the coconut coir pyrolysis process.

The generic rate equation can be given by the below equation

$$\frac{dC}{dt} = kC \tag{2}$$

wherein C denotes the concentration, k is the reaction rate constant at any temperature and t is the time.

Now we rearrange the terms and integrate both sides

Fig. 1 Conversion % versus time plot for the given pyrolysis reaction
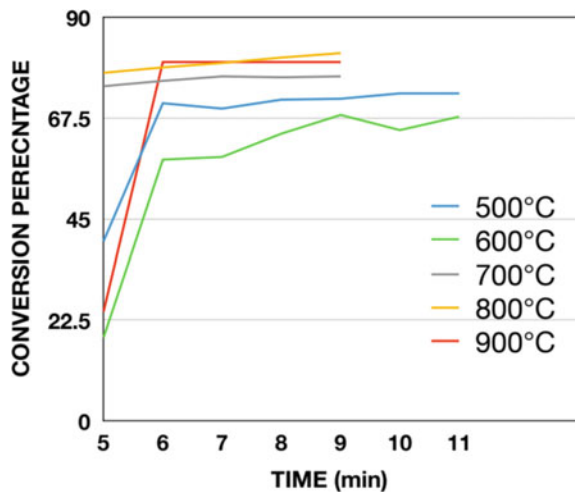
$$\int_{Co}^{C} dC/C = \int_{0}^{t} kdt$$

Co is the initial concentration

$$\ln(C) - \ln(Co) = kt$$

$$\ln(C/Co) = kt$$

Now we convert concentration in terms of initial concentration and conversion which is given by

$$C = Cox - Ea/RT$$

Therefore, we get

$$\ln(x) = kt \tag{3}$$

Here x denotes the fractional conversion.

We plot a graph between ln(x) versus t in Fig. 2, this equation is in the form of y = mx, after plotting the graph we determine the slope = k.

Then we use the Arrhenius equation

$$k = Ae^{-Ea/RT} \tag{4}$$

Now apply natural logarithm (ln) both sides, we get

Fig. 2 F(x) versus time plot for the given pyrolysis reaction
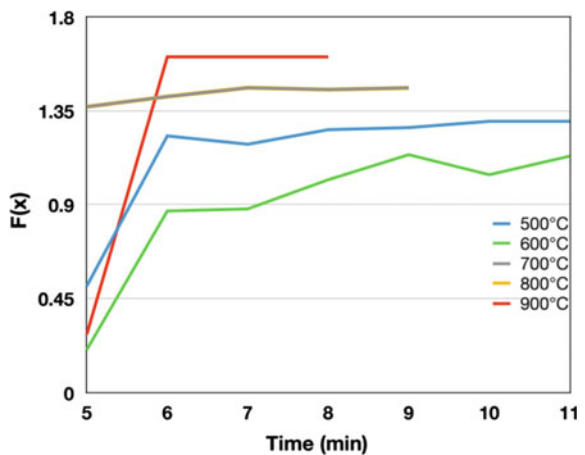
Fig. 3 Arrhenius plot
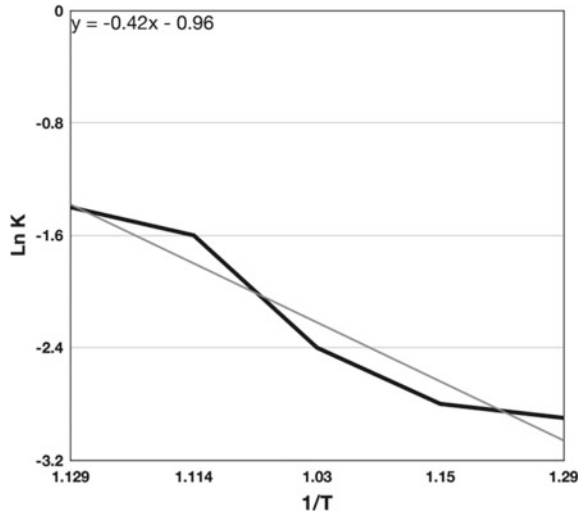
$$\ln(k) = \ln(A) - (Ea/RT) \tag{5}$$

Using the Arrhenius plot in Fig. 3, we verified the order of biomass pyrolysis reaction.

From the graph we get,

$$y = -0.42x + (-0.96) \tag{6}$$

By comparing Eqs. (5) and (6) we get,

$$Slope = -0.42 = Ea/R$$

$$Ea = 3.38 \, KJ/mol$$

$$\ln(A) = (-0.96)$$

$$A = \exp(-0.96)$$

$$A = 0.383$$

$$Rate = 0.383 * \exp(3.38 \, KJ/RT) \, g \, char/g \, cat \, min$$

Thus, we evaluated the conversion, order, Arrhenius parameter, activation energy and the rate of the coconut coir pyrolysis reaction.

5 Simulation

Figure 4 describes the simulation on DWSim. Peng-Robinson was the chosen thermodynamic model since it is the most used method for thermochemical processes as per literature (Molino et al. 2016). The real life pyrolizers by virtue are isothermal and function at a steady state.

The closest possible reactor setup and environment that can be generated on DWSIM is the RGIBBS reactor since it calculates results based on reduction of overall Gibbs energy. Bio char has been considered solid comprising of only fixed carbon (Hassan et al. 2016). Coconut shell biomass (coir) are heavily composed of cellulose and lignin as shown in Table 3. A decomposition reaction of cellulose and lignin has been thereby carried out. The reaction is a conversion of nonconventional components within a simulator to conventional components (White et al. 2011). Decomposition counts for high necessity since reactors in DWSIM cannot perform calculations based on phase and chemical equilibrium for nonconventional components.

As cellulose and lignin are non-conventional compounds and hence need to be created using the compound creator in DSWIM. Since the software doesn't have any provision to accept ultimate and proximate analysis of the compound as in ASPEN, we opted for an alternative route. The software DWSim demands certain data requirements such as CASID, molecular weight and generic molecular formula, and on feeding the required data the resultant important data such as enthalpy of formation, breakdown etc. are calculated automatically (French and Czernik 2010). Further, for more precision in data input, the software also has a flowsheet, which allows selection of bonds (aldehyde, ketonic, carboxylic, double and triple carbon bonds) which has been used with reference from the literature. Table 4 depicts the properties taken into consideration to create compounds to thereby perform the simulations.

Fig. 4 Simulation on DWSim
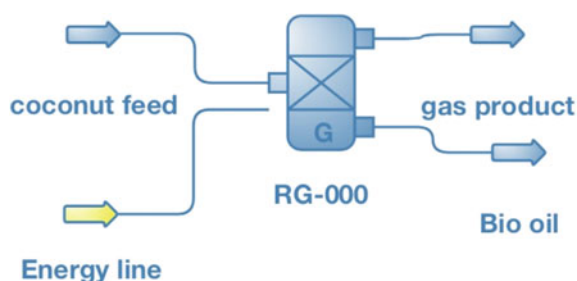
5.1 Observation and Analysis

It is observed that from Fig. 5 for reaction temperature less than 550 °C carbon dioxide (CO_2) has the maximum yield (%) while hydrogen gas (H_2) being the least and for the reaction temperature greater than or equal to 550 °C the carbon monoxide (CO) has the maximum yield (%) while hydrogen gas (H_2) being the least.

From Fig. 6 it is observed that for pressure less than 3 atm carbon monoxide has the maximum yield while carbon dioxide being the least and for pressure greater than 3 atm. Hydrogen gas (H_2) has the maximum yield while CO_2 being the least. From Fig. 7 it is observed that as the pressure increases the yield of bio-gas increases
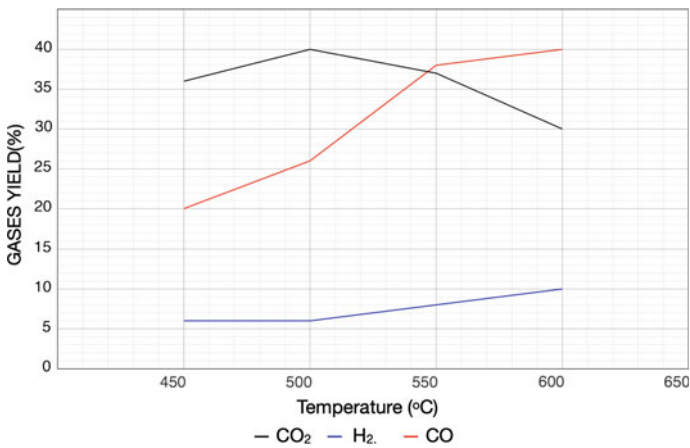
Fig. 5 Effect of reaction temperature on gas yield
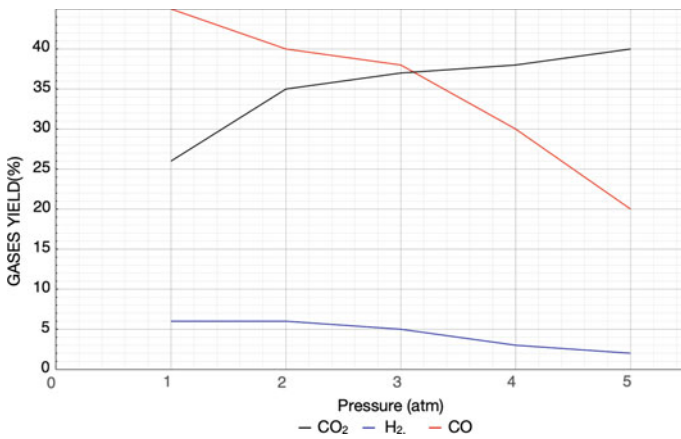
Fig. 6 Effect of pressure on gas yield
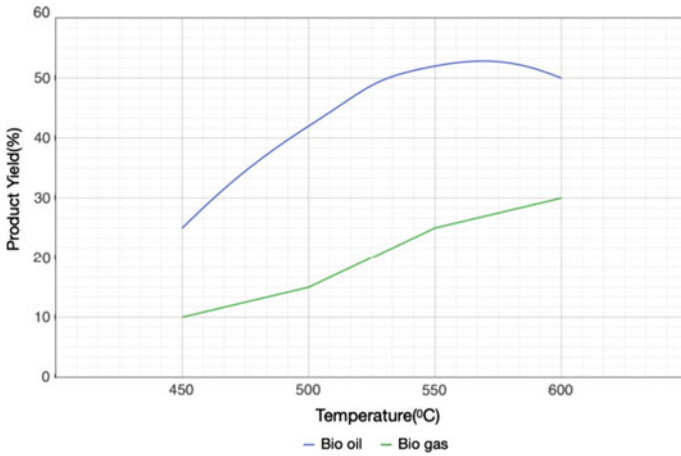
Fig. 7 Effect of temperature on product yield

and the yield (percentage) of bio-oil decreases. From Fig. 8 it can be concluded that, as the temperature increases the yield (percentage) of Biogas increases while the yield (percentage) of bio-oil increases until temperature less than 575 °C and then decreases on further increase in temperature.

The product yield was calculated according to the following equation

$$\text{Product Yield}\ (\%) = \frac{\text{kg Product}}{\text{kg Biomass}} \tag{7}$$
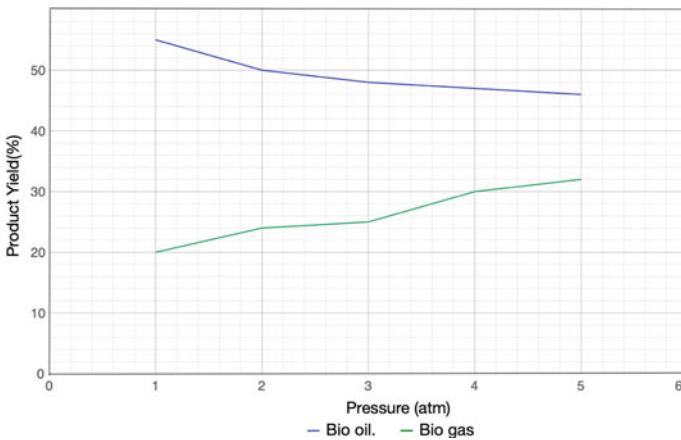
Fig. 8 Effect of pressure on product yield

It can be safely concluded that temperature is the strongest influencing parameter between the two. Pyrolysis above 550 °C encourages gasification, that is the yield of biogas increases and bio oil decreases. This is primarily due to occurrence of secondary decomposition (Bridgwater 2011; Burhenne et al. 2013; Mohanty et al. 2011; Bulushev and Ross 2011; Yaman 2004). The results show that a moderate balance between the two is the optimum condition. The ideal condition for maximum production of bio oil over biogas is 550 °C at one atmosphere. The graphs tend give us a replicated version of the actual experimentation (Czernik and Brigdwater 2004). It gives the approximate values of production that we can expect accordingly and hence shall help us maximize the production with the use of idle catalyst. The simulated temperature might be difficult to achieve, but upon using catalyst and in an in-situ environment we can succeed in lowering the threshold value to around 500 °C and hence improve the economic feasibility of the process.

6 Results

Due to lack of experimental data to carry out simulations, certain assumptions were made to carry out the simulation in limited scope for a near accurate result. Feedstock studies showed Cellulose and Lignin were the major components of coconut shell biomass hence the pyrolysis process was replicated as a Lignin/Cellulose decomposition reaction by creating these compounds on DWSim compound creator. From the simulation process, certain key observations were made in regards with trends of pyrolysis product yields with respect to temperature and pressure. It could be clearly observed that at temperatures up to 550 °C the product yields of both bio-oil and biogas were increasing, at 550–575 °C maximum yield of bio-oil can be obtained and at temperatures above 575 °C biogas remains predominant. It could also be observed that at one atm pressure, the bio oil yield is maximum and biogas yield is minimum and as the pressure increases, the Bio-oil yield goes on decreasing and the bio-gas yield goes on decreasing. Further as certain key reactants were missing from the Simulation considerations due to data limitations, the predominant product from the simulation tends to be gaseous and hence the gaseous yield with respect to temperature and pressure were observed.

7 Conclusions

Simulations replicated as Decomposition of Lignin and Cellulose showed the product yields were predominantly gaseous components like Carbon monoxide, Carbon-dioxide and Hydrogen gas and that the product lacked furfurals, phenols that form the major part of Bio-oil liquid product. Simulation results on the other hand did make us understand the reaction parameters that would be needed to carry out the Pyrolysis experiments. From the observation, it can be concluded that a reaction temperature of

550 °C and 1 atm pressure would be the ideal condition. Although creating a 550 °C environment tends to remain a highly energy intensive process, the point to note here is that simulations don't involve the use of catalyst, hence for a practical purpose using the catalyst ZSM-5 would drastically reduce the energy needs hence thereby making it a feasible process. The novelty of our project is that existing research only includes work on either Biomass pyrolysis to produce Bio-oil or external stabilization of Biomass derived pyrolysis oil using catalysts, our project if successful would be a one of its kind where the the pyrolysis as well as the stabilization and purification of the Bio-oil pyrolysis product could be achieved within a single system hence reducing the energy intensity and providing an economical solution. In conclusion, we were able to obtain the desired results with the limited scope of data available with us and now we plan to perform the experiments at the university and compare the simulated results and hence design a process that would generate alternative fuels on a commercial scale from biomass. Furthermore, we also plan to develop a kinetic model to strengthen the technical foundation of our project, which would then help us understand the true potential of our project for future endeavors.

References

Bridgwater AV (2011) Review of fast pyrolysis of biomass and product upgrading. Biomass Bioenergy 38:68–94

Bulushev DA, Ross JRH (2011) Catalysis for conversion of biomass to fuels pyrolysis and gasification: a review. Catal Today 171:1–13

Burhenne L, Messmer J, Aicher T, Laborie MP (2013) The effect of the biomass components lignin, cellulose and hemicellulose on TGA and fixed bed pyrolysis. J Anal Appl Pyrol 101:177–184

Czernik S, Brigdwater AV (2004) Overview of applications of biomass fast pyrolysis oil. Energy Fuels 12:590–598

French R, Czernik S (2010) Catalytic pyrolysis of biomass for bio fuels production. Fuel Process Technol 91:25–32

Hassan H, Lim JK, Hameed BH (2016) Recent progress on biomass co-pyrolysis conversion into high quality bio-oil. Bioresour Technol 221:645–655

Islam MR, Islam MN, Nabi MN (2004) Design, fabrication and performance study of a biomass solid waste pyrolysis system for alternative liquid fuel production. J Energy Environ 3:103–117

Lesage D, Graaf TV (2010) Global energy governance in a multipolar world. Imprint Routledge, London

Meng A, Chen S, Zhou H, Long Y, Zhang Y, Li Q (2015) Pyrolysis and simulation of typical components in wastes with macro-TGA. Fuel 157(3):1–8

Mohanty P, Pant KK, Naik SN, Das LN, Vasudevan P (2011) Fuel production from biomass: Indian perspective for pyrolysis oil. J Sci Ind Res 70:668–674

Molino A, Chianese S, Musmarra D (2016) Biomass gasification technology: the state of the art overview. J Energy Chem 25(1):10–25

Nematollahi O, Hoghooghi H, Rasti M, Sedaghat A (2016) Energy demands and renewable energy resources in the Middle East. Renew Sustain Energy Rev 54:1172–1181

Richardson Y, Drobek M, Julbe A, Blin J, Pinta F (2015) Biomass gasification to produce syngas. In: Recent advances in thermo-chemical conversion of biomass, pp 213–245

Shen Y, Wang J, Ge X, Chen M (2016) By-products recycling for syngas cleanup in biomass pyrolysis—an overview. Renew Sustain Energy Rev 59:1246–1268

Sivakumar K, Mohan NK (2010) Performance analysis of downdraft gasifier for agri-waste biomass materials. Indian J Sci Technol 3(1):58–60

Tanneru SK, Steele PH (2015) Direct hydrocracking of oxidized bio oil to hydrocarbons. Fuel 154:268–274

White JE, Caterllo WJ, Legendre BL (2011) Biomass pyrolysis kinetics: a comparative critical review with relevant agricultural residue case studies. J Anal Appl Pyrol 91:1–33

Xianjun X, Zongkang S, Peiyong M, Jin Y, Zhaobin W (2015) Establishment of three components of biomass pyrolysis yield model. Energy Procedia 66:293–396

Yaman S (2004) Pyrolysis of biomass to produce fuels and chemical feedstocks. Energy Convers Manage 45:651–671

Zakir HM, Hasna HQ, Uddin MM, Ahmed MT (2014) Municipal solid waste (MSW) as a source of renewable energy in Bangladesh: revisited. Renew Sustain Energy Rev 39:35–41

Zhang Y, Brown TR, Hu G, Brown RC (2013) Techno economic analysis of two bio oil-upgrading pathways. Chem Eng J 225:895–904

Zhao YH, Wen H, Xu ZH (2006) Conceptual design and simulation study of a co-gasification technology. Energy Convers Manage 47(11–12):1416–1428

Zheng HX, Kaliyan N, Morey RV (2010) Aspen plus simulation of biomass-integrated gasification combined cycle systems at corn ethanol plants. Biomass Bioenergy 56:197–210

Study of Some Magnetic Effects of Mg Substituted Hexaferrite in Nano Range

Jasvinder Singh

Abstract The constitution and magnetic effects Y-Type of Hexaferrite have been explored for the manufactured material $Ba_2Mg_2Al_{x/2}Cr_{x/2}Fe_{12-x}O_{22}$, using FTIR, XRD and VSM. The acquisition of granule size that remains in nano area is well supported from the VSM analysis. Existence of two different noticeable spikes near around 550–600 cm^{-1} directed toward 500–600 cm^{-1}. FTIR analysis clearly demonstrates the creation of hexaferrite. Further from VSM study, it has been noticed that with rising the number of co-dopants the escalation in retentivity and magnetization for x = 0 along with x = 0.5. From graph it was clearly noticed that zero coercivity reveals the super-paramagnetic nature is present in the material.

Keywords Nanomaterials · Materials characterization · Sol-gel auto combustion method · Nano-ferrites · Hexaferrite

1 Basic Survey

Advancement of ferrites materials is a great advancement in the various branches of the nanotechnology in last few decades. The swap of Barium in hexaferrite has major meaningful finding for the modern science as a result of they are part and parcel of a collection of electrical gadgets passed down in many parts of surgical accompaniments, transmission, dissemination and production of sound energy, telephonic ringers and image processing (Jotania and Virk 2012). Hexaferrite or commonly known as Y-type hexagonal ferrite has been a pioneered material for this type operations and it is being lucrative for scientists from long time. These ferrites are level headed of Y-type Magnesium hexagonal, continuing a hexagonal configuration, along with the easy lines of magnetization onward with the c-axis. Though, Co_2Y, Mg Y are famous as ferroxplana ferrites as they have a basal plane of magnetization (Haijun et al. 2002).

J. Singh (✉)
VSS University of Technology, Burla, India
e-mail: jpsvirdi@gmail.com

833

To study characteristics of Nano-ferrites many approaches have used in past like oxidation in nitric acid, solution-gel auto combustion method, co-precipitation, ammonium nitrate melt, etc. Though further to this, many synthetic procedures such as spray pyrolysis, combustion or ignition method, micro-emulsion technique, hydrothermal reaction sintering, glass crystallization, mechanical grinding has been explored widely (Sözeri 2009; Virdi 2018; Radwan et al. 2007; Sözeri et al. 2011; Junliang et al. 2009; Ren et al. 2006; Liu et al. 1998, 1999; Rezlescu et al. 1993; Jin et al. 1998). The solution–gel method auto combustion arrangement is leading, easier and low cost extensively used for the preparation of hexagonal ferrites. By using solution–gel arrangement auto combustion method, it is conceivable to extract to structure of microscopic particles for securing useful possessions for nanoparticles.

This work, explored the accouterment for Mg replacement of Ba_2^+ in barium exchanged Y-type hexagonal ferrites ($Ba_2Mg_2Al_{x/2}Cr_{x/2}Fe_{12-x}O_{22}$) manufactured by solution gel approach. In this work constitutional and magnetic properties is explored using Fourier Transform Infrared Spectroscopy (FTIR), X-ray diffraction (XRD) and Vibrating sample magnetometer (VSM).

2 Characterization Techniques

The sample that we prepared ($Ba_2Mg_2Al_{x/2}Cr_{x/2}Fe_{12-x}O_{22}$) i.e. the Y-type hexagonal ferrites powders have been symphonized via solution–gel approach along with Barium Nitrate ($Ba(NO_3)_2$), ($Al(NO_3)_3 \cdot 9H_2O$) Aluminum Nitrate nona hydrate, ($Cr(NO_3)_3 \cdot 9H_2O$) Chromium Nitrate nona hydrate, ($Fe(NO_3)_3 \cdot 9H_2O$) Ferric nitrate nona hydrate and ($C_6H_8O_7 \cdot H_2O$) Monohydrate citric acid. ($Mg(NO_3)_2 \cdot 6H_2O$) Magnesium Nitrate Hexahydrate, Aqueous solution of metal salts and iron are refined independently in stoichiometric ratio by rendering them with water.

Salt solution along with aqueous solution of citric acid is mixed to the further with cations to citric acid molar ratio of 1:1.5. To maintain the 7 pH values of this mixture, we further add ammonium hydroxide solution as drop by drop. Now this solution kept in oven at 80–85 °C almost for 4–6 h with continued exhilarating with help of magnetic stirrer. This liquid now changing in the direction of through to a uniform brown colored gel as the evaporation of prepared liquid starts. Then this solution is dried by using a hot plate at 280–300 °C at least minimum for 3 h to form the forerunner material. Now for continuous 2 h pre-sintering is done at 500 °C. At last the forerunner material is calcined at different temp such as 750, 950, 1150 and 1250 °C minimum for 5 h. Now we use some equipment's to know the accouterment of symphonized Y-type hexagonal ferrites.

3 Outcomes and Discussion

3.1 Constitutional Effects

3.1.1 FTIR Study

FTIR Spectroscopy clearly demonstrates the change in, constitutional and phase transfer present in the material in the course of combustion along with sintered operation.

For the prepared sample $Ba_2Mg_2Al_{x/2}Cr_{x/2}Fe_{12-x}O_{22}$, the infrared spectra of prepared was recorded in the domain 4000–400 cm^{-1}. The ideal spectra for the chosen material $Ba_2Mg_2Fe_{12}O_{22}$ is displayed in Fig. 1 at pH = 7. The band has the domain of 4000–400 cm^{-1}. We can here observe presence of dominant absorption bands at domain of 400–600 cm^{-1}, along with 1250–1600 and 3600–4000 cm^{-1}. Furthering addition to this, the band in the territory of 1250–2000 cm^{-1} indicates the existence of carboxylic acid and nitrile. We can observe for the sample descending spike at 2400 cm^{-1} which is due to existence of OH$^-$. The band from range 3400 to 4000 cm^{-1} displays the expanding of hydroxyl group which clearly demonstrates the existence of free or absorbed moisture in the material.

Correspondingly Spectra corresponding to sample $Ba_2Mg_2Al_{0.25}Cr_{0.25}Fe_{11.5}O_{22}$ is displayed in Fig. 2 at pH = 7. In the territory of 4000–400 cm^{-1}, we can see the band. Similarly in the territory of 400–600 cm^{-1}, along with 1250–1600 cm^{-1} and also 3500–3900 cm^{-1} we can observe the dominant absorption band. Further we can see some band authorized to be responsible for widening of metal oxygen bonding in the territory of 400–600 cm^{-1}, which is the characteristics of hexaferrites. Further, indication the existence of carboxylic acid and nitrile in the band in the territory of

Fig. 1 FTIR spectra of $Ba_2Mg_2Fe_{12}O_{22}$

1250–1700 cm^{-1}. At last the band from territory 3400–4000 cm^{-1} shows existence of free or absorbed moisture that exhibit the expansion of hydroxyl group.

Likewise, the spectrum for the sample $Ba_2Mg_2Al_{0.5}Cr_{0.5}Fe_{11}O_{22}$ is plotted in Fig. 3 at pH = 7. The band is in the territory of 4000–400 cm^{-1}. It is clearly visible that in territory of 400–600 cm^{-1}, along with 1250–1600 cm^{-1}, and also 3500–3900 cm^{-1}. It has the dominant absorption band. The widening of metal oxygen bonding which is the properties of hexagonal ferrites is in the territory of 400–600 cm^{-1}. Again, the band in the territory of 1250–1800 cm^{-1} demonstrates the existence of carboxylic acid and nitrile.

Fig. 3 FTIR spectra of
$Ba_2Mg_2Al_{0.5}Cr_{0.5}Fe_{11}O_{22}$
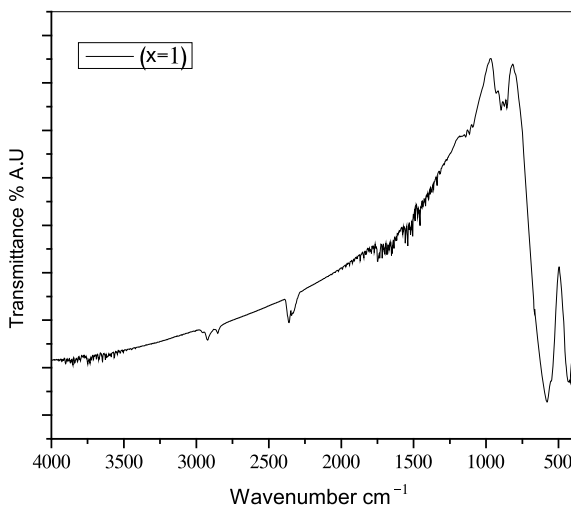
3.1.2　XRD Study

For the given material $Ba_2Mg_2Al_{x/2}Cr_{x/2}Fe_{12-x}O_{22}$ ($x = 0, 0.5, 1.0$) nanoparticles we studied the X ray diffraction pattern in Fig. 4. For continuous 6 h at a temperature of 1000 °C. The standard crystallite dimension of the nano-crystalline hexagonal ferrite symphonized at distinct molar ratios of substitution for the spikes was estimated from the XRD data applying the Scherrer formula.

$$D = \frac{k\lambda}{\beta \cos\theta} \tag{1}$$

Here D is known as crystallite dimension. λ is known as X-ray wavelength (1.54 Å). For hexagonal systems, the shape factor of K could be from the range 0.62 to 2.08 and is usually taken as about 0.89. It was observed practically erect out at 44.9434 nm for $x = 0$, and simultaneously 57.9684 nm for $x = 0.5$ along with 38.379 nm at $x = 1$.

For calculation of the cell volume (V) and the lattice constant (a and c) with given formula below.

$$\frac{1}{d_{hkl}^2} = \frac{4}{3}\left[\frac{h^2 + hk + k^2}{a^2}\right] + \frac{l^2}{c^2} \tag{2}$$

$$V = 0.8666a^2c \tag{3}$$
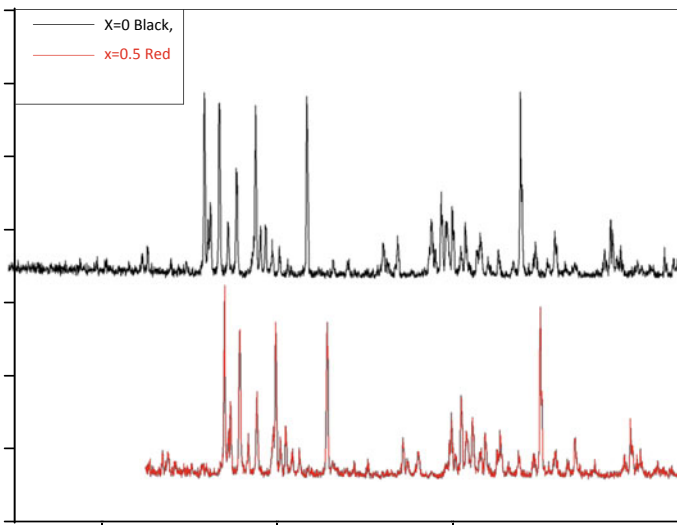
Fig. 4 XRD arrangement of hexagonal ferrite $Ba_2Mg_2Al_{x/2}Cr_{x/2}Fe_{12-x}O_{22}$ at distinct composition

Table 1 For hexaferrite, values of distinct parameter

S. No.	1	2	3
Materials	X = 0	X = 0.5	X = 1
Lattice constant (Å)	4.40	5.85	5.87
Lattice constant (Å)	47.86	44.432	39.76
Cell volume (Å)	802.956	1317.12	1187.24

For all given samples with different concentrations, the lattice parameters of symphonized material were calculated and is shown in Table 1 at pH = 7. It was clearly visible that with increase in dopants there is decrease in c and increase in a.

3.1.3   VSM Study

Figures 5, 6 and 7 demonstrates the room temperature hysteresis loop graphs. For all the Nano dimension samples, at least for 6 h at 1000 °C is sintered with the chemical formula of $Ba_2Mg_2Al_{x/2}Cr_{x/2}Fe_{12-x}O_{22}$. From the loops, the amount of saturation magnetization (Ms) along with coercivity (Hc) for all given material were accomplished, From figure it is clear that, the saturation magnetization was moderately raised with by an increase in substitution content It is found that coercivity is zero for the value $x = 0$ and $x = 0.5$, which clearly demonstrates sample is super-paramagnetic in essence and where for $x = 1$, it is 838.7025. With rise in substitution values of the retentivity also gets increasing. All parameters are shown in Table 2 for each sample.
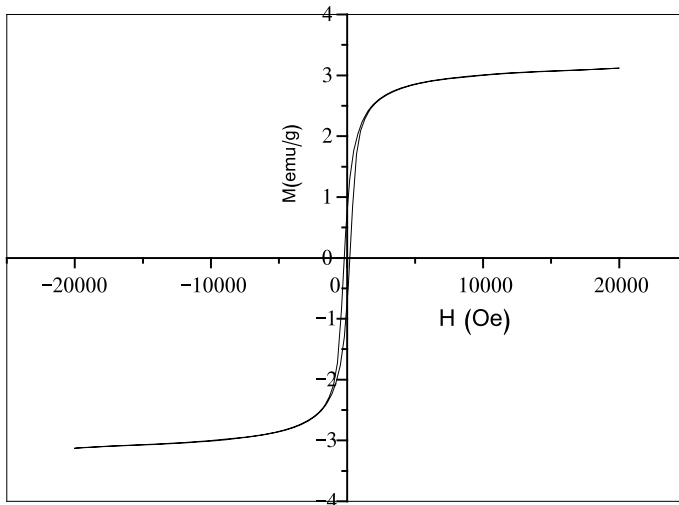
Fig. 5 Magnetic-hysteresis curve for $x = 0$
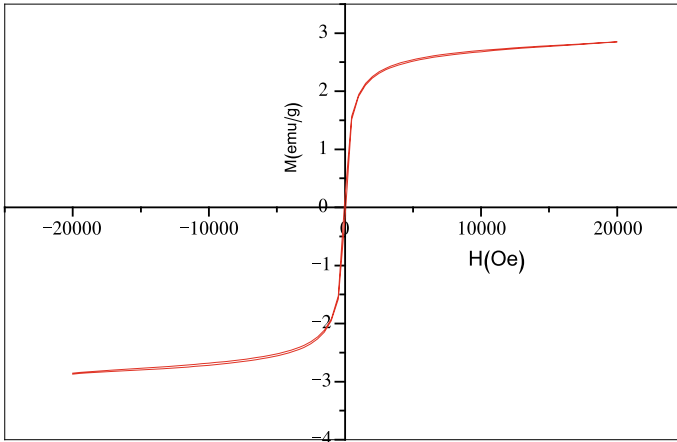
Fig. 6 Magnetic-hysteresis curve for $x = 0.5$
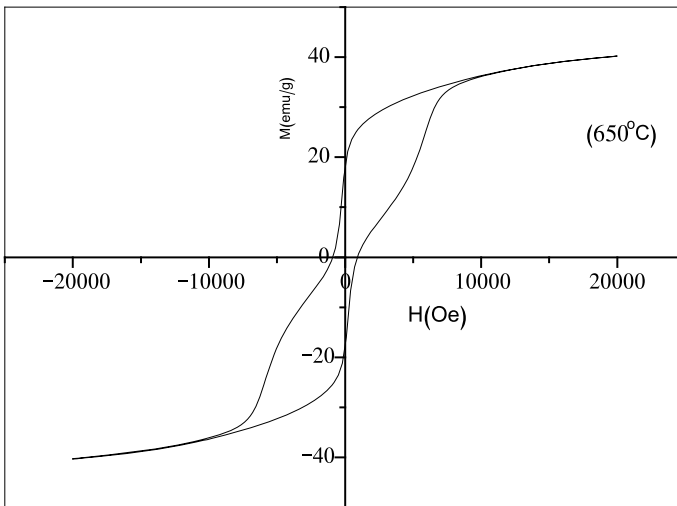
Fig. 7 Magnetic-hysteresis curve for $x = 1$

Table 2 The value of calculated saturation magnetization retentivity, and for coercivity ($x = 0$, 0.5, and 1)

S. No.	1	2	3
Materials	X = 0	X = 0.5	X = 1
Retentivity (Mr) (emu/g)	4609.39	5183.01011	9628.5168
Coercivity (Hc) (Oe)	0	0	838.7025
Saturation magnetization (Ms) (emu/g)	19,441.4095	19,796.5037	21,510.5163

4 Concluding Remarks

The sample has been symphonized using sol–gel auto combustion method technique and was analyzed by using VSMFTIR and XRD. This work clearly demonstrates that the granule dimension lies in nano range from X-ray analysis. FTIR demonstrates the formation of hexaferrite. From existence of two noticeable spikes near 550–600 to 400–600 cm^{-1}. Finally it is confirmed that the sample is super-paramagnetic in nature for coercivity is zero for $x = 0$ along with $x = 0.5$ using VSM plots, further It is observed that with increasing the amount $Al - cr$ the saturation magnetization, retentivity and rise in coercivity, that confirms material is super-paramagnetic in character.

References

Haijun Z, Xi Y, Liangying Z (2002) J Eur Ceram Soc 22:835
Jin Z, Tang W, Zhang J, Lin H, Du Y (1998) J Magn Magn Mater 182:231
Jotania RB, Virk HS (2012) Solid State Phenom 189:209
Junliang L, Wei Z, Cuijing G, Yanwei G (2009) J Alloys Compd 479:863
Liu X, Wang J, Gan LM, Ng SC, Ding J (1998) J Magn Magn Mater 184:344
Liu X, Wang J, Gan LM, Ng SC (1999) J Magn Magn Mater 195:452
Radwan M, Rashad MM, Hessien MM (2007) J Mater Process Technol 181:106
Ren P, Guan J, Cheng X (2006) Mater Chem Phys 98:90
Rezlescu L, Rezlescu E, Popar PD, Rezlescu N (1993) J Magn Magn Mater 193:288
Sözeri H (2009) J Magn Magn Mater 321:2717
Sözeri H, Kucuk I, Ozcan H (2011) J Magn Magn Mater 323:1799
Virdi JPS (2018) IOP Conf Ser Mater Sci Eng 360:012053

Eco-Friendly Ceramic Membranes from Inexpensive Raw Materials and Their Applications

S. Lakshmi Sandhya Rani and R. Vinoth Kumar

Abstract Ceramic membranes provide several advantages over polymeric membranes owing to their outstanding chemical, mechanical and thermal stability, fouling resistance, and longer lifetime. However, industrial applications of commercial ceramic membranes are limited owing to economic constraints, including high-priced raw materials and the necessity of elevated sintering temperatures. Therefore, the fabrication of ceramic membranes from inexpensive and locally abundant raw materials has been gaining interest in recent times. Therefore, several research studies were carried out to produce highly porous and stable ceramic membranes by selecting suitable low-cost raw materials with appropriate additives, including pore formers, binders, and plasticizers. In the present chapter, the recent research studies on the fabrication of ceramic membranes from inexpensive raw materials including kaolin, ball clay, bentonite, perlite, fly ash, rice husk ash, natural pozzolan, etc., are discussed elaborately. Furthermore, the applications of low-cost ceramic membranes are also highlighted in this chapter.

Keywords Ceramic membrane · Inexpensive · Raw materials · Applications

1 Introduction

A membrane is generally described as a selective/semipermeable barrier present between two phases and that allows specific components from one side to another side under the influence of a driving force. This driving force might be a gradient in pressure, temperature, concentration, electric potential, etc. A virtual representation of a basic membrane separation process is given in Fig. 1. Membranes can be categorized concerning different viewpoints. According to the nature of the membrane, they can be classified into biological or synthetic membranes. Synthetic membranes can be broadly differentiated into polymeric (organic) and inorganic membranes

S. Lakshmi Sandhya Rani · R. Vinoth Kumar (✉)
Department of Chemical Engineering, National Institute of Technology Andhra Pradesh, Tadepalligudem, Andhra Pradesh 534101, India
e-mail: vinoth@nitandhra.ac.in
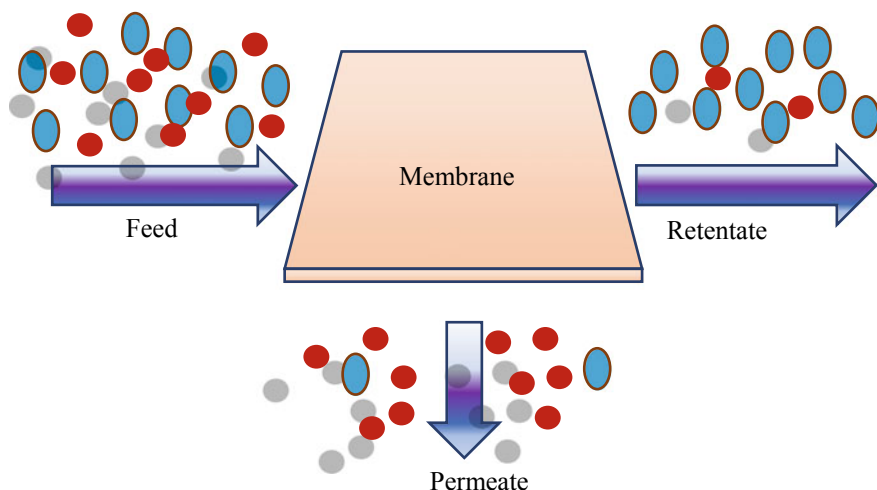
Fig. 1 Schematic representing basic membrane separation process

(glass, metal, ceramics, etc.). Among them, ceramic membranes provide excellent thermal and mechanical stability, high chemical resistance. These properties allow the regeneration of the membrane by using harsh chemicals and mechanical means, which leads to a longer lifetime of the membrane.

Based on the structure of the membrane, they can be classified into asymmetric and symmetric membranes. In asymmetric membranes, the bottom macro-porous layer usually provides mechanical support, whereas the relatively dense and thin top layer does actual separation. Therefore, intermediate layers are placed between support and selective top layer to reduce the pore size gradually.

Titania, alumina, silica, and zirconia are few inorganic precursors that are commonly used to fabricate commercial ceramic membranes. However, the aforementioned materials are highly expensive, causing the rise in the overall price of the membranes (500–3000 $/m^2). In addition, they require high sintering temperatures more than 1200 °C for the membrane manufacturing process, which leads to high operating costs. To avoid these economic constraints, several researchers are focusing on preparing ceramic membranes using inexpensive raw materials.

In recent times, the usage of inexpensive raw materials in ceramic membrane fabrication is gaining interest because valuable ceramic membranes can be prepared at a relatively lower price. This chapter presents the recent studies on the fabrication of ceramic membranes using various low-cost precursors, including kaolin, ball clay, bentonite, rice husk ash, etc. In addition, applications of ceramic membranes were presented in detail.

2   Raw Materials

To replace the highly-priced inorganic precursors, various low-cost and highly abundant raw materials are chosen by several researchers. Natural earth minerals including kaolin clay, bentonite, dolomite, perlite, pozzolan, etc. have been used to synthesize ceramic membranes. A few research studies focused on the fabrication of ceramic membranes from waste materials such as coal fly ash, sugarcane bagasse ash, and rice husk ash. These alternative raw materials are gaining popularity because the ceramic membranes synthesized using these materials perform well exhibiting excellent mechanical stability, high chemical resistance, and operability at elevated temperatures. Further, this chapter discusses these alternative or low-cost raw materials as follows:

2.1   Kaolin

Kaolin ($Al_2Si_2O_5$ $(OH)_4$) is one of the most abundant mineral clay which is being extensively used for ceramic membrane preparation (Nandi et al. 2008; Hubadillah et al. 2018b). It is also called soft clay and China clay. It is odorless and white to yellowish. Kaolin mainly contains a mineral called kaolinite ($Al_2O_3(SiO_2)_2$ $(H_2O)_2$), along with other minerals including dickite, halloysite, nacrite, and anauxite. It has unique special properties such as finer particle size, brightness, glossiness, abrasiveness, viscosity, and excellent hydrophilicity (Indian Bureau of Mines 2016). Kaolin is widely available in various countries, namely; China, Germany, India, and Malaysia, at a much lower cost. The melting point of kaolin is very high in the order of 740–1785 °C. When kaolin group minerals are heated, there will be two heat effects: endothermic at nearly 550 °C and exothermic at approximately 950 °C. The endothermic effect occurs because of the dissociation of kaolin minerals into water vapor and an amorphous mixture of alumina and silica.

In contrast, the exothermic effect occurs due to the crystallization of alumina (Insley and Ewell 1935). A study demonstrated that significant endothermic mass loss was observed between 450 and 600 °C temperatures. Minimum weight loss was identified above 500 °C. Endothermic mass loss below 500 °C is due to the dehydration of kaolin to produce amorphous metakaolin ($Al_2Si_2O_7$), Eq. (1). This process continues upto 925 °C (Wang et al. 2011).

$$2Al_2Si_2O_5(OH)_4 \rightarrow 2Al_2Si_2O_7 + 4H_2O \tag{1}$$
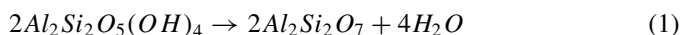
Amorphous metakaolin turns into crystalline form when the sintering temperature exceeds 925 °C (Insley and Ewell 1935). After that, kaolin transforms into a mullite phase. Mullite is the most desirable material for the preparation of ceramic membranes as it offers enhanced thermal stability, mechanical strength, less thermal expansion coefficient, and low thermal conductivity.

2.2   Ball Clay

Ball clay consists of kaolinite, mica, and quartz. This clay differs from kaolin in terms of plasticity. It has very high plasticity, binding power, and tensile strength. In general, ball clay used to be mixed with non-plastic clay to attain desired plasticity (Indian Bureau of Mines 2016). As a result, the availability of ball clay is relatively less when compared to kaolin. In total, 83.39 million tonnes are available in India, out of which 16.78 million tonnes are reserves. Nearly 62% of resources are in Andhra Pradesh's state, whereas 38% are in Rajasthan.

In a study, ball clay was used to prepare hollow fiber ceramic membranes using a phase inversion fabrication method. Membranes sintered at 1250 °C showed an excellent combination of membrane properties. At this sintering temperature, the membrane has exhibited a mechanical strength of 55.8 MPa and porosity of 50.5% with 0.61 μm pore size (Abd Aziz et al. 2019). In another study, the ceramic membrane was prepared from a mixture of ball clay and corn starch by compaction method, followed by sintering at 1200 °C. In this study, 20–25 wt.% of starch content was reported as optimum to get desired porosity with enough flexural strength (Bazin et al. 2014). Other research studies on kaolin, ball clay-based ceramic membranes are summarized in Table 1.

2.3   Bentonite

Bentonite is naturally available plastic clay. It was first discovered in Benton, America, and named bentonite. Like Fuller's earth, it has inherent bleaching properties. Therefore, it is also called bleaching clay. Sodium bentonite and calcium bentonite are the two forms of bentonite clay. Generally, sodium bentonite is known as bentonite; calcium bentonite is Fuller's earth based on its swelling properties. As per the reports of the UNFC (United Nations Framework Classification) system, 568 million tonnes of bentonite resources are available in India. Of which 424 million tonnes are in the state of Rajasthan; 134 million tonnes are in the state Gujarat and the rest in the states of Tamil Nadu, Jharkhand, Jammu, and Kashmir (Indian Bureau of Mines 2016). It mainly consists of a clay mineral called montmorillonite, a hydrous aluminium silicate, along with other minerals such as quartz, feldspar, gypsum, volcanic glass, and organic matter (Clem 1961). Montmorillonite adsorbs water to a large extent—industrial applications of bentonite result from its swelling action in the water. Based on the water to clay ratio, a wide variety of applications are available. When the water ratio is less, the mixture will have adhesive properties. If the water ratio is increased, the plastic properties of the system increase. Very high water to clay ratio forms suspensions in which particle size of the bentonite clay decreases as available surface area increases because of the availability of oxygen atoms on the surface of montmorillonite which are highly reactive over other compounds.

Table 1 Low-cost ceramic membranes prepared from kaolin and ball clay as raw materials

Raw materials	Preparation method	Sintering temperature (°C)	Pore former	Binder	Pore size (μm)	Porosity (%)	Flexural strength (MPa)	Cost ($/m^2)	Application	References
Kaolin, quartz, sodium carbonate (Na$_2$CO$_3$), boric acid	Paste casting	850–1000	CaCO$_3$	Sodium metasilicate	0.55–0.81	33–42	3–8	130	MF	Nandi et al. (2008)
Kaolin, quartz, feldspar, boric acid	Paste casting	900	Na$_2$CO$_3$	Sodium metasilicate	0.285	23.6	–	220	MF of mosambi juice	Nandi et al. (2009a)
Kaolin, pyrophyllite ball clay, feldspar quartz	Uniaxial compaction	850–1000	CaCO$_3$	Polyvinyl alcohol (PVA)	0.87–1.10	41–46	25–32	10	MF	Monash and Pugazhenthi (2011)
Kaolin, quartz, boric acid, Na$_2$CO$_3$, sodium meta silicate	Uniaxial dry compaction	900–1000	CaCO$_3$	PVA	2.6–4.94	22–40	22–31	67	–	Vasanth et al. (2011)
Kaolin, quartz, titanium dioxide	Uniaxial compaction	900	CaCO$_3$		0.45–1.3	23–30	10–34	–	MF of the oil–water emulsion	Vasanth et al. (2013)

(continued)

Table 1 (continued)

Raw materials	Preparation method	Sintering temperature (°C)	Pore former	Binder	Pore size (μm)	Porosity (%)	Flexural strength (MPa)	Cost ($/m^2)	Application	References
Kaolin, quartz, boric acid, sodium metasilicate, Na_2CO_3	Uniaxial dry compaction	900	$CaCO_3$	PVA	0.89–1.85	35.4–39.4	7.81–11	78	Mosambi juice clarification	Emani et al. (2013)
Kaolin, quartz, ball clay, pyrophyllite, feldspar	Extrusion	950	$CaCO_3$		0.309	53	12	4	Oily waste water treatment	Vinoth Kumar et al. (2015)
Kaolin, feldspar, quartz, boric acid, titanium dioxide	Paste casting	850–950	Activated carbon	Sodium metasilicate	1.59–2.56	5.59–18.88	–	92	MF	Das et al. (2016)
Kaolin, sand	Extrusion	1250	Starch	–	–	28–48	5–20 MPa	–	Algal concentration	Issaoui et al. (2017)
Kaolin	Dry pressing	1150	Powdery high-density polyethylene	–	–	62	18 MPa	–	MF	Obada et al. (2017)
Kaolin	Extrusion	1000–1250	Starch	–	0.9–1.4	46–60	4–24	–	Support for MF membrane	Bouzerara et al. (2009)

Mixtures with different water to bentonite ratios can be used for bonding, plasticizing, and suspending industries. Sodium montmorillonite absorbs more moisture than calcium montmorillonite which leads to high disaggregation in water and greater viscosity. For this reason, sodium bentonites are used as emulsion stabilizers, drilling muds, and retardant gels. Calcium bentonites are extensively used for the decolorization of oils. In a study, bentonite clay powder and hydrophilic polymer sulfonated polyether ether ketone (SPEEK) was utilized to synthesize polyethersulfone and cellulose acetate membranes. It was reported that the modified membrane provided increased water uptake rate and flux, higher rejection of COD [Chemical Oxygen Demand], and turbidity (Kiran et al. 2015). A few other current research studies on low-cost ceramic membranes fabricated from bentonite clay are illustrated in Table 2.

2.4 Perlite

Perlite is an amorphous aluminosilicate rock formed by the rapid cooling of volcanic lava. In general, they are chemically bonded with water. Based on the water content in the perlites, they can be classified into three types: obsidian (water content <2 wt.%), perlite (water content 2–5 wt.%), and pitchstone (water content more than 5 wt.%) (Maxim et al. 2014). Perlite has a unique property of 4–20 folds expansion when heated at 760–980 °C. Expanded perlite has lower bulk density and thermal conductivity, high surface area, chemical inertness, and thermal resistance. Both crude perlite and expanded perlite have several applications in various fields. One of those applications includes filter aid for wastewater treatment, clarification of fruit and vegetable juices.

In a study, Flat ceramic membrane was prepared from natural Moroccan perlite with the help of a few organic additives and sintered at 1000 °C (Majouli et al. 2011). The prepared membrane is 42% porous having an average pore size of 6.64 μm. Later, they have extended their previous work by preparing perlite-based tubular ceramic membranes to treat tannery, textile effluents, and dicing wafer effluents produced by electronic industries. Initially, tubular ceramic support with perlite was prepared; later, the MF layer of the same material was placed over the ceramic support using the slip casting technique. Obtained MF layer exhibited an average pore size of 0.27 μm (Majouli et al. 2012). In another study, flat perlite ceramic membranes using the dry pressing technique were prepared by Saja et al., to remove turbidity from industrial effluents. Membrane sintered at a temperature of 950 °C shown 1.7 μm average pore size and 52.11% porosity. As a result, they achieved turbidity rejection of 97% for the agro-food industry and 96% rejection for the tannery industry (Saja et al. 2018).

Table 2 Low-cost ceramic membranes fabricated from bentonite

Raw materials	Technique	Sintering temperature (°C)	Pore former	Binder	Pore size (μm)	Porosity (%)	Flexural strength (MPa)	Application	References
Kaolin, bentonite, talc, sodium borate, barium carbonate	Simple pressing	1000	Carbon black	Polyethylene glycol	0.65–1.25	34–44	32–58	Oily waste water treatment	Eom et al. (2014)
Diatomite, kaolin, bentonite, talc, sodium borate, barium carbonate	Simple pressing	1000–1100		Polyethylene glycol	0.29–0.67	34.6–36.3	28–32	Oily wastewater treatment	Eom et al. (2015)
Bentonite extracted near Nador, Morocco	Uniaxial pressing	950	Starch		1.7	32.12	22	Textile industry effluent treatment	Bouazizi et al. (2016)
Bentonite clay from Gabes (Southern Tunisia), Amijel	Extrusion	950–1100	Starch	Methocel	0.8–2.3		9.28–67.61	–	Chihi et al. (2019)

2.5　Natural Pozzolan

An asymmetric tubular ceramic membrane was elaborated in a study from natural pozzolan material to pretreat seawater for desalination. Support and MF layers were prepared using the same pozzolan material with different particle sizes (particle size of $\leq 200\,\mu$m for support and $\leq 40\,\mu$m for MF layer) (Achiou et al. 2017). In this study, the extrusion method fabricated porous ceramic support, whereas the MF layer was deposited inside the tubular support by cross-flow filtration technique. The whole membrane was sintered at 950 °C. Pore sizes of support and MF layer were reported as 8.18, 0.36 μm.

In another study, Beqqour et al. tried to enhance the porosity of low-cost pozzolan ceramic membrane with micronized phosphate. The influence of sintering temperature and composition of micronized phosphate (wt.%) on the properties of the membrane were analyzed. It was reported that with an increment in temperature, porosity was initially increased and further decreased due to partial vitrification of pozzolan particles; as a result, water permeability also decreased at temperatures beyond 1050 °C. Optimum membrane properties (1.33 μm pore size, 32.07% porosity) were observed at 20 wt.% micronized phosphate and sintering temperature 1050 °C (Beqqour et al. 2019).

2.6　Other Earth Minerals

Multilayer ceramic membrane was synthesized from Tunisian natural illite clay by Khemakhem et al. Support was fabricated by extrusion. In contrast, slip casting and powder suspension techniques prepared the intermediate microfiltration and top ultrafiltration layers (Khemakhem et al. 2007). In another study, porous inorganic membranes were manufactured using natural Moroccan clay and phosphate. They studied the influence of starch on pore size, water permeability, and air permeability. In addition, dye retention experiments were conducted with a membrane having optimum starch content to remove methyl orange as well as potassium chromate (Palacio et al. 2009). Furthermore, Jana et al. fabricated ceramic membranes with dried raw muddy clay collected from Guwahati (India). They reported that increased flux was observed with the addition of boric acid, Na_2CO_3, and sodium metasilicate (Jana et al. 2010).

Local Moroccan magnesite was prepared by uniaxial pressing technique to prepare a low-cost, flat ceramic membrane (Manni et al. 2020). The influence of temperature used for sintering on membrane characteristics was studied by changing the temperature from 900 to 1200 °C. The membrane sintered at 1100 °C possessed a pore size of 1.12 μm and 48.12% porosity and achieved turbidity rejection of 99.9% and COD removal of 69.7% from textile effluent. Furthermore, Lorente-Ayza et al. synthesized microfiltration ceramic membranes using Spanish clay mixture as a mullite precursor, chamotte from fired tile scraps as a filler, calcite, and potato

starch as inorganic, organic pore formers, respectively (Lorente-Ayza et al. 2015). In another work, Barrouk et al. prepared 3-layer asymmetric membrane by using Moroccan apatite to remove dye molecules from pretreated textile effluent (Barrouk et al. 2015).

In a study, kyanite was used as a primary precursor, and $Al(OH)_3$ was added as a pore-forming agent to prepare porous mullite ceramic support (Guo et al. 2016). The influence of initial feed composition and sintering temperature on the characteristics of the membrane was studied. It was observed that needle-like mullite structure forming skeletal interwoven network appeared during the sintering process, which improves apparent porosity and enhances the membrane's mechanical strength. Mouiya et al. prepared a ceramic membrane with Moroccan clay as the main component and natural phosphate as a pore-forming agent by dry compaction (Mouiya et al. 2018). They concluded that the optimum mass ratio of clay to phosphate was identified as 3:2. Saikia et al. prepared microfiltration ceramic membranes with locally available (Assam, India) potter's clay, stone quarry dust, and tea waste by paste pressing method. It was reported that 0.49 μm pore diameter and 52.5% porosity were observed for membrane sintered at 900 °C (Saikia et al. 2019).

2.7 Rice Husk Ash (RHA)

Rice husk is a major agricultural waste readily available in rice-producing countries. India is the second-largest country which produces nearly 104 million tons per year. About 21.84 million tons of rice husk are generated yearly. Rice husk is not used as cattle feed because of its low cellulose and other sugar contents. Most rice husk is either dumped or burned in open space, which generates a vast amount of RHA. RHA contains silica, carbon, and few other mineral oxides. As the melting point of silica is high, membranes synthesized from RHA are thermally stable.

In a study, RHA was utilized to prepare ceramic hollow fiber membranes from RHA through the immersion-induced phase inversion/sintering method and efficiently removed heavy metal ions from water. In this study, Arlacel was used as a dispersant, N-methyl pyrrolidone solution, and polyethersulfone were used as a solvent and binder. Finally, the fabricated membrane was sintered at 1200 °C (Hubadillah et al. 2017). Furthermore, Mohammed et al. fabricated a porous ceramic membrane using RHA as a silica source and alumina powder as a pore-forming agent. They observed that porosity was increased with an increase in RHA content, whereas mechanical strength was initially decreased and then increased at 30 wt.%, 50 wt.% of RHA (Ali et al. 2017).

The burning of rice husk at high temperatures will convert silica from amorphous to crystalline form. In a study, rice husk combustion at 600 °C resulted in amorphous RHA, and the combustion at 1000 °C generated crystalline RHA (Hubadillah et al. 2018a). It was reported that hollow fibers prepared with 37.5 wt.% crystalline rice husk ash and sintered at a temperature of 1200 °C showed an excellent mechanical

strength of 71.2 MPa with 0.55–2.3 µm ranged pore size distribution and 43.1% porosity.

2.8 Fly Ash

Fly ash is a significant waste generated from coal combustion in power plants and remains a major environmental problem in many countries because of disposal issues. Finding alternative applications from this waste would be beneficial. Fly ash has produced various essential materials, namely cement, ceramics, concretes, and glasses. Fly ash has been primarily studied as an inexpensive raw material for making MF and UF ceramic membranes in recent years.

In a study, mullite ceramic supports were fabricated using fly ash and calcined bauxite. Pure titania was added to enhance the sintering process. On the incorporation of titania, sintering was suppressed at low temperatures. However, this additive improved the sintering at high temperatures. It was reported that the highest porosities were obtained for membranes with 0–6.0 wt.% of titania, sintered at a temperature of 1450 °C (Dong et al. 2010). Suresh et al. observed that an increase in TiO_2 content, porosity, and mechanical strength of the membrane was increased (Suresh and Pugazhenthi 2016). A comparative study was carried out between low-cost polymeric nylon mesh and ceramic bagasse fly ash membranes by Tewari et al. for wastewater treatment in a submerged membrane bioreactor. Fly ash filter showed higher critical flux in comparison with the commercially available ceramic membranes (Tewari et al. 2010). Fang et al. prepared composite tubular membranes using three types of fine fly ashes. Macroporous support was prepared using extrusion technique followed by sintering at 1190 °C; intermediate, and top layers were fabricated by slip casting with dispersant. They studied the effect of withdrawal speed, slip concentration, contact time. A pore size of 0.77 µm with a narrower pore size distribution was observed for a double-coated membrane (Fang et al. 2011).

In a study conducted by Rawat and Bulasara, five ceramic membranes were prepared by changing the weight ratio of kaolin to fly ash (0:1–1:0). However, a constant sintering temperature of 900 °C was maintained. The water permeation studies observed that with increased kaolin content, membrane porosity, mechanical strength as well as chemical resistance were increased and pore size was decreased. A membrane with 25% fly ash and 50% kaolin was chosen as the optimum membrane. This membrane offered a decent combination of porosity, pore size, mechanical and chemical strength to perform acid removal experiments (Rawat and Bulasara 2018). Furthermore, Wang et al. prepared porous cordierite ceramic membranes using fly ash, magnesite, and quartz as raw materials. The influence of sintering temperature and magnesite composition on phase transformation was studied. It was concluded that an increase in magnesite content increased porosity and the number of pores but decreased mechanical strength (Wang et al. 2019). Zou et al. proposed a co-sintering process for the fabrication of ceramic membranes. In their study, fly ash was utilized

as a primary raw material, and mullite fibers were added to reduce the shrinkage rate of support (Zou et al. 2019).

3 Applications

The application of membrane technology in various fields is gaining interest in recent times as it is energy-efficient and environmentally friendly. Literature studies reveal that the low-cost ceramic membranes have been efficiently used for various applications, including separation of oily wastewater emulsions, fruit juice processing, wastewater treatment, etc. In addition, they also served as porous support in the fabrication of micro and ultrafiltration membranes.

3.1 As Porous Support for Microfiltration (MF) and Ultrafiltration (UF) Membranes

From the reported works of literature, it can be observed that membranes fabricated from inexpensive raw materials mostly fall in the MF range (Tables 1, 2 and 3), as the average pore size of the membranes is in the range of 0.1–10 μm. Therefore, they are perfect to use as coarse porous supports for micro and ultrafiltration membranes. For example, in a study, tubular ceramic support was fabricated from Moroccan clay. Intermediate ZrO_2 MF layer possessing an average pore size of 0.23 μm and top TiO_2-$ZnAl_2O_4$ UF layer having an average pore size of 5 nm were coated on the ceramic support by sol-gel process (Saffaj et al. 2006). In another study, Jedidi et al. fabricated tubular porous support from fly ash by extrusion having an average pore size of 4.5 μm and 51% porosity (Jedidi et al. 2009). Ceramic supports from low-cost precursors were fabricated from locally available clay (Indian Institute of Technology, Guwahati), and the UF chitosan layer was deposited on the support by dip-coating technique. This UF membrane was subjected to remove heavy metal ions Hg (II) and As (II) with the aid of Poly Vinyl Alcohol as a chelating agent and achieved up to 100% removal efficiency at very low pressures (Jana et al. 2010). In another study, the uniaxial pressing method prepared MF supports with bentonite powder and micronized phosphate. UF layers of TiO_2 were deposited on prepared supports by spin-coating technique. The obtained UF layer possessed a 72 nm pore diameter and was tested for dye removal (Bouazizi et al. 2017).

Table 3 Low-cost ceramic membranes fabricated from fly ash

Raw materials	Other additives	Fabrication method	Sintering temperature (°C)	Pore former	Pore size (μm)	Porosity (%)	Flexural strength (MPa)	Cost ($/m²)	Application	References
Fly ash	Methocel, Amijel	Extrusion	1100–1130	Starch	4–4.9	48–56	9.8–22.9		Support for MF and UF	Jedidi et al. (2009)
Fly ash	Na_2CO_3, boric acid, sodium metasilicate	Paste casting	800–1000	Calcium carbonate	1.2–2.3	35–40	8–20	17.3	Oil–water emulsion treatment	Singh and Bulasara (2015)
Fly ash, quartz	Titania (weight ratio of titania to fly ash varied from 0 to 1.5)	Uniaxial dry compaction	1100	Calcium carbonate	1.32–2.97	21–48	6.02–13.82	15–40	Oil–water emulsion treatment	Suresh and Pugazhenthi (2016)

3.2 Fruit Juice Processing

Fruit juices are primarily acidic and lie in a pH range of 3–5. Therefore, processing fruit juices using ceramic membranes would be more beneficial than polymeric membranes as they are chemically more stable. Mosambi juice clarification by using low-cost ceramic membranes was first reported in a study by Nandi et al. (2009a). It is stated that fresh juice pre-treated with pectinase enzyme followed by centrifugation improved the quality and clarity of the permeate juice while retaining its valuable parameters, including acidity, total soluble solids (TSS), and density. Furthermore, it is proved that processed juice can be stored for 30 days under refrigeration. They have continued their studies and fabricated four membranes with different compositions of raw materials for mosambi juice clarification. In addition, they studied the influence of membrane morphological parameters and operating pressure on the flux and quality of the permeate, reported optimum conditions (Nandi et al. 2011). Furthermore, another study by Emani et al. also strongly recommended enzymatic pretreatment before centrifugation to minimize irreversible fouling (Emani et al. 2013).

In another study, the clarification of kiwi fruit juice was done with tubular fly ash-based membranes. They prepared three membranes with a different particle size of raw material fly ash using the extrusion method which was followed by sintering at 950–1190 °C. Membrane obtained with a pore size of 1.25 μm and influential permeable area factor $\varepsilon_m d_m^2$ of 0.64 μm^2 was reported as optimum. A clarity of 86.2–90% was obtained while retaining valuable parameters like acidity, TSS, density (Qin et al. 2015).

3.3 Separation of Oil–Water Emulsions

Oily wastewater is a significant effluent from pharmaceuticals, food, metallurgical, chemical, petrochemical industries, and oil refineries. The wastewater contains high molecular weight hydrocarbons, suspended solids, and other impurities. Therefore, it is necessary to treat effluents before discharge to avoid health and environmental hazards. Vinoth Kumar et al. used a tubular kaolin-based ceramic membrane to treat oily wastewater and achieved a rejection of 99.88% for a feed having a concentration of 100 mg/L (Vinoth Kumar et al. 2016). Emani et al. prepared membranes from kaolin by uniaxial dry compaction and applied them for oil–water emulsion treatment. A rejection of 98.52% was obtained at a transmembrane pressure of 207 kPa. Fly ash-based ceramic membranes were prepared by Singh et al. to treat oil–water emulsions, and they achieved a maximum rejection of 99.2% (Emani et al. 2014).

In most oil–water separation studies, the membrane is usually cleaned after each run to regain its permeability. Several cleaning procedures are adapted to clean

the membrane. Firstly, the membrane is generally washed with tap water to eliminate loosely bounded oil droplets from the membrane surface. After that, sonication was carried out to remove the inner particles of the membrane. Finally, alkali wash/detergent wash/backflushing was performed to remove oil droplets inside the pores, followed by cleaning with tap water again (Das et al. 2017). After the proper cleaning of the membrane, hydraulic permeability can be evaluated to know the fouling index by the following expression Eq. (2),

$$\text{Fouling index} = \frac{PW_c - PW_f}{PW_c} \times 100 \tag{2}$$

where, PW_c and PW_f are hydraulic permeabilities of cleaned and new membranes, respectively (Lu et al. 2021).

3.4 Industrial Wastewater Treatment

Several researchers applied low-cost ceramic membranes for treating the wastewater generated from various industries (Sandhya Rani and Kumar 2021). Kumar et al. synthesized tubular ceramic membranes using naturally available clays by extrusion technique. They treated wastewater from the dairy industry with the help of prepared ceramic membranes and reduced the COD of feed to a permissible limit (Kumar et al. 2016). A low-cost ceramic microfiltration membrane was fabricated by Mouiya et al. from Moroccan clay. The membrane was used to treat tannery beam house effluent, and it has exhibited a turbidity removal efficiency of 99.8% (Mouiya et al. 2018). Furthermore, Manni et al. prepared a membrane from Moroccan magnesite and treated textile wastewater. Efficient rejection of turbidity and COD rejection of 99.9% and 69.7%, respectively, were exhibited by this membrane (Manni et al. 2020).

4 Conclusions

Ceramic membranes are becoming viable over polymeric membranes owing to their intrinsic and unique properties. Fabrication of ceramic membranes using low-cost precursors enables the industrial application of ceramic membranes to offer desired properties at a lower cost. Researchers selected several low-cost raw materials and fabricated membranes by various methods. Mainly the selection of raw materials is in accordance with local abundance. Following the literature studies, ceramic membranes fabricated from low-cost raw materials exhibit high porosity, mechanical stability, and chemical stability. Accordingly, these membranes can be efficiently applied in several applications, including industrial wastewater treatment, fruit juice clarification, protein separation, etc. However, the fabrication process of ceramic

membranes and parameters optimization need to be improved further for full-pledged application industries.

Declaration of Competing Interest The authors declare that they have no known competing financial interests or personal relationships that could have appeared to influence the work reported in this paper.

References

Abd Aziz MH, Othman MHD, Hashim NA, Adam MR, Mustafa A (2019) Fabrication and characterization of mullite ceramic hollow fiber membrane from natural occurring ball clay. Appl Clay Sci 177:51–62

Achiou B, Elomari H, Bouazizi A, Karim A, Ouammou M, Albizane A et al (2017) Manufacturing of tubular ceramic microfiltration membrane based on natural pozzolan for pretreatment of seawater desalination. Desalination 419:181–187

Ali MS, Hanim MAA, Tahir SM, Jaafar CNA, Mazlan N, Amin Matori K (2017) The effect of commercial rice husk ash additives on the porosity, mechanical properties, and microstructure of alumina ceramics. Adv Mater Sci Eng 2017

Barrouk I, Alami Younssi S, Kabbabi A, Persin M, Albizane A, Tahiri S (2015) Elaboration and characterization of ceramic membranes made from natural and synthetic phosphates and their application in filtration of chemical pretreated textile effluent. J Mater Environ Sci 6(8):2190–2197

Bouazizi A, Breida M, Karim A, Achiou B, Ouammou M, Calvo JI, Aaddane A, Khiat K, Younssi SA (2017) Development of a new TiO2 ultrafiltration membrane on flat ceramic support made from natural bentonite and micronized phosphate and applied for dye removal, Ceram. Int. 43:1479–1487

Bazin MM, Ahmat MA, Zaidan N, Ismail AF, Ahmad N (2014) Effect of starch addition on microstructure and strength of ball clay membrane. J Teknol Sci Eng 69(9):117–120

Beqqour D, Achiou B, Bouazizi A, Ouaddari H, Elomari H, Ouammou M et al (2019) Enhancement of microfiltration performances of pozzolan membrane by incorporation of micronized phosphate and its application for industrial wastewater treatment. J Environ Chem Eng 7(2):102981

Bouazizi A, Saja S, Achiou B, Ouammou M, Calvo JI, Aaddane A et al (2016) Elaboration and characterization of a new flat ceramic MF membrane made from natural Moroccan bentonite. Application to treatment of industrial wastewater. Appl Clay Sci 132–133:33–40

Bouzerara F, Harabi A, Condom S (2009) Porous ceramic membranes prepared from kaolin. Desalin Water Treat 12(1–3):415–419

Chihi R, Blidi I, Trabelsi-Ayadi M, Ayari F (2019) Elaboration and characterization of a low-cost porous ceramic support from natural Tunisian bentonite clay. Comp Rend Chim 22(2–3):188–197

Clem AG (1961) Industrial applications of bentonite. Clays Clay Miner 10(1):272–283

Das B, Chakrabarty B, Barkakati P (2016) Preparation and characterization of novel ceramic membranes for micro-filtration applications. Ceram Int 42(13):14326–14333

Das B, Chakrabarty B, Barkakati P (2017) Separation of oil from oily wastewater using low cost ceramic membrane. Korean J Chem Eng 34(10):2559–2569

Dong Y, Hampshire S, Zhou J, Lin B, Ji Z, Zhang X et al (2010) Recycling of fly ash for preparing porous mullite membrane supports with titania addition. J Hazard Mater 180(1–3):173–180

Emani S, Uppaluri R, Purkait MK (2013) Preparation and characterization of low cost ceramic membranes for mosambi juice clarification. Desalination 317:32–40

Emani S, Uppaluri R, Purkait MK (2014) Cross flow microfiltration of oil-water emulsions using kaolin based low cost ceramic membranes. Desalination 341(1):61–71

Eom JH, Kim YW, Yun SH, Song IH (2014) Low-cost clay-based membranes for oily wastewater treatment. J Ceram Soc Japan 122(1429):788–794

Eom JH, Yeom HJ, Kim YW, Song IH (2015) Ceramic membranes prepared from a silicate and clay-mineral mixture for treatment of oily wastewater. Clays Clay Miner 63(3):222–234

Fang J, Qin G, Wei W, Zhao X (2011) Preparation and characterization of tubular supported ceramic microfiltration membranes from fly ash. Sep Purif Technol 80(3):585–591

Guo H, Li W, Ye F (2016) Low-cost porous mullite ceramic membrane supports fabricated from kyanite by casting and reaction sintering. Ceram Int 42(4):4819–4826

Hubadillah SK, Othman MHD, Harun Z, Ismail AF, Rahman MA, Jaafar J (2017) A novel green ceramic hollow fiber membrane (CHFM) derived from rice husk ash as combined adsorbent-separator for efficient heavy metals removal. Ceram Int 43(5):4716–4720

Hubadillah SK, Othman MHD, Matsuura T, Rahman MA, Jaafar J, Ismail AF et al (2018a) Green silica-based ceramic hollow fiber membrane for seawater desalination via direct contact membrane distillation. Sep Purif Technol 205:22–31

Hubadillah SK, Othman MHD, Matsuura T, Ismail AF, Rahman MA, Harun Z et al (2018b) Fabrications and applications of low cost ceramic membrane from kaolin: a comprehensive review

Indian Bureau of Mines (2016) Indian minerals yearbook 2015. Part-III: mineral reviews, 54th edn, pp 1–9

Insley H, Ewell RH (1935) Thermal behavior of the kaolin minerals. J Res Natl Bur Stand 14(5):615

Issaoui M, Limousy L, Lebeau B, Bouaziz J, Fourati M (2017) Manufacture and optimization of low-cost tubular ceramic supports for membrane filtration: application to algal solution concentration. Environ Sci Pollut Res 24(11):9914–9926

Jana S, Purkait MK, Mohanty K (2010) Preparation and characterization of low-cost ceramic microfiltration membranes for the removal of chromate from aqueous solutions. Appl Clay Sci 47(3–4):317–324

Jedidi I, Khemakhem S, Larbot A, Ben Amar R (2009) Elaboration and characterisation of fly ash based mineral supports for microfiltration and ultrafiltration membranes. Ceram Int 35(7):2747–2753

Khemakhem S, Ben Amar R, Larbot A (2007) Synthesis and characterization of a new inorganic ultrafiltration membrane composed entirely of Tunisian natural illite clay. Desalination 206(1–3):210–214

Kiran SA, Arthanareeswaran G, Thuyavan YL, Ismail AF (2015) Influence of bentonite in polymer membranes for effective treatment of car wash effluent to protect the ecosystem. Ecotoxicol Environ Saf 121:186–192

Kumar RV, Goswami L, Pakshirajan K, Pugazhenthi G (2016) Dairy wastewater treatment using a novel low cost tubular ceramic membrane and membrane fouling mechanism using pore blocking models. J Water Process Eng 13:168–175

Lorente-Ayza MM, Mestre S, Menéndez M, Sánchez E (2015) Comparison of extruded and pressed low cost ceramic supports for microfiltration membranes. J Eur Ceram Soc 35(13):3681–3691

Lu C, Bao Y, Huang JY (2021) Fouling in membrane filtration for juice processing, Curr. Opin. Food Sci. 42:76–85

Majouli A, Younssi SA, Tahiri S, Albizane A, Loukili H, Belhaj M (2011) Characterization of flat membrane support elaborated from local Moroccan perlite. Desalination 277(1–3):61–66

Majouli A, Tahiri S, Alami Younssi S, Loukili H, Albizane A (2012) Elaboration of new tubular ceramic membrane from local Moroccan perlite for microfiltration process. Application to treatment of industrial wastewaters. Ceram Int 38(5):4295–4303

Manni A, Achiou B, Karim A, Harrati A, Sadik C, Ouammou M et al (2020) New low-cost ceramic microfiltration membrane made from natural magnesite for industrial wastewater treatment. J Environ Chem Eng 8(4):103906

Maxim LD, Niebo R, Mcconnell EE (2014) Perlite toxicology and epidemiology—a review. Inhal Toxicol 26(5):259–270

Monash P, Pugazhenthi G (2011) Development of ceramic supports derived from low-cost raw materials for membrane applications and its optimization based on sintering temperature. Int J Appl Ceram Technol 8(1):227–238

Mouiya M, Abourriche A, Bouazizi A, Benhammou A, El Hafiane Y, Abouliatim Y et al (2018) Flat ceramic microfiltration membrane based on natural clay and Moroccan phosphate for desalination and industrial wastewater treatment. Desalination 427:42–50

Nandi BK, Uppaluri R, Purkait MK (2008) Preparation and characterization of low cost ceramic membranes for micro-filtration applications. Appl Clay Sci 42(1–2):102–110

Nandi BK, Das B, Uppaluri R, Purkait MK (2009) Microfiltration of mosambi juice using low cost ceramic membrane. J Food Eng 95(4):597–605

Nandi BK, Uppaluri R, Purkait MK (2011) Identification of optimal membrane morphological parameters during microfiltration of mosambi juice using low cost ceramic membranes. LWT Food Sci Technol 44(1):214–223

Obada DO, Dodoo-Arhin D, Dauda M, Anafi FO, Ahmed AS, Ajayi OA (2017) Physico-mechanical and gas permeability characteristics of kaolin based ceramic membranes prepared with a new pore-forming agent. Appl Clay Sci 150:175–183

Palacio L, Bouzerdi Y, Ouammou M, Albizane A, Bennazha J, Hernández A et al (2009) Ceramic membranes from Moroccan natural clay and phosphate for industrial water treatment. Desalination

Qin G, Lü X, Wei W, Li J, Cui R, Hu S (2015) Microfiltration of kiwifruit juice and fouling mechanism using fly-ash-based ceramic membranes. Food Bioprod Process 96:278–284

Rawat M, Bulasara VK (2018) Synthesis and characterization of low-cost ceramic membranes from fly ash and kaolin for humic acid separation. Korean J Chem Eng 35(3):725–733

Saffaj N, Persin M, Younsi SA, Albizane A, Cretin M, Larbot A (2006) Elaboration and characterization of microfiltration and ultrafiltration membranes deposited on raw support prepared from natural Moroccan clay: application to filtration of solution containing dyes and salts. Appl Clay Sci 31(1–2):110–119

Saikia J, Sarmah S, Bora JJ, Das B, Goswamee RL (2019) Preparation and characterization of low cost flat ceramic membranes from easily available potters' clay for dye separation. Bull Mater Sci 42(3):1–13

Saja S, Bouazizi A, Achiou B, Ouammou M, Albizane A, Bennazha J et al (2018) Elaboration and characterization of low-cost ceramic membrane made from natural Moroccan perlite for treatment of industrial wastewater. J Environ Chem Eng 6(1):451–458

Sandhya Rani SL, Kumar RV (2021) Insights on applications of low-cost ceramic membranes in wastewater treatment: a mini-review. Case Stud Chem Environ Eng 4:100149

Singh G, Bulasara VK (2015) Preparation of low-cost microfiltration membranes from fly ash. Desalin Water Treat 53(5):1204–1212

Suresh K, Pugazhenthi G (2016) Development of ceramic membranes from low-cost clays for the separation of oil–water emulsion. Desalin Water Treat 57(5):1927–1939

Tewari PK, Singh RK, Batra VS, Balakrishnan M (2010) Membrane bioreactor (MBR) for wastewater treatment: filtration performance evaluation of low cost polymeric and ceramic membranes. Sep Purif Technol 71(2):200–204

Vasanth D, Uppaluri R, Pugazhenthi G (2011) Influence of sintering temperature on the properties of porous ceramic support prepared by uniaxial dry compaction method using low-cost raw materials for membrane applications. Sep Sci Technol 46(8):1241–1249

Vasanth D, Pugazhenthi G, Uppaluri R (2013) Cross-flow microfiltration of oil-in-water emulsions using low cost ceramic membranes. Desalination 320:86–95

Vinoth Kumar R, Kumar Ghoshal A, Pugazhenthi G (2015) Elaboration of novel tubular ceramic membrane from inexpensive raw materials by extrusion method and its performance in microfiltration of synthetic oily wastewater treatment. J Memb Sci 490:92–102

Vinoth Kumar R, Monash P, Pugazhenthi G (2016) Treatment of oil-in-water emulsion using tubular ceramic membrane acquired from locally available low-cost inorganic precursors. Desalin Water Treat 57(58):28056–28070

Wang H, Li C, Peng Z, Zhang S (2011) Characterization and thermal behavior of kaolin. J Therm Anal Calorim 105(1):157–160

Wang S, Wang H, Chen Z, Ji R, Liu L, Wang X (2019) Fabrication and characterization of porous cordierite ceramics prepared from fly ash and natural minerals. Ceram. Int. 45:18306–18314

Zou D, Qiu M, Chen X, Drioli E, Fan Y (2019) One step co-sintering process for low-cost fly ash based ceramic microfiltration membrane in oil-in-water emulsion treatment. Sep Purif Technol 210:511–520

Therapeutic Potential of Seleno-Compounds in Cancer—An Overview

Anu Radha Pathania and Swati Sharma

Abstract Researchers are looking for natural agents to tackle high-prevalence cancer cases, for this Selenium (Se) becoming a promising contender because it inhibits the growth of the tumor. Selenium (Se) is a well-known necessary trace component that has been propagated (spread and promote) by non-metallic. Selenium (Se) as a cancer therapeutic agent a report was documented 100 years ago after that another research claimed that selenium (Se) is a carcinogen and an early study claiming that selenium (Se) played role in the prevention of cancer. As an outcome, this remarkable oxygen family member has a wide range of health impacts, including acting as a cancer preventive agent, also act as a toxin and a carcinogen. Numerous clinical trials showed no important significant benefit of selenium (Se) in tumor suppression, the scientists have found that only a few species of selenium (Se) have significant anticancer activities. By suppressing metastasis organic selenium (Se) compounds aid in the treatment of cancer but in comparison with inorganic compounds, they have several disadvantages. The scientists are working on the challenge to improve the Selenium efficacy with toxicity effect. For this nanotechnology has become a solution. The nanoparticle of selenium (SeNPs) is used against various malignant diseases as curative agents. In this review paper, selenium species categorize into three types (Se nanoparticles, organic and inorganic) and an outline of their function in the curing of cancer. To give reliable information on selenium capabilities in the treatment of tumors so it is necessary to review the state of selenium and selenium compounds.

Keywords Selenium · Nanoparticles · Cancer · Organic · Inorganic · Diseases

1 Introduction

Selenium (Se) is a trace component in micronutrition, humanoid, nutrition. Berzelius in 1917 identified this family member of oxygen (Ali et al. 2018). In 1911, Colloidal

A. R. Pathania (✉) · S. Sharma
UIS-Chemistry, Chandigarh University, Gharuan, Punjab, India
e-mail: anuradha.appsci@cumail.in

Se with low harmful damage with an eosin carrier have anticancer activity in mice and humans but in comparison to the first report of colloidal selenium (Se) cancer treatment success the further studies were not satisfied (Berzelius 1817; Bhattacharya 2011). Following that in 1933 in another toxicology study of selenium was noticed, it has been noticed that livestock has a harmful impact this is due to because livestock consumed plants that have a higher ability for accumulating more selenium (Se) from soil (Bilek et al. 2019). In times of recession intake, certain tissue and gene-specific processes guarantee that the most important organs, such as the brain and endocrine tissues, are preferred supplied, and that the most important selenoproteins are preferentially involved in the pathogenesis (Brodin et al. 2020). This enzyme cannot function without it, and it helps in the prevention of oxidative stress damage. As a result of its potential to influence the activity of the enzyme glutathione peroxidase, Se is thought to be necessary for the organism. The level of selenium in fish is high, whereas it is modest in vegetables and wheat. Selenoprotein P is implicated in free radical pathology as well as protein and selenium trafficking. It has some biological impact based on its restricted daily consumption range. It will not be able to perform helpful functions below this limited range of daily consumption, and it will be poisonous over this range. The tumor mortality rate survey in the United States demonstrates that persons living in a part of the United States that has forage crops with a large concentration of Se had lower cancer mortality rates. Cancer fatalities will be increased in persons living in low-forage Selenium regions. This discovery prompted Shamberger and Frost (1969) to report that (Se) may have a function in tumor prevention (Brozmanova et al. 2010). As a result, the danger of selenium (Se)-related disorders (cancer, kashin, keshan) is greater among those who live in low selenium areas. According to Schrauzer and his colleagues, selenium has a function in tumor protection agents (Burk et al. 2006). A modest dietary dose of selenium was shown to protect against certain types of tumors. In one research, subjects were given a small portion or dosage of antioxidant vitamins and minerals regularly to demonstrate its protective impact. According to the findings of this study, as compared to persons who received a placebo, persons who received antioxidants had a decreased risk of prostate cancer development (vitamins, minerals). Another research found that consuming selenium in one's diet decreases the risk of cancer and has some protective benefits in the case of human lung cancer (Cao et al. 2004). It has a part in the treatment of a variety of degenerative disorders, and the scientist is attracted by its recent data report on the mechanism of selenium in the inhibition of cancer (Cavalu et al. 2016; Chakraborty et al. 2017; Chen 2012). Because of selenium's (Se) dualistic nature (antioxidant or prooxidant) it is used in the curing and prevention of cancer. Its dual chemopreventive or antitumor function has been widely discussed by several researchers (Chen et al. 2008; Combs et al. 1997). Selenium can be found in a variety of forms in nature. Several experimental researchers have discovered that only some types of selenium are considered to be of primary significance for anticancer activity via various mechanisms (Cui et al. 2019). Both organic and inorganic forms of selenium cause the death of tumorous cells after inducing apoptosis. Organic selenium (Se) is not widely available and it is primarily present in food. As compared to inorganic selenium the organic selenium is absorbed better (Domínguez-Álvarez et al.

2014). The toxicity of selenium inorganic form is higher than that of organic or nano form. Selenite promotes the genetic expression of glutathione peroxidase-containing antioxidant enzymes (an inorganic form of selenium) (El-Sayed et al. 2016). One of the issues with selenium is the narrow line between dangerous and necessary doses for dietary and healing benefits, as well as the quantity required for dietary purposes or medicinal impacts. Nanotechnology provides a solution for demonstrating selenium effectiveness while reducing toxicity. Presently, the nanoparticles of Se are mostly used for different medical applications. Nanoparticles of selenium act as effective nanocarriers for targeting cancer administration medications to tumor cells by extending their therapeutic effect and lowering the medication dosage (Ertilav et al. 2019; Çetin et al. 2016). The nanoform of (Se) with low harmful damage for normal cells has an anticancer function, as anew anti-tumor mediator it drew a great deal of interest. In addition, the class of selenocompounds, i.e., selenocyanates, has also anticancer effects (Frieben et al. 2019).

The earliest cancer prevention tests in China have been conducted by Selenium (Se). Many citizens under this study received table salt containing sodium selenite and Selenium (Se) up to 30–50 mg for 8 years. The findings of this study revealed that for residents who get table salt the prevalence of primary liver cancer has been lowered (Fu et al. 2016). There is a decrease in 50% cancer death rate when people consumed brewer's yeast which contains selenium mainly Selenomethionine (Oldfield 1987). This resulted in the experiment [SELECT] that recruited [selenomethionine] for the inhibition of male's prostate carcinoma (Ganesan 2015). The outcome of this study indicated that Se cannot suppress prostate cancer (Gao et al. 2014). Few people reported that utilizing a low effectual form of Se could be the reason for study failure (Gorain et al. 2018; Hariharan et al. 2012; Hu et al. 2019). Several have proposed that it is because of high intake when compared to the necessary optimum dosage of Selenium for cancer inhibition (Jain et al. 2016; Johnson et al. 2008). This has opened a lot of doors in researching the tumor prevention mechanism to determine why it helps to prevent or toxic tumors in certain situations or certain instances.

2 Selenium (Se) Enhancing Anticancer Properties of Therapeutic Agent

Several processes, including increased cellular apoptosis, cell retention, detoxification of the tumor-causing substance, activation of the immune system, angiogenesis-prevention, and redox-state regulations, have been offered for interpretations (Kalishwaralal et al. 2016; Khan et al. 2019; Khurana et al. 2019). From all these various mechanisms of selenium, the recommended one is apoptotic for the prevention of cancer via selenium compounds. Selenium (Se) leads to oxidative DNA damage and damage on mitochondria, after a mitochondrial malfunction, and with caspase-dependent/independent apoptosis, with mitochondria malfunction. The selenium

(Se) antitumor pathway is not yet well understood, which means it is controversial, but much research has shown that it can prevent cancerous cells development and assist normal cell proliferation (Klein et al. 2001; Kora and Rastogi 2016).

According to Song et al. (Kumar et al. 2015) study which state that the effect of Selenium on the improvement of gynecologic tumor carboplatin anticancer property. Huge levels of selenium help in the prevention of the growth of antimitotic resistance in mouse ovarian cancer. The Selenium (Se) combination is safe and tolerated in antimitotic products and has no influence on antimitotic drugs. So that this result demonstrates that the combination of antimitotic medicine (paclitaxel, carboplatin) and Se (Selenium) acid is safe to treat gynecological carcinoma patients. According to Wang et al. (Le Province Medicale 1912) report which states that the anticancer action of β-lactoglobulin is enhancing by selenium (Se). In humans, Seleno-β-lactoglobulin played the role of anticancer agent to (MCF-7) or (MDA-MB-231) breast cancerous cell. Due to the formation of reactive oxygen species via mitochondrial arbitered pathway the Seleno-β-lactoglobulin results in a decrease in the growth of human breast cancerous cells. The cytotoxic activity of Seleno-β-lactoglobulin to breast carcinomatous cells depends on the concentration. According to Freiben et al. (Li et al. 2011) report the Selenium (Se) also increasing the anticancer activity of isothiocyanates. Against some human carcinoma, the Isothiocyanates show some antitumor activity. They have been changed to isoselenocyanates to improve their anticancer function. According to Esin et al. (Le Province Medicale 1912), Ca^{2+} signaling aids tumor cell proliferation, and the importance of Ca^{2+} signaling has led to the investigation that suggests Ca^{2+} channel inhibitors have the potential to treat a few malignancies. The combination of selenium (Se) with cisplatin induces apoptosis in cancerous breast cells. This results in a reduction in calcium buildup (Le et al. 2016). According to Riva et al. (Lippman et al. 2009), in human epithelial cancer cells, *Arthrospira platensis* adorned with Selenium and in combination with (oxaliplatin, docetaxel) exhibits its influence on cell growth, ROS production, and cause death. Selenium or the presence of selenium in *Arthrospira platensis* did not affect vitality. When cancer cells are incubated with (Se-OXA) (Se-OTX) supplemented with *Arthrospira platensis*, by triggering apoptosis mediated by capase (3) as well as a reduction in reaction oxygen species (ROS) production then there is raised in the cytotoxicity of the dosage. The [Se—anticancer medicine rich with *Arthrospira platensis*] utilizes *Arthrospira platensis* as a possible delivery system for antitumor drugs. As a result, the selenium-anticancer medication supplemented with *Arthrospira platensis* demonstrates a novel approach to the creation of a low harmful and effective treatment for carcinoma. According to Ertilay et al. (Lü et al. 2016), the Selenium enhanced the anticancer capabilities of docetaxel which is a therapeutic agent by activation of TRMP2 channel in the cancer cell. There is an increase in apoptosis, reactive oxygen species (ROS) generation on treating with Se + DTX (DBTRG) glioblastoma cells. Due to this rise in the level of apoptosis and also in reactive oxygen species (ROS) mitochondrial generation on curing with Se + DTX. TRMP2 channel is activated. Se + DTX inhibits cell propagation by inducing [oxidative mitochondrial stress], which leads to raised calcium entry by the TRPM2 and cell death. More research is

needed to fully comprehend the DTX + Se functioning and how it leads to the death of glioblastoma cells.

3 Reported Work on Selenium

3.1 Inorganic Selenium

Sodium Selenite

The inorganic type or form of selenium (Se) aids in cancer prevention via a variety of mechanisms. One of these pathways is the formation of reactive oxygen species (ROS) and the degradation of mitochondria in cancerous cells.

Inhibition of Cancer by the Formation of (ROS) Reactive Oxygen Species

According to Wu et al. (Li et al. 2000) selenite has a function in the suppression of peritoneal cancer in mice, and its mode of action is also appropriate. Injected selenite can prevent or destroy cancer cells in the peritoneal cavity, leading to the spread of Se in cancer cells and their transformation to SeNP. The selenium nanoparticles then sequester the GSH connected Trx–Grx systems, resulting in the production of (ROS) reactive oxygen species and the killing of cancerous cells. As a result, selenite acts as an anticancer agent in the treatment of peritoneal carcinomatosis. According to Li et al. (2009) sodium selenite boosts antioxidant enzymes in healthy tissue, which aids in twofold shielding. Thus, the dosage of inorganic type causes a 50% reduction in the new cancer cases in Chinese people residing in high-risk locations.

3.2 Organic Selenium as Anti-cancer

An organic form of Selenium (Se), acts as a good source of a supplement of selenium (Se). It also seems the low hazardous and organic type of selenium is absorbed better than the inorganic form of Se (selenium). The cell's death with intact suicidal genes by apoptosis is promoted by L-selenomethionine whereas L-selenomethionine causes death by triggering apoptosis of cancerous mutated cells (Lindshield et al. 2010).

It comprises the L-methionine which is a natural amino acid and it is selenium (Se) organic complex. So, it drives the decrease in the cancer cell's growth at a larger rate than the normal cells (Liong et al. 2009). As result, there has been a rise in the interest in supplements selenium to inhibit cancer. Clark was attempting to inhibit cancer of the skin by using pills of 200 mcg L-selenomethionine (Li et al. 2011). But for few types of skin cancer, the result was ineffective in inhibiting the cancer cell growth, these patients were saved from death by a 50% decrease in cancer cells (Li et al. 2011). Selenomethionine is often integrated with proteins in a non-specific manner rather than methionine (Met). L-selenomethionine solely causes the death
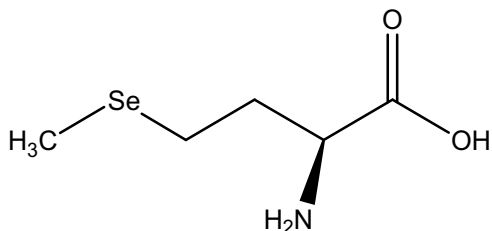
of cells with undamaged suicidal genes via apoptosis, but l-selenocysteine led to the death of malignant altered cells via apoptosis.

According to Spallholz et al. (Liu et al. 2015) Selenomethionine has demonstrated exceptional cytotoxicity (Cell toxicity) against a wide range of cancer cells, including lung, breast, and colorectal. Cancerous cells undergo apoptosis as a result of ROS generation. When Selenium methylated substances (selenomethionine or Se-methylselenocystein) are exposed to their corresponding enzyme gamma or beta lyases, methylselenide is formed, which inadequate concentrations are toxic. Apoptosis is due to the generation of reactive oxygen species (ROS).

It is a prooxidant and has toxicity to the living cell, which is proved by the formation of reactive oxygen species (ROS) and DNA damage which further leads to (mitochondrial) apoptosis in various cancers including (lung, breast, cervical, and liver cancer).

Fig. 2 Structure of selenium-methyl L-selenocysteine (selenocysteine)
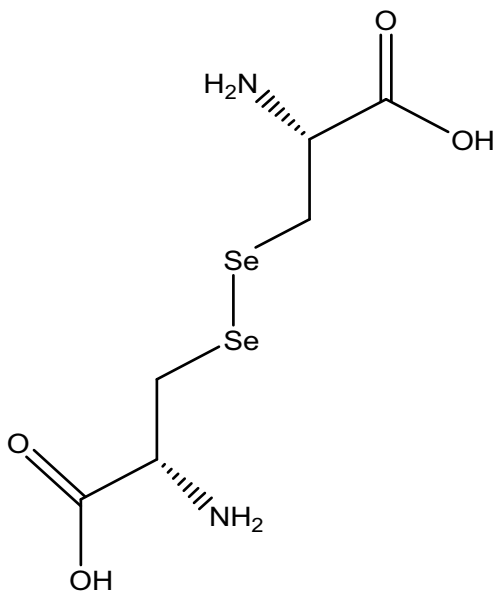
In plants such as onion Selenium-methyl L-selenocysteine which is discovered recently as a significant Selenium (Se) form (Luesakul et al. 2018). It prevents new blood vessel production or leads to angiogenesis (Liu et al. 2015, 2019; Luesakul et al. 2018; Li et al. 2019). The growth of cancer is reduced by this effect. When combined with the anticancer drug like tamoxifen, enhances that drug's capacity to suppress breast cancer cell development in mice. Moreover, this organic form has an inhibitory potential for colon, head, and neck tumors (Oldfield 1987; Misra et al. 2016; Peters and Takata 2008; Rotruck et al. 1973).

3.3 Selenium Nano-Particle as an Anti-cancer

There is a thin gap between beneficial and hazardous qualities of high dose of selenite (inorganic form), nanotechnology solves the problem of a thin gap between beneficial and hazardous qualities. Numerous studies stated that selenium nanoparticles (SeNPs) have superior biotic activities, low toxicity, and also show greater bioavailability (Richie et al. 2014; Riva and Oreal 2016; Redman et al. 1998; Ranjitha et al. 2019; Sugiura and Benedict 1929). The harmful effects of selenium (Se) are due to the production of reactive oxygen species (ROS) or by its mechanism (Shamberger and Frost 1969). Comparing with the organic or inorganic form it has low harmful damage. 0.7 mg Se/kg of SeNPs are required to halt the propagation of tumorous cells without showing toxic damage (Schrauzer et al. 1977). Xu et al. in 2008 had exposed nanoparticles of selenium (SeNPs) that can act as chemopreventive agents with low toxicity damage (Sanmartín et al. 2009). Thus, for cancer nanoparticles of selenium (Se) play the role of therapeutic mediator (Gangadoo et al. 2017). SeNPs nanoparticle of selenium possess enhanced and effective anti-tumor action on cancerous cells (Song et al. 2018; Suzuki et al. 2010; Spallholz 2019). Nanoforms of Selenium have anticancer qualities because nanoparticles of selenium (SeNPs) play the role of prooxidant for cancer cells at the inner side and also cause apoptosis (Srivastava and Kowshik 2016; Menon 2018). The procedure for preparing NPs in the biological or chemical procedure and lessening of multifaceted chemical to the harmless elemental form of NPs is the principle that both biological or chemical method follows. stabilizers and Modifiers are involved in the method of chemical reduction (Sun et al. 2014; Song et al. 2017) and low toxic green synthesis has bio-molecular-lessening mediators with increased control over structure and dimension (Sun et al. 2013, 2014). The anti-cancer curation based on nanoforms is auspicious because of the small size of the nanoparticle (NPs) so that they can enter and iterate within the cell surface. The cellular absorption or dispersion of nanoparticles is affected by nanoparticle dose or size. As a result of these features, the size and dose of nanoforms are essential variables in the suppression of malignant cell proliferation (Tan et al. 2012). Nanoparticles (NPs) [12.5 nm] induced apoptosis in many tumor cell lines, that is equal to methylselenic acid, however, bigger size nanoparticle is failed to decrease the growth of cancer cells. A dose of [0.4 mg/kg] per day is appropriate

to prevent the growth of cancer cells this is examined by Vekariya et al. in an anti-tumor treatment of breast tumorous cells. Nanoparticles of selenium [SeNPs] stop the growth of cancerous cell [HCT-8] growth in the concentration more than [50 μm] this demonstrating that a huge amount of these nanoparticles increase apoptosis level (Tan et al. 2009). Zheng et al. demonstrate that the small size of nanoparticles is the cause for the departure from the cell system (reticuloendothelial) this minor size of nanoparticles is also responsible for their rejection by macrophages. Activation of [caspase-3,8,9] demonstrates that a Se nanoparticle fixed with ATP induces apoptosis in [tumorous-HepG2-cells] via a mitochondrial-mediated route. Selenium nanoparticles possess a huge drug-storage capacity and low toxicity impact with the better antitumor property this is caused to their large surface-to-volume ratio (Valdiglesias et al. 2010). The major endocytosis pathway is responsible for nanoparticles being accepted by cells. The cell type and dimension influenced the intracellular uptake. These nanoparticles are easily blended in an aqueous mixture to increase their magnitude so that prevent their endocytosis (Vekariya et al. 2012). By their combination with a biocompatible polymer, the cellular absorption of anticancer medicine occurs via the endocytic pathway which is proceeded by dilapidation. The cellular absorption via receptor arbitrated endocytosis-clathrin arbitrated route is improved by the addition of folic acid to the surface of nanoparticles (Waters and Chiang 2018). Increased cytotoxicity occurs when drugs are delivered to an unsuspecting place (Wu et al. 2014). Drugs loaded on the surface of selenium nanoparticles (SeNPs) will enhance these inadequacies (Wu et al. 2019). To resolve the issue of medication distribution to an unknown location Cancer-targeting drugs can be coupled with selenium nanoparticles, and the combination form binds to the tumor cell membrane receptor. The process of nanoparticle absorption is enhanced by the combination form which is accumulation in tumor-bearing organs and is also useful in lowering the cytotoxic effect on a normal cell. A combination of nanoparticles with antitumor drugs prepared the drug targeted delivery system and this system serves as a source for anticancer medicine transportation to antitumor cells (Wang et al. 2009). A study which reported that [Se + curcumin nanoparticle] show a decrease in cancer cell production and there are no decrease in normal [HaCaT] cells, this study shows the Selectivity of nanoparticle (NPs) towards tumor cells (Wadhwani et al. 2016). Random delivery arises the Limitation of this system. Difference of tumorous cell is to be low when compared with normal cells, the difference help in the reduction of hazardous effect in the normal cell by drug delivery system [pH] (Wang et al. 2015). The drug delivery to cancerous cells via encapsulated drug release is facilitated by the degradation of nanoparticles (Wang et al. 2016). Nanoparticles of Selenium (SeNPs) boost the formation of reactive oxygen species (ROS). After that, the mitochondrial membrane potential is disrupted, and the mitochondrial arbitrated apoptotic pathway is initiated.

To achieve high tumor-directed capacity, several targeted residues, like hyaluronic acid (HA), are coated with nanoforms (Wang et al. 2014) the functions of therapeutic drugs are enhanced by loading them on the surface of modified nanoparticles of selenium. The modified nanoparticle (NPs) with negligible toxicity damage has an anti-tumor agent function for various types of cancers. Functionalized or modified

nanoparticles are a solution to the issue of nanoparticle targeting to unexpected sites, which causes plenty of negative consequences. By combining functionalized nanoparticles with bio-adhesive polysaccharides, drug absorption can be improved or drug occupancy duration can be extended (Wang et al. 2012).

3.4 Functionalized Se Nanoparticle Possesses Enhanced Cytotoxicity

For prevention of [Bel-7402] cancer cell growth, functionalized nanoform of [Adriamycin or SeNPs] demonstrates more efficient anticancer activity in a dosage-dependent manner. For hepatic tumor cell lines, this combination of functionalized-selenium nanoparticles promotes apoptosis (Wang et al. 2015).

There is a harmful effect of the combination of [selenium nanoparticles and anti-cancer medicine] on the cancerous cell by causing apoptosis and cell cycle arrest at distinct stages of the cell cycle. Toxicity effects are mainly caused via the formation of reactive oxygen species (ROS) (Wu et al. 2012; Xu et al. 2019). Apoptosis can take two pathways. The first is extrinsic, which is initiated by combining a pro-apoptotic ligand with a death-receptor, and this conjugate acts via caspase-8, which is located on the cell membrane, whereas the second is intrinsic, which is initiated by fewer types of stress among cells, due to DNA impairment, and is initiated within the cell via caspase-9 (Xia et al. 2018). For the cellular uptake process, the surface charge plays an important role. The NH_3^+ groups of chitosan improve the stability of selenium nanoparticles in water. This group has enhanced the cellular absorption of chitosan. Nanoparticles of selenium in combination with chitosan enhanced the apoptosis process in [A375] melanoma, cancer cells (Xia et al. 2019a, b). Antiviral effects have been discovered in functionalized selenium nanoparticles conjugated with antiviral medicine. Nanoparticles of Selenium (Se) in combination with antiviral drug (functionalized nanoparticles) [SeNPs@OT] boost the antiviral function of the medication (oseltamivir) and might be a potent antiviral drug agent (Xia et al. 2019b). According to Tang et al. (Yoshizawa et al. 1998), the (Arabinogalactans) conjugated with selenium nanoparticles generate functionalized selenium nanoparticles, i.e. [LAG + SeNPs]. This compound, which consists of functionalized selenium nanoparticles of varying sizes, aids in the prevention of tumor cell proliferation by triggering apoptosis in [A549] adenocarcinomas human alveolar epithelial cells. Liu et al. (Yu et al. 1991) demonstrated the possession of better stability and longer residence for [PSP]—polysaccharide-protein complexes coupled with selenium nanopart, as the good applicants for breast cancer therapy. The reason for greater stability is the adsorption on the external portion of the selenium nanoparticle by hydroxyl or other groups of (polysaccharides). Apoptotic process in MCF cells is enhanced by this conjugate by activate [caspase-7,8,9] [functionalized-selenium nanoparticle]. By an arbitrary intrinsic (mitochondrial) pathway apoptotic brain tumor cell's killing happens.

Sun et al. (Zhuo et al. 2004) observed that combining of [Luminescent-Ru (II)-thiol + SeNPs] shows low adverse effects aids to suppress cancer development or assists through suppression of mitochondrial membrane potential in angiogenesis and ROS in a [HepG2] tumor mice model. The promotion of S-phase detention and promotion of apoptosis in (MCF-7) cancerous cells via a mitochondrial arbitrated mechanism, is helped by folic acid in conjunction with SeNPs. According to Jou et al. (Zinicovscaia et al. 2016), the Selenium Nanoform may be produced using the Selenium nanoparticles Surface Efficacies Rule to reduced toxicity and for the better anti-cancer property. via activation of caspase and the mechanism of mitochondrial dysfunction the growth of cancer cells is inhibited in the mouse model and this does not affect organs. According to Jou et al. (Zhang et al. 2008) for low toxicity effect and for enhancing the anticancer functions of paclitaxel Hyaluronic acid—A modified form of selenium nanoparticle (HA@PTX) is used. For preparing HA@PTX SeNPs with hyaluronic acid (HA) are binding and enriched with paclitaxel (PTX) to increase the features of paclitaxel. By clathrin endocytosis, these modified nanoforms became able to penetrate the A549 which is a cancer cell. Or by the release of PTX in tumorous cells and they prevent the spread, migration of cancer cells A549 and result in the apoptosis of these cancer cells. [HA]—(Se@PTX) has properties for the prevention or treating cancer cells of the lung. According to Liu et al. (Zhang et al. 2012) report that for enhancing the stability of antitumor action of selenium nanoparticle (SeNPs) a nanocomposite was made with the use of CPA, Na_2SeO_3 by a redox reaction. By HeLa cells, this nanocomposite is taken via clathrin endocytosis resulting in the prevention of cancer cells. CPA embellish selenium nanoparticle (SeNPs) by an intrinsic path, promotes HeLa cancer cell apoptosis triggering intracellular reactive oxygen species (ROS) generation and membrane potential dysfunction.

According to Baskar et al. (Zhang et al. 2008) by binding asparaginase to selenium, nanoparticles enhance anticancer properties of L-asparaginase resulting in the creation of nanocomposite of selenium. On testing of these Se nanocomposites on human osteosarcoma cell lines, colon liver found that it helps in decreasing cancer in these cancer lines. In cancer treatment, this nanobiocomposite acts as a potential. TiO_2 nanotubes coated with selenium nanoparticles can be used in the inhibition of cancer cell growth as well as also used for infection due to bacteria. These nanotubes coated with selenium nanoparticles (SeNPs) can be prepared with the help of sodium selenite and glutathione (Zhang et al. 2013).

Bilek et al. find that the anticancer action of Vγ9Vδ2 T cells is increased by Selenium nanoparticles (SeNP). Comparison with the Gamma and Delta T cells alone, Gamma and Delta T cells possess has a greater effect in decreases of cancer growth when combined with selenium nanoparticle (SeNP). A steady microtubule network in selenium nanoparticles (SeNPs) pretreated Gamma and Delta T cells boost (cellular)-organelle transmissions, which cause in promotes in death of a cancerous cell. Crocin is dispersed around cancerous tissue in an acidic environment for probable cancer treatment because Polyethylene glycol—SeNPs is a pH-mediated delivery system. Crocin in combination with PEG + SeNP optimizes the cytotoxicity of a lung cancer cell by generating apoptosis via a mitochondrial-mediated mechanism. Moreover, in the nude mouse model the combination of crocin with PEG + SeNPs aids in the

prevention of cancer cell production. This combination plays the role of a therapeutic agent for many types of human carcinoma.

According to Xia (Zhong et al. 2019) report modified SeNPs with galactose plays a role of the delivery vehicle of doxorubicin (chemopreventive agent) to the hepatocellular cell which is a cancerous cell. Preparation of GA-Se@DOX with fewer toxicity effects is done by modification of selenium nanoparticle (SeNPs) with galactose, after that on the surface of galactose selenium nanoparticle, there is the addition of doxorubicin. For enhancing the effectiveness of doxorubicin in the treatment of hepatocellular carcinoma the GA-Se@DOX is prepared. By pathway i.e. (clathrin—endocytosis) GA-Se@DOX comes into cancerous cells and release antimitotic drug doxorubicin in HepG2 (cancer cells) and help in growth and death (apoptosis) of these cancerous cells by caspase signaling. When comparison with antimitotic drugs alone or with (SeNPs + DOX) this modification of SeNPs has better antitumor properties. For treatment of hepatocellular carcinoma (GA + Se@DOX) has good potential.

According to Xia et al. (Zhang et al. 2019) report the [HA-SeNPs + DOX] which is a functionalized SeNPs used for delivery of doxorubicin which is antimitotic medication to cervical cancer cells. This functionalized SeNPs [HA-SeNPs + DOX] prepared with low toxicity damage when (Se-NPs) combined with [hyaluronic-HA] acid and formed [HA + SeNPs] and it is used to load doxorubicin (DOX) (antimitotic medication). [HA-SeNPs + DOX] helps in the prevention of cancer cell production by suppressing the augmentation of tumor cells and inducing apoptosis of tumor cells. When there is a comparison between [SeNPs + DOX] and with antimitotic medication, [HA-SeNPs + DOX] has a higher effective antitumor function. That is why [HA-SeNPs + DOX] is an auspicious anticancer mediator in treating cervical cancer. According to Liu et al. (Zou et al. 2019) report that state that functionalized selenium nanoparticles with polyethylene glycol helping in the delivery of sesamol which is an antimitotic medication in the liver cancer cell. The modification form [sesamol + PEG + selenium nanoparticles] is prepared by using polyethylene glycol-(PEG) and nanoparticles of antimitotic agents by combining that is [sesamol, Se]. This modified form [Sesamol + PEG + SeNPs] possesses high antimitotic function than [PEG + SeNP] or sesamol alone by boosting the prevention of growth of cancer cells [HepG2]. This functionalized form of nanoparticle increased cancer cell apoptosis (cell death), which may be advantageous in the development of antimitotic medicine. According to Ranjitha et al.'s study which showed bio-conjugated SeNPs peptide preparation is done when biosynthesized selenium nanoparticles (SeNPs) and peptides combine by cysteine conjugation. As compared to both the peptide and the nanoparticle (NP) alone the [bioconjugated-SeNPs] showed increased cytotoxic action. This functionalized nanoparticle conjugate [bio-conjugated-SeNPs] was tested for its toxicity action in contradiction of [HT29] which is tumorous cells and caused in cancerous cell apoptosis (death). More researches are required for knowing the pathway of this functionalized nanoparticle [bio-conjugated-SeNPs-peptide] cytotoxicity in contrast to colon cancer cells (Tang et al. 2019). According to Khan et al. propose that hydroxyapatite with doped selenium can be used for curing Osteosarcoma because of its known antimitotic functions. Selenium—hydroxyapatite nanoparticles interactions with catechins-CC as catechins-CC enhanced the antitumor properties of these

modified nanoparticles of selenium because it has high therapeutic value in curing cancer. Modification of Se-hydroxyapatite nanocomposites with Catechins [CC/Se + HAp] has increased antitumor properties so that it aids in producing apoptosis of cancer cells via the formation of reactive oxygen species of (ROS). By combining of hydroxyapatite-HAp nanoparticles with Se, CC-catechins are prepared.

4   Conclusion

Selenium nanoparticles have been studied for their potential in the treatment of a variety of disorders, with cancer therapy being one of the most pressing study topics. Selenium or its type has chemopreventive properties against cancer but selenium's form (inorganic and organic) is unable to show their efficacy with less toxicity damage to cancer cells. Selenium also aids in the improvement of therapeutic agent anticancer efficacy. To give reliable information on the Se—capacity in tumor suppression, the state of selenium and selenium forms must be re-evaluated. Less toxicity effect and effectiveness of selenium is a huge task for scientists. But presently nanotechnology has provided a solution to this problem because they have properly [high surface/volume ratio, minor dimension] they can reach to the cell surface or has high drug storage capacity with a low hazardous impact. Insignificant toxic effects of modified selenium (Se) nanoparticles are used to increased the features of antimitotic drugs by putting them on the surface of SeNPs. More research is still needed to understand completely the cytotoxic mechanism of different functionalized nanoparticles of selenium.

Author Contribution   A.R.P. had the idea for the article, A.R.P had performed the literature search and data analysis, and A.R.P and S.S. had drafted and critically revised the work.

Data Availability   All data generated or analyzed during this study are included in this article.

Declarations   Ethics approval and consent to participate: Not applicable.

Consent for Publication   Not applicable.

Conflict of Interest   The authors declare no competing interests.

References

Ali W, Álvarez-Pérez M, Marć MA, Salardón-Jiménez N, Handzlik J, Domínguez-Álvarez E (2018) The anticancer and chemopreventive activity of selenocyanate-containing compounds. Curr Pharmacol Rep 4(6):468–481

Berzelius JJ (1817) Sur deux métaux nouveaux (litium et sélénium). Schweigger J 2:1818–1823

Bhattacharya A (2011) Methylselenocysteine: a promising antiangiogenic agent for overcoming drug delivery barriers in solid malignancies for therapeutic synergy with anticancer drugs. Expert Opin Drug Delivery 8(6):749–763

Bilek O, Fohlerova Z, Hubalek J (2019) Enhanced antibacterial and anticancer properties of Se-NPs decorated TiO$_2$ nanotube film. PLoS ONE 14(3)

Brodin O, Hackler J, Misra S, Wendt S, Sun Q, Laaf E, Stoppe C, Björnstedt M, Schomburg L (2020) Selenoprotein P as a biomarker of selenium status in clinical trials with therapeutic dosages of selenite. Nutrients 12(4):1067

Brozmanova J, Manikova D, Vlckova V, Chovanec M (2010) Selenium: a double-edged sword for defense and offense in cancer. Arch Toxicol 84:919–938

Burk RF, Norsworthy BK, Hill KE, Motley AK, Byrne DW (2006) Effects of chemical form of selenium on plasma biomarkers in a high-dose human supplementation trial. Cancer Epidemiol Biomark Prev 15(4):804–810

Cao S, Durrani FA, Rustum YM (2004) Selective modulation of the therapeutic efficacy of anticancer drugs by selenium-containing compounds against human tumor xenografts. Clin Cancer Res 10(7):2561–2569

Cavalu S, Laslo V, Banica F, Vicas SI (2016) Naturally derived matrix for controlled selenium nanoparticles delivery. Key Eng Mater 695:284–288. https://doi.org/10.4028/www.scientific.net/KEM

Çetin ES, Nazıroğlu M, Çiğ B, Övey İS, Koşar PA (2016) Selenium potentiates the anticancer effect of cisplatin against oxidative stress and calcium ion signalling-induced intracellular toxicity in MCF-7 breast cancer cells: involvement of the TRPV1 channel. J Recept Signal Transduct 37(1):84–93

Chakraborty M, Mitra MK, Chakraborty J (2017) One-pot synthesis of CaAl-layered double hydroxide–methotrexate nanohybrid for anticancer application. Bull Mater Sci 40(6):1203–1211

Chen T (2012) Surface decoration by spirulina polysaccharide enhances the cellular uptake and anticancer efficacy of selenium nanoparticles. Int J Nanomed. https://doi.org/10.2147/IJN.S28278

Chen T, Wong YS, Zheng W, Bai Y, Huang L (2008) Selenium nanoparticles fabricated in *Undaria pinnatifida* polysaccharide solutions induce mitochondria-mediated apoptosis in A375 human melanoma cells. Colloids Surf B Biointerfaces 67:2631. https://doi.org/10.1016/j.colsurfb.2008.07.010

Combs GF Jr, Clark LC, Turnbull BW (1997) Reduction of cancer mortality and incidence by selenium supplementation. Med Klin (munich) 92(Suppl 3):42–45

Cui D, Ma J, Liang T, Sun L, Meng L, Liang T, Li Q (2019) Selenium nanoparticles fabricated in laminarin polysaccharides solutions exert their cytotoxicities in HepG2 cells by inhibiting autophagy and promoting apoptosis. Int J Biol Macromol. https://doi.org/10.1016/j.ijbiomac.2019.07.031

Domínguez-Álvarez E, Plano D, Font M, Calvo A, Prior C, Jacob C, Palop JA, Sanmartín C (2014) Synthesis and antiproliferative activity of novel selenoester derivatives. Eur J Med Chem 12(73):153–166

El-Sayed WM, Aboul-Fadl T, Lamb JG, Roberts JC, Franklin MR (2016) Effect of selenium-containing compounds on hepatic chemoprotective enzymes in mice. Toxicology 220(2–3):179–188

Ertilav K, Nazıroğlu M, Ataizi ZS, Braidy N (2019) Selenium enhances the apoptotic efficacy of docetaxel through activation of TRPM2 channel in DBTRG glioblastoma cells. Neurotox Res. https://doi.org/10.1007/s12640-019-0009-5

Frieben E, Amin S, Sharma AK (2019) Development of isoselenocyanate compounds' syntheses and biological applications. J Med Chem. https://doi.org/10.1021/acs.jmedchem.8b01698

Fu X, Yang Y, Li X, Lai H, Huang Y, He L, Zheng W, Chen T (2016) RGD peptide-conjugated selenium nanoparticles: antiangiogenesis by suppressing VEGF-VEGFR2-ERK/AKT pathway. Nanomed Nanotechnol Biol Med 12:1627–1639

Ganesan V (2015) Biogenic synthesis and characterization of selenium nanoparticles using the flower of *Bougainvillea spectabilis* willd. Int J Sci Res (IJSR) 4:690–695

Gangadoo S, Stanley D, Hughes RJ, Moore RJ, Chapman J (2017) The synthesis and characterization of highly stable and reproducible selenium nanoparticles. Inorg Nano-Met Chem

Gao F, Yuan Q, Gao L, Cai P, Zhu H, Liu R, Wang Y, Wei Y, Huang G, Liang J, Gao X (2014) Cytotoxicity and therapeutic effect of irinotecan combined with selenium nanoparticles. Biomaterials 35(31):8854–8866

Gorain B, Choudhury H, Pandey M, Kesharwani P (2018) Paclitaxel loaded vitamin E-TPGS nanoparticles for cancer therapy. Mater Sci Eng C 91:868–880

Hariharan H, Al-Harbi N, Karuppiah P, Rajaram S (2012) Microbial synthesis of selenium nanocomposite using *Saccharomyces cerevisiae* and its antimicrobial activity against pathogens causing nosocomial infection. Chalcogenide Lett 9(12):509–515

Hu Y, Liu T, Li J, Mai F, Li J, Chen Y, Jing Y, Dong X, Lin L, He J, Xu Y, Shan C, Hao J, Yin Z, Chen T, Wu Y (2019) Selenium nanoparticles as new strategy to potentiate γδ T cell anti-tumor cytotoxicity through upregulation of tubulin-α acetylation. Biomaterials. https://doi.org/10.1016/j.biomaterials.2019.119397

Jain R, Dominic D, Jordan N, Rene ER, Weiss S, van Hullebusch ED, Hübner R, Lens PN (2016) Higher Cd adsorption on biogenic elemental selenium nanoparticles. Environ Chem Lett 14(3):381–386. https://doi.org/10.1007/s10311-016-0560-8

Johnson WD, Morrissey RL, Kapetanovic I, Crowell JA, McCormick DL (2008) Subchronic oral toxicity studies of Se-methylselenocysteine, an organoselenium compound for breast cancer prevention. Food Chem Toxicol 46(3):1068–1078

Kalishwaralal K, Jeyabharathi S, Sundar K, Muthukumaran A (2016) A novel one-pot green synthesis of selenium nanoparticles and evaluation of its toxicity in zebrafish embryos. Artif Cells Nanomed Biotechnol 44(2):471–477. https://doi.org/10.3109/21691401.2014.962744

Khan S, Ullah MW, Siddique R, Liu Y, Ullah I, Xue M, Yang G, Hou H (2019) Catechins-modified selenium-doped hydroxyapatite nanomaterials for improved osteosarcoma therapy through generation of reactive oxygen species. Front Oncol 9:499. https://doi.org/10.3389/fonc.2019.00499

Khurana A, Tekula S, Saifi MA, Venkatesh P, Godugu C (2019) Therapeutic applications of selenium nanoparticles. Biomed Pharmacother 111:802–812

Klein EA, Thompson IM, Lippman SM, Goodman PJ, Albanes D, Taylor PR, Coltman C (2001) SELECT: the next prostate cancer prevention trial. J Urol 166(4):1311–1315

Kora AJ, Rastogi L (2016) Biomimetic synthesis of selenium nanoparticles by *Pseudomonas aeruginosa* ATCC 27853: an approach for conversion of selenite. J Environ Manage 181:231–236. https://doi.org/10.1016/j.jenvman

Kumar S, Tomar MS, Acharya A (2015) Carboxylic group-induced synthesis and characterization of selenium nanoparticles and its anti-tumor potential on Dalton's lymphoma cells. Colloids Surf B Biointerfaces 126:546–552. https://doi.org/10.1016/j.colsurfb.2015.01.009

Le PN, Nguyen NH, Nguyen CK, Tran NQ (2016) Smart dendrimer-based nanogel for enhancing 5-fluorouracil loading efficiency against MCF7 cancer cell growth. Bull Mater Sci 39(6):1493–1500

Le Province Medicale (1912) In references to a publication to the use of selenium to treat a tongue epithelioma, 6 May 1912

Li W, Zhu Y, Yan X et al (2000) The prevention of primary liver cancer by selenium in high-risk populations. Chin J Prev Med 34(6):336–338

Li Z, Carrier L, Belame A et al (2009) Combination of methylselenocysteine with tamoxifen inhibits MCF-7 breast cancer xenografts in nude mice through elevated apoptosis and reduced angiogenesis. Breast Cancer Res Treat 118(1):33–43

Li Y, Li X, Wong YS, Chen T, Zhang H, Liu C, Zheng W (2011) The reversal of cisplatin-induced nephrotoxicity by selenium nanoparticles functionalized with 11-mercapto-1-undecanol by inhibition of ROS-mediated apoptosis. Biomaterials 32(34):9068–9076. https://doi.org/10.1016/j.biomaterials.2011.08.001

Li H, Liu D, Li S, Xue C (2019) Synthesis and cytotoxicity of selenium nanoparticles stabilized by α-D-glucan from *Castanea mollissima* Blume. Int J Biol Macromol

Lindshield BL, Ford NA, Canene-Adams K, Diamond AM, Wallig MA, Erdman Jr JW (2010) Selenium, but not lycopene or vitamin E, decreases growth of transplantable dunning R3327-H rat prostate tumors. PLoS ONE 5(4):10423

Liong M, Lu J, Kovochich M, Xia T, Ruehm SG, Nel AE, Tamanoi F, Zink JI Multifunctional inorganic nanoparticles for imaging, targeting, and drug delivery. ACS Nano 2:889–896 (2009). https://doi.org/10.1021/nn800072t

Lippman SM, Klein EA, Goodman PJ, Lucia AS, Thompson IM, Ford LG, Parnes HL, Minasian LM, Gaziano JM, Hartline JA, Parsons JK, Bearden JD, Crrawford ED, Goodman GE, Claudio J, Winquist E, Cook ED, Karp DD, Walther P, Lieber MM, Kristal AR, Darke AK, Arnold KB, Ganz PA, Santella RM, Albanes D, Taylor PR, Probstfield JL, Jagpal TJ, Crowley JJ, Meyskens FL, Baker LH, Coltman CA (2009) Effect of selenium and vitamin E on risk of prostate cancer and other cancers. JAMA 301(1):39–51

Liu T, Zeng L, Jiang W, Fu Y, Zheng W, Chen T (2015) Rational design of cancer targeted selenium nanoparticles to antagonize multidrug resistance in cancer cells. Nanomed Nanotechnol Biol Med 11:947–958. https://doi.org/10.1016/j.nano.2015.01.009

Liu F, Liu H, Liu R, Xiao C, Duan X, McClements DJ, Liu X (2019) Delivery of sesamol using polyethylene glycol-functionalized selenium nanoparticles in human liver cells in culture. J Agric Food Chem. https://doi.org/10.1021/acs.jafc.8b06924

Lü J, Zhang J, Jiang C, Deng Y, Özten N, Bosland MC (2016) Cancer chemoprevention research with selenium in the post-SELECT era: promises and challenges. Nutr Cancer 68(1):1–7

Luesakul U, Puthong S, Neamati N (2018) Muangsin: pH-responsive selenium nanoparticles stabilized by folate-chitosan delivering doxorubicin for overcoming drug-resistant cancer cells. Carbohydr Polym 181:841–850. https://doi.org/10.1016/j.carbpol.2017.11.068

Menon S et al (2018) Colloids Surf B Biointerfaces 170:280–292

Misra S, Boylan M, Selvam A, Spallholz JE, Bjornstedt M (2016) Redox-active selenium compounds—from toxicity and cell death to cancer treatment. Nutrients 7:35–36

Oldfield JE (1987) The two faces of selenium. J Nutr 117(12):2002–2008

Peters U, Takata Y (2008) Selenium and the prevention of prostate and colorectal cancer. Mol Nutr Food Res 52(11):1261–1272

Ranjitha R, Muddegowda U, Rai VR (2019) Potent activity of bioconjugated peptide and selenium nanoparticles against colorectal adenocarcinoma cells. Drug Dev Ind Pharm 1–21. https://doi.org/10.1080/03639045.20191634090

Redman C, Scott JA, Baines AT et al (1998) Inhibitory effect of selenomethionine on the growth of three selected human tumor cell lines. Cancer Lett 125(1–2):103–110

Richie Jr JP, Das A, Calcagnotto AM, Sinha R, Neidig W, Liao J, Lengerich EJ, Berg A, Hartman TJ, Ciccarella A, Baker A, Kaag MG, Goodin S, DiPaola RS, El-Bayoumy K (2014) Comparative effects of two different forms of selenium on oxidative stress biomarkers in healthy men: a randomized clinical trial. Cancer Prev Res 7(8):796–804

Riva C, Oreal H (2016) Selenium-enriched *Arthrospira platensis* potentiates docetaxel, oxaliplatin, and topotecan anticancer activity in epithelial tumors. J Appl Phycol 28(6):3371–3377

Rotruck JT, Pope AL, Ganther HE, Swanson AB, Hafeman DG, Hoekstra WG (1973) Selenium: biochemical role as a component of glutathione peroxidise. Science 179:588–590

Sanmartín C, Plano D, Domínguez E, Font M, Calvo A, Prior C, Encio I, Palop JA (2009) Synthesis and pharmacological screening of several aroyl and heteroaroyl selenylacetic acid derivatives as cytotoxic and antiproliferative agents. Molecules 14:3313–3338

Schrauzer GN, White DA, Schneider CJ (1977) Cancer mortality correlation studies. III. Statistical association with dietary selenium intakes. Bioinorg Chem 7:35–56

Shamberger RJ, Frost DV (1969) Possible protective effect of selenium against human cancer. Can Med Assoc J 100:682

Song D, Li X, Cheng Y, Xiao X, Lu Z, Wang Y, Wang F (2017) Aerobic biogenesis of selenium nanoparticles by *Enterobacter cloacae* Z0206 as a consequence of fumarate reductase mediated selenite reduction. Sci Rep 7:32–39. https://doi.org/10.1038/s41598-017-03558-3

Song M et al (2018) Phase I trial of selenium plus chemotherapy in gynecologic cancers. Gynecol Oncol. https://doi.org/10.1016/j.ygyno.2018.07.001

Spallholz JE (2019) Selenomethionine and methioninase: selenium free radical anticancer activity. In: Methionine dependence of cancer and aging: methods and protocols, pp 199–210

Srivastava P, Kowshik M (2016) Anti-neoplastic selenium nanoparticles from Idiomarina sp. PR58-8. Enzyme Microb Technol 95:192–200. https://doi.org/10.1016/j.enzmictec.2016.08.002.S

Sugiura K, Benedict SR (1929) The action of certain dyestuffs on the growth of transplantable tumors. J Cancer Res 13(4):340–358

Sun D, Liu Y, Yu Q, Zhou Y, Zhang R, Chen X, Hong A, Liu J (2013) The effects of luminescent ruthenium (II) polypyridyl functionalized selenium nanoparticles on bFGF-induced angiogenesis and AKT/ERK signalling. Biomaterials 34:171–180. https://doi.org/10.1016/j.biomaterials.2012.09.031

Sun D, Liu Y, Yu Q, Qin X, Yang L, Zhou Y, Chen L, Liu J (2014) Inhibition of tumor growth and vasculature and fluorescence imaging using functionalized ruthenium-thiol protected selenium nanoparticles. Biomaterials 35(5):1572–1583. https://doi.org/10.1016/j.biomaterials.2013.11.007

Suzuki M, Endo M, Shinohara F, Echigo S, Rikiishi H (2010) Differential apoptotic response of human cancer cells to organoselenium compounds. Cancer Chemother Pharmacol 66(3):475–484

Tan L, Jia X, Jiang X, Zhang Y, Tang H, Yao S, Xie Q (2009) In vitro study on the individual and synergistic cytotoxicity of adriamycin and selenium nanoparticles against Bel7402 cells with a quartz crystal microbalance. Biosens Bioelectron 24:2268–2272. https://doi.org/10.1016/j.bios.2008.10.030

Tan H, Mo H-Y, Lau A, Xu Y-M (2012) Selenium species: current status and potentials in cancer prevention and therapy. Int J Mol Sci 20(1):75. https://doi.org/10.3390/ijms20010075

Tang S, Wang T, Jiang M et al (2019) Construction of arabinogalactans/selenium nanoparticles composites for enhancement of the antitumor activity. Int J Biol Macromol. https://doi.org/10.1016/j.ijbiomac.2019.01.152

Valdiglesias V, Pásaro E, Méndez J, Laffon B (2010) In vitro evaluation of selenium genotoxic, cytotoxic, and protective effects: a review. Arch Toxicol 337–351. https://doi.org/10.1007/s00204-009-0505-0

Vekariya KK, Kaur J, Tikoo K (2012) ERα signaling imparts chemotherapeutic selectivity to selenium nanoparticles in breast cancer. Nanomed Nanotechnol Biol Med 8:1125–1132. https://doi.org/10.1016/j.nano.2011.12.003

Wadhwani SA, Shedbalkar UU, Singh R, Chopade BA (2016) Biogenic selenium nanoparticles: current status and future prospects. Appl Microbiol Biotechnol 100:2555–2566. https://doi.org/10.1007/s00253-016-7300-7

Wang, L, Bonorden, MJ, Li, GX et al (2009) Methyl-selenium compounds inhibit prostate carcinogenesis in the transgenic adenocarcinoma of mouse prostate model with survival benefit. Cancer Prev Res 2(5):484–495

Wang Y, Ma J, Zhou L, Chen J, Liu Y, Qiu Z, Zhang S (2012) Dual functional selenium-substituted hydroxyapatite. Interface Focus 2:378–386. https://doi.org/10.1098/rsfs.2012.0002

Wang X, Sun K, Tan Y, Wu S, Zhang J (2014) Efficacy and safety of selenium nanoparticles administered intraperitoneally for the prevention of growth of cancer cells in the peritoneal cavity. Free Radic Biol Med 72:1–10. https://doi.org/10.1016/j.freeradbiomed.2014.04.003

Wang Y, Chen P, Zhao G, Sun K, Li D, Wan X, Zhang J (2015) Inverse relationship between elemental selenium nanoparticle size and inhibition of cancer cell growth in vitro and in vivo. Food Chem Toxicol 85:71–77. https://doi.org/10.1016/j.fct.2015.08.006

Wang L, Wang J, Liu X, Liu Q, Zhang G, Liang L (2016) Association between selenium intake and the risk of pancreatic cancer: a meta-analysis of observational studies. Biosci Rep 36. https://doi.org/10.1042/BSR20160345e00395-e00395

Waters DJ, Chiang EC (2018) Five threads: how U-shaped thinking weaves together dogs, men, selenium, and prostate cancer risk. Free Radic Biol Med. https://doi.org/10.1016/j.freeradbiomed. 2017.12.039

Wu H, Li X, Liu W, Chen T, Li Y, Zheng W, Man CW-Y, Wong M-K, Wong KH (2012) Surface decoration of selenium nanoparticles by mushroom polysaccharides–protein complexes to achieve enhanced cellular uptake and antiproliferative activity. J Mater Chem 22(19):9602–9610

Wu TT, Peters AA, Tan PT et al (2014) Consequences of activating the calcium-permeable ion channel TRPV1 in breast cancer cells with regulated TRPV1 expression. Cell Calcium 56:59–67

Wu X, Zhao G, He Y, Wang W, Yang CS, Zhang J (2019) Pharmacological mechanisms of the anticancer action of sodium selenite against peritoneal cancer in mice. Pharmacol Res 147:104360

Xia Y, Xu T, Wang C, Li Y, Lin Z, Zhao M, Zhu B (2018) Novel functionalized nanoparticles for tumor targeting co-delivery of doxorubicin and siRNA to enhance cancer therapy. Int J Nanomed 13:143–159

Xia Y, Xiao M, Zhao M, Xu T, Guo M, Wang C, Liu H (2019a) Doxorubicin-loaded functionalized selenium nanoparticles for enhanced antitumor efficacy in cervical carcinoma therapy. Mater Sci Eng C 110100

Xia Y, Zhong J, Zhao M, Tang Y, Han N, Hua L, Zhu B (2019b) Galactose-modified selenium nanoparticles for targeted delivery of doxorubicin to hepatocellular carcinoma. Drug Deliv 26(1):1–11. https://doi.org/10.1080/10717544.2018.1556359

Xu X, Feng Y, Chen X, Wang Q, Meng T, Liu A (2019) Antitumor effects of seleno-β-lactoglobulin on human breast cancer MCF-7 and MDA-MB-231 cells in vitro. Toxicol In Vitro 104607

Yoshizawa K, Willett WC, Morris SJ et al (1998) Study of prediagnostic selenium level in toenails and the risk of advanced prostate cancer. J Natl Cancer Inst 90(16):1219–1224

Yu SY, Zhu YJ, Li WG, Huang QS, Huang CZ, Zhang QN et al (1991) A preliminary report on the intervention trials of primary liver cancer in high-risk populations with nutritional supplementation of selenium. Biol Trace Elem Res 29(3):289–294

Zhang J, Wang X, Xu TT (2008) Elemental selenium at nano size (Nano-Se) as a potential chemopreventive agent with reduced risk of selenium toxicity: comparison with se-methylselenocysteine in mice. Toxicol Sci 101:2231. https://doi.org/10.1093/toxsci/kfm221

Zhang P, Hu L, Yin Q, Zhang Z, Feng L, Li Y (2012) Transferrin-conjugated polyphosphoester hybrid micelle loading paclitaxel for brain-targeting delivery: synthesis, preparation and in vivo evaluation. J Control Release 159:429–434

Zhang Y, Li X, Huang Z, Zheng W, Fan C, Chen T (2013) Enhancement of cell permeabilization apoptosis-inducing activity of selenium nanoparticles by ATP surface decoration. Nanomed Nanotechnol Biol Med 9:74–84. https://doi.org/10.1016/j.nano.2012.04.002

Zhang Z, Du Y, Liu T, Wong KH, Chen T (2019). Biomater Sci. https://doi.org/10.1039/C9BM01 104H

Zhong J, Xia Y, Hua L, Liu X, Xiao M, Xu T, Zhu B, Cao H (2019) Functionalized selenium nanoparticles enhance the anti-EV71 activity of oseltamivir in human astrocytoma cell model. Artif Cells Nanomed Biotechnol 47(1):3485–3491. https://doi.org/10.1080/21691401.2019.164 0716

Zhuo H, Smith AH, Steinmaus C (2004) Selenium and lung cancer: a quantitative analysis of heterogeneity in the current epidemiological literature. Cancer Epidemiol 771–778

Zinicovscaia I, Rudi L, Valuta A, Cepoi L, Vergel K, Frontasyeva MV, Safonov A, Wells M, Grozdov D (2016) Biochemical changes in nostoc linckia associated with selenium nanoparticles biosynthesis. Ecol Chem Eng S 23:559–569. https://doi.org/10.1515/eces-2016-0039

Zou J, Su S, Chen Z, Liang F, Zeng Y, Cen W, Huang D (2019) Hyaluronic acid-modified selenium nanoparticles for enhancing the therapeutic efficacy of paclitaxel in lung cancer therapy. Artif Cells Nanomed Biotechnol 47(1):3456–3464

Photocatalytic Degradation of Amaranth Dye from Water Using TiO$_2$-BiOI Nanocomposite

Sunidhi and Surinder Singh

Abstract Due to rapid and uncontrolled development, industrialization and population shift towards cities and discharge of wastes into water bodies the contamination of water takes place. This has led to release of diversity of chemical species like aromatic and inorganic compounds, pigments, colorants and dyes, phenols and catechol etc. compounds into water bodies. The present study incorporates the synthesis of TiO$_2$/BiOI nano-composite, its characterization, and further photocatalytic application of the nanostructure for amaranth dye removal. Commercial TiO$_2$, P25 Degussa was used and BiOI nanosheets were synthesized in laboratory using the precipitation process. TiO$_2$/BiOI nanostructure was prepared through the calcination method and was further characterized using different analytical techniques. Catalytic activity of the prepared TiO$_2$/BiOI nano-composite was assessed for the degradation of amaranth dye utilizing visible solar light. The influence of various process parameters e.g. catalyst dose, pH, initial dye concentration, contact time and scavengers effect on the degradation efficiency of amaranth dye degradation was examined. Around 91% degradation of amaranth dye was achieved at pH 6, utilizing catalyst dose of 25 mg/L, initial dye concentration of 10 mg/L in 40 min. Scavenger studies showed that h$^+$, e$^-$, and OH$^-$ were the most reactive chemical species responsible for the photo-catalytic degradation process.

Keywords Photocatalysis · Degradation · Visible light · Catalyst · Nanocomposite

1 Introduction

Water is a vital and exceptionally imperative resource for maintaining satisfactory nourishment and beneficial environment for all life forms. As human population is expanding and economies growing, the freshwater demand has been expanding quickly all over the world. With reference to the threatening water scarcity, water

Sunidhi · S. Singh (✉)
Dr. S. S. Bhatnagar University Institute of Chemical Engineering and Technology, Panjab University, Chandigarh, India
e-mail: sonuunos@gmail.com

deficiencies have reduced the biodiversity in both sea-going and earthly ecosystems. The harmful effects of worldwide population increment, climate change based impacts, and lifestyle changes have burdened the crucial water resources driving to far-reaching water inadequacy in numerous nations. Water is basic to life, since it intensely impacts health of the citizens along with standard of their living. Be that as it may, water is unequally distributed throughout the world (Ritika et al. 2019a).

The contamination water bodies occur when harmful chemical species like organic and inorganic compounds, pathogens and microorganisms enter these resources. The industrial discharge contains many of the toxic and hazardous chemicals which are sometime carcinogenic like heavy metals and in general are highly toxic for the aquatic organisms. The common pollutants which are discharged into water bodies includes pigments, drugs, cosmetics and personal care products released from different chemical process industries and cause a great harm to the water resources (Sood et al. 2015a; Ritika et al. 2019b). Domestic sewage is additionally a major source of plant supplements, primarily nitrates, and phosphates which can cause episode like algal bloom.

Such substances when present in water obstruct sunlight into water thereby affecting the aquatic life and ecosystem and hamper the photosynthesis activity. The ingestion and use of these harmful substances can affect the human health and can cause various kinds of acute and chronic ailments and water borne health effects. These substances not only affect the biodiversity, but cause various other ill effects such as microbial resistance, bio-magnification and deterioration of soil layers and plant growth. Hence the efficient removal of these toxic compounds from water bodies is a matter of critical concern (Sood et al. 2015b; Kumar and Bansal 2010b).

Varied types of water treatment methods have been practiced such as adsorption, membrane separation, flocculation, coagulation and advanced oxidation processes (AOPs) like photo-Fenton, chemical precipitation, ozonolysis and photocatalysis. The AOPs are supposed to be highly efficient techniques as they offer to degrade or treat harmful contaminants and can convert them into simple non-toxic compounds. Photocatalysis is further sub-divided into homogeneous and heterogeneous sub-categories. Homogeneous photocatalysis involves the use of suitable molecular catalysts in UV or solar light based environment wherein the catalysts degrade the pollutions in a single phase (solution) utilizing oxidizing and reduction of the contaminants. Whereas the heterogeneous photocatalysis reaction involves two phases and involves the photon energy to degrade the harmful contaminants. Heterogeneous photocatalysis offers great potential and is widely utilized by the researchers due to its benefits like environmentally benign, low cost and highly effective in mineralizing the harmful contaminants present in the wastewater (Sood et al. 2015c, 2016; Majhi et al. 2019; Naik et al. 2017).

Synthetic dyes have complex aromatic structures, these bear resistant to heat, illumination and oxidizing agents, and also are non-biodegradable (Tamilarasan et al. 2016). The various processes included within the tanning, chrome plating and textile industry happen to be responsible for the discharge of huge amounts of dyes, pigments and colorants, heavy metals, and synthetic compounds. The release of dyestuffs from these diverse industries is stacked with high amounts of organic and

inorganic compounds with steady complex structures. The effluents from industrial units of dyes consuming plants contain pigments, overwhelming toxic metal particles, dyes, amino and amine compounds, surfactants, bleaching agents, solvents, salts, disinfectants, and conditioners. These compounds collectively make the water bodies polluted with heavy amounts of dyestuffs and colorants (Meng et al. 2019). Different dyes are having different affinity and chemical bonding with water which determines the complexity of the dyes and their removal potential from water bodies.

These dyes cause a large BOD load in the water bodies and their biological removal causes depletion of the dissolved oxygen (DO) and more need for oxygen in the aquatic bodies for their removal (Anwer et al. 2019). The correlation between BOD and COD was studied by Kumar et al. (2005). The conventional water treatment methods like precipitation, adsorption, coagulation/flocculation, ultra-filtration, incineration etc. are also utilized but all of these have some limitations e.g. these methods cannot induce complete degradation of dye stuffs, due to which the use of AOP based techniques like photocatalysis is very much viable and useful for wastewater treatment (Bansal 2012; Cai et al. 2019; Chen et al. 2020; Dai et al. 2019; Kaur et al. 2017, 2018, 2019). Titanium dioxide (TiO_2), a transition metal has extraordinary characteristics like tunable bandgap, wide photo-response, great mobility, high conductivity, easy abundance, chemical inertness, high quantum efficiency, excellent catalytic activity, cost-effectiveness, and non-toxic nature. Due to the peculiar features, it is extensively employed in air pollution control, wastewater treatment, catalysis, energy storage devices, lithium batteries, super capacitors, sensing, and so forth (Al-Mamun et al. 2019).

Marchelek et al. (2018) synthesized $TiO_2/SrTiO_3$ (binary) and $TiO_2/SrTiO_3/BiOI$ nanocomposites by stepwise procedure. The finest catalytic ability for degradation of phenol was exhibited by $TiO_2/SrTiO_3/BiOI^{-4}$ run, thereby degrading 30.2% phenol within one hour using solar visible irradiation. Liu et al. (2019) utilized surface of TiO_2 nanotube clusters by SILAR technique. The prepared photo-electro-catalytic (PEC) catalyst ($BiOI/TiO_2$ nanotubes) was utilized for degradation of Rhodamine B, methylene blue and methyl orange dyes and Cr (VI) ions. CFD simulations of immobilized-titanium dioxide based annular photocatalytic reactor were studied and reported by Kumar and Bansal (2015). Enhancement of photocatalytic activity and hydrophilicity of self-cleaning cement containing microsized TiO_2 was reported by Ratan and Saini (2019) and Saini et al. (2020). Degradation of meropenem antibiotic in aqueous solution using UV, UV/H_2O_2, UV/TiO_2 and $UV/TiO_2/H_2O_2$ was reported by Verma and Kumar (2014).

Jyotsna et al. (2020) synthesized β-$AgVO_3/TiO_2$ nano-heterojunction utilizing facile hydrothermal strategy for the photocatalytic decay of Rhodamine B (RhB) and drug ciprofloxacin (using normal pH) utilizing visible solar light. The experimental results illustrated that synthesized β-$AgVO_3/TiO_2$ hetero-composite degraded 93% dye as compared to 43% done by virgin TiO_2. Based on the literature review and capability of binary nanocomposites, in the present work $TiO_2/BiOI$ nanocomposite was utilized for degradation of amaranth dye using solar light driven photocatalysis.

2   Materials and Methods

All the chemicals used were of analytical grade purity and were utilized without any further treatment process. Double distilled water has been used throughout the experimental study. Bismuth (III) nitrate pentahydrate ($Bi(NO_3)_3 \cdot 5H_2O \geq 98\%$) was procured from Sigma-Aldrich, India. Potassium Iodide (KI, $\geq 99\%$), sodium hydroxide (NaOH), hydrochloric acid (HCl, 36.5–38%), sodium chloride (NaCl, $\geq 99\%$), formic acid (FA/HCOOH, ≥ 98–100%), isopropanol (IPA), p-benzoquinone (p-BQ/$C_6H_4O_2$, $\geq 98\%$), isopropyl acetate, methanol (CH_3OH), and Acetic acid ($C_2H_4O_2$) were purchased from Merck, India. Ethanol (C_2H_5OH, $\geq 99.9\%$) was procured from S.D. fine, India. TiO_2 P25 from Degussa (Germany) was procured.

The pH of different solutions was measured using a Mettler-Toledo pH-meter (FEP20) and pH was adjusted using 0.1 M HCl and NaOH solutions. The ultra-violet–visible (UV–vis) spectrum was recorded on a Systronics-2202 UV–vis spectrophotometer for measuring the absorbance of the sample.

3   Synthesis and Characterization of the Nanocomposite

3.1   Synthesis of BiOI

The synthesis of BiOI catalyst was done using 1.4552 g of $Bi(NO_3)_3 * _5H_2O$, which was added to 50 mL distilled water. After stirring for 30 min, 30 mL of H_2O containing 0.4980 g KI was added further and slowly into the earlier solution (Luévano-Hipólito et al. 2019). The obtained solution was then stirred for 1.5 h at ambient temperature. Further, the solution products were separated utilizing filtration, after that it was washed with water and ethanol thoroughly, and then dried at temperature of 60 °C (Wang et al. 2018).

3.2   Synthesis of TiO$_2$-BiOI Nanocomposite

The synthesis of TiO_2/BiOI nanostructure was carried out via a calcination-assisted mechano-chemical approach. For the preparation of TiO_2/BiOI, 0.5 g of TiO_2 (P25 commercial, used directly) and 0.5 g of BiOI was mixed and grounded for 30 min in a mortar-pestle until the red powder is formed. Thereafter, the crucible was placed in a muffle furnace for the calcination process. The calcination was done at 450 °C for 2 h (Ali et al. 2018).

3.3 Characterization of Nanocomposite

The prepared samples were characterized in detail using multiple spectroscopic and analytical techniques. X-ray diffraction (XRD; PANanalytical XpertPro.), with Cu-Kα radiation ($\lambda = 1.54178$ Å) at 45 kV and 40 mA in the 2θ ranging from 4 to 80° was used to determine the structural and crystal properties. The presence of different functional groups was investigated by using Fourier transform infrared spectroscopy (FTIR; Perkin Elmer-Spectrum RX-IFTIR) ranging from 250 to 4000 cm^{-1}. The morphology of the prepared sample was determined by high-resolution transmission electron microscopy [HRTEM: Technai $G_2$20 (FEI) S-Twin]. The diffuse reflectance spectrum (DRS) was taken on a UV–vis spectrophotometer (UV-2600, Shimadzu). The general morphology of the prepared sample was observed by field emission scanning electron microscopy (FESEM; Hitachi-8010). Photo-luminescence (PL) spectra of prepared catalyst samples were analyzed utilizing a fluorescence based spectrophotometer (Hitachi F-7000; 5j1-004 model).

3.4 Photocatalytic Degradation Experiments

The catalytic capability of as-prepared TiO$_2$/BiOI heterostructure was monitored for decontamination of amaranth dye utilizing solar illumination. Solar light intensity of around 75 K lux was recorded utilizing a digital light meter. Catalytic reactions were employed utilizing an appropriate weight of catalyst added into 100 mL of dye mixed solution. The solution was kept under stirring in the dark space for about 30 min to attain an adsorption–desorption based equilibrium attainment between catalyst and dye mixture. Then the solution was kept beneath solar illumination source and the sample aliquots (of 2 mL volume) were taken from flask at predetermined time intervals. Catalyst was removed from dye solution utilizing filtration through a 0.45-µm Chromafil syringe filter. Further filter absorbance was analyzed utilizing Systronics make UV–vis spectrophotometer.

3.5 Scavengers Study

The performance or interference of reactive chemical species during the catalytic photo-degradation of organic pollutants was ascertained by scavengers based study. In order to perform scavenger studies, 0.01 M of different scavengers like formic acid, sodium chloride, isopropyl alcohol and benzoquinone were mixed with aqueous solution of dye before adding photocatalyst. The role of superoxide ($O_2^{\cdot -}$) was also confirmed utilizing benzoquinone technique. Catalytic photo-degradation reaction employed 38 µL of IPA along with fixed amount of the synthesized catalyst which was added to 100 mL of isopropyl alcohol and then kept in solar illumination. At

pre-determined intervals, reaction samples were taken out, filtered utilizing chromophil syringe filter, and analyzed using excitation wavelength of 520 nm by using a fluorescence spectrophotometer.

4 Results and Discussion

4.1 XRD of the Nanocomposite

XRD technique was utilized to examine the crystallographic and phase analysis of the samples prepared (Fig. 1). A sharp diffraction pattern of $2\theta = 29.7°$, $31.8°$, $45.5°$, and $51.5°$ was shown in the typical BiOI XRD pattern, with which BiOI crystalline structure of the Würtze-tetragonal phase could be indexed to (012), (110), (020) and (114) planes (JCPDS card no. 73-2062) (Odling and Robertson 2017). The TiO_2/BiOI heterostructure XRD pattern, together with BiOI, also observed the TiO_2 peaks at $2\theta = 25.4°$, $37.9°$, $48.2°$, and $55.1°$ which could be related to the TiO_2 anatase-phase planes (101), (004), and (105), respectively (JCPDS card no. 40-0548) (Teng et al. 2016; Li et al. 2018). The XRD TiO_2/BiOI heterostructure diffractogram revealed that the synthesized composite contains individual components TiO_2 and BiOI. No characteristic peak related to other phases and impurities was observed which confirmed the high purity and superior crystallinity of the prepared samples.
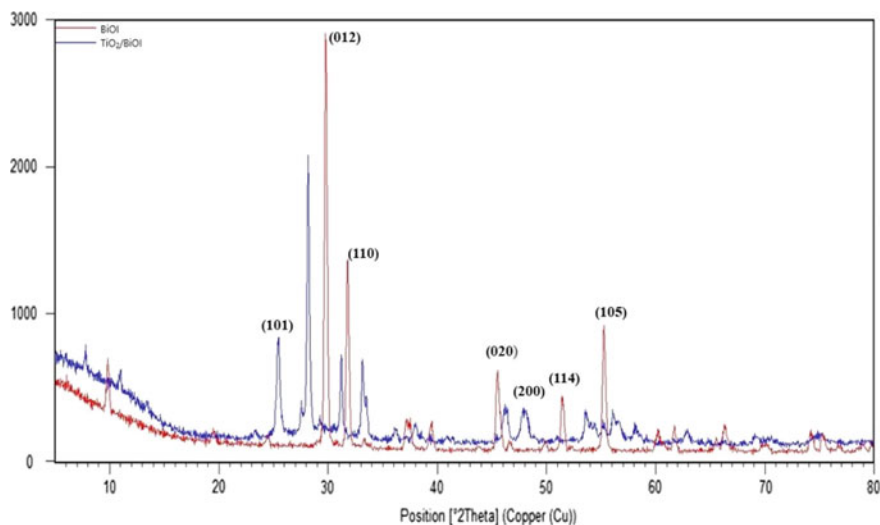
Fig. 1 XRD spectrum of TiO_2/BiOI heterostructure

4.2 FT-IR Analysis

The FTIR analysis as shown in Fig. 2, reveals that the peaks at 1050–1700 cm^{-1} for the BiOI sample were attributed to the vibration bending absorption of chemically adsorbed water, and the 3000–3450 cm^{-1} absorption bands were attributed to the absorption of the surface hydroxyl group by deepening vibration with H bond interactions (Li et al. 2018; Küçük et al. 2018). The band observed at 3434 cm^{-1} is due to the extended vibrations in the catalyst of the OH group. C$^{1/4}$O and C–O, which may be due to the presence of precursors and solvents, are due to sharp peaks in 1631.88 and 1386.1 cm^{-1}. Due to the Ti–O stretching of TiO$_2$, the peak of 670.99 cm^{-1} is observed (Sood et al. 2015b, c).

Fig. 2 FTIR spectrum of TiO$_2$/BiOI
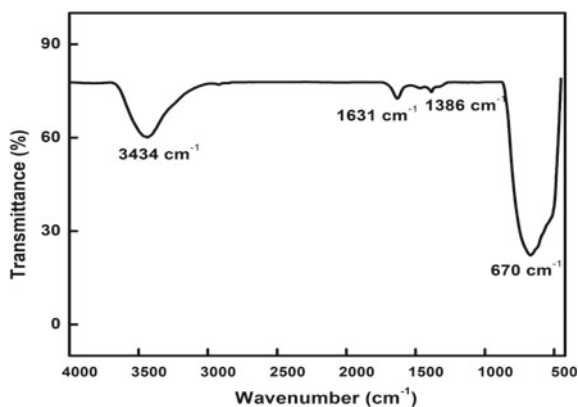
Fig. 3 PL spectrum of TiO$_2$/BiOI heterostructure
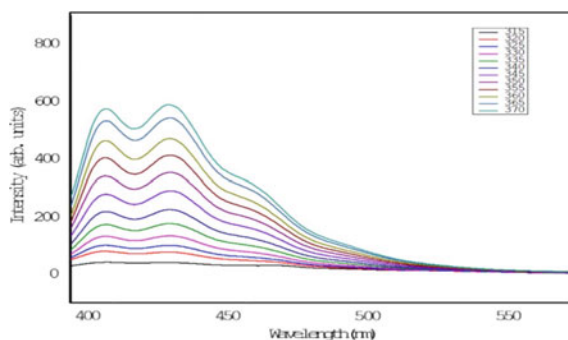
4.3 Photoluminescence (PL) Spectra

The photoluminescence (PL) spectrum is shown in Fig. 3 for further exploration of the transfer and separation performance of photo-induced carriers (Wu et al. 2018). A high PL intensity represents usually rapid recombination of electrons and hole pairs and reduces the photocatalytic activity of electron–hole pairs. The TiO_2/BiOI composites' PL emission intensity is lower, which indicated that they recombined at the lowest photogenerated electron–hole rate. Given the above analysis, the hetero-junctions from TiO_2/BiOI can effectively extend the life of the electron–hole photo-generated pairs. The wavelength of arousal was 365 nm. It is obvious that the radiative recombinant e^- hole pairs process for self-induced excitation could be attributed from the PL spectrum.

4.4 UV–Vis DRS Spectroscopy

UV–vis DRS spectroscopy was used to analyze the light absorption capacity of the synthesized samples. The band gap was estimated using Eq. 1 as

$$(\alpha h\nu)^n = A(h\nu - E_{bg}) \tag{1}$$

where α, h, ν, A, and E_{bg} represent coefficient of absorption, Planck's constant, light frequency, constant of proportionality and band gap energy respectively. Here, n is dependent on the semiconductor optical transition and n = 2 represent direct bandgap semiconductor. The UV DRS graph between absorbance and wavelength for the prepared hetero-composite is displayed in Fig. 4. The energy band gap for pure BiOI and TiO_2/BiOI hetero-structures was found to be 1.86 eV and 2.92 eV, respectively. For TiO_2/BiOI heterostructure (Chaturvedi et al. 2019), there was little decline in band gap as compared to pure BiOI, which showed that the prepared heterostructure was better photo-absorbed.

Fig. 4 UV–Vis DRS of TiO_2/BiOI heterostructure
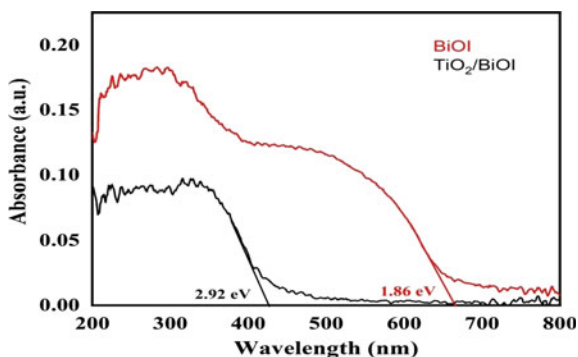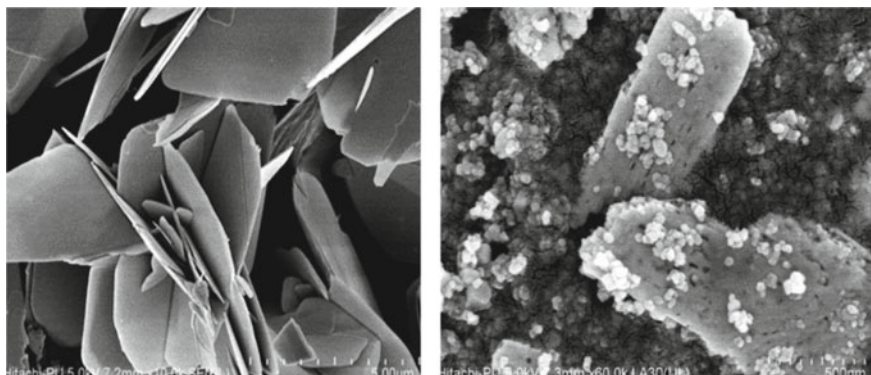
Fig. 5 FESEM of TiO$_2$/BiOI heterostructure

4.5 FE-SEM

Pure BiOI had a 3-dimensional floral structure with an average diameter of about 5 µm, assembled with the average thickness of around 30 nm from the BiOI nanosheets. And these nanosheets of BiOI were stacked and crossed (Li et al. 2018b). The TiO$_2$/BiOI composite surface morphology was measured by utilizing FESEM as shown in Fig. 5. The TiO$_2$ particles are carefully packed on the BiOI nanosheet surface. Furthermore, the more TiO$_2$ particles cover the BiOI nanosheet with the increased TiO$_2$ content.

4.6 EDS-Mapping

The elemental mapping analysis was carried out to further verify information on spatial element distribution of the photocatalyst. The Bi and Ti elements were well defined and distributed evenly as shown in the peaks for the image of the sample as depicted in Fig. 6. The O element mapping shows a sparse distribution and does not correspond to the number of Bi and Ti atoms. The elementary mapping of measurement elements with less than 11 atomic numbers is attributable to the inaccurate spectral analysis. EDS spectrum analysis figure shows Ti, O, Bi, and I elements. Bi, I, and Ti have 42.52, 46.35, and 3.02 atomic %, respectively, as determined by theoretical elements within the heterostructure TiO$_2$/BiOI (Li et al. 2018a). Cross-fringes of TiO$_2$ nanoparticles with BiOI nanosheet appeared in the interface of hetero-structure. It was proven that sample prepared was TiO$_2$/BiOI composite material and was also consistent with the XRD analysis.
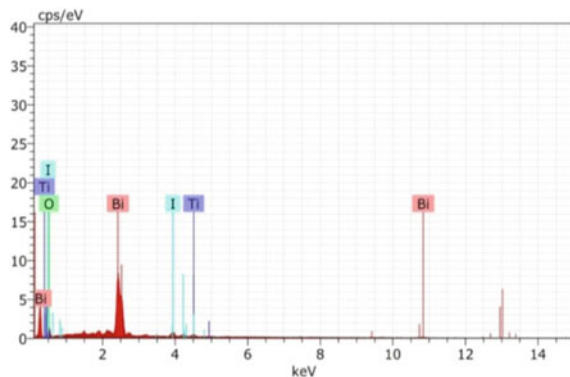
4.7   HRTEM

HRTEM further explained the detailed structure of the composite and the results are presented in Fig. 7. The random distribution of numerous TiO$_2$ particles on the BiOI nanosheets were observed (Malathi et al. 2018), and the calculated fringe distance of TiO$_2$ was 0.35 nm and could be attributed to the (101) TiO$_2$ plane. The TiO$_2$/BiOI heterostructure consisted of BiOI and TiO$_2$ as shown in the lattice fringes and an interplanar distance of 0.28 nm was observed. Well-defined structure of the TiO$_2$/BiOI heterostructure crystals were visible in the exposed facets of TiO$_2$ and BiOI.

Results of photocatalytic decomposition of amaranth dye using the nanocomposite
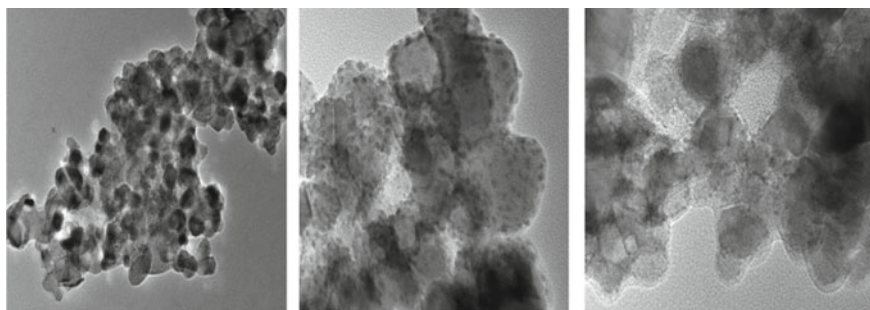
Fig. 7   HRTEM of TiO$_2$/BiOI heterostructure

Fig. 8 Effect of pH on the degradation efficacy of amaranth dye utilizing TiO_2/BiOI heterostructure
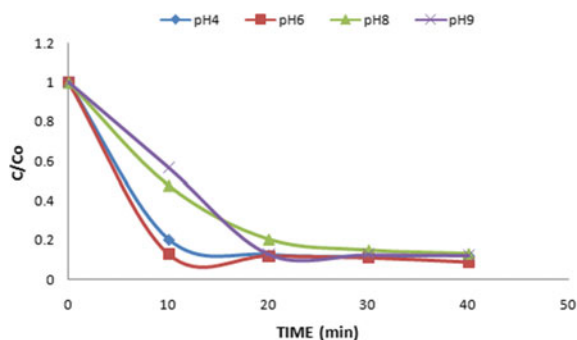
4.8 Effect of pH

The effect of pH for amaranth dye photo-degradation in the presence of solar light utilizing TiO_2/BiOI heterostructure was analyzed. The influence of pH on the photocatalytic degradation of amaranth dye was investigated by altering pH between 4 and 9 (Lamba et al. 2015) utilizing a catalyst dosage of 25 g/L and a dye concentration of 10 mg/L. The % degradation of amaranth dye as a pH function is shown in Fig. 8. It was found that 87% amaranth dye degradation occurred at pH of 8 and 9. At pH of 4, the degradation rate increased to 87.7%. The maximum efficiency of dye degradation at pH 6 was observed and an amaranth decontamination of approximately 91.12% in 40 min was achieved.

4.9 Effect of Catalyst Dose

The influence of catalyst dose (at pH 6 and initial dye concentration 10 mg/L), was also studied utilizing the TiO_2/BiOI catalyst by degradation of amaranth dye. From Fig. 9, it can be seen that with the catalyst dose increase from 5 to 50 mg/L, it showed a huge increase of 66–87% in the photocatalytic effectiveness of the TiO_2/BiOI

Fig. 9 Effect of catalyst dose on the degradation efficacy of amaranth dye utilizing TiO_2/BiOI heterostructure
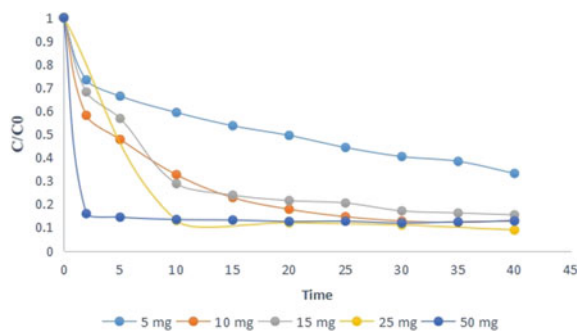
Fig. 10 Effect of initial dye concentration on the degradation efficacy of amaranth dye utilizing TiO_2/BiOI heterostructure
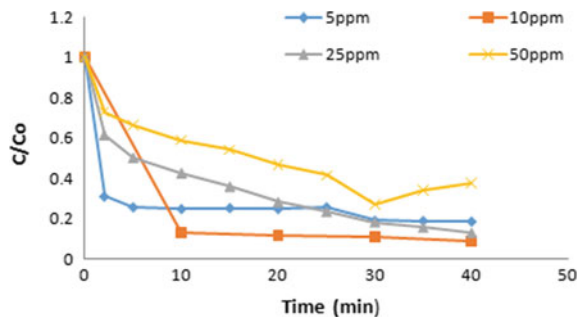
heterostructure, because there were more active sites on the catalyst surface, resulting in higher dye adsorption (Chaturvedi et al. 2019; Kaur et al. 2015). With an increased catalyst load up to 25 mg/L, the degradation rate increased to 91% and the optimum catalytic dose for photocatalytic decontamination was 25 mg/L.

4.10 Effect of Initial Dye Concentration

At the optimized pH and catalyst dose, the photo-catalytic impact of the initial dye concentration was investigated. The concentration of dye was kept between 5 and 50 mg/L, and the results are illustrated in Fig. 10. At a concentration of 10 mg/L, the efficiency of degradation of 91% was achieved. For other dye concentrations, varying from 5 to 50 mg/L respectively, the degradation efficacy decreased from 81 to 62%.

4.11 Photolysis and Adsorption of Amaranth Dye Using TiO_2/BiOI Catalyst

In the presence of solar light without the addition of the catalyst, a control experiment was also carried out and 2% degradation in reaction time of 40 min was observed. TiO_2/BiOI heterostructure based adsorption of amaranth dye without solar light was performed in the adsorption experiment. The amaranth dye removal using TiO_2/BiOI heterostructure using adsorption was 36.08%. The effect of photolysis, adsorption and photocatalysis is shown in Fig. 11. The experiments for adsorption and photolysis concluded that the efficient degradation of the amaranth dye is based on essential elements consisting of both light and the catalyst (Kaur et al. 2017).

Fig. 11 Photolysis/adsorption/photocatalys for the decomposition of amaranth dye using TiO$_2$/BiOI catalyst
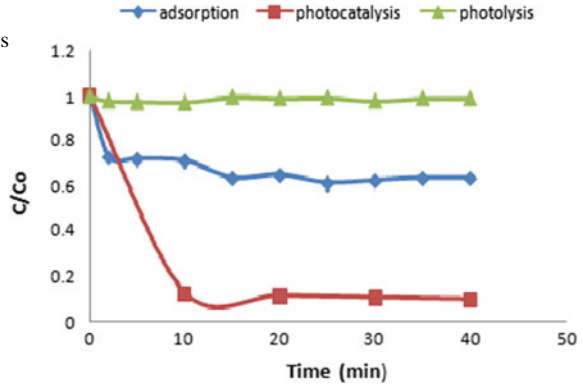
4.12 Comparison with the Bare Catalyst Components

Compared with pure BiOI and commercial TiO$_2$ (P-25) based dye degradation, efficacy of prepared TiO$_2$/BiOI heterostructure was also studied (Ma et al. 2021) as shown in Figs. 12 and 13. The synthesized TiO$_2$/BiOI heterostructure showed an

Fig. 12 Bare TiO$_2$ for the decomposition of amaranth dye
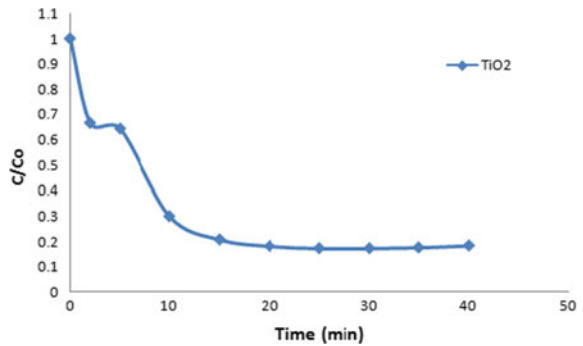
Fig. 13 Bare BiOI for the decomposition of amaranth dye
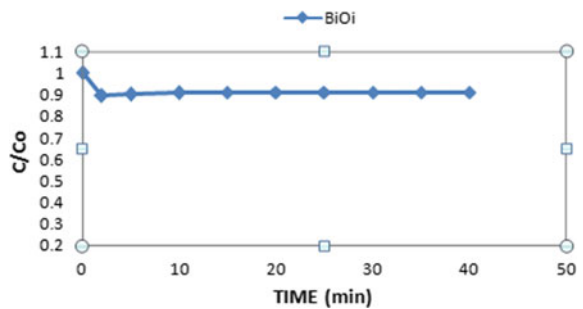
Fig. 14 Effect of various scavengers on the photo-degradation of amaranth dye using TiO_2/BiOI
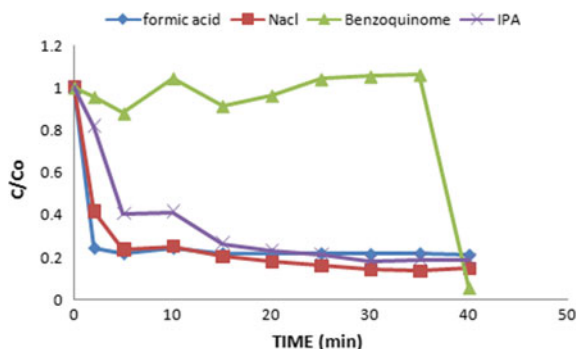
improved photocatalytic performance (91%) as compared to pure BiOI (8.6%) and TiO_2 PC-25 under optimized reaction conditions (81%).

4.13   Role of Reactive Oxygen Types in the Breakdown

During the photocatalytic decomposition of the amaranth dye, various scavengers were used to determine the role of reactive species involved. Various quenchers such as NaCl (h^+) and HCOOH (e^-) were chosen to study the inhibitory effects (Li et al. 2018b). The results are presented in Fig. 14 for amaranth dye photo-degradation by using different scavengers over the synthesized solar-illuminated TiO_2/BiOI photocatalyst. It has been found that, by the addition of NaCl and HCOOH, the pivotal contribution of h^+ and e^- in the degradation process has been significantly reduced from 91% (without scavenger), respectively, to 85% and 79.1%. During photocatalytic reactions, isopropanol was checked for the formation of hydroxyl radicals. It was concluded by the experiments of scavengers that the photocatalytic degradation of amaranth dyes was dominated by e^-, h^+ and $\cdot$OH radicals.

4.14   Recyclability Studies of TiO_2/BiOI Photocatalyst

For utilizing the practical application of the prepared nano catalyst, the reusability and stability of photocatalyst play a key role. The reusability test of TiO_2/BiOI was therefore conducted. The photocatalyst was utilized and recycled three times as shown in Fig. 15, following the photocatalytic reaction (Kaur et al. 2016). Over the three repeated reaction cycles, degradation and selectivity had no apparent change. The hetero-structured TiO_2/BiOI revealed good re-usability for three reaction cycles and maintained high photocatalytic potential. The results showed that the photochemical stability of the heterostructure was excellent and it can be reused again comfortably for repeated cycles.

Fig. 15 Recyclability of the TiO$_2$/BiOI heterostructure
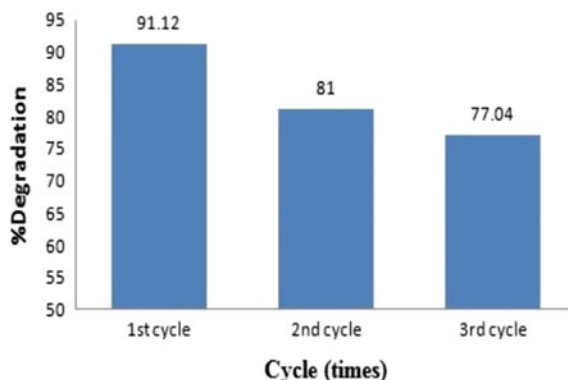
5 Conclusions

The TiO$_2$/BiOI structure demonstrated the successful loading of nano-sheets of BiOI to the surface of TiO$_2$ nanoparticles. In addition, the prepared hetero-structure of TiO$_2$ and BiOI acted as a powerful catalyst for amaranth dye degradation under solar light. Around 91% degradation of amaranth dye was accomplished within 40 min of photocatalytic response with the optimum catalyst loading of 25, 10 mg/L initial dye concentration at pH of 6 which was much higher than the virgin TiO$_2$ (81%) and BIOI (8.6%). The results of the scavengers based study ensured that h$^+$, e$^-$, and OH were among the most reactive chemical species for the photocatalytic degradation processes. The PL results showcased that TiO$_2$/BiOI heterostructure was stable and thus the quantum effect of the heterostructure was enhanced. The hetero-structured TiO$_2$/BiOI revealed with good reusability for three reaction cycles (77%) and maintained high photocatalytic performance. The results showed excellent photochemical stability of the hetero-structure which is vital for practical applications of the photocatalytic degradation.

Conflict of Interest The authors declare no conflict of interest.

References

Al-Mamun MR, Kader S, Islam MS, Khan MZH (2019) Photocatalytic activity improvement and application of UV-TiO$_2$ photocatalysis in textile wastewater treatment: a review. J Environ Chem Eng 7(5):2213–3437

Ali I, Suhail M, Alothman ZA, Alwarthan A (2018) Recent advances in syntheses, properties and applications of TiO_2 nanostructures. RSC Adv 8:30125–30147

Anwer H, Mahmood A, Lee J, Kim KH, Park JW, Yip ACK (2019) Photocatalysts for degradation of dyes in industrial effluents: opportunities and challenges. Nano Res 12(5):955–972

Bansal JKA (2012) Photodegradation of amaranth in aqueous solution catalyzed by immobilized nanoparticles of titanium dioxide. Int J Environ Sci Technol 9:479–484

Cai L, Yao J, Li J, Zhang Y, Wei Y (2019) Sonochemical synthesis of $BiOI$-TiO_2 heterojunction with enhanced visible-light-driven photocatalytic activity. J Alloys Compd 783:300–309

Chaturvedi G, Kaur A, Kansal SK (2019) CdS-decorated MIL-53(Fe) microrods with enhanced visible light photocatalytic performance for the degradation of ketorolac tromethamine and mechanism insight. J Phys Chem C 123(27):16857–16867

Chen R, Wang H, Wu H, Sheng J, Li J, Cui W, Dong F (2020) $SrTiO_3$/$BiOI$ heterostructure: interfacial charge separation, enhanced photocatalytic activity, and reaction mechanism. Chin J Catal 41(4):710–718

Dai B, Zhang A, Zhang D, Liu Z, Li H, Wang R, Zhang X (2019) Effect of preparation method on the structure and photocatalytic performance of $BiOI$ and Bi_5O_7I for Hg^0 removal. Atmos Pollut Res 10:355–362

Jyotsna, Kaur A, Kansal SK, Umar A (2020) β-$AgVO_3$ nanowires/TiO_2 nanoparticles heterojunction assembly with improved visible light driven photocatalytic decomposition of hazardous pollutants and mechanism insight. Sep Purif Technol 251:1383–5866

Kaur A, Umar A, Kansal SK (2015) Sunlight-driven photocatalytic degradation of non-steroidal anti-inflammatory drug based on TiO_2 quantum dots. J Colloid Interface Sci 459:257–263

Kaur S, Sharma S, Kansal SK (2016) Synthesis of ZnS/CQDs nanocomposite and its application as a photocatalyst for the degradation of an anionic dye, ARS. Superlattices Microstruct 98:86–95

Kaur A, Salunke DB, Umar A, Mehta SK, Sinha ASK, Kansal SK (2017) Visible light driven photocatalytic degradation of fluoroquinolone levofloxacin drug using Ag_2O/TiO_2 quantum dots: a mechanistic study and degradation pathway. New J Chem 41(20):12079–12090

Kaur A, Umar A, Anderson WA, Kansal SK (2018) Facile synthesis of CdS/TiO_2 nanocomposite and their catalytic activity for ofloxacin degradation under visible illumination. J Photochem Photobiol A Chem 360:34–43

Kaur A, Anderson WA, Tanvir S, Kansal SK (2019) Solar light active silver/iron oxide/zinc oxide heterostructure for photodegradation of ciprofloxacin, transformation products and antibacterial activity. J Colloid Interface Sci 557:1–844

Küçük Ö, Teber S, Cihan Kaya İ, Akyıldız H, Kalem V (2018) Photocatalytic activity and dielectric properties of hydrothermally derived tetragonal $BaTiO_3$ nanoparticles using TiO_2 nanofibers. J Alloys Compd 765:82–91

Kumar J, Bansal A (2010a) Photocatlytic degradation of amaranth dye in aqueous solution using sol-gel coated cotton fabric. In: Proceedings of the world congress on engineering and computer science, vol 2, pp 20–22

Kumar J, Bansal A (2010b) Photocatalytic degradation of amaranth dye over immobilized nano-crystals of TiO_2. In: International conference on energy & environment, Cambridge, pp 129–133

Kumar J, Bansal A (2015) CFD simulations of immobilized-titanium dioxide based annular photocatalytic reactor: model development and experimental validation. Indian J Chem Technol 22:95–104

Kumar J, Jana AK, Bansal A, Garg R (2005) Development of correlation between BOD and COD for refinery waste. Indian J Environ Prot 25(5):405

Lamba R, Umar A, Mehta SK, Anderson WA, Kansal SK (2015) Visible-light-driven photocatalytic properties of self assembled cauliflower-like AgCl/ZnO hierarchical nanostructures. J Mol Catal A Chem 408:189–201

Li B, Chen X, Zhang T, Jiang S, Zhang G, Wu W, Ma X (2018a) Photocatalytic selective hydroxylation of phenol to dihydroxybenzene by $BiOI$/TiO_2 p-n heterojunction photocatalysts for enhanced photocatalytic activity. Appl Surf Sci 439:1047–1056

Li Q, Qin H, Zhao H, Zhao X, Cheng X, Fan W (2018b) Facile fabrication of a BiOI/TiO$_2$ p-n junction via a surface charge-induced electrostatic self-assembly method. Appl Surf Sci 457:59–68

Liu Z, Wang Q, Tan X, Wang Y, Jin R, Gao S (2019) Enhanced photocatalytic performance of TiO$_2$ NTs decorated with chrysanthemum-like BiOI nanoflowers. Sep Purif Technol 215:565–572

Luévano-Hipólito E, Torres-Martínez LM, Cantú-Castro LVF (2019) Self-cleaning coatings based on fly ash and bismuth-photocatalysts: Bi$_2$O$_3$, Bi$_2$O$_2$CO$_3$, BiOI, BiVO$_4$, BiPO$_4$. Constr Build Mater 220:206–213

Ma Y, Li M, Jiang J, Li T, Wang X, Song Y, Dong S (2021) In-situ prepared MIL-53(Fe)/BiOI photocatalyst for efficient degradation of tetracycline under visible-light driven photo-Fenton system: investigation of performance and mechanism. J Alloys Compd 870:159524

Majhi D, Samal PK, Das K, Gouda SK, Bhoi YP, Mishra BG (2019) α-NiS/Bi$_2$O$_3$ nanocomposites for enhanced photocatalytic degradation of tramadol. ACS Appl Nano Mater 2:395–407

Malathi A, Arunachalam P, Madhavan J, Al-Mayouf AM, Ghanem MA (2018) Rod-on-flake α-FeOOH/BiOI nanocomposite: facile synthesis, characterization and enhanced photocatalytic performance. Colloids Surf A 537:435–445

Marchelek M, Grabowska E, Klimczuk T, Lisowski W, Mazierski P, Zaleska-Medynska A (2018) Visible light photocatalysis employing TiO$_2$/SrTiO$_3$-BiOI composites: surface properties and photoexcitation mechanism. Mol Catal 452:154–166

Meng A, Zhang L, Cheng B, Yu J (2019) Dual cocatalysts in TiO$_2$ photocatalysis. Adv Mater 31(30):1–31

Naik AP, Salkar AV, Majik MS, Morajkar PP (2017) Enhanced photocatalytic degradation of amaranth dye on mesoporous anatase TiO$_2$: evidence of C-N, NN bond cleavage and identification of new intermediates. Photochem Photobiol Sci 16(7):1126–1138

Odling G, Robertson N (2017) SILAR BiOI-sensitized TiO$_2$ films for visible-light photocatalytic degradation of Rhodamine B and 4-Chlorophenol. ChemPhysChem 18(7):728–735

Ratan JK, Saini A (2019) Enhancement of photocatalytic activity of self-cleaning cement. Mater Lett 244:178–181

Ritika, Kaur M, Umar A, Mehta SK, Kansal SK (2019a) BiF$_3$ octahedrons: a potential natural solar light active photocatalyst for the degradation of Rhodamine B dye in aqueous phase. Mater Res Bull 112:376–383

Ritika, Kaur M, Umar A, Mehta SK, Kansal SK, Khan MA, Algarni H (2019b) Enhanced solar light-mediated photocatalytic degradation of brilliant green dye in aqueous phase using BiPO$_4$ nanospindles and MoS$_2$/BiPO$_4$ nanorods. J Mater Sci Mater Electron 30(11):20741–20750

Saini A, Arora I, Ratan JK (2020) Photo-induced hydrophilicity of microsized-TiO$_2$ based self-cleaning cement. Mater Lett 260:126888

Sood S, Kumar S, Umar A, Kaur A, Mehta SK, Kansal SK (2015a) TiO$_2$ quantum dots for the photocatalytic degradation of indigo carmine dye. J Alloys Compd 650:193–198

Sood S, Umar A, Mehta SK, Sinha ASK, Kansal SK (2015b) Efficient photocatalytic degradation of brilliant green using Sr-doped TiO$_2$ nanoparticles. Ceram Int 41(3):3533–3540

Sood S, Umar A, Mehta SK, Kansal SK (2015c) Highly effective Fe-doped TiO$_2$ nanoparticles photocatalysts for visible-light driven photocatalytic degradation of toxic organic compounds. J Colloid Interface Sci 450:213–223

Sood S, Mehta SK, Sinha ASK, Kansal SK (2016) Bi$_2$O$_3$/TiO$_2$ heterostructures: synthesis, characterization and their application in solar light mediated photocatalyzed degradation of an antibiotic, ofloxacin. Chem Eng J 290:45–52

Tamilarasan R, Sureshkumar V, Kumar M (2016) Biosorption of victoria blue using *Zizyphus oenoplia* seed: evaluation of experimental and modeling studies. In: 1st international conference on emerging trends in engineering, technology and science, ICETETS 2016—proceedings. ISBN 978-1-4673-6725-7

Teng Q, Zhou X, Jin B, Luo J, Xu X, Guan H, Wang W, Yang F (2016) Synthesis and enhanced photocatalytic activity of a BiOI/TiO$_2$ nanobelt array for methyl orange degradation under visible light irradiation. RSC Adv 6(43):36881–36887

Verma P, Kumar J (2014) Degradation and microbiological validation of meropenem antibiotic in aqueous solution using UV, UV/H$_2$O$_2$, UV/TiO$_2$ and UV/TiO$_2$/H$_2$O$_2$ processes. Int J Eng Res Appl 4(7):58–65

Wang N, Shi L, Yao L, Lu C, Shi Y, Sun J (2018) Highly improved visible-light-induced photocatalytic performance over BiOI/Ag$_2$CO$_3$ heterojunctions. RSC Adv 8(1):537–546

Wu J, Zhang J, Xu W, Qu C, Guan Y, Qi X, Ling Y, Zhou X, Xu K, Zhu L (2018) One-pot synthesized BiOI/TiO$_2$ heterostructure with enhanced photocatalytic performance and photocatalytic treatment of gas-phase Hg^0. Catal Lett 148(8):2337–2347

Reduction of Fluoride from Domestic Waste Water by Using Activated Diatomaceous Earth

Pawan Kumar and Pankaj Gupta

Abstract In this present study, a fixed-mattress column adsorption device was transformed into implemented. The pH Point of Zero Charges (pHPZC), Scanning Electron Microscopy (SEM) and BET surface area examination had been carried through for adsorbent to demonstrate the techniques of significant reduction of fluoride by absorption. On the whole functioning, the column was assessed at usual space heat, a constant initial concentration, and bed level. The highest breakdown capability of 71.97 mg/kg was transformed into accomplished for DE at particle sizes of 1 mm, 850 µm, 600 µm, and 500 µm respectively. The Bradley equation is used to determine the isothermal information and, a dose that is an adsorbent. The statistical analyses were done Langmuir that is using and equations until isotherm studies had been carried out. To investigate the adsorption process, two simplified kinetic models were used. A series of experiments were conducted using diatomaceous earth in raw form, as received from mines and activated form for the adsorption of fluoride ions present in water. This experiment shows that the diatomaceous earth clay works as a filtration media for the elimination of 20.73% fluoride from water. The fluoride removal potential that is the majority of 71.97 mg/kg was found into DE at particle dimensions of 850 mm. Pre-heated diatomaceous earth clays were highly active to form a complex with fluoride. Adsorption through less heated diatomaceous earth had been less significant. There was a slight change in pH, it would increase by 0.1% in the sample while there was negligible change in TDS of water after adding activated absorbent. This paper depicts the fluoride elimination from treated wastewater and groundwater that can be accomplished with the aid of using diatomaceous earth clay. The absorbance convenience of DE is 20.73% when utilized as being filtration materials. While 71.97%, when activated diatomaceous earth clay, is used as a sorbent.

Keywords Adsorption · De-fluoridation · Diatomaceous Earth

P. Kumar (✉)
Department of Chemistry, Sunrise University, Alwar, Rajasthan, India
e-mail: kvspwn@gmail.com

P. Gupta
Faculty of Science, Sunrise University, Alwar, Rajasthan, India

1 Introduction

The supply that is for plenty of population is groundwater for the large array of outlying communities in nations like India. Excess fluoride present in portable water had disturbed vitamins and mineral enzymes, protein, lipid, and carbohydrate burning this is certainly fat whenever found in large amounts (Adeyemo et al. 2017). The countless supply is popular of water is groundwater for the huge population of countries like India (BIS 2012). For more strong teeth, the desired concentration of fluoride levels must be maintained as per WHO norms. The adsorbent is the part that is many that are essential of defluoridation system this is certainly adsorption-based. The ability associated with the selection of adsorbents, both changed and normal, to eliminate fluoride is analyzed (Anthony et al. 2016). No end is last the analysis into possible de-fluoridation yields. It's better for the merchandise utilized as an adsorbed become common in the neighborhood market, many, and affordable. Diatomaceous earth (DE) is a material that can be investigated that is beneficially associated with aspects. DE is rich and non-toxic. Over the previous several periods, diatomaceous earth has acknowledged considerable attention in pollutant treatment (Berger et al. 2016). Diatomaceous Earth has a highly affordable surface, simple accessibility, great technical fat, and supply in big amounts. Adsorption convenience of adsorbents centered on batch safety pays to provide information that is fundamental to your adsorbents' effectiveness. Nevertheless, the full total link between medical team studies never is highly relevant to procedures being constant that the contact time essential to achieve security is insufficient. Because of this, numerous tests also expose that constant procedures mode yields trustworthy facts. Diatomaceous earth (DE) can be a research that is effective in its abundance and non-toxic (Aoudj et al. 2017). DE has a highly affordable surface, simple supply, great technical weight, and offers in big amounts. The power of the selection of adsorbents, both normal and altered, to get rid of fluoride is analyzed. They also compared the adsorption characteristics of adsorbent particles with and without activation of DE. This study aims to find an easily available material for de-fluoridation of water that has high adsorption capacity to remove this harmful material from groundwater or drinking water. We do the experiment with DE in raw form as well as Activated form (Mishra et al. 2020). The aim would be to verify the designs' sustainability and efficiency for the design of flow-through techniques employed by the Thomas designs and Adams–Bohart (Tsuzuki et al. 2004).

2 Experiment

2.1 Material and Methods

Diatomaceous earth clay was gathered from mines situated around 100–150 km surrounding Barmer and Jodhpur City Centre, in Jodhpur and Barmer area of
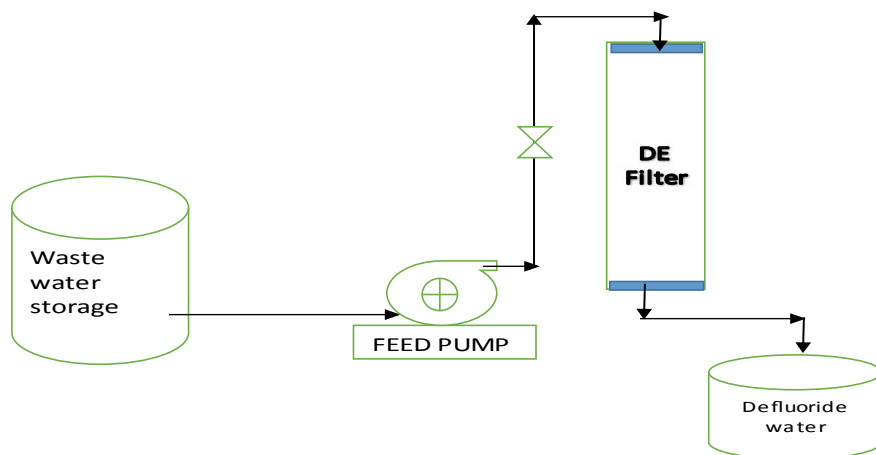
Fig. 1 Lab-scale adsorbent filter model setup for Diatomaceous Earth

Rajasthan State, India. Given that these rocks in many cases are found in Rajasthan, the supply can be easily available in surrounding areas of Rajasthan. These materials were collected from mines for an experiment (Kumar et al. 2014).

2.2 Sample Preparation

The DE supplied for the research deposits which are normal in the Rajasthan, districts Barmer and Jodhpur. DDW or demineralized water were washed aided by the primary test. The centrifugation eventually ends up being particles that can be usual can be broken up, the suspension system being colloidal. The DE is heated to and heated, including 110 °C for 6–8 h (Subbaiah et al. 2014), to virtually be tested in just a range. "Then cooled in a dryer before it is often crushed right into a ball mill (Swapnila et al. 2017) before the particles are passed via a 250 micron size sieve test out of tangled containers to prevent humidity (Fig. 1).

2.3 Experimental Setup and Procedures for Column Adsorption

The efficient performance of planetary fluoride treatment is assessed utilizing a constant line in fixed-bed studies (Cherukumilli et al. 2018). A tiny cylindrical movement that is a small-size test having a clear bed amount of 515 cm³ plus an inside diameter of 8.1 cm was done. "These columns have actually in reality been

placed several adsorbents with various particle sizes (silt: 0.075 mm; dust: 0.075–0.425 mm and sand that is moderate mm). Whenever pH and flow price parameters have already been analyzed, the particulate that is the same is used. The sleep was finished by training with water deionized (pH: 7.00–7.30), which also prevents the function of the channeling that can be done creeping occasion which could notably influence the performance associated with the line. The top is adsorbed tightly packed for 12 h (overnight) (Kır et al. 2016). Fluoride, artificially produced at a 10 concentration that is mg/l was moved to the packed up-flow sleep line to avoid gravity channeling. Nonetheless, a variable pump that is peristaltic has been used in all these experiments to maintain a constant movement (MS-REGALO, Labortechnik-Analytics, Zürich, Switzerland). At space temperature (25 °C), the test had been carried out. The constant flow expense was confirmed by the collection and quantification of an affluent answer over regular durations. The relative line task ended up being stopped when fluoride levels in the effluent were more than 90% for the amounts understood (Aoudj et al. 2017). The level of fluoride was quantified with the help of an ion electrode, make U.S.A, model HQ440D. For measuring levels of fluoride in the selection of 0.2–200 mg/l. Which works as a maximum quantity acceptable to normal water according to the WHO's suggestion. The final results of the experimental Particle (0.075–0.425 mm sludge), influential solution PH (2.00, 4.00, 6.00, and 8.00), influential volumetric movement rate (1.21, 2.50, and 3.75 ml/min) on percussion and fluoride reduction were finally analyzed. (Silt: 0.075–0.414 mm and Sand, moderated 0.075–0.425 mm) (He et al. 2013).

3 Results and Discussion

3.1 Physicochemical Analysis of Adsorbent

Analysis examples had been available in a cooking pot of tungsten carbide with a particle size of 75 mm (Godboley et al. 2016). To evaluate the increased loss that is fat Ignition (LOI) values, heating examples, and temperatures a part of an assortment and extra muffle furnace are completed as much as the temperature at 1000 °C. 1 gm of sample ended up being mixed with six g of lithium tetraborate flux and mixed at 1050 °C along the way of fabricating cup that is fused. The test ended up being completed by having a PVA binder squeezed for trace element analysis in an aluminum cup (Kumar and Gupta 2021). Table 1 shows the outcomes which are overall terms of the part oxide with this element. The DE's main constituents are alumina and silica, based on the findings (Ngulube et al. 2016).

Table 1 Physicochemical parameters of Diatomaceous Earth

S. No.	Oxide	Composition %
1	pH	8.65
2	Fe_2O_3	2.85
3	Na_2O	0.60
4	K_2O	0.72
5	TiO_2	0.16
6	CaO	0.21
7	MgO	0.12
8	MnO	0.05
9	P_2O_5	0.04
10	Al_2O_3	3.96
11	SiO_2	85.62
12	LOI	7.55
13	VM	0.07

3.2 SEM Analysis

"Electron scanning research that is scanning and recorded on the CDU lead sensor using an electric scanning tool, which is a micro-powered production of 25 kV and which examines the DE housing across the whole area. CIQTEK—SEM3000—SEM (Scanning Electron Microscope)—Scanning Electron Microscope by Chinainstru and Quantumtech (Hefei) Co., Ltd China. A series of pores in the rectangular pattern, typical of this void tube are arranged every diatom, as shown in Fig. 2" (Nehra et al. 2020).

3.3 BET Analysis

"In the Brunauer–Emmett–Teller (BET) method, the pore level, zone, and pore width of the 250 m diameter DE particles were determined (Rabelani et al. 2017). The following dimensions are shown in micrometric TriStar II surface area and porosity (Kumar and Gupta 2021; Mishra et al. 2021)" (Table 2).

Higher the BET surface area indicates that Diatomaceous Earth can become a good adsorbent. When we used raw DE as a filtration media that also remove some fluoride as explain in the below result data, while we activate the DE, it remove more fluoride from water. That is due to on activation of DE, the surface area increased, as shown by BET analysis.
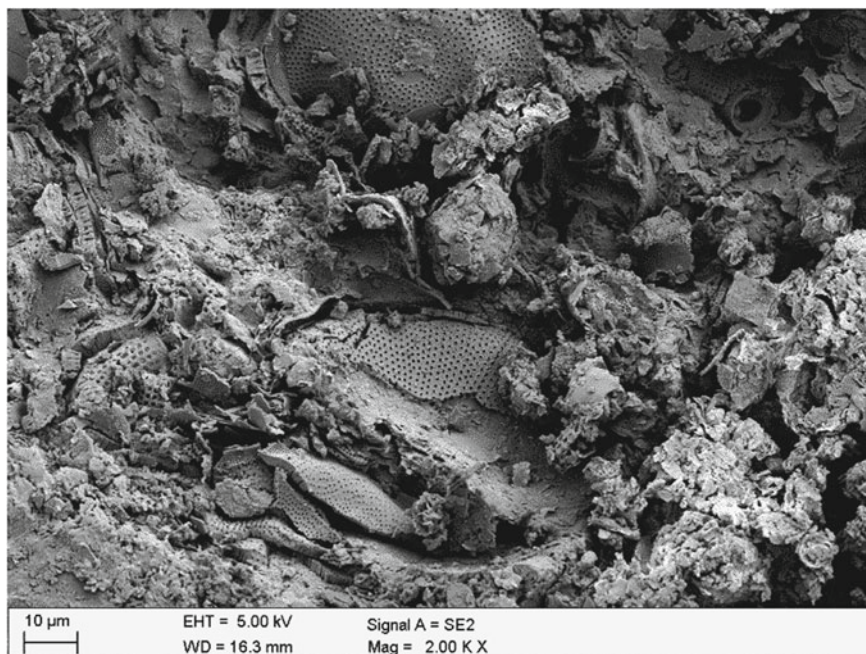
Fig. 2 Scanning of the raw diatomaceous earth's electron microscope view

Table 2 BET surface area measurement of Diatomaceous Earth

S. No.	Parameters	Area (m^2/g)
1	Single point surface area	31.174
2	BET surface area of activated DE	31.8861

3.4 Batch Adsorption Test

The approach to batch adsorption balance was utilized to research the adsorption of fluoride on DE (Zhang et al. 2016). In a container synthetic of the measurement that is ml 50 ml of solutions of fluoride have indeed been pipetted away. Apply 0.1 M HCl or 0.1 M NaOH to the calibration of the pH, while the acid or alkali used are supervised in several masses of adsorbent. With the addition of water to your solution that is deionized, it is increased by 50 ml (Steier et al. 2016). "After complete dilution, a fix that is 10-fluoride is mg/l is the final mg/l concentration. In a water shower shaker, corked bottles had been shaken" (Kumar and Gupta 2021). Have trend that is thermostatic is suspensions that may be blended for 5000 rpm after a centrifuge device is balanced. TISAB III finishes with a power that is ionic and maintains pH between 5.2 and 5.5 by adding 1:10 quantities of the supernatants of aluminum fluoride or iron (III) structures. The weather is stirred plus the complete response has been permitted to stay for the hour that is complete. Using an electrode

that is ion-selective Hack, HQ440D, the U.S.A. creates a selectable electrode fluoride ion meter cross-checked with all the standard of fluoride and Iron (III). Fluoride and Iron (III) were contained in a ratio of 1:10 in the samples (Kumar and Gupta 2021).

The proportion of total fluoride removal was evaluated by Eq. (1).

$$\text{Fluoride removal (\%)} = \frac{[C_o - C_t]}{C_o} \times 100 \tag{1}$$

3.5 PH and Zero-Point Charges (pHPZC) Determination

Adsorbents According to the procedure (WHO Guideline for drinking water 2011) that is standard pH was used electronically in a ratio of 1:10 by adsorbent and water. An SOP finally looked for the pH of adsorbents through the asking that is actual (pHPZC). In a 298 K vessel 250 ml 0.01 M NaCl solution had been utilized (Roy et al. 2017) and N_2 had been purged in solution for pH intact by maintaining CO_2 from dissolving through oxygen. The electrolyte of 25 ml is added to 6 Erlenmeyer flasks and pH is adjusted to your desired value with 0.1 M NaOH (Wu et al. 2016) or 0.1 M HCl (2.00, 4.00, 6.00, 8.00, and 10.00) (Uddin et al. 2018). The technique is the same method used for the blank electrolyte (0.01 M NaCl). Every beaker has been shaken for 48 h, receiving 0.25 g of rock examples. The pH-filtered suspension system was established (Berger et al. 2016). At the intersection point, the pH in which the initial pH ends was plotted was the idea of zero charges (pHPZC) (Fig. 3).
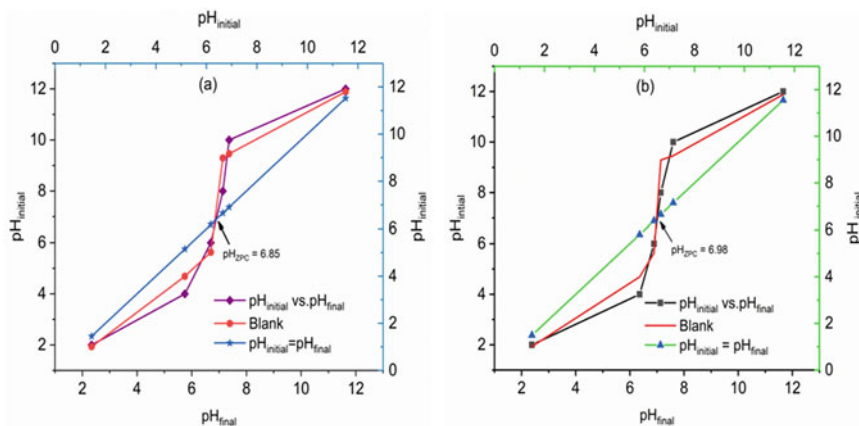
Fig. 3 pH (pHPZC) measured for zero charge. **a** Raw DE, **b** activated DE

Table 3 Observed Langmuir isothermal data

Intercept	Slope	q max (mg/g)	KL	RL	R^2
0.04824	0.00422	20.72968491	11.43128	0.001747	0.98312

Equation	y = a + b*x
Plot	1/qe
Weight	No Weighting
Intercept	0.04824 ± 0.0124
Slope	0.00422 ± 2.7574
Residual Sum of Squ	5.7253E-4
Pearson's r	0.99365
R-Square (COD)	0.98734
Adj. R-Square	0.98312
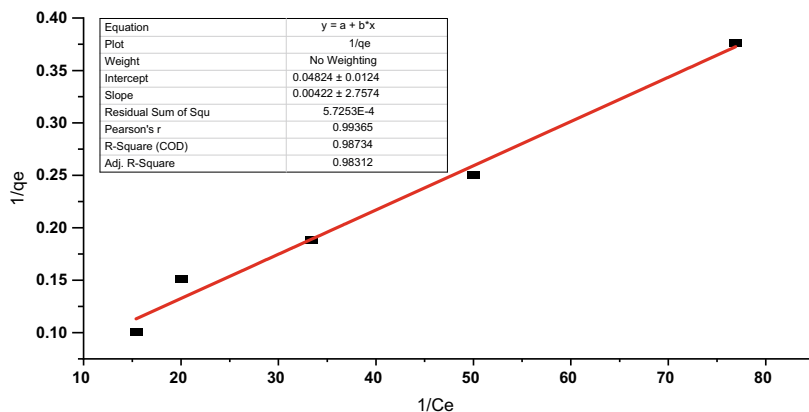
Fig. 4 Langmuir adsorption isotherm

3.6 Adsorption Isotherm

"Adsorption isotherms were expressed using the Langmuir and Freundlich isotherm models" (Kumar and Gupta 2021) (Table 3).

According to the Langmuir model: (Prathibha et al. 2015)

$$\frac{Ce}{Qe} = \frac{1}{[qLxkL]} + \frac{Ce}{qL} \tag{2}$$

The Freundlich isotherm explained below (Fig. 4).

$$\log qe = \log Kf + \frac{1}{n}\log Ce \tag{3}$$

These research schemes for fluoride elimination from treated aqueous solutions of the wastewater adsorption have been analyzed, which means that the diatomaceous earth system filters used, and the diatomaceous earth is activated as an absorbent. The XRD, ICP-OES, BET, XRF, and FTIR equipment (Yu et al. 2018) were used to demonstrate the techniques of adsorption, which are therefore suitable for fluoride therapy with adsorbents (Ece et al. 2019). The pHPZC is 6.98 for natural DE if it is used as an adsorbent and filters 6.85 for activated DE. The results of procedure parameters including a particle that is adsorbent, influential pH and influential flow rate, volumetric to your adsorption procedure performance, were examined in a single line.

"To your smaller solution pH (2.00) and low cost (1.25 ml/min) of particles 0.075–0.425 mm and 0.075 mm, correspondingly" (Nehra et al. 2020). The reduction that is optimal for raw DE ended up being 20.73 mg/kg while the optimum removal ability of activated DE ended up being 71.97 mg/kg. The rising within the size of adsorbent particles, fluid pH, and movement rates lowers the column-sleep breakthrough and saturation some time, therefore, decreases the fluoride extraction by normal DE. Activated DE has received fatigue that is the high breakthrough time of 0.075–0.425 mm in particle dimensions (Hamamoto et al. 2015), and a low pH solution and flow rate, the same as normal DE. Thus, for the procedure about the adsorption column, you'll attain performance that is optimally suited to parameters that can be experimental. "For the calculation of breakthrough curves and the choosing of the contour having a parameter that is fixed-bed Thomas and Adams-Bohar model was used" (Anthony et al. 2016). Both the Adam-Bohart and Thomas models may well anticipate the spot of all of the breakthrough curves so that you can decrease fluoride by activated DE and fluoride that is normal (Adeyemo et al. 2017). The results reveal that natural DE and triggered DE enable you to remove fluoride that is additional water in adsorption that is fixed. While adsorbents are affordable, the fee that is general of the treatment system, as it impacts the viability of this adsorption strategy, (Dhillon et al. 2017) is important (both theoretically and economically). Enabling a secure, sustainable and assessment that is extra linked with adsorbents, including representative exemplar tests for prospective structure, mineralogy, and textural changes to guarantee the defluoridation regarding the groundwater and wastewater with Diatomaceous Earth. Due to weathering, lixiviation tests, competition, and recharging options (Fig. 5 and Table 4).
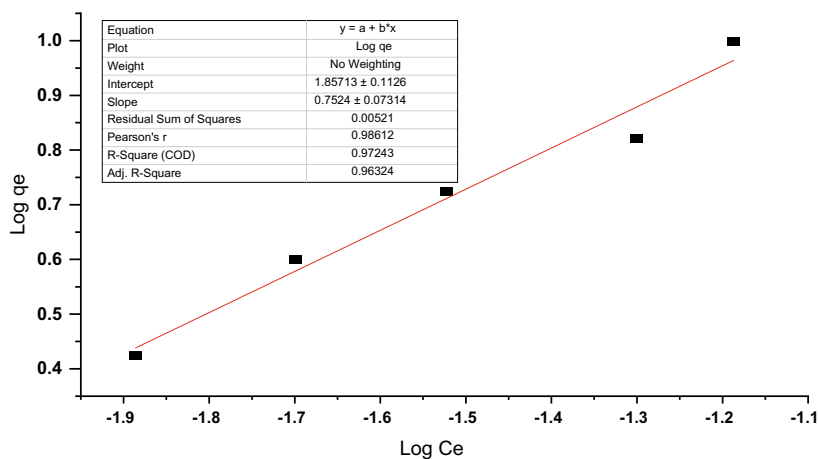
Fig. 5 Freundlich Adsorption isotherm

Table 4 Observed Freundlich parameters

		Intercept	Slope	1/n	Kf	R^2
MCBB	ASV	1.85713	0.7524	0.7524	71.9664	0.96324

4 Conclusions

The reduction of fluoride from wastewater was analyzed by constant adsorption, the fixed bed column matrix system. Diatomaceous Earth was useful for the goal of filtering fluoride from the water as an adsorbent. The pHPZC is 6.98 when utilized being a filter for normal DE and 6.85 for activated DE. Based on this study we conclude that when raw DE is used as a filtration media, 20.73 mg/kg fluoride had been reduced, while when we used Activated DE as an adsorbent the Activate DE happen attained at a particulate size of 0.075–0.425 mm having a capacity to reduce fluoride up to 71.97 mg/kg. DE is therefore an adsorbent for the defluoridation of water that would work and is simply available. The main cause of the adaptation absorbance technique is its straightforwardness of define and operation. Even more, investigation associated with the adsorbent, including regeneration options, is needed to make sure diatomaceous earth DE fluoridation of domestic water is just a secure and eco-friendly process.

Conflicts of Interest None.

References

Adeyemo AA, Adeoye IO, Bello OS (2017) Adsorption of dyes using different types of clay: a review. Appl Water Sci 7:543–568. https://doi.org/10.1007/s13201-015-0322-y

Anthony IA, Gitari MW, Gumbo RJ (2016) Desalination and Water Treatment 36:16745–16757

Aoudj S, Khelifa A, Drouiche N (2017) Removal of fluoride, SDS, ammonia and turbidity from semiconductor wastewater by combined electrocoagulation–electroflotation. Chemosphere 180:379–387. https://doi.org/10.1016/j.chemosphere.2017.04.045

Berger T, Mathurin F, Drake H, Åström M (2016) Fluoride abundance and controls in fresh groundwater in quaternary deposits and bedrock fractures in an area with fluoride-rich granitoid rocks. Sci Total Environ 569–570:948–960. https://doi.org/10.1016/j.scitotenv.2016.06.002

BIS (Bureau of Indian Standards) (2012) Specification for drinking water IS 10500:2012, New Delhi

Cherukumilli K, Maurer T, Hohman J, Mehta Y, Gadgil A (2018) Effective remediation of groundwater fluoride with inexpensively processed Indian bauxite. Environ Sci Technol 52. https://doi.org/10.1021/acs.est.7b05539

Dhillon A, Sapna, Kumar D (2017) Dual adsorption behavior of fluoride from drinking water on Ca-Zn(OH)$_2$CO$_3$ adsorbent. Surf Interf 6:154–161

Ece UD, Ceyhun A, Çağdaş G, Yasin Ö (2019) Enhancing treatability of tannery wastewater by an integrated process of electrocoagulation and fungal via using RSM in an economic perspective. Process Biochem 84:124–133. https://doi.org/10.1016/j.procbio.2019.06.016

Godboley B, Nagarnaik P (2016) Groundnut shell: effective adsorbent for defluoridation from aqueous solution 7:51–60

Hamamoto S, Kishimoto N, Ueki M (2015) Mechanistic consideration of fluoride removal using aluminum sulfate. J Water Environ Technol 13:15–24

He Z, Zhang G, Xu W (2013) Enhanced adsorption of fluoride from aqueous solution using an iron-modified attapulgite adsorbent. Water Environ Res A Res Publ Water Environ Fed 85:167–174. https://doi.org/10.2175/106143012X13560205144218

Kır E, Oruc H, Kır I, Sardohan-Koseoglu T (2016) Removal of fluoride from aqueous solution by natural and acid-activated diatomite and ignimbrite materials. Desalin Water Treat 57:21944–21956

Kumar P, Gupta P (2021) DE Fluoridation of domestic waste water by using activated diatomaceous earth in fixed mattress column adsorption system. Oriental J Chem 37(3):594–601. https://doi.org/10.13005/ojc/370311

Kumar SP, Yesha A, Kaliaperumal S (2014) Defluoridation using biomimetically synthesized nano zirconium chitosan composite: kinetic and equilibrium studies. J Hazard Mater 276:232–240. https://doi.org/10.1016/j.jhazmat.2014.05.038

Mishra KU, Siddiqi A, Meikap H (2020) J Cleon Prod 381:120917

Mishra KU, Siddiqi A, Meikap H (2021) J Cleon Prod 279:123645

Nehra S, Raghav S, Kumar D (2020) Biomaterial functionalized cerium nanocomposite for removal of fluoride using central composite design optimization study. Environ Pollut 113773. https://doi.org/10.1016/j.envpol.2019.113773

Ngulube T, Gitari MW, Tutu H (2016) Defluoridation of groundwater using mixed Mukondeni clay soils. Water Sci Technol 17:480–492

Prathibha C, Sharma B, Chunduri LAA, Aditha SK, Rattan TM, Venkataramaniah K (2015) Nano calcium-aluminum mixed oxide: a novel and effective material for defluoridation of drinking water. Sep Sci Technol 50:1915–1924

Rabelani M, Mugera WG, Segun AA, Titus A, Makudali M (2017) Synthesis and physicochemical characterization of MnO_2 coated Na-bentonite for groundwater defluoridation: adsorption modeling and mechanistic aspect. Appl Surf Sci 422:745–753. https://doi.org/10.1016/j.apsusc.2017.05.194

Roy S, Das P, Sengupta S (2017) Thermodynamics and kinetics study of defluoridation using Ca-SiO_2-TiO_2 as adsorbent: column studies and statistical approach. Korean J Chem Eng 34:179–188

Steier L, Steier R, Steier G (2016) Intersections of dental health and food law: the conflict of systemic fluoridation as a public health instrument to prevent tooth decay. Int Food Law Policy 291–318. https://doi.org/10.1007/978-3-319-07542-6_13

Subbaiah MP, Natrayasamy V, Sankaran M (2014) Defluoridation of water using chitosan assisted ethylenediamine functionalized synthetic polymeric blends. Int J Biol Macromol 70:621–627. https://doi.org/10.1016/j.ijbiomac.2014.07.016

Swapnila R, Shubhalakshmi S, Papita D (2017) Integral approach of adsorption and chemical treatment fluoride-containing wastewater: batch and optimization using RSM. J Environ Chem Eng 5(1):274–282. https://doi.org/10.1016/j.jece.2016.12.003

Tsuzuki T, McCormick PG (2004) Mechanochemical synthesis of nanoparticles. J Mater Sci 39:5143–5146. https://doi.org/10.1023/B:JMSC.0000039199.56155.f9

Uddin MK, Salah MM (2018) Statistical analysis of Litchi Chinensis adsorption behavior toward Cr(VI). Appl Water Sci 8:140. https://doi.org/10.1007/s13201-018-0784-9

WHO guideline for drinking water (2011) 4th ed, Geneva 978:154815

Wu L, Zhang G, Tang D (2016) A novel high efficient Mg–Ce–La adsorbent for fluoride removal: kinetics, thermodynamics and reusability. Desalin Water Treat 57:23844–23855

Yu X, Chen J, Li Y, Liu H, Hou C, Zeng Q, Cui Y, Zhao L, Li P, Zhou Z, Pang S, Tang S, Tian K, Zhao Q, Dong L, Xu C, Zhang X, Zhang S, Liu L, Wang A (2018) Threshold effects of

moderately excessive fluoride exposure on children's health: a potential association between dental fluorosis and loss of excellent intelligence. Environ Int. https://doi.org/10.1016/j.envint.2018.05.042,118,(116-124)

Zhang S, Lyu Y, Su X, Bian Y, Yu B, Zhang Y (2016) Removal of fluoride ion from groundwater by adsorption on lanthanum and aluminum loaded clay adsorbent. Environ Earth Sci 75:401

An Inside for the Treatment of Tannery Industry Effluent

Harshika Suman and Vikas K. Sangal

Abstract The tanning industry includes the process of animal skins and hides to make leather. The tannery process generates a lot of wastewater in almost every step, different processes have different wastewater characteristics. Although many health hazards exist at tanneries, such as acute and chronic musculoskeletal injury, falls, and skin wounds from trauma, chemical hazards are of great importance. There are several norms decided by regularity authorities for discharge effluents in streams. Traditional wastewater treatment approaches are already available for treating tannery wastewater. But they are not fully successful for the treatment of tannery wastewater, so advanced and integrated processes are now in trend. This chapter provides an insight into the tannery industry and treatment approaches for the wastewater generated from the tannery industry.

Keywords Tannery industry · Treatment technology · Pollutants · Standards and regulations

1 Introduction

With the exponential rise of the human population, demand for leather items has increased, resulting in continued growth in the tanning industry sector, which is one of the most water-intensive sectors. Treatment of tannery effluent is a major environmental problem nowadays because of the high concentration of organic load and limited biodegradability (Mwinyihija 2010). The leather industry is a major economic carrier in many emerging countries, has seen rapid expansion in the tanning and processing of leather. The amount of water required is determined by the type of the manufacturing process, as well as the processing chemicals, raw materials, and finished products (Saxena et al. 2016). Because tannery wastewater is unsuited for any use in its raw condition, it is a major concern in today's water management. High

H. Suman · V. K. Sangal (✉)
Chemical Engineering Department, Malaviya National Institute of Technology Jaipur, Jaipur, Rajasthan 302017, India
e-mail: vksangal.chem@mnit.ac.in

909

organic and inorganic material in form of phosphates, nitrates, and other impurities in tannery wastewater is one of the primary causes of eutrophication in several water bodies, as well as poses serious health risks and having a significant impact on the local ecosystem, killing natural plants and animals (Sawalha et al. 2020). Furthermore, the wastewater's black colour blocks sunlight from entering the water body, inhibiting plant photosynthesis. As a result, the amount of dissolved oxygen in the water drops, causing the aquatic life in the water body to suffer. As a response, treating tannery wastewater to the quality levels needed by different regulatory agencies is critical for biotic or abiotic health.

The treatment of pollutants is a serious challenge for the industry because of the lack of efficient wastewater treatment technology, huge operational costs, and the strict requirements set by numerous environmental and governmental regulatory authorities. Low capacity of the plant, lower efficiency in handling large intake loads, treatment process constraints or inability to remove biorefractory contaminants, and inefficiency of the process because of the current practice for mixing various effluents generated from many places, Industrial wastewater is not completely treated in the common effluent treatment plant (Yadav et al. 2019). Regulatory authorities, such as India's Central Pollution Control Board, strive to reduce industrial effluent from being discharged into the environment by applying a variety of regulatory restrictions, For example, enacting strict legislation requiring the closure of industrial units or the enforcement of large fines as compensation for harming the environment if they strive to fulfill wastewater discharge regulations. Furthermore, the government has granted subsidies for the development of CETPs, but these actions will be ineffective unless technology for the treatment of the recalcitrant pollutants, as well as different technical challenges such as highly strung and operating costs, is created. Traditional wastewater treatment approaches such as physical and chemical flocculation, adsorption/ion exchange, precipitation, and biological anaerobic and aerobic digestion (Aber et al. 2010; Tiravanti et al. 1997; Ayoub et al. 2011; Lofrano et al. 2013; Wang et al. 2011) processes have failed to completely treat tannery effluent due to its complex nature. Chemical treatment technologies of many kinds such as Advance Oxidation, Photochemical, Sonochemical and Electrochemical (Sivagami et al. 2018; Oturan and Aaron 2014; Caliari et al. 2021) approaches, have been investigated in the recent decade for their potential application in treating tannery effluents. This study summarized the aspects of the tannery industry and wastewater treatment processes.

2   Tannery Industry Process

The tannery industry is a major polluting industry in the world. Because during the leather processing a variety of Chemicals are used (Sivaram and Barik 2019). There are two types of leather processing, one is vegetable tanning and the other is chrome tanning. Vegetable tanning is the conventional technique for processing leather, it used vegetable extracts but it is very time-consuming so that chrome tanning is the

Fig. 1 Steps involved in a tanning process
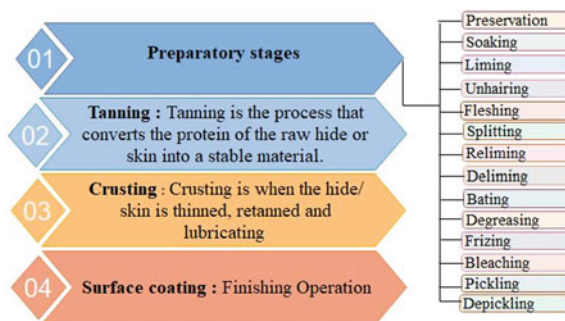
most popular among industries for this reason, it uses chromium salt for tanning operation (Sreeram and Ramasami 2003). Animals like buffaloes, goat and sheep hide/skin is used for manufacturing the leather. Skins of the goat and sheep are the byproducts of the meat industry because in India cow slaughter is banned so naturally dead animals hide are used mostly.

Leather processing can be divided into four categories:

(1) Preservation
(2) Tanning
(3) Crusting
(4) Finishing and Surface Coating

Preparatory stage, tanyard and crusting or post tanning operations are referred to as the wet processes, which are performing in the large drums. After crusting the leather subject to the dry finishing operation. The series of processes and chemicals used for the manufacturing of leather material can be changed depending on the raw materials used and what are the desired products. So the environmental impact of these tannery operations can be varying from industry to industry. Figure 1 shows the steps involve in the tanning process.

3 Tannery Pollutants Characteristics

Tannins, chromium salts, organic matter, phenolics, among different products, are regularly being released into the environment in the tannery wastewater (Marichamy et al. 2021). Untreated sewage, industrial effluents, and agricultural pollutants are frequently dumped into bodies of water. The contaminated water spread a variety of water-borne illnesses. These bodies of water have an impact on the agricultural lands that surround them. The many forms of heavy metals carried by wastewater effluent are freely discharged into surrounding rivers, contaminating them. Groundwater has total dissolved solids content of 17,000 mg/l. Sodium chloride is the most prevalent component in groundwater, rendering it unfit for drinking and irrigation (Saxena et al. 2018). A single tannery can pollute groundwater in a radius of 7–8 km. The

Table 1 Characteristics of tannery waste contents

Characteristics	
Solids	(a) Suspended solids
	(b) Setteleable solids
	(c) Gross solids
Oxygen demand	(a) BOD (biological oxygen demand)
	(b) COD (chemical oxygen demand)
Nitrogen	(a) Total kjeldahl nitrogen
	(b) NH_4-N
Sulfides	
Neutral Salts	(a) Sulphates
	(b) Chlorides
Oil and grease	
pH value	
Chromium compounds	(a) Chrome 3 + (trivalent chrome)
	(b) Chrome 6 + (hexavalent chrome)

types of characteristics that are used to identify tannery waste contents are shown in Table 1.

Table 2 shows typical characteristics of tannery effluent, high BOD, COD, sodium sulfide, and suspended particles are found in tannery wastewater. The properties of tannery effluent vary greatly depending on the size of the plant, the chemicals employed in a particular process, the volume of used water, and the final product type. Different locations and Different industrial processes have different tannery characteristics. As a result, the tannery wastewater streams should be treated to minimize the additional impacts of tannery effluents.

4   Standards and Regulations

With growing legal and societal demands, No tanner can manage to be ignorant of the man problems and environmental preservation concepts that apply to tanneries. Pollution reduction is still the most important goal because it leads to cheaper treatment costs. Despite all the precautions, end-of-pipe techniques are still required to handle a significant quantity of pollution. Excessive pollutant levels, which are prevalent in tannery effluents, can have serious consequences.

Limits for various pollutants in the effluent are set in principle in two ways: based on widely used standards that have been found to be generally acceptable, and based on standards that have not been widely used but have been found to be generally acceptable (i.e. tends to ignore specific individual situations). The magnitude of dilution in the actual recipient is also taken into consideration, as is its capacity to cope with contamination from other sources, based on the mass balance of key

Table 2 Wastewater characteristics of tannery effluent

pH	COD (mg/L)	BOD	TOC	Total suspends solids (mg/L)	SS	TDS (mg/L)	Chromium total (mg/L)	Turbidity (mg/L)	Sulfides (mg/L)	Chlorides (mg/L)	Surfactants (mg/L)	Kjeldahl Nitrogen total (mg/L)	TN (mg/L)	TP (mg/L)	Conductivity (mS/cm)	References
8.1 ± 0.4	3350 ± 150	–	–	1374 ± 10	–	14,250 ± 130	21 ± 2	337 ± 20	38 ± 4	72 ± 4	640 ± 20	460 ± 15	–	–	–	Marichamy et al. (2021)
6.3 ± 0.8	8800 ± 700	700 ± 42	–	589 ± 21	–	–	–	–	–	1150 ± 100	–	–	978 ± 60	9.1 ± 1.2	7.4 ± 2.4	Azarian et al. (2018)
11.41	–	–	–	12,518	–	24,267	30.11 Cr^{6+} 6.95	902	66.13	–	–	–	–	–	–	Moradi and Moussavi (2018)
3.7–4.3	9922–10,180	528	1800–1950	445–530	30	–	Cr^{6+} < 0.11	–	< 28.9	1239	–	–	849	7.86	6.3–9.1	Isarain-Chávez et al. (2014)
7.2 ± 0.2	11,267.5 ± 30.3	6543.9 ± 12.5	1463.2 ± 15.7	–	–	–	–	–	–	–	–	–	754.2 ± 8.4	12.0 ± 0.3	–	Luu et al. (2019)
8–8.30	450–550	–	–	–	–	–	Cr^{3+} and Cr^{6+} 4–4.5	–	1.8–2.0	4500–4600	–	–	–	–	–	Rao et al. (2001)
7.9 ± 0.5	CODt 3600 ± 100 CODd 2500 ± 100	BODt 1550 ± 100 BODd 1425 ± 100	900–1050	–	4200 ± 100	13,000 ± 150	–	–	–	10,700 ± 80	2400 ± 60	–	–	–	–	Iyappan et al. (2014)
4.0	–	–	1005.0	–	–	–	49.8	–	–	787.0	–	–	–	–	6.1	Regina et al. (2008)

(continued)

Table 2 (continued)

pH	COD (mg/L)	BOD	TOC	Total suspends solids (mg/L)	SS	TDS (mg/L)	Chromium total (mg/L)	Turbidity (mg/L)	Sulfides (mg/L)	Chlorides (mg/L)	Surfactants (mg/L)	Kjeldahl Nitrogen total (mg/L)	TN (mg/L)	TP (mg/L)	Conductivity (mS/cm)	References
3.74 ± 0.08	1823.23 ± 2.04	–	576.04 ± 0.17	–	–	–	69.12 ± 0.19 Cr^{3+} 118 and Cr^{6+} 7.04 ± 0.09	–	–	–	–	–	–	–	–	Vilardi et al. (2018)
7.2–7.5	8800–10,080	2800–3200	2290–2583	17,450–19,950	–	18,850–20,370	–	–	–	–	–	–	–	–	–	Saxena et al. (2018)
8.4	4947	–	–	2239	–	–	–	–	–	7601	–	–	–	4	–	Ates et al. (1997)
10.5	3114	1126	–	–	1147	17,737	83	–	55	–	–	–	–	–	–	Ram et al. (1999)
7.5–9	5000–10,000	1500–2000	–	–	–	–	100	–	–	–	–	–	–	–	–	Song et al. (2000)
–	8000	930	–	–	2004	15,152	11.2	–	228	–	–	–	–	–	–	Koteswari and Ramanibai (2003)
7.81	1785	–	–	460	–	14,825	15–65	–	70	6440	–	–	–	4.3	21,000	Dogruel et al. (2004)
8.7	7270	–	–	2210	–	7040	28.0	–	480	–	–	–	112	12.4	–	Alemu et al. (2016)

Table 3 Effluent discharged from typical tannery industry and standards (CPCB)

Parameter	Avg. total pollution load	Effluent limits
COD (chemical oxygen demand)	7200	125–250
BOD$_5$ (biological oxygen demand)	3600	20
SS (suspended solids)	4800	35–100
Total chromium (Cr)	200	1.5–2.0
S^{2-}	200	1–2
SO$_4{}^{2-}$	3200	Locally specific
Cl$^-$	7200	Locally specific
TKN	560	50
Oil and grease	400	10
TDS (total dissolve solids)	16,000	Locally specific
pH	6–9	6–9

All mg/l

pollutants, i.e. the quality of the recipient water after receiving and mixing with the effluent (IL&FS Ecosmart Limited Hydrabad 2010). Table 3 shows Effluent Discharged from typical tannery industry and their standards set by the regulatories.

5 Health and Safety Aspects

Leather processing is linked to a number of significant environmental issues. As can be seen a significant volume of wastewater is generated during the tanning process at various stages (Suman et al. 2021). The notorious smell of tanneries, as well as the presence of unused harmful chemicals in the effluent, demonstrates their contaminating character. The waste produced during the tanning process at various stages, Liquid effluents discharged by tanneries, which contain high organic and inorganic suspended particles, high COD, and possibly hazardous metals, are of greater concern to environmentalists (Kanagaraj et al. 2008). In Table 4 Toxic chemicals used in leather industries and use of the that toxic compound with the target organs are described.

The toxicity of the effluent discharge from the industries is a very complex subject because there are wide varieties of aquatic life and effluent contains many components which may be different in nature and have different degradation rate. Thus specific data for these are lacking. However specification for the effect of a particular component or complex on fish, invertebrates, algae and daphina etc. is not possible.

Table 4 Toxic chemicals used in the leather industry (Saxena et al. 2016; Sivaram and Barik 2019; Dixit et al. 2015)

Name	Chemical formula	Molecular weight	Use of the toxic compound	Target organs
– Bis(2-ethylhexyl) phthalate	– $C_{24}H_{38}O_4$	390.6	Used as plasticizers	– Liver – Testes
– Azo dyes (Acid Black 210)	– $C_{34}H_{28}KN_{11}O_{11}S_3$	901.94	– For dyeing	– Blood – Liver – Testes – Carcinogen
– Benzyl butyl phthalate	– $C_{19}H_{20}O_4$	312.4	– For the production of a micro porous artificial leather coating	– Eyes – Lungs – Liver – Reproductive system
– Anthracene	– $C_{14}H_{10}$	178.23	– As a tanning agent	– Kidney – Liver – Fat – Carcinogen
– Chromium	– Cr	51.996	– Used as tanning agent	– Kidney – CNS – Hematopoietic system
– Cobalt dichloride	– $CoCl_2$	129.84	– Dyeing and finishing	– Lungs – Liver – Kidney – Heart – Skin
– Di-butyl phthalate	– $C_{16}H_{22}O_4$	278.34	– Used as a phthalate plasticizer	– Eyes – Lungs – Gastrointestinal tract – Testes
– Formaldehyde	– CH_2O	30.026	– Finishing	– Eyes – Lungs – Carcinogen
– Heavy metals Arsenic	– As	74.92159	– Finishing	– Liver – Kidneys – Skin – Lungs – Lymphatic system – Carcinogen
– Methyl isothiazolinone	– C_4H_5NOS	115.16	– Biocide, microbiological protection	– Skin – Eyes – Carcinogen
– N-Methyl pyrrolidone	– C_5H_9NO	99.13	– Coalescence, plasticizers, wetting agent	– Eyes – Kidney – Lymphatic system – Liver – Lung – Testes

(continued)

Table 4 (continued)

Name	Chemical formula	Molecular weight	Use of the toxic compound	Target organs
– Nonyl phenol	– $C_{15}H_{24}O$	220.35	– Finishing	– Blood – Lungs – Eyes – Skin – Cns – Kidneys – Low biodegradability
– Organotin compounds- dibutyltin oxide	– $C_8H_{18}OSn$	248.94	– As a catalyst	– Gastrointestinal tract – Liver – Carcinogen
– Short chain chlorinated paraffins	– C_{10-13}		– Additive and leather oiling agent	– Liver – Kidney – Thyroid – Carcinogen
– Sodium dichromate	– $Na_2Cr_2O_7$	261.97	– It is Chrome-tanning salts	– Blood – Kidneys – Heart – Lungs – Eyes – Carcinogen
– Pentachlorophenol	– C_6HCl_5O	266.3	– Biocide in preservation	– Eyes – Nose – Skin – Respiratory tract – Blood – Kidney – Liver – Immune system – Reproductive system – Carcinogen

The LD50, or lethal dosage, is a toxicity metric that represents the dose that would kill 50% of a sample species. Not every species reacts to a particular exposure in the same way, and the kind of reaction to an identical dosage of a toxin might vary greatly. The species under test should be specified when values are reported, and the evaluation period should generally be 24 or 96 h or 14 days. (Hauber and Buljan 2000) Environmental quality criteria, based on fate, behavior, and aquatic toxicity, are also employed to assess the preservation of aquatic life. Much of this extremely sensitive data is derived from study data from many sources and species. When there aren't enough facts to make a decision, expert judgment may be used instead. Environmental quality standards may be described as the maximum concentration of a chemical that must not be surpassed in order to sustain a specified aquatic use.

6 Wastewater Treatment Options

Physical, chemical, and biological treatments are commonly used to treat tannery effluent. Adsorption, coagulation, precipitation, flocculation, sedimentation, filtration, ion exchange, and chemical oxidation are some of the chemical processes used to treat organic wastewater (Aber et al. 2010; Tiravanti et al. 1997; Ayoub et al. 2011; Lofrano et al. 2013; Wang et al. 2011; Sivagami et al. 2018; Oturan and Aaron 2014; Caliari et al. 2021). The tannery industry has long relied on coagulation to decrease COD and suspended solids. The adsorption process is used to remove chromium and ammonia from the effluent. Only easily degradable organics are suitable for the biological treatment of industrial effluents. However, for effluents containing refractory (i.e. resistant to biological treatment) organic contaminants, these approaches are useless. Although traditional technologies have been utilized in the tannery sector for many years, they have limitations and cannot fulfill the severe pollution control board regulations. As a result, manufacturers are being compelled to seek out alternative treatment technologies in order to successfully treat tannery effluent. Advanced oxidation techniques have already been applied for the treatment of refractory organics in industrial wastewater (Sivagami et al. 2018; Rameshraja and Suresh 2011). Table 5 shows the classification of the Wastewater Treatment Process.

In Fig. 2. Common layout of an Effluent Treatment Plants (ETPs) is shown, most of the industries follow this process for treatment. It's vital to remember the following before moving on to treatment: There are never too identical effluent treatment plants (ETPs) since their design is always adapted to the needs of a given location. Pollutants in wastewater cannot be removed; they can only be transformed into something that is more ecologically friendly or simpler to dispose of (sludge). Surprisingly, the obvious is commonly overlooked: reducing water usage while maintaining the same amount of pollutants results in a lower hydraulic load (volume) but a higher concentration, which is harder to treat. To decrease the total cost of treatment, a tanner must grasp the relationship between the leather technology used and wastewater treatment (Hansen et al. 2021). Wastewater treatment is a multi-stage procedure that purifies wastewater before it is discharged into a body of natural water, applied to land, or reused. Because each receiving body of water can only accept a

Table 5 Wastewater treatment process

Treatment options		
1. Coagulation and flocculation		
2. Biological treatment	a. Aerobic processes b. Anaerobic processes c. Wetlands and ponds	
3. Emerging treatment technologies	a. Membrane processes b. Membrane bioreactors c. Advanced oxidation processes	c (i). Fenton based processes c (ii). Photooxidation processes c (iii). Ozone based processes c (iv). Photocatalysis c (v). Electrochemical treatment
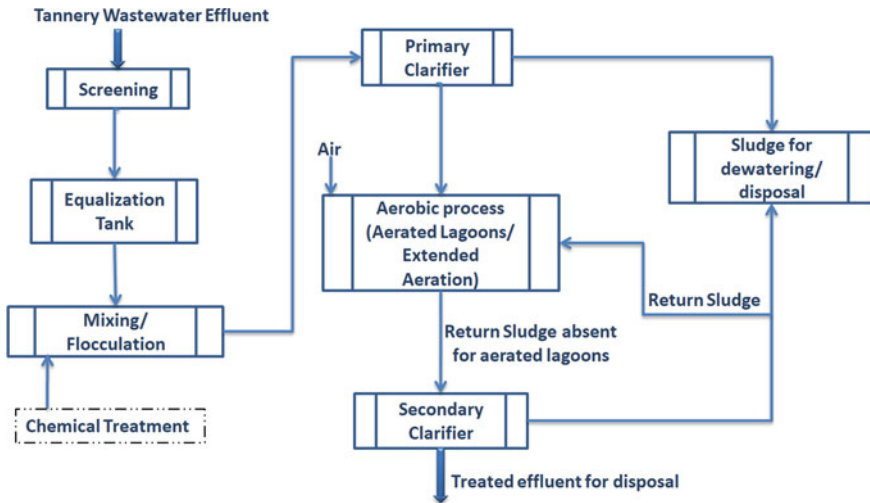
Fig. 2 A common layout of an effluent treatment plants (ETPs)

limited amount of contaminants without degrading, the objective is to minimize or eliminate organic matter, sediments, nutrients, Cr, and other pollutants. As a result, each effluent treatment plant must conform to discharge regulations, which are often established by the appropriate environmental authority as permissible levels of pollutants represented as BOD_5, COD, suspended solids (SS), Cr, total dissolved solids (TDS), and others for practical reasons (IL&FS Ecosmart Limited Hydrabad 2010). The three major types of tannery effluent, each with its own set of properties, are: Liming, deliming/bating, and water from fleshing and splitting machinery emitted from the beam-house include sulfides, have a high pH, but are chrome-free. Tanyard effluents (tanning and re-tanning, sammying) have a high Cr concentration and are acidic. Low Cr concentration from soaking and other general effluents, primarily from post-tanning processes (fat-liquoring, dyeing) (Suman et al. 2021).

6.1 Recent Attraction

A considerable portion of a tannery's operations are wet operations, which use a lot of water, chemicals, and energy and result in a lot of polluted water. Although "process integrated" methods can significantly reduce water consumption and pollution, tanneries continue to produce wastewater that requires special treatment. When the potential for "process integrated" solutions has been exhausted, additional pollution reduction must be found in the enhancement of end-of-pipe controls. Process integrated or hybrid treatment technology is now in trend (Deghles and Kurt 2016; Suganthi et al. 2013). In hybrid treatment technology, conventional and advanced

treatment processes are combined to achieve higher removal efficiencies. Successful and effective demonstration of a new integrated and compact biological and physical treatment plant for tannery wastewater treatment. Table 6 Summarise AOP methodologies used in the treatment of tannery effluent with the parameters employed and

Table 6 A summary of advanced oxidation techniques used in tannery wastewater treatment

Technology	Parameters	Removal efficiency (%)	References
Fenton oxidation	Temperature = 40–45 °C pH = 3.5 $H_2O_2/FeSO_4$ = 600/750 (mg/mg)	COD = 80–90 UV_{254} = 80–95 UV_{280} = 80–95	Lofrano et al. (2007)
Ozonation	pH = 4 O_3 concentration = 1.6 mg/l Time = 0–60 Min	Decolourization = 98	Srinivasan et al. (2009)
Photocatalytic TiO_2 coating	Time = 3 h pH—2.5	TOC = 49.1	Bordes et al. (2015)
Green synthesized TiO_2 nanoparticle	Time = 5 h	COD = 82.26	Goutam et al. (2017)
Electro-fenton (EF) oxidation	pH = 3 H_2O_2 Conc. = 1670 mgl^{-1} Power consumption = 15 W Contact time = 12 min	COD = 70	Kurt et al. (2007)
AOP – UV/H_2O_2 – $TiO_2/H_2O_2/UV$ – TiO_2/UV	H_2O_2 Concentration = 500 mg/l	– UV/H_2O_2 COD = 10–20 – $TiO_2/H_2O_2/UV$ COD = 60–70 – TiO_2/UV COD = 80–90	Sauer et al. (2006)
Ozonation	pH = 4 O_3 flow rate = 4 × 10^{-3} m^3/min	Decolourization = 90–100 COD = 60–80 BI = 0.49	Preethi et al. (2009)
Fenton reaction, UV/H_2O_2 reactions	Fenton reaction (pH = 3.5 $H_2O_2/FeSO_4$ Conc. = 100/150 mgl^{-1}) UV/H_2O_2 reactions (pH = 3 H_2O_2 Conc. = 1020 mgl^{-1})	COD ≥ 60 TOC ≥ 45	Schrank et al. (2005)
Fenton process photo Fenton process	Fenton reaction (H_2O_2 = 600 $FeSO_4$ = 1000) Photo-fenton reaction (H_2O_2 = 150 $FeSO_4$ = 400) Reaction time—30 min pH = 3 ± 0.2 Temp. = 40–45 °C	Fenton process COD = 72 UV_{254} = 86 UV_{280} = 77 Photo fenton process COD = 80 UV_{254} = 90 UV_{280} = 90	Lofrano et al. (2010)
Ozonation	1.5 g of O_3/g of COD pH = 7.6	COD = 60	Saranya and Shanthakumar (2020)

Table 6 (continued)

Technology	Parameters	Removal efficiency (%)	References
Electro-oxidation	Current density = 0.065 A/cm^2 Time = 2 h Temp = 30 °C pH = 12.5 NaCl = 10,000 mg/l	Synthetic (TOC = 86.2 TKN = 77.2) Real (TOC = 84.4 TKN = 71.2)	Vijayalakshmi and Sarvananan (2015)
One-compartment filter-press Electrochemical flow cell	Current density = 20 A/cm^2 Time = 2–5 h Temp = 25 °C pH = 3.3 NaCl = 500 mmol/l	Phenolic compounds = 100 TOC = 44.6	Costa and Olivi (2009)
Electrochemical treatment	Current = 0–10 A Voltages = 0–30 V pH = 6.5–9.0 Time = 30–45 min	COD = 51–56 TSS = 30–70 Cr ≥ 98 Turbidity ≥ 96	Espinoza-Quinones et al. (2009)
Electro-coagulation	Current density = 4 A/dm^2 pH = 3, 7, 11 Time = 30 min Chloride concentration = 0, 8 NaCl L^{-1}	Ammonium = 78.9 COD = 26.0	Min et al. (2004)
Electro-coagulation	Current density = 50 mA/cm^2 pH = 7 Time = 25 min	Iron electrodes COD = 63.3 Total chrome = 99.7 Color = 82 Aluminum electrode COD = 64.4 Total chrome = 99 Color = 88	Abdalhadi Deghles and Ugur Kurt (2015)
Coagulation + EO Coagulation + H$_2$O$_2$/UV + EO	pH = 8 Current = 3 A/dm^2	Coagulation COD = 57–74 EO COD = 53–73.1 UV/H$_2$O$_2$ COD = 77.7–86 Coagulation + H$_2$O$_2$/UV + EO COD = 97	Naumczyk and Kucharska (2017)
Hybrid US treatment (US + Fenton US + H2O2)	Amplitude = 40% Ultra sonocation time = 2 h	Ultra sonocation COD = 23.68 Ultra sonocation + fenton COD = 66.96 Ultra sonocation + H$_2$O$_2$ COD = 36.82	Saxena et al. (2021)

removal efficiency. It can be seen from the table tannery wastewater can be treated with multiple techniques.

7 Conclusion

The aspects of tannery wastewater were summarized in this review which includes the Tanning process, effluent standards, health and safety, characteristics of pollutants, and wastewater treatment options. The tannery business discharges enormous amounts of hazardous chemicals into the environment due to the use of underdeveloped and traditional technologies. Found the feasibility of the Advanced Oxidation method for the treatment of effluent from leather industry. Technical Barriers, Economic Barriers, Social Barriers, Inadequate Legislation, and a Lack of Monitoring Facilities are all obstacles in the tannery business. Leather companies are using different contemporary technologies on the manufacturing side as well as in the management of effluents to limit pollutants discharged into the environment and minimize waste creation. The leather industry's effluents include a greater proportion of hazardous compounds and heavy metals, severely degrading the environment.

References

Aber S, Salari D, Parsa MR (2010) Employing the Taguchi method to obtain the optimum conditions of coagulation–flocculation process in tannery wastewater treatment. Chem Eng J 162(1):127–134

Alemu T, Lemma E, Mekonnen A, Leta S (2016) Performance of pilot scale anaerobic—SBR system integrated with constructed wetlands for the treatment of tannery wastewater. Environ Process 3(4):815–827 https://doi.org/10.1007/s40710-016-0171-1

Ates E, Orhon D, Tünay O (1997) Characterization of tannery wastewaters for pretreatment selected case studies. Water Sci Technol 36(2–3):217–223. https://doi.org/10.1016/S0273-1223(97)00390-9

Ayoub GM, Hamzeh A, Semerjian L (2011) Post treatment of tannery wastewater using lime/bittern coagulation and activated carbon adsorption. Desalination 273:359–365. https://doi.org/10.1016/j.desal.2011.01.045

Azarian G, Miri M, Nematollahi D (2018) Combined electrocoagulation/electrooxidation process for the COD removal and recovery of tannery industry wastewater. Environ Prog Sustain Energy 37(2):637–644

Bordes MC, Vicent M, Moreno R, García-Montaño J, Serra A, Sánchez E (2015) Application of plasma-sprayed TiO$_2$ coatings for industrial (tannery) wastewater treatment. Ceram Int 41(10):14468–14474. https://doi.org/10.1016/j.ceramint.2015.07.083

Caliari PC, Pacheco MJ, Ciríaco L, Lopes A (2021) Treatment of tannery effluent by chemical coagulation combined with batch-recirculated electro-oxidation at different anode materials. Environ Sci Pollut Res 28(19):24138–24149

Central Pollution Control Board, Ministry of environment, forest and climate Govt. of India

Costa CR, Olivi P (2009) Electrochimica acta effect of chloride concentration on the electrochemical treatment of a synthetic tannery wastewater. Electrochim Acta 54(7):2046–2052

Costa CR, Botta CM, Espindola EL, Olivi P (2008) Electrochemical treatment of tannery wastewater using DSA ® electrodes. J Hazard Mater 153(1–2):616–627

Deghles A, Kurt U (2016) Treatment of raw tannery wastewater by electrocoagulation technique: optimization of effective parameters using Taguchi method. Desalin Water Treat. https://doi.org/10.1080/19443994.2015.1074622

Deghles A, Kurt U (2016) Treatment of tannery wastewater by a hybrid electrocoagulation/electrodialysis process. Chem Eng Process 104:43–50

Dixit S, Yadav A, Dwivedi PD, Das M (2015) Toxic hazards of leather industry and technologies to combat threat: a review. J Clean Prod 87:39–49

Dogruel S, Genceli EA, Babuna FG, Orhon D (2004) Ozonation of nonbiodegradable organics in tannery wastewater. J Environ Sci Health Part A 39(7):1705–1715. https://doi.org/10.1081/ESE-120037871

Espinoza-Quinones FR, Fornari MMT, Módenes AN, Palácio SM, da Silva FG, Szymanski N, Kroumov AD, Trigueros DEG (2009) Pollutant removal from tannery effluent byelectrocoagulation. Chem Eng J 151(1–3):59–65

Goutam SP, Saxena G, Singh V, Yadav AK, Bharagava RN, Thapa KB (2018) Green synthesis of TiO$_2$ nanoparticles using leaf extract of *Jatropha curcas* L. for photocatalytic degradation of tannery wastewater. Chem Eng J 336:386–396. https://doi.org/10.1016/j.cej.2017.12.029

Hansen É, de Aquim PM, Gutterres M (2021) Current technologies for post-tanning wastewater treatment: a review. J Environ Manage 294:113003

Hauber C, Buljan J (2000) Regional programme for pollution control in the tanning industry in South–East Asia

Isarain-Chávez E, De La Rosa C, Godínez LA, Brillas E, Peralta-Hernández JM (2014) Comparative study of electrochemical water treatment processes for a tannery wastewater effluent. J Electroanal Chem 713:62–69

Iyappan K, Basha CA, Saravanathamizhan R, Vedaraman N, Tahiyah Nou Shene CA, Begum SN (2014) Electrochemical treatment of tannery effluent using a battery integrated DC–DC converter and solar PV power supply—an approach towards environment and energy management. J Environ Sci Health Part A 49(10):1149–1162.

Kanagaraj J, Babu NC, Mandal AB (2008) Recovery and reuse of chromium from chrome tanning waste water aiming towards zero discharge of pollution. J Clean Prod 16(16):1807–1813

Koteswari YN, Ramanibai R (2003) The effect of tannery effluent on the colonization rate of plankters: a microcosm study. Turk J Biol 27(3):163–170

Kurt U, Apaydin O, Gonullu MT (2007) Reduction of COD in wastewater from an organized tannery industrial region by electro-fenton process. J Hazard Mater 143(1–2):33–40. https://doi.org/10.1016/j.jhazmat.2006.08.065

Min KS, Yu JJ, Kim YJ, Yun Z (2004) Removal of ammonium from tannery wastewater by electrochemical treatment. J Environ Sci Health Part A 39(7):1867–1879. https://doi.org/10.1081/ESE-120037884

Lofrano G, Meric S, Inglese M, Nikolau A, Belgiorno V (2010) Fenton oxidation treatment of tannery wastewater and tanning agents: synthetic tannin and nonylphenol ethoxylate based degreasing agent. Desalin Water Treat 23(1–3):173–180. https://doi.org/10.5004/dwt.2010.1991

Lofrano G, Meriç S, Zengin GE, Orhon D (2013) Chemical and biological treatment technologies for leather tannery chemicals and wastewaters: a review. Sci Total Environ 461:265–281. https://doi.org/10.1016/j.scitotenv.2013.05.004.23735721

Lofrano G, Meriç S, Belgiorno V, Napoli RMA (2007) Fenton's oxidation of various-based tanning materials. Desalination 211(1–3):10–21. https://doi.org/10.1016/j.desal.2006.03.589

Luu TL, Djeuga D, Stephane F, Minh NH, Canh ND, Thanh BX (2019) Electrochemical oxidation as a post treatment for biologically tannery wastewater in batch reactor. Water Sci Technol 1–12

Marichamy MK, Kumaraguru A, Jonna N (2021) Particle size distribution modeling and kinetic study for coagulation treatment of tannery industry wastewater at response surface optimized condition. J Clean Prod 297:126657

Moradi M, Moussavi G (2019) Enhanced treatment of tannery wastewater using the electrocoagulation process combined with UVC/VUV photoreactor: parametric and mechanistic evaluation. Chem Eng J 358:1038–1046. https://doi.org/10.1016/j.cej.2018.10.069

Mwinyihija M (2010) Main pollutants and environmental impacts of the tanning industry. In: Ecotoxicological diagnosis in the tanning industry, pp 17–35. Springer, New York

Naumczyk JH, Kucharska MA (2017) Electrochemical treatment of tannery wastewater—Raw, coagulated, and pretreated by AOPs. J Environ Sci Health Part A 52(7):649–664. https://doi.org/10.1080/10934529.2017.1297140

Oturan MA, Aaron JJ (2014) Advanced oxidation processes in water/wastewater treatment: principles and applications. A review. Crit Rev Environ Sci Technol 44(23):2577–2641

Preethi V, Parama Kalyani KS, Iyappan K, Srinivasakannan C, Balasubramaniam N, Vedaraman N (2009) Ozonation of tannery effluent for removal of cod and color. J Hazard Mater 166(1):150–154. https://doi.org/10.1016/j.jhazmat.2008.11.035

Ram B, Bajpai PK, Parwana HK (1999) Kinetics of chrome-tannery effluent treatment by the activated-sludge system. Process Biochem 35(3–4):255–265. https://doi.org/10.1016/S0032-9592(99)00062-X

Rameshraja D, Suresh S (2011) Treatment of tannery wastewater by various oxidation and combined processes. Int J Environ Res 5(2):349–360

Rao NN, Somasekhar KM, Kaul SN, Szpyrkowicz L (2001) Electrochemical oxidation of tannery wastewater. J Chem Technol Biotechnol: Inter Res Process Environ Clean Technol 76(1):1124–1131

Saranya D, Shanthakumar S (2020) An integrated approach for tannery effluent treatment with ozonation and phycoremediation: a feasibility study. Environ Res 183:109163. https://doi.org/10.1016/j.envres.2020.109163

Sauer TP, Casaril L, Oberziner ALB, Jos´e HJ, Moreira RdFPM (2006) Advanced oxidation processes applied to tannery wastewater containing direct black 38—elimination and degradation kinetics. J Hazard Mater 135(1–3):274–279. https://doi.org/10.1016/j.jhazmat.2005.11.063

Sawalha H, Al-Jabari M, Elhamouz A, Abusafa A, Rene ER (2020) Tannery wastewater treatment and resource recovery options. In: Waste biorefinery, pp 679–705. Elsevier

Saxena G, Chandra R, Bharagava RN (2016) Environmental pollution, toxicity profile and treatment approaches for tannery wastewater and its chemical pollutants. Rev Environ Contam Toxicol 240:31–69

Saxena S, Saharan VK, George S (2018) Enhanced synergistic degradation efficiency using hybrid hydrodynamic cavitation for treatment of tannery waste effluent. J Clean Prod 198:1406–1421. https://doi.org/10.1016/j.jclepro.2018.07.135

Saxena S, Saharan VK, George S (2021) Studies on the efficacy of ultrasonication processes in combination with advanced oxidizing agents for alum pretreated tannery waste effluent. J Environ Chem Eng 9(1):104678. https://doi.org/10.1016/j.jece.2020.104678

Schrank SG, Jos´e HJ, Moreira RFPM, Schr¨oder HF (2005) Applicability of fenton and H2O2/UV reactions in the treatment of tannery wastewaters. Chemosphere 60(5):644–655. https://doi.org/10.1016/j.chemosphere.2005.01.033

Sivagami K, Sakthivel KP, Nambi IM (2018) Advanced oxidation processes for the treatment of tannery wastewater. J Environ Chem Eng 6(3):3656–3663

Sivaram NM, Barik D (2019) Toxic waste from leather industries. In: Energy from toxic organic waste for heat and power generation. pp 55–67, Woodhead Publishing. https://doi.org/10.1016/B978-0-08-102528-4.00005-5

Song Z, Williams CJ, Edyvean RGJ (2000) Sedimentation of tannery wastewater. Water Res 34(7):2171–2176. https://doi.org/10.1016/S0043-1354(99)00358-9

Sreeram KJ, Ramasami T (2003) Sustaining tanning process through conservation, recovery and better utilization of chromium. Resour Conserv Recycl 38(3):185–212

Srinivasan SV, Rema T, Chitra K, Balakameswari KS, Suthanthararajan R, Maheswari BU, Ravindranath E, Rajamani S (2009) Decolourisation of leather dye by ozonation. Desalination 235(1–3):88–92. https://doi.org/10.1016/j.desal.2007.07.032

Suganthi V, Mahalakshmi M, Balasubramanian B (2013) Development of hybrid membrane bioreactor for tannery effluent treatment. Desalination 309:231–236

Suman H, Sangal VK, Vashishtha M (2021) Treatment of tannery industry effluent by electrochemical methods: a review. Mater Today Proc 47:1438–1444

Technical EIA guidance manual for leather/skin/hide processing industry prepared for the Ministry of Environment and Forests Government of India by IL&FS Ecosmart Limited Hydrabad August 2010

Tiravanti G, Petruzzelli D, Passino R (1997) Pretreatment of tannery wastewaters by an ion exchange process for Cr(III) removal and recovery. Water Sci Technol 36(2–3):197–207

Vijayalakshmi P, Sarvananan P (2015) Treatment of organics containing from leather processing unit using electro—oxidation—a noval approach. Int J ChemTech Res 7(7):3004–3012

Vilardi G, di Palma L, Verdone N (2018) On the critical use of zero valent iron nanoparticles and Fenton processes for the treatment of tannery wastewater. J Water Process Eng 22:109–122. https://doi.org/10.1016/j.jwpe.2018.01.011

Wang H, Wang Y, Zhou L (2011) Purification and recycling of tannery degreasing wastewater by ultrafiltration with polyimide membrane. In: 2011 international conference on remote sensing, environment and transportation engineering. 569–572. IEEE

Yadav A, Raj A, Purchase D, Ferreira LFR, Saratale GD, Bharagava RN (2019) Phytotoxicity, cytotoxicity and genotoxicity evaluation of organic and inorganic pollutants rich tannery wastewater from a common effluent treatment plant (CETP) in Unnao district, India using vigna radiata and allium cepa. Chemosphere 224:324–332

Enrichment of Anammox in Sequencing Batch Reactor (SBR)

Ashma Parween and S. K. Patidar

Abstract Disposal of wastewater rich in nutrients harms aquatic ecosystems. Strict effluent standards are being implemented to restrict excess nutrient disposal in water bodies and therefore, there is need for developing efficient and effective methods for nutrient removal. Conventional nitrification–denitrification has been used for biological nitrogen removal from wastewaters. Anammox (anaerobic ammonium oxidation) is a novel, promising and efficient method for removal of nitrogen from wastewater. It has advantages of lesser operational costs, no chemical demand and lesser sludge handling. In this process, ammonium is oxidized anaerobically to nitrogen gas in presence of nitrite as electron acceptor. Since its discovery, it is being studied extensively. In the present paper, anammox process and factors affecting enrichment of anammox are discussed. A summary of various studies involving enrichment of anammox using sequencing batch reactor (SBR) is also presented.

Keywords Nitrification–denitrification · Biological nitrogen removal · Anammox (anaerobic ammonium oxidation) · Sludge handling

1 Introduction

Anaerobic ammonium oxidation (ANAMMOX) was discovered in denitrifying fluidized bed reactor treating effluent from a methanogenic reactor in Delft, The Netherland in 1995 (Mulder et al. 1995). It is novel, promising and cost-effective alternative to conventional nitrification-denitrification process (Graaf et al. 1996). It is a chemo-autotrophic process, requires no oxygen, chemicals in form of organic matter and also biomass yield is very low, so less sludge production (Strous et al. 1997b; Graaf et al. 1996) and thus have advantage over conventional nitrification-denitrification process. Anammox oxidizes ammonium anaerobically to nitrogen gas

A. Parween (✉) · S. K. Patidar
NIT Kurukshetra, Kurukshetra 136119, India

S. K. Patidar
e-mail: skpatidar@nitkkr.ac.in

927

by using nitrite as the electron acceptor (Graaf et al. 1996). Anammox has very slow growth yield with multiplying time of 11–30 days. The specific activity of Anammox is more than seven times lower than the specific activity reported for aerobic ammonium oxidation (Lotti et al. 2015; Strous et al. 1998). Strous et al. (1998) reported maximum specific growth rate of $0.0027\ h^{-1}$. The maximum growth rate as high as $0.334\ d^{-1}$ was observed at 30 °C by Lotti et al. (2015). The application of anammox in mainstream wastewater treatment plant is difficult due to its extremely slow growth (Ding et al. 2017).

The biochemical reaction of anammox as given by Strous et al. (1998) is as following:

$$NH_4^+ + 1.32NO_2^- + 0.066HCO_3^- + 0.13H^+ \rightarrow 1.02N_2 + 0.26NO_3^- + 0.066CH_2O_{0.5}N_{0.15} + 2.03H_2O.$$
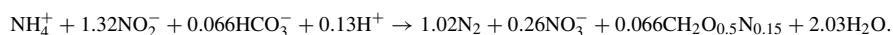
Enrichment of anammox from conventional sludge takes place through changes in sludge due to exposed system conditions. Based on removal performance of ammonium and nitrite, the start-up process of anammox can be divided in mainly three phases: denitrification phase, anammox start phase (propagation phase) and stable activity phase (stationary phase) (Araujo et al. 2011; Chamchoi and Nitisoravut 2007; Ding et al. 2017; Wang et al. 2011). Duration of each phase depends on operating conditions, sludge taken and sludge pretreatment.

Denitrification Phase During this phase, lysis of sludge takes place in which dominant bacteria is killed and break down of organic nitrogen to ammonium takes place. The nitrite removal during this phase may be zero and ammonium removal may be negative with high ammonium in effluent than influent. Denitrification takes place in this phase in which aerobic bacteria may be killed due to low DO (dissolved oxygen) concentration and provides organic matter for denitrification.

After lysis of aerobic bacteria, lysis of denitrifying bacteria takes place due to lack of organic matter.

Propagation Phase During this phase, there is variation in ammonium removal efficiency. In this phase consumption of ammonium starts with first sign of anammox activity. In this phase the sludge goes through transition. Ammonium removal efficiency increases with increase in growth and activity.

Stationary Phase During this phase, nitrogen removal efficiency is reached at its maximum level with maximum anammox activity.

2   Factors Affecting Enrichment of ANAMMOX

The operational conditions affecting anammox enrichment and performance are pH, temperature, dissolved oxygen (DO), substrate concentration, solids retention time (SRT) and organic matter (Cho et al. 2020). DO is critical during anammox enrichment (Strous et al. 1997a).

2.1 pH

The optimal pH range for enrichment of anammox is 6.7–8.3 (Strous et al. 1999). Jetten et al. (2001) suggests optimal pH of 6.7–8.5 with maximum activity at pH 8. The change in culture pH can influence the anammox process greatly owing to the accumulation of toxic compounds which inhibits anammox activity. The effect of pH on Anammox process has been studied by Strous et al. (1997b) and results have shown that the specific anammox activity at pH of 9 was only 1/5 of that at of pH 8. Performance failure of anammox reactors may occur when reactors are operated under such high pH for a longer time. High pH is accompanied by high free ammonia (FA) concentration which could inhibit anammox performance (Tang et al. 2009).

2.2 Temperature

Temperature influences cell growth and metabolic activity. Cell grows faster at higher temperature. It is one of the most important factors for enrichment of anammox. Anammox generally takes place at temperatures from 6 °C to 43 °C, however the reaction rate drops rapidly at temperatures lower than 15 °C or higher than 40 °C (Zhu et al. 2008). Strous et al. (1999) reported physiological temperature range of 20–43 °C for anammox. Decrease in nitrogen removal was reported when temperature decrease from 30 °C to 15 °C, but recovery in efficiency was achieved with increase in temperature (Li et al. 2018; Wang et al. 2018).

2.3 Dissolved Oxygen (DO)

DO is a critical parameter for anammox growth. DO must be strictly controlled in anammox, especially during enrichment to avoid DO inhibition. It was reported that anammox activity was inhibited temporarily at DO of 0.2 mg/L and complete inhibition between DO of 0.2–1 mg/L (Strous et al. 1997a). Ammonium removal and anammox activity increases with decrease in DO less than 0.2 ppm (Jetten et al. 2001; Jung et al. 2007). Lotti et al. (2012) reported no inhibition in anammox activity with DO exposure of 5 mg/L for 1 h. Adaptability of anammox can be increased by gradually increasing DO in the system. By stepwise increase in DO, anammox culture adapted the high DO concentration of 8 mg/L without much decrease in activity (Liu et al. 2008). Anammox can coexist with aerobic bacteria. Aerobic bacteria consume DO and toxic nitrite and contributes to nitrogen removal (Liu et al. 2008; Ma et al. 2016).

2.4 Substrate Concentration

Anammox bacteria requires ammonia and nitrite as substrate. Ammonia (the substrate for anammox) and nitrate (the substrate by-product) do not appear to inhibit anammox bacteria at concentrations less than 500 mg/L (Lotti et al. 2012). However, anammox bacteria are inhibited by nitrite at lower concentration. The anammox process was completely inhibited by nitrite concentrations higher than 0.1 g of nitrogen per liter (Strous et al. 1999). During enrichment lower nitrogen load is preferable. Availability of nitrite and ammonia in excess during start up inhibits anammox activity. Anammox reaction activated when concentration of nitrite and ammonia was changed from 70 mg/L to 25 and 35 mg/L respectively (Jung et al. 2007). Enrichment of anammox was successful when nitrite was supplied at low concentration (25 mg/L) in initial days and then progressively increase to 150 mg/L (Connan et al. 2016).

Nitrite

Nitrite is a substrate for anammox but it can inhibit its activity if present in excess, especially during startup phase. Nitrite inhibition is reversible and activity can be reversed once nitrite concentration is reduced. However, Strous et al. (1999) reported complete loss of activity when nitrite concentration was higher than 100 mg/L. Inhibition by nitrite is reported to be more severe for suspended and flocculant biomass than biomass grown on carriers and granular biomass (Lotti et al. 2012). Highest nitrite concentration of 1000 mg/L has been tested which resulted in activity loss by 93–94% (Lotti et al. 2012). Higher activity loss due to nitrite occurs in absence of ammonium (Lotti et al. 2012).

Ammonium

It has been reported anammox activity was not inhibited by ammonium concentration up to 1 g N/L (Strous et al. 1999). It has been found that free ammonia (FA) is inhibitor rather than ammonium. Maximum tolerable FA concentration was reported to be 150 mg/L (Aktan et al. 2012). The concentration of free ammonia nitrogen (NH_3–N) can be calculated using following formula:

$$NH_3 - N = \frac{Total\ ammonia\ nitrogen}{1 + 10^{(pK_a - pH)}} \tag{1}$$

$$pK_a = 0.09018 \frac{2729.92}{T + 278.15} \tag{2}$$

where, pK_a is the dissociation constant for ammonium ion, and T is temperature in °C (Aktan et al. 2012).

Free ammonia concentration is dependent more on pH and temperature than ammonia concentration (Aktan et al. 2012). With increase in pH, FA concentration increases. Jung et al. (2007) reported FA concentration to be below 2 mg/L for enrichment of anammox without inhibition. Fernandaz et al. (2012) studied short term and long-term effect of FA on anammox activity. For short term effect, FA concentration of 38 mg/L decreases specific anammox activity by 50% and for long term effect FA concentration between 35–40 mg/L leads to loss of operation and zero removal efficiency.

2.5 SRT

Because anammox has slow growth rate and low biomass yield, a long sludge age is critical for this process (Zhu et al. 2008). For good retention of anammox SRT should be more than doubling time. Anammox bacteria have been retained in a membrane bioreactor operated at 30 °C with a SRT of 3 days. However, the maximum volumetric specific nitrite removal rate decreased by almost 3 times when SRT decreased from 12 to 3 days (Lotti et al. 2015). Longer SRT favors anammox growth and activity.

2.6 Organic Matter

Anammox are chemoautotrophic microorganisms that uses inorganic carbon. Availability of bicarbonate is important for cultivation of anammox bacteria. Addition of inorganic carbon can promote the growth of anammox bacteria and increases it activity. Liao et al. (2008) reported maximum anammox activity of 66.4 mg N/(Ld) at bicarbonate concentration of 1.5–1.75 mg/L. However, anammox activity was inhibited at bicarbonate concentration of 1 mg/L and 2 mg/L (Liao et al. 2008). Organic matter was thought to be inhibitory for anammox but coexistence of anammox with heterotrophic bacteria has been reported by many researchers (Dapena-Mora et al. 2004). However, existence of heterotrophs can outcompete anammox due to slow growth rate of anammox (Jin et al. 2012).

2.7 Other Factors

Apart from above factors, anammox is inhibited by toxic organic matter (phenols, alcohol, aldehydes, antibiotics), salinity, toxic and heavy metals (copper, zinc, lead, mercury, nickel, cadmium, chromium), phosphate and sulphides (Jin et al. 2012).

3 Summary of Studies on Enrichment of Anammox

Enrichment of anammox from different conventional sludges has been reported by researchers (Chamchoi and Nitisoravut 2007; Ding et al. 2017; Ganesan and Vadivelu 2019; Wang et al. 2018). A summary of studies on enrichment of anammox from different conventional sludges in SBR is presented in Table below.

Summary of studies on enrichment of anammox:

S. No.	Seeding sludge	Operating conditions and system	Factor studied for enrichment	Anammox activity start	Observations	References
1	Activated sludge	SBR Vol 1.3 L; T 34–35 °C; HRT 24 h; pH 7.5	–	3 months	Nitrite and ammonium removal 70–95%	Araujo et al. (2011)
2	Sludge of UASB, activated sludge process and anaerobic sludge digestor	3 SBR each Vol 7 L; pH 7.7–8.4; MLSS 1500 mg/L; T 33–34 °C	–	120 d	Nitrite removal 100%, ammonia removal 80%	Chamchoi and Nitisoravut (2007)
3	Activated sludge	Vol 1 L; pH 7.8–8; T 35 °C; HRT 0.62 d	–	100 d	Nitrogen removal 82%	Dapena-Mora et al. (2004)
4	Aerobic sludge, denitrification sludge and anaerobic sludge	SBR Vol 5 L; H/D 4:1; pH 7.5–8; T 34 ± 1 °C; HRT 2 d; DO <0.2 ppm	–	Aerobic sludge 240 d, denitrification 150 d and anaerobic failed	N removal in aerobic sludge 50–60%, 80% in denitrification sludge	Ding et al. (2017)
5	Combined anaerobic and nitrification sludge	SBR Vol 2 L; pH 7.3 ± 0.1; T 35 °C; MLVSS 700 ± 20 mg/L	Effect of hydrazine on startup time	49 d	Ammonium removal 88% and nitrite removal 87%	Ganesan and Vadivelu (2019)
6	Activated anaerobic sludge	Vol 1.2 L; pH 7.58; T 30 ± 1 °C; HRT 0.6–0.81 h	–	57 d	Nitrogen removal >90%	Jin et al. (2008)
7	Methanogenic anaerobic granular sludge	Vol 7 L; pH 7.58.3; T 35 °C; HRT; 30 d	Effect of inorganic carbon	90 d	Ammonium removal 83.6%; nitrite removal 100%	Liao et al. (2008)

(continued)

S. No.	Seeding sludge	Operating conditions and system	Factor studied for enrichment	Anammox activity start	Observations	References
8	Mixed activated sludge from landfill leachate treatment plant, urban wastewater treatment plant and leachate treatment of urban solid wastes	Vol 20 L; pH 7.58, 100 rpm; HRT 3.6 d; T 362 ± 0.3 °C	–	105 d	Ammonium removal 79%; nitrite removal 96%	López et al. (2008)
9	Anoxic activated sludge	Vol SBR1 8 L and SBR2 4 L; 7.2 ± 0.2; T 28 ± 3 °C; VSS 2210 mg/L	Effect of DO	90 d	Total nitrogen removal in SBR 1 and 2 85.36% and 89.43% respectively	Saricheewin et al. (2010)
10	Activated sludges from a landfill leachate treatment plant (S1), municipal sewage treatment plant (S2) and monosodium glutamate (MSG) wastewater treatment plant (S3)	3 SBR (R1, R2, R3) Vol 2.5 L each; pH 7.5–8; T 30 ± 1 °C; HRT 3 d; SRT 100 d	–	360 d	Ammonium removal 69.2%, 70.5% and 74.1%, and nitrite removal efficiencies of 70.6%, 72.4% and 77.6% in R1, R2 and R3 respectively	Shen et al. (2012)
11	Anaerobic granular sludge	Vol 10 L; pH 7.57.8; T 30 ± 1 °C; DO < 0.2 mg/L	–	67 d	Total nitrogen removal 90%	Sobooka et al. (2017)
12	Aerobic granular sludge	Vol 3 L; pH 8 ± 0.3; T 31 ± 1 °C; DO < 1 mg/L; HRT 2 d; VSS 0.3 g/L	–	147 d	Ammonium removal 83.7%; nitrite removal 92.5%	Tao et al. (2012)

(continued)

(continued)

S. No.	Seeding sludge	Operating conditions and system	Factor studied for enrichment	Anammox activity start	Observations	References
13	Activated sludge	SBR Vol 1 L; T 3536 °C; pH 7.8; HRT 1 d	–	105 d	N conversion of 0.6 kgNm^{-3}d^{-1}	Third et al. (2005)
14	Mixture of aerobic and anaerobic sludge	Vol 4 L; pH 8; T 37 °C; DO 0.1–0.5 mg/L; HRT 5 d	–	95 d	Total nitrogen removal 85%	Verma et al. (2021)
15	Sludge of labscale membrane bioreactor (MBR) (A), labscale SBR (B), and wastewater treatment plant (C)	pH 7–8; HRT 2 d; T 35 °C	–	95 d	Only sludge a showed anammox activity; TN removal 99.68%; nitrite removal 99.94%	Wang et al. (2011)
16	Mixture of aerobic activated sludge and nitrifying activated sludge	Vol 4.8 L; pH 7.88.2; T 35 °C; HRT 2 d; 100 rpm; DO < 0.05 mg/L	–	101 d	Nitrogen removal rate of ammonium and nitrite were 130.3 and 161.7 mg N^{-1}L^{-1}d^{-1} respectively	Wang et al. (2012)
17	Return sludge of anaerobic-anoxic–oxic (A2/O) process	Vol 4 L; pH 7.7 ± 0.3; T 25 ± 2 °C; 50 rpm; SRT 2030 d	–	107 d	Total nitrogen removal rate of 32.46 mg/(Lh)	Yao et al. (2020)
18	Endogenous denitritation sludge	Vol 2.5 L; T 35 ± 1 °C; DO < 0.5 mg/L	–	93 d	Ammonium removal 75.4%; nitrite removal 55.7%,	Yuan et al. (2010)

4   Conclusions

Enrichment of anammox is very difficult as it cannot be inoculated with conventional techniques like petri dish. Moreover, enrichment of anammox and its growth is a very slow process. Successful enrichment and growth are possible by controlling physiological conditions favorable for anammox growth with reactor configuration supporting biomass retention. However, after enrichment physiological conditions may be changed slowly to allow the sludge to get acclimized without having adverse effect on overall growth of anammox bacteria. DO (Dissolved Oxygen) is one of the critical parameters during startup period and should be controlled below 0.2 ppm to prevent DO inhibition and growth of other microorganisms. Enrichment of anammox requires complete control on operating conditions and environment.

Conflict of Interest Statement   The authors declare that there is no conflict of interest.

References

Aktan CK, Yapsakli K, Bulent Mertoglu B (2012) Inhibitory effects of free ammonia on anammox bacteria. Biodegradation 23(5):751–762

Araujo JC, Campos AC, Correa MM, Silva EC, Matté MH, Matté GR, Von Sperling M, Chernicharo CAL (2011) Anammox bacteria enrichment and characterization from municipal activated sludge. Water Sci Technol 64(7):1428–1434

Chamchoi N, Nitisoravut S (2007) Anammox enrichment from different conventional sludges. Chemosphere 66(11):2225–2232

Cho S, Kambey C, Nguyen VK (2020) Performance of anammox processes for wastewater treatment: a critical review on effects of operational conditions and environmental stresses. Water 12(1):20

Connan R, Dabert P, Khalil H, Bridoux G, Béline F, Magrí A (2016) Batch enrichment of anammox bacteria and study of the underlying microbial community dynamics. Chem Eng J 297:217–228

Dapena-Mora A, Van Hulle SWH, Campos JL, Méndez R, Vanrolleghem PA, Jette M (2004) Enrichment of anammox biomass from municipal activated sludge: experimental and modelling results. Chem Technol Biotechnol 79(12):1421–1428

Ding Z, Ventorino V, Panico A, Pepe O, van Hullebusch ED, Pirozzi F, Bourven I, Guibaud G, Esposito G (2017) Enrichment of anammox biomass from different seeding sludge: process strategy and microbial diversity. Water Air Soil Pollut 228(1):1–13

Fernández JD, Fajardo C, Campos JL, Mosquera-Corral A, Méndez R (2012) Short- and long-term effects of ammonium and nitrite on the anammox process. J Environ Manage 95:S170–S174

Ganesan S, Vadivelu VM (2019) Effect of external hydrazine addition on anammox reactor start-up time. Chemosphere 223:668–674

Jetten MSM, Wagner M, Fuerst J, Van Loosdrecht M, Kuenen G, Strous M (2001) Microbiology and application of the anaerobic ammonium oxidation ('anammox') process. Curr Opin Biotechnol 12(3):283–288

Jin RC, Zheng P, Hua AH, Mahmood Q, Hua BL, Jilani G (2008) Performance comparison of two anammox reactor: SBR and UBR. Chem Eng J 138(1–3):224–230

Jin RC, Yang GF, Yu JJ, Zheng P (2012) The inhibition of the Anammox process: a review. Chem Eng J 197:67–79

Jung JY, Kang SH, Chung YC, Ahn DH (2007) Factors affecting the activity of anammox bacteria during start up in the continuous culture reactor. Water Sci Technol 55(1–2):459–468

Li Q, Wang S, Zhang P, Yu J, Qiu C, Zheng J (2018) Influence of temperature on an anammox sequencing batch reactor (SBR) system under lower nitrogen load. Biores Technol 269:50–56

Liao D, Li X, Yang Q, Zeng G, Guo L, Yue X (2008) Effect of inorganic carbon on anaerobic ammonium oxidation enriched in sequencing batch reactor. J Environ Sci 20(8):940–944

Liu S, Yang F, Xue Y, Gong Z, Chen H, Wang T, Su Z (2008) Evaluation of oxygen adaptation and identification of functional bacteria composition for anammox consortium in non-woven biological rotating contactor. Biores Technol 99(17):8273–8279

López H, Puig S, Ganigu´e R, Ruscalleda M, Balaguer MD, Colprim J (2008) Start-up and enrichment of a granular anammox SBR to treat high nitrogen load wastewaters. Chem Technol Biotechnol Int Res Process Environ Clean Technol 83(3):233–241

Lotti T, van der Star WRL, Kleerebezem R, Lubello C, van Loosdrecht MCM (2012) The effect of nitrite inhibition on the anammox process. Water Res 46(8):2559–2569

Lotti T, Kleerebezem R, Abelleira J, Abbas B, van Loosdrecht MCM (2015) Faster through training: the anammox case. Water Res 81:261–268

Ma B, Wang S, Cao S, Miao Y, Jia F, Du R, Peng Y (2016) Biological nitrogen removal from sewage via anammox: recent advances. Biores Technol 200:981–990

Mulder A, van de Graaf AA, Robertson LA, Kuenen JG (1995) Anaerobic ammonium oxidation discovered in a denitrifying fluidized bed reactor. FEMS Microbiol Ecol 16(3):177–184

Saricheewin K, Sirivithayapakorn S, Noophan PL, Wantawin C, Techkarnjanaruk S, MunakataMar J (2010) Nitrogen removal of anammox cultures under different enrichment conditions. J Environ Sci Health Part A 45(14):1832–1838

Shen LD, Hu AH, Jin RC, Cheng DQ, Zheng P, Xu XY (2012) Enrichment of anammox bacteria from three sludge sources for the startup of monosodium glutamate industrial wastewater treatment system. J Hazard Mater 199–200:193–199

Sobotka D, Tuszynska A, Kowal P, Ciesielski S, Czerwionka K, Makinia J (2017) Long-term performance and microbial characteristics of the anammox-enriched granular sludge cultivated in a bench-scale sequencing batch reactor. Biochem Eng J 120:125–135

Strous M, van Gerven E, Kuenen JG, Jetten MSM (1997a) Effects of aerobic and microaerobic conditions on anaerobic ammonium-oxidating (anammox) sludge. Appl Environ Microbiol 63(6):2446–2448

Strous M, van Gerven E, Zheng P, Kuenen JG, Jetten MSM (1997b) Ammonium removal from concentrated waste streams with the anaerobic ammonium oxidation (anammox) process in different reactor configurations. Water Resour 31(8):1955–1962

Strous M, Heijnen JJ, Kuenen JG, Jetten MSM (1998) The sequencing batch reactor as a powerful tool for the study of slowly growing anaerobic ammonium-oxidizing microorganisms. Appl Microbiol Biotechnol 50(5):589–596

Strous M, Kuenen JG, Jetten MSM (1999) Key physiology of anaerobic ammonium oxidation. Appl Environ Microbiol 65(7):3248–3250

Tang C, Zheng P, Mahmood Q, Che J (2009) Start-up and inhibition analysis of the anammox process seeded with anaerobic granular sludge. J Ind Microbiol Biotechnol 36(8):1093–1100

Tao Y, Gao DW, Fu Y, Wu WM, Ren NQ (2012) Impact of reactor configuration on anammox process startup: MBR versus SBR. Biores Technol 104:73–80

Third KA, Paxman JM, Schmid M, Strous M, Jetten MSM, Cord-Ruwisch R (2005) Enrichment of anammox from activated sludge and its application in the CANON process. Microbial Ecol 49(2):236–244

Van de Graaf AA, de Bruijn P, Robertson LA, Jetten MSM, Kuenen JG (1996) Autotrophic growth of anaerobic ammonium oxidizing micro-organisms in fluidized bed reactor. Microbiology 142(8):2187–2196

Verma S, Daverey A, Lin JG (2021) Successful start-up of anammox process from activated sludge and anaerobic sludge in a sequencing batch reactor using an unconventional strategy. Int Biodeterior Biodegradation 156:105132

Wang T, Zhang H, Gao D, Yang F, Yang S, Jiang T, Zhang G (2011) Enrichment of anammox bacteria in seed sludges from different wastewater treating processes and start-up of anammox process. Desalination 271(1–3):193–198

Wang T, Zhang H, Gao D, Yang F, Zhang G (2012) Comparison between MBR and SBR on anammox startup process from the conventional activated sludge. Biores Technol 122:78–82

Wang G, Zhang D, Xu Y, Hua Y, Dai X (2018) Comparing two start up strategies and the effect of temperature fluctuations on the performance of mainstream anammox reactors. Chemosphere 209:632–639

Yao R, Yuan Q, Wan K (2020) Effective inhibition prevention strategy for the enrichment of anammox bacteria with low concentrations of substrates at 25 °C. J Water Process Eng 37:101514

Yuan Y, Huang Y, Deng H, Li Y, Pan Y (2010) Research on enrichment for anammox bacteria inoculated via enhanced endogenous denitrification. In: Life science modelling and intelligent computing, vol 6330, pp 700–707. Springer, Berlin, Heidelberg

Zhu G, Peng Y, Li B, Guo J, Yang Q, Wang S (2008) Biological removal of nitrogen from wastewater. Rev Environ Contam Toxicol 192:159–195

Overview of Gel Casted Fused Silica Ceramics

Rakesh Kanakam, P. Subhash Chandra Bose, G. Raghavendra, S. Ojha, G. Dheeraj, B. Anjireddy, B. Aswani kumar, and Harsha vardhan

Abstract The current review mainly emphasizes about the importance of water, low cost water filtration applications and fabrication technique. Pressure driven ceramic membranes are widely accepted for water purification/filtration applications. These membranes are processed using conventional techniques such as slip casting, dip coating and pressure casting, however they have processing difficulties for complex shapes. As a result, gel casting process has received significant attention in the scientific community for the fabrication of ceramic membrane. Gel casting process has an advantage to fabricate complex shapes, exhibiting homogeneous microstructure and better strength to weight ratio compared to the other conventional processes. Gel casting processing is one of the forming techniques developed to address the constraints of prolonged binder burnout, geometry and range of size and non-uniform density issues associated with traditional complex forms. In lieu of this, the current paper reviews the gel casting processed silica members and their applications for the purification/filtration applications.

Keywords Ceramic membranes · Water filtration · Fused silica

R. Kanakam · P. Subhash Chandra Bose · G. Raghavendra (✉) · G. Dheeraj
Department of Mechanical Engineering, NIT, Warangal, Telangana, India
e-mail: raghavendra.gujjala@nitw.ac.in

S. Ojha
Department of Mechanical Engineering, KITS, Warangal, Telangana 506004, India

B. Anjireddy
Chemical Engineering, Dr. B R Ambedkar NIT, Jalandhar, Punjab 144011, India

B. Aswani kumar
Mechanical/Biomedical Engineering, Munster Technological University, cork, Ireland

H. vardhan
Mechanical Engineering, PVKK Institute of Technology, Ananthapuramu, Andhra Pradesh, India

1   Introduction

In 2010, the General Assembly of the United Nations officially declared the human right to water and sanitation. Water extensively affects all parts of human existence including yet not restricted to health, food, energy, and economy. It is assessed that 10–20 million individuals pass on consistently because of waterborne and nonfatal disease causes demise of in excess of 200 million individuals consistently (www.Prb.org). In the current scenario ceaselessly rising human population growth has led to the demand for clean water. Currently available conventional resources such as ground water, impoundment, brackish water etc. are not sufficient to fulfil human requirements. Consequently, various methods have been adopted to reuse the waste water generated from various chemical treatment. Some common methods such as sedimentation and filtration (membranes, media filtration), coagulation, pH adjustments, addition of anti-scalants and acids are used for waste water treatment (El-Ghonemy 2012).

Membranes are classified as organic and inorganic; wherein organic membranes are generally used for water treatment which contains mild pollutants. These membranes are difficult to process with a porosity amenable for filtration applications. Albeit, various materials are also in use for the filtration process which are produced from poly-sulphone, polyamide or cellulose but these materials are not sustain in high pollutant concentrations. Subsequently, the application of ceramic membranes is vast, in particular for the food, pharmaceutical, chemical and petro-chemical sectors, in precipitation, pickling and degreasing, drinks (in particular wines and brews) and mining processes, and in metal separation (Hakami et al. 2020). In recent years, ceramic membranes received significant attention among the mostly available materials, specifically silica or sand one of the most common ceramic material which is most preferred for purification of water. Among them, the fused-silica sintered at high temperature is a preferred ceramic material which is comprises of fused-silica powder or sand.

Due to the significant physical properties of fused-silica such as low coefficient of thermal expansion, good thermal stability and high specific strength, it could be applicable for medium–high temperature applications. Such type of materials is suitable for the fabrication of refractories and structural materials. The gel-casting (Porozova 2002) and slip-casting (Wall et al. 2000) are few of the most widely used methods for preparation of fused-silica materials. Different types of fabrication techniques with their advantages and drawbacks are listed Table 1. Ceramic components are traditionally fabricated by using forming methods such as hot pressure, slipping, cold isostatic pressing, band casting, frozen casting, pressure slip casting, pressure slip casting, aqueous injection moulding, hydrolysis assisted Solidification and lately gel casting. Various fabrication techniques and their advantages and drawbacks are listed Table 2.

As discussed, different types of conventional methods, here is a detailed comparison tabulated on slip casting, injection molding, pressure casting, gel casting and their process parameters for the fabrication.

Table 1 Different wet fabrication techniques benefits and drawbacks (Rak 2001)

S. No.	Fabrication techniques	Benefits	Drawbacks
1	Gelcasting (polymer)	Great green strength and established process	Toxicity problems, costly reagents
2	Gelcasting (natural additives)	Safe eco-friendly, water based technique	Low green strength
3	Freeze casting	Water based method, unique sublimation technique	Low green strength
4	Aqueous injectionmoulding	Fast, eco-friendly	Size limitation, high viscosity
5	Centrifugal slip casting	One step process for filters	Additional equipment required
6	Direct coagulation casting	No size and wall thickness issues, high green density	Poor green strength, costly additives
7	Electrophoretic casting	Suitable for functionally graded composites and coatings	Sensitive to current parameters
8	Hydrolysis assisted solidification	Fast, high green density	Gaseous product formation, poor green strength
9	Pressure slip casting	Fast, eco-friendly	Drying, additional equipment needed
10	Temperature induced forming	Simple	Heat transfer, Gaseous product formation

Table 2 Comparisons of different ceramic forming techniques (Guo 2011)

Property	Gelcating	Slip casting	Injection molding	Pressure casting
Molding time	5–60 min	1–10 h	10–60 s	10 min–5 h
Strength (dried)	Very high	Less	–	Less
Mold materials	Metal, glass, polymer wax	Plaster	Metal	Porous plastic
Binder burnout	2–3 h	2–3 h	7 days	2–3 h
Maximum Part dimension	>1 m	>1 m	About 30 cm, 1 dimension must ≤1 cm	About 1 m
Molding defects	Minimum	Minimum	Significant	Minimum
War page during drying/binder-burnout	Minimum l	Minimum	Possibly be severe	Minimum
Thick/thin sections	Both are ok	Thick section requires more casting time	Issues with binder removal for thick section	Thick section requires more casting time

During early days, processing silica-based ceramics was done by slip casting followed by a little modification in the processing parameters. But this as an industrial advantage has lost its grasp due to the various pre and post processing of ceramic components, such as producing complex shapes and obtaining desired porosity. Hence, new class of forming techniques referred to as gel casting has been introduced by the scientific community. Gel casting process is found to most amenable method to fabricate membranes for water purifiers. These membranes require good porosity to eliminate various other waste from the water, this requirement takes the advantage of the gel casting process. Gel casting is one of the best manufacturing processes for high quality porous ceramic components, which can be used for various industry applications (Vandeperre et al. 2003; Tari 2003; Adolfsson 2006; Nangrejo and Edirisinghe 2002). Gel casting process is more suitable for synthesis of classic ceramics and polymer chemicals (Janney et al. 1998). It has been utilized to develop a wide range of ceramic systems for materials (Yi et al. 2002; Hu et al. 2008; Santacruz et al. 2009; Ramay and Zhang 2003). Moraes et al. have studied effect of biopolymers as a gelling agent using gel casting as fabrication method for silicon nitride foams fabrication (Moraes et al. 2021). It was also used in porous ceramic preparations (Tulliani et al. 2009; Park et al. 2002; Chen et al. 2007; Wang et al. 1999; Liu et al. 2001; Zhang et al. 2006). The Gel casting technology has been employed to generate porous silica ceramics with fine pores, high porosity and high strength. Gel casting does not require costly moulds, it simply uses modest amounts of organic binder; it uses water as a suspension medium, includes no significant removal of binder and may be utilized for both prototypes and small-scale production processes. The technology is at the industrial applicability threshold.

The advantages of Gel casting can be articulated:

- Reduced capital expenditure.
- Cost-effective mould material Possibility for mass-production deployment.
- Green strength.
- Excellent green machinery should be used.
- Extremely uniform qualities of material.
- Generic approach for both powder and metal powder.

2 Methodology

Gel casting was accepted as an intuitive forming technology that can fabricate large and complex structural components with a uniform microstructure when compared to the existing techniques. Gel casting sometimes referred to a similar with the slip casting technique because of their nature of fabricating complex shapes. It has become one of the high-quality, complex ceramic component manufacturing techniques, which greatly reduce the serious repercussions of machining, colloidal in shape. It has since developed into an attractive process for the production of near-net-shaped ceramic parts with defined threshold strength.

Gel casting process can be explained with the help of Fig. 1 which discourses the processing of silica to green component. Initially, the silica being thixotropic and monomer, adding water makes it polymer retaining thixotropic during grinding process. Grinding process is where exactly the ceramic slurry is prepared. A 24 h grinding with Fe balls at 1400 rpm is most preferable. Further catalyst is added to form the perfect gelation configuration at fixed temperature. The sol gel derived is poured into the die and casted for one hour at 180 °C. The wet cast sample is dried at room temperature until cracks or any voids present in the cast sample is released. The binder burnout process is than carried out to remove the polymers from the as cast ceramic sample. The voids created due to the burning of polymers produces voids in ceramic sample, as a result, further sintering is done at 1200–2100 °C at various intervals for 24 h, this process is also referred as densification and the sample is called green sample. The same process is referred in the flow chart mentioned in Fig. 2.

During the 1990s at Oak Ridge National Laboratory (ORL), United States, Gelcasting was first developed for hard metals later adopted this method for ceramics (Omatete et al. 1997).

According to author, procedure adopted was very simple and fits for most of the ceramic materials. Slurry-based techniques are thought to be a good way to fill moulds and get high-green-strength pieces, which are then sintered. It is critical to characterize ceramic materials and add additives to a homogeneous ceramic slurry in order to achieve this goal. It's difficult to get optimal properties when ceramic materials, dispersants, monomers, and other additives don't have the right features. The goal of the experiment was to look at several SiO_2 ceramic suspension systems and
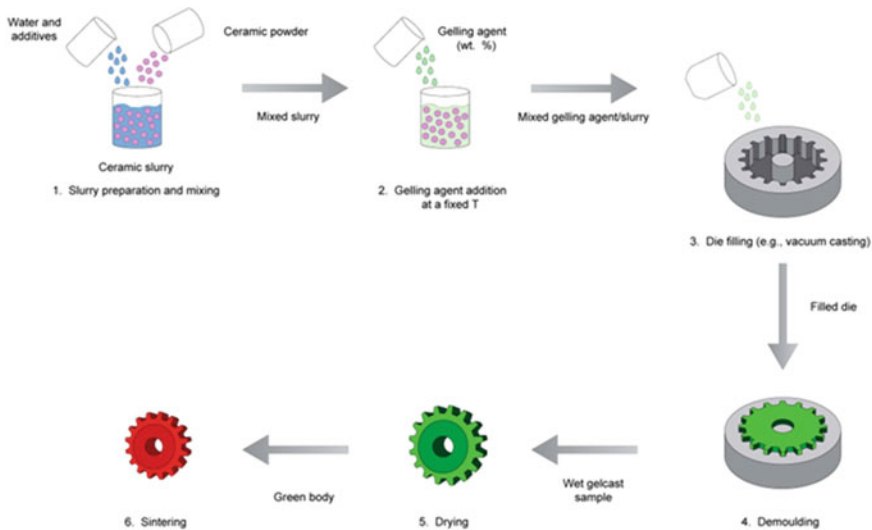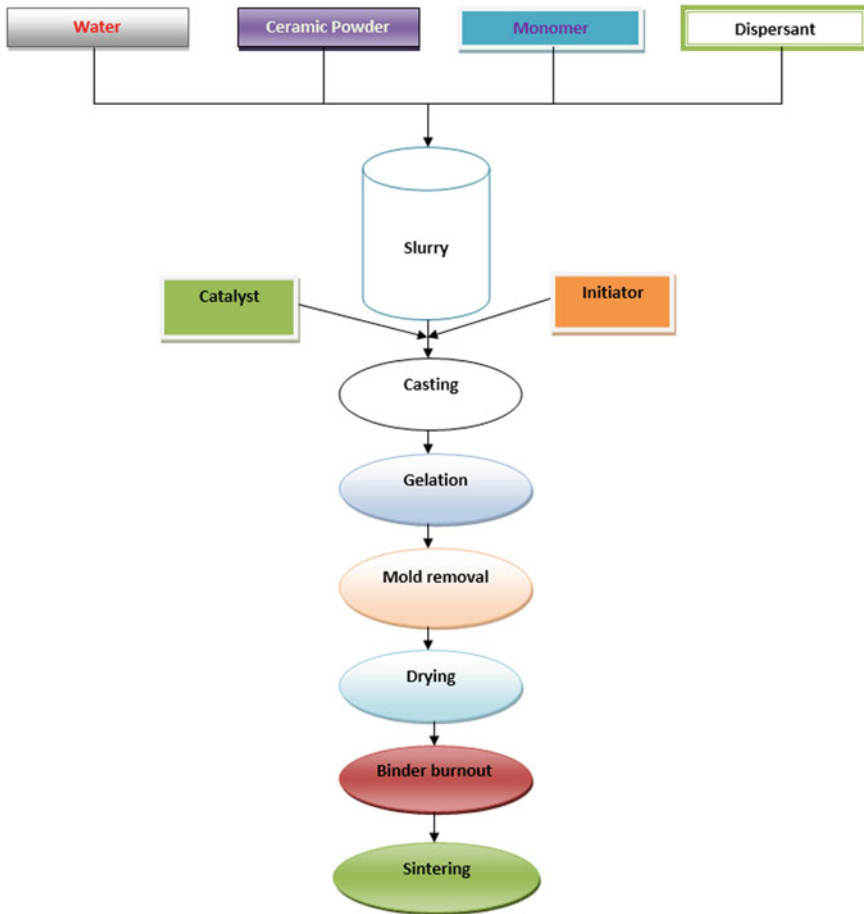

Fig. 1 Schematic diagram of the gel casting process (Omatete et al. 1997)

Fig. 2 The gel casting process flow chart

find the best composition for making near net form ceramic components. Methacrylamide (MAM) and N, N'-Methylenebisacrylamide (MBAM) were mixed in distilled water with a dispersant to make a premix solution. In order to maintain the optimum solid loading of the suspensions, ceramic powders and additives were added to the premix solution. The suspensions were agitated in a magnetic stirrer to break down agglomerates and obtain high consistency.

The pH was adjusted with hydrochloric acid and ammonia, and the results were monitored with a pH meter. The resulting suspension was deaired for 5–10 min with a desiccator linked to a vacuum pump, and then an initiator (10 wt% aqueous solution of ammonium per-sulfate, APS) and a catalyst (Tetramethylethylenediamine, TEMED) were added. The suspension was immediately cast into a nonporous mould and cured in an oven at a regulated humidity. The samples were binder-burned and sintered in

Fig. 3 SEM image of the fused silica
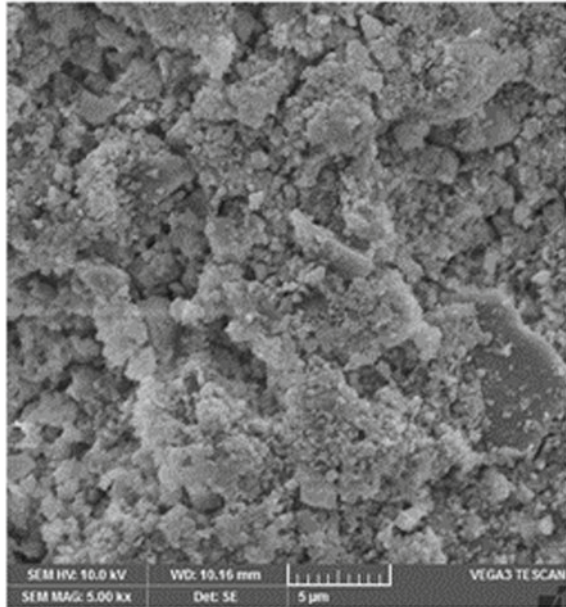
an argon environment, then naturally cooled in a High Temperature Muffle furnace (Punugupati et al. 2020a; Wan et al. 2014a). The flow chart of the process in Fig. 2. Explains the steps involved which were described above. SEM micrograph in Fig. 3 (Punugupati et al. 2020b) of the fused silica ceramic is displayed indicating the uniform porosity is achieved when fabricated using gel casting method.

3 Results and Discussions

Kishore et al. (2016) have fabricated Fused silica ceramics with low warpage, low shrinkage and high flexural strength, by using Gelcasting method. They have studied the effect of monomer content ratio on gel casting process and obtained good results. Wan et al. (2014a) manufactured fused silica ceramics through Gelcasting technique with minimum toxic acrylamide and toxicity 2-hydroxyethyl methacrylate system. In this article, the influence of sintering temperature on thermal shock resistance, mechanical properties, microstructure, and dielectric properties were reported. Yu et al. (2010) have studied the fabrication of porous Si_3N_4 ceramics using gel casting method. They noted that increased porosity with the increasing monomer content. It is noticed that the adjustment in the monomers ratio, the shrinkage and warpage of the green body is enhanced efficiently. Porous silica powders produced through Gelcasting with N, N-dimethyl acrylamide (DMAA) as gelling agent and multigrade poles as starting material have been examined by Yin et al. (2020). Results indicated

a very strong correlation between fine grain and rough grain, solid load and sintering temperature with the microstructure and characteristics of fused silica ceramics.

Wan et al. (2014b), were fabricated the silica-based ceramics with minimum porosity and low dielectric constant at higher strength through Gelcasting techniques with a minimum toxicity N'N-dimethyl acrylamide (DMAA) gel system. The influence on the rheological characteristics of slurries, sintered and green ceramics were examined. The influence of solid loads in aqueous Gelcasting of colloidal silica-fused ceramics was examined in Manivannan et al. by filling nano-silica particles in the interstitial position of the Green Body, the physical and mechanical properties of fused silica were improved (Manivannan et al. 2013). Wan et al. (2014a) have studied the effect of sintering temperature on green samples fabricated by gel casting method. They have used low toxicity DMAA gel system instead of AM. They have noticed that fused silica has critical effect on the silica ceramic properties. Densification has been improved to certain level and flexural strength was increased. Wan et al. (2013) studied the effect of water soluble and non-toxic monomer NN-dimethylacrylamide (DMAA) as a gelling agent in Gelcasting of fused silica. The selected dispersant is acrylic acid 2-acrylamide 2-methypropane sulphonic acid co polymer (AAAMPS) which is used to increase the maximum vol% of solid loading as well as minimum viscous slurries.

In the beginning stages of gel casting, the method was not highlighted from a manufacturing or industrial point of view due to the presence of organic toxic additives like acrylamide (AM). Later, it was highlighted because of the design of low organic toxic additive like (2-hydroxyethyl methacrylate (HEMA), egg white (He et al. 2011), glutinous rice flour (Nayak and Bera 2012), curdlan (Wan et al. 2014c), and ISOBAM, because of which there have been sudden and massive transformation from laboratory level production to industrial level applications (Yao et al. 2018; Sun et al. 2014).

4 Conclusions

This review article mainly focused on the fused silica based ceramics through gel casting fabrication technique even though traditional techniques are available because of its advantages it poses such as lesser equipment and simple procedures. Gel casting method was successfully implemented on ceramic based membranes/components using different solid loading, monomers, gelling agents and sintering temperatures. Silica is the most widely used ceramic for water filtration applications from olden days because of its advantages. This article also deals with optimization of properties of ceramics for the commercial applications and achieved better results compared to traditional methods. Microstructural studies conferred the network of uniform porosity indicating the feasibility of the gel casting technique. Therefore, the gel casted fused silica ceramics are preferred and promising for the water filtration applications from the various literature studies.

References

Adolfsson E (2006) Gelcasting of zirconia using agarose. J Am Ceram Soc 89(6):1897–1902

Chen R, Huang Y, Wang CA, Qi J (2007) Ceramics with ultra-low density fabricated by gelcasting: an unconventional view. J Am Ceram Soc 90(11):3424–3429

de Moraes EG, Innocentini MDM, Biasetto L, de Oliveira AN, Hotza D, Colombo P (2021) Gel casting of silicon nitride foams using biopolymers as gelling agents. Open Ceram 8:100183

El-Ghonemy AK (2012) A small-scale brackish water reverse-osmosis desalination system used in northern Saudi Arabia: a case study. Renew Sustain Energy Rev 16(7):4597–4605

Guo X (2011) Gel casting of high strength ceramics

Hakami MW, Alkhudhiri A, Al-Batty S, Zacharof MP, Maddy J, Hilal N (2020) Ceramic microfiltration membranes in wastewater treatment: filtration behavior, fouling and prevention. Membranes 10(9):248

He X, Su B, Zhou X, Yang J, Zhao B, Wang X, Qiu H (2011) Gelcasting of alumina ceramic using an egg white protein binder system. Ceramics-Silikáty 55(1):1–7

Hu Y, Wang Z, Lu J (2008) Study on the gel casting of fused silica glass. J Non-Cryst Solids 354(12–13):1285–1289

Janney MA, Omatete OO, Walls CA, Nunn SD, Ogle RJ, Westmoreland G (1998) Development of low-toxicity gelcasting systems. J Am Ceram Soc 81(3):581–591

Kandi KK, Punugupati G, Pal SK, Rao Chilakalapalli SP (2016) Effect of monomers content and their ratio on gelcasting of fused silica ceramics. Trans Indian Ceram Soc 75(3):185–188

Liu YF, Liu XQ, Wei H, Meng GY (2001) Porous mullite ceramics from national clay produced by gelcasting. Ceram Int 27(1):1–7

Manivannan R, Kumar A, Subrahmanyam C (2013) Aqueous gelcasting of fused silica using colloidal silica binder. J Am Ceram Soc 96(8):2432–2436

Nangrejo MR, Edirisinghe MJ (2002) Porosity and strength of silicon carbide foams prepared using pre-ceramic polymers. J Porous Mater 9(2):131–140

Nayak JP, Bera J (2012) Bioactive porous silica ceramics prepared using rice husk ash by gelcasting method. Adv Mater Res 548:12–16

Omatete OO, Janney MA, Nunn SD (1997) Gelcasting: from laboratory development toward industrial production. J Eur Ceram Soc 17(2–3):407–413

Park JK, Lee JS, Lee SI (2002) Preparation of porous cordierite using gel casting method and its feasibility as a filter. J Porous Mater 9(3):203–210

Porozova SE (2002) Optimized composition of the slip for preparing high-porosity permeable quartz ceramics. Refract Ind Ceram 43(7):269–272

Punugupati G, Bose PSC, Raghavendra G, Rao CSP (2020a) Response surface modeling and optimization of gelcast fused silica micro hybrid ceramic composites. SILICON 12(7):1513–1528

Rak ZS (2001) Advanced forming techniques in ceramics. Klei/Glas/Keramiek 22

Ramay HR, Zhang M (2003) Preparation of porous hydroxyapatite scaffolds by combination of the gel-casting and polymer sponge methods. Biomaterials 24(19):3293–3302

Santacruz I, Nieto MI, Binner J, Moreno R (2009) Gel casting of aqueous suspensions of BaTiO$_3$ nanopowders. Ceram Int 35(1):321–326

Sun Y, Shimai S, Peng X, Dong M, Kamiya H, Wang S (2014) A method for gelcasting high-strength alumina ceramics with low shrinkage. J Mater Res 29(2):247–251

Tari G (2003) Gelcasting ceramics: a review. Am Ceram Soc Bull 82(4):43–46

Tulliani JM, Bartuli C, Bemporad E, Naglieri V, Sebastiani M (2009) Preparation and mechanical characterization of dense and porous zirconia produced by gel casting with gelatin as a gelling agent. Ceram Int 35(6):2481–2491

Vandeperre LJ, De Wilde AM, Luyten J (2003) Gelatin gelcasting of ceramic components. J Mater Process Technol 135(2–3):312–316

Wall CA, Kirby GH, Janney MA, Omatete OO et al (2000) Gel-casting methods. US Patent US6066279

Wan W, Yang J, Zeng J, Qiu T (2013) Gelcasting of fused silica glass using a low-toxicity monomer DMAA. J Non-Cryst Solids 379:229–234

Wan W, Huang CE, Yang J, Zeng J, Qiu T (2014a) Effect of sintering temperature on the properties of fused silica ceramics prepared by gelcasting. J Electron Mater 43(7):2566–2572

Wan W, Yang J, Zeng J, Yao L, Qiu T (2014b) Effect of solid loading on gelcasting of silica ceramics using DMAA. Ceram Int 40(1):1735–1740

Wan W, Huang CE, Yang J, Qiu T (2014c) Study on gelcasting of fused silica glass using glutinous rice flour as binder. Int J Appl Glas Sci 5(4):401–409

Wang HT, Liu XQ, Zheng H, Zheng WJ, Meng GY (1999) Gelcasting of La0. 6Sr0. 4Co0. 8Fe0. 2O3-δ from oxide and carbonate powders. Ceram Int 25(2):177–181

www.Prb.org. Available online: https://www.prb.org/Population-trends-and-challenges-in-the-middle-east-and-north-Africa (2020)

Yao Q, Zhang L, Jiang Z, Huang G, Zhou T, Ben Y, Wang Y (2018) Isobam assisted slurry optimization and gelcasting of transparent YAG ceramics. Ceram Int 44(2):1699–1704

Yi ZZ, Xie ZP, Huang Y, Ma JT, Cheng YB (2002) Study on gelcasting and properties of recrystallized silicon carbide. Ceram Int 28(4):369–376

Yin S, Guo L, Pan L, Yan S, Qiao H, Zhang S, Jinqiong T, Huihua M, Qiu T, Wan W, Yang J (2020) Porous fused silica ceramics prepared by gelcasting using multi-grade fused silica powders. J Alloy Compd 819:152982

Yu J, Wang H, Zhang J, Zhang D, Yan Y (2010) Gelcasting preparation of porous silicon nitride ceramics by adjusting the content of monomers. J Sol-Gel Sci Technol 53(3):515–523

Zhang FZ, Kato T, Fuji M, Takahashi M (2006) Gelcasting fabrication of porous ceramics using a continuous process. J Eur Ceram Soc 26(4–5):667–671

Curing of Epoxy Resin by Using Commercial Amine/hydrazine and Its Effect on Ultra Violet Spectrum

Prince Ranpara and **Pravin Narayan Bhalerao**

Abstract Modified Epoxy resin found applicable in various application. Cured epoxy resin material has been prepared by thermal treatment of epoxy resin and the aromatic amine/aromatic hydrazine at high temperature in hot air oven. The characterization was performed on the basis of FTIR and UV analysis. Cured epoxy resin was found high stability towards organic solvents, strong acids (Con. HCl and HNO$_3$), and basic (NaOH) solution. Commercially available curing agent, solvent and simple high temperature epoxy curing is key features of our method. Very Few reports on epoxy curing with hydrazine functional group found in literature. In addition, the curing performed on the glass Petri plate and epoxy resin coating on the glass Petri dish will be observed. Epoxy curing with various solvents at different temperature with aromatic amine/hydrazine studied. Effect of UV–Visible study on curing of epoxy resin studied and compared.

Keywords Aromatic amine · Epoxy resin · Thermal treatment

1 Introduction

Epoxy resin act as excellent properties and thus epoxy resin and cured epoxy resin are applicable to various areas and there are various epoxy hardeners known for epoxy opening (Yu et al. 2020; Strzelec 2007; Chen et al. 2017). Some applications related to our coating work are cited. Krzysztof Strzelec reported the polythiourethene curing agent, and cured epoxy resin found improvement in properties like scratchresistance, pencil hardness, flexibility, adhesion and chemical resistance. Strzelec (2007) Organic coating is important to prevent corrosion, and also found anticorrosion in engineering applications. Chen et al. (2017) Epoxy resin composite have wide range

P. N. Bhalerao
Department of Chemistry, Marwadi University Gauridhad, Rajkot 360003, India

P. Ranpara (✉) · P. N. Bhalerao
Department of Chemical Engineering, Marwadi University Rajkot, Rajkot 360003, India
e-mail: prince.ranpara1111@gmail.com

of application in various area aerospace civil and other, this is due excellent thermal stability, durable mechanical properties, good adhesion, low sinkage and good chemical resistance properties at variety of environmental condition (Maljaee et al. 2017). Amines are very common in curing of epoxy resins than other functional group like carboxylic acid, anhydride and alcohols. Biobased amines are more relevant and significant over other due to eco-friendly nature, recently, Stéphane Grelie and group disclosed new methylated divanillydiamine by using simple vanillin. Cured resin observed good thermal and mechanical properties (Savonnet et al. 2019).

Certain resin cure without high temperature term as cold curing resin, this type of epoxy resins is used for construction industry. Such cold cure epoxy resins are good mechanical properties and sustainable to different environmental conditions such as moisture, humidity and temperature (Maljaee et al. 2017). Tiziana Benelli and group reported eco-friendly cured epoxy resin using biobased amine L-tryptophan and aromatic heterocycles as reaction promotors. Bio-based resin was observed with high Tg (Stefano Merighi et al. 2021).

There are various applications for epoxy resin and cured epoxy is known in literature. Resin cross linked by curing agent or hardener and then use in coating application. It was reported that curing bisphenol A and epichlorohydrin cured at room temperature by using amines and polyamides and used in heavy coating for ships, oil rigs, storage tanks and water pipes (Oldring 2003).

Polythiourethane cured resin found very good chemical resistant, and very good in adhesion properties, of resin to metal surface compared to common epoxy resin. Presence of polar group on the curing agent led to improve properties of cured resin material (Chen et al. 2017).

Haichao Zhao reported poly (o-phenylenediamine) nano particles coating on epoxy resin. In this poly (o-phenylenediamine) nano particle was synthesized by oxidative polymerization o-phenylenediamine mono-hydrochloride salt with reacting ammonium persulfate by ultrasonication method. Epoxy curing was performed by using poly (o-phenylenediamine) nano particle in presence of amine hardener. Chen et al. (2017) Epoxy resin use in coating, colorant and in paint, P. Schlack (Oldring 2003) file patent on epoxy resin and prepare by condensation reaction of bisphenol A and epichlorohydrin, thus epoxy resin epoxy group at both end and several hydroxyl functional group.

Huang and Nei (2016) reported modified GGEAB resin with hydrazine functional group. Amino group present in hydrazine underwent epoxy ring opening on epoxy resin further removal of water molecule from primary amine and hydroxyl group give stable alkene resin. Properties of modified resin observe since cross linking of epoxy resin such properties cross linking density and plasticization effect. Patel (2008) reported epoxy curing by using aromatic hydrazine, synthesis of Arylhydrazino-bismaleimides (AHBM), curing for commercial epoxy resin. Author observe cured epoxy warrant good chemical resistant, mechanical propertied and low conductivity. Zhang and co-workers use platinum catalyzed hydrosiliation reaction of epoxy curing with halloysites to improve mechanical properties of hyperbranched epoxy resin (Zhang et al. 2013).

Our method for curing was on the basis of literature data, we have studied the functional groups responsible for epoxy curing is amine like aliphatic and aromatic amines. Most of that are diamines which lead to curing of epoxy resin which is due to cross linking structure. On the basis our interest to develop new commercially available aromatic diamine/hydrazine in the method of curing of epoxy resin, we though to use aromatic ortho-phenylenediamine and aromatic phenyl hydrazine.

2 Material and equipment's Used

Diglycidyl ether of bisphenol A (DGEBA) Epoxy resin (epoxy value of DGEBA, 5.46 eq/kg) was purchase from Chemdye corporation chemical supplier in INDIA Product code: EP0004, Ortho-phenylenediamine and phenyl hydrazine, purchase from Loba Chemie, MW 108.14, MW 198 respectively. Hot air Oven ISO 9001:2008 Patel scientific Instrument PVT. Petridish Borosilicate Glass-S-line.

3 Method for Curing of Epoxy Resin for Aromatic Diamine and Aromatic Hydrazine

Preparation procedure for cured epoxy system for both diamine and hydrazine derivatives is describe below.

Diglycidyl ether of bisphenol A (DGEBA) that is Epoxy resin (1 mL) was degassed by using nitrogen and dissolved in solvent acetone. Then various % of o-phenylenediamine was added to this at room temperature, the reaction mixture was spread on the petridish (Glass-dish) uniformly. The petridish was kept in pre heated hot air oven at temperature at 150 °C. Then after 5–10 min. the temperature rate rise to 30 s per degree (°C) and at the temperature 160 °C the cured epoxy resin was coated on the glass petri plate. The glass plate was taken out and the wash with water. Coated epoxy resin was difficult to remove from glass plate. Thus, the cured material was crush by using knife and the material taken as a particle for spectroscopic characterization (FTIR and UV). The coated petriplate subjected to heat at high temperature (up to 210 °C) to check thermal resistant of epoxy coating on petridish. In our observation, no degradation of the epoxy coating on glass petridish (Borosilicate glass) observed.

4 Result and Discussion

Opening of epoxy resin by sing aromatic amines are well known, (Yu et al. 2020; Strzelec 2007; Chen et al. 2017; Huang and Nie 2016; Patel 2008) here in our

method ortho-di substituted aromatic amine utilized for epoxy ring opening as well as cross linking of epoxy resin. Epoxy curing using o-phenylenediamine was performed at different temperature and different percentages, however our best result is for 0.250 mg ortho-phenylenediamine, 1 gm epoxy resin at temperature 160 °C for 5–10 min condition.

Chemical reaction scheme on resin material: Reaction with aromatic diamine: The epoxy resin heated with aromatic diamine, epoxy group present in epoxy resin underwent epoxy functional group opening and forms alcohols Fig. 1 (Scheme 1). This reaction was in acetone medium and under heat. Cured epoxy resin was found in the form of the coating on the surface of glass petri plate.

In above observation, the same experiment with different percentage for o-phenylenediamine at temperature 160 °C has been carried out the coating result are shown in Table 1.

In Table 1 various percentage of o-phenyldiamine shown, curing of epoxy resin was observed from 17 weight % of ortho-phenylenediamine, no epoxy curing observed at 9, 11 and 13% at high temperature (200 °C).In our experiments other organic solvent also we use for curing of epoxy resin, in that we use acetonitrile as solvent but unfortunately no curing of epoxy resin was observed.
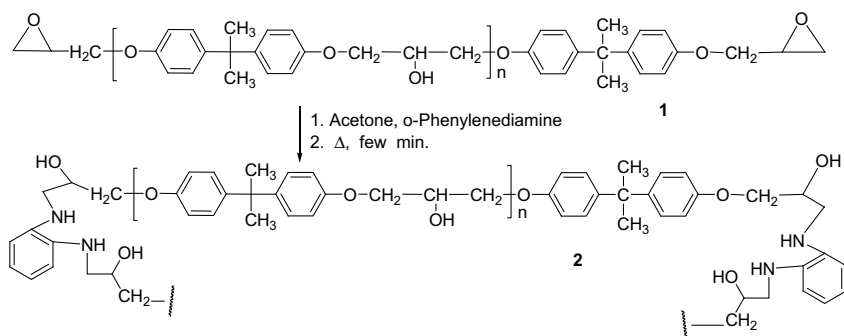
Scheme 1: Possible orientation of epoxy opening by using the o-phenelenediamine
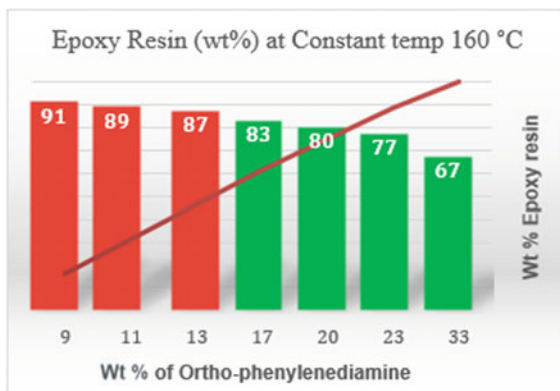
Fig. 1 Reaction of ortho-phenylenediamine with epoxy resin

Table 1 Different percentage of o-phenylenediamine and epoxy resin

S. No.	O-phenylenediamine (wt%)	Epoxy resin (wt%)	Temp. (°C)	Coating
1	9	91	160	No
2	11	89	160	No
3	13	87	160	No
4	17	83	160	Yes
5	20	80	160	Yes
6	23	77	160	Yes
7	33	67	160	Yes

Fig. 2 Graph showing % of ortho-phenylenediamine and epoxy resin

On the basis of above result we thought to use hydrazine functional group for epoxy curing because literature study shown that hydrazine R-NH-NH$_2$ can use as curing agent to improve properties of cured epoxy material. Very few authors reported hydrazine derivative as a curing agent for epoxy resin (Huang and Nie 2016; Patel 2008).

Commercially available material phenyl hydrazine we use for epoxy curing as applying above same method: 1 gm epoxy resin (liquid) and phenyl hydrazine (0.250 mg), and 5 mL acetone was taken in Petri plate (borosilicate) and the material was subjected to heat treatment (in oven) for 5 min. The proper curing on the petridish was not seen. Then increase curing time in 10 min and thus coating was observed. The petridish was wash with water and cured epoxy resin used for UV characterization.

Graphical representation with different wt% of epoxy resin and ortho-phenylenediamine shown in Fig. 2. Graph red lines indicate no curing on petridish, while green line indicate curing of epoxy resin with o-phenylenediamine on petridish.

The above epoxy curing method develop for aromatic diamine and aromatic hydrazine which is commercially available in market. Repeated same above-mentioned procedure for epoxy curing for hexamethylene diamine and aromatic secondary amine (diphenylamine) but unfortunately method was unsuccessful. There was no curing of epoxy resin on petridish with solvent at high temperature (200 °C). This may due to solubility problem of curing agent with solvent acetone.

5　FTIR and UV Study of Orthophenylene Diamine Epoxy Cured Material

On the basis of FTIR (Fig. 3) study for epoxy resin IR spectrum (Neat) shows peak at 3510 cm^{-1} and 918 cm^{-1} wavenumber peaks those peaks indicate presence of hydroxyl group and epoxy groups present in structure. Curing of epoxy resin
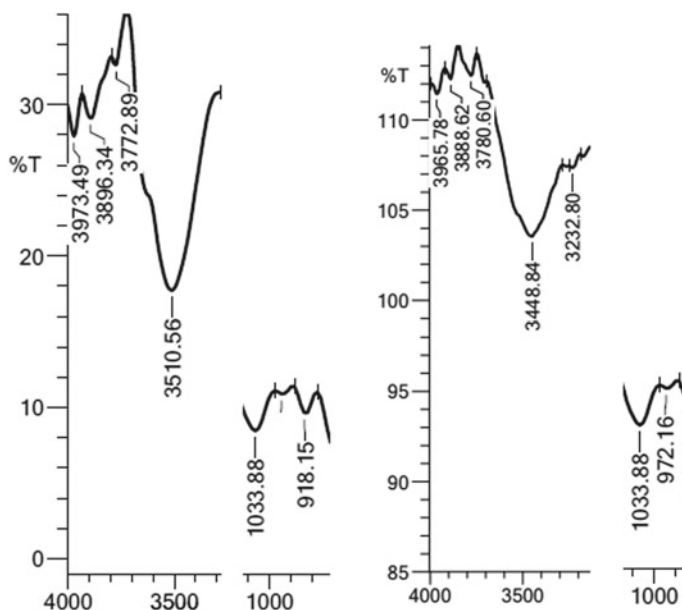
Fig. 3 Grpah for epoxy resin IR graph for cured epoxy resin

with ortho-phenylenediamine lead to opening of the epoxy groups and addition of aromatic amine group in the epoxy structure. It was confirmed on the basis of FTIR study of cured epoxy resin with o-phenylenediamine (FTIR, KBr) FTIR of the cured epoxy resin shows extra peak appearance at 3232 cm^{-1} wave number, which is from N–H secondary amine stretching vibration, cured epoxy resin also show peak at 3448 cm^{-1} due to primary hydroxy group, and there were no peaks at 918 cm^{-1} (peak due to epoxy group). On comparing the study of epoxy resin spectrum and cured (o-phenylene diamine) epoxy resin new peak appears at 3232 cm^{-1} and in cured epoxy resin no peak observed at 918 cm^{-1} for epoxy group.

On the basis of Ultra Violate-visible spectroscopy spectrum of o-phenylenediamine absorption show at two band respectively for n–π* and π–π* at λ_{max} 240 nm and 219 nm. UV of pure epoxy found to be λ_{max} 276 nm (π–π*) absorption. After curing of epoxy resin on petridish λ_{max} was found increase to λ_{max} 325 nm n–π*. It was observed that due to addition of phenylene group on the chain of the polymer lead to increase λ_{max} thus we have absorption due may due to π–π* transition in the o-phenylenediamine ring. Water absorption capacity of cured epoxy resin ofortho-phenylenediamine.

6 Water Absorption Capacity of Cured Epoxy Resin by Ortho-phenylenediamine

Water absorption capacity of cured epoxy resin was carried out using literature known procedure, (Hu et al. 2015) and by using following formula (Hu et al. 2015).

$$W_a\% = \frac{W_n \times W_d}{W_d} \times 100$$

Wa is water absorption in percentage, Wn weight of cured epoxy resin after water absorb, and Wd is initial dry weight of cured epoxy resin. To carry out above experiment the piece of cured epoxy resin, was deep in 20 mL of water in petridishat ambient temperature. There was no weight change in initial and final material weight for cured epoxy resin. So, no water absorption was shown by the cured epoxy material.

7 Chemical Resistant Test

To detect the corrosion resistance and chemical resistance the Con. HCl, Con HNO$_3$ and Con. H$_2$SO$_4$ and saturated NaOH, was added to epoxy resin coated petridish and kept for 24 h. Only in case of Con. H$_2$SO$_4$ coating degradationand removal was observed. In case of other HCl, HNO$_3$ and NaOH there was no effect on epoxy coating.

8 Conclusion

Commercially available orthophenylene diamine and phenyl hydrazine used for epoxy resin curing on petridish. In case of cured epoxy with orthophenylene diamine which lead to improvement of chemical resistance in acids (Con. HCl, Con. HNO$_3$), base (NaOH) and organic solvents for 24 h. The method is very quick for curing on petriplate and readily available material. Method may possible to as a corrosion protection, chemical protection covey.

References

Chen C, Qiu S, Qin S, Yan G, Zhao H, Wang L (2017) Anticorrosion performance of epoxy coating containing reactive poly (o-phenylenediamine) nanoparticles. Int J Electrochem Sci 12

Hu J, Shan J, Zhao J, Tong Z (2015) Water resistance and curing kinetics of epoxy resins with a novel curing agent of biphenyl-containing amine synthesized by one-pot method. Thermochim Acta 606:58–65

Huang J, Nie X (2016) A simple and novel method to design flexible and transparent epoxy resin with tunable mechanical properties. Polym Int 65:835–840

Maljaee H, Ghiassi B, Lourenço PB (2017) Effect of synergistic environmental conditions on thermal properties of a cold curing epoxy resin composites part B; (b) Frigione M, Lettieri M, Mecchi M (2006) Environmental effects on epoxy adhesives employed for restoration of historical buildings. J Mater Civ Eng 18(7):715–722

Oldring PKT (2003) Coating, colourant and paints. In: Encyclopedia of physical science and technology, pp 175–190

Patel SV (2008) Electric conductivity of cured aryhydrazino bismaleimide-epoxy resins. Int J Chem Sci 6(4):2194–2201

Savonnet E, Coz CL, Grau E, Grelier S, Defoort B, Cramail H (2019) Divanillin-based aromatic amines: synthesis and use as curing agents for fully vanillin-based epoxy thermosets. Front Chem 7:606

Stefano Merighi S, Mazzocchetti L, Benelli T, Giorgini L (2021) Evaluation of novel bio-based amino curing agent systems for epoxy resins: effect of tryptophan and guanine. Processes 9:42

Strzelec K (2007) Studies on the properties of epoxy resins cured with polythiourethanes. Int J Adhes Adhes 27:92–101

Yu S, Li X, Zou M, Guo X, Ma H, Wang S (2020) Effect of the aromatic amine curing agent structure on properties of epoxy resin-based syntactic foams. ACS Omega 5:23268−23275; (b) Curing agents for epoxy resin, three bond technical news (1990); (c) Pramanik MEW, Rawlins JW J Coat Technol Res. https://doi.org/10.1007/s11998-013-956

Zhang D, Liang E, Li T, Chen S, Zhang J, Cheng X, Zhou J, Zhang A (2013) Environment-friendly synthesis and performance of a novel hyperbranched epoxy resin with a silicone skeleton. RSC Adv 3:3095–3102

An Introduction to Bioenergy, Biofuel, and Bio Refining

T. Srinivas, G. Vijay Samuel, R. Govindarajan, Poulami Patra, Kakumanu Pooja Sri, Abhishek Varadarajan, Johncy Saji Mathew, and R. Sudarshan

Abstract Fossil fuel resources are finite and not environmentally benign. Hence, the development of bio-based energy resources is inevitable. Globally, intense research is being currently pursued on the manufacture of biofuels, bio-electricity and platform chemicals from organic matter. In India, bio-resources are available from the agricultural sector, food processing industries, and process industries. The effective utilization of these resources is essential for sustainable development. The main aspects that need to be focused include the identification of suitable feedstock, production methods, cost reduction, scale-up, and process intensification. This chapter aims to address all these issues.

Keywords Bio-energy · Bio-electricity · Cost reduction · Scale-up · Process intensification · Bio-fuel

1 Biomass

Biomass gas energy production is an application of organic matter energy production; sustainable energy is a form of power generation. This is a type of solar energy that is obtained actively or passively from the photosynthesis of green leaves. It is an infinite and limitless power source. The primary application of forestry and agricultural organic matter, hazardous effluent, but also town waste as raw resources, direct burning or anaerobic digestion, and electricity production, such as forestry and agricultural garbage gasification Direct combustion energy production, waste thermal decomposition of forestry and agricultural garbage, landfill gas electricity production, and biogas electricity production (Holdren et al. 2000). Mostly with continuous

T. Srinivas
Department of Chemical Engineering, B V Raju Institute of Technology, Narsapur, Medak, India

G. Vijay Samuel (✉) · R. Govindarajan · P. Patra · K. Pooja Sri · A. Varadarajan · J. S. Mathew · R. Sudarshan
Department of Chemical Engineering, Hindustan Institute of Technology and Science, Chennai, India
e-mail: vijaysamjuly@gmail.com

957

progress of the high population growth and period, energy crisis is becoming a globally must deal with the challenges, to accomplish the reasonable use through power usage of new technologies is becoming the provinces facing investigators topic, which produces power through biomass development can ultimately solve that issue and introduced the wonderful beginning for the underprivileged (Wang et al. 2010).
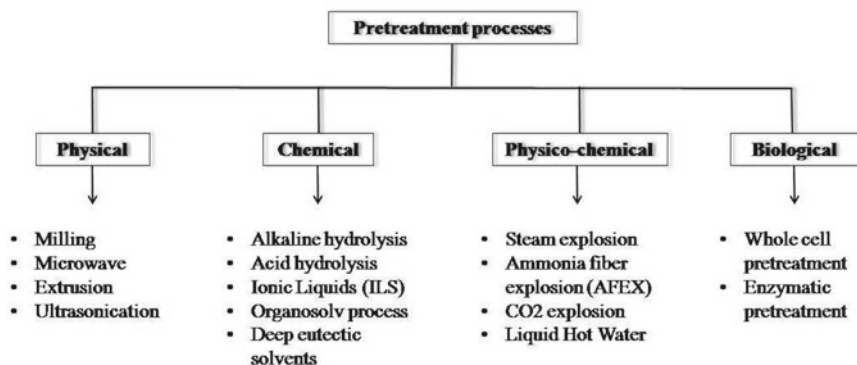
2 Lignocellulosic Biomass

The polysaccharides cellulose and hemicellulose make up most cellulosic materials (Fig. 1). Because the polysaccharides are significantly more strong and the pentose carbohydrates are not immediately fermentable by Saccharomyces cerevisiae, using lignocelluloses is much more challenging than using very next biomass feedstocks. To transform lignocellulose biomass (Fig. 2) to fossil fuels, the polysaccharides should first be hydrolyzed (broken down) toward carbohydrates employing acid or enzymes. Numerous bioengineering methods have been used to address these issues, including the development of Saccharomyces cerevisiae strains capable of fermenting pentoses, as well as the use of additional yeast species capable of fermenting pentose sugars, and the development of enzymes capable of destroying cellulose and hemicelluloses via simple sugars (Liu et al. 2004).

The pulp and paper industry uses lignocellulosic biomass as a raw material. The segregation of the lignin and cellulosic divisions of biomass is the priority of this electricity industry. Lignocellulosic biomass is the world's largest most cost-effective and renewable common resource. The production of sustainable power derived from lignocellulosic biomass as a replacement for fossil fuels is critical for humanity's survival. Lignocellulose is a complicated matrix made up of a variety of proteins, polysaccharides and phenolic polymer. Cellulose, a glucan polysaccharide embedded

Fig. 1 Structure of lignocellulosic biomass (Khanal 2009)
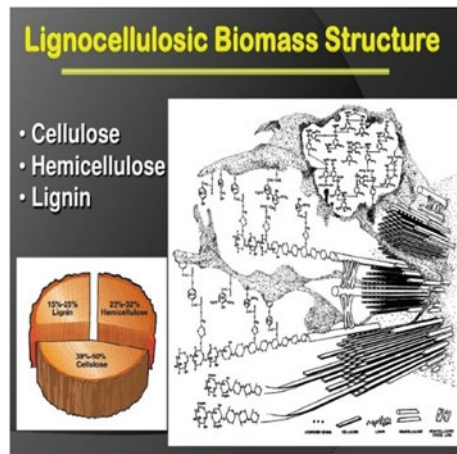
Fig. 2 Pretreatment of lignocellulosic biomass (Baruah et al. 2018)

in the terrestrial plantscell walls, is indeed a massive energy repository with immense potential for bioenergy production (Beylier et al. 2011). Lignocellulosic biomass is made up of a wide range of materials that have distinct chemical and physical properties. It is really the fibrous portion of the plant that isn't made up of starch. The potential of first-generation fossil fuels (typically made from agricultural crops like seeds, sugar beets, and oil seeds) to meet oil-product replacement, tackling climate change, and economic development goals is small. Their long-term viability is being scrutinized, as is the risk of generating unfair rivalry for food and fiber manufacturing water and land. The combined effects of certain issues have piqued efforts in improving non-food biomass-based alternative fuels. Bagasse, cereal straw, vegetative grasses and forest residues and sustainably managed forests are all examples of lingo-cellulosic fuel sources. Such second-generation fossil fuels may escape many of the issues that plague very next alternative fuels, as well as potentially lower costs in the long run (Climent and Feliu 2018).

The main potential feedstock for bioenergy is agricultural residues (corn stover, crop straws, and bagasse), herbaceous crops (alfalfa, switch grass), short rotation woody crops, forestry leftovers, wastepaper, and other wastes (municipal and industrial). The development of bioethanol from these fuel sources may be a viable option for disposing of these wastes. Furthermore, lignocellulosic fuel sources do not jeopardize food security. Furthermore, in terms of energy stability, environmental concerns, job opportunities, agricultural productivity, foreign exchange gains, social challenges, and other considerations, bioethanol is vital for both rural and urban areas (Rapp 2018).

3 Bioethanol

3.1 *Process*

Sugar fermentation, distillation, dehydration, and denaturing are really the initial requirements in massive production of bioethanol (optional). Few crops involve carbohydrates hydrolysisalso includingstarch and celluloseinto sugars prior to fermentation. Cellulolytic refers to the hydrolysis of cellulose (see Fig. 3). Starch is converted to sugar with the aid of enzymes (Alafif and Linke 2019).

3.1.1 Fermentation

The sugar is fermented by bacteria to manufacture ethanol. At this moment, bacteria will only be able to directly ferment carbohydrates. Starch and cellulose, two of the most important components of plants, are mostly made up of sugars and can thus be converted to sugars by fermentation. At the moment, only the sugar (e.g., sugar cane) and starch (e.g., maize) elements of the crop can be commercialised. The process of decomposing cellulose in plants to sugars and subsequently converting them to ethanol is known as cellulosic ethanol (Asif 2012).

Fig. 3 Bioethanol production from lignocellulosic biomass (Paulová et al. 2013)
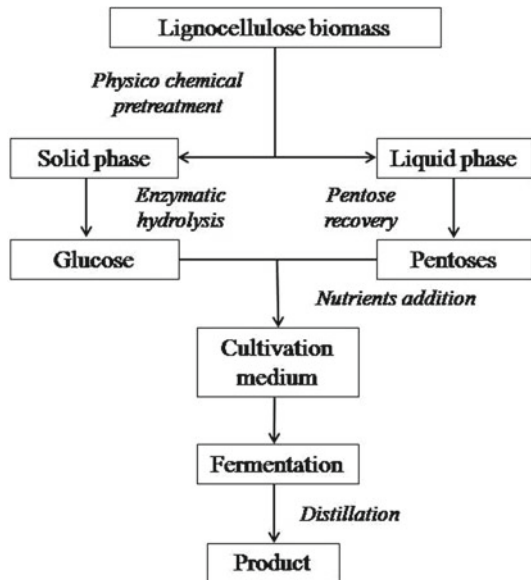
3.1.2 Distillation

Water should be extracted from ethanol before it can be used as fuel. Distillation removes most of the vapor. Because of a low-boiling water–ethanol azeotrope, quality is restricted to 95–96%. It can be used as a standalone fuel, but unlike anhydrous ethanol, it is immiscible in gasoline, meaning it cannot be mixed with other fuels like E85. The water proportion is generally removed in a subsequent step to burn in conjunction with gasoline in petrol engines (Feng et al. 2010).

3.1.3 Dehydration

The most extensively used purification method is a physical absorption procedure that uses a molecular sieve, such as the ZEOCHEM Z3-03 (a special 3A molecular sieve for EtOH dehydration). Azeotropic distillation, on the other hand, is enhanced by applying the hydrocarbon benzene, then denatured proteins the ethanol as well (to render it undrinkable for duty purposes). Calcium oxide is used as a desiccant in a third form (Fozer et al. 2019).

3.2 The Advantages of Bioethanol

Owing to government support and reduced taxes, the value of bioethanol/petroleum fuels would remain low. Which has been shown to promote the use of a clean energy, considering consumer demand is high enough to establish a substantial demand for bioethanol and alcohol-powered vehicles. When bioethanol is burned, it produces only carbon dioxide and water as pollutants (Fig. 4), and the carbon dioxide emitted during fermentation and combustion is equal to the carbon dioxide removed from the atmosphere while the crop grows. Ethanol is typically used to power cars, but it can also be used to power farm equipment, planes, and ships. While using higher mixes of Bioethanol energy in vehicles, similar to Biodiesel, engine beginning could be affected (Janke et al. 2015).
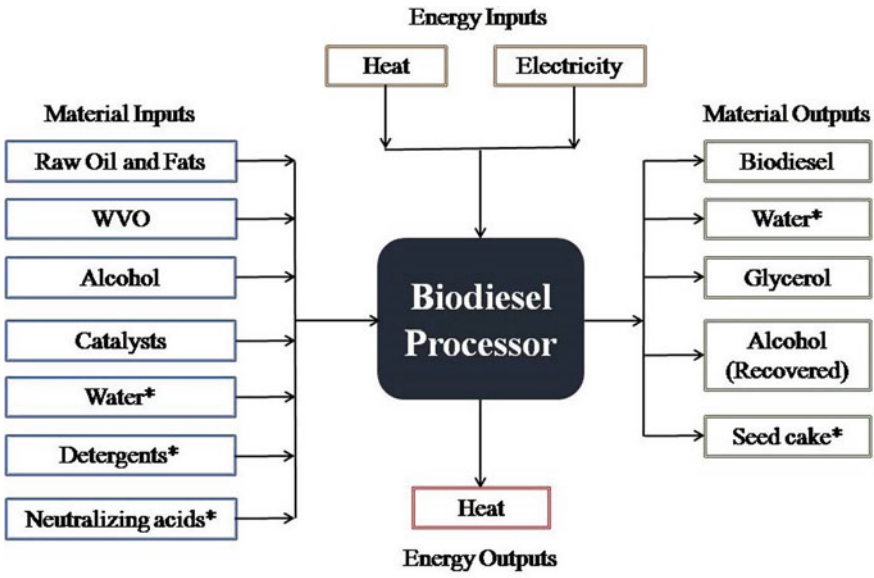
4 Biodiesel Production Process

4.1 Process

Feedstock Pre-Treatment
Pretreatment is required because most biodiesel feedstocks are of poor quality and contain additional chemicals that reduce catalyst performance during Transesterification (Fig. 5).

Fig. 4 Process of Bioethanol production (Janke et al. 2015)

Fig. 5 Biodiesel production process (Faruque et al. 2020)

Transesterification (Acid Esterification)

The most crucial reaction in the manufacture of biodiesel is the transformation of triglycerides and/or fatty acids into methyl esters. Yields, raw material quality, catalyst selection (Sodium Methoxide, Sulphuric Acid, or Enzyme), technique routes, energy consumption, and other aspects all contribute to the value of transformation.

Glycerin Recovery

To obtain technical grade or pharmaceutical grade glycerin, the glycerin produced from biodiesel processing must be refined, refined, and distilled.

Methanol Recovery

Excess methanol from the different sources is extracted and used in the transesterification reaction once more.

Biodiesel Purification

The methyl ester step is washed and dried in the bio-diesel purification process. Methyl ester distillation may be needed for better biofuel quality.

4.2 Advantages of Biodiesel

Generated from Renewable Resources: Unlike other petroleum-based goods, biodiesel energy source (Fig. 6). It can even be made on demand which produces less emissions than petroleum diesel because it is produced from vegetable and animal fat. Biodiesel can be used in diesel engines with next to no changes, making this the most favored main transportation source of energy. Biofuel could be used entirely
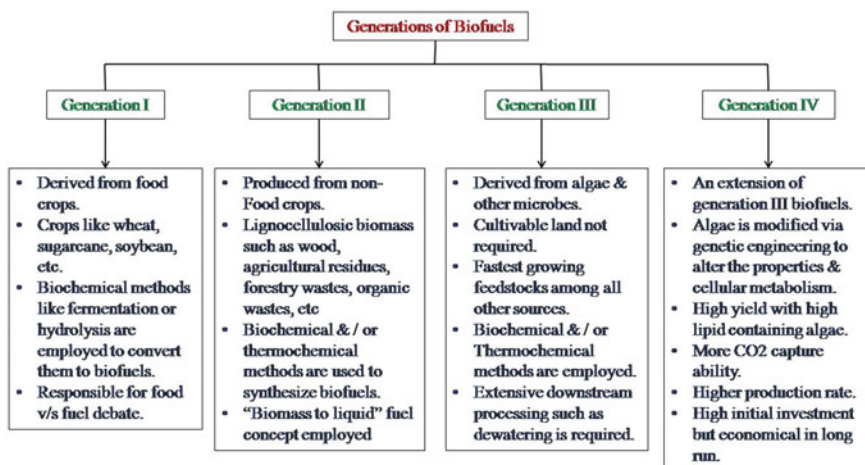

Fig. 6 Generations of biofuels (Sikarwar et al. 2017)

(B100) or in combination with diesel fuel. B20, for example, is a biodiesel/diesel fuel mix that contains 20% biodiesel and 80% diesel. Since it is virtually sulphur-free, it enhances engine lubrication and extends life of the engine.

5 Pyrolysis

Pyrolysis (Fig. 7) is a thermochemical process it can be used on any organic (carbon-based) material. It can be applied to both pure products and mixtures. In this treatment, the substance is heated to a high temperature and then separated into various molecules chemically and physically in the absence of oxygen. Decomposition occurs due to the reduced thermal stability of chemical bonds in materials, allowing them to be collapsed with heat. The formation of new molecules occurs because of thermal degradation. This enables the delivery of goods with a distinct, and sometimes superior, character than the initial residue. Pyrolysis is becoming an exceedingly essential matter for today's industry as a result of this function, as it permits for much quality product to be extracted from specific materials and waste. Thermal therapy is often connected by pyrolysis. However, unlike combustion and gasification, which require completely or partially oxidation of the product, pyrolysis relies on heating in the oxygen—free environment. As a result, it is primarily an endothermic process that ensure that the goods obtained have a high energy density. Solids (charcoal, biochar), liquids, and non-condensable gases are often generated by pyrolysis (H_2, CH_4, C_nH_m, CO, CO_2, and N_2). Since the liquid phase is only removed from pyrolysis gas during cooling, these two phases should be used together in the same implementations when supplying hot syngas straight to the burning or oxidation container. A substance molecule is heating from ambient to a given temperature while pyrolysis. The substance is held within the pyrolysis machine and conveyed at a given speed by a screw conveyor on until process is finished. The formulation and yields of pyrolysis products (pyrolysis oil, syngas, and char) are determined by the temperature of pyrolysis (Jin et al. 2015).
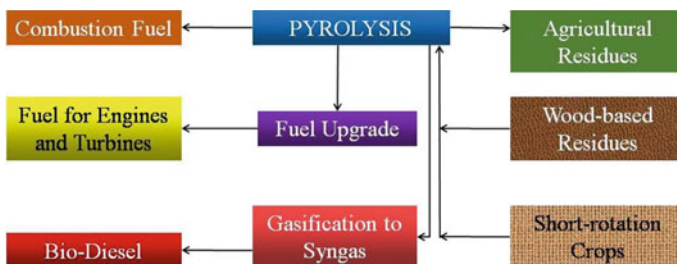

**Fig. 7** Pyrolysis process (Zafar 2020)

6 Biogas Technology

Applied science the degradation of biodegradable material in the absence of oxygen produces biogas, which is a mixture of various gases (Table 1). Agriculture waste, fertilizer, agricultural waste, urban, organic matter, sewage, green waste, and food waste are all examples of raw materials that can be used to make biogas (Sathish et al. 2019). It is a source of energy that is renewable. Methanogens (methane-producing bacteria) degrade material in a closed environment, or biodegradable materials are fermented to create it. Methane could be used for heating, energy generation, and vehicle fueling as CNG (compressed natural gas) (Vijay Samuel and Srinivas 2019).

Biogas, bioethanol, biodiesel, and biobutanol seem to be the most appealing biofuels. Most of these biofuels are likely to play an important mostly in development of renewable energy carriers as viable alternative sources of energy that will support the environment worldwide. Anaerobic digestion of organic wastes produces biogas, which mainly includes biomethane (Figs. 8 and 9). Biogas appears to be the simplest of the biofuels manufacturing processes even though it does not require sterilization, can indeed be processed in standard reactors at moderate temperatures using a

Table 1 General composition of biogas (Sathish et al. 2019)

Compound	Molecular formula	Percentage composition
Methane	CH_4	50–75
Carbon dioxide	CO_2	25–50
Nitrogen	N_2	0–10
Hydrogen	H_2	0–1
Hydrogen sulphide	H_2S	0–3
Oxygen	O_2	0–0
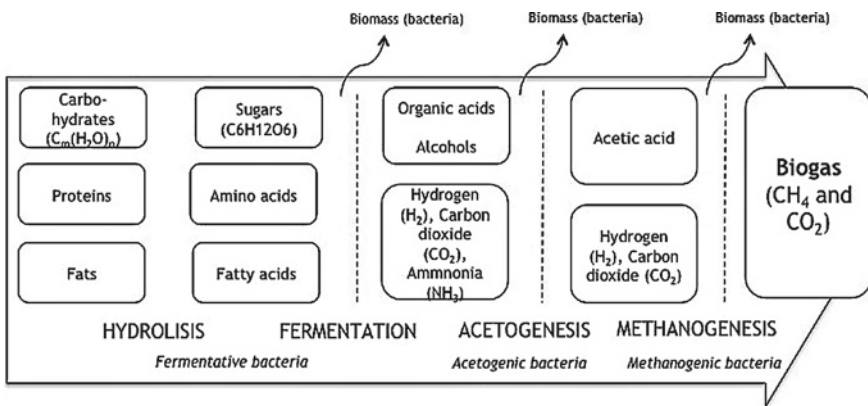
**Fig. 8** Anaerobic digestion of biogas (Spuhler 2010)

natural consortium of microorganisms found in nature including certain manure, and therefore does not require a sophisticated extraction and purification process. Fortunately, it is much more difficult than it exists now, particularly whenever a higher biogas yield is desired. When compared to other biofuels, biogas processing has the most complicated microbiology and biochemistry since four different processes, namely hydrolysis, acidogenesis, acetogenesis, and methanogenesis, are carried out in parallelly by a consortium of various bacteria. Besides that, the biogas substrates are a combination of various components with varying degradation properties. Strong wastes, such as rural, urban, and food industrial wastes, as well as wastewater, are the most common feedstocks (Logan 2007).

Bio-slurry is a fertilizer that could be used in agriculture and aquaculture (Fig. 10).

7 Microbial Fuel Cell

Microbial fuel cells (MFCs) are anaerobic bioreactors that transform energy stored in organic compound chemical bonds to electrical power thru catalytic reactions of microorganisms. For many years, researchers have known that bacteria can decompose organic material and generate electricity directly (Sophia and Saikant 2016). The current energy crisis has reignited enthusiasm in MFCs between academic researchers to produce electricity or hydrogen from biomass without releasing net carbon into the environment. MFCs can be used to decompose the organic in sewage treatment plants as well. They have also been looked into for use as biosensors, including certain sensors for measuring amount of dissolved oxygen. The groups of
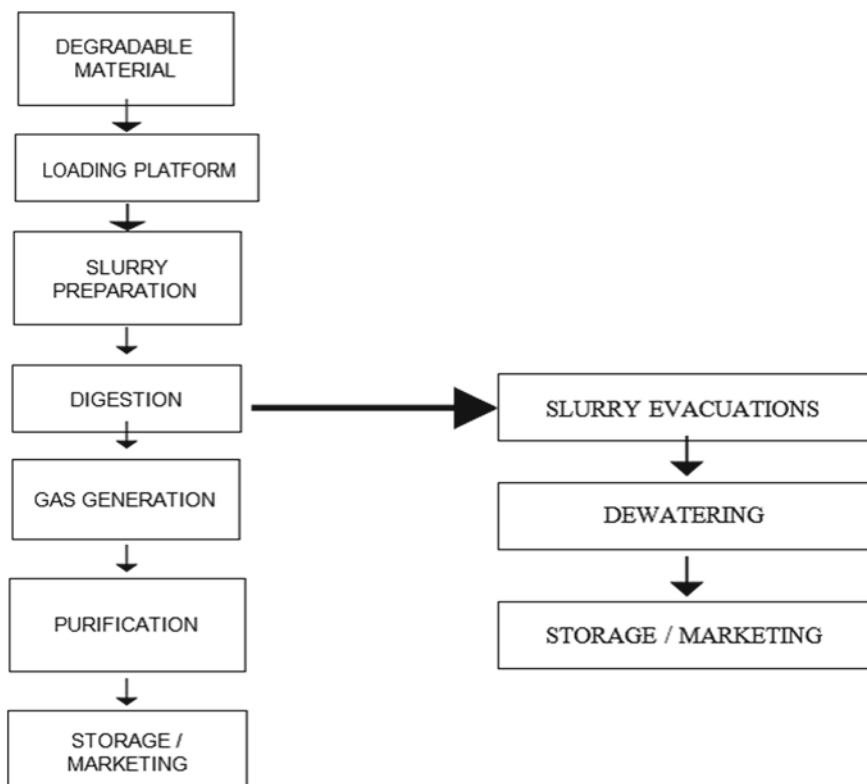
Fig. 10 Flow chart (Logan 2007)

microorganisms in an MFC's anode compartment, the MFC's design, and operational parameters all have a major impact on power production and Coloumbic performance. Due to various their low switching frequency of many thousand mW/m^2, MFCs are currently constrained in their real-world applications. MFC performance is being improved while building and operating costs are being reduced (Mathuriya 2014).

Microorganisms catalyze reactions at the anode and/or cathode in MFCs, which are newer technologies. MFC research is rapidly progressing, and several different approaches using various electron donors and acceptors have been already established. When anodes and cathodes are combined in an MFC, new inefficiencies and possibilities emerge. It is critical to reduce internal energy losses while increasing efficiency while using MFCs. Membranes are essential for high efficiency and pure materials, but they also enhance the internal resistance of MFCs. Future MFC analysis should give more importance to the relation between MFC-produced chemicals and fuels and current manufacturing processes (Mwinyihija and Mwinyikione 2010). Anode, cathode, proton exchange membrane (PEM), and electrical circuit constitute the basic MFC configuration (Fig. 11). The microbial population in the anode compartment of an MFC uses organic material as feedstock to generate electrons
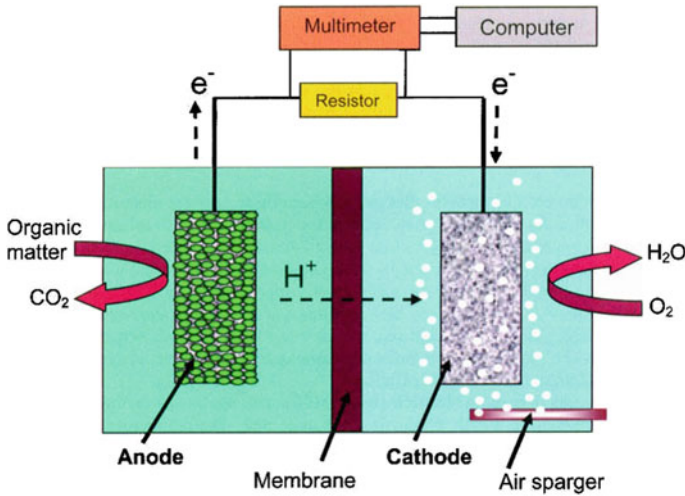
Fig. 11 Diagrammatic representation of MFCs (Ahemad 2014)

and protons via biochemical reactions. All of these electrons are identified by the energy transfer chain's nicotinamide adenine dinucleotide (NADH) and subsequently transferred to the breakdown of organic molecules like nitrate, sulphate, and oxygen before reaching the outer membrane proteins. Bacteria eventually transfer such electrons to an anode, where they travel to the cathode via an external electrical circuit, resulting in an electric current that may be measured with a voltmeter or ammeter coupled to the device. The induced protons diffuse to the cathode via the PEM, where they combine with the electrons and oxygen to form water. The anode section is often maintained anaerobic because oxygen inhibits power generation, whereas the cathode section is released into the environment. The electrode reaction is defined as the degradation of the degradable substrate into water and carbon dioxide, as well as the creation of energy using acetate as a substrate (Ahemad 2014).

$$\text{Reaction at anode}: \ CH_3COO^- + 2H_2O \ 2CO_2 + 7H^+ + 8e^-$$

$$\text{Reaction at cathode}: \ O_2 + 4e^- + 4H^+ \rightarrow 2H_2O$$
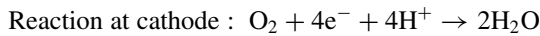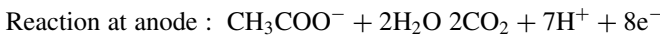
8 Conclusion

India's bioenergy strategy is a new-comer-friendly sector—based industrial policy that emphasizes on assisting and attracting entrants into the green field. Export

and import of bioenergy are prohibited in the country, and domestically generated biodiesel is exempt from tariffs and taxes, however there are few positive and empowering measures for bioenergy mixers and distributors to protect the industry from external and market shocks. Although India's move to advanced biofuels is commendable, certain bio refineries' technologies and performance are still in their infancy. The government also has dedicated to funding support of up to 40% for infrastructure development, concentrating on private operators. A total of Rs. 50 billion has been pledged (Rs. 5000 crore). However, given that the building of a 100 kilolitres per day (klpd) bio-refinery would require approximately Rs. 800–900 crore in capital investment, this amount of money is insufficient to maintain 2G/3G bioenergy refineries. The phase of retail industry follows bio refineries. The government and non-governmental Oil Marketing Companies are in charge of the last mixing of ethanol with fossil fuel (OMCs). The six public service OMCs—Indian Oil Corporation Ltd (IOCL), Hindustan Petroleum Corporation Ltd (HPCL), Bharat Petroleum Corporation Ltd (BPCL), Numaligarh Refinery Ltd (NRL), Mangalore Refinery and Petrochemicals Ltd (MRPL), and Bharat Oman Refineries Ltd (BORL), as well as some private companies such as Shell, Essar, and Reliance—handle consumer marketing. The OMCs are expected to invest about Rs. 100 billion in the construction of 12 2G bio refineries (Rs. 10,000 crore). Fortunately, despite sufficient infrastructure development in remote areas, appropriate bioenergy marketing, and supply chain, this growth will not translate into increased progress. Green industrial policies are rife with mistakes, which are unavoidable. In fact, making too few errors indicates poor results. To be efficient, a green project must have efficiency, effectiveness, and credibility. If any of these interconnected elements is missing, the policy will fail. What's required is a collection of methods for finding defects and revising policies as necessary. The National Biofuel Committee, for example, and other regulatory bodies must better direct policy. Given the country's biomass production capability, available technologies, incentives, and expenditure, biofuel as a policy goal may be difficult to achieve. According to experts, India might attain a goal of roughly 6% blending with petrol and 4% blending with diesel by 2030 if advanced biofuels are used. The Spice Jet flight's 25% ethanol blending was a one-time stunt that India pulled off admirably and garnered international attention. India must, therefore, incorporate the economic, environmental, and market aspects of bioenergy production for the policy to be effective. Financing for green industries is still scarce, and this is where the government must step in to support the sustainable sector by encouraging private investment.

References

Ahemad M (2014) Bacterial mechanisms for Cr(VI) resistance and reduction: an overview and recent advances. Folia Microbiol 59:321–332

Alafif R, Linke B (2019) Biogas production from three-phase olive mill solid waste in lab-scale continuously stirred tank reactor. Energy 171:1046–1052

Asif M (2012) Energy crisis in Pakistan: origins, challenges, and sustainable solutions. OUP Catalogue 121:1034–1041

Baruah J, Nath BK, Sharma R, Kumar S, Deka RC, Baruah DC, Kalita E (2018) Recent trends in the pretreatment of lignocellulosic biomass for value-added products. Front Energy Res 6:141. https://doi.org/10.3389/fenrg.2018.00141

Beylier MR, Balaguer MD, Colprim J, Pellicer-Nàcher C, Ni B-J, Smets BF, Sun S-P, Wang RC (2011) Biological nitrogen removal from domestic wastewater. In: Comprehensive biotechnology, 2nd edn. vol 6, pp 285–296

Climent V, Feliu JM (2018) Encyclopedia of interfacial chemistry

Faruque MO, Razzak SA, Hossain MM (2020) Application of heterogeneous catalysts for biodiesel production from microalgal oil—a review. Catalysts 10:1025. https://doi.org/10.3390/catal1009 1025

Feng XM, Karlsson A, Svensson BH, Bertilsson S (2010) Impact of trace element addition on biogas production from food industrial waste—linking process to microbial communities. FEMS Microbiol Ecol 74(1):226–240

Fozer D, Kiss B, Lorincz L, Szekely E, Mizsey P, Nemeth A (2019) Improvement of microalgae biomass productivity and subsequent biogas yield of hydrothermal gasification via optimization of illumination. Renew Energy 138:1262–1272

Holdren JP, Smith KR, Kjellstrom T, Streets D, Wang X, Fischer S (2000) Energy, the environment, and health. In: Goldemberg J, Baker JW, Khatib H (eds) World energy assessment. United Nations Development Program, New York, pp 61–110

Janke L, Leite A, Nikolausz M, Schmidt T, Liebetrau J, Nelles M, Stinner W (2015) Biogas production from sugarcane waste: assessment kinetic challenges for process designing. Int J Mol Sci 16(9):20685–20703

Jin Y, Chen T, Chen X, Yu Z (2015) Life-cycle assessment of energy consumption and environmental impact of an integrated food waste-based biogas plant. Appl Energy 151:227–236

Khanal S (2009) Biomass conversion to biofuel and biobased product. The REIS Seminar Series at the University of Hawaii at Manoa

Liu H, Ramnarayanan R, Logan BE (2004) Environ Sci Technol 38(7):2281–2285

Logan BE (2007) Microbial fuel cells. John Wiley Publications

Mathuriya AS (2014) Enhanced tannery wastewater treatment and electricity generation in microbial fuel cell by bacterial strains isolated from tannery waste. Environ Eng Manage J 13(12):2945–2954

Mwinyihija, Mwinyikione (2010) Ecotoxicological diagnosis in tanning industry. Springer-Verlag New York

Paulová L, Patáková P, Rychtera M, Melzoch K (2013) Production of 2nd generation of liquid biofuels, liquid, gaseous and solid biofuels—conversion techniques (Fang Z, ed). IntechOpen. https://doi.org/10.5772/53492

Rapp BE (2018) Encyclopedia of interfacial chemistry

Sathish S, Vijay Samuel G, Balaji K, John Presin Kumar A (2019) Experimental investigation of methane gas generation using textile effluents. Int J Ambient Energy. https://doi.org/10.1080/014 30750.2019.1636878

Sikarwar VS, Zhao M, Fennell PS, Shah N, Anthony EJ (2017) Progress in biofuel production from gasification. Prog Energy Combust Sci 61:189–248

Sophia AC, Saikant S (2016) Reduction of chromium (VI) with energy recovery using MFC technology. J Water Process Eng 11:39–45

Spuhler D (2010) Anaerobic digestion (general). Further resources: wastewater treatment

Vijay Samuel G, Srinivas T (2019) Effluent treatment technologies and cost research. Int J Eng Adv Technol (IJEAT) 9(1):6745–6751

Wang S, Dai G, Yang H, Luo Z (2010) National renewable energy laboratory: biomass energy basics. Prog Energy Combust Sci 62:33–86

Zafar S (2020) Biomass pyrolysis process. BioEnergy Consult Powering a Greener Future

Optimization of Extraction Parameters and Evaluation of Functional Properties of Protein Isolateobtained from Cottonseed Meal

Akash Sharma, Surinder Singh, and Sushil Kumar Kansal

Abstract In the present work, alkaline extraction, acidic precipitation and physical separation was used to extract protein from the defatted cottonseed flour. The process parameters affecting the extraction e.g. pH, extraction time, flour to solvent ratio, temperature and centrifugal speed were optimized. Different suspensions of 1:10, 1:20, 1:30 (w/v) flour to water ratio were prepared during the extraction. Each suspension was subjected to different temperatures i.e. 45 °C, 55 °C and 60 °C for different time intervals i.e. 30, 40, 50 and 60 min. The extraction process was carried out at pH 11 and the iso-electric point of protein isolate was obtained at pH 4.5. The protein isolates were characterized by using Scanning Electron Microscopy (SEM). The protein content in the samples prepared for different flour to water ratios i.e. 1:10, 1:20 and 1:30 (w/v) was found out to be 81.487 ± 0.016, 82.612 ± 0.025, 86.162 ± 0.034 respectively. Maximum yield (86%) of protein was obtained at pH 11, flour to water ratio 1:30 (w/v) at 60 min extraction time, centrifugal speed of 7000 rpm and temperature of 30 °C. The obtained protein isolate was found to be very useful to enhance the protein content for different food/feed applications.

Keywords Cottonseed meal · Extraction · Protein isolate · Acid precipitation

1 Introduction

Proteins are the basic and fundamental building blocks for tissues formation in animals and humans (Wu 2016). Proteins happen to be the vital components for growth of bones, blood, cartilage and skin. Apart from the growth of bones and adipose tissue, the proteins account for three-fourth of the dry weight of human tissues. Proteins are known to be the important macronutrients along with the carbohydrates and fats which are required by our body in large amounts. Proteins are useful in generating enzymes, hormones and many other chemicals for the body.

A. Sharma · S. Singh (✉) · S. K. Kansal
Dr. S.S. Bhatnagar University Institute of Chemical Engineering and Technology, Panjab University, Chandigarh 160014, India
e-mail: sonuunos@gmail.com

Regarding the chemical composition, the proteins are made up of carbon, hydrogen, nitrogen, oxygen and sulfur compounds. Proteins are large sized heteropolymeric macromolecules having one or more polypeptides. Polypeptides are the chains made up of amino acids, which are linked in series through peptide bonds. For a healthy adult who has limited physical activity, the recommended dietary protein allowance is 0.8 g of protein per kg of body weight per day and 1.6 g protein per kg body weight everyday for person doing extreme physical activity, in order to fulfill functional requirements that include skeletal muscle protein accretion and physical strength. Long term protein intake at 2 g/kg of body weight per day is considered safe for healthy adults (Wu 2016). The sources of proteins include legumes, nuts and seeds, whole grains, fruits and vegetables, poultry products like eggs, meat and fish etc. (Yu et al. 2007). The common proteins found in the human body includes haemoglobin, insulin, enzyme urease, iso-citrate dehydrogenase and pyruvate dehydrogenate complex. The functions of the proteins inside the body include growth and maintenance, carrying out biochemical reactions in body, acting as chemical messengers, maintaining pH, controlling body fluids, strengthening immunity, transporting materials and storing of nutrients and act as anti-fungal agents (Phillips et al. 2015; Baden and Kubilus 1984; Hamm et al. 2015; Hankins 2006; Li et al. 2007; Diallinas 2014; Carbone et al. 2014; Wong et al. 2010). The seeds which are grown primarily for the production of edible oils are categorized as oilseeds. In India, oilseeds are considered as the backbone of the agriculture economy. The oilseeds which are grown in India include cottonseed, groundnut, sesame, soybean, mustard, sunflower, niger, castor and linseed. Oilseeds are good source of energy due to their high percentage oil and protein. Oilseeds are good source of vitamins (vitamin E, folate and niacin), fiber, minerals (iron, phosphorus and iron), polyunsaturated and monounsaturated fatty acids. Nutritional value of oilseed meal is largely dependent on the process of oil extraction. Severe heat during the extraction of oil from oilseeds may lead to the destruction of amino acids present in the oilseeds, which leads to the reduction in oil content in the meal (Gupta and Gupta 2016). Cotton is primarily grown for the production of fiber. Cottonseed is recovered from the cotton plant after the removal of cotton lint. Cottonseeds are of great economic value, as they provide valuable oil, possess good protein content and many other nutrients and vitamins. The production of the cottonseed in the world has increased at a great pace in the last decade. India is the largest producer of cottonseed and produces about one third of the total world's production (Shah 2012). Cottonseed is a good source of protein. Cottonseed kernel contains up to 30–40% of protein. Protein components are primarily globulins (60%), albumins (30%) and lower quantity of prolamins (8.6%) and glutelins (0.5%) (Gahlawat et al. 2017). The essential proteins in the body, albumin and globulin, are found abundantly in the liquid portion of the blood. Albumin's primary function is to regulate and maintain oncotic pressure (force that pushes fluid into blood circulation) and thus prevents excess fluid from collecting in the tissues of the body and other areas of the body. These proteins help in the liver function, blood clotting and fighting various infections (Coulthard 2015). Cottonseed is also a good source of ionizable amino acids like aspartic acids, glutamic acid, histidine, arginine, and lysine. Arginine and lysine are vital amino acids present in protein that induce body

growth, strengthens blood vessels, helps in lowering the blood pressure and reduces heart disease risk. Glutamic acid, another amino acid found in the cottonseed helps in the functioning of nervous system. In the human body, it turns into glutamate a chemical that allows nerve cells in brain to send and receive signals from other cells in the body by transferring neurons to maintain acid and base balance in body tissues and blood. Histidine another amino acid is responsible for maintaining normal pH in the body. It is also important in maintaining hemoglobin level which helps in the movement of oxygen in the blood vessels (Buffo and Han 2005). The fatty acid profile of cottonseed typically consists of 70% unsaturated fatty acids, including 52% poly-unsaturated and 18% mono unsaturated fatty acids and 26% saturated fatty acids. The three main fatty acids in cottonseed oil are oleic acid, palmitic acid and linoleic acid along with myristic, lignoceric, cis-vaccenic, sterculic, malvalic, behenic and arachidic in small amounts (Sekhar and Rao 2011; Sharif et al. 2019). Cottonseed produces much more food for humans and feed for animals than its fiber. Cottonseed hulls generate the fiber and linters, while the kernel includes protein, starch, oil and other components such as minerals, lecithin, sterols etc. Cottonseed oil is derived from the kernel of cottonseed. Cottonseed protein contains important fats and water soluble vitamins and other minerals (Hathcock 1997; Ravisankar et al. 2015; Brown and Reynolds 1963). Cottonseed is among the most unsaturated edible oils and is termed as "heart oil" (Agarwal et al. 2003). The various products from cottonseed after its crushing consist of 45% meal, 27% hull, 8% linters, 16% oil and 8% waste. If there is a good utilization of the products that are obtained after the extraction of oil from the cottonseed then, the cottonseed meal can be used as a raw material for various industries. The chemical composition of soy and cottonseed protein have been documented by He et al. (2015), the global contribution of cottonseed protein has been reported by Kumar et al. (2021), functionality of oilseed proteins by Moure et al. (2006) and proteins availability form various oilseeds by Bajjalieh (2002). There is a great potential of using cottonseed meal in the production of wood adhesives, super-absorbent, bioplastics, protein adhesives, low gossypol protein and hydrogels (Zhuge et al. 1988; Cheng et al. 2013; Yue et al. 2012). The foaming and emulsi-fying properties of cottonseed protein isolates are very important for the produced isolates and have useful applications in food supplements which have been reported by various researchers (Tsaliki et al. 2002, 2004; Cherry et al. 1978; Leah and John 1981). The methods of extraction of cottonseed protein include alkaline extraction and acidic precipitation, enzymatic extraction, ultra-filtration and aqueous extraction (He et al. 2013; Stroher et al. 2011; Cui 2005; Rosenthal et al. 1998). In the present study alkaline extraction and acidic precipitation method were employed to extract protein from the cottonseed. The parameters affecting the protein extraction were optimized and functional properties of protein isolate were also evaluated.

2 Materials and Methods

2.1 Materials

Defatted cottonseed flour was used as the main raw material and was procured from the local market. Chemicals i.e. sodium hydroxide (NaOH) and hydrochloric acid (HCl) were procured from Merck Life Science Private Limited (Merck India Ltd.) and double distilled water was prepared in the laboratory to prepare stock solutions. All the chemicals and reagents used were of analytical grade.

2.2 Extraction of Protein from Defatted Cottonseed Flour

The extraction of protein from the defatted cottonseed flour was conducted by taking required flour to solvent (alkali) ratio (i.e. 1:10, 1:20 and 1:30) and varying the process parameters like temperature (45, 55 and 60 °C), digestion period (i.e. 30, 40, 50 and 60 min) and centrifugal speed (5000–7000 rpm). To determine the optimum parameters; flour to solvent ratio, temperature, extraction time and centrifugal speed were varied during the experiments.

The criteria for the selection of different level of parameters was to take attest three levels of low, medium and high values of parameters as studied from the literature. In case of extraction time and centrifugal speed one more value of parameter was taken to study the effect of increased time and centrifugal speed to get the optimum values. The process parameters were optimized using one factor at a time method (OFAT) thereby varying one parameter and fixing the all others for one set of experiments. The procedure adopted for the extraction of protein from the defatted cottonseed flour after preparing the cottonseed flour and water suspension consisted of adjusting the suspension first to a pH of 11.0 by using 1.0 N of sodium hydroxide (NaOH) and then digesting it for a certain time period at a fixed temperature. The suspension was constantly stirred during the digestion and cottonseed protein isolate was formed. It was then centrifuged at fixed rpm for 25 min. After collecting the supernatant, the iso-electric pH 4.5 was attained by using 1.0 N hydrochloric acid (HCL). It was again centrifuged at fixed rpm for 25 min and precipitates were collected and dried and kept in refrigerator for further use. A hot air oven was used to dry the precipitates obtained from the above procedure. The precipitates were dried overnight at a temperature of 50 °C. The dried precipitates were collected and grinded well and then kept for further testing and analysis.

2.3 Characterization of Cottonseed Protein Isolate

Various techniques were used to characterize the prepared cottonseed protein isolates. The structural and crystal properties were examined by powder X-ray diffraction (XRD; PAN analytical X'pert Pro.), with Cu-Kα radiation ($\lambda = 1.54178$ Å) at 45 kV and 40 mA in the 2θ ranging from 10° to 80°. The size and general morphologies of prepared samples were analyzed by scanning electron microscopy (SEM; JSM-6010LA, JEOL Co. U.S.A). The chemical composition of prepared sample was determined using Fourier transform infrared spectroscopy (FTIR; Thermo scientific Nicolet iS50) equipped with a diamond ATR at room temperature with KBrpellet as a reference ranging from 450 to 4000 cm^{-1}.

2.4 Determination of Functional Properties and Proximate Analysis of Protein Isolate

The functional properties of the prepared protein isolates i.e. water holding capacity, oil holding capacity, foaming capacity and moisture and ash content were determined. The water holding capacity and oil holding capacity were determined using the method of Ma et al. (2018) and foaming capacity was determined using the method of Shao et al. (2016). CHNS analysis was used for the determination of carbon, hydrogen, nitrogen and sulfur content of the protein sample. This analysis was performed by using elementary CHNS analyzer [Thermo scientific (FLASH 2000) based on Pregl-Dumas method (Fadeeva et al. 2008). The proximate analysis including ash content, acid insoluble ash content was determined by the method described by Kadam et al. (2013)] and the moisture content was determined using standard reported method (Babayan et al. 1978).

3 Results and Discussion

3.1 Characterization of Protein Sample Using XRD

Figure 1 represents the X-ray diffraction pattern of extracted protein isolate from cottonseed flour. The two characteristic peaks of cottonseed protein isolate were centered at approximately 2θ = 9.2° and 20.0°, which corresponded to the d-spacing of 0.92 nm and 0.43 nm, indicating crystalline nature (He et al. 2018).

3.2 Scanning Electron Microscopy (SEM) Analysis

1. SEM image of defatted cottonseed flour

The morphological properties were revealed using SEM images of defatted cotton-seed flour and cottonseed protein isolate as shown in Figs. 2 and 3. The surface of defatted cottonseed flour was more porous whereas the protein isolate from cotton-seed flour showed flatter and tighter structures with sharp angles. Moreover, there were no open pores observed (Zhang et al. 2018).
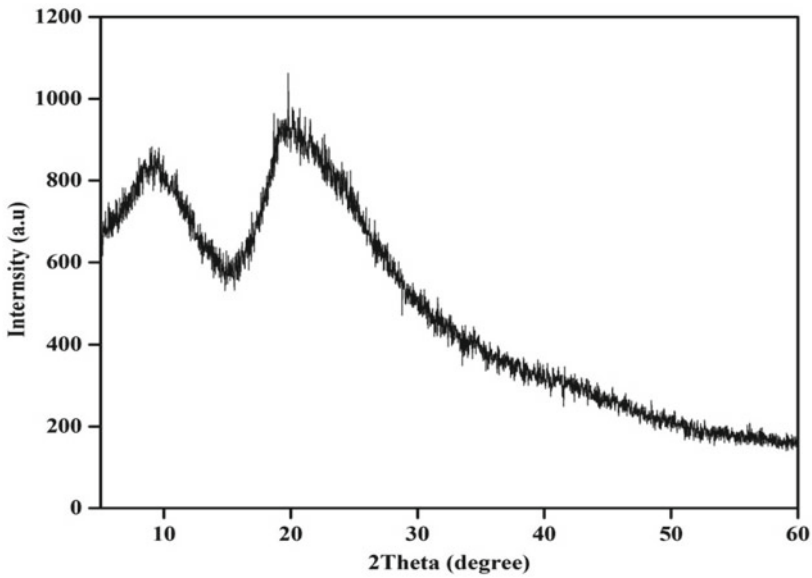
2. SEM images of cottonseed protein isolate

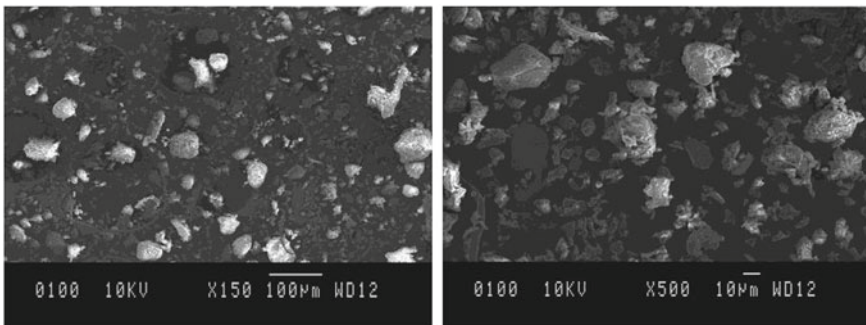**Fig. 1** X-ray diffraction analysis of cottonseed protein isolate

Fig. 2 SEM images of defatted cottonseed flour
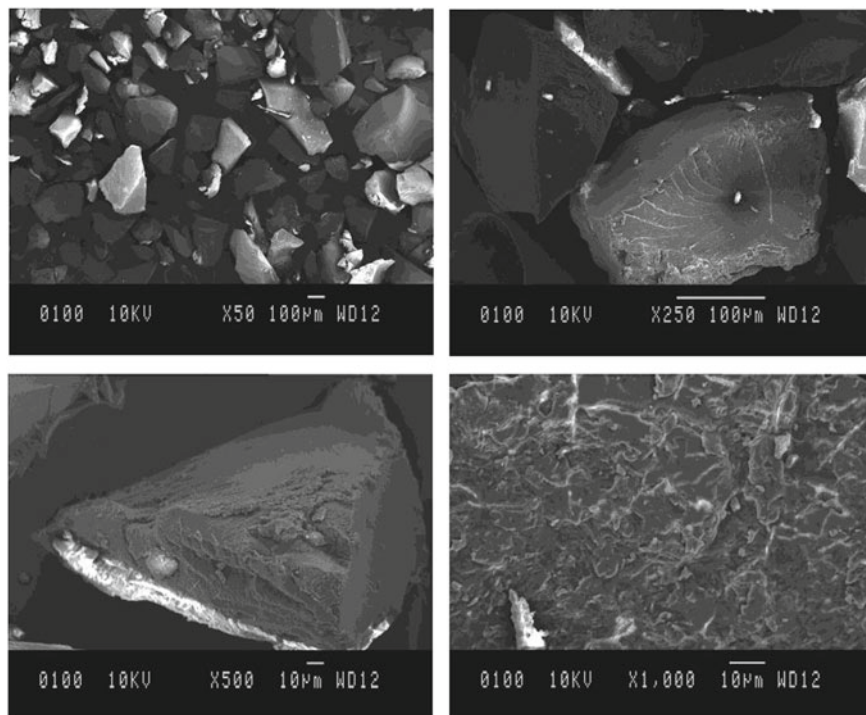
Fig. 3 SEM images of cottonseed protein isolate

3.3 FT-IR Analysis

The presence of functional groups and surface composition were analyzed by Fourier transformation Infra-red spectroscopy as shown in Fig. 4. The spectrum of both cottonseed flour and cottonseed protein isolate was quite similar. In the FT-IR spectrum of cottonseed protein isolate, the absorption peaks at $3433.4\,cm^{-1}$, $1646.4\,cm^{-1}$, $1545.4\,cm^{-1}$ and $1387.9\,cm^{-1}$ indicated the amide I (C=O and C-N stretching), amide II (C-N stretching and N-H bending), amide III (C-N stretching in primary amines) and amide A bands (free O-H and N-H group in protein) respectively (Chen et al. 2019). Whereas the peak at $2928.1\,cm^{-1}$ and $1059.2\,cm^{-1}$ could be attributed to C–H symmetrical and asymmetrical stretching and carbohydrate, which is main component of cottonseed flour (Liu et al. 2018). The difference between defatted cottonseed flour and cottonseed protein isolate spectrum revealed that alkaline extraction of protein improved the spectrum of protein isolate over cottonseed flour.

Fig. 4 FT-IR spectrum of cottonseed flour and cottonseed protein isolate
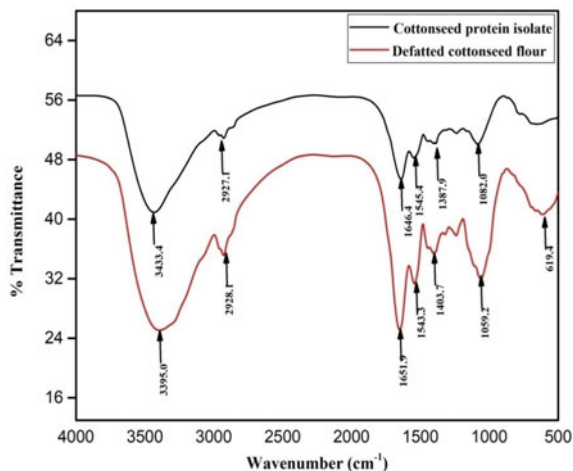
3.4 Optimization of Process Variables Affecting the Extraction Process

3.4.1 Effect of Extraction Time with Varying Temperatures on the Protein Yield

The influence of extraction time on the extraction of the protein was evaluated at different time intervals i.e. 30, 40, 50 and 60 min respectively. It was observed that with the increase of time, extraction rate of protein increased as shown in Figs. 5, 6 and 7. The maximum extraction was found at 60 min and hence 60 min was chosen as optimum value. It was also seen that with the increase of temperature, extraction rate of protein increased. When temperature increased molecules moved with higher speed, which increased the mass transfer rate among the solid and liquid interface. Moreover, with increase in temperature, viscosity decreased and mass transfer rate increased (Zhang et al. 2009).

However, at further high temperatures beyond 60 °C, protein activity decreased which led to denaturation of protein. Also further increase in temperature leads to darkening of the extracted protein. This was due to the saturation limit of protein extracted at 60 °C. Therefore, 60 °C was adjudged as the optimum temperature.

3.4.2 Effect of pH on the Extractability of Protein

Defatted cottonseed flour was mixed with water in the ratios of 1:10, 1:20, 1:30 (w/v) respectively and the pH used was in the range of 4.0–12.0. The pH was adjusted using 1.0 N sodium hydroxide (NaOH) and 1.0 N hydrochloric acid (HCl). The result showed a rapid rise in the yield between pH 6.0 and pH 11.0 as shown in
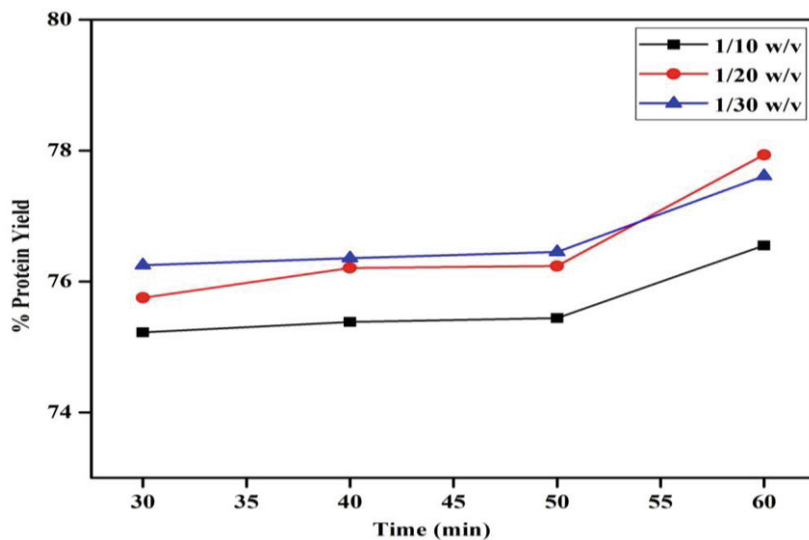
Fig. 5 Extraction time versus % protein yield at 45 °C
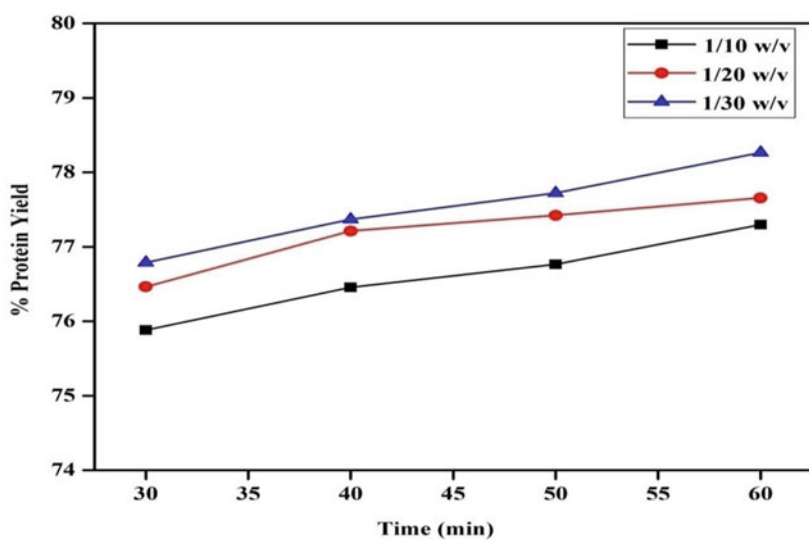
Fig. 6 Extraction time versus % protein yield at 55 °C

Fig. 8. Further, it is difficult to keep the protein under strong alkaline conditions as it degrades and denatures the cottonseed protein so the optimum pH for protein extraction was selected as pH 11.
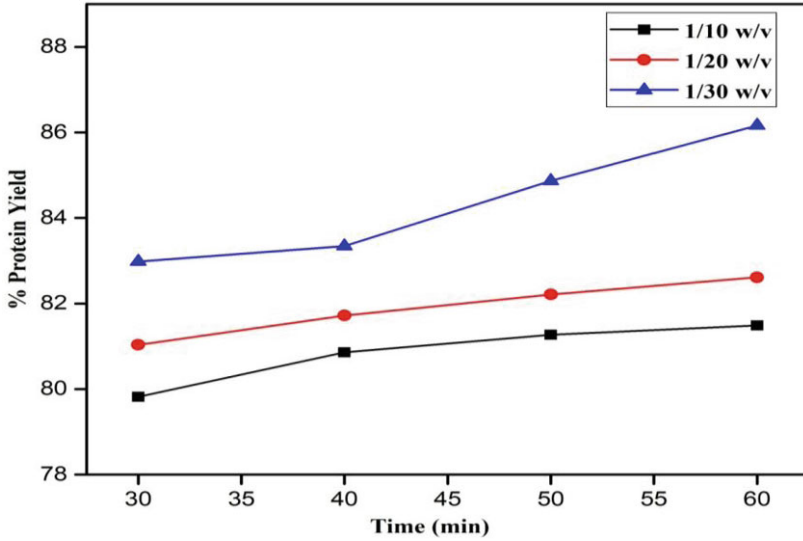
Fig. 7 Extraction time versus %protein yield at 60 °C
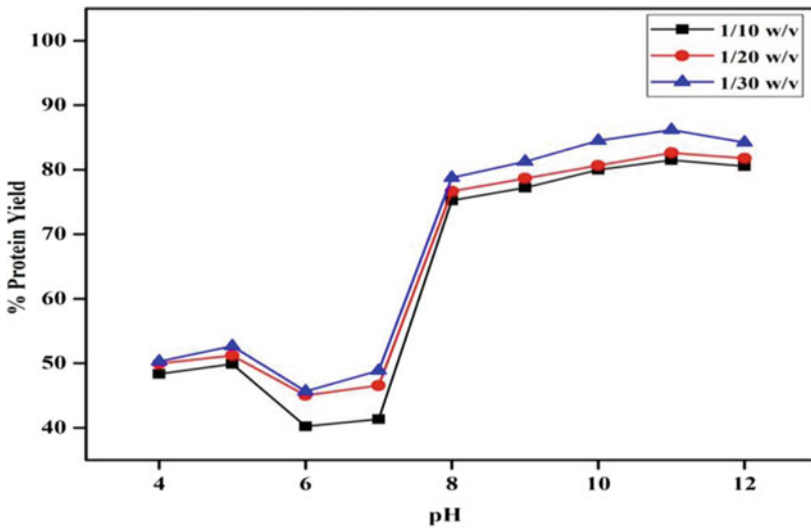
Fig. 8 Extraction pH versus % protein yield

3.4.3 Effect of Flour to Water Ratio on Protein Yield

The influence of flour to water ratio on protein yield was also investigated. Three different flour to water ratios i.e. 1:10, 1:20 and 1:30 were used for the extraction of protein at optimum pH value of 11 and optimum temperature of 60 °C. When

Fig. 9 Flour to water ratio versus % protein yield
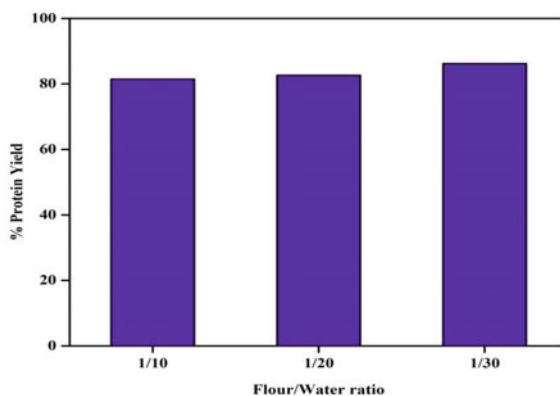
the flour to water ratio was low, due to water adsorption cottonseed flour swelled up which increased the viscosity and the obtained protein amount was found to be low as compared to higher flour to water ratio. Results indicated that there was an increase in protein yield when we increased flour to water ratio from 1:10 to 1:20 and then to flour to water ratio of 1:30 as shown in Fig. 9. Further, increase in flour to water ratio does not produce significant difference as it would produce less amount of protein from extraction (Zhang et al. 2009).

3.4.4 Effect of Centrifugal Speed on Protein Yield

The effect of centrifugal speed was studied to observe its effect on protein extraction. Different centrifugal speeds were tested at 5000, 6000, 6500, 7000 rpm. The results obtained showed that as centrifugal speed increases from 5000 to 7000 rpm, there was significant increase in the protein yield as shown in Fig. 10. At the centrifugal speed of 7000 rpm, maximum amount of protein got deposited in the centrifuge tubes. Hence 7000 rpm centrifugal speed was taken as the optimum speed.

The progressive increase in the protein yield might be due to higher compaction rate of solid phase as centrifugal speed was increased (Kain et al. 2009).

3.5 Functional Properties of Cottonseed Protein Isolate

3.5.1 Water Holding Capacity

Water holding capacity is a very important functional property which is used in determining how the protein interacts with water. This assessment of the protein provides a good idea about how the protein interacts with the food stuff like breads, gravies and sauces. Table 1 indicates the water holding capacity of the defatted
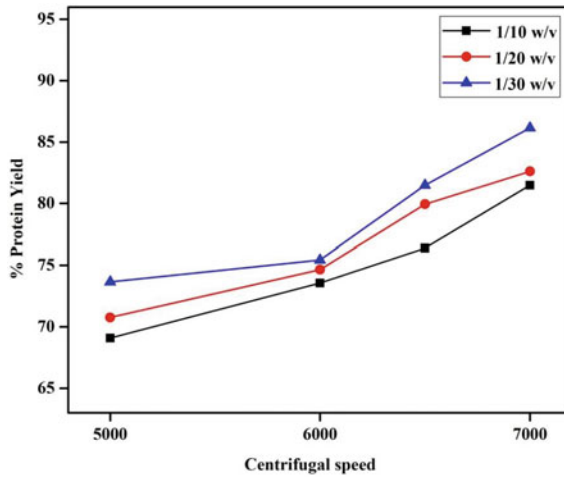
Fig. 10 Centrifugal speed versus % protein yield

Table 1 Water holding capacity

S. No.	Samples	Water holding capacity (g of water/g of protein)
1	Defatted flour	4.42 ± 0.03
2	1:10	3.3 ± 0.22
3	1:20	3.36 ± 0.46
4	1:30	3.61 ± 0.34

cottonseed flour and protein samples at different flour to water ratios. The results indicated that protein samples hold almost similar water content when compared with each other but certainly less as compared to the defatted cottonseed flour.

The water holding capacity is linked with the suitable amino acid composition, proportion of surface polarity to surface hydrophobicity and the structure of protein (Yu et al. 2020).

3.5.2 Oil Holding Capacity

The oil holding capacity is a very important functional property as the oil -protein interactions have an impact on the emulsifying abilities, texture and flavor of food. It is the composition of amino acids, protein conformation and surface polarity which affects the oil holding capacity of food proteins. Table 2 shows the oil holding capacities of the defatted cottonseed flour and protein samples prepared at different flour to water ratios. The result showed improvement in the oil holding capacities of the protein isolate samples over defatted cottonseed flour. The oil binding capacities can

Table 2 Oil holding capacity

S. No.	Samples	Oil holding capacity (g of oil/g of protein)
1	Defatted flour	4.8 ± 0.02
2	1:10	5.4 ± 0.4
3	1:20	5.2 ± 0.36
4	1:30	± 0.27

be linked to diverse protein type and hydrophobicity of cottonseed protein isolates (Malik et al. 2017).

3.5.3 Foaming Capacity

Foaming capacity was determined for the defatted cottonseed flour and the cottonseed protein isolate. Foaming formation is governed by penetration, transportation and reorganization of molecules (Ma et al. 2018). Figure 11 below shows the foaming capacity results which indicated improvement in the foaming capacity of the cottonseed protein isolate as compared to the defatted cottonseed flour. The obtained foaming capacity for cottonseed protein isolate was found to be 49%. The improved foaming capacity could be linked to heating, as on heating the structure of protein unfolds and exposes hydrophobic sites which may be absorbed more quickly to air-water interface, decreases interfacial tension and increasing the foaming capacity by trapping more air (Mauer 2003). The foaming capacity was calculated by measuring the foam volume after whipping using Eq. 1 below.

$$\text{Foam capacity \%} = [V_{foam}(f)/V_i] \times 100 \tag{1}$$

Fig. 11 Time versus foam volume
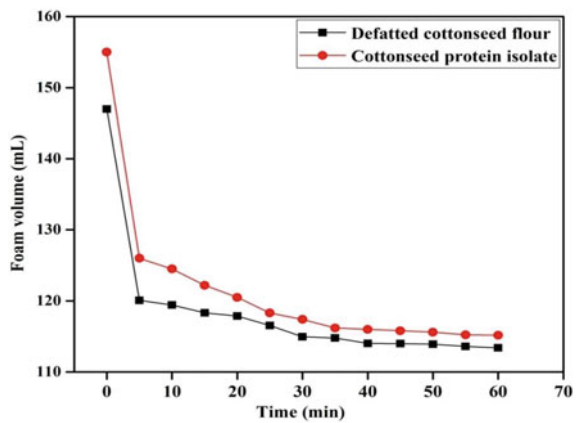
where $V_{foam}(f)$—Volume of foam after whipping and V_i—Initial volume.

3.5.4 CHN Analysis

CHN analysis was conducted for the defatted cottonseed flour and the protein isolates at different flour to water ratios (F/W). The results of CHN analysis for the defatted cottonseed flour are shown in Table 3 and Fig. 12. The results of CHN analysis for

Table 3 Elemental analysis of the defatted cottonseed flour

S. No.	Retention time (min)	Component	Element percentage
1	0.792	Nitrogen	7.519
2	1.267	Carbon	41.766
3	6.450	Hydrogen	5.864
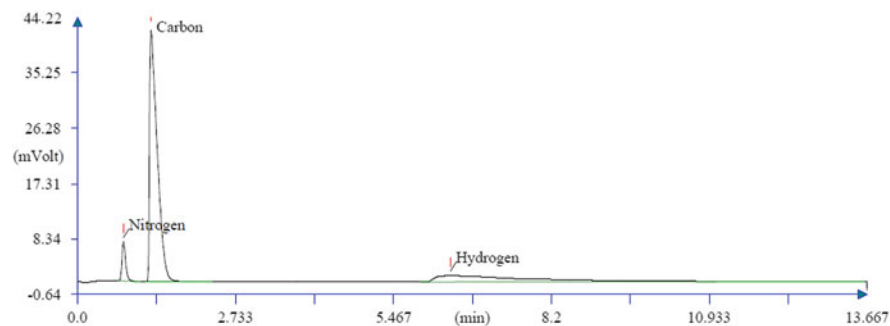
Fig. 12 Graphical representation of elemental analysis (CHN) of defatted cottonseed flour

Table 4 Elemental analysis of 1:10 (F/W) cottonseed protein isolate

S. No.	Retention time (min)	Component	Element percentage
1	0.792	Nitrogen	13.038
2	1.267	Carbon	46.650
3	6.467	Hydrogen	6.635

Table 5 Elemental analysis of 1:20 (F/W) cottonseed protein isolate

S. No.	Retention time (min)	Component	Element percentage
1	0.758	Nitrogen	13.218
2	1.192	Carbon	45.953
3	5.692	Hydrogen	5.434

1:10, 1.20 and 1.30 flour to water ratios are shown in Tables 4, 5 and 6, and Figs. 13, 14 and 15.

1. CHN analysis for defatted cottonseed flour
2. CHN analysis of 1:10 (F/W) cottonseed protein isolate
3. CHN analysis of 1:20 (F/W) cottonseed protein isolate
4. CHN analysis of 1:30 (F/W) cottonseed protein isolate

Nitrogen is the main amino acid element and amino acids are the construction blocks of all the proteins. The above mentioned results of CHN analysis provided

Table 6 Elemental analysis of 1:30 (F/W) cottonseed protein isolate

S. No.	Retention time (min)	Component	Element percentage
1	0.800	Nitrogen	13.786
2	1.233	Carbon	45.287
3	5.567	Hydrogen	8.062
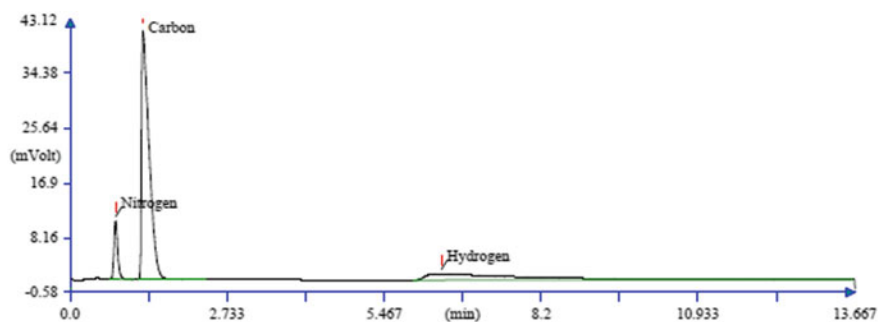
Fig. 13 Graphical representation of elemental analysis of 1:10 (F/W) cottonseed protein isolate
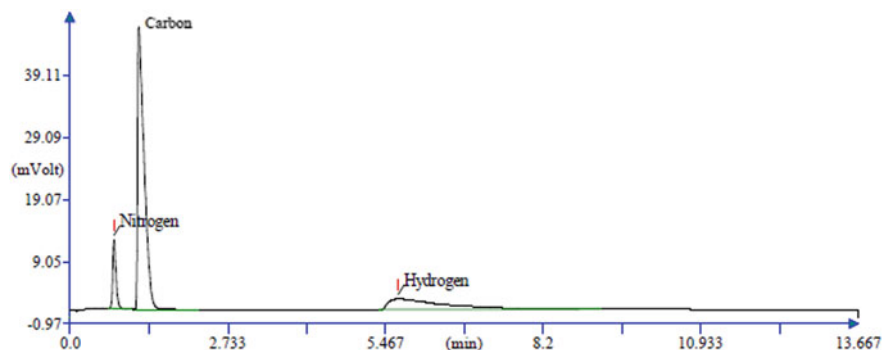
Fig. 14 Graphical representation of elemental analysis of 1:20 (F/W) cottonseed protein isolate
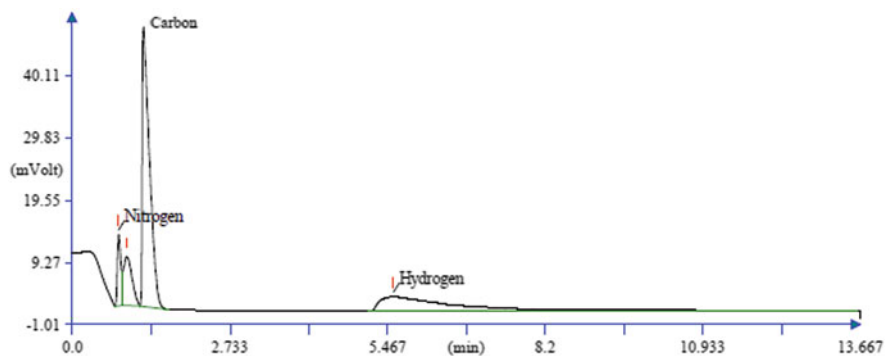
Fig. 15 Graphical representation of elemental analysis of 1:30 (F/W) cottonseed protein isolate

the elemental percentage of nitrogen in each protein/flour sample. The maximum percentage of nitrogen was obtained at 1:30 (w/v) cottonseed protein isolate.

3.5.5 Determination of Protein Content for Different Cottonseed Protein Isolates and Flour

For calculation of protein content in each sample the nitrogen content in each the sample was multiplied with a factor of 6.25 (nitrogen conversion factor). The results of protein content in the cottonseed flour and protein isolate samples are shown in Table 7.

As per standards of Food Safety and Standards Authority of India (FSSAI) (2011), crude protein content should be equal to or more than 47% by weight. Defatted cottonseed flour did not meet the standards as protein content is less than 47% but the cottonseed protein isolates have a very high value and thus meet the standards of FSSAI.

Table 7 Protein content for different samples

S. No.	Sample	Nitrogen %	Protein % (N% * 6.25)
1	Defatted cottonseed flour	7.519	46.993
2	1:10	13.038	81.487
3	1:20	13.218	82.612
4	1:30	13.786	86.162

Table 8 Ash content analysis

S. No.	Samples	Ash content (%)
1	Defatted flour	8.03 ± 0.02
2	1:10	1.09 ± 0.14
3	1:20	1.03 ± 0.26
4	1:30	0.97 ± 0.17

Table 9 Ash insoluble ash content (%)

S. No.	Samples	Acid insoluble ash content (%)
1	Defatted flour	1.41 ± 0.07
2	1:10	0.83 ± 0.11
3	1:20	0.88 ± 0.05
4	1:30	0.79 ± 0.06

3.6 Proximate Analysis

3.6.1 Ash Content

Ash content test was conducted on the defatted cottonseed flour and the protein isolate samples which were prepared at different flour to water ratio that is 1:10, 1:20 and 1:30 (w/v) using method of Kadam et al. (2013). Table 8 shows the results of ash content test and it clearly indicated that there was a significant change in the ash content in the protein isolates as compared to the defatted cottonseed flour but there was no significant difference between the ash content of different protein isolates. As per standards of Food Safety and Standards Authority of India (FSSAI) (2011), the maximum limit of total ash content is 5% by weight and obtained results were well within the limit.

3.6.2 Acid Insoluble Ash Content

Acid insoluble ash content was determined using the ash received from the ash content test which was conducted on the flour and different protein samples. Table 9 shows the results of acid insoluble ash content.

3.6.3 Moisture Content

Moisture content was obtained for defatted cottonseed flour and the protein isolate samples which were prepared at different flour to water ratios that are 1:10, 1:20 and 1:30 (w/v). Table 10 shows the values of the moisture content for all the above mentioned samples. The results showed that the moisture content in the defatted

Table 10 Moisture content analysis

S. No.	Samples	Moisture content (%)
1	Defatted flour	7.7 ± 0.08
2	1:10	5.4 ± 0.14
3	1:20	5.39 ± 0.11
4	1:30	5.46 ± 0.09

cottonseed flour and the protein samples is almost comparable and there is no considerable difference. The observed results were in accordance with the standards of Food Safety and Standards Authority of India (FSSAI) (2011), where the maximum limit of moisture content is 8% by weight.

4   Conclusions

The extraction of cottonseed protein isolate from defatted cottonseed flour was performed utilizing alkaline extraction and acidic precipitation method. The optimum conditions obtained for precipitation of cottonseed protein isolate included pH-11, iso-electric point obtained was at pH-4.5, extraction time-60 min, temperature 60 °C and 1:30 (w/v) flour to water ratio and 7000 rpm centrifugal speed.

The protein content in defatted flour was found to be 46.99% while the protein content in the isolate prepared using optimum flour to water ratio [1:30 (w/v)] was 86.16%. Water holding capacity for defatted flour obtained was 4.42 (g of water/ g of protein), while for the protein isolate prepared using optimum flour to water ratio was 3.61 (g of water/g of protein) respectively. Oil holding capacity for the defatted flour obtained was 4.8 (g of oil/ g of protein) while for the protein isolate prepared using optimum flour to water ratio was 5.49 (g of oil/ g of protein) respectively.

The functional properties of cottonseed protein isolates like water holding capacity, oil holding capacity, foaming volume and proximate analysis showed significant improvement of quality as compared to the cottonseed flour utilized and it was concluded that the protein isolates can be used effectively for producing food products.

Conflict of Interest The authors declare no conflict of interest.

References

Agarwal DK, Singh P, Chakrabarty M, Shaikh AJ, Gayal SG (2003) Cottonseed oil quality utilization and processing; CICR Technical Bulletin No. 25. Central Institute for Cotton Research Nagpur: Maharashtra, India, pp 1–16

Babayan VK, Koottungal D, Halaby GA (1978) Proximate analysis, fatty acid and amino acid composition of Nigella sativa L. seeds. J Food Sci 43(4):1314–1315

Baden HP, Kubilus J (1984) A comparative study of the immunologic properties of hoof and nail fibrous proteins. J Investig Dermatol 83(5):327–331

Bajjalieh N (2002) Proteins from oilseeds. Protein sources for the animal feed industry, pp 141–159

Brown GM, Reynolds JJ (1963) Biogenesis of the water-soluble vitamins. Ann Rev Biochem 32(1):419–462

Buffo RA, Han JH (2005) Films and coatings from plant origin proteins. In: Innovations in food packaging, pp 277–300

Carbone JW, Pasiakos SM, Vislocky LM, Anderson JM, Rodriguez NR (2014) Effects of short-term energy deficit on muscle protein breakdown and intramuscular proteolysis in normal-weight young adults. Appl Physiol Nutr Metab 39(8):960–968

Chen W, Ding J, Yan X, Yan W, He M, Yin G (2019) Plasticization of cottonseed protein/polyvinyl alcohol blend films. Polymers 11(12):2096

Cheng HN, Dowd MK, He Z (2013) Investigation of modified cottonseed protein adhesives for wood composites. Ind Crops Prod 46:399–403

Cherry JP, Berardi LC, Zarins ZM, Wadsworth JI, Vinnett CH (1978) Cottonseed protein derivatives as nutritional and functional supplements in food formulations. In: Nutritional improvement of food and feed proteins, pp 767–796

Coulthard MG (2015) Oedema in kwashiorkor is caused by hypoalbuminaemia. Paediatr Int Child Health 35(2):83–89

Cui Z (2005) Protein separation using ultrafiltration- an example of multi-scale complex systems. China Particuol 3(6):343–348

Diallinas G (2014) Understanding transporter specificity and the discrete appearance of channel-like gating domains in transporters. Front Pharmacol 5:207

Fadeeva VP, Tikhova VD, Nikulicheva ON (2008) Elemental analysis of organic compounds with the use of automated CHNS analyzers. J Anal Chem 63(11):1094–1106

Food safety and standards (food products standards and food additives) Regulations, 2011. https://www.fssai.gov.in/upload/uploadfiles/files/Compendium_Food_Additives_Regulations_08_09_2020-compressed.pdf

Gahlawat SK, Salar RK, Siwach P, Duhan JS, Kumar S, Kaur P (2017) Plant biotechnology: recent advancements and developments. In: Plant biotechnology: recent advancements and developments, pp 1–390

Gupta RD, Gupta SK (2016) Strategies for increasing the production of oilseed on a sustainable basis. In: Breeding oilseed crops for sustainable production: opportunities and constraints, pp 1–18

Hamm LL, Nakhoul N, Hering-Smith KS (2015) Acid-base homeostasis. Clin J Am Soc Nephrol 10(12):2232–2242

Hankins J (2006) The role of albumin in fluid and electrolyte balance. J Infus Nurs 29(5):260–265

Hathcock JN (1997) Vitamins and minerals: efficacy and safety. Am J Clin Nutr 66(2):427–437

He Z, Cao H, Cheng HN, Zou H, Hunt JF (2013) Effects of vigorous blending on yield and quality of protein isolates extracted from cottonseed and soy flours. Modern Appl Sci 7(10):79–88

He Z, Zhang H, Olk DC (2015) Chemical composition of defatted cottonseed and soy meal products. PLoS ONE 10(6):1–13

He Z, Cheng HN, Olanya OM, Uknalis J, Zhang X, Koplitz BD, He J (2018) Surface characterization of cottonseed meal products by SEM, SEM-EDS, XRD and XPS analysis. J Med Sci Res 7(1):28–40

Kadam VB, Momin RK, Wadikar MS, Andhale SB (2013) Determination of acid insoluble ash values of some medicinal plants of genus Sesbania. J Biomed Pharmaceut Res 2(5):31–34

Kain RJ, Chen Z, Sonda TS, Abu-Kpawoh JC (2009) Study on the effect of control variables on the extraction of peanut protein isolates from peanut meal (Arachishypogaea L.). Am J Food Technol 4(1):47–55

Kumar M, Tomar M, Punia S, Grasso S, Arrutia F, Choudhary J, Singh S, Verma P, Mahapatra A, Patil S, Dhumal S (2021) Cottonseed: A sustainable contributor to global protein requirements. Trends Food Sci Technol 111:100–113

Leah CB, John PC (1981) Functional properties of co-precipitated protein isolates from cottonseed, soybean and peanut flours. Can Inst Food Sci Technol J 14(4):283–288

Li P, Yin YL, Li D, Kim SW, Wu G (2007) Amino acids and immune function. Br J Nutr 98(2):237–252

Liu M, Wang Y, Wu Y, He Z, Wan H (2018) Greener adhesives composed of urea-formaldehyde resin and cottonseed meal for wood-based composites. J Clean Prod 187:361–371

Ma M, Ren Y, Xie W, Zhou D, Tang S, Kuang M, Wang Y, Du SK (2018) Physicochemical and functional properties of protein isolate obtained from cottonseed meal. Food Chem 240:856–862

Malik MA, Sharma HK, Saini CS (2017) High intensity ultrasound treatment of protein isolate extracted from dephenolized sunflower meal: effect on physicochemical and functional properties. Ultrasonics Sonochem 39:511–519

Mauer L (2003) Protein| heat treatment for food proteins. In: Encyclopedia of food sciences and nutrition, pp 4868–4872

Moure A, Sineiro J, Domínguez H, Parajó JC (2006) Functionality of oilseed protein products: a review. Food Res Int 39(9):945–963

Phillips SM, Fulgoni VL III, Heaney RP, Nicklas TA, Slavin JL, Weaver CM (2015) Commonly consumed protein foods contribute to nutrient intake, diet quality and nutrient adequacy. Am J Clin Nutr 101(6):1346–1352

Ravisankar P, Reddy AA, Nagalakshmi B, Sai O, Kumar BV, Anvith PS (2015) The comprehensive review on fat soluble vitamins. IOSR J Pharm 5(11):12–28

Rosenthal A, Pyle DL, Niranjan K (1998) Simultaneous aqueous extraction of oil and protein from soybean: Mechanisms for process design. Food Bioprod Process: Trans Inst Chem Eng Part C 76(4):224–230

Sekhar SC, Rao BVK (2011) Cottonseed oil as health oil. Pertanika J Trop Agric Sci 34(1):17–24

Shah DK (2012) Bt cotton in India: a review of adoption, government interventions and investment initiatives. Indian J Agric Econ 67(3):67854

Shao YY, Lin KH, Kao YJ (2016) Modification of foaming properties of commercial soy protein isolates and concentrates by heat treatments. J Food Qual 39(6):695–706

Sharif I, Farooq J, Chohan SM, Saleem S, Kainth RA, Mahmood A, Sarwar G (2019) Strategies to enhance cottonseed oil contents and reshape fatty acid profile employing different breeding and genetic engineering approaches. J Integr Agric 18(10):2205–2218

Stroher R, Stenzel M, Pereira NC, Zanin GM (2011) Enzymatic extraction of protein from toasted and not toasted soybean meal. Procedia Food Sci 1:463–469

Tsaliki E, Kechagia U, Doxastakis G (2002) Evaluation of the foaming properties of cottonseed protein isolates. Food Hydrocolloids 16(6):645–652

Tsaliki E, Pegiadou S, Doxastakis G (2004) Evaluation of the emulsifying properties of cottonseed protein isolates. Food Hydrocolloids 18(4):631–637

Wong JH, Ng TB, Cheung RC, Ye XJ, Wang HX, Lam SK, Liu F (2010) Proteins with anti-fungal properties and other medicinal applications from plants and mushrooms. Appl Microbiol Biotechnol 87(4):1221–1235

Wu G (2016) Dietary protein intake and human health. Food Funct 7(3):1251–1265

Yu J, Ahmedna M, Goktepe I (2007) Peanut protein concentrate: Production and functional properties as affected by processing. Food Chem 103(1):121–129

Yu N, Jiang C, Ning F, Hu Z, Shao S, Zou X, Xiong H (2020) Protein isolate from Staunto-niabrachyanthera seed: chemical characterization, functional properties, and emulsifying performance after heat treatment. Food Chem 345:128542

Yue HB, Cui YD, Shuttleworth PS, Clark JH (2012) Preparation and characterisation of bioplastics made from cottonseed protein. Green Chem 14(7):2009–2016

Zhang B, Cui Y, Yin G, Li X, Zhou X (2009) Alkaline extraction method of cottonseed protein isolate. Modern Appl Sci 3(3):48–51

Zhang Z, Wang Y, Dai C, He R, Ma H (2018) Alkali extraction of rice residue protein isolates: Effects of alkali treatment conditions on lysinoalanine formation and structural characterization of lysinoalanine-containing protein. Food Chem 261:176–183

Zhuge Q, Posner ES, Deyoe CW (1988) Production study of a low-gossypol protein product from cottonseed meal. J Agric Food Chem 36(1):153–155

MOF Encapsulated Beads for Fluoride Removal from Water

Ranjana Kumari, Anil Kumar, and Subhankar Basu

Abstract Drinking of fluoride-containing groundwater is reported to cause dental and skeletal fluorosis. However, fluoride is also essential for bone mineral density. The world health organization (WHO) has recommended that 1–1.5 mg F/L is safe for human consumptions. Although several treatment methods have been reported over the years, adsorption is the most widely reported technology till date. However, using powder materials as an adsorbent is often challenging to scale up, regenerate, and reuse. Thus, deter its broader applications. Recently, some of the porous metal-organic frameworks (MOFs) have shown super adsorption of fluoride in water. However, MOFs are usually unstable in water and at room temperature. Recently, Aluminium fumarate (AlFu) MOF has been found to be effective in fluoride removal from water. In this study, AlFu was synthesized and study its applicability in water treatment. It has been encapsulated in the polymer matrix as porous beads with well-defined channels for water diffusion. The capsules of the AlFu-polymer mix were solidified in a water bath by the phase-inversion process. The material was studied in batch reactors and fixed column bed reactors under optimized conditions for maximum removal. The results show complete removal of fluoride from water within few hours of study. Thus, encapsulation of AlFu shows a way forward to reuse and regenerate the materials.

Keywords Aluminium Fumarate · Encapsulation · Fluoride · Removal · Reuse

1 Introduction

Fluoride contamination of groundwater is a serious issue worldwide (Ayoob and Gupta 2006). The sources of fluoride in groundwater are geogenic and anthropogenic (human activities). The weathering of rocks (fluorspar, chlorite, muscovite, and apatite) resulted in the dissolution of fluoride in groundwater. Fluoride (0.7 mg/L)

R. Kumari · A. Kumar · S. Basu (✉)
Department of Applied Sciences and Humanities, National Institute of Advanced Manufacturing Technology (NIAMT), Ranchi, Jharkhand, India
e-mail: subhankarb@niamt.ac.in

in drinking water is considered beneficial for bone growth and preventing dental caries. However, excess fluoride in drinking water causes dental and skeletal fluorosis. The world health organization (WHO) has recommended fluoride concentration in drinking water as 1.0–1.5 mg/L. In rural areas of developing countries, the groundwater is directly consumed from artesian wells and hand pumps, without any water purification steps. The average fluoride concentration in groundwater is reported up to 30 mg/L (Karmakar et al. 2017).

Many technologies have been developed for fluoride removal from contaminated water. They may be broadly classified into four categories (i) electro-coagulation and coagulation (Hu et al. 2005), (ii) chemical precipitation (Turner et al. 2005), (iii) membrane process (reverse osmosis, ion-exchange) (Ndiaye et al. 2005; Durmaz et al. 2005), and (iv) adsorption (Zhang et al. 2014a; Wu et al. 2007; Tripathy et al. 2006; Sahli et al. 2007). Out of these, ion exchange and reverse osmosis are expensive to use and mainly used in household water filters and small urban community water supply systems. On the other hand, the adsorption process is widely used because it is eco-friendly and can remove fluoride effectively at a low cost (Dhillon et al. 2017). Activated alumina (Chatterjee and De 2014), alum impregnated with activated alumina (Tripathy et al. 2006), hydrous zirconium oxide (Dou et al. 2012), and calcium oxide modified activated alumina (Camacho et al. 2010) and aluminium hydroxide impregnated limestones (Jain and Jayaram 2009) are some of the adsorbents that can be used for defluoridation.

The adsorption process is pH sensitive, slow rate of adsorption and low fluoride uptake capacity compared to the recently developed fluoride adsorption materials e.g. metal–organic frameworks (MOFs). MOFs are characterized by high surface area to volume ratio, multifunctional groups, and highly ordered atomic arrangements (Karmakar et al. 2016). ZIF-7, ZIF-8, AlFu, MIL-96(Al), MIL-88A (Fe), MIL-53(Cr), MIL-53(Fe), UiO-66 and MOF-801 are some of the MOFs that have been effectively used for fluoride adsorption (Karmakar et al. 2016; Kumar et al. 2017; Zhao et al. 2014; Lin et al. 2016; Zhang et al. 2014b; Ke et al. 2016). AlFu MOF shows the highest adsorption capacity (600 mg/g) (Karmakar et al. 2016).

AlFu MOF is highly stable in water and at room temperature. It contains boundless Al-OH-Al chains joined with fumarate linkers. It has high fluoride adsorption capacity because of its high surface area (1156 m^2/g), wide pH stability, and microporous structure. However, disposal of saturated power adsorbents is challenging. Unlike powder activated carbon which is used for removal of organics, and regenerated by thermal activation, MOFs used to remove fluoride are not possible to regenerate by the same process. Also, the nano-sized MOFs tend to agglomerate in water. Further, desorption of fluoride from saturated MOFs using organic solvents and further recovering those solvents is not cost-effective. Some of the current methods of overcoming such issues are (i) MOF-electrospinning nanofibers (Dou et al. 2020) and (ii) encapsulation of nanoparticles (Munoz and Nieto-Sandoval 2021). It helps in regenerating the MOFs after use and could be used repeatedly.

The motivation of this study was to prepare an easy-to-use material that could be used for the removal of fluoride from water, and it could be regenerated for repeated use. In this study, AlFu MOF has encapsulated in a polyethersulfone (PES) matrix and

solidified in the water bath. The resulting material appears as porous adsorbent beads. The fluoride removal performance of the beads was studied at different adsorbent doses, adsorption timing, initial fluoride concentration, and temperature in batch reactors. A continuous flow system was studied in a fixed-bed column reactor. The adsorption performance and its reusability were investigated.

2 Materials and Methods

2.1 Materials

N,N-Dimethyl formamide (DMF), sodium fluoride (NaF) and aluminium sulphate 16-hydrate $[Al_2(SO_4)_3.16H_2O]$ were purchased from Merck Life Science Pvt. Ltd. Fumaric acid was purchased from Loba Chemie Pvt. Ltd. Sodium hydroxide (NaOH) and hydrochloric acid were purchased from HiMedia Laboratories Pvt. Ltd. Polyethersulfone (PES) was purchased from Tech. Inc. Ltd. Chennai India. All the chemicals were of analytical grade and were used as received from the suppliers.

2.2 Preparation of AlFu MOF and Adsorbent Beads

The AlFu MOF was prepared by adding solution B in solution A. Solution A was prepared by dissolving 18.55 g of $[Al_2(SO_4)_3.16H_2O]$ in 79.5 mL deionized water. The solution was heated at 60 °C for 1 h in an orbital shaker (Yorco Sales, Delhi, India). Similarly, solution B was prepared by adding 6.45 g of fumaric acid and 4.75 g of NaOH in 95.5 mL deionized water. The solutions were mixed and heated at 60 °C for 2 h in an orbital shaker at 60 rpm. The white precipitated AlFu MOF was washed with deionized water for several times in a centrifuge at 2000 rpm for 30 min. The material was dried in hot air oven (i-therm, Mumbai, India) at 105 °C. It was then mortar pestle into a fine powder (Lakra et al. 2021).

Required amount of AlFu MOF (0, 0.5, 1.0, 1.5, 2.0, 2.5 g) powder was added in 1 g PES and 10 mL DMF solution. The resulting solution was stirred for 8 h and then kept idle for de-bubbling. The solution was filled in a 50 mL syringe and the solution was added drop wise in the water bath at room temperature. Immediately phase inversion between water and DMF took place, resulted in the solidification of the beads. The beads were left in the water bath for an hour. The floating beads were then separated from the water. Hereafter the beads are termed as C0 (AlFu: 0 g), C5 (AlFu: 0.5 g), C10 (AlFu: 1.0 g), C15 (AlFu: 0.5 g), C20 (AlFu: 2.0 g), and C25 (AlFu: 2.5 g). The beads were washed with DI water several times.

2.3   Batch Adsorption Experiments

Stock solution of 100 mg/L of fluoride was prepared by dissolving 0.22 g NaF salt in 1L deionized water. Feed solutions 4 to 10 mg/L were prepared by dissolving the stock solution. Batch adsorption experiments were conducted in 500 mL plastic container. Prepared beads were added in 100 mL synthetic fluoride solutions and kept in an orbital incubator shaker at 110 rpm for desired time and temperature. After that the adsorbents were separated from the fluoride containing solution. The fluoride concentrations of initial and final solutions were measured by Fluoride Meter (Extech Instruments, FL700, USA). The fluoride removal efficiency (R%) was calculated using Eq. (1),

$$R(\%) = (C_o - C_f)x100/C_o \tag{1}$$

where C_o and C_f are the initial and final fluoride concentrations respectively.

Optimum conditions for maximum fluoride removal was determined by varying the (1) percentage of beads (0–25 wt%), adsorbent dose (2.5–15 g/L), adsorption time (1–5 h), initial fluoride concentration (4–10 mg/L) and operating temperature (30–45 °C). Effect of pH on the adsorbent performance was conducted by adjusting the pH of the synthetic fluoride solution from 2.5 to 12 using HCl (0.1 M) and NaOH (0.1 M).

2.4   Reusability Study

In order to check the reusability performance of the prepared AlFu-beads, first 1 g beads were added in 100 mL synthetic feed solution with fluoride concentration 10 mg/L, and then put in an orbital shaker at optimized operating condition. However, the spent adsorbent was dipped into the deionized water for 5 min for its regeneration and then added in new fluoride solution ($C_0 = 10$ mg/L). This process was repeated for at least 5 cycles.

2.5   Continuous Column Study

Continuous column study was carried out in a lab scale borosilicate glass cylindrical tube of height 50 cm and diameter 1 cm. The beads were packed in the column. 500 mL of fluoride solution ($C_0 = 25$ mg/L and pH = 6) was pumped upward with a flow velocity of 100 mL/min through the fixed bed of different bed heights (7.5, 15, 30 and 45 cm). Fluoride removal (%) was measured at varying reaction time. Figure 1 shows the schematic representation of the set-up.
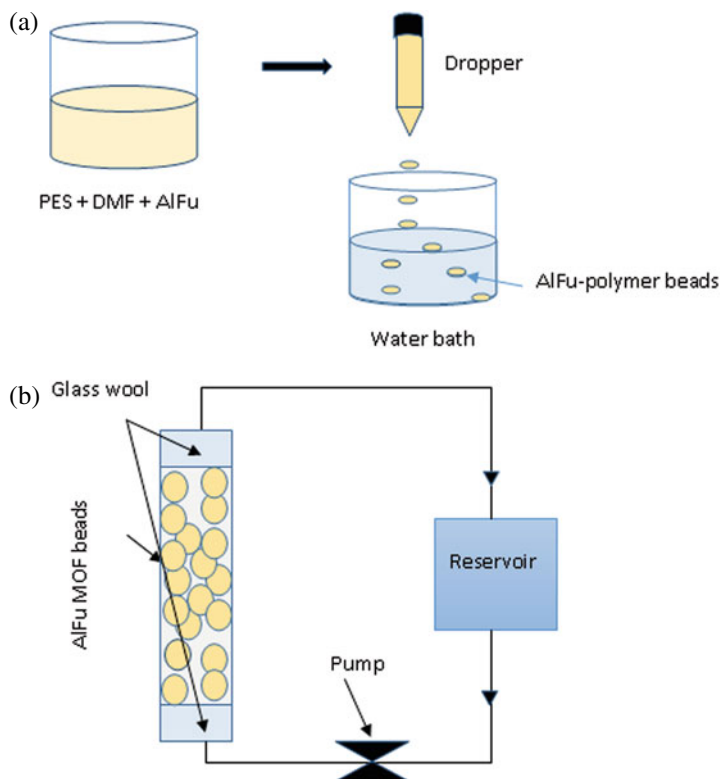
Fig. 1 Schematic representation of **a** preparation of AlFu MOF beads, **b** column study

3 Results and Discussion

3.1 *Characterization of the AlFu MOF Beads*

The characteristics (powder X-ray diffraction (XRD) patterns, Fourier-transform infrared-attenuated total reflection (FTIR-ATR) spectroscopy, scanning electron microscopy image, surface area of AlFu MOF is published in our earlier work (Lakra et al. 2021). In this study, Fig. 2a shows that the AlFu MOF beads size ranges between 3 and 5 mm. The beads are spherical in shape. The cross-section view of the beads shows the distribution of AlFu MOF in the polymer matrix (Fig. 2b). The presence of pores in the structure indicates pore channels through which water can pass inside the beads. The surface of the beads is rough at $50\times$ (Fig. 2c). The images (Fig. 2b) and (Fig. 2c) were obtained using OLYMPUS Optical Microscope VX 52, Germany.
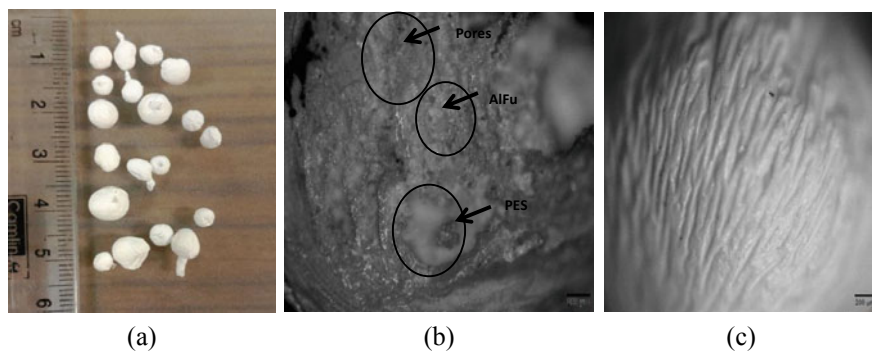
Fig. 2 AlFu MOF beads (**a**), cross section view of beads (50×) (**b**), surface morphology of beads (50**X**) (**c**)

3.2 Performance of Beads in Batch Study

The effect of AlFu concentration on the beads performance was studied with C_0 = 10 mg F/L, t = 5 h, T = 35 °C, and pH = 6 (Fig. 3a). Co shows no fluoride removal. The fluoride removal (%) increased as the beads content increased in the column. It was noticed that the beads with MOF concentration of 15 wt% (C15) or more (C20 and C25) effectively reduced fluoride concentration within the WHO standards of drinking water. The effect of beads dosage on fluoride removal was studied with C15 beads, C_0 = 10 mg F/L, t = 5 h, T = 35 °C, and pH = 6 (Fig. 3b). The optimum adsorption of fluoride occurred after 10 g/L (96%). Therefore, 10 g/L was fixed to carry out the subsequent experiments. The effect of reaction time on fluoride uptake was studied with C15 beads, C_0 = 10 mg F/L, beads dosage = 10 g/L, T = 35 °C, pH = 6 (Fig. 3c). After 3 h of the experiment, the fluoride concentration of feed solution was reduced to 0.6 mg/L. The adsorption process was rapid due to the high intra-particle diffusion of fluoride in AlFu MOF (intra-particle diffusion constant: 12.42 mg g^{-1} h$^{-0.5}$) (Karmakar et al. 2016). The performance of C15 beads was studied at four different fluoride solutions of 4, 6, 8 and 10 mg F/L (Fig. 3d). Experiment was carried out at beads dosage = 10 g/L, t = 3 h, T = 35 °C and pH = 6. For all the solutions (4, 6, 8 and 10 mg F/L), fluoride concentration reduced to the WHO permissible limit. The effect of reaction temperature (30 °C - 45 °C) on fluoride removal was studied with C_0 = 10 mg F/L, beads dosage = 10 g/L, t = 3 h and pH = 6 (Fig. 3e). At all the studied temperature, more than 90% fluoride was removed. The fluoride uptake rate was increased with temperature. It was because of negative values of Gibbs free energy at all the reaction temperatures (Karmakar et al. 2016). The effect of pH on fluoride uptake was studied with C_0 = 10 mg F/L, beads dosage = 10 g/L, t = 3 h, T = 35 °C. At pH 2–14, beads are stable and the isoelectric point (pH$_{zpc}$) was at pH 8.1 (Karmakar et al. 2016). Figure 3f shows that fluoride removal efficiency decreased with increased pH (2.5 to 12) of the solution. At pH 2.5, 4, 6 and 7.5 fluoride concentration reduced to <1.5 mg/L. However, only
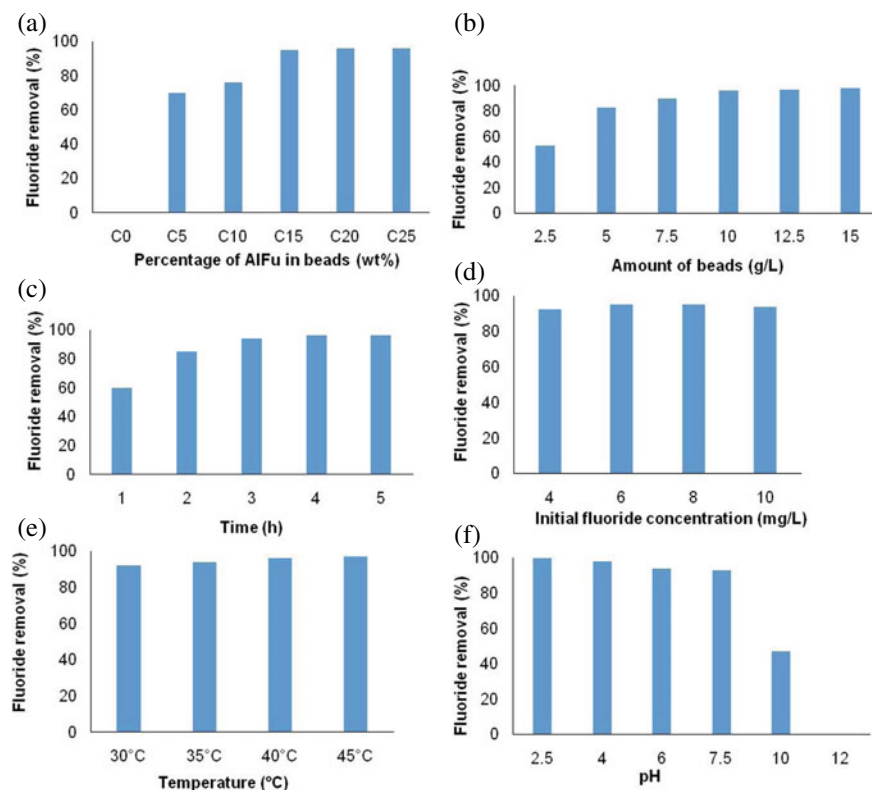
Fig. 3 Fluoride removal of beads at different, **a** AlFu content, **b** amount of beads, **c** reaction time, **d** initial fluoride concentration, **e** temperature, and **f** pH

47% removal was achieved at pH 10. It may be because at higher pH concentration of OH^- ion increased. Hence, the competition between fluoride ion and OH^- ion was increased for active sites on AlFu beads.

3.3 Reuseability of Beads

Figure 4 represents the ability of AlFu-MOF beads to be reused. The initial fluoride concentration was 10 mg/L. After each cycle of operation, the beads were dipped in deionized water for 5 min. The fluoride removal for the first three cycles C1, C2, and C3 was within the WHO standards for drinking water. After three cycles of use, the fluoride removal decreases 72% compared to 94% at C1. Thus, periodic cleaning of the beads extends the potential of its applications.
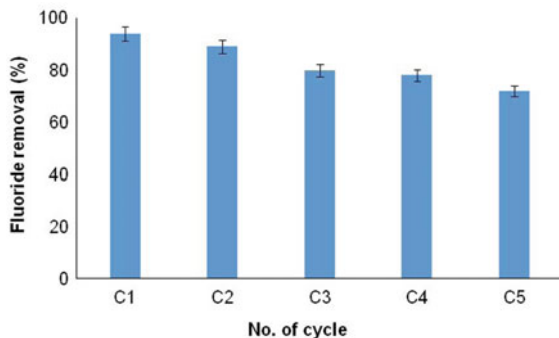
Fig. 4 Reuseability study of AlFu MOF beads for five successive cycles (pH 6, 35 °C)

3.4   Continuous Column Study

Figure 5 shows that the fluoride removal percentage at different bed heights (7.5, 15, 30 and 45 cm) in fixed bed column reactor at $C_o = 25$ mg F/L, pH $= 6$ and flow velocity 100 mL/min. In this study the reaction time at which the fluoride concentration of the treated water was reduced to WHO standards for different bed height's of AlFu MOF beads was reported. The fluoride concentration for bed height of 7.5 cm reduced to 1.5 mg/L within 34 h, for bed height of 15 cm the fluoride content reduced to 0.9 mg/L within 10 h, similarly for bed height of 30 cm it reduced
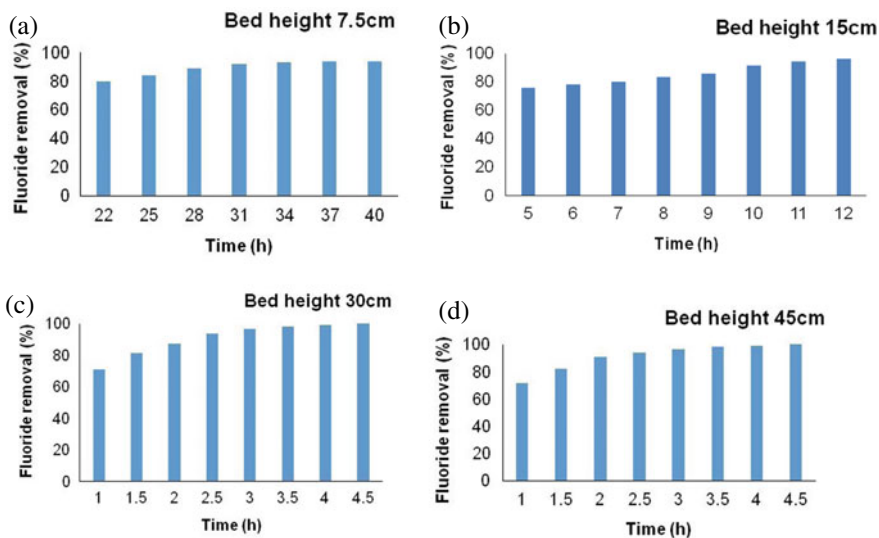
Fig. 5 Removal of fluoride in fixed bed reactor with beads bed height of (a) 7.5, (b) 15, (c) 30 and (d) 45 cm respectively

to 1 mg/L within 2.5 h, and for bed height of 45 cm the fluoride content reduced to 1.1 mg/L within 3 h of reaction time. The fluoride removal increased with an increase in bed height of beads. This is due to the increased adsorption sites with more beads in the column. Thus, the optimum bed height is 30 cm, in which at 2.5 h the fluoride removal is within WHO standards for drinking water.

4 Conclusions

AlFu MOF-PES/DMF beads were prepared and studied for the removal of fluoride from water. Batch experiments show that the beads are stable at a wide pH range and temperature. The beads also show high removal of fluoride from water with the WHO guidelines for drinking water. Furthermore, the beads could be reused several times with periodic cleaning in water. Fixed bed column study with beads at different heights showed that high removal of fluoride at 30 cm column height is possible within 2.5 h of reaction time. Thus, the present study shows that AlFu MOF encapsulated in PES effectively remove fluoride from water and could be easily regenerated and reused. The technique is suitable for treating fluoride contaminated ground water and use for drinking purposes. Further, it could be scale-up for practical applications.

References

Ayoob S, Gupta AK (2006) Fluoride in drinking water: a review on the status and stress effects. Crit Rev Environ Sci Technol 36:433–487. https://doi.org/10.1080/10643380600678112

Camacho LM, Torres A, Saha D, Deng S (2010) Adsorption equilibrium and kinetics of fluoride on sol–gel-derived activated alumina adsorbents. J Colloid Interface Sci 349:307–313. https://doi.org/10.1016/j.jcis.2010.05.066

Chatterjee S, De S (2014) Adsorptive removal of fluoride by activated alumina doped cellulose acetate phthalate (CAP) mixed matrix membrane. Sep Purif Technol 125:223–238. https://doi.org/10.1016/j.seppur.2014.01.055

Dhillon A, Soni SK, Kumar D (2017) Enhanced fluoride removal performance by Ce–Zn binary metal oxide: adsorption characteristics and mechanism. J Fluor Chem 199:67–76. https://doi.org/10.1016/j.jfluchem.2017.05.002

Dou X, Mohan D, Pittman CU, Yang S (2012) Remediating fluoride from water using hydrous zirconium oxide. Chem Eng J 198–199:236–245. https://doi.org/10.1016/j.cej.2012.05.084

Dou Y, Zhang W, Kaiser A (2020) Electrospinning of metal-organic frameworks for energy and environmental applications. Adv Sci 7:1902590–1902611. https://doi.org/10.1002/advs.201902590

Durmaz F, Kara H, Cengeloglu Y, Ersoz M (2005) Fluoride removal by donnan dialysis with anion exchange membranes. Desalination 177:51–57. https://doi.org/10.1016/j.desal.2004.11.016

Hu CY, Lo SL, Kuan WH, Lee YD (2005) Removal of fluoride from semiconductor wastewater by electrocoagulation-flotation. Water Res 39:895–901. https://doi.org/10.1016/j.watres.2004.11.034

Jain S, Jayaram RV (2009) Removal of fluoride from contaminated drinking water using unmodified and aluminium hydroxide impregnated blue limestone waste. Sep Sci Technol 44:1436–1451. https://doi.org/10.1080/01496390902766074

Karmakar S, Dechnik J, Janiak C, De S (2016) Aluminium fumarate metal-organic framework: a super adsorbent for fluoride from water. J Hazard Mater 303:10–20. https://doi.org/10.1016/j.jhazmat.2015.10.030

Karmakar S, Bhattacharjee S, De S (2017) Experimental and modeling of fluoride removal using aluminum fumarate (AlFu) metal organic framework incorporated cellulose acetate phthalate mixed matrix membrane. J Environ Chem Eng 5:6087–6097. https://doi.org/10.1016/j.jece.2017.11.035

Ke F, Luo G, Chen P, Jiang J, Yuan Q, Cai H, Peng C, Wan X (2016) Porous metal-organic frameworks adsorbents as a potential platform for defluoridation of water. J Porous Mater 23:1065–1073. https://doi.org/10.1007/s10934-016-0164-5

Kumar P, Pournara A, Kim KH et al (2017) Metal-organic frameworks: challenges and opportunities for ion-exchange/sorption applications. Prog Mater Sci 86:25–74. https://doi.org/10.1016/j.pmatsci.2017.01.002

Lakra R, Balakrishnan M, Basu S (2021) Development of cellulose acetate-chitosan-metal organic framework forward osmosis membrane for recovery of water and nutrients from wastewater. J Environ Chem 9:105882. https://doi.org/10.1016/j.jece.2021.105882

Lin KYA, Liu YT, Chen SY (2016) Adsorption of fluoride to UiO-66-NH$_2$ in water: stability, kinetic, isotherm and thermodynamic studies. J Colloid Interface Sci 461:79–87. https://doi.org/10.1016/j.jcis.2015.08.061

Munoz M, Nieto-Sandoval J et al (2021) Carbon-encapsulated iron nanoparticles as reusable adsorbents for micropollutants removal from water. Sep Purif Technol 257:117974. https://doi.org/10.1016/j.seppur.2020.117974

Ndiaye PI, Moulln P, Dominguez L, Millet JC, Charbit F (2005) Removal of fluoride from electronic industrial effluent by RO membrane separation. Desalination 173:25–32. https://doi.org/10.1016/j.desal.2004.07.042

Sahli MAM, Annouar S, Tahaikt M, Mountadar M, Soufiane A, Elmidaoui A (2007) Fluoride removal for underground brackish water by adsorption on the natural chitosan and by electrodialysis. Desalination 212:37–45. https://doi.org/10.1016/j.desal.2006.09.018

Tripathy SS, Bersillon JL, Gopal K (2006) Removal of fluoride from drinking water by adsorption onto alum-impregnated activated alumina. Sep Purif Technol 50:310–317. https://doi.org/10.1016/j.seppur.2005.11.036

Turner BD, Binning P, Stipp SLS (2005) Fluoride removal by calcite: evidence for fluorite precipitation and surface adsorption. Environ Sci Technol 39:9561–9568. https://doi.org/10.1021/es0505090

Wu X, Zhang Y, Dou X, Yang M (2007) Fluoride removal performance of a novel Fe-Al-Ce tri-metal oxide adsorbent. Chemosphere 69:1758–1764. https://doi.org/10.1016/j.chemosphere.2007.05.075

Zhang S, Lu Y, Lin X, Su X, Zhang Y (2014a) Removal of fluoride from groundwater by adsorption onto La(III)–Al(III) loaded scoria adsorbent. Appl Surf Sci 303:1–5. https://doi.org/10.1016/j.apsusc.2014.01.169

Zhang N, Yang X, Yu X, Jia Y, Wang J, Kong L, Jin Z, Sun B, Luo T, Liu J (2014b) Al-1,3,5-benzenetricarboxylic metal–organic frameworks: a promising adsorbent for defluoridation of water with pH insensitivity and low aluminum residual. Chem Eng J 252:220–229. https://doi.org/10.1016/j.cej.2014.04.090

Zhao X, Liu D, Huang H, Zhang W, Yang Q, Zhong C (2014) The stability and defluoridation performance of MOFs in fluoride solutions. Micropor Mesopor Mat 185:72–78. https://doi.org/10.1016/j.micromeso.2013.11.002

Non-catalytic and Catalytic Co-pyrolysis of Lignocellulosic-Lignocellulosic Waste

Sourav Poddar and J. Sarat Chandra Babu

Abstract The present investigation involves non-catalytic and catalytic co-pyrolysis. The mixture of sesame oil cake and jute waste sacks in the ratio 1:1 was examined573K to 1173 K for 1 h. Al_2O_3 catalyst was verified to achieve the highest level of performance active catalyst amongst all the catalysts. The yield of co-pyro oil (29 wt% $\rightarrow$ 30.5 wt%) increases with the use of catalyst. The specific surface area of the co-pyro-char increased from 3.435 (non-catalytic) to 5.921 $m^2\,g^{-1}$ (catalytic). The pH values of the co-pyro-oil observed that co-pyro-oil is acidic, but the presence of catalyst makes the co-pyro-oil basic may be due to the absorbance of the catalyst in the oil. GC detected the formation of co-pyro-gas. Therefore, it finds its utilization as liquid fuel from syngas. The present investigation proves that this biomass (the mixture of sesame oil cake and jute waste) without and with catalyst can be used for a large scale pyrolyzer for municipal areas of large metropolitan cities.

Statement of Novelty

The investigation examines non-catalytic and catalytic co-pyrolysis of lignocellulosic-lignocellulosic biomass feedstock. The feed stocks were mixed in the ratio 1:1 and co-pyrolyzed without and with metal oxide and salt catalyst dependence of copyrolytic temperature from the Indian scenario.

S. Poddar · J. Sarat Chandra Babu (✉)
Department of Chemical Engineering, National Institute of Technology Tiruchirappalli,
Tiruchirappalli, Tamil Nadu, India
e-mail: sarat@nitt.edu

S. Poddar
e-mail: spoddar@nitt.edu

Graphical Abstract
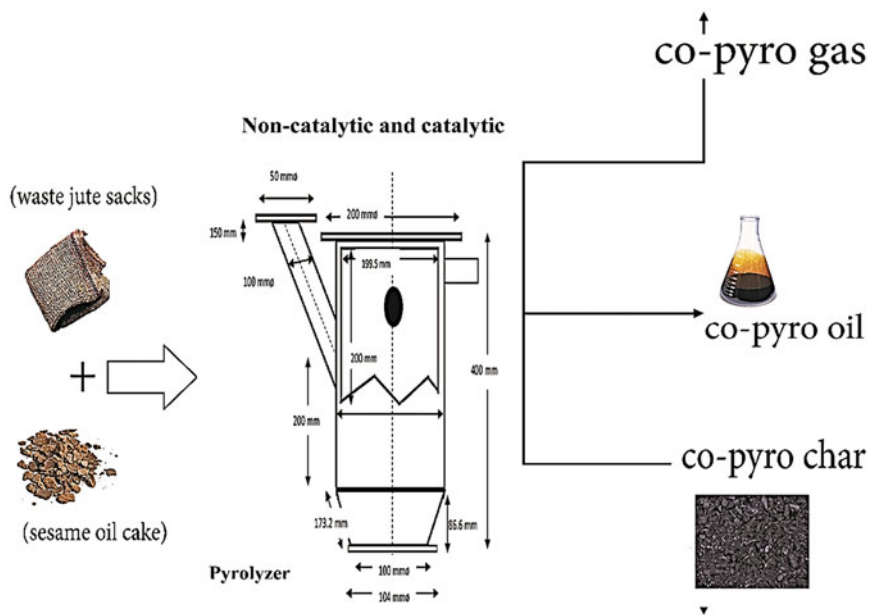
1 Introduction

With the rise of global energy demand, humanity has a severe environmental problem, considering accelerated industrialization, population growth and enhancing lifestyle. The accretion of garbages and the "throw-away philosophy" culminated in severe issues related to the environment, health, freedom and peril and avert sustainable development regarding resource readjustment and recycling waste materials (Özsin and Pütün 2018). Considering the above facts, the conversion of lignocellulosic wastes into biofuels and chemicals has gained importance due to low emission and carbon neutral advantages (Chen et al. 2019). Such conversion technologies have been a feasible waste management blueprint in establishing sustainable waste disposal modes. They are competent for conveying clean energy and contributing better-finished products than other known ways (Özsin and Pütün 2018; Shen et al. 2016). Under such methods, availability and economic and environmental benefits become a crucial factor; it can be seen that biomass wastes, mainly lignocellulosic, have received importance in the recent few years (Özsin and Pütün 2018; Poddar et al. 2015, 2014; Dewangan et al. 2016; Ning et al. 2013). There are mainly two types of methods, thermochemical and biochemical. The thermochemical techniques (Processing 2011) comprise combustion (>573 K), slow pyrolysis (623–1073 K),

torrefaction (473–573 K), fast pyrolysis (673–873 K), flash pyrolysis (573–1073 K), gasification (973–1773 K), etc. Contrary to this, biochemical techniques include fermentation, aerobic and anaerobic digestion, enzyme and normal hydrolysis, etc. (Bhattacharjee and Biswas 2019). Amidst all the methods mentioned, pyrolysis is gaining importance due to its ability to produce pyro-char, pyro-oil, and pyro-gas (Poddar et al. 2015, 2021) and flexible due to conveniently manipulated process parameters maximize the product yield based on preferences.

Through pyrolysis operation, long-chain polymer molecules of the lignocellulosic biomass into small, lesser complex molecules by being heated in an inert atmosphere (Poddar et al. 2014, 2015, 2015, 2021; Wang et al. 2021; Sharuddin et al. 2016; Chowdhury et al. 2014; Li et al. 2014). The solid product of the pyrolytic process is known as pyro-oil. It is applicable in the boiler, in soil amendment (Poddar 2019), biofertilizer (Ahmad et al. 2014), adsorption of organic and inorganic contaminants and reduction of trace-gas emissions from soil and atmosphere (Chen et al. 2016; Lu et al. 2012; Zhao et al. 2018). The liquid product of the above-said process is known as pyro-oil. It is applicable in boilers and diesel engines for power generation, transportation, stock material for other chemicals, electricity generation through boilers, furnaces, engines and turbines (Uzun and Sarioğlu 2009). Lastly, the gaseous product (pyro-gas is a mixture of carbon oxides, light hydrocarbons, and hydrogen) finds its applicability in electricity generation, stock material for other chemicals, gas to liquid conversion (Poddar 2020) etc.

The production of fuels (synthetic) and value-added intermediate chemicals from biomass, mainly lignocellulosic, seems alluring considering the nature of the biomass, which is renewable with the aim of maximum oil yield and boosted properties (Dorado et al. 2015; Hasan et al. 2017).

As lignocellulosic biomass is transformed into solid, liquid, and gaseous fuel, its calorific value, elemental makeup, etc., pose the most significant danger. Therefore, the quality of the pyrochar, oil and gas products was improved by using additional procedures such as hydro-pyrolysis, hydrothermal treatment, or catalytic co-pyrolysis.

The present investigation focuses on the use of mixed bio-waste sesame oil cake and jute sacks in catalytic and non-catalytic co-pyrolysis. The rationale of the selected feedstocks is that India produces 10,990 thousand bales of jute (Board 2020) and 225,606 tons of sesame seed (Indian Sesame Seeds-Market Review & Forecast 2018–2020) yearly. It is worthy enough even if 10% of the waste is considered for energy recovery, which is equivalent to 100 MWh.

2 Experimental Concepts

The studies include the characterization of feestock for proximate and ultimate analyses, estimation of heating value (HHV and LHV), evaluation of the product quality, char characterization etc. An experimental setup is fabricated to carryout the pyrolysis of feedstock and also instrumented to control the heating rate and reactor temperature. Details are given in following sections.

2.1 Feedstock

The materials for this experiments are procured from local market and sun dried for two weeks. The samples were crushed and sieved to less than 500 μm. The feedstock is mixed in 1:1 ratio by mass and stocks of 2 kg are prepared for experiments. The residual moisture removed by heating the stock of 2 kg each in hot air oven at 120 °C for four hours before the experiment.

2.2 Catalysts and Experimental Procedure

Aluminium oxide [Al_2O_3], Zinc oxide [ZnO], sodium chloride [NaCl], potassium chloride [KCl] and sodium aluminosilicate [$NaAl(SiO_3)_2$] were procured from Merck India. These catalyst combinations are selected in this study and are based on the encouraging performance in terms of yield as reported by Poddar et al. (2015). The catalyst is prepared as per the procedure given by Poddar et al. (2015).

2.3 Methods for Characterization of Waste (A Mixture of Sesame Oil Cake and Jute Waste), Co-pyrolytic Oil and Co-pyrolytic-Gas

2.3.1 Analyze Proximal and Ultimate

The moisture, ash, volatile matter, and fixed carbon contents of the scanned samples (biomass) and co-pyro char were determined using the ASTM D 3172 -07a method.

2.3.2 Higher Heating Value (HHV) and Lower Heating Value (LHV)

The results from the CHNS and O (by difference method calculation) were used to determine the LHV and HHV of the biomass sample, and co-pyro char calculated by the model Eqs. (1) and (2) found elsewhere (Shayan et al. 2018)

$$LHV\left(\frac{MJ}{kg}\right) = \frac{0.0041868(1 + 0.15[O])\left(7837.667[C] + 33888.89[H] - \frac{[O]}{8}\right)}{1000}$$

(1)

$$HHV\left(\frac{MJ}{kg}\right) = \frac{LHV + 21.97[H]}{1000}$$

(2)

The HHV and LHV of co-pyro-oil were given by the formula (3) (Hamilton and Kennedy 1992) and (4) (Oasmaa et al. 1997) as shown below:

$$HHV\left(\frac{MJ}{kg}\right) = 338.2 * C + 1442.8 * \left(H - \frac{O}{8}\right) \tag{3}$$

$$LHV\left(\frac{MJ}{kg}\right) = HHV - 218.3 * H\%(wt\%) \tag{4}$$

The HHV and LHV of the co-pyro-gases given as (5) and (6), which are found elsewhere (Waldheim and Nilsson 2001)

$$HHV\left(\frac{MJ}{Nm^3}\right) = 12.622 * X_{CO} + 39.782 * X_{CH_4} + 12.769 * X_{H_2}$$
$$+ 58.059 * X_{C_2H_2} + 69.693 * X_{C_2H_6} + 101.242 * X_{C_3H_8} \tag{5}$$

$$LHV\left(\frac{MJ}{Nm^3}\right) = 12.622 * X_{CO} + 35.814 * X_{CH_4} + 10.788 * X_{H_2}$$
$$+ 56.078 * X_{C_2H_2} + 63.748 * X_{C_2H_6} + 93.215 * X_{C_3H_8} \tag{6}$$

2.3.3 Physical Properties of the Co-pyrolytic Oil

The co-pyrolytic oil was tested for its initial and final boiling point, according to ASTM D2887-08, and its pH at various temperatures (573–1173 K).

2.3.4 Fourier-Transform Infrared Spectroscopy (FTIR) Assessment of Co-pyrolytic Oil

VERTEX 70 (series no. A213748) of Shimadzu Company FTIR with a resolution of 4 cm^{-1} was used to confirm the functional group in the spectrum dimension between 4000 and 400 cm^{-1} of the co-pyrolytic oil.

2.3.5 Gas Chromatography Coupled Mass Spectrometry (GC–MS) Assessment of Co-pyrolytic Oil

Gas chromatography coupled mass spectrometry(Agilent 6890 armed with 5973 MSD and HP5 column with dimension 2.5e−7 m * 30 m * 0.00025 m) evaluated the non-catalytic and catalytic co-pyrolytic oil. The instrument was initially programmed at 343 K for 0.0667 h, then incremented to 573 K at a continual heating rate of 300 K h^{-1} and retained for 0.5 h. First, a homogeneous solution was prepared

by mixing 100 µL of co-pyrolytic oil and 0.005 L of ethyl alcohol of HPLC grade and finally filtered before injecting the solution into the instrument. Then, to the non-polar column, roughly 1.2 µL of the mixture were injected at a flow rate of 0.09 lph of helium carrier gas. Next, the ionization energy of 72 eV was inserted into the instrument to ionize the chemical compounds present in the co-pyrolytic oil. The ion source and the contact were maintained at 475 K and 515 K, respectively. According to the statistics, Scanner MS started at 42 m/z and concluded at 802 m/z. The components of the co-pyrolytic oil at various retention times were achieved using gas chromatography-mass spectrometry analysis and determined from the NIST library that came as anallusion.

2.3.6 Gas Chromatography (GC) Assessment of Co-pyrolytic Gas

The composition of co-pyrolytic gas obtained from co-pyrolysis of non-catalytic and catalytic feedstocks was determined using gas chromatography (GC-Make-Varian-Model-CP3800) [ASTM E 112 method]. First, the gas chromatography is equipped with FID and Splitless Capillary Inlet to detect the various gases in the co-pyrolytic gas. Next, the oven was registered to hold at 333 K for 0.1167 h and then increased the intensity at a continual heating rate of 1200 Kh^{-1} to 543 K and retained for another 0.4167 h. Finally, the detectors were held at 433 K for quantification of various mixtures of gas used. The gas components at different retention times were detected and compared with the NIST library that came as anallusion.

2.3.7 Surface Morphology of Raw Sample, Co-pyrochar Without and with the Usage of Catalyst

Distinct components present in the raw sample (mixture of sesame oil cake and jute waste) and co-pyrochar were evaluated in a JEOL-JSM 5200. In addition, an SEM–EDX analyzer (JEOL-JSM 5200 integrated with ULTIMA-II RIGAKU MAKE) was used to observe the morphological variations happening previously and later the co-pyrolysis operation without and with catalysts. The images were scanned at 150X magnification for the co-pyrolytic char without and with catalyst.

2.3.8 XRD of Co-pyrolytic Char Without and with the Usage of Catalyst

The XRD of the powder mixture of sesame oil cake and jute waste and co-pyrochar were evaluated through an ULTIMA-II RIGAKU MAKE diffractometer using Ni-filtered CuKa radiation (λ: $1.52e^{-10}$ m) source. In the 2θ range of 278–353 K, the diffraction arrangement was measured at 17,580 K/h. The detailed investigation is represented by Fig. 4b.

2.3.9 Brunauer–Emmett–Teller (BET) Assessment of Co-pyrolytic Char Without and with the Usage of Catalyst

The nitrogen adsorption or desorption isotherms on the NOVA 1000e quantachrome analyzer were used to determine the surface area and pore volume of a combination of sesame oil cake and jute waste co-pyrochar using Brunauer–Emmett–Teller (BET) methods. Before analysis, around 20 mg of waste sample (biomass) and co-pyro char were put in sampling tubes with a diameter of 0.009 m and degassed for two hours at 473 K under 0.5333 Pa pressure before being weighed out. The detailed investigation is represented by Table 2.

2.3.10 Experimental System

The non-catalytic and catalytic co-pyrolysis experiments were investigated in a lab-scale semi-batch pyrolyzer 0.4 m in length and an internal and external diameter of 0.1195 mø and 0.2 mø respectively. The pyrolyzer has three openings, the first one of 0.05 mø for inputting biomass, another for washing and implanting catalysts of 0.2 mø and the final opening of B24 to collect the volatiles. The pyrolyzer was covered from outside with glass wool insulation for heating with an 800 W (3 phase AC). The temperature inside the pyrolyzer was audited and controlled with the help of a Nickel-Chromium thermocouple connected to a proportional–integral–derivative detector of K-type, as displayed in Fig. 1. Nitrogen gas was supplied to the pyrolyzer from the bottom with a flow rate of 0.04998 m³/h throughout the experiment to sweep the volatiles produced during co-pyrolysis and control the pyrolyzer's inert atmosphere. The volatiles obtained from the co-pyrolysis reaction passes through the
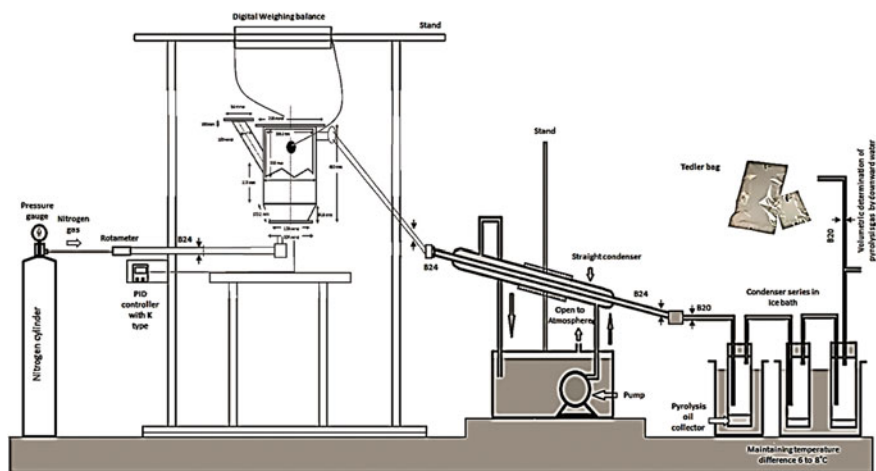
Fig. 1 Schematic diagram of a non-catalytic and catalytic pyrolysis setup

B24 opening (stainless steel pipe) followed by the straight condenser. The condenser was maintained at a temperature of 281–285 K. Coldwater is pumped directly into the condenser through a tiny submersible pump, resulting in the condensing of volatiles into co-pyrolytic oil, as represented in Fig. 1.

Three condensers were placed in a salt and ice mixture between 273 and 271 K were engaged to condense the maximum amount of volatiles into co-pyro oil. The co-pyrolytic oil collected into the condenser was then relocated into 0.025 L vials for further analysis. The co-pyrolytic char obtained from the pyrolyzer cooled at room temperature and then moved into plastic packets for further research. Volumetric measurements followed downward water displacement in a one-litre measuring container for non-condensable gases (assembled). For additional compositional analysis, the gases were transferred to a 1-L "Tedlar bag." According to GC results, the exact weight and mole percent of different gases were determined in the co-pyrolytic gas.

2.3.11 Loss of Mass

The section of the pyrolyzer associating with the straight condenser was 0.1016 m long, as displayed in Fig. 1 and inclined at an angle of 75° (with padding). After the non-catalytic and catalytic co-pyrolysis experiment, the pyrolyzer, condensers, and the vents connecting the three salt and ice bath condensers were rinsed thoroughly with lab-grade ethyl alcohol to maximize the co-pyrolytic oil yield. The homogeneous mixture (benzene and co-pyro-oil mixed in the ratio 10:1) was collected in a 0.25 L separating funnel kept for 8–10 h and separated using a vacuum evaporator. After the evaporation of benzene from the co-pyrolytic oil, the weight is recorded and combined with the previous oil weight and subjected to further analysis. The co-pyro-vapours, which remains weighty inside the pyrolyzer, condensed on the semi-batch pyrolyzer wall containing co-pyrolytic char and, therefore, endured uncollected and emerged as a mass loss.

2.3.12 Experimental Strategy

The non-catalytic and catalytic co-pyrolysis investigations were examined in three distinct batches to cross-check the outcomes of various operating parameters (573–1173 K) on the product yield. The inert atmosphere for pyrolysis is ensured by purging the pyrolyzer, after loading with the feestock, for 90 min with nitrogen gas $(0.006 m^3/h)$. Subsequently, the pyrolyzer temperature is raised to set value with a fixed heating rate at 600 K/h for all the experiments. The pyrolyzer temperature is varied between 573 and 1173 K. The temperature corresponding to the maximum yield of co-pyrolytic oil is regarded as optimum operating temperature.

3 Result and Discussion

3.1 Feed Characterization

The proximate, ultimate analysis, empirical formula, HHV, LHV, and other properties present in the sesame oil cake and waste jute sacks, are represented in Table 1.

Table 1 The elemental analysis of sesame oil cake and waste jute sacks

Properties	Sesame oil cake	Jute wastes
Moisture (w%)	7.41	10.025
Volatile Matter (w%)	85.72	77.15
Ash (w%)	3.8	2.59
Fixed Carbon (w%)	3.07	10.235
C% (w/w)	45.19	49.79
H% (w/w)	7.55	6.02
O% (w/w) [a]	39.20	41.37
N% (w/w)	7.26	0.19
Cl% (w/w)	0.08	0.05
S% (w/w)	0.721	0.05
Lower heating value (MJ /kg)	17.57	17.92
Higher heating value (MJ /kg)	17.73	18.05
Bulk density (kg/m^3)	460	110
H/C	0.17	0.12
O/C	0.87	0.83
N/C	0.00 [b]	0.00 [b]
Cl/C	0.00 [c]	0.00 [c]
S/C	0.00 [d]	0.00 [d]
Empirical formula	**$CH_{0.17}O_{0.87}$**	**$CH_{0.12}O_{0.83}$**
Molecular weight (g/mol)	26.26	25.52
Surface area (m^2/g)	0.65	0.69
Pore volume	$3.85 * 10^{-3}$	$3.97 * 10^{-3}$

[a] By difference
[b] 0.0034 (jute waste); 0.14 (sesame oil cake)
[c] 0.00034 (jute waste); 0.0006 (sesame oil cake)
[d] 0.0005 (jute waste); 0.006 (sesame oil cake)

Table 2 Specific surface area of pyro char (pyrolysis at 873 K)

Pyrolysis process	The specific surface area of char (m^2/g)
Non-catalytic	3.435
Catalytic	5.921

The moisture content of sesame oil cake is 7.41 wt%, and for jute, it is 10.025 wt%, which is within the tolerable limit of 10 wt%, resulting in downsize the thermal conversion efficiency. But, contrarily, it can create additional heat requirements resulting in more expense processes (Bhattacharjee and Biswas 2019; Asadullah et al. 2007).

The high volatile content of the samples (jute waste and sesame oil cake) was 85.72 wt% and 77.15 wt%, which finds application in high reactivity and easy devolatilization during the non-catalytic and catalytic co-pyrolysis of the mixture of sesame oil cake and jute waste. Moreover, as ash content (3.8 wt% for sesame oil cake and 2.59 wt% for jute waste) are lower compared to other feedstocks in the case of pyrolysis, catalytic pyrolysis and co-pyrolysis (Poddar et al. 2015; Bhattacharjee and Biswas 2019; Chowdhury et al. 2014; Varma and Mondal 2017; Blasi et al. 1999). Therefore, minor operation issues can be caused by low ash content, such as slag development, corrosion inside the pyrolyzer and fouling, and a reduced burn rate.

CHNS and O concentrations in sesame oil cake and jute waste were found to be virtually identical to other feedstocks in the final analysis (Table 1) (Poddar et al. 2015; Bhattacharjee and Biswas 2019; Chowdhury et al. 2014; Blasi et al. 1999; Miranda et al. 2009; Alvarez et al. 2018).

The critical feedstock characteristics are found to be similar for the the feedstock under study. The molar ratios of H/C and O/C, respectively for sesame oil cake and jute waste, are (0.17 and 0.87) and (0.12 and 0.83). Simiarly, the HHV and LHV too are comparable at (17.57 and 17.73) for sesame oil cake and (17.92 and 18.05) for jute waste respectively. The empirical formula of sesame oil cake and jute waste are $CH_{0.17}O_{0.87}$ and $CH_{0.12}O_{0.83}$ respectively with corresponding average molecular weights 26.56 g/mol and 25.52 g/mol. The close magnitudes of these critical characteristics suggests to mix could be of any ratio, however, the current study considers the feedstock mix at 1:1 mass ratio.

The less liberating SO_X and NO_X during the non-catalytic and catalytic co-pyrolysis process is because the sesame oil cake and jute waste comprise lower S and N content than bituminous coal (4.7 and 1.5 wt%) (Sudiro and Bertucco 2007).

3.2 Pyro-product Characterization

The co-pyro products viz., co-pyro-char, co-pyro-oil, and co-pyro-gas obtained for different pyrolysis temperature are expressed as percentage of the total product produced for one hour. The results are reported in Fig. 2a–c for product yield with different catalysts and at different pyrlosis temperature.

According to Fig. 2a, Co-pyro char is influenced significantly by pyrolysis temperature and found to decrease with increase in temperature. However, the relative magnitude of decrement varies with the catalyst type. The alumina is found to result in large variation in char production with temperature. Similarly, non-catalytic pyrolysis is too resulted in significant variation in char production as is the case with the catalyst alumina.
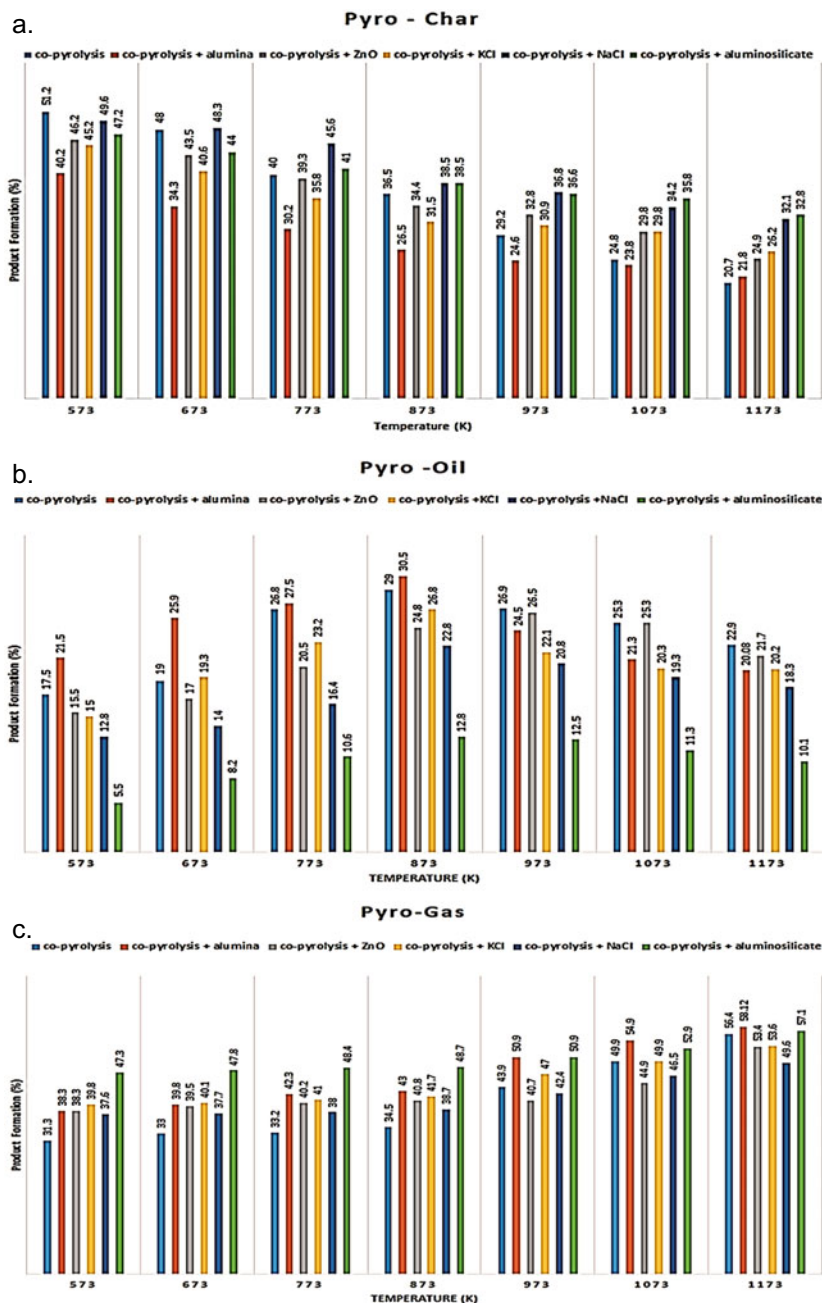
Fig. 2 a The output of co-pyro char at different co-pyrolysis temperatures in the absence and presence of the catalyst, **b** the output of co-pyro oil at different co-pyrolysis temperatures in the absence and presence of the catalyst and **c** the output of co-pyro gas at different co-pyrolysis temperatures in the absence and presence of the catalyst

The yield of Co-pyro-oil is found to show a maximum at 873 K according to Fig. 2b but with a catalyst for which the maximum is found to be at 973 K. The degree of variation with temperature is influenced by the type of catalyst. The alumina catalyst is found to result in maximum yield at 30.2%. The catalyst alumina-sililcate seems to be less influenced by temperature with yield varying from 5.5 to 10.2% over the temperature range.

The yield of co-pyro-gas is expected to increase with increase in temperature and is observed a similar trend as seen in Fig. 3c. The influence of temperature seems to be less significant upto 873 K, however, there seems to be sharp rise in gas yield beyond 873 K. Alumina has shown to influence strongly on gas yield beyond 873 K while the influence of alumina-silicate seems to be less significant.

It appears that aluminium oxide is a compelling catalyst followed by potassium chloride and then rest. However, implementing sodium chloride and aluminosilicate on catalytic co-pyro-oil is not authoritative as the output is relatively low. A similar conclusion had been reported by previous researchers (Hoekstra et al. 2012) during their experimentation on the pyrolysis of pinewood in the presence of sodium and potassium catalyst. During the rapid pyrolysis of wood and agricultural wastes in the presence of salt and potassium catalysts, another study (Oasmaa et al. 2010) observed a reduction in oil production. Thus, aluminium oxide and aluminosilicate exhibited a more significant catalytic impact than other materials. The outcomes impacted secondary or tertiary tar cracking reactions or polymerization reactions involved amongst the newly formed products. Recently Alvarez et al. (2019) experimented with the co-pyrolysis effect on biomass and tyre waste, where they tested in a bench-scale plant. The co-pyro char yield for biomass, tyres and maximized copyrolysed were 18 wt%, 38wt% and 35 wt%, respectively.

Similarly, the oil yield observed were 74 wt%, 60 wt% and 62 wt%, respectively, for biomass, tyres and maximized copyrolysed. Furthermore, the gas yield was 10 wt%, 8 wt% and 10 wt %, respectively, for biomass, tyres and maximized copyrolysed. Thus, the results obtained by them showed maximum oil yield followed by char and then gas. But in our case, there is a proportion amongst char, oil and gas formation, making the co-pyrolysis process more prominent than others. Thus, proving the current research more superior with aluminium oxide catalysts than the previous ones reported. The conclusion represented that the co-pyrolysis of lignocellulosic–lignocellulosic biomass without and with catalysts, lacking in the literature.

Figure 3 suggests that HHV (Fig. 3a) and LHV (Fig. 3b) of the co-pyro-char and co-pyro-oil were obtained during the non-catalytic and catalytic co-pyrolysis process. Figures (both a and b) show that the non-catalytic and catalytic co-pyro-char values increase with co-pyrolytic temperature. In contrast, the values of the co-pyro oil also increase. The detailed effects depend on the compound's compound's %Carbon, %Hydrogen, and %Oxygen, presented in Sect. 3.5.
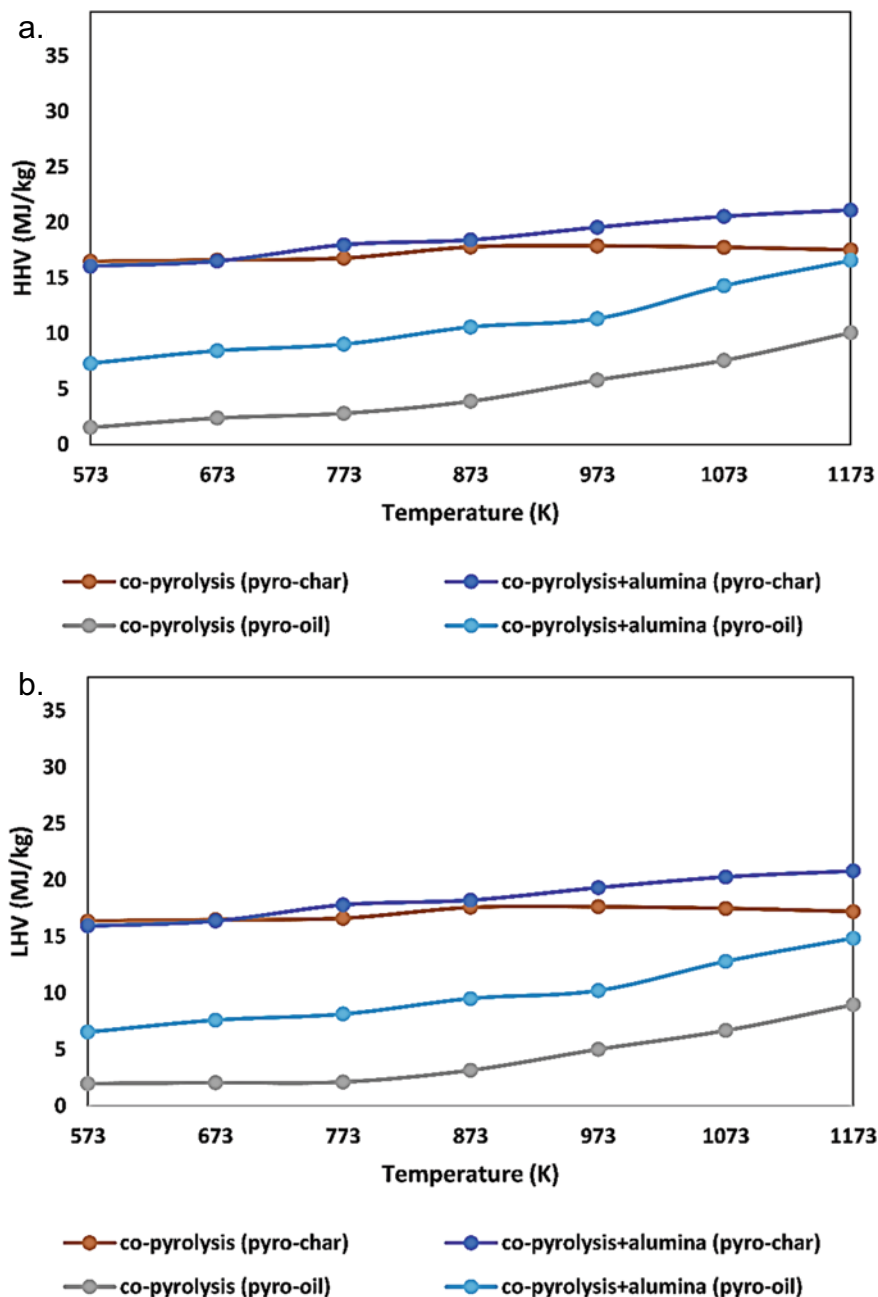
Fig. 3 Pictorial representation of HHV (**a**) and LHV (**b**) of the co-pyro-char and co-pyro-oil obtained during co-pyrolysis operation in the absence and presence of the catalyst
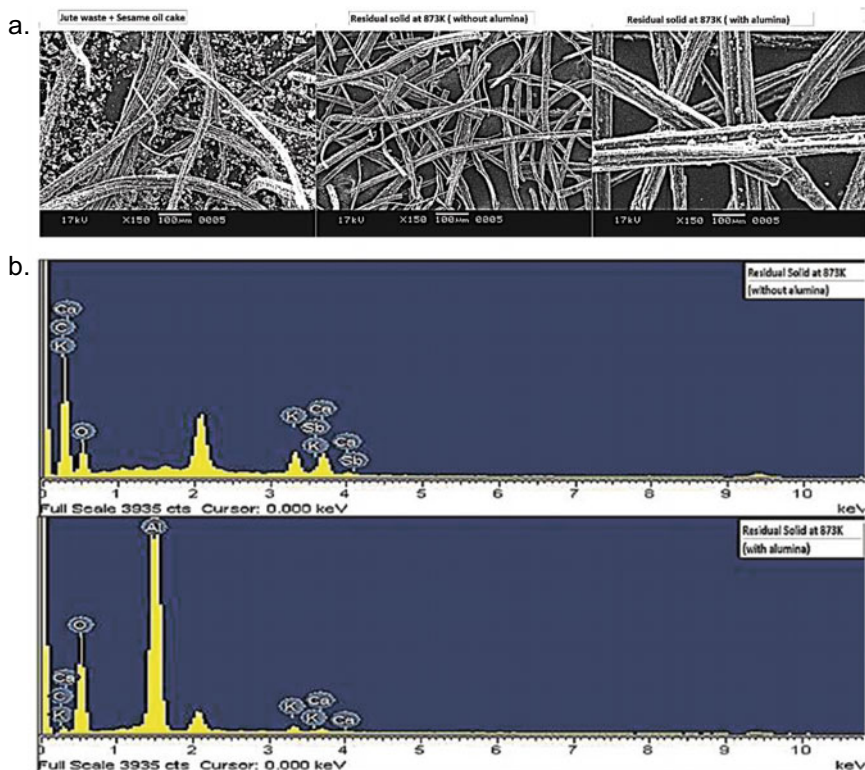
Fig. 4 **a** SEM images of actual co-mixed waste and the solid obtained at 873 **K**, in the absence and presence of alumina catalyst. **b** EDX spectra of the solid residue obtained at 873 K for the spectrum 10 in the absence and presence of catalyst

3.3 Aluminium Oxide Bed Porosity and Catalytic Activity

Figure 4a displays the SEM photograph of the actual mixture of sesame oil cake and jute waste and the solid residue obtained at 873 K, without and with an aluminium oxidecatalyst. The picture clearly illustrates the increase in porosity that occurs when a catalyst is present. The results demonstrate the catalytic movement mechanism proposed for co-pyro-char production by increasing the surface area. To calculate the surface area per mass of co-pyrochar, the BET technique measured the surface area per mass of a combination of sesame oil cake and jute waste at 873 K. The results are shown in Table 2. It also verifies that the specific surface area of co-pyro-char obtained through catalytic co-pyrolysis (5.921 m^2 g^{-1}) is higher than that of co-pyro-char of non-catalytic co-pyrolysis (3.435 m^2 g^{-1}) at the exact value of reaction temperature. Furthermore, the specific surface area of co-pyro-char of non-catalytic co-pyrolysis is proportionate to those observed by previous researchers during their

studies on pyrolysis of sawdust, wheat, and flax straws ($<5 \, m^2 \, g^{-1}$) (Azargohar et al. 2014).

According to Fig. 4b, char yield decreases with temperature for both noncatalytic and catalytic co-pyrolysis procedures. Co-pyro-char produced without catalyst includes potassium, calcium, and a tiny quantity of "Antimony", whereas catalytic co-pyrochar contains potassium, calcium, and a considerable amount of alumina. Figure 4b illustrates the results of EDX experiments. Co-pyrolysis with alumina, on the other hand, shows a more significant decline. This discovery might be explained by the substantial catalyzing impact on co-pyro-oil evolution.

3.4 pH and Distillation Characterization of Co-pyro-Oil

Figure 5a shows the pH values of non-catalytic and catalytic co-pyrolytic oils. During non-catalytic co-pyrolysis of jute and sesame oil cake, co-pyrolytic oil's pH rises to 5 at 973 K. Afterwards, it remains constant until 1173 K has been achieved. In the past, experts have seen a similar tendency (Poddar et al. 2015) on catalytic and non-catalytic pyrolysis of waste jute sacks. On the other hand, for catalytic pyrolysis, the aluminium oxide catalyst fluctuates between 7 and 7.85. Thus, the pH value of co-pyro-oil is acidic, whereas the pH value of catalytic pyro-oil is basic; the rest catalyst showed the basic effect. Therefore, the outcomes may be due to the presence of the catalyst, which absorbs the basic impact. Similar observations were represented by Veses et al. (2020) during their catalytic co-pyrolysis of Waste (a mixture of sesame oil cake and waste jute) is co-pyrolyzed; its initial boiling point (IBP) and final boiling point (FBP) will vary, as shown in Fig. 5b. The ASTM D86 (Aboyade et al. 2012) technique determines the co-pyrolysis oil distillation properties at different co-pyrolysis temperatures. The figure shows that greater IBP and FBP values were achieved when catalysts were used. Thus, more excellent carbon content is produced by utilizing catalytic co-pyrolysis of the same feedstock than by using non-catalytic co-pyrolysis, as stated in Sect. 3.5.

3.5 Effects of Al_2O_3 on Carbon–Hydrogen–Oxygen Content of Co-pyro-Char and Co-pyro-Oil

3.5.1 Pyro-Char

The elemental, mainly Carbon-Hydrogen-Oxygen, the composition of the co-pyro char, is the essential criterion for using co-pyro-char as a fuel. Co-pyro char's heating value increases with increasing carbon and hydrogen content, whereas a more effective oxygen content results in lower heating values, leading to higher polymerization, etc. Pictured is a diagram depicting Fig. 6a. Carbon, Hydrogen, and Oxygen content of
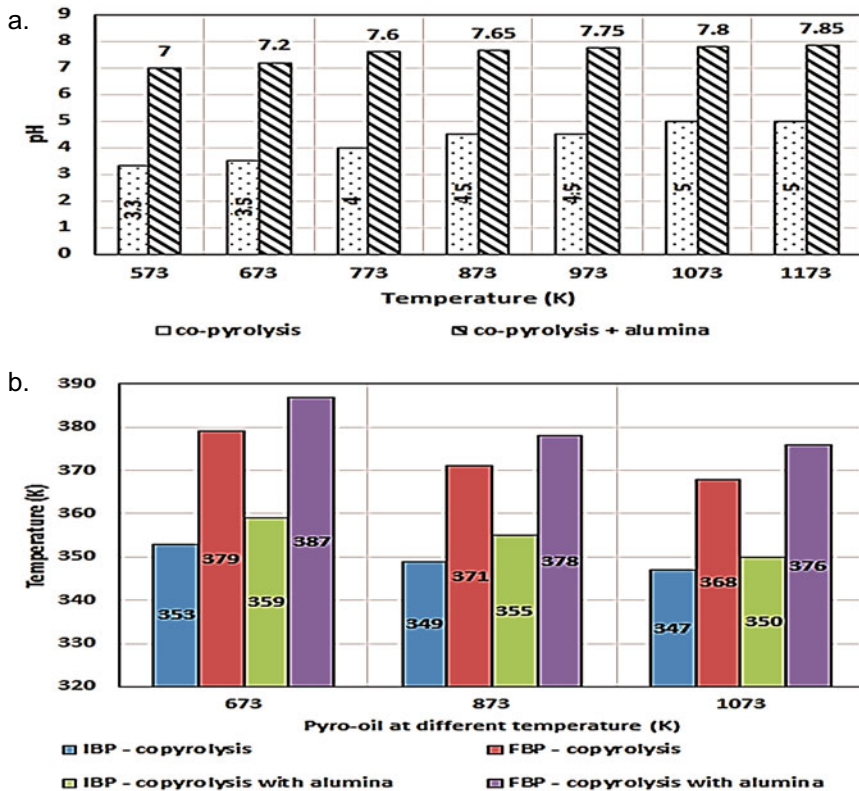
Fig. 5 **a** Dependence of pH of co-pyro-oil against co-pyrolytic temperature in the absence and presence of the catalyst, **b** variation of IBP and FBP of co-pyro-oil against co-pyrolytic temperature in the absence and presence of the catalyst

co-pyro char of feedstock are shown. The figure shows that when co-pyrolysis temperature increases, the per cent carbon increases and the per cent oxygen drops. With an increase in co-pyrolysis temperature, the difference in per cent Hydrogen is minimal. This co-pyrolysis is catalytic, and the outcomes are better than non-catalytic co-pyrolysis. A similar trend of observations is observed by previous researchers while experimenting with woodchips (Laidy et al. 2014) and catalytic and non-catalytic pyrolysis of waste jute sacks (Poddar et al. 2015; Chowdhury et al. 2014).

3.5.2 Pyro-Oil

Figure 6b along with Table 3 represents the elemental (Carbon-Hydrogen-Oxygen) composition of co-pyro oil as a function of co-pyrolytic temperature for both non-catalytic and catalytic biomass feedstock. The figure clarifies that the carbon content in the co-pyro-oil decreases as the co-pyrolytic temperature increases for

Fig. 6 **a** Plot of wt% of the components exists in co-pyro-char against temperature in the absence, and the presence of the catalyst, **b** the plot of wt% of compounds presents in co-pyro-oil against temperature in the absence and the presence of the catalyst
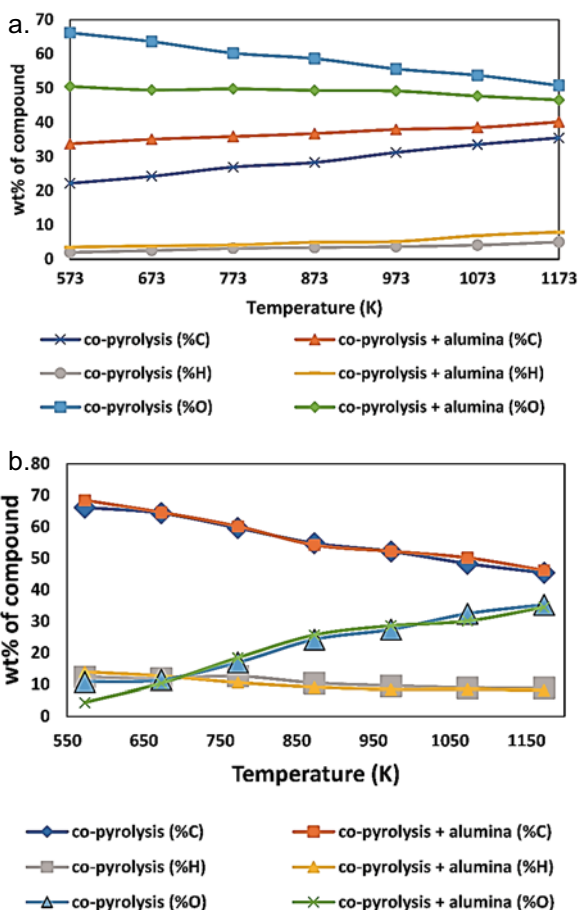
both catalytic and non-catalytic reactions. Similar observations were inferred by Poddar et al. (2014) and Yang et al. (Yang et al. 2015), when empty fruit bunches are hydrolyzed enzymatically, and when waste jute bags are pyrolyzed catalytically or non-catalytically.

The outcomes after non-catalytic and catalytic co-pyrolysis infer that the properties of the co-pyro-oil are in the range, concerning the researchers Varma et al. (2018) and Dhyani and Bhaskar (2018). Catalytic oil has a greater carbon concentration than non-catalytic oil, up to 873 K. The importance of hydrogen is not responsive to temperature and is not altered by the existence of alumina in the feedstock; similar observations were inferred by Wang et al. (2017) in their review article about the lignocellulosic biomass mechanism. The magnitude of oxygen, on the other hand, decreases as the co-pyrolytic temperature is increased. However, up to 873 K, the oxygen content in co-pyro oil is reduced due to catalyst (aluminium oxide).

Table 3 FTIR functional groups and the indicated compounds of co-pyro-oil in the absence and the presence of the catalyst (Chu et al. 1999)

Frequency range (cm^{-1})	Groups	Class of compounds
3600–3200	O–H stretching	Polymeric O–H
3050–2800	C–H stretching	Alkanes
1775–1650	C = O stretching	Ketones, aldehydes, carboxylic acids
1680–1575	C≡C stretching	Alkenes
1550–1475	– NO$_2$ stretching	Nitrogenous compounds
1490–1325	C–H stretching	Alkanes
1300–950	C–O stretching, O–H bending	Primary, secondary and tertiary alcohols Phenols, esters, ethers
900–650	–	Aromatic compounds
900–650	–	Aromatic compounds

Overall, it can be inferred from the figure that alumina exhibits a positive effect on the improvement of the elemental proportion of co-pyro oil up to 873 K. Similar trends of experimental observations were inferred by Yang et al. (Liu et al. 2019) and Kim et al. (Xie et al. 2020), respectively, during their pyrolysis of lignin and woody biomass. Similarly to Gao et al. (2020a), who reviewed the thermochemical conversion of sludge, the results may be due to carbon enrichment in the non-condensable lower molecular weight gaseous components produced during the splintering of co-pyro oil at higher temperatures. The magnitude of carbon content is higher for the catalytic one in correlation to the non-catalytic one. It is depicted as a temperature function that increases up to 873 K in co-pyro oil. Naqvi and others During non-catalytic pyrolysis of rice husk in the temperature range of 723–873 K, Naqvi et al. (2014) likewise achieved similar results. Attributed to a decrease in carbon content in co-pyro oil, an increase in oxygen concentration may also be due to a transfer of elemental carbon from the non-condensable gaseous products to the non-condensable gaseous products. From the outcomes of GC/MS analysis of catalytic and non-catalytic co-pyro oil at 873 K, furnished in Table 4, it is clear that the co-pyro-oil comprises many constituent components with oxygen as their primary molecule.

Further analysis of the stoichiometry of the assemblage of reactions occurring during the primary and secondary co-pyrolysis may edify the basic fact behind the decline and enhancement of %Carbon and %Oxygen, respectively, as a function of co-pyrolytic temperature. Alumina has a favourable impact on the elemental composition of co-pyro oil up to 873 K. It turns blackish-brown in hue and has a smokey smell (Bhattacharjee and Biswas 2019).

Table 4 GC/MS analysis of the pyro-oil of non-catalytic co-pyrolyzed feed material

	Retention time	Name of compound	Molecular weight	Usages
1	3.35	2-octanone ($C_8H_{16}O$)	128	Used in alcohol preparation (Carceller et al. 2020) Used for bioprocesses (Oda 2020)
2	5.18	Decane ($C_{10}H_{22}$)	174	For nanoparticle synthesis (Long et al. 2020)
3	7.02	Cyclodecane ($C_{10}H_{20}$)	140	In polymeric industry (Even et al. 2020)
4	8.16	2-dodecanone ($C_{12}H_{24}O$)	184	In pharmaceutical industry (Fraaije et al. 2004)
5	8.95	7-tridecanone ($C_{13}H_{26}O$)	198	Used in mushroom industry (Hao et al. 2020)
6	9.45	8-heptadecene ($C_{17}H_{34}$)	238	Used for aquatic biomass and increases bio-oil production (Ma et al. 2020)
7	9.92	Levoglucosenone ($C_6H_6O_3$)	126	3-hydroxy-cis, cis-muconate is produced by reacting hydroxyquinol with oxygen (Shafizadeh and Chin 1977)
8	10.43	Phenol (C_6H_6O)	94	Making cosmetics such as sunscreens and hair dyes (Phenol 2020) and skin lightening preparation (Phenol 2020)
9	11.38	Methyl hydroquinone ($C_6H_6O_2$)	110	Used for dermal analysis (Rustemeyer et al. 2020)

Table 4 (continued)

	Retention time	Name of compound	Molecular weight	Usages
10	12.62	Guaiacol ($C_7H_8O_2$)	124	Guaiacol is used as flavorants, such as eugenol (Jadhav et al. 2004) and vanillin (Walton et al. 2003). In addition, its compounds are employed as expectorants, antiseptics, and local aesthetics in medicine and dentistry
11	13.89	4-ethyl phenol ($C_8H_{10}O$)	218	used as an indicator of the yeast's presence (Liu et al. 2019; Cheynier et al. 2010)
12	14.38	Pyrocatechol ($C_6H_6O_2$)	110	Used for coffee industry (Funakoshi-Tago et al. 2020)
13	14.58	Phenol 2-methoxy 4-methyl ($C_8H_{10}O_2$)	138	For carceral treatment (Xie et al. 2020; Gonzalez-Coloma et al. 2013)
14	15.55	3-methoxycatehol ($C_7H_8O_3$)	140	Used for environmental microbiology (Higson and Focht 1992)
15	15.76	4-ethyl guaiacol ($C_9H_{12}O_2$)	152	Used in perfume industry (Jeleń et al. 2019)
16	15.91	4-methyl catechol ($C_7H_8O_2$)	124	In the agriculture and chemical food industry (Arsad et al. 2020)
17	16.96	2,6-dimethoxyphenol ($C_8H_{10}O_3$)	154	Used as a mediator for lignin modification (Kwiatos et al. 2020)

(continued)

Table 4 (continued)

	Retention time	Name of compound	Molecular weight	Usages
18	17.05	Eugenol ($C_{10}H_{12}O_2$)	164	Fragrances and essential oils often include this ingredient. Additionally, it is a local antiseptic, as well as an anaesthetic (Allen and Gates 1955); used in the pharmaceutical industry (Jadhav et al. 2004)
19	17.20	2-methoxy-4-propylphenol ($CH_3OC_6H_3(CH_2CH_2CH_3)$ OH)	166	Used as a supercritical fluid (Antipova et al. 2020)
20	17.94	Vanillin ($C_8H_8O_3$)	152	1. To conceal undesirable scents or tastes in medications, animal feed, cleaning products and cleaning supplies (Walton et al. 2003) 2. Pharmaceutical and other exemplary compounds are produced from this chemical intermediate. Over half of the world's vanillin production in the 1970s was used to make other compounds (Davis et al. 2019; Hocking 1997). In 2004, however, vanillin's market share was barely 13% (Davis et al. 2019)
21	18.78	Isoeugenol ($C_{10}H_{12}O_2$)	164	Anti-carceral agent (Tatsuzaki et al. 2006)

Table 4 (continued)

	Retention time	Name of compound	Molecular weight	Usages
22	19.52	4′-hydroxy-3′-methoxyacetophenone ($C_9H_{10}O_3$)	166	NADPH oxidase inhibition is used to treat atherosclerosis by preventing the formation of reactive oxygen species. This inhibits the endothelial cells from developing an illness (Hart et al. 1990)
23	20.31	2-propanone, 1-(-hydroxy-3-methoxyphenol) ($C_{10}H_{12}O_3$)	180	Used for esterification purpose (Hu 2019)
24	23.22	3,5-dimethoxy-4'-hydroxy acetophenone ($C_{10}H_{12}O_4$)	196	For improving bleaching activity (Jiao et al. 2020)
25	24.49	Syringaldehyde ($C_9H_{10}O_4$)	182	Utilized in the fragrance business, fragrances, medications, animal feed, and cleaning goods to mask undesirable odours or tastes (Walton et al. 2003)

3.6 FTIR Assessment of the Jute Waste and Sesame Oil Cake Waste Are Co-pyrolyzed to Produce Catalytic and Non-catalytic Co-pyro Oil

Figures 7a(i–iii), b(i–iii) represents the composition of the liquid products along with Table 3. There are also water impurities and other polymers in the table.

The figure shows that the peak in the IR spectrum at 3565.2 cm^{-1} (without and with catalyst) depicts a strong absorbance indicating the presence of O-H stretching in phenol. Torres-Garcia and Brachi (Naqvi et al. 2014) described a similar trend of observations during grape marc is pyrolyzed non-isothermally. Two sharp and narrow bands at 2922.6 cm^{-1} and 2851.8 cm^{-1} for non-catalytic co-pyrolysis and 2922.5 cm^{-1} and 2851.7 cm^{-1} for catalytic co-pyrolysis, described C-H bonds in alkane groups are stretched.

As observed from the identified region of the FTIR spectrum, the presence of peaks at 1770.8 cm^{-1} (both non-catalytic and catalytic co-pyrolysis) suggests a presence of C = O stretching of non-conjugated carbonyl groups like ketones, aldehydes, carboxylic acids. The absorption band at 1650.2 cm^{-1} (both for non-catalytic and

Table 5 Pyro-oil from catalytic co-pyrolyzed feedstock GC/MS analysis

S. No.	Retention time	Name of compound	Molecular weight	Usages
1	4.12	Acetaldehyde (C_2H_4O)	44	Used for in biochemistry (Kitakaze et al. 2020)
2	5.45	Methanol (CH_3OH)	32	In nanoparticle synthesis (Gao et al. 2020b)
3	7.10	2,3 Butanedione ($C_4H_6O_2$)	86	Used in food industry (Li et al. 2020)
4	8.32	Pyrimidine, 5-methyl ($C_4H_4N_2$)	80	Used for medicinal chemistry (Bailly et al. 2020)
5	9.05	Levoglucosenone($C_6H_6O_3$)	126	uses hydroxyquinol as a substrate with oxygen to produce 3-hydroxy-cis,cis-muconate (Shafizadeh and Chin 1977)
6	9.65	2-Hydroxy-3-oxobutanal ($C_4H_6O_3$)	102	No investigation to date
7	10.03	Succinaldehyde ($C_4H_6O_2$)	86	Beneficial for plant growth (Mcknight and Payborn 2020)
8	10.78	2(5H) – Furanone ($C_4H_4O_2$)	84	Used for drinking disinfection (Richardson et al. 2020)
9	11.42	4-Hydroxy-5,6-dihydro-(2H)-pyran-2-one ($C_5H_6O_3$)	114	Used for nanoparticle synthesis (Ziyaadini et al. 2020)
10	12.71	Guaiacol ($C_7H_8O_2$)	124	Guaiacol is a precursor to several flavorants, including eugenol and menthol (Jadhav et al. 2004) and vanillin (Davis et al. 2019; Bailly et al. 2020). Its compounds are employed as expectorants, antiseptics, and local aesthetics in medicine and dentistry
11	13.99	D-limonene ($C_{10}H_{16}$)	136	Usage of cosmetics (Sobel 2019) Biofuel/cleaning solvent/paint solvent (Power and to Showcase External Combustion Engine at SAE Event 2020)

(continued)

Table 5 (continued)

| S. No.	Retention time	Name of compound	Molecular weight	Usages
12	14.40	p-cresol (C_7H_8O)	108	In bacterial treatment (Londry et al. 1999) Used for pharmaceutical industry (Hsu et al. 2019) Used in nanotechnology (Vagts et al. 2020)
13	14.65	Cresol (C_7H_8O)	108	Used for nanotechnology (Vagts et al. 2020)
14	15.61	4-Ethyl guaiacol ($C_9H_{12}O_2$)	152	Used for alcohol industry (Jeleń et al. 2019)
15	15.83	4-vinyl guaiacol ($C_9H_{10}O_2$)	150	used as a flavouring agent (Jeleń et al. 2019)
16	16.02	5-(Hydroxymethyl)-2-furancaboxldehyde ($C_6H_6O_3$)	126	Used as an antioxidant and antiproliferative agent (Zhao et al. 2013)
17	17.12	Syringol ($C_8H_{10}O_3$)	154	Used for alcohol industry (Flynn 2020)
18	17.45	4-Vinylsyringol ($C_{10}H_{12}O_3$)	180	Used for carbon tracking (Kaal et al. 2020)
19	17.52	N-Nitrosonornicotine ($C_9H_{11}N_3O$)	177	Tobacco curing, ageing, processing, and smoking (Hecht 2020)
20	18.24	Vanillin ($C_8H_8O_3$)	152	1.To conceal undesirable scents or flavours in medications, livestock feed, and cleaning goods. (Walton et al. 2003) 2. Pharmaceutical and other exemplary compounds are produced using this chemical intermediate. To synthesize other compounds, more than half of the world's vanillin output was utilized in 1970 (Davis et al. 2019; Hocking 1997). In 2004, however, vanillin's market share was barely 13% (Walton et al. 2003)
21	19.07	Isoeugenol ($C_{10}H_{12}O_2$)	164	Anti-carceral agent (Tatsuzaki et al. 2006)
22	19.59	4′-hydroxy-3′-methoxyacetophenone ($C_9H_{10}O_3$)	166	For improving bleaching activity (Jiao et al. 2020)
23	21.47	2-propanone, 1-(-hydroxy-3-methoxyphenol) ($C_{10}H_{12}O_3$)	180	No investigation reported till date

Table 5 (continued)

S. No.	Retention time	Name of compound	Molecular weight	Usages
24	22.98	5-Phenylisooxazoline (C_9H_7NO)	145	No investigation reported to date

catalytic co-pyrolysis) inferred that α, β-unsaturated ($=$ conjugated) carbonyl group ($C = C–C = O$) fluctuations; the comparable weak $C = C$ stretching absorbs near 1640 cm^{-1} but is consistently masked by the O– H curving fluctuations of water at the same frequency (i.e., 1631 cm^{-1}) (Torres-Garcia and Brachi 2020; Bellamy 1975). Aromatic compounds characterize the spectrum band occurring between 1600 and 1300 cm^{-1}, were the band associated with the aromatic skeleton fluctuations in the lignin content may be present in the bio-oil, with various classified compounds like alkenes with $C\equiv C$ stretching, nitrogen compounds mainly with -NO_2 stretching and lastly, alkanes with C–H stretching. Precisely, in content with Torres-Garcia and Brachi (2020) and Xiong et al. (2017), the spectrum bands at 1650.2 cm^{-1} were referred to as the alkenes with $C\equiv C$ stretching; they made such inference. In contrast, the band at 1523.6 cm^{-1} was attributed to nitrogen compounds mainly with –NO_2 stretching, which was different from them, as they inferred the C–C stretching of the aromatic skeleton, whereas the spectrum band at 1457.8 cm^{-1} was ascribed to alkanes with C–H stretching, which were similar to their observations.

Again, the spectrum band observed between 1300 and 950 cm^{-1} describes the presence of primary, secondary and tertiary alcohols, phenols, esters, ethers may be with C–O stretching and/or O–H bending. In context to the previous researchers, Torres-Garcia and Brachi (2020), Xiong et al. (2017), and, Crini and Badot (2010), where they reported that the band at 1322 and 1162 cm^{-1} were correlated with syringyl units vibration and aromatic C–H in-plane deformations in syringyl unit, respectively. According to the present investigation, 1315.4 and 1269 cm^{-1} for non-catalytic co-pyrolysis and 1314.6 and 1269.1 cm^{-1} for catalytic co-pyrolysis suggest that the band were associated with primary, secondary and tertiary alcohols, phenols, esters, ethers with C–O stretching and/or O–H bending. Categorically, the spectrum band at 1015.9 and 1017.1 cm^{-1} for non-catalytic and catalytic co-pyrolysis infers the presence of primary, secondary and tertiary alcohols, phenols, esters, ethers with C–O stretching and/or O–H bending. At the band spectrum at 1040 cm^{-1}, which conforms to the stretching fluctuations of the side of C–OH groups (primary alcohols), infers that the co-pyro-oil may contain similar compounds in terms of cellulose and hemicelluloses as recommended by Torres-Garcia and Brachi (2020), where they suggested the dissymmetric lengthening of C–O–C glycosidic bonds in cellulose and hemicelluloses but this is beyond the scope of the present investigation.

Finally, the band spectrum at 716.8 and 666.8 cm^{-1} for non-catalytic co-pyrolysis and 718.8 and 667.1 cm^{-1} refers to aromatic compounds, similar to the observations Torres-Garcia and Brachi (2020), where they inferred about the presence of C-H fluctuations of unsaturated fragments. As seen in Fig. 7a, b, the co-pyro-oil produced
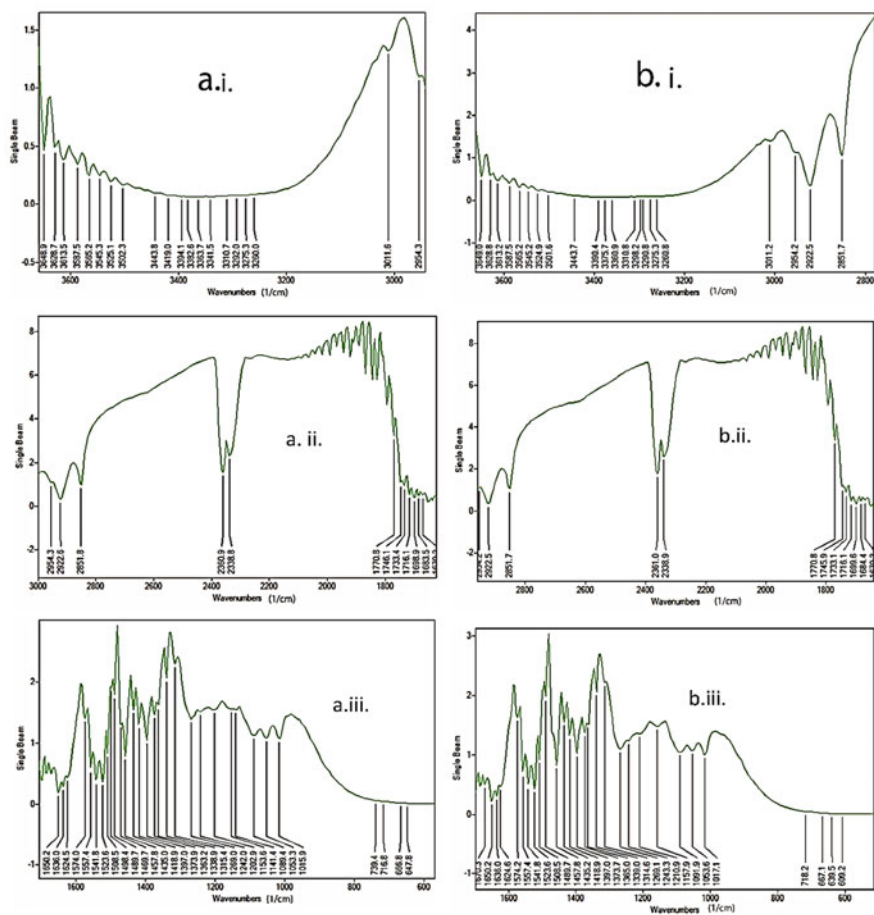
Fig. 7 **a** (i–iii) FTIR analysis of the co-pyro oil of jute waste and sesame oil cake and **b** (i–iii) FTIR analysis of the co-pyro oil of jute waste and sesame oil cake in the presence of alumina

from non-catalytic and catalytic co-pyrolysis, according to several studies, might be utilized as a fuel in the future.

3.7 GC/MS Analysis of Co-pyro-Oil

An Agilent 6890 equipped with a 5973 MSD and HP5 column (2.5e−7 m * 30 m * 0.00025 m) was used to characterize the co-pyro oil (qualitatively and quantitatively). As shown in Tables 4 and 5, the components contained in the co-pyro-oil produced from the co-pyrolysis of sesame oil cake and jute waste at 873 K are non-catalytic and catalytic, respectively. Compound lists with

Table 6 GC analyses the pyro-gas derived from non-catalytic and catalytic co-pyrolysis of sesame oil cake and waste jute sacks

Product distribution	(volume %)	(volume %)	(volume %)	(volume %)	(volume %)	(volume %)	(volume %)	
	CO_2	CO	CH_4	H_2	C_2H_2	C_2H_6	C_3H_8	CO/H_2
Feedstock	52.4	4.32	14.41	8.43	8	6.5	5.94	1:1.95
Feedstock presence of catalyst	55.8	3.64	16.12	8.35	6	4.5	5.59	1:2.29

retention times and future uses are shown in the Tables. These included D-limonene, furfuryl- and propanol-containing compounds, and 1-hydroxymethyl-1,3-dimethyl- and cyclopentane-containing compounds with aromatic and aliphatic characteristics. Interessant is also that pyro-oil has a wide variety of chemical compounds that have diverse applications. By activating the pyrolysis process. To make even more valuable chemical compounds using the techniques of deoxygenation and acid neutralization, etc.

3.8 GC Analysis

According to gas chromatography examination, the catalytic co-pyro-gas generated from the mixture of sesame oil cake and jute waste had a greater proportion of chemicals than the non-catalytic one. In terms of chemical composition, pyro-gas is composed of CO, CO_2, H_2O, CH_4, C_2H_2, C_2H_6, and C_3H_8. Table 6 provides a thorough analysis. In the table, CO/H_2 ratio, HHV (MJ/kg) and LHV (MJ/kg) are predicted to be 1:1.95, 22.54, and 20.22 MJ m^{-3} for non-catalytic feed material, and 1:2.29, 20.78, and 18.58 for catalytic feedstock at 873 K (Bhattacharjee and Biswas 2019; Poddar 2020; Alvarez et al. 2018).

4 Conclusion

On a 1:1 ratio of jute waste to sesame oil cake, the co-pyrolysis was examined at temperatures ranging from 573 to 1173 K for one hour. The Al_2O_3 catalyst found to be the most effective of all the catalysts employed in this study. As the catalyst used, the production of co-pyro oil (29–30.5 wt%) rises. The deoxygenation and increase in carbon content in co-pyrooil are responsible for the results. On the other hand, Al_2O_3 is a dominant catalyst in co-pyro-char surface area. There was an increase from 3.435 m^2 (non-catalytic) to 5.921 m^2 (catalytic). Due to the catalyst's absorption in the oil, the co-pyro-pH oil's values were measured and found to be acidic, whereas the catalytic one is basic. This is based on GC/MS analysis of the co-pyrolytic oil;

a GC/MS study of co-pyrolytic oil supports this conclusion. As a result, it is best to separate the oil before using it. Co-pyro-gas generation may be calculated and identified with the use of GC. The data revealed that the gas has a CO/H_2 ratio, HHV (MJ/kg) and LHV (MJ/kg) of 1:1.95, 22.54 and 20.22 MJ m^{-3} non-catalytic feedstock and 1:2.29, 20.78 and 18.58 for catalytic feedstock at 873 K and finds its utilization as liquid fuel production from syngas. The present investigation proves that this biomass (the mixture of sesame oil cake and jute waste) without and with catalyst can be used for a large-scale pyrolyzer without and with catalyst. Pyrolyzers of this sort find their most significant value in municipal regions of major cities.

Conflicts of Interest There are no conflicts to declare.

Credit Authorship Contribution Statement
Dr Sourav Poddar: Conceptualization, Data curation, Formal analysis, Investigation, Software utilization, Validation, Visualization, Writing, review, and editing—original and final manuscript.
Prof. (Dr.) J. Sarat Chandra Babu—Funding acquisition, Project Administration, Supervision, Validation, Visualization, Writing—review and editing.

References

Aboyade AO, Carrier M, Meyer EL, Knoetze JH, Görgens JF (2012) Model fitting kinetic analysis and characterisation of the devolatilization of coal blends with corn and sugarcane residues. Thermochim Acta. https://doi.org/10.1016/j.tca.2011.12.007

Ahmad M, Rajapaksha AU, Lim JE, Zhang M, Bolan N, Mohan D, Vithanage M, Lee SS, Ok YS (2014) Biochar as a sorbent for contaminant management in soil and water: a review. Chemosphere. https://doi.org/10.1016/j.chemosphere.2013.10.071

Allen CFH, Gates JW Jr (1955) o-Eugenol. Org Synth 3:418

Alvarez J, Hooshdaran B, Cortazar M, Amutio M, Lopez G, Freire FB, Haghshenasfard M, Hosseini SH, Olazar M (2018) Valorization of citrus wastes by fast pyrolysis in a conical spouted bed reactor. Fuel 224:111–120. https://doi.org/10.1016/j.fuel.2018.03.028

Alvarez J, Amutio M, Lopez G, Santamaria L, Bilbao J, Olazar M (2019) Improving bio-oil properties through the fast co-pyrolysis of lignocellulosic biomass and waste tyres. Waste Manage 85:385–395. https://doi.org/10.1016/j.wasman.2019.01.003

Antipova ML, Petrenko VE, Odintsova EG, Bogdan TV (2020) Study of solvation of substituted propylbenzene in ethanol-water solutions under subcritical conditions by molecular dynamics. J Supercrit Fluids. https://doi.org/10.1016/j.supflu.2019.104649

Arsad SS, Zainudin MAM, De Gobba C, Jongberg S, Larsen FH, Lametsch R, Andersen ML, Lund MN (2020) Quantitation of protein cysteine-phenol adducts in minced beef containing 4-methyl catechol. J Agric Food Chem. https://doi.org/10.1021/acs.jafc.9b07752

Asadullah M, Rahman MSA, Ali MM, Rahman MSA, Motin MA, Sultan MB, Alam MR (2007) Production of bio-oil from fixed bed pyrolysis of bagasse. Fuel 86:2514–2520. https://doi.org/10.1016/j.fuel.2007.02.007

Azargohar R, Nanda S, Kozinski JA, Dalai AK, Sutarto R (2014) Effects of temperature on the physicochemical characteristics of fast pyrolysis bio-chars derived from Canadian waste biomass. Fuel. https://doi.org/10.1016/j.fuel.2014.01.083

Bailly C, Hecquet PE, Kouach M, Thuru X, Goossens JF (2020) Chemical reactivity and uses of 1-phenyl-3-methyl-5-pyrazolone (PMP), also known as edaravone. Bioorg Med Chem

Bellamy LJ (1975) The infra-red spectra of complex molecules. Infra-Red Spectra Complex Molecules. https://doi.org/10.1007/978-94-011-6017-9

Bhattacharjee N, Biswas AB (2019) Pyrolysis of orange bagasse: comparative study and parametric influence on the product yield and their characterization. J Environ Chem Eng. https://doi.org/10.1016/j.jece.2019.102903

Blasi D, Colomba GS, Di Russo C, Rea G (1999) Product distribution from pyrolysis of wood and agricultural residues. Ind Eng Chem Res 38:2216–2224. https://doi.org/10.1021/ie980711u

Board, National Jute. 2020. Production at Glance. https://jute.com/web/guest/products-suppliers/supplier-database/production-capacity. Accessed 6 Apr

Carceller JM, Mifsud M, Climent MJ, Iborra S, Corma A (2020) Production of chiral alcohols from racemic mixtures by integrated heterogeneous chemoenzymatic catalysis in fixed bed continuous operation. Green Chem. https://doi.org/10.1039/c9gc04127c

Chen D, Chen X, Sun J, Zheng Z, Kexin F (2016) Pyrolysis polygeneration of pine nut shell: quality of pyrolysis products and study on the preparation of activated carbon from biochar. Biores Technol 216:629–636. https://doi.org/10.1016/j.biortech.2016.05.107

Chen H, Xie Y, Chen W, Xia M, Li K, Chen Z, Chen HYY, Chen H, Xie Y, Chen W, Xia M, Li K, Chen Z, Chen Y, Yang H (2019) Investigation on co-pyrolysis of lignocellulosic biomass and amino acids using TG-FTIR and Py-GC/MS. Energy Convers Manage 196:320–329. https://doi.org/10.1016/j.enconman.2019.06.010

Cheynier V, Schneider R, Salmon J-M, Fulcrand H (2010) Chemistry of wine. In: Comprehensive natural products II, vol 3, pp 1119–1172. https://doi.org/10.1016/B978-008045382-8.00088-5

Chowdhury R, Poddar S, De S (2014) Kinetic modelling of non-catalytic pyrolysis of waste jute in a fixed bed pyrolyzer. APCBEE Procedia 9:18–24. https://doi.org/10.1016/j.apcbee.2014.01.004

Chu PM, Guenther FR, Rhoderick GC, Lafferty WJ (1999) The NIST quantitative infrared database. J Res Nat Inst Stand Technol 104:59–81. https://doi.org/10.6028/jres.104.004

Crini G, Pierre-Marie B (2010) Sorption processes and pollution: conventional and non-conventional sorbents for pollutant removal from wastewaters. Presses Universitaires de Franche-Comté, Besançon

Cyclone Power to Showcase External Combustion Engine at SAE Event (2020) BioAge Group, LLC. https://www.greencarcongress.com/2007/09/cyclone-power-t.html. Accessed 3 Feb

Davis K, Rover MR, Salvachúa D, Smith RG, Beckham GT, Wen Z, Brown RC, Jarboe LR (2019) Promoting microbial utilization of phenolic substrates from bio-oil. J Ind Microbiol Biotechnol. https://doi.org/10.1007/s10295-019-02208-z

Dewangan A, Pradhan D, Singh RK (2016) Co-pyrolysis of sugarcane bagasse and low-density polyethylene: influence of plastic on pyrolysis product yield. Fuel 185:508–516. https://doi.org/10.1016/j.fuel.2016.08.011

Dhyani V, Bhaskar T (2018) A comprehensive review on the pyrolysis of lignocellulosic biomass. Renew Energy. https://doi.org/10.1016/j.renene.2017.04.035

Dorado C, Mullen CA, Boateng AA (2015) Origin of carbon in aromatic and olefin products derived from HZSM-5 catalyzed co-pyrolysis of cellulose and plastics via isotopic labeling. Appl Catal B 162:338–345. https://doi.org/10.1016/j.apcatb.2014.07.006

Even M, Hutzler C, Wilke O, Luch A (2020) Emissions of volatile organic compounds from polymer-based consumer products: Comparison of three emission chamber sizes. Indoor Air 30:40–48

Flynn NE (2020) Chemistry of aged beer and spirits: symposium introduction. J Agric Food Chem. https://doi.org/10.1021/acs.jafc.9b07007

Fraaije MW, Kamerbeek NM, Heidekamp AJ, Fortin R, Janssen DB (2004) The prodrug activator EtaA from mycobacterium tuberculosis is a baeyer-villiger monooxygenase. J Biol Chem. https://doi.org/10.1074/jbc.M307770200

Funakoshi-Tago M, Nonaka Y, Tago K, Takeda M, Ishihara Y, Sakai A, Matsutaka M, Kobata K, Tamura H (2020) Pyrocatechol, a component of coffee, suppresses LPS-induced inflammatory responses by inhibiting NF-κB and activating Nrf2. Sci Rep. https://doi.org/10.1038/s41598-020-59380-x

Gao N, Kamran K, Quan C, Williams PT (2020a) Thermochemical conversion of sewage sludge: a critical review. Prog Energy Combust Sci. https://doi.org/10.1016/j.pecs.2020.100843

Gao H, Zhai C, Nianqing F, Yukou D, Kevin Y, Zhu M (2020b) Synthesis of Pt nanoparticles supported on a novel 2D bismuth tungstate/lanthanum titanate heterojunction for photoelectrocatalytic oxidation of methanol. J Colloid Interface Sci 561:338–347

Gonzalez-Coloma A, Reina M, Diaz CE, Fraga BM, Santana-Meridas O (2013) Natural product-based biopesticides for insect control☆ BT—reference module in chemistry, molecular sciences and chemical engineering. Ref Mod Chem Molecul Sci Chem Eng 3:237–268

Hamilton LA, Kennedy JF (1992) Sourcebook of methods of analysis for biomass and biomass conversion processes. In: Carbohydrate polymers. Springer Netherlands, Netherlands. https://doi.org/10.1016/0144-8617(92)90167-o

Hao X, Zhao J, Yang J, Xie J, Zhang N, Jiang J (2020) Effects of apple and pear wood vinegar components on pleurotus ostreatus mycelium growth. BioResources 15:2961–2970

Hart T, Bert A, Simons JM, Shoshan KS, Bakker NPM, Labadie RP (1990) Antiarthritic activity of the newly developed neutrophil oxidative burst antagonist apocynin. Free Radical Biol Med. https://doi.org/10.1016/0891-5849(90)90115-Y

Hasan MDM, Wang XS, Mourant D, Gunawan R, Chunlong Y, Xun H, Kadarwati S et al (2017) Grinding pyrolysis of Mallee wood: effects of pyrolysis conditions on the yields of bio-oil and biochar. Fuel Process Technol 167:215–220. https://doi.org/10.1016/j.fuproc.2017.07.004

Hecht SS (2020) Metabolism and DNA adduct formation of carcinogenic tobacco-specific nitrosamines found in smokeless tobacco products. Smokeless Tobacco Prod. https://doi.org/10.1016/b978-0-12-818158-4.00007-8

Higson FK, Focht DD (1992) Utilization of 3-chloro-2-methylbenzoic acid by Pseudomonas cepacia MB2 through the meta fission pathway. Appl Environ Microbiol. https://doi.org/10.1128/aem.58.8.2501-2504.1992

Hocking MB (1997) Vanillin: Synthetic flavoring from spent sulfite liquor. J Chem Educ. https://doi.org/10.1021/ed074p1055

Hoekstra E, Westerhof RJM, Brilman W, Van Swaaij WPM, Kersten SRA, Hogendoorn KJA, Windt M (2012) Heterogeneous and homogeneous reactions of pyrolysis vapors from pine wood. AIChE J. https://doi.org/10.1002/aic.12799

Hsu YH, Huang HP, Chang HR (2019) The uremic toxin p-cresol promotes the invasion and migration on carcinoma cells via Ras and mTOR signaling. Toxicol in Vitro. https://doi.org/10.1016/j.tiv.2019.03.029

Hu X (2019) Stabilization of bio-oil via esterification. In: Santillan-Jimenez MCE (ed) Chemical catalysts for biomass upgrading. Wiley Online Library

Indian Sesame Seeds-Market Review & Forecast (2018–2020)

Jadhav BK, Khandelwal KR, Ketkar AR, Pisal SS (2004) Formulation and evaluation of mucoadhesive tablets containing eugenol for the treatment of periodontal diseases. Drug Dev Ind Pharm. https://doi.org/10.1081/DDC-120028715

Jeleń HH, Majcher M, Szwengiel A (2019) Key odorants in peated malt whisky and its differentiation from other whisky types using profiling of flavor and volatile compounds. LWT. https://doi.org/10.1016/j.lwt.2019.02.070

Jiao J, Fang G, Liang F, Deng Y, Shen K, Tian Q, Han S, Zhu B (2020) Bleachability improvement of eucalypt mechanical pulps using hydrogen peroxide in ethanol-water media. BioResources 15:1370–1383

Kaal J, Plaza C, Rodriguez MP, Biester H (2020) Towards understanding ecological disaster in the Harz Mountains (Central Germany) by carbon tracing: pyrolysis-GC-MS of biological tissues and their water-extractable organic matter (WEOM). Anal Pyrol Lett 8:1–17

Kitakaze T, Yuan S, Inoue M, Yoshioka Y, Yamashita Y, Ashida H (2020) 6-(Methylsulfinyl)hexyl isothiocyanate protects acetaldehyde-caused cytotoxicity through the induction of aldehyde dehydrogenase in hepatocytes. Arch Biochem Biophys. https://doi.org/10.1016/j.abb.2020.108329

Kwiatos N, Jędrzejczak-Krzepkowska M, Krzemińska A, Delavari A, Paneth P, Bielecki S (2020) Evolved fusarium oxysporum laccase expressed in Saccharomyces cerevisiae. Sci Rep. https://doi.org/10.1038/s41598-020-60204-1

Laidy E, Mena H, Pecora AAB, Beraldo AL (2014) Slow pyrolysis of bamboo biomass: analysis of biochar properties. Chem Eng Trans 37:115–120

Li S, Chen X, Liu A, Wang L, Guangsuo Y (2014) Study on co-pyrolysis characteristics of rice straw and Shenfu bituminous coal blends in a fixed bed reactor. Biores Technol. https://doi.org/10.1016/j.biortech.2013.12.119

Li P, Chen Z, Tan M, Mei J, Xie J (2020) Evaluation of weakly acidic electrolyzed water and modified atmosphere packaging on the shelf life and quality of farmed puffer fish (Takifugu obscurus) during cold storage. J Food Saf. https://doi.org/10.1111/jfs.12773

Liu X, Jiang Z, Feng S, Zhang H, Li J, Changwei H (2019) Catalytic depolymerization of organosolv lignin to phenolic monomers and low molecular weight oligomers. Fuel. https://doi.org/10.1016/j.fuel.2019.01.117

Londry KL, Suflita JM, Tanner RS (1999) Cresol metabolism by the sulfate-reducing bacterium Desulfotomaculum sp. Strain Groll. Can J Microbiol. https://doi.org/10.1139/w99-041.

Long L, Zhou W, Qiu Y, Lan Z (2020) Coking and gas products behavior of supercritical n-decane over NiO nanoparticle/nanosheets modified HZSM-5. Energy 192:116540

Lu X, Jordan B, Berge ND (2012) Thermal conversion of municipal solid waste via hydrothermal carbonization: comparison of carbonization products to products from current waste management techniques. Waste Manage 32:1353–1365. https://doi.org/10.1016/j.wasman.2012.02.012

Ma C, Geng J, Zhang D, Ning X (2020) Hydrothermal liquefaction of macroalgae: influence of zeolites based catalyst on products. J Energy Inst. https://doi.org/10.1016/j.joei.2019.06.007

Mcknight GD, Payborn RL (2020) Compositions for increasing nitrogen sources life span in plant growth mediums and methods of making. United States: United States

Miranda R, Bustos-Martinez D, Sosa Blanco C, Gutiérrez Villarreal MH, Rodriguez Cantú ME (2009) Pyrolysis of sweet orange (Citrus sinensis) dry peel. J Anal Appl Pyrol 86:245–251. https://doi.org/10.1016/j.jaap.2009.06.001

Naqvi SR, Uemura Y, Yusup SB (2014) Catalytic pyrolysis of paddy husk in a drop type pyrolyzer for bio-oil production: the role of temperature and catalyst. J Anal Appl Pyrol 106:57–62

Ning SK, Hung MC, Chang YH, Wan HP, Lee HT, Shih RF (2013) Benefit assessment of cost, energy, and environment for biomass pyrolysis oil. J Clean Prod 59:141–149. https://doi.org/10.1016/j.jclepro.2013.06.042

Oasmaa A, Solantausta Y, Arpiainen V, Kuoppala E, Sipilä K (2010) Fast pyrolysis bio-oils from wood and agricultural residues. Energy Fuels. https://doi.org/10.1021/ef901107f

Oasmaa A, Leppämäki E, Koponen P, Levander J, Tapola E (1997) Physical characterisation of biomass-based pyrolysis liquids application of standard fuel oil analyses. VTT Publications. 1st edn. Espoo: VTT Technical Research Centre of Finland. https://doi.org/10.1016/s0140-6701(98)97220-4

Oda S (2020) Microbial transformation of water-insoluble substrates by two types of novel interface bioprocesses, tacky liquid–liquid interface bioreactor and non-aqueous sporular bioconversion system. World J Microbiol Biotechnol 36:57

Özsin G, Pütün AE (2018) A comparative study on co-pyrolysis of lignocellulosic biomass with polyethylene terephthalate, polystyrene, and polyvinyl chloride: synergistic effects and product characteristics. J Clean Prod 205:1127–1138. https://doi.org/10.1016/j.jclepro.2018.09.134

Phenol (2020). https://cosmeticsinfo.org/ingredient/phenol-0. Accessed 3 Apr

Poddar S (2019) Energy and environmental analysis (EEA) of a 100 tpd waste jute pyrolysis plant: parametric sensitivity of energy return on energy investment (EROEI) and CO_2 avoidance (ACO$_2$). DJ J Eng Chem Fuel 4:40–53. https://doi.org/10.18831/djchem.org/2019011004

Poddar S (2020) Novel simulation and optimization for the production of green products I.E., green gasoline, green diesel and green waxes. Int J Innov Technol Explor Eng 9:1428–1436. https://doi.org/10.35940/ijitee.F4569.049620

Poddar S, Biswas R, Chowdhury R, De S (2014) Product characterization and kinetic study of co-pyrolysis of waste jute sacks and sesame oil cake. In: 2014 Power and energy systems conference: towards sustainable energy. In: PESTSE 2014. https://doi.org/10.1109/PESTSE.2014.6805290

Poddar S, Biswas R, De S, Chowdhary R (2015) Analysis of tar by catalytic pyrolysis of waste jute. J Adv Mech Eng Sci 1:12–19. https://doi.org/10.18831/james.in/2015011002

Poddar S, De S, Chowdhury R (2015) Catalytic pyrolysis of lignocellulosic bio-packaging (jute) waste-kinetics using lumped and DAE (distributed activation energy) models and pyro-oil characterization. RSC Adv 5(Royal Society of Chemistry):98934–98945. https://doi.org/10.1039/c5ra18435e

Poddar S, Sarat Chandra Babu J, Sarat Chandra Babu J, Sarat Chandra Babu J (2021) Modelling and optimization of a pyrolysis plant using swine and goat manure as feedstock. Renew Energy 175:253–269. https://doi.org/10.1016/j.renene.2021.04.120

Richardson SD, Dong H, Cuthbertson AA (2020) Effect-directed analysis (EDA): a promising tool for nontarget identification of unknown disinfection by products in drinking water. Environ Sci Technol 54:1290–1292

Rustemeyer T, Frosch PJ, Johansen J, Rustemeyer T, Elsner P, Maibach H (2020) Occupational contact dermatitis in dental personnel. In: Kanerva's occupational dermatology, Springer, Cham. https://doi.org/10.1007/978-3-319-68617-2_143

Shafizadeh F, Chin PPS (1977) Preparation of 1,6-anhydro-3,4-dideoxy-β-D-glycero-hex-3-enopyranos-2-ulose (levoglucosenone) and some derivatives thereof. Carbohyd Res. https://doi.org/10.1016/S0008-6215(00)83406-0

Sharuddin A, Dayana S, Abnisa F, Daud WMAW, Aroua MK (2016) A review on pyrolysis of plastic wastes. Energy Convers Manage 115:308–326. https://doi.org/10.1016/j.enconman.2016.02.037

Shayan E, Zare V, Mirzaee I (2018) Hydrogen production from biomass gasification; a theoretical comparison of using different gasification agents. Energy Convers Manage 159:30–41. https://doi.org/10.1016/j.enconman.2017.12.096

Shen Y, Linville JL, Patricia AA, Leon I-d, Schoene RP, Urgun-Demirtas M (2016) Towards a sustainable paradigm of waste-to-energy process: enhanced anaerobic digestion of sludge with woody biochar. J Clean Prod 135:1054–1064. https://doi.org/10.1016/j.jclepro.2016.06.144

Sobel A (2019) What is limonene? Everything You Need to Know. Healthline

Sudiro M, Bertucco A (2007) Synthetic fuels by a limited CO_2 emission process which uses both fossil and solar energy. Energy Fuels 21:3668–3675. https://doi.org/10.1021/ef7003255

Tatsuzaki J, Bastow KF, Nakagawa-Goto K, Nakamura S, Itokawa H, Lee KH (2006) Dehydrozingerone, chalcone, and isoeugenol analogues as in vitro anticancer agents. J Nat Prod. https://doi.org/10.1021/np060252z

Thermochemical Processing (2011)

Torres-Garcia E, Brachi P (2020) Non-isothermal pyrolysis of grape marc. J Therm Anal Calorim 139:1463–1478

Uzun BB, Sarioğlu N (2009) Rapid and catalytic pyrolysis of corn stalks. Fuel Process Technol 90:705–716. https://doi.org/10.1016/j.fuproc.2009.01.012

Vagts J, Weiten A, Scheve S, Kalvelage K, Swirski S, Wöhlbrand L, Neidhardt J, Winklhofer M, Rabus R (2020) Nanomolar responsiveness of an anaerobic degradation specialist to alkylphenol pollutants. J Bacteriol. https://doi.org/10.1128/JB.00595-19

Varma AK, Shankar R, Mondal P (2018) A review on pyrolysis of biomass and the impacts of operating conditions on product yield, quality, and upgradation. In: Recent advancements in biofuels and bioenergy utilization. https://doi.org/10.1007/978-981-13-1307-3_10

Varma AK, Mondal P (2017) Pyrolysis of sugarcane bagasse in semi batch reactor: effects of process parameters on product yields and characterization of products. Ind Crops Prod 95:704–717. https://doi.org/10.1016/j.indcrop.2016.11.039

Veses A, Parejo S, Navarro MV, Lopez JM, Murillo R, Callen MS, Garcia T (2020) From laboratory scale to pilot plant: Evaluation of the catalytic co-pyrolysis of grape seeds and polystyrene wastes with CaO. Catal Today

Waldheim L, Nilsson T (2001) Heating value of gases from report prepared for: IEA bioenergy agreement. English 1–61

Walton NJ, Mayer MJ, Narbad A (2003) Vanillin. Phytochemistry. https://doi.org/10.1016/S0031-9422(03)00149-3

Wang S, Dai G, Yang H, Luo Z (2017) Lignocellulosic biomass pyrolysis mechanism: a state-of-the-art review. Prog Energy Combust Sci. https://doi.org/10.1016/j.pecs.2017.05.004

Wang Z, Burra KG, Lei T, Gupta AK (2021) Co-pyrolysis of waste plastic and solid biomass for synergistic production of biofuels and chemicals—a review. Prog Energy Combust Sci 84:1–51. https://doi.org/10.1016/j.pecs.2020.100899

Xie Y, Jiang C, Chen X, Hongfei W, Bi S (2020) Preparation of oligomeric phenolic compounds (DHPs) from Coniferin and Syringin and characterization of their anticancer properties. BioResources 15:1791–1809

Xiong F, Han Y, Wang S, Li G, Qin T, Chen Y, Chu F (2017) Preparation and formation mechanism of renewable lignin hollow nanospheres with a single hole by self-assembly. ACS Sustain Chem Eng. https://doi.org/10.1021/acssuschemeng.6b02585

Yang HM, Appari S, Kudo S, Hayashi JI, Norinaga K (2015) Detailed chemical kinetic modeling of vapor-phase reactions of volatiles derived from fast pyrolysis of lignin. Ind Eng Chem Res. https://doi.org/10.1021/acs.iecr.5b01289

Zhao L, Chen J, Jianyu S, Li L, Songqing H, Li B, Zhang X, Zhenbo X, Chen T (2013) In vitro antioxidant and antiproliferative activities of 5-hydroxymethylfurfural. J Agric Food Chem. https://doi.org/10.1021/jf403098y

Zhao Y, Wang Y, Duan D, Ruan R, Fan L, Zhou Y, Dai L, Lv J, Liu Y (2018) Fast microwave-assisted ex-catalytic co-pyrolysis of bamboo and polypropylene for bio-oil production. Biores Technol 249:69–75. https://doi.org/10.1016/j.biortech.2017.09.184

Ziyaadini M, Bakhsh NN, Roudbaraki SJ, Ghashang M (2020) Zn2SnO4-SnO2 nano-composite promoted ultrasonic-assisted synthesis of pyran derivatives. Polycyclic aromatic compounds

Separation of Congo Red Dye from Water Using AgNPs Based Hybrid UF Membrane

Subhankar Basu, Reshma Lakra, Ranjana Kumari, Wasim A. Shaikh, and Sukalyan Chakraborty

Abstract Congo red dye (CRD) is used in several industries and scientific applications. Discharge of CRD in receiving water bodies without complete removal from the effluent has toxic effects on aquatic life. This study reports the preparation of ultrafiltration (UF) membranes containing biosynthesis (extract of *Azadirachta indica* leaves) silver nanoparticles (AgNPs), called a hybrid membrane. Different polysulfone (PSF 3500) membranes were prepared, and its water flux was studied. PSF 18% was selected for preparing the hybrid membranes containing AgNPs: 0.0, 0.2, 0.4, 06, and 0.8 w/v. To avoid membrane defects, the PSF-AgNPs membranes were coated with hydrophilic chitosan (CS) (0.25, 0.5, and 1%). The membrane porosity, pore size, water flux, and CRD rejection were studied. The contact angle decreased from 80° to 32° with CS coating. The SEM cross-section image of the membrane indicates an asymmetric membrane structure with porous support over lined by a thin separation layer. The AgNPs were evenly distributed in the support layers providing selective water flow channels. The hydrophilic nature of the CS results in an enhanced water flux and reduced membrane fouling, and complete retention of CRD, compared to the bare membrane. Thus, the hybrid membrane could be used in industries to separate the CRD and reuse the dye for another application.

Keywords AgNPs · Ultra-filtration membrane · Chitosan · Congo red dye · Improved flux and retention

1 Introduction

Dyes are used in textile, personal care products, paper industry, paint, pharmaceutical, food items, cart, and printing industries. The presence of dyes in wastewater

---

S. Basu (✉) · R. Lakra · R. Kumari
National Institute of Advanced Manufacturing Technology (NIAMT), Ranchi, Jharkhand 834003, India
e-mail: subhankarb@niamt.ac.in

W. A. Shaikh · S. Chakraborty
Birla Institute of Technology (BIT) Mesra, Ranchi, Jharkhand 835215, India

produces dark colour and their by-products during chemical reactions are toxic, cancer-causing, and causes genetic-disorder to life forms. This causes skin diseases. The dyes are stable in natural water bodies for a long time, and this makes them non-biodegradable. Congo red dye ($C_{32}H_{22}N_6Na_2O_6S_2$) (CRD) is an anionic dye, and it is used widely in industries. CRD is stable and non-biodegradable. Adsorption (e.g., nano-zerovalent manganese/biochar composite; metal-organic framework) and chemical coagulation (e.g., phytogenic aluminium sulphate nano coagulant) are the most widely reported technologies for the removal of CRD from wastewater (Iqbal et al. 2021; Fu et al. 2021; Garvasis et al. 2020). The uptake capacity and photo-degradation activity of CRD using zeolite, ZnO, ZnO-NP, and ZnO-Ze were studied. More than 90% CRD removal was observed in ZnO-Ze with Langmuir isotherm and 2nd order kinetics (Madan et al. 2019). Waste materials like eggshells, activated carbon, cabbage waste powder, and surfactant modified zeolites were reported for CRD removal (Pravin et al. 2019; Ma et al. 2020; Wekoye et al. 2020; Nodehi et al. 2020). However, considering the limitations of these technologies (generation of chemical sludge and reduced regeneration capacity), they have not been adopted in most industries. Membrane technology is reported to be one of the suitable technologies to separate dye from wastewater (Madan et al. 2019) with no such limitations.

Ultrafiltration (UF) membrane made of polysulfone (PSF) is reported for the removal of CRD. However, membrane fouling is one of the major drawbacks due to the hydrophobic interaction between foulants and membrane surface, which eventually leads to flux decline and shortening of membrane life span. This problem was overcome by the addition of hydrophilic polymer blending (polyvinyl alcohol) and adsorbents (*L. Camara* plants waste) in the PSF polymer matrix (Lavanya et al. 2019; Khumalo et al. 2019). The presence of 20% *C. Odorata* particles in polyethersulfone membranes resulted in high separation of CRD from water (Zwane et al. 2018). In a similar study, Jammun (*Syzgium Cumini*) leaf ash was used for the uptake of CRD (Tirkey et al. 2018). Table 1 shows the separation efficiency of the various studies reported recently for the removal of CRD from water.

Biosorbents as adsorbent prepared from biological materials, are reported to have good uptake capacity for CRD (Shaikh et al. 2018). It also reduces the overall treatment cost. However, the problem of chemical sludge handling remains. The present study reports the preparation of a UF membrane containing biosynthesis (extract of *Azadirachta indica* leaves) silver nanoparticles (AgNPs), called hybrid membrane, to separate of CRD from water streams.

2 Materials and Methods

2.1 Materials

The materials were purchased from: CRD (Qualigens); PSF 3500 (Solvay Specialty Polymers); N-Methyl 2 Pyrrolidone (NMP) (Loba Chemie Pvt. Ltd.); CS flakes,

Table 1 The separation efficiency of studied materials reported for CRD from water

S. No.	Material	Material content	Separation efficiency	Observations
1	ZnO and Zeolite (ZnO-Ze)	1 g/L	90%	CRD removal of 90% was observed in ZnO-Ze at dose of 0.05 g, pH 3, 20 min, initial CRD 300 mg/L, Langmuir isotherm, second order kinetics, reusability high
2	PSF/PVA containing ZnO, SiO$_2$	1 g/L	53.5%	Less fouling, ZnO NPs showed better than SiO$_2$ NPs for CRD removal, both adsorption and rejection was studied, hydrophilicity increased
3	PSF-Caramel	50 mg/L	90%	Fouling reduced from 91 to 56%, hydrophilic, 100% recovery using ethanol
4	*C. odorata* stems	1 g/L	CO 92% CO + PES 84% PES 24%	PES + 20% *C. odorata* at pH 2, at 270 min, 99.5% removal reported, Freundlich isotherm, second order kinetics, low cost, eco-friendly
5	Egg Shells	1 g/L	98%	Cheap, easily available, Langmuir isotherm, second order kinetics, adsorption at pH 4.5 dosage 7.5 mg/L
6	Activated Carbon (1329 m^2/g)	200 mg/L	94.7%	Second order order kinetics, acidic condition is best at pH 2, Temp = 30 °C
7	PSF- *L. carama*	100 mg/L	99.5%	Natural, low cost plant, best at pH 4, (1% *L. carama*) has high hydrophilicity, permeability increased by 91%

(continued)

Table 1 (continued)

S. No.	Material	Material content	Separation efficiency	Observations
8	Cabbage powder	0.02 g/mL	91%	Maximum adsorption dosage at 2.5 g was 91%, Pseudo second order kinetics, Langmuir isotherm
9	Surfactant modified zeolite (SMZ) particles, and natural zeolite	1 g/L	99.9%	Equilibrium time was 240 min by SMZ, 99.9% uptake at 140 g/L dosage, Langmuir isotherm and Pseudo second order kinetics

acetic acid, glutaraldehyde (GA) (Merck Life Science Pvt. Ltd.,), silver nitrate (Merck emplura grade) and Polypropylene sheet Novatex 2471 (Freudenberg, Germany). All the chemicals and materials were used as received.

2.2 Synthesis of Hybrid Membranes

AgNPs was synthesized according to earlier reported study (Shaikh et al. 2018). Leaves of *A. indica* were collected from the institute campus and washed in tap water to remove the dust particles. The leaves were then cleaned several times with distilled water and dried at room temperature. The dried leaves were crushed into powder and put into the distilled water (25%). The extract was obtained by centrifuged and filtered through Whatman filter paper and stored in the refrigerator. AgNPs was prepared by addition of silver nitrate solutions in the leaf extract. The mixture was stirred continuously in a conical flask at room temperature under dark condition. The experiment was stopped after the appearance of dark colour of the solution. The AgNPs were separated and stored at room temperature.

PSF was dissolved in NMP (12, 14, 16, 18, and 20%) and the hybrid membranes were prepared via phase inversion process, with tap water in a coagulation bath. Hybrid membranes containing AgNPs: 0.0, 0.2, 0.4, 0.6, 0.8 w/v were prepared with PSF 18%. PSF-AgNPs membranes were coated with chitosan (CS) (0.25%, 0.5%, and 1%). CS was prepared in acetic acid and crosslinked with GA. The prepared membranes were tested in a dead-end filtration unit (Tech Inc. Ltd., Chennai) with N_2 gas as applied pressure. 20 mg CRD/L solution was prepared as feed solution using 0.02 g of CRD in 1L of deionized water. The characteristic of the membranes water flux and CRD (20 mg/L) retention (λ 540 nm) via UV-Vis spectrophotometer was studied in a dead-end filtration cell at 2 bar feed pressure. The water flux (J_w) was calculated using Eq. (1) and retention (R) was determined by Eq. (2).

The photograph of the bare, AgNPs, and hybrid membrane is shown in Fig. 1.
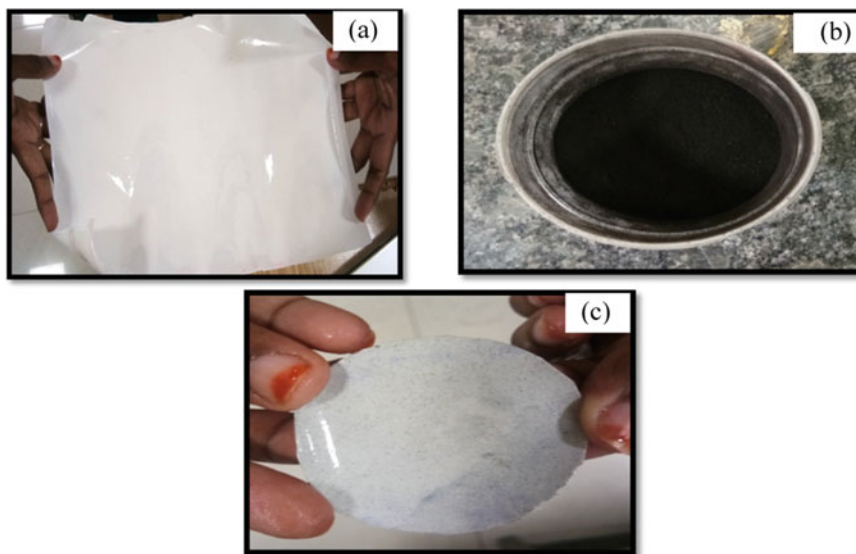
Fig. 1 Photograph of the **a** PSF membrane, **b** AgNPs, and **c** PSF-AgNPs (18%-0.6 w/v) hybrid membrane

$$J_w(LMH) = V/Axtx P \tag{1}$$

$$R(\%) = (C_o - C_f)x100/C_o \tag{2}$$

where V is the permeate volume (L), A is the effective membrane area (m^2), t is the time of filtration (h), and P is the feed pressure (bar). C_o and C_f are the feed and permeate concentrations of the CRD solution respectively.

2.3 Membrane Characterization

The membrane porosity of the samples was determined by soaking the membranes overnight in water. The wet weight was measured using an analytical balance. The membrane samples were then dried at room temperature overnight and weighed the following day to obtain the dry weight. All weights were recorded multiple times on an analytical balance, and the thickness was measured using a digital Vernier calliper twice on each side of the samples. The values were then used in the following Eq. (3) to calculate the porosity,

$$P_r = (M_s - M_d)/\rho x Axt \tag{3}$$

where P_r is the membrane porosity, M_s is the wet membrane weight, M_d is the dry membrane weight, ρ is the density of water, A is the surface area of membrane and t is the membrane thickness. The pore size was determined by the Guerout-Elford-Ferry Eq. (4).

$$r_m = \sqrt{(2.9 - 1.75\varepsilon)x\,8\eta l\,Q/(ex\,Ax\,\Delta P)} \tag{4}$$

where r_m is the mean pore radius (m), h is the water viscosity, l is the membrane thickness (m), Q is the volume of the permeate water per unit time (m^3/s), A is the effective area of the membrane (m^2), e is the porosity, and P is the operational pressure (Pa).

The water wettability of the membranes was studied by contact angle measurements (Tech Inc. Ltd., Chennai), and membrane morphology was studied by scanning electron microscope (SEM) (Zeiss-EVO/MA10 instrument). The property of AgNPs is mentioned in Shaikh et al. (2018).

3 Results and Discussion

3.1 Pore Characteristics of Hybrid Membranes

Table 2 shows the porosity and pore radius of the PSF and PSF containing AgNPs of different concentrations. The study shows that the porosity and pore radius of the hybrid membranes improved with increased concentration of AgNPs. This indicates

Table 2 Porosity and pore radius of developed membranes

Membrane containing	Porosity (%)	Pore radius (μm)
AgNPs loading 0.1 gm (PSF 18%)	84.2	1.604
AgNPs loading 0.2 gm (PSF 18%)	86.6	1.942
AgNPs loading 0.4 gm (PSF 18%)	87.4	0.581
AgNPs loading 0.6 gm (PSF 18%)	93.4	0.606
AgNPs loading 0.8 gm (PSF 18%)	96.7	0.607
PSF 12%	49	0.612
PSF 14%	49.3	0.610
PSF 16%	52	0.748
PSF 18%	53	0.589
PSF 20%	57	0.614

development of supplementary channels in the hybrid membranes with the introduction of AgNps. Similar results were also reported with multi walled carbon nanotubes (MWCNT) (Basu et al. 2018).

3.2　Performance of Hybrid Membranes

Figure 2a shows the water flux of the different PSF (12, 14, 16, 18, and 20) membranes. The water flux decreases with increased PSF content, which indicates the development of the dense structure. The SEM image in Fig. 2b shows an asymmetric structure formed via phase separation of NMP and water, resulted in a thin separation layer and a support layer. Figure 2c shows that the porosity of the membrane
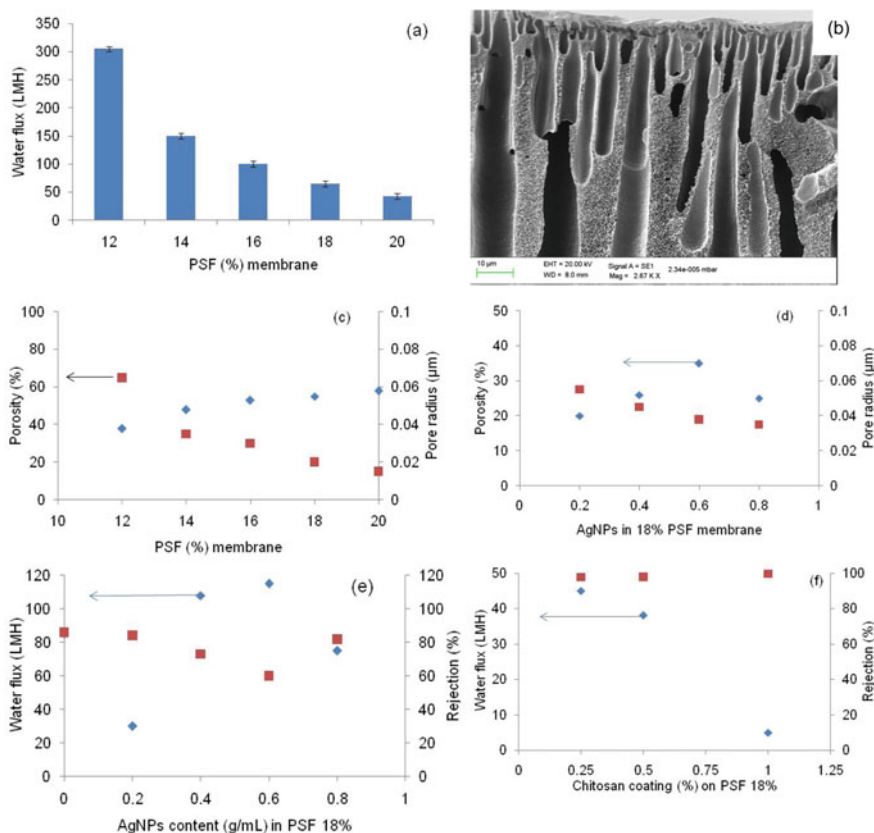
Fig. 2 The water flux of PSF membranes (**a**); SEM cross section view of PSF 18% membrane (**b**); porosity and pore radius of: PSF membranes (**c**) and AgNPs in 18% PSF membranes (**d**); Water flux and CRD rejection of: AgNPs containing in PSF membranes (**e**) and chitosan coated PSF 18% membranes (**f**)
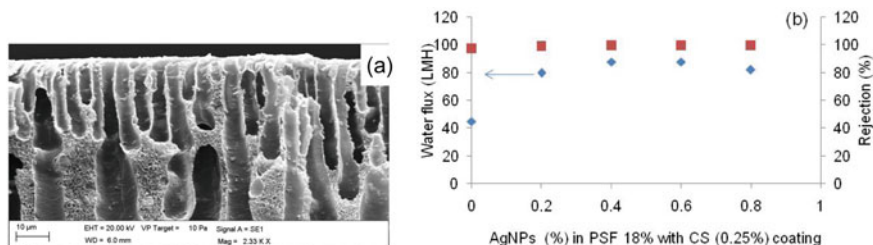
Fig. 3 **a** SEM image of PSF 18% membrane with 0.6% AgNPs and **b** water flux and CRD rejection of PSF 18% membrane with different contents of AgNPs and coated with 0.25% CS

reduces with increased concentration of PSF, which again indicates the formation of a dense membrane structure. Figure 2d shows that different amount of AgNPs is added into the PSF polymer matrix with an intension to produce supplementary water flow channels and thereby increases the water flux. However, the porosity decreases with increased AgNPs content. PSF 18% was selected, as at higher concentration the mixture is difficult to cast, while at lower concentration the AgNPs settle down during the degassing period. The decreased porosity indicates densification of the mixture with increased AgNPs addition in the solution. Figure 2e shows an irregular pattern of water flux and CRD retention.

Further, in 0.4 and 0.6 AgNPs, there occurs increased water, but decreased CRD retention compared to the bare membrane. This indicates defects on the membrane surface, which could be due to the incompatibility between the AgNPs and the polymer matrix. This resulted in increased water flux, but the retention decreased. This problem was overcome by coating with a hydrophilic CS layer. Different concentration of CS was used to coat the PSF 18% membrane, in order to determine the optimal concentration. Figure 2f shows complete retention of CRD, but the water flux reduced to 45 LMH when PSF 18% was coated. Further, the CS coating resulted in decreased water wettability (80^0 to 32^0) as the contact angle measurements. Figure 3a shows that the AgNPs are well distributed in the polymer matrix. This has resulted in over all increased water flux at 0.6 AgNPs and 0.25% CS coating on PSF 18% hybrid membrane to 88 LMH and complete rejection of CRD (Fig. 3b).

3.3 Overall Performance of the Hybrid Membrane

Figure 4 shows the overall performance of the newly developed hybrid membrane. The treated water shows complete retention of the CRD, and clear water was obtained after filtration. Thus, the membranes could be scaled to different module and use it for the retention of CRD, which could be reused, and the clear water could be reused in the industry. This supports the zero-liquid discharge of water and reduces the dependence on fresh water.

Before filtration

After filtration

Retentate of CRD

Treated water
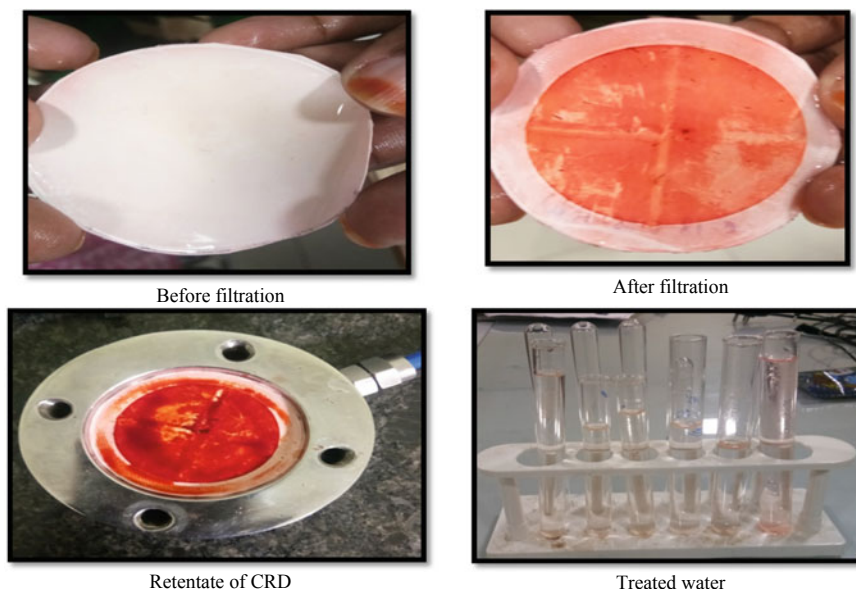
Fig. 4 The overall performance of the CRD wastewater treatment process

4 Conclusions

The study shows the development of a defect-free hybrid UF membrane. PSF (18%) membrane containing 0.6% biosynthesis AgNPs membrane with 0.25% CS coating resulted in higher water flux and complete retention of CRD compared to the bare membrane. Therefore, this membrane could be used in industries handling dyes in its manufacturing processes, and it can recover (i) the dyes and (ii) freshwater for reuse.

References

Basu S, Mukherjee S, Balakrishnan M, Deepthi M, Sailaja VRRN (2018) Polysulfone/nanocomposites mixed matrix ultrafiltration membrane for the recovery of Maillard reaction products. Membr Water Treatm 9(2):105–113. https://doi.org/10.12989/mwt.2018.9.2.105

Fu Q, Lou J, Zhang R, Peng L, Zhou S, Yan W, Mo C, Luo J (2021) Highly effective and fast removal of Congo red from wastewater with metal-organic framework Fe-MIL-88NH$_2$. J Solid State Chem 294:121836. https://doi.org/10.1016/j.jssc.2020.121836

Garvasis J, Prasad AR, Shamsheera KO, Jaseela PK, Joseph A (2020) Efficient removal of Congo red from aqueous solutions using phytogenic aluminum sulfate nano coagulant. Mater Chem PhyS 251:123040. https://doi.org/10.1016/j.matchemphys.2020.123040

Iqbal J, Shah NS, Sayed M, Niazi NK, Imran M, Khan JA, Khan ZUH, Hussien AGS, Polychronopoulou K, Howari F (2021) Nano-zerovalent manganese/biochar composite for the adsorptive and oxidative removal of Congo-red dye from aqueous solutions. J Hazard Mater 403:123854. https://doi.org/10.1016/j.jhazmat.2020.123854

Khumalo NP, Vilakati GD, Mhlanga SD, Kuvarega AT, Mamba BB, Li J, Dlamin DS (2019) Dual-functional ultrafiltration nano-enabled PSf/PVA membrane for the removal of Congo red dye. J. Water Process Engg. 31:100878. https://doi.org/10.1016/j.jwpe.2019.100878

Lavanya C, Khantong S, Jyothi MS, Balakrishna RG (2019) Environmental friendly and cost effective caramel for congo red removal, high flux, and fouling resistance of polysulfone membranes. Sep Purif Technol 211:348–358. https://doi.org/10.1016/j.seppur.2018.10.006

Ma M, Ying H, Cao FF, Wang Q, Ai N (2020) Adsorption of Congo red on mesoporous activated carbon prepared by CO_2 physical activation. Chin J Chem Eng 28:1069–1076. https://doi.org/10.1016/j.cjche.2020.01.016

Madan S, Shaw R, Tiwari S, Tiwari KS (2019) Adsorption dynamics of Congo red dye removal using ZnO functionalized high silica zeolitic particles Appl. Surf Sci 487:907–917. https://doi.org/10.1016/j.apsusc.2019.04.273

Nodehi R, Shayesteh H, Kelishami AR (2020) Enhanced adsorption of congo red using cationic surfactant functionalized zeolite particles. Microchem J 153:104281. https://doi.org/10.1016/j.microc.2019.104281

Pravin S, Biswas KB, Rahman A, Rahman H, Anik S, Uddin R (2019) Study on adsorption of Congo red onto chemically modified egg-shell membrane. Chemosphere 236:124326. https://doi.org/10.1016/j.chemosphere.2019.07.057

Shaikh WA, Chakraborty S, Islam RU (2018) UV-assisted photo-catalytic degradation of anionic dye (Congo red) using biosynthesized silver nanoparticles: a green catalysis. Desal Water Treat 130:232–242. https://doi.org/10.5004/dwt.2018.23004

Tirkey P, Bhattacharya T, Chakraborty S (2018) Optimization of fluoride removal from aqueous solution using Jamun (Syzygiumcumini) leaf ash. Process Saf Environ 115:125–138. https://doi.org/10.1016/j.psep.2017.10.022

Wekoye JN, Wanyony WC, Wangil PT, Tonui MK (2020) Kinetic and equilibrium studies of Congo red dye adsorption on cabbage waste powder. J Environ Chem Ecotoxicol 2:24–31. https://doi.org/10.1016/j.enceco.2020.01.004

Zwane S, Kuvarega AT, Mhlanga SD, Dlamini DS (2018) Hydrophilic polysulfone/Lantana camara mixed matrix membranes for the removal of dyes from water. Surf Interfaces 13:216–223. https://doi.org/10.1016/j.surfin.2018.10.001

Synthesis and Characterization of Copper (II) Schiff Base Metal Complex for Environmental Remediation

Hemant Kumar, Amandeep Kaur, and Amit Rai

Abstract The present work is focused on the synthesis and characterization of Schiff base ligand along with its metal complex from dialdehyde and primary amine. Repeated melting temperature and spectrum studies such as IR and ^{1}HNMR were used to analyse the synthesised Schiff base and its corresponding metal complex. The photocatalytic degradation of Methylene blue (MB) dye was studied in the presence of an oxidising agent such as H_2O_2, spectrophotometrically by the synthesized Cu(II) metal complex on irradiation of visible light radiation. The degradation of MB dye was studied in terms of regular time interval. The outcomes clearly reveals that the MB dye can be degraded and almost mineralized completely by using the synthesised copper metal complex as a catalyst. The photocatalysis of complex were studied using various parameters including the impact of light irradiation period, concentration of catalyst, substrate concentration (MB dye), amount of H_2O_2 as oxidising agent, and effect of pH. The percentage degradation of MB was found more than ninety percentages in the visible light irradiation.

Keywords Schiff base ligand · Copper metal complex · Photocatalytic degradation · Methylene blue dye

1 Introduction

One of humanity's most pressing issues is water. According to WHO data, almost a billion people do not have access to water (due to poor hygiene), and water supplies are mismanaged, resulting in hundreds of thousands of fatalities each year. As a result of advancements in the industrial and agricultural sectors, large amounts of

H. Kumar (✉) · A. Kaur
Department of Chemistry, Sant Longowal Institute of Engineering and Technology, Longowal, Sangrur,, Punjab 148106, India
e-mail: hemantk1331@gmail.com

A. Rai
Department of Chemical Engineering, Sant Longowal Institute of Engineering and Technology, Longowal, Sangrur, Punjab 148106, India

wastewater containing harmful chemicals have been generated. Organic dyes effluent coming out from textile industries are considered as one of the leading pollutants found in textile industry wastes (Forgacs et al. 2004). Different physical process such as pollutants separation, reverse osmosis, adsorption and others do not result in a complete process of mineralization; instead, they merely move contaminants from one phase to next, resulting in secondary contamination. Due to the resistance of azo dyes to aerobic degradation and the inclusion of carcinogenic aromatic amines in their composition, biological treatment approaches have proven ineffective (Habibi et al. 2005). The various advanced oxidation processes (AOPs) have been successfully employed for water treatment over the last decades to address limitations in existing research treatment approaches and the development of innovative technologies. Out of various methods, the photocatalytic degradation is most promising advanced oxidation processes (AOPs) because of simple and cost-effective nature (Lodha et al. 2008a). Creating OH$^\bullet$ hydroxyl free radicals and subsequently reacting with them using a combination of intense UV radiation and an oxidizing reagent are examples of these approaches. Several oxidation techniques are adopted like UV/TiO$_2$, UV/H$_2$O$_2$, and UV/O$_3$. AOPs involve the Photo- Fenton reaction and its variations, as well as H$_2$O$_2$/UV or ozonization (Kuo 1992; EI-Akabi et al. 1993; Arslan and Balcioglu 1999; Arslan et al. 2000; Herrera et al. 1999). Fenton's reagent only works in acidic (pH 2–4) conditions, and certain dyes are not completely destroyed (Gregor 1992; Nerud et al. 2001). Heterogeneous photocatalysis has been found to be one of the significant processes in AOPs as this process completely mineralized the waste water toxic dyes from the industries in a laboratory scale. Various Schiff-base complexes are used to catalyses AOPs for the degradation and mineralization of industrial watercourse (Abdou et al. 2018). As Schiff-base complex possess highly stable framework, classified electronic environment, and a space effect that can be appropriately and carefully changed by selecting the nature of ligand or by changing the metal ion (Ruck and Jacobsen 2002; Gupta and Sutar 2008; Liu et al. 2011). Nowadays several copper based metal complexes are used for highly selective catalytic oxidative processes of different groups particularly in homogenous processes have been reported (Sedai et al. 2011; Booblan et al. 2012; Zahng et al. 2012). However, only a few researches have been concentrated on the mineralization of hazardous organic contaminants in water treatment when exposed to visible light such as lignin, polycyclic aromatic hydrocarbons, and synthetic dyes (Cao et al. 2001; Watanabe et al. 1998; Gabriel et al. 2000; Salem 2000; Jyoti and Kumar 2019). More surprising its capacity to generate a hydrophobic microenvironment, imitate enzyme catalytically character, and inhibit axisymmetric agglomeration and decomposition is even more remarkable. The flexibility to function at pH 3–9 and the high specificity of the substrate are the real advantages of such systems (Zahng et al. 2012; Cao et al. 2001). In our previous studies the synthesized Cu(II) complex was used for degradation and mineralization of dyes in visible light conditions (Kumar and Kaur 2021). Therefore in present study different parameters are optimized and applied for the degradation and almost complete mineralization of MB dye.

2 Experimental

2.1 Materials

Himedia-company supplies Copper (II) acetate monohydrate salt and were used as received. 2-hydroxybenzaldehyde, 2-aminophenol, and Methylene blue (MB) dye were purchased from Sigma-Aldrich and utilized without additional purification. Freshly distilled solvents were properly refluxed on desiccants according to conventional techniques and maintained under vacuum. Hydrogen peroxide (30%) solution was used as a reagent to carry out this work. Millipore water was used to dissolve the H_2O_2 and dye solution. Double-distilled water was carried out during the experiments.

2.2 Instruments Used

FT-Infrared spectrophotometer model RZX (Perkin Elmer) was used to record the FTIR spectra with a KBr disk in range of 4000–400 cm^{-1}. FT-NMR spectrometer 400 MHz Bruker recorded ^1H and ^{13}C NMR analyses in DMSO solvent. A UV-Vis spectrometer UV-1800 (Shimadzu) was used to record the absorbance spectra in the range of 400–800 nm.

2.3 Synthesis

2.3.1 Preparation of 2, 2′-(Ethane-1, 2-Diylbis(Oxy)) Dicarbaldehyde (EDDC)

As reported by the literature (Reddy et al. 2014), the synthesizing methodology for EDDC was adopted as shown in Fig. 1.
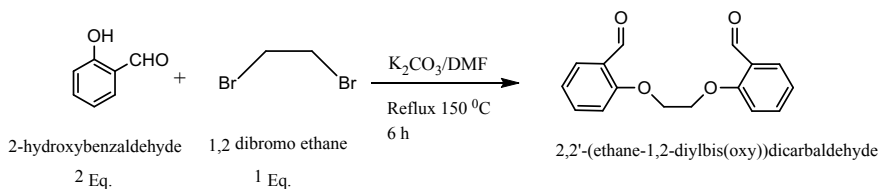
Fig. 1 Preparation of 2, 2′-(ethane-1, 2-diylbis(oxy))dicarbaldehyde (EDDC)
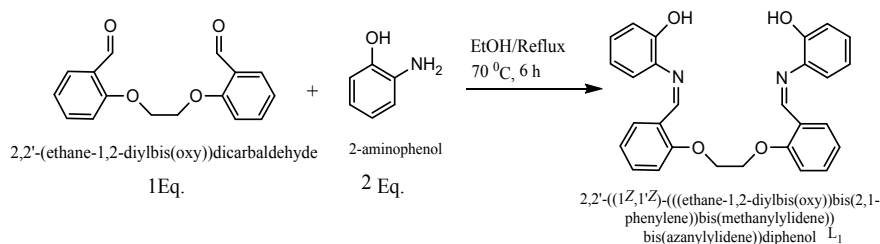
Fig. 2 Preparation of ligand L_1
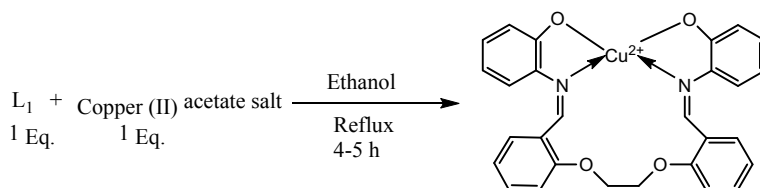
Fig. 3 Preparation of ML_1

2.3.2   Preparation of Ligand (L_1)

The ligand L_1 was synthesized by dissolving ethanolic solution of 0.0018 mol 2-aminophenol (0.196 gm) to the ethanolic solution of dicarbaldehyde (EDDC) (0.0009 mol, 0.243 gm). The reaction mixture was allowed to reflux for six hours at 70 °C. Suction filtration was used to recover the solid that formed after stirring. The desired product was obtained after recrystallization from hot ethanol as shown in Fig. 2 (Kumar and Kaur 2021).

2.3.3   Preparation of Metal Complex (ML_1)

0.001 mol of copper acetate salt solution in ethanol was transferred to the 0.001 mol solution of ligand in ethanol. After that, the mixture was refluxed for 4–5 h. Upon using a rotary evaporator to evaporate the solvent, the solid mass was obtained which further washed with C_2H_5OH and CH_3OCH_3 after that dried over vacuum desiccator (Fig. 3).

2.3.4   Photocatalytic Activity

Photocatalytic demineralization of aqueous solution of MB was conducted spectrophotometrically with Cu(II) complex of ligand (L_1) under visible light irradiation. The reaction mixture and the light source were separated by 5 cm^{-1}. The stock solutions of MB dye at different concentrations (mol/L) were prepared in Millipore

water. In a photo reactor, 50 mL of dye solution containing $Cu(II)(L_1)$ as catalyst and an appropriate amount of H_2O_2 (mL) were placed in a cylinder-shaped glass apparatus for photodegradation tests. The above solution was placed in the dark for 1 h to establish the adsorption and desorption equilibrium. To investigate the effect of the irradiation period, photocatalytic degradation studies were carried out for 10 to 50 min. At fixed time intervals, the rate of mineralization of MB was evaluated using Cu(II)photocatalyst. A spectrum was recorded in the 500–800 nm range on a UV-Visible spectrometer. $Cu(II)(L_1)$ activity with degradation of MB dye was investigated at various time intervals.

The following equation was used to calculate the percentage of dye degradation:

$$\text{Dye degradation } (\%) = \frac{[A_0 - A]}{[A_0]} \times 100 \tag{1}$$

where A_0 and A are the initial absorbance and A is the given time absorbance of solution.

The given below pseudo first order kinetics was used to interpret dye mineralization:

$$\ln(c_o/c_i) = k_{obs}t \tag{2}$$

where, k = rate constant, c_o = initial concentration of solution, t = time (min.), c_i = concentration of solution at given time.

A linear relationship was obtained when plotting $\ln(c_o/c)$ versus irradiation time t.

3 Results and Discussion

3.1 *Infrared Spectral Studies (FT-IR)*

The L_1 as shown in (Fig. 4) exhibited the primary peak of azomethine linkage of $^v_{CH=N}$ at 1618 cm^{-1} and peak $^v_{OH}$ of free ligand was attributed at 3405 cm^{-1}. As compared in complex there is a decrease in the value of 21 cm^{-1} from 1618 cm^{-1} ($^v_{CH=N}$) to 1597 cm^{-1} and also the frequency of ^{v}OH of the free ligand which was attributed at 3405 cm^{-1} decreases to frequency at 3285 cm^{-1} after complexation. As there is coordination linkage of nitrogen (–CH = N) and deprotonated oxygen (–OH) with copper ion the frequency of peaks shift to the lower region.
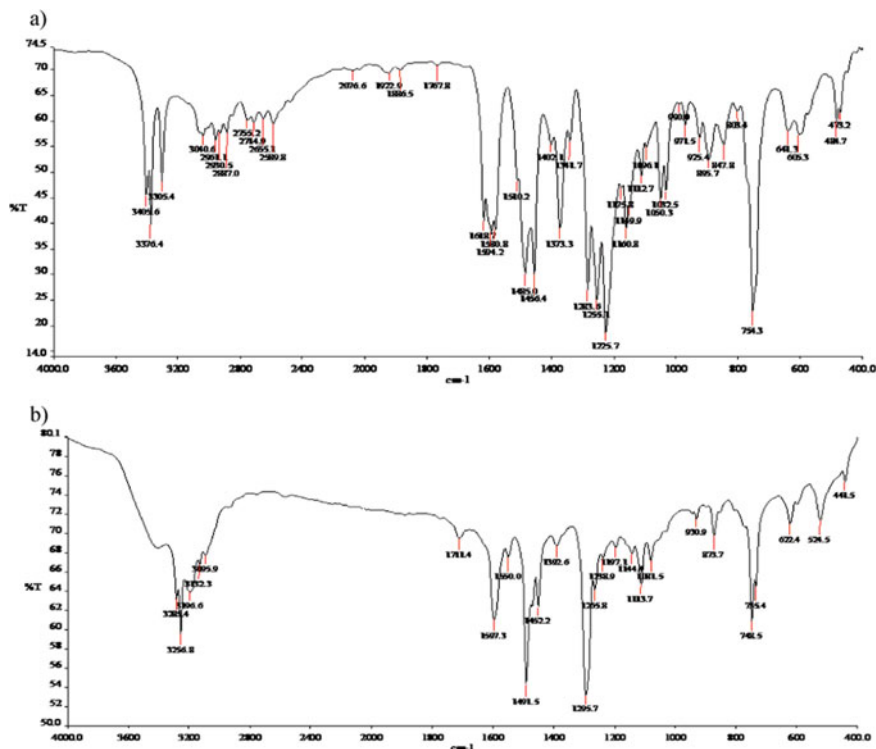
Fig. 4 IR spectra of **a** L$_1$, **b** ML$_1$

3.2 ^{1}H NMR Spectrum of Ligand L$_1$

In DMSO as a solvent, the ^{1}H NMR spectrum of the ligand, L$_1$ (Fig. 5) was obtained. The singlet 8.89 δ ppm is verified to phenoxy hydrogen-OH of free ligand while the presence of azomethine proton-CH $=$ N is attributed by singlet 8.21 δ ppm in the ^{1}H NMR data. This peaks indicates the formation of ligand. Aromatic ring protons are involved for multiplets ranging from 8.21 to 6.67 δ ppm, while bridging O-CH$_2$ functionality is observed for the singlet at 4.55 δ ppm.

3.3 Photo-Catalytic Mineralization Studies of MB Dye

3.3.1 Effect of Time of Irradiation

The effect of irradiation time on MB dye degradation and mineralization was investigated by considering the time ranging from 10 to 50 min. The maximum MB dye mineralization can be obtained within 50 min, according to the results, as shown in
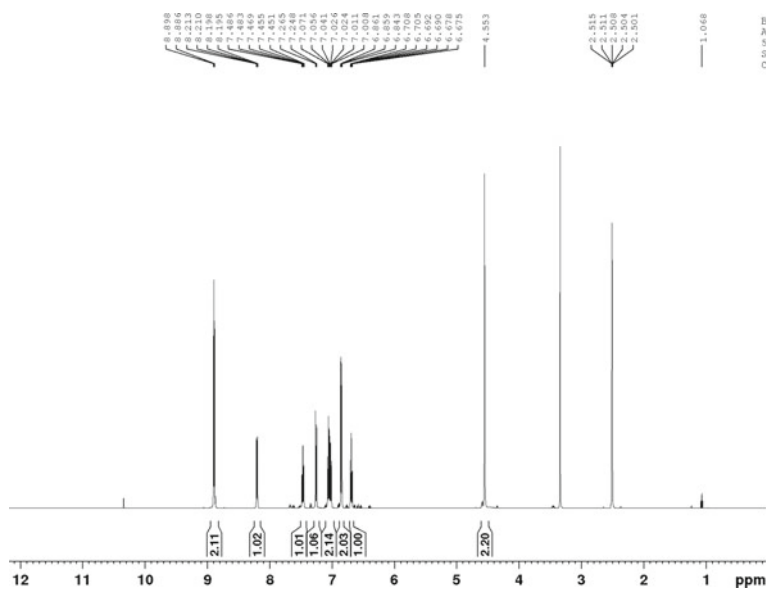
Fig. 5 ^{1}H NMR Spectrum of L$_1$

Fig. 6 and after that the rate is almost constant. The MB dye was almost completely degraded and subsequently mineralized after 50 min of visible light impact. Based on linear graph fitting of MB dye mineralization, the rate constant calculated was found to be k $= 2.20\ 10^{-2}\ min^{-1}$. The Cu(II)(L$_1$) was found to act as a catalyst for the oxidation of MB dye by activating H$_2$O$_2$. The maximum absorbance 660.00 nm

Fig. 6 Percentage of photo-degradation of MB under visible light irradiation
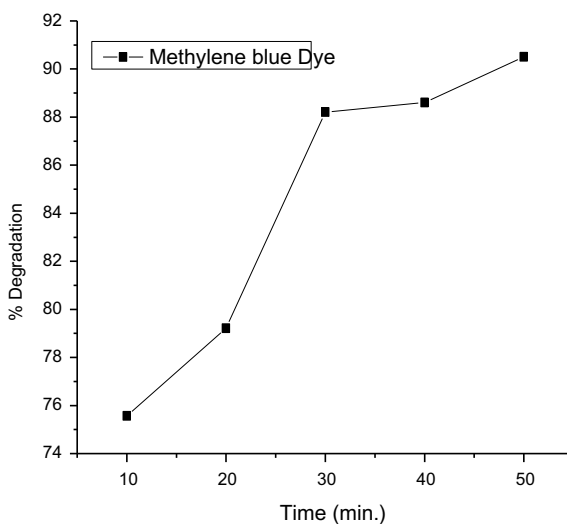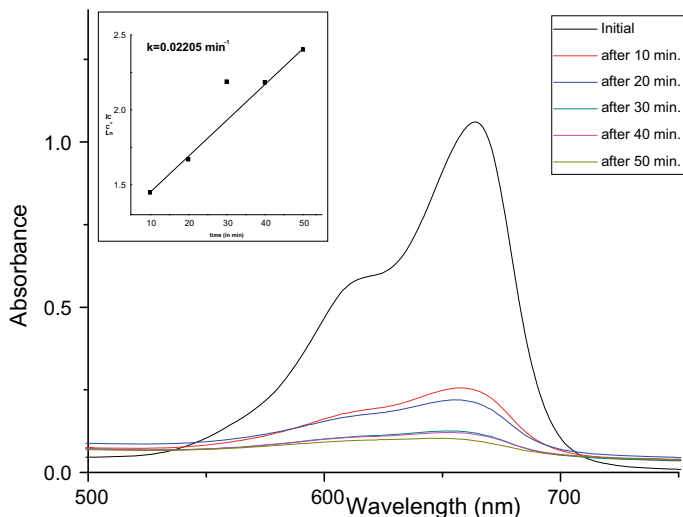
Fig. 7 Effect of irradiation time on MB degradation under visible light irradiation

(λmax) of MB dye was continuously reduced during the reaction process, indicating that the dye's conjugation ring was destroyed (Fig. 7).

3.3.2 Effect of Catalyst Concentration

The effect of concentration of complex was investigated by gradually increasing $Cu(II)(L_1)$ concentrations to have the optimal catalyst concentration for effective photodegradation and mineralization. It also decrease excessive photocatalyst usage. The concentration of substrate was maintained constant (1.50×10^{-5} mol/L) throughout the experimental procedure. Figure 8 depicted that degradation efficiency

Fig. 8 Effect of catalyst dosage on MB dye degradation
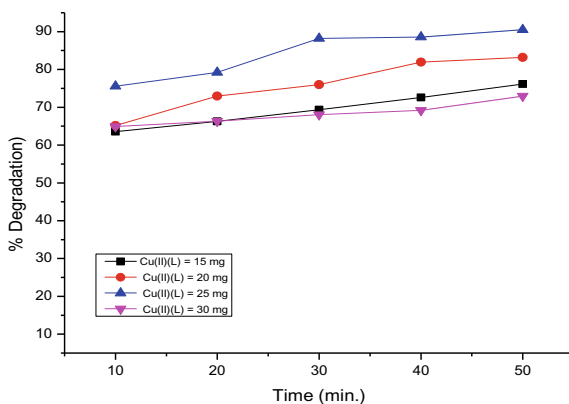
improves as it approaches up to 25 mg/50 mL of dye solution and after that it starts to decrease. As on increasing the dose concentration, the substrate molecules are insufficient to adsorb the increasing molecules of $Cu(II)(L_1)$ catalyst (Subramani et al. 2007). The rate does not rise when the catalyst concentration increases because the increasing catalyst quantity is unaffected by the catalyst's activities. Particles agglomerate on increasing the concentration of $Cu(II)(L_1)$, reducing the area between the reaction mixture and the catalyst. As a result, there is decrease in the number of active sites on the surface of the catalyst. The extra photocatalyst presence makes the turbid solution, and the loss in degradation efficiency might be attributed to the excess $Cu(II)(L_1)$ quantity causing a reduction in light penetration. In this present investigation, the optimal dose of catalyst concentration of $Cu(II)(L_1)$ complex was 25 mg for maximum MB dye degradation.

3.3.3 Effect of Substrate Concentration

At concentrations ranging from 1.0×10^{-5} to 2.5×10^{-5} mol/L, effect of substrate concentration on MB dye degradation was examined. The experimental data, which show that the rate of photocatalytic decolorization and mineralization is dependent on the initial concentration of MB dye as shown in Fig. 9. The rate of degradation was found to improve when the dye concentration was increased to 1.5×10^{-5} mol/L. An increase in dye concentration slows down the rate of degradation beyond this point. The solution gets more brightly colored as the dye concentration increases, and the path length of photons entering the solution reduces as fewer photons reach the catalyst surface. As a result, hydroxyl radical generation is decreased, and photo degradation efficiency is reduced (Subramani et al. 2007). The colloidal frequency between MB dye molecules rises as concentration rises, but the colloidal frequency between the $OH^\bullet$ free radical and dye molecules reduces (Lodha et al. 2008b). As a

Fig. 9 Influence of substrate concentration on MB dye degradation
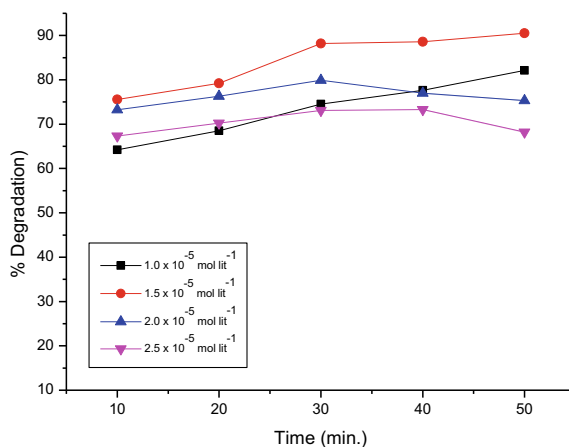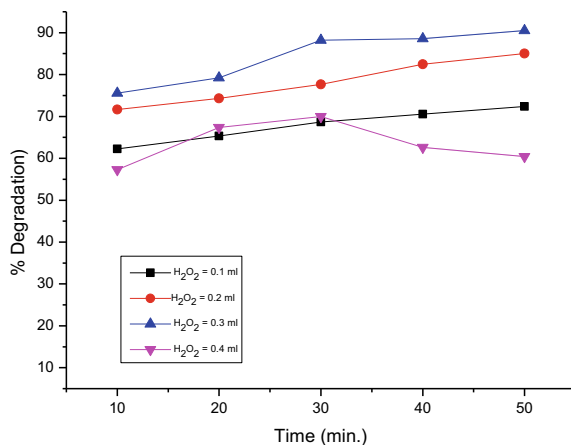
consequence, the optimal MB dye substrate concentration in the current study was
1.5×10^{-5} mol/L.

3.3.4 Effect of Hydrogen Peroxide

The variation of adding different amount of H$_2$O$_2$ was investigated by increasing
the H$_2$O$_2$ concentration in the system from 0.1 to 0.4 mL while maintaining the
optimal catalyst concentration and starting substrate concentration. Figure 10 shows
the variation in MB dye photodegradation rate as a function of H$_2$O$_2$ concentration.
The degradation of MB dye by adding0.3 $_{mL}$ of H$_2$O$_2$ was the fastest, and further
the rate of degradation of MB dye was insignificant after that. When H$_2$O$_2$ is added
to a heterogeneous system, the concentration of OH$^{\bullet}$ radicals rises. The maximum
degradation was attained within 50 min. In this investigation, the optimal amount of
H$_2$O$_2$ was found to be 0.3 $_{mL}$. Furthermore, excess H$_2$O$_2$ absorbs hydroxyl radicals
and acts as a hydroxyl radical scavenger when H$_2$O$_2$ concentration rises (Shintre and
Thakur 2008).

3.3.5 Effect of pH

To investigate the effect of pH conditions, the mineralization of MB dye using Cu(II)
complex as a photocatalyst and H$_2$O$_2$ was performed under visible light irradiation
at various pH levels as shown in Fig. 11. It was concluded that the pH of the solution
when raised from 5 to 12, the degradation and decolorization of the solution increases
upto pH 9. Degradation and decolorization were reduced as the pH was increased
more. When the pH of the solution reaches 12, the MB dye adsorption on the surface
of the catalyst increases, resulting in light penetration inhibition. The results showed
that the catalyst had greater catalytic activity for MB dye degradation at basic pH than
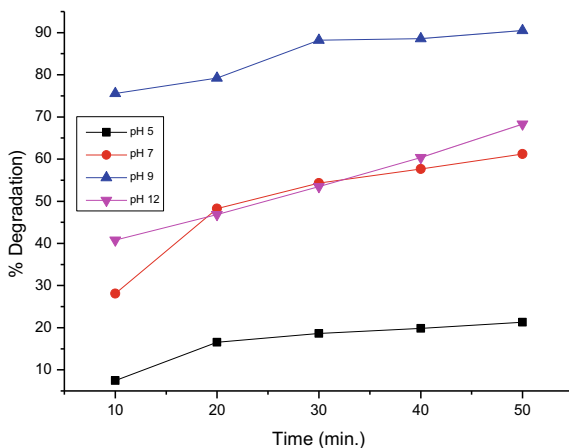
at acidic pH. Cu(II)(L$_1$) crosses the limitation of pH and extended the pH range in the photocatalytic system when exposure to visible light irradiation. The effectiveness of photocatalyst for degrading dye enhanced and MB dye degraded completely within 50 min. at pH 9 (Lodha et al. 2008a).

4 Conclusions

The synthesized Copper complex can be used as a photocatalyst to degrade hazardous dyes in waste water systems when exposed to visible light irradiation. The Cu(II)(L$_1$) catalyst can easily activate H$_2$O$_2$ to produce OH$^\bullet$ free radical, which effectively mineralized MB dye as it possess strong oxidizing potential. The analysis revealed that addition of hydrogen peroxide expedited degradation and mineralization process and the MB dye was degrade within 50 min after that the amount reaches to a certain critical point, that the degradation rate becomes independent. The amount of H$_2$O$_2$ that finally worked was 0.3 mL. At alkaline pH, the catalyst had greater catalytic activity for MB dye degradation than at acidic pH. The optimal MB dye substrate concentration was found to be as 1.5×10^{-5} mol/L. As per the studies, 25 mgL^{-1} amount of photocatalyst Cu(II)(L$_1$) in MB dye solution was shown to be the optimal amount for maximal dye degradation. The experimental results of this work clearly revealed the necessity of determining the appropriate degradation characteristics that are required for successful completion of photocatalytic oxidation for complete degradation and treatment of practical industrial wastewater.

References

Abdou SN, Faheim AA, Alaghaz A-N (2018) Synthesis, spectral characterization, cyclic voltammetry, molecular modeling and catalytic activity of sulfa-drug divalent metal complexes. Curr Synth Syst Biol 2(2):1–8

Arslan I, Balcioglu IA (1999) Degradation of commercial reactive dyestuffs by advanced oxidation process: a comparative study. Dyes Pigm 43:95–108

Arslan I, Balcioglu IA, Bahnemann DW (2000) Advanced chemical oxidation of reactive dyes in simulated dyehouse effluents by ferrioxalate-Fenton/UV-A and TiO_2/UV-A processes. Dyes Pigm 47:207–218

Booblan R, Lee G-H, Chen C (2012) Copper complex of aminoisoborneol Schiff base Cu_2(SBAIB-d)$_2$: an efficient catalyst for direct catalytic asymmetric nitroaldol (Henry) reaction. Adv Synth Catal 354(13):2511–2520

Cao TT, Zou CQ, Li RP, Huang YP (2001) Heterogenous degradation of toxic organic pollutants by hydrophobic iron(Ó) Schiff base complex under visible irradiation. Chem J Chin Univ 1:105–112

EI-Akabi H, Butters B, Delany D, Holden W, Powell T, Story J (1993) In: Ollis DF, AI-Ekabi H (eds) Photocatalytic purification and treatment of water and air. Elsevier Science Publishers, Amsterdam, pp 665–673

Forgacs E, Cserhati T, Oros G (2004) Removal of synthetic dues from wastewater: a review. Environ Int 30:953–971

Gabriel J, Shah V, Nesmerak K, Baldrian P, Nerud F (2000) Degradation of polycyclic aromatic hydrocarbons by the Copper(II) hydrogen peroxide system. Folia Microbiol 45(6):573–575

Gregor KH (1992) In: Eckenfolder WW, Bowers AR, Roth JA (eds) Oxidative decolourization of textile waste water with advanced, chemical oxidation technologies for the nineties, Lancaster, Basel, pp 161–193

Gupta KC, Sutar AK (2008) Catalytic activities of Schiff base transition metal complexes. Coord Chem Rev 252:420–1450

Habibi MH, Hassanzadeh A, Mahdavi S (2005) The effect of operational parameters on the photocatalytic degradation of three textile azo dyes in aqueous TiO_2 suspensions. J Photochem Photobiol a: Chem 172:89–96

Herrera F, Kiwi J, Lopez A, Nadtochenko V (1999) Photochemical decoloration of remazol brilliant blue and uniblue A in the presence of Fe^{3+} and H_2O_2. Environ Sci Technol 33:3145–3151

Jyoti D, Kumar H (2019) Role of copper Schiff-base complex for photocatalytic degradation of methylene blue under visible irradiation. J Emerg Technol Innov Res 6(5):70–82

Kumar H, Kaur A (2021) Synthesis of metal complex for photocatalytic degradation of dyes under visible light irradiation. IOP Conf Ser: Earth Environ Sci 785:012017

Kuo WG (1992) Decolorizing dye wastewater with Fenton's reagent. Water Res 26:881–886

Liu L, Jiang D, McDonald A, Hao Y, Millhauser GL, Zhou F (2011) Copper redox cycling in the prion protein depends critically on binding mode. J Am Chem Soc 133:12229–12237

Lodha S, Jain A, Sharma VK, Punjabi PB (2008a) Photocatalytic degradation of rhodamin-b using metal complexes and hydrogen peroxide. Indonesian J Chem 42:42–46

Lodha S, Vaya D, Ameta R, Punjabi PB (2008b) Photocatalytic degradation of phenol red using complexes of some transition metals and hydrogen peroxide. J Serb Chem Soc 73:631–639

Nerud F, Baldrian P, Gabriel J, Ogbeifun D (2001) Decolorization of synthetic dyes by the Fenton reagent and the Cu/pyridine/H_2O_2 system. Chemosphere 44:957–961

Reddy GR, Balasubramanian S, Chennakesavulu K (2014) Zeolite encapsulated Ni(II) and Cu(II) complexes with tetradentate N_2O_2 schiff base ligand: catalytic activity towards oxidation of benzhydrol and degradation of rhodamine-B. J Mater Chem A 2:15598–15610

Ruck RT, Jacobsen EN (2002) Asymmetric catalysis of hetero-ene reactions with tridentate Schiff base chromium(III) complexes. J Am Chem Soc 124:2882–2883

Salem IA (2000) Kinetic of the oxidative color removal and degradation of bromophenol blue with hydrogen peroxide catalyzed by Copper (II)-supported alumina and zirconia. Appl Catal b: Environ 28:153–162

Sedai B, Diaz-Urrutia C, Baker RT, Wu R, Silks LK. "Pete", Hanson SK (2011) Comparison of copper and vanadium homogeneous catalysts for aerobic oxidation of lignin models. ACS Catal 1:794–804

Shintre NS, Thakur PR (2008) Photo-catalyzed degradation of p-nitrophenol employing TiO_2 and UV radiations. J Environ Sci Eng 50:299–302

Subramani K, Byrappa K, Ananda S, Rai K (2007) Photocatalytic degradation of indigo carmine dye using TiO_2 impregnated activated carbon. Bull Mater Sci 30:37–41

Watanabe T, Koller K, Messner K (1998) Copper-dependent depolymerization of lignin in the presence of fungal metabolite, pyridine. J Biotechnol 62(3):221–230

Zahng Z, Li X, Wang C, Zhang C, Liu P, Fang T, Xiong Y, Xu W (2012) A novel dinuclear Schiff-base copper(II) complex modified electrode for ascorbic acid catalytic oxidation and determination. Dalton Trans 41:1252–1258

Environmental Impact Assessment of Potato Cultivation in Northern India

Rohit Kumar, Arvind Bhardwaj, and Lakhwinder Pal Singh

Abstract Potato (Solanum tuberosum) is a staple food crop and a major agricultural product in the northern part of India. However, the provinces are confronted with issues such as water scarcity, nitrate contamination, and plant disease outbreaks. Potato production has also imposed a significant environmental burden, especially when we consider the usage of resources and the environmental impact of the production of fertilizers, pesticides, and electricity. The cradle to gate approach was used, which included agricultural activities as well as machinery used, time of service, amount of seed potatoes, fertilizers, pesticides, used gasoline, and water. The Sima Pro version 9.0 along with CML 2 baseline 2000 method were used to assess the environmental correlations of all the inputs and outputs included in the LCA research and estimate their possible environmental impact. The results revealed that the fertilization phase had the highest negative impact on the environment. In the present study, some agriculture practice approaches are recommended while potato production includes environmental thresholds using agri-environmental indicator scores and their relationships.

Keywords Life cycle assessment · Potato production · Sima pro · Agricultural · Environmental impact assessment

1 Introduction

Agriculture is a dynamic area that offers a vast variety of products that are valuable to society. The agricultural sector contributes 6.4% ($5,084,800 million) to global economic production, in which India is responsible for 7.39% of global agricultural output, and is the second-largest contributor after China. Agriculture is the primary source of livelihood for about 58% of India's population. Moreover, Gross Value Added by agriculture, forestry, and fishing was estimated at Rs. 19.48 lakh crore (US$ 276.37 billion) in FY20 (IBEF 2020). The basic meaning of the term agriculture

R. Kumar (✉) · A. Bhardwaj · L. P. Singh
Dr B R Ambedkar National Institute of Technology, Jalandhar, Punjab 144011, India
e-mail: rohitk.ip.19@nitj.ac.in

Table 1 Impact Categories associated with Agriculture Production

Impact category	Indicators	Units	References
Ecosystem	Climate change Acidification potential Eutrophication potential Ozone depletion potential Ozone creation potential	[kg CO_2eq] [kgSO_2 eq] [kg Phosphate eq] [kg R11 eq] [kg ethane eq]	Guinée et al. (2001) Guinée et al. (2001) Guinée et al. (2001) Guinée et al. (2001) Tilman et al. (2001)
Resources	Water5Consumption Energy Use	[m^3] [MJ net calorific]	Bayart et al. (2010) N/A—inventory level indicator
Human Health	Human. Toxicity Potential Ecotoxicity potential	[kg 1,4-DB eq] [kg 1,4-DB eq]	Rosenbaum et al. (2008) Rosenbaum et al. (2008)

from Merriam-Webster is science, art, or practice of planting soil, growing crops, and raising livestock as well as planning and selling the resulting goods. According to the United Nations world population prospects as the global population is anticipated to exceed 9.6 billion by 2050, this would intensify the need for resources. This Intense demand for the resources needed for agricultural production would lead to insufficient land, water, mineral resources, fuels, and so on. To support the projected human population growth, agriculture would need to generate expanded food, fiber and biomass energy products within the constraints of these finite resources, while at the same time reducing the associated environmental impacts (Guinée et al. 2001). Moreover, Modern agronomy, plant breeding, inorganic chemicals such as pesticides and fertilizers, and advancement in technology have raised yields sharply, thereby causing extensive ecological and environmental damage (Shafiq and Rehman 2000).

On a Global basis, agriculture production feeds more than 7 billion people; however, it is also a significant source of different forms of environmental pollution and thus produces immense environmental costs (Clark and Tilman 2017; Tilman et al. 2001). To satisfy food demand while simultaneously encouraging sustainable agriculture, an effective approach including a range of sustainable agricultural practices is required. The agriculture sector contributes to a wide range of different environmental effects, including ecosystem, human health, and resources (Notarnicola et al. 2015). As indicated in Table 1, some of the most significant impact indicators are listed there. These Impact categories help us to make actionable statements about how emissions influence the environment.

1.1 Environmental Impacts Associated with Agriculture

Agriculture production requires enormous amounts of resources such as water, fossil fuels, and agricultural chemicals, all of which damage the environment in different ways (Shafiq and Rehman 2000). Overuse of pesticides pollutes the environment by

releasing greenhouse gases into the atmosphere and by contaminating water supplies. Drainage and leaching of nitrates from agricultural land, as well as the overuse and abuse of chemical pesticides, contaminate India's freshwater resources (Anju et al. 2010). In a recent study by Bosona and Gebresenbet (2018), they used the life cycle assessment method in conjunction with the SimaPro8.2 software to investigate the cumulative energy demand and global warming potential of organic tomatoes grown and consumed in Sweden by taking the system boundary of the cradle-to-consumer gate into consideration. After the quantification of the indicators, the post-harvest and transportation phases were identified as hotspot stages for both energy use and climate impact. Similarly, recent research by Sreekumar et al. (Sreekumar et al. 2020) presented a systematic LCA of a novel process to produce ethanol from rice straw in India. The results indicate that the global warming potential (GWP), one of the impact categories of concern, is 2.82 kg CO_2eq. per liter of ethanol. According to their research, electricity is responsible for 86% of the overall impact. This implies that there is a huge potential to substantially decrease the total effect by switching to a more sustainable energy source, such as solar or hydro. Aside from that, frequent ploughing has also a significant impact on the overall quality and structure of the soil. Moreover, Kowalczyk and Cupiał (2020) found significant conclusions by a comparison study of traditional and organic carrot processing technologies in the scope of their effect on the environment in the south of Poland. Some sustainability ideas were suggested in their studies with respect to locally produced organic carrot supply chains. Vegetables, like potatoes, are grown using various technologies, each with a different environmental effect, depending on the cultivation area, yield designation, soil quality, mechanization techniques, and so on, necessitating extensive analysis.

1.2 Environmental Impact Assessment Tools

Environmental impact assessment tools are used to determine the environmental, social, and economic consequences of a project prior to decision-making. The main objective is to promote the awareness of environmental concerns in planning and decision-making and eventually to take action that is more environmentally compatible (Tukker 2000). Environmental impact assessment is broadly classified into three categories Management based tools (Environmental audits, Law and policy, Environmental performance evaluation, etc.), Process-based tools (Environmental technology Assessment, Toxic use reduction, Eco-efficiency), Product based tools (Eco-labeling, Industrial ecology, Life cycle assessment). Among the variety of evaluation methods, life-cycle assessment (LCA) is known to be one of the most informative tools for evaluating the environmental impacts of farm products (Vries and Boer 2010). A variety of software packages, such as SimaPro, OpenLCA, Gabi, and Umberto, etc., may be used to conduct a comprehensive impact assessment of the process or product (Iswara et al. 2020). As the obtained results are not dependent

on the choice of software (Speck et al. 2016), Sima Pro version 9.1.1 is utilized for impact assessment owing to its availability.

1.3   Potato as a Crop

Potatoes (Solanum Tuberosum L.) is a significant agricultural crop in the Region of Punjab, India, and a staple meal for numerous people. The favorable climate conditions of this crop are the usual mean air temperature between 15 and 18 °C throughout the growing season and rainfall or irrigation provides optimum water. Potatoes are planted in the rabi season (October to December) at a seed rate of 1.40 kg per 10 m^2. Planting distances for potato crops are 50×20 cm and 60×25 cm. Moreover, the plant is characterized by a high nutritional and energy value per unit of the area (Zangeneh et al. 2010).

Despite this, the state is facing problems like as water shortages, nitrate contamination, and an outbreak of plant diseases. The purpose of this research was to investigate the environmental impact assessment of potato farming operations in the Indian state of Punjab.

1.4   Life Cycle Assessment

Life-cycle assessment is considered to be one of the most informative techniques available for assessing the environmental effects of agricultural products (Vries and Boer 2010). The life cycle assessment technique is extensively utilized to aid in the development of sustainable solutions. Life cycle impact assessment is a comprehensive technique for assessing environmental impacts associated with a product over its entire lifetime, from resource extraction through processing, manufacturing, distribution, use, and disposal or recycling. A common governing standard can be found in ISO 14040 and ISO 14044 for such an assessment, which was last reviewed and confirmed in 2016. These standards specify the requirements and provide guidelines for life cycle assessment. The Environment-damaging impacts of crop cultivation result not only came from field activities, but also from the extraction and manufacture of inputs (fuels, fertilizers, and pesticides), as well as the transportation of these inputs. To conduct a comprehensive assessment of the system, all of these aspects must be taken into consideration. The LCA method analyses consist of a boundary in which all inputs and outputs are cross for a certain production system. The reference unit, which denotes the useful output, is referred to as the functional unit and has a specified quantity and quality, such as 1 ton of wheat producing bread. By understanding environmental hotspots, you may help to minimize the environmental load caused by agricultural production. Moreover, by comparing products, life cycle assessment may assist farmers in increasing their revenue and productivity by implementing the alternatives recommended by the LCA model. So, in order to
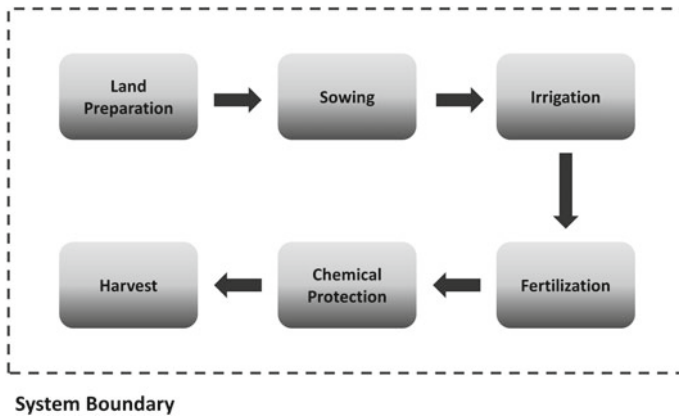
Fig. 1 System boundary of potato production

make conscientious decisions we have to measure or compare the environmental impacts with the aid of life cycle assessment.

2 Methodology

2.1 Goal and Scope

The description of the goals and scope of the LCA is the first stage in the process. A decision is made at this step about both the goals of the LCA research as well as the limitations or scope of the LCA analysis. The environmental impact of potato production per hectare is the functional unit taken in the study. In the present study farm gate was taken as a system boundary which encompasses agriculture practices such as land preparation, sowing, irrigation, fertilization, chemical protection, and harvesting. The system boundary of the potato cultivation system is shown in Fig. 1.

2.2 Life Cycle Inventory

New data for agricultural productivity were obtained, and while the number of farms was small, it was discussed with experts, so it is thought to be of reasonable quality. The median data values from five potato cultivation farms (less than five hectares) were used in this study. The inventory data were gathered directly from farmers and agriculture experts via face-to-face set of questionnaires. The data on the production of faming inputs and energy carriers (agrochemical production, power generation, transportation, and so on) was obtained from the Eco-invent 3.7 database. A number

Table 2 Description of inputs for one hectare of potato cultivation system

Inputs	Unit	Value
Ploughing	Liter diesel/ha	10
Rotavator	Liter diesel/ha	6
Leveler	Liter diesel/ha	16
Seed Potatoes	Kg	2500
Planter (tractor implement)	Liter diesel/ha	17.5
Diammonium phosphate	kg/ha	300
Muriate of potash	kg/ha	185
Urea	kg/ha	125
Mancozeb	kg/ha	2
Irrigation	m^2/ha	2500
Transportation	km	50
Harvester	liter diesel /ha	30
Emission to Air (Taken from Literature roots et al. 2009)		
NPK fertilizers	kg CO_2e/kg N	6.8
Diesel	kg CO_2e/MJ diesel	0.004

of inputs of potato cultivation were collected through face-to-face interviews with potato farmers. Identical units were used (as shown in Table 2) to acquire data for specific materials, raw materials, energy, processes, etc.

2.3 System Inputs

Table 2 lists all of the inputs, as well as all of the agricultural practices, that were utilized throughout the potato production process. This also includes information on the amount of fuel used by agricultural activities, as well as the amount of fertilizer and pesticides applied per hectare of land. The production of diesel fuel utilized in machine operations was included, and the overall diesel fuel consumption was estimated using information about the required operations. An average distance of 50 km was estimated for the transportation of fertilizers, insecticides, and seeds from the point of sale to the farm.

3 Results and Discussion

The objective of an LCA is to provide results that may be used to assist in making a wise decision or to provide you with a comprehensible conclusion. The result

shows the ten impact indicators including Abiotic depletion, Ozone layer depletion, Eutrophication potential, Global warming potential, Acidification potential, Photochemical oxidation potential, Human toxicity potential, Terrestrial ecotoxicity potential, Freshwater and marine aquaticecotoxicity potential.

To suit the demands of their study, each researcher selects a number of them. Three impact categories Abiotic depletion, Ozone layer depletion, and global warming potential, were used for this present study. In the one-hectare potato agricultural system, the effect groups' categorization indices for abiotic depletion, global warming, potential, and Ozone layer depletion are 16.22097 kg Sb eq, 2013.815 kg CO_2 eq, and 0.000304 kg CFC-11 eq, respectively. The global warming potential (GWP) is a measurement of how much a range of gases released by farming systems contribute to environmental concerns and climate change which encompass mainly three major gases i.e., carbon dioxide, nitrous oxide and methane (Brentrup et al. 2004). In the present study major hotspot of greenhouse gas is fertilizer production which is 917.92 kg CO_2 eq as showing in Fig. 2. By optimizing nitrogen fertilizer usage and raising organic fertilizer use, as well as planting legumes in rotation, may assist to minimize the usage of synthetic fertilizers and the greenhouse impacts they generate.

The abiotic depletion was 16.22 kg Sb eq., which was mostly caused by fertilization and sowing practices as showing in Table 3. According to Williams et al., the major cause of ADP in potato production, as determined by simulation and system modeling, was the use of chemical fertilizers and energy (Williams et al. 2010). The utilization of low-power, high-efficiency technologies, alternative growing practices
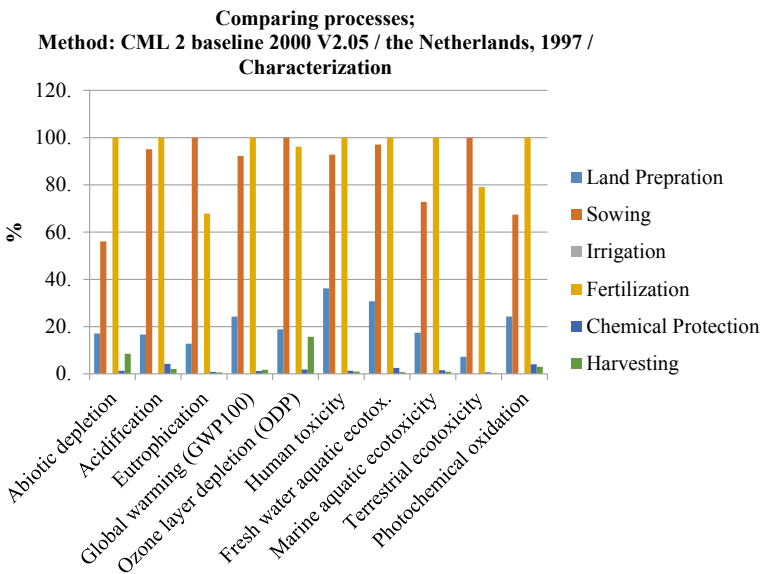
Fig. 2 Comparison of agriculture practices results w.r.t per hectare of potato production

Table 3 Total life cycle impact assessment related to one hectare of potato production

Impact indicators	Unit	Land preparation	Sowing	Fertilization	Chemical protection	Harvesting
Abiotic Depletion	kg Sb eq	1.511085	4.972081	8.862243	0.117512	0.75805
Acidification	kg SO_2 eq	1.341672	7.648354	8.042092	0.341181	0.169844
Eutrophication	kg PO4-eq	0.426247	3.334738	2.26152	0.029238	0.021255
Global warming (GWP100)	kg CO_2 eq	222.2898	846.4524	917.9269	11.07921	16.06623
Ozone Layer depletion (ODP)	kg CFC-11 eq	2.47E-05	0.000131	0.000126	2.44E-06	2.05E-05
Human toxicity	kg 1,4-DB eq	375.4736	961.8723	1036.284	13.71931	10.37586
Fresh water aquatic ecotoxicity	kg 1,4-DB eq	101.595	320.8347	330.5957	8.420882	2.513293
Marine aquatic ecotoxicity	kg 1,4-DB eq	141,299.5	590,402.6	811,364.8	12,715.92	7383.749
Terrestrial ecotoxicity	kg 1,4-DB eq	0.880279	12.16294	9.619982	0.085126	0.049189
Photochemical oxidation	kg C2H4 eq	0.082706	0.229274	0.340194	0.013899	0.010206

and precision farming can help to mitigate the harmful environmental impacts caused by this indicator.

Aside from that, one hectare of potato cultivation results in the release of 0.000304 kg of CFC-11 emissions into the atmosphere, which is a significant amount of emissions released into the atmosphere. According to Iriarte et al. (2010) most significant causes influencing ozone layer depletion were the manufacturing of chemical fertilizer and diesel fuel. Diesel fuel, which accounts for 55% of all emissions, is the primary source of these harmful pollutants. Pesticide usage and emission into the atmosphere are contributing significantly to ozone layer depletion. So, It is critical to prepare ahead of time for the use of diesel fuel and pesticides, particularly in potato production.

4   Conclusion

In order to establish a sustainable agro-ecosystem and safeguard natural resources, there must be alternative and optimized agriculture practices need to be presented. Based on the research findings, it has been determined that:

- Replacing flood irrigation with contemporary technologies like pressured irrigation may minimize water use, which in turn reduces power consumption and greenhouse gas emissions.
- Energy and chemical fertilizer management, as well as the precise timing of these fertilizers, can help to mitigate the negative effects of potato production.
- Particularly in potato production, it is important to prepare adequately for the use of diesel fuel and pesticides.

References

Anju A, Ravi SP, Bechan S (2010) Water pollution with special reference to pesticide contamination in India. J Water Resource Protect

Bayart JB, Bulle C, Deschênes L, Margni M, Pfister S, Vince F, Koehler A (2010) A framework for assessing off-stream freshwater use in LCA. Int J Life Cycle Assessm 15(5):439–453

Bosona T, Gebresenbet G (2018) Life cycle analysis of organic tomato production and supply in Sweden. J Clean Prod 196:635–643

Brentrup F, Küsters J, Kuhlmann H, Lammel J (2004) Environmental impact assessment of agricultural production systems using the life cycle assessment methodology: I. Theoretical concept of a LCA method tailored to crop production. Eur J Agron 20(3):247–264

Clark M, Tilman D (2017) Comparative analysis of environmental impacts of agricultural production systems, agricultural input efficiency, and food choice. Environ Res Lett 12(6):064016

De Vries M, de Boer IJ (2010) Comparing environmental impacts for livestock products: a review of life cycle assessments. Livest Sci 128(1–3):1–11

Guinée JB, Huppes G, Heijungs R (2001) Developing an LCA guide for decision support. Environ Manage Health

IBEF (2020) http://www.ibef.org/industry/agriculture-india.aspx Assessed on 20 Jan 2020

Iriarte A, Rieradevall J, Gabarrell X (2010) Life cycle assessment of sunflower and rapeseed as energy crops under Chilean conditions. J Clean Prod 18(4):336–345

Iswara AP, Farahdiba AU, Nadhifatin EN, Pirade F, Andhikaputra G, Muflihah I, Boedisantoso R (2020) A comparative study of life cycle impact assessment using different software programs. In: IOP conference series: earth and environmental science, vol. 506, no. 1. IOP Publishing, p 012002

Kowalczyk Z, Cupiał M (2020) Environmental analysis of the conventional and organic production of carrot in Poland. J Clean Prod 269:122169

Notarnicola B, Salomone R, Petti L, Renzulli PA, Roma R, Cerutti AK (eds) Life cycle assessment in the agri-food sector: case studies, methodological issues and best practices. Springer (2015)

Rosenbaum RK, Bachmann TM, Gold LS, Huijbregts MA, Jolliet O, Juraske R, Hauschild MZ (2008) USEtox—the UNEP-SETAC toxicity model: recommended characterisation factors for human toxicity and freshwater ecotoxicity in life cycle impact assessment. Int J Life Cycle Assessm 13(7):532–546

Shafiq M, Rehman T (2000) The extent of resource use inefficiencies in cotton production in Pakistan's Punjab: an application of data envelopment analysis. Agric Econ 22(3):321–330

Speck R, Selke S, Auras R, Fitzsimmons J (2016) Life cycle assessment software: selection can impact results. J Ind Ecol 20(1):18–28

Sreekumar A, Shastri Y, Wadekar P, Patil M, Lali A (2020) Life cycle assessment of ethanol production in a rice-straw-based biorefinery in India. Clean Technol Environ Policy 22(2):409–422

Tilman D, Fargione J, Wolff B, D'antonio C, Dobson A, Howarth R, Swackhamer D (2001) Forecasting agriculturally driven global environmental change. Science 292(5515):281–284

Tukker A (2000) Life cycle assessment as a tool in environmental impact assessment. Environ Impact Assess Rev 20(4):435–456

Williams AG, Audsley E, Sandars DL (2010) Environmental burdens of producing bread wheat, oilseed rape and potatoes in England and Wales using simulation and system modelling. Int J Life Cycle Assessm 15(8):855–868

Zangeneh M, Omid M, Akram A (2010) A comparative study on energy use and cost analysis of potato production under different farming technologies in Hamadan province of Iran. Energy 35(7):2927–2933

Evaluation of Drugs as Corrosion Inhibitors for Metals: A Brief Review

Shveta Sharma, Richika Ganjoo, Suresh Kumar, and Ashish Kumar

Abstract The use of chemical inhibitors is crucial to keep corrosion in check. Various inorganic and organic compounds are used as inhibitors, although their usage is being phased out in favors of newer and less toxic inhibitor types that produce desired results. For this purpose, the drugs are considered an excellent alternative to the toxic inhibitors, as the drug molecules contain heteroatoms oxygen, nitrogen, and sulfur, and they are less hazardous to the environment. Drugs are successfully inhibiting the corrosion of various metals like Steel, Zn, Cu, Al, etc. and generally, their corrosion inhibition efficiency is verified by employing the Weight Loss Technique, Electrochemical Analysis, and surface morphology are investigated by Scanning Electron Microscopy, Atomic Force Microscopy, etc. In this review article majority of the literature's past studies on the usage of drugs as corrosion inhibitors for different metals are summarized along with the main techniques used for corrosion inhibition study.

Keywords Corrosion · Corrosion inhibitor · Drugs

1 Introduction

Over the past many years, hazardous, biodegradable, and corrosion inhibitor contaminants released into the environment have become a major concern. Corrosion inhibitors must be non-polluting, safe, and cost-effective for a variety of reasons, including safety, environmental pollution, and economics (Nathiya et al. 2018). Gray inhibitors are those that are harmful to the environment, whereas green inhibitors are those that are beneficial to the environment. For several metals, non-toxic "green" corrosion inhibitors have been described. Organic chemicals, amino acids, plant

S. Sharma (✉) · S. Kumar
Govt. P.G. College Una, Una, India
e-mail: drashishchemlpu@gmail.com

R. Ganjoo · A. Kumar (✉)
Department of Chemistry, School of Chemical Engineering and Physical Sciences, Lovely Professional University, Phagwara, Punjab 144411, India

extracts, and rare earth metal compounds are among them (Ameh and Sani 2016). Organic compounds generally have N, O, S as heteroatoms, and pi-electron clouds present in molecules are often employed to safeguard metals and alloys and are thought to be excellent corrosion inhibitors (Fayomi et al. 2018a). The substructures of many widely used medicines are very similar to the overwhelming majority of these organic compounds like pyridines, isoxazoles, etc. This characteristic has led researchers all around the world to look into the use of medicines as corrosion inhibitors. Due to their non-toxic qualities and minimal to no environmental impact, drugs have emerged as potential alternatives to hazardous corrosion inhibitors (Bashir et al. 2020a). Also they are cost effective as compare to other organic compounds to be utilized as inhibitors and the expired drugs can also be utilized, which can also solve the problem of disposal of these expired drugs. Moreover, preparation of these medications is also a simple process. Drugs forms a thin protective layer on the top of metallic sample under investigation. Either electrostatic interaction is there between sample and drug molecule or electrons are donated by employing the hetero atoms, π bonds of the drug towards sample, which are also called as donor-acceptor interactions and chances of back donation from the metallic sample to drug molecules are also there. In the past studies many antibiotic and antibiotic derivatives were already investigated for reducing the corrosion of different metals (Karthikeyan 2016; Pathak and Mishra 2016). Drugs have been employed to mitigate corrosion for different metals in varied conditions, according to a significant number of research papers (Fayomi et al. 2018b). Sometimes the limitation of using the drug molecule as corrosion inhibitor is their larger size, which creates the solubility problem. As a result, we have concentrated and tries to give an overview on the use of medicines for reducing corrosion in different solutions for iron, aluminium, zinc, and copper metals (Nwanonenyi et al. 2019).

2   Drugs as Corrosion Inhibitors for Mild Steel in Corrosive Medium

Due to two main factors cost effectiveness and mechanical strength, mild steel is widely employed in numerous sectors and in industries generally acids are employed for descaling process, which cause the deterioration of structures made up of mild steel. For mitigating the corrosion of mild steel structures, the organic compounds were preferred because of the presence of pi electron cloud, ring structures, heteroatoms, which help in the better physical or chemical adsorption of these compounds on the metallic surface. But due to hazardous and toxic nature of organic compounds, the research is shifting towards the use of drug molecules as corrosion inhibitors. In Table 1 few recent researches in which drugs were effectively employed on mild steel in different media are summarized (Singh et al. 2017, 2019a; Palaniappan et al. 2019; Xu et al. 2017; Gupta et al. 2017).

Table 1 Inhibition efficiency of recently studied drugs against Mild Steel Corrosion

S. No.	Name of the drug	Medium	Adsorption isotherm	Inhibition efficiency (%)
1	Atorvastatin	1 M HCl	Langmuir adsorption isotherm	96.3% at 150 ppm
2	Rabeprazolesodium, Domperidone and Benfotiamine	3.5% NaCl	–	98%
3	Dapsone	0.5 M H_2SO_4	Langmuir adsorption isotherm	95.67% and 94.23%, increased to o 99.03% and 97.98% after adding KI
4	Biotin	15% HCl	Langmuir adsorption isotherm	98% at 500 ppm
5	Atenolol and Nifedipine	1 M HCl	–	91.30 and 93.91% at 200 ppm

3 Drugs as Corrosion Inhibitors for Aluminum in Corrosive Medium

Aluminum is extensively utilized as the container for a variety of industrial processes, including chemical reactions, pipelines, equipment, and chemical batteries, due to its corrosion resistance. The development of a protective surface oxide layer is responsible for aluminum's corrosion resistance. Aluminum and its alloys, on the other hand, are easily corroded by strong acid assault. The first line of defense against corrosion is the employment of organic inhibitors. The organic inhibitors create a thin layer on the metallic surface that isolates, protects and shields it from corrosion. Drugs are the most promising alternative options for protecting aluminium against corrosion in acidic solutions since they are usually of biological origin, have a strong inhibitory performance at low concentrations, and are biodegradable. Several drugs that have been tested and confirmed in the past as efficient corrosion inhibitors for aluminium in acidic environments are summarized in Table 2 (Bashir et al. 2020b, 2020c; Su et al. 2020; Akande et al. 2020; Udeh et al. 2021).

4 Drugs as Corrosion Inhibitors for Copper in Corrosive Medium

Copper and its alloys are often utilized in industries because of their noble qualities, mechanical workability, and high electrical and thermal conductivity. Copper and its alloys are used as a conductor in electronic industries and communications, pipelines for industrial and residential water utilities as well as seawater, heat exchangers and conductors, and other applications. As a result, copper corrosion and its prevention

Table 2 Inhibition efficiency of recently studied drugs against Aluminium corrosion

S. No.	Name of the drug	Medium	Adsorption isotherm	Inhibition efficiency (%)
1	Nicotinamide	0.5 M HCl	Langmuir adsorption isotherm	94.5 at 4000 ppm
2	Bronopol	0.5 M HCl	Langmuir adsorption isotherm	93.89% at 4000 ppm
3	Theophylline	1 M NaOH	–	91% at 2.5% of inhibitor
4	Suphtrim	0.5 M H_2SO_4	Freundlich isotherm	52.55% at 20 ml of inhibitor
5	Kolestran	1 M H_2SO_4	–	78.57 at 0.8 g/l

Table 3 Inhibition efficiency of recently studied drugs against copper corrosion

S. No.	Name of the drug	Medium	Adsorption isotherm	Inhibition efficiency
1	Cefotaxime	0.1 mol L^{-1} HCl	Langmuir's adsorption isotherm	91.5%12 $\times 10^{-5}$ mol/L
2	Meropenem	1 M HNO_3	Temkin adsorption isotherm	98.7 at 300 ppm
3	Nafcillin	1 M HCl	Temkin adsorption isotherm	98.28% at 0.0001 g
4	Cephradine	0.9% NaCl solution	Langmuir adsorption isotherm	92.4% at 5 $\times 10^{-3}$ M
5	Cefadroxil	1 M HNO_3	Langmuir isotherm	94% at 2 mM

have gotten a lot of press. Several chemical medications have been studied as copper corrosion inhibitors in acidic solutions. The drugs with exceptional copper inhibition efficiency are summarized in Table 3 (El-Haddad 2016; Fouda et al. 2016; Shahraki et al. 2017; Tasic et al. 2018; Yao and Trokourey 2019).

5 Drugs as Corrosion Inhibitors for Zinc in Corrosive Medium

Zinc is generally used for preparing anodes and for coating steel sheets. But it is one of the non-ferrous materials, which disintegrates in an acidic or basic medium very easily. Also in the pickling and descaling processes, the acid used increases the corrosion process manifolds (Pais and Rao 2019; Abdallah et al. 2019; Khalil 2014; Sun et al. 2017). Zinc corrosion is more pronounced below 6.5 and above pH of 12 and it deteriorates by forming white rust (Mahida and Chaudhari 2012; Shanbhag et al. 2011). Therefore to reduce the Zinc metal mitigation and to decrease

Table 4 Inhibition efficiency of recently studied drugs against Zinc Corrosion

S. No.	Name of drug	Medium (M HCl)	Adsorption isotherm	Inhibition efficiency
1	Seroquel	0.1	Temkin adsorption isotherm	84.38% at 1000 ppm
2	Paromomycin, streptomycin and spectinomycin	1	Temkin adsorption isotherm	93.03%,91.46%, 89.66% at 500 ppm
3	Clotrimazole	0.1	Langmuir isotherm	80.34% at 500 ppm
4	Guaifenesin	2	–	81% at 300 ppm
5	Tenofovir disproxil Fumarate	0.1	Langmuir isotherm	43.36% at 10 ppm

economical loss, and improve human safety, the researchers are trying to discover various ways, out of which one is the use of drugs as a corrosion inhibitor (Pais and Rao 2021). In Table 4 few types of research on the effect of different drug molecules on zinc metal are summarized (Guruprasad et al. 2019, 2020; Abdallah et al. 2016; Adil 2015; Hebbar et al. 2015).

6 Theoretical and Experimental Approaches for the Study of Corrosion Inhibition by Drugs

The objective of corrosion research is to look into the drug molecules both theoretically and experimentally. Weight loss study, Potentiodynamic Polarization measurements, EIS, energy dispersive X-ray spectroscopy, UV–vis, surface morphological analysis such as AFM and SEM in addition to XPS techniques are used to investigate the behaviour of the drug molecules as well as their adsorption efficiency. Second, the theoretical analysis involves quantum chemical measurements to evaluate electronic properties.

6.1 The Experimental Approach

6.1.1 Weight Loss Experiments

To figure out the rate of corrosion, CR (mm year^{-1}) of metal in diverse concentrations of corrosive media at different drug concentrations, after a few hours, weight loss tests are conducted by immersion of metal in the corrosive medium at a temperature of 25 °C or higher temperatures. The CR and weight loss inhibition efficiency values are, were calculated with Eqs. (1) and (2). The weight loss experiments are conducted to analyze the consequence of the temperature on the performance of protection of drug

molecules and the Studies show that with the rise in the temperature the inhibition competence of the drugs generally decreases and this is because of desorption of inhibitor molecules adsorbed initially. The formulas for calculating the corrosion rate and inhibition efficiency are following:

$$CR = (87.6 \times W)/(A \times T \times D) \tag{1}$$

$$I.E.(\%) = \frac{w_0 - w_1}{w_0} \times 100 \tag{2}$$

where W_0 denotes initial weight, W_1 specifies the final weights, CR denotes the corrosion rate, A, T, and D specifies area, immersion time, and density of metal respectively (Bashir et al. 2019a).

6.1.2 Surface Morphological Analysis

Surface morphological experiments of metal surfaces are carried out to examine the morphology of metal surfaces in the existence and lack of inhibitors. The surface morphologies are analyzed using techniques of scanning electron microscopy (SEM) as well as atomic force microscopy (AFM). The exterior exposed mild steel surface was heavily degraded as well as weakened as a result of the violent corrosive attack due to immersion in the test solution. It is clear from Fig. 1 extracted from the literature that the metallic surface appeared very rough with many pits and cracks. Metallic specimens with surfaces inhibited by drug as inhibitor was cleaner as well as less affected or corroded. SEM helps to identify the surface changes with and without the inhibitor (Guruprasad et al. 2019; Singh et al. 2019b).

A similar conclusion may be drawn from observations of metallic surfaces using atomic force microscopy. AFM provides three-dimensional topographs of the sample which clearly shows the heavily corroded unprotected surface with strong surface
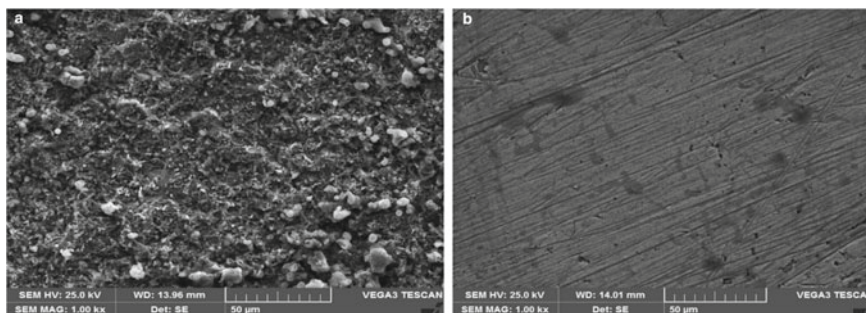
Fig. 1 SEM images of metallic surface in the absence and presence of optimized concentration of seroquel drug molecule as inhibitor in test solution. Adapted from Ref. Guruprasad et al. (2019)

roughness. The average roughness, root mean square roughness values of protected surface comes out to be low as compared to unprotected surface (Bashir et al. 2019b).

6.1.3 Electrochemical Measurements

Electrochemical Impedance Spectroscopy (EIS)

EIS evaluation is a valuable method for assessing corrosion behaviour and mechanism (Singh et al. 2019b). This approach is necessary to obtain additional knowledge regarding a compound's corrosion inhibition. EIS uses AC excitation signals to calculate a material's resistance and capacitance properties. Variable frequency ranges are used to build the continuum and impedance spectroscopy is used in the determination of capacitance of double-layer (C_{dl}) as well as charge-transfer resistance (R_{ct}). The inhibition performance is also measured using these parameters. The reaction of charge transfer and the electrical double layer that forms on the surface of the metal can be linked to the capacitive loop in EIS plots. Double layer capacitance and inhibition efficiency can be calculated by employing the following formulas

$$C_{dl} = Y_0 (2\pi f_{max})^{n-1} \tag{3}$$

C_{dl} Stands for the capacitance of double layer, and f_{max} denotes the frequency at which the impedance's imaginary element approaches its maximum value.

$$IE(\%) = \frac{R'_{ct} - R_{ct}}{R'_{ct}} \times 100 \tag{4}$$

Here R'_{ct} and R_{ct} reflect the Resistance of Charge Transfer in the existence of corrosion inhibitor as well as in the lack of an inhibitor, respectively (Bashir et al. 2019b; Sharma and Kumar 2020). In general, we plot two forms of graphical displays using data obtained from the EIS instrument to provide additional clarity on the corrosion protection mechanism known as the Nyquist as well as Bode plot as given in Fig. 2a, b. Figure 2a taken from the literature is Nyquist plot when sulphuric acid was selected as test solution in the varying concentration of coffee senna extract and Fig. 2b was the graph between phase angle and log of frequency (Akalezi et al. 2012). The higher R_{ct} values of the inhibited system than the unprotected, implying that the investigated drugs prevent corrosion in test solution against the metallic sample. At high concentrations of inhibitor, increased R_{ct} values result in increased impedance to electrochemical corrosion, and this was validated with the increased size of semicircular loops in the Nyquist plot.

Fig. 2 Electrochemical impedance spectra of metallic sample in the absence and presence of inhibitor **a** Nyquist and **b** bode phase angle plots. Adapted from Ref. Akalezi et al. (2012)
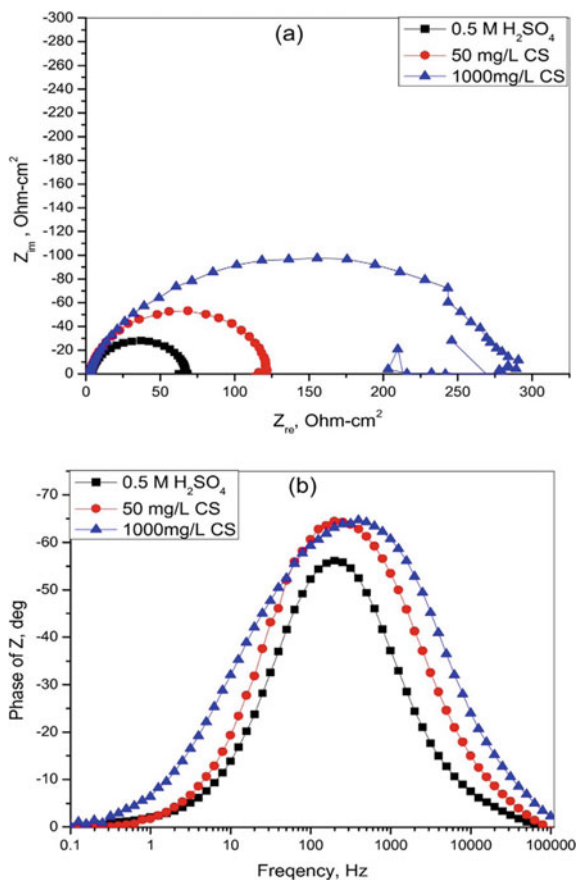
Potentiodynamic Polarization Techniques

Polarization analysis is an excellent and practical method for investigating corrosion processes. Polarization is the Deviation of potential from equilibrium potential because of current flow (net charge flow).Polarization is quantified by overvoltage. With the assistance of polarization curves, the kinetics of anodic and cathodic reactions are readily known. The readings are calculated in a certain range of potential with a specific scan rate. The kinetics of corrosion reactions can be calculated using polarization techniques. To measure electrochemical parameters Polarization technique is utilized. The mechanism of inhibition will decide if the inhibition is through cathodic or anodic reactions and whether the E_{corr} value is decided by the form of the inhibitor to be used. When the curve is moved to a lower current density this displays a decrease in the frequency of corrosion. The inhibition efficacy (%IE) was estimated from the calculated (I_{corr}), values employing the equation

$$\% \, IE = 100\left(\frac{i_{\mathrm{corr}}^{0} - i_{\mathrm{corr}}^{i}}{i_{\mathrm{corr}}^{0}}\right) \tag{5}$$

where i_{corr}^{0} and i_{corr}^{i} denotes the values attributed to the density of corrosion current in lack as well as the existence of inhibitors correspondingly (Bashir et al. 2018). Figure 3 is the pictorial representation of Tafel plots when sulphamic acid was taken as a test solution and polyethylene glycol cross-linked chitosan was considered as an inhibitor. It was validated in the study that the value of corrosion current density decreased with the increased value of inhibitor concentration (Parveen et al. 2019; Chauhan et al. 2018).

6.2 Theoretical Methods

The theoretical methods include computational studies which are further comprised of the quantum chemical calculations in addition to Molecular dynamic simulation studies. DFT experiments are used to determine metal surface interactions and active chemical centers. The binding energies and orientations of adsorbate ions on metal surfaces are determined using molecular dynamic simulations. Following equations are used to find the values of ionization potential. Electron affinity, electronegativity, and global hardness (Bashir et al. 2018, 2020d).

$$IE = -E_{\mathrm{HOMO}} \tag{6}$$

$$EA = -E_{\mathrm{LUMO}} \tag{7}$$

$$\chi = \frac{IP + EA}{2} \tag{8}$$

$$\eta = \frac{IP - EA}{2} \qquad (9)$$

7 Conclusion

The current study compiles several previous studies on medicines that have already been tested and verified as efficient corrosion inhibitors for metallic corrosion in acid solutions. The medicines are excellent and environmentally acceptable candidates to replace conventional harmful corrosion inhibitors, as shown by the current debate. Weight loss, electrochemical investigations were well in agreement with each other to confirm the results. Drug molecules are successfully mitigating the corrosion which was also confirmed by surface morphological techniques employed in various researches. Several medicines and their derivatives have been successfully studied as corrosion inhibitors for mild steel, Aluminium, Zinc, and Copper alloys, as well as their alloys in acidic solution, according to a comprehensive literature review. Because of their complex chemical structures and the inclusion of many heteroatoms such as nitrogen, oxygen, and sulphur atoms, as well as non-bonding and π electrons in their structures, the medicines had a comparatively greater inhibitory effectiveness.

References

Abdallah M, Zaafarany IA, Al Jahdaly BA (2016) Corrosion inhibition of zinc in hydrochloric acid using some antibiotic drugs. J Mater Environ Sci 7(4):1107–1118

Abdallah M, Ahmed SA, Altass HM, Zaafarany IA, Salem M, Aly AI, Hussein EM (2019) Competent inhibitor for the corrosion of zinc in hydrochloric acid based on 2, 6-bis-[1-(2-phenylhydrazono) ethyl] pyridine. Chem Eng Commun 206(2):137–148

Adil H (2015) Corrosion inhibition of zinc metal in 2M hydrochloric acid solution by using guaifenesindrug as an inhibitor and theoretical calculations. Al-Nahrain J Sci 18(1):60–65

Akalezi CO, Enenebaku CK, Oguzie EE (2012) Application of aqueous extracts of coffee senna for control of mild steel corrosion in acidic environments. Int J Indus Chem 3(1):1–2

Akande IG, Fayomi OS, Oluwole OO (2020) Anticorrosion potential of inhibitive suphtrim drug on aluminium alloys in 0.5 MH 2 SO 4. J Bio-Tribo-Corros 6(4):1–8

Ameh PO, Sani UM (2016) Cefuroxime axetil: a commercially available drug as corrosion inhibitor for aluminum in hydrochloric acid solution. Port Electrochim Acta 34(2):131–141. https://doi.org/10.4152/pea.201602131

Bashir S, Sharma V, Lgaz H, Chung IM, Singh A, Kumar A (2018) The inhibition action of analgin on the corrosion of mild steel in acidic medium: a combined theoretical and experimental approach. J Mol Liq 263:454–462

Bashir S, Lgaz H, Chung IM, Kumar A (2019a) Potential of Venlafaxine in the inhibition of mild steel corrosion in HCl: insights from experimental and computational studies. Chem Pap 73(9):2255–2264

Bashir S, Thakur A, Lgaz H, Chung IM, Kumar A (2020a) Corrosion inhibition performance of acarbose on mild steel corrosion in acidic medium: an experimental and computational study. Arab J Sci Eng 45(6):4773–4783

Bashir S, Sharma V, Kumar S, Ghelichkhah Z, Obot IB, Kumar A (2020b) Inhibition performances of nicotinamide against aluminum corrosion in an acidic medium. PortugaliaeElectrochimica Acta 38(2):107–123

Bashir S, Lgaz H, Chung IM, Kumar A (2020d) Effective green corrosion inhibition of aluminium using analgin in acidic medium: an experimental and theoretical study. Chem Eng Commun 21:1

Bashir S, Thakur A, Lgaz H, Chung IM, Kumar A (2019) Computational and experimental studies on phenylephrine as anti-corrosion substance of mild steel in acidic medium. J Mol Liq 293:111539

Bashir S, Thakur A, Lgaz H, Chung IM, Kumar A (2020) Corrosion inhibition efficiency of bronopol on aluminium in 0.5 M HCl solution: insights from experimental and quantum chemical studies. Surf Interf 20:100542

Chauhan DS, Srivastava V, Joshi PG, Quraishi MA (2018) PEG cross-linked chitosan: a biomacromolecule as corrosion inhibitor for sugar industry. Int J Indus Chem 9(4):363–377

El-Haddad MN (2016) Inhibitive action and adsorption behavior of cefotaxime drug at copper/hydrochloric acid interface: electrochemical, surface and quantum chemical studies. RSC Adv 6(63):57844–57853. https://doi.org/10.1039/c6ra03316d

Fayomi OS, Akande IG, Popoola AP (2018) Corrosion protection effect of chitosan on the performance characteristics of A6063 alloy. J Bio-Tribo-Corros 4(4):1–6.O.S.I. https://doi.org/10.1007/s40735-018-0192-6

Fayomi OS, Anawe PA, Daniyan A (2018) The impact of drugs as corrosion inhibitors on aluminum alloy in coastal-acidified medium. Corrosion inhibitors, principles and recent applications 79. https://doi.org/10.5772/intechopen.72942

Fouda AS, Rashwan SM, Kamel M, Badawy AA (2016) Unused meropenem drug as corrosion inhibitor for copper in acidic medium; experimental and theoretical studies. Int J Electrochem Sci 11:9745–61. https://doi.org/10.20964/2016.11.36

Gupta NK, Gopal CS, Srivastava V, Quraishi MA (2017) Application of expired drugs in corrosion inhibition of mild steel. Int J Pharm Chem Anal 4(1):8–12

Guruprasad AM, Sachin HP, Swetha GA, Prasanna BM (2019) Adsorption and inhibitive properties of seroquel drug for the corrosion of zinc in 0.1 M hydrochloric acid solution. Int J Indus Chem 10(1):17–30

Guruprasad AM, Sachin HP, Swetha GA, Prasanna BM (2020) Corrosion inhibition of zinc in 0.1 M hydrochloric acid medium with clotrimazole: experimental, theoretical and quantum studies. Surf Interf 19:100478

Hebbar N, Praveen BM, Prasanna BM, Venkatesha VT (2015) Inhibition effect of an anti-HIV drug on the corrosion of zinc in acidic medium. Trans Indian Inst Met 68(4):543–551

Karthikeyan S (2016) Drugs/antibiotics as potential corrosion inhibitors for metals—a review. Int J Chem Tech Res 9:251–259

Khalil KS (2014) Corrosion inhibition of zinc in hydrochloric acid solution using ampicillin. Iraqi J Sci 55(2)

Mahida M, Chaudhari H (2012) Aromatic amines as corrosion inhibitors for zinc in hydrochloric acid. J Chem Pharm Res 4:5195–5201

Nathiya RS, Perumal S, Murugesan V, Raj V (2018) Expired drugs: environmentally safe inhibitors for aluminium corrosion in 1 MH 2 SO 4. J Bio-Tribo-Corros 4(1):1–3. https://doi.org/10.1007/s40735-017-0120-1

Nwanonenyi SC, Obasi HC, Eze IO (2019) Hydroxypropyl cellulose as an efficient corrosion inhibitor for aluminium in acidic environments: experimental and theoretical approach. Chem Afr 2(3):471–482. https://doi.org/10.1007/s42250-019-00062-1

Pais M, Rao P (2019) Biomolecules for corrosion mitigation of zinc: a short review. J Bio-Tribo-Corros 5(4):1–1

Pais M, Rao P (2021) An up-to-date review on industrially significant inhibitors for corrosion control of zinc. J Bio-Tribo-Corros 7(3):1–3

Palaniappan N, Alphonsa J, Cole IS, Balasubramanian K, Bosco IG (2019) Rapid investigation expiry drug green corrosion inhibitor on mild steel in NaCl medium. Mater Sci Eng B 249:114423

Parveen G, Bashir S, Thakur A, Saha SK, Banerjee P, Kumar A (2019) Experimental and computational studies of imidazolium based ionic liquid 1-methyl-3-propylimidazolium iodide on mild steel corrosion in acidic solution. Mater Res Express 7(1):016510

Pathak RK, Mishra P (2016) Drugs as corrosion inhibitors: a review. Int J Sci Res 5(4):671–677

Shahraki M, Habibi-Khorassani SM, Noroozifar M, Yavari Z, Darijani M, Dehdab M (2017) Corrosion inhibition of copper in acid medium by drugs: experimental and theoretical approaches. Iran J Mater Sci Eng 14(4):35. https://doi.org/10.22068/ijmse.14.4.35

Shanbhag AV, Venkatesha TV, Prabhu RA, Praveen BM (2011) Inhibition effects of acetyl coumarines and thiazole derivatives on corrosion of zinc in acidic medium. Bull Mater Sci 34(3):571–576

Sharma S, Kumar A (2020) Recent advances in metallic corrosion inhibition: a review. J Mol Liq 114862

Singh P, Chauhan DS, Srivastava K, Srivastava V, Quraishi MA (2017) Expired atorvastatin drug as corrosion inhibitor for mild steel in hydrochloric acid solution. Int J Indus Chem 8(4):363–372

Singh P, Chauhan DS, Chauhan SS, Singh G, Quraishi MA (2019) Chemically modified expired Dapsone drug as environmentally benign corrosion inhibitor for mild steel in sulphuric acid useful for industrial pickling process. J Mol Liq 286:110903

Singh A, Soni N, Deyuan Y, Kumar A (2019) A combined electrochemical and theoretical analysis of environmentally benign polymer for corrosion protection of N80 steel in sweet corrosive environment. Results Phys 13:102116

Su P, Li L, Li W, Huang C, Wang X, Liu Y, Singh A (2020) Expired drug theophylline as potential corrosion inhibitor for 7075 aluminum alloy in 1 M NaOH solution. Int J Electrochem Sci 15:1412–1425

Sun CX, Chen YM, Xu HW, Huang CS, Zhang M, Wu JY, Chen M, Xue M (2017) Research on the corrosion inhibitors of zinc in hydrochloric acid. In: IOP conference series: materials science and engineering, vol 213, no. 1, p 012043. IOP Publishing

Tasic ZZ, Mihajlovic MB, Radovanovic MB, Simonovic AT, Antonijevic MM (2018) Cephradine as corrosion inhibitor for copper in 0.9% NaCl solution. J Mol Struct 1159:46–54. https://doi.org/10.1016/j.molstruc.2018.01.031

Udeh BC, Onukwuli OD, Omotioma M (2021) Corrosion control of aluminium in H_2SO_4 medium using kolestran (cholestyramine) drug as inhibitor. World Sci News 159:95–107

Xu X, Singh A, Sun Z, Ansari KR, Lin Y (2017) Theoretical, thermodynamic and electrochemical analysis of biotin drug as an impending corrosion inhibitor for mild steel in 15% hydrochloric acid. Roy Soc Open Sci 4(12):170933

Yao JS, Trokourey A (2019) Thermodynamic and DFT studies on the behavior of cefadroxil drug as effective corrosion inhibitor of copper in one molar nitric acid medium. J Mater Environ Sci 10:926–38. http://www.jmaterenvironsci.com

Groundwater Quality Assessment by Using Water Quality Index for Block Abohar, District Fazilka in Punjab

Kaleem Ahmad, Amit Rai, and Dinesh Chand

Abstract The Abohar block of district Fazilka, Punjab is one of the highest fertilizers consuming block. This is the biggest cotton-producing belt in Punjab. The economy of the this area is basically depends up on cultivated crops because about 75% of populationsare maily involve in agricultural activities. The paposedwork is mainly focus on assessing the groundwater quality of the Abohar block. The samples of groundwater from the different stations of different villages were taken for a comprehensive physiochemical analysis. Nine water quality parameters were considered as pH, Bicarbonate, Total hardness, Calcium, Chloride, Nitrate, Sulphate, Magnesium, and Fluoride. This work demonstrates the qualityof groundwater with reference to water quality index (WQI).The water quality index were found in the range of 16.26–66.276 during pre-monsoon season. Current studywarrants that the groundwater of the Abohar block required special water treatment facility to make it suitable and safe for consumption and alsoneeds to be protected from dangerous bacteria.

Keywords Water quality · Groundwater · Fluoride

1 Introduction

India is one of the country which have rich and cyclopean diversity of natural resources such as water in term of underground and surface (Mangukiya et al. 2012). Water is a prime natural resource and behaves like the chief constituent of the

K. Ahmad (✉) · A. Rai
Department of Chemical Engineering, Sant Longowal Institute of Engineering and Technology, Longowal, Dist-Sangrur, Punjab 148106, India

A. Rai
e-mail: amit@sliet.ac.in

D. Chand
Additional Advisor, Ministry of Drinking Water and Sanitation, ParyavaranBahwan, CGO Complex Lodhi Road, New Delhi 110003, India

1083

ecosystem (Tyagi et al. 2013). The freshwater is of main concern for mankind due to the direct linkage with human being (Yogendra and Puttaiah 2008). it also plays a key and very important role in the growth and development of the nation along with securing the necessities of life. However, the groundwater is being polluted due to rapid industrialization, urbanization, unregulated growth of the population, and other developmental activities (Gangwar et al. 2013). Intense agricultural pursuits are more responsible to contaminate the groundwater in the Punjab region, where the intensity of cultivating crops in a year is quite high (Mittal and Sharma 2008). In tern, the higher use of fertilizer and pestiside along with unsanitary conditions also threatenedhuman health (Ramakrishnaiah et al. 2009). The qualityof water is a critical part of human health and life, that must be monitored regularly. Although, health effects are generally linked with long-term exposures due to chemical contaminants(Hamid et al. 2013).

The information about the quality of any water body can be assess by the WQI because it is offer a simple, stable, reproducible unit of measure. Its behaves like a most efficacious tools to transfuse information on the quality of any sourse of waterto the concerned citizens and policymakers (Reza and Singh 2010). Hence, it is very important and crucial parameter for the assessment and management of surface water (Chauhan and Singh 2010). It demonstrates by a single number generates using a mathematical equation through a large number of water quality data (Reza and Singh 2010), which is one of the most influential waysto describe the quality of water (Tyagi et al. 2013). The data set of water quality into simple information is the prime concern of WQI that is comprehensible and useable by the people (Alam and Pathak 2010). Brown et al. 1970 have developed this index and improved by Deininger (Horton 1965), praposed that the several water quality data could be aggregated into an overall index. There are various research has been conducted on the WQI of different water sourse such as rivers (Ramakrishnaiah et al. 2009; Samantray et al. 2009), taluka or blocks (Yogendra and Puttaiah 2008; Reza and Singh 2010; Brown et al. 1972). Deepika and Singh (2015) estimated the WQI of Bhalswa Lake located in New Delhi by considering twelve important parameters likesalts (calcium, magnesium, sulfate, chloride, nitrate), BOD, and DO, pH, TDS, TSS, alkalinity, hardness and reported the WQI 107.72 and 119.67 for pre-monsoon and post-monsoon respectively which showed the unsuitability of water quality for the human being.

Ramakrishnaiah et al. (Gangwar et al. 2013) assessed groundwater of Tumkur taluka with 12 parametersfor 269 samples and found the range of WQI from 89.21 to 660.56. Exceeds the value of WQI in these areas mainly due to higher values of nitrate, iron, fluorides, bicarbonate, chloride, and manganese in the groundwater which need at least primary treatments before taking in use. In simple words, one can observed that water quality indices incorporate data from multiple water quality parameters into a mathematical equation that rates the fitness of water with a number (Thakor et al. 2011). The objective of the current study is to evaluate, assess, and discusses the appropriateness of groundwater for humanconsumption as per values computed of the WQI.

2 Materials and Methodology

2.1 Water Quality Index (WQI)

A water quality index is a popular tool thatreflects the conjoint effects of several parameters. Generally used to monitorand assess the pollutionof surface as well as groundwater and helps to design and implementation of water quality upgrading programs (Alam and Pathak 2010). Understanding the condition of water quality in terms of number is the prime objective of WQI.

2.2 Study Area

Abohar is a municipal committee located in the districtFazilka of the Indian state of Punjab, northeast of Sri Ganganagar and southeast of Fazilka block. Haryanaand Rajasthanare neighboring states of Punjab that touching the territory of Abohar, near the international border with Pakistan. It is well known for biggest cotton producer of north India and the production of a Kinno. It extends from 29°57′49.2″ N to 30° 15′ N 58″ latitude and 73° 57′38″ E to 74° 26′ 58″ E longitude (PUPDA 2011). There are 57 villages and 99 habitations (IMIS 2014–2015) with a population of 145,238, including 76,840 malesand 68,398 females as per the census 2011. Big sand dunes (sand mounds) are covered on the surface of Abohar which mostly comprises of sandy soil. Vast topographical changes were experienced connected with the green revolution, the water table has been rising in the area comprising blocks ofLambi, Kot Bhai, KhuiyanSarwar, and Abohar creating water at many places (Chopra and Krishan 2014). To get more cultivated land underthe green revolution the previously existingsand dunesin the rural areas have been leveledby former (Fig. 1).

2.3 Sampling Sites

To assess the variation in water quality at five sites within the Abohar Tehsil in the Fazilka district of Punjab. The samples of groundwater were collected from five different locations during the pre-monsoon. The analysis of each sample were performed to evaluate the WQI with reference to nine parameters as discussed previously by using standard procedures recommended by the American public health association (APHA) (1998). Details of sampling stations along with theirWell number are tabulated in Table 1.

The sample of groundwater were collected in anplastic container prewash with acid to eliminate the chances uncertain changes in characteristics as suggested in standard procedures of APHA (1998). To assess the quality of water, the drinking water quality standard suggested by World health organization (WHO) (2008) and
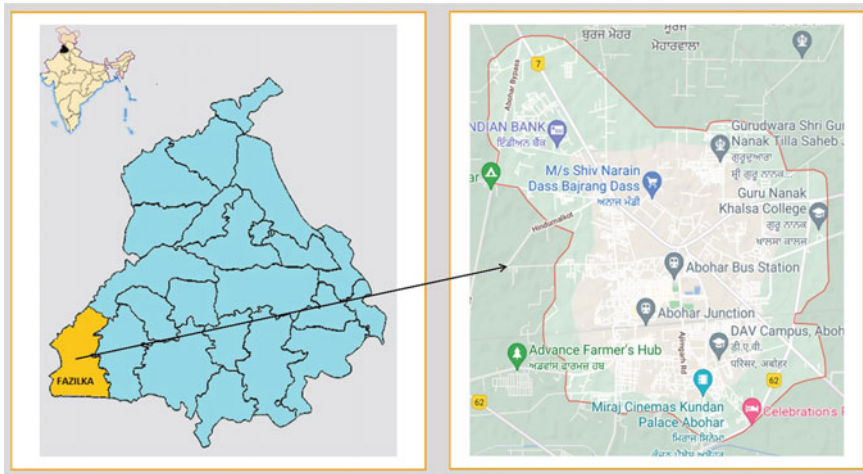
Fig. 1 Geographical map of Abohar Tehsil, Fazilka district of Punjab

Table 1 Sampling location with their Well number

S. No	Station No	Well No	Location
1	S_1	44 J-4A4	Abohar
2	S_2	44 J-4A5	Alamgarh
3	S_3	44 J-4A6	WaryamKhera
4	S_4	44 J-4B3	Sitogana
5	S_5	44 J-4B4	Kundal

Bureau of Indian Standards (BIS) (2012) have been taken as basis for calculation (Al-hadithi 2012).

2.4 Availability of Data

In the current study, the groundwater quality data from five stations were taken for current study from the Central Ground Water Board (CGWB) between Feb 2012 and Apr-2012.

2.5 Data Analysis

The assessment of surface water quality is cumbersome and challenging task because there are lot of parameter that affect the quality of water. Hence, the WQI has been

calculated based on analysis of available data for spatial variation (Prasada and Siddaraju 2012). Several researchers have calculated the WQI using weighed Arithmetic index method (Yogendra and Puttaiah 2008; Gangwar et al. 2013; Reza and Singh 2010; Thakor et al. 2011; Brown et al. 1972) as perthe following steps. Let 'n'is the water quality parameters, and 'Q_n' is the quality ratingcorresponding to an nth parameter which reflectsthe relative value of this parameter in the water sample. It was calculated by using a standard relationship as follow:

$$Q_n = \frac{100(V_n - V_i)}{(V_s - V_i)} \tag{1}$$

V_s = Standard base value, V_n = Observed value, V_i = Ideal value.

Generally $V_i = 0$, except in calculation of pH, dissolved oxygen (Al-Mashagbah 2015) as shown by Eqs. (2) and (3).

$$Q_{pH} = \frac{100(V_{pH} - 7.0)}{(8.5 - 1.0)} \tag{2}$$

and

$$Q_{DO} = \frac{100(V_{DO} - 14.6)}{(15.0 - 14.6)} \tag{3}$$

Unit weight calculation: The unit weight (W_n) is inversely proportional to the recommended standards for the corresponding parameters and given by $W_n = k/S_n$. Where, 'S_n'is the standard permissible value for the nth parameter and 'k' is proportionalityconstant (Mahesh and Raju 2012). WQI was calculated by Eq. (4).

$$WQI = \frac{\sum_{n=1}^{n} Q_n W_n}{\sum_{n=1}^{n} W_n} \tag{4}$$

In this current study, the upper and lower limit of WQI was categorizedby considering the permissibility for human consumption or uses. The maximum permissible limit was set as 300 for WQI for the drinking water (Table 2).

Table 2 The classification of water quality based on WQI value (Gangwar et al. 2013)

WQI level	Description
< 50	Excellent
50–100	Good water
100–200	Poor water
200–300	Very poor water
>300	Unsuitable for drinking

Table 3 Standards for drinking water and relative weight of parameters (all values are in mg/l, except pH)

Parameter	BIS standard	Remarks	WHO standard
pH	6.5–8.5	May be relaxed up to 9.2	7.0–8.0
Bicarbonate	245	No specification	No specification
Total hardness (TH)	300	May be extended up to 600	100
Calcium	75	May be extended up to 200	75
Magnesium	30	May be extended up to 100	30
Chloride	250	May be extended up to 1000	250
Nitrate	45	No relaxation	50
Sulphate	200	May be extended up to 400	500
Fluoride	1	0.6–1.5	1.5

Sources WHO (2008), BIS (2012)

Standards limit of parameters introduced by recommending agencies BIS and WHO. Table 3 contains parameters, their standard limits for assessing the WQI (Deepika and Singh 2015).

3 Results and Discussion

The physicochemical characterization of Abohal block during the premonsoon season was observed as concise in Table 4 (All values are in mg/l except pH). Most of the samples were found in the range of excellent categories. Percolation of water through dissolution of minerals from a lithological composition including the addition of several pollutants from anthropogenic activities, areas may be a prime cause of groundwater contaminations. WQI values of S_1: Abohar, S_2: Alamgarh, S_3: WaryamKhera, S_4: Sitogana, S_5: Kundal, are 58.834, 42.28, 66.276, 20.428, and 16.26 respectively. Due to the weathering and leaching of fluoride-rich minerals and rocks (Reza and Singh 2010), the soil of these locations got highly affected by fluoride, chloride, and total hardness. Which are responsible to get a high value of WQI at

Table 4 Water quality values at various sampling stations

S. No	Station No	Well No	pH	HCO$_3$	Cl	SO$_4$	NO$_3$	Ca	Mg	TH (CaCO$_3$)	F
1	S1	44 J-4A4	8.34	96	1509	2100	326	161	114	872	0.49
2	S2	44 J-4A5	8.01	299	267	320	140	71	69	461	0.33
3	S3	44 J-4A6	8.51	114	42	87	81	43	43	284	0.59
4	S4	44 J-4B3	8.12	84	793	1500	42	172	224	1352	0.1
5	S5	44 J-4B4	7.68	169	542	100	126	256	72	934	0.08

S1: Abohar, S2: Alamgarh, S3: WaryamKhera, S4: Sitogana, S5: Kundal

Table 5 Calculation of WQI of Sampling Station 1 (S$_1$)

Parameter	Observed value (V_n)	St. value (S_n)	Unit weight (W_n)	Quality rating (Q_n)	$W_n Q_n$
pH	8.34	6.5–8.5	0.0977	89	8.7
HCO$_3$	96	245	0.0034	80	0.272
Cl	1509	250	0.0033	84	0.393
SO$_4$	2100	200	0.0042	100	0.42
NO$_3$	326	45	0.0185	280	5.18
Ca	161	75	0.0111	81	0.899
Mg	114	30	0.0033	113.3	0.374
TH (CaCO$_3$)	872	300	0.0028	91	0.455
F	0.49	1	0.8312	49	40.7
			$\sum W_n = 0.9755$		$\sum W_n Q_n = 57.393$

Water Quality Index (WQI) $= \sum W_i Q_i / \sum W_i = 58.834$

these stations. The higher values of calcium magnesium are significantly interrelated to the hardness of the water in nature (Tables 5, 6, 7, 8 and 9).

4 Conclusion

Based onanalysis of several parameters, it has been concluded that the water quality of Aboharblock is fit for drinking purposes. WQI may be used as an indicator to know the quality of water. The discharging of wastewater from domestic, industrial, and various anthropogenic activities are the prime factors to get contaminated the surface water in the Abohar region. Hence, regular monitoring of water is required to maintain the quality and control the big changes in physicochemical characteristics of water in Abohar.

Table 6 Calculation of WQI of Sampling Station 2 (S_2)

Parameter	Observed value (V_n)	St. value (S_n)	Unit weight (W_n)	Quality rating (Q_n)	$W_n Q_n$
pH	8.01	6.5–8.5	0.0977	67	6.55
HCO$_3$	299	245	0.0034	8.12	0.276
Cl	267	250	0.0033	106.8	0.2352
SO$_4$	320	200	0.0042	160	0.672
NO$_3$	140	45	0.0185	89	1.65
Ca	71	75	0.0111	95	1.055
Mg	69	30	0.0033	93	3.069
TH (CaCO$_3$)	461	300	0.0028	120	0.336
F	0.33	1	0.8312	33	27.4
			$\sum W_n = 0.9755$		$\sum W_n Q_n = 41.243$

Water Quality Index (WQI) $= \sum W_i Q_i / \sum W_i = 42.28$

Table 7 Calculation of WQI of Sampling Station 3 (S_3)

Parameter	Observed value (V_n)	St. value (S_n)	Unit weight (W_n)	Quality rating (Q_n)	$W_n Q_n$
pH	8.51	6.5–8.5	0.0977	101	9.87
HCO$_3$	114	245	0.0034	46.5	0.158
Cl	42	250	0.0033	96.8	0.319
SO4	87	200	0.0042	143.5	0.6027
NO$_3$	81	45	0.0185	180	3.33
Ca	43	75	0.0111	57.3	0.636
Mg	43	30	0.0033	143	0.4719
TH (CaCO$_3$)	284	300	0.0028	94.7	0.265
F	0.59	1	0.8312	59	49
			$\sum W_n = 0.9755$		$\sum W_n Q_n = 64.653$

Water Quality Index (WQI) $= \sum W_i Q_i / \sum W_i = 66.276$

Table 8 Calculation of WQI of Sampling Station 4 (S_4)

Parameter	Observed value (V_n)	St. value (S_n)	Unit weight (W_n)	Quality rating (Q_n)	$W_n Q_n$
pH	8.12	6.5–8.5	0.0977	74.7	7.2
HCO^3	84	245	0.0034	75	0.255
Cl	793	250	0.0033	117.2	0.387
SO_4	1500	200	0.0042	92	0.386
NO_3	42	45	0.0185	93.3	1.73
Ca	172	75	0.0111	96	1.066
Mg	224	30	0.0033	80	0.264
TH ($CaCO_3$)	1352	300	0.0028	117.3	0.328
F	0.1	1	0.8312	10	8.312
			$\sum W_n = 0.9755$		$\sum W_n Q_n = 19.928$

Water Quality Index (WQI) $= \sum W_i Q_i / \sum W_i = 20.428$

Table 9 Calculation of water quality index of Sampling Station 5 (S_5)

Parameter	Observed value (V_n)	St. value (S_n)	Unit weight (W_n)	Quality rating (Q_n)	$W_n Q_n$
pH	7.68	6.5–8.5	0.0977	45.3	4.39
HCO_3	169	245	0.0034	69	0.2346
Cl	542	250	0.0033	96.8	0.319
SO_4	100	200	0.0042	50	0.21
NO_3	126	45	0.0185	137.8	2.549
Ca	256	75	0.0111	74.7	0.829
Mg	72	30	0.0033	140	0.462
TH ($CaCO_3$)	934	300	0.0028	78	0.2184
F	0.08	1	0.8312	8	6.65
			$\sum W_n = 0.9755$		$\sum W_n Q_n = 15.862$

Water Quality Index (WQI) $= \sum W_i Q_i / \sum W_i = 16.26$

References

Alam M, Pathak JK (2010) Rapid assessment of water quality index of Ramganga River, Western Uttar Pradesh (India) using a computer programme. Nat Sci 8(11):1–8

Al-hadithi M (2012) Application of water quality index to assess suitability of groundwater quality for drinking purposes in Ratmao—Pathri Rao watershed, Haridwar District, India. Am J Sci Ind Res 3(6):395–402

Al-Mashagbah AF (2015) Assessment of surface water quality of King Abdullah Canal using physico-chemical characteristics and water quality index, Jordan. J WaTer Res Prot 7:339–352

APHA (1998) American Public Health Association, Standard method for the examination of water and waste water, 20th edn. Washington DC

BIS (Bureau of Indian Standards) (2012) 10500, Indian standard drinking water- specification, 2nd revision, New Delhi

Brown RM, McClelland NI, Deininger RA, Tozer RG (1970) A water quality index: do we dare? Water Sewage Works 117:339–343

Brown RM, McClelland NI, Deininger RA, O'Connor MA (1972) Water quality index—crashing the psychological barrier. Environ Sci Res 1:173–182

Chauhan A, Singh S (2010) Evaluation of Ganga Water for drinking purpose by water quality index At Rishikesh, Uttarakhand, India 2(9):53–61

Chopra RPS, Krishan G (2014) Assessment of ground water quality in Punjab India. Earth Sci & Climatic Change 5(10):1000243

Deepika SS, Singh SK (2015) Water quality index assessment of Bhalswa lake, New Delhi. Int J Adv Res 3(5):1052–1059

Gangwar RK, Singh J, Singh AP, Singh DP (2013) Assessment of water quality index: a case study of river Ramganga at Bareilly U.P. India. Int J Sci Eng Res 4(9):2325–2330

Hamid A, Yaqub G, Sadiq Z, Tahir A (2013) Noor ul Ain intensive report on total analysis of drinking water quality in Lahore. Int J Environ Sci 3(6):2161–2171

Horton RK (1965) An index number system for rating water quality. J-Water Pollut Control Fed 37(3):300–306

IMIS: Integrated Management Information System 2014–2015

Mahesh AK, Raju BSN (2012) A comparative study of water quality indices of River Godavari. Int J Eng Res Dev 2(3):29–34

Mangukiya R, Bhattacharya T, Chakraborty S (2012) Quality characterization of groundwater using water quality index in Surat city, Gujarat, India. Int Res J Environ Sci 1(4):14–23

Mittal S, Sharma S (2008) Assessment of drinking ground water quality at Moga, Punjab (India): an overall approach. J Environ Res Dev 3(1):1–2

Prasada AGD, Siddaraju K (2012) Application of CCME Water Quality Index (CWQI) to the Lakes of Mandya, Karnataka State. India Int Interdisc Res J 2(1):108–114

PUPDA (2011) Report, Punjab Urban Planning and Development Authority

Ramakrishnaiah CR, Sadashivaiah C, Ranganna G (2009) Assessment of water quality index for the groundwater in Tumkur Taluk, Karnataka State, India. J Chem 6(2):523–530

Reza R, Singh G (2010) Assessment of ground water quality status by using water quality index method in Orissa India. World Appl Sci J 9(12):1392–1397

Samantray P, Mishra BK, Panda CR, Rout SP (2009) Assessment of water quality index in Mahanadi and Atharabanki rivers and Taldanda canal in Pradip area. Indian J Hum Ecol 26(3):153–161

Thakor FJ, Bhoi DK, Dabhi HR, Pandya SN, Chauhan NB (2011) Water quality index (W.Q.I.) of Pariyej Lake Dist. Kheda—Gujarat. Curr World Environ 6(2):225–231

Tyagi S, Sharma B, Singh P, Dobhal R (2013) Water quality assessment in terms of water quality index. Am J Water Resour 1(3):34–38

WHO (2008) Guidelines for drinking water quality recommendations, Geneva and World Health Organ 3(1):491–493

Yogendra K, Puttaiah ET (2008) Determination of water quality index and sustainability of an urban waterbody in Shimoga town, Karnataka. In: Proceedings of taal 2007: the 12th world lake conference, pp 342–345

Sustainable Approach to Biodiesel Production Using Hydrodynamic Cavitation Route

Birupakshya Mishra, Atharv Thakare, Anupam Mukherjee, Aditi Mullick, Siddhartha Moulik, and Anirban Roy

Abstract Complete reliance on fossil fuels has to lead to skyrocketing prices with detrimental environmental conditions. This drove the search for an alternative source of energy with low emissions and higher energy. In this regard, biodiesel has gained importance over the last few years as a clean, sustainable, and renewable energy resource. However, for producing biodiesel commercially it is important to recognize technologies that are sustainable, energetically feasible, and technologically viable. In this context, Hydrodynamic cavitation provides ample scope for the synthesis of biodiesel in the simplest, energy-efficient, and environmentally friendly with high yield. In, the present work, a detailed analysis of intensified biodiesel production using HC is explained. The present chapter begins with a discussion on the acquisition of feedstock and the role feedstock played in the characterization of biodiesel. Furthermore, it also highlights the reaction mechanism for transesterification reaction employed chiefly for the production of biodiesel. The chapter further delves into biodiesel production using different reactors and their technological advancements. The chapter then proceeds to discuss the state of art HC technology and its use in biodiesel production. The chapter ends with the recent trends and future perspectives of biodiesel production concluding biodiesel prepared by this technology is scalable, energy-efficient, and eco-friendly.

Keywords Hydrodynamic cavitation · Sustainability · Biodiesel · Renewable energy · Transesterification

B. Mishra · A. Thakare · A. Mukherjee (✉) · A. Mullick · S. Moulik (✉)
Cavitation and Dynamics Lab, Department of Process Engineering and Technology Transfer, CSIR-Indian Institute of Chemical Technology, Hyderabad 500007, India
e-mail: p20170408@goa.bits-pilani.ac.in

S. Moulik
e-mail: smoulik@iict.res.in

A. Roy
Water-Energy Nexus Lab, Department of Chemical Engineering, BITS Pilani Goa Campus, Goa 403726, India
e-mail: anirbanr@goa.bits-pilani.ac.in

1 Introduction

With the exponential population growth, there has been extensive stress levied on fossil fuels to bridge the gap between demand and supply. Over the years, the development of a more and more energy-efficient system and lower losses has tried to seal the gap which demands additional cost for development. This invisible ballet performed by usage of fossil fuels can be eased by an alternate fuel which preferably is generated from animal fats or vegetable oils can solve the current world fuel crisis and provide with biofuel (Mukherjee et al. 2021b). It can also be synthesized from free fatty acid (FFA) from vegetable oils with alcohols such as ethanol or methanol by transesterification reaction. Typically biodiesel has 13–23 long carbon chains and is produced by polymerization of short-chain alcohols. Since biodiesel possesses properties similar to conventional fuels it can be used by conventional engines without any modification. Moreover, the superior properties of biodiesel such as higher flash point, reduction in greenhouse gas emissions, high cetane no, energy-efficient, sulfur-free, low cost, and toxicity when compared to diesel makes biodiesel comparable a better alternative from conventional fuels (Demirbas 2009).

Biodiesel is a promising biofuel as an alternative in reducing our dependability on fossil fuels. Biodiesel produces cleaner exhaust emissions compared to petrodiesel. In general, fossil fuel consumption by the transportation sector has contributed to environmental and health problems. Biodiesel becomes one of the most preferred biofuels for the transportation sector due to its biodegradability, non-toxicity, and low harmful exhaust gas emission. However, the major drawback of biodiesel is in its economic sector, it becomes costly for general usage. Maintaining the balance between economy and quality of fuel produced depends on the type of feedstock used which further affects its calorific properties. Math et al. (Math et al. 2010) in the study have shown the usage of non-edible fats, oils, and grease (FOG) such as animal fats, used cooking oil (UCO), yellow or brown grease, and sludge oil for effective production of biodiesel. Methods like this can reduce pollution and landfills and also directly be obtained from municipal and industrial waste. Production of long-chain methyl or ethyl esters is generally preferred because of its biodegradability. The drawback of such products is a higher requirement of energy. By conventional means as by stirring supercritical methanol and microwave heating which demand higher energy the cost of biodiesel production also increases. Thus, the search for an energy efficient method for production of biodiesel has taken up and for the incorporation of the same in ot the industrial scale is being tried (Ghayal et al. 2013; Pal et al. 2010; Zhou et al. 2020). Alcoholysis can be carried out with or without the presence of catalysts which only aids in achieving the equilibrium (Ji et al. 2006; Stavarache et al. 2005; Macedo et al. 2006; Patil et al. 2011). In a reaction, the catalyst can be present as in homogenous catalyst which provides higher reaction rate and separation but lower reuse or can be the heterogenous type where separation and reuse of catalysts are sufficient;y high but the reaction rate is slower as compared to homogenous one but in each case have acceptable limits.

Here in this chapter, the economic and ecological viewpoint is exploited for feedstock acquisition and is graded on these two parameters as to which suits the best. Temperature plays an integral part in the transesterification reaction as increasing the temperature results in higher solubility but sufficient increase can cause alcohol present to flash and thereby limit its contact with oil leading to lower yields. It is well-reported (Nguyen et al. 2015; Patil et al. 2019; Singh et al. 2020) that hydrodynamic cavitation (HC) is an energy-efficient technique for biodiesel production. It is one of the novel methods of wastewater treatment and biofuel generation. Passing the fluid from high pressure to low pressure causes it to form cavities filled with air which implodes to provide energy (Mukherjee et al. 2021a). The process intensive approach of the HC technique can bring about a higher conversion of triglycerides up to 90% at intervals twenty min of the reaction period. The catalyst used for biodiesel synthesis process, particularly for cavitation, has a lot of importance relating to conversion and its use (Gardy et al. 2017; Gryglewicz 2011). It has several advantages over conventional methods such as low chemical dependency, lower energy consumption, and closed-loop operation hence a higher safety index. These combined with higher yield and lower reaction time have led to further research and attention for the development of better methods in HC. Furthermore, the lower reaction time and continuous operation mode make it ideal for being able to scale up to industrial scale and economic production of biodiesel.

2 Feedstock for Biodiesel Production

Biodiesel is produced chiefly by transesterification reaction. Biodiesel production uses natural and organic resources as feedstock like animal fats, oils, or lipids. Feedstock can be classified into several types, broadly as (i) first, (ii) second, (iii) third, (iv) the fourth generation, upon which the characteristics of biodiesel depend. For example, Palm oil, rapeseed, and soybean are profoundly used as feedstock belongs to the first generation.

Biomass and edible vegetable oils belong to the 1st-generation feedstock extraction. Due to the good availability to sustain biodiesel demand sufficiently, 1stgeneration feedstocks are extensively utilized which might lead to inflation in food prices. This supply to demand ratio between food and the fuel industry incites a cost battle for raw materials. The palatable oil markets are usually cost-effective when compared with the fuel sector. This makes the profit margin of biodiesel from 1st generation feedstock to be very slim. The demand for rigorous plantation of the feedstocks causes ecological issues. Some of the environmental issues caused by first-generation feedstock planting include food instability, water paucity, soil deterioration, deforestation, as well as loss of biodiversity.

A variety of sources contribute to the non-edible 2nd-generation feedstocks. Some of them can be produced from non-edible plant oil, grease, trash cooking oil, and waste animal fats. These crops require less plantation acreage and can be grown to utilize mixed crop production. As per Hums et al. (2016), Reduction in landfill areas

and environmental deterioration due to toxic gases from conventional fuels can be addressed by utilizing waste as a source of energy. The second-generation feedstocks are available at an economical price than first-generation feedstocks. According to the reports of Yang et al. and Sakthivel et al. (2018) the quality of fuels prepared from 2nd generation feedstock is higher than that of 1st generation as they are non-corrosive, cleaner, and possess a higher cetane number. However, the fuel from 2nd generation feedstock has a low yield (Sakthivel et al. 2018) and possesses poor cold few fuel properties along with inadequate technological advancements with additional bio-security concerns (Alptekin and Canakci 2011) as was highlighted in previous studies.

For the biodiesel feedstocks, some varieties of oil-impregnated plants are preferable for usage, namely Calophyllum inophyllum (Bintagor), Azadirachta indica (Neem), Jatropha curcas (Jatropha), and Pongamia pinnata (Karanja) (). Cultivation in their natural habitat makes the plant containing oil be used as feedstock to be available for oil extraction round the year. The biodiesel obtained from 1st and 2nd generation feedstock is said to possess similar characteristics. Additionally, the biodiesel produced from 2nd gen feedstock possesses low Sulphur and aromatic content thereby reducing the toxic emissions into the environment. Despite the high oil quantity, the yield of 2nd gen feedstock biodiesel is low as compared to 1st gen where coconut and palm oil produce 5000 and 2670 kg oil/ha while 1590,2250, and 2670 kg oil/ha were generated by jatropha, neem, and Karanja respectively. Due to the high viscosity a density of oils produced from 2nd gen feedstock, they pose a higher environmental risk due to the higher release of particulate matter and NOx because of incomplete combustion. Extensive studies on Genetically Modified Plants (GMPs) for higher oil generation by suppression or over-expression of particular genes in genetic material, yielding to higher biodiesel production.

Used cooking oil (UCO), yellow or brown grease, animal fat, and soapstock which is a by-product in refining vegetable oil are all examples of waste oil (FOG). They may be obtained from trash generated in both household and industrial sectors. As per Math et al. (2010) global FOG production is estimated to be in the millions of tons per year. Yet, the disposal of FOG through household and industrial drains poses significant health and environmental risks. The existence of an oil film on top of river water prevents oxygen dissolution. This puts the life of aquatic plants and creatures in jeopardy. In a study conducted by Jafari (2010), the mixture of oil and water causes the chemical oxygen demand to increase in an aquatic body thereby poisoning it. Additionally, the fear of access to the food chain through ingestion of fishes who could have taken in the carcinogenic substance cannot be ignored and is capable of causing serious health issues. These potential issues can be addressed by using FOG as a biodiesel feedstock. Producers of vegetable oils now have multiple options of either producing biodiesel or vegetable oil for food supply as biodiesel can be produced from higher quality food-grade vegetable oils such as palm, rapeseed, and soybean oil. Hence the usage of FOG could eliminate such dilemmas. Economically, the lower price of biodiesel compared to Petro-diesel prevalent in the consumer market encourages its usage (Khan et al. 2019). FOG can initiate saponification reaction due to the high percentage of FFA which decreases the yield by inhibiting the production

of biodiesel. Additionally, it also prevents the separation of biodiesel, glycerol, and washes water. To avoid this, FFA is converted to an ester which is further passed onto transesterification reaction via a base catalyst.

Algal biomass constitutes the 3rd-generation feedstocks. Algae are categorized into two kinds: macro algae and microalgae. Algae can grow in tight spaces and for thriving require ample sunshine, water, CO_2, and little nutrition. In terms of oil content, certain algae are productive. Per kg growth of Algal biomass consumes 1.8 kg of CO_2, generously reducing the greenhouse effect. Chlorella species may generate up to 70% of their dry weight in oil. Oil makes beyond 80% of the dry weight of some microalgae. To place things in context, the oil of sunflower seed has 55% oil per dry weight, whereas oil-palm oil comprises just 50%. 3rd-generation feedstocks, like feedstocks from earlier generations, have some disadvantages. Algae production needs a huge quantity of water. For most portions of the year, water is limited or frozen in certain regions. As a result, growing algae in such nations is tricky. Algae cultivation is also a relatively recent technique. It is probably impossible to scale up and industrialize algal biodiesel, and prevailing technology is too costly. The kinds, features, and drawbacks of each feedstock production are depicted in Fig. 1. By considering all of the needs, merits, and drawbacks of various feedstock classes, the forthcoming biodiesel synthesis is seen as relying on a union of all feedstock generations rather than a single kind of feedstock. Climate, crop availability, technologies, price stability, and regulations policy may all play a role in the biodiesel feedstock selection process. Synthetic biology's latest advancements have laid the groundwork for the fourth-generation feedstock. A sustainable and cost-effective biodiesel feedstock may be created by combining the intent-designed biological system with solar power. One or a combination of three methods can be used to synthesize fourth-through the manufacture of photovoltaic and microbic fuel, and/or (iii) through the production of artificial cells. Generation biodiesel feedstock: (i) by the development of photosynthetic (Table 1).
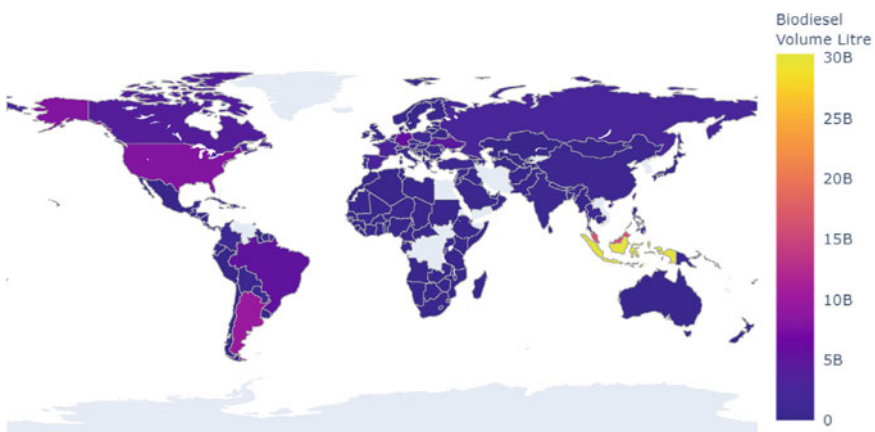
Fig. 1 Maximum biodiesel production volume (in billion liters)

Table 1 Comparison of types of feedstocks (Singh et al. 2020; Shah et al. 2018; Hajjari et al. 2017)

Generation	Advantages	Limitations
First	• Environmentally friendly • Higher cost than the second generation • Economic and social security	• First-generation biofuels are directly related to biomass that is generally edible • Limited feedstocks (food vs fuel crisis) • Blended partially with petroleum diesel
Second	• Not competing with food • Reduced cost of conversion • They are perennial and so energy for planting need only be invested once • Environmentally friendly • They are fast-growing and can usually be harvested a few times per year • They have relatively low fertilizer needs • Waste oil can decrease engine life if not properly refined • They grow in marginal land	• Low yield • Fuel properties not conforming to international standards • Low cold flow fuel properties • Bio-safety issues with animal-sourced feedstocks
Third	• Algae can use a diverse array of carbon sources • Total carbon emissions would be reduced substantially • Ease of scale-up • Technology readily available • High flexibility to strain selection (closed system cultivation) • No caustic chemicals are needed in oil separation from algal biomass	• A minor drawback regarding algae is that biofuel produced from them tends to be less stable than biofuel produced from other sources • The oil found in algae tends to be highly unsaturated. Unsaturated oils are more volatile, particularly at high temperatures, and thus more prone to degradation • The cost of algae-based biofuel is much higher than fuel from other sources • Scalability • Technology not demonstrated on a large scale
Fourth	• More lipid contents • More CO_2 absorbing ability • High energy content • Rapid growth rate	• High initial investment • Research still on infancy level

The biodiesel characteristics are influenced by the feedstock quality, particularly the free fatty acid (FFA) concentration, and fatty acid composition. Using a standard base catalyst transesterification method, the large quantity of FFA in oil leads to a relatively poor yield of biodiesel. The lipid content of the feedstock oil influences several of the biodiesel's important qualities, such as cetane number, cold flow features, flashpoint, oxidation stability, and so on. For long-chain fatty acids, the cetane number is high, and saturation is increased. Various investigations carried out on the relationship between biodiesel characteristics and fatty acid content have

found that cetane numbers are low for considerably unsaturated components (C18:2) and (C18:3). Grape seed oils, oil of sunflower seeds, and soya bean oils are all abundant in unsaturated fatty acids. As a consequence, the inclusion of glutinous fatty acids such as palmitic acid (C16:0) and octadecanoic acid (C18:0), palm seed oil biofuel has a quite large cetane number. Olive, cottonseeds, rapeseed, walnut kernel, kernels of hazelnut, benne seed, and other oils with high C18:1 and C20:1 cetane numbers are similar to biodiesel of palm oil in cetane numbers. Because the quantity of saturated fatty acids like palmitic acid and octadecanoic acid present is minimal, the cloud point of fatty acid alkyl esters (FAAE) produced from oils like soya bean, flaxseed, and corn kernels have been much less or closer to 0 °C. Due to the presence of significant quantities of lipids in cattle tallow, the cloud point of biofuel made using the animal fat is greater, that of biofuel made using soybean. Since the alkyl esters of palmitic and octadecanoic acids are the earliest to settle as biodiesel cools, they commonly clog biodiesel fuel filters. Biodiesel made from palm oil, which has a high proportion of octadecanoic acid along with palmitic acid, has supreme cold flow plugging points (CFPP), but biofuel made from groundnut, which contains a considerable percentage of lengthy-chain saturated fatty acids of alkyl esters, has the least cold flow clogging point(CFPP). The flash point of biodiesel is generally high (150 °C or above). Biodiesel having a length of hydrocarbon of somewhere around 12 has less flashpoint than biodiesel with C16 and C18 chain lengths. Another notable aspect of biodiesel, which is based upon polyunsaturated oil molecules, is its oxidation stability. Vegetable oils ample in saturated fatty acids, along with palm kernel oil and olive oil, have higher methyl ester stability. Biodiesel's viscosity is less, that of vegetable oils. It rises in proportion to the number of carbon atoms in the chain and the alcohol moiety. The degree of saturation also affects the viscosity. The cis double-bond configuration has less viscosity than the trans-double-bond structure. This is advantageous for biodiesel production from trash cooking oil, since, this oil is generally hydrogenated to a certain magnitude and includes a significant amount of trans fatty acid chains. Besides, it is been observed that the existence of one single double bond increments viscosity, but the presence of 2 or 3 double bonds causes viscosity to decrease. Viscosity is similarly affected by branching in the ester chain, perhaps to a lesser amount than unsaturation. The occurrence of hydroxy groups within molecules of oil (as in castor oil) increases viciousness as well.

Availability, opportunity, and shortcomings of biodiesel feedstock:

Biodiesel feedstock abundance in every nation is determined by its environmental conditions, local soil, geographical region, and farming techniques. When comparing different feedstocks, it's critical to take into account a certain aspect. Each feedstock should undergo a full life-cycle assessment, which incorporates the straight financial worth of the feedstocks, their effects on quality of air, availability of land, supply of energy, insecticide use, biodiversity value losses, job creation, cultivation practices, water necessity, soil degradation, supply chain costs, and so on. For the growth of oil feedstocks, biodiesel manufacturing needs a considerable amount of water. Water use has sparked discussions over drinking vs driving and is partly to blame for the severity of the water shortages. Varying varieties of crops require diverse amounts of

water to flourish. When compared to soybeans (602 m^3/t) and sunflower (972 m^3/t), palm (1502 m^3/t) and rapeseed (1460 m^3/t) needs greater amount of water to grow. Oil content and high yield per hectare are key considerations when choosing a biodiesel feedstock. Cooking oils including soya beans, seeds of sunflower, coconut, palm seed oil, safflower, groundnut, and rapeseed were among the first crops utilized to make biodiesel. Many nations, including Germany, Malaysia, and the USA, have built plantations of these feedstocks. Currently, fats and oils create 95% of the world's biodiesel. Oilseed rape (16%), soya (26%), oil of palm tree (35%), ruminant fats (7%), leftover edible oil (11%) and rest (3%) are the most often utilized feedstocks for biodiesel production globally. However, using edible or cooking oil sources for biodiesel production raises issues such as food versus fuel conflicts, soil resource degradation, and deforestation, to name a few. Furthermore, the biodiesel industry's economics has been impacted by the dramatically increased pricing of edible oils in the previous ten years. Moreover, due to the growing disparity among both production and consumption in many biodiesel-producing nations, using these edible oils for biofuel synthesis isn't practical in the long run. One approach for reducing biodiesel production's reliance upon edible oil is to utilize non-edible oil. Non-edible oils are making resurgence nowadays on account of their widespread availableness in many regions around the globe, particularly in wastelands where food oil plants are not appropriate. This minimizes food conflict, improves efficiency and productivity, reduces deforestation, and makes them more cost-effective than edible oils. Jatropha, castor oil, babassu tree, rice husk, mahua, jojoba, oil from tobacco seeds, karanja, cottonseed, neem, nagchampa, coffee powder, kusum, eucalypt oils, and other inedible oils are the most common. Feedstocks of biodiesel include animal oils such as poultry fat, animal fats, fish oil, and fat, as well as waste oils such as waste cooking oil, date pit oil, and the waste of leather tanning. Considering their advantages above edible oils in regard of FFA content, humidity, and different contaminants, these oils are substandard to edible oils concerning FFA content, moisture, and other residues. During biodiesel manufacturing, non-edible oils containing higher FFA undergoes process of esterification or are processed in a 2-step technique of esterification/transesterification. The expense of pre-treatment for non-edible oils should indeed be maintained lesser than the savings gained through feedstock selection. Besides the oil quality the cost of producing biodiesel is determined by the end-use of non-edible feedstocks such as kernel cakes of palm oil, shell and fiber, agricultural residues, trunk, and leaves, among other things. As a result, palm fruit oil has co-products that have energy potentiality. Chemical, cosmetics, pharma, and fertilizers sectors all provide prospects. Nonetheless, most uses of non-edible oil co—products are still in the dawning stages of development, and their financial viability will be determined by opportunity, pricing, and need. The larger the market for co-products, the better the chances of effectiveness. Palm trees, in broad sense, have a lot of potential to generate a broad array of products, lowering financial risk. Various non-edible feedstocks, such as jatropha, rapeseed, karanja, and jojoba, would be used to make candles, cleansers, cosmetics, tanned leather, glowing oil, lubricating oils, water-paint binding agent, and insecticides, in a similar way. It's important to realize that non-edible oils such as karanja, jatropha, and castor oils have production costs

of 0.39, 0.25, and 0.12 USD/kg, respectively, but soya bean oil has a manufacturing cost of 1.64 USD/kg. Whereas, oil of palm fruit and rapeseed oil may be capable of competing on price with the abovementioned non-edible oils, they suffer from a number of additional drawbacks that have already been highlighted. Microalgae has recently emerged as a viable biodiesel source. Water, CO2, and sunshine are all used by photosynthetic bacteria to produce algal biomass, but they do it more efficiently than plants. When tried to compare between edible and non-edible oils, microalgae are a dormant feedstock because of their high lipid composition and profitability. Microalgae have the opportunity to manage the issue of food and biofuel synthesis. Furthermore, it is the only source that has the ability to meet global transport fuels needs while still being sustainable. Being created at a rapid pace, their high manufacturing costs are the primary roadblocks to development and commercialization. Expenses associated with obtaining high-oil-yielding algae strains, as well as the need for a significant volume of water freshwater, as well as huge, efficacious bioreactors. Microalgae have been shown to thrive on exhaust gas and so utilize greenhouse gas emissions as such a feedstock in several investigations. Switch grass, big bluestem, poplar and miscanthus are all genetically modified plants that might be used as novel biodiesel feedstocks. Because these novel bioenergy crops are unrelated to food crops, they have the potential to be a long-term biodiesel feedstock. To summarize, edible oils, despite their low FFA concentration, can't be utilized for long-term biodiesel synthesis, even though it is commercially viable, due to the food versus fuel argument. As a result, non-edible oils are superior biofuel feedstocks than edible oils since they are more agronomically acceptable and ecologically benign. Jatropha, karanja, and castor oil are other viable options. If the obstacles to commercial exploitation can be overcome in the future, Microalgae may be proposed as potential measure for long-term biofuel synthesis.

a. **Availability, opportunity, and shortcomings of biodiesel feedstock**

Biodiesel feedstock abundance in every nation is determined by its environmental conditions, local soil, geographical region, and farming techniques. When comparing different feedstocks, it's critical to take into account a certain aspect. Each feedstock should undergo a full life-cycle assessment, which incorporates the straight financial worth of the feedstocks, their effects on quality of air, availability of land, supply of energy, insecticide use, biodiversity value losses, job creation, cultivation practices, water necessity, soil degradation, supply chain costs, and so on. For the growth of oil feedstocks, biodiesel manufacturing needs a considerable amount of water. Water use has sparked discussions over drinking vs driving and is partly to blame for the severity of the water shortages. Varying varieties of crops require diverse amounts of water to flourish. When compared to soybeans ($602 \text{ m}^3/\text{t}$) and sunflower ($972 \text{ m}^3/\text{t}$), palm ($1502 \text{ m}^3/\text{t}$) and rapeseed ($1460 \text{ m}^3/\text{t}$) needs a greater amount of water to grow. Oil content and high yield per hectare are key considerations when choosing a biodiesel feedstock. Cooking oils including soya beans, seeds of sunflower, coconut, palm seed oil, safflower, groundnut, and rapeseed were among the first crops utilized to make biodiesel. Many nations, including Germany, Malaysia, and the USA, have built plantations of these feedstocks. Currently, fats and oils create 95% of the world's

biodiesel. Oilseed rape (16%), soya (26%), oil of palm tree (35%), ruminant fats (7%), leftover edible oil (11%) and rest (3%) are the most often utilized feedstocks for biodiesel production globally. However, using edible or cooking oil sources for biodiesel production raises issues such as food versus fuel conflicts, soil resource degradation, and deforestation, to name a few. Furthermore, the biodiesel industry's economics has been impacted by the dramatically increased pricing of edible oils in the previous ten years. Moreover, due to the growing disparity among both production and consumption in many biodiesel-producing nations, using these edible oils for biofuel synthesis isn't practical in the long run. One approach for reducing biodiesel production's reliance upon edible oil is to utilize non-edible oil. Non-edible oils are making a resurgence nowadays on account of their widespread availability in many regions around the globe, particularly in wastelands where food oil plants are not appropriate. This minimizes food conflict, improves efficiency and productivity, reduces deforestation, and makes them more cost-effective than edible oils. Jatropha, castor oil, babassu tree, rice husk, mahua, jojoba, oil from tobacco seeds, karanja, cottonseed, neem, nagchampa, coffee powder, kusum, eucalypt oils, and other inedible oils are the most common. Feedstocks of biodiesel include animal oils such as poultry fat, animal fats, fish oil, and fat, as well as waste oils such as waste cooking oil, date pit oil, and the waste of leather tanning. Considering their advantages above edible oils in regard of FFA content, humidity, and different contaminants, these oils are substandard to edible oils concerning FFA content, moisture, and other residues. During biodiesel manufacturing, non-edible oils containing higher FFA undergoes a process of esterification or are processed in a 2-step technique of esterification/transesterification. The expense of pre-treatment for non-edible oils should indeed be maintained lesser than the savings gained through feedstock selection. Besides the oil quality, the cost of producing biodiesel is determined by the end-use of non-edible feedstocks such as kernel cakes of palm oil, shell and fiber, agricultural residues, trunk, and leaves, among other things. As a result, palm fruit oil has co-products that have energy potentiality. The Chemical, cosmetics, pharma, and fertilizers sectors all provide prospects. Nonetheless, most uses of non-edible oil co-products are still in the dawning stages of development, and their financial viability will be determined by opportunity, pricing, and need. The larger the market for co-products, the better the chances of effectiveness. Palm trees, in a broad sense, have a lot of potentials to generate a broad array of products, lowering financial risk. Various non-edible feedstocks, such as jatropha, rapeseed, karanja, and jojoba, would be used to make candles, cleansers, cosmetics, tanned leather, glowing oil, lubricating oils, water-paint binding agent, and insecticides, similarly. It's important to realize that non-edible oils such as karanja, jatropha, and castor oils have production costs of 0.39, 0.25, and 0.12 USD/kg, respectively, but soya bean oil has a manufacturing cost of 1.64 USD/kg. Whereas oil of palm fruit and rapeseed oil may be capable of competing on price with the abovementioned non-edible oils, they suffer from several additional drawbacks that have already been highlighted. Microalgae have recently emerged as a viable biodiesel source. Water, CO_2, and sunshine are all used by photosynthetic bacteria to produce algal biomass, but they do it more efficiently than plants. When tried to compare between edible and non-edible oils, microalgae

are a dormant feedstock because of their high lipid composition and profitability. Microalgae have the opportunity to manage the issue of food and biofuel synthesis. Furthermore, it is the only source that can meet global transport fuels needs while still being sustainable. Being created at a rapid pace, their high manufacturing costs are the primary roadblocks to development and commercialization. Expenses are associated with obtaining high-oil-yielding algae strains, as well as the need for a significant volume of water freshwater, as well as huge, efficacious bioreactors. Microalgae have been shown to thrive on exhaust gas and so utilize greenhouse gas emissions as such a feedstock in several investigations. Switch grass, big bluestem, poplar, and miscanthus are all genetically modified plants that might be used as novel biodiesel feedstocks. Because these novel bioenergy crops are unrelated to food crops, they have the potential to be a long-term biodiesel feedstock. To summarize, edible oils, despite their low FFA concentration, can't be utilized for long-term biodiesel synthesis, even though it is commercially viable, due to the food versus fuel argument. As a result, non-edible oils are superior to biofuel feedstocks than edible oils since they are more agronomically acceptable and ecologically benign. Jatropha, karanja, and castor oil are other viable options. If the obstacles to commercial exploitation can be overcome in the future, Microalgae may be proposed as a potential measure for long-term biofuel synthesis.

3　Reaction Mechanism of Transesterification

It's indeed essential to comprehend the mechanisms of reactions transpiring in the syntheses to successfully increase the pace of biodiesel production, utilizing any process optimization technique. For homogenous, the reacting process is traditionally almost the same, which is also true for approaches that are heterogeneous and supercritical. The pace of reactions is determined by the active ions used to initiate the synthesis and, also more importantly, by the oil-methanol inter-facial encounter. The first active ions are created using a catalyst, but in supercritical oxidation, active ions are generated owing to supercritical circumstances, which include extremely high cumulative temperature and pressure. The rate of emulsification amongst the two compounds is determined by the produced inter-facial vicinity and therefore the degree of mass transfer, which is reliant on the kind of reactors employed for synthesizing. A rotary agitator is often employed in traditional methods to generate an emulsion among the insoluble heterogeneous aqueous phases of oil and methanol.

Three main stages are involved in the transesterification process. (1) Formation of alcohol anion through basic catalyst withdrawal of the proton from alcohol and intrusion of this negatively charged anion on the carbonylic carbon of the triglyceride molecule to generate tetrahedral intermediates (2) interaction of tetrahedral intermediate with alcohol to reinstate the anion of alcohol and (3) The tetrahedral intermediate is rearranged to yield a fatty acid ester and a diglyceride. Below are some examples of reaction mechanisms shown by Eqs. (1)–(4).

The very first step: Synthesis of the active species, like $R'O^-$
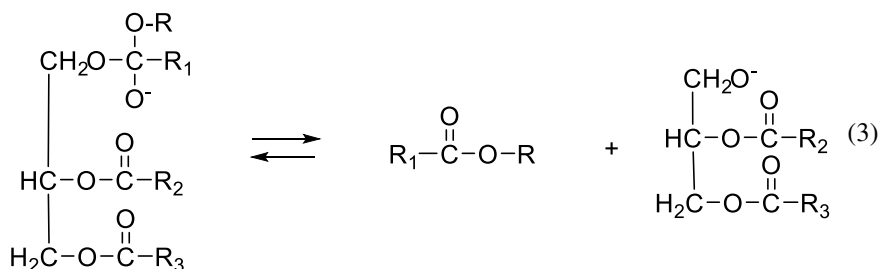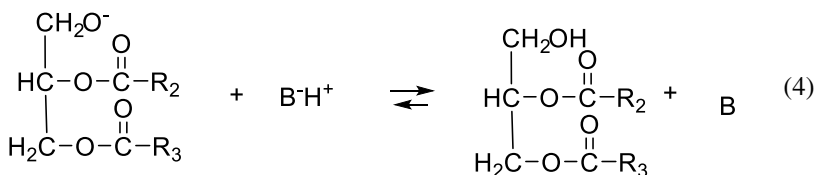
$$B + R'OH \rightleftharpoons R'O^- + BH^+ t \tag{1}$$

2nd Step: Generating a tetrahedral intermediate by nucleophilic attack on triglycerides of RO^- on the carbonylic group.

$$
\begin{array}{l}
CH_2-O-\overset{\overset{\displaystyle O}{\|}}{C}-R_1 \\[2mm]
HC-O-\overset{\overset{\displaystyle O}{\|}}{C}-R_2 \qquad + \qquad R'O- \qquad \longleftrightarrow \\[2mm]
H_2C-O-\overset{\overset{\displaystyle O}{\|}}{C}-R_3
\end{array}
\qquad
\begin{array}{l}
CH_2O-\overset{\overset{\displaystyle O-R}{|}}{\underset{\underset{\displaystyle O^-}{|}}{C}}-R_1 \\[2mm]
HC-O-\overset{\overset{\displaystyle O}{\|}}{C}-R_2 \\[2mm]
H_2C-O-\overset{\overset{\displaystyle O}{\|}}{C}-R_3
\end{array}
\tag{2}
$$
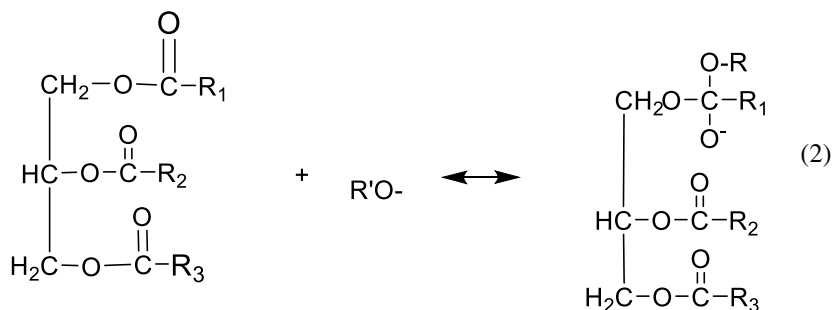
3rd Step: Breakdown of the reaction intermediate.

$$
\begin{array}{l}
CH_2O-\overset{\overset{\displaystyle O-R}{|}}{\underset{\underset{\displaystyle O^-}{|}}{C}}-R_1 \\[2mm]
HC-O-\overset{\overset{\displaystyle O}{\|}}{C}-R_2 \\[2mm]
H_2C-O-\overset{\overset{\displaystyle O}{\|}}{C}-R_3
\end{array}
\rightleftharpoons
R_1-\overset{\overset{\displaystyle O}{\|}}{C}-O-R
\quad + \quad
\begin{array}{l}
CH_2O^- \\[2mm]
HC-O-\overset{\overset{\displaystyle O}{\|}}{C}-R_2 \\[2mm]
H_2C-O-\overset{\overset{\displaystyle O}{\|}}{C}-R_3
\end{array}
\tag{3}
$$

4th Step: Regeneration of $R'O^-$ active species.

$$
\begin{array}{l}
CH_2O^- \\[2mm]
HC-O-\overset{\overset{\displaystyle O}{\|}}{C}-R_2 \\[2mm]
H_2C-O-\overset{\overset{\displaystyle O}{\|}}{C}-R_3
\end{array}
\quad + \quad B^-H^+ \quad \rightleftharpoons \quad
\begin{array}{l}
CH_2OH \\[2mm]
HC-O-\overset{\overset{\displaystyle O}{\|}}{C}-R_2 \\[2mm]
H_2C-O-\overset{\overset{\displaystyle O}{\|}}{C}-R_3
\end{array}
\quad + \quad B
\tag{4}
$$

R and R1 are alkyl groups, while B is the catalyst. Methanol is fragmented into the active species in the supercritical technique, as shown in Eq. (5) while leaving the rest mechanism being identical to that shown in Eqs. (2)–(4):

$$R'OH \rightleftharpoons R'O^- + H^+ \tag{5}$$

The whole proceeding is usually broken down into three successive phases. Diglyceride is obtained during the first stage, which then is transformed into a monoglyceride in the 2nd step, and ultimately glycerin is produced in the 3rdstep. Equation (6) gives the stoichiometric relationship for the complete reaction.

$$
\begin{array}{c}
R1COOH2 \\
|\\
R1COOCH + 3CH3OH \\
|\\
R1COOCH2
\end{array}
\;\rightleftharpoons\;
\begin{array}{c}
HOCH_2 \\
|\\
HOCH + \\
|\\
HOCH_2
\end{array}
\begin{array}{c}
R1\text{-}COOCH3 \\
R2\text{-}COOCH3 \\
R3\text{-}COOCH3
\end{array}
\qquad (6)
$$
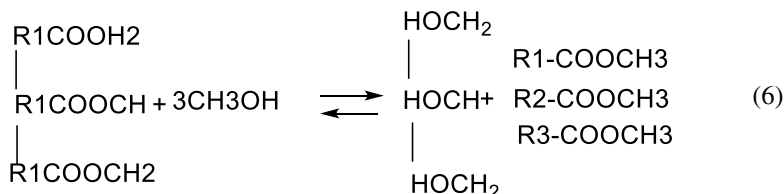
Stoichiometry requires a molar ratio of 1:3for oil to alcohol, which could be observed from the entire process. Because the reaction is restricted by the state of equilibrium, an excess of methanol is commonly utilized to impel the reaction forwards. The forward reaction is typically pseudo-first-order in the occurrence of spare alcohol, but the reverse reaction is of 2ndorder. The molar ratio, the temperature of the reaction, and catalyst concentration are all essential factors that influence the reaction's state of equilibrium. Excessive methanol, while driving the reaction in a positive direction, causes severe difficulties in downstream processes including separation issues. The synthesis procedure has a substantial impact on the total profitability of biofuel synthesis The majority of processing costs are incurred in the upstream and downstream stages.

The presence, of alkali separation and purification of glycerol demand additional processing in homogeneous catalysis, which necessitates a large volume of water. The expense of treating the wastewater adds to the overall production value. The utilization of heterogeneous and supercritical techniques can help reduce the expenditure of pre- and post-processing. Heterogeneously catalyzed transesterification provides several benefits over homogeneously catalyzed transesterification, including a greater yield the elimination of soap formation, the generation of FFA, and high glycerin quality with low moisture content. However, because of the reduced reactivity of the catalyst, this technique has certain drawbacks, including a higher molar ratio of methanol to oil, a long reaction period, and elevated temperature and pressure parameters.

The supercritical technique outperforms both homogeneous and heterogeneous techniques. Mass transfer regulates the pace of reaction involving oil and methanol. Oil is dissolved into methanol at supercritical settings. It forms a single phase due to the high solubility of oil as well as supercritical methanol, which accelerates the pace of reactions. The pressure and temperature factor impact the merging of polar methanol with oil. This procedure offers numerous benefits over all other procedures, including (1) no soap formation, (2) FFA inclusion does not affect ultimate product quality, and (3) less reaction period. As by-products of an innovative supercritical technique utilizing dimethyl carbonate, important intermediate compounds including glycerol carbonate and citramalic acid were produced. The economic value of glycerol carbonate is higher than that of glycerol. One of the primary drawbacks of

utilizing supercritical settings is that it is tough to scale up reactors regarding safety and production optimization.

Based on a comprehensive study of the reaction process and frequently used methodologies for biofuel synthesis it could be inferred that the implementation of process optimization technologies that can produce greater biodiesel yields while using less extra methanol can provide considerable cost savings. In addition, if the technology aids in reaching a lesser process operating temperature, the potent energy needs could be reduced as tried to compare with traditional techniques.

The process intensifying technique relying on sonochemical reactors may solve the conditions like elevated temperature and high pressure, encountered while utilizing supercritical technologies for intensification. In certain situations, equivalent equilibrium yields could be achieved with a lesser excess of alcohols, resulting in a reduced separation load and, as a consequence, cheaper separation costs.

4   Reactors for Biodiesel Synthesis: Technological Advancements

For biodiesel production, various kinds of reactors of varied designs are used. Some of them are elucidated as follows.

4.1   Rotating Reactor

Multiple rotating elements like impellers, disks, or tubes make the rotating reactor which is rated by the rotational parameter such as power and speed. Effective heat and mass transfer conditions are provided by the agitation made by these agitators. Stirred tank reactor (STR), rotating tube reactor (RTR), and spinning disk reactor (SDR) are some examples of rotational reactors (Tabatabaei et al. 2019). The design of STR comprises of a vessel, either a single or a combination of stirrers connected to an axial shaft and a temperature regulator element. Temperature can be regulated by both coils and jackets but later is preferred for lower fouling, no interference with mixing, and ease of maintenance (Stitt 2002). STR further can be classified based on operation as (i) batch stirred tank reactor (BSTR), or (ii) continuous stirred tank reactor (CSTR).

Bearing a similar agitation mechanism as in batch-type reactors, CSTR can be termed to be an extension of the batch-type reactors. Continuous production of biodiesel is also achievable in CSTR for small setups. During batch production of biofuel commercially minute variations occur in every batch. CSTR can be used in a steady-state continuous system by the attachment of a mechanical stirrer and reactants and products are added and removed simultaneously. The attached stirrer provides adequate energy input into the system and proper mixing. As simple CSTR

might be to scale up but is capital demanding as large tanks are required which raises the capital investment by a substantial amount thereby making it not viable for commercial usage. Multiple stage CSTRs are generally used where a reactor and a phase separator are present. To increase the production of biodiesel, partial conversion of alcohol and triglycerides into biodiesel is done initially and glycerol is removed. This shifts the chemical equilibrium thereby promoting the transesterification reaction. By a highly efficient production and separation system, a single-stage reactor can ensure the complete conversion of oil.

Darnoko and Cheryan (2000) developed a two-stage CSTR system and produced biofuel from RBD palm oil with the second stage being a separator used for glycerol removal. It requires a residence time of 40 min during initialization in batch mode followed by the introduction of feedstock and methanol by feed pumps at a consistent rate. The mixture is moved by another feed pump to a separator for glycerol removal by phase separation. The initial yield was found to be 82.7% which on subsequent runs dropped to 58.8%. A maximum of 97.3% yield was obtained in steady-state and optimization to residence time set to 60 min, bearing 6:1 oil molar ratio and 60 °C optimum temperature with a catalyst loading of 1 wt%.

In RTR, the reactants and catalyst are pumped together into the tube which rotates not higher than 1000 rpm thereby creating a thin film of liquid on the inner walls of the reactor between 0.7 and 1.4 mm (Tabatabaei et al. 2019). Owing to the film formed, the heat and mass transfer becomes efficient and the surface area to volume ratio becomes high leading to residence times as low as 8 times that of CSTR. Glycerol and biodiesel were separated in the reactor's tube because of the high pressure. An additional condenser is also fitted to condense the vaporized reactant to ensure the ratio of reactant to be kept constant throughout the reactor. This made the reactor much compact and be of simple design. The high energy demand is the downside of the reactor.

Effective mass and heat transfer can also be obtained by SDR where reactants were added at the center of a rotating disk and are dispersed. This dispersion of the liquid reactants causes the liquid reactants to form a film radius and thickness being controlled by the rotational speed of the disk and the reactant flow rate which in turn controls the amount of product formed and residence time. The thickness of the film formed is around 100 µm (Visscher et al. 2013). Scaling-up in an SDR can be done via (i) incorporation of additional disks and (ii) increasing the disk size. Increasing the disk size would incur more power requirements (Meeuwse et al. 2012). The residence time of SDR is around 20–40 times lower as compared to BSTR (Qiu et al. 2012). Similar to RTR, the process is energy demanding.

4.2 Microchannel Reactor

To overcome the issues of the low contact surface-to-volume ratio, Microchannel reactors or microreactors were designed (Natarajan et al. 2019). They can further be categorized as, microtubular reactors, zig-zag microchannel reactors, etched

microchannel reactors, and micro fluidic laminated lab chips. For the reacting channels, meso or micro-scale geometry are used bearing hydraulic diameters in the range of 100–1000 μm. The ratio of surface area to volume is high because of the narrow channels which decrease the diffusion lengths and increases the mass transfer for elevated reaction rates. In comparison to conventional lab vessels and production vessels having a surface-to-volume ratio of 100 m^2/m^3 and 1000 m^2/m^3 respectively the microreactors possess surface to volume ratio of 10,000–50,000 m^2/m^3 (Maddikeri et al. 2012). As these have higher rates of reaction which reduces the energy requirement, hence they are operated in milder conditions. Compared to other biodiesel reactors, microchannel reactors have smaller footprints leading to reduced investment and lower cost of pumping in biodiesel production (Madhawan et al. 2018). Micromixers are generally used for agitation inside microreactors where two or more liquids need to be mixed leading to enhanced microscale mixing efficiency. The micro mixers can be of the active type or static type wherein electric or magnetic excitation allows the operation in the former and pressure differences in the latter for operation. These are used in different applications based on production capacities and mixing speeds (Santana et al. 2015). Intensification can be of two types being (i) convection which creates a heterogeneous mixture or (ii) homogenous mixture due to the diffusion of adjacent layers.

Different types of Micromixers viz. T-junction, J-junction, rectangular interdigital micromixer (RIMM), and slit interdigital micro mixers (SIMM) were studied for static mixers by Sun et al. (2010). For studying the hydrodynamics of mixing two liquid streams interdigital Micromixers are used as they create liquid lamellae periodically from alternating feed channels (Hardt and Schönfeld 2003). In the study, the outlet was connected to a transparent polytetrafluoroethylene (PTFE) tube with an internal diameter of 1.2 mm to observe the formation of oil droplets and flow patterns. To avoid phase separation, stainless steel Dixon rings with a high surface area to volume ratio were packed in the reacting channels. RIMM and SIMM were considered to be better mixers than T-junction and J-junction micro mixers with a roughly double yield of biodiesel as can be concluded from the study.

4.3 Plug Flow Reactor (PFR)

The mixing of reactants happens during a pipe or passage once they're discharged into the reactor and therefore the the} product is collected at the gap and thence may be known as one among the only of chemical reactors. The turbulence inside the pipes and fittings aids the blending process. The regulation of body of water pressure will cause changes in duration and length of the reactor. For effective handling of extremely viscous materials reactor is fitted with injection devices, mechanical mixers, and static mixers along side the piping. the dimensions of the reactor was also regulated with the fluid behavior (Santacesaria et al. 2012). The most effective thanks to utilize PFR is by subjecting it beneath air mass and continuous mode or a gradual flow of chemicals and catalysts. With this, the optimum energy spent on the method is

overcome by biodiesel yield. Compared to alternative vessel and tank-based reactors, PFR provides additional economic and economical reactant commixture for a reactor. From a maintenance viewpoint, PFR comparatively desires less period of time and maintenance. The house demand and initial opportunity cost for PFR are relatively lower compared to other forms of the reactor (Wong et al. 2019). Nonetheless, PFR suffers from temperature and pressure variation among its long pipe. Temperature and pressure drop were determined between the reactor's recess and outlet attributable to the fluid viscosity, internal fittings, and therefore the length to diameter magnitude relation of the reactor. This consequently resulted in inefficient heat and mass transfer.

5   Hydrodynamic Cavitation in Biodiesel Synthesis

HC method has seen its glorified applications in the field of wastewater treatment and fatty acid alkyl ester synthesis by alcoholysis of oil and alcohol. HC is devoid of any additional steps such as separation which makes it time-efficient. Studies were conducted by Ghayal et al. (2013) on used frying oil with KOH catalyst in a closed loop with a 10 L reservoir and a centrifugal pump. It was concluded that geometry plays a significant role in the intensification. A similar study was conducted by Pal et al. (2010) using HC wherein alcoholysis of thumba oil was studied with methanol 1% by weight of oil and NaOH as a catalyst. CH3OH and NaOH were mixed with oil and introduced to the feed tank. It yielded up to 80% in the first 30 min and on further studies on the number of orifices yield increased further and finally became constant for all types of plates.

Studies conducted on transesterification of waste cooking oil by Mohamad et al. (2017) with homogenous catalyst obtained high conversion rates during the initial stages. It was done in a setup consisting of a centrifugal pump with main and bypass lines with ball valves leading into the tank with an orifice plate in the main line. Pressure difference was measured by the addition of gauges in the line. The reaction was optimized to the temperature being 60 °C and KOH concentration (1.5% (w/w) of oil) with 60–90 min of reaction time. TiO_2–Cu_2O nanocomposites were used as a catalyst in the study conducted by Patil et al. (2020) where the preparation of alkyl ester from thumba seed oil was performed using HC in which they confirmed that reverse reaction was favored by the formed biodiesel resulting in incomplete conversion. Waste cooking oil was utilized by Bargole et al. (2019) who studied the process intensity of ether synthesis by varying the ratio of throat diameter to cross-sectional area. The yield of alkyl ester obtained was as high as 99% in 5 min under optimized conditions such as temperature 65 °C, reaction period = 20 min, and NaOH concentration of 1% (w/w) of oil. Chuah et al. (2017) used waste cooking oil for methyl ester synthesis in HC via alkali catalyzed alcoholysis which gave rise to cleaner biodiesel. Here, thumba methyl esters are considered to be synthesized from thumba oil by HC using TiO_2 as a catalyst. Cavitation intensity was varied by orifice plates and venturi tubes by varying pressure from 3 to 5 bars. The performance of synthesized biodiesel was evaluated via parameters such as reaction period, alcohol

to oil ratio, temperature, cavitation number, and inlet pressure as all these affect the conversion to biodiesel (Table 2).

5.1 Variation in Reaction Period

The conversion of thumba oil into biofuel was increased with increase in time and catalyst loading. Samani et al. (2021), observed an increase of 5.5% upon increasing the reaction time from 30 to 60 s. With the increase of catalyst concentration from 0.75 to 1.25% the yield decreased by 2.68%. The above can be explained by the fact that with the increased distance between rotor and stator, the blending decreased due to decreased effect of shear force. Patil et al. (2021), report the delayed response of catalyst during initial phases mainly due to the dominance of esterification at optimized conditions (Temperature = 65 °C and pressure = 2 bar). With the increase of catalysts and time alcoholysis of thumba oil increased. In the first hour, the conversion remains unchanged even with varying loadings of catalyst.

5.2 Alcohol to Oil Ratio

Triglyceride conversion increased upon increasing the ratio up to a certain value beyond which the conversion decreases. This was due to inadequate separation of biodiesel from formed glycerol, a by-product of reaction (Ghayal et al. 2013; Patil et al. 2018; Bokhari et al. 2016). For a short reaction period, methanol was considered to be an excess reactant and hindered in achieving equilibrium. It is reported that the 1:6 ratio for acid catalysis and 1:9 for alkaline catalysis is considered to be optimum for transesterification reactions. Meher et al. (2006) have reported 1:6 as suitable oil to alcohol molar ratio for the transesterification using an acid catalyst. Ghayal et al. (2013) has reported six as suitable alcohol to oil ratio for biodiesel production of used frying oil. Using NaOH as catalyst Pal et al. (2010) examined the alcoholysis of thumba oil and found the optimum ratio to be 1:4.5 for thumba oil with that of methanol. Patil et al. (2018) reported 1:6 as the optimum molar feed ratio in the ultrasonication method for biofuel synthesis using a catalyst as Amberlyst-15. Vegetable oils in presence of catalysts are transesterified in the range of 1:6–1:40. The highest conversion of 75% was achieved using an orifice plate at a 1:6 molar ratio. As esterification reaction dominates at initial conditions hence lower ratios do not show promising results.

Beyond the 1:6 molar ratio, the conversion decreased as more and more glycerol was obtained. Patil et al. (2018) and Chuah et al. (2017) both reported similar results with the former using the US method whereas later uses HC. Maddikeri et al. (2014) obtained the optimum at 1:12 ratio with 89% yield in HC reactor. Gole et al. (2013) in his studies reported similar results using venturi for HC. Mohod et al. (2017)

Table 2 Comparison of methods followed by various authors

Parameters	Mohammad et al. (Mohamad et al. 2017)	Bargole et al. (Bargole et al. 2019)	Chuah et al. (Chuah et al. 2016)	Innocenzi et al. (Innocenzi and Prisciandaro 2021)	Maddikeri et al. (Maddikeri et al. 2014)	Kolhe et al. (Kolhe et al. 2017)
Optimized process conditions	Molar ratio: 1:6, TiO_2 concentration of = 1.2%, operating temperature = 65 °C within 60 min at 5 bar	Catalyst concentration of = 1%, operating temperature = 35 °C within 15 min at 7 bar	Catalyst concentration of = 1%, operating temperature = 60 °C within 15 min at 2 bar	Catalyst concentration of ¼ 1%, operating temperature = 60 °C within 60 min	Molar Ratio:1:12, catalyst concentration of = 1.%, operating temperature = 60 °C at 3 bar	Molar Ratio:1:4.5, catalyst concentration of = 0.55%, operating temperature = 45 °C
Catalyst	TiO_2 (heterogeneous) First of its kind with HC	NaOH	KOH	$NaOCH_3$	KOH	KOH
Methodology	Hydrodynamic cavitation	Hydrodynamic cavitation	Hydrodynamic cavitation	Hydrodynamic cavitation and mechanical stirring	Hydrodynamic cavitation	Hydrodynamic cavitation
Highest conversion	75% conversion	98% yield	97.5% conversion	96% yield	91% yield	94% conversion
Time of reaction	60 min	15 min	15 min	60 min	Not reported	120 min
Orifice plate details	2 holes (2 mm in size)	100 holes (0.5 mm in size)	21 holes (1 mm in size)	N/A	1 hole (2 mm in size)	16 holes (3 mm in size)
Oil to alcohol ratio	1:2–1:10	1:4–1:8	1:4–1:7	1:5	1:10–1:14	1:3–1:6
Catalyst reuse	Possible	Not possible	Not possible	Not possible	Not possible	Not possible

investigated the alcoholysis of cooking oil through a high-speed homogenizer in HC within the optimum value of 1:12 and a yield of 95%.

5.3 Temperature

Temperature nearing the boiling point of alcohol is said to favor the transesterification reaction thereby leading to higher conversion of triglyceride to biodiesel (Ghayal et al. 2013; Pal et al. 2010; Patil et al. 2018; Bokhari et al. 2016). Ghayal et al. (2013) and Pal et al. (2010) individually concluded 60 °C to be optimum for biodiesel synthesis in the alkaline pathway. Similar studies (Demirbas 2009; Jain and Sharma 2010) have reported temperature closer to the boiling point of alcohol is taken to be optimum for biofuel synthesis as heating beyond this point would incur in alcohol readily vaporize thereby reducing the contact with oil inside the reactor. At 65 °C methanol vaporized, which led to minimal contact with the oil thereby resulting in decreased conversion. 98% conversion in HC and 97% with the conventional stirring method was obtained upon maintaining the temperature at 60 °C observed by Bokhari et al. (2016) implicating the higher temperature increased the solubility which also increased the rate of reaction. Through a high-speed homogenizer as HC reactor, Mohod et al. (2017) concluded that for conversion of waste oil into biofuel 50 °C was optimum at which 95% conversion was observed.

Using thumba oil, 65 °C was considered to be optimum wherein 75% conversion was achieved in the orifice plate. This was achieved because of the small orifice plate area resulting in high-intensity cavitation as compared to orifice meters. Hydrodynamic cavitation proved to be an efficient method over ultrasonication when yields were compared.

5.4 Cavitation Number

Cavitation number Cv is used to predict the hydraulic characteristics in HC reactor (Mukherjee et al. 2020a). Cv can be altered by changing the inlet pressure. For the generation of cavities to be more or the cavitation process to be optimum Cv should remain less than one (Mukherjee et al. 2020b). To balance it at optimum, flow rate and velocity were increased along with the inlet pressure. It can be measured by

$$C_v = \frac{P_2 - P_V}{0.5\left(\rho \times V_O^2\right)} \tag{7}$$

where P2 is pressure across the downstream side, P_v is the vapor pressure of the reaction mixture depending upon the individual moles of alcohol and oil, V_O is

the velocity of the reaction mixture, ρ is the liquid density of the reaction mixture depending upon the individual moles of alcohol and oil.

6 Trends and Perspectives

6.1 A Techno-Economic Evaluation

The present biofuel production capacity, as seen in Fig. 1, shows that only a very a few nations, including the United States, France, Poland, Thailand, Brazil, China, Argentina, Indonesia, Germany, and Spain, make a significant contribution over a billion liters of biofuel manufacture in bulk every year. The combined yield of the abovementioned nations amounts to 25.6 billion liters or 74.8% of entire global manufacturing.

Because of the diversity of biofuel feedstock, several other nations on the continent have an enormous potential for biodiesel synthesis. As a result, as shown in Fig. 1, a statistics-driven prediction algorithm was utilized to estimate the utmost biofuel production output of hundred and fifty-five nations. The model is based on primary information from the United Nations Statistics Division's Food and Agriculture Organization, Index Mundi, and the USA Energy Information Administration. Aside from the aforementioned nation, eight others, including Russia, Ukraine, Canada, the Netherlands, Malaysia, Colombia, the Philippines, and Belgium, have an enormous capacity for biofuel production volumes above a billion liters per year. Given the availability of palm feedstock, Southeast Asia nations such as Indonesia and Malaysia have the potential to achieve up to 16.3 and 30.3 billion liters of biofuel annually. Figure 2 depicts the optimum biofuel blend levels which may be achieved for the 155 nations based on their fuel consumption levels. Biodiesel can supersede all diesel fuel use (B100) in just one nation, Malaysia, assuming that the economic scenario is conducive to biodiesel synthesis. Other nations with the competency to adopt B10 to B100 mixtures are positioned between the black and red lines, whereas countries appropriate for B1 to B10 blends are seen across blue and black lines, and nations with no potential above B1 are located just beneath the blue colored line.

There are 25, 41, and 23 nations, correspondingly, which can volumetrically substitute 10–100%, 1–10%, and less than 1% biofuel blends in diesel. Because of the enormous amount of diesel use across nations like Japan, Indonesia, and China, implementing a greater biofuel blending ratio entirely with domestically sourced feedstock is challenging.
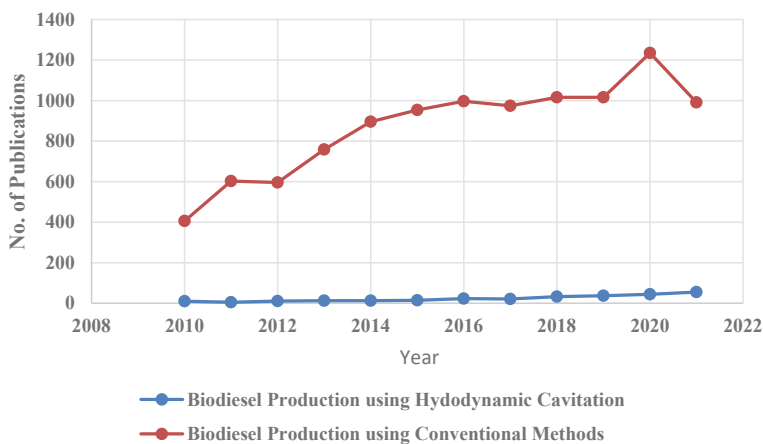
Fig. 2 Comparison between the number of articles in the previous decade (2010–2020) on Biodiesel production using Hydrodynamic cavitation and with conventional methods has been surveyed and exhibited in the interleaved diagram

6.2 Policies, Standards, and Emissions Analyses for Biodiesel

Long-chain alkyl esters from methyl, ethyl, or propyl esters are present in biofuel produced from plant oil or animals' fat. Because leftover frying oil is frequently treated to be reused as a raw material for biofuel manufacturing, that is made from both vegetable and animal fat, the grade of the feedstock can vary greatly. As a result, the grade of biofuel must be monitored while manufacturing to guarantee that it meets international requirements.

The tropical environment of Malaysia entails a better total storage temperature, culminating in a much more rigorous need for gasoline flashpoints. This did help to ease tensions in Malaysia, which adopted a mandated 10% biodiesel blend for conventional fuels in December 2018 to take advantage of the nation's capacity to minimize unexported raw palm oil while also improving energy security.

The standards are intended to give requirements for the biodiesel's physio-chemical properties. The American Standards for Testing Materials (ASTM D6751) and the European Standards for Biofuel are the 2 basic global biodiesel benchmarks (EN14214). Several biodiesel-producing nations use the ASTM and EN criteria as a basis for developing their biodiesel norms. In India, the National Policy on Biofuels (NPB) of 2009 and the newly authorized National Policy on Biofuel (NPB) of 2018 provide explicit directions for addressing the biodiesel trilemma's impact on food, energy and resources, and the ecology. The Indian government is concentrating on cultivating bushes and plants yielding non-edible feedstock to create biofuel on waste and impaired woodland and non-forest grounds. Biofuel is mostly made in the nation from molasses, a by-product of the cane sugar industry. Non—edible materials would be used to fuel the next era of technology in the long term. As a

result, the debate over fuel versus food security is irrelevant in India. The Indian govt is also focused on reducing Greenhouse gas by 33–35% by 2030 compared to 2005 levels, as well as transitioning to green biodiesel and a minimal-carbon economy, by 2023, improving fuel efficiency requirements and upgrading cars from BS-IV to BS-VI fuel compatibility regulations would help to combat harmful emissions and their impact on the environment. Major developing issues for the IPCC AR6 cycles are anticipated to include (1) transaction between ground use for biofuel production, food and fiber manufacturing, and ecological integrity preservation, and (2) co-delivery of bioenergy-based climatic change avoidance.

Rigorous emission restrictions have been a major impetus in the last several years to promote the use of ecologically benign fuel in IC engines. When contrasted to regular fuel oil, biodiesel fuel undoubtedly can reduce the main emissions from internal combustion. Coconut biodiesel had the greatest decrease in emissions since it is the solitary feedstock that accomplished all four reductions in releases, as well as the greatest drop in smoke density, which is linked to particulate material content. Even though most biofuel produced from various feedstocks reduces emissions, raw materials including olives and rice straw may not be ideal choices for biodiesel production due to their lower emissions efficacy.

6.3   Practical Implications of This Study

The most common batch-type reactor is compared to various types of biofuel manufacturing reactors. Nevertheless, because the biofuel yield and time of response are the only parameters to be evaluated, the comparison is frequently unfair. As a result, for a comprehensive comparison, additional more essential aspects such as processing capabilities, energy efficacy, space requirements, ecological effect, and technology adaptability must be considered. Conventional flow production in microreactors is inefficient due to the nature of the two-behavior involving alcohol and oil, which decreases their mixability during the start of the transesterification process. Because of the increased surface-to-volume ratio, both the droplet and pulsing methods in the microreactor have been shown to boost yield. Because of their ease of use, homogeneous catalysts are presently preferred in hydrodynamic reactors. The advancement of heterogeneous catalysts and cosolvent-assisted transesterification can resolve the concern of higher Lipid biofuel raw materials while also lowering alcohol and catalyst needs. Furthermore, because it functions as a boundary among the polar and non-polar phases, the addition of cosolvent can increase the solubility of the oil and methanol throughout transesterification. Extraction of cosolvent, on the other hand, will entail significant operational costs, which will be prohibitively expensive. Cosolvent has likewise proven promising about improving phase splitting amongst biofuel and glycerol by increasing the specific gravity as well as the relative viscosity difference amongst the 2 phases. When it's used in conjunction with another intensification approach, the microwave reactor has proved to be more successful. Industrial microwave reactors, on the other hand, operate at a set of 2.45 GHz, therefore, due

to their limited depth of penetration, may not be suitable for large-scale biodiesel production. As a result, microwave-assisted biofuel reactors are constrained to limited batch production, posing a scaling problem and manufacturing slower biodiesel. As a result, a continuous reactor is used to maximize biodiesel productivity while reducing residence time to account for the microwave reactor's smaller footprint.

Aside from the scientific hurdles of biodiesel synthesis, the present fiscal condition is also a key issue in the biofuel sector. As the techno-economic study indicates, several nations, like Malaysia and Indonesia, have the enormous capability for biofuel manufacturing and utilization, however, there is no financial benefit to replace traditional fuel at a better mix level since the sector is unprofitable. Because the emission levels of different biodiesels can differ by a substantial margin, material selectivity can increase the efficiency of biodiesel as a motivator to decrease greenhouse emissions.

7   Conclusion

In the current study, authors have traced the importance of feedstock on the quality of biofuel produced. Feedstock produced by different methods si potent to cause variations in the quality of biofuel and would also affect the socio-economic aspect of biodiesel production. Apart from feedstock variation in the reaction can also be due to the catalysts chosen. Alcholysis reaction is used for the production of biodiesel and can progress in presence of various catalysts such as acidic, basic, or heterogenous. Generally, heterogenous catalysts are chosen for ease in separation and recycle and reuse of the same. A varied number of conventional reactors were discussed with advantages and disadvantages to establishing a clear balance of the type of reactor and usage. A novel idea of the generation of biofuel by employing the methods of hydrodynamic cavitation was discussed in detail. Generation of biodiesel using hydrodynamic cavitation can be profitable and the running cost of the same would be less. It was observed the peak in the yield of the biodiesel was observed at a particular condition. Moreover, the requirement of chemicals decreases and residence time decreases, leading to an economic and time-efficient process. Additionally, the fuel generated is also compared side by side to the commercially available gasoline or diesel and was found to possess less smoke potential and lower the release of toxic gases. Also, the generated biodiesel from other sources was found to be effective and had a better performance as compared to current fuels. Various trends observed in biofuel production and studies were highlighted and also the expectations of future technologies basing on current growth and developmental pathway were discussed.

References

Alptekin E, Canakci M (2011) Optimization of transesterification for methyl ester production from chicken fat. Fuel 90:2630–2638. https://doi.org/10.1016/j.fuel.2011.03.042

Bargole S, George S, Kumar Saharan V (2019) Improved rate of transesterification reaction in biodiesel synthesis using hydrodynamic cavitating devices of high throat perimeter to flow area ratios, Chem Eng Process Process Intensif 139:1–13. https://doi.org/10.1016/j.cep.2019.03.012

Bokhari A, Chuah LF, Yusup S, Klemeš JJ, Kamil RNM (2016) Optimisation on pretreatment of rubber seed (Hevea brasiliensis) oil via esterification reaction in a hydrodynamic cavitation reactor. Bioresour Technol 199:414–422. https://doi.org/10.1016/j.biortech.2015.08.013

Chuah LF, Klemeš JJ, Yusup S, Bokhari A, Akbar MM, Chong ZK (2017) Kinetic studies on waste cooking oil into biodiesel via hydrodynamic cavitation. J Clean Prod 146:47–56. https://doi.org/10.1016/j.jclepro.2016.06.187

Chuah LF, Yusup S, Abd Aziz AR, Bokhari A, Abdullah MZ (2016) Cleaner production of methyl ester using waste cooking oil derived from palm olein using a hydrodynamic cavitation reactor. J Clean Prod 112:4505–4514. https://doi.org/10.1016/j.jclepro.2015.06.112

Darnoko D, Cheryan M (2000) Continuous production of palm methyl esters, JAOCS. J Am Oil Chem Soc 77:1269–1272. https://doi.org/10.1007/s11746-000-0199-x

Demirbas A (2009) Progress and recent trends in biodiesel fuels, Energy Convers. Manag 50:14–34. https://doi.org/10.1016/j.enconman.2008.09.001

Gardy J, Hassanpour A, Lai X, Ahmed MH, Rehan M (2017) Biodiesel production from used cooking oil using a novel surface functionalised TiO2 nano-catalyst. Appl Catal B Environ 207:297–310. https://doi.org/10.1016/j.apcatb.2017.01.080

Ghayal D, Pandit AB, Rathod VK (2013) Optimization of biodiesel production in a hydrodynamic cavitation reactor using used frying oil. Ultrason Sonochem 20:322–328. https://doi.org/10.1016/j.ultsonch.2012.07.009

Gole VL, Naveen KR, Gogate PR (2013) Hydrodynamic cavitation as an efficient approach for intensification of synthesis of methyl esters from sustainable feedstock. Chem. Eng. Process. Process Intensif. 71:70–76. https://doi.org/10.1016/j.cep.2012.10.006

Gryglewicz S (2011) Simulateur EIRL Notice Et Exemple Commenté 70:1–16

Hajjari M, Tabatabaei M, Aghbashlo M, Ghanavati H (2017) A review on the prospects of sustainable biodiesel production: a global scenario with an emphasis on waste-oil biodiesel utilization. Renew Sustain Energy Rev 72:445–464. http://doi.org/10.1016/j.rser.2017.01.034

Hardt S, Schönfeld F (2003) Laminar mixing in different interdigital micromixers: II. Numerical Simulations, AIChE J. 49:578–584. https://doi.org/10.1002/aic.690490305

Hums ME, Cairncross RA, Spatari S (2016) Life-Cycle Assessment of Biodiesel Produced from Grease Trap Waste. Environ Sci Technol 50:2718–2726. https://doi.org/10.1021/acs.est.5b02667

Innocenzi V, Prisciandaro M (2021) Technical feasibility of biodiesel production from virgin oil and waste cooking oil: Comparison between traditional and innovative process based on hydrodynamic cavitation. Waste Manag 122:15–25. https://doi.org/10.1016/j.wasman.2020.12.034

Jafari N (2010) Review of Pollution Sources and Controls in Caspian Sea Region 2:25–29

Jain S, Sharma MP (2010) Prospects of biodiesel from Jatropha in India: A review. Renew Sustain Energy Rev 14:763–771. https://doi.org/10.1016/j.rser.2009.10.005

Ji J, Wang J, Li Y, Yu Y, Xu Z (2006) Preparation of biodiesel with the help of ultrasonic and hydrodynamic cavitation. Ultrasonics 44. https://doi.org/10.1016/j.ultras.2006.05.020

Khan HM, Ali CH, Iqbal T, Yasin S, Sulaiman M, Mahmood H, Raashid M, Pasha M, Mu B (2019) Current scenario and potential of biodiesel production from waste cooking oil in Pakistan: An overview, Chinese. J Chem Eng 27:2238–2250. https://doi.org/10.1016/j.cjche.2018.12.010

Kolhe NS, Gupta AR, Rathod VK (2017) Production and purification of biodiesel produced from used frying oil using hydrodynamic cavitation. Resour Technol 3:198–203. https://doi.org/10.1016/j.reffit.2017.04.008

Macedo CCS, Abreu FR, Tavares AP, Alves MB, Zara LF, Rubim JC, Suarez PAZ (2006) New heterogeneous metal-oxides based catalyst for vegetable oil trans-esterification. J Braz Chem Soc 17:1291–1296. https://doi.org/10.1590/S0103-50532006000700014

Maddikeri GL, Pandit AB, Gogate PR (2012) Intensification approaches for biodiesel synthesis from waste cooking oil: A review. Ind Eng Chem Res 51:14610–14628. https://doi.org/10.1021/ie301675j

Maddikeri GL, Gogate PR, Pandit AB (2014) Intensified synthesis of biodiesel using hydrodynamic cavitation reactors based on the interesterification of waste cooking oil. Fuel 137:285–292. https://doi.org/10.1016/j.fuel.2014.08.013

Madhawan A, Arora A, Das J, Kuila A, Sharma V (2018) Microreactor technology for biodiesel production: a review, Biomass Convers. Biorefinery. 8:485–496. https://doi.org/10.1007/s13399-017-0296-0

Math MC, Kumar SP, Chetty SV (2010) Technologies for biodiesel production from used cooking oil - A review, Energy Sustain. Dev 14:339–345. https://doi.org/10.1016/j.esd.2010.08.001

Meeuwse M, van der Schaaf J, Schouten JC (2012) Multistage rotor-stator spinning disc reactor. AIChE J 58:247–255. https://doi.org/10.1002/aic.12586

Meher LC, Vidya Sagar D, Naik SN (2006) Technical aspects of biodiesel production by transesterification—a review. Renew Sustain Energy Rev 10:248–268. https://doi.org/10.1016/j.rser.2004.09.002

Mohamad M, Ngadi N, Wong SL, Jusoh M, Yahya NY (2017) Prediction of biodiesel yield during transesterification process using response surface methodology. Fuel 190:104–112. https://doi.org/10.1016/j.fuel.2016.10.123

Mohod AV, Gogate PR, Viel G, Firmino P, Giudici R (2017) Intensification of biodiesel production using hydrodynamic cavitation based on high speed homogenizer. Chem Eng J 316:751–757. https://doi.org/10.1016/j.cej.2017.02.011

Mukherjee A, Mullick A, Teja R, Vadthya P, Roy A, Moulik S (2020a) Performance and energetic analysis of hydrodynamic cavitation and potential integration with existing advanced oxidation processes: a case study for real life greywater treatment. Ultrason Sonochem 66:105116. https://doi.org/10.1016/j.ultsonch.2020.105116

Mukherjee A, Mullick A, Vadthya P, Moulik S, Roy A (2020b) Surfactant degradation using hydrodynamic cavitation based hybrid advanced oxidation technology: a techno economic feasibility study. Chem Eng J 398:125599. https://doi.org/10.1016/j.cej.2020.125599

Mukherjee A, Mullick A, Moulik S, Roy A (2021a) Oxidative degradation of emerging micropollutants induced by rotational hydrodynamic cavitating device: a case study with ciprofloxacin. J Environ Chem Eng 9:105652. https://doi.org/10.1016/j.jece.2021.105652

Mukherjee A, Satish A, Mullick A, Rapolu J, Moulik S, Roy A, Ghosh AK (2021b) Paradigm shift toward developing a zero liquid discharge strategy for dye-contaminated water streams: a green and sustainable approach using hydrodynamic cavitation and vacuum membrane distillation. ACS Sustain Chem Eng 9(19):6707–6719. https://doi.org/10.1021/acssuschemeng.1c00619

Natarajan Y, Nabera A, Salike S, Dhanalakshmi Tamilkkuricil V, Pandian S, Karuppan M, Appusamy A (2019) An overview on the process intensification of microchannel reactors for biodiesel production. Chem. Eng. Process. - Process Intensif. 136:163–176. https://doi.org/10.1016/j.cep.2018.12.008

Nguyen VK, Lee MH, Park HJ, Lee JU (2015) Bioleaching of arsenic and heavy metals from mine tailings by pure and mixed cultures of Acidithiobacillus spp. J Ind Eng Chem 21:451–458. https://doi.org/10.1016/j.jiec.2014.03.004

Pal A, Verma A, Kachhwaha SS, Maji S (2010) Biodiesel production through hydrodynamic cavitation and performance testing. Renew Energy 35:619–624. https://doi.org/10.1016/j.renene.2009.08.027

Patil P, Gude VG, Pinappu S, Deng S (2011) Transesterification kinetics of Camelina sativa oil on metal oxide catalysts under conventional and microwave heating conditions. Chem Eng J 168:1296–1300. https://doi.org/10.1016/j.cej.2011.02.030

Patil AD, Baral SS, Dhanke PB, Madankar CS, Patil US, Kore VS (2018) Parametric studies of methyl esters synthesis from Thumba seed oil using heterogeneous catalyst under conventional stirring and ultrasonic cavitation. Mater. Sci. Energy Technol. 1:106–116. https://doi.org/10.1016/j.mset.2018.06.004

Patil A, Dhanke P, Kore V, Kanse N (2019) Thumba methyl ester production using prepared novel TiO2 nano-catalyst in ultrasonic cavitation reactor. Mater. Today Proc. 18:4322–4329. https://doi.org/10.1016/j.matpr.2019.07.391

Patil A, Baral SS, Dhanke P, Kore V (2020) Biodiesel production using prepared novel surface functionalised TiO2 nano-catalyst in hydrodynamic cavitation reactor. Mater. Today Proc. 27:198–203. https://doi.org/10.1016/j.matpr.2019.10.009

Patil A, Baral S, Dhanke P (2021) Hydrodynamic cavitation for process intensification of biodiesel synthesis—a review. Curr Res Green Sustain Chem 4:100144. https://doi.org/10.1016/j.crgsc.2021.100144

Qiu Z, Petera J, Weatherley LR (2012) Biodiesel synthesis in an intensified spinning disk reactor. Chem Eng J 210:597–609. https://doi.org/10.1016/j.cej.2012.08.058

Sakthivel R, Ramesh K, Purnachandran R, Mohamed Shameer P (2018) A review on the properties, performance and emission aspects of the third generation biodiesels. Renew Sustain Energy Rev 82:2970–2992. https://doi.org/10.1016/j.rser.2017.10.037

Samani BH, Behruzian M, Najafi G, Fayyazi E, Ghobadian B, Behruzian A, Mofijur M, Mazlan M, Yue J (2021) The rotor-stator type hydrodynamic cavitation reactor approach for enhanced biodiesel fuel production. Fuel 283:118821. https://doi.org/10.1016/j.fuel.2020.118821

Santacesaria E, Turco R, Tortorelli M, Russo V, Di Serio M, Tesser R (2012) Biodiesel Process Intensification by Using Static Mixers Tubular Reactors. Ind Eng Chem Res 51:8777–8787. https://doi.org/10.1021/ie201640w

Santana HS, Silva JL, Taranto OP (2015) Numerical simulation of mixing and reaction of Jatropha curcas oil and ethanol for synthesis of biodiesel in micromixers. Chem Eng Sci 132:159–168. https://doi.org/10.1016/j.ces.2015.04.014

Shah SH, Raja IA, Rizwan M, Rashid N, Mahmood Q, Shah FA, Pervez A (2018) Potential of microalgal biodiesel production and its sustainability perspectives in Pakistan. Renew Sustain Energy Rev 81:76–92. http://doi.org/10.1016/j.rser.2017.07.044

Singh D, Sharma D, Soni SL, Sharma S, Kumar Sharma P, Jhalani A (2020) A review on feedstocks, production processes, and yield for different generations of biodiesel. Fuel 262:116553. https://doi.org/10.1016/j.fuel.2019.116553

Stavarache C, Vinatoru M, Nishimura R, Maeda Y (2005) Fatty acids methyl esters from vegetable oil by means of ultrasonic energy. Ultrason Sonochem 12:367–372. https://doi.org/10.1016/j.ultsonch.2004.04.001

Stitt E (2002) Alternative multiphase reactors for fine chemicals. Chem Eng J 90:47–60. https://doi.org/10.1016/S1385-8947(02)00067-0

Sun P, Wang B, Yao J, Zhang L, Xu N (2010) Fast synthesis of biodiesel at high throughput in microstructured reactors. Ind Eng Chem Res 49:1259–1264. https://doi.org/10.1021/ie901320s

Tabatabaei M, Aghbashlo M, Dehhaghi M, Panahi HKS, Mollahosseini A, Hosseini M, Soufiyan MM (2019) Reactor technologies for biodiesel production and processing: A review. Prog Energy Combust Sci 74:239–303. https://doi.org/10.1016/j.pecs.2019.06.001

Visscher F, van der Schaaf J, Nijhuis TA, Schouten JC (2013) Rotating reactors – A review. Chem Eng Res Des 91:1923–1940. https://doi.org/10.1016/j.cherd.2013.07.021

Wong KY, Ng J-H, Chong CT, Lam SS, Chong WT (2019) Biodiesel process intensification through catalytic enhancement and emerging reactor designs: a critical review. Renew Sustain Energy Rev 116:109399. https://doi.org/10.1016/j.rser.2019.109399

Zhou Y, Schulz S, Lindoy LF, Du H, Zheng S, Wenzel M, Weigand JJ (2020) Separation and recovery of rare earths by in situ selective electrochemical oxidation and extraction from spent fluid catalytic cracking (FCC) catalysts. Hydrometallurgy 194:105300. https://doi.org/10.1016/j.hydromet.2020.105300

Electrochemical Treatment of Sulphidic Spent Caustic Waste Stream Generated from Petroleum Refineries

Merin Susanna James and Anurag Garg

Abstract The objective of present study was to assess the performance of electro-Fenton (EF) process for treatment of the simulated sulphidic SCS (sulphide concentration = 10 g/L and pH = 13.7) using iron electrodes. The experimental runs were performed with simulated wastewater at an adjusted pH of ~ 5 with varying H_2O_2 dosages of 0.31–1.56 M. The current density, electrode spacing and agitation speed were maintained at 1 mA/cm^2, 3 cm and 500 rpm, respectively. The treatment process resulted in complete degradation of sulphides, though the chemical oxygen demand (COD) was not fully removed (upto ~91%). It was observed that the addition of super-stoichiometric H_2O_2 dosage (i.e., 1.56 M) even caused a decrease in the COD removal. Mere adjustment of wastewater pH to 5 resulted in ~ 48% sulphide removal due to H_2S stripping which is just almost 50% of the overall sulphide removal during EF process. Hence, EF process can be considered a potential alternative for the removal of sulphides from spent caustic stream.

Keywords Electro-Fenton oxidation · Sulphidic spent caustic · Wastewater treatment

1 Introduction

Spent caustic is one of the challenging waste streams generated from petroleum refineries. The various products manufactured during petroleum refining consists substantial quantities of sulphur compounds as impurities inhibiting the direct usage of these products (Alipour and Azari 2020; Paulino and Afonso 2012). In order to eliminate these detrimental compounds, mercaptans oxidation (MEROX) process is used commercially for product sweetening and extraction (Pino-Cortés et al. 2020). In this unit, caustic scrubbing with sodium hydroxide is carried out leading to elimination of hydrogen sulphides and mercaptans from the stream.

M. S. James · A. Garg (✉)
Environmental Science and Engineering Department, Indian Institute of Technology (IIT) Bombay, Mumbai, Maharashtra 400076, India
e-mail: a.garg@iitb.ac.in

Table 1 Chemical composition of sulphidic SCS

Parameter	Value
pH	12–14
Chemical oxygen demand (COD) (g/L)	10–200
Total organic carbon (TOC) (g/L)	6–20
Sulphides (weight %)	0.1–4
Mercaptans (weight %)	0.1–4
Phenols (g/L)	0–5
NaOH (weight %)	2–5

$$RSH + NaOH \rightarrow RSNa + H_2O \tag{1}$$

$$H_2S + 2NaOH \rightarrow Na_2S + 2H_2O \tag{2}$$
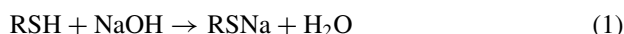
The discarded caustic solution from this unit is termed as spent caustic stream (SCS). The SCS is highly alkaline (pH > 12) with 5–12 weight % NaOH, phenols, sulphides (0.1–4 weight %), mercaptans, various organic and inorganic compounds rendering the stream hazardous for disposal. The characteristics of SCS differ depending on the product being manufactured. Depending on the composition, SCS can be classified into three types: (i) sulphidic SCS—generated from liquefied petroleum gas or ethylene gas scrubbing unit, (ii) naphthenic SCS—generated from diesel/kerosene scrubbing and (iii) cresylic SCS – effluent from gasoline scrubbing.

The present study focused on the treatment of sulphidic SCS which contains sulphides and mercaptans in considerably high concentrations as compared to the cresylic and naphthenic streams (Rathore et al. 2011). The typical composition of sulphidic SCS is given in Table 1. Due to its hazardous nature, direct biological treatment is unviable, hence a suitable pre-treatment has to be performed. Wet oxidation is widely adopted by refineries to serve this purpose. However, the requirement of high operating conditions (i.e., temperature and pressures) is the main disadvantage with the hydrothermal treatment process hence there is a need to find alternate techniques for the treatment of SCS (Seyedin and Hassanzadeganroudsari 2018; Rodriguez et al. 2008).

Electrochemical methods are gaining importance due to their high potential for oxidising the organics and inorganics present in aqueous phase at ambient conditions with less sludge production. During the electrochemical reactions, strong oxidising agents such as hydroxyl radicals (OH·) are released at the cathode which lead to the oxidation of organic and inorganic contaminants (Bhagawan et al. 2016). Electro-Fenton (EF) is an electrochemical technique in which Fenton's reagent ($Fe^{2+} + H_2O_2$) is also used to oxidise the pollutants. This process is a combination of the conventional Fenton and electrochemical oxidation process. Anodic oxidation reactions produce ferrous ions which can be regenerated by the cathodic reduction. The hydrogen peroxide added to the system, reacts with ferrous ions to produce OH· radicals which oxidise the pollutants (Nidheesh and Gandhimathi 2012; Gameel et al. 2015; Nuñez

et al. 2009). This method overcomes some limitations of the conventional Fenton's process such as higher chemical requirement as well as sludge generation and lower regeneration of Fe^{2+}. Various factors which may affect performance of EF process includes wastewater pH, current density, H_2O_2 dose, inter-electrode spacing and reaction time (Ribeiro and Nunes 2021).

Although several studies have been reported on treatment of different types of wastewater by EF process, the potential of EF on SCS treatment is in the progressing stage. Only few studies have been reported on EF treatment of SCS waste stream.

Nunez et al. (Nuñez et al. 2009) performed EF for treating SCS with sulphide concentration and chemical oxygen demand (COD) of 21.5 g/L and 125.8 g/L, respectively. They reported an overall sulphide and COD removals of 97% and 93%, respectively, within 60 min of reaction. Gameel et al. (2015) performed EF treatment on SCS (S^{2-} = 3.3–3.9 weight %, COD = 24 g/L) using iron and stainless steel as anode and cathode, respectively. The reaction time, current density and H_2O_2 dose were 60 min, 3.3 mA/cm^2 and 1.88 g/L, respectively. A similar study on EF using iron electrodes as both anode and cathode was conducted by Davarnejad and Bakhshandeh (2018). The researchers treated SCS (COD = 14.2 g/L, S^{2-} = 6.82 g/L, phenol = 0.4 g/L) obtained from olefin plants at current density, reaction time and H_2O_2/SCS of 20–80 mA/cm^2, 10–90 min and 0.3–2.14 mL/L, respectively. Both the studies reported considerably good removal efficiencies of sulphides (~99%) and COD (~83%). Nasr Esfahani et al. (2019) investigated the potential of electro-photo Fenton for the removal of COD from SCS (initial COD = 22.5 g/L). A COD removal of 97% was obtained after 80 min reaction at current intensity and H_2O_2/COD of 16.6 mA/cm^2 and 0.69, respectively. However, limited studies have looked into leaching and regeneration of Fe^{2+}, as well as H_2O_2 consumption during the overall process of SCS treatment.

In the view of available literature, the present study was aimed to assess the performance of EF process using iron electrodes for the treatment of simulated SCS wastewater prepared in laboratory. In addition to removal of sulphides and COD, the change in residual iron and H_2O_2 concentrations was also analysed. Moreover, an effort was made to understand possible routes for sulphide removal from the wastewater. Therefore, the removal of sulphides from wastewater only by adjusting pH was also studied.

2 Materials and Methods

2.1 Materials and Simulated Wastewater

Analytical grade (AR) sodium sulphide ($Na_2S.xH_2O$) (60% purity) purchased from Loba Chemie Pvt.Ltd, Mumbai, was used to prepare the simulated sulphidic SCS. The other reagents or chemicals such as H_2O_2 (50% w/v), H_2SO_4 and NaOH were purchased from Merck Chemicals Private Limited, Mumbai. Potassium titanium

Table 2 Wastewater characteristics and operating conditions

Parameter	Value
Initial sulphides	10 g/L
Initial COD	19.65 g/L
Initial pH	13.7
Adjusted pH	~ 4.5
Area of electrodes immersed	56 cm^2
Current density	1 mA/cm^2
H_2O_2 dose	0.94–1.56 M
Inter-electrode spacing	3 cm
Stirring speed	500 rpm
Reaction time	2 h

oxalate used for H_2O_2 measurement after EF process, was procured from Sigma Aldrich, Germany. Iron electrodes (10.5 cm × 4.5 cm × 0.2 cm) were purchased from a local vendor. The DC power supply machine (0–2 A and 0–32 V) was supplied by Testronix Ltd, Mumbai.

The simulated wastewater with sulphide concentration of 10 g/L was prepared for the experimental work. The wastewater characteristics are shown in Table 2. The initial pH and COD of the wastewater were 13.7 and 19.65 g/L, respectively.

2.2 Experimental Methodology

The EF experimental study was performed with 250 mL simulated wastewater (sulphide concentration = 10 g/L) in 1 L capacity glass beaker for a period of 2 h. Before the run, the wastewater pH was adjusted to 4.5 using H_2SO_4 and the solution was agitated by means of magnetic stirring for an initial period of 30 min. From the previous studies, it has been reported that the wastewater pH has to be adjusted in the range of 3–5 for effective Fenton-based oxidation process. H_2O_2 is highly unstable at high pH which leads to its decomposition in water and oxygen. Moreover, iron is precipitated out as ferric hydroxide at higher pH values. A pH lower than 3 is also not suitable since the decomposition of H_2O_2 to OH$^·$ radicals is not happended and H_2O_2 is likely to transform into oxonium ions ($H_3O_2^+$) by capturing one proton (Nidheesh and Gandhimathi 2012). Thus, a wastewater pH of ~4.5 was chosen for the study. Iron electrodes were then immersed into the wastewater such that the inter-electrode spacing was maintained at 3 cm and the net electrode area was 56 cm^2. Pre-calculated amount of H_2O_2 was added to the reactor to commence the oxidation process. The EF runs were performed with H_2O_2 dosages of 1.25 M (stoichiometric), 0.94 M, 0.625 M, 0.31 M and 1.56 M. A current density and stirring speed of 1 mA/cm^2 and 500 rpm, respectively were maintained throughout the runs.

All the experiments were conducted at ambient conditions (i.e., at 25 °C temperature). The treated samples were withdrawn at regular time intervals and 1 M NaOH solution was added immediately to quench the reaction as reported in earlier studies (Khatri et al. 2018). The treated samples were analysed for COD, sulphides, residual H_2O_2, total iron and ferrous ions. All the runs were performed in duplicate.

Table 2 summarizes the wastewater characteristics and reaction parameters adopted in this study.

2.3 Analytical Methods

pH of the untreated and treated water samples was measured with a digital pH meter (Polmon, LP-139S, India). COD was determined by standard closed reflux dichromate titration method (APHA 2017). The sulphide was measured by iodometric titration method as per the standard procedure (APHA 2017). Standard 1, 10-phenanthroline colorimetric method was used to analyse the concentrations of total iron and Fe^{2+} present in the treated samples. Residual H_2O_2 in the treated samples was determined by potassium titanium oxalate spectrophotometric analysis (APHA 2017).

# 3 Results and Discussion

3.1 Sulphides and COD Removal

It has been mentioned earlier that the EF batch experiments were conducted for 2 h duration with varying H_2O_2 doses at an adjusted pH of ~4.5. The aqueous samples were withdrawn at regular intervals of 10, 30, 60, 90 and 120 min. From Fig. 1a, it can be observed that sulphides were completely eliminated by the end of 60 min with all doses of H_2O_2. However, complete removal of COD was not observed in the process (Fig. 1b). The COD removal increased with change in H_2O_2 dosage from 0.31 M to 0.625 M. It was found to decrease with further increase in H_2O_2 dose. A maximum COD removal of 91% was obtained with H_2O_2 concentration of 0.625 M. The lower COD removal suggests partial oxidation of sulphides. Thus, the formation of one or more of the intermediates like thiosulphates, tetrathionates, trithionates and sulphites is expected (Zopfi et al. 2004). Oxidation of sulphides takes place due to $OH^{\cdot}$ radicals which are likely to generate from ferrous ion produced at the anode Eqs. (3) and (4) (Rodriguez et al. 2008).

$$Fe^0 \rightarrow Fe^{2+} + 2e^- \tag{3}$$

$$Fe^{2+} + H_2O_2 \rightarrow Fe^{3+} + OH^{\cdot} + OH^- \tag{4}$$
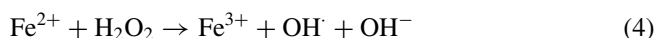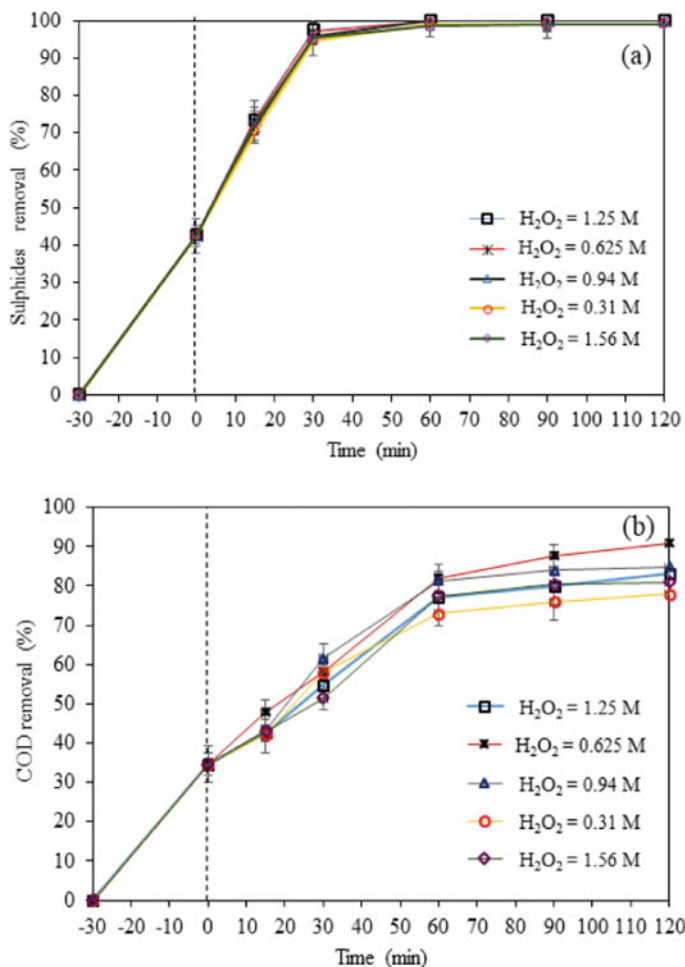
Fig. 1 Effect of H_2O_2 dose on: (a) sulphide removal, and (b) COD removal (S^{2-} concentration = 10 g/L, adjusted pH = 4.5, current density = 1 mA/cm^2, inter-electrode spacing = 3 cm, stirring speed = 500 rpm, reaction time = 2 h)

The production of OH$^·$ radicals increases with H_2O_2 dose resulting in the improved sulphide removal efficiency. However, excess H_2O_2 dose can be detrimental to the overall effectiveness of the process due to two major reasons (Nidheesh and Gandhimathi 2012; Nasr Esfahani et al. 2019): (i) excess H_2O_2 concentration can lead to recombination of OH$^·$ to H_2O_2 (Eq. 5), thereby reducing the availability of OH$^·$ radicals for oxidation, (ii) scavenging effect, i.e., H_2O_2 and OH$^·$ radicals can react to form weaker hydroperoxyl radicals (Eq. 6). Hence, the decrease in COD removal would have happened beyond 0.625 M H_2O_2 dose.

$$2OH^{\cdot} \rightarrow H_2O_2 \qquad (5)$$

$$OH^{\cdot} + H_2O_2 \rightarrow HO_2^{\cdot} + H_2O \qquad (6)$$
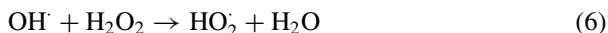
3.2 Determination of Residual Iron and H₂O₂ Concentration

Time based concentrations of the residual total and ferrous ions present in the treated wastewater samples are shown in Fig. 2a,b. After 2 h reaction, their concentrations in the treated sample were ~200 mg/L and ~100 mg/L, respectively. The presence of ferrous ions indicates occurrence of oxidation reaction at anode (Eq. 3) and its regeneration should occur at the cathode (Eq. 7). More regeneration of Fe^{2+} assists in the production of more OH· radicals (Brillas et al. 2009). From the results, it can be inferred that sufficient Fe^{2+} ions were present in the system for oxidation reaction
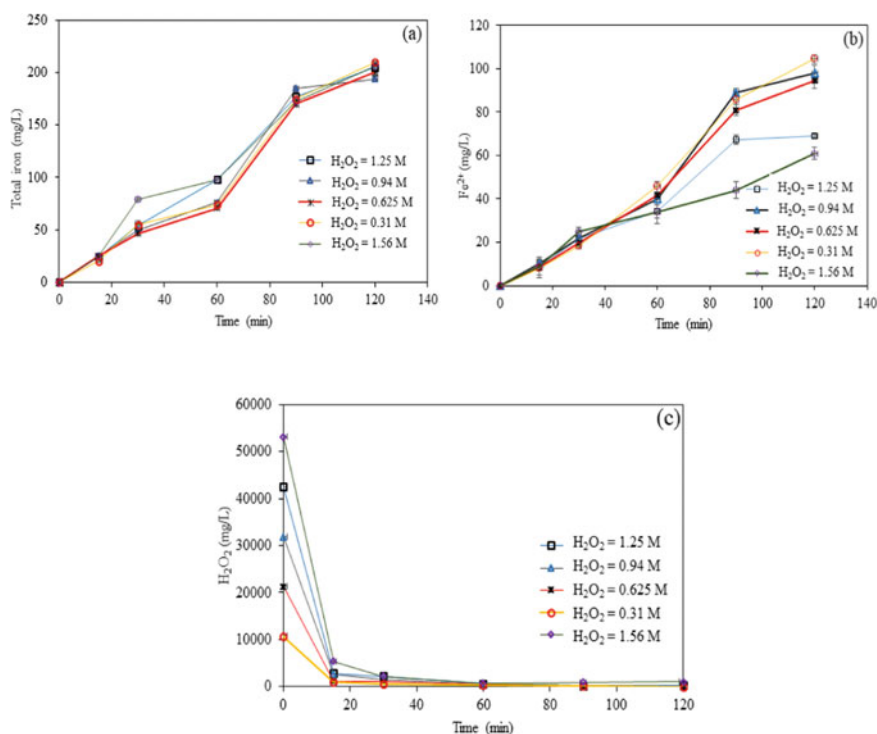
Fig. 2 Effect of EF on **a** residual total iron, **b** ferrous ion, and **c** H_2O_2 present in the treated samples ($S^{2-} = 10$ g/L, adjusted pH = 4.5, current density = 1 mA/cm², inter-electrode spacing = 3 cm, stirring speed = 500 rpm, reaction time = 2 h)

to occur. The maximum Fe^{2+} concentration was recorded during the run conducted with 0.31 M H_2O_2 dose which indicates that the H_2O_2 dose was not sufficient for producing enough $OH^{.}$ radicals.

$$Fe^{3+} + e^- \rightarrow Fe^{2+} \tag{7}$$

The results showed complete consumption of H_2O_2 when its dose was 0.31–0.94 M. From Fig. 2c, it is evident that more than 90% of the H_2O_2 was consumed within 15 $_{min}$ after the start of reaction irrespective of initial H_2O_2 dose. Higher initial dose resulted in small quantities of residual H_2O_2, which might be due to the recombination of $OH^{.}$ to H_2O_2 as mentioned in Eq. 5.

3.3 Effect of Wastewater pH on Sulphide and COD Removals

To understand the effect of pH, one run was also performed with wastewater having original pH of 13.7. The stoichiometric H_2O_2 dose (i.e., 1.25 M) was used for this run while keeping all other reaction conditions (such as current density, inter-electrode spacing and run duration) same as mentioned previously. An overall sulphide and COD removals of only 28% and 24%, respectively were obtained at the end of 2 h in comparison to 100% sulphide and ~ 90% COD removals recorded during EF treatment process. In alkaline conditions, the sulphides can also get oxidised to sulphates by reacting with H_2O_2 according to Eq. 8. The H_2O_2 was completely disappeared within 5 $_{min}$ after addition since the alkaline condition results in decomposition of H_2O_2 to water and oxygen (Eq. 9).

$$S^{2-} + 4H_2O_2 \rightarrow SO_4^{2-} + H_2O \tag{8}$$

$$2H_2O_2 \rightarrow 2H_2O + O_2 \tag{9}$$
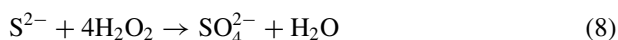
3.4 Effect of Neutralisation on Sulphides and COD Removals

The contribution of H_2S stripping in the overall removal of sulphides and COD was also determined by neutralising the solution in pH range of 1.5–10. The decrease in reaction pH from 10 to 1.5 led to increased removal of sulphide and COD (maximum removals = 48% and 43%, respectively) (Fig. 3). Decreasing the pH below 5 exhibited insignificant change in the sulphide and COD removal efficiencies. As the pH approached in acidic range, sulphides are expected to escape as H_2S gas resulting in unpleasant odours (Hawari et al. 2015).
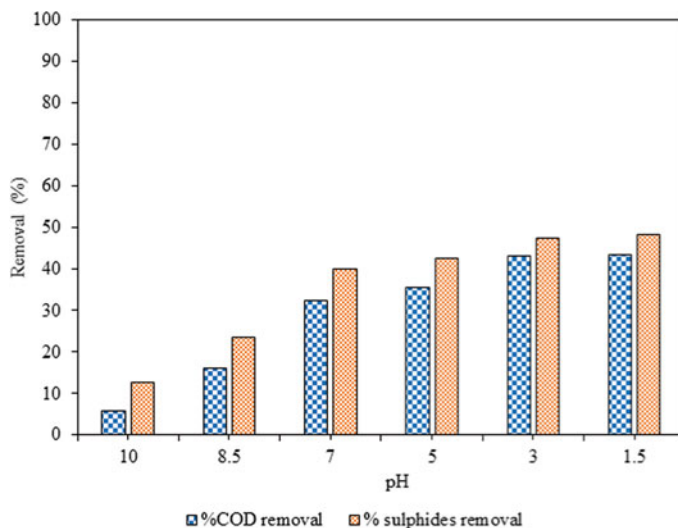
Fig. 3 Effect of neutralisation on COD and sulphide removals

4 Conclusions

In the present study, the performance of EF process on the removal of sulphides and COD for different doses of H_2O_2 was investigated. It was observed that sulphides were completely removed within 60_{min} after the start of reaction while COD was not completely eliminated. Higher doses of H_2O_2 caused decrease in the sulphide removal. The H_2O_2 was completely consumed within 15_{min} for all H_2O_2 doses. The presence of trace amounts of residual H_2O_2 could be observed after the runs with its higher doses. Neutralisation to pH ~5 could remove 48% and 43% of sulphides and COD respectively, which can be due to the escape of sulphides as H_2S. Thus, it can be presumed that sulphide oxidation and H_2S stripping are the core reasons for sulphide removal. From the present study, it can be concluded that EF has great potential for sulphidic SCS. In future, the EF studies should be carried out on simulated wastewater containing phenol and sulphides as well as real wastewater.

Conflict of Interest Declaration of Conflict of Interest: We declare that there is no conflict of interest.

References

Alipour Z, Azari A (2020) COD removal from industrial spent caustic wastewater: a review. J Environ Chem Eng 8:19. https://doi.org/10.1016/j.jece.2020.103678

American Public Health Association (APHA) Handbook (2017) Standard methods for the examination of water and wastewater, 23rd edn, Washington

Bhagawan D, Poodari S, Golla S, Himabindu V, Vidyavathi S (2016) Treatment of the petroleum refinery wastewater using combined electrochemical methods. Desalin Water Treat 57:3387–3394

Brillas E, Sirés I, Oturan MA (2009) Electro-Fenton process and related electrochemical technologies based on Fenton's reaction chemistry. Chem Rev 109:6570–6631

Davarnejad R, Bakhshandeh M (2018) Olefin plant spent caustic wastewater treatment using electro-Fenton technique. Egypt J Pet 27:573–581

Gameel A, Malash G, Mubarak AA, Hussein M (2015) Treatment of spent caustic from ethylene plant using electro-Fenton technique. Am J Environ Eng Sci 2:37–46

Hawari A, Ramadan H, Abu-Reesh I, Ouederni M (2015) A comparative study of the treatment of ethylene plant spent caustic by neutralization and classical and advanced oxidation. J Environ Manage 151:105–112

Khatri I, Singh S, Garg A (2018) Performance of electro-Fenton process for phenol removal using Iron electrodes and activated carbon. J Environ Chem Eng 6:7368–7376

Nasr Esfahani K, Farhadian M, Solaimany Nazar AR (2019) Interaction effects of various reaction parameters on the treatment of sulfidic spent caustic through electro-photo-Fenton. Int J Environ Sci Technol 16:7165–7174

Nidheesh PV, Gandhimathi R (2012) Trends in electro-Fenton process for water and wastewater treatment: an overview. Desalination 299:1–15

Nuñez P, Hansen HK, Rodriguez N, Guzman J, Gutierrez C (2009) Electrochemical generation of fenton's reagent to treat spent caustic wastewater. Sep Sci Technol 44:2223–2233

Paulino JF, Afonso JC (2012) New strategies for treatment and reuse of spent sulfidic caustic stream from petroleum industry. Quim Nova 35:1447–1452

Pino-Cortés E, Montalvo S, Huiliñir C, Cubillos F, Gacitúa J (2020) Characteristics and treatment of wastewater from the mercaptan oxidation process: a comprehensive review. Processes 8:425, 23. https://doi.org/10.3390/pr8040425

Rathore V, Gupta S, Thorat TS, Rao PVC, Choudary NV, Biju G (2011) Catalytic oxidation of spent caustic. Pet Technol Q 16:1–6

Ribeiro JP, Nunes MI (2021) Recent trends and developments in Fenton processes for industrial wastewater treatment—a critical review. Environ Res 197

Rodriguez N, Hansen HK, Nuñez P, Guzman J (2008) Spent caustic oxidation using electro-generated Fenton's reagent in a batch reactor. J Environ Sci Health Part A Toxic/Hazard Subst Environ Eng 43:952–960

Seyedin S, Hassanzadeganroudsari M (2018) Evaluation of the different methods of spent caustic treatment. Int J Adv Res Sci Eng Technol 5:5275–5283

Zopfi J, Ferdelman TG, Fossing H (2004) Distribution and fate of sulfur intermediates—Sulfite, tetrathionate, thiosulfate, and elemental sulphur—in marine sediments. Spec Paper Geol Soc Am 379:97–116

Lignin Based Hydrogel Production and Their Applications

Jatinderpal Singh, Subhrajeet Dash, Anjireddy Bhavanam, Poonam Gera, D. Giribabu, and Nitin Naresh Pandhare

Abstract When the world's population grows, so does resource scarcity, resource demand, and pollution. Polymers are one of the better sources that can be used in place of chemicals derived from fossils. Polymers derived from biomass have recently piqued the attention of the scientific community due to inherent properties such as biodegradability, low density, low cost, and low abrasiveness, low weight, facile synthesis, resistant to chemicals, radar absorbent, thermally and electrical insulating, easier to clear etc. We will learn about lignin, which is the second most abundant biopolymer in plants, in this article. The literature on lignin hydrogels is growing, particularly in the scientific community. There are many technical papers and public reports available that describe things from an engineering standpoint. The aim of this article is to review the literature on lignin extraction processes, hydrogel production techniques, and lignin-based hydrogel production processes, as well as their applications. In this article, acrylic acid is grafted onto the backbone of lignosulfonate in the presence of MBA as an initiator to form lignosulfonate acrylic acid hydrogel. Lignin PVA hydrogel is made by combining lignin and PVA in the presence of NaOH and the cross-linker ECH in a single pot reaction. Lignin-agarose hydrogels are made from lignin and agarose solutions that have been cross-linked with ECH. Similarly, this article discusses the preparation of lignin-based hydrogels, which are used for dye, Cu (II), Pb (+2), and other ion extraction from waste water, making slow-release fertilisers, biosensors, drug delivery, and agriculture harvesting, among other applications.

Keywords Hydrogel · Lignin · Applications · Production techniques etc.

J. Singh · S. Dash · A. Bhavanam (✉) · P. Gera · D. Giribabu · N. N. Pandhare
Department of Chemical Engineering, Dr. B. R. Ambedkar National Institute of Technology, Jalandhar, Punjab 144011, India
e-mail: bhavanama@nitj.ac.in

1131

1 Introduction

As the world's population expands, so does the depletion of resources. This has ignited a surge of interest in seeking a modern, safe, and globally accessible resource (Rico-García 2020). Polymers are one of the clean sources when we talk about clean sources. Polymer can be used to replace metal and inorganic materials in our setting. Polymers were considered as an alternate source because to their qualities such as low density, low cost, low abrasiveness, low weight, easy synthesis, chemical resistance, radar absorbent, thermally and electrically insulating, and easier to remove. Polymers have a number of drawbacks, including strength to size ratio is less, can't withstand high temperature, can't be machined easily, less heat capacity, difficult to disposure etc. Due to characteristics like as eco-friendliness, low cost, and biodegradability, bio regenerated polymers are garnering the interest of the research community. By replacing conventional materials with bio sustainable polymers such as lignocelluloses materials, energy consumption and emissions can be minimised. Cellulose, hemi-cellulosic, lignin, and inorganic material are the primary constituents of lignocelluloses materials. Because of their drawbacks, such as low chemical resistance and hydrolysis, plant lignocelluloses content must be modified with different treatments (Ricciardi et al. 2004). cellulose (40–45 wt%), hemicelluloses (25–35 wt%), lignin (15–30 wt%), and inorganic components (up to 10 wt%) make up the plant biomass (Rico-García 2020). Lignin is an in-expansive source since it is a by-product of the paper industry and ethanol industry. Coconut has 45% lignin, rice husk has 35% lignin, and wood has 10–35% lignin.

Hydrogel has been characterised in a variety of ways by different researchers, but the most common is that it is a water-swollen and cross-linked polymeric network formed by polymerization of monomers or modification of existing polymers. Hydrogels made of biopolymers are one form of bio renewable polymer-based material. These hydrogels have benefits such as being quickly degraded in water, the ability to stimulate natural tissues, and so on. Lignin-based hydrogel is one of the bio renewable polymer-based hydrogel. Hardwood contains approximately 48–50% cellulose, 25–27% hemicelluloses and 19–23% lignin, while softwood contains 42–45% cellulose, 20–31% hemicelluloses and 25–28% lignin (Ricciardi et al. 2004).
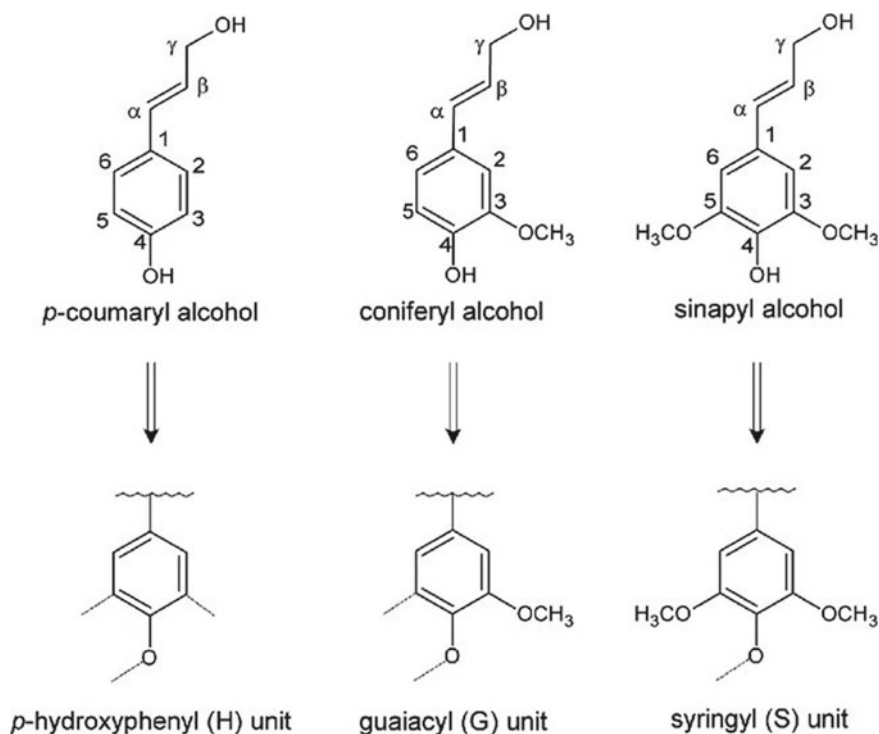
2 Lignin

Lignin is the most prevalent aromatic natural complex polymer on earth, behind cellulose (Chern 2006). It is branched bio macromolecule with molecular masses ranging from 1000 to 20,000 g/mol (Rico-García 2020) and it is obtained from plant species and it may make up as much as 30% of a plant's biomass (Thakur et al. 2016), for instance, Hardwood consists around 19–23% lignin and softwood consist around 25–28% lignin. It binds with cellulose and hemicelluloses to give plant cells toughness, stability, and inflexibility (Chern 2006). There is no fixed lignin

structure because the lignin structure is extremely complex. Different structures and repeated units make up lignin's structure, which varies depending on the plant's species, position, growth length, and the extraction method used to distinguish it from cellulose and hemi-cellulose. P'-hydroxyphenyl (H), Guaiacyl (G), and Syringyl (S) are the three components of lignin. Sinapyl alcohol, coniferyl alcohol and Coumaryl alcohol are three different phenyl propane monomers that yield P'-hydroxyphenyl (H), Guaiacyl (G), and Syringyl (S) units as shown is Fig. 1.

Softwood lignin consistsof P'-hydroxyphenyl (H), Guaiacyl (G) and Syringyl (S), these are connected with each other with different bonds as shown in Fig. 2.

Lignin, like other biodegradable polymers, has a number of advantages, including antioxidant properties, biodegradability, CO_2 neutrality, antimicrobial properties, and the ability to be obtained in large amounts as a waste by-product. In lignin, different monomers form various forms of carbon–carbon and carbon–oxygen bonds. The parent cellulosic materials and organisms decide the amount of lignin in a given substance. Fungi and bacteria determine the biodegradability of lignin-based products. Fungi have been demonstrated to be more effective than bacteria at breaking down lignin, whereby fragmentation is slower and more restricted. Extracellular

Fig. 1 Monolignols in Lignin Structure Reprinted with permission from Schoenherr S et al. (2018), Copyright (2018)
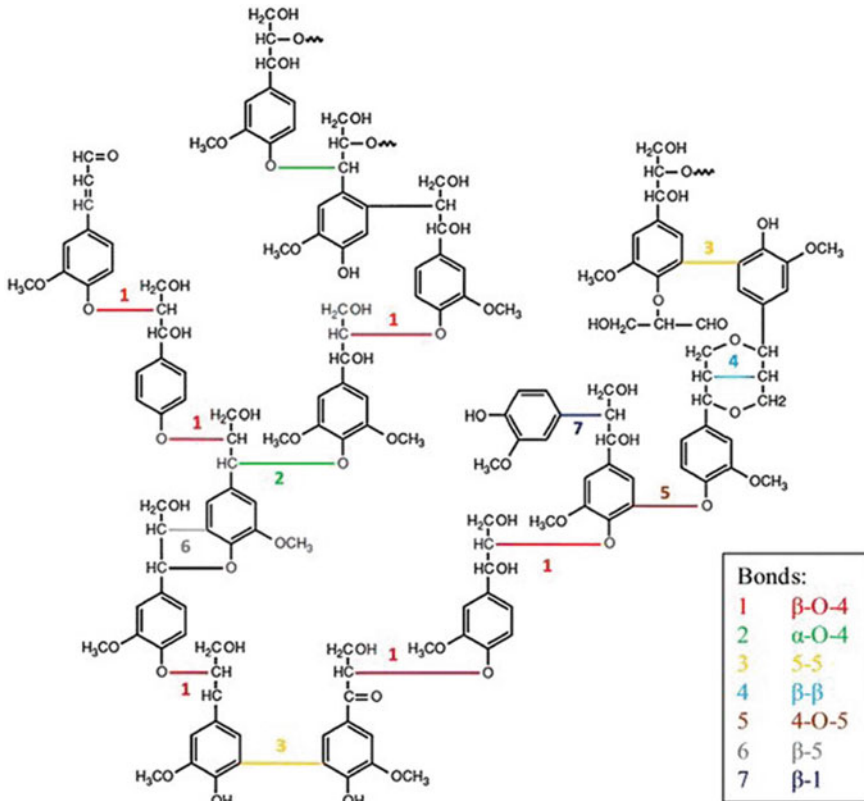
Fig. 2 Main Linkages in the structure of Lignin Reprinted with permission from Thakur VK et al. (2015), Copyright (2015)

enzyme systems that use radical-based oxidative processes to break down lignin are found in microorganisms that breakdown lignin (Bian et al. 2018).

2.1 Process of Production of Different Type of Lignin

Lignin, cellulose and semi-cellulose are separated by pre-treatment as shown in Fig. 3 and following method can be used (Rico-García 2020).

a. Alkali lignin from Kraft process.
b. Organosolv lignin from Organosolv process.
c. Hydrolytic lignin from enzymatic hydrolysis.
d. Lignosulfonates from sulphite process.
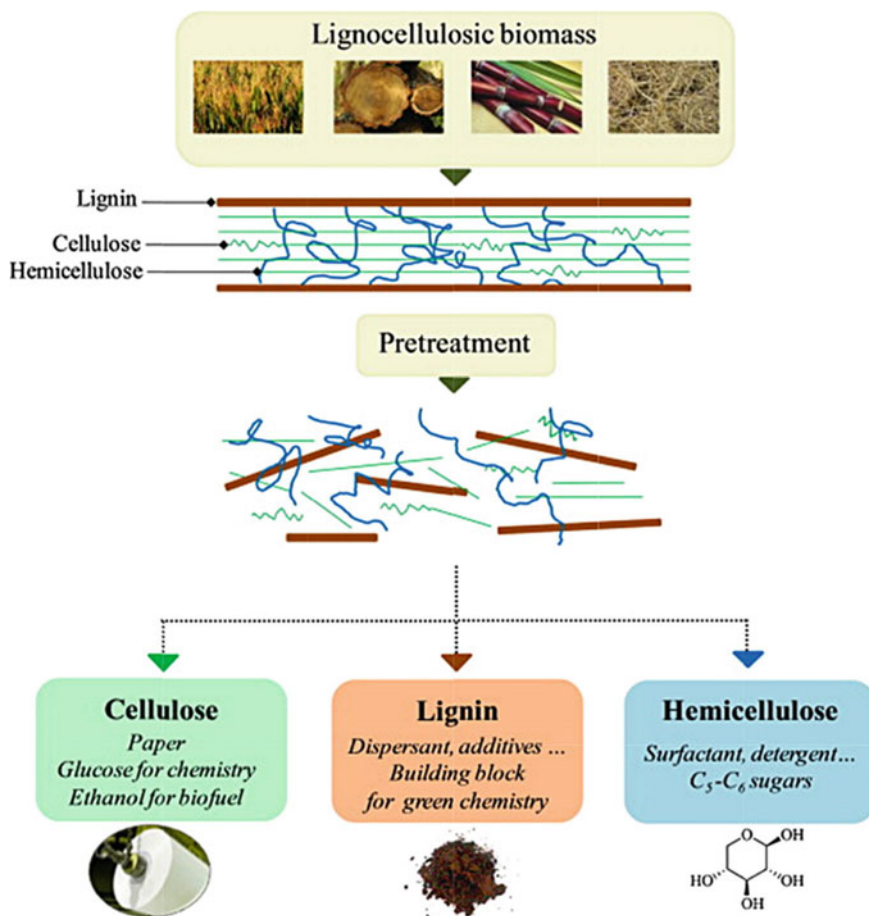
Fig. 3 Pretreatment processes reprinted with permission from Thakur VK et al. (2015), Copyright (2015)

2.1.1 Kraft Process

Wood is transformed to wood chips, which are then treated in a digester with white liquor (an aqueous solution of sodium hydroxide (NaOH) and sodium sulphate (Na_2S)) at high pressure and temperatures of 170 °C. White liquor reacts with wood to disrupt the bonds that hold lignin, cellulose, and hemicelluloses together, resulting in the formation of lignin. This method is mostly used for softwood (Rico-García 2020).

2.1.2 Enzymatic Process

Cellulolytic enzymes hydrolyze the wood sugars, leaving lignin as an insoluble residue. A series of enzymes are used to force complete hydrolysis and degradation of the cellulose and hemicellulose carbohydrates, resulting in a higher amount of insoluble recoverable lignin. This process yields lignin that is 65–80% lignin, 7–8% carbohydrates, and free of contaminants (Rico-García 2020).

2.1.3 Organosolv Process

To extract the lignin from the cellulose, organic solvents are used. In most cases, a rotary digester is used, with the wood dust being treated with ethanol and sulphuric acid (H_2SO_4). This procedure is only used to extract lignin from hardwoods (Rico-García 2020).

2.1.4 Sulphite Process

Lignin is extracted using sulphuric acid and a sulphite salt containing magnesium, calcium, sodium, or ammonium at various pH values. Hardwood and bagasse are processed in this manner (Rico-García 2020).

3 Hydrogel

Hydrogels are three-dimensional networks of naturally or artificially cross-linked hydrophilic polymeric materials formed by modifying an existing polymer or polymerization and simultaneously cross linking one or more monomers. Its water-swelling and compression-resistance capabilities are well-known.
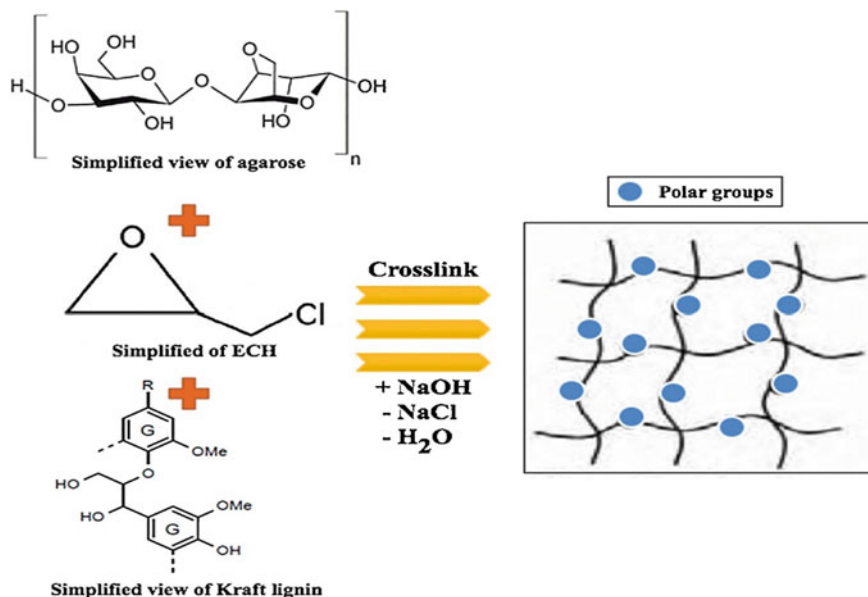
3.1 Method of Hydrogel Synthesis

The Synthesis of polymeric hydrogel is done by two ways (Mathur et al. 1996).

1. Hydrophilic monomer polymerization
2. Polymeric modification of existing polymers.

3.1.1 Polymerization of Hydrophilic Monomers

The polymerization of hydrophilic monomers is done by following techniques (Thakur and Thakur 2015).

Fig. 4 Lignin agarose polymerization Reprinted with permission from Sathawong S et al. (2018), Copyright (2018)

Bulk Polymerization

This is used to polymerize undiluted monomers. A soluble imitator is combined with a pure monomer in a liquid state to produce this. As indicated in Fig. 4, the mixture is heated to polymerization temperature while being constantly stirred. Heating is ceased when reactions begin due to their exothermic nature (Kuchanov and Bort 1973). Polyvinyl chloride, Polystyrene, low density polyethylene and polymethyl for instance, are all produced.

Solution Polymerization

The polymer is created when the monomers and initiator are dissolved in the solvent, but the polymer remains dissolved in the mixture. The mixture is continually agitated and held at polymerization temperature as shown in Fig. 5. Polymers are isolated after the reaction is completed by evaporating the solution (Sathawong et al. 2018). For example, the manufacture of polyacrylamide, polyvinyl alcohol, and polybutadiene.
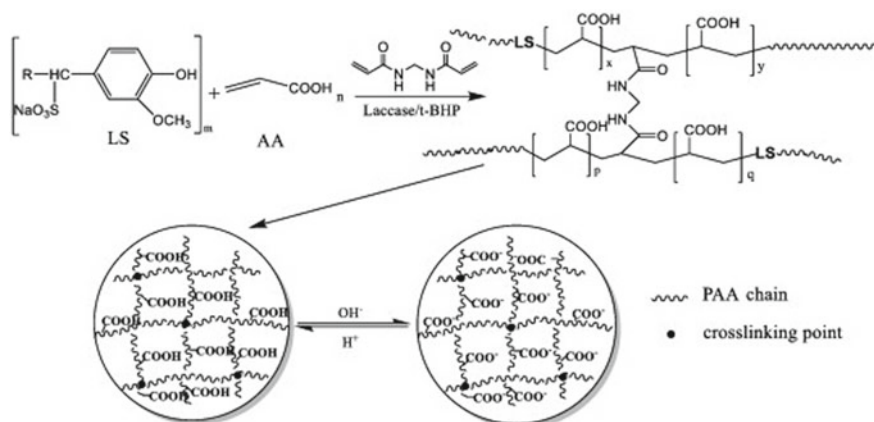
Fig. 5 Schematic synthesis of LS-g-AA hydrogel Reprinted with permission from Yu C et al. (2016), Copyright (2016)

Suspension Polymerization

Polymers are generally produced by a free-radical process in commercial suspension polymerisation. In the liquid process, dissolved monomers are combined with an initiator that is soluble in monomers. Droplets of monomers vary in size from 50 to 200 μm in diameter. Continuous agitation maintains the dispersion, and small quantities of stabilisers, such as PVA, gelatin, cellulose, magnesium silicate, aluminium hydroxide, and others, prevent the droplets from coalescing. Polymerization happens inside the droplet, and the substance is divided into spherical pearls or polymer beads as shown by Fig. 6 (Brooks 2010). Polystyrene, PVC, Polyvinyl acetate and Styrene-divinyl benzene copolymers beads are only a few examples.

Emulsion Polymerization

To achieve emulsion polymerisation, free radicals react with nonnumeric units in a high sequence of distinct polymer particles (1016–1018 dm^{-3}) spread in a continuous aqueous phase. Water-insoluble monomers, a dispersion medium, an emulsifying agent or surfactants, and a water-soluble initiator are all used in this method. In the aqueous phase, the monomer is spread in a uniform emulsion. Depending on temperature and agitation intensity, monomer droplets range in size from 0.5 to 10 μm in diameter. The monomer emulsion in water is stabilised by a surfactant (Schoenherr et al. 2018). Some examples are Polystyrene, PVC and synthetic styrene-butadiene-rubber (SBR).
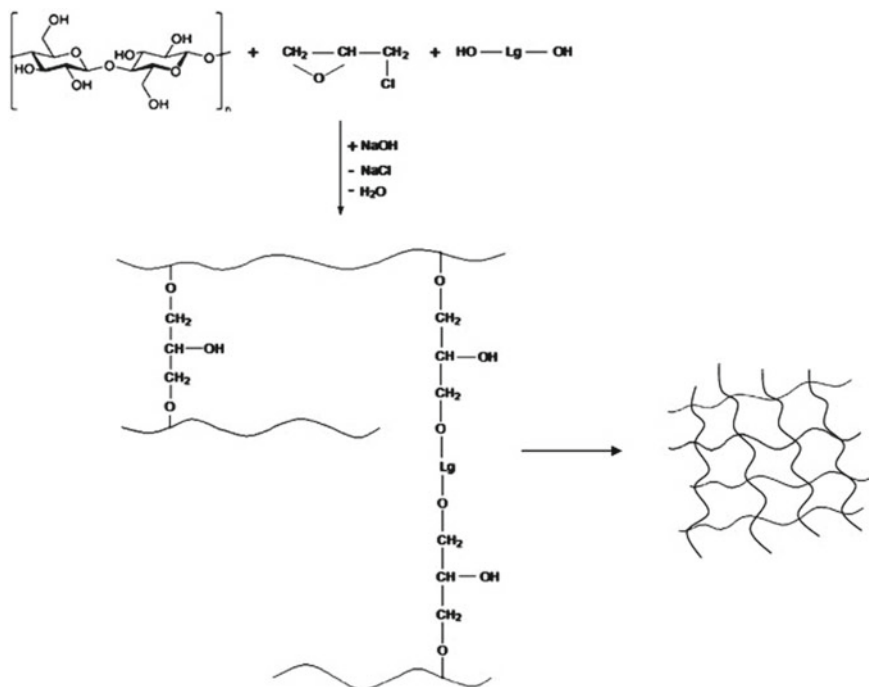
Fig. 6 Cellulose Lignin Hydrogel Synthesis Pathway Reprinted with permission from Ciolacu et al. (2012), Copyright (2012)

Polymerization by Irradiation

This is used to render unsaturated compounds. To prepare the hydrogels, ionising radiation such as gamma rays and electron beams were used as an initiator. Irradiating an aqueous polymer solution allows radicals to form on the polymer chains. The formation of hydroxyl radicals from the radiolysis of water molecules attacks the polymer chains, resulting in the formation of macro-radicals. Recombination of macro-radicals on various chains results in the formation of covalent bonds, resulting in the formation of a cross-linked structure (Thakur and Thakur 2015), as seen in polyvinyl alcohols, polyethylene glycol, and polyacrylic acid, for example.

Advantages and disadvantages of above methods are given by Table 1.

3.1.2 Modification of Existing Polymers

Hydrogel can be prepared by the modification of existing polymers (Mathur et al. 1996).

Table 1 Different Methods of Polymerization

Polymerisation method	Type of reaction	Advantages	Disadvantages
Bulk polymerisation	Homogeneous reaction	• Yield a high pure end-product • The final product has a high level of optical clarity • Molecular weight distribution can easily change	• As the viscosity of the reaction mass rises, heat transport and mixing become more difficult • It is possible to obtain molecules with extremely low molecular weights
Solution polymerisation	Homogeneous reaction	• Heat and mass transfer is easy • Stirring is also simple because the resulting product has a low viscosity • Resulting liquid product, can be used as a solid simply by drying	• It is not possible to acquire a high molecular weight • The real rate of polymerisation is slowed when a solvent is present • Complete removal of solvent is difficult
Suspension polymerisation	Heterogeneous reaction	• High economical and more environmentally friendly • Little catalyst is used to get 100% solid final product • Temperature and viscosity control is fairly easy	• Only used for water-insoluble monomers • Continuous agitation required • Contamination by the stabilizer
Emulsion polymerisation	Heterogeneous reaction	• There are no issues with the chain or heat transfer • Within 1–2 h, a high molecular weight product can be produced	• Yield a less pure end-product • To recover emulsion polymers in solid form, a significant technological investment is required • Used surfactants are difficult to remove • High water usage, thus lower yield-per-reactor volume

Table 1 (continued)

Polymerisation method	Type of reaction	Advantages	Disadvantages
Polymerisation by irradiation	–	• Cross-linking doesn't change with chemical structure of polymer and doesn't significantly affect with temperature • Cross-linking depends on the dose of radiations	–

Hydrogels from Natural Polymers and Their Derivatives

Natural polymers, such as macromolecules derived from animal collagen, seeds, and sea wood, can be used to produce hydrogels. These polymers can be modified to create hydrogels. Poly-saccharides, for example, are carbonate polymers containing glycosidic repeating units.

Hydrogel from Modification of Synthetic Polymers

Existing synthetic polymers can be modified to produce hydrogels. Polyvinyl alcohol, for example, is made by hydrolysis of polyvinyl alcohol (vinyl acetate).

4 Why We Use Lignin for Production of Hydrogel?

We use lignin for production of hydrogel, because of following reasons (Thakur and Thakur 2015).

- Due to a Chemical reaction with aromatic pollutants, phenolic rings found in lignin may help to increase organic pollutant retention.
- The hydrogel's ability to absorb contaminants may be aided by the pH sensitivity of lignin and its counter monomers.
- Lignin improves the hydrogel's thermal stability, biocompatibility, and biodegradability.
- Lignin controls the hydrogel's absorption, hydrophilicity, and mechanical characteristics.
- Lignin has antioxidant capacity due to their polyphenolic structure.
- Lignin is the world's second most abundant biopolymer.
- Lignin has dispersing, binding, complexing, and emulsion-stabilizing properties.
- Lignin has anti-Carcinogenic, apoptosis, inducing antibiotic and anti-HIV activities.

5   Technique Used for Production of Lignin-Based Hydrogel

5.1   Hydrogel Production by Polymerization

5.1.1   Synthesis of Lignin Based Polyurethane Hydrogels

"Chemical bonding with isocyanate group-terminated polyurethane ionomers could be employed to produce hydrogels out of acetic acid and lignin," as mentioned in Peng and Chen (2011). The addition of lignin to the hydrogels improves their heat stability. pH sensitivity was seen in the hydrogels. The hydrogels could be used as coating materials in the production of slow-release fertilisers. Lignin depending polyurethane hydrogel is prepared by following method.

Materials: Dimethylol-propionic acid (DMPA), polyethylene glycol (PEG 2000), 1,4-dioxane, 2,4-toulene diisocyanate(2,4-TDI).

Production: Polyethylene glycol (PEG 2000), dimethyl Ol -propionic acid (DMPA), and 1,4-dioxane were used as reactants in the lignin-based polyurethane hydrogel synthesis. In a three-necked flask, a reflux condenser, and a thermometer set at 40° Celsius, these reactants are mixed with continual stirring. As a catalyst, 2,4-toluene diisocyanate (2,4-TDI) containing ditin n-butyl dilaurate was used. This catalyst is added to the mixture in a ratio of 1:5:1 according to the isocyanate index. IPUI is produced when a flask is heated to 80 °C and left there for 2 h. After that, the flask is filled with acetic acid lignin, and the reaction is kept at 60 °C for an hour. The flask is then heated to 80 °C and permitted to cool for two hours. The hydrogel is generated once the dioxane is extracted. Acetone is added to the solution to separate cross-linked samples and eliminate soluble components.

5.1.2   Synthesis of Lignin Based Polyvinyl Alcohol Hydrogel

According to Wu et al. (2019), lignin based PVA hydrogel is produced by below method.

Material: Lignin, polyvinyl alcohol (PVA), NaOH Solution, ECH. polyvinyl alcohol (PVA), NaOH.

Swelling and mechanical characteristics of polyvinyl alcohol are poor. When lignin is added to polyvinyl alcohol, however, the water swelling and mechanical properties of the material significantly improve. A one-pot technique is used to create the lignin-PVA hydrogel. The instructions below will show you how to make a hydrogel with 5% PVA and 5% lignin by following the steps below. PVA was added to a 9 g 4% NaOH solution, which was then heated to 90 °C and swirled continuously with a magnetic field at 400 RPM until the PVA was entirely dissolved. When the PVA in the solution is completely mixed, 0.5 g of lignin is added, and the solution is agitated at room temperature with a magnetic field to form a homogeneous solution.

At room temperature, ECH (0.03 g) is added to the solution and mixed again. Before forming a firm and homogeneous Lignin-PVA hydrogel, the solution is heated at 75 °C for 20 min.

A three-level two-factorial strategy to optimise the production conditions of lignin-based PVA hydrogels was given in Wu et al. (2019). The PVA and lignin concentrations had a substantial impact on the lignin waste during the washing stage, as well as the swelling capacity of the synthesised hydrogels, according to the statistical analysis. Physical cross-linked hydrogels with up to 800% water retention and a lignin waste of 40–50% were generated using the most sophisticated synthetic techniques. When lignin was injected, SEM pictures revealed a unique porous microstructure, which was responsible for the considerable swelling capacity. As amorphous lignin was integrated, XRD analyses revealed the loss of some crystalline areas, which was corroborated by DSC and TGA techniques. Despite the fact that the Young's modulus decreased by more than half as the lignin percentage increased, compression tests revealed that all of the hydrogels maintained their integrity even when stretched to 80% of their original thickness. Finally, two approaches were used to create physically cross-linked greener lignin hydrogels with high water retention and good thermal and mechanical properties."

5.1.3   Synthesis of Lignin-Agarose Hydrogel

According to Oveissi et al. (2018), Lignin—agarose hydrogel produced by following method.

Materials: Lignin, distilled water, NaOH, Agarose, Epichlorohydrin (ECH).

Preparation: We'll need to make agarose and lignin solutions. By dissolving agarose in distilled water and boiling the solution to 682 oC for 30 min, we may generate agarose solutions with concentrations of 1, 3, and 5% (W/V). The solution is continually swirled at 120 RPM. Dissolve 100 grammes of lignin in 400 mL of water and stir for 60 min at 85 °C to make a 20% lignin solution. While stirring, 15 mL of 30 wt. percent NaOH aqueous solution is added to the solution until pH 12 is attained. Following the preparation of the lignin and agarose solutions as shown in Fig. 7, the cross-linker ECH (epichlorohydrin) is applied to both solutions, resulting in a composite solution of 1 ml to 10 ml. The solution is then stirred for 30 min at 120 RPM. We coated the beaker with a plastic film to prevent solvent evaporation during stirring.

When the pH was reduced to 3, lignin was extracted in great yield and purity. Furthermore, variations in pH have an impact on COD reduction. As lower the pH, the more efficient the elimination. To confirm the qualities of isolated lignin samples, multiple analytical techniques were used to characterise them. The researchers discovered that the lignin produced may be used to create a lignin-based hydrogel with good gel strength and mechanical properties. It offers an opinion on possible future developments.

5.1.4   Synthesis of Lignosulfonate-Acrylic Acid Hydrogel (LS-G-AA)

Polyacrylic acid can be added to the backbone of lignosulfate by grafting acrylic acid by free radical polymerization, according to Yu C et al. (2016). Catalyzed oxidation, reducing or oxidising, propagation, and termination are the four stages of radical polymerization. To begin, we must generate phenoxy radicals on lignosulfate using an oxidation method. We then used organic peroxide to oxidise reduced peroxide to produce alkoxy or peroxyl radicals. Acrylic acid monomers are covalently attached to the polyacrylic acid chain's free radical sites, allowing the polyacrylic acid chain to propagate until it is terminated. A cross-linker is used to finish the phenoxy radical.

Material: Lignosulfonate, laccase(1000U/ml), Acrylic acid N, N'-methylene-bis-acrylamide (MBA).

Production of Lignosulfonate: In 30 ml acetate buffer (0.1 mol/L, pH = 4.5), 0.34 g lignosulfonate and 4 g acrylic acid are combined. Laccase (20U) and t-BHP (40**U) are applied to the solution. A cross-linker of 24 g MBA is used to prepare the solution for cross-linking as shown in Fig. 8. Protons and other ions can be present in the substance. As a result, we deprotonated the liquid by adding NaOH drop by drop and washing with distilled water until the pH of the solution was neutral. The hydrogel is removed from the neutral solution by soaking it in acetone for 24 h at room temperature. The hydrogels are dried to a constant weight in an oven at 50 degrees Celsius.

The LS-g-AA hydrogels have a high MB absorption capacity due to the carboxylic acid groups added to them (equilibrium absorption 2013 mgg1). As a result, the Freundlich model and pseudo-2nd-order framework best fit the absorption isotherm and kinetics observed in the experiments. In general, in a mild acid solution, the MB-absorbed hydrogels could be successfully regenerated.

5.1.5   Synthesis of Polyvinyl Alcohol-Lignin Containing Cellulose Nano Fibril-Reinforced Hydrogel

According to Sathawong et al. (2018), The PVA-LCNF hydrogel is made in one pot as follows. LCNF solution (0.25–2.0 wt %) made by dissolving LCNF in distilled water. The LCNF solution is poured into a conical flask, which is then stirred for 30 min at room temperature. PVA powder is added to the flask as a 4% wt. solution. In order to prevent the formation of PVA lumps, the solution is stirred for 30 min. When the PVA powder fully swells, the solution is heated to 90 °C in an oil or water bath, and the flask is stirred with magnetic stirring for 2 h. To prevent water evaporation, the flask is sealed before heating. The solution is cooled to room temperature until it has become homogeneous. To prevent air bubbles, the solution is put in an ultrasonic water bath for 5 min. The solution is moved to a plastic beaker, which is then frozen for 12 h at −18 °C.

In a process developed by the authors, it is possible to produce a super-absorbent hydrogel from lignin and PVA using a cross-linker ECH. When the lignin content of

the polymer was increased from 0 to 5%, the swelling ratio of the polymer went from 92 to 456 g/g. Softwood lignin, hardwood lignin and corncob lignin could be used to make a lignin-PVA hydrogel with a phenomenally high swelling coefficient, and a lignin-dependent hydrogel made from a higher molecular weight PVA molecule had better swelling efficiency in water. The Lignin-PVA hydrogel adsorbed 196 mg/g of rhodamine 6G, 179 mg/g of crystal violet, and 169 mg/g of methylene blue. The Lignin-PVA hydrogel could be useful in agriculture for soil water retention, seed cultivation, and dye pollution reduction.

LCNF-reinforced PVA hydrogels were successfully created in an aqueous media without the use of initiators or chemicals. Integrating three types of cellulose nanofibrils (i.e., CNF, LCNF-lL, and LCNF-hL) into PVA aqueous systems greatly improved the viscoelastic properties and specific Young's modulus of composite hydrogels, particularly when using the LCNF with a high lignin concentration of 17%. The well-distributed LCNF in the polymer matrix served as versatile cross-linking agents, strengthening the bonds between LCNF and PVA. Lignin, specifically lignin nanoparticles extracted from LCNF during the manufacturing process, served as nano-spacers, inhibiting polymer aggregation and enhancing PVA porosity. The mechanical and rheological properties of LCNF reinforced PVA hydrogels can be changed by changing the LCNF loading and lignin content. Because LCNF may be produced more sustainably than CNF with a larger production and without bleaching, this discovery has practical implications in boosting the use of lignocellulosic materials for a wide range of applications."

5.1.6 Synthesis of Cellulose-Lignin Hydrogel

According to Bian et al. (2018), cellulose-lignin hydrogel is prepared via a cross-linking reaction as follow.

Materials: Alkaline lignin (AL), NaOH, urea, microcrystalline cellulose (MMC), deionized water.

Preparation: A solution of 100 g NaOH (6 wt%)/urea (4 wt%) is combined with 3.8 g Microcrystalline cellulose (MCC) and filtered through a G2 sand filter. The solution is treated for 12 h at $-30\,°C$ after uniform mixing. The frozen solid is thawed and then mixed at room temperature. Stir in 1.0 ml ECH and a little amount of AL (0.05, 0.1, and 0.2 g) at 30 °C for 2 h. As indicated in Fig. 9, pour the completely mixed solution into the system and let it at 60 °C for 12 h to allow the cross-linking reaction to occur. This hydrogel may contain urea and sodium hydroxide, which can be removed by washing it with deionized water.

Alkaline lignin was used as a functional cross-linker in the preparation of lignin-containing cellulose (Cell-AL) hydrogels, which allowed the hydrogel to be mechanically strengthened while enabling certain lignin molecules to be absorbed or filtered (Bian et al. 2018). This fractionation procedure extracted lignin with a high concentration of aliphatic structures and a low number of phenolic structures without lignin

linkage cleavage, according to structural characterisation. The ratio of lignin functional cross-linker is a crucial predictor of hydrogel network development, as well as hydrogel characteristics and lignin fractionation efficiency, according to the findings. The Cell-AL hydrogel can also be used again.

5.1.7 Synthesis of Lignin Based Hyaluronan Hydrogel

According to Musilová et al. (2018), The following is a summary of how to make a hydrogel.

Materials: Hyaluronan (NaHY), crosslinking agent N-(3-di-methylaminopropyl- N_ ethyl carbodiimide hydrochloride (EDC), formaldehyde solution 37% (w/w), glycine (98.5%), sodium acetate trihydrate (99.5%), acetic acid (99.0%).

Preparation: Preparation consists of two steps.

1.   Glycine-formaldehyde Modification of Kraft Lignin

Water does not dissolve lignin. As a result, lignin must be altered. 4 g methanol kraft lignin is combined with a 0.08 mol sodium acetate trihydrate solution in acetic acid. At 50o C, 1.6 ml 37% formaldehyde is added to the lignin/glycine solution at a rate of 500 micro-L/min. The pH of the solution is changed to pH = 2 after dissolving the lignin in water for 4 h. Ethyl acetate is then used to coagulate the lignin. After that, the lignin is vacuum-dried at 60 °C. Water soluble Kraft lignin (WS/KL) is the name for this form of lignin.

2.   Preparation of Hydrogels

Preparation of WS/KL solution: Modified lignin is slowly applied to Milli-Q water with constant stirring for 24 h at 50 °C, until the WS/KL solution concentration reaches 1% (w/w). PTFE Syringe filters with a pore size of 0.45 m were used to filter the prepared WS/KL solution (Millipore).

Sodium salt of hyaluronic acid solution: Hyaluronan is mixed with Milli-Q water and swirled continuously at 50 °C for 24 h until the sodium salt of hyaluronic acid solution reaches 1% (w/w). The WS/KL solution is mixed for 1 h at 50 °C with a 1% (w/w) hyaluronan solution. As a cross linker, EDC was added to the hyaluronan-lignin solution and mixed continuously for 1 h at 25 °C. By stirring in 0.1 M HCl solution, the pH of the solution is altered to 4.5–4.7. This solution was frozen for 60 h at 18 degrees Celsius in a polystyrene container, then freeze-dried with a freeze-dryer to generate a porous hydrogel with a diameter of 28 mm and a height of 5 mm.

The stability, swelling capacity, and viscoelastic properties of the NaHy/lignin hydrogels have been demonstrated to be easily mixed, which could have a substantial impact on their applicability. Furthermore, adding lignin to hyaluronan hydrogels had no influence on the final product's cytotoxicity. This favourable outcome, in combination with the cells' ability to migrate into the structure and multiply within the body of the sample under investigation, qualifies a hyaluronan and lignin-based product for tissue engineering and other biomedical applications."

5.1.8 Silicate-Lignin Based Hydrogel

According to Burrs et al. (2013), Prepare a saponite hydrogel and then combine it with modified cationic lignin to produce a silicate lignin-based hydrogel.

Silicate-based hydrogel synthesis: Saponite and laponite clay are mixed with 2% Deionization water and agitated for 12–18 h to make homogenous solutions. To make the sol–gel solution, 5 g Tetraethyl orthosilicate (TEOS), 4.325 g H_2O, and 2.3 g HCl (0.04 M) are combined at 22 °C in a closed vessel and shaken for 30 min. The sol–gel solution is combined with the Saponite and Laponite clay solution to create a Saponite and Laponite clay hydrogel.

Lignin-based hydrogel synthesis: A fermentation broth from a cellulosic bioethanol process was utilised to extract lignin. The residues are composed of 60–70% lignin, 10–20% carbohydrate, and 10% protein. To obtain high purity lignin, alkaline extraction, organosolvent extraction, and enzyme hydrolysis were used. Ethyl trimethyl ammonium chloride (ETAC) adds quaternary ammonium groups to lignin to generate cationic lignin groups. When cationic lignin is combined with a 1.25% (wt.) saponite hydrogel, a lignin-Saponite based hydrogel is generated.

These hydrogel-nonmaterial composite sheets offer a new method for immobilising enzymes on metal electrodes that is both sustainable and long-lasting. The most difficult aspect of creating these devices is immobilising proteins while keeping their tertiary structure. Researchers will be able to better comprehend the bio-nano interaction in enzyme biosensors thanks to the findings of Burrs et al. (2013). Understanding the fundamental electron transport pathways at this interface is crucial not only for biosensors, but also for biofuel cells, implanted medication delivery devices, and medical monitoring."

5.1.9 Preparation of Hydrogels and Films of Chitosan-Alkali Lignin

According to Ravishankar, et al. (2019), A chitosan-alkali lignin-based hydrogel is made by combining a chitosan solution with an alkali lignin solution.

Chitosan solution: 2.5 g of chitosan is dissolved in 100 ml of 2.5 v/v percent acetic acid to create it.

Alkali lignin solution: One gram of alkali lignin is dissolved in ten millilitres of water to make it.

Chitosan and alkali lignin gels are washed with a 1 M NH_4OH solution to neutralise and eliminate any unbound alkali lignin. To make chitosan and alkali lignin xerogels, the neutralised gel was freeze-dried. Many of the tests were carried out on powdered and dried gels. To make cross-linked films, cast chitosan films were immersed in a 10% w/v solution of alkali lignin for three hours. It was then rinsed in distilled water and dried overnight at 65 °C in a hot air oven.

Ionotropic cross-linking of chitosan and alkali lignin produced hydrogels and cross-linked films of the two components. Electro-kinetic potential and solubility

investigations, among other things, were used to confirm the nature of cross-linking. These biocompatible materials provided an optimal environment for cell adhesion and proliferation, making them ideal for tissue engineering and wound healing scaffolds. Its attraction is reinforced even more by the reusability and low cost of the systems. While tissue engineering and regenerative medicine have great potential, more research into the reasons and circumstances of biocompatibility is needed."

5.1.10 Production of Methylvinylether and Maleic Acid Copolymer (GAN), Polyethylene Glycol/ Glycerol (PEG/GLY) and Lignin Based Hydrogel

According of Ahmed (2015),

Materials: lignin, methylvinylether and maleic acid copolymer (GAN), polyethylene glycol/ Glycerol (PEG/GLY) and Lignin.

Hydrogel Synthesis: A solution of 70% Ethanol/water, 10% (w/w) LIG, 5% (w/w) GAN, and 5% (w/w) GLY or PEG is prepared.

These mixtures are poured into a 5 cm × 5 cm mould and let to be dried for at least 48 h. After that, the films were chopped into smaller pieces with a cork borer (diameter 1 cm) and baked at 80 °C for 24 h. The films were immersed in an ethanol/water (70% v/v) solution for 1 week to remove unreacted chemicals. On a regular basis, this solution was updated.

Hydrogels were also made using a MW-assisted approach. In this procedure, which is similar to the one previously discussed, the thermal process (80 °C for 24 h) was substituted by a MW aided process. "In a Panasonic NN-CF778S MW oven, samples were cooked for 1 h at full power (1000 W).

It is possible to make LIG-based hydrogels in a simple and environmentally friendly manner (Ahmed 2015). Because it does not require the use of harmful solvents, it is one of the most important components of the absorption capabilities of up to 500%. When PEGs with greater molecular weights of 14,000 and 10,000 were employed, the maximum LIG content and swelling capacities were discovered. The material hydrogel can be reused. After mixing the bio molecule with GAN, a polyacid, and PEG in an esterification technique, LIG hydrogels were successfully generated. The molecular weight of the PEG had an impact on the final LIG concentration and water uptake capacity of the hydrogel. When PEGs with greater molecular weights of 14,000 and 10,000 were employed, the maximum LIG content and swelling capacities were discovered. The hydrogels were capable of releasing hydrophobic chemicals for up to 4 days after being loaded with them.

PEG hydrogels with a molecular weight of 10,000 had the best drug loading and release qualities. S. aureus and P. mirabilis, two prevalent bacteria responsible for medical device-related diseases, were used to assess the antimicrobial properties of LIG-based hydrogel materials cross-linked with PEG 10,000. When compared to PVC and similar hydrogels that do not include LIG, the results of these trials revealed that LIG-based hydrogels demonstrated exceptional resistance to bacterial adherence.

Because of their resistance to infection and ability to distribute medications over several days, LIG-based hydrogels offer potential as medicinal material coverings."

5.2 Modification of Existing Monomers

5.2.1 Polysaccharides and Lignin-Based Hydrogel

According to Farhat et al. (2017),

Material: kraft lignin, citric acid (CA), sodium hypophosphite (SHP).

A micro-extruder is used to make reactive extrusion hydrogels, which allows the feed to be exposed to the atmosphere. There is a recirculation thread in the extruder.

By altering the citric acid (CA) level from 20 to 200%, we were able to create a variety of formulations. (wt lignin: wt CA) We sought to add sodium hypophosphite (SHP) in some formulations so that it accounted for 20% of the CA in the final product (wt SHP: wt CA). With a screw rotation speed of 120 rpm, the extruder recirculation time was either 2 or 5 min. In the extruder, a temperature of 120 °C is maintained.

Hydrogels were produced from biomolecules, starch, hemicelluloses, and lignin via reactive extrusion with and without SHP catalyst under the influence of citric acid. The hydrogels' equilibrium swelling reached 1380%. The swelling behaviour of the produced hydrogels might vary significantly depending on the material composition and the pH of the media. Due to electrostatic repulsion generated by the ionised citric acid moieties grafted to the polymer, the swelling degree of hydrogels increased at high pH levels. Furthermore, the citric acid concentration during the reactive extrusion process, as well as the molecular weight of the polymeric substance, have a significant impact on the weight loss of such a material in physiological solution. These plant-based biopolymers may be used in a variety of biomedical applications due to the characteristics of the hydrogels generated."

6 Hydrogels and They Suggest that Hydrogels Have Wide Applications

1. **Dye's adsorption**: Rhodamine 6G, methylene blue, crystal violet, and methyl orange are among the dyes that are toxic to marine life and the environment. These must be separated from industrial waste water. Hydrogel may be used to extract dyes from waste water in the manufacturing industry. A super-absorbent called lignin-PVA hydrogel is used to extract dyes from industrial waste water (Thakur 2017).

2. **Slow-release fertilizer**: Hydrogel has the ability to swell and hold large amounts of water when swollen. Hydrogel is used to produce a slow-release fertiliser

because of these properties. Ammonium sulphate $((NH_4)_2SO_4)$ is applied to the lignin-polyurethane solution to produce slow-release fertiliser. The coating method is uniformed by swirling the mixture. After the dioxane is removed, the slow-release fertiliser is collected. Slow-release fertiliser is used in agriculture to reduce fertiliser use while also reducing emissions. In contrast to ammonium sulphate without coating, ammonium sulphate coated with gel has control-release properties, and the release ratios increase as the mass ratio of AAL to IPUI increases from 0 to 0.35. The graph below shows how the release ratio has changed over time as the mass ratio of AAL to IPUI has increased.

3. **Drug Delivery and medical material coating**: The polymeric network of a lignin-based hydrogel has a porous structure, which allows drugs to be inserted within and thus protect them from the environment. Lignin has antiviral, immunomodulatory, antibacterial, anti-bacterial, and anti-parasite properties. As a result, we use lignin-based hydrogels for drug delivery and coating medical materials. For drug delivery, polysaccharides and lignin-based hydrogels are used.

4. **Wound healing medication**: Dispersing, binding, complexing, emulsion stabilisation, anti-biotic properties, and so on are all properties of lignin. Because of their properties, lignin-based hydrogels boost lap sheer adhesiveness and processability, and are thus used for wound healing medicine. Hydrogels based on Na/Hg lignin are used to treat wounds.

5. **Agriculture for retention of water**: Hydrogels produced of synthetic polymers can hold moisture from irrigation or rainfall and release it in response to crop water demands, but they have a short functional lifetime and can generate a by-product that is safe for plants but pollutes the soil environment.

7 Future Perspective and Conclusions

The abundance of lignin in nature, as a by-product of the pulp and paper industries, ethanol industries, and other industries, has piqued the interest of the research community in lignin-based materials.

Lignin has a few flaws:

- Since lignin contains a limited amount of hydroxyl groups, it is difficult to crosslink with other molecules.
- The structure of lignin is complex and sporadic. So, it's difficult to find novel applications of lignin-based product.

Lignin needs to be repurposed. Companies nowadays are concerned about environmental issues. Industries have discovered low-cost treatments to remove toxic waste (lignin). Thus, the manufacture of hydrogel from lignin will add value to industries by opening up new business opportunities and allowing for the free removal of lignin. The importance of research in this area is underscored by the fact that each year, a large number of groups plan various presentations.

References

Ahmed EM (2015) Hydrogel: Preparation, characterization, and applications: a review. J Adv Res 6:105–121

Athawale VD, Lele V (1998) Graft copolymerization onto starch. II. Grafting of acrylic acid and preparation of it's hydrogels. Carbohydr Polym 35:21–27

Bian H et al (2018) Lignin-containing cellulose nanofibril-reinforced polyvinyl alcohol hydrogels. ACS Sustain Chem Eng 6:4821–4828

Brooks B (2010) Suspension polymerization processes. Chem Eng Technol 33

Brown ME, Chang MCY (2014) Exploring bacterial lignin degradation. Curr Opin Chem Biol 19:1–7

Brzonova I et al (2017) Production of lignin based insoluble polymers (anionic hydrogels) by C. versicolor. Sci Rep 7:17507

Burrs SL, Jairam S, Vanegas DC, Tong Z, McLamore ES (2013) Lignin and silicate based hydrogels for biosensor applications. In: Proceedings of SPIE vol 8719

Chern CS (2006) Emulsion polymerization mechanisms and kinetics. Prog Polym Sci 31:443–486

Ciolacu D, Oprea AM, Anghel N, Cazacu G, Cazacu M (2012) New cellulose–lignin hydrogels and their application in controlled release of polyphenols. Mater Sci Eng C 32:452–463

Dai L et al (2019) A lignin-containing cellulose hydrogel for lignin fractionation. Green Chem 21:5222–5230

Domínguez-Robles J, Peresin MS, Tamminen T, Rodríguez A, Larrañeta E, Jääskeläinen AS (2018) Lignin-based hydrogels with "super-swelling" capacities for dye removal. Int J Biol Macromol 115:1249–1259

Farhat W et al (2017) Polysaccharides and lignin based hydrogels with potential pharmaceutical use as a drug delivery system produced by a reactive extrusion process. Int J Biol Macromol 104:564–575

Feng Q, Chen F, Wu H (2011) Preparation and characterization of a temperature-sensitive lignin-based hydrogel. Bioresour 6(4)

Heidarian P et al (2020) Dynamic plant-derived polysaccharide-based hydrogels. Carbohydr Polym 231:115743

Kuchanov SI, Bort DN (1973) Kinetics and mechanism of bulk polymerization of vinyl chloride. Polym Sci USSR 15:2712–2736

Larrañeta E et al (2018) Synthesis and characterization of lignin hydrogels for potential applications as drug eluting antimicrobial coatings for medical materials. ACS Sustain Chem Eng 6:9037–9046

Liu H, Chung H (2017) Lignin-based polymers via graft copolymerization. J Polym Sci Part A Polym Chem 55

Mathur AM, Moorjani SK, Scranton AB (1996) Methods for synthesis of hydrogel networks: a review. J Macromol Sci Part C 36:405–430

Mazloom N, Khorassani R, Zohury GH, Emami H, Whalen J (2020) Lignin-based hydrogel alleviates drought stress in maize. Environ Exp Bot 175:104055

Moreno A, Sipponen MH (2020) Lignin-based smart materials: a roadmap to processing and synthesis for current and future applications. Mater Horizons 7:2237–2257

Mujumdar AN, Young SG, Merker RL, Magill JH (1990) A study of solution polymerization of polyphosphazenes. Macromolecules 23:14–21

Musilová L et al (2018) Hyaluronan hydrogels modified by glycinated Kraft lignin: morphology, swelling, viscoelastic properties and biocompatibility. Carbohydr Polym 181:394–403

Oveissi F, Naficy S, Le TYL, Fletcher DF, Dehghani F (2018) Tough and processable hydrogels based on lignin and hydrophilic polyurethane. ACS Appl Bio Mater 1:2073–2081

Peng Z, Chen F (2011) Synthesis and properties of lignin-based polyurethane hydrogels. Int J Polym Mater Polym Biomater 60:674–683

Ravishankar K et al (2019) Biocompatible hydrogels of chitosan-alkali lignin for potential wound healing applications. Mater Sci Eng C Mater Biol Appl 102:447–457

Ricciardi R, Auriemma F, Gaillet C, De Rosa C, Lauprêtre F (2004) Investigation of the crystallinity of freeze/thaw poly(vinyl alcohol) hydrogels by different techniques. Macromolecules 37:9510–9516

Rico-garc D, Ruiz-rubio L, Leyre P (2020) Lignin-based hydrogels : synthesis and applications, pp 1–23

Rico-García D et al (2020) Lignin-based hydrogels: synthesis and applications. Polymers 12

Sathawong S, Sridach W, Techato K (2018) Lignin: Isolation and preparing the lignin based hydrogel. J Environ Chem Eng 6:5879–5888

Schoenherr S, Ebrahimi M, Czermak P (2018) Lignin degradation processes and the purification of valuable products

Shi R, Li B (2016) Synthesis and characterization of cross-linked starch/lignin film. Starch Stärke 68:1224–1232

Thakur VK, Thakur MK (2015) Recent advances in green hydrogels from lignin: a review. Int J Biol Macromol 72:834–847

Thakur S, Pandey S, Arotiba OA (2016) Development of a sodium alginate-based organic/inorganic superabsorbent composite hydrogel for adsorption of methylene blue. Carbohydr Polym 153:34–46

Thakur S, Govender P, Mamo M, Tamulevičius S, Thakur VK (2017) Recent progress in gelatin hydrogel nanocomposites for water purification and beyond. Vacuum 146

Wu L et al (2019) Synthesis and characterization of biomass lignin-based PVA super-absorbent hydrogel. Int J Biol Macromol 140:538–545

Yu C, Wang F, Zhang C, Fu S, Lucia LA (2016) The synthesis and absorption dynamics of a lignin-based hydrogel for remediation of cationic dye-contaminated effluent. React Funct Polym 106:137–142